Shashank Bishnoi *Editor*

Calcined Clays for Sustainable Concrete

Proceedings of the 3rd International Conference on Calcined Clays for Sustainable Concrete

Springer

Calcined Clays for Sustainable Concrete

RILEM BOOKSERIES

Volume 25

RILEM, The International Union of Laboratories and Experts in Construction Materials, Systems and Structures, founded in 1947, is a non-governmental scientific association whose goal is to contribute to progress in the construction sciences, techniques and industries, essentially by means of the communication it fosters between research and practice. RILEM's focus is on construction materials and their use in building and civil engineering structures, covering all phases of the building process from manufacture to use and recycling of materials. More information on RILEM and its previous publications can be found on www.RILEM.net.

Indexed in SCOPUS, Google Scholar and SpringerLink.

More information about this series at http://www.springer.com/series/8781

Shashank Bishnoi
Editor

Calcined Clays for Sustainable Concrete

Proceedings of the 3rd International Conference on Calcined Clays for Sustainable Concrete

Springer

Editor
Shashank Bishnoi
Department of Civil Engineering
Indian Institute of Technology Delhi
New Delhi, Delhi, India

Contents

RILEM Publications

The following list is presenting the global offer of RILEM Publications, sorted by series. Each publication is available in printed version and/or in online version.

RILEM Proceedings (PRO)

PRO 1: Durability of High Performance Concrete (ISBN: 2-912143-03-9; e-ISBN: 2-351580-12-5; e-ISBN: 2351580125); *Ed. H. Sommer*

PRO 2: Chloride Penetration into Concrete (ISBN: 2-912143-00-04; e-ISBN: 2912143454); *Eds. L.-O. Nilsson and J.-P. Ollivier*

PRO 3: Evaluation and Strengthening of Existing Masonry Structures (ISBN: 2-912143-02-0; e-ISBN: 2351580141); *Eds. L. Binda and C. Modena*

PRO 4: Concrete: From Material to Structure (ISBN: 2-912143-04-7; e-ISBN: 2351580206); *Eds. J.-P. Bournazel and Y. Malier*

PRO 5: The Role of Admixtures in High Performance Concrete (ISBN: 2-912143-05-5; e-ISBN: 2351580214); *Eds. J. G. Cabrera and R. Rivera-Villarreal*

PRO 6: High Performance Fiber Reinforced Cement Composites - HPFRCC 3 (ISBN: 2-912143-06-3; e-ISBN: 2351580222); *Eds. H. W. Reinhardt and A. E. Naaman*

PRO 7: 1st International RILEM Symposium on Self-Compacting Concrete (ISBN: 2-912143-09-8; e-ISBN: 2912143721); *Eds. Å. Skarendahl and Ö. Petersson*

PRO 8: International RILEM Symposium on Timber Engineering (ISBN: 2-912143-10-1; e-ISBN: 2351580230); *Ed. L. Boström*

PRO 9: 2nd International RILEM Symposium on Adhesion between Polymers and Concrete ISAP '99 (ISBN: 2-912143-11-X; e-ISBN: 2351580249); *Eds. Y. Ohama and M. Puterman*

PRO 10: 3rd International RILEM Symposium on Durability of Building and Construction Sealants (ISBN: 2-912143-13-6; e-ISBN: 2351580257); *Ed. A. T. Wolf*

PRO 11: 4th International RILEM Conference on Reflective Cracking in Pavements (ISBN: 2-912143-14-4; e-ISBN: 2351580265); *Eds. A. O. Abd El Halim, D. A. Taylor and El H. H. Mohamed*

PRO 12: International RILEM Workshop on Historic Mortars: Characteristics and Tests (ISBN: 2-912143-15-2; e-ISBN: 2351580273); *Eds. P. Bartos, C. Groot and J. J. Hughes*

PRO 13: 2nd International RILEM Symposium on Hydration and Setting (ISBN: 2-912143-16-0; e-ISBN: 2351580281); *Ed. A. Nonat*

PRO 14: Integrated Life-Cycle Design of Materials and Structures - ILCDES 2000 (ISBN: 951-758-408-3; e-ISBN: 235158029X); (ISSN: 0356-9403); *Ed. S. Sarja*

PRO 15: Fifth RILEM Symposium on Fibre-Reinforced Concretes (FRC) - BEFIB'2000 (ISBN: 2-912143-18-7; e-ISBN: 291214373X); *Eds. P. Rossi and G. Chanvillard*

PRO 16: Life Prediction and Management of Concrete Structures (ISBN: 2-912143-19-5; e-ISBN: 2351580303); *Ed. D. Naus*

PRO 17: Shrinkage of Concrete – Shrinkage 2000 (ISBN: 2-912143-20-9; e-ISBN: 2351580311); *Eds. V. Baroghel-Bouny and P.-C. Aïtcin*

PRO 18: Measurement and Interpretation of the On-Site Corrosion Rate (ISBN: 2-912143-21-7; e-ISBN: 235158032X); *Eds. C. Andrade, C. Alonso, J. Fullea, J. Polimon and J. Rodriguez*

PRO 19: Testing and Modelling the Chloride Ingress into Concrete (ISBN: 2-912143-22-5; e-ISBN: 2351580338); *Eds. C. Andrade and J. Kropp*

PRO 20: 1st International RILEM Workshop on Microbial Impacts on Building Materials (CD 02) (e-ISBN 978-2-35158-013-4); *Ed. M. Ribas Silva*

PRO 21: International RILEM Symposium on Connections between Steel and Concrete (ISBN: 2-912143-25-X; e-ISBN: 2351580346); *Ed. R. Eligehausen*

PRO 22: International RILEM Symposium on Joints in Timber Structures (ISBN: 2-912143-28-4; e-ISBN: 2351580354); *Eds. S. Aicher and H.-W. Reinhardt*

PRO 23: International RILEM Conference on Early Age Cracking in Cementitious Systems (ISBN: 2-912143-29-2; e-ISBN: 2351580362); *Eds. K. Kovler and A. Bentur*

PRO 24: 2nd International RILEM Workshop on Frost Resistance of Concrete (ISBN: 2-912143-30-6; e-ISBN: 2351580370); *Eds. M. J. Setzer, R. Auberg and H.-J. Keck*

PRO 25: International RILEM Workshop on Frost Damage in Concrete (ISBN: 2-912143-31-4; e-ISBN: 2351580389); *Eds. D. J. Janssen, M. J. Setzer and M. B. Snyder*

PRO 26: International RILEM Workshop on On-Site Control and Evaluation of Masonry Structures (ISBN: 2-912143-34-9; e-ISBN: 2351580141); *Eds. L. Binda and R. C. de Vekey*

PRO 27: International RILEM Symposium on Building Joint Sealants (CD03; e-ISBN: 235158015X); *Ed. A. T. Wolf*

PRO 28: 6th International RILEM Symposium on Performance Testing and Evaluation of Bituminous Materials - PTEBM'03 (ISBN: 2-912143-35-7; e-ISBN: 978-2-912143-77-8); *Ed. M. N. Partl*

PRO 29: 2nd International RILEM Workshop on Life Prediction and Ageing Management of Concrete Structures (ISBN: 2-912143-36-5; e-ISBN: 2912143780); *Ed. D. J. Naus*

PRO 30: 4th International RILEM Workshop on High Performance Fiber Reinforced Cement Composites - HPFRCC 4 (ISBN: 2-912143-37-3; e-ISBN: 2912143799); *Eds. A. E. Naaman and H. W. Reinhardt*

PRO 31: International RILEM Workshop on Test and Design Methods for Steel Fibre Reinforced Concrete: Background and Experiences (ISBN: 2-912143-38-1; e-ISBN: 2351580168); *Eds. B. Schnütgen and L. Vandewalle*

PRO 32: International Conference on Advances in Concrete and Structures 2 vol. (ISBN (set): 2-912143-41-1; e-ISBN: 2351580176); *Eds. Ying-shu Yuan, Surendra P. Shah and Heng-lin Lü*

PRO 33: 3rd International Symposium on Self-Compacting Concrete (ISBN: 2-912143-42-X; e-ISBN: 2912143713); *Eds. Ó. Wallevik and I. Níelsson*

PRO 34: International RILEM Conference on Microbial Impact on Building Materials (ISBN: 2-912143-43-8; e-ISBN: 2351580184); *Ed. M. Ribas Silva*

PRO 35: International RILEM TC 186-ISA on Internal Sulphate Attack and Delayed Ettringite Formation (ISBN: 2-912143-44-6; e-ISBN: 2912143802); *Eds. K. Scrivener and J. Skalny*

PRO 36: International RILEM Symposium on Concrete Science and Engineering – A Tribute to Arnon Bentur (ISBN: 2-912143-46-2; e-ISBN: 2912143586); *Eds. K. Kovler, J. Marchand, S. Mindess and J. Weiss*

PRO 37: 5th International RILEM Conference on Cracking in Pavements – Mitigation, Risk Assessment and Prevention (ISBN: 2-912143-47-0; e-ISBN: 2912143764); *Eds. C. Petit, I. Al-Qadi and A. Millien*

PRO 38: 3rd International RILEM Workshop on Testing and Modelling the Chloride Ingress into Concrete (ISBN: 2-912143-48-9; e-ISBN: 2912143578); *Eds. C. Andrade and J. Kropp*

PRO 39: 6th International RILEM Symposium on Fibre-Reinforced Concretes - BEFIB 2004 (ISBN: 2-912143-51-9; e-ISBN: 2912143748); *Eds. M. Di Prisco, R. Felicetti and G. A. Plizzari*

PRO 40: International RILEM Conference on the Use of Recycled Materials in Buildings and Structures (ISBN: 2-912143-52-7; e-ISBN: 2912143756); *Eds. E. Vázquez, Ch. F. Hendriks and G. M. T. Janssen*

PRO 41: RILEM International Symposium on Environment-Conscious Materials and Systems for Sustainable Development (ISBN: 2-912143-55-1; e-ISBN: 2912143640); *Eds. N. Kashino and Y. Ohama*

PRO 42: SCC'2005 - China: 1st International Symposium on Design, Performance and Use of Self-Consolidating Concrete (ISBN: 2-912143-61-6; e-ISBN: 2912143624); *Eds. Zhiwu Yu, Caijun Shi, Kamal Henri Khayat and Youjun Xie*

PRO 43: International RILEM Workshop on Bonded Concrete Overlays (e-ISBN: 2-912143-83-7); *Eds. J. L. Granju and J. Silfwerbrand*

PRO 44: 2nd International RILEM Workshop on Microbial Impacts on Building Materials (CD11) (e-ISBN: 2-912143-84-5); *Ed. M. Ribas Silva*

PRO 45: 2nd International Symposium on Nanotechnology in Construction, Bilbao (ISBN: 2-912143-87-X; e-ISBN: 2912143888); *Eds. Peter J. M. Bartos, Yolanda de Miguel and Antonio Porro*

PRO 46: ConcreteLife'06 - International RILEM-JCI Seminar on Concrete Durability and Service Life Planning: Curing, Crack Control, Performance in Harsh Environments
(ISBN: 2-912143-89-6; e-ISBN: 291214390X); *Ed. K. Kovler*

PRO 47: International RILEM Workshop on Performance Based Evaluation and Indicators for Concrete Durability (ISBN: 978-2-912143-95-2; e-ISBN: 9782912143969); *Eds. V. Baroghel-Bouny, C. Andrade, R. Torrent and K. Scrivener*

PRO 48: 1st International RILEM Symposium on Advances in Concrete through Science and Engineering (e-ISBN: 2-912143-92-6); *Eds. J. Weiss, K. Kovler, J. Marchand and S. Mindess*

PRO 49: International RILEM Workshop on High Performance Fiber Reinforced Cementitious Composites in Structural Applications (ISBN: 2-912143-93-4; e-ISBN: 2912143942); *Eds. G. Fischer and V. C. Li*

PRO 50: 1st International RILEM Symposium on Textile Reinforced Concrete (ISBN: 2-912143-97-7; e-ISBN: 2351580087); *Eds. Josef Hegger, Wolfgang Brameshuber and Norbert Will*

PRO 51: 2nd International Symposium on Advances in Concrete through Science and Engineering (ISBN: 2-35158-003-6; e-ISBN: 2-35158-002-8); *Eds. J. Marchand, B. Bissonnette, R. Gagné, M. Jolin and F. Paradis*

PRO 52: Volume Changes of Hardening Concrete: Testing and Mitigation (ISBN: 2-35158-004-4; e-ISBN: 2-35158-005-2); *Eds. O. M. Jensen, P. Lura and K. Kovler*

PRO 53: High Performance Fiber Reinforced Cement Composites - HPFRCC5 (ISBN: 978-2-35158-046-2; e-ISBN: 978-2-35158-089-9); *Eds. H. W. Reinhardt and A. E. Naaman*

PRO 54: 5th International RILEM Symposium on Self-Compacting Concrete (ISBN: 978-2-35158-047-9; e-ISBN: 978-2-35158-088-2); *Eds. G. De Schutter and V. Boel*

PRO 55: International RILEM Symposium Photocatalysis, Environment and Construction Materials (ISBN: 978-2-35158-056-1; e-ISBN: 978-2-35158-057-8); *Eds. P. Baglioni and L. Cassar*

PRO 56: International RILEM Workshop on Integral Service Life Modelling of Concrete Structures (ISBN 978-2-35158-058-5; e-ISBN: 978-2-35158-090-5); *Eds. R. M. Ferreira, J. Gulikers and C. Andrade*

PRO 57: RILEM Workshop on Performance of cement-based materials in aggressive aqueous environments (e-ISBN: 978-2-35158-059-2); *Ed. N. De Belie*

PRO 58: International RILEM Symposium on Concrete Modelling - CONMOD'08 (ISBN: 978-2-35158-060-8; e-ISBN: 978-2-35158-076-9); *Eds. E. Schlangen and G. De Schutter*

PRO 59: International RILEM Conference on Site Assessment of Concrete, Masonry and Timber Structures - SACoMaTiS 2008 (ISBN set: 978-2-35158-061-5; e-ISBN: 978-2-35158-075-2); *Eds. L. Binda, M. di Prisco and R. Felicetti*

PRO 60: Seventh RILEM International Symposium on Fibre Reinforced Concrete: Design and Applications - BEFIB 2008 (ISBN: 978-2-35158-064-6; e-ISBN: 978-2-35158-086-8); *Ed. R. Gettu*

PRO 61: 1st International Conference on Microstructure Related Durability of Cementitious Composites 2 vol., (ISBN: 978-2-35158-065-3; e-ISBN: 978-2-35158-084-4); *Eds. W. Sun, K. van Breugel, C. Miao, G. Ye and H. Chen*

PRO 62: NSF/ RILEM Workshop: In-situ Evaluation of Historic Wood and Masonry Structures (e-ISBN: 978-2-35158-068-4); *Eds. B. Kasal, R. Anthony and M. Drdácký*

PRO 63: Concrete in Aggressive Aqueous Environments: Performance, Testing and Modelling, 2 vol., (ISBN: 978-2-35158-071-4; e-ISBN: 978-2-35158-082-0); *Eds. M. G. Alexander and A. Bertron*

PRO 64: Long Term Performance of Cementitious Barriers and Reinforced Concrete in Nuclear Power Plants and Waste Management - NUCPERF 2009 (ISBN: 978-2-35158-072-1; e-ISBN: 978-2-35158-087-5); *Eds. V. L'Hostis, R. Gens and C. Gallé*

PRO 65: Design Performance and Use of Self-consolidating Concrete - SCC'2009 (ISBN: 978-2-35158-073-8; e-ISBN: 978-2-35158-093-6); *Eds. C. Shi, Z. Yu, K. H. Khayat and P. Yan*

PRO 66: 2nd International RILEM Workshop on Concrete Durability and Service Life Planning - ConcreteLife'09 (ISBN: 978-2-35158-074-5; ISBN: 978-2-35158-074-5); *Ed. K. Kovler*

PRO 67: Repairs Mortars for Historic Masonry (e-ISBN: 978-2-35158-083-7); *Ed. C. Groot*

PRO 68: Proceedings of the 3rd International RILEM Symposium on 'Rheology of Cement Suspensions such as Fresh Concrete (ISBN 978-2-35158-091-2; e-ISBN: 978-2-35158-092-9); *Eds. O. H. Wallevik, S. Kubens and S. Oesterheld*

PRO 69: 3rd International PhD Student Workshop on 'Modelling the Durability of Reinforced Concrete (ISBN: 978-2-35158-095-0); *Eds. R. M. Ferreira, J. Gulikers and C. Andrade*

PRO 70: 2nd International Conference on 'Service Life Design for Infrastructure' (ISBN set: 978-2-35158-096-7, e-ISBN: 978-2-35158-097-4); *Ed. K. van Breugel, G. Ye and Y. Yuan*

PRO 71: Advances in Civil Engineering Materials - The 50-year Teaching Anniversary of Prof. Sun Wei' (ISBN: 978-2-35158-098-1; e-ISBN: 978-2-35158-099-8); *Eds. C. Miao, G. Ye and H. Chen*

PRO 72: First International Conference on 'Advances in Chemically-Activated Materials – CAM'2010' (2010), 264 pp., ISBN: 978-2-35158-101-8; e-ISBN: 978-2-35158-115-5, *Eds. Caijun Shi and Xiaodong Shen*

PRO 73: 2nd International Conference on 'Waste Engineering and Management - ICWEM 2010' (2010), 894 pp., ISBN: 978-2-35158-102-5; e-ISBN: 978-2-35158-103-2, *Eds. J. Zh. Xiao, Y. Zhang, M. S. Cheung and R. Chu*

PRO 74: International RILEM Conference on 'Use of Superabsorsorbent Polymers and Other New Addditives in Concrete' (2010) 374 pp., ISBN: 978-2-35158-104-9; e-ISBN: 978-2-35158-105-6; *Eds. O. M. Jensen, M. T. Hasholt and S. Laustsen*

PRO 75: International Conference on 'Material Science - 2nd ICTRC - Textile Reinforced Concrete - Theme 1' (2010) 436 pp., ISBN: 978-2-35158-106-3; e-ISBN: 978-2-35158-107-0; *Ed. W. Brameshuber*

PRO 76: International Conference on 'Material Science - HetMat - Modelling of Heterogeneous Materials - Theme 2' (2010) 255 pp., ISBN: 978-2-35158-108-7; e-ISBN: 978-2-35158-109-4; *Ed. W. Brameshuber*

PRO 77: International Conference on 'Material Science - AdIPoC - Additions Improving Properties of Concrete - Theme 3' (2010) 459 pp., ISBN: 978-2-35158-110-0; e-ISBN: 978-2-35158-111-7; *Ed. W. Brameshuber*

PRO 78: 2nd Historic Mortars Conference and RILEM TC 203-RHM Final Workshop – HMC2010 (2010) 1416 pp., e-ISBN: 978-2-35158-112-4; *Eds. J. Válek, C. Groot and J. J. Hughes*

PRO 79: International RILEM Conference on Advances in Construction Materials Through Science and Engineering (2011) 213 pp., ISBN: 978-2-35158-116-2, e-ISBN: 978-2-35158-117-9; *Eds. Christopher Leung and K. T. Wan*

PRO 80: 2nd International RILEM Conference on Concrete Spalling due to Fire Exposure (2011) 453 pp., ISBN: 978-2-35158-118-6, e-ISBN: 978-2-35158-119-3; *Eds. E. A. B. Koenders and F. Dehn*

PRO 81: 2nd International RILEM Conference on Strain Hardening Cementitious Composites (SHCC2-Rio) (2011) 451 pp., ISBN: 978-2-35158-120-9, e-ISBN: 978-2-35158-121-6; *Eds. R. D. Toledo Filho, F. A. Silva, E. A. B. Koenders and E. M. R. Fairbairn*

PRO 82: 2nd International RILEM Conference on Progress of Recycling in the Built Environment (2011) 507 pp., e-ISBN: 978-2-35158-122-3; *Eds. V. M. John, E. Vazquez, S. C. Angulo and C. Ulsen*

PRO 83: 2nd International Conference on Microstructural-related Durability of Cementitious Composites (2012) 250 pp., ISBN: 978-2-35158-129-2; e-ISBN: 978-2-35158-123-0; *Eds. G. Ye, K. van Breugel, W. Sun and C. Miao*

PRO 84: CONSEC13 - Seventh International Conference on Concrete under Severe Conditions – Environment and Loading (2013) 1930 pp., ISBN: 978-2-35158-124-7; e-ISBN: 978-2- 35158-134-6; *Eds. Z. J. Li, W. Sun, C. W. Miao, K. Sakai, O. E. Gjorv and N. Banthia*

PRO 85: RILEM-JCI International Workshop on Crack Control of Mass Concrete and Related issues concerning Early-Age of Concrete Structures – ConCrack 3 – Control of Cracking in Concrete Structures 3 (2012) 237 pp., ISBN: 978-2-35158-125-4; e-ISBN: 978-2-35158-126-1; *Eds. F. Toutlemonde and J.-M. Torrenti*

PRO 86: International Symposium on Life Cycle Assessment and Construction (2012) 414 pp., ISBN: 978-2-35158-127-8, e-ISBN: 978-2-35158-128-5; *Eds. A. Ventura and C. de la Roche*

PRO 87: UHPFRC 2013 – RILEM-fib-AFGC International Symposium on Ultra-High Performance Fibre-Reinforced Concrete (2013), ISBN: 978-2-35158-130-8, e-ISBN: 978-2-35158-131-5; *Ed. F. Toutlemonde*

PRO 88: 8th RILEM International Symposium on Fibre Reinforced Concrete (2012) 344 pp., ISBN: 978-2-35158-132-2, e-ISBN: 978-2-35158-133-9; *Ed. Joaquim A. O. Barros*

PRO 89: RILEM International workshop on performance-based specification and control of concrete durability (2014) 678 pp., ISBN: 978-2-35158-135-3, e-ISBN: 978-2-35158-136-0; *Eds. D. Bjegović, H. Beushausen and M. Serdar*

PRO 90: 7th RILEM International Conference on Self-Compacting Concrete and of the 1st RILEM International Conference on Rheology and Processing of Construction Materials (2013) 396 pp., ISBN: 978-2-35158-137-7, e-ISBN: 978-2-35158-138-4; *Eds. Nicolas Roussel and Hela Bessaies-Bey*

PRO 91: CONMOD 2014 - RILEM International Symposium on Concrete Modelling (2014), ISBN: 978-2-35158-139-1; e-ISBN: 978-2-35158-140-7; *Eds. Kefei Li, Peiyu Yan and Rongwei Yang*

PRO 92: CAM 2014 - 2nd International Conference on advances in chemically-activated materials (2014) 392 pp., ISBN: 978-2-35158-141-4; e-ISBN: 978-2-35158-142-1; *Eds. Caijun Shi and Xiadong Shen*

PRO 93: SCC 2014 - 3rd International Symposium on Design, Performance and Use of Self-Consolidating Concrete (2014) 438 pp., ISBN: 978-2-35158-143-8; e-ISBN: 978-2-35158-144-5; *Eds. Caijun Shi, Zhihua Ou and Kamal H. Khayat*

PRO 94 (online version): HPFRCC-7 - 7th RILEM conference on High performance fiber reinforced cement composites (2015), e-ISBN: 978-2-35158-146-9; *Eds. H. W. Reinhardt, G. J. Parra-Montesinos and H. Garrecht*

PRO 95: International RILEM Conference on Application of superabsorbent polymers and other new admixtures in concrete construction (2014), ISBN: 978-2-35158-147-6; e-ISBN: 978-2-35158-148-3; *Eds. Viktor Mechtcherine and Christof Schroefl*

PRO 96 (online version): XIII DBMC: XIII International Conference on Durability of Building Materials and Components (2015), e-ISBN: 978-2-35158-149-0; *Eds. M. Quattrone and V. M. John*

PRO 97: SHCC3 – 3rd International RILEM Conference on Strain Hardening Cementitious Composites (2014), ISBN: 978-2-35158-150-6; e-ISBN: 978-2-35158-151-3; *Eds. E. Schlangen, M. G. Sierra Beltran, M. Lukovic and G. Ye*

PRO 98: FERRO-11 – 11th International Symposium on Ferrocement and 3rd ICTRC - International Conference on Textile Reinforced Concrete (2015), ISBN: 978-2-35158-152-0; e-ISBN: 978-2-35158-153-7; *Ed. W. Brameshuber*

PRO 99 (online version): ICBBM 2015 - 1st International Conference on Bio-Based Building Materials (2015), e-ISBN: 978-2-35158-154-4; *Eds. S. Amziane and M. Sonebi*

PRO 100: SCC16 - RILEM Self-Consolidating Concrete Conference (2016), ISBN: 978-2-35158-156-8; e-ISBN: 978-2-35158-157-5; *Ed. Kamal H. Kayat*

PRO 101 (online version): III Progress of Recycling in the Built Environment (2015), e-ISBN: 978-2-35158-158-2; *Eds. I. Martins, C. Ulsen and S. C. Angulo*

PRO 102 (online version): RILEM Conference on Microorganisms-Cementitious Materials Interactions (2016), e-ISBN: 978-2-35158-160-5; *Eds. Alexandra Bertron, Henk Jonkers and Virginie Wiktor*

PRO 103 (online version): ACESC'16 - Advances in Civil Engineering and Sustainable Construction (2016), e-ISBN: 978-2-35158-161-2; *Eds. T. Ch. Madhavi, G. Prabhakar, Santhosh Ram and P. M. Rameshwaran*

PRO 104 (online version): SSCS'2015 - Numerical Modeling - Strategies for Sustainable Concrete Structures (2015), e-ISBN: 978-2-35158-162-9

PRO 105: 1st International Conference on UHPC Materials and Structures (2016), ISBN: 978-2-35158-164-3, e-ISBN: 978-2-35158-165-0

PRO 106: AFGC-ACI-fib-RILEM International Conference on Ultra-High-Performance Fibre-Reinforced Concrete – UHPFRC 2017 (2017), ISBN: 978-2-35158-166-7, e-ISBN: 978-2-35158-167-4; *Eds. François Toutlemonde and Jacques Resplendino*

PRO 107 (online version): XIV DBMC – 14th International Conference on Durability of Building Materials and Components (2017), e-ISBN: 978-2-35158-159-9; *Eds. Geert De Schutter, Nele De Belie, Arnold Janssens and Nathan Van Den Bossche*

PRO 108: MSSCE 2016 - Innovation of Teaching in Materials and Structures (2016), ISBN: 978-2-35158-178-0, e-ISBN: 978-2-35158-179-7; *Ed. Per Goltermann*

PRO 109 (2 volumes): MSSCE 2016 - Service Life of Cement-Based Materials and Structures (2016), ISBN Vol. 1: 978-2-35158-170-4, Vol. 2: 978-2-35158-171-4, Set Vol. 1&2: 978-2-35158-172-8, e-ISBN : 978-2-35158-173-5; *Eds. Miguel Azenha, Ivan Gabrijel, Dirk Schlicke, Terje Kanstad and Ole Mejlhede Jensen*

PRO 110: MSSCE 2016 - Historical Masonry (2016), ISBN: 978-2-35158-178-0, e-ISBN: 978-2-35158-179-7; *Eds. Inge Rörig-Dalgaard and Ioannis Ioannou*

PRO 111: MSSCE 2016 - Electrochemistry in Civil Engineering (2016), ISBN: 978-2-35158-176-6, e-ISBN: 978-2-35158-177-3; *Ed. Lisbeth M. Ottosen*

PRO 112: MSSCE 2016 - Moisture in Materials and Structures (2016), ISBN: 978-2-35158-178-0, e-ISBN: 978-2-35158-179-7; *Eds. Kurt Kielsgaard Hansen, Carsten Rode and Lars-Olof Nilsson*

PRO 113: MSSCE 2016 - Concrete with Supplementary Cementitious Materials (2016), ISBN: 978-2-35158-178-0, e-ISBN: 978-2-35158-179-7; *Eds. Ole Mejlhede Jensen, Konstantin Kovler and Nele De Belie*

PRO 114: MSSCE 2016 - Frost Action in Concrete (2016), ISBN: 978-2-35158-182-7, e-ISBN: 978-2-35158-183-4; *Eds. Marianne Tange Hasholt, Katja Fridh and R. Doug Hooton*

PRO 115: MSSCE 2016 - Fresh Concrete (2016), ISBN: 978-2-35158-184-1, e-ISBN: 978-2-35158-185-8; *Eds. Lars N. Thrane, Claus Pade, Oldrich Svec and Nicolas Roussel*

PRO 116: BEFIB 2016 – 9th RILEM International Symposium on Fiber Reinforced Concrete (2016), ISBN: 978-2-35158-187-2, e-ISBN: 978-2-35158-186-5; *Eds. N. Banthia, M. di Prisco and S. Soleimani-Dashtaki*

PRO 117: 3rd International RILEM Conference on Microstructure Related Durability of Cementitious Composites (2016), ISBN: 978-2-35158-188-9, e-ISBN: 978-2-35158-189-6; *Eds. Changwen Miao, Wei Sun, Jiaping Liu, Huisu Chen, Guang Ye and Klaas van Breugel*

PRO 118 (4 volumes): International Conference on Advances in Construction Materials and Systems (2017), ISBN Set: 978-2-35158-190-2, Vol. 1: 978-2-35158-193-3, Vol. 2: 978-2-35158-194-0, Vol. 3: ISBN:978-2-35158-195-7, Vol. 4: ISBN:978-2-35158-196-4, e-ISBN: 978-2-35158-191-9; *Eds. Manu Santhanam, Ravindra Gettu, Radhakrishna G. Pillai and Sunitha K. Nayar*

PRO 119 (online version): ICBBM 2017 - Second International RILEM Conference on Bio-based Building Materials, (2017), e-ISBN: 978-2-35158-192-6; *Ed. Sofiane Amziane*

PRO 120 (2 volumes): EAC-02 - 2nd International RILEM/COST Conference on Early Age Cracking and Serviceability in Cement-based Materials and Structures, (2017), Vol. 1: 978-2-35158-199-5, Vol. 2: 978-2-35158-200-8, Set: 978-2-35158-197-1, e-ISBN: 978-2-35158-198-8; *Eds. Stéphanie Staquet and Dimitrios Aggelis*

PRO 121 (2 volumes): SynerCrete18: Interdisciplinary Approaches for Cement-based Materials and Structural Concrete: Synergizing Expertise and Bridging Scales of Space and Time, (2018), Set: 978-2-35158-202-2, Vol.1: 978-2-35158-211-4, Vol.2: 978-2-35158-212-1, e-ISBN: 978-2-35158-203-9; *Eds. Miguel Azenha, Dirk Schlicke, Farid Benboudjema and Agnieszka Knoppik*

PRO 122: SCC'2018 China - Fourth International Symposium on Design, Performance and Use of Self-Consolidating Concrete, (2018), ISBN: 978-2-35158-204-6, e-ISBN: 978-2-35158-205-3; *Eds. C. Shi, Z. Zhang and K. H. Khayat*

PRO 123: Final Conference of RILEM TC 253-MCI: Microorganisms-Cementitious Materials Interactions (2018), Set: 978-2-35158-207-7, Vol.1: 978-2-35158-209-1, Vol.2: 978-2-35158-210-7, e-ISBN: 978-2-35158-206-0; *Ed. Alexandra Bertron*

PRO 124 (online version): Fourth International Conference Progress of Recycling in the Built Environment (2018), e-ISBN: 978-2-35158-208-4; *Eds. Isabel M. Martins, Carina Ulsen and Yury Villagran*

PRO 125 (online version): SLD4 - 4th International Conference on Service Life Design for Infrastructures (2018), e-ISBN: 978-2-35158-213-8; *Eds. Guang Ye, Yong Yuan, Claudia Romero Rodriguez, Hongzhi Zhang and Branko Savija*

PRO 126: Workshop on Concrete Modelling and Material Behaviour in honor of Professor Klaas van Breugel (2018), ISBN: 978-2-35158-214-5, e-ISBN: 978-2-35158-215-2; *Ed. Guang Ye*

PRO 127 (online version): CONMOD2018 - Symposium on Concrete Modelling (2018), e-ISBN: 978-2-35158-216-9; *Eds. Erik Schlangen, Geert de Schutter, Branko Savija, Hongzhi Zhang and Claudia Romero Rodriguez*

PRO 128: SMSS2019 - International Conference on Sustainable Materials, Systems and Structures (2019), ISBN: 978-2-35158-217-6, e-ISBN: 978-2-35158-218-3

PRO 129: 2nd International Conference on UHPC Materials and Structures (UHPC2018-China), ISBN: 978-2-35158-219-0, e-ISBN: 978-2-35158-220-6;

PRO 130: 5th Historic Mortars Conference (2019), ISBN: 978-2-35158-221-3, e-ISBN: 978-2-35158-222-0; *Eds. José Ignacio Álvarez, José María Fernández, Íñigo Navarro, Adrián Durán and Rafael Sirera*

PRO 131 (online version): 3rd International Conference on Bio-Based Building Materials (ICBBM2019), e-ISBN: 978-2-35158-229-9; *Eds. Mohammed Sonebi, Sofiane Amziane and Jonathan Page*

PRO 132: IRWRMC'18 - International RILEM Workshop on Rheological Measurements of Cement-based Materials (2018), ISBN: 978-2-35158-230-5, e-ISBN: 978-2-35158-231-2; *Eds. Chafika Djelal, Yannick Vanhove*

PRO 133 (online version): CO2STO2019 - International Workshop CO2 Storage in Concrete (2019), e-ISBN: 978-2-35158-232-9; *Eds. Assia Djerbi, Othman Omikrine-Metalssi, Teddy Fen-Chong*

RILEM Reports (REP)

Report 19: Considerations for Use in Managing the Aging of Nuclear Power Plant Concrete Structures (ISBN: 2-912143-07-1); *Ed. D. J. Naus*

Report 20: Engineering and Transport Properties of the Interfacial Transition Zone in Cementitious Composites (ISBN: 2-912143-08-X); *Eds. M. G. Alexander, G. Arliguie, G. Ballivy, A. Bentur and J. Marchand*

Report 21: Durability of Building Sealants (ISBN: 2-912143-12-8); *Ed. A. T. Wolf*

Report 22: Sustainable Raw Materials - Construction and Demolition Waste (ISBN: 2-912143-17-9); *Eds. C. F. Hendriks and H. S. Pietersen*

Report 23: Self-Compacting Concrete state-of-the-art report (ISBN: 2-912143-23-3); *Eds. Å. Skarendahl and Ö. Petersson*

Report 24: Workability and Rheology of Fresh Concrete: Compendium of Tests (ISBN: 2-912143-32-2); *Eds. P. J. M. Bartos, M. Sonebi and A. K. Tamimi*

Report 25: Early Age Cracking in Cementitious Systems (ISBN: 2-912143-33-0); *Ed. A. Bentur*

Report 26: Towards Sustainable Roofing (Joint Committee CIB/RILEM) (CD 07) (e-ISBN 978-2-912143-65-5); *Eds. Thomas W. Hutchinson and Keith Roberts*

Report 27: Condition Assessment of Roofs (Joint Committee CIB/RILEM) (CD 08) (e-ISBN 978-2-912143-66-2); *Ed. CIB W 83/RILEM TC166-RMS*

Report 28: Final report of RILEM TC 167-COM 'Characterisation of Old Mortars with Respect to Their Repair (ISBN: 978-2-912143-56-3); *Eds. C. Groot, G. Ashall and J. Hughes*

Report 29: Pavement Performance Prediction and Evaluation (PPPE): Interlaboratory Tests (e-ISBN: 2-912143-68-3); *Eds. M. Partl and H. Piber*

Report 30: Final Report of RILEM TC 198-URM 'Use of Recycled Materials' (ISBN: 2-912143-82-9; e-ISBN: 2-912143-69-1); *Eds. Ch. F. Hendriks, G. M. T. Janssen and E. Vázquez*

Report 31: Final Report of RILEM TC 185-ATC 'Advanced testing of cement-based materials during setting and hardening' (ISBN: 2-912143-81-0; e-ISBN: 2-912143-70-5); *Eds. H. W. Reinhardt and C. U. Grosse*

Report 32: Probabilistic Assessment of Existing Structures. A JCSS publication (ISBN 2-912143-24-1); *Ed. D. Diamantidis*

Report 33: State-of-the-Art Report of RILEM Technical Committee TC 184-IFE 'Industrial Floors' (ISBN 2-35158-006-0); *Ed. P. Seidler*

Report 34: Report of RILEM Technical Committee TC 147-FMB 'Fracture mechanics applications to anchorage and bond' Tension of Reinforced Concrete Prisms – Round Robin Analysis and Tests on Bond (e-ISBN 2-912143-91-8); *Eds. L. Elfgren and K. Noghabai*

Report 35: Final Report of RILEM Technical Committee TC 188-CSC 'Casting of Self Compacting Concrete' (ISBN 2-35158-001-X; e-ISBN: 2-912143-98-5); *Eds. Å. Skarendahl and P. Billberg*

Report 36: State-of-the-Art Report of RILEM Technical Committee TC 201-TRC 'Textile Reinforced Concrete' (ISBN 2-912143-99-3); *Ed. W. Brameshuber*

Report 37: State-of-the-Art Report of RILEM Technical Committee TC 192-ECM 'Environment-conscious construction materials and systems' (ISBN: 978-2-35158-053-0); *Eds. N. Kashino, D. Van Gemert and K. Imamoto*

Report 38: State-of-the-Art Report of RILEM Technical Committee TC 205-DSC 'Durability of Self-Compacting Concrete' (ISBN: 978-2-35158-048-6); *Eds. G. De Schutter and K. Audenaert*

Report 39: Final Report of RILEM Technical Committee TC 187-SOC 'Experimental determination of the stress-crack opening curve for concrete in tension' (ISBN 978-2-35158-049-3); *Ed. J. Planas*

Report 40: State-of-the-Art Report of RILEM Technical Committee TC 189-NEC 'Non-Destructive Evaluation of the Penetrability and Thickness of the Concrete Cover' (ISBN 978-2-35158-054-7); *Eds. R. Torrent and L. Fernández Luco*

Report 41: State-of-the-Art Report of RILEM Technical Committee TC 196-ICC 'Internal Curing of Concrete' (ISBN 978-2-35158-009-7); *Eds. K. Kovler and O. M. Jensen*

Report 42: 'Acoustic Emission and Related Non-destructive Evaluation Techniques for Crack Detection and Damage Evaluation in Concrete' - Final Report of RILEM Technical Committee 212-ACD (e-ISBN: 978-2-35158-100-1); *Ed. M. Ohtsu*

Report 45: Repair Mortars for Historic Masonry - State-of-the-Art Report of RILEM Technical Committee TC 203-RHM (e-ISBN: 978-2-35158-163-6); *Eds. Paul Maurenbrecher and Caspar Groot*

Report 46: Surface delamination of concrete industrial floors and other durability related aspects guide - Report of RILEM Technical Committee TC 268-SIF (e-ISBN: 978-2-35158-201-5); *Ed. Valerie Pollet*

About the Editor

Shashank Bishnoi is currently a Chair Professor in the Department of Civil Engineering at IIT Delhi. He holds a Bachelor's degree in Civil Engineering from IIT Kanpur, a Master's degree from the University of Tokyo, and a PhD from Institute of Materials, Ecole Polytechnique Fédérale de Lausanne (EPFL). He has served as a post-doctoral fellow at Laval University, Canada and at EPFL, Switzerland. His areas of research interest include experimental and numerical studies into hydration of cement and supplementary cementitious materials, sustainability, resource utilization, durability, repair and life-cycle costs of concrete structures.

The Experience of Cuba TRC on the Survey of Kaolinitic Clay Deposits as Source of SCMs—Main Outcomes and Learned Lessons

Adrián Alujas Díaz, Roger S. Almenares Reyes, Florencio Arcial Carratalá, Luis A. Pérez García, Carlos A. Leyva Rodríguez and José F. Martirena Hernández

Abstract Kaolinitic clays are among the most abundant source of highly reactive pozzolans and constitute a strategic mineral resource for the development of cements with high clinker replacement and reduced environmental impact. However, despite its abundance, suitable kaolinitic clay deposits are frequently uncharted or not properly identified, due partially to the absence of selection criteria and to the relatively high mineralogical complexity of kaolinitic clays. In this paper, the main findings in the accumulated experience of Cuba Technical Regional Center in the search and assessment of kaolinitic clay deposits are summarized. Through the study of selected samples from several kaolinitic clay deposits of different geologic origins, the relationship between chemical and mineralogical composition, and potentialities as a source of highly reactive SCMs are established, and experience-based guidelines for the preliminary assessment of kaolinitic clay deposits as a source of SCMs are proposed.

Keywords Kaolinitic clays · Geological survey

1 Introduction

Clay minerals from the kaolinite group, when properly activated, are among the most reactive SCMs known to man. Its abundance, low activation temperature and large thermal activation window in comparison with other clay minerals are advantageous factors for its processing at industrial scale [1]. Moreover, calcination products of clay

A. A. Díaz (✉) · J. F. M. Hernández
Universidad Central de Las Villas, 54830 Santa Clara, Cuba
e-mail: adrianad@uclv.edu.cu

R. S. A. Reyes · L. A. P. García · C. A. L. Rodríguez
Instituto Superior Minero Metalúrgico de Moa, 83330 Moa, Cuba

F. A. Carratalá
Empresa Geominera del Centro, 54800 Santa Clara, Cuba

minerals from the kaolinite group are an excellent source of reactive alumina, a particular feature that allows to increase the volume of clinker substitution while maintaining mechanical and durability performance by combining alumina-rich phases with limestone [2].

However, despite its abundance, the excellent potentialities offered by kaolinitic clay deposits as source of highly reactive SCMs are frequently overlooked, partly because the approaches for the identification and classification of this type of mineral resources obey to criteria derived mainly from the ceramics, paper or pigment industries, where selection parameters are very rigorous as regards to the absence of mineral impurities that may affect color and/or plasticity [3, 4]. On the other hand, the absence of selection criteria adapted to the evaluation of the potentialities of kaolinitic clay deposits as a source of pozzolanic materials limits their proper identification and exploitation. The present paper intends to summarize the accumulated experience of Cuba Technical Regional Center in the search and preliminary assessment of kaolinitic clay deposits as source of SCMs and to propose experience-based guidelines for the preliminary assessment of kaolinitic clay deposits as a source of SCMs.

2   Discussion

2.1   Kaolin and Kaolinitic Clays

A common mistake made by even experience professionals when looking for kaolinitic clays as source of SCMs is not to distinguish properly between kaolin and kaolinitic clays, both related terms but of a different meaning. Kaolin is a commercial term, coined by the ceramic industry, and mainly used to describe a claystone comprised mostly kaolinite or related clay minerals, characterized by being white or nearly white, even when calcined, with its commercial value determined by its whiteness and particle size [5]. Originally prized for its use in the manufacture of whiteware ceramics, nowadays is mainly used in paper coating and filling, and, as a filler in paints, rubber and plastics and in the manufacture of refractories [6]. Industrial-grade kaolin deposits are relatively few in number and represent just a small fraction of global kaolinitic clay deposits, a factor which is reflected in the limited availability and relative high prices for metakaolin, the product of calcination of high-grade kaolin [5].

On the other hand, kaolinitic clay is a much more comprehensive term, as it is derived from the rock mineralogical composition and not from its industrial value. It is commonly used to refer to rocks where clay minerals from the kaolinite group are a dominant portion within its mineralogical constitution, although upper and lower limits are no well established, and therefore much broader ranges of concentration for kaolinite minerals are accepted in comparison with industrial-grade kaolin. Kaolinitic clays are not necessarily white or nearly white, and may contain large

amounts of other clay and non-clay minerals. Usual mineralogical composition of kaolinitic clays includes kaolinite and its isochemical polytype nacrite and dickite, and its relatively common hydrated polymorph halloysite. Other clay minerals that could be associated with kaolinitic clay deposits are micas, smectites and chlorites. Iron oxides and hydroxides and aluminum hydroxides are also frequently associated with kaolinite clay minerals, while quartz and feldspars are common in the coarse fraction. Depending on its genesis, minor amounts of carbonates, sulfides, sulfates and phosphates could also be present [7]. The commercial value of kaolinitic clays as source of SCM is directly related to the content of kaolinite clay minerals in the rock.

2.2 Geological Survey of Kaolinitic Clays

For minerals that occur in such diverse and heterogeneous environments such as clay minerals, a representative sampling and an adequate understanding of the characteristics of the clay deposit are of paramount importance. Any conclusions that may be derived from the use of the state-of-the-art characterization techniques are meaningless unless one is certain that the sample is truly representative of the clay deposit that it is intended to characterize. Although there are no fixed rules for geological survey, sampling and exploration of kaolinitic clay deposits, some general considerations could be useful for readers with a non-geological formation.

Geological research of a clay deposit could be summarized in three stages [8]. First, the information is collected from documental sources and the areas of interest are identified. It should be taken into account that suitable kaolinitic clay deposits may be uncharted or not properly identified, because geological studies and classification of kaolinite ores have for long been focused just on the finding of high-grade kaolin deposits. Therefore, the existence of kaolinitic clay deposits appropriated as source of SCMs is not self-evident and in most case should be deduced from existing data. Some relevant points to consider at this stage are the local geological features (type of rocks, soils, landscape morphology) and the reported existence in the area of clay quarries of kaolin or related denominations (flint clay, fire clay, refractory clay). For the selection of areas of interest, some additional points related to economical feasibility should be considered as, for example, distance of the calcination unit from the clay quarry.

In a second stage, preliminary exploration of the selected areas and a grid of sampling points should be established, adapted to landscape morphology and trying to cover all relevant lithological features in order to keep representability during sampling. Both basic and composite samples are analyzed not only according to their chemical and mineralogical composition but also in terms of their potential behavior as pozzolans.

The third stage, geological exploration, is at the same time the most expensive and the one that provides the higher level of information, and it only makes sense if the results of the previous stages justify a deeper evaluation of the clay deposit as source

of pozzolans. To rationalize resources and minimize exploration costs, the size of the explored area must be selected to comply with the amount of resources that are needed according to the foreseeing intensity of exploitation. At the end of this stage, a greater degree of knowledge about mineralogical composition and mineralogical variability is achieved. This is a key information for a further rational industrial exploitation of the clay deposit.

Another point that should be considered regarding geology of clay deposits is that, more often than not, information generated at the field is not properly considered when samples are analyzed at the laboratory. However, for such a complex material such as clays, this information should be not only preserved but actively used when interpreting the results of characterization techniques. Kaolinitic clays may occur in a large variety of geological environments, each one determining the mineralogical composition of the sample and indirectly influencing its pozzolanic reactivity when calcined. Therefore, an in-deep knowledge of the genesis and geological features of the clay deposit is very useful when designing sample preparation procedures and analyzing the results.

One of the most common kaolinitization processes is that related to hydrothermal alteration zones of rocks with acid/acid-medium composition, where surface rocks have undergone a transformation process resulting from the action of hydrothermal fluids that ascend to the surface by existing faults in the upper crust. The type of minerals formed hereby is dependent on a series of parameters such as composition of the parent rock, temperature, chemical composition and pH of the hydrothermal fluids, and distance to the heat source. All these factors put together give rise to a zoning pattern characteristic of this type of geological environment. Specifically, the formation of clay mineral from the kaolinite group is favored under acidic conditions and relatively moderate temperatures [9]. Among the minerals of the kaolinite group, it is not uncommon to find nacrite and dickite. Relatively high contents of sulfides and aluminum sulfates such as alunite could be found, depending on the distance to the heat source [5]. Occurrence of iron oxides or hydroxides will depend on their content in the parent rock. Many industrially valuable high-grade kaolin deposits are associated with this type of geological environment.

Weathering is maybe the most important route for the formation of kaolinitic clays at a global scale. In these processes, the most soluble components of rocks, such as alkalis, are leached out, while the most insoluble components, such as iron and aluminum oxides and hydroxides, remain. Weathering-related kaolinitization is especially favorable in tropical and subtropical climatic zones, where abundant rainfall and high temperatures favor the development of weathering crusts that could reach thicknesses of tens of meters of useful kaolinite content [10]. In these types of clay deposits, mineralogical composition is variable over depth, obeying to the sequence of weathering phenomena. Kaolinite minerals appear associated, especially at surface levels, with iron and aluminum oxides and hydroxides; hence, they are often reddish in color. Toward the bottom of the profile, there is usually an increase in the content of 2:1 clays, which is partially related to the drain of solutions rich in alkaline and alkaline earth ions [10]. Due to its complex mineralogical composition and usual presence of iron-rich phases, these clay deposits are usually considered to have low

industrial value, as regards to the traditional industrial applications of kaolinitic clays. In some cases, weathering could be superimposed over hydrothermal alteration. Thus, some kaolinitic clay deposits have a mixed origin, first a primary alteration occurs through hydrothermal routes, and then weathering of the hydrothermally altered rock continues the kaolinitization process.

Another important environment for the formation of kaolinitic clay deposits is that related to flood plains, deltas, among others, where fine-grain sediments could be redeposited. Kaolinitic clay deposits could also be formed by transport and deposition of fine-grain sediment by fluvial currents, glaciations or related phenomena, slowly forming large deposits with relatively high kaolinite mineral content. This type of clay deposits usually has a layer structure, with a variable mineralogical composition as a function on the depth [5]. At the contrary of primary kaolinitization environments, sometimes the presence of these secondary kaolinitic clay deposits could not be related to its surrounding geological environment because the sediments could be dragged out hundreds of kilometers from its source before being redeposited.

2.3 Identification of Criteria

The absence of selection criteria adapted to the evaluation of kaolinitic clay deposits as a source of raw materials for obtaining pozzolanic materials is a major limitation for their identification and industrial exploitation. Although there are currently no specific criteria that respond to the use of kaolinitic clays as a source of SCMs, a minimum content of kaolinite clay minerals of 40% has been proposed by several authors [11, 12], including the authors of this paper, based on the minimum content of reactive material needed to achieve a mechanical performance comparable to OPC by a 30% substitution of OPC by calcined kaolinitic clay or by a 50% substitution of clinker by a calcined clay–limestone addition in a limestone–calcined clay cement (LC3) [12].

The direct relationship between mineralogical and chemical compositions has been successfully used in the past to establish selection criteria of a given mineral resource for a specific technological application [13, 14]. Instead of mineralogical composition, chemical composition is easier to use when dealing with most of the existing local geological databases, due to the fact that they often include quantitative chemical composition of sampling points, while just qualitative mineralogical description is offered in most cases. Minerals of the kaolinite group are distinguished from other clay or non-clay minerals by their high contents of Al_2O_3, high Al/Si ratio, relatively high loss of ignition (LOI), associated with the dehydroxilation process of the clay minerals, and low alkali content, since these elements are normally lixiviated during kaolinitization process [9]. The relation between the above-mentioned chemical parameters and the content of clay minerals from the kaolinite group, calculated on dry weight basis, is depicted in Fig. 1 for 20 clay deposits of different geological origins. From this comparison, the following chemical constraints could be established for the selection of a suitable kaolinitic clay, likely to contain
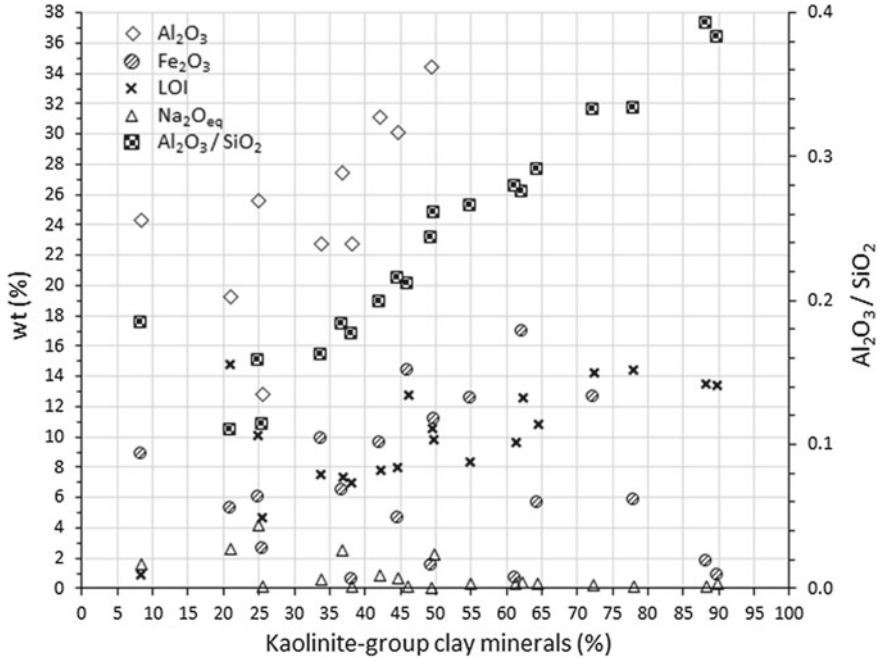
Fig. 1 Relationship between chemical composition and content of clay minerals from the kaolinite group

at least 40% of kaolinite clay minerals: (i) % $Al_2O_3 > 18.0$, (ii) $Al_2O_3/SiO_2 > 0.3$, (iii) % LOI > 7.0 and (iv) % $Na_2O_{eq} < 3.0$. It is important to point out that, for a successful selection process, all the above-mentioned criteria should be fulfilled as a whole and not just individually.

Other chemical criteria should be also developed related to the potential harmful companion minerals. The presence of relatively moderate amounts of calcite may adversely affect the pozzolanic reactivity of the calcined clay if it is calcined at temperatures above 800 °C, due to the formation of alumina-rich, non-crystalline phases of low specific surface [15, 16]. In the case of sulfides or sulfates, such as pyrite or alunite, its partial overlapping with the decomposition process of kaolinite clay minerals may negatively affect its dehydroxilation kinetics [17]. Moreover, its presence in the raw materials is also related to the unwanted emission of SO_x gases during the thermal activation process. Therefore, it is proposed to limit both the CaO and the SO_3 values to a maximum of 3.0%. As for iron-rich phases, as could be observed in Fig. 1, its content moves within a wide range, independently of the content of kaolinite minerals. Therefore, for kaolinitic clays, contrary to what is normally believed, the color of the clay is not related to its useful kaolinite content. While it is true that a reddish color of the cement by the addition of iron-rich pozzolans is usually undesirable, this is a criterion that varies greatly depending on the regional

culture or on the merchandizing strategy. Moreover, development of color in iron-rich materials is a process that could be addressed by using appropriate calcination technologies [18].

The above-stated criteria about the use of kaolinitic clays as a source of pozzolans are much more flexible if compared with the chemical requirements established for current main industrial applications of kaolinitic clays [14]. Several conclusions could be drawn from this comparison: (I) It is possible to find materials suitable as a source of pozzolans among the mining tails of kaolinitic clay quarries already closed or currently under operation that were or are dedicated to the supply of raw materials for the ceramic, refractory or paper industry; (II) suitable materials may occur naturally in some sectors nearby the existing area of exploitation, since these sectors are often found and rejected in the preliminary geological exploration by not complying with the chemical requirements of the current industrial use of kaolinitic clays; (III) given their lower requirements in terms of chemical and mineralogical composition, kaolinitic clay deposits suitable to be used as a source of SCMs should be much more abundant in comparison with industrial kaolin deposits. However, it is important to keep in mind that the use of chemical criteria, although allows to identify suitable candidates, is not, per se, a sufficient criterion, and further mineralogical analysis is needed to complete the selection process, once the preselected candidates have been narrowed to a reasonable number.

3   Conclusions

To describe those clay deposits suitable to be used as source of SCMs, kaolinitic clay is a much more comprehensive term than the industrial coined kaolin, as it is derived from the rock mineralogical composition and not from its industrial value for a specific application. The commercial value of kaolinitic clays as source of SCM is directly related to the content of kaolinite clay minerals in the rock.

Due to the high mineralogical complexity of clay deposits, to guarantee meaningful results when characterizing point samples and to assure a proper and rational exploitation of the deposits, general stages for geological research should be followed, and geological information should be used as an additional criterion to have sound results.

The direct relationship between mineralogical and chemical compositions could be successfully used to identify kaolinitic clay deposits suitable to be used as source of SCMs. Key chemical criteria are related to the percent of Al_2O_3, LOI (proportionally related to kaolinite clay minerals) and alkalis (inversely related to kaolinite clay minerals). The color of the clay or the iron-rich phase content is not related to its useful kaolinite content.

The chemical criteria used to define the suitability of kaolinitic clays as a source of pozzolans are much more flexible when compared to the chemical requirements established for current main industrial applications of kaolinitic clays. Therefore,

suitable kaolinitic clays include not only those related to unexplored clay deposits but also the mining tails or previously rejected areas of kaolinitic clay quarries used as source of high-grade kaolin.

References

1. Tironi, M., Trezza, A., Scian, E.: Irassar, Kaolinitic calcined clays: factors affecting its performance as pozzolans. Constr. Build. Mater. **28**, 276–281 (2012)
2. Antoni, M., Rossen, J., Martirena, F., Scrivener, K.: Cement substitution by blends of metakaolin and limestone. Cem. Concr. Res. **42**, 1579–1589 (2012)
3. Chandrasekhar, S., Ramaswamy, S.: Influence of mineral impurities on the properties of kaolin and its thermally treated products. Appl. Clay Sci. **21**, 133–142 (2002)
4. Murray, H.: Industrial Clays Case Study, IIED and WBCSD. MMSD-Indiana University (2002)
5. Pruett, R.J.: Kaolin deposits and their uses: Northern Brazil and Georgia, USA. Appl. Clay Sci. (2015)
6. Brigatti, M.F., Galan, E., Theng, B.K.G.: Structures and mineralogy of clay minerals. In: Bergaya, F., Theng, B.K.G., Lagaly, G. (eds.), Handbook of Clay Science. Developments in Clay Science, vol. 1, 1st edn., pp. 19–86. Elsevier Ltd., Amsterdam (2006)
7. Dill, H.G.: Kaolin: soil, rock and ore from the mineral to the magmatic, sedimentary, and metamorphic environments. Earth Sci. Rev. (2016)
8. Arcial, F.: Informe de exploración detallada de caolín La Loma y orientativa de Bañadero y Loma Sur. Instituto de Geología y Paleontología, La Habana, Cuba (2007)
9. Galán, E.: Genesis of clay minerals. In: Bergaya, F., Theng, B.K.G., Lagaly, G. (eds.) Handbook of Clay Science, 1st edn, pp. 1129–1161. Elsevier Ltd., Amsterdam (2006)
10. Righi, D., Meunier, A.: Origin of clays by rock weathering and soil formation. In: Velde, B. (ed.) Origin and Mineralogy of Clays, pp. 43–161. Springer, Berlin Heidelberg (1995)
11. Alujas, A., Fernández, R., Quintana, R., Scrivener, K.L., Martirena, F.: Pozzolanic reactivity of low-grade kaolinitic clays: influence of calcination temperature and impact of calcination products on OPC hydration. Appl. Clay Sci. **108**, 94–101 (2015)
12. Avet, F., Snellings, R., Alujas, A., Ben, M., Scrivener, K.: Development of a new rapid, relevant and reliable (R3) test method to evaluate the pozzolanic reactivity of calcined kaolinitic clays. Cem. Concr. Res. **85**, 1–11 (2016)
13. U.S. Geological Survey: Mineral commodity summaries 2017: U.S. Geological Survey, Virginia, USA (2017)
14. Díaz, A., Ramírez, J.: Compendio de rocas y minerales industriales en el Perú, INGEMMET, Boletín, Serie B: Geología Económica **19**, 482 (2009)
15. Trindade, M.J., Dias, M.I., Coroado, J., Rocha, F.: Mineralogical transformations of calcareous rich clays with fi ring: a comparative study between calcite and dolomite rich clays from Algarve, Portugal. Appl. Clay Sci. **42**, 345–355 (2009)
16. Traoré, K.: Structural transformation of a kaolinite and calcite mixture to gehlenite and anorthite. J. Mater. Res. **18**, 475–481 (2003)
17. Lozano, A., Antoni, M.: Evaluation of calcined clays from Boyaca-Colombia containing alunite as Supplementary Cementitious Materials. In: Martirena, F., et al. (eds.), Calcined Clays for Sustainable Concrete, RILEM Bookseries, vol. 16, pp. 286–292 (2017)
18. Lemke, J., Berger, C.: Thermal processing of calcined clay. In: Martirena, F., et al. (eds.), Calcined Clays for Sustainable Concrete, RILEM Bookseries, vol. 16, pp. 286–292 (2017)

Potential of Selected South African Kaolinite Clays for Clinker Replacement in Concrete

Emmanuel S. Leo and Mark G. Alexander

Abstract Growth of the world's population is projected to add 2.5 billion people to the urban population by 2050, with nearly 90% of the increase concentrating in Asia and Africa. This will result in an immense demand for urban concrete infrastructure, leading to more global anthropogenic carbon-dioxide emissions. The most promising strategy for Africa entails the partial substitution of Portland cement clinker with additions of kaolinite clay and limestone to make cement and concrete. Kaolinite content is an important indicator of clay suitability. Results obtained by X-ray fluorescence, X-ray diffraction and thermogravimetric analysis indicate the potential of clay from two South African sources for clinker replacement in cement and concrete, showing that one source is very suitable, while the other is not.

Keywords Kaolinite clay · Calcination · Clinker replacement

1 Introduction

The production process of plain Portland cement (PC) involves grinding and calcining a mixture of limestone (>60%) and clay to form clinker, at high temperatures of about 1450 °C. This process generates about 900 kg of CO_2 per ton of clinker [15]. Currently, it is estimated that the manufacture of cement contributes about 8% of global anthropogenic CO_2 emissions [4, 20, 22], and about 40% of cement that is produced is used to make concrete [27].

According to the United Nations [32], the overall growth of the world's population is projected to add 2.5 billion people to the urban population by 2050, with almost 90% of the increase concentrating in Asia and Africa. At the same time, the proportion of the world's population living in urban areas is expected to reach 66% by 2050. For Africa, the proportion is estimated to reach 56% by 2050, South Africa and

E. S. Leo (✉) · M. G. Alexander
Concrete Materials and Structural Integrity Research Unit (CoMSIRU), Department of Civil Engineering, University of Cape Town, Cape Town, South Africa
e-mail: lxxemm003@myuct.ac.za

Tanzania being among the top 10 contributors to population increase [31]. This will result in an immense demand for urban infrastructure including housing, sewerage networks, marine infrastructure such as ports and transport infrastructure such as bridges. These structures are usually made of concrete as it is a relatively low-cost durable construction material with an intrinsically low environmental impact. However, due to the anticipated high demand for concrete, it will contribute more to global CO_2 emissions. Therefore, Africa has a role in ensuring a significant reduction of global CO_2 emissions through the use of low-clinker cements in concrete.

It is believed that PC will continue to dominate in the coming decades due to [27]: (i) the economies of scale which results in low-cost cement, (ii) the widespread availability of raw materials; (iii) ease of use enabled by workability time before setting; and (iv) confidence in long-term durability based on prolonged usage of these cements. In view of this, a very effective strategy to reduce CO_2 emissions is to substitute some of the PC clinker with supplementary cementitious materials, abbreviated as SCMs, which also improve the durability of the concrete [13, 17, 25, 26].

The most widely used SCMs, granulated blast furnace slag and fly ash, are limited worldwide, especially in most African countries [15, 24, 27, 29]. In Tanzania, there are no sources of fly ash or slag, although there are certain volcanic ashes available in Mbeya, Moshi and Arusha regions [16]. In South Africa, there are large amounts of fly ash generated by burning coal to produce electricity. However, the burning of coal to produce electricity is also the largest source of CO_2 emissions [23, 27], so in the long term the availability of fly ash is also in doubt. On the other hand, Africa has abundant reserves of clays, which when calcined, make extremely good SCMs [2, 9, 26]. Kaolinite clays produce reactive minerals when calcined to around 800 °C [12]. The use of calcined kaolinite clay in concrete reduces the amount of energy used in the production of clinker and CO_2 emissions. Energy saving occurs because the calcination temperature of clays is lower than that of clinker and they are also easy to grind. On the other hand, a great quantity of CO_2 is emitted in the decomposition of limestone during clinker production, whereas calcination of kaolinitic clays emits only water vapour. Moreover, the high-alumina content of calcined kaolinite clays makes them particularly suitable for co-substitution with limestone to replace clinker in cement or concrete [5]. This means that with this combination, it is possible to have a more sustainable and durable concrete for future projects. Figure 1 shows the estimated availability of common SCMs that have been used in concrete mixes.

Potential selected deposits of kaolinite clay in South Africa and Tanzania are given in Table 1. The Pugu deposit is believed to be the largest in Africa [1]. For this project, only South African clays were sourced initially, but the intention is also to source Tanzanian clays later.

Fig. 1 Estimated availability of SCMs versus amount of cement produced [27]
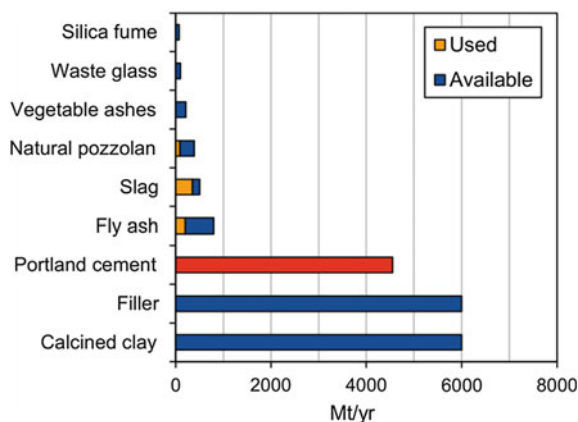
Table 1 Potential selected kaolinite clay deposits in South Africa and Tanzania

Country	Deposit—Location	Estimated amount
South Africa [10, 11, 14]	Hopefield—Western Cape	500 million tons
	Grahamstown—Eastern Cape	60 million tons
	Bronkhorstspruit—Gauteng	>35 million tons
Tanzania [11, 18]	Pugu—Kisarawe Coast Region	2 billion tons
	Matamba—Makete Njombe Region	56 million tons
	Malangali—Mufindi Iringa Region	Unknown

2 Materials and Methods

Thus, the objective of this paper was to study the suitability of the clay from Grahamstown (G-Clay) and Bronkhorstspruit (B-Clay) deposits for clinker replacement in concrete. A sample of G-Clay graded as Kaolin A was supplied to the University of Cape Town (UCT) by Serina Trading, and a sample of B-Clay was supplied to UCT by AfriSam. G-Clay was beneficiated to produce a clean, off-white, low iron and high-alkali content product. Both clays had particle size d90 < 45 µm. Before carrying out measurements, both samples were dried at 200 °C for 24 h to remove moisture. Chemical compositions of both clays were obtained using Panalytical Axios wavelength-dispersive XRF spectrometer and are presented in Table 2.

X-ray diffraction (XRD) and thermogravimetric analysis (TGA) were used to determine the mineralogical composition of clay. XRD measurements were obtained using Bruker D8 Advance powder diffractometer with Vantec detector and fixed divergence and receiving slits with Co-Ka radiation. To improve data quality, XRD measurements were taken for 90 min. The phases were identified using Bruker Topas 4.1 software and the relative phase amounts were estimated using the Rietveld method. A SDT 650 TA instrument was used to investigate thermal behaviour of the clays. Thermogravimetric measurements were taken from room temperature to

Table 2 Chemical composition and LOI for the G-clay and B-clay

Sample	SiO_2 (wt%)	TiO_2 (wt%)	Al_2O_3 (wt%)	Fe_2O_3 (wt%)	MnO (wt%)	MgO (wt%)	CaO (wt%)	Na_2O (wt%)
B-clay	51.52	1.57	31.59	1.14	0.07	0.46	1.64	0.25
G-clay	68.53	0.77	20.58	0.52	0	0.27	b.d	0.38
Na_2O (wt%)	K_2O (wt%)	P_2O_5 (wt%)	SO_3 (wt%)	Cr_2O_3 (wt%)	NiO (wt%)	H_2O (wt%)	LOI (wt%)	Total (wt%)
0.25	0.35	0.12	0.06	0.02	0.01	0.08	11	99.9
0.38	2.74	0.02	b.d	0.01	0.01	0.06	5.15	99

"b.d." is an abbreviation of "below detection" meaning that the concentration of the element was too low to quantify (generally <0.01 wt% for major elements)

1000 °C, at a heating rate of 10 °C/min, using alumina crucibles with no lids under a 10 ml/min flow of nitrogen gas. The mass change over the kaolinite-dehydroxylation interval was used to determine the kaolinite content of the clay.

3   Results and Discussions

It has been indicated that a suitable clay for clinker replacement should have a kaolinite content of at least 40%, and secondary minerals have less influence on the reactivity of the clay [3, 6, 7]. This means that kaolinite content is an important indicator of clay suitability. As for the case of SCM in the first days of the mix, the presence of secondary minerals such as quartz also contributes in offsetting the initial hydration reaction of the clinker components by filler effect [19, 21]. Chemical composition of clay obtained by XRF can give an indication of the suitability of the clay. However, the presence of other minerals in the clay may affect the results of chemical composition. Therefore, more conclusive results can be obtained from TGA and quantitative XRD (QXRD).

3.1   G-Clay

The results of TGA and QXRD for the sample of G-Clay are presented in Figs. 2 and 4, respectively. The TGA curve shows that there is a negligible mass loss between room temperature and 200 °C due to dehydration. The endothermic peak on the DTG curve also confirms this. The endothermic peak between 400 and 600 °C with a maximum peak at 498 °C corresponds to the dehydroxylation of kaolinite and the formation of metakaolin [3, 12, 28, 30]. From the TGA curve, the mass change over the kaolinite-dehydroxylation interval (400–600 °C) is 4.2%. From this mass loss and the molecular weights of kaolinite and water, the percentage of kaolinite is
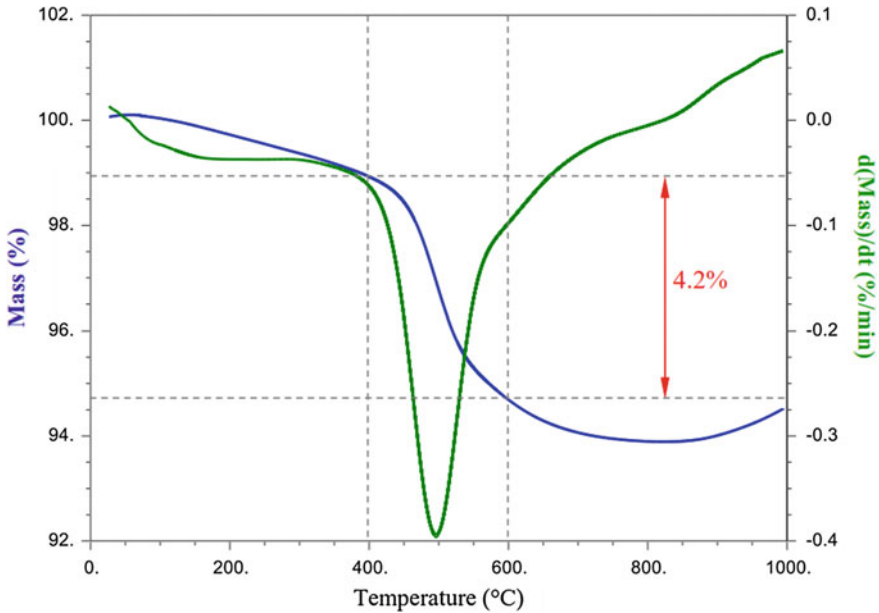
Fig. 2 TGA and DTG curves of the sample of G-clay

estimated at 30.1%. Loss of mass after 600 °C is related to the dehydroxylation of illite [12]. The mass gain after 850 °C as can be seen on the TGA curve corresponds to the transformation of metakaolin to form spinel [8].

3.2 B-Clay

The results of TGA and QXRD for the B-Clay are presented in Figs. 3 and 5, respectively. As in the case of G-Clay, there is a negligible mass loss between room temperature and 200 °C due to dehydration. The endothermic peak is maximum at 506 °C. From the TGA curve, the mass change over the kaolinite-dehydroxylation interval (400–600 °C) is 9.6%. From this mass loss, the percentage of kaolinite is estimated at 68.8%. The mass gain after 800 °C as can be seen on the TGA curve corresponds to the formation of spinel [8]. This is also confirmed by the endothermic peak at 950 °C on the DTG curve (Fig. 4).
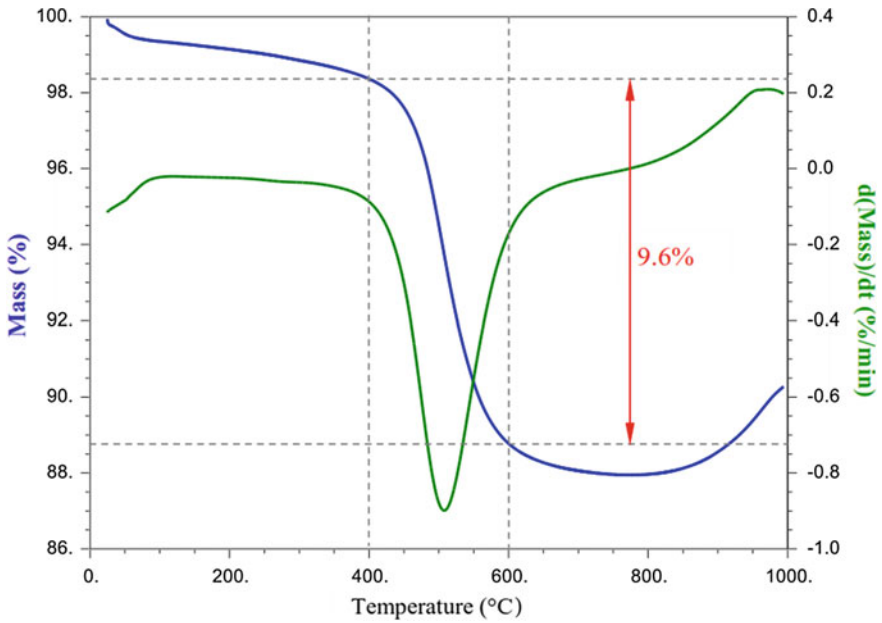
Fig. 3 TGA and DTG curves of the sample of B-clay
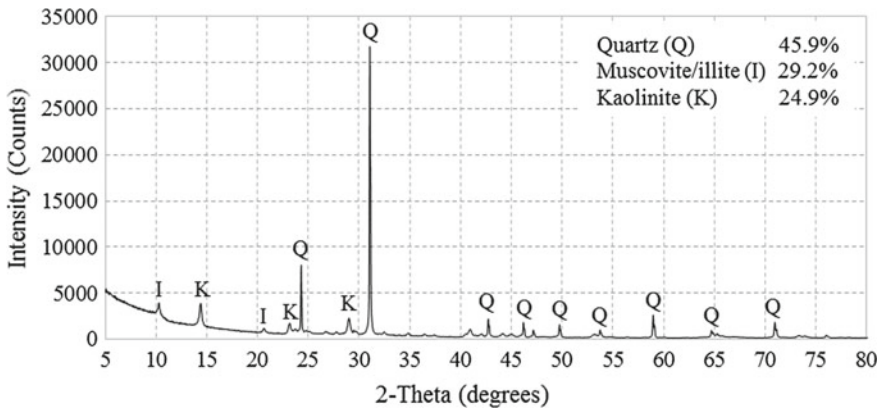
Fig. 4 XRD pattern of the sample of G-clay

4   Conclusion

Kaolinite clays from Grahamstown and Bronkhorstspruit deposits in South Africa were studied for their potential application in cement or concrete. According to the results, both clays are composed mainly of quartz, kaolinite and muscovite/illite. In
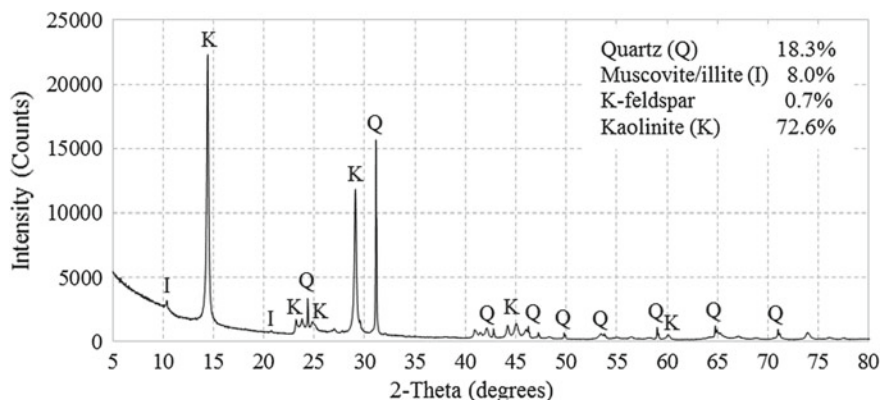
Fig. 5 XRD pattern of the sample of B-clay

general, the XRF results are in good agreement with the mineralogical composition obtained by QXRD and TGA.

Currently, clay from the two deposits is not used in the cement and concrete industry. It has been pointed out that a suitable clay for clinker replacement is one with a kaolinite content of at least 40%. In this case, the B-Clay has about 70% kaolinite content based on TGA and QXRD results, making it potentially suitable to be used in cement and concrete. By contrast, the G-Clay has about 30.1% kaolinite content from TGA and 24.9% from QXRD results and therefore is not suitable for use in cement and concrete.

References

1. Akwilapo, L.D., Wiik, K.: Ceramic properties of Pugu kaolin clays. Part I: porosity and modulus of rupture. Bull. Chem. Soc. Ethiop. **17**(2), 147–154 (2004)
2. Almenares, R.S., Vizcaíno, L.M., Damas, S., Mathieu, A., Alujas, A., Martirena, F.: Industrial calcination of kaolinitic clays to make reactive pozzolans. Case Stud. Constr. Mater. **6**, 225–232
3. Alujas, A., Fernández, R., Quintana, R., Scrivener, K.L., Martirena, F.: Pozzolanic reactivity of low grade kaolinitic clays: influence of calcination temperature and impact of calcination products on OPC hydration. Appl. Clay Sci. **108**, 94–101 (2015)
4. Andrew, R.M.: Global CO_2 emissions from cement production. Earth Syst. Sci. Data **10**, 195–217 (2018)

5. Antoni, M., Rossen, J., Martirena, F., Scrivener, K.: Cement substitution by a combination of metakaolin and limestone. Cem. Concr. Res. **42**(12), 1579–1589 (2012)

6. Avet, F.: Investigation of the grade of calcined clays used as clinker substitute in limestone calcined clay cement (LC3), Ph.D. thesis. EPFL (2017)

7. Avet, F., Snellings, R., Alujas Diaz, A., Ben Haha, M., Scrivener, K.: Development of a new rapid, relevant and reliable (R3) test method to evaluate the pozzolanic reactivity of calcined kaolinitic clays. Cem. Concr. Res. **85**, 1–11 (2016)

8. Brown, I.W.M., Mackenzie, K.J.D., Bowden, M.E., Meinhold, R.H.: Outstanding problems in the kaolinite-mullite reaction sequence investigated by 29Si and 27Al solid-state nuclear magnetic resonance: 11, high-temperature transformations of metakaolinite. J. Am. Ceram. Soc. **68**(6), 298–301 (1985)

9. Castillo, R., Fernández, R., Antoni, M., Scrivener, K., Alujas, A., Martirena, J.F.: Activación de arcillas de bajo grado a altas temperaturas. Revista Ingeniería de Construcción **25**(3), 329–352 (2010)

10. Cole, D.I., Ngcofe, L., Halenyane, K.: Mineral Commodities in the Western Cape Province, South Africa. Council for Geoscience, Western Cape Regional Office, Report 12 (2014)

11. Ekosse, G.E.: Kaolin deposits and occurrences in Africa: geology, mineralogy and utilization. Appl. Clay Sci. **50**(2), 212–236 (2010)

12. Fernandez, R., Martirena, F., Scrivener, K.L.: The origin of the pozzolanic activity of calcined clay minerals: a comparison between kaolinite, illite and montmorillonite. Cem. Concr. Res. **41**(1), 113–122 (2011)

13. Habert, G., Billard, C., Rossi, P., Chen, C., Roussel, N.: Cement production technology improvement compared to factor 4 objectives. Cem. Concr. Res. **40**(5), 820–826 (2010)

14. Hosterman, J.W., Patterson, S.H., Good, E.E.: World nonbauxite aluminum resources; alunite (No. 1076-A) (1978)

15. Klee, H., Roland, H., van der Rob, M., Richard, W.: Getting the numbers right: a database of energy performance and carbon dioxide emissions for the cement industry. Greenhouse Gas Measur. Manag. **1**(2) (2011)

16. Lema, E.A., Lweikiza, S.J.: Use of Local Pozzolan for Stabilization of Subbase and Basecourse for Road Construction in Tanzania: Case Study of TANZAM Highway (Chalinze-Melela Section). Annual Road Convention, Dar es Salaam, Tanzania, 27–28 Nov 2014, p. 31 (2014)

17. Lothenbach, B., Scrivener, K., Hooton, R.D.: Supplementary cementitious materials. Cem. Concr. Res. **41**(12), 1244–1256 (2011)

18. Ministry of Energy and Minerals: Industrial Minerals in Tanzania—An Investor's Guide (2008)

19. Moosberg-Bustnes, H., Lagerblad, B., Forssberg, E.: The function of fillers in concrete. Mater. Struct./Materiaux et Constructions **37**(266), 74–81 (2004)

20. Müller, N., Harnisch, J.: A Blueprint for a Climate-Friendly Cement Industry: How to Turn Around the Trend of Cement Related Emissions in the Developing World. World Wide Fund for Nature, Gland, Switzerland (2008)

21. Oey, T., Kumar, A., Bullard, J.W., Neithalath, N., Sant, G.: The filler effect: the influence of filler content and surface area on cementitious reaction rates. J. Am. Ceram. Soc. **96**(6), 1978–1990 (2013)

22. Olivier, J.G.J., Schure, K.M., Peters, J.A.H.W.: Trends in global CO_2 and total greenhouse gas emissions. PBL Netherlands Environmental Assessment Agency (2017)

23. Pretorius, I., Piketh, S., Burger, R., Neomagus, H.: A perspective on South African coal fired power station emissions. J. Energy Southern Africa **26**(3), 27–40 (2015)

24. Proske, T., Rezvani, M., Palm, S., Müller, C., Graubner, C.A.: Concretes made of efficient multi-composite cements with slag and limestone. Cem. Concr. Compos. **89**, 107–119 (2018)

25. Schneider, M., Romer, M., Tschudin, M., Bolio, H.: Sustainable cement production-present and future. Cem. Concr. Res. **41**(7), 642–650 (2011)

26. Scrivener, K.L.: Options for the future of cement. Indian Concr. J. **88**(7), 11–21 (2014)

27. Scrivener, K.L., John, V.M., Gartner, E.M.: Eco-efficient cements: Potential economically viable solutions for a low-CO_2 cement-based materials industry. Cem. Concr. Res. **114**, 2–26 (2018)

28. Shvarzman, A., Kovler, K., Grader, G.S., Shter, G.E.: The effect of dehydroxylation/amorphization degree on pozzolanic activity of kaolinite. Cem. Concr. Res. **33**(3), 405–416 (2003)
29. Snellings, R.: Assessing understanding and unlocking supplementary cementitious materials. RILEM Tech. Lett. **1**, 50–55 (2016)
30. Snellings, R., Mertens, G., Elsen, J.: Supplementary cementitious materials. Rev. Miner. Geochem. **74**, 211–278 (2012)
31. UN: The Demographic Profile of African Countries. United Nations, Economic Commission for Africa, Addis Ababa (2016)
32. UN: World Urbanization Prospects: The 2014 Revision, Highlights. United Nations, Department of Economic and Social Affairs, Population Division, New York (2014)

Potential for Selected Kenyan Clay in Production of Limestone Calcined Clay Cement

Joseph Mwiti Marangu, Kyle Riding, Anfal Alaibani, Abla Zayed, Joseph Karanja Thiong'o and Jackson Muthengia Wachira

Abstract The potential for calcined clay, and in particular Limestone Calcined Clay Cement (LC^3), to be used in concrete in Kenya was examined in this study. Locations of clay sources and existing mining infrastructure were examined for potential development. Potential sources of clay were obtained and characterized for kaolinite content and reactivity. Results showed that there is significant potential for development and use of calcined clays in Kenya. Product development issues going forward in Kenya is also discussed.

Keywords Cement · Clay · Compressive strength · Limestone · Pozzolana

1 Introduction

There is an increasing demand for affordable housing in most part of the world. Cement accounts for more than 50% of the total cost of construction materials used in housing. Commercial Ordinary Portland Cement (OPC) is expensive cement due to the fact that energy in excess of 1300 °C is required during the clinkerization process. This has made OPC unaffordable in many developing countries, Kenya being one of them. Majority of the citizens in developing countries, especially where the governments do not have an established housing and shelter system, cannot afford

J. M. Marangu (✉)
Department of Physical Sciences, Meru University of Science and Technology, Meru, Kenya
e-mail: jmarangu@must.ac.ke

K. Riding · A. Alaibani
Department of Civil and Coastal Engineering, University of Florida, Gainesville, FL, USA

A. Zayed
Department of Civil and Environmental Engineering, University of South Florida, Tampa, FL, USA

J. K. Thiong'o
Department of Chemistry, Kenyatta University, Nairobi, Kenya

J. M. Wachira
Department of Physical Sciences, University of Embu, Embu, Kenya

the cement, which is a major building binder for housing and construction [1]. This has led to the mushrooming of urban slums such as Kibera, Mukuru kwa Njenga, Mathare, Kawangware, Huruma and Korogocho in Nairobi-Kenya among others. There is an increasing demand for decent housing as the shanty houses pose various health challenges such as jigger menace [1].

During hydration of OPC, it is estimated that more than 20% of calcium hydroxide (CH) is produced. CH present in hydrated cement forms a weak point of attack that makes the structure susceptible to degradation especially in the presence of aggressive media such chlorides, sulfates, carbon dioxide and water among others. The blending of supplementary cementitious materials (SCMs) with OPC to produce blended cements has been reported to increase the overall compressive strength of cement, though often after a longer period of curing than it is for plain OPC. SCMs such as calcined clays have been found to consume CH produced during hydration of cement to form secondary calcium-silicate-hydrate (C-S-H). C-S-H is a cementitious compound which is mainly responsible for strength in cementitious materials. The formation of additional C-S-H as a result of pozzolanic reaction also reduces the permeability of the hydrated cement matrix. Reduced permeability results in decreased ingress of the aggressive ions such as chlorides [2] and carbon dioxide [3] into the cement mortar. Calcined clays also improve thermal resistance in blended cements [4] which results in increased durability.

In Kenya, Portland Pozzolana Cement (PPC) is the main blended cement used for various construction activities. The PPC is made from volcanic ash also known as Kenyan Tuff as pozzolana. This has resulted in massive agglomeration of cement industries in Athi River town in Kenya. Transportation of manufactured cement to other parts of Kenya has also resulted in increased cement prices. Moreover, the availability of volcanic ash is low compared to that of clays. The present study aimed at investigating the potential of selected clays from Kenya for production of Limestone Calcined Clay Cement (LC^3). The cement is potentially affordable in Kenya due to low clinker content and abundance of raw materials such as clay and limestone. LC^3 is also eco-friendly since it can effectively reduce the CO_2 emissions by 30% [5].

2   Materials and Methods

2.1   Materials

Raw clays were sampled from three different sites located within Mukurweini in Nyeri County in Kenya. From each sampling site, about 5 kg of clay was obtained at a depth of 30 m below the ground level. The sampled clays were mechanically blended to form a homogeneous mix. Limestone and clinker were supplied by East Africa Portland Cement Company (EAPCC) located in Athi River in Kenya. The chemical composition of raw clay, limestone and clinker obtained from X-ray fluorescence

Table 1 Chemical composition of clay, limestone, clinker and gypsum

Oxide	Oxide composition (%)			
	Clinker	Raw clay	Limestone	Gypsum
SiO_2	22.88	64.79	6.38	2.56
Al_2O_3	5.44	29.93	0.45	0.88
Fe_2O_3	3.85	2.36	0.30	0.82
CaO	62.52	0.18	61.13	35.56
MgO	1.03	0.27	27.89	1.86
SO_3	2.06	0.31	0.00	39.97
K_2O	0.7	1.08	0.10	0.04
Na_2O	0.21	0.17	0.20	0.07
H_2O	2.22			
Sum ($SiO_2 + Al_2O_3 + Fe_2O_3$)		97.08		
Loss on ignition (LOI)	0.88			12.88

Table 2 Description of OPC, PPC and LC^3 materials

Cement type	Description
OPC	Ordinary Portland Cement (OPC) [42.5 N/mm]. OPC was prepared by blending and inter-grinding of clinker and 5% gypsum in a laboratory ball mill
PPC	Portland Pozzolana Cement (PPC) [32.5 N/mm] commercially available in Kenya. Prepared by inter-grinding of clinker, volcanic ash (Kenya Tuff) and gypsum in a laboratory mill
LC^3	Was prepared by blending of 50% of clinker, 30% of ground calcined clay, 15% limestone and 5% gypsum inter-ground in a laboratory ball mill

(XRF) analysis is presented in Table 1. The description OPC, PPC and LC^3 materials used in this work is given in Table 2.

2.2 Methods

The sampled clay was heated in an electrical muffle furnace at 850 °C for one hour. The calcined clay was then allowed to cool to room temperature. The cooled clay was finely ground in a laboratory ball mill to ensure that more than 90% of the clay particles had particle size less than 45 µm.

Samples of oven-dried and calcined clay were prepared for the thermogravimetric analysis (TGA). An approximately 51 mg of each sample was placed on 150 μL aluminum crucible and enclosed in gas tight furnace with nitrogen as the purging gas with a rate of 30–50 mL/min the samples were heated from 30 to 950 °C at a rate of 20 °C/min.

R3 test approach was used to evaluate the pozzolanic reactivity of the calcined clay. Mixture ingredients of calcined clay, portlandite and limestone as a binder were prepared with a mixing solution of deionized water, potassium hydroxide and potassium sulfate. The ingredient was prepared with a portlandite to calcined clay ratio of 3, portlandite to binder ratio of 1/9, and deionized water to binder ratio of 1.2. Prior to mixing all ingredients were stored overnight at 40 °C. Using the overhead mixer, duplicate samples of paste were mixed for 2 min at 1600 rpm and 15 g of the paste was casted in a sealed glass vial and placed inside the isothermal calorimeter (TAM Air) for 13 days at 40 °C to measure the cumulative heat of reaction.

Mortar prisms measuring 160 mm × 40 mm × 40 mm were prepared using the LC^3 test cement. The mortar prisms were placed in a humidity cabinet maintained at a temperature of 22 ± 1 °C for 24 h. After 24 h, the mortar prisms were demolded, marked for identification purposes and immersed in water contained in a curing tank. Compressive test were conducted at 1, 3, 7 and 28 days of curing.

3 Results and Discussion

The analysis results of the raw clay show that between 500 and 600 °C, there is an endothermic peak where the dehydroxylation process went through. Assuming that pure kaolinite has a mass loss of 13.95% [6] during complete dehydroxylation, the TGA results show that the clay has a kaolinite content of 54.4%. The calcined clay showed no dehydroxylation in TGA which means that the clay was activated and fully calcined (Fig. 1).

The R3 test results and the amount of heat released shown in Fig. 2 showed the pozzolanic reactivity in the calcined clay. While the heat developed is lower than that observed for other calcined clays with similar percentages of kaolin clay [7], the clay still showed adequate performance for use in LC^3 mixtures.

The compressive test results obtained after curing of mortar prisms for 1, 3, 7 and 28 days are presented in Fig. 3. The LC^3 mixture showed higher strength than the currently used pozzolan in the Kenyan market, showing its potential to improve the economics and durability of Kenyan concrete. The compressive strength was observed to increase with increased curing. This could be attributed to continue
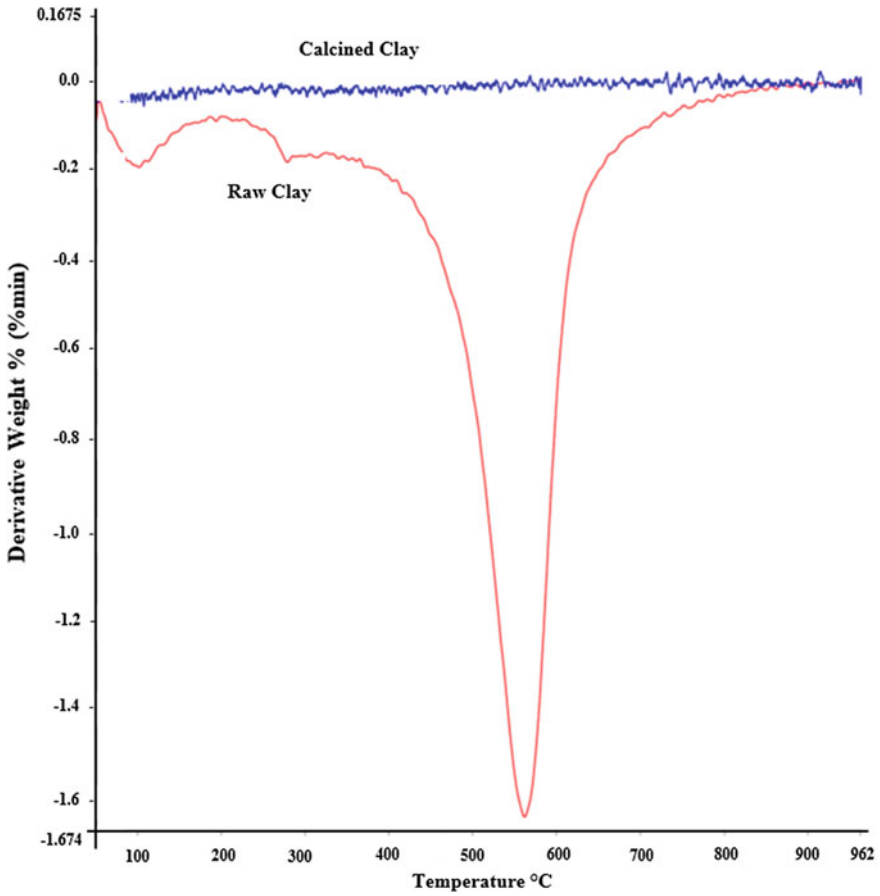
Fig. 1 DTG analysis of raw and calcined clay

hydration process taking place in the cements as a result of curing. The compressive strength of OPC was observed to be higher than that of blended cements (LC^3 and PPC) since the latter contains lower proportions of C_3S and C_2S, which upon hydration produce C-S-H.
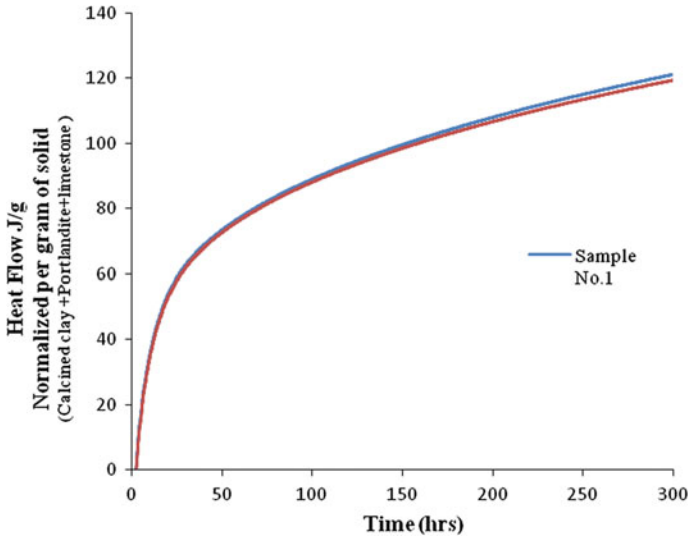
Fig. 2 Cumulative heat flow for calcined clay at 40 °C
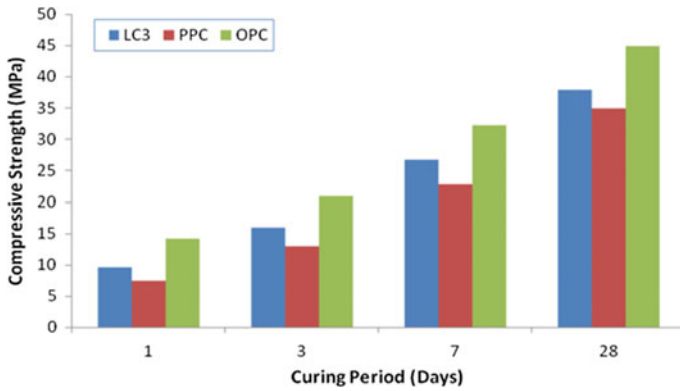
Fig. 3 Compressive strength results

4   Conclusions

In conclusion, the LC[3] mortars were found to exhibit higher compressive strength than commercial PPC. On the basis of kaolin content, pozzolanic activity and compressive strength, LC[3] is therefore a potentially viable cementitious material for local manufacture in Kenya. Future work will focus on material durability and in demonstration projects of LC[3] to encourage its production and use.

References

1. Marangu, J.M., Wachira, M.J., Wa-Thiong'o. J.K.: Performance of potential pozzolanic cement in chloride media. IOSR J. Appl. Chem. **7**(2), 36–44 (2014)
2. Marangu, J.M., Thiong'o, J.K., Wachira, J.M.: Chloride ingress in chemically activated calcined clay-based cement. J. Chem. **2018**, 1–8 (2018)
3. Marangu, J.M., Thiong'o, J.K., Wachira, J.M.: Review of carbonation resistance in hydrated cement based materials. J. Chem. **2019**, 1–6 (2019)
4. Mwiti, M.J., Karanja, T.J., Muthengia, W.J.: Thermal resistivity of chemically activated calcined clays-based cements. In: Martirena, F., Favier, A., Scrivener, K. (eds.) Calcined Clays for Sustainable Concrete, vol. 16, pp. 327–333. Springer, Netherlands, Dordrecht (2018)
5. Martirena, F., Scrivener, K.: Low carbon cement LC3 in Cuba: ways to achieve a sustainable growth of cement production in emerging economies. In: Martirena, F., Favier, A., Scrivener, K. (eds.) Calcined Clays for Sustainable Concrete, vol. 16, pp. 318–321. Springer, Netherlands, Dordrecht (2018)
6. Brindley, G.W., Nakahira, M.: The kaolinite-mullite reaction series: II, metakaolin. J. Am. Ceram. Soc. **42**(7), 314–318 (1959)
7. Avet, F., Snellings, R., Alujas Diaz, A., Ben Haha, M., Scrivener, K.: Development of a new rapid, relevant and reliable (R3) test method to evaluate the pozzolanic reactivity of calcined kaolinitic clays. Cem. Concr. Res. **85**, 1–11

Feasibility Study for Calcined Clay Use in the Southeast USA

Brandon Lorentz, Hai Zhu, Yuriy Stetsko, Kyle A. Riding and Abla Zayed

Abstract The Southeast USA contains very large reserves of clay that could be used for supplementary cementitious material (SCM) production. A feasibility study has been performed recently to determine the viability of this clay for use as an SCM. Samples were taken from currently operating mines in Florida and analyzed for clay content, particle size, reactivity, and strength development potential. This paper discusses results with a focus on clay quality, material processing needs for use, and availability.

Keywords Supplementary cementitious materials · Calcined clay · Specifications

1 Introduction

There exists a plethora of clay resources spanning the Southeast USA, especially in the state of Florida where kaolin may be found in large quantities among other minerals. Low-purity clays with kaolin mineral contents as low as 40 wt% in the presence of limestone yield cements with excellent strength and durability performance [1]. However, amorphous content, chemical, and mineralogical composition, and calcination temperature of the clay can affect the quality of the resulting pozzolanic material. In Florida, low-quality kaolin clays are predominantly sold for brick manufacturing, road, and construction base materials, or mined as overburden during the excavation of sand, limestone, dolomite, and other natural minerals [2]. These clays are accompanied by large quantities of sand of various composition and size. This study examined availability, processing requirements, and use of Florida's kaolin clays as SCMs in terms of mineralogy, reactivity, and compressive strength.

B. Lorentz (✉) · H. Zhu · Y. Stetsko · A. Zayed
University of South Florida, Tampa, FL 33620, USA
e-mail: bxl@mail.usf.edu

K. A. Riding
University of Florida, Gainesville, FL 32611, USA

2 Materials and Methods

2.1 *Sample Collection and Characterization*

Geological reports and databases that document clay resources across the state of Florida are available [3–6]. The Florida Department of Environmental Protection maintains the integrated habitat network (IHN) [7] with a 2D graphical interface that maps out the natural and anthropogenic geological resources of the state. Sites were analyzed and noted as possible locations were kaolin clays may exist in large quantities or as auxiliary minerals to the more dominantly present materials such as sand, limestone, fuller's earth, dolomite, phosphate, and fill materials. Sampling and full characterization of any materials of interest were necessary to get detailed material compositions.

Roughly 1 kg of each sample as received from the field was wet sieved through sieve No. 325. The passing and retained materials were dried of free water at 110 °C in a box furnace until constant mass was achieved and deemed each samples' clay and sand fraction, respectively. 30 clays were excavated from 13 active and inactive mining locations across Florida with various mineralogies and physical characteristics. Each sample was crushed, mixed, and dried in a box furnace at 110 °C until constant mass. All samples were then sieved with a No. 325 (45 μm) sieve and analyzed using X-ray diffraction (XRD) to screen samples for further study. XRD scans were according to ASTM C1365 [8] using a Phillips X'Pert PW3040 Pro diffractometer equipped with an X'Celerator Scientific detector and a Cu-Kα X-ray source. Tension and current were set to 45 kV and 40 mA, respectively; 5 mm divergence and anti-scatter slits were used in the automatic mode. Scans were collected for the 4°–70° 2θ angular range, and the sample was rotated at 30 rpm during scanning. Corundum (standard reference material 676a) obtained from the National Institute of Standards and Technology (NIST) was used as the external standard. The mass absorption coefficient (MAC) of corundum was 30.91 cm^2/g. MAC values for the clays were calculated based on their respective elemental oxide compositions. Loss on ignition content was attributed to release of water. The collected diffraction patterns were analyzed using HighScore Plus v. 4.5 for phase identification and Rietveld refinement. The following parameters were refined during Rietveld analysis: scale factors, lattice parameters, zero shift, fifth-order regular polynomial for background fitting, preferred orientation for all kaolin-group phases in the (001) direction, peak shape parameters w, coordinates of atoms, and a defined Fe–Al substitution parameter x [9]. The value of the substitution parameter, x, was controlled by comparison of the amount of the main oxides, SiO_2, Al_2O_3, and Fe_2O_3, determined by the Rietveld analysis with that of the XRF analysis.

For 10 samples selected for further analysis, X-ray fluorescence (XRF) was performed according to ASTM C114 and thermogravimetric analysis (TGA). TGA measurements were performed using a SDT Q600 series simultaneous TGA/differential scanning calorimeter (DSC) manufactured by TA Instruments. Approximately 5 mg of each sample was scanned in an open alumina crucible in a nitrogen atmosphere

using a heating rate of 20 °C/min to 1000 °C. Kaolin dehydroxylation was identified on a TGA thermogram by weight loss using the tangential method in the range of 400–800 °C depending on particle size and degree of disorder of kaolinite, as well as measurement conditions [10, 11].

2.2 Calcination

Unsieved clay samples were calcined in ceramic crucibles by heating at 20 °C/min to 600 °C for 1 h in a box furnace and allowed to cool to room temperature [2]. After calcination, the material was ground by hand with mortar and pestle. The calcined material was sieved through a 45 µm sieve, and the fraction finer than 45 µm was analyzed by XRD to ensure complete calcination for each sample.

2.3 Mortar Compressive Strength

Pozzolanic activity of the 10 calcined clays was evaluated by mortar compressive strength at 7 and 28 days following ASTM C109 [12] and ASTM C305 [13], with a fixed water-to-cementitious materials (w/cm) ratio of 0.485. A 10% cement replacement with each sample's clay fraction from the wet-sieving analysis was used, adjusting the standard sand requirement by the sand fraction that would accompany this amount of clay. A Type I/II portland cement with 1.3% limestone fines was used in this study. The following naming convention was used for the mix designs: 10X-600-1, where 10 was the cement replacement level (percent by weight), X was the name of the calcined material, 600 was the calcination temperature, (°C) and 1 referred to the duration of calcination (hours) [2]. In an effort to isolate the filler effect caused by inclusion of each clays' sand content, individual control mixtures were prepared for the first five calcined clays that contained only portland cement as binder with the same portion of standard sand and sand from the calcined material as in the respective calcined clay mortars [2]. These controls were tested at 7 days.

3 Results and Discussion

3.1 Sand Content

Wet-sieving analysis of all 10 as received kaolin clays showed sand contents ranging from 65 to 90% and clay contents ranging 10–35% [14]. The sand content must be separated from the clay portion or ground to an appropriate fineness in order to be included with clay and considered feasible as natural pozzolans for use in modern concrete.

3.2 Elemental Oxide Composition

The XRF composition of all 10 clay fractions may be seen below in Table 1. It may be observed that all clays predominantly consist of Al_2O_3 (30–38%) and SiO_2 (34–46%), which is generally consistent with the chemical composition of kaolin ($Al_2O_3 \cdot 2SiO_2 \cdot 2H_2O$, 39.5 wt% Al_2O_3, 46.5 wt% SiO_2, and 14.0 wt% H_2O) [2]. The high loss on ignition content (LOI) is assumed to be due to the water chemically combined in kaolin minerals which is lost during the calcination process. The Fe_2O_3 content of the clay fractions varies from 0.9–10.2%. All the clays meet the ASTM C618 requirement of a minimum of 70.0% for $SiO_2 + Al_2O_3 + Fe_2O_3$ [14]. Additionally, the SO_3 content of all the clays is very low, below 0.1%, which is well below the maximum limit of 4% specified by ASTM C618 [14].

3.3 XRD Mineralogy

Several approaches for Rietveld analysis of cementitious materials have been proposed in the literature that yield good results [15–18]. However, refinement and quantification of natural clays are more complicated due to the varying degree of disorder of the kaolin-group minerals. The main kaolin-group minerals found in Florida include kaolinite, dickite, and nacrite which are polymorphs that differ in the stacking of adjacent clay layers [19]. It was observed that fitting of the clay XRD patterns, regardless of the degree of order/disorder, was significantly improved when the kaolin content of the sample was considered to be equal to the sum of the kaolinite, dickite, and nacrite [9]. In addition to variability in stacking, kaolin can have a variable amount of isomorphous substitution of Al^{3+} in its crystal structure by Fe^{3+}, Mg^{2+}, Ti^{4+}, and V^{3+}, which can affect the quantification of this phase [19–21]. Since the amount of MgO and TiO_2 identified by XRF was low compared to Fe_2O_3, and vanadium was not found, only Fe^{3+} substitution was considered. A general formula of $(Al_2O_3)_{(1-x)}(Fe_2O_3)_x(SiO_2)_2(H_2O)_2$, was adopted for kaolin, where x was the Fe–Al substitution parameter for all kaolin polymorphs. Refinement of Fe^{3+} substitution in kaolin's structure during Rietveld analysis was previously implemented by Prandel et al. [20, 21]. The authors pointed out that substitution of Fe^{3+} for Al^{3+} results in an increase in kaolin unit cell volume which causes hydrogen bonds stretching, increasing the degree of structural disorder [22]. Structural disorder will affect calcined clay reactivity although its influence is not fully understood. The refined mineralogy of all 10 kaolin clay fractions is reported in Table 2. Table 2 presents that the total kaolin content in the selected samples ranged from approximately 70–90 wt%. All of these clay fractions are expected to have high reactivity upon calcination due to their high kaolin contents. Hematite was identified in all the clays, except A1 and B1, and was responsible for their red color. Small amounts of quartz were also detected in the clay fractions, ranging from 0.4 to 3.8%, except for clay E, where the amount of quartz was 10.3%. The amorphous/unidentified content of the samples may be

Table 1 Elemental oxide compositions of the clay fractions [9]

Clay ID	A1	B1	B2	B3	B4	C	D1	F	E	G
Analyte	wt%	wt%	wt%	wt%	wt%	wt%	wt%	wt%	wt%	wt%
SiO_2	46.0	42.5	43.3	37.1	41.1	34.1	38.5	42.6	43.7	43.8
Al_2O_3	37.7	35.9	34.3	33.1	33.3	33.1	31.3	34.9	30.1	32.5
Fe_2O_3	0.9	1.6	3.0	10.2	5.4	6.6	8.9	4.6	6.5	5.5
CaO		0.1			0.2	1.1	0.1		0.4	
MgO	0.2	0.4	0.2	0.3	0.3	0.3	0.5	0.2	0.3	0.2
Na_2O	0.1			0.1	0.1	0.2	0.1			
K_2O	0.2	0.2	0.2	0.2	0.2	0.2	0.2	0.1	0.2	0.3
TiO_2	0.3	1.5	2.5	1.5	1.7	1.1	1.4	1.1	1.8	1.2
P_2O_5	0.1	0.7	0.4	0.8	1.1	5.4	1.3	0.2	0.3	0.8
SrO		0.1	0.1	0.1	0.2	0.5	0.2			0.2
BaO		0.1	0.1	0.1	0.1	0.3	0.1			0.2
L.O.I (950 °C)	14.2	16.1	15.1	16.5	15.6	16.3	16.6	15.4	15.7	14.4
Total	99.7	99.2	99.2	100	99.3	99.2	99.2	99.1	99.0	99.1
Na_2O_{eq}	0.2	0.2	0.2	0.2	0.2	0.4	0.2	0.1	0.1	0.2

Table 2 Kaolin clay fraction [9]

Clay	Kaolinite (wt%)	Nacrite (wt%)	Dickite (wt%)	Sum (Kaolin wt%)	Fe^{3+} Substitution, x	Illite (wt%)	Crandallite (wt%)	Hematite (wt%)	Gibbsite (wt%)	Anatase (wt%)	Quartz (wt%)	Amorphous (wt%)
A1	59.5	9.9	20.2	**89.6**	0.003	0.6					1.7	8.2
B1	49.4	14.1	23.9	**87.4**	0.013		1			1.1	0.4	10.2
B2	57.9	9	17.6	**84.5**	0.047		0.8	0.5		1.6	1.9	10.7
B3	54.4	17.7	11.2	**83.3**	0.187		1	0.7		1.1	1.2	12.7
B4	41	18.1	23	**82.1**	0.069		1.2	0.1		1.2	2	13.5
C	49.7	10.2	10.4	**70.2**	0.005		2.6	0.4	1.3	0.7	0.6	24.2
D1	51.8	10.6	16	**78.4**	0.154		1.5	0.1		1	2.4	16.6
E	51.4	12.4	7.6	**71.4**	0.013		0.5	1	3.3	0.9	10.3	12.5
F	62.6	12.8	10.5	**85.9**	0.014		0.1	1		0.8	1.5	10.8
G	55.6	11.9	10.2	**77.7**	0.031		0.9	1.4		0.8	3.8	15.4

due to the presence of allophane, which is a general name for amorphous, hydrous aluminosilicates and short-ranged order-oxides and hydroxides commonly found in natural clays [9, 23–25].

3.4 Thermogravimetric Analysis

Thermal decomposition of kaolin clays may be divided into 3 general stages: dehydration, dehydroxylation, and recrystallization [2, 26, 27]. The computed kaolin contents using TGA compared similarly to that determined during refinement with a maximum error of 5.4% in clay E and 7.8% in clay B3 with and without accounting for iron substitution, respectively [9]. Thus, the TGA- and XRD-determined kaolin quantification techniques corroborated one another and are deemed reliable [9].

3.5 Mortar Compressive Strength

Figure 1 shows the compressive strength results for all the calcined clay mixtures and the cement control. Additionally, the strength activity indices for all the clay mixtures may be observed by the bold lines in Fig. 1 marking 75% of the control's strength. It can be seen that at 7 days, compressive strengths of the calcined clay mortars were greater than 75% for all the samples, except 10B3-600-1. However, by 28 days, the strength activity index was above 76% for all the mixtures making them eligible as Class N pozzolans according to ASTM C618 [14].
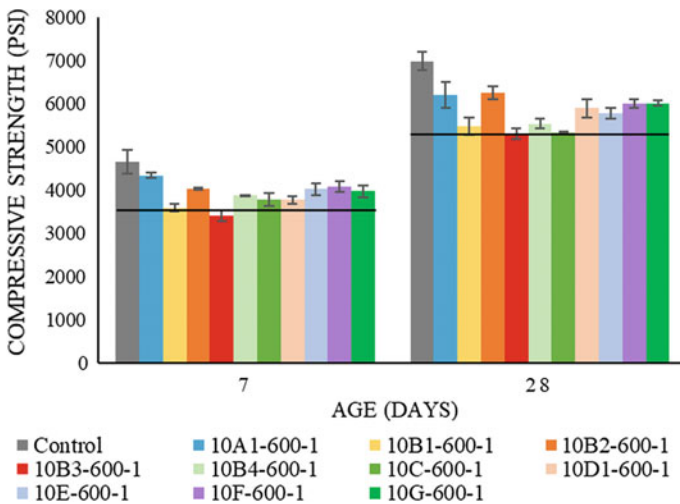
Fig. 1 Compressive strength of 10% calcined clay mortar cubes [18]

In order to isolate the filler effects of the sand used with each calcined clay, compressive strengths of the first five calcined clay mixtures were compared to their respective individual controls where a portion of the standard sand was replaced with the sand coming from the calcined material. This comparison showed the 7-day strength activity indices of the calcined clay mortars were higher than 75%, even for the 10B3-600-1 mortar revealing an index of 84%. Compressive strengths of the individual controls of A1, B2, and B4 were very similar to that of the common control mixture, while the compressive strengths of the individual control B1 and B3 were lower, which is consistent with the trend observed in Fig. 1 at 7 days, where 10B1-600-1 and 10B3-600-1 mixtures had the lowest compressive strengths. Nevertheless, isolating the filler effect of the first five calcined clay mortars allows for their 7-day strength performance to surpass the ASTM C618 requirements for Class N pozzolans [14].

4   Conclusions

A number of potential clay sources were identified in the state of Florida. The obtained field samples contained 65–90% sand (material retained on the 45 μm sieve). The sand content must be separated from the clay portion or ground to an appropriate fineness in order to be included with clay and considered feasible as natural pozzolans for use in modern mortar and concrete. Alternatively, this sand may be treated as a replacement for fine aggregate used during mortar and concrete construction. The fraction passing the 45 μm sieve met the chemical oxide composition requirements of ASTM C618: minimum of 70.0% for $SiO_2 + Al_2O_3 + Fe_2O_3$ and SO_3 content of less than 4%. The kaolin content of the clay fractions was determined by XRD and TGA accounting for structural disorder by means of kaolin polymorph stacking and impurity iron isomorphic substitution. Both mineralogical quantification techniques revealed the Florida clays that were composed of approximately 70–94% kaolin, indicating the potential for these clays to be high-quality pozzolanic materials post calcination. The pozzolanic activity of the clays calcined at 600 °C showed that the Florida kaolin clays obtained are capable of producing a pozzolanic material that meet the Class N requirements of ASTM C618 using a 10% cement replacement level.

References

1. Vizcaíno, L., Antoni, M., Alujas A., Martirena, F., Scrivener, K.: Industrial manufacture of a low-clinker blended cement using low-grade calcined clays and limestone as SCM: the Cuban experience. In: Calcined Clays for Sustainable Concrete, RILEM, pp. 347–358. Springer (2015)
2. Zayed, A., Shanahan, N., Sedaghat, A., Stetsko, Y., Lorentz, B.: Development of calcined clays as pozzolanic additions in Portland cement concrete mixtures, Florida (2018)
3. Calver, J.L.: Florida kaolins and clays, Tallahassee (1949)
4. Matson, G.C.: Clays of Florida (1908)
5. The Southeastern Geological Society: Ochlocknee mine and little river mine, Tallahassee (2013)
6. Bishop, E.W., Dee, L.L.: Guide to rocks and minerals of Florida. Florida Bureau of Geology, Tallahassee (1961)
7. Florida Department of Environmental Protection Agency, Map direct: integrated habitat network (IHN). [Online]. Available: https://ca.dep.state.fl.us/mapdirect/?focus=ihn. Accessed 2 Feb 2017
8. ASTM C1365-06 (Reapproved 2011): Standard Test Method for Determination of the Proportion of Phases in Portland Cement and Portland-Cement Clinker Using X-Ray Powder Diffraction Analysis. ASTM International, West Conshohocken, PA (2006)
9. Lorentz, B., Shanahan, N., Stetsko, Y.P., Zayed, A.: Characterization of Florida kaolin clays using multiple-technique approach. Appl. Clay Sci. (2018)
10. Shvarzman, A., Kovler, K., Grader, G.S., Shter, G.E.: The effect of dehydroxylation/amorphization degree on pozzolanic activity of kaolinite. Cem Concr Res (2003)
11. Vyazovkin, S.: Thermogravimetric analysis. In: Characterization of Materials, pp. 177–211 (2012)
12. ASTM C109-16a: Standard Test Method for Compressive Strength of Hydraulic Cement Mortars (Using 2-in. or [50-mm] Cube Specimens), p. 10. ASTM International, West Conshohocken, PA (2016)
13. ASTM C305-14: Standard Practice for Mechanical Mixing of Hydraulic Cement Pastes and Mortars of Plastic Consistency. ASTM International, West Conshohocken, PA (2014)
14. ASTM C618-17a: Standard Specification for Coal Fly Ash and Raw or Calcined Natural Pozzolan for Use in Concrete. ASTM International, West Conshohocken, PA (2017)
15. Snellings, R., Bazzoni, A., Scrivener, K.: The existence of amorphous phase in Portland cements: Physical factors affecting Rietveld quantitative phase analysis. Cem. Concr. Res. **59**, 139–146 (2014)
16. Álvarez-Pinazo, G., et al.: Rietveld quantitative phase analysis of Yeelimite-containing cements. Cem. Concr. Res. **42**(7), 960–971 (2012)
17. Le Saôut, G., Kocaba, V., Scrivener, K.: Application of the Rietveld method to the analysis of anhydrous cement. Cem. Concr. Res. **41**(2), 133–148 (2011)
18. Stetsko, Y.P., Shanahan, N., Zayed, A.: Quantification of supplementary cementitious content in blended Portland cement using an iterative Rietveld–PONKCS technique research papers, pp. 1–10 (2017)
19. Brigatti, M.F., Galan, E., Theng, B.K.G.: Structures and mineralogy of clay minerals. In: Bergaya, F., Theng, B.K.G., Lagaly, G. (eds.) Developments in Clay Science, vol. 1, pp. 19–86. Elsevier Ltd. (2006).
20. Prandel, L.V., Dias, N.M.P., da Costa Saab, S., Brinatti, A.M., Giarola, N.F.B., Pires, L.F.: Characterization of kaolinite in the hardsetting clay fraction using atomic force microscopy, X-ray diffraction, and the Rietveld method. J. Soils Sediments **17**(8), 2144–2155 (2017)
21. Prandel, L.V., Saab, S.C., Giarola, N.F.B., Brinatti, A.M.: Analysis of kaolinite isomorphic substitution and microstrain in hardsetting soils horizons through X-ray diffraction and the Rietveld method. In: Proceedings of the International Symposium on Crystallography, p. 65 (2015)
22. Bich, C., Ambroise, J., Péra, J.: Influence of degree of dehydroxylation on the pozzolanic activity of metakaolin. Appl. Clay Sci. **44**(3–4), 194–200 (2009)

23. Bergaya, F., Lagaly, G.: General introduction: clays, clay minerals, and clay science. Dev. Clay Sci. **5**, 1–19 (2013)
24. Dill, H.G.: Kaolin: soil, rock and ore: from the mineral to the magmatic, sedimentary and metamorphic environments. Earth-Sci. Rev. **161**, 16–129 (2016)
25. Russell, J., Fraser, A.: Infrared Methods. In: Wilson, M.J. (ed.) Clay Mineralogy: Spectroscopic and Chemical Determinative Methods, pp. 11–67. Chapman & Hall, Oxford, UK (1994)
26. Mohammed, S.: Processing, effect and reactivity assessment of artificial pozzolans obtained from clays and clay wastes: A review. Constr. Build. Mater. (2017)
27. Kakali, G., Perraki, T., Tsivilis, S., Badogiannis, E.: Thermal treatment of kaolin: The effect of mineralogy on the pozzolanic activity. Appl. Clay Sci. **20**(1–2), 73–80 (2001)

An Approach for the Evaluation of Local Raw Material Potential for Calcined Clay as SCM, Based on Geological and Mineralogical Data: Examples from German Clay Deposits

Matthias Maier, Nancy Beuntner and Karl-Christian Thienel

Abstract This study gives an overview over the geological and spatial distribution of German clay deposits visualized in a GIS map, which is based on the map of mineral resources and the geological map of Germany, and supplemented by active clay pits. The clays are classified regarding their geological context. Representative clays for a certain geological formation are examined closely. Detailed clay mineralogy is determined using XRD. Optimal calcination temperature is defined using TG/DTG. The calcined clays are characterized by XRD and BET. Pozzolanic reactivity is assessed by R^3 calorimetry test and solubility of Al and Si ions in alkaline solution. A correlation between geological origin, chemical–mineralogical composition and pozzolanic reactivity is discussed. The study shows that a rough estimation of pozzolanic reactivity based on geological data or chemical composition is possible. For a detailed assessment, an elaborate determination of mineralogical phase content or a direct determination of reactivity is necessary.

Keywords Calcined clay · Clay deposits · Clay mineralogy · Pozzolanic reactivity

1 Introduction

One of the most effective attempts to lower the ecological impact of cement production due to CO_2 emissions is the partial substitution of cement clinker. Since established supplementary cementitious materials (SCM) like fly ash and slag stagnate or even decrease in many industrialized countries, the demand for alternative materials will rise in the future [1]. The probably most promising alternative materials are calcined clays. Much research has been done in the past years, focusing primarily on metakaolin [2]. Recently, the focus shifted on calcined natural clays [3, 4] which, from an economic point of view, form the most interesting group of new SCM. The pozzolanic reactivity in dependence of the mineralogical clay composition, primarily kaolinite content, has been subject of many studies [5, 6], which already allows drawing conclusions on the reactivity based on the mineralogy. In

M. Maier (✉) · N. Beuntner · K.-C. Thienel
University of the Bundeswehr Munich, Werner-Heisenberg-Weg 39, 85577 Neubiberg, Germany
e-mail: matthias.maier@unibw.de

order to enhance the evaluation of clay deposits for the use as SCM, it is important to better understand the influence of mineralogy on reaction behavior and to relate these parameters to the geological setting of the deposit. This could help for a rough assessment of clay deposits based on geological data and maps, which exist for many parts of the world.

In Germany, the current main application fields for clays are the brick, the ceramic and the refractory industry. Lower quantities are used as sealing clays. Kaolin mainly serves as ceramic raw material, filler for paper, plastics, rubber or colors. In 2015, 5.3 million tons of raw kaolin have been mined leading to 1.1 million tons of kaolin products available for sale. On the other side, there were 6.4 million tons of special clay being used for the ceramic and refractory industry plus another 12 million tons of clay used in the brick industry [7].

This study gives an overview over the clay deposits in Germany, including an evaluation of characteristic samples, regarding their applicability as calcined clays as SCM, based on mineralogical characterization and assessment of pozzolanic reactivity.

2   Spatial Analysis of Clay Deposits and Selection of Clays

On the basis of the maps of mineral resources [8] and geology of Germany [9], a base map (Fig. 1) was created using *ESRI ArcGIS*. *ArcGIS* is a geographic information system, which allows to collect, analyze and present spatial data. Active clay pits and cement plants were added. Areas with a concentration of clay deposits were described geologically. From each area, at least one sample was selected for further investigation.

Orange areas and the small orange dots represent clay and claystone, which are not further classified, as they are provided by the map of mineral resources of Germany. The manually added open clay pits are divided in brick clays, special clays, kaolin and washing sludges. Brick clays are clays which are mainly used for the production of masonry bricks, roof tiles, facing bricks or clinker. Special clays represent the raw material for refractories, acid-resistant and technical ceramics or fine ceramics. Primary kaolin deposits which are further processed to high-grade products are referred to as kaolin. Washing sludges are residues from processing of other raw materials, for example, sand, gravel or also coal. Table 1 gives an overview over the selected clays with reference to their geological origin.

The geographic location of clay deposits plays an important role regarding a use as SCM, since the distance from the pits to potential customers defines a major part of the costs. Beyond that, the geographic location can be referenced with geological maps, as it was done in this study, to get a first idea about the suitability of the clays.
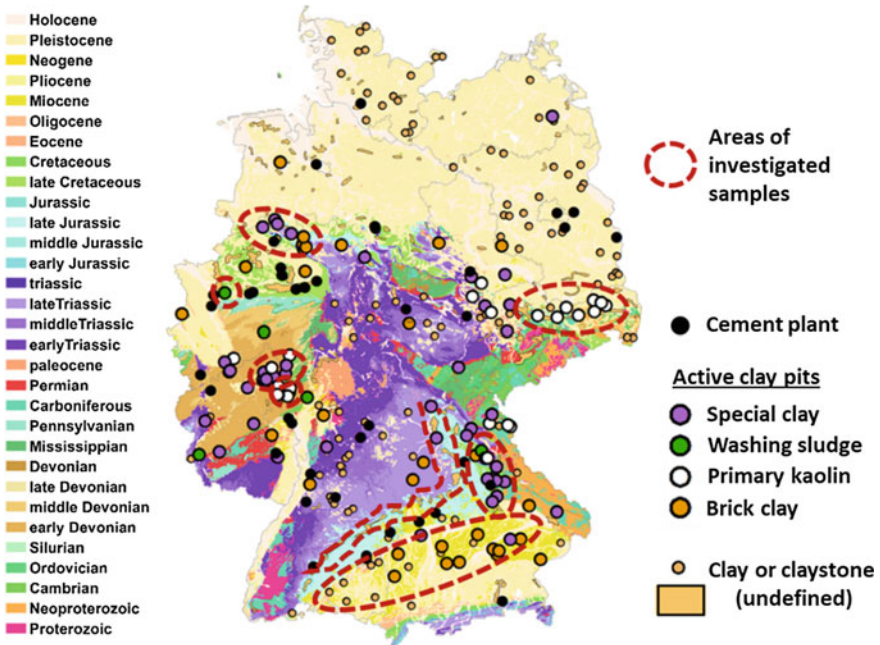
Fig. 1 Geological map of Germany 1:1,000,000 [9] with deposits of clay and claystone [8] and active clay pits

Table 1 Clays selected for investigations and their geological description

Short name	Long name	Geological description
KT	Raw Kaolin Taunus	Primary kaolin deposit accrued by Eocene and Oligocene weathering of Devonian chlorite-rich shale [10]
KUP	Raw Kaolin Upper Palatinate	Primary kaolin deposit formed from Eocene until Miocene by weathering of Carboniferous granite [10]
FUP	Fireclay Upper Palatinate	Sedimentary kaolin-rich clays deposited in the Miocene [11]
RKUP	Recycling Kaolin Upper Palatinate	Secondary component of a Jurassic sandstone, enriched by technical wet processing [10]
AC	Amaltheen Clay	Early Jurassic marine sediments of a continental shelf [12]
SW	Shale Westerwald	Devonian slate which outcrops in Westerwald clay deposits [13]

<div align="right">(continued)</div>

Table 1 (continued)

Short name	Long name	Geological description
SCW	Stoneware Clay Westerwald	Tertiary weathering products of fine-grained Devonian rocks deposited in Eocene until Miocene [12]
CCW	Coal-bearing Clay Westphalia	Secondary component of Upper Carboniferous coal beds [13]
MOSM	Marl Upper Freshwater Molasse	Upper Eocene to the Upper Miocene sediments resulting from erosion processes of the alps which were deposited in the foreland basin [13]
SLS	Shale Lower Saxony	Cretaceous shale [12]
KS	Kaolin Saxony	Tertiary kaolinisation of a Permian quartz-porphyry—purified by wet processing [11]

3 Experimental Procedure

The chemical composition of the raw clays was analyzed by means of ICP-OES (*Varian ICP-OES 720 ES*) on solutions of lithium metaborate flux fusions. The clay minerals were identified by XRD (*PANalytical Empyrean, Bragg-BrentanoHD monochromator, PIXcel1D linear detector*) on oriented mounts of the particle fraction smaller than 2 µm following [14]. The samples were measured in air-dried and in glycolated condition in order to account for swellable clay minerals. Bulk mineralogy of raw and calcined clays was analyzed on side-loaded powder mounts in order to reduce preferred orientation effects. The quantitative phase composition was calculated by Rietveld refinement using Profex BGMN [15]. For the determination of the amorphous fraction of the calcined samples, the external standard method was applied according to [16]. Thermal decomposition of the clays was investigated using TG/DTG (*Netzsch STA 449 F3 Jupiter*) with a heating rate of 2 K/min. The calcination temperature was defined by adding 100 K to the offset temperature of the main dehydroxylation reaction. The clays were calcinated for 30 min in a laboratory muffle furnace using platinum crucibles. The calcined clays were ground in a vibratory disk mill with a speed of 700 min^{-1} for 10 min, using an agate grinding tool. Specific surface area (BET) was measured in a *Horiba S-9601 MP* using nitrogen as absorption gas. The solubility of Al and Si ions was determined by elution of the calcined material in NaOH-solution (10%) [17]. Pozzolanic reactivity was assessed following the R^3 calorimetry test at 40 °C [18, 19].

4 Results

4.1 Chemical and Mineralogical Properties of the Raw Clays

The investigated raw clays are plotted in a ternary diagram (Fig. 2) based on their contents of SiO_2, Al_2O_3 and $CaO + MgO$, normalized to the sum of these components. The relevant silica-rich region of the diagram is enlarged.

The three clays in the alumina-rich right corner are sedimentary kaolinitic clays and technically processed primary kaolin (FUP, SCW and KS). The marl (MOSM) and the calcite-bearing Amaltheen clay (AC) can be differentiated by their $CaO + MgO$ content. The low-grade kaolinitic clays plot in the silica-rich half of the SiO_2-Al_2O_3-axis and cannot be differentiated in this way. Ternary diagrams based on the chemical composition can help to separate the kaolinite-rich clays from the low kaolinite clays (if there is no other major Al_2O_3 source) or marls from lime-free clays but are unsuitable to differentiate between different low-grade kaolinitic clays with several other clay minerals. Nevertheless, chemical compositions are often provided by clay-suppliers and can be used for a first rough classification.

The mineralogical composition of the different clays are presented in Table 2 and is discussed together with the reactivity below point 4.3.
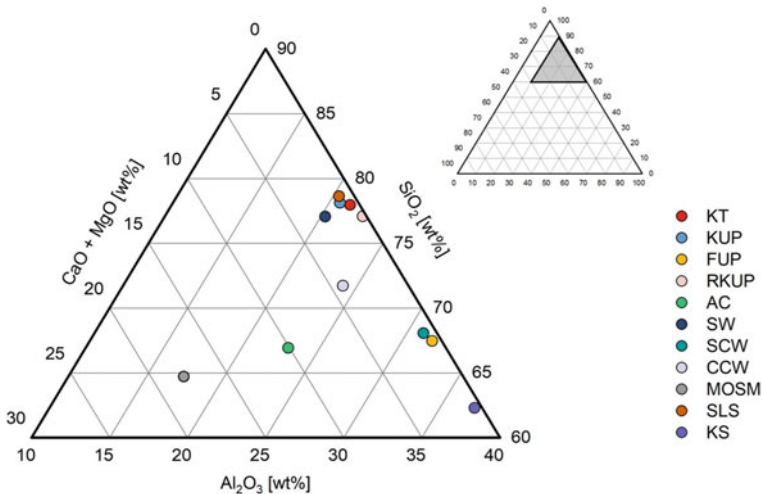
Fig. 2 Plot of the investigated raw clays in the ternary diagram based on the contents of Al_2O_3, SiO_2 and $CaO + MgO$ normalized to the sum of them

Table 2 Mineralogical composition of the analyzed clays

	FUP	SW	CCW	KT	AC	MOSM	RKUP	KUP	SLS	SCW	KS
Qtz	12	21	16	38	20	18	48	33	37	18	16
K_{md}	–	7	–	20	–	8	17	26	7	–	25
K_{hd}	74	–	10	–	23	–	28	–	–	40	59
Ill	3	–	11	–	–	–	–	–	–	–	–
I-S	8	–	24	–	32	–	–	–	40	20	–
Sm	–	–	–	–	–	25	–	–	–	–	–
Ms	–	51	–	36	5	19	3	36	15	18	–
Chl	–	19	1	–	6	5	–	–	–	–	–
Cc	–	–	<1	–	7	7	–	–	–	–	–
Dol	–	–	1	–	1	10	–	–	–	–	–
Fsp	–	–	–	–	4	7	–	–	–	–	–
Rt	1	1	–	1	<1	1	–	1	–	2	–
An	1	–	0	–	2	–	<1	–	1	–	1
Py	–	–	–	–	1	–	–	–	–	–	–
He	–	–	<1	–	–	–	<1	–	–	2	–
Goe	–	–	–	5	–	–	3	4	–	1	–
Sid	–	–	1	–	–	–	–	–	–	–	–
Am	–	–	35	–	–	–	–	–	–	–	–

Qtz = Quartz, K_{md} = moderately disordered kaolinite, K_{hd} = highly disordered kaolinite, Ill = illite, I-S = illite–smectite, Sm = smectite, Ms = muscovite, Chl = chlorite, Cc = calcite, Dol = dolomite, Fsp = feldspar, Rt = rutile, An = anatase, Py = pyrite, He = hematite, Goe = goethite, Sid = siderite and Am = amorphous

4.2 Characterization of Calcined Clays

Table 3 gives the X-ray-amorphous content after calcination, the specific surface area after grinding and the calcination temperatures that were defined based on the end set temperatures of the main dehydroxylation reaction in the DTG data.

4.3 Reactivity

The heat release of the different calcined clays during the R^3 calorimetry test is shown in Fig. 3. The first 1.2 h are cut off, according to Li et al. [19]. Quartz powder was used as an inert reference. The investigated materials show a broad variation, regarding the quantitative heat release as well as the reaction kinetics. The high-grade kaolinitic clays cause two maxima which are differently pronounced, referring to the silicate and aluminate reaction. The sedimentary kaolinitic clays (FUP and SCW) provide a fast reaction with a first heat flow maximum below 8 h, which probably results from a faster release of especially Al ions due to the high amount of disordered kaolinite and a high specific surface area. The primary kaolins (KS, KT and KUP) and the recycling kaolin (RKUP), which show a higher degree of order and therefore also a lower surface area, provide a slower reaction and the two maxima merge to one. The clays with lower amount of kaolinite react clearly slower with one broad reaction maximum, which is due to the lower release of Al ions.

The correlation between Al_2O_3 content and reactivity (Fig. 4) is good for high kaolintite contents, where other clay minerals do not play an important role. Clays with lower kaolinite content do not differ significantly in Al_2O_3 content which is why this parameter cannot be used to assess them. As has been shown before [5, 6], the decisive criterion for reactivity is the overall kaolinite content of the raw clay. If it exceeds about 40 wt%, the contribution of other components to the heat flow is nearly negligible. In the area of lower kaolinite contents, the role of the other clay minerals gains significance. This is shown by the clays with a kaolinite content below 30 wt%. Here, clays containing significant amounts of illite, smectite or illite–smectite mixed-layer minerals provide a clearly higher heat development during the R^3 calorimetry test than those containing mainly mica and quartz. This is in good consistency with investigations on reactivity of single phyllosilicates [20].

Table 3 Calcination temperatures, amorphous content and BET after calcination and grinding

	FUP	SW	CCW	KT	AC	MOSM	RKUP	KUP	SLS	SCW	KS
T_{calc} [°C]	650	810	660	800	680	700	680	620	740	620	650
Am. [wt%]	76	37	49	19	43	31	33	23	36	56	81
BET [m^2/g]	44.1	9.1	40.2	10.0	30.2	17.3	8.4	8.7	16.5	32.2	n.d
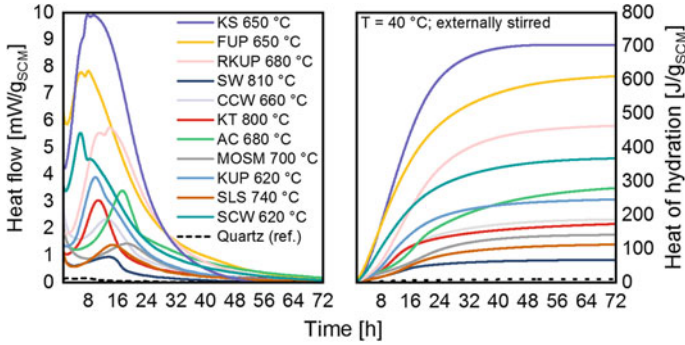
Fig. 3 Development of the heat release normalized per gram of calcined clay during R³ calorimetry test (left) and cumulative heat (right) from 1.2 to 72 h
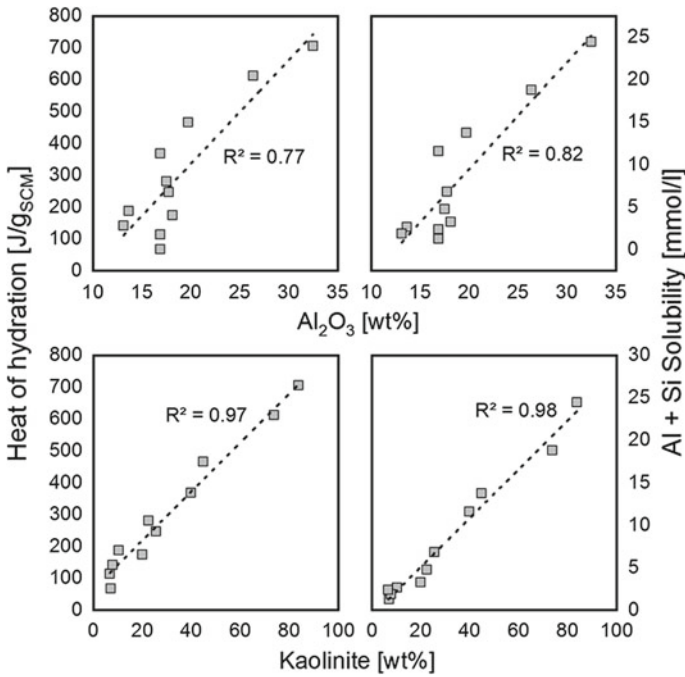
Fig. 4 Influence of Al₂O₃ (top) and kaolinite (bottom) content on heat of hydration during R³ calorimetry test (left) and on solubility of Si and Al ions (right)

5   Conclusion

Geological data can allow conclusions on the type of clay deposits and therefore help for a rough estimation of suitability. In order to derive a more precise assessment, a comprehensive mineralogical analysis is requisite. Particularly for low-grade kaolinitic clays, the impact of other clay minerals is significant. An evaluation based on the chemical composition does not work for low-grade kaolinitic clays, since the difference in Al_2O_3 content is not significant. For the assessment of pozzolanic reactivity, the R^3 calorimetry test and the solubility of Al and Si ions show very good consistency.

References

1. Snellings, R., Mertens, G., Elsen, J.: Supplementary cementitious materials. Rev. Mineral. Geochem. **74**, 211–278 (2012)
2. Sabir, B.B., Wild, S., Bai, J.: Metakaolin and calcined clays as pozzolans for concrete: a review. Cem. Concr. Compos. **23**(6), 441–454 (2001)
3. Danner, T., Norden, G., Justnes, H.: Characterisation of calcined raw clays suitable as supplementary cementitious materials. Appl. Clay. Sci. **162**, 391–402 (2018)
4. Beuntner, N., Thienel, K.-C.: Properties of calcined lias delta clay—technological effects, physical characteristics and reactivity in cement. In: Scrivener, K., Favier, A. (eds.) 1st International Conference Calcined Clays for Sustainable Concrete, pp. 43–50. Springer, Netherlands (2015)
5. Tironi, A., Trezza, M.A., Scian, A.N., Irassar, E.F.: Kaolinitic calcined clays: factors affecting its performance as pozzolans. Constr. Build. Mater. **28**(1), 276–281 (2012)
6. Avet, F., Scrivener, K.: Investigation of the calcined kaolinite content on the hydration of limestone calcined clay cement (LC3). CCR **107**, 124–135 (2018)
7. Lorenz, W., Gwosdz, W.: Handbuch zur geologisch-technischen Bewertung von mineralischen Baurohstoffen. Geologisches Jahrbuch Sonderhefte. Bundesanstalt für Geowissenschaften und Rohstoffe (2003)
8. Dill, H.G., Röhling, S.: Map of Mineral Resources of Germany 1:1,000,000 (BSK1000). BGR, Hannover (2007)
9. Toloczyki, M., et al.: Geological Map of Germany 1:1,000,000 (GK1000). BGR, Hannover (2006)
10. Elsner, H.: Kaolin in Deutschland. BGR, Hannover (2007)
11. Radczewski, O.-E.: Die Rohstoffe der Keramik. Springer, Heidelberg (1968)
12. Börner, A., et al.: Steine- und Erden-Rohstoffe in der Bundesrepublik Deutschland. Geologisches Jahrbuch, Sonderhefte, Heft SD 10. BGR, Hannover (2012)
13. Meschede, M.: Geologie Deutschlands, 2nd edn. Springer Spektrum, Berlin (2018)
14. Moore, D.M., Reynolds, R.C.: X-ray Diffraction and the Identification and Analysis of Clay Minerals, 2nd edn. Oxford University Press, Oxford
15. Döbelin, N., Kleeberg, R.: Profex: a graphical user interface for the Rietveld refinement program BGMN. J. Appl. Crystallogr. **48**, 1573–1580 (2015)
16. O'Connor, B.H., Raven, M.D.: Application of the Rietveld refinement procedure in assaying powdered mixtures. Powder Diffr. **3**, 2–6 (1988)
17. Buchwald, A., Kriegel, R., Kaps, C.H., Zellmann, H.-D.: Untersuchungen zur Reaktivität von Metakaolinen für die Verwendung in Bindemittelsystemen. In: Proceedings Bauchemie, Munich (2003)
18. Avet, F., Snellings, R., Diaz, A.A., Ben Haha, M., Scrivener, K.: Development of a new rapid, relevant and reliable (R^3) test method to evaluate the pozzolanic reactivity of calcined kaolinitic clays. Cem. Concr. Res. **85**, 1–11 (2016)

19. Li, X., et al.: Reactivity tests for supplementary cementitious materials: RILEM TC 267-TRM phase 1. Mater. Struct. **51**(151), 1–14 (2018)
20. Scherb, S., Beuntner, N., Thienel, K.-C.: Reaction kinetics of basic clay components present in natural mixed clays. In: Martirena, M., Favier, A., Scrivener, S. (eds.) Proceedings 2nd International Conference on Calcined Clays for Sustainable Concrete, pp. 427–433. Springer, Netherlands (2018)

Clay Deposits from the Northeastern of Cuba: Characterization, Evaluation, and Use as a Source of Supplementary Cementitious Materials

Roger S. Almenares Reyes [ORCID]**, Adrián Alujas Díaz, Carlos A. Leyva Rodríguez, Lisandra Poll Legrá, Luis A. Pérez García, Sergio Betancourt Rodríguez, Florencio Arcial Carratalá and José F. Martirena Hernández**

Abstract Three clay deposits from northeastern Cuba were characterized by X-ray fluorescence, X-ray diffraction, and thermogravimetric analysis. The clay deposits present high content of aluminum oxide and loss on ignition. Kaolinite was identified as a main clay mineral, and iron and aluminum phases as impurities. The clays were preliminarily selected by chemical and mineralogical criteria and then activated by stationary calcination at 750 °C. The pozzolanic reactivity was determined by strength activity index in standardized mortars. Three blended cements containing calcined clay, limestone, clinker, and gypsum were formulated and assessed. Formulated cements were used to produce hollow blocks of concrete and hydraulic tiles. Finally, it is concluded that the three clayey deposits are presented with high potential for use as source of supplementary cementitious materials. Chemical criteria and kaolinite content are a useful tool to predict the potential of clay deposits to be used as source of supplementary cementitious materials. Samples with higher kaolinite content present the best pozzolanic activity. Ternary cements assessed can replace Portland cement in the manufacture of hollow concrete blocks and hydraulic tiles.

R. S. Almenares Reyes (✉) · L. Poll Legrá
Departamento de Metalurgia—Química, Instituto Superior Minero Metalúrgico de Moa, 83330 Moa, Cuba
e-mail: ralmenares@ismm.edu.cu

A. Alujas Díaz
Centro de Estudios de Química Aplicada, Universidad Central de Las Villas, 54830 Santa Clara, Cuba

C. A. Leyva Rodríguez · L. A. Pérez García
Departamento de Geología, Instituto Superior Minero Metalúrgico de Moa, 83330 Moa, Cuba

S. Betancourt Rodríguez
Facultad de Construcciones, Universidad Central de Las Villas, 54830 Santa Clara, Cuba

F. Arcial Carratalá
Empresa Geominera del Centro, 54800 Santa Clara, Cuba

J. F. Martirena Hernández
Centro de Investigación y Desarrollo de Estructuras y Materiales, Universidad Central de Las Villas, 54830 Santa Clara, Cuba

Keywords Calcined clays · Kaolinitic clays · Pozzolanic reactivity

1 Introduction

In Cuba, there is growing interest in the use of clays as sources of supplementary cement materials (SCMs). There are several experiences that have shown the potentialities of the use of these materials in the production of cements with a high level of clinker substitution [1–3].

In the northeastern region of Cuba there is an important industrial mining activity. In recent times, aluminum-rich weathering crusts as raw material for the production of refractory materials and ceramic bricks have been considered as an alternative in their future development [4], although their potential can go beyond these applications indicated.

Several investigations show the prospects of the use of the clay deposits of the region as source of raw material for the production of SCMs [5, 6]. However, the only industrial use of the clay deposits lying of the weathering crusts over gabbros of this northeastern region has been as a raw material for small productions of ceramic bricks [7].

This issue has been limited in part, because the availability and potentialities of the clay deposits have not been demonstrated. Therefore, the goal of this paper is to present the results of the characterization, evaluation, and use as a source of supplementary cementitious materials from three new clay deposits from the northeastern region of Cuba.

2 Materials and Methods

The area of interest of this research is the region of Moa, Holguín Province, where there are numerous clay deposits. Three deposits lying in weathering crusts on gabbroic rocks were selected at Centeno (C1), La Delta (C2), and Cayo Guam (C3) deposits.

The chemical composition was analyzed by X-ray fluorescence (XRF) on a Bruker AXS S4 spectrometer. Mineralogical composition was determined by X-ray diffraction (XRD) using a PANalytical X'Pert Pro MPD diffractometer.

Thermogravimetric analysis (TGA) was used to quantify the kaolinite content, applying the equation reported in Alujas et al. [8] and modified for the temperature range between 350 and 750 °C. This method assumes that weight loss in this temperature range is mainly related to kaolinite dehydroxylation. Chemical and mineralogical composition was used for the preliminary assessment based on the procedure reported in Alujas et al. [8].

The clay samples were heated at 750 °C for 60 min, cooled, and ground in a ball mill until reaching about 90% passed in the sieve 90 μm. The calcination was

carried out in a heat-treating furnace. The pozzolanic activity of calcined clays was measured by strength activity index [9].

After reactivity assessing of calcined clays, ternary cementitious systems were formulated according to the Cuban standard NC 1208 [10]. Ternary blends were formulated based on a mixture of calcined clay (30%) and limestone (15%) with clinker (50%) and gypsum (5%). Blends were termed as LC^3-50 (47%) (2:1) C1, LC^3-50 (57%) (2:1) C2 and LC^3-50 (80%) (2:1) C3 where LC^3-50 is the name of blend and the values in parentheses (equivalent kaolinite content) (proportion of calcined clay: limestone) and finally the name assigned to the clay.

The compressive strength of ternary cement mortars was determined by the Cuban standard NC 506 [11]. Ordinary Portland cement was used as a reference.

Main applications of LC^3-50 (47%) (2:1) C1 and LC^3-50 (80%) (2:1) C3 were the manufacture of hollow concrete blocks having size $400 \times 150 \times 200$ mm and hydraulic tiles of 250×250 mm. Hollow concrete blocks and hydraulic tiles were produced under standard manufacturing conditions at a local plant in northeastern of Cuba. The quality was assessed through the Cuban standards [12, 13].

3 Results and Discussion

3.1 Characterization of Raw Materials

Chemical composition is shown in Table 1. The three deposits, products of the weathering of basic rocks, have high aluminum contents, mainly associated with clay mineral, and iron and aluminum phases as impurities. A relatively high content Al_2O_3 in the clays is very important for LC^3 blended systems due to synergy with the calcium carbonate [14].

The kaolinite content and main impurities identified in the samples are summarized in Table 2. The possible interferences of the thermally active associated minerals on the quantification of kaolinite were considered negligible.

3.2 Preliminary Assessment Based on Chemical and Equivalent Kaolinite Content

In agreement with the chemical composition criteria (Table 3) and the identification of kaolinite with content higher than 40%, the three clay deposits are suitable as source of SCMs. These results show, preliminarily, that the characterized clay deposits present potentialities to be used as source of SCMs.

R. S. Almenares Reyes et al.

Table 1 Chemical composition of original clay, %

Clay	SiO$_2$	Al$_2$O$_3$	Fe$_2$O$_3$	CaO	MgO	SO$_3$	Na$_2$O	K$_2$O	Others	PPI
C1	46.52	21.27	16.98	0.12	0.39	0.10	0.12	0.22	3.47	10.81
C2	39.02	33.52	12.05	0.04	0.19	0.06	0.14	0.12	2.82	12.04
C3	39.44	30.25	13.03	0.03	0.48	0.08	0.10	0.21	2.05	14.33

Table 2 Kaolinite content and associated minerals of the raw clays

Clay	C1	C2	C3
Kaolinite content, %	47	75	80
Impurities	Hematite Goethite Hercynite	Hematite Goethite Gibbsite	Hematite Goethite Quartz

Table 3 Selection criteria based on chemical composition

	Criteria	C1	C2	C3
Al_2O_3	>18.00%	21.27	33.52	30.25
CaO	<5.00%	0.12	0.04	0.03
SO_3	<3.00%	0.10	0.06	0.08
Al_2O_3/SiO_2	>0.30	0.46	0.86	0.77
LOI	>7.00%	10.81	12.04	14.33
Kaolinite content	>40	47	75	80

3.3 Assessment of the Pozzolanic Reactivity of the Calcined Clays

Table 4 presents the strength activity index for the three calcined clays. The results are globally in agreement with the equivalent kaolinite content of clays (Fig. 1). Clays rich in kaolinite have the best pozzolanic activity. These results confirm the good potential of clay deposits to produce SCMs.

Table 4 Strength activity index, %

C1	C2	C3
95.21	101.09	105.78
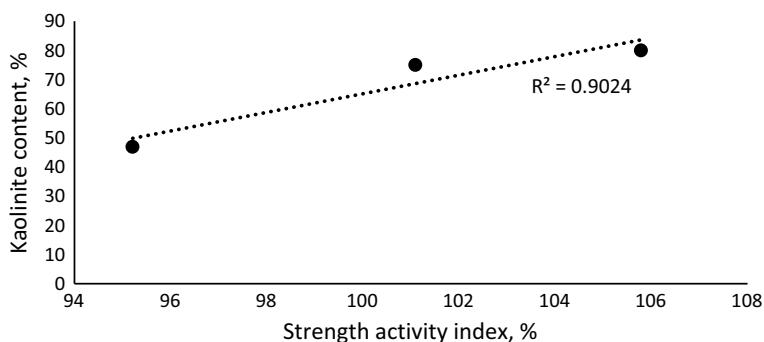
Fig. 1 Correlation between the kaolinite content and the strength activity index
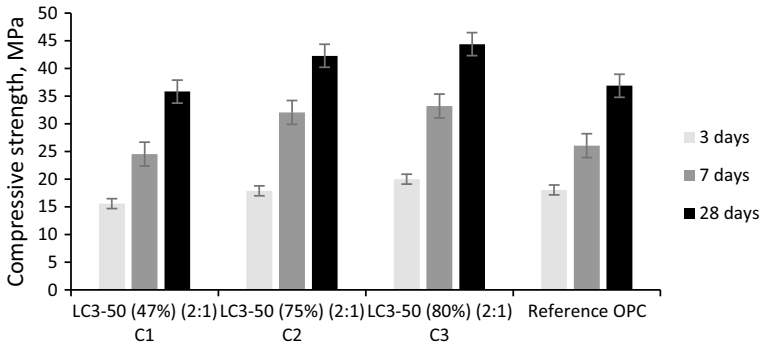
Fig. 2 Compressive strength of ternary blends and the reference

3.4 Assessment of the Compressive Strength of Ternary Blended Cements

The average compressive strength of the ternary and reference cements is presented in Fig. 2. From three days, LC3-50 (75%) (2:1) C2 and LC3-50 (80%) (2:1) C3 show upper values of compressive strength than the control series. Similar behavior is evident at 7 and 28 days, although no significant differences are observed between LC3-50 (75%) (2:1) C2 and LC3-50 (80%) (2:1) C3. Generally, the evolution of the resistance seems to be in correspondence with the reactivity of the calcined clays and the kaolinite content in the original clay.

All series of blended cement mortars meet the compressive strength requirements standardized by the Cuban standard NC 1208 for TAC-35 ternary cements.

3.5 Assessment of the Ternary Blended Cements in the Precast Manufacture

Small format precast products were manufactured for application in housing construction. Table 5 presents the results of the assessment of hollow concrete blocks and hydraulic tiles made with blended cements as well as the standard specifications. The experimental blocks and hydraulic tiles met the standard requirements for strength and water absorption. No major difference between the performances of precast is observed. These results show that the ternary cement containing kaolinite between 47 and 80% seems to give hollow blocks and hydraulic tiles with similar performance, thus indicating that the ternary cements assessed can replace Portland cement in this kind of industrial application.

Table 5 Strength and absorption of hollow blocks and hydraulic tiles

	Average compressive strength at 7 days, MPa	Average compressive strength at 28 days, MPa	Water absorption of blocks, %, w/w	Average flexural strength, MPa	Water absorption of hydraulic tiles, % w/w
Blocks C1	4.41	5.62	8.13	–	–
Blocks C3	5.60	6.96	7.76	–	–
Tiles C1	–	–	–	3.00	7.20
Tiles C3	–	–	–	3.30	6.70
Specifications	4.00	5.00	<10	2.80	<8.00

4 Conclusions

In this study, three new clay deposits of the northeastern Cuba were characterized and assessed as SCMs. Main conclusions can be drawn:

- Chemical criteria and kaolinite content allow a preliminary assessment of the potentialities of clay deposits as source of supplementary cementitious materials.
- Pozzolanic activity of the calcined clays evaluated by compressive strength tests confirms that samples with higher kaolinite content present the best reactivity.
- Three deposits were found suitable to be used as SCMs to the production of cement with high level of clinker replacement.
- Ternary blends can be applied to the production of hollow concrete blocks and hydraulic tiles, which represents a promising alternative for its production in northeastern Cuba.

References

1. Vizcaíno, L., Sánchez, S., Pérez, A., Damas, S., Scrivener, K., Martirena, F.: Industrial trial to produce low clinker, low carbon cement. Materiales de Construcción **65**, e045 (2015). https://doi.org/10.3989/mc.2015.00614
2. Almenares, R.S., Vizcaíno, L.M., Damas, S., Mathieu, A., Alujas, A., Martirena, F.: Industrial calcination of kaolinitic clays to make reactive pozzolans. Case Stud. Constr. Mater. **6**, 225–232 (2017). https://doi.org/10.1016/j.cscm.2017.03.005
3. Martirena, F., Scrivener, K.: Low carbon cement LC3 in Cuba: ways to achieve a sustainable growth of cement production in emerging economies. In: Martirena, F., Favier, A., Scrivener, K. (eds.) Calcined Clays for Sustainable Concrete, pp. 318–321. Springer, Dordrecht (2018). https://doi.org/10.1007/978-94-024-1207-9_51

4. Njila, T., Díaz-Martínez, R.: Estudio químico-mineralógico de los perfiles lateríticos fer-rosialíticos en los sectores Téneme Farallones y Cayo Guam en el noreste de Cuba. Revista Geológica de América Central **54**, 67–83 (2016). https://doi.org/10.15517/rgac.v54i0.21149

5. Almenares-Reyes, R.S., Alujas-Díaz, A., Poll-Legrá, L., Bassas-Noa, P.R., Betancourt-Rodríguez, S., Martirena-Hernández, J.F., et al.: Evaluación de arcillas caoliníticas de Moa para la producción de cemento de base clínquer – arcilla calcinada – caliza (LC3). Minería y Geología **32**, 63–76 (2016)

6. Poll-Legrá, L., Almenares-Reyes, R.S., Romero-Ramírez, Y., Alujas-Díaz, A., Leyva-Rodríguez, C.A., Martirena-Hernández, J.F.: Evaluación de la actividad puzolánica del material arcilloso del depósito La Delta Moa, Cuba. Minería y Geología **32**, 15–27 (2016)

7. Njila, T., Díaz, R., Orozco, G., Rojas, L.A.: An overview of non-nickeliferous weathering crusts in Eastern Cuba. Minería y Geología **26**, 14–34 (2010)

8. Alujas Díaz, A., Almenares Reyes, R.S., Arcial Carratalá, F., Martirena Hernández, J.F.: Proposal of a methodology for the preliminary assessment of kaolinitic clay deposits as a source of SCMs. In: Martirena, F., Favier, A., Scrivener, K. (eds.) Calcined Clays for Sustainable Concrete, pp. 29–34. Springer, Dordrecht (2018). https://doi.org/10.1007/978-94-024-1207-9_5

9. NC/CTN22, NC TS 527:2013: Cemento hidráulico-Métodos de ensayo-Evaluación de las puzolanas 20. www.nc.cubaindustria.cu (2013)

10. NC/CTN22, NC 1208:2017: Cemento Ternario - Especificaciones 9. www.nc.cubaindustria.cu (2017)

11. NC 506: 2013: Cemento hidráulico. Método de ensayo. Determinación de la resistencia mecánica 26. www.nc.cubaindustria.cu (2013)

12. NC/CTN37, NC 247:2010: Bloques huecos de hormigón - Especificaciones 18. www.nc.cubaindustria.cu (2010)

13. NC/CTN37, NC 237:2009: Baldosas hidráulicas de terrazo - Especificaciones 31. www.nc.cubaindustria.cu (2009)

14. Antoni, M., Rossen, J., Martirena, F., Scrivener, K.: Cement substitution by a combination of metakaolin and limestone. Cem. Concr. Res. **42**, 1579–1589 (2012). https://doi.org/10.1016/j.cemconres.2012.09.006

Potential of Marine Clay for Cement Replacement and Pozzolanic Additive in Concrete

Hongjian Du, Anjaneya Dixit and Sze Dai Pang

Abstract Marine clay is a low-grade kaolinsite clay commonly occurring in the coastal areas globally. Produced during excavation works, they are characterized by high silt and low kaolinite content, and hence, have little value for industrial applications. Since, the legislation in Singapore does not allow for disposal of these waste clays in the landfill, coupled with the acute shortage of space, marine clay poses a nuisance for handling and environmental issues. This project investigates the valorization of marine clay as a cement replacing agent and studies its pozzolanic potential. The clay after calcination at 600, 700 and 800 °C was used to replace ordinary Portland cement. Thermo-gravimetric analyses and isothermal calorimetry results indicate the potential of pozzolanic reactions with the consumption of calcium hydroxide and release of additional heat, respectively. Comparable strength was obtained at 28 days even at 30% by wt cement replacement. Furthermore, the 28-days compressive strength was not substantially affected with the calcination temperatures.

Keywords Kaolinite · Calcined clay · Hydration · Pozzolan

1 Introduction

The production of cement clinker is associated with a severe environmental concern of anthropogenic carbon emission. It is a well-established fact that every ton of cement produced results in an equivalent amount of CO_2 is being released in the atmosphere. This emission is partly due to the breakdown of limestone (calcium carbonate, $CaCO_3$) which is a raw ingredient in cement production, and partly due to the fuel required for high-temperature kiln firing. On a global perspective, the

H. Du

Department of Civil and Environmental Engineering, National University of Singapore, Singapore 117576, Singapore

A. Dixit (✉) · S. D. Pang
Department of Civil and Environmental Engineering, National University of Singapore, Singapore 117576, Singapore
e-mail: anjaneya.dixit@u.nus.edu

production of cement is currently responsible for 5–8% of the total carbon emission. As per a recent report by the International Energy Agency, the projected increase in cement production is 12–23% by 2050 [1], which will proportionally increase the carbon emissions in the absence of alternative means of cement production. A successful strategy to curtail the clinker requirement in cement is the use of supplementary cementitious materials (SCM), which react with the hydration products of the clinker to produce additional calcium silicate hydrate (CSH) gel. Common SCMs included fly ash, blast furnace slag, silica fume, etc. However, a common problem associated with numerous SCM, such as silica fume and slag, is their long-term availability to be considered as a viable source for cement replacement. In this regard, calcined clays can be a viable option due to their ease of availability and abundance around the globe [2].

Clays are rich in kaolinite, montmorillonite and illite. These minerals become reactive upon calcining at different temperatures (600–1000 °C). The most reactive calcined product of the three, metakaolin, is formed by the de-hydroxylation of kaolinite above 600 °C. The reason for reactivity is the loss of crystallinity in the kaolinite structure, exposing the aluminium groups for reactions with portlandite in the cement matrix [3]. The limiting factor in the pozzolanicity of calcined clay is the availability of high kaolinite containing clays. Nonetheless, studies have been conducted on the potential of clays with low and moderate kaolinite content [4–6]. The findings of Alujas et al. [4] revealed that the calcined clay favours the formation of AFm phases and calcium silicate aluminate hydrates (CASH) having longer chains. In another study by Zhou et al. [5], low kaolinite London clay (26% kaolinite content) was calcined at 800–900 °C to activate the kaolinite. A 30% cement replacement with calcined London clay resulted in higher 28-days strength compared to the reference mix. Indirect kaolinite sources like dredging sediments have also been investigated, wherein it was found that though the calcined sediments were inferior to metakaolin, they performed better than siliceous fly ash [6].

Marine clay is another such low-grade kaolinite clay in the coastal regions. It is characterized by high silt and low kaolinite content, which makes it unsuitable for industry applications (ceramics, etc.). In Singapore's context, an abundant amount of this clay is distributed throughout the island, and is therefore, found in the excavation works in large quantities. For instance, in 2011, the amount of excavated works in Singapore was approximately 8.5 million cubic meters, with marine clay being the major constituent [3]. Although some of the excavated clay is used for land reclamation and soil stabilization works, the large amount of unused volume creates a nuisance for disposal, as Singapore legislation prohibits the dumping of marine clay in landfills.

Given the acute shortage of space for waste disposal in Singapore, and the fact that calcined low-grade kaolinite clay has also shown promising results as a SCM, this study has been undertaken to study the use of calcined marine clay in concrete as a possible avenue towards sustainable construction material. Marine clay as obtained from excavation works of underground tunnels was calcined at different temperatures. The activated clays were then used to replace cement at 30% by wt and studied

for their pozzolanic potential. The effect on hydration was investigated using isothermal calorimetry and thermo-gravimetric analysis. This was followed by comparing the compressive strength of the concrete containing marine clay with the reference mix. It is expected that the results from this study would be beneficial for countries with resource and land deficiencies and to utilize waste clays as a valorized product in sustainable concretes.

2 Materials and Methodology

2.1 Materials

The cement used in this study was CEM I 52.5N. To compare with the calcined clay, fine quartz powder was used as inert filler. The marine clay used in this study was obtained from Ulu Pandan, Singapore. The clay, supplied as big lumps, was dried at 50 °C for three days, pulverized manually and then grounded in a ball mill (RESTCH PM 400) for 30 min. The fine powder obtained was then calcined at a designated temperature (600, 700 and 800 °C) for 1 h in a furnace. The heating ramp was maintained at 10 °C/min from room temperature to the calcination temperature. Thereafter, the clay was removed and quickly cooled down by spreading in a metal tray at room temperature. The densities as determined using an automatic density analyser (ULTRAPYC 1200e) for cement, quartz filler and marine clay were 3.25, 2.65 and 2.87, respectively. Fifty mm mortar cubes for compression tests were prepared with cement: sand ratio of 1:3. The mortar mixes were formed using river sand of fineness of 2.95 and specific gravity of 2.65. The water–cement ratio was kept at 0.50. The cement was replaced with calcined clay 30% by wt for the three calcination temperatures. All mortar samples were stored in water till testing.

2.2 Test Methodologies

The raw materials (cement, quartz filler and clay) were characterized using a laser diffractometer (HORIBA LA-960) for particle size distribution and X-ray fluorescence (XRF) to determine the elemental composition.

The heat of hydration of paste samples was monitored for 28 days using a TAM air isothermal calorimeter. Apart from the reference sample with 100% cement, three samples with calcined clay replacing cement and one sample with quartz filler to distinguish between the filler effect of clay (replacement level at 30% by wt) were tested.

To quantify the de-hydroxylation of clay minerals, thermo-gravimetric analysis (TGA) was carried out in a N_2 environment from 30 to 950 °C. TGA was also carried out on hardened cement paste samples to ascertain portandite consumption.

Hydration in the samples was stopped by immersion in a 2-Propanol solution for three days, followed by vacuum drying for 24 h. This was crushed to a fine powder to determine portlandite content using TGA. The loss of moisture during heating was measured using the tangent method.

The compressive strength of the mortar cubes was determined as per the ASTM C109 [7] at 1, 3, 7, 14 and 28 days of age. The average values of three cube specimens have been reported.

3   Results and Discussion

3.1   Material Characterization

The particle size distribution of the raw materials is shown in Fig. 1. The marine clay contained a lot of inert particles like silt and grounded gravel which caused it to have a higher fraction of coarser particles than cement. XRF results of cement and marine clay are shown in Table 1. It was observed that marine clay had large fractions of silica from clay and the inert constituents mentioned above.

The results from the TGA on the uncalcined marine clay are shown in Fig. 2. A clear loss of mass between 400 and 650 °C can be seen, characteristic to the de-hydroxylation of kaolinite [8] and the formation of metakaolin, as given by Eq. (1). Using this equation and tangent method, the kaolinite content of the untreated marine clay was found to be 19.5%.

$$Al_2Si_2O_5(OH)_4 \rightarrow Al_2Si_2O_7 + 2H_2O \tag{1}$$
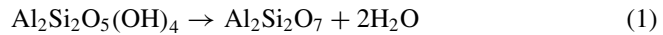
Fig. 1 Particle size distribution of raw materials used in the study
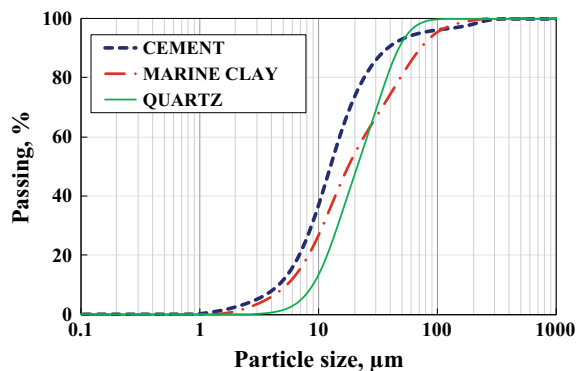
Table 1 Compositional analysis of cement and marine clay

Compound	SiO_2	Al_2O_3	CaO	Fe_2O_3	K_2O	MgO	Na_2O	SO_3	Total
Cement	19.02	4.69	66.48	3.35	0.53	1.31	0.41	3.64	99.43
Marine clay	75.42	20.11	0.11	1.23	0.92	0.40	1.44	0.03	99.66

Fig. 2 TGA curve for mass loss in uncalcined marine clay
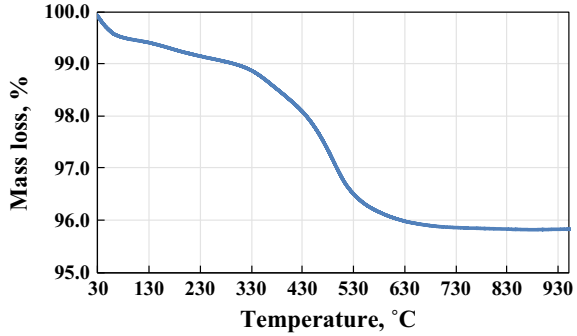
3.2 Puzzolanic Effects of Calcined Marine Clay on Cement Hydration

The results from the hydration tests are shown in Fig. 3. It is observed that while paste with quartz does not cause any major shift in the hydration peak, the pastes with calcined clay show discernable acceleration. Additionally, they also increase the second and third peaks associated with C_3S and C_3A hydration, respectively. The rise in C_3A peak is due to the exothermic reaction of calcium aluminate phases, a characteristic of metakaolin-rich SCMs.

From the cumulative heat of hydration for 28 days shown in Fig. 4, it is evident that the presence of quartz and calcined clay improves the hydration due to their filler effect. For calcined clay, additional heat is generated compared to pastes with quartz, indicating pozzolanic reaction occurring primarily after 3 days. Another observation is the effect of calcination temperature: marine clay calcined at 600 °C shows lesser heat evolution than 700 °C or 800 °C, suggesting that better activation is obtained at 700 °C.

Fig. 3 Rate of heat evolution for different pastes. (Number following 'MC' in the legend indicates the calcination temperature for the clay.)
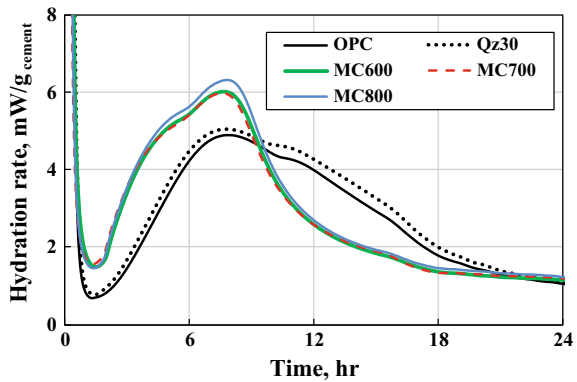
Fig. 4 Cumulative heat of hydration for different pastes
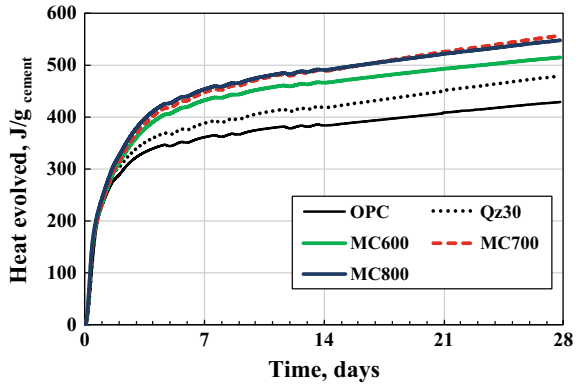
Fig. 5 Portlandite content at various ages for the pastes
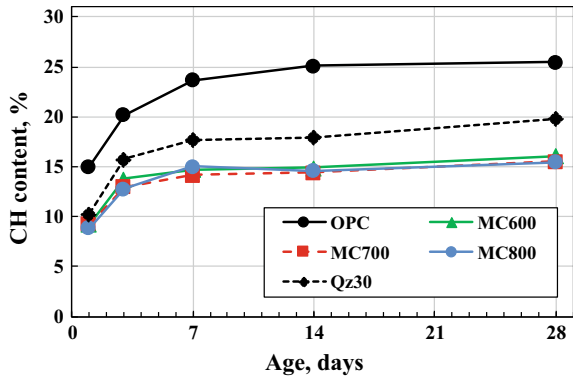
The change in quantity of portlandite (CH) in different pastes with age, determined from the TGA results, is shown in Fig. 5. The amount of CH in pure cement and cement + quartz pastes were found to increase with age, though the rate of increase plateaued after 14 days. Since, the paste with quartz had lesser cement, the amount of CH is found less than the reference paste (with 100% cement). Sharp decrease in CH content can be seen for pastes with calcined marine clay, attributed to the pozzolanic behaviour of the clay. However, due to low kaolinite content of the clay, CH content remains constant beyond 7 days, with a minute increase at 28 days. This suggests that the pozzolanic reactions were completed within first 7–10 days.

3.3 Effect of Calcined Marine Clay on the Compressive Strength of Mortar

Figure 6 shows the development of strength in various mortar samples with age. Compared to the reference mortar with 100% cement, the largest reduction in strength

Fig. 6 Development of compressive strength in different mortars
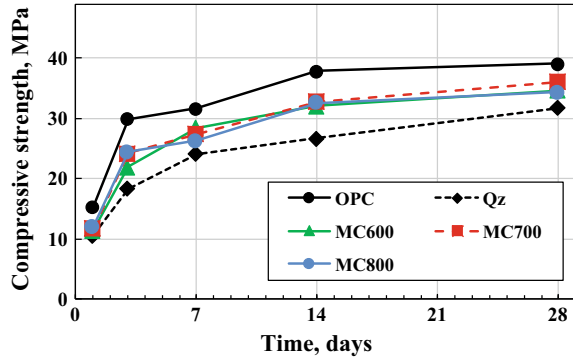
at 28 days was observed for mortar with 30% quartz by wt, primarily due to dilution effect. Though mortar with calcined marine clay displayed inferior strength at 1 day, the strength for mortar with clay calcined at 700 °C was 93% of the reference mortar at 28 days. This indicates that the dilution effect caused by replacing cement was balanced by the development of CASH and CAH gels due to the pozzolanic reactions in clay mortars, filling up the capillary pores in the matrix and also strengthening the interfacial transition zones.

4 Conclusion

Based on the findings of the study presented herein, it is demonstrated that the thermal activation of marine clay above 600 °C can yield a potential SCM. The clay used in this study was low-grade kaolinite clay (20%) excavated during construction works in Singapore. The clay was calcined at 600, 700 and 800 °C and used to replace 30% by wt of cement. From the tests conducted, strong evidences of pozzolanic reactions were obtained. It was found that calcined clay improved the hydration rate, with a clear increase in the C_3A peak as well as the total heat of hydration after 28 days. The CH content in samples with calcined clay was also found to be substantially less in samples with 100% cement. However, the consumption of CH stopped beyond 7 days due to the completion of pozzolanic reactions. The mortars with 30% by wt calcined clay replacing cement showed reduction in strength. Mortar with MC700, however, showed comparable strength as that of the reference mortar. With these results, it is demonstrated that calcined marine clay can help tackle two problems at the same time: solve the waste disposal problems in Singapore and also help towards a sustainable and long-term viable approach in reducing the carbon footprint of concrete.

References

1. International Energy Agency: Technology roadmap: low-carbon transition in the cement industry (2018)
2. Scrinever, K.: Options for the future of cement. Indian Concr. J. **88**, 11–21 (2014)
3. Hongjian, D., Pang, S.D.: Value-added Utilization of marine clay as cement replacement for sustainable concrete production. J. Clean. Prod. **198**, 867–873 (2018)
4. Alujas, A., Fernández, R., Quintana, R., Scrivener, K.L., Martirena, F.: Pozzolanic reactivity of low grade kaolinitic clays: influence of calcination temperature and impact of calcination products on OPC hydration. Appl. Clay Sci. **108**, 94–101 (2015)
5. Zhou, D., Wang, R., Tyrer, M., Wong, H., Cheeseman, C.: Sustainable infrastructure development through use of calcined excavated waste clay as a supplementary cementitious material. J. Clean. Prod. **168**, 1180–1192 (2017)
6. Snellings, R., et al.: Properties and pozzolanic reactivity of flash calcined dredging sediments. Appl. Clay Sci. **129**, 35–39 (2016)
7. ASTM C 109/109M: Standard Test Method for Compressive Strength of Hydraulic Cement Mortars (Using 2-in. or [50-mm] Cube Specimens), pp. 1–10. American Society for Testing and Materials (2016)
8. Fernandez, R.: Calcined Clayey Soils as a Potential Replacement for Cement in Developing Countries. EPFL (2016)

Evaluation of Ceramic Waste from Goa as SCM

Harald Justnes, Christian J. Engelsen, Tobias Danner and Monica N. Strøm

Abstract Tourism is a very important contributor to Goa's GDP. In 2017, 6.9 million domestic tourists and 0.89 million foreign tourists visited Goa. This leads to a need for refurbishment of hotel rooms which is a significant contributor to the C&D waste generation in Goa. Around one ton of waste is on average generated per rehabilitated hotel room. The contents of tiles and bathroom fittings are around 20–25%. In this study, two different ceramic samples (wall tiles and sanitary ware) have been collected from C&D waste dumping sites in Goa. In addition, broken Mangalore roof tiles have been collected as a third ceramic waste. These three ceramics are made from clayey raw materials, most likely kaolin. The samples were split, size reduced and pulverized for the different analyses. In the preliminary study, all samples were analysed for the composition by XRF/XRD, characterized in terms of particle size distribution and tested for pozzolanic reactivity using the R^3 test. The reaction products from the R^3 test were investigated by XRD and DTA/TG.

Keywords Ceramic waste · Reactivity · SCM

1 Introduction

The state of Goa, India, has stated an ambitious goal of zero landfill. However, tourism is a very important contributor to Goa's GDP. In 2017, 6.9 million domestic tourists and 0.89 million foreign tourists visited Goa. This leads to a need for refurbishment of hotel rooms which is a significant contributor to the C&D waste generation in Goa. Around one ton of waste is on average generated per rehabilitated hotel room. The contents of tiles and bathroom fittings are around 20–25%. Although there are on-going projects on recycling of concrete and bricks, ceramic waste has not been developed. Since the ceramics usually are based on sintered clay, there is a good chance they may be pozzolanic when ground fine enough and could be added as a

H. Justnes (✉) · T. Danner
SINTEF Community, Høgskoleringen 7b, 7034 Trondheim, Norway
e-mail: harald.justnes@sintef.no

C. J. Engelsen · M. N. Strøm
SINTEF Community, Forskningsveien 3b, 0373 Oslo, Norway

67

pozzolan to concrete. Although this potential SCM source may not matter too much globally in terms of reducing CO_2 emission, it may help to solve waste issues locally.

Ground tile as pozzolan is not new since apparently the Romans found it beneficial to add it to the lime mortars as strength improvement. Literature is however scarce on using ground ceramic waste as a pozzolan, but plentiful on using it as fine or coarse aggregate where its porosity and water absorption are a challenge to tackle. A few examples of using ceramic fines are listed in Refs. [1–5], but findings may not apply to any local material as the composition can vary widely.

2 Experimental

Three ceramic wastes from the state of Goa, India, were selected: wall tile, sanitary ware and Mangalore roof tile, denoted P1-wall, P2-WC and P3-roof tile, respectively. The ceramic wastes were milled down in a disc mill to a particle size of about d_{90} ≤ 40 µm for the main experiment. To check the effect of particle size on reactivity, the materials were milled down for 30 s extra to obtain a $d_{90} \leq 25$ µm. The particle size distribution of the materials was measured (Table 1), as well as the chemical composition by XRF (Table 2) and qualitative mineralogy by XRD (Fig. 1). Fly ash and limestone were used as a reference for the R^3-test, and their compositions are given in Table 2 as well. A silica fume used as reactivity reference consisted of 94% SiO_2 and a specific surface (BET) of 22 m^2/g.

Calcium hydroxide ($Ca(OH)_2$), calcium carbonate ($CaCO_3$), potassium sulphate (K_2SO_4) and potassium hydroxide (KOH) used in the R^3 test were of laboratory grade. The reaction products from the R^3 test were characterized by XRD and DTA/TG.

Qualitative *X-ray diffraction* (*XRD*) was performed on a Bruker D8-Advance equipped with a Lynx Eye detector and a Cu-Kα X-Ray source. A fixed divergence slit of 0.2 mm was used. Measurements were taken from 5° to 75° 2θ with a step size of 0.2° 2θ and a step time of 1 s.

X-ray fluorescence (*XRF*) was performed on homogenized samples compressed under pressure according to EN 15309.

Particle size distribution (*PSD*) was performed with a Horiba Partica LA-960. The powders were dispersed in water by ultrasonic sound for 1 min prior to analysis.

Table 1 Particle size distribution (PSD) of investigated materials

Materials	d_{10}	d_{50}	d_{90}
P1-wall	0.7	10.7	38.6
P2-WC	0.7	14.1	40.5
P3_Roof tile	0.7	8.2	38.8
P1-wall_30s	0.4	6.7	21.8
P2-WC_30s	0.5	7.3	25.4
P3-roof tile_30s	0.7	5.4	25.1

Table 2 Chemical composition of the investigated ceramic wastes

Oxide (%)	P1-wall	P2-WC	P3-roof	Fly ash	Limestone
SiO_2	65.1	75.4	82.7	55.2	13.2
Al_2O_3	18.9	16.0	8.1	21.6	3.4
Fe_2O_3	3.7	0.5	3.4	6.8	1.7
CaO	3.9	0.9	0.8	5.3	43.8
K_2O	2.3	3.1	0.6	2.1	0.7
Na_2O	1.4	0.5	0.1	1.0	0.2
MgO	2.6	1.4	1.3	2.2	1.7
TiO_2	0.8	1.0	1.5	0.9	0.2
LOI	0.18	0.11	0.54	3.3	33.4

Fig. 1 XRD profiles of the ceramic wastes
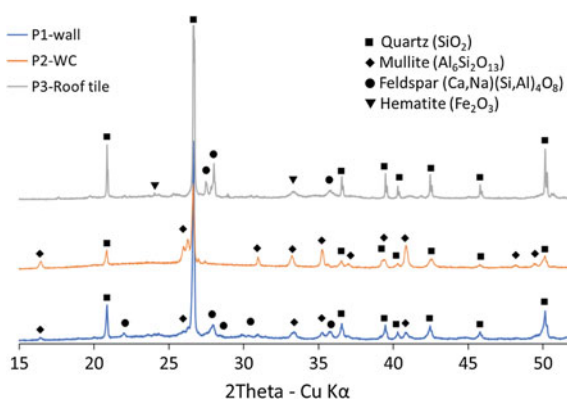
Thermogravimetric analysis (*TGA*) was performed with a Mettler Toledo TGA/SDTA 851. Samples were analysed with a heating rate of 10 °C/min between 40 and 1100 °C. All measurements were performed in nitrogen atmosphere with a flow rate of 50 ml/min.

To test the reactivity of the different ceramic wastes, a R^3 test was performed as described by Avet et al. [6]. The mix proportions of the powder for the R^3 test were 22% ceramic waste, 11% $CaCO_3$, 65% $Ca(OH)_2$, 1% K_2SO_4 and 0.25% KOH. The powder blend was mixed with water to binder ratio of 1.2, and samples were hydrated for 6 days at 20 °C and 2 days at 40 °C, respectively. Prior to mixing, the powder and the deionized water were equilibrated at the desired temperature for 24 h. About 10 g of paste was produced, and mixing was performed with a Vortex SA6 model at 4500 rpm for 1 min. Hydration was stopped by solvent exchange. If necessary, samples were milled down by hand to particle sizes <0.5 mm and immersed in 100 ml iso-propanol for 15 min. After filtration, the powder was immersed in 20 ml diethyl ether and filtrated. This step was repeated two times. As the last step, the sample was dried for 8 min at 40 °C. The amount of bound water was determined by TGA

analysis from the weight loss between 40 and 350 °C and calculated in per cent by weight at 350 °C. The calorimetric part of the R^3-test was omitted at this stage.

3   Results and Discussion

Data extracted from the particle size distributions of the ceramic wastes are listed in Table 1, while their element compositions obtained by XRF are listed as the respective oxides in Table 2 together with the reference materials fly ash and limestone filler.

Figure 1 shows the qualitative XRD data of the investigated ceramic wastes. The main phases in the ceramic wastes are quartz, mullite (typical thermal transformation product from kaolin), plagioclase feldspars and some haematite in P3-roof tile. P2 appears to contain more mullite than the other two wastes and less feldspar compared to P1 and P3. There is only a weak increase of the background in the range 20°–35° 2θ indicating a small amount of amorphous material, perhaps most pronounced for P2-WC.

The chemical bound water from the R^3 test is given in Table 3. The Mangalore roof tile (P3) fines appeared to be the most reactive and when cured for 6 days at 20 °C it nearly reached the level of silica fume, while the P1-wall and P2-WC reached the reactivity level of siliceous fly ash. When cured for 2 days at 40 °C, the Mangalore roof tiles (P3) gained less bound water and failed to reach the increased level for silica fume cured under the same conditions. P1-wall and P2-WC both increased the amount of bound water when cured for 2 days at 40 °C relative to 6 days at 20 °C and nearly reached the same level of bound water as for fly ash again. As a rule of thumb, the chemical reaction will double their rate for every 10 °C increase in temperature, so 2 days at 40 °C should correspond to 4 days at 20 °C (6 days in the R^3 test).

The differential thermogravimetry curves (TG/DTG) for the ceramic fines cured 6 days at 20 °C and 2 days at 40 °C, respectively, are shown in Fig. 2, while sections of their XRD profiles focusing on hydration products are plotted in Fig. 3. It is clear from Fig. 2 that the hydration products of P3-roof tile are altered when cured at 40 °C relative to 20 °C, explaining the reduction in bound water. From Fig. 3, it can be seen

Table 3 Results of the R^3 reactivity test of the different ceramic wastes compared to reference materials in terms of bound water

	Ceramic wastes			Reference materials		
	P1-wall	P2-WC	P3-roof	Silica fume	Fly ash	Limestone filler
Bound water 6 d at 20 ℃	2.6	2.5	6.8	7.1[a]	2.3	1.3
Bound water 2 d at 40 ℃	3.1	2.9	6.3	10.6[a]	3.4	1.3

[a]Silica fume appeared not perfectly dispersed in the paste which may have an influence on the amount of bound water measured
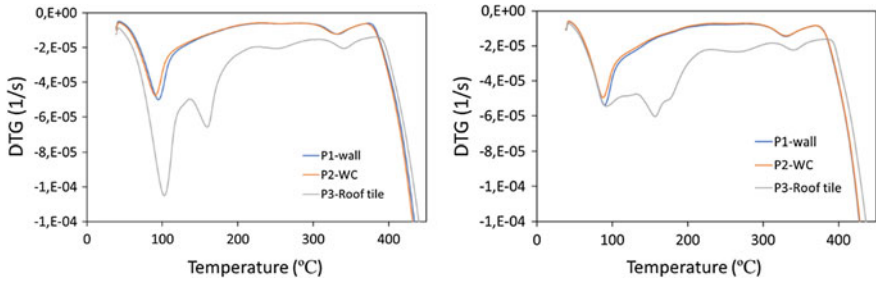
Fig. 2 TGA analysis of R^3 pastes hydrated at 20 °C for 6 days (Left) and at 40 °C for 2 days (Right)
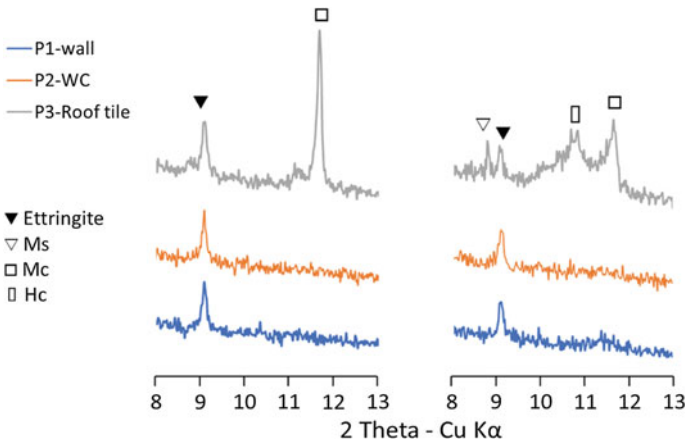
Fig. 3 XRD of R^3 pastes hydrated at 20 °C for 6 days (Left) and at 40 °C for 2 days (Right)

that a pure calcium monocarboaluminate hydrate at 20 °C has changed into a mix mono- and hemicarboaluminate hydrate at 40 °C and that the ettringite present as the sole sulphate mineral at 20 °C has partly reacted to a calcium monosulphoaluminate hydrate. Both these observations indicate that the SCM has reacted more, feeding extra aluminate into the system, but at the same time less water is chemically bound (32 crystal water in AFt and 12 in AFm). For the P1-wall and P2-WC, ettringite is stable at both 20 and 40 °C, and only a marginal sign of carboaluminates formed for P1-wall.

The effect of 30 s additional grinding of the ceramic fines on the chemical bound water when cured for 2 days at 40 °C is listed in Table 4. It is clear that only 30 s extra grinding compared to "normal" grinding has a large effect on the reactivity, in particular for P2-WC. The differential thermogravimetry curves for the ceramic fines ground 30 s extra are directly compared to the same samples after "normal" grinding when cured for 2 days at 40 °C in Fig. 4. Evidently, there are hydration products with broader peaks indicating a larger variety of hydration products for P3-roof tiles,

Table 4 Effect of 30 s additional grinding on the R^3 reactivity of ceramic fines

Sample	30 s extra	Normal	Δ (%)
P1-wall	3.7% water	3.1% water	+19.4
P2-WC	4.2% water	2.9% water	+44.8
P3-roof tile	8.5% water	6.3% water	+34.9

Fig. 4 Effect of 30 s extra milling time on the hydration products of ceramic fines
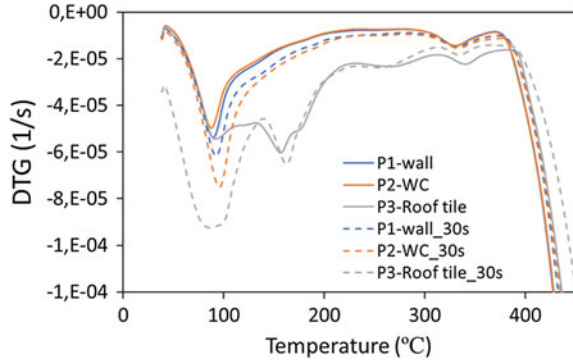
while the nature of the hydration products seems to be unchanged for P1 and P2 even though the amount has increased.

Based on these observations, it was decided to cast mortars where 20, 35 and 50% of the cement was replaced by P3-roof tiles to start with. However, the strength results of these will not meet the paper deadline, but will be presented at the conference.

4 Conclusion

Three types of ceramic wastes from the state of Goa have been finely ground, and their reactivity has been evaluated with respect to function as supplementary cementitious material.

The best material, fines of Mangalore roof tiles, had a reactivity comparable to silica fume when cured for 6 days at 20 °C according to chemical bound water in the R^3 test. The chemical bound water went down when cured for 2 days at 40 °C since the increased reactivity released more aluminate destabilizing AFt and forming AFm with less crystal water.

The other two materials, wall tiles and sanitary ware, had reactivity comparable to siliceous fly ash according to the R^3 test. Their amount of chemical bound water increased when cured for 2 days at 40 °C compared to 2 days at 20 °C.

Increasing the milling time with only 30 s increased the reactivity of all three ceramic wastes substantially, and in particular, for the sanitary ware.

References

1. Pacheco-Torgal, F., Jalali, S.: Reusing ceramic wastes in concrete. Constr. Build. Mater. **24**, 832–838 (2010)
2. Lavat, A.E., Trezza, M.A., Poggi, M.: Characterization of ceramic roof tiles wastes as pozzolanic admixture. Waste Manage. **29**, 1666–1674 (2009)
3. Silva, J., De Brito, J., Veiga, R.: Incorporation of fine ceramics in mortars. Constr. Build. Mater. **23**, 556–564 (2009)
4. Naceri, A., Hamina, M.C.: Use of waste brick as a partial replacement of cement in mortar. Waste Manage. **29**, 2378–2384 (2009)
5. Medina, C., Manfill, P.F.G., Sánches de Rojas, M.I., Frías, M.: Rheological and calorimetric behaviour of cement blended with containing sanitary ware and construction/demolition waste. Constr. Build. Mater. **40**, 822–831 (2013)
6. Avet, F., Snellings, R., Alujas Diaz, A., Ben Ha Ha, M., Scrivener, K.: Development of a new rapid, relevant and reliable (R^3) test method to evaluate pozzolanic reactivity of calcined kaolinitic clays. Cem. Concr. Res. **85**, 1–11 (2016)

Potential of Calcined Recycling Kaolin from Silica Sand Processing as Supplementary Cementitious Material

Matthias Maier, Benjamin Forster, Nancy Beuntner and Karl-Christian Thienel

Abstract Suitability of calcined kaolinitic filter cake arising from the production of high-quality silica sand as SCM was tested. The investigation comprises two different grades of materials. The first one represents a cross section from one week of sand production. The other sample has been subsequently prepared by sedimentation on a laboratory scale in order to investigate the impact of lower sand content. Chemical and mineralogical compositions of both samples were determined by means of ICP-OES, XRD and FTIR. The laboratory sample yielded higher kaolinite and a lower quartz content in comparison with the industrial product. The dehydroxylation behavior was determined using TG/DTG. After thermal activation, the reactivity was investigated by measuring the solubility of Al- and Si-ions in alkaline solution. It turned out that a calcination temperature of at least 650 °C is required for a complete dehydroxylation. Heat of hydration was studied by isothermal calorimetry using a substitution of 20 wt% of cement by the calcined product. The same substitution was chosen for the determination of strength activity index on mortar bars. Both materials provided a significant acceleration of the early hydration by promoting the aluminate reaction. After 28 days, the higher kaolinite content of the laboratory sample leads to a higher activity index of 121% in comparison with 102% of the industrial product.

Keywords Metakaolin · SCM · Calcined clay · Recycling kaolin

1 Introduction

The high pozzolanic reactivity of metakaolin has been the subject of many studies [1]. A wide use is yet impeded by the high price, caused by the costly purification process and the high demand by competing industries like ceramic or paper industry. This reason shifted the focus of research on naturally occurring kaolinite-bearing clay as a raw material for pozzolanic cement substitutes [2]. Beyond that, clay minerals

© RILEM 2020
S. Bishnoi (ed.), *Calcined Clays for Sustainable Concrete*, RILEM Bookseries 25,
https://doi.org/10.1007/978-981-15-2806-4_9

also exist as minor components in many sand or gravel deposits. During the raw material processing, which often includes a washing process, the clay-bearing fine fractions are separated as a water–solid mixture and end up as backfill in most cases. In Central Europe, 50 million tons of mineral washing sludge are produced every year [3]. Only a small percentage of it is used as raw material by the ceramic industry (e.g., less than 100,000 t per year in Germany [4]). The material investigated in the course of this study represents a residue from the washing process of a kaolin-bearing Jurassic silica sand, which is dewatered after the separation. The produced filter cake is partly used as supplementary clay for the production of clay bricks but its application is limited. This study covers first calcination trials based on a comprehensive raw material characterization, complemented by reactivity tests for an application as a supplementary cementitious material.

2   Materials and Methods

The investigated material is a fine-grained, secondary component of a siliceous sandstone, which is located in the Upper Palatinate (Bavaria, Germany) and has been exposed in several open-pit mines (Fig. 1). The outcropping sandstones exhibit a thickness of up to 30 m and are of white color, due to low iron contents. Locally, higher iron contents cause yellow, brown and red colors. The sediments belong to the geological formation of the dogger sandstone [5] with an age of approximately 171 million years [6]. Figure 1 shows on the left the sequence of the various quartz sand layers. The uppermost layer consists of brownish-colored limonite sand. Pink-colored so-called flamingo sands follow these on the bottom. The lowest layers are defined as glass sand or glass sand equivalent. These layers are characterized by their white color and high proportion of finest grain sizes (0–0.180 mm).

After transportation to the plant, the extracted sand is cleaned from interfering sediments, such as kaolinitic clays and iron and titanium-bearing minerals, in a multistage cleaning and classifying process (Fig. 2). The water required for the process is recycled in an in-house water treatment during which the washed-out

Fig. 1   Sequence of sand layers (left) and aerial view of the mining area (right)
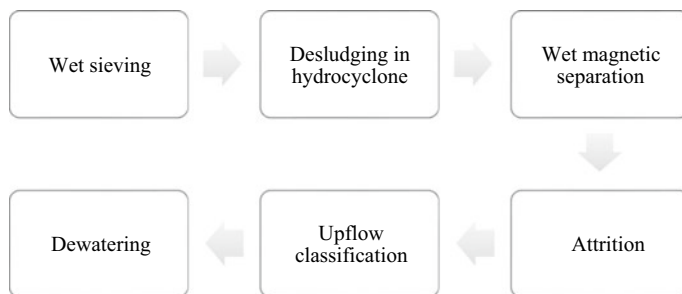
Fig. 2 Processing scheme of the quartz sands

residual substances are separated. In the course of this process, the finest sand fraction is separated from the process water in a sedimentation cone and returned to the treatment process. The clay minerals are coagulated in the washing water by adding flocculants (anionic polyacrylamide). The settling and thickening of these flocked fine fractions are performed in the two circular thickeners. The settled fine clay gets pumped out and dewatered on chamber filter presses to a residual moisture content of approx. 20 wt%. The filter cake obtained in this process is the subject of investigation in this study.

Two grades of raw materials were investigated. The first one represented a cross section of one week of production. The second one was prepared by sedimentation on a laboratory scale. For this purpose, 1 m^3 of the sludge was removed from the storage tank of the filter press and diluted to a solid concentration of 20 wt%. Separation was executed using an 80 mm hydrocyclone test rig. The de-sanded material in the overflow of the hydrocyclone was collected in a tank together with the process water and precipitated using flocculants. The separated fine quartz was discharged via the underflow of the hydrocyclone. After a resting period of 24 h, the excess water was removed and the remaining material was dried at 105 °C in a drying cabinet.

The chemical composition of both grades of clay was measured by means of ICP-OES and is shown in Table 1. The mineralogical composition was determined by XRD (PANalytical Empyrean, Bragg-BrentanoHD monochromator, PIXcel1D linear detector) on sideloaded powder mounts to reduce preferred orientation effects, which are pronounced in well crystalline kaolinite-bearing samples. The quantitative phase composition was calculated by Rietveld refinement using Profex BGMN [7], complemented by the external standard method [8] in order to consider poorly crystalline and amorphous components after calcination. Kaolinite degree of order was analyzed from FTIR spectra of powder samples (ThermoFisher Scientific Nicolet iS10) according to Bich et al. [9] and by using models of ordered and disordered kaolinite for Rietveld refinement [10]. Calcination temperature was derived from dehydroxylation behavior, which was analyzed by means of TG/DTG (Netzsch STA 449 F3 Jupiter). For the thermal treatment, the samples were placed in platinum crucibles and calcined for 30 min in a laboratory muffle furnace. After calcination, the materials were ground in a vibratory disk mill with a speed of 700 min^{-1} for 10 min,

Table 1 Chemical composition of the raw materials

Constituent (wt%)	Industrial grade	Laboratory grade	Cement[a]
SiO_2	67.1	57.3	20.7
Al_2O_3	19.8	26.2	4.9
Fe_2O_3	5.4	6.7	2.9
CaO	0.1	0.1	65.3
MgO	0.1	0.1	1.5
MnO	n.d	n.d	0.1
TiO_2	0.9	1.1	0.3
K_2O	0.3	0.3	0.7
Na_2O	<0.1	<0.1	0.1
SO_3	<0.1	<0.1	2.9
Cl	n.d	n.d	0.1
LOI	6.3	8.2	2.3

[a]Provided by supplier

using an agate grinding tool. The calcination process was verified using FTIR and XRD. Solubility of Al- and Si-ions was measured by ICP-OES (Varian ICP-OES 720 ES) after elution of the samples for 20 h in 10% NaOH solution [11]. Heat of hydration was measured using a TAM air isothermal calorimeter at 25 °C for 48 h. For the determination of the activity index on mortar bars according to DIN EN 196–1 and for calorimetry, a CEM I 42.5 N with the chemical composition given in Table 1 was used with a substitution rate of 20 wt% and a water–solid ratio of 0.5.

3 Results

3.1 Dehydroxilation Behavior

The mass loss at approximately 280 °C (Fig. 3) could be attributed to the decomposition of iron hydroxide (e.g., Goethite). Dehydroxylation of kaolinite starts with onset between 430 and 435 °C for both samples. The reaction is accompanied by a loss of mass due to the elimination of the crystal water, which is 5.6 wt% for the industrial sample and 8.0 wt% for the laboratory sample, indicating a higher content of kaolinite for the latter.

After calcination at 550 °C, Al–OH stretching bands (Fig. 4), which indicate an incomplete dehydroxylation, are still visible. After 650 °C, Al–OH bands are no longer present.
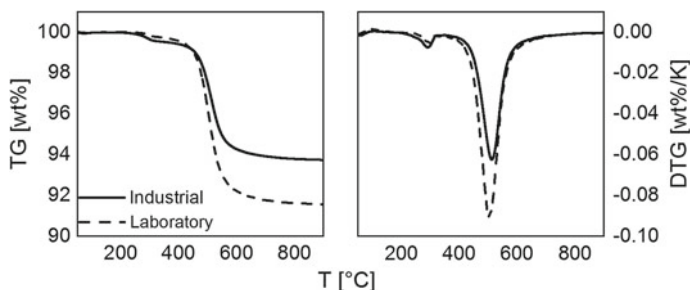
Fig. 3 Thermogravimetric analysis of the two different grades
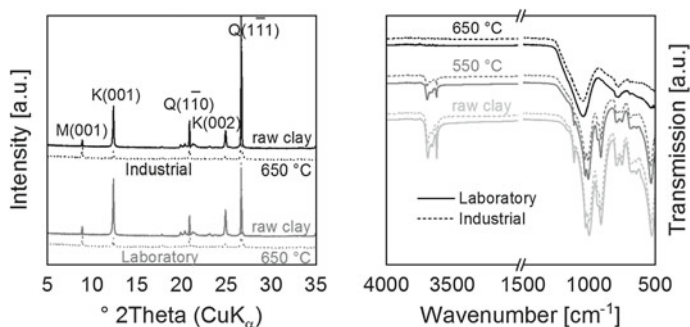
Fig. 4 X-ray diffractogram (left) and FTIR spectra (right) of the two different grades in dependence of calcination temperature (M = Muscovite, K = Kaolinite, Q = Quartz)

3.2 Mineralogical Properties

The secondary hydrocyclone reduced the quartz content from 47.3 to 29.3 wt%, while increasing the kaolinite content from 44.5 to 62.3 wt%. The complete mineralogical composition before and after calcination is given in Fig. 5 (left). Based on the ratios of the Al–OH bands in the FTIR spectra in the range between 3600 and 3700 cm^{-1}, the degree of order of the kaolinite was determined by calculating the indexes P0 (0.97) and P2 (1.02), which implicate an intermediate degree of order according to Bich et al. [8]. The results from Rietveld refinement reveal a mixture of ideally ordered and stacking disordered kaolinite (Fig. 5, right).

While the FTIR spectra indicate a complete dehydroxylation at 650 °C, the diffraction patterns still show small kaolinite reflexes which can be quantified to 6.9 wt% for the industrial and 7.7 wt% for the laboratory sample. Since no more OH vibrations can be detected, these reflexes may also represent relics of a dehydrated kaolinite lattice, which did not break down completely during calcination.
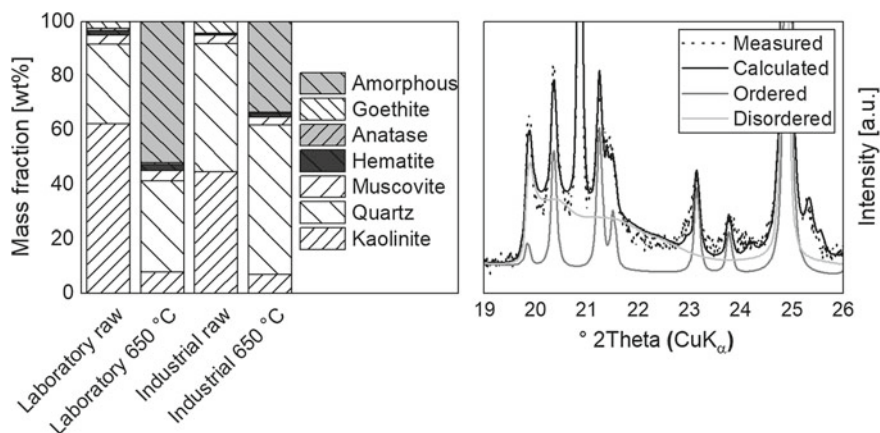
Fig. 5 Quantitative phase composition of two different samples before and after calcination (left) and refinement of structure models of ordered and stacking disordered kaolinite (right)

3.3 Reactivity

Solubility of Al- and Si-Ions

The pozzolanic reactivity of calcined clay depends to a large extent on the amount and proportion of soluble aluminum and silicon ions in alkaline solution. The solubilities are shown in Fig. 6 for both samples and both calcination temperatures. The bars show the total solubility of Al- and Si-ions in mmol/l. The numbers above the bars indicate the Si–Al ratio and are close to 1 for all samples, which is typical for metakaolin. As already seen from the FTIR spectra, almost complete dehydroxylation of the kaolinite is only ensured at a temperature of at least 650 °C, which is reflected in an Al and Si solubility being more than twice as high compared to 550 °C. The laboratory sample exhibits a solubility of Al- and Si-ions that is about 50% higher

Fig. 6 Solubility of Al- and Si-ions after elution in 10% NaOH solution for 20 h
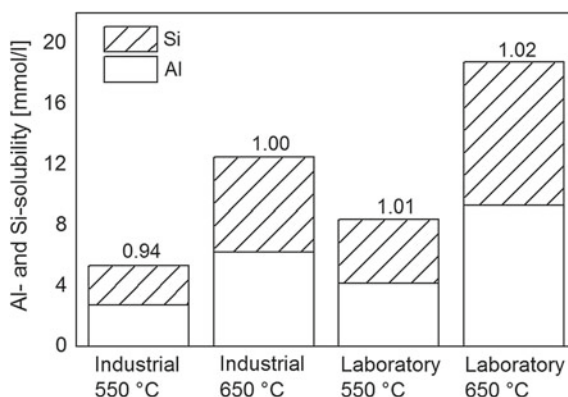
than that of the industrial sample for both calcination temperatures. Due to these results, calorimetric and strength measurements were only conducted for the 650 °C samples.

Heat of Hydration

Within the first hours, both substituted samples have a similar course of heat flow as the reference (Fig. 7), whereby the samples with calcined clay show a slightly higher heat flow in the dormant period and a slightly faster acceleration period relative to the cement content. In the reference sample, the aluminate reaction is recognizable as a clear shoulder of the silicate heat peak. The influence of the calcined clays can be seen in the acceleration and amplification of the aluminate reaction, which leads to a superposition of the two reactions for the laboratory sample. The heat of hydration after 48 h is 236 J/g_{cement} for the reference, 252 J/g_{cement} for the substitution with 20 wt% industrial grade and 269 J/g_{cement} for the substitution with 20 wt% laboratory grade. From this, a clear contribution of both calcined materials to the early hydration can be derived.

Activity Index

The development of compressive strength related to the reference is shown in Fig. 8. After two days, a significant strength contribution was detected for both samples. This contribution slows down until 7 days but is still present as the activity index exceeds 80% for both systems. After 28 days, the compressive strength of the mortar substituted with the industrial grade sample corresponds approximately to that of the reference while the mortar substituted with the laboratory grade sample reaches an activity index of 121% of the reference strength.
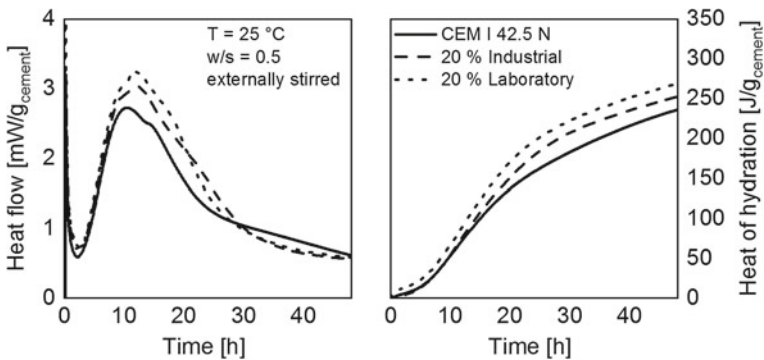
Fig. 7 Comparison of heat flow and cumulative heat during the first 48 h of hydration

Fig. 8 Comparison of
activity indexes after 2, 7 and
28 days
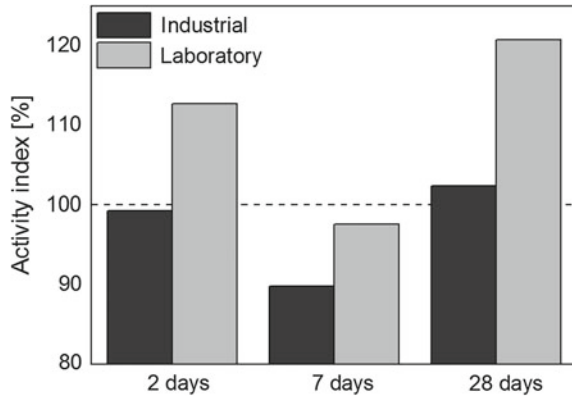
4 Conclusion

Both investigated samples show a high potential regarding the use as SCM. The
pozzolanic reactivity indicated by the high solubilities of Al- and Si-ions could
be confirmed by a significant contribution to the early hydration and the strength
activity indexes within the first 28 days. As expected, the laboratory grade material
provides a higher reactivity due to a higher proportion of kaolinite, reached by the
supplementary sedimentation process. While a calcination temperature of 550 °C
is not yet sufficient, an almost complete conversion from kaolinite to metakaolin
takes place at 650 °C. For further studies, the temperature will be raised to 680 °C to
ensure complete dehydroxylation. Nevertheless, the activation temperature is still in
a very interesting range from an ecological and economical point of view. This study
confirms that clay-bearing mineral residues can provide a high potential as resource-
efficient raw materials for the production of SCM and should get high attention in
the search for appropriate materials.

References

1. Sabir, B.B., Wild, S., Bai, J.: Metakaolin and calcined clays as pozzolans for concrete: a review.
   Cem. Concr. Compos. **23**(6), 441–454 (2001)
2. Scrivener, K., Martirena, F., Bishnoi, S., Maity, S.: Calcined clay limestone cements (LC3).
   Cem. Concr. Res. **114**, 49–56 (2018)
3. Schmitz, M., Röhling, S., Dohrmann, R.: Waschschlamm: Ein vernachlässigtes heimisches
   Rohstoffpotenzial? Gesteinsperspektiven **8**, 16–18 (2011)
4. Krakow, L.: Resource efficiency in the clay brick and roofing tile industry Part I: general
   introduction. ZI Ziegelindustrie International **01–02**(12), 15–24 (2012)
5. Börner, A.: Steine- und Erden-Rohstoffe in der Bundesrepublik Deutschland, 1st edn. E.
   Schweizerbart'sche Verlagsbuchhandlung, Hannover (2012)
6. Elsner, H.: Kaolin in Deutschland. Federal Institute for Geosciences and Natural Resources,
   Hannover (2017)

7. Döbelin, N., Kleeberg, R.: Profex: a graphical user interface for the Rietveld refinement program BGMN. J. Appl. Crystallogr. **48**, 1573–1580 (2015)
8. O'Connor, B.H., Raven, M.D.: Application of the Rietveld refinement procedure in assaying powdered mixtures. Powder Diffr. **3**, 2–6 (1988)
9. Bich, C., Ambroise, J., Péra, J.: Influence of degree of dehydroxylation on the pozzolanic activity of metakaolin. Appl. Clay. Sci. **44**(3–4), 194–200 (2009)
10. Ufer, K., Kleeberg, R., Monecke, T.: Quantification of stacking disordered Si-Al layer silicates by the Rietveld method: application to exploration for high-sulphidation epithermal gold deposits. Powder Diffr. **30**(S1), 1–8 (2015)
11. Buchwald, A., Kriegel, R., Kaps, C., Zellmann, H.-D.: Untersuchung zur Reaktivität von Metakaolinen für die Verwendung in Bindemittelsystemen. In: 7th Gesellschaft Deutscher Chemiker e.V –Jahrestagung, München (2003)

Comparison of Brick Clays and a Kaolinitic Clay Regarding Calcination and Performance in Blended Cement Mortars

Nsesheye Susan Msinjili, Patrick Sturm, Hans-Carsten Kühne and Gregor J. G. Gluth

Abstract Two brick clays (rich in 2:1 clay minerals) and a low-grade kaolinitic clay were studied regarding their transformations during calcination and their performance in blended cement mortars. The mortars with calcined clays exhibited decreased workability (slump flow), but this effect could be mitigated by employment of a conventional superplasticizer; however, compressive strength of the hardened mortar was lowered in some cases. While the kaolinitic clay generally yielded the highest strength, the performance of a brick clay could be increased by grinding to higher fineness and by mixing it with the kaolinitic clay.

Keywords Calcined clays · Blended cements · Workability · Compressive strength

1 Introduction

Calcined clays have emerged as one of the most promising supplementary cementitious materials (SCMs) due to their global availability and often good performance in blended cements [1]. The majority of research is focused on kaolinitic clays because of their higher reactivity compared to illitic or smectitic clays (rich in 2:1 minerals) [2]. The latter clays are, however, available at lower cost and therefore may provide an economically more feasible option for use as SCMs in cement production. The present work aims to investigate the potential of brick clays (illitic clays) by studying their calcination and their performance in blended cement mortars and comparison with a low-grade kaolinitic clay. Cement substitution rates considered in the study were 15 and 25 wt%. The effect of a polycarboxylate-based superplasticizer on the workability of blended cement mortars was studied at the higher substitution rate.

N. S. Msinjili · P. Sturm · H.-C. Kühne · G. J. G. Gluth (✉)
Bundesanstalt für Materialforschung und-prüfung (BAM), Division 7.4 Technology of
Construction Materials, Unter den Eichen 87, 12205 Berlin, Germany
e-mail: gregor.gluth@bam.de

2 Materials and Methods

2.1 Starting Materials

A Portland cement, CEM I 42.5 R (PC; $Na_2O_{eq} = 0.88\%$), and three clays (I1, I2 and K1), extracted from deposits in Central Germany, were used in this study. I1 and I2 can be classified as brick clays (major clay mineral: illite), while K1 was a low-grade kaolinitic clay with only minor amounts of 2:1 minerals. Quartz powder (Q) was used for comparison with the calcined clays in blended cement mortars. CEN standard sand was used for production of the mortar specimens. The chemical, mineral and physical properties of the raw materials used in this study are summarized in Table 1.

Table 1 Chemical, mineralogical and physical properties of cement, quartz filler and raw clays

Component (wt%)	PC	Q	I1[a]	I2[a]	K1
SiO_2	19.82	99.40	76.74	68.06	54.60
Al_2O_3	4.56	0.10	10.40	12.50	24.27
Fe_2O_3	1.97	0.03	1.79	5.66	2.44
TiO_2	0.13	0.07	1.43	1.34	2.79
CaO	62.87	–	0.36	0.84	1.51
MgO	1.73	–	0.50	1.32	0.54
Na_2O	0.31	–	0.32	0.93	0.26
K_2O	0.86	–	1.80	2.76	1.31
SO_3	3.26	–	0.25	0.08	0.68
P_2O_5	0.20	–	0.19	0.37	0.30
Mn_2O_3	0.02	–	0.01	0.06	0.01
LOI[c]	3.57	0.15	5.89	5.70	10.81
Residual	0.74	–	0.35	0.43	0.48
Kaolinite[b]			16.7	18.0	54.8
Illite[b]			16.3	31.1	1.1
Smectite[b]			–	5.2	–
Quartz[b]			62.5	36.3	40.4
Apparent density[d], ρ (g/cm^3)	3.15	2.65	2.58	2.66	2.54
Median particle size[e], d_{50} (µm)	4.87	12.17	13.29	20.48	10.70
Specific surface area[f], a_s (m^2/g)	1.07	0.45	16.74	15.50	35.64

[a] Average of chemical compositions of samples from three locations within the deposit
[b] Determined on separate clay batches by Rietveld QPA after micronizing, using 10% zincite as internal standard [3]
[c] Loss on ignition at 1000 °C determined according to DIN EN 196-2
[d] Determined by He-pycnometry according to DIN 66137-2
[e] Determined by laser granulometry after wet dispersion in propan-2-ol
[f] Determined by N_2 sorption (BET method) according to ISO 9277

A commercial polycarboxylate-based superplasticizer (PCE SP) with a solid content of 41.8% was employed in selected mortars.

In addition, a mix of I1 and K1 was produced by homogenizing the clays at a 1:1 weight ratio for 2 h in a 75-L concrete mixer. The blended clay was named B1 and calcined and ground like the other clays, as described in Sect. 2.2. In what follows, sample name affixes '_yyy' are used to denote calcined clays, where yyy indicates the calcination temperature in °C.

2.2 Methods

Calcination of the clays was performed in a laboratory-scale rotary kiln with a tube length of 2 m. Two heating regimes were selected, following results obtained in previous work with a muffle furnace to determine optimum temperatures [3]: the brick clays (I1 and I2) were calcined at 850 and 900 °C; the low-grade kaolinitic clay (K1) and the blended clay (B1) were calcined at 650 and 900 °C. The feeding rate was kept constant at 1.2 kg/h, and the measured throughput (T_{clay}) and retention time (t_R) were calculated according to Eq. 1 and Eq. 2, respectively.

$$T_{clay} = \left(\frac{m_{t1} - m_{t2}}{t_2 - t_1} \right) \times 60 \tag{1}$$

$$t_R = \left(\frac{m_{final}}{T_{clay, final}} \right) \times 0.7 \tag{2}$$

where m_{t1} and m_{t2} are the masses (in kg) of calcined clay collected from the kiln at time t_1 and time t_2 (in minutes), respectively, m_{final} is the final mass collected after the final feed and $T_{clay,final}$ is the final throughput recorded. The factor 0.7 in Eq. 2 corresponds to the percentage of the heated zone in the kiln (i.e. 1.4 m).

Qualitative phase analysis of the raw and calcined clays (collected at each measured throughput) was carried out on a Rigaku Ultima IV diffractometer in Bragg–Brentano geometry using CuKα radiation ($\lambda = 1.541874$ Å) and a divergence slit of 0.5°. The X-ray tube was operated at 40 kV and 40 mA; patterns were recorded with a sampling interval of 0.02° 2θ and a scan rate of 0.5° 2θ min^{-1}. The scanning range was 5–65° 2θ. The samples were front-loaded into sample holders and spun at 15 rpm.

The calcined clays collected from the rotary kiln were ground in a screening ball mill at a grinding capacity of 5 kg/h and screened through a sieve mesh of 125 μm. A fraction of I1 calcined at 850 °C was further ground in a planetary ball mill at a grinding capacity of 0.5 kg/h and screened through a sieve mesh of 63 μm (i.e. to a higher fineness; material designated I1*_850).

Standard mortar prisms (160 mm × 40 mm × 40 mm) were produced at a substitution rate of 15 and 25 wt%, with a constant water/binder ratio of 0.50 (as in

DIN EN 196-1) for all mortars. The higher substitution rate was only employed for I1*_850 and for K1_900 with use of PCE SP.

Through trials, an amount of 0.36% PCE SP by weight of binder was identified as sufficient to obtain a workable mix similar to that of plain Portland cement mortar. The PCE SP was added 90 s after the start of the mixing, and the bulk mixing water was corrected for the water content of the SP. The workability of the fresh mortar with and without the presence of PCE SP was investigated by mini-slump flow using a Haegermann cone and a jolting table according to DIN EN 1015-3.

Curing of the mortars was done at 23 °C, immersed in water. Compressive strength measurements on the hardened mortars were carried out after 2, 7 and 28 days of curing on a 10-kN ToniPRAX strength-testing device according to DIN EN 196-1.

3 Results and Discussion

3.1 Transformation of the Clays Due to Calcination

The measured T_{clay} and t_R for all clays during the calcination period varied in the range 0.5–1 kg/h and ~1–3 h, respectively. Due to the tendency of I2 to exhibit sintering and/or excessive agglomeration, presumably caused by its high Fe content (Table 1) [3], the kiln was adjusted to a maximum retention time of ~1 h for this clay to avoid sticking of the material in the interior of the kiln. Figure 1 shows the XRD patterns of the calcined clays at various retention times per calcination temperature and the respective raw clays.

At 650 °C and above, the major kaolinite peaks were absent in the diffractograms of all clays, demonstrating kaolinite's complete dehydroxylation and amorphization [2–4]. The basal smectite peak in I2 was absent after calcination at 850 °C, indicating its complete dehydroxylation [3]. The diffractograms of the low-grade kaolinitic clay (K1) and the blended clay (B1) reveal incomplete dehydroxylation of the illite at 650 °C, evidenced by the fact that the shift of its 004 reflection from ~5.00 Å (~17.8° 2θ) to 5.04 Å (17.6° 2θ) was only partial at this temperature [3]. However, at 900 °C, a complete shift of the peak to lower Bragg angles was detected, owing to complete dehydroxylation of the illite [3, 5]. This was observed for I1 and I2, calcined at 850 or 900 °C, as well. The intensity of the basal reflection (and other reflections) of illite in I1 was considerably diminished after calcination, compared to the raw clay (Fig. 1a). On the contrary, the illite peaks were only moderately diminished after calcination in the other clays (Fig. 1b–d). This may possibly indicate a higher degree of amorphization of the illite in the calcined I1 or may be related to transformation to new (high temperature) phases. However, close inspections of the diffractograms revealed that, in all clays and at all calcination conditions, no spinel phase was present after calcination. No significant differences were observed between the major reflections of the clay minerals in the clays calcined at different
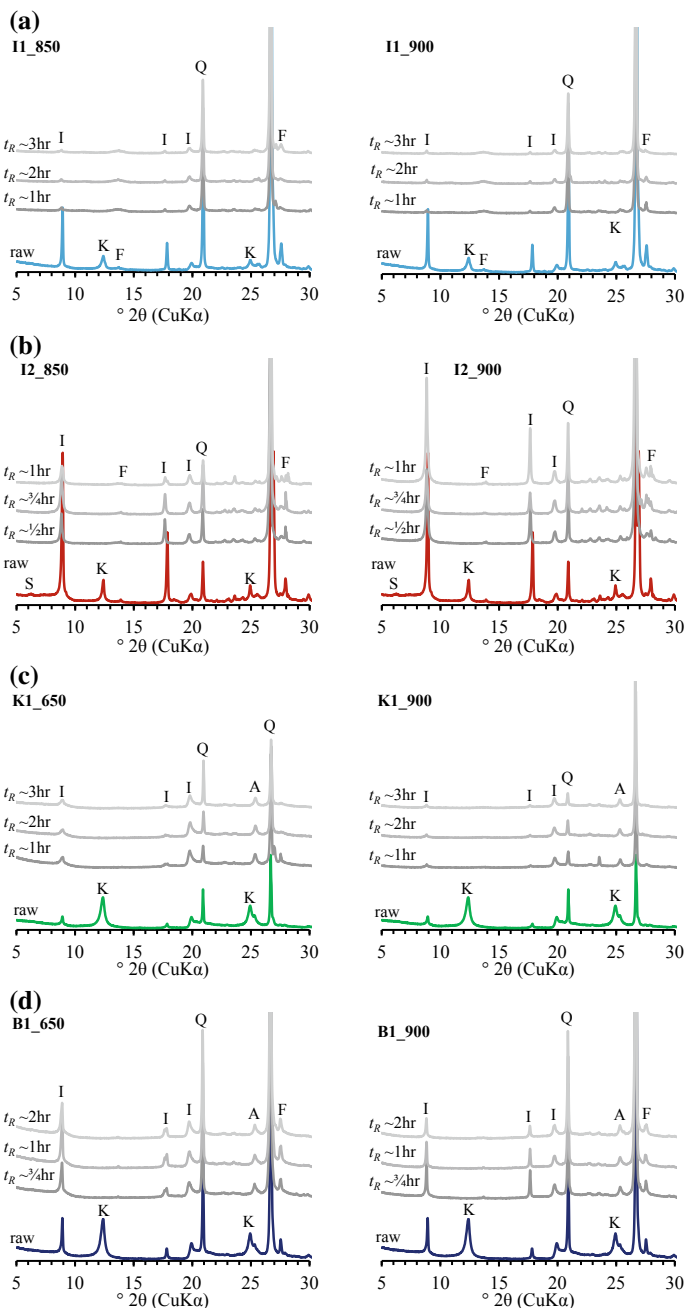
Fig. 1 Comparison of X-ray diffractograms (5–30° 2θ range) of raw and calcined clays at various retention times and calcination temperatures for **a** I1, **b** I2, **c** K1 and **d** B1 (I-illite/dehydroxylated illite; K-kaolinite; S-smectite; Q-quartz; F-feldspar; A-anatase)
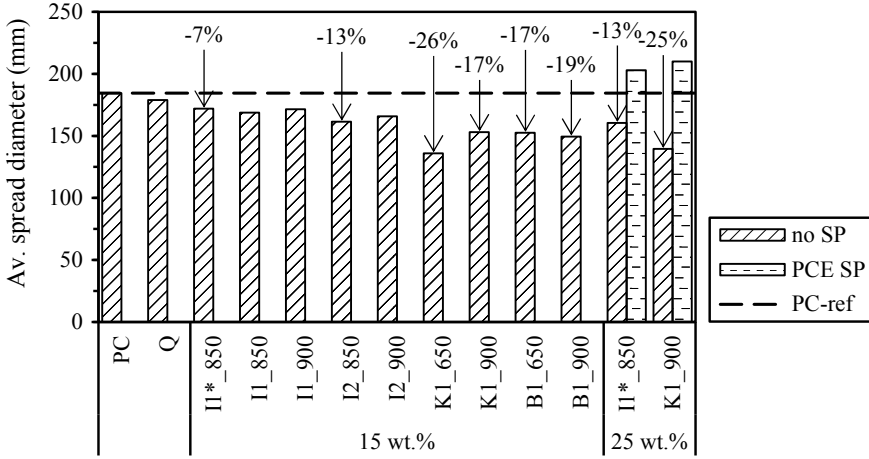
Fig. 2 Slump flow of plain Portland cement mortars and blended cement mortars with 15 wt% or 25 wt% substitution rate and influence of PCE SP on selected blends

retention times, indicating that extending the retention time above ~1 h does not contribute to increased reactivity.

3.2 Workability of the Blended Cement Mortars

The slump flows of all blended cement mortars with 15 wt% substitution rate, and selected blends with 25 wt% substitution rate, are shown in Fig. 2. Compared to the plain Portland cement mortar, the slump flow was lower for all blended cement mortars without PCE SP. This was most pronounced for K1, due to its high kaolinite content and high specific surface area (Table 1), in line with previous reports on calcined kaolinitic clays [6]. When K1 was calcined at 650 °C, the workability of the corresponding blended cement mortar was reduced by 26%, but at 900 °C, the workability was reduced by only 17%, which is likely related to changes in morphology of the clay particles (agglomeration), caused by the higher calcination temperature [3]. In the presence of PCE SP, the blended mortars exhibited higher flowability, compared to the plain Portland cement mortar, owing to the dispersing ability of the superplasticizer.

3.3 Compressive Strength of the Blended Cement Mortars

Figure 3 shows the evolution of the compressive strength of the blended cement mortars at 15 wt% substitution rate. The brick clays (I1 and I2) show no pozzolanic
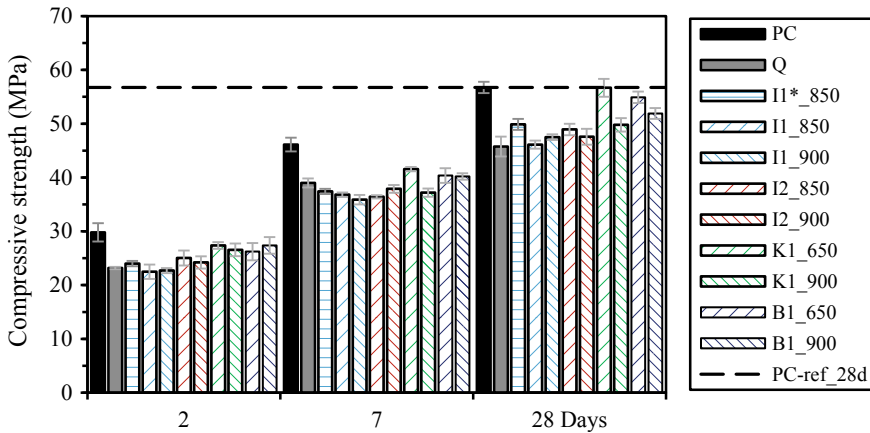
Fig. 3 Compressive strengths of Portland cement mortar and blended cement mortars with 15 wt% substitution rate versus curing time

activity at early ages (i.e. strength similar to quartz powder-blended reference at 2 and 7 days). However, the low-grade kaolinitic clay (K1) and the blended clay (B1) show an increase of ~7%, compared to the quartz powder-blended reference, at 2 days.

After 28 days of hydration, K1_650 and B1_650 were the blended cement mortars with the highest strengths. The mortars with calcined brick clays (I1 and I2) generally exhibited only slightly higher strengths than the Q mortar. The present results differ from previously reported strengths of blended cement pastes, in which I1 performed considerably better than I2 [3]; the reasons for this discrepancy are currently not clear, but are possibly related to material inhomogeneities within the clay deposit. However, the mortar with the more finely ground brick clay I1*_850 exhibited considerably higher strength than the mortars with the coarser brick clays, demonstrating the beneficial effect of grinding to increase the specific surface area.

A higher substitution rate of 25 wt% was studied for I1*_850 and K1_900 and quartz powder for comparison. Table 2 shows the relative compressive strengths, referred to the strength of the PC mortar, of these blended cement mortars after 28 days of hydration with and without the presence of PCE SP. Without PCE SP, the brick clay and the low-grade kaolinitic clay exhibited a relative strength increase

Table 2 Effect of PCE SP on the relative strengths of blended cement mortars with 25 wt% substitution rate after 28 days of hydration

Mortar	Relative compressive strength at 28 days (%)	
	No SP	With PCE SP
PC	100	–
Q	65	–
I1*_850	84	75
K1_900	91	91

of 19% and 26%, respectively, compared to the Q mortar, owing to their pozzolanic reaction. In the presence of PCE SP, the strength remained unchanged for K1_900, whereas the strength of the mortar with I1*_850 was decreased, despite the improved workability caused by the addition of the superplasticizer (Fig. 2). However, the strength of this mortar still exceeded that of the quartz powder-blended reference mortar.

4   Summary

For the two brick clays (I1 and I2) and the low-grade kaolinitic clay (K1) studied in the present work, calcination for more than 1 h did not lead to substantial further changes of their phase assemblage as observed by XRD, indicating that it does not contribute to increased reactivity.

The workability (slump flow) of all blended cement mortars with calcined clays was lower than those of mortars with plain Portland cement or binders with quartz powder. This effect was most pronounced for the kaolinitic clay, because of its higher surface area. Employment of a conventional polycarboxylate-based superplasticizer could fully mitigate this effect on workability; however, in one case it led also to a decrease in the strength of the hardened mortar.

The calcined brick clays generally performed not as good as the kaolinitic clay in terms of compressive strength of blended cement mortars. However, two strategies could be applied to increase the performance of brick clay I1: grinding to higher fineness (I1*_850) and mixing of the brick clay with the kaolinitic clay (B1). In both cases, the strengths of blended cement mortars were significantly higher than without these measures, and the mortar with the mixed clay had a strength that was comparable to that of the mortar with only K1.

References

1. Scrivener, K.L., John, V.M., Gartner, E.M.: Eco-efficient cements: potential, economically viable solutions for a low-CO_2, cement-based materials industry. United Nations Environment Programme, Paris (2016)
2. Fernandez, R., Martirena, F., Scrivener, K.L.: The origin of the pozzolanic activity of calcined clay minerals: a comparison between kaolinite, illite and montmorillonite. Cem. Concr. Res. **41**, 113–122 (2011)

3. Msinjili, M.S., Gluth, G.J.G., Sturm, P., Vogler, N., Kühne, H.-C.: Comparison of calcined illitic clays (brick clays) and low-grade kaolinitic clays as supplementary cementitious materials. Mater. Struct. **52**, 94 (2019)
4. Alujas, A., Fernández, R., Quintana, R., Scrivener, K.L., Martirena, F.: Pozzolanic reactivity of low grade kaolinitic clays: influence of calcination temperature and impact of calcination products on OPC hydration. Appl. Clay Sci. **108**, 94–101 (2015)
5. Garg, N., Skibsted, J.: Pozzolanic reactivity of a calcined interstratified illite/smectite (70/30) clay. Cem. Concr. Res. **79**, 101–111 (2016)
6. Trümer, A., Ludwig, H.-M., Rohloff, K.: Investigation into the application of calcined clays as composite material in cement. ZKG Int. **67**(9), 52–57 (2014)

Utilization of Clay Brick Waste Powder for Partial Replacement with Cement in Cement Mortar

Hemraj R. Kumavat, Narayan R. Chandak and Dhananjay J. Jadhav

Abstract Partial replacement of cement with crushed burnt clay brick waste powder (CBP) could reduce CO_2 emission, enhance the conservation of natural resources, and decrease the cost of waste disposal sites. The aim of this study is to investigate the use of CBP as a partial replacement for cement in the production of cement mortar. Clinker was replaced by CBP in different proportions (0, 5, 10, 15, and 20%) by weight for cement. The physicochemical properties of cement at the anhydrous state and the hydrated state thus compressive strengths after 7, 28, and 90 days for the mortar were studied. Thermogravimetry analysis (TGA), Differential thermal analysis (DTA) and Thermogravimetry (TG) tests were conducted to investigate the development of cement hydration reactions in the presence of these wastes. Particle size distributions were obtained from laser granulometry (LG) of CBP and cement used in this study. Considering the proportions levels studied, the results indicated that the use of CBP in mixture accelerated the hydration reactions, and there was an indication of pozzolanic activity, particles packing density and compressive strength were maintained. Compressive strength decreased as the replacement level and average particle size increased. The CBP mixture at 20% level had similar or even higher mechanical properties than controlled mortar.

Keywords Clay brick waste · Pozzolana · Thermal analysis

1 Introduction

The use of pozzolanic materials in mortar as additional cementing material is beneficial due to significant energy savings and the decrease of solid waste [1]. These materials can enhance the final mortar product's characteristics. The pozzolanic products may be of natural or industrial origin [2]. Pozzolanic materials are defined as silica and aluminum materials with little or no cemented significance but which

H. R. Kumavat (✉) · N. R. Chandak
Department of Civil Engineering, MPSTME, NMIMS, Shirpur, India
e-mail: kumavathr1981@gmail.com

D. J. Jadhav
Department of Civil Engineering, R C Patel Institute of Technology, Shirpur, India

respond chemically with calcium hydroxide at normal temperatures in a finely split shape in the presence of moisture to form compounds with cemented characteristics [3]. Pozzolans have amorphous silica that respond to $Ca(OH)_2$. This is beneficial because pozzolans generate a more resistant material and less portlandite which can be drained during chemical attack, thereby decreasing the porosity of the final product and making the substance more compact [4].

The differential thermal analysis (DTA) and thermogravimetric analysis (TGA) methods are most popular in the research of cement hydration [5]. TGA is a method that examines a sample's mass shift depending on temperature and/or time. TG assessment enables CH content to be estimated from weight loss. While the temperature difference between a sample and a reference material is measured in DTA, heat absorption is recorded during endothermic reactions or heat emission during exothermic reactions [6].

Calcium hydroxide (CH) is one of the main hydrated goods in a completely cured cement paste that comprises more than 20% of the hydrated goods [7]. Calcium hydroxides (CH) and calcium silicate hydrate (C–S–H) are the end products of alite and belite water response [8]. Calcium hydroxide occurs predominantly in the form of well-defined crystals and a exactly determined structure, so that the assessment of the CH content determines both the features of hydration and the degree of hydration of the cement paste. The formation and alteration of CH quantities created in hydrated Portland cement not only determine the proportion of reaction hydration, but also affect the paste's ultimate mechanical characteristics [9].

Brick waste can be used for partial replacement of cement and sand in mortar as an alternative material. The significant content and chemical, physical characteristics of brick waste material are comparable to cement and sand, so we can use this material as one of the building materials in the construction industry to meet the industry's present requirement and guarantee sustainable building. The use of brick waste product for experimental work is gathered from various brick plant locations in the district of Jalgaon and Dhule and sampling of brick waste with varying proportions of fly ash and clay used for brick production.

2 Experimental Program

2.1 Material

The Ordinary Portland Cement (OPC) for controlled mortar was used in this study. The main properties are listed in Table 1.

Table 1 Chemical properties of Ordinary Portland Cement

Chemical requirements	CaO − 0.70SO$_3$/(2.8SiO$_2$ + 1.2Al2O$_3$ + 0.65Fe$_2$O$_3$)	Al$_2$O$_3$/Fe$_2$O$_3$	Insoluble residue [%]	Magnesia [%]	Sulfuric anhydride [%]	Loss on ignition [%]	Chloride [%]
Test results	0.88	1.21	1.15	1.01	2.46	2.96	0.005

2.2 Particle Size Distribution

The particle size distribution of cement and clay brick waste was shown in Fig. 1. The figure shows that cement is very fine than clay brick waste, because some coarser particles stay after clay brick waste has been crushed. The distribution of cement particle size starts from 200 microns, but clay brick particle size from 400 microns depends on that particle density as well.

Compressive strength and elasticity modulus are key parameters for determining the bearing capacity and deformation of the load-bearing mortar and masonry prism. Several experiments were performed to assess the uniaxial compressive stress–strain curves of brick units, mortar cubes, and mortar prisms built with mortar grade 1:4. The replacement mortar experimental lead compared to the controlled mortar (0% replacement). The compressive strength of cement mortar cubes (size $7.07 \times 7.07 \times 7.07$ cm) of 1:4 proportions was prepared using clay brick waste with 0, 10, 20, 30, and 40% replacement of cement with clay brick waste. After casting of mortar cube,

Ordinary Portland cement
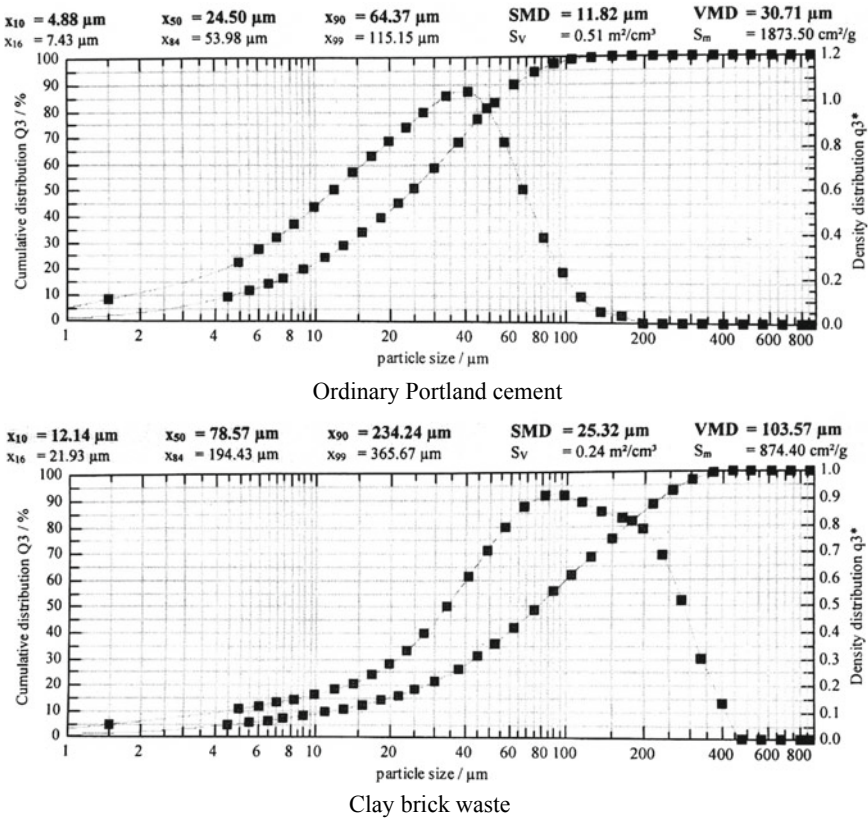
Clay brick waste

Fig. 1 Particle size distribution of cement and clay brick waste

Fig. 2 Axial load on cube
specimen in CTM

they are cured in water for 3, 7, and 28 days. Mortar specimen was placed on the computerized universal testing machine, and the axial compressive load was applied. The specimens were subjected to an axial load up to failure of the test specimen as shown in Fig. 2.

3 Result and Discussion

3.1 Thermo Gravimetric Analysis (TGA)

The TGA is a technique used to measure a sample's mass shift as a function of temperature increase. Thermal modifications lead to mass changes in cement-based products that can be measured by a thermogravimetric analyzer [10]. The TGA was carried out primarily to study the impact of the presence of clay brick waste on the degree of cement hydration, which is a function of the content of calcium hydroxide. TGA was performed on samples subject to temperatures of up to $1000°$ C, with a heating rate of 18 °F/min (10 °C/min) in the atmosphere of helium. Controlled mortar (0% replacement) was prepared using the 1.5:1 water-to-cement ratio. The blend was stirred, and the sample was filtered using a quantitative filter paper after 48 h of hydration. The residue was cleaned twice with isopropyl alcohol and acetone, dried for 30 min in the vacuum oven at 60 °C, then sieved using a 90 m sieve, and then placed in a desiccator. The thermogravimetric measurements were performed in the non-isothermal circumstances from room temperature to 1000 °C at heating levels

of 10 °C/min by a Perkin Elmer concurrent DTA/TG analyzer, the Pyris Diamond
model, in the nitrogen atmosphere with a flow rate of 300 ml/min.

Changes in mass involve dehydration of products for hydration. This method is
useful in assessing changes in the structure of cement-based products in order to
predict their behavior when exposed to fire. Typical TGA curve plots for controlled
and substituted cement mortars with corresponding mass loss are shown in Figs. 3
and 4.

TGA curves indicate that there are three areas in each curve. Zone I includes
the 100–500 °C variety and is ascribed to C–S–H and ettringite dehydration. Zone
II is ascribed to calcium hydroxide dehydration, ranging from 500 to 700 °C. The
loss of calcium hydroxide in CM and clay brick waste mortar amounts to 4.8% and
6.27%, respectively. The full C–S–H decomposition is indicated by an endotherm
after 700 °C. The calcium hydroxide peak is 470–485 °C in all specimens (cement
mortar, clay brick waste mortar specimens), indicating that there is no change in stage
chemistry for distinct mixtures [11]. However, there is an insignificant variation in
the content of calcium hydroxide between controlled and substituted cement mortars.
The decomposition method of $Ca(OH)_2$ is ascribed to an endothermic peak of about
420 °C on the DTA curve and mass loss in the temperature range of 340–460 °C on
the TG curve [12].
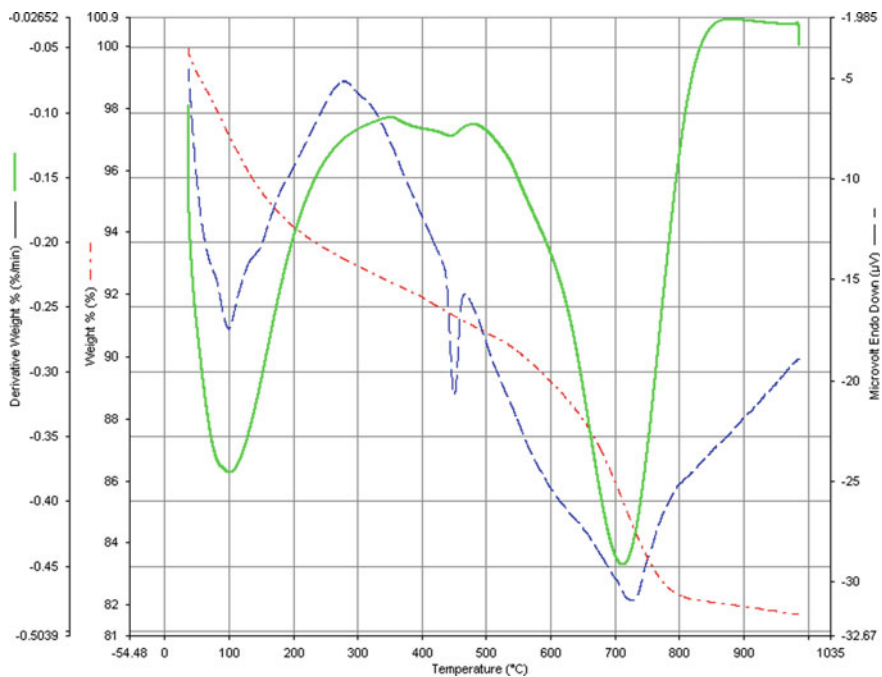
Fig. 3 DTG/DTA/TG curve of controlled mortar
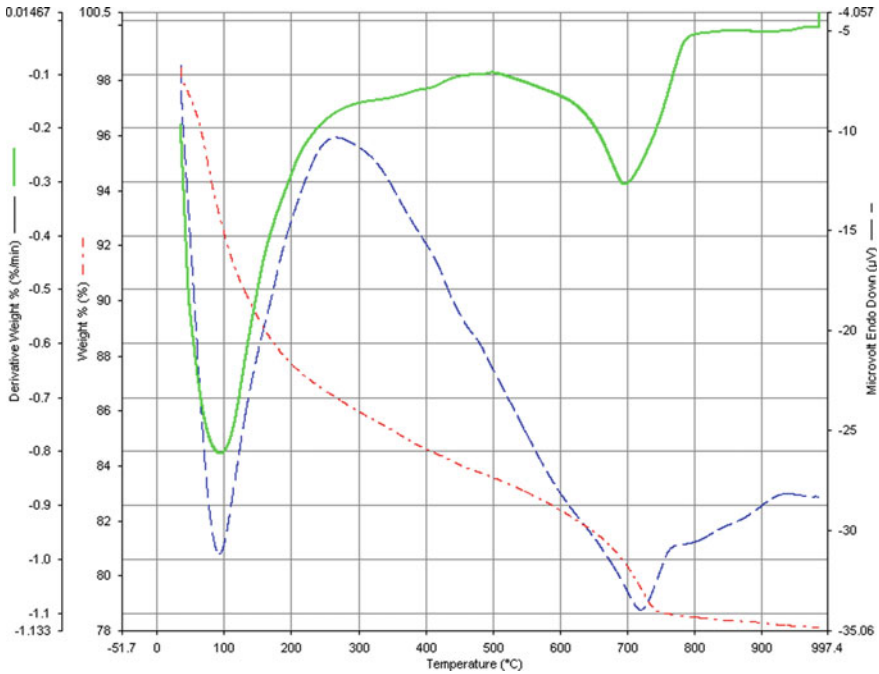
Fig. 4 DTG/DTA/TG curve of 20% brick waste replaced in cement mortar

3.2 Heat Flow and Mass Change (%)

Figures 3 and 4 for all studied samples show the outcomes for the heat flow and relative weight change (percent) for specimens with variable quantities of burnt clay brick waste at a specified temperature. Several heat flow peaks happen in Fig. 4, and the size of these peaks differs with the quantity of burnt clay brick waste in the samples.

The two heat flow peaks in the 25–250 °C temperature interval correspond to the release of physically bound water from pores, plus the dehydration responses owing to water loss from the gel of calcium silicate (C–S–H) and also the decomposition of ettringite in specimens. Throughout the study, C–S–H gel and ettringite dehydration were observed near 110 °C temperature. It was likely triggered before measurement by distinct ages of the samples studied, hydration products formed, temperature program selected, or preparation processes.

An important mass loss is connected with the responses in this temperature range. It is about 6.5% for the controlled mortar. The mass loss then reduces with a growing quantity of burnt clay brick waste and reaches up to 2.9% for replacement by 40%. There is another peak associated with the decomposition of $Ca(OH)_2$ in the temperature range of 400–480 °C, which is also followed by a mass loss. The temperature

point for the specimens being studied is 600 °C, where quartz transformation α–β occurs. A sharp endothermic heat flow peak and a volume shift accompany this response. There is no mass change during the quartz transition. The small peak in the reference sample is visible at the temperature around 700 °C, but it is only triggered by measurement inaccuracy. The decomposition of $CaCO_3$ is initiated in the temperature range 650–760 °C. This impact is followed by a greater mass loss compared to the decomposition of $Ca(OH)_2$.

There are two exothermal peaks corresponding to a crystallization process after reaching temperatures above 800 °C. The pozzolanic reaction causes it, and its size corresponds to the degree of crystallization between Ca and Si. It was noted that the healing era was increasing. With the quantity of burnt clay shale, the temperature of this peak rises. For samples with higher amounts of burnt clay brick waste, the heat flow peak moves to higher temperatures around 950 °C.

4   Conclusion

Based on this experimental study, the following conclusions can be drawn:

1. It is inferred from TGA results that the samples have a stable structural state up to 500 °C, while the exposure to higher temperatures results in a remarkable decomposition of the hydration products.
2. The loss of calcium hydroxide in CM and clay brick waste mortar amounts to 4.8%, 6.27%, respectively. The full CSH decomposition is indicated by an endotherm after 700 °C.
3. The two heat flow peaks in the temperature interval of 25–250 °C correspond to the expulsion of physically bound water from pores, plus the reactions to dehydration due to water loss from the calcium silicate gel CSH and also the decomposition of ettringite in samples.
4. The mass loss then decreases as the amount of burnt clay brick waste increases and reaches up to 2.9% for replacement by 40%.
5. $CaCO_3$ decomposition is initiated in the 650–760 °C temperature range. Compared to $Ca(OH)_2$ decomposition, this effect is followed by a higher mass loss.

References

1. Heikal, M., El-Didamony, H., Morsy, M.S.: Limestone-filled pozzolanic cement. Cem. Concr. Res. **30**, 1827–1834
2. Donatello, S., Tyrer, M., Cheeseman, C.R.: Comparison of test methods to assess pozzolanic activity. Cem. Concr. Compos. **32**, 121–127 (2010)
3. ASTM C125–14: Standard Terminology Relating to Concrete and Concrete Aggregates. ASTM International, West Conshohocken, PA (2014)

4. Sha, W., Pereira, G.B.: Differential scanning calorimetry study of ordinary Portland cement paste containing metakaolin and theoretical approach of metakaolin activity. Cem. Concr. Compos. **23**(6), 455–461 (2001, December)
5. Ramachandran, V.S., James, J.B.: Handbook of Analytical Techniques in Concrete Science and Technology. Institute for Research in Construction National Research Council of Canada Ottawa, Ontario, Canada (2001)
6. Ramachandran, V.S.: Concrete Admixtures Handbook, Properties, Science, and Technology, 2nd edn, Noyes Publications. Institute for Research in Construction National Research Council of Canada Ottawa, Ontario, Canada
7. Jelica, Z., Leticija U., Drazan, J.: Application of thermal methods in the chemistry of cement: kinetic analysis of portlandite from non-isothermal thermogravimetric data. In: The first International Proficiency Testing Conference, Sinaia, Romania, 11th–13th October 2007
8. Jacques, M., Dale, P.B., Eric, S., Yannick, M.: Influence of calcium hydroxide dissolution on the transport properties of hydrated cement systems, Reprinted from Materials Science of Concrete: Calcium Hydroxide in Concrete, Special Volume, Proceedings. American Ceramic Society. In: Workshop on the Role of Calcium Hydroxide in Concrete, November 1–3, 2000, Holmes Beach, Anna Maria Island, Florida, 113–129 pp. (2001)
9. Chen, D., Dollimore, D.: Kinetic analysis of the calcium hydroxide formed in the hydration of pure C3S and with addition of $Ca(NO_3)_2$. J. Thermal Anal. **44**, 1001–1011 (1995)
10. DeJong, M., Ulm, F.: The nanogranular behavior of C-S-H at elevated temperatures (up to 700 °C). Cem. Concr. Res. **37**, 1–12 (2007). https://doi.org/10.1016/j.cemconres.2006.09.006
11. AbdElmoaty, M.: Mechanical properties and corrosion resistance of concrete modified with granite dust. Constr. Build. Mater. **47**, 743–752 (2013). https://doi.org/10.1016/j.conbuildmat.2013.05.054
12. Jeyaprabha, B., Elangovan, G., Prakash, P.: Strength and microstructure of mortar with sand substitutes, Građevinar **68**(1), 29–37 (2016). https://doi.org/10.14256/JCE.1245.2015

Qualifying of Low Grade Clay for Geopolymer Mortar: A Preliminary Assessment

Sreedevi Lekshmi, Reesha Bharath, Sunitha K Nayar and J Sudhakumar

Abstract This paper reviews the feasibility of using low grade clay for developing geopolymer mortar by partially replacing conventional source material. The study intends to develop a framework for identification, classification and utilization of various clays and suggest suitable processing techniques to qualify for geopolymerization. The influence of source clay based on the reactivity of silica, physical, chemical and mineralogical characteristics on the properties of geopolymer mortar is extensively studied based on existing literature. Characteristics of clay after various treatment methods (calcining and lime treatment) are also reviewed so as to identify the extent of its effectiveness on geopolymers. Characteristics based on micro-structural studies such as energy dispersive X-ray analysis (EDX), Fourier transform infrared spectroscopy (FTIR), scanning electron microscopy (SEM) and X-ray diffraction spectroscopy (XRD) along with geotechnical characterization are reviewed. The paper highlights the significant characteristics of clay that is significant for geopolymerization and its implication on the properties of geopolymer mortar. The manifestation of geopolymer characteristics and its relation to crystallography and microstructure is explored to develop strategies for the qualification of clays. The influence of parameters such as alkali concentration and sodium silicate to sodium hydroxide ratio on compressive strength is presented. Based on the review, an attempt has been made to characterize different types of clay obtained from few sources in India, and a study has been conducted to assess the qualification technique proposed.

Keywords Geopolymerization · Fly ash · Clay · Characterization

S. Lekshmi (✉) · R. Bharath · J. Sudhakumar
NIT Calicut, Calicut, Kerala, India

S. K. Nayar
IIT Palakkad, Palakkad, Kerala, India

1   Introduction

The global demand for concrete as a construction material has increased the demand for Portland cement. The massive production of cement results in considerable emission of carbon dioxide to the atmosphere which results in climatic change as a result of global warming [1]. In this context, the relevance of geopolymer concrete is well recognized. Geopolymers are aluminosilicate binder (source material) having cementitious property synthesized by the reaction achieved by the alkaline activation of aluminosilicate rich materials. The term geopolymer was coined by Davidovits [2]. Geo the prefix in geopolymer symbolize the relationship of binder to geological materials such as natural stones and minerals [3]. Commonly used source materials are fly ash, metakaolin, ground granulated blast furnace slag, etc., which are aluminosilicate rich sources. Typical alkaline activators are sodium hydroxide (NaOH) in combination with sodium silicate (Na_2SiO_3) [4]. As metakaolin is chemically simpler and more amorphous than fly ash, geopolymerization of metakaolin has yielded more reliable results in comparison; however, fly ash has gained global interest due to its cost-effectiveness [5]. The objective of this paper is to explore the possibility of utilizing raw clay from different sources as the source material for the production of fly ash-based geopolymers and to review the possible scope of using lime and thermally treated clay in geopolymers.

Clay can be defined as cohesive soil which is mostly plastic in nature with finely grained particles of size less than 0.002 mm. For synthesizing geopolymer, the most commonly used clay mineral is kaolinite with chemical formula $Al_2O_3 \cdot 2SiO_2 \cdot 2H_2O$ [2, 6]. It has been reported that the alumina (Al_2O_3) and silica (SiO_2) contents in clay meet the criteria to be used as source material in geopolymers similar to that of fly ash.

From literature, it is evident that mechanical properties of geopolymer specimens are enhanced after lime treatment and calcining. Ogundiran et al. (2015), reported that calcined clay accelerated dissolution/ hydrolysis of fly ash, whereas fly ash controlled the exothermic reaction that resulted in alkaline dissolution/hydrolysis of calcined clay. Consequently, it is suggested that the addition of calcined clay to fly ash enhanced early dissolution of fly ash, even at a low content of 25%, and as a proportion of calcined clay increases, early dissolution also increases.

As reported by Duxon and Provis [7] and Ming et al. [2], in the dissolution process of aluminosilicates, the hydroxyl ions present in the alkaline medium release silicates and aluminate species to permit polymerization process to take place. The phenomenon of geopolymerization is exothermic in nature. Rate and extent of dissolution depend on ion exchange capacity, fineness and nature of source material and concentration of alkaline solution. Continuous rearrangement of gel phase occurs upon curing which results in the formation of zeolitic crystals. In this model, initial gel phase is represented by solidification and hardening and final gel phase represented by gel rearrangement and crystallization, respectively, and as a result, more ordered phases are formed as end product. During the process of geopolymerizaton,

Si–O–Si and Si–O–Al bond breaks down in the presence of alkaline medium. In the final stage, the midway product which is rich in Al content transforms to a Si dominated gel product.

But a large quantity of subsurface clay is being dumped on earth's surface as a result of excavation activities carried out in relation with construction industries which is a menace. Since most of the clay is rich in aluminosilicates, it can be regarded as an excellent geopolymer binder. Hence, by using clay as a source material by partially or fully replacing fly ash, the adverse effects of subsurface clay accumulation on earth's surface can be rectified to a great extent. Along these lines, the current study is a preliminary investigation of the possible classification of low grade clay for utilization for geopolymerization.

2 Investigations on Utilization of Low Grade Clay

2.1 Materials

The clay used in this study was collected from few sources of Kerala. Two types of clay were considered in this study, one is clay filled flood soil and other is paddy clay which is shown in Fig. 1. For the present study, pulverized clay passing through 300 μ IS sieve was used for partially replacing fly ash. Fine aggregate used in geopolymer mortar was locally available siliceous river sand. Geopolymer mortar specimens were prepared for both class F and class C fly ash as source material in which clay is used up to 50% by partial replacement of fly ash.
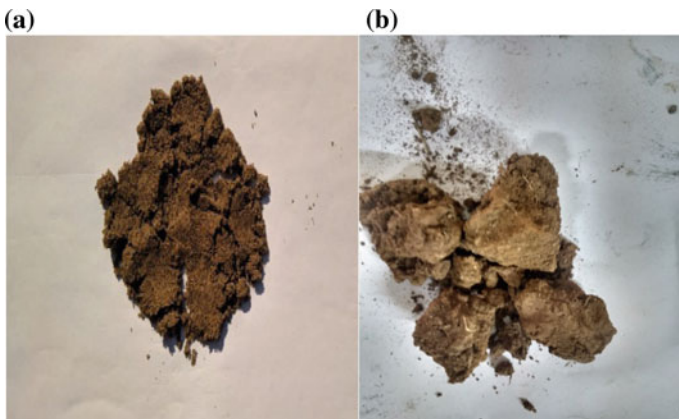
Fig. 1 **a** Clay filled flood soil **b** paddy clay

2.2 Material Characterization

Functional groups present in clay were identified by Fourier transform infrared spectroscopy (FTIR), morphology of clay was identified using scanning electron microscopy (SEM), chemical composition is revealed using energy dispersive X-ray analysis (EDX) and X-ray diffraction spectroscopy (XRD) and are reported in Figs. 2, 3, 4 and 5.

Visual characteristics such as colour, odour, texture and dry strength of the clay are reported in Table 1. It is examined that clay filled flood soil is of sandy type with medium dry strength, pale brown colour and earthy odour. Also, paddy clay is fine-grained cohesive clay with stiff dry strength, brown colour and has the odour of paddy field.

Geotechnical characterization such as specific gravity and index properties was studied and is given in Table 2. Since the flood soil is a kind of clay filled sandy soil, tests for investigating index properties could not be performed. Specific gravity (IS
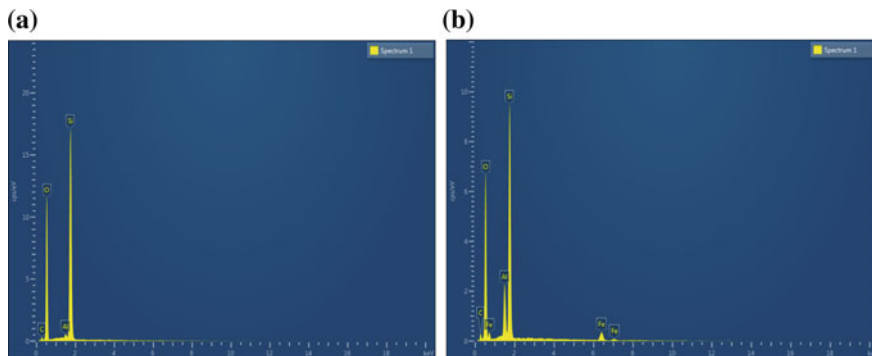
Fig. 2 EDX results of **a** clay filled flood soil **b** paddy clay
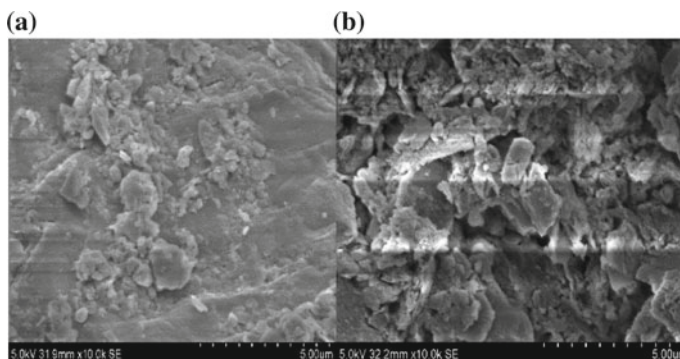
Fig. 3 SEM images of **a** clay filled flood soil **b** paddy clay

(a)

(b)
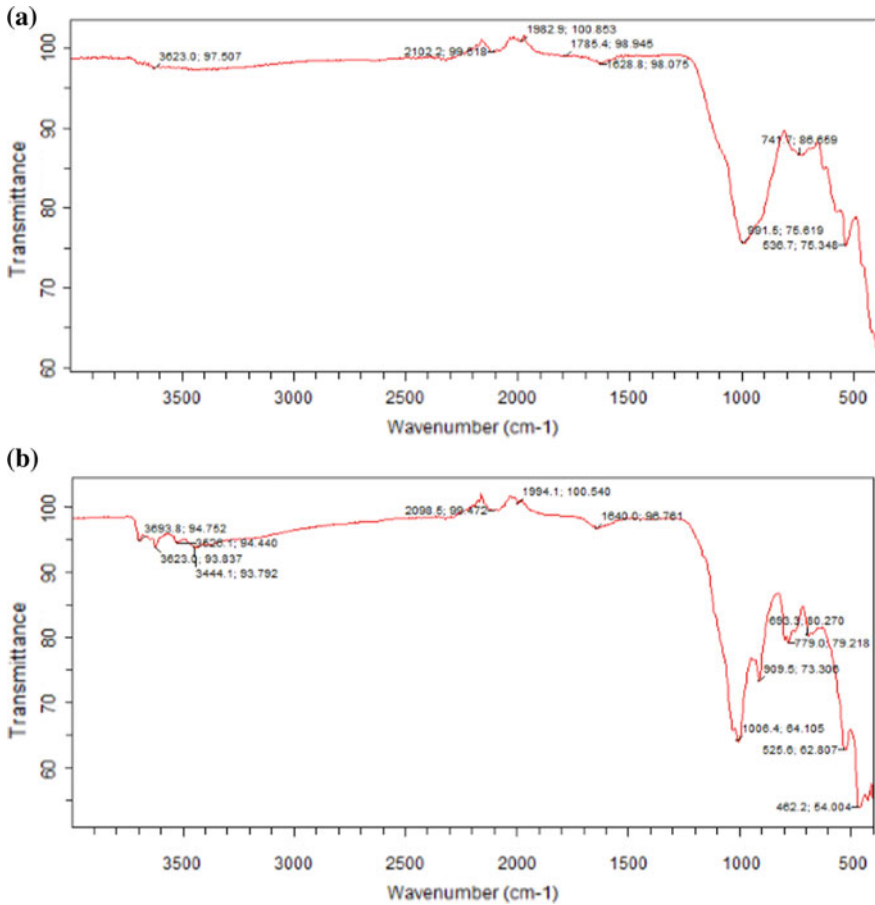
Fig. 4 FTIR analysis of **a** clay filled flood soil **b** paddy clay

2720, part 3) of flood soil and paddy clay is 2.07 and 2.13, respectively, which is less than 2 which implies that both clays are of porous type. The pH values for flood soil and paddy clay are 7.13 and 7.38, respectively, which is slightly greater than 7 and hence shows a trend towards alkaline side. The pozzolanic activity index (ASTM C311) of flood soil and paddy clay is 79.48% and 75.84%, respectively, which shows both clays are pozzolanic in nature. Loss on ignition (ASTM D7348-08) of clay filled flood soil and paddy clay is 16.4% and 15.1%, respectively.

Chemical composition of flood soil and paddy clay is revealed by EDX in Fig. 2. EDX spectra show dominant peaks of Si, O, Al and C for flood soil and Si, O, Al, C and Fe for paddy clay implying that these elements are the main constituents of these clays and their percentage weight is reported in Table 3.

The morphological aspect of both clays such as shape and size of particles is determined using SEM as shown in Fig. 3. The SEM analysis of clay filled flood
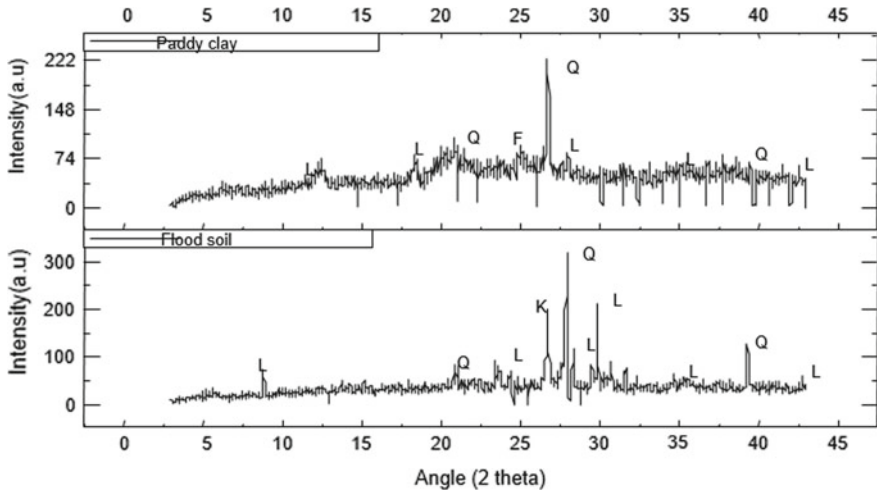
Fig. 5 XRD results of clay filled flood soil and paddy clay

Table 1 Visual characterization of clay filled flood soil and paddy clay

Characteristics	Clay filled flood soil	Paddy clay
Colour	Pale brown	Brown
Odour	Earthy	Slight odour of paddy
Texture	Sandy	Fine grain
Dry strength	Medium	Stiff

Table 2 Geotechnical characterization of paddy clay

Index properties	Clay filled flood soil	Paddy clay
Flow index	–	11.205
Liquid limit	–	50.19
Plastic limit	–	32.3%
Plasticity index	–	17.89%
Liquidity index	–	0.97
Consistency index	–	0.028
Toughness index	–	1.596
Shrinkage limit	–	57.94%

Table 3 Percentage weight of elements present in clay based on EDX result

Element	Clay filled flood soil (wt%)	Paddy Clay (wt%)
C	1.72	10.02
O	15.04	51.82
Al	0.13	5.99
Si	8.19	27.41
Fe		4.76

soil and paddy clay reveals that there are numerous large micro-aggregates of size 5 μm. Also, it is evident from the image that for clay filled flood soil, these particles are with rounded and nodular morphology, and paddy clay has platy, rounded and nodular morphologies.

The relevant functional groups present in both clays are analyzed using FTIR as shown in Fig. 4. In Fig. 4, for both clay filled flood soil and paddy clay, the bands between 3500 and 2300 cm^{-1} indicate stretching vibrations of structural OH bonds and bands between 1650 and 1630 cm^{-1} indicate bending vibration of OH bonds due to adsorbed water. For calcined clay and fly ash, the adsorption peak around 1088 cm^{-1} is associated with asymmetric stretching of Si–O–Si and Al–O–Si bond [10]. During the process of geopolymerization, the strong band (band with high wave number) shifts towards the low wave number and is correlated to the partial replacement of SiO_4 by AlO_4 which results in the change in chemical environment of Si–O bond. High Al penetration intensity from glassy part of fly ash into SiO_4 is represented by a large shift which is similar to that of zeolites [6].

XRD results of clay filled flood soil and paddy clay are reported in Fig. 5 (L—Illite, Q—Quartz (SiO_2), F—Iron Oxide (Fe_2O_3), K—Kaolinite). Major peaks of crystalline silica (quartz), illite, iron oxide and kaolinite are observed in both clays.

2.3 Geopolymer Synthesis

Sodium hydroxide activators were prepared by dissolving NaOH pellets in water, and activator solution was prepared for 6, 7, 8, 9 and 10 M NaOH solutions. Geopolymer mortar specimens were prepared with 50% of clay for both types of clay and its suitability being observed for both class F and class C type of fly ash. Experiments were designed using central composite design of response surface methodology in which a set of 20 experiments were obtained for 50% replacement of fly ash with clay. For each trial, six numbers of 50 mm cube specimens were casted for testing compressive strength. The workability of fresh mortar for each trial was determined using flow table test and the flow values were noted as an average of three measurements for each trial, for which the flow values observed were within the permissible range (ASTM C1437-15). The specimens were oven cured for one day at 90 °C after a dissolution time of 24 h in room temperature, for which the effect of molarity of NaOH solution and ratio of sodium silicate to sodium hydroxide solution on compressive strength is observed.

3 Results and Discussions

Figure 6 shows the compressive strength of geopolymer mortar with source material, class C and class F fly ash, which is partially replaced to 50% by clay filled flood soil and paddy clay, which is cured at 90 °C in hot air oven for a curing period

(a) Class C fly ash   (b) Class F fly ash
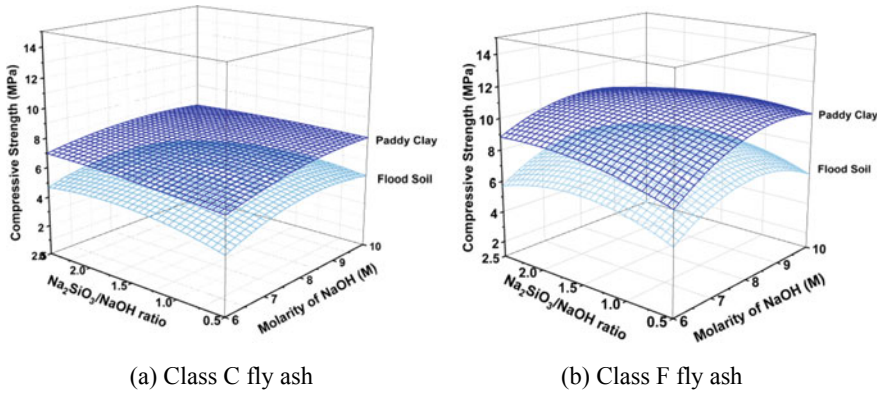
Fig. 6 Compressive strength of geopolymer mortar containing clay with **a** class C **b** class F fly ash

of one day. The factors considered for the present study are molarity of NaOH solution, temperature of curing, percentage of clay and ratio of sodium silicate to sodium hydroxide. Percentage of clay and temperature of curing are kept constant as 50% and 90 °C, respectively. The results of ANOVA for the dependent variables demonstrated that the model was significant for response variables such as molarity of NaOH, ratio of sodium silicate to sodium hydroxide and temperature of curing.

The models of compressive strength for clay filled flood soil and paddy clay for class F and class C fly ash are statistically significant as P-value is less than 0.05. It is observed that molarity of NaOH is a significant factor which affects compressive strength as its P-value is less than 0.005. Hence, it can be summarized that molarity of NaOH is a major factor contributing towards development of compressive strength of geopolymer mortar when compared with other abovementioned factors. The ANOVA results of compressive strength are summarized in Tables 4 and 5.

For both class C and class F fly ash, for both types of clay such as flood soil and paddy clay, it is observed that compressive strength increases with increase in molarity of NaOH solution to an optimum value and decreases further and the same

Table 4 ANOVA for compressive strength of class C fly ash-based geopolymers

	Mean value		F value		P value	
Factors	FS	PC	FS	PC	FS	PC
Model	1.50	1.08	72.73	16.79	<0.0001	<0.0001
Molarity-A	1.57	3.67	43.42	41.32	<0.0001	<0.0001
Na_2SiO_3/NaOH-B	0.02	0.21	0.22	0.55	0.8906	0.4719
Temperature-C	0.57	0.97	0.50	2.51	0.4914	0.1371
A^2	5.73	2.47	5.03	6.37	0.0429	0.0254
B^2	3.51	0.56	3.08	1.43	0.1027	0.2530
C^2	1.98	0.39	1.74	0.99	0.2102	0.3371

Table 5 ANOVA for compressive strength of class F fly ash-based geopolymers

	Mean value		F value		P value	
Factors	FS	PC	FS	PC	FS	PC
Model	1.55	1.01	78.26	16.16	<0.0001	<0.0001
Molarity-A	0.46	2.57	22.93	41.32	0.0001	<0.0001
$Na_2SiO_3/NaOH$-B	0.15	0.24	0.75	3.82	0.3984	0.0724
Temperature-C	0.063	0.064	3.18	1.04	0.0914	0.3275
A^2	0.13	2.66	6.68	42.79	0.0187	<0.0001
B^2	0.044	0.52	2.21	8.44	0.1548	0.0123
C^2	0.46	0.58	23.10	9.26	0.0001	0.0094

trend is observed for sodium silicate to sodium hydroxide ratio. The reason behind this is that at a sustained high temperature of 90 °C, with increase in sodium silicate to sodium hydroxide ratio and molarity of NaOH, the geopolymerization process is enhanced, and as a result, the polymerization products will get filled in the void space which makes the matrix dense and stiff, which increases dry density and hence compressive strength. With further increase in temperature or exposure to sustained high temperature, the formation of micro-cracks results in lowering compressive strength. From Fig. 6, it is evident that clay filled flood soil and paddy clay show better strength performance in class F fly ash-based geopolymers, which is attributed to the Si/Al ratio of class F fly ash which enhances polymerization process at elevated temperature [6, 7].

Increment in compressive strength is generally attributed to the amount of reactive silica in clay which helps in geopolymerization at a high temperature of 90 °C for all combinations of molarity of NaOH solution and ratio of sodium silicate to sodium hydroxide [8, 9]. The presence of reactive silica in both clays is evident from the XRD results. Further, strength can be achieved through treating the clay by calcination or using lime, by which the crystalline phase of silica in clay can be converted to amorphous [6]. In highly plastic soil, clay particles absorb majority of alkaline solution, and hence, the strength gain becomes unnoticeable. Strength of geopolymer is affected by specific surface area of clay particles [8].

4 Conclusion

Based on the experiments carried out in the present study, the following conclusions are drawn;

a. It is revealed that low grade clay can be employed as source material for the synthesis of geopolymers in fly ash (both class C and class F)-based geopolymers by partial replacement of fly ash. Performance of clay minerals and hence

the mechanical properties of geopolymers can be further improved by lime and thermal stabilization of clay.

b. Molarity of NaOH solution and percentage of clay are the significant factors that affect strength parameters of geopolymer mortar. Compressive strength increases with increase in molarity of NaOH solution and ratio of sodium silicate to sodium hydroxide to an optimum value and then decreases at 50% replacement of class C and class F fly ash with different types of clay.

c. The compressive strength obtained was in the range of 5–9.5 MPa at 50% clay, which is expected to increase by lowering the clay percentage. The optimum mix was obtained at sodium silicate to sodium hydroxide ratio of 1.5 and NaOH molarity of 8 M. Paddy clay exhibited better performance in terms of compressive strength than flood soil in both class F and class C fly ash.

d. The optimum mix obtained can be used for developing alkali-activated blocks for constructing non-structural members such as compound walls and garden tiles and also as repair material for filling cracks and patchworks on RC structures. The scope of this study in developing structural members can be explored by lowering clay percentage and by thermal and chemical treatment.

References

1. Vora, P.R., Dave, U.V.: Parametric studies on compressive strength of geopolymer concrete. Procedia Eng. **51**, 210–219 (2013)
2. Ming, L.Y., Yong, H.C.: Structure and properties of clay based geopolymer cements: a review. Prog. Mater. Sci. **83**, 595–629 (2016).
3. Buchwad, A., Hohann, M.: The suitability of thermally activated illite/smectite clay as raw material for geopolymer binder. Appl. Clay Sci. **46**, 300–304 (2009)
4. Pavithra, P., Srinivasula Reddy, M.: A mix design procedure for geopolymer concrete with fly ash. J. Cleaner Prod. **133**, 117–125 (2016)
5. Oh, J.E., Jong, Y., Jeong, Y.: Characterization of geopolymers from compositionally and physically different class F fly ashes. Cem. Concr. Compos. **50**, 16–26 (2014)
6. Ogundiran, M.B.: Synthesis of fly ash calcined clay geopolymers: reactivity, mechanical strength, structural and microstructural characteristics. Appl. Clay Sci. **125**, 450–457 (2016)
7. Duxson, P., Provis, J.: Designing precursors for geopolymer cements. J. Am. Ceram. Soc. **91**(12), 3864–3869 (2008)
8. Priyadershini, P., Ramamurthy, K., Robinson, R.G.: Excavated soil waste as fine aggregate in fly ash based geopolymer mortar. Appl. Clay Sci. **146**, 81–91 (2017)
9. Xu, H., Van Deventer J.S.J.: The geopolymerization of aluminosilicate minerals. Int. J. Miner. Process. **59**, 247–266 (2000)
10. Ogundiran, M.B., Kumar, S.: Synthesis and characterization of geopolymer from Nigerian clay. Appl. Clay Sci. **108**, 173–181 (2015).

Alkaline Activation of Blended Cements with Calcined Illitic Clay Using Glass Powder Wastes

Mónica A. Trezza, Edgardo F. Irassar and Viviana F. Rahhal

Abstract Previous studies revel that calcined illitic clay acts as potentially supplementary cementitious materials in Portland cement. Packing and workability are improved; the hydration products are like that corresponding to Portland cement and it also produces a pore size refinement improving the mechanical performance at later ages. The illitic clays have a high activation temperature and its pozzolanic activity is slow; however, it is the most abundant type of clay in several regions of the world, and therefore, their used as supplementary cementitious materials must be improved. Therefore, compression resistance values denote the effect of dilution at early ages. On the other hand, materials containing silica and alumina can be activated in an alkaline form, which would help to compensate the dilution generated by the addition. In this work, the alkaline activation of cement mixtures with calcined illitic clays is presented. As an alkaline activator, finely ground discarded glass is used. The finely ground glass, due to its amorphous nature, reacts quickly contributing to early hydration, while providing the alkalis necessary for an alkaline activation. In this paper, the blended cements with 30% of calcined illitic clays were analyzed and the effect of different percentages of replace by glass powder wastes was studied.

Keywords Illite clay · Blended cements · Glass powder · Hydration · Calorimetric

1 Introduction

High grade calcined kaolinitic clays as supplementary cementitious materials (SCM) to ordinary Portland cement are widespread recommendation to reduce CO_2 emission. But there are not abundant; as a consequence, several studies have been carried out on different types of clays to know their thermal behavior and to analyze their potential use as pozzolanic addition in cement industry.

When calcined clay is incorporated to blended cements, several simultaneous effects occur such as filler and dilution effects and pozzolanic reactions that improve

M. A. Trezza (✉) · E. F. Irassar · V. F. Rahhal
Facultad de Ingeniería, CIFICEN (UNCPBA-CONICET-CICPBA), Av. del Valle 5737, Olavarría, Argentina
e-mail: mtrezza@fio.unicen.edu.ar

the cement-based material. The main shortcoming of these SCM is the large water demand [1].

Among the natural clays, illite clays conserve the order of their structure layers despite the thermal treatment, even after dehydroxylation [2]. As a consequence, illitic clays have a high activation temperature. But considering the abundance of illitic clays in several regions of the world, in recent years, their potential use as SCM in blended cements has been widely investigated [3–6].

The illite is a clay mineral from the group of hydrated micas; they differ from micas by having silicon substituted by aluminum and part of these ions displaced by iron or magnesium ions, by containing water and having part of the potassium substituted by calcium and magnesium [7].

Previous works [3–6] have allowed to know the thermal behavior of these clays and to determine the optimum calcination temperature for their use as SCM. When calcined clays are used as SCM in blended cements, they act in two different ways during hydration: as filler in the first ages and later as a pozzolanic addition. It has been demonstrated that the pozzolanic contribution of calcined illitic clays is moderate and delayed in time with respect to other clays, especially kaolinitic ones. Therefore, compressive strength values denote the effect of dilution at early ages.

On the other hand, alkaline activation is a technology that has been used for a long time [8–10] for the formulation of alkaline cements based on slag and fly ash (containing reactive species as SiO_2 and Al_2O_3), from alkaline solutions specially designed for that purpose. However, waste materials such as glass that containing alkalis and they are not totally recycled or are used in other industries [11] can also be used. The finely ground glass, due its amorphous nature, reacts quickly contributing to early hydration, while providing the alkalis necessary for an alkaline activation. The application of this technology, in addition to promoting the use of waste and/or industrial by-products as raw materials, reduces energy consumption and the levels of emissions.

In this paper, blended cements with 30% of calcined illitic clays were analyzed and the effect of different percentages of replace by glass powder wastes (between 5 and 30%) was studied. The early hydration was described by calorimetric isothermal conductivity test, and the performance of blended cements mortars was evaluated by fluidity test and by measurement of compressive strength. The pozzolanicity activity of each mixture was evaluated by the Frattini test at different ages.

2 Materials and Methods

An ordinary Portland cement (PC), calcined illitic clay (IC) and ground white bottle glass were used. The glass was ground until retained on sieve 45 µm (# 325) was less than 12%, using a laboratory ball mill. The IC was calcined al 950 °C for this activation and then was ground until retained on sieve 45 µm (# 325) was less than 12%.

The chemical composition of materials was determined by inductively coupled plasma atomic emission spectroscopy (ICP-AES) analysis in an external laboratory (ALS, Argentine). The mineralogical composition was identified by X-ray diffraction (XRD) using a Philips PW 3710 diffractometer operating with Cu Kα radiation at 40 kV and 20 mA. The size distribution curves were determined using Malvern Mastersizer 2000 laser particle size analyzer, and the d90, d50 and d10 diameters were calculated.

The reference clay blended cement was made in proportion 30:70 (IC:PC) and then the IC was replaced in 5–30% by mass by glass powder (GP). The name given to each sample was: CIG0 (the reference, with 70% of PC, 30% of IC and 0% of GP), CIG5, CIG10, CIG15, CIG20, CIG25 and CIG30, being 5–30 the replacement percentages of the illite calcined clay by the ground glass, respectively.

The heat evolution rate and the cumulative heat released during the early hydration (first 48 h) of different pastes with water/cementitious material ratio of 0.5 (w/cm = 0.5) were registered by isothermal conduction calorimetry at 20 °C.

Pozzolanic activity was determined by Frattini test according to the procedure described in EN196-5 at 2, 7 and 28 days. This test evaluates the pozzolanic activity of blending cements measuring its reaction with the $Ca(OH)_2$ released during the cement hydration. The result is considered positive when the points are located below the calcium hydroxide solubility isotherm at 40 °C.

The workability of mortar was determined using the flow table test according to ASTM C1437 as the diameters of spread mortar measured along four lines and expresses in percentage. Mortars were cast in 40 × 40 × 160 mm molds and then compacted in two layers, covered with plastic sheet to prevent water loss and stored at 20 ± 2 °C. Standard siliceous sand and w/cm = 0.50 were used. After 24 h, specimens were removed from the molds and tightly covered with plastic sheets and stored until the test age was reached. From different blended cements, the compressive strength was determined at 2, 7, 28 and 90 days. The reported results are the average of six compression tests.

3 Results and Discussion

3.1 Characterization of Materials

The chemical composition and physical properties of the raw materials are presented in Table 1. The mineralogical composition of the cement is: 63.6% C3S, 15.1% C2S, 2.8% C3A and 15.0% C4AF. The predominant mineral in clay is illite (75.4%) and quartz (23.0%) [3]; the whole set is impregnated with iron oxide that determines the color of calcined clay, being classified as a ferruginous shale [12]. The glass was obtained from discarded bottles. Both IC and GP have higher specific surface than PC and lower density.

Table 1 Chemical composition and physical properties of materials

	SiO$_2$	Al$_2$O$_3$	CaO	Fe$_2$O$_3$	Na$_2$O	K$_2$O	SO$_3$	MgO	LOI
PC	20.41	3.86	63.30	4.50	0.16	0.85	2.28	0.70	3.26
IC	66.30	16.28	0.33	9.23	0.08	5.60	–	1.46	0.58
GP	70.91	1.55	10.75	0.26	13.80	0.89	0.21	0.10	1.14
Physical Properties					PC		IC		GP
Density (g/cm^3)					3.13		2.58		2.50
Specific surface (m^2/kg)					354		552		609
Particle size distribution (μm)				d90	60.7		35.6		24.6
				d50	18.7		7.4		7.5
				d10	2.7		1.3		1.6

3.2 Calorimetry Studies

Figure 1 plots the rate of heat release (dQ/dt) as a function of time during the first 48 h of hydration and Table 2 shows a summary of the singular points for the PC and CIG0, CIG15 and CIG30 samples.

At the beginning of hydration, the heat release rate of PC is high and then decreases reaching the first minimum at 140 min with an intensity of 0.22 mW/g. All the other samples needed greater times until they reach the first minimum (between 140 and 150 min) and have lower intensities (from 0.18 to 0.16 mW/g).
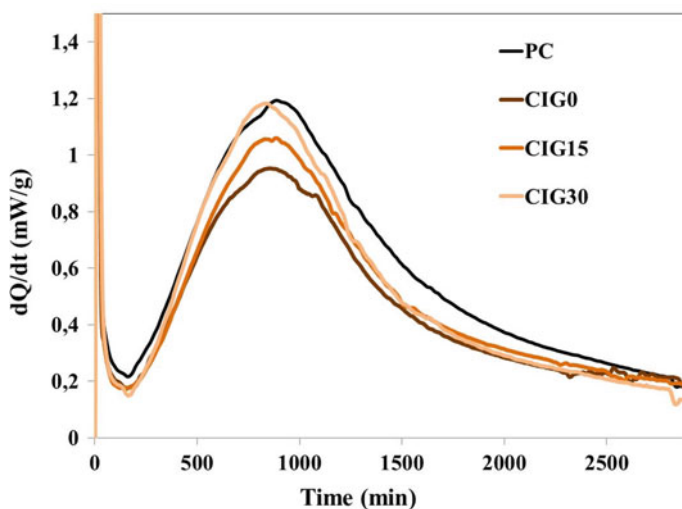
Fig. 1 Rate of heat release (dQ/dt) for PC, CIG10, CIG20 and CIG30 samples, during the first 48 h of hydration

Table 2 Singular points and total heat

Samples	1st minimum		2nd maximum		Qt (J/g)
	Age (min)	Intensity (mW/g)	Age (min)	Intensity (mW/g)	
PC	140	0.22	875	1.19	102.03
CIG0	140	0.18	850	0.95	83.95
CIG15	145	0.17	840	1.05	87.67
CIG30	150	0.16	820	1.18	92.07

These differences are mainly because of dilution generated by the replacement. Less cement particles require more time to saturate the pore solution and to resume the hydration reactions. Since the total replacement level is always 30%, the IC/GP combination shows that the higher the content of calcined clay, the intensity of the first minimum increases and as the content of GP increases, increases the time in which this occurs.

Hydration continues with the formation of calcium silicate hydrate and with an increase in the intensity, reaching the second maximum for PC at 875 min with an intensity of 1.19 mW/g. The samples CIG0–CIG30 reach it before (between 820 and 850 min $\approx$ 14 h) and with lower intensities (from 0.95 to 1.18 mW/g).

The IC/GP combination shows that as the content of IC increases, the intensity of the second maximum decreases and as the content of GP increases decreases the time that it occurs. The two additions stimulate the hydration of the cement, but GP does it with greater intensity, possibly by the liberation of alkalis (Na_2Oeq: 14.39% the ground glass and 3.76% the calcined clay).

At this moment, the parameters that can be related are: (a) the end of setting time, which should be lower than of PC and decrease with the increase in GP content; (b) the $[OH^-]$ measured at the first hours following the methodology of Frattini test (see point 3.4), which should be greater than that of the PC and increase with the content of GP.

Table 2 also shows that the total heat released during the first 48 h of hydration of the CIG samples, although it is lower than that of the PC, in all cases, is greater than that corresponding to 70% of the PC (71.42 J/g), which shows the effect of early stimulation by the two additions, the greater being that generated by the ground glass.

This parameter can be related to: (a) the $[OH^-]$ measured at 24 and 48 h following the methodology of the Frattini test (see point 3.4), which should increase with the increment in the content of GP; (b) the compressive strength at two days, which should be greater than that corresponding to 70% of the PC.

The above mentioned shows the synergy between both additions that mildly stimulate early hydration; the incorporation of GP instead of IC improves the *Qt* in the first 48 h, which helps to reduce the dilution effect generated in the first ages.

3.3 Flow and Compressive Strength

The results of fluidity and compressive strength, in percentages relative to the PC mortar, are presented in Table 3 for all the mortars studied.

The flow value of the PC mortar was 125% and the strength values were: 18.6, 34.8, 46.6 and 53.7 MPa at the ages of 2, 7, 28 and 90 days, respectively.

Table 3 shows that the fluidity of mortars GIC0 to GIC30 is lower than that of PC mortar, and as the IC is replaced by GP, the fluidity decreases. However, the ratio w/cm remains constant and equals to 0.5 for all mortars, and both additions are not reactive at an early age.

This behavior may be due in part to the fact that the particles of IC, which replace those of PC and those of GP that replace the IC, have larger specific surfaces than PC and IC, respectively. Consequently, they require more water to wet the surface (see Table 1), leaving less water to act as a lubricant for the particles. To this must be added the lower density of the IC with respect to that of PC and that of GP with respect to that of IC (see Table 1).

Both effects (the smaller particle size and the lower density) contribute to the lower fluidity recorded by the mortars with replacements by IC at first and subsequently by GP.

Table 3 presents too, the results of compressive strength with respect to the PC mortar. In general, the resistance is greater than 70% of the resistance of the PC mortar at two days. This percentage increases with age, exceeding 75% at seven days and 100% at 28 and 90 days.

At two days, mortars with CIG0–CGI30 show compressive strength values affected firstly by the dilution due to the lower cement content and by the greater porosity caused by the increase in the effective w/c, which changes to 0.5 for the PC mortar at 0.71 for mortars CIG0–CIG30. Consequently, the expected resistance would be less than 70%, a fact that did not happen, but quite the opposite, which is consistent with the Qt reached by the pasta at the age of 48 h, as previously stated.

Table 3 Fluidity and compressive strength relative to PC mortar

Mortars	Flow (%)	Compressive strength (%)			
		Age (days)			
		2	7	28	90
PC	100	100	100	100	100
CIG0	93	77.4	86.4	101.3	109.8
CIG5	92	78.1	86.1	113.8	112.3
CIG10	89	73.7	82.9	109.4	109.7
CIG15	89	72.2	78.9	109.5	112.9
CIG20	89	80.6	86.3	107.4	120.0
CIG25	85	75.6	76.0	108.9	103.0
CIG30	82	68.6	75.2	107.9	101.4

After seven days, there was a considerable increase in the compressive strength overcoming the effect of dilution (all mortars had a compressive strength greater than 70% of the PC mortar). This effect can be attributed to the best packaging by the incorporation of particles of smaller sizes than those of cement (see Table 1), and chemical stimulation produced by the pozzolanic reaction of both: the IC and the GP.

At 28 and 90 days, the mortars CIG0–CIG30 reach and overcome the compressive strength of the PC mortar, showing a moderate pozzolanic activity of the IC, the normal pozzolanic activity of the GP and the synergy produced between both additions, especially in CIG20 (10% IC and 20% GP).

3.4 Pozzolanicity

The results of the Frattini test are shown in Fig. 2. The solubility isotherm of calcium hydroxide delimits the non-pozzolanic (above) and pozzolanic (below) response zones.

For the CIG0–CIG30 samples at early ages (12, 24 and 48 h), the values obtained in the Fratini test indicate a consumption of [CaO] by the pozzolanic reaction, although they are still located above the solubility isotherm (non-pozzolanic zone). They also show an increase in [OH$^-$] with age, due to the release of alkalis by both additions. The [OH$^-$] grows especially with the increase of GP.

This is consistent with the shorter time required by the pastes to reach the second maximum of the calorimetric curve as GP content increases.

From seven days, CIG0–CIG30 samples show positive results; that is, their representative points are located below the solubility isotherm; decreasing the [CaO] and increasing the [OH$^-$], both movements are recorded when the GP content increases. This confirmed the compressive strength results after seven days and the synergy between both additions.

In Fig. 3, it can be observed the alkalis released with ages, by GP principally and the CaO consumption by GP and IC with age, principally by GP.

4 Conclusions

With the materials and methodologies used in this work, can be concluded regarding the incorporation of GP as partial replacement of IC in blending cements that:

The heat released in the first hours of hydration, followed by isothermal conduction calorimetry, shows that the effects of dilution are only partially compensated with the early stimulation generated by the additions. The replacement of GP by IC increases the degree of compensation.
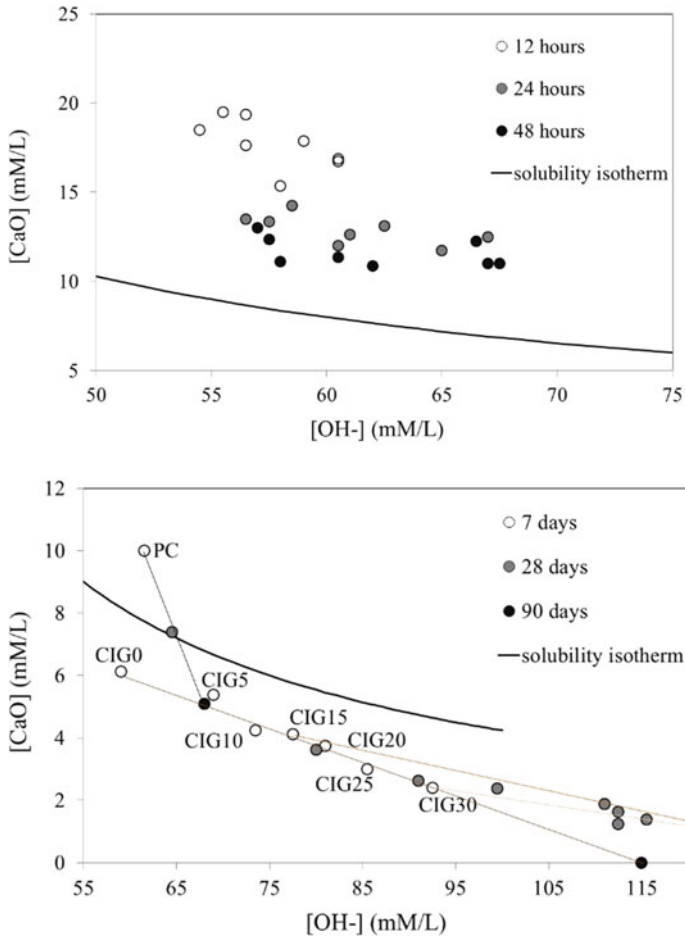
Fig. 2 Results of Frattini test at: 12, 24 and 48 h (up) and 7, 28 and 90 days (down)

The compressive strength at 28 days, of all mortars, exceeds the PC one. The replacement of GP by IC improves the values reached by CIG0 overcoming it by around 10% for GIG20.

The Frattini test from 12 h to 90 days shows, in addition to the pozzolanic activity, the alkali leaching from the GP, which contributes to the alkaline activation.

The replacement of GP by IC causes an additional stimulation of the hydration reactions of the PC and contributes along with the IC to the pozzolanic activity. This additional stimulation was attributed to the alkaline self-activation as consequence of alkali leaching from the GP.

Consequently, replacement percentages between 5% and no greater than 20% of GP by IC are adequate to improve the compressive strength, without excessive alkali release.
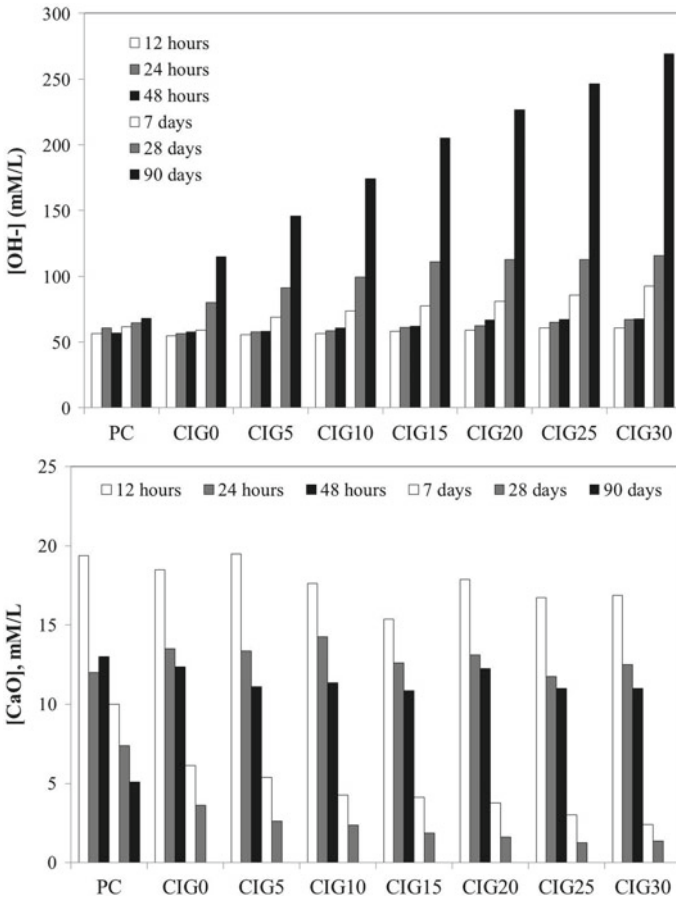
Fig. 3 Results of Frattini test: alkalis released (up) and CaO consumption (down)

References

1. Sabir, B.B., Wild, S., Bai, J.: Metakaolin and calcined clays as pozzolans for concrete: a review. Cem. Concr. Comp. **23**(6), 441–454 (2001). https://doi.org/10.1016/S0958-9465(00)00092-5
2. He, C., Osbaeck, B., Makovicky, E.: Pozzolanic reactions of six principal clay minerals: activation, reactivity assessments and technological. Cem. Concr. Res. **25**(8), 1691–1702 (1995). https://doi.org/10.1016/0008-8846(95)00165-4
3. Trezza, M.A, Tironi, A., Irassar, E.F.: Estabilidad térmica y actividad puzolánica de una arcillita illítica. Memorias VII Congreso Internacional- 21 RT- AATH, pp. 505–512 (2016)
4. Marchetti, G., Pokorny, J., Tironi, A., Trezza, M.A., Rahhal, V.F., PavlÍk, Z., Černý, R., Irassar, E.F.: Blended cements with calcinedillitic clay: workability and hydration. In: Martirena, F., Favier, A., Scrivener, K. (eds.) Calcined Clays for Sustainable Concrete. RILEM Bookseries, vol. 16, pp. 310–317. Springer, Dordrecht (2018). https://doi.org/10.1007/978-94-024-1207-9_50

5. Trezza, M.A., Tironi, A., Irassar, E.F.: Thermal activation of two complex clays (kaolinite-pyrophillite-illite) from tandilia system, buenos aires, argentina. In: Martirena, F., Favier, A., Scrivener, K. (eds.) Calcined Clays for Sustainable Concrete. RILEM Bookseries, vol. 16, pp. 469–474. Springer, Dordrecht (2018)
6. Lemma, R., Castellano, C.C., Bonavetti, V.L., Trezza, M.A., Rahhal, V.F., Irassar, E.F.: Thermal transformation of illitic-chlorite clay and its pozzolanic activity. In: Martirena, F., Favier, A., Scrivener, K. (eds.) Calcined Clays for Sustainable Concrete. RILEM Bookseries, vol. 16, pp. 266–272. Springer, Dordrecht (2018)
7. Biondolillo, M.P.: Manual para el ceramista. Cap. II: Mineralogía de las arcillas. Univ. Nac. de Cuyo-EdiUNC (2000)
8. Fernández, J.A., Puertas, F.: Alcali-activated slag cements: kinetic studies. Cem. Concr. Res. **27**(3), 359–368 (1997)
9. Robayo, R.A., Mulford, A., Munera, J., Mejía de Gutiérrez, R.: Alternative cements based on alkali-activated red clay brick waste. J. Con. Build. Mater. **128**, 163–169 (2016)
10. Puertas, F., Barba, A., Gazulla, M.F., Gómez, M.P., Palacios, M., Martínez, R.S.: Residuos cerámicos para su posible uso como materia prima en la fabricación de clinker de cemento Pórtland: caracterización y actividad alcalina. Mater. Constr. **56**(281), 73–84 (2006)
11. Trezza, M.A., Rahhal, V.F.: Comportamiento del residuo de vidrio molido en cementos mezcla: Estudio comparativo con microsílice. MATERIA, en prensa no vol. 23, no.1 (2018)
12. Maiza, P.J.: Informe Petrográfico de Arcillas. Dpto. de Geología, Universidad Nacional del Sur, Argentina (2016)

Why Low-Grade Calcined Clays Are the Ideal for the Production of Limestone Calcined Clay Cement (LC^3)

Sreejith Krishnan, D. Gopala Rao and Shashank Bishnoi

Abstract Clinker substitution by a combining multiple supplementary cementitious materials has been established as the most promising solution for combating the greenhouse gas emissions from the cement industry. Limestone calcined clay cement is a ternary cement in which clinker is partially replaced using calcined clay and limestone. This paper discusses the importance of using low-grade kaolinite clay for producing limestone calcined clay cements. While it appears that higher grade clay would be more beneficial at higher substitution levels, it is seen that the availability of portlandite becomes the limiting factor in LC^3 cements having low clinker factors. Additionally, the reduction in the long-term clinker hydration, which has been reported in LC^3 systems, is not observed in the presence of low-grade kaolinite clay.

1 Introduction

Recent studies have highlighted the importance of developing sustainable alternatives to ordinary Portland cements to mitigate greenhouse gas emissions from the cement industry [1–3]. Decomposition of limestone in the rotary kiln is the major source of carbon dioxide emission during the production of clinker. Hence, partially replacing clinker with supplementary cementitious materials (SCMs) such as calcined clay or fly ash has emerged as a promising solution to produce sustainable cements. Considering the significant demand for cement, it is important to choose SCMs that are available in sufficient quantities worldwide. Calcined clay and limestone appear to be the favourable choices for partial clinker replacement due to their widespread availability [4, 5]. It has been reported that the presence of high levels of clinker substitutions can be achieved by combining limestone and calcined clay (also known as limestone calcined clay cement or LC^3). LC^3 having a composition of 50% clinker, 30% calcined clay, 15% limestone and 5% gypsum has been widely investigated by various researchers [6–10].

S. Krishnan (✉) · D. Gopala Rao · S. Bishnoi
Department of Civil Engineering, IIT Delhi, New Delhi, India

One of the significant advantages offered by ternary cement blends is the ability to customize the blend composition depending on the end-user requirements. There are various factors that can be modified, such as the clinker factor, grade of the kaolinite clay, the type of limestone, etc. that can be optimized to produce an LC^3 blend with desirable properties. Generally, it is believed that using higher grade calcined clay would be beneficial while producing blended cements. This paper tries to highlight why using lower-grade clays would be beneficial for producing limestone calcined clay cements.

2   Why Lower-Grade Clays?

High levels of clinker substitution levels can be achieved in LC^3 systems due to the synergy between clinker, calcined clay and limestone. The fast pozzolanic reaction of the calcined clay improves the early age strength development in the LC^3 despite having lower clinker factors. The reaction of limestone leads to the formation of carboaluminate phases that prevent the transformation of ettringite to monosulphate, leading to improve space filling by the hydration products. Both the reactions can be combined into a single equation, as shown in Eq. 1. It should be noted that the composition of the C-A-S-H gel formed in the system was measured using SEM–EDS analysis, and this composition can vary depending on various parameters such as alkali content, clinker factor, etc. [11, 12].

$$0.5AS_2 + 2.75CH + 0.38Cc + 5.43H \rightarrow C_{1.61}A_{0.12}SH_4 + 0.38C_4AcH_{11} \quad (1)$$
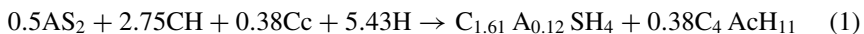
In most LC^3 systems, the availability of portlandite is the limiting factor. Hence, the optimum composition is considered to be the one where the entire portlandite is consumed in the reaction with calcined clay and limestone, leaving behind no unreacted metakaolin. This also becomes important in case of lower clinker factors, since the availability of portlandite is directly dependent on the amount of clinker present in the systems as well as the degree of hydration of clinker phases. Table 1 shows the details of three LC^3 blends have clinker factor of 0.55, 0.70 and 0.85. The cements were prepared using a clinker having 48.1% C3S, 29.4% C2S, 4.34% C3A and 17.67% C4AF. The calcined clay used for preparing these blends contained approximately 56.5% amorphous content. The compressive strengths of the three blends are shown in Table 2.

Table 1 Details of LC^3 blends having different clinker factor

S. No.	Blend name	Cement (%)	Calcined clay (%)	Limestone (%)
1	LC^3-55	55	30	15
2	LC^3-70	70	20	10
3	LC^3-85	85	10	5

Table 2 Compressive strengths of LC^3 blends having different clinker factors

Blend name	7 days (MPa)	28 days (MPa)	90 days (MPa)
LC^3-55	34	41.2	43
LC^3-70	31.1	42.4	43.7
LC^3-85	30.7	41	45.2

It is interesting to observe that, despite the differences in clinker factors, the strength development in all the three LC^3 blends is similar. The reason for these trends become clearer when examining the amount of portlandite remaining in these systems at different ages (Fig. 1). In the LC^3-55 system, the no significant amount of portlandite is observed after three days, whereas, in LC^3-70 system, a gradual reduction of the portlandite is seen until 90 days. This indicated that the pozzolanic reaction continues in the LC^3-70 system even up to 90 days. However, the portlandite content was observed to increase continuously in the LC^3-85 system, which indicates that the pozzolanic reaction in this system is completed by three days. It should be once again noted here that the calcined clay contains only 56.5% amorphous content. Therefore, the actual reactive content from calcined clay in LC^3-85, LC^3-70 and LC^3-55 was 16.95%, 11.3% and 5.65%, respectively. This suggests that using higher grade clay would be beneficial in the case of LC^3-85 for obtaining higher compressive strengths. This would be beneficial in completely consuming the portlandite available in this system. On the other hand, utilizing lower-grade clay would be beneficial in the LC^3-55 since there is not enough portlandite forming in this system to completely consume the available metakaolin from the calcined clay.

Table 3 shows the details of three LC^3-55 blends produced using different grades calcined clay. The numbers in the bracket correspond to the amount of reactive metakaolin present in the calcined clays. Figure 2 shows the compressive strength development in LC^3-55 blends produced with different grades of clays. The influence

Fig. 1 The amount of portlandite present in the different LC^3 systems estimated using QXRD
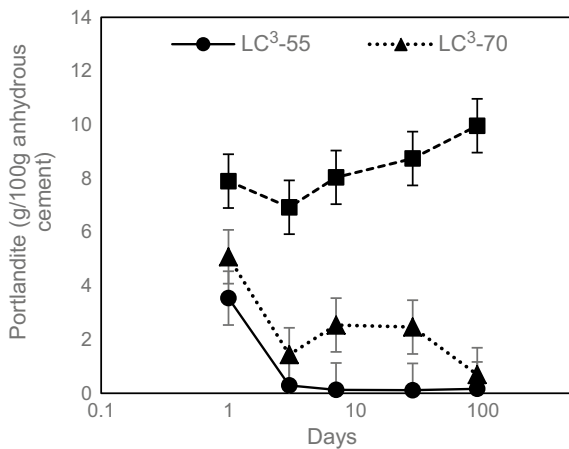
Table 3 Details of LC^3-55 blends having produced with different grades of calcined clays

S. No.	Blend name	Cement (%)	Calcined clay (%)	Limestone (%)	Quartz (%)
1	LC^3-55(27%)	55	30	15	0
2	LC^3-55(56.5%)	55	30	15	0
3	LC^3-55(80%)	55	30	15	0
4	LC^3-55(Q:L)	55	0	15	30
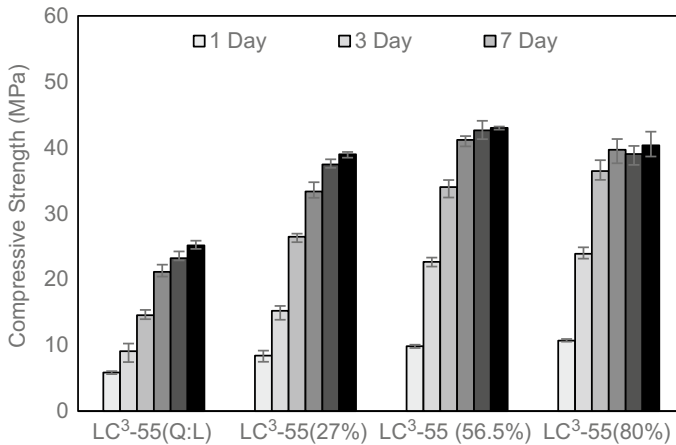
Fig. 2 The compressive strength development in the LC^3 blends prepared with different grades of kaolinite clay

of calcined clay in improving the compressive strengths in LC^3 systems is clearly seen in the strength results. Even when a lower-grade calcined clay is used, which was the case in LC^3-55(27%), the seven-day compressive strength was greater than the 90 days strength of LC^3-55(Q:L). The impact of having higher grade calcined clay in the LC^3 appears to be limited to the early ages (up to seven days). This is very apparent in the compressive strength at three and seven days, with an increase of nearly 30% in strength when higher grade calcined clay is used. Higher strengths were observed for LC^3-55(56.5%) and LC^3-55(80%) up to 28 days when compared to LC^3-55(27%), but the 90-day strengths were similar and within 10% value of each other. From the trends observed, it is clear that the grade of calcined clay appears to affect the rate at which strength development takes place in LC^3-55 systems and not the ultimate strength itself. The addition of the higher grade calcined clays improves the strength at initial ages, but the final age strengths are very similar across the three blends.

Once again, the reason for such a trend appears to be the additional clinker hydration observed in the LC^3-55 (27%) compared to other two blends where clinker hydration remains more or less same from 28 to 90 days (Fig. 3). This is also reflected

Fig. 3 The degree of hydration of belite in the LC³ blends with different grade of kaolinite clays estimated using QXRD
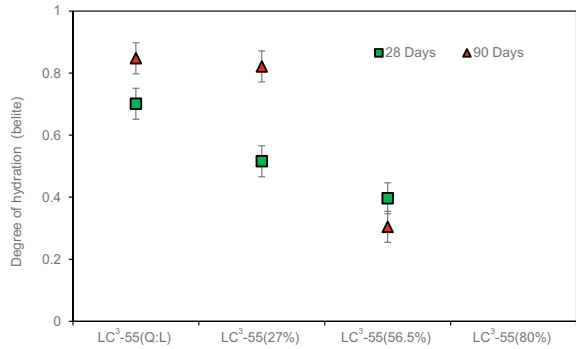
in the strength development trends, where only a marginal strength gain was observed from 28 to 90 days in LC³ blends with higher grade clays. It should be noted here that the 90-day strength of LC³-55 (80%) was slightly lower than LC³-55 (56.5%), but the difference in strengths was still within 10% variation. From the compressive strength results, it is clear that use of higher grade clay may not translate into higher compressive strengths.

3 Conclusions

It is clear that using lower-grade clay would be beneficial in blended cements. This is especially critical in the case of blended cements having low clinker factors since the availability of portlandite becomes the limiting factor in these systems. Additionally, it is also seen that higher grade clay also reduces the long term hydration of clinker phases. Therefore, using higher grade clay leads to inefficient clinker utilization in low clinker cements. Such a reduction was not observed when lower-grade clay was used. The later age compressive strengths were observed to be similar in the LC³ blends studied irrespective of the grade of calcined clay used. However, higher grade clay can be used in blends with higher clinker factors so as to completely consume the portlandite.

References

1. Gartner, E.: Industrially interesting approaches to "low-CO_2" cements. Cem. Concr. Res. **34**, 1489–1498 (2004). https://doi.org/10.1016/j.cemconres.2004.01.021
2. Gartner, E., Sui, T.: Alternative cement clinkers. Cem. Concr. Res. (2018)
3. Imbabi, M.S., Carrigan, C., McKenna, S.: Trends and developments in green cement and concrete technology. Int. J. Sustain. Built Environ. **1**, 194–216 (2012). https://doi.org/10.1016/j.ijsbe.2013.05.001
4. Krishnan, S., Emmanuel, A.C., Shah, V., et al.: Industrial production of limestone calcined clay cement: experience and insights. Green Mater. **7**, 15–f LC (2019)
5. Scrivener, K., Martirena, F., Bishnoi, S., Maity, S.: Calcined clay limestone cements (LC^3). Cem. Concr. Res. **114**, 49–56 (2018). https://doi.org/10.1016/j.cemconres.2017.08.017
6. Antoni, M., Rossen, J., Martirena, F., Scrivener, K.: Cement substitution by a combination of metakaolin and limestone. Cem. Concr. Res. **42**, 1579–1589 (2012). https://doi.org/10.1016/j.cemconres.2012.09.006
7. Krishnan, S., Kanaujia, S.K., Mithia, S., Bishnoi, S.: Hydration kinetics and mechanisms of carbonates from stone wastes in ternary blends with calcined clay. Constr. Build. Mater. **164**, 265–274 (2018). https://doi.org/10.1016/j.conbuildmat.2017.12.240
8. Krishnan, S., Emmanuel, A.C., Bishnoi, S.: Hydration and phase assemblage of ternary cements with calcined clay and limestone. Constr. Build. Mater. **222**, 64–72 (2019). https://doi.org/10.1016/j.conbuildmat.2019.06.123
9. Krishnan, S., Bishnoi, S.: Understanding the hydration of dolomite in cementitious systems with reactive aluminosilicates such as calcined clay. Cem. Concr. Res. **108**, 116–128 (2018). https://doi.org/10.1016/j.cemconres.2018.03.010
10. Dhandapani, Y., Santhanam, M.: Assessment of pore structure evolution in the limestone calcined clay cementitious system and its implications for performance. Cem. Concr. Compos. **84**, 36–47 (2017). https://doi.org/10.1016/j.cemconcomp.2017.08.012
11. Dai, Z., Tran, T.T., Skibsted, J.: Aluminum incorporation in the C-S-H phase of white portland cement-metakaolin blends studied by 27 Al and 29 Si MAS NMR spectroscopy. J. Am. Ceram. Soc. **97**, 2662–2671 (2014). https://doi.org/10.1111/jace.13006
12. Avet, F., Boehm-Courjault, E., Scrivener, K.: Investigation of C-A-S-H composition, morphology and density in Limestone Calcined Clay Cement (LC^3). Cem. Concr. Res. **115**, 70–79 (2019). https://doi.org/10.1016/j.cemconres.2018.10.011

The Effect of Calcite in the Raw Clay on the Pozzolanic Activity of Calcined Illite and Smectite

Tobias Danner, Geir Norden and Harald Justnes

Abstract The pozzolanic reactivity of four calcined natural clays (two being rich in illite and two being rich in smectite) was investigated by means of 28 days compressive strength of mortars and calcium hydroxide (CH) consumption in pastes of calcined clay and CH. The materials were characterized by XRD, XRF, BET, SEM and TG/DTG. Hydrated pastes of clay and CH were investigated by means of XRD, DTG and SEM. Besides clay minerals, two of the investigated raw clays contained 15 and 25% calcite, respectively. At optimum calcination temperature, calcined clays containing smectite and calcite, and illite and calcite in the raw clay had higher pozzolanic reactivity than clays containing smectite and illite alone. Results indicate that in clays containing high amounts of calcite, the formation of a glass phase upon calcination contributes to the pozzolanic reactivity.

Keywords Clay · Illite · Smectite · Calcite · Pozzolanic reactivity

1 Introduction

Depending on clay mineralogy, calcination of clays between 600 and 900 °C leads to the formation of amorphous or disordered metastable phases with high pozzolanic activity [1]. The pozzolanic activity usually increases in the order illite, smectite, kaolinite. Additionally, recent studies showed that the coupled substitution of cement by blends of calcined clay and limestone allows for total substitution levels up to 45% due to a strong synergetic effect [2, 3]. On the other hand, only few studies covered investigations on natural clays already containing high amounts of calcium carbonate before calcination. A recent study showed that marl (47% calcium carbonate in the raw material) can be a good pozzolanic material when calcined between 400 and 800 °C [4]. Calcareous clay is often regarded as not suitable for the production of burnt clay products (e.g., bricks and lightweight aggregate) due to concerns about

---

T. Danner (✉) · H. Justnes
SINTEF Building and Infrastructure, 7034 Trondheim, Norway
e-mail: tobias.danner@sintef.no

G. Norden
Leca International, Årnesvegen 1, 2009 Nordby, Norway

the decomposition of $CaCO_3$ to CaO after burning. During service, CaO may react with moisture to form $Ca(OH)_2$ which can result in so-called pop outs. Thus, these types of clays are not yet exploited by other industries and can serve as a large SCM resource to produce blended cements.

Results from the following investigations indicate that calcite impurities in the raw clay can increase the pozzolanic activity of otherwise low reactive smectite and illite clays.

2   Materials

Tables 1 and 2 show the bulk mineralogy of crystalline phases of the raw clays before calcination and the chemical composition of the different clays calcined at 800 °C, respectively. Two of the investigated clays are rich in smectite (Sm) while the other two investigated clays are rich in illite (Ill). All clays contain carbonate minerals (calcite, dolomite, siderite) while two of the investigated clays contain considerable higher amounts of calcite than the others (Sm-Ca and Ill-Ca). There are additional differences in the amount of other clay and non-clay minerals.

Calcium hydroxide (CH) used in pastes with calcined clay was of laboratory grade. The cement used in mortar tests was a CEM I 42.5 R.

For artificial pore water, potassium and sodium hydroxide of analytical grade were mixed with water. The artificial pore water used in pastes of calcined clay and CH had a pH of 13.2 and a KOH:NaOH ratio of 2:1.

Table 1 Mineralogical composition of raw clays before calcination

	Sm	Sm-Ca	Ill	Ill-Ca
Kaolinite (%)	1.0	8.4	5.2	8.0
Smectite (%)	42.5	53.5	0.2	2.0
Illite (%)	5.6	4.4	39.6	33.0
Chlorite (%)	1.0	–	9.1	–
Quartz (%)	32.6	4.3	17.1	22.0
K-feldspar (%)	8.2	–	4.8	4.0
Plagioclase (%)	–	–	6.5	4.0
Calcite (%)	4.6	24.7	2.8	15.0
Siderite (%)	4.4	3.1	–	–
Dolomite (%)	–	–	–	4.0
Pyrite (%)	–	1.3	–	–
Hematite (%)	–	–	14.7	–
Goethite (%)	–	–	–	8.0

Table 2 Chemical composition of the clays calcined at 800 °C

Oxide (%)	Sm	Sm-Ca	Ill	Ill-Ca
SiO_2	61.4	48.7	56.1	57.4
Al_2O_3	19.5	17.8	20.1	15.7
Fe_2O_3	6.9	10.4	9.9	8.0
CaO	3.2	13.8	1.1	9.2
K_2O	3.1	2.4	5.0	3.9
Na_2O	0.1	0.7	–	0.2
MgO	3.0	2.8	5.0	3.1
TiO_2	1.1	1.0	0.9	0.8
LOI (1100 °C)	1.7	2.4	1.1	1.7

3　Methods

The raw clays were calcined in a pilot-scale natural gas heated rotary kiln at IBU-Tec advanced materials AG (Weimar, Germany) with a residence time of 45 min. In earlier investigations, the clays were calcined at different temperatures between 600 and 1100 °C and their pozzolanic reactivity was investigated in dependence of the temperature [5, 6]. Although the calcination temperature of highest pozzolanic reactivity can depend considerably on the clay mineralogy, Sm, Sm-Ca, Ill and Ill-Ca, all showed their highest pozzolanic reactivity close to 800 °C [5].

Qualitative *X-ray diffraction (XRD)* was performed on a Bruker D8-Advance equipped with a Lynx Eye detector and a Cu-Kα X-Ray source. A fixed divergence slit of 0.2 mm was used. Measurements were taken from 5°–65° 2θ with a step size of 0.2° 2θ and a step time of 1 s. Quantitative Rietveld analysis of the raw clays was performed as described in [6].

X-ray fluorescence (XRF) was performed on molten glass disks with a Bruker AXS S8 Tiger WDXRF with a 4 kW generator.

BET specific surface area was measured with a Micromeritics Tristar 3000. Prior to analysis, the samples were degassed.

Scanning electron microscopy (SEM) was performed on a JEOL JXA-8500F electron probe microanalyzer (EPMA) equipped with five wavelength dispersive X-ray spectrometers (WDS) and an energy dispersive X-ray spectrometer (EDS). Samples were cast in epoxy resin, polished and surface coated with carbon. Analysis was done in backscattered electron imaging (BEI) modus with an accelerating voltage of 15 kV.

Thermogravimetric analysis (TGA) was performed with a Mettler Toledo TGA/SDTA 851. The powdered paste samples were analyzed with a heating rate of 10 °C/min between 40 and 1100 °C. All measurements were performed in nitrogen atmosphere with a flow rate of 50 ml/min. The CH consumption in pastes after 28 days of hydration was calculated from the weight loss temperature interval of CH decomposition using the horizontal tangents method.

Pozzolanic activity was tested according to an internal SINTEF procedure. Calcined clay and CH were mixed in a ratio of 1:1 with water to binder ratio of 0.9. Artificial pore water was used as mixing water and pastes were mixed for 1 min by hand with a plastic spatula. The mixed pastes were stored sealed at 20 °C for 28 days. The hydration of the pastes was stopped by crushing the samples to a fine powder and washing it several times in ethanol. After filtration, the samples were dried at about 35% relative humidity (RH) in a closed desiccator upon $CaCl_2$ saturated water.

Compressive strength of mortars was tested with 20% substitution of Portland cement (PC) by calcined clay according to NS-EN 196-1. The water to binder ratio (w/b) was held constant at 0.5 in all mortar mixes and the consistency was determined using a flow table. To keep the flow within ±5% of the reference mortar, the consistency was adjusted with superplasticizer when necessary. The mortar mixes were cast in three $40 \times 40 \times 160$ mm molds and stored in a cabinet for 24 h at 23 ± 2 °C and 90% RH. After 24 h, the mortar prisms were removed from the molds and stored in saturated CH water for 28 days.

4   Results and Discussion

4.1   Changes upon Calcination

The mineralogical changes of all investigated clays upon calcination are documented in detail in [5]. At 800 °C, all clay minerals were completely dehydroxylated and smectite and kaolinite were transformed to metastable phases. Illite, on the other hand, showed still a distinct peak in the XRD diffractograms of the clays indicating an incomplete breakdown of the structure [5]. Increased background observed in XRD diffractograms after calcination indicated higher amorphization of samples Sm-Ca and Ill-Ca compared to Sm and Ill. XRD and FT-IR analysis showed that in sample Sm-Ca, small amounts of undecomposed calcite (3–5%) were left after calcination at 800 °C [5, 6].

A typical difference between the samples containing high and low amounts of calcite was the formation of a glass phase upon calcination in samples with high calcite content (Fig. 1). Figure 1 shows the BEI images of Sm-Ca and Ill-Ca before and after calcination. The formation of a glass phase after calcination at 800 °C was not observed in samples Sm and Ill with only small amounts of calcite in the raw clay.

The formation of a glass phase in calcite containing clays was also observed in other studies [7, 8]. Due to the formation of the glass phase, the BET surface area decreased significantly for samples Sm-Ca and Ill-Ca upon calcination (Table 3).
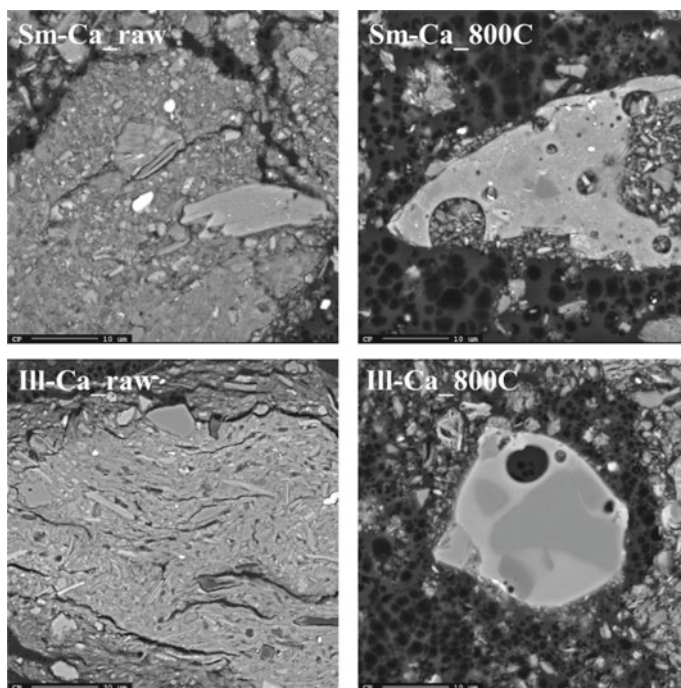
Fig. 1 BEI images of Sm-Ca and Ill-Ca not calcined (left) and calcined at 800 °C (right)

Table 3 BET specific surface area of the investigated clays before and after calcination at 800 °C

	Sm	Sm-Ca	Ill	Ill-Ca
BET surface (m²/g)—raw clay	21	71	41	48
BET surface (m²/g)—800 °C	30	15	23	9

4.2　Calcium Hydroxide Consumption

Table 4 shows the results of measured CH consumption of pastes of calcined clay and CH hydrated for 28 days at 20 °C. The highest pozzolanic activity in terms of CH consumption was measured in clay Sm-Ca, which was about double as high as

Table 4 CH consumption and bound water of pastes of calcined clay and CH hydrated for 28 days at 20 °C measured with TGA

	Sm	Sm-Ca	Ill	Ill-Ca
Consumed (g CH/g clay[1])	0.26	0.52	0.23	0.34
Bound water (by dry weight at 350 °C)	6.2	11.4	5.9	7.9

[1]STDEV <0.05

the CH consumption in clay Sm. Clay Ill-Ca had a higher CH consumption than clay Ill but lower than SM-Ca. The CH consumption of clay Sm and Ill was about equal. For comparison, laboratory grade pure metakaolin had a CH consumption of about 0.7 g CH/g clay.

Figure 2 shows the formation of hydration products in the pastes of calcined clay with CH as analyzed with DTG and XRD. The DTG results confirmed that clay Sm-Ca had the highest CH consumption (peak at 500 °C) and formed the highest amount of hydration products from the pozzolanic reaction. The peak at around 160 °C is typical for the formation of AFm phases. Ill-Ca forms more hydration products than Ill and Sm but less than Sm-Ca. As seen in the XRD diffractograms, monocarboaluminate (Mc) is the main hydration product in all pastes. This might be due to small amounts of calcite left in the calcined clays or small impurities of calcite in the CH. XRD confirms the DTG results showing that Sm-Ca formed the highest amount of hydration products. In addition to monocarboaluminate, a peak for hemicarboaluminate (Hc) is visible. In addition, the peak between hemicarboaluminate and monocarboaluminate in sample Sm-Ca might reflect Fe-substituted carboaluminate hydrate [9, 10].

The results show that besides the smaller BET surface area after calcination, the clays initially containing higher amounts of calcite (Sm-Ca and Ill-Ca) have a higher pozzolanic reactivity than the clays with small amounts of calcite before calcination. One reason for the high pozzolanic activity of Sm-Ca might be that there was about 5% calcite left in the clay after calcination. It is known that calcite together with the metastable clay minerals contributes to a synergetic effect increasing the amount of bound water [2]. Furthermore, SEM observations indicate that the glass phase in Sm-Ca and Ill-Ca calcined at 800 °C contributed to the pozzolanic reaction. Figure 3 shows BEI images of the paste of Sm-Ca and CH after hydration for 28 days. To the left, a large calcite particle is shown. The right picture shows a glass particle. Both calcite and the glass phase have a clear reaction rim with the formation of hydration products at the edges. EDX phase analysis confirmed the formation of carboaluminate hydrate (Fig. 3-left) and a C-A-S-H phase (Fig. 3-right), respectively.
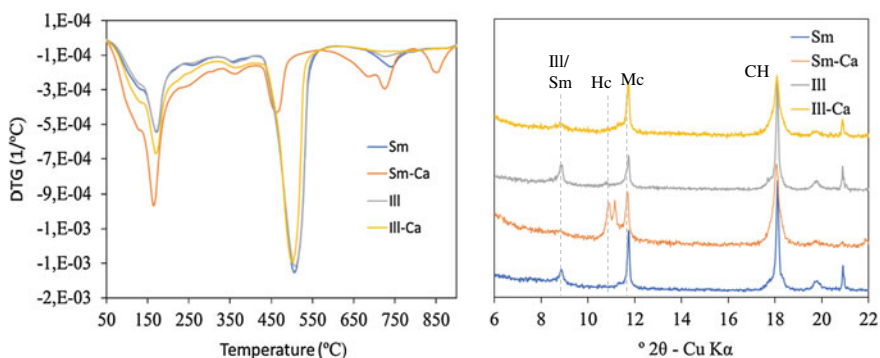
Fig. 2 DTG (left) and XRD (right) of pastes of calcined clay and CH hydrated for 28 days at 20 °C
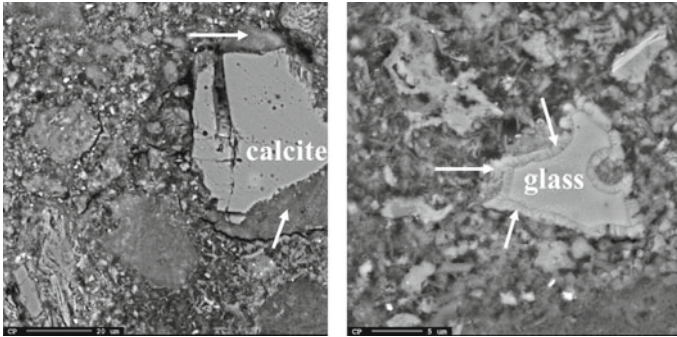
Fig. 3 BEI images of paste of Sm-Ca_800 with CH hydrated for 28 days. White arrows indicate reaction rims around calcite (left) and glass phase (right)

Still, Sm-Ca and Ill-Ca do also contain slightly higher amounts of kaolinite in the raw clay compared to Sm and Ill. Upon calcination, small amounts of metakaolin might also contribute to reactivity.

4.3 Compressive Strength of Mortars

Figure 4 shows the relative compressive of mortars with 20% replacement of cement by the respective calcined clay. It can be seen that the clays initially containing high amounts of calcite show better performance in mortar testing than the clays with only small amounts of calcite. The mortar with 20% Sm-Ca reached 113% of the strength of the reference, while the mortar with 20% Ill-Ca had about the same 28-day strength as the reference mortar. Mortars with 20% Sm and 20% Ill had about 95 and

Fig. 4 28 day relative compressive of mortars with 20% replacement of cement by the respective calcined clay
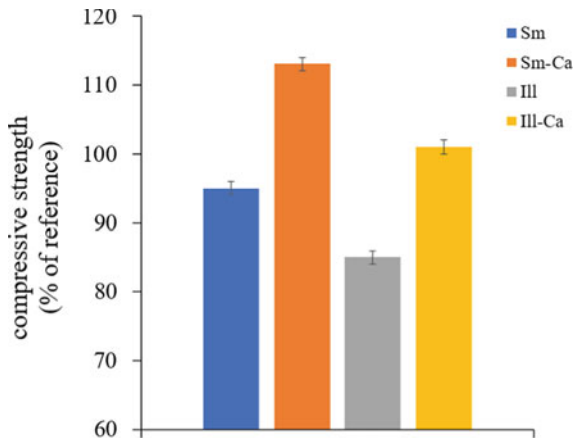
85% of the reference strength after 28 days. As expected, clays rich in Illite are less reactive than clays rich in smectite [1]. The results indicate that calcite impurities in raw clays can have a positive effect on the pozzolanic activity when calcined at optimum temperature.

5   Conclusions

- Calcareous clays have the potential to be used as a SCM in cement production.
- Clays with a calcite content between 15 and 25% in the raw clay appear to form a reactive glass phase upon calcination.
- Results indicate that the reactivity of illite and smectite rich clays can be increased when calcite is present in the raw clays.

References

1. Fernandez, R., Martirena, F., Scrivener, K.L.: The origin of the pozzolanic activity of calcined clay minerals: a comparison between kaolinite, illite and montmorillonite. Cem. Concr. Res. **41**(1), 113–122 (2011)
2. Antoni, M., et al.: Cement substitution by a combination of metakaolin and limestone. Cem. Concr. Res. **42**(12), 1579–1589 (2012)
3. Scrivener, K., John, V., Gartner, E.M.: Eco-efficient cements: potential economically viable solutions for a low-CO_2 cement-based materials industry. In: Green Concrete Conference 2018. Taastrup, Denmark
4. Rakhimov, R.Z., et al.: Properties of Portland cement pastes enriched with addition of calcined marl. J. Build. Eng. **11**, 30–36 (2017)
5. Danner, T.: Reactivity of calcined clays. Doctoral Thesis, 2013:218, Norwegian University of Science and Technology—NTNU, p. 229 (2013)
6. Danner, T., Norden, G., Justnes, H.: Characterisation of calcined raw clays suitable as supplementary cementitious materials. Appl. Clay Sci. **162**, 391–402 (2018)
7. Duminuco, P., Messiga, B., Riccardi, M.P.: Firing process of natural clays. Some microtextures and related phase compositions. Thermochim. Acta **321**(1), 185–190 (1998)
8. Nodari, L., et al.: Hematite nucleation and growth in the firing of carbonate-rich clay for pottery production. **27**, 4665–4673 (2007)
9. Danner, T., Østnor, T.A., Justnes, H.: Calcined Marl as a Pozzolan for sustainable development of the cement and concrete industry. In: 12th International Conference on recent Advances in Concrete Technology and Sustainability Issues. American Concrete Institute, Prague (2012)
10. Dilnesa, B.Z.: Fe-containing hydrates and their fate during cement hydration thermodynamic data and experimental study. EPFL

Activated Calcined Clays as Cement Main Constituent

Simone Elisabeth Schulze, Roland Pierkes and Joerg Rickert

Abstract Within three research projects, VDZ was able to show the performance of several calcined impure clays as supplementary cementitious materials (SCM). The used kaolinitic, illitic, and chloritic clays indicated low ceramic qualities and represented typical clays of cement plant quarries. Even suitable calcination conditions led to acceptable pozzolanic reactivity of the calcined clays. Illitic clay of low quality was mixed with few amounts of CaO added as limestone and calcined at different temperatures to investigate the influences of CaO addition on pozzolanic activation of the clay. The obtained samples were analyzed concerning their mineralogical composition and their amounts of reactive components. These activated calcined clays were used as SCM to mix laboratory cements with 20 and 40 mass % of calcined clay and were subjected to cement performance tests. The procedure may offer an opportunity to improve the quality of calcined clays for use as SCM produced with clays of lower quality. Currently, research is done to use, e.g., bypass dusts as clay activating calcium source to find another suitable valorization of by-products from the clinker production.

Keywords Calcined clay · Reactivity · Compressive strength

1 Introduction

Although suitable raw material resources exist in Europe, calcined clays have rarely been used in cements upto now. The influence of the chemical and mineralogical composition of clays on their suitability as a supplementary cementitious material (SCM) has been successfully investigated in the recent past. In a completed research program, VDZ investigated a couple of different kaolinitic, illitic, and chloritic clays, partially of low ceramic quality [1, 2]. For each type of clay, it was possible to meet the requirements of the European Standard EN 197-1 for a natural calcined pozzolana applying appropriate calcination conditions. At laboratory scale, pozzolanic

S. E. Schulze (✉) · R. Pierkes · J. Rickert
Cement Chemistry Department, Research Institute of the Cement Industry, VDZ gGmbH,
Tannenstrasse 2, 40476 Duesseldorf, Germany
e-mail: Simone.Schulze@vdz-online.de

cements were produced using these calcined clays in portions of 20 or 40 mass %, respectively. The cements performed well in crucial cement properties like workability and strength development. In a further research project, the potential of cement optimization by adjusting the components clinker, calcined clay, and sulfate carrier was investigated [3, 4]. To prove the applicability of such cements in concrete, their performance, especially with regard to durability, was shown. The performance of the tested binder systems was comparable to cements with other SCMs like limestone, slag, or fly ash [5, 6].

In the present research, a clay of low ceramic quality (illitic clay with high amounts of quartz), which is hard to activate by thermal treatment, was doped with CaO to increase its amount of reactive components. The obtained activated pozzolanic materials were investigated concerning their mineralogical composition and their amounts of reactive phases. Pozzolanic cements with 20 and 40 mass % of the activated calcined clays were produced on laboratory scale. Their phase development during hydration and their compressive strength were tested.

2   Experimental Procedure

Mixtures of an illitic clay (T7) and varying amounts of CaO (5, 9, and 17 mass %) added as limestone were calcined at 900, 1000, 1100, and 1200 °C under oxidizing burning conditions according to Schulze and Rickert [1] to increase the amount of reactive compounds of the clay. Table 1 shows the mineralogical composition of the used clay, which consisted of high amounts of quartz beside the clay minerals illite/muscovite and kaolinite.

The calcined samples were ground in a laboratory ball mill to achieve an equal level of fineness. After that the amounts of reactive compounds was determined acc. to Surana [7]. To get the mineralogical composition of the samples, XRD measurements were carried out by means of PANalytical X'Pert Pro using Cu Kα radiation, and evaluated with the TOPAS® Rietveld Software.

Pozzolanic cements with 20 and 40 mass % calcined clay, respectively, were produced at laboratory scale by mixing the clays with an OPC (CEM I 52,5 R). Their

Table 1 Mineral composition of the used illitic clay T7

Mineral group	T7–illitic
Quartz	+++
Kaolinite	++
Illite/Muscovite	+++
Mixed layer	+
Feldspar	+
Calcite	(+)

+++/++ = main constituent, + = minor constituent, (+) = trace

Table 2 Mortar compressive strength acc. EN 196-1 of the OPC (CEM I 52,5 R) used as clinker component

	Compressive strength, MPa
2 days	41
7 days	58
28 days	66

compressive strength was determined on $40 \times 40 \times 160$ mm^3 mortar prisms with a water/cement ratio of 0.50 according to EN 196-1. Table 2 shows the compressive strength data of the used OPC.

Cement samples with 40 mass % calcined clay were hydrated with water/solid ratio of 0.50. After stopping the hydration process by acetone and diethyl ether, the hydrated samples were examined by means of XRD.

3 Results and Discussion

3.1 Calcined Clay Samples

Figure 1 shows as an example of the mineralogical phase composition of clay T7 with an addition of 9 mass % CaO as limestone and calcined in the range from 900 up to 1200 °C. Kaolinite, as well as mixed-layer clays ($< 8°$ 2θ) were destroyed completely at 900 °C. Some remaining illite structure and few amounts of calcite were still visible at that temperature. Most of the added limestone was calcined to free lime, but some free calcium, alumina, and silica were already forming new CAS phases like feldspar and gehlenite. At 1000 °C, the primary feldspar started to convert into anorthite, and the free lime was consumed with additional silica forming wollastonite. At 1100 °C,
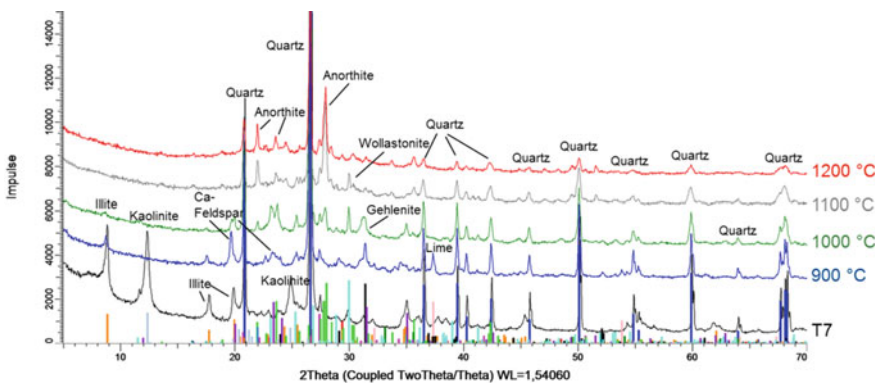
Fig. 1 Phase composition of clay T7 calcined with 9 mass % CaO in dependency on calcination temperature (XRD), the black curve shows the phase composition of pure T7

gehlenite and wollastonite started to form further anorthitic feldspar. The increased resorption of quartz was visible at each temperature step. At 1200 °C, only anorthite and some residual quartz could be determined clearly as crystalline phases. A broad hump in the background level (15°–35° 2θ) indicated an increasing amount of X-ray amorphous phases. It is expected that all mentioned CAS phases formed during the calcination do not support the pozzolanic reactivity of the calcined clays.

By calcination of pure T7 (no figure), all clay minerals were destroyed at the temperatures mentioned above and only very small amounts of the Ca-free phases, sillimanite and hematite, were built as high-temperature phases.

It could be shown in [1] that the determination of reactive Si and Al according to Surana's method [7] is very sensitive to variations in the burning conditions during the calcination of clays. Figure 2 shows the results of the determination of reactive Si (left) and reactive Al (right) for T7 without CaO addition and also with 5, 9, and 17 mass % CaO after calcination at different temperatures. The data were referred to the clay content of the samples, to eliminate a dilution effect. It is obviously that except after the calcination at 1200 °C with increasing amount of CaO the amounts of reactive Si and Al decreased. The amounts of reactive Si and Al also decreased up to a calcination temperature of 1100 °C; however, there seemed to be a small growth at 1200 °C.

As described above, the addition of CaO did not lead to the formation of reactive hydraulic phases like belite, but phases like feldspar and gehlenite were formed already at 900 °C. At higher temperatures, wollastonite and further anorthitic feldspar were formed, which also bound Si and Al. As a result, the amounts of reactive Si and Al decreased at higher calcination temperatures. Increasing amounts of CaO did result in higher amounts of the mentioned stable phases; therefore, the pozzolanic reactivity of the samples decreased.
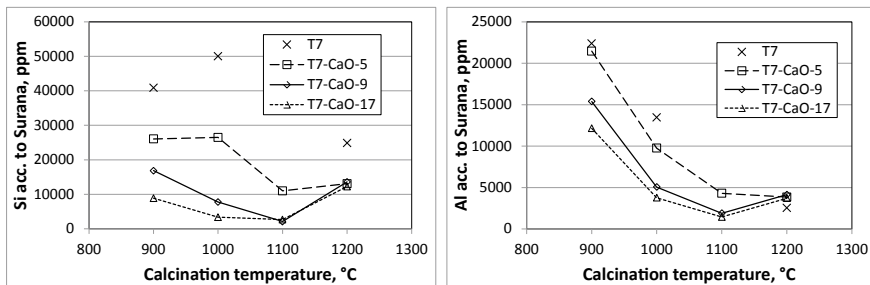
Fig. 2 Reactive Si and Al acc. to Surana's method [7] dependent on amount of added CaO and calcination temperature, data referred to the clay content of the calcined samples

3.2 Cements Containing Calcined Clay Samples

The XRD investigation on the hydration products of pozzolanic cements showed some influence of the doped calcined clay T7 on the hydration of the clinker. Figure 3 presents the diffraction pattern of the cement pastes hydrated for 28 days (OPC and mixtures with 40 mass % T7 with 9 mass % CaO calcined at different temperatures). Even taking into account the dilution of the OPC, there seemed to be a slight increase in hydration of the clinker, leading to some stronger decrease in alite content. The strongest effects were visible for the sample with the clay calcined at 900 °C (green pattern), that also shows the highest amounts of reactive Si and Al (see Fig. 2). Beside the strongest alite consumption especially the conversion from ettringite to monosulfate and the amounts of other CAH phases like hemicarbonate (diffraction area on 9°–12° 2θ) were significantly increased in that sample. The same effects were already visible after 2 days of hydration as well as within the samples with 20 mass % calcined clay. Obviously the higher availability of reactive Al led to the increased formation of Al-bearing hydration phases and alite consumption. As shown in Fig. 2, the alumina reactivity of the calcined clays decreased with higher calcination temperatures. Beside this, it is known that the lower the calcination temperature, the higher the surface area of calcined clay is [2], which could be an additional reason for the higher reactivity of the sample calcined at 900 °C and its enhancement of the clinker reaction by working as nucleating agent.

In Fig. 4, the relative compressive strength data of pozzolanic cements consisting of OPC and 20 or 40 mass % calcined clay T7 with 9 mass % CaO are given. All data is referred to the compressive strength data of the used OPC (see Table 2). The filled markers on the left show the relative compressive strength data of the respective mixtures with calcined clay T7 without addition of CaO. For both groups of samples (20 and 40 mass % calcined clay), the results of the compressive strength were within the area of the reference cement with T7 without CaO addition.
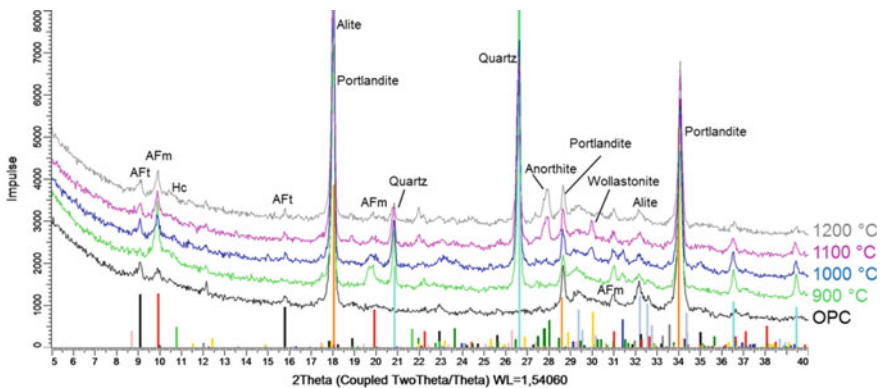
Fig. 3 X-ray diffraction pattern of 28 days hydrated OPC (black curve) and cement with 60 mass % OPC and 40 mass % calcined clay (T7 with 9 mass % CaO calcined at different temperatures)
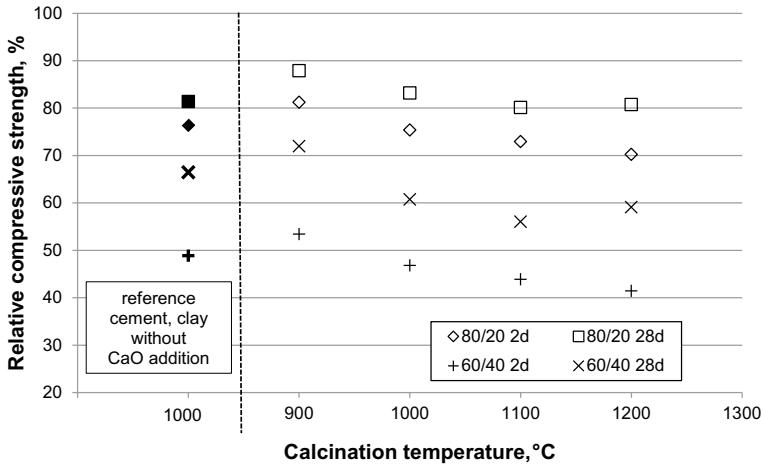
Fig. 4 Compressive strength of the laboratory cements after 2 and 28 days of hydration with 20 and 40 mass % calcined clay with 9 mass % CaO related to strength development of the respective OPC

After 2 days of hydration, the pozzolanic reaction had not started yet. Nevertheless a significant strength contribution of the calcined clay could be observed, especially in the mixtures with 40 mass % calcined clay. This strength contribution could be traced to the enhancement of the clinker reaction by the calcined clay described above. With increasing calcination temperature, the surface area of the clay decreased and thus, the compressive strength of the respective pozzolanic cement decreased.

The growth of compressive strength between 2 and 28 days of hydration was higher for the samples with 40 mass % calcined clay, which is an evidence for a strong pozzolanic reactivity of all calcined clays. The calcination at 1200 °C had a positive impact also on the compressive strength of the pozzolanic cements (see Fig. 4) following the positive effect on their amount of reactive Si and Al (see Fig. 2). As mentioned in the discussion of the phase composition of the clay calcined with 9 mass % CaO (see Fig. 1), a high amount of X-ray amorphous reactive phases could be detected in this sample, which could be an explanation for this behavior.

4 Conclusions

The valorization of low-quality clays with impurities of quartz and calcite becomes more and more in the focus of the cement industry. Within a current research project, VDZ tested the suitability of such clays as SCMs, which were calcined with CaO at different temperatures to achieve activated pozzolanic material.

The results showed that in the temperature range between 900 and 1100 °C, no hydraulic phases were built in the clay samples doped with 9 mass % CaO and also the

amounts of reactive Si and Al decreased. However after the calcination at 1200 °C, an increasing amount of X-ray amorphous phases and a respective higher amount of reactive Al and Si could be detected.

XRD investigation on the hydration products of pozzolanic cements with the doped calcined clays showed an increase in hydration of the clinker, particularly with the sample calcined at 900 °C, leading to some stronger increase in alite consumption. This positive effect on the clinker hydration was also reflected in the compressive strength development. Furthermore, the amounts of reactive Al and Si according to Surana correlate clearly with the calcined clays' contribution to the compressive strength of the cement.

The presented approach may offer an opportunity to use even lower quality clays as raw material for SCM production. Beside CaO from limestone, other by-products from the clinker production like bypass dusts are conceivable calcium sources and are investigated within a current research project.

References

1. Schulze, S.E., Rickert, J.: Suitability of natural calcined clays as supplementary cementitious material. Cem. Concr. Compos. **95**, 92–97 (2019)
2. Schulze, S.E., Rickert, J.: Pozzolanic activity of calcined clays. In: Proceedings of the Twelfth International Conference on Recent Advances in Concrete Technology and Sustainability Issues, pp. 277–287. American Concrete Institute (2012)
3. Pierkes, R., Schulze, S.E., Rickert, J.: Optimization of cements with calcined clays as supplementary cementitious materials. In: Scrivener, K., Favier, A. (eds.) Proceedings of the 1st International Conference on Calcined Clays for Sustainable Concrete (Lausanne 23.-25.06.2015), pp. 59–66 (2015)
4. Schulze, S.E., Pierkes, R., Rickert, J.: Optimization of cements with calcined clays as supplementary cementitious materials. In: Proceedings of the 14th International Congress on the Chemistry of Cement, ICCC (Beijing 13.-16.10.2015)
5. Pierkes, R., Schulze, S.E., Rickert, J.: Durability of composite cements with calcined clay. Int. Cem. Rev. **12**, 34–36 (2018)
6. Pierkes, R., Schulze, S.E., Rickert, J.: Durability of concretes made with calcined clay composite cements. In: Martirena, F., Scrivener, K., Favier, A. (eds.) Proceedings of the 2nd International Conference on Calcined Clays for Sustainable Concrete (Havana City 05.-07.12.2017), pp. 366–371 (2017)
7. Surana, M.S., Joshi, S.N.: Spectrophotometric method for estimating the reactivity of pozzolanic materials. Adv. Cem. Res. **1**, 238–241 (1988)

Simple and Reliable Quantification of Kaolinite in Clay Using an Oven and a Balance

François Avet and **Karen Scrivener**

Abstract This study investigates the feasibility of using an oven and a balance to determine the kaolinite content in clay. The mass of 14 clays was recorded after three heating steps at 200 °C, 400 °C, and 600 °C. The two upper temperatures permit to accurately consider the kaolinite dehydroxylation, whereas the step at 200 °C considers the moisture state of the clay. The protocol of the test was optimized with an adequate sample mass of 10 g and finer than 4 mm. The correlation with thermogravimetric analyses (TGA) results shows a very high correlation coefficient ($R^2 = 0.99$). Since TGA is not available in all laboratories, this alternative method permits to characterize the clay without any expensive equipment.

Keywords Clay characterization · Kaolinite · Oven

1 Introduction

The demand for cement and construction materials will keep increasing in the next decades. This increase will lead to significantly higher levels of CO_2 emissions if no alternatives to conventional cement are developed. One of the most promising approach to decrease the emissions related to concrete production is the decrease of the clinker content in cement [1–3]. The combination of calcined kaolinitic clays and limestone permits to decrease the clinker content to 50% in limestone calcined clay cements (LC^3) [4]. The performance of these blends is highly dependent on the kaolinite content of clay [5, 6]. In terms of strength development, kaolinite content as low as 40% is sufficient to reach similar strength to plain cement [7]. The kaolinite content of clay is usually determined by thermogravimetric analysis (TGA). The water loss corresponding to the dehydroxylation of kaolinite is monitored and its content permits to calculate the kaolinite content of clay. The main drawback of TGA is that the device is not available in all laboratories. X-ray diffraction (XRD) combined with Rietveld method is also common. However, some deviations were observed by comparing XRD–Rietveld and TGA [6]. XRD–Rietveld requires skilled

F. Avet (✉) · K. Scrivener
Laboratory of Construction Materials, EPFL, 1015 Lausanne, Switzerland
e-mail: francois.avet@epfl.ch

operators for the quantification and issues are often faced due to preferred orientation, structural defects, and sometimes poor crystallinity [8–11]. Thus, a novel way of quantifying kaolinite would permit to provide this key information more universally. The weight loss over calcination was proposed to estimate the quality of clay [12], not only focusing on kaolinite nor correlating it with XRD or TGA. In this study, the development of a relevant test to determine the kaolinite content is investigated, using simply a balance and an oven. The critical parameters are identified and investigated to establish a robust protocol of the test. This protocol was then applied to a wide range of kaolinitic clays and the results were compared with the kaolinite content obtained by TGA.

2 Materials and Methods

2.1 Clay Characterization

In this study, 14 clays from 9 countries were used. TGA was used as reference technique for the kaolinite content determination. The kaolinite content $wt\%_{kaolinite}$ is obtained from the mass loss during kaolinite dehydroxylation $wt\%_{kaol-OH}$ according to Eq. 1, where $M_{kaolinite}$ ($258.16\,g\,mol^{-1}$) and M_{water} ($18.02\,g\,mol^{-1}$) refer to kaolinite and water molecular weights, respectively. The influence of moisture is considered in $wt\%_{kaol-OH,}$ since the mass loss is normalized by the mass of kaolinite at 200 °C.

$$wt\%_{kaolinite} = wt\%_{kaol-OH} \times \frac{M_{kaolinite}}{2M_{water}} \qquad (1)$$

For TGA experiments, 50 mg of powder sample is enough for the quantification. All samples were tested using a Mettler Toledo TGA/SDTA 851 balance. A constant nitrogen flow of $30\,ml\,min^{-1}$ has to be used to prevent carbonation. A heating rate of $10\,°C\,min^{-1}$ is used to get an experiment time of approximately 2 h, including cooling down. The horizontal method of TGA consists of considering the direct mass loss difference between approx. 400 to 600 °C for kaolinite. However, the influence of other phases dehydroxylating over the same temperature range cannot be discarded using the horizontal method. For a better accuracy, tangent method is used.

The kaolinite content and the secondary phases present in the clay are shown in Table 1. XRD was used for the identification of the secondary phases. The range of kaolinite goes from 7.5 to 93.4 wt%. The chemical composition of the clays by X-ray fluorescence is shown in Table 2.

Table 1 Origin, kaolinite content, and secondary phases of the 14 clays

Clay	Origin	Kaolinite content (wt.%)	Secondary phases
1	Middle East	7.5	Quartz, Illite
2	South Asia	17.5	Quartz, Goethite
3	Europe	28.0	Quartz, Muscovite
4	Central America	33.2	Quartz, Calcite
5	South America	39.1	Quartz, Gibbsite
6	West Africa	41.6	Quartz, Microcline
7	South America	45.7	Quartz, Anatase
8	Latin America	53.1	Quartz, Goethite
9	Southeast Asia	53.8	Muscovite, Anatase
10	Central America	63.3	Quartz, Anatase
11	South Asia	63.6	Quartz, Muscovite
12	South Asia	72.0	Muscovite, Anatase
13	South Asia	83.9	Muscovite
14	North America	93.4	Anatase

2.2 Novel Robust Method to Determine the Kaolinite Content of Clay

For the oven method, different parameters are needed to be assessed to define a robust protocol. First, the boundary temperatures for kaolinite dehydroxylation had to be chosen. 20 mL alumina crucibles were weighed and filled with 10 g of clay. These crucibles were ignited at 1000 °C prior to testing. Three replicas were used for each clay. The samples were heated upto 200 °C for 1 h, cooled down, and weighed again. These heating and cooling down steps were repeated from 350 to 850 °C, with 50 °C increment, and the weight of each crucible was measured after cooling down for each step.

Moreover, the influence of three parameters was investigated. For a higher sample mass or a coarser sample, some temperature non-uniformity could occur and cause a shift, and a broadening of the kaolinite dehydroxylation. First, the influence of the sample mass was determined: 1, 5, 10, and 50 g were compared with 50 mg used for TGA experiment. For the impact of sample fineness, particles from 10 up to 16 mm were used and the kaolinite content was compared with the reference

Table 2 XRF chemical composition of the 14 clays

Clay	SiO_2	Al_2O_3	Fe_2O_3	CaO	MgO	SO_3	Na_2O	K_2O	TiO_2	P_2O_5	MnO	Others	LOI
1	57.3	17.7	8.0	0.5	0.4	0.2	1.0	3.2	1.5	0.7	0.0	0.7	8.7
2	62.8	17.3	9.3	0.7	0.6	0.0	0.0	2.3	0.7	0.0	0.0	0.1	6.2
3	57.5	21.1	9.6	0.2	0.6	0.0	0.1	2.7	1.2	0.0	0.0	0.1	6.8
4	43.6	18.7	12.2	8.6	0.7	0.0	0.0	0.0	1.0	0.0	0.5	0.2	14.3
5	60.1	24.4	1.5	2.2	0.1	0.0	0.3	0.2	0.4	0.0	0.0	0.1	9.8
6	54.1	24.3	7.2	0.4	0.6	0.0	0.4	1.5	1.2	0.2	0.1	0.3	9.4
7	46.7	23.3	14.0	1.6	0.7	0.0	0.1	0.1	1.0	0.3	0.2	0.5	11.5
8	42.0	26.1	17.0	0.1	0.6	0.0	0.5	0.1	0.6	0.2	0.0	0.2	12.6
9	39.3	31.0	12.6	1.3	0.6	0.1	0.3	0.1	2.0	0.3	0.1	0.0	10.8
10	56.1	24.6	6.4	0.1	0.1	0.1	0.0	0.1	1.8	0.1	0.0	0.2	10.3
11	53.6	29.1	0.8	1.5	0.3	0.0	0.1	0.3	1.6	0.2	0	0	11.6
12	47.4	34.6	1.1	0.5	0.6	0.0	0.2	0.7	1.4	0.2	0	0	12.4
13	43.2	39.7	1.5	0.1	0.0	0.0	0.1	0.1	2.1	0.0	0.0	0.0	11.7
14	45.8	38.4	0.4	0.0	0.1	0.0	0.2	0.3	1.1	0.0	0.0	0.1	13.6

value obtained by TGA. Finally, moisture conditions can also influence the kaolinite content determination in clay. Thus, the moisture was also studied, by preparing a slurry with 1:1 clay to water ratio and comparing it with laboratory-stored clay.

3 Results

3.1 Temperature Boundaries

The mass evolution with temperature by TGA or using the oven is shown in Fig. 1 for clays 2, 4, 9, and 13. Very similar mass evolutions are obtained using these two techniques. Thus, the oven permits to replicate the data obtained by TGA. The main differences are observed below 200 °C, and are due to moisture difference which comes from clay environment or storage conditions. To determine the boundary conditions for the determination of the kaolinite content, the different reactions taking place with the increase of temperature are separated. In addition to kaolinite, the dehydroxylation of goethite or gibbsite occurs from approx. 200 to 350 °C. 2:1 clays partially dehydroxylate from 550 to 650 °C. Finally, calcite decarbonation occurs from about 650 to 750 °C. Thus, 400 °C and 600 °C are used as lower and upper limits for considering kaolinite dehydroxylation. Lower boundaries would cause interference with iron or aluminum hydroxide dehydroxylation. Higher boundary would then cover 2:1 clay dehydroxylation.
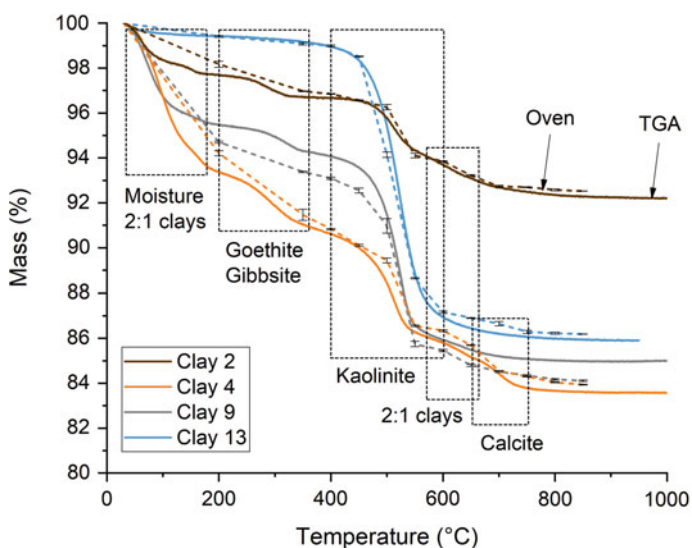
Fig. 1 Mass loss monitored with temperature increase measured by TGA and oven
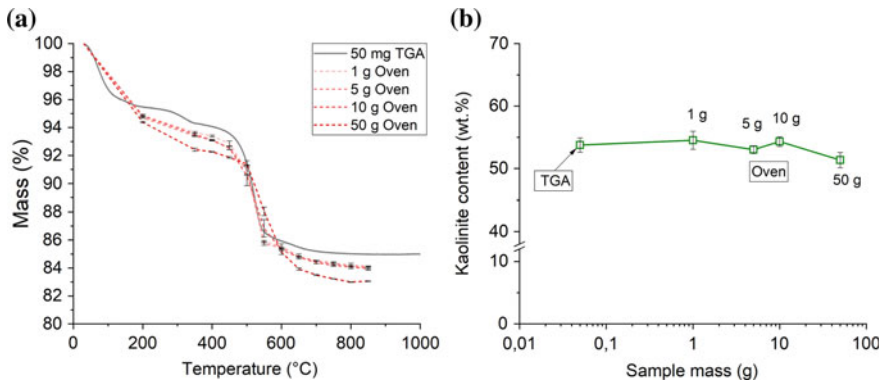
Fig. 2 Influence of sample mass on the mass change with temperature (**a**) and the kaolinite content (**b**)

The kaolinite content can thus be estimated according to Eq. 2, considering the mass loss from 400 °C, $wt_{400°C}$ to 600 °C, $wt_{600°C}$. The weight at 200 °C is used as normalization factor to consider differences in moisture content of each clay. The mass of the powder is determined as the difference of the mass of the crucible with the sample at 200 °C, $wt_{200°C}$, and the mass of the empty crucible, wt_i.

$$wt\%_{kaolinite} = \frac{wt_{400°C} - wt_{600°C}}{wt_{200°C} - wt_i} \times \frac{M_{kaolinite}}{2M_{water}} \times 100 \qquad (2)$$

3.2 Influence of Sample Mass

The influence of samples mass is shown in Fig. 2a. Oven results are slightly shifted compared with TGA due to slight moisture difference. Using 1 g, 5 g, or 10 g does not cause any shift of the position of the kaolinite dehydroxylation. For 50 g, inertia causes some shift of the kaolinite transition. This is shown in Fig. 2b where the kaolinite content estimation using the oven starts deviating from the TGA reference for 50 g of sample. Due to the shift of the dehydroxylation, part of it is not considered in Eq. 2. Thus, 10 g is chosen to be as representative of the clay as possible.

3.3 Influence of Sample Fineness

The influence of the particle size on the mass loss curves is shown in Fig. 3. From 15 μm to an upper limit of 16 mm, extremely similar mass loss evolution with temperature is observed. There is no clear evidence of any mass influence on the
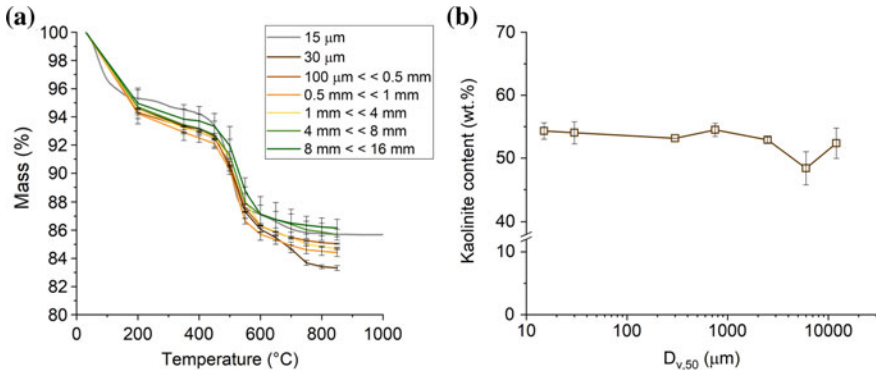
Fig. 3 Influence of particle size on the mass change with temperature (**a**) and the kaolinite content (**b**)

shift of the kaolinite peak. The kaolinite content determination is shown in Fig. 3b. Above an upper limit of 4 mm (maximum of sand size), higher deviations are observed without significantly impacting the kaolinite content. Thus, it is recommended not to overcome this size of 4 mm in order to keep a good reproducibility of the measurement.

3.4 Protocol for the Kaolinite Content Determination

The final protocol is summarized in Fig. 4. For each clay, 3 ignited crucibles are weighed and filled with 10 ± 0.1 g of clay. The sample does not need to be dried before testing. The crucibles are then placed in an oven at 200 °C for 1 h. After drying at 200 °C, the crucibles are left in the oven for cooling down to 100 °C. Each crucible weight is then measured. The material is then heated up to 400 °C for 1 h. After cooling down to 100 °C, each crucibles mass is measured again. The crucibles are then heated up again to 600 °C for 1 h. Each crucible weight is measured once more after cooling. The kaolinite content can then be estimated using Eq. 2. Since three measurements are obtained for each clay, an average kaolinite content is calculated, and the standard deviation indicates the error of measurement.

The duration of test is about 5.5 h. A TGA experiment usually takes 2.5 h, including cooling. The advantage of the oven test is that several samples can be run at the same time, whereas only one sample can be tested with TGA.
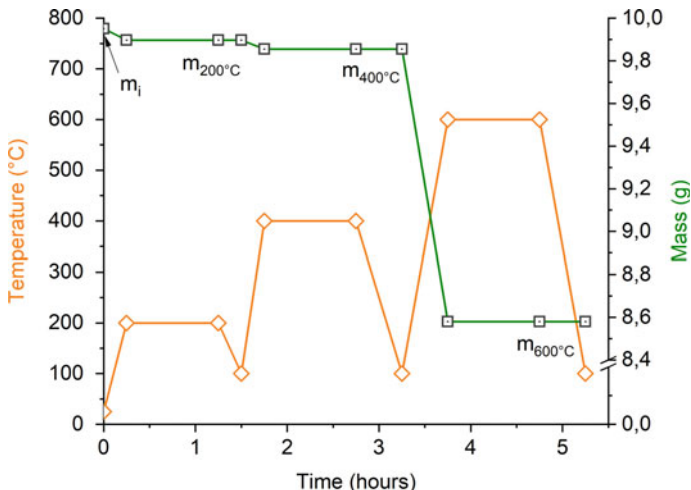
Fig. 4 Protocol used for the determination of the kaolinite content in clay using an oven

3.5 Application to Calcined Clays

The protocol was then applied to the other clays, covering the whole range of kaolinite content. Figure 5 shows the correlation between the kaolinite content obtained by TGA using tangent method and the kaolinite content obtained with the oven. A very high correlation coefficient $R^2 = 0.99$ is obtained. In order to better understand this correlation, Fig. 6 shows the comparison of the determination of the kaolinite content by TGA and using the oven. Using tangent method, the kaolinite content could be thought to be lower than the oven method using direct mass difference from the two

Fig. 5 Correlation between the kaolinite content determined by TGA using tangent method and the oven test
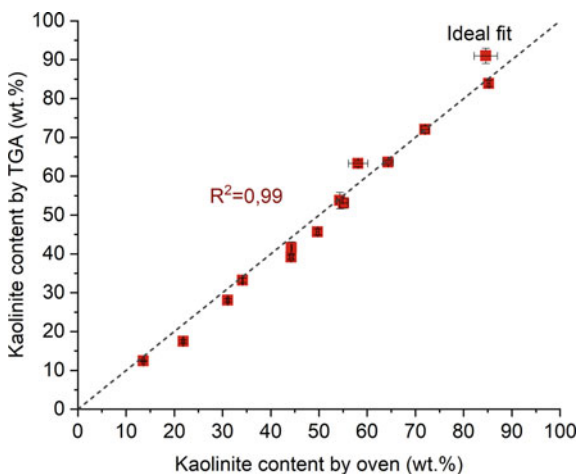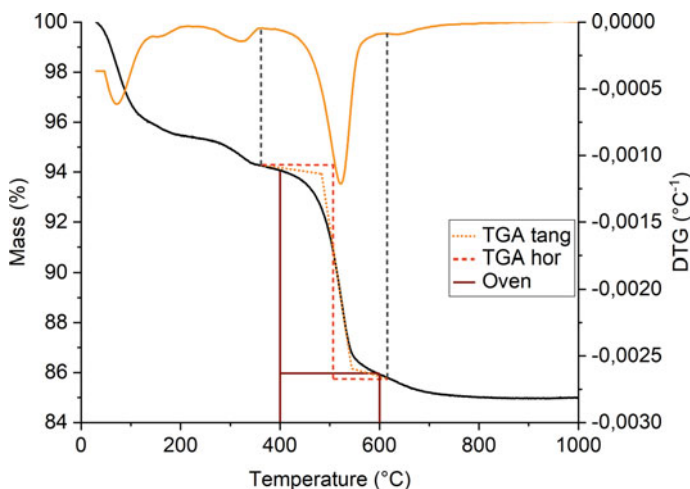
Fig. 6 Methods to determine the kaolinite content: horizontal TGA, tangential TGA, and oven with fixed temperature boundaries

temperature boundaries. However, this is compensated by the narrower boundaries used for the oven method. For TGA, the boundaries are defined by the inflection points, which permit to separate kaolinite dehydroxylation from the reactions of other phases. This explains why such excellent correlation is obtained despite the different ways of determining the kaolinite content.

4   Conclusion

– The boundary temperatures for the oven steps are defined at 200, 400, and 600 °C. This permits to consider the moisture content of the clay and to isolate the kaolinite dehydroxylation.
– An optimal mass of sample of 10 g was defined. Inertia influences the results for a higher mass of material.
– In terms of fineness, it is not necessary to grind the clay below 4 mm. Higher deviations are observed for coarser particle sizes.
– The correlation with TGA is excellent, with a correlation coefficient of 0.99. This shows that the oven can be used instead of TGA.

References

1. IEA, World Business Council for Sustainable Development: Technology Roadmap Low Carbon Transition in the Cement Industry, p. 66 (2018)
2. Scrivener, K.L., John, V.M., Gartner, E.M.: Eco-efficient cements: potential economically viable solutions for a low-CO_2 cement-based materials industry (2016)
3. Damtoft, J.S., Lukasik, J., Herfort, D., et al.: Sustainable development and climate change initiatives. Cem. Concr. Res. **38**, 115–127 (2008). https://doi.org/10.1016/j.cemconres.2007.09.008
4. Scrivener, K., Martirena, F., Bishnoi, S., Maity, S.: Calcined clay limestone cements (LC^3). Cem. Concr. Res. 1–22 (2017). https://doi.org/10.1016/j.cemconres.2017.08.017
5. Maraghechi, H., Avet, F., Wong, H., et al.: Performance of Limestone Calcined Clay Cement (LC^3) with various kaolinite contents with respect to chloride transport. Mater. Struct. **51**, 125 (2018). https://doi.org/10.1617/s11527-018-1255-3
6. Scrivener, K., Avet, F., Maraghechi, H., et al.: Impacting factors and properties of Limestone Calcined Clay Cements (LC^3). Green Mater. 1–49 (2018). https://doi.org/10.1680/jgrma.18.00029
7. Avet, F., Scrivener, K.: Investigation of the calcined kaolinite content on the hydration of Limestone Calcined Clay Cement (LC^3). Cem. Concr. Res. **107**, 124–135 (2018). https://doi.org/10.1016/j.cemconres.2018.02.016
8. Aparicio, P., Galan, E.: Mineralogical interference on kaolinite crystallinity index measurements. Clays Clay Miner. **47**, 12–27 (1999)
9. Brigatti, M.F., Galan, E., Theng, B.K.G.: Chapter 2 Structures and mineralogy of clay minerals. Dev. Clay Sci. 1, 19–86 (2006). https://doi.org/10.1016/S1572-4352(05)01002-0
10. Hart, R.D., Gilkes, R.J., Siradz, S., Singh, B.: The nature of soil kaolins from Indonesia and Western Australia. Clays Clay Miner. **50**, 198–207 (2002)
11. Lorentz, B., Shanahan, N., Stetsko, Y.P., Zayed, A.: Characterization of Florida kaolin clays using multiple-technique approach. Appl. Clay Sci. **161**, 326–333 (2018). https://doi.org/10.1016/j.clay.2018.05.001
12. Díaz, A.A., Almenares Reyes, R.S., Carratalá, F.A., Martirena Hernández, J.F.: Proposal of a methodology for the preliminary assessment of kaolinitic clay deposits as a source of SCMs. In: Martirena, F., Favier, A., Scrivener, K. (eds.) Calcined Clays for Sustainable Concrete, pp 29–34. Springer, The Netherlands, Dordrecht (2018)

Improving the Behaviour of Calcined Clay as Supplementary Cementitious Materials by a Combination of Controlled Grinding and Particle Selection

Franco Zunino and Karen L. Scrivener

Abstract This project explores the use of grinding aids to control the resulting particle-size distribution of calcined clay and limestone. It was observed that after grinding, calcined clays exhibit a strongly bimodal particle-size distribution, where the clay minerals concentrate mainly in the finer particle population. A significant increase in compressive strength at early age was observed in systems incorporating alkanolamines. The effect appears to be restricted to the aluminate reaction, as the silicate peak remains virtually unmodified. Particle classification (air separation) techniques were applied to remove the impurities (mainly quartz and iron oxides) and, therefore, increase the amount of kaolinite in the resulting material. An increase in the kaolinite content from 29 to 45% by mass was achieved in one step and without pre-dispersion of the particles.

Keywords Alkanolamines · Air separation · Kaolinite

1 Introduction

Calcined clays are a promising opportunity to lower clinker levels in cements because of their widespread availability and their excellent reactivity in blended cements. The combination of metakaolin and limestone in OPC-based systems produces a synergy that enables the production of high-performance cement with a significantly lower clinker factor. Clays are mixtures of clay minerals (such as kaolinite, illite and montmorillonite) and other impurities, such as quartz, iron oxide and other rock forming minerals. Due to this inherent heterogeneity of the material, the grinding of clays results in a characteristic bimodal particle-size distribution. This characteristic distribution is observed when grinding both raw and calcined clay and also at industrial-scale grinding setups. This opens the possibility of applying particle classification processes to increase the kaolinite content in low-grade clays.

F. Zunino (✉) · K. L. Scrivener
Laboratory of Construction Materials, IMX, École Polytechnique Fédérale de Lausanne (EPFL), 1015 Lausanne, Switzerland
e-mail: franco.zunino@epfl.ch

Grinding aids (GAs) are incorporated during comminution of clinker to reduce electrostatic forces and minimize agglomeration of clinker and SCM grains [1]. Such additions are commonly used to increase cement fineness and compressive strength for given specific energy consumption (Ec) of the grinding mill [1–3]. After the grinding process, GAs may not preserve their original molecule structures. However, they do remain adsorbed onto the cement particles to entail variations of cement properties whether in the fresh or hardened state [1]. Thus, grinding aids may have beneficial effects on rheology and hydration of limestone calcined clay cements (LC^3).

2 Materials and Methods

The effect of grinding aids on the agglomeration of calcined clay during grinding was studied using unground calcined clay passing #8 sieve, and a lab-scale rotary jar mill. The clay had a calcined kaolinite content of 62%. The grinding was performed in controlled conditions of time and load of the mill, incorporating different dosages of commercial grinding aids based on polycarboxylate ether (PCE), glycol or amines. As the clay was calcined before grinding, the workability of LC^3 cast using these clays was assessed using the mini-cone slump test, while hydration kinetics was studied using isothermal calorimetry.

To assess the potential of particle classification as a mean to increase the kaolinite content of ground clays, a natural clay with 30% kaolinite content was selected. Two different particle classification techniques, gravimetric precipitation and air separation, were applied over the same material. The first one is a classic and accurate method normally used by geologists on soil science, while the second one has the biggest potential for industrial scalability. The procedure was applied to a previously grounded and dried batch of raw clay. A Hermle Z 206 lab centrifuge was used with 50 mL tubes. The clay dispersion was composed of raw ground clay as solute and sodium metaphosphate (0.1%) aqueous solution in water-to-solid ratio of 6. At the end of the centrifugation, the liquid solution was placed in plastic container. The containers were placed in a 60 °C oven to speed-up the evaporation and to allow the retrieval of the dry samples. The gravimetric separation was performed to obtain 5 batches with their own target separation size (the limit size between particles sedimented and in suspension): 0.8, 3, 5, 11 and 50 microns. The time required to achieve the desired separation limit was established using the Stoke's law adapted for centrifugation [4].

Cement plants normally perform grinding in close circuit configuration, combining a mill with an air classifier that controls the particle size of the output. In order to demonstrate the potential for clay concentration using this technology, a lab-scale air separator was used. The speed of the classifier was initially adjusted using a limestone calibration curve. Afterwards, a clay curve was constructed based on experimental results. The reactivity of the fine and rejected (coarse) fractions of clay was analysed

by means of the R^3 test [5], while their physical (particle-size distribution by laser diffraction and specific surface area by nitrogen adsorption) and chemical (kaolinite content by TGA) properties were also assessed.

3 Results and Discussion

3.1 Effect of the Incorporation of Grinding Aids in the Agglomeration of Clay During Grinding

Calcined clay was ground in the conditions described above for 60 min in order to observe the effects of grinding aids incorporation on the strong agglomeration observed in clays without the addition of these molecules. The three commercial grinding aids were included in the dosages recommended by the manufacturer. As observed in Fig. 1, all of the products used showed a strong effect on reducing the clay covering layer of the mill walls and grinding media, which impacts the efficiency of the process. Particle-size distribution of samples collected every 15 min during the grinding process allowed to observe that fine clay is obtained faster with the use of grinding aids. However, the ultimate fineness is similar as this is mainly controlled by the mill geometry and the grinding media load.

Particle-size distribution and specific surface area measurements of the samples were collected every 15 min and compared. It was observed that the increase in the surface area as a function of particle size is almost negligible (2% increase of surface area, for a DV50 reduction from 50 to 10 m), in contrast to what is normally observed in cement and other SCMs. This is explained as the main source of surface area from clays is their internal porosity, which is independent of the particle size over the range explored in this study.

Fig. 1 Photographs of ground clay after 60 min incorporating (from left to right) no GA, PCE-based GA, Amine-based GA and Glycol-based GA

3.2   Effect of the Incorporation of Grinding Aids on Workability and Hydration

The effect of the grinding aids addition on the workability of LC^3 is illustrated on Fig. 2. Results are presented as slump versus addition of a commercial PCE super-plasticizer, and compared against a reference OPC w/c 0.5 mixture. As observed, the incorporation of some grinding aids can improve the flowability of LC^3 to levels approaching the behaviour of OPC. The most effective grinding aid is the PCE based. For this reason, another batch of clay was ground with an increased dosage of this product to see if the effects could be further increased. Thus, the addition of PCE both in the solids or during mixing as a regular superplasticizer is effective to increase the slump of LC^3-based mixtures.

Regarding the effects of grinding aids on LC^3 hydration, it was observed that alkanolamines (TEA, TIPA and DEIPA) have a strong effect on the intensity of the aluminate (second) peak of hydration. The effect seems to be more intense in the system containing DEIPA, followed by TIPA and finally TEA. Previous research has suggested that this heat increase is linked to the complexation of iron contained in calcined clay, preventing the formation of a solid ferrous hydroxide phase that prevents further dissolution of clay. In order to confirm this hypothesis, model systems with synthetic iron-free clay (prepared by mixing quartz and pure metakaolin to match the grade of the natural clay used) and also incorporating white OPC instead of grey cement were tested. Each system was intended to test the effect of alkanolamines on the aluminate peak in LC^3 mixtures with iron-free clays and iron-free clays and
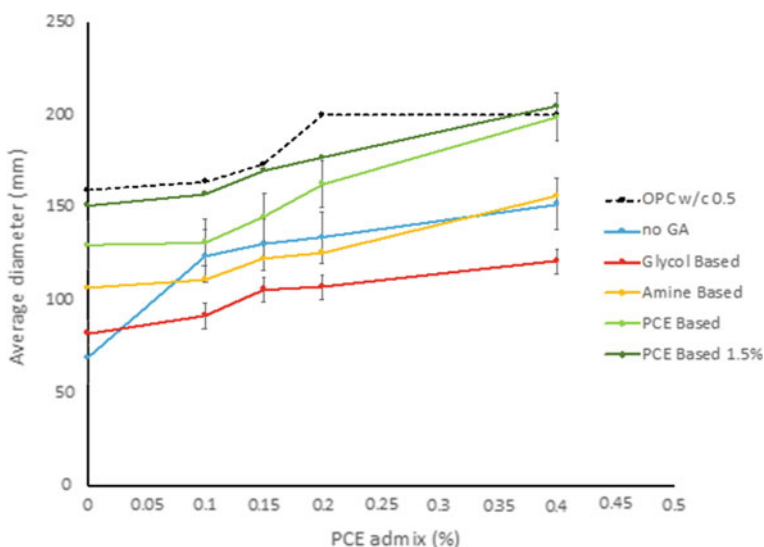
Fig. 2 Slump of LC^3-50 paste versus PCE superplasticizer addition, comparing systems with clays ground with different commercial grinding aids

cement. Results show that in the iron-free clay system, the effects of TEA, TIPA and DEIPA are comparable as the one observed in the natural (iron rich) clay LC^3. On the other hand, the complete iron-free system (synthetic clay and white OPC) showed a very minor effect of the molecules studied. This confirms that the interaction is indeed related to the presence of iron, but not sourced from calcined clay. In contrast, the effect appears to be linked to the iron contained in cement, in particular, C$_4$AF.

3.3 Particle Classification of Ground Clay to Increase the Kaolinite Content

The measurements of kaolinite content on the fine fraction collected after gravimetric separation showed that it is concentrated in the fine fraction of the particle-size distribution, corresponding typical first bump observed between about 0.1 and 1 m. This is linked to the different grindability of kaolinite and the impurities normally found on clays (quartz and rock forming minerals). In this regard, clay minerals become finer quicker generating the characteristic bimodal distribution, while the impurities remain concentrated in the coarser fraction. Thus, particle classification techniques based on size difference could provide a technically suitable way to concentrate kaolinite in low-grade natural clays.

A consolidated plot containing the results of characterization of the fine fraction obtained by air separation is shown on Fig. 3. It can be observed that, as gravimetric separation, air separation is effecting in removing the impurities (mainly quartz) from the raw materials and concentrating the kaolinite in the remaining one. The amount
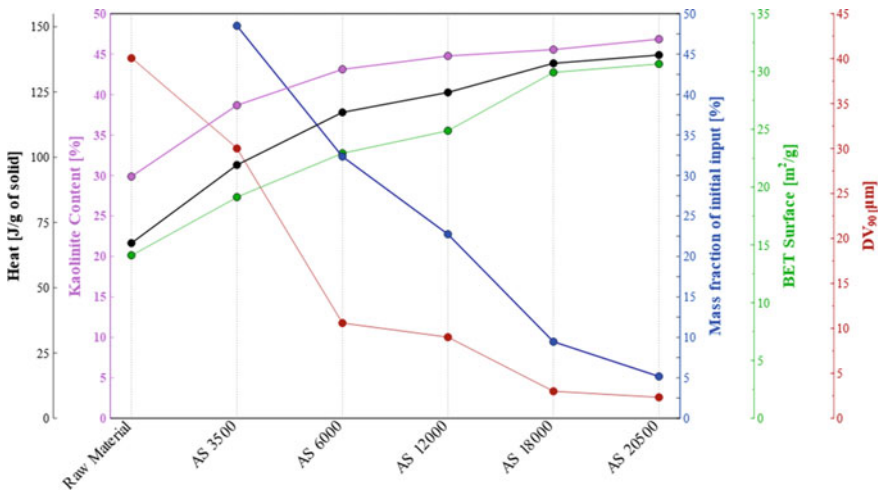
Fig. 3 Consolidated results of particle separation trials using a lab-scale air classifier. Results shown represent values measured over the fine fraction of material obtained

of kaolinite was increased from 30% in the raw clay to about 45% under the most restrictive conditions. However, the reactivity as measured by the R^3 test shows an increase on the heat release at 24 h from 70 to 130 J/g of solids. This is explained due to the simultaneous increase of kaolinite content and specific surface area of the final material as compared to the initial clay.

4 Conclusions

Based on the presented results, the following conclusions can be drawn:

- The incorporation of grinding aids effectively reduces the agglomeration of clays upon grinding. This leads to a reduction of the time required to reach a fine material suitable for LC^3 manufacture under the same grinding energy conditions.
- The incorporation of grinding aids in calcined clay can lead in some cases to significant improvements in the flowability of fresh LC^3.
- Alkanolamines have a strong impact on the aluminate reaction during LC^3 hydration. This effect is linked to the interaction between alkanolamines and iron-bearing phases of OPC.
- Kaolinite is concentrated in the finer portion of the particle-size distribution of ground clays. Particle classification techniques can be used to remove part of the (coarser) impurities in order to increase the kaolinite content of the final material.

References

1. Assaad, J.J., Issa, C.A.: Effect of clinker grinding aids on flow of cement-based materials. Cem. Concr. Res. **63**, 1–11 (2014). https://doi.org/10.1016/j.cemconres.2014.04.006
2. Katsioti, M., Tsakiridis, P.E., Giannatos, P., Tsibouki, Z., Marinos, J.: Characterization of various cement grinding aids and their impact on grindability and cement performance. Constr. Build. Mater. **23**, 1954–1959 (2009). https://doi.org/10.1016/j.conbuildmat.2008.09.003
3. Sohoni, S., Sridhar, R., Mandal, G.: The effect of grinding aids on the fine grinding of limestone, quartz and Portland cement clinker. Powder Technol. **67**, 277–286 (1991). https://doi.org/10.1016/0032-5910(91)80109-V
4. Hathaway, J.C.: Procedure for clay mineral analyses used in the sedimentary petrology laboratory of the USGS. US. Geol. Surv. Methods, 8–13 (1955)
5. Avet, F., Snellings, R., Alujas Diaz, A., Ben Haha, M., Scrivener, K.: Development of a new rapid, relevant and reliable (R3) test method to evaluate the pozzolanic reactivity of calcined kaolinitic clays. Cem. Concr. Res. **85**, 1–11 (2016). https://doi.org/10.1016/j.cemconres.2016.02.015

Calcined Clay: Process Impact on the Reactivity and Color

Mariana Canut, Steven Miller and Morten Jolnæs

Abstract The use of calcined clay fits well with the cement industry scenario where the goal is to produce sustainable and low CO_2 products. In addition, calcined clay draws special attention due to the high availability and improvement of mechanical strength of cement with addition of calcined clay. The trend toward clay calcination stresses the importance to find alternative processes that focus on efficiency and quality of the final product. Temperature, retention time and atmospheric conditions are process parameters which must be under control during the clay calcination, and those will be responsible for the quality and color of the final materials. FLSmidth investigations using two different processes—(1) soak calcination by rotary kiln and (2) flash calcination by gas suspension calciner—show that the flash calcination process gives a uniform heating with a better control of temperature and residence time of clay, which has an impact on the final quality of the clay product. FLSmidth has developed and patented a process which enables to obtain grayish color clays and to recover heat from the finished product more efficiently than traditional kiln process design.

Keywords Sustainability · Calcined clay · Process · Quality and color

1 Introduction

Preventing catastrophic climate change, most studies agree, will mean reducing the level of CO_2 in the atmosphere. The cement industry today is responsible for about 8% of the man-made carbon dioxide, and approximately 55% of the CO_2 emitted by cement production comes from the decarbonation of limestone ($CaCO_3$), when clinker is produced. Substituting clinker by other materials is one of the sustainable ways to decreases the CO_2 footprint from the cement industry. Clays are particularly interesting due to their high availability, low associated CO_2 emissions and product

M. Canut (✉) · M. Jolnæs
FLSmidth, 2650 Valby, Denmark
e-mail: Mariana.Canut@flsmidth.com

S. Miller
FLSmidth, Bethlehem, USA

quality. Clays are aluminum silicates which are in general weathering products of feldspar and other primary minerals and are typically found in sedimentary rocks. According to EN 197 standard, up to 35% of calcined clay can be used in the cement. Several studies have shown that heat treatment of clay at high temperatures (500–900 ℃) to form amorphous synthetic clay will significantly increase the pozzolanic activity of the clays. Other requirement is the color of the clay; FLSmidth has developed and patented the process control for color of clay where grayish color can be obtained by applying the right setting and conditions during the clay calcination and cooling process.

In the past years, FLSmidth has been studying different types of clays and the optimum calcination condition (temperature, retention time, gas flow) using pilot calciner plant and has developed characterization test applied for clay characterization and performance. From these analyses, it is possible to design the proper calciner system for the desired raw materials and provide guarantees of not only production but also heat consumption, energy consumption and color of the final product.

Nowadays, FLSmidth has the know-how to support and advise customers in the area of calcined clay, and the main focus is to combine high efficiency with a high-quality product:

- Convert **locally available** clay raw materials into **high-quality** clay products and to optimize the local cement production at any given site to the **highest possible CO₂ reduction** using an efficient system for clay calcination
- Give guarantee on the energy consumption, process and quality of the final material.

2   Can I Make Calcined Clay?

A laboratory protocol based on physical and chemical characterization tests are used to measure the potential of clays in being used as cementitious materials. Special techniques such as thermogravimetric analyses (TGA) and X-ray diffraction are used to find the appropriated dehydroxylation temperature and mineralogy of clays; these analyses will help in determining the optimum process conditions to obtain a high-quality product. A pilot calciner plant using gas suspension calciner (flash calcination) is used to calcine and confirm the process conditions to be implemented on site. Quality control tests are used to show the final quality of calcined clay according to the international cement standards (Fig. 1).

3   How is the Calcination System and Process?

A process, specifically designed for activation of clays, has been developed by FLSmidth. The process is based on flash gas suspension calciner, and it combines pretreatment, activation and cooling of the clay into one compact, integrated plant as shown in the calcined clay production system illustration, Fig. 2.
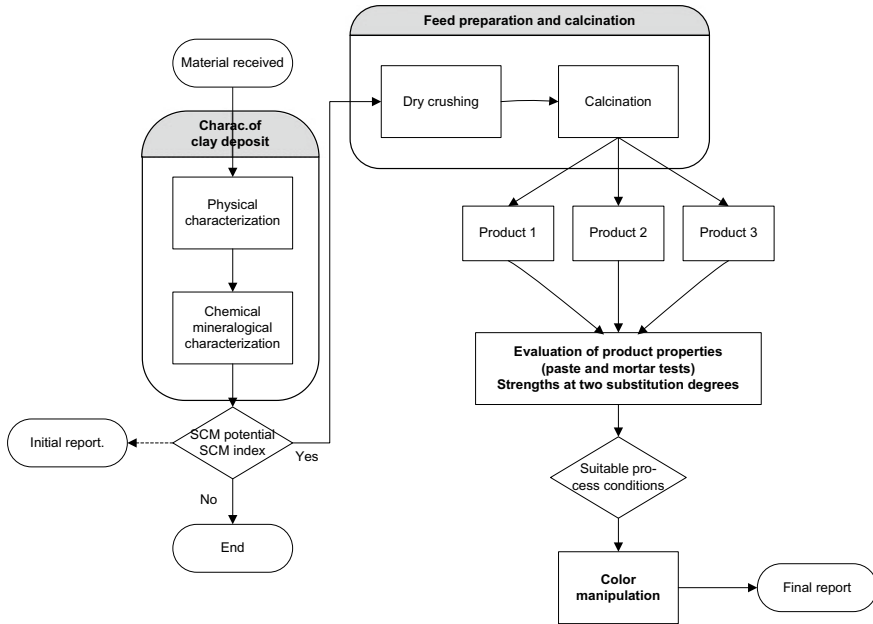
Fig. 1 Laboratory protocol from FLSmidth to ensure an optimum process to obtain a high-quality product

The material pretreatment step breaks up the lumps and removes the moisture (free water) from the raw clay material. The material is then activated through heat treatment in a flash gas suspension calciner, which more efficiently controls the heat applied to the material compared to that which can be achieved in a rotary kiln. With moisture content up to 15%, flash calciner utilizes less than 700 kcal/kg. As a result, by replacing 30% of the clinker with calcined clay, the overall carbon footprint of the traditional cement producing process is reduced by approximately 25%. Moreover, the integrated cooler recuperates heat from the material under controlled reducing conditions, thus preventing a discoloration of the final product. The result is a highly reactive product with a color similar to cement, allowing for high substitution rates in cement, see Fig. 3.

Numerous raw clays from global sources have been used to produce calcined clay in our pilot scale calciner system (flash calcination) and kiln system (soak calcination). When testing the material quality, the product produced in the calciner system outperforms the product from the kiln system, see Table 1. Figure 4 clearly shows the high reactivity of clay calcined by calcination using a flash gas suspension calciner, where up to approximately 90% of the calcium hydroxide from cement product with 30% of clay is reacted at temperatures between 800–900 °C, while in soak calcination (kiln), only 60% was reacted at approximately 600 °C
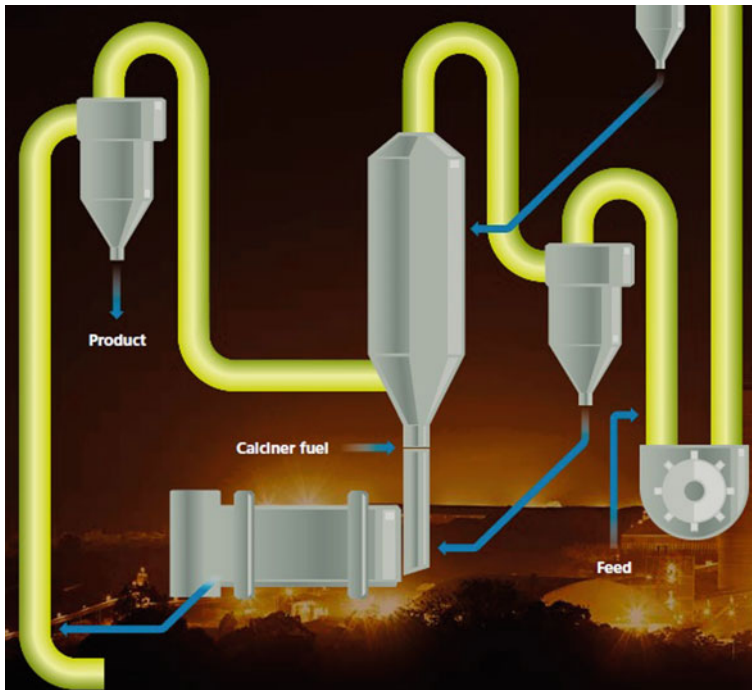
Fig. 2 Flash calcination process developed by FLSmidth

Table 1 Rotary kiln (soak calcination) versus flash gas suspension calciner

	Rotary kiln (soak calcination)	Flash gas suspension calciner
Cost	100% capital cost power cons. maintenance	~75% of kiln capital cost power cons. maintenance
Energy	670–720 kcal/kg	620–660 kcal/kg
Power consumption	~12 kW/t	~17 kW/t
Maintenance	US$3/t	<US$1/t
Color	Reddish color	Cement color
Reactivity	Low reactivity (10% less)	High reactivity
Degree of clay substitution	15–25% substitution	30–40% substitution

4 Main Remarks

FLSmidth is investing in sustainable initiatives for the cement industry, and an important one is the clay calcination system where lower energy costs and emissions without compromising the final quality of the material. A laboratory protocol was prepared to evaluate the feasibility of the raw clay to be used as clinker substitute. A flash gas suspension calciner has shown more advantages over a soak kiln calcination

1. Is the raw material
2. Is calcined material without Color control
3. Are calcined material with color control optimized

Fig. 3 (1) Raw material (2) Calcined material without Color control (3) Calcined material with color control process (Patent from FLSmidth)
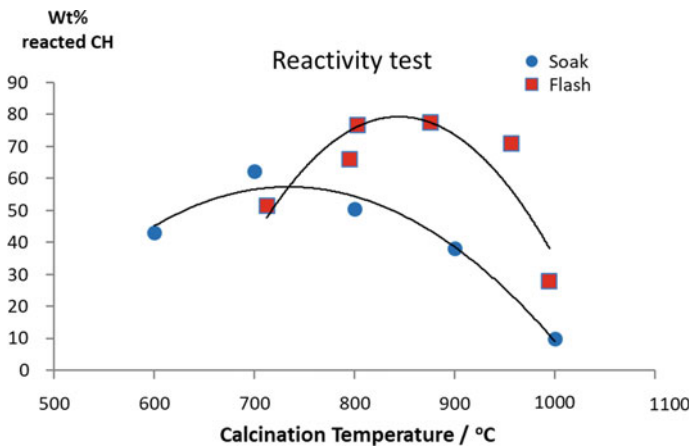
Fig. 4 Amount of CH (calcium hydroxide) in the cement product with 30% clay calcined at different temperatures and using two calcination processes: soak and flash

application due to lower OPEX cost and high quality of the final material (reactivity and color). FLSmidth has developed and patent the process for controlling the color of clay resulting in a grayish cement color clay.

A Flexible Technology to Produce Gray Calcined Clays

Luiz Felipe de Pinho, Luis Felipe Von Rainer Fabiani and Natália Bernardi Ghisi Celeghini

Abstract The use of calcined clays as a substitute for clinker in the cement manufacturing is of great interest among the industries of cement and concrete due to many reasons, such as lower cost of production, lower CO_2 emission rate and great availability of clay material. However, there are different kinds of clays available, regarding chemical and mineralogical composition. Processing clays with high iron content results in reddish or pinkish pozzolan, and cements with reddish and pinkish hues are misjudged as low-quality material. A color change technology to produce gray pozzolan from high iron content clays has been developed by Dynamis and proved in both laboratorial and industrial scales. This work presents the advance of this technology, proving that it can be applied to different kinds of clays and also that it can be implemented with the use of a flash dryer and a rotary kiln or considering only the kiln that can be a refurbished equipment. The technology also enables the production of pozzolan without the color change issue but also in an efficient and economically viable way. Using a combustion technology developed for clay activation, it is possible to control the calcination temperature and to obtain a controlled atmosphere, which is the key to the color change process. Industrial-scale tests proved that the technology is viable and versatile, regarding the types of processed clays.

Keywords Pozzolan · Clay color · Reducing atmosphere · Industrial scale · Calcined clay · Rotary kiln · Flash dryer

1 Introduction

Clays that possess required chemical and mineralogical composition can be calcinated at temperatures between 700 and 900 °C which modify its properties and favor its application as pozzolanic material.

The utilization of calcined clays in Brazil is regulated by ABNT and there are three main cement classifications that contain pozzolan: CP II Z with 6–14% of pozzolan,

L. F. de Pinho (✉) · L. F. Von Rainer Fabiani · N. B. G. Celeghini
Dynamis Engenheria e Comércio, São Paulo, Rua Padre Chico, 85 Cj 11, São Paulo, SP CEP 05008-010, Brasil
e-mail: luiz.pinho@dynamis-br.com

CP IV with 15–50% of pozzolan, CP IV with 15–50% of pozzolan and CP V ARI RS with maximum of 25% of pozzolan.

Hence, the calcined clays market in Brazil can be estimated in 5 million tons/year in the current market. Despite that, processing high iron content clays is still a problem to this market.

Such clays, when calcined, turn into reddish and pinkish pozzolan, and this is not well accepted because it affects the final color of produced cement. In Brazil, reddish and pinkish cements are misjudged as low-quality material, once the consumers tend to believe that this material is mixed with raw material, as sand or raw clay.

Therefore, Dynamis has developed a technology that enables the production of gray pozzolan using as raw material high iron content red clays.

Clay activation occurs in temperatures between 700 and 900 °C, when crystallized water is removed, changing the crystalline structure of the material, resulting in a product with hydraulic activity. The calcination temperature varies according to its mineralogical composition. In this same range of temperature, the hematite resident in the clay, when in contact with oxygen, will become even more reddish.

The technology consists in performing the activation and color changing processes in an atmosphere with low oxygen content concentration, without carbon monoxide (CO) emission. Using a D-Gasifier (Dynamis patented burning equipment), the drying and calcination process can take place in a rotary kiln, flash dryer and rotary kiln or fluidized bed kiln. The technology comprises the following steps:

- Heating and Drying: Heating the raw clays to a temperature between 100 and 350 °C to obtain a material with 0–5% moisture. This step can be done in the initial length of a long rotary kiln, in a flash dryer or in a fluidized bed.
- Mixing: In this stage, the dried clay is mixed with a solid fuel, according to the iron content.
- Calcination: Heating the mixture of dried raw material and fuel to a temperature between 700 and 900 °C in a low oxygen environment. In this step, the localized reducing atmosphere is obtained from the solid fuel that will be consuming the oxygen from the environment to burn completely. This localized reducing atmosphere will transform the hematite in magnetite ($FeO \cdot Fe_2O_3$) that possesses a dark greyish hue.
- Cooling: This step is important because cooling slowly the gray pozzolan in oxygen-rich environment will transform back the magnetite in hematite, and the material will become reddish again. Therefore, this step consists in rapidly cooling the product until 600 °C, and after that, the cooling can be slow until 120 °C. Those processes can take place in rotary cooler, using air and water. The water can be used directly or indirectly, as in the external surface of the cooler.

The combustion equipment applied in those processes, D-Gasifier, has its crucial importance to the technology owing to the following reasons:

- It allows a sub-stoichiometric combustion of the fuels (solid, liquid or gas). The D-Gasifier is coupled in the kiln's discharge and will generate hot gaseous fuel with high content of CO. The amount of oxygen necessary to burn completely this CO

will be supplied by secondary air, preheated in the rotary cooler, and the complete combustion will take place inside the kiln, maintaining a low O_2 environment.

- The D-Gasifier generates a gas flame, which is shorter than a solid fuel flame that allows the installation of metallic lifters in the first portion of the kiln length. In this case, former long wet process kilns can be refurbished in a one equipment dryer/kiln.
- The kind of shorter flame generated in the D-Gasifier is more suitable to a dusty atmosphere formed inside the pozzolan kilns.
- Temperature control in the calcination zone is possible through regulation of the primary air rate. Working with a sub-stoichiometric combustion allows lower temperatures, under 900 °C, that is an adequate temperature for clay's calcination and for the kiln's operation. Once pozzolan kilns do not have coating such as clinker kilns, maintaining a lower temperature is important.
- The D-Gasifier can also be applied to generate hot drying gases for a flash dryer.

2 Experimental Study

2.1 First Run Tests

In the first run, two types of clays were processed in the Instituto de Pesquisas Tecnológicas (IPT), dried in stove at 105 °C and, after that, grinded in a disk mill to 0.150 mm. After that, a mix of clays containing 30% addition of coke were prepared and homogenized in a rotary shaker and calcined in a rotary pilot-scale rotary kiln, such as described in [1].

The same two types of clay were calcined in an industrial plant designed by Dynamis in 2009 to produce calcined clay for Cimento Planalto (CIPLAN), in Brazil [2, 3]. The pozzolan activation line has a countercurrent rotary kiln of Ø3.0 m × $L = 52$ m. The calcined clay was cooled by a rotary cooler (that also preheats the combustion air), and the de-dusting was done by high efficiency cyclones and a baghouse filter. The combustion system is a D-Gasifier that burns 100% grinded petroleum coke. The industrial trials processed 25 t/h of raw clays in a period of more than twelve hours (Table 1).

Table 1 First run raw materials

Composition	Clay 1	Clay 2
Loss on ignition (LOI)	12.2	13.9
Silicic anhydride (SiO$_2$)	55.0	47.5
Aluminum oxide (Al$_2$O$_3$)	23.2	27.6
Iron oxide (Fe$_2$O$_3$)	7.8	9.0

Fig. 1 Bik Gardner's color guide sphere d/8 (CIELAB)
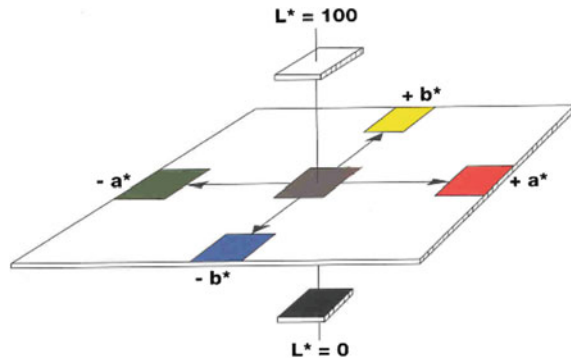
Fig. 2 Raw clay and pozzolan produced in industrial trial

Raw Clay   Pozzolan

In order to evaluate the color of the produced pozzolan, the samples are analyzed by a colorimeter, according to Bik Gardner's parameters. A desirable material must have the parameter "*a*" under 5.0 (Figs. 1 and 2; Tables 2 and 3).

2.2 Second Run Tests

For the second run of tests, three different types of clay were mixed and calcined both in laboratorial and industrial scales. The laboratorial trials also took place in IPT, with the same methodology applied in the first run. Industrial scale tests were performed in the same CIPLAN's plant, but was done a 10 days trial, processing 5.000 t of clay. The "Clay 4" possesses a higher iron content, and the "Clay 5" is the more reactive one. With the objective to obtain an optimized mix, considering iron content, reactivity and cost were tested in two mixes. The Mix 1 contains 90% of Clay 3 and 10% of Clay 5, and Mix 2 contains 85% of Clay 3 and 15% of Clay 4.

Table 2 First run results—color change

Coordinates	Cement CPV	Clay 2—raw	Clay 2—calcined without coke	Nonmetallic fraction of calcined clay 2 (NFM)	Mix 35% NFM + 65% CPV	Mix 45% NMF + 55% CPV
L	58.8	40.4	39.1	40.5	50.5	49.1
a	1.1	21.0	23.6	−0.1	0.8	0.7
b	10.5	23.4	25.4	−0.6	6.4	5.4
Sample						

Table 3 First run results—strengths—pozzolanic activity index (PAI)

Time	Compression resistance (MPa)—100% cement CP V	Compression resistance (MPa)—cement CP V with 30% of pozzolan
3 days	43.7	37.8
7 days	50.8	49.5
28 days	59.7	59.6

Pozzolanic activity index (PAI): 105%

3 Industrial Plant

Both the industrial tests were performed in a plant consisted of a rotary kiln with two stages; the first portion of the length is the drying section, with metallic lifters, and the final portion of the length is the calcining section, with refractory bricks. The cooler is a rotary cylinder that also preheats the secondary air. The cooling is supplemented with water in the cooler shell.

However, the same color changing technology is now being applied in a plant using a flash dryer–rotary kiln system. In this case, a D-Gasifier is used to provide hot drying gases to a flash dryer. The dried clays are mixed with coal and fed in the kiln, which now is only used for the calcining step, and possesses refractory lining along all its length. In the discharge of the kiln, there is another D-Gasifier, working with a sub-stoichiometric flow of primary air, in order to supply necessary heat for calcining and maintaining a low O_2 atmosphere (around 3%).

The cooler is also a rotary cylinder working with secondary air and a water flow outside the shell (Fig. 3).

Industrial production was also made in the flash dryer–rotary kiln installation, processing the Clay 3 indicated in Table 4. Very satisfactory results were obtained, resulting in gray pozzolan with loss on ignition below 3%. Figure 6 shows an Erlenmeyer containing a solution with laboratory-scale calcined clay (color changing
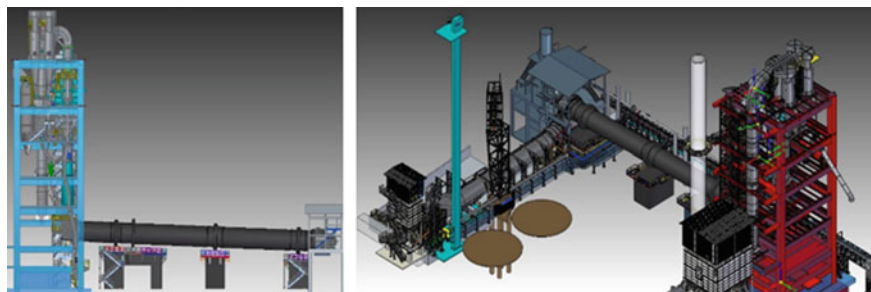
Fig. 3 Industrial plant with flash dryer

Table 4 Second run raw materials

Composition	Clay 3	Clay 4	Clay 5	Mix 1	Mix 2
Loss on ignition (LOI)	7.55	10.4	11.5	7.73	8.55
Silicic anhydride (SiO_2)	62.8	50.9	64.2	72.0	60.0
Aluminum oxide (Al_2O_3)	15.9	19.9	22.1	13.8	20.6
Iron oxide (Fe_2O_3)	8.3	17.4	3.8	5.17	9.12

Fig. 4 Industrial plant with flash dryer–rotary kiln system

technology not applied) that becomes completely red and a flask containing a solution with the industrial calcined clay that becomes gray due to the color changing technology (Figs. 4 and 5; Tables 5 and 6).

4 Conclusion

The color change technology has been tested in more than one industrial and laboratorial trials and proves to be a viable solution for the application of reddish and pinkish clays in the production of pozzolan. The method is versatile and can be applied in long rotary kilns, such ones that can be refurbished from wet process, new kilns that combine drying and calcining and also considering flash dryer. Drying the raw material with a flash is interesting because it provides smaller footprints considering the same size of a project. Besides, the flash dryer, once is an static equipment, can offer a more economic solution, with low maintenance, when compared with a rotary kiln.

Fig. 5 Comparison between laboratory-scale calcined clay and industrial calcined clay
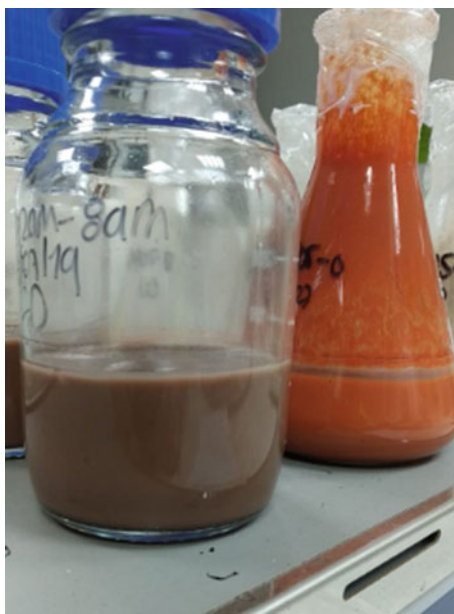
Fig. 6 Grinded pozzolan obtained in industrial trials

Table 5 Second run industrial results—color change

Coordinates	Mix 1—raw	Mix 2—raw	Mix 1—industrial calcined	Mix 2—industrial calcined	70% cement 30% mix 1	70% cement 30% mix 2
L	6.23	60.4	55.5	50.2	40.5	50.5
a	14.7	15.3	6.5	4.7	−0.1	0.8
b	22.2	23.7	14.5	10.6	−0.6ç	6.4
Sample						

Table 6 Second run industrial results—pozzolanic activity index with lime

Composition	Mix 1	Mix 2
Loss on ignition (LOI)	7.73	8.55
Strength at 7 days with lime	8.2 MPa	10.3 MPa
Minimum strength allowed	6.5 MPa	

References

1. Chotoli, F.F., Quarcioni, V.A., Lima, S.S., Ferreira, J.C., Ferreira, G.M.: Clay activation and color modification in reducing calcination process: development in lab and industrial scale. In: International Conference on Calcined Clay Fos Sustainable Concrete (2015)
2. Fabiani, L.F., Ferreira, G.M.: Pozzolan: a green solution. World Cement (2010)
3. Pinho, L.F., Ferreira, J.C.: Comparativo de Tecnologias para Calcinação de Argilas Pozolânicas. Congresso Brasileiro de Cimento (2016)

Research and Design of Suspension Calcining Technology and Equipment for Kaolin

Shengliang Tang, Jianjun Wu, Huating Song, Bin Wang and Tongbo Sui

Abstract A new large-scale suspension calcination process and key equipment suitable for dehydration and calcination of kaolin clay are introduced. The pretreatment process can be designed to meet various raw materials with different moisture contents, and the burning system has high heat transfer efficiency with a five-stage cyclone preheater, a suspension calciner and a fluidization cooling system. Moreover, the thermal process of materials in the production line can be accurately controlled as required necessarily; especially, the temperature of calciner can be controlled at a fluctuation of less than ± 10 °C. Pilot production results show that suspension calcined clay has good activity and workability as a kind of supplementary cementing materials, indicating that suspension calcination technology has a good application prospect in the field of producing calcined clay for cement.

Keywords Suspension calcining technology · Process design · Calcined clay · Performance

1 Introduction

There are different traditional calcination processes of kaolin, e.g., fixed bed process (such as tunnel kiln, down flame kiln, shuttle kiln, push plate kiln and heat preservation cylinder), moved bed process (such as shaft kiln, rotary kiln and multilayer open hearth furnace) [1–4]. But, there are more or less intractable disadvantages in these modes. Due to the advantages of preferable gas–solid contact effect, high thermal efficiency and being suitable for mass production, suspension calcination technology has been successfully applied in the fields of cement, alumina, magnetization roasting, lime and so on [5, 6]. Based on the comprehensive investigation and analysis of the application status and the existing problems of suspension calcination technology in these industries, we creatively developed a suspension calcining process and complete set of equipment which can be applied to kaolin calcining. The successful application of this technology is also attributed to our rich experience in

S. Tang (✉) · J. Wu · H. Song · B. Wang · T. Sui
Sinoma International Engineering Co., Ltd., Nanjing 211100, People's Republic of China
e-mail: tangshengliang@sinoma-ncdri.cn

engineering design of preheating and pre-decomposition suspension state calcination system. The production line with an output of 300 t/d magnesium oxide (MgO) has been established in Jiangsu province, which is also a demonstration line of 600 t/d for kaolin calcination. This paper will briefly introduce the development process and equipment matching and trial production of suspension CC (calcined clay).

2 Technological Design

On the basis of the experimental research and theoretical analysis, the processing parameters are calculated and subsequently applied to the technological design. Some proprietary technical equipments are also developed to meet the technical requirements.

2.1 Raw Material Pretreatment

The vertical roller mill (VRM) is used for the raw material grinding. The kaolin with water content less than 14% is fed into the mill by a bucket elevator. The material is grinded, dried and subsequently separated by the classifier in the VRM. The technological process is shown in Fig. 1. Dynamic separator is used; the fineness of raw meal can be controlled by regulating the speed of separator. Powder that meet the requirements (90 μm mesh residue ≤12%, the product moisture ≤1%) from the mill enters the bag filter along with the airflow. The collected powder is discharged
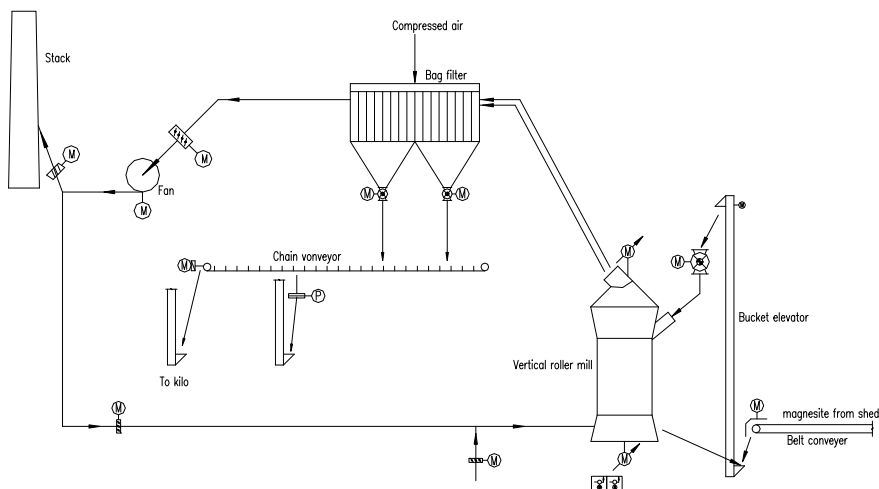
Fig. 1 Process of raw material pretreatment

to the chain conveyed and bucket elevator and then sent to the raw meal storage. The heat source for drying the raw mill is the hot exhaust gas which comes from the preheater. The air out of the mill is induced by the fan. Part of the exhaust gas through the fan returns to the raw mill as recycle air, and the other is discharged into chimney. When the raw material with water content is more than 20% or no need for grinding, another production process will be adopted (due to limited space, this article only introduces some of the main overviews of the technology).

2.2 Suspension Burning and Cooling System

The suspension burning and cooling system may be divided into five parts, including raw meal feeding, preheating and calcining of raw meal, metakaolin cooling, waste gas treatment and product conveyance (Fig. 2). The preheating, calcining and cooling processes of material are completed in suspension state. This ensures good mass transfer and heat transfer efficiency.

The raw meal unloaded from the storage is measured and then is successively transported through the air slide, bucket elevators and the preheater top chute. Finally, the raw meal is fed into the preheater. The preheating system uses four-stage preheaters and an on-line calciner which includes cyclones, connecting pipes, feeding pipes, calciner, etc. The top cyclone is class 1, namely C_1, and the bottom cyclone is class 4, namely C_4. The specifications of preheater C_1, C_2, C_3 and C_4 are Ø2700, Ø3000, Ø3000 and Ø3350 mm, respectively. The raw meal powder sent into the C_2 cyclone gas outlet pipe is immediately dispersed and suspended in gas flow by the agency of the gas flow. And with the gas flow, raw meal enters the C_1, in which gas–solid separation is finished. Then, the separated solid powder enters into C_3 cyclone gas outlet pipe through a heavy flap damper after the separation material out off gas, and with gas flow, enters into C_2, C_3 and C_4 cyclone successively.

Thus, after four-stage heat exchange, the preheated raw meal powder is fed into the calciner. Four burners are arranged for the calciner. The temperature in calciner can be controlled about 700–950 °C. This heating causes the dehydroxylation of kaolin and leads to the production of metakaolin. By controlling the retention time of the kaolin in the calciner, the reaction is fully completed. This process takes only a few seconds. The product follows the airflow into the C_5 cyclone, and after separation, it will be fed into the fluidized bed cooling system which includes three cyclones and two fluidized bed coolers. The use of fluidized bed cooler guarantees the cooling effect and the safety of the system. The product is eventually cooled to less than 120 °C, and then conveyed to silo. And, the waste gas will rise along with various cyclones and gas outlet pipes and finally is discharged by one gas duct and induced by high temperature induce draft fan to a vertical roller mill and waste gas treating system. Exhaust gas of C_8 also goes to the waste gas treatment system of burning system. The demonstration line for suspension calcination has been constructed (Fig. 3).
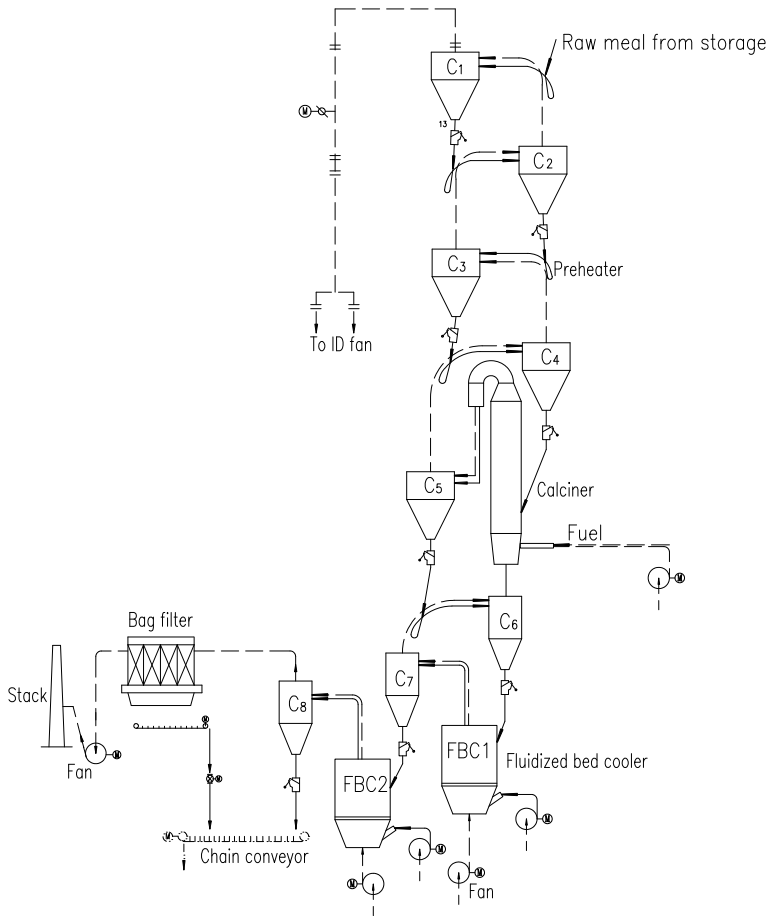
Fig. 2 Process of the suspension burning and cooling system

2.3 Waste Gas Treating System

The waste gas treatment system uses large bag filter (as shown in Fig. 4). The dust concentration of the purified gas is less than 20 mg/Nm^3. The gas is discharged into atmosphere by induced fan and stack. The dust collected by bag filter is discharged into chain conveyer and then enters into the raw meal storage by the elevator.

Fig. 3 Demonstration production line of suspension calcining and cooling system
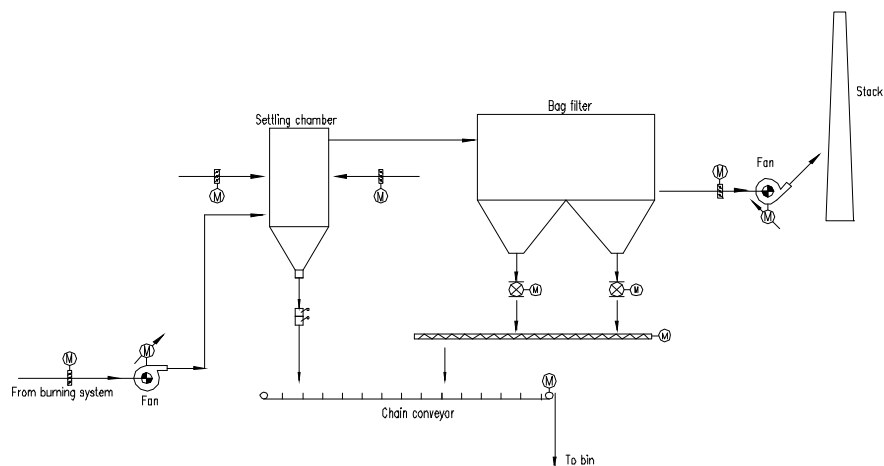
Fig. 4 Process of exhaust gas treating system

3 Pilot Production

3.1 Raw Material Analysis

The raw materials used in the project are collected from Beihai. Chemical composition (Table 1) was determined with X-ray fluorescence spectrometer. XRD analysis was performed on X'pert Powder equipment, and the results are shown in Fig. 5. The contents of kaolin and other minerals were estimated. The result (Table 2) shows that the raw material has a low kaolin content of 50.7%. Quartz and muscovite are the main impurities.

The dehydroxylation test was conducted by using SDT Q600 which simultaneously measured the heat flow changes (by DSC) and weight changes (by TGA) associated with transitions in a material as a function of temperature (heating rate: 20 K/min) and time in a well-controlled atmosphere. Figure 6 shows that the initial dehydroxylation temperature of kaolin is about 400 °C, and the fast dehydroxylation of kaolinite occurs in the temperature range of 500–550 °C.

Table 1 Chemical composition (dry basis) of the Beihai kaolin

Chemical	SiO_2	Al_2O_3	Fe_2O_3	TiO_2	K_2O	MgO	CaO	P_2O_5	LOI	Total
Content (wt%)	52.42	31.53	1.32	0.19	3.62	0.33	0.19	0.06	9.36	99.02

LOI: loss on ignition (measured by thermogravimetry)
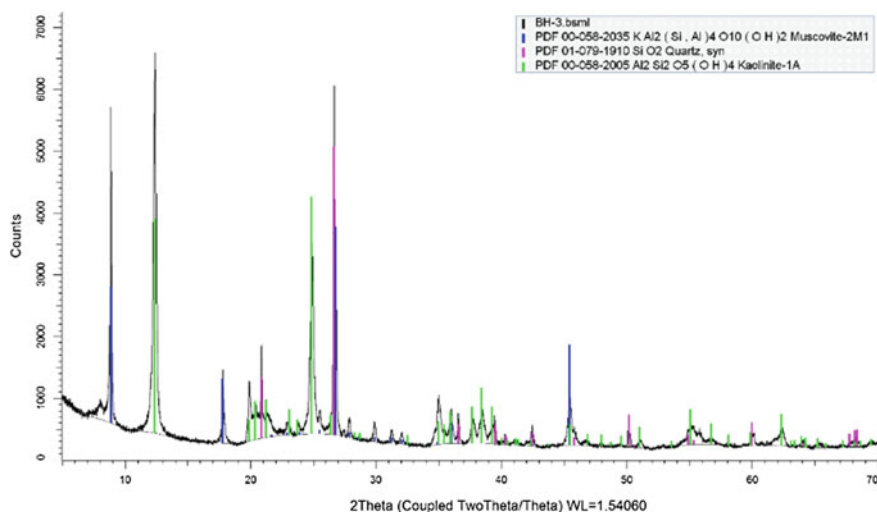
Fig. 5 X-ray diffraction patterns of the kaolin

Table 2 Mineral composition of the Beihai kaolin

Mineral	Kaolin	Quartz	Muscovite	Total
Content (wt%)	50.7	15.2	34.1	100
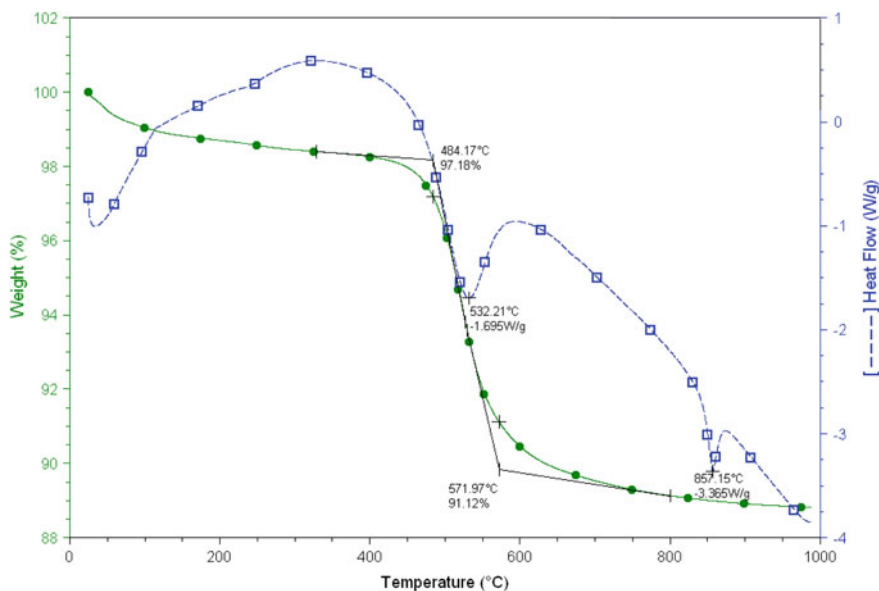
Fig. 6 Thermogravimetric analysis curves of kaolinite

Table 3 Analysis and elemental analysis of coal

Items	Coal analysis				Qnet/(kJ/kg)	Elemental analysis				
	M_{ad}	A_{ad}	V_{ad}	FC_{ad}		C_{daf}	H_{daf}	O_{daf}	N_{daf}	S_{daf}
Values	2.27	13.60	30.78	53.35	23,023	62.00	4.20	16.00	3.00	0.49

3.2 Fuel Analysis

According to the requirements of product quality, different fuels can be used. In this project, the coal with low ash is selected and used. Coal analysis and elemental analysis of coal fuel were determined by using chemical analysis based on stoichiometry (Table 3).

3.3 Suspension Calcined Clay Analysis

3.3.1 Reactivity of Calcined Clay

Beihai kaolin was thermally treated in the demonstration line to produce calcined clay. Different outlet temperatures of calciner were controlled to analyze the relationship with temperature, loss on ignition and pozzolanic activity of calcined clay. The calcining temperature and physical performance of cement mixtures with 30% calcined clay used as SCM according to the standards of EN 196-1 can be seen in Fig. 7. It shows that the best burning temperature as can be seen is around 740 °C, and calciner temperature can be controlled accurately, and the range of temperature fluctuation is very small.
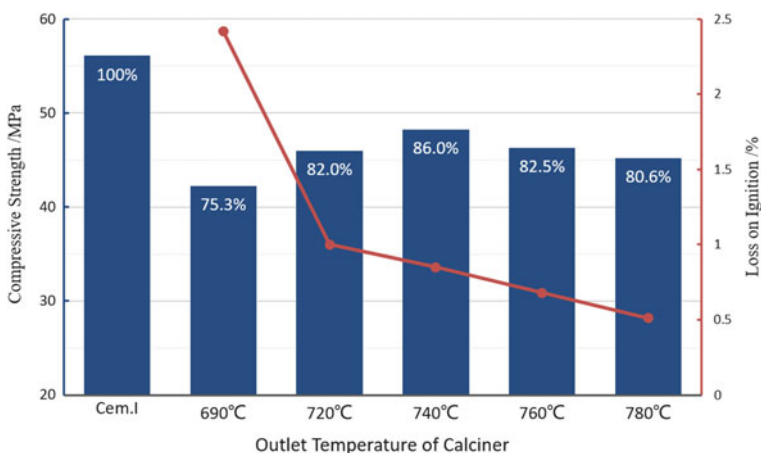
Fig. 7 Mortar strength, reactivity index and L.O.I of calcined clay at different temperatures
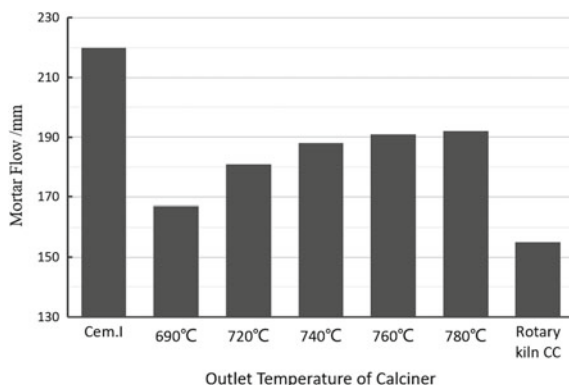
Fig. 8 Mortar flow of calcined clay at different temperatures

3.3.2　Workability of Suspension Calcined Clay Cement Mortar

The comparison of mortar flow (0.50 w/c) of reference cement, blended cement mixtures with 30% calcined clay at different temperatures and blended cement with rotary kiln calcined clay (same raw kaolin from Beihai) can be seen in Fig. 8. It shows that the blended cement with 740–780 °C suspension CC performs good workability with around 190 mm flow which is much higher than rotary kiln CC.

3.3.3　Micromorphology of Suspension Calcined Clay

Scanning electron microscopy (SEM) was used to observe the micromorphology of calcined clay powders and to analyze the influence on physical properties. As can be seen in Fig. 9, suspension calcining technology produced a number of spherical and smooth surface metakaolin unlike the layered original kaolinite structure of rotary kiln CC that has a significant positive effect on reducing the high water demand of calcined clay blended cement.

4　Technical and Economical Indexes

The theoretically designed heat consumption of the burning system was 580 kcal/kg at a design production capacity of 600 tons per day. The total power consumption is 60 kwh/t. The exhaust gas temperature of the C_1 outlet can be controlled at 250 ± 40 °C. The pressure drop of system is only about 7000 Pa. The project covers an area of 40,000 m^2, and the total investment is about 60 million.
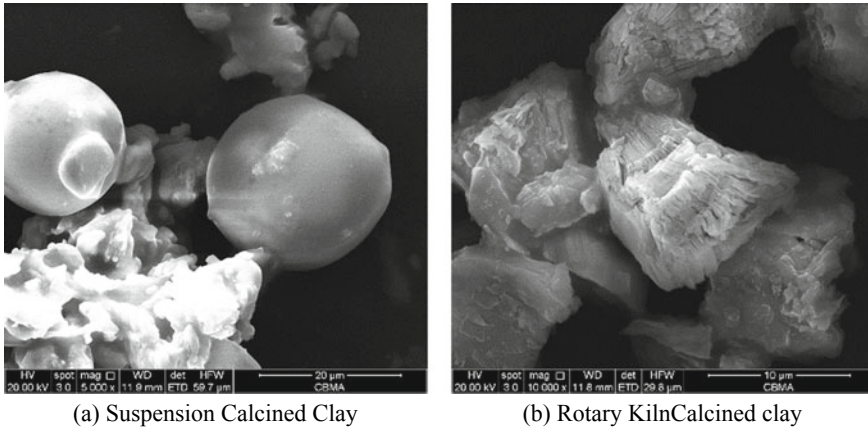
(a) Suspension Calcined Clay   (b) Rotary KilnCalcined clay

Fig. 9 Micromorphology of calcined clay

5 Conclusions

The first demonstration production line with suspension calcining technology has been completed in China. The design, construction process and the first trial calcining kaolin clay production results show:

(1) The suspension calcining technology can meet the processing requirements of raw materials with different moisture contents.
(2) The production process of rapid decomposition reaction with suspension calciner, preheating and fluidization cooling has the characteristics of fast heat transfer and high heat exchange rate. The heat consumption is below 580 kcal/kg at a design 600 tpd production capacity.
(3) The calciner temperature can be easy to adjust and control, and the range of temperature fluctuation is less than $\pm 10\,^{\circ}\mathrm{C}$.
(4) The suspension calcined clay has good pozzolanic activity and less water demand due to its spherical metakaolin particles than rotary kiln calcined clay.

References

1. Teklay, A., Yin, C., Rosendahl, L., Bojer, M.: Calcination of kaolinite clay particles for cement production: a modeling study. Cem. Concr. Res. **61–62**, 11–19 (2014)
2. Salvador, S., Pons, O.: A semi-mobile flash dryer/calciner unit to manufacture pozzolana from raw clay soils-application to soil stabilization. Constr. Build. Mater. **14**(2), 109–117 (2000)

3. Wang, Z.: Design and manufacture of kaolinic direct-fired calcining kiln. Mech. Manag. Develop. **24**(2), 34–36 (2009)
4. Wang, Z., Li, H.: Study on suspension calcination technology of kaolin from coal measures. Non-Met. Mines **30**(2), 45–47 (2007)
5. Zhao, B., Chen, Y.: Study on process control of suspended calcining production line of calcium carbonate residue. Inorg. Chem. Ind. **45**(11), 38–40 (2013)
6. Yang, Q.: Energy-saving reconstruction of fluidized bed cooler of gas suspension calciner. Non-Ferrous Metall Equip. **3**, 44–47 (2016)

Elements for the Design of Experimental Plant for LC^3 Cement Production

L. I. Machado, M. I. Herrera and F. Martirena

Abstract Associated with cement manufacturing processes, large amounts of carbon dioxide (CO_2) are released into the atmosphere, and it is estimated that between 0.65 and 0.90 tons of CO_2 are emitted per ton of cement manufactured. By 2050, the demand for this binder is expected to exceed 5000 million tons, which would contribute to an increase of more than 3% of emissions. However, the emissions can be reduced by using supplementary cementitious materials (SCMs); in this sense, calcined clays have a great potential for the reduction of emissions in the manufacture of cement. This has been studied in recent years with low carbon cement or LC^3, developed by a joint team of the University of Lausanne and the Central University of Las Villas. The main results are the expansion of production by achieving clinker substitutions of up to 50%. In this sense, the Center for Research and Development of Technologies and Materials (CIDEM) in conjunction with the company *IPIAC NERY* has committed to the development of a small pilot plant that makes the manufacture of limited quantities of LC^3, which allows the study of the process by interacting different sources of raw materials. In this paper, some calculations were for designing a pilot plant, taking into account the balance of mass and energy necessary for its proper functioning, which in turn allows to specify the technology for the scaling of the production in any new industrial plant or adaptation of capacities installed.

Keywords Mass · Energy · Low carbon cement · Clay

1 Introduction

A new technology based on the replacement of clinker by high volumes of supplementary cementitious material, in this case thermally activated clay (TAC, in Spanish AAT), has been investigated in recent years by researchers of the international team "Low Carbon Cement." The new proposal is officially recognized by the scientific

L. I. Machado (✉) · M. I. Herrera · F. Martirena
Central University Marta Abreu de Las Villas, Center for Research and Development of Structures and Materials (CIDEM), Santa Clara, Cuba
e-mail: ivanm@uclv.edu.cu

community as LC^3, whose results and advances are documented in scientific journals, being in this sense very important the expansion of production to achieve clinker substitutions of up to 50% [1].

The LC^3 is an appropriate option because it considerably reduces CO^2 emissions into the atmosphere by reducing energy consumption, which is economically advantageous [2]. Recently, through the management of *IPIAC-NERY* the demand for LC^3 commercial production plants has skyrocketed. However, perform the essential industrial tests, although necessary to perform tests in real conditions can be very expensive.

In this sense, this work exposes some elements of the design of a small pilot plant where tests can be carried out in industrial conditions, with the advantage of obtaining reduced yields; however, these small plants replicated in a conscious way can be equivalent to the investment in a large cement plant. The first IPIAC–CIDEM plant will be put into operation in facilities of the Central University of Las Villas; its location is shown in Fig. 1.

The balance of mass and energy that is established in the calciner by achieving the thermal modification of the clay is also analyzed. At temperatures between 100 and 400 °C approximately, clay minerals give up their free water (not combined) and adsorbed water, including interlaminar water, at higher temperatures, between 400 and 750 °C, and depending on the types of clay minerals present in the raw material, water combined chemically in the form of hydroxyl groups is released (dehydroxylation).

In the case of kaolinite, the process of mass loss of the material during thermal activation is defined as a function of the activation temperature by the following expressions [3].

$$Al_4\big[(OH)_8Si_4O_{10}\big] \rightarrow 2(Al_2O_3 \cdot 2SiO_2) + 4\,H_2O \tag{1}$$

$$Al_2O_3.2SiO_2(OH)_4 \rightarrow Al_2O_3 + 2\,SiO_2 + 2\,H_2O \tag{2}$$
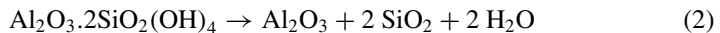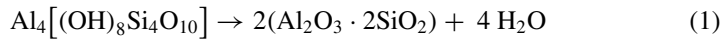
In the dehydration, clays influence factors such as the type of clay minerals, the nature and quantity of impurities, the size of the particles, the degree of crystallization of the clays, the gaseous atmosphere, and others.

The pilot plant IPIAC–CIDEM for the design of experimental tests is conceived to obtain a production flow of TAC of 100 kg/h by dry process, in this work to facilitate the design tasks in terms of mass and energy balances. Data are obtained from the bibliography consulted or from estimates made. The theoretical–methodological approach is exposed to perform the mass and energy balance, within the control limits determined for the kiln system. Figure 2 shows the flow of the process established in the pilot plant for the production of LC^3.

Fig. 1 Location of the pilot plant IPIAC–CIDEM, Central University of Las Villas, Faculty of Constructions, Villa Clara, Cuba

2 Analysis and Results

An optimal design of the rotary kiln can considerably reduce the assembly cost of the plant from the initial assumption of the desired production levels. Table 1 shows a summary with the projection in time of the expected production level.

2.1 The Rotary Kiln—Sizing

The rotary kiln consists of a cylindrical tube resting on rolling stations, which has a certain slope with respect to the horizontal and which rotates at speeds of rotation between 1.8 and 3.5 revolutions per minute (rpm).

Low carbon cement manufacture process flow chart

1	Rotary kiln	6	Additive storage silos
2	Balls mill	7	Centrifugal blowers
3	Heat exchanger	8	Endless screw
4	S-G separators (cyclones)	9	Burner
5	Conveyor belt	T	Temperature sensor
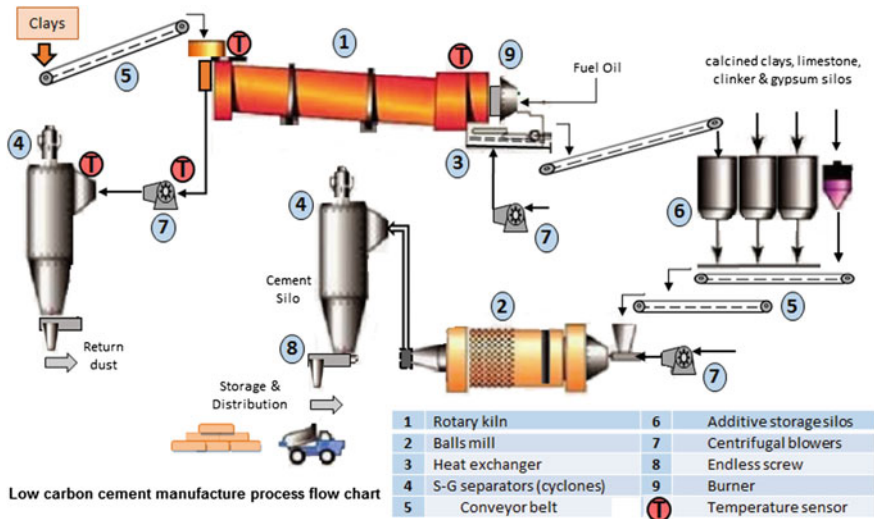
Fig. 2 Flow of the process established in the pilot plant for the production of LC^3. *Source* Esparza (2020)

Table 1 Estimated TAC production when carrying out the design calculations of the pilot plant *IPIAC–CIDEM*

Productivity calcination—TAC		CaCO$_3$	LC^2	P35	LC^3
100	Kg/hours	67	167	167	333
800	Kg/8 h	533	1333	1333	2666.7
2400	Kg/24 h	1600	4000	4000	8000
72,000	Kg/month	48,000	120,000	120,000	240,000
720,000	Kg/year	480,000	1,200,000	1,200,000	2,400,000
720	Tons per year	480	1200	1200	2400

The slope is determined for which there is no rigid rule, its value ranges between 2 and 6%, and most furnaces are installed with slopes between 2 and 4% in relation to the horizontal. As a result of the experience of operating rotary kilns, the optimum ratio between slope and filling coefficient (ϕ) has been obtained [4].

For the present design, a slope of 2° is established with a coefficient ϕ of 11%. In addition, the revolutions per minute (rpm) of the rotary kiln will be in the order of 2.5 rpm and a flow rate of 0.045 m^3 of clay/hours.

The calculation of different furnace design parameters is based on the law of transport of material inside an inclined rotary tube given by the US Bureau of Mines, which is expressed by Eq. 1:

$$Q = 1,48 * n * \text{Di}^3 * \Phi * \rho a * \text{tag}(\beta) \tag{3}$$

where Q is the transport capacity per hour (kg/h), n is the speed of rotation (rpm), Di is the inner diameter (m), ϕ is the filling degree, ρa is the density of the material, and β is the movement of the resulting material (°).

Transformed (1)—it is possible to obtain an expression for the determination of the inner diameter of the calciner rotary kiln according to 2 [5]:

$$D = \sqrt{\frac{ws \cdot 4 \cdot t}{L \cdot gr \cdot \pi \cdot \rho}} \tag{4}$$

where ws is the solid flow (kg/min), L is the length of the kiln (m), gr is the furnace filling degree (%), p is the kiln slope (in %), and t is the total time of residence of the material inside the kiln (min).

The residence time of the clay material that has to be dehydroxylated is possible to obtain from Eq. 3, however, there are many other expressions for the calculation of the residence time [4]. The residence time will determine the flow of material inside the kiln, so this is one of the basic parameters for the design. When setting this variable, others can be calculated for the sizing of the kiln.

$$t = \frac{10.62 * L}{p * d * n} \tag{5}$$

where t is the time of permanence (minutes), L is the length of the rotary kiln (m), d is the inner diameter (m), n is the rotation speed (rpm), and p is the inclination slope of the kiln.

The residence time is inversely proportional to the rotation speed and diameter of the kiln, being directly proportional to the length of the oven. The length and diameter of the furnaces are related by empirical laws such as $L/D = 10-13$, for long furnaces with different types of support; however, prototypes with relation (4–12) can be found [6], in this work, we have opted for a relationship in the environment of 5. Table 2 shows the values of the coefficients and factors assumed, as well as the final dimensions adopted.

Table 2 Main working parameters and dimensions of the rotary kiln *IPIAC–CIDEM* for obtaining thermally activated clay

Di	L	t	Q	n	ϕ	p	β
0.42	3.745	11	100	2.5	11	2	2.751

Fig. 3 Calcination of clays
in a pilot plant. Analysis and
borders. *Source* Self-made

Clay   Gases

Rotatory
Kilnt

Fuels

Air   cooler

TAC
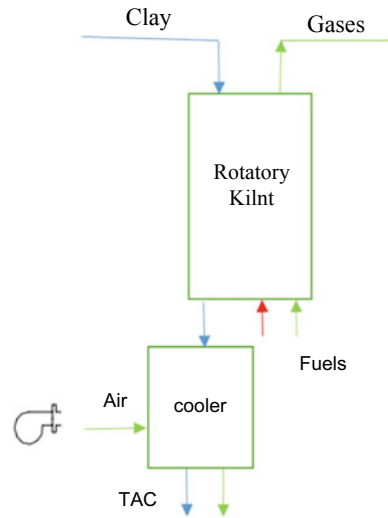
2.2 Thermal Design

The analysis of the flow processes begins with the choice of the spatial region called
"control volume." In the diagram represented in Fig. 3, the border or edge of the
analysis performed in this work is shown.

If the estimated flow of material to be treated is taken into account and that the
natural humidity of the clay is 6%, then the following can be considered

$$M \text{ initial } + E = M \text{ final } + \text{losses} \tag{6}$$

The thermal balance is defined from the mass balance that occurs in the process,
taking into account the elimination of free water and adsorbed water (up to 400 °C),
and in the decomposition or loss of the OH-of the clay (up to ≈850 °C), given by the
equations described above (see 1 and 2). The loss of mass due to the natural humidity
of the clay is approximately 6–7%, and also the loss of mass due to decomposition
or dehydroxylation of clay is 14%.

According to the thermal balance of the rotary kiln (see Fig. 4, the heat that comes
from the burning of the fuel is equal to the heat consumed in the clay transforma-
tion process plus the losses through different routes. Thermal balance is essentially
conducted based on energy and mass conservation laws.

$$E_{in} = E_{out} \tag{7}$$

$$E_{in} = Q_1 = E_{out} = Q_2 + Q_3 + Q_4 \tag{8}$$

Fig. 4 Energy balance.
Source Self-made
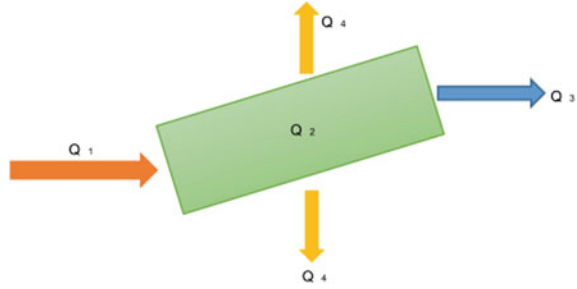
where Q_1 is the heat delivered to the kiln; Q_2 the heat needed for the clay transformation process; Q_3 the heat losses with the hot gases through the chimney; and Q_4 the radiation heat losses.

$$Q_1 = m_F * \text{LHV}/\eta_{\text{comb}} \tag{9}$$

where m_F is the fuel mass in kg/h; LHV the low heating value (MJ/kg); and η_{comb} the combustion efficiency adopted for this case 90%.

$$Q_2 = K_{\text{cap}} * Q_e \tag{10}$$

where K_{cap} is the kiln capacity in kg/h and in this case kiln capacity is 100 kg/h; Q_e is the specific energy needed for clay transformation in the sinterization process, and in this case is adopted the value of 0.81 MJ/kg reported by Mayorga and Rodriguez [7] and Machado et al. [8].

$$Q_3 = 0.001 * m_g * \overline{Cp} * \Delta t \tag{11}$$

where m_g is the exit gas mass in kg/h; $\overline{Cp}$ is the average specific heat of the exit gases in the given window temperature in kJ/kgK; Δt is the difference of the exit gas temperature (t_{out}) and the environment temperature (t_{env}).

$$Q_4 = 0.11 * Q_1 \tag{12}$$

Taking the criteria that the maximum acceptable value of radiation losses is 11% [9, 10]

$$m_g = m_F * m_e \tag{13}$$

where m_e is the specific mass of gases per kilogram of fuel burned in kg/kgF; this is calculated by combustion energy and mass balance based on fuel properties and combustion condition.

Table 3 Calculation result
and data

Results and data	Value
m_F (kg/h) [lts/h]	(3.16) [3.76]
K_{cap} (kg/h)	100
Tg$_{out}$ (°C)	600
T_{env} (°C)	29
Q_e (MJ/kg)	1
LHV (MJ/kg)	42.8
η_{comb}	0.9
Radiation losses	0.11
m_e (kg/kgF)	17
$\overline{Cp}$ (kJ/kgK)	1.10

Combining Eqs. 7–13 can calculate the fuel mass needed for the kiln and complete
the energy balance.

$$m_F = \frac{K_{cap*Q_e}}{\text{LHV} * \eta_{comb} - 0.105 * \text{LHV} * \eta_{comb} - 0.001 * m_{e*\overline{Cp}} * \Delta t} \quad (14)$$

The results given by Eq. 14 and the value of the variable for the resolution are
summarized in Table 3. Calculating the fuel mass consumption can complete the
thermal balance, as shown in Fig. 5.

Q_2 expressed in % represents the kiln efficiency with a value of 66% for the
analyzed rotatory kiln. The heat losses with the exit gases are considerable; this
is the biggest loss representing 23% of the heat input; some way to use this heat,
for example in a clay dryer, could lead to important benefits in fuel saving and
overall efficiency. The fuel consumption for an 8 h working day is 8 * 3.76 lts/h =

Fig. 5 Thermal balance
results (MJ/h). $Q_1 =$
150.4 MJ/h
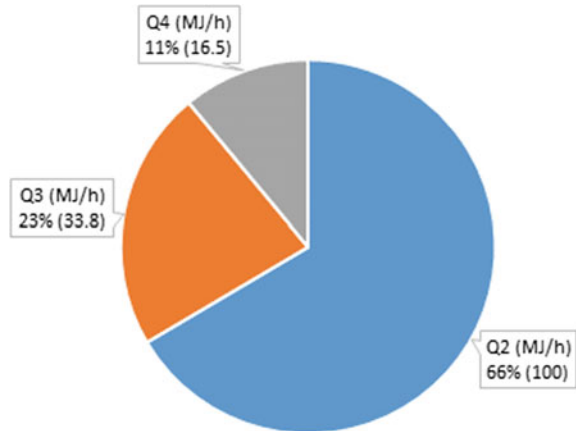
30.1 lts/day equivalent to 25.3 kg/day; on this base can be estimated an emotion of 25.3 kgfuel/day * 3.1 KgCO$_2$/kgfuel = 78.2 kg/day of CO$_2$.

However, other previous calculations made for this equipment report a significantly higher fuel consumption (IPIAC Technical Department), which must be verified exhaustively during the start-up and operation of the plant.

3 Conclusions

The design of a rotary kiln for the treatment and thermal modification of clays is advantageous since this technology allows continuous production, by obtaining the optimal sizing according to the desired productivity and characteristics of the material to be obtained; the best behavior of parameters such as fuel consumption and heat losses can be used and extrapolated, for the design and construction of facilities with diverse production capacities.

The simulation of the rotary kiln allows to obtain different dwell times, by varying parameters such as its inclination and its speed of rotation; these parameters can be correlated with the degree of pozzolanic reactivity of the thermally activated clay.

References

1. Vizcaíno, L., Sánchez, S., Damas, S., Pérez, A., Scrivener, K., Martirena, F.: Industrial trial to produce a low clinker, low carbon cement. Materiales de Construccion **65**(317), 045 (2015). ISSN-L: 0465–2746. https://doi.org/10.3989/mc.2015. 00614. (2015)
2. Dairon, J.A.C.: Evaluación económica y ambiental de plantas prototipo de pequeño y mediano tamaño para la producción de cemento LC^3. Facultad de Construcciones. CIDEM. Santa Clara. Cuba. 2017, Universidad Central Marta Abreu de Las Villas, TD (2017)
3. Orihuela, E.M.: Análisis energético de las diversas alternativas aplicables a una planta de clinkerizacion y producción de cemento Escuela Superior de Ingenieros. Sevilla, Universidad de Sevilla. TD Ingeniería Energética y Mecánica de Fluidos (2007)
4. Duda, W.: Manual tecnológico del cemento. Traducido por Antonio Sarabia González. España: Editores técnicos asociados (1977)
5. . Colina, F.G., Caballero, I., López, J.C.: Diseño básico de hornos rotatorios para el tratamiento de minerales. Ingenieria Quimica. Julio, Agosto 2016 Dpto Universitat de Barcelona de Ingeniería Química y Metalurgia (2016)
6. Aros Oñate, N.: Control predictivo no lineal de un horno rotatorio Ier Congreso Iberoamericano de ingeniería de proyectos. Antofagosta, Chile (2010)
7. Mayorga, E., Rodriguez, L.: Técnicas de construcción de hornos artesanales para quema de ladrillos, Lima. ITDG, Perú (2000)
8. Machado, L.I., Herrera, M.I., Martirena, F.: Improvements on the energy efficiency of fired clay bricks production by the employment of densified lignocellulosic material as biofuel. Revista Ingeniería de Construcción, vol. 26 No. 2 Agosto 2011 Disponible en: https://www.ing.puc.cl/ric/PDFRIC/RICVol26N2.pdf
9. Radwan, M.: Different possible ways for saving energy in the cement production. Adv. Appl. Sci. Res. **3**(2), 1162–1174 (2012)

10. Moya, J.A., Pardo, N., Mercier, A.: The potential for improvements in energy efficiency and CO_2 emissions in the EU27 cement industry and the relationship with the capital budgeting decision criteria. J. Clean. Prod. **19**(11), 1207–1215 (2011)
11. Machado-Lopez, I., Bacallao, F., Moya, I.H., Martirena-Hernandez, J.F.: Considerations for the Energy Balance and Preliminary Design of an Experimental LC3 Cement Pilot Plant. In: Martirena-Hernandez J., Alujas-Díaz A., Amador-Hernandez M. (eds) Proceedings of the International Conference of Sustainable Production and Use of Cement and Concrete. RILEM Bookseries, vol 22. Springer, Cham (2020)

Effectiveness of Amphoteric PCE Superplasticizers in Calcined Clay Blended Cements

Marlene Schmid, Ricarda Sposito, Karl-Christian Thienel and Johann Plank

Abstract This study highlights the suitability of amphoteric (zwitterionic) polycarboxylate-based superplasticizers for a naturally occurring mixed-layer clay used as pozzolanic cement substitute after calcination. After a successful synthesis, dispersing performance tests reveal that amphoteric superplasticizers are a promising type of superplasticizer to address both calcined clays and cement. Tailor-made terpolymers can be applied to vary the initial slump by integration of different ratios of cationic monomer. Furthermore, heat flow calorimetry tests with amphoteric superplasticizers point out a less pronounced retardation in cement hydration compared to a standard anionic polymer. Zwitterionic superplasticizers are seen as potential alternatives for common anionic superplasticizers, especially for the advancing replacement of cement clinker with calcined clays of various mineralogical composition. Calcined mixed-layer clays are particularly promising as supplementary cementitious materials (SCMs) as they can be fluidized at low dosages of superplasticizers comparable to cement.

Keywords Amphoteric polymers · Cement hydration · Dispersing performance · Polycarboxylate ether · Workability

1 Introduction

Optimizing the ecological and energetic properties of concrete asks for the use of pozzolanic cement constituents instead of ordinary Portland cement clinker [1]. The only type of SCM which is available in sufficiently high amounts nearly all over the world is calcined clay. These thermally activated clays are ascribed to have an appreciable potential to contribute to the reduction of cement-derived carbon dioxide emissions as well as of thermal energy required during processing [2–4].

M. Schmid · J. Plank (✉)
Chair of Construction Chemistry, Department of Chemistry, Technical University of Munich, Garching, Germany
e-mail: sekretariat@bauchemie.ch.tum.de

R. Sposito · K.-C. Thienel
Institute for Construction Materials, University of the Federal Armed Forces, Neubiberg, Germany

However, cements substituted with calcined clays suffer from a very high water demand and consequently evoke a limited workability of mortars and concretes [5]. To overcome this disadvantage and to avoid a loss on mechanical properties and durability when increasing the water-to-binder (w/b) ratio, the addition of superplasticizers is essential [6].

While in the literature [7, 8], many studies do not consider the interaction with water-reducing admixtures in the assessment of low-grade calcined clays, the present study reports on a calcined naturally available mixed-layer clay as SCM and its accessibility for amphoteric superplasticizers.

Our previous investigations [9] pointed out that the present clay can be dispersed well with anionic polycarboxylate ethers (PCEs) and cationic polymers. Moreover, zeta potential measurements suggested that this clay exhibits particles with positive and negative surface charges [10].

Hence, amphoteric (zwitterionic) PCE superplasticizers exhibiting different ratios of anionic/cationic monomer were synthesized, characterized *via* gel permeation chromatography (GPC) and tested in cement blended with this calcined clay on dispersing effectiveness and influence on cement hydration.

2 Materials and Methods

2.1 Materials

Calcined Clay As a clay sample, a naturally occurring mixed-layer clay was investigated. The raw material originates from a Lias delta layer in Bavaria (Germany). It is composed of approximately 25 wt% kaolinite and 45 wt% 2:1 clay minerals (especially mica, illite and chlorite). Quartz and feldspar (around 30 wt%) are included as inert components. Calcination at 750 °C in a three-part rotary kiln for around 30 min results in a material with 61 wt% amorphous content. The mineralogical composition of the calcined material is summarized in Table 1. The calcined clay (CC) exhibits a specific surface (BET surface) area of 3.9 m^2/g and a particle density of 2.63 g/cm^3.

Cement An ordinary Portland cement (OPC) CEM I 42.5 R from Schwenk Zement K.G. (Allmendingen, Germany) is used for the production of cements blended with the calcined clay. The *Blaine* value is 2.918 cm^2/g, and the particle density is 3.16 g/cm^3. Its mineralogical analysis is shown in Table 2.

Characteristic particle size parameters, i.e., d_{10}, d_{50} and d_{90} values of the CC and the OPC sample are given in Table 3.

The particle size distribution of the OPC and the calcined mixed-layer clay was measured *via* laser granulometry and is presented in Figs. 1 and 2.

CC exhibits a unimodal distribution. For the OPC, the volume of finer particles is larger than that of CC, but it also includes coarse particles (higher d_{90} value compared to CC).

Table 1 Mineralogical composition of the calcined mixed-layer clay sample

Phase	[wt%]
Quartz	16.2
Muscovite	2.2
Calcite	0.6
Illite	4.6
Chlorite	0.4
Feldspar	6.0
Secondary silicates	6.3
Hematite	0.6
Ores	1.1
Sulfates	1.6
X-ray amorphous	60.8
Total	100.4

Table 2 Phase composition of the CEM I 42.5 R sample

Mineral phase	[wt%]
C_3S, m	52.4
C_2S, m	19.9
C_3A, c	3.3
C_3A, o	3.2
C_4AF	11.8
CaO	0.7
MgO	0.7
Anhydrite	1.4
Hemihydrate[a]	1.9
Dihydrate[a]	1.3
Calcite	1.6
Quartz	0.4
Dolomite	1.4
Total	100.0

[a]Determined by thermogravimetry

Table 3 d_{10}, d_{50} and d_{90} values of the OPC and the CC

Sample	[μm]		
	d_{10}	d_{50}	d_{90}
CC	4.0	13.2	37.0
OPC	1.5	18.5	48.7

Fig. 1 Cumulative particle size distribution of the calcined clay and OPC samples (d_{10}, d_{50} and d_{90} values are marked with a cross)
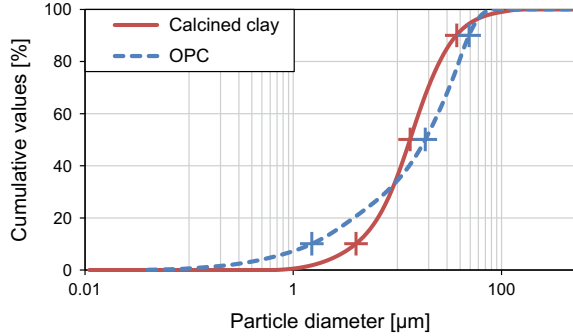
Fig. 2 Frequency distribution of the calcined clay and OPC samples
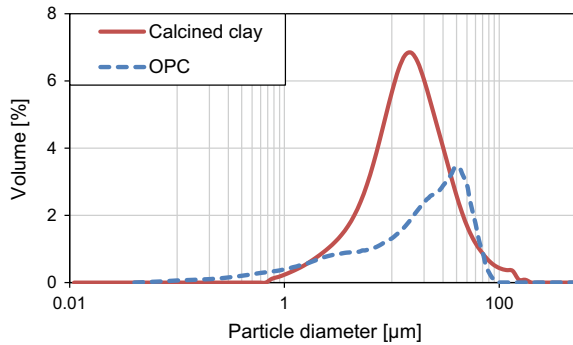
Superplasticizers As amphoteric (zwitterionic) superplasticizers, four terpolymers were prepared *via* aqueous free radical copolymerization of the monomers methacrylic acid (MAA), MPEG-methacrylate macromonomer (ω-methoxy polyethylene glycol methacrylate ester with a chain length (n_{EO}) of 45) and 3-trimethylammonium propyl methacrylamide chloride (MAPTAC). The polymerization was initiated with ammonium peroxydisulfate and controlled with 3-mercaptopropionic acid as chain transfer agent. After neutralization with sodium hydroxide solution, the polymers were obtained as yellowish and slightly viscous polymer solutions with a solid content of ~25%.

For comparison, a standard anionic PCE (MAA-45MPEG (6:1)) was investigated. The chemical structures of the polymers are shown in Fig. 3.

All terpolymers were characterized by gel permeation chromatography. The molecular weights (M_w and M_n) and polydispersity indexes (PDIs) of the polymers obtained from these measurements are summarized in Table 4.

MAA-45MPEG-MAPTAC: x = 0.5, 1, 3, 6   MAA-45MPEG (6:1)
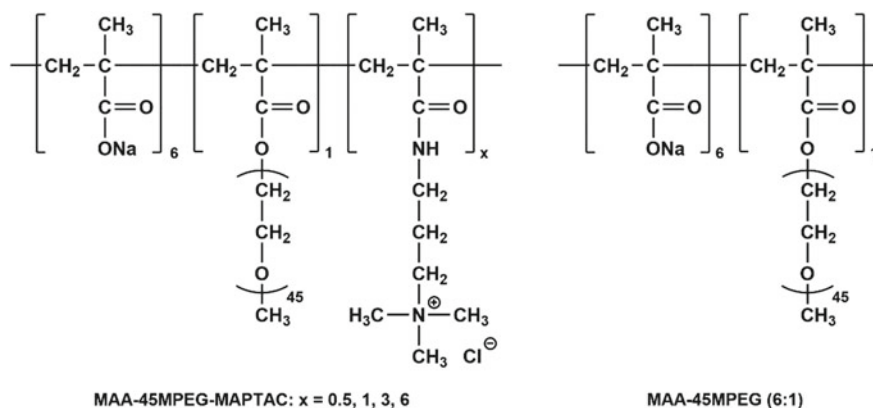
Fig. 3 Chemical structures of the synthesized amphoteric PCE samples and the anionic reference polycarboxylate ether

Table 4 Molecular properties and macromonomer conversion of the synthesized polymers

Polymer sample	M_w [g/mol]	M_n [g/mol]	PDI	Conversion [%]
MAA-45MPEG-MAPTAC (6:1:6)	15,000	9700	1.5	76.9
MAA-45MPEG-MAPTAC (6:1:3)	18,000	9600	1.9	84.7
MAA-45MPEG-MAPTAC (6:1:1)	22,000	11,000	2.0	89.1
MAA-45MPEG-MAPTAC (6:1:0.5)	21,000	9400	2.2	86.0
MAA-45MPEG (6:1)	14,900	7400	2.0	91.9

2.2 Methods

Dispersing Performance of Synthesized Polymers Dispersing effectiveness of the synthesized superplasticizer samples in CC, neat OPC and OPC blended with CC suspensions was assessed *via* a modified (adapted from DIN EN 1015-3 [11]) mini-slump test using a *Vicat* cone (bottom diameter: 8.0 cm, top diameter: 7.0 cm, height: 4.0 cm). The substitution rate for the cement was set at 20 wt%.

In this test, the cone was filled with the paste and the spread diameter was recorded after removing the cone. The average value of two spread diameters perpendicular to each other was reported as the test result. The w/b ratios of the pastes without polymer were set to give a spread flow of 18 ± 0.5 cm and were 0.77, 0.48 and 0.55 for pure CC, neat cement and blended cement paste, respectively. At those w/b ratios, the dosages of the superplasticizers required to reach a spread flow of 26 ± 0.5 cm were determined.

Isothermal Heat Flow Calorimetry Hydration kinetics were monitored by isothermal heat flow calorimetry (TAM AIR, Thermometric, Järfälla, Sweden) at 20 °C. All pastes of the blended cement (OPC:CC 80:20) were prepared from 4.0 g of binder and

2.2 g of distilled water (w/b = 0.55). The dosages of the superplasticizers were those which were required to achieve a spread flow of 26 ± 0.5 cm in the mini-slump tests in order to ensure comparable rheological properties and avoid segregation of the paste during the hydration process. The heat released during hydration was reported over a period of 48 h.

3   Results and Discussion

3.1   *Dispersing Effectiveness of Amphoteric Superplasticizers*

Generally, in the calcined clay suspension always the highest dosages of the novel superplasticizers were required to achieve a spread flow of 26 ± 0.5 cm when compared with neat cement or the OPC/CC blend. In light of this, it was quite surprising that in the blended cement lower or the same dosages of the amphoteric superplasticizers were required to achieve the same spread flow as in the neat cement paste (Fig. 4).

Among the MAPTAC-modified samples, polymer MAA-45MPEG-MAPTAC synthesized at a molar ratio of 6:1:1 performs best, implying that an anionic to cationic charge ratio of 6:1 seems to be the most efficient composition for these terpolymers.
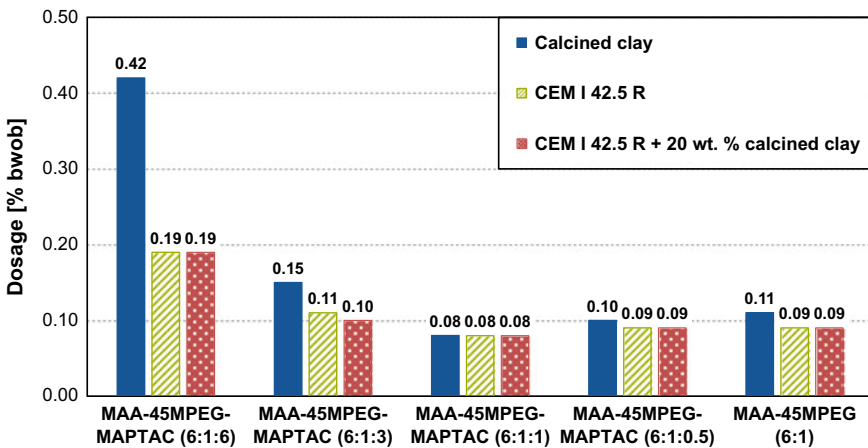
Fig. 4 Dosages of synthesized superplasticizers required to obtain a target slump flow of 26 ± 0.5 cm in calcined clay, cement and an 80:20 blend of cement and calcined clay
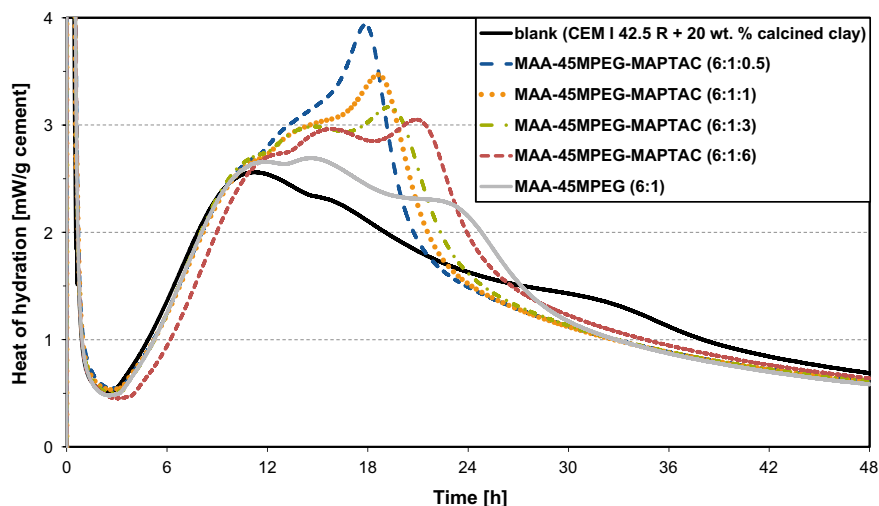
Fig. 5 Heat evolution during hydration of CEM I 42.5 R blended with 20 wt% calcined clay (w/b = 0.55) admixed with superplasticizers (polymer dosage as shown in Fig. 4)

3.2 Impact of Amphoteric Superplasticizers on Cement Hydration

The effect of the synthesized amphoteric terpolymers on the hydration of the blended cement was studied *via* isothermal heat flow calorimetry (Fig. 5). When the amphoteric comb polymers are added, no (e.g., sample MAA-45MPEG-MAPTAC (6:1:0.5)) or only a slight (~2 h, e.g., sample MAA-45MPEG-MAPTAC (6:1:6)) delay in the induction period was observed, indicating no influence on the silicate clinker hydration.

Moreover, for all zwitterionic polymers the deceleration period exhibits a much higher exothermic rate which leads to a shorter period of heat evolution, indicating a faster kinetics of the early hydration compared to an anionic MAA-45MPEG (6:1).

4 Conclusions

In the present study, four amphoteric comb copolymers composed of methacrylic acid, MPEG macromonomer and MAPTAC as cationic monomer were synthesized and their ability to disperse OPC blended with a calcined naturally occurring mixed-layer clay was investigated.

It can be concluded that optimal dispersing effectiveness is achieved at a low content of cationic monomer.

Moreover, the investigations revealed that zwitterionic polymers show no or only a minor retarding effect on early cement hydration and can even shorten the heat evolution period in the first 48 h compared to conventional anionic polycarboxylates.

The authors are aware that for a better understanding of the influence of a cationic monomer on the dispersing mechanism, adsorption and zeta potential measurements have to be conducted. Moreover, heat flow calorimetry results have to be proven and underpinned by compressive strength measurements.

References

1. Chen, C., Habert, G., Bouzidi, Y., Jullien, A.: Environmental impact of cement production: detail of the different processes and cement plant variability evaluation. J. Clean. Prod. **18**(5), 478–485 (2010)
2. UN Environment, Scrivener, K.L., John, V.M., Gartner, E.M.: Eco-efficient cements: potential economically viable solutions for a low-CO_2 cement-based materials industry. Cem. Concr. Res. **114**, 2–26 (2018)
3. Miller, S.A., John, V.M., Pacca, S.A., Horvath, A.: Carbon dioxide reduction potential in the global cement industry by 2050. Cem. Concr. Res. **114**, 115–124 (2018)
4. Scrivener, K., Martirena, F., Bishnoi, S., Maity, S.: Calcined clay limestone cements (LC^3). Cem. Concr. Res. **114**, 49–56 (2018)
5. Beuntner, N., Thienel K.-C.: Performance and properties of concrete made with calcined clays. In: Tagnit-Hamou, A. (ed.) 10th ACI/RILEM International Conference on Cementitious Materials and Alternative Binders for Sustainable Concrete, ACI SP 320, pp. 7.1–7.12. Sheridan Books, Montreal (2017)
6. Akhlaghi, O., Aytas, T., Tatli, B., Sezer, D., Hodaei, A., Favier, A., Scrivener, K., Menceloglu, Y.Z., Akbulut, O.: Modified poly(carboxylate ether)-based superplasticizer for enhanced flowability of calcined clay-limestone-gypsum blended Portland cement. Cem. Concr. Res. **101**, 114–122 (2017)
7. Schulze, S.E., Rickert, J.: Suitability of natural calcined clays as supplementary cementitious material. Cem. Concr. Comp. **95**, 92–97 (2019)
8. Tironi, A., Scian, A.N., Irassar, E.F.: Blended cements with limestone filler and Kaolinitic Calcined clay: filler and Pozzolanic effects. J. Mater. Civ. Eng. **29**(9), 04017116/1–04017116/8 (2017)
9. Schmid, M., Beuntner. N., Thienel, K.-Ch., Plank, J.: Colloid-chemical investigation of the interaction between PCE superplasticizers and a calcined mixed layer clay. In: Martirena, F., Favier, A., Scrivener, K. (eds.) Calcined Clays for Sustainable Concrete. Proceedings of the 2nd International Conference on Calcined Clays for Sustainable Concrete, pp. 434–439. RILEM Bookseries 16, Cuba (2017)

10. Schmid, M., Beuntner, N., Thienel, K.-C. Plank, J.: Amphoteric superplasticizers for cements blended with a calcined clay. In: Liu, J., Wang, Z., Holland, T.C., Huang, J., Plank, J. (eds.) 12th International Conference on Superplasticizers and Other Chemical Admixtures in Concrete, ACI SP 329, pp. 41–54. Beijing (2018)
11. European Norm DIN EN 1015-3: Methods of test for mortar for masonry—Part 3: determination of consistence of fresh mortar (by flow table), DIN Deutsches Institut für Normung e. V

Effect of Clay Mineralogy, Particle Size, and Chemical Admixtures on the Rheological Properties of CCIL and CCI/II Systems

Brandon Lorentz, Hai Zhu, Dhanushika Mapa, Kyle A. Riding and Abla Zayed

Abstract A major challenge of calcined clay cements is the flow properties. This research addresses binary and ternary CCIL (calcined clay blended with an ASTM C595 Type IL cement at the ready-mixed plant) and CCI/II systems and the effect of particle size and chemical admixtures on rheological characteristics. The effects of six different calcined clays and a superplasticizer and viscosity reducing admixture on the static and dynamic yield stress and viscosity of the blended paste were measured. While calcined clay systems alter the cementitious system flowability, modern chemical admixtures can custom-tailor the concrete rheological properties for robust placement and consolidation.

Keywords Supplementary cementitious materials · Specifications

1   Introduction

Calcined clay has been shown to be a viable supplementary cementitious material, and when used in conjunction with ground limestone fines, it is capable of significantly reducing the concrete clinker factor and carbon footprint [1, 2]. It also improves concrete strength, resistance to ASR, pore structure, and chloride penetrability [3, 4]. Limestone calcined clay cements (LC^3) have been promoted for use in many markets as a pre-blended product optimized for performance and use. For some regions, however, the market may prefer the flexibility of adding the calcined clay separately at the ready-mixed plant with an ASTM C595 Type IL cement. This system called calcined clay Type IL cement (CCIL) can provide durability and sustainability benefits of LC^3 systems [5]. CCIL systems however will not have grinding aids optimized to compensate for reductions in flowability caused by the calcined clay. Chemical admixtures need to be added at the ready-mixed plant to adjust the rheological properties of CCIL.

B. Lorentz (✉) · H. Zhu · D. Mapa · A. Zayed
University of South Florida, Tampa, FL 33260, USA
e-mail: bxl@mail.usf.edu

K. A. Riding
University of Florida, Gainesville, FL 32611, USA

Rheometers are used to measure the fundamental flow properties of cement and concrete systems. These properties include the relationship between shear stress and shear rate and thixotropy. The relationship between shear stress and shear rate for concrete is often idealized using a linear Bingham model with the yield stress, the stress needed to initiate flow, and the plastic viscosity, the slope of the shear stress and shear rate relationship. Rheometers cannot directly measure cement paste shear rate or shear stress. Instead, they measure a linear velocity and force for paste moving between parallel plates or rotational velocity and torque for concentric cylinders. These measurements are then used to calculate the shear rate and shear stress using analytical transformations. For other rheometer geometries, transformation to fundamental rheological properties is indirect and, in any cases, empirical. Rheometer geometry choice and data misinterpretation can sometimes lead researchers to conclude that cement paste is shear thinning or shear thickening [6].

Calcined clay can cause stiffening of paste through particle flocculation, trapping water and causing high mixture thixotropy [7]. Clay particles can have positively charged edges and negatively charged faces that contribute to the flocculation. It is believed that particle size, clay type and amount should influence the clay surface charge, flocculation, and rheological properties that can be overcome through the use of admixtures [8]. This study examines the effects of calcined clay particle size, type, and amount on rheological properties of CCIL systems.

2 Materials

An ASTM C595 Type IL10 and a Type I/II Portland cement with 1.3% limestone were used in this study. Six different kaolin clays obtained from the USA southeast were used. The clay composition was measured using x-ray diffraction with Rietveld refinement as shown in Table 1. Clays A1, F, G, and D1 were calcined in an electric furnace at 600 °C, while clays B1 and B4 were calcined at 850 °C. All clays were

Table 1 Clay composition as determined by x-ray diffraction with Rietveld refinement

	B1	A1	F	G	D1	B4
Kaolin (wt%)	93.1	89.6	85.9	77.7	78.4	65.5
Fe substitution x			0.01	0.03	0.15	
Illite (wt%)	0.3	0.6				0.1
Crandallite (wt%)	0.3		0.1	0.9	1.5	
Hematite (wt%)			1.0	1.4	0.1	
Gibbsite (wt%)						24.0
Anatase (wt%)	0.7		0.8	0.8	1.0	1.1
Quartz (wt%)	0.9	1.7	1.5	3.8	2.4	0.2
Amorphous/unidentified (wt%)	4.6	8.2	10.8	15.4	16.6	9.1
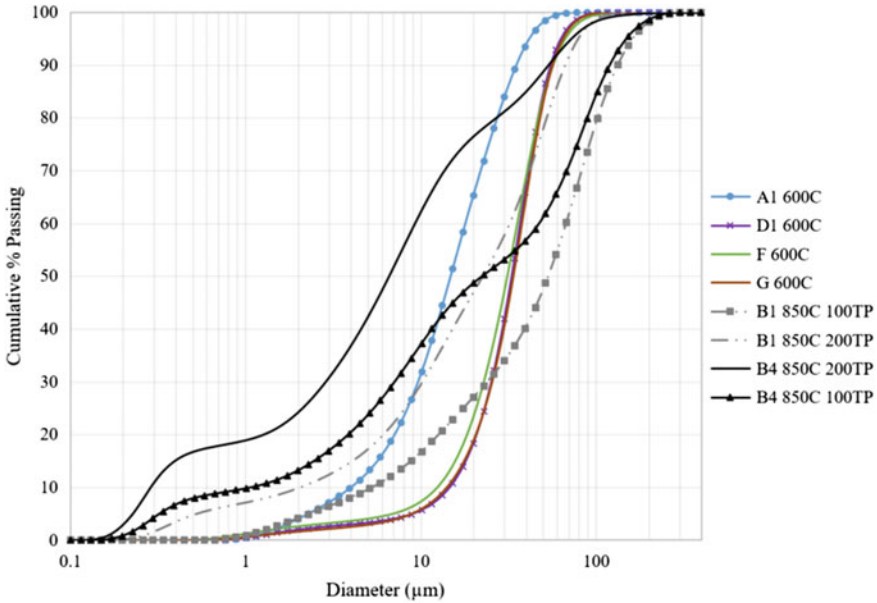
Fig.1 Calcined clay particle size distribution

ground using a mortar and pestle and measured using laser particle size analysis as shown in Fig. 1. Clays B1 and B4 were ground to different fineness levels. Cement pastes used in this study were made using a water–cementitious material ratio (w/cm) of 0.485 with 20% weight replacement of calcined clay. Mixtures with Type I/II mix designs were made using calcined clays A1, D1, F, and G with their naturally mined fine aggregate separated between sieves No. 200 (75 µm) and No. 325 (44 µm) during grading. Six calcined clays were also tested with a Type IL cement. An ASTM C494 Type F high-range water-reducing (HRWR) admixture was used [9]. When used, HRWR was at a dosage of 650 mL/100 kg cementitious material.

3 Methodology

Cement pastes were mixed for 3 min using a low shear mixer. After mixing, the IL10 cement pastes were placed in the rheometer concentric cylinders. After the sample was placed in the container, the following steps were performed to measure the cement paste rheological properties:

1. Condition sample in testing cup at 10 s^{-1} shear rate for 10 s
2. Let the paste rest in testing cup for 2 min
3. Measure paste static yield stress by rotating at low shear rate (0.005 s^{-1}) for 1 min

4. Breakdown agglomerates by rotating for 1 min at 70 s^{-1} shear rate
5. Flow sweep down from 70 to 0.1 s^{-1} to calculate fluid dynamic yield stress and plastic viscosity

A TA Instruments Discovery Hybrid rheometer (DHR-2) was used to measure the cement paste rheological parameters. The average results of three independently mixed samples are reported in this study. Sample temperature was maintained at 23 °C using a Peltier module in the rheometer.

The zeta potential of the Type I/II cementitious systems was measured using a Malvern Instrument nano-series Zetasizer following Smoluchowski's expression [10]. Reported electrokinetic data are based on the average of data obtained from three independently mixed pastes. Methods used for paste analysis were similar to those reported by Safi et al. and Talero et al. where 1 cm^3 of fresh paste as prepared for rheological study was diluted with 30 cm^3 of water and analyzed as an aqueous solution [11–13]. Mixtures tested for zeta potential were made with Type I/II cement. Paste rheological measurements made with Type I/II cement were made using a helical ribbon and were measured by pre-shearing at 50 s^{-1}, allowing the paste to sit in the cup for 2 min and then using the ascending branch to compute the yield stress.

4   Results

Figure 2 shows the static yield stress of the Type IL cements vs. clay kaolin content for the clays tested. A linear relationship was seen between the clay kaolin content and static yield stress for the calcined clays with similar particle sizes (D1, F, G, B1-fine). When the particle size was significantly smaller (clay A1) or the composition
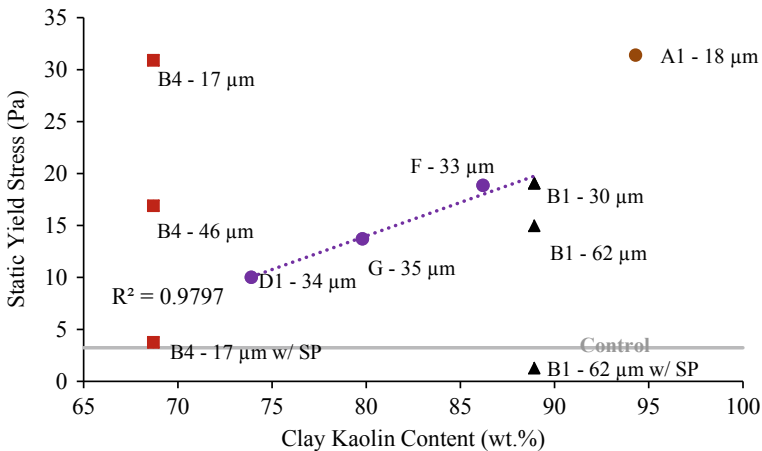
Fig. 2 Type IL Static yield stress for calcined clays. Clay type and mean diameter is given next to each data point
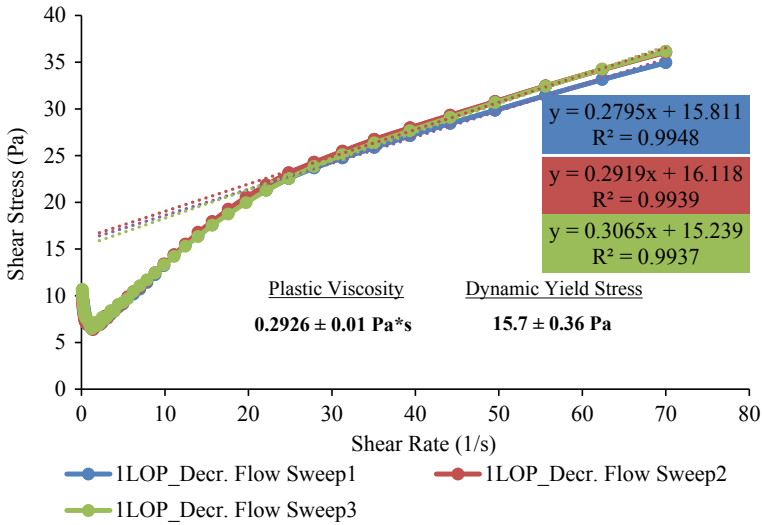
Fig. 3 Measured shear rate vs. shear stress for Type IL cement control mixture

was significantly different (clay B4 with 24% Gibbsite), the static yield stress deviated from this relationship. The presence of Gibbsite in the raw clay is expected to decompose to an amorphous alumina phase after the calcination procedure employed which results in a similar influence on rheological properties as calcined kaolin, an amorphous aluminosilicate [14, 15]. Figure 3 shows the measured shear rate vs. shear stress values measured for the control Type IL cement paste mixture. The cement pastes tested showed very linear behavior at high shear rates, indicating Bingham fluid behavior. At low shear rates, a significant nonlinear behavior was found because of plug flow. The Bingham model was fit to the linear portion of the curves to avoid this measurement artifact. Figure 4 shows a rheograph for the Type IL paste mixtures tested. The calcined clay increased the plastic viscosity and dynamic yield stress in a similar ratio, regardless of the clay type and particle size tested. The use of HRWR reduced the yield stress significantly more than the plastic viscosity. HRWR was able to successfully increase the paste flow properties to a level comparable to the control.

Figure 5 shows the relationship between the zeta potential of the Type I/II binary and ternary (20% fine aggregate replaced for clay) cements and clay kaolin content, while Fig. 6 shows the paste yield stress and viscosity with zeta potential for all Type I/II pastes. It is noted that the inclusion of each clays' natural fine aggregate slightly improved the rheological performance. However, the development of a ubiquitous trend between admixture kaolin content, yield stress, and zeta potential was not observed when replaced as part of the clay portion. This has been attributed to the inability of kaolin content to account for the bimodal mixing effects caused by the aggregates during mixing, facilitating thixotropic and structural breakdown. However, Fig. 6 presents a strong relationship between yield stress and viscosity with
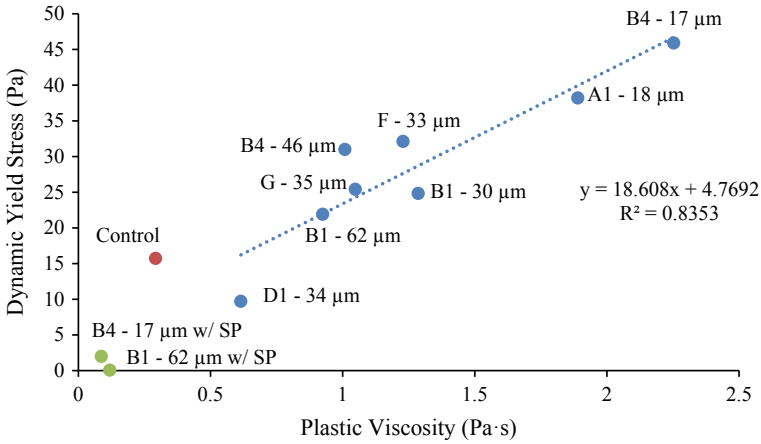
Fig. 4 Rheograph of dynamic yield stress versus plastic viscosity for Type IL paste mixtures
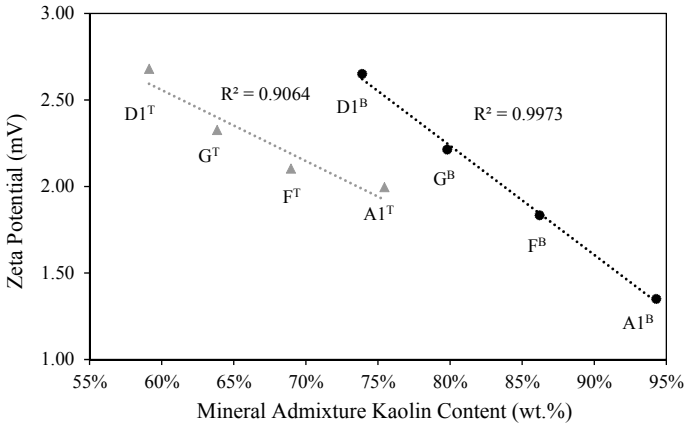
Fig. 5 Zeta potential of Type I/II cements with admixture kaolin content (superscripts noted: B ≡ Binary, T ≡ Ternary)

all pastes' zeta potentials, indicating that the charged surfaces of the clay particles, having a Lewis-Basic character post calcination, are the ultimate driving force behind the flow reduction [16, 17]. This is corroborated by the trends presented in Fig. 5 where kaolin content strongly influences system zeta potential. Zeta potential is shown to ubiquitously account for mineralogical and bimodal mixing effects calcined clays and their fine aggregates have on rheological properties.
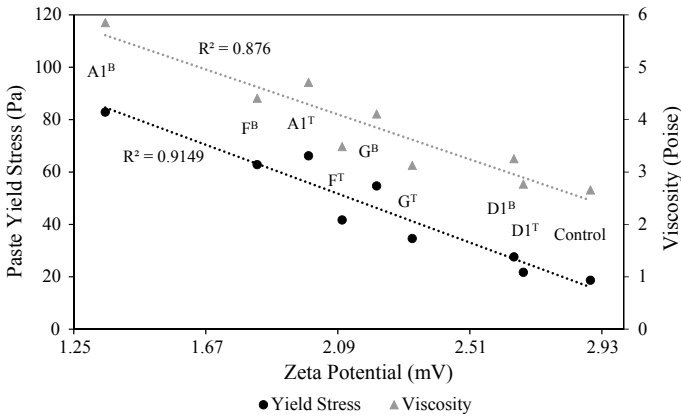
Fig. 6 Zeta potential influence on Type I/II cements yield stress and viscosity

5 Conclusions

The poor flowability of CCIL systems is widely known and has been recognized in the experimental studies presented in this research. Based on the experimental results from this study, kaolin quality, nature, and content of impurities all have important implications on rheological performance. The Lewis—Basic and surface characteristics of calcined clay minerals control paste rheology via colloidal interactions. The effect of particle size is a significant driver of workability issues and inclusion of fine aggregate and clays with varying fineness clearly exposed pastes' rheological performance to deviate from a purely mineralogical influence. The effects of both mineralogy and particle size must be considered when optimizing calcined clay cements' for flow performance, and zeta potential measurements are an effective means of capturing their confounding influence. Although there are serious concerns with these systems rheological behavior, superplasticizers may be used to custom-tailor their flow characteristics to an appreciable level.

References

1. Vizcaíno-Andrés, L.M., Sánchez-Berriel, S., Damas-Carrera, S., Pérez-Hernández, A., Scrivener, K.L., Martirena-Hernández, J.F.: Industrial trial to produce a low clinker, low carbon cement. Mater. Construcción **65**(317), e045 (2015)
2. Cancio Díaz, Y. et al.: Limestone calcined clay cement as a low-carbon solution to meet expanding cement demand in emerging economies. Dev. Eng. **2**, 82–91 (2017)

3. Maraghechi, H., Avet, F., Wong, H., Kamyab, H., Scrivener, K.: Performance of limestone calcined clay (LC3) with various kaolinite contents with respect to chloride transport. Mater. Struct. **51**(125), 1–17 (2018)
4. Avet, F., Scrivener, K.: Investigation of the calcined kaolinite content on the hydration of limestone calcined clay cement (LC3). Cem. Concr. Res. (2018)
5. ASTM C595/C595M-16: Standard Specification for Blended Hydraulic Cements. ASTM International, West Conshohocken, PA (2016)
6. Wallevik, O. H., Feys, D., Wallevik, J. E., Khayat, K. H.: Avoiding inaccurate interpretations of rheological measurements for cement-based materials. Cem. Concr. Res. (2015)
7. Tregger, N.A., Pakula, M.E., Shah, S. P.: Influence of clays on the rheology of cement pastes. Cem. Concr. Res. (2010)
8. Teh, E.J., Leong, Y.K., Liu, Y., Fourie, A.B., Fahey, M.: Differences in the rheology and surface chemistry of kaolin clay slurries: the source of the variations. Chem. Eng. Sci. (2009)
9. A.C.-13: Standard Specification for Chemical Admixtures for Concrete. ASTM International, West Conshohocken, PA (2013)
10. Berghout, S.: The Einstein Smoluchowski equation in the one dimensional exclusion process. Independent (2013)
11. Safi, B., Benmounah, A., Saidi, M.: Rheology and zeta potential of cement pastes containing calcined silt and ground granulated blast-furnace slag. Mater. Constr. **61**(303), 353–370 (2011)
12. Talero, R., Pedrajas, C., Rahhal, V.: Performance of fresh Portland cement pastes—determination of some specific rheological parameters. In: Rheology—New Concepts, Applications and Methods, INTECHOpen, p. 24 (2013)
13. Talero, R., Pedrajas, C., González, M., Aramburo, C., Blázquez, A., Rahhal, V.: Role of the filler on Portland cement hydration at very early ages: rheological behaviour of their fresh cement pastes. Constr. Build. Mater. (2017)
14. Yusiharni, E., Gilkes, R.: Rehydration of heated gibbsite, kaolinite and goethite: an assessment of properties and environmental significance. Appl. Clay Sci. **64**, 61–74 (2012)
15. Kloprogge, J.T., Ruan, H.D., Frost, R.L.: Thermal decomposition of bauxite minerals: Infrared emission spectroscopy of gibbsite, boehmite and diaspore. J. Mater. Sci. **37**(6), 1121–1129 (2002)
16. Moulin, E., Blanc, P., Sorrentino, D.: Influence of key cement chemical parameters on the properties of metakaolin blended cements. Cem. Concr. Compos. **23**(6), 463–469 (2001)
17. Pardo, P., Christensen, P.V., Keiding, K., Herfort, D., Skibsted, J.: Surface properties of calcined clays and their dispersion in blended Portland cement pastes. In: 13th International Congress on the Chemistry of Cement, pp. 1–7 (2011)

On the Workability of Mortar and Concrete Mixtures Containing Calcined Clay Blends

Klaus-Juergen Huenger, Ingolf Sander and Natalia Zuckow

Abstract Calcined clays can be used in mortar and concrete as a part of a binder (LC^3) or as a supplementary cementing material (SCM). The aim here is to substitute fly ash as an additive in concrete recipes. A stable mixture between two regionally available clays, burnt together with a certain ratio of 60:40 wt% at 650–680 °C, could be produced. Such metaclays produced in larger amounts were investigated in different mortar and concrete mixtures. The production indicates an important problem with the workability of the fresh concrete mixtures. That is why different superplasticizers were tested. It could be found that especially a mixture between a PCE-based material and a special additive developed for loam sands provides very good results. The workability increases from less than 200 mm slump on a value of about 300 mm. The combination of calcined clay materials and specially developed superplasticizer mixtures allows producing concrete with very different properties. It can be a closed system for the production of durable concrete structures.

Keywords Calcined clay mixtures · Supplementary cementing material · Workability · Superplasticizers mixtures · Precast concrete elements

1 Introduction

The goal of the performed investigations is to substitute fly ash as an additive in concrete recipes. Already in some years, one type of certificated fly ash in Germany will then no longer be available as the power plant will be closed. Therefore, it is necessary to find substitute materials with same or even better properties. One of them can be calcined clay.

Calcined clay is the main term for a group of substances consisting of thermally treated clay materials. An important representative of this group is metakaolin. The formation of metakaolin, the common material used as a pozzolanic reactant in

K.-J. Huenger (✉) · I. Sander
Brandenburg University of Technology Cottbus-Senftenberg, 03046 Cottbus, Germany
e-mail: huenger@b-tu.de

N. Zuckow
Mattig & Lindner Company, 03149 Forst, Germany

cement or concrete structures, is connected to relatively pure raw clays consisting of kaolinite with a content of more than 90%. Because of the calcination process at approximately 750–800 °C, metakaolin is formed by destruction of the crystal structure of the kaolinite mineral. Other clay materials which are not so pure and consist of different clay structures are also in the focus of the international research. Here, in this paper, the name "metaclay" is used for such materials.

During the last decade, many researchers have dealt with metaclay materials in order to reduce CO_2 emissions and to increase the strength and durability of mortars and concrete [1–3]. Already in 1995, 25 years ago, this subject was a part of the research work summarized in [4]. Investigations of special mixtures of clay minerals were performed too to improve the pozzolanic properties [5, 6]. Exactly, this idea was taken up for the research presented here. The first results have been described in [7].

In the meantime, a stable mixture between two regionally available clays, burnt together with a certain ratio of 60:40 wt% at 650–680 °C, could be developed. In cooperation with a regional company, the production reaches a technical scale of approximately several 100 kilograms of calcined clay materials. With this amount, larger formatted concrete samples are also available.

What works in the laboratory does not have to work in the field. The large production indicates an important problem with the workability of the fresh concrete mixtures. This is a problem described in the literature too. Certain "old" and "new" superplasticizers were tested, and obviously different results were obtained. In [8], a good workability was reached by using superplasticizers based on lignosulphonate. Another researcher [9] reported on the good effectiveness of PCE-based superplasticizers added to calcined clay limestone cement mixtures.

Because of contradictory results by using superplasticizers in combination with calcined clay mixtures, each calcined clay material requires obviously its special component. That is why a comprehensive program for testing different superplasticizers was performed.

2 Materials Used

The investigations were made with four different groups of superplasticizers.

- on the basis of PCE from different producers,
- on the basis of Lignosulphonate,
- on the basis of mixtures between both,
- and additionally a special additive developed for loam containing sands (sand blocker system).

The reference recipes were well-known fly ash containing concrete mixtures. The new mixture should indicate a same or better workability behavior.

The workability was measured very easily by determining the slump using the so-called Haegermann table for mortar and a larger spreading table for concrete mixtures.

Table 1 Superplasticizers chosen

Material	SP1	SP2	SP3	SP4	SP5
Name	ACE455	334 BV	22 BV	SBS 8005	18 BV
Basis	PCE	Na-Lignosulphonate	PCE + Lignosulphonate	Sand blocker system	Mg-Lignosulphonate
Effect as	FM	BV	VZ/BV/FM	SB	BV

FM superplasticizers; *BV* condenser; *VZ* retarder; *SB* sand blocker

On selected mixtures, additionally, the setting behavior was pursued by using the ultrasonic technique. Investigations in the laboratory and also investigations in the field (performed in cooperation with the company) were realized. Mortar prisms and also concrete samples were produced to find out the best recipes or the most effective SP materials. Table 1 summarizes the superplasticizers used in the laboratory and also in the field.

It is very difficult to get information on the composition of superplasticizers used in this project. The manufacturer advertises, for example, with a specially developed sand blocker system for layer silicate structure substances, which are very useful for highly clay containing sands. The focus lays also on the use of substances containing lignin sulphonate because of results and advertises from the literature.

To determine the influence of the cement strength, two cements with a strength class of 42.5 N/mm^2 and 52.5 N/mm^2 according to the European standard EN 197 were selected. Data of the calcined clay material used here as a substitute for fly ash can be taken from [7].

3 Performance

Investigations were performed not only in the laboratory (slump experiments) but also in the field (in cooperation with the company). The last one means that large concrete samples were produced under real production conditions. Table 2 contains

Table 2 Recipes of the laboratory investigations

Cement type	42.5/52.5	42.5/52.5	42.5/52.5
Volume [L]	0.77	0.77	0.77
Cement [g]	450	450	450
Water [g]	225	250	250
Aggregate	1056	850	850
Fly ash	–	112	–
Calcined clay	–	–	112
$w/(z + k*f)$	0.5	0.5 (f = 0.4)	0.5 (f = 0.4)

Table 3 Dosages of superplasticizers

	min.[wt]	min.[g]	med.[wt%]	med.[g]	max.[wt%]	max.[g]
MS SBS 8005	0.20	0.90	0.85	3.82	1.50	6.74
MP 18 BV	0.10	0.45	0.50	2.25	0.90	4.04
MP 22 BV	0.20	0.90	1.10	4.94	2.00	8.98
MP 334 BV	0.10	0.45	0.55	2.47	1.00	4.49

the recipes for determination of the slump in the laboratory. In the first step, the pure substances were tested and the slump was determined. The activity index f was defined with 0.4, equal to fly ash. In the second step, because of an economic view the mixtures of superplasticizers were investigated.

The dosages of superplasticizers used can be taken from Table 3. According to the information of the producers, the amount varies from SP to SP. Additionally, min-, med- and max-values were selected for producing mortar prisms.

Additionally, mixtures between different SPs in all possible ratios (min-min, min-med and min–max) were investigated.

Based on the results in the laboratory, a large investigation program was performed in cooperation with the practical partner. Recipes are summarized in Table 4.

Table 4 Investigation in cooperation with the company

Components	SP [wt% of cement]	Volume	density ϱ	Mass for 1 m^3 concrete	Mass for 30 L mixture
Units		dm^3	kg/dm^3	kg	kg
Sand, 0–2 mm		259.70	2.63	683	20.49
Gravel sand 2–8		102.67	2.62	269	8.07
Gravel 8–16		321.29	2.63	845	25.35
CEM I 52.5 R		90.32	3.1	280	8.4
Freshwater		162.00	1	162	4.86
Fly ash or calcined clay		32.41	2.16	70	2.1
ACE 455	0.7	1.81	1.08	1.96	0.0588
MS SBS 8005	0.4	1.02	1.1	1.12	0.0336
Air void		28.78	0	0	0
Sum		1000		2312.08	69.39
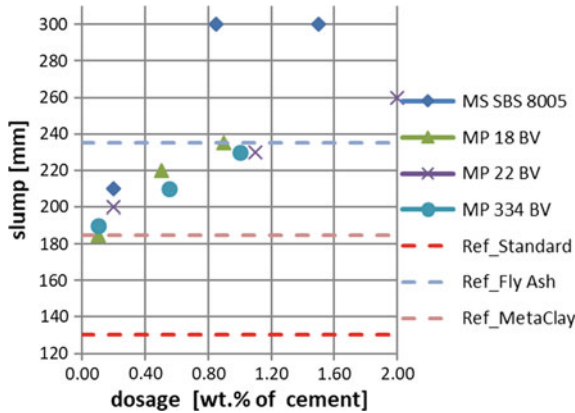
Fig. 1 Slump of samples produced with different superplasticizers

4 Results

4.1 Slump/Spreading Behavior

Figure 1 shows the results of the slump of samples produced in the laboratory. It can be observed that an effect to improve the workability can be measured with every material. Especially, MS SBS 8005 shows a strong increase of the slump, and also the other substances reach the reference mixture with fly ash. In general, the values are a little bit too high because of the high amount of water inside the mixtures

Because of the fact that MS SBS 8005 provides very good results, also mixtures between some SP were investigated. The background here is an economical view too because SBS 8005 is very expensive. Figure 2 shows the results of these investigations. A minimum concentration of SBS 8005 combined with a middle concentration of MP BV 22 or 334 provides results, which are equal to the reference recipe with fly ash.

Therefore, the amount of SBS 8005 can be reduced and extended by a cheaper SP substance.

4.2 Dynamic Modulus of Elasticity of Mortar Samples

Figure 3 shows data of the evaluation of the dynamic modulus of elasticity of the produced mortar samples. The behavior is equal to the reference mixtures and confirms the principle suitability of recipes developed in the laboratory.
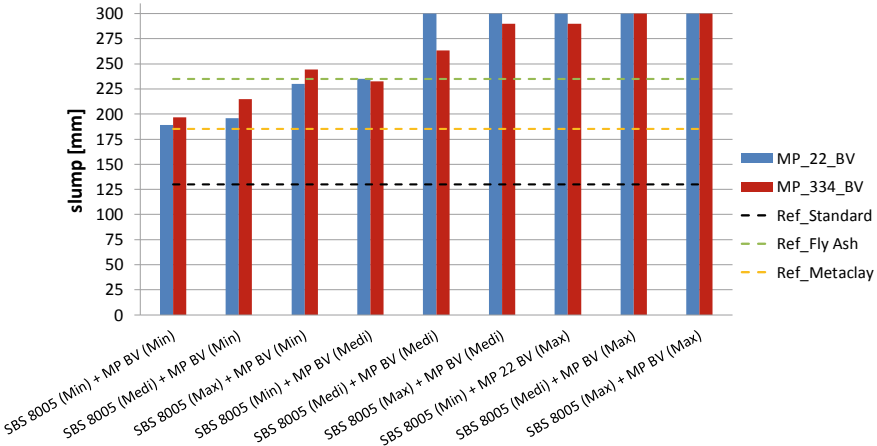
Fig. 2 Slump of samples produced with different superplasticizers in mixtures
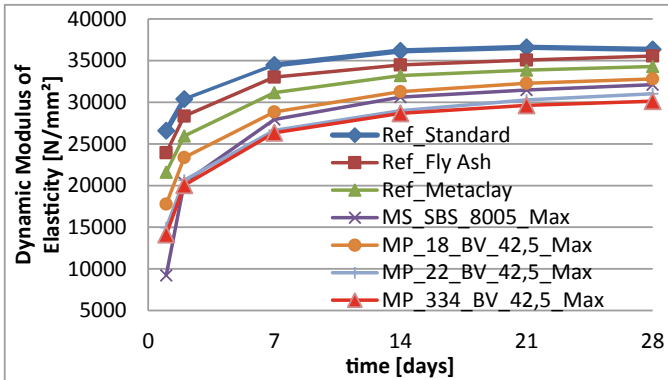
Fig. 3 Dynamic modulus of elasticity of mortar samples investigated

4.3 Production of Precast Concrete Samples

Table 5 summarizes experiences of the company when dealing with different superplasticizers. SPs were also used in mixtures based on the results of the laboratory investigations. In total, more than 20 different recipes were tested by the company. Three of them were selected producing larger formatted concrete samples. Because of many years of use, the superplasticizers ACE 455 was also included in the study program.

Concrete samples (see Fig. 4) were produced using recipe No. 1, No. 16 and No. 18 because of the best workability and stability values. There are no significant differences in the concrete structure of the precast elements produced with different

Table 5 Recipes for practical use

No.	Recipe	Superplasticizer	SP type	Dosage [wt%]	Slump [cm]	Observations
1	**Ref fly ash**	**ACE 455**	**FM**	**0.9**	**62**	**Good cohesiveness**
2	FDW recipe metaclay	ACE 455	FM	0.9	50	Good cohesiveness
3	FDW recipe metaclay	MP 334 BV	BV	0.9	34	Not suitable, stiff
4	FDW recipe metaclay	MP 22 BV	VZ/BV/FM	0.9	31	Not suitable, stiff
5	FDW recipe metaclay	SBS 8005	SBS	0.9	52	Good cohesiveness
16	**FDW recipe metaclay**	**ACE 455**	**FM**	**0.7**	**58**	**Good cohesiveness**
		SBS 8005	**SBS**	**0.4**		
18	**FDW recipe metaclay**	**MP 22 BV**	**VZ/BV/FM**	**1.5**	**53**	**Very soft, particular frothed**
		SBS 8005	**SBS**	**0.5**		

Fig. 4 Precast elements produced with different recipes

recipes, however visible differences of the surface quality of the samples exist. The surface has a great importance for the production of precast elements that is why different technologies to smooth the surfaces were applied (with hand, with a plate or an impeller smoother). One half of the plates were produced with, the other without any reinforcement.

Values of the compressive strength are satisfactory. While recipe No. 1 (reference with fly ash) reaches values of approximately 62–64 N/mm^2, the values of the recipes No 16 and No 18 are a little bit among them and reach 57 N/mm^2 (No. 16) and 53 N/mm^2 (No. 18). Actually, precast elements produced store under the same conditions as the normal produced one to compare the shrinkage and durability behavior.

5 Conclusions

1. A specially developed calcined clay mixture between two different clays, burnt at temperature of approximately 650–680 °C, is suitable for using SCM in concrete.
2. Because of the calcined clay structure, sometimes the workability is a problem for producers of precast concrete elements.
3. Different superplasticizers with different compositions and molecule structures were tested because some information from the literature is contradictory.
4. The combination of calcined clay materials and specially developed superplasticizers mixtures allows producing concrete with different properties.
5. Results obtained in the laboratory cannot transform in a direct way to the conditions in the company, that's why the recipes from the laboratory have to be tested under production conditions.
6. It can be summarized that a substitution of fly ash by calcined clay materials using a special mixture of superplasticizers is possible and allows producing large formatted precast elements with equal properties.

References

1. Fernandez, R., Martirena, F., Scrivener, K.L.: The origin of the pozzolanic activity of calcined clay minerals: A comparison between kaolinite, illite and montmorillonite. Cem Concr Res **41**, 113–122 (2011)
2. Tironi, A., Trezza, M.A., Scian, A.N., Irassar, E.F.: Incorporation of calcined clays in mortars: porous structure and compressive strength. Procedia Materials Science **1**, 366–373 (2012)
3. Tironi, A., Trezza, M.A., Scian, A.N., Irassar, E.F.: Assessment of pozzolanic activity of different calcined clays. Cement Concr Compos **37**, 319–327 (2013)
4. He, Ch., Osbaeck, B., Makovicky, E.: Pozzolanic reactions of six principal clay minerals: activation, reactivity, assessments and technological effects. Cem Concr Res **25**, 1691–1702 (1995)
5. Taylor-Lange, S.C., Lamon, E.L., Riding, K.A., Juenger, M.C.G.: Calcined kaolinite–bentonite clay blends as supplementary cementitious materials. Appl Clay Sci **108**, 84–93 (2015)
6. Garg, N., Skibsted, J.: Pozzolanic reactivity of a calcined interstratified illite/smectite (70/30) clay. Cem Concr Res **79**, 101–111 (2016)

7. Huenger, K.-J., Gerasch, R., Sander, I., Brigzinsky, M.: On the reactivity of calcined clays from lower Lusatia for the production of durable concrete structures. In: Proceedings of the 2nd International Conference on Calcined Clays for Sustainable Concrete, RILEM 16, pp. 205–211, Habana (2017)
8. Sposito, R., Duerr, I., Thienel, K.-Ch.: Lignosulfonates in cementitious systems blended with calcined clays. In: 2nd workshop on the durability and sustainability of concrete structures Moscow (Russia) SP 17-1 (2018)
9. Akhlaghi, O., Aytas, T., Tatli, B., Sezer, D., Hodaei, A., Favier, A., Scrivener, K., Menceloglu, Y.Z., Akbulut, O.: Modified poly(carboxylate ether)-based superplasticizer for enhanced flowability of calcined clay-limestone-gypsum blended Portland cement. Cem Concr Res **101**, 114–122 (2017)

Studying the Rheological Behavior of Limestone Calcined Clay Cement (LC^3) Mixtures in the Context of Extrusion-Based 3D-Printing

Mirza A. B. Beigh, Venkatesh N. Nerella, Christof Schröfl and Viktor Mechtcherine

Abstract Ensuring sustainability of printable concretes while complying with the complex requirements to their rheological properties in the fresh state is challenging yet absolutely essential. In this context, the limestone calcined clay cement (LC^3) is of high relevance. In the study at hand, the structural build-up of LC^3 paste was investigated by using the single batch testing approach. Two different calcined clays (CC), one from India and one from Germany, were studied, which were characterized by 58 and 66% amorphous phase, respectively. Both CCs enhanced the static yield stress of the cementitious materials, showing benefits of their use for digital concrete construction. However, the structural build-up of LC^3 made with Indian CC was significantly more pronounced in comparison with that made of the German CC. Most likely, such quick and intense structural build-up can be attributed to the presence of kaolinite in the Indian CC which interacts with the high-range water-reducing admixture used in a particular way.

Keywords Digital concrete construction · 3D-printing · Calcined clays · Rheology · Structural build-up

1 Introduction

Extrusion-based DC has seen a surge in the research efforts and innovations in recent years [1, 2]. 3D-printable cementitious materials (3PCs) for the extrusion-based digital construction (DC) should possess sufficiently high initial static yield stress (SYS) to yield the required buildability. Furthermore, the rate of increase in SYS must be in well-balanced proportion to the vertical printing rate which increases the static pressure [3] of the lower printed layers. From material composition perspective, there are two ways to meet the requirement of high static yield stress: (1) use of chemical admixtures such as accelerators [4, 5] and/or (2) addition of secondary supplementary materials (SCMs) which increase the rate of flocculation at early age and hence enhance the structural build-up [6, 7]. The type and amount of the SCMs

M. A. B. Beigh · V. N. Nerella · C. Schröfl · V. Mechtcherine (✉)
Institute of Construction Materials, Technische Universität Dresden, Dresden, Germany
e-mail: mechtcherine@tu-dresden.de

affect directly the overall sustainability of digital construction and therefore must be considered while designing concrete compositions for such seminal technologies as 3D-printing. While compositions with fly ash and silica fume are more sustainable than those with Portland cement only, the availability of such SCMs is limited. Therefore, the use of alternative SCMs in 3PCs must be fostered. Chen et al. [8] suggested the usage of calcined clay along with limestone powder as SCMs for developing sustainable 3PCs with low CO_2 footprint. The key literature on LC^3 [9, 10] suggests that a mixture consisting of limestone and calcined clay with a mass ratio of 1:2 not only can replace higher amounts of clinker but also can generate carbo-aluminate hydrates which can fill the capillary pores. Note that the calcined clay serves as a pozzolanic material [11] while the limestone powder primarily serves as a rheology modifier [12]. In the article at hand, the rheology of LC3 cement pastes is investigated, while two different sources of clay were used denoted as Indian calcined clay (ICC) and German calcined clay (GCC). The concept of using 1:2 mass ratio proportions of limestone and calcined clay is followed. The influence of CC replacements on the structural build-up is assessed in comparison with a reference paste that has only Portland cement as a binder [13]. The early age structural build-up evolution of cement pastes in time is characterized by linear evolution [14] until a characteristic age of t_c and is exponential thereafter as described by Perrot's model [15] in (Eq. 1).

$$\tau_0(t_{rest}) = \tau_{0,0} + A_{thix}.t_c(e^{t_{rest}/t_c} - 1)$$ (1)

where $\tau_{0,0}$ is the static yield stress at the beginning of the rest period, t_{rest} is the resting time and A_{thix} is the structuration parameter.

2 Experimental Investigation

2.1 Materials

Two LC^3 paste mixtures were investigated based on the reference cement paste (Ref) presented in the prior work by authors [13]. The LC^3 mixtures were prepared by replacing 52.5 wt% Portland cement CEM I 52.5 R ft, denoted CEM, by limestone and calcined clay used in the ratio of 1:2 [10, 16]. All cement pastes had an equivalent water-to-cement ratio $(w/c)_{eq}$ of 0.42, calculated according to EN 206-1 [17]. As a high-range water-reducing admixture (HRWRA), MasterGlenium SKY 593 produced by BASF Construction Solutions GmbH, Trostberg/Germany, was used. Mineralogical compositions of both calcined clays and limestone powder were determined using powder X-ray diffraction (XRD) operating with CuKα radiation. Clays were inherently hydrous aluminosilicates [18]. XRD disclosed that GCC contained a higher amount of amorphous phase of 66% as compared to ICC, which had approximately 58%. Besides, ICC contained 25% calcite and 9.2% kaolinite. The

Table 1 Mineralogical composition of GCC (wt%)

Quartz	Mica	Feldspar	Anhydrite	Calcite	Amorphous phase %
18.8	6.6	4.9	1.8	1.8	65.7

Table 2 Mineralogical composition of ICC (wt%)

Quartz	Anatase	Tricalcium aluminate	Gypsum	Kaolinite	Calcite	Amorphous phase %
1.8	1.2	0.9	3.3	9.2	25.4	58.2

high amount of kaolinite in ICC, which is absent in GCC, can be very important with respect to the performance of HRWRA. The GCC and the ICC were obtained from external providers who had prepared them using proprietary processes (Tables 1 and 2).

The particle size distribution (PSD) of the dry constituents was measured using a laser diffraction technique, and the cumulative plot is shown in Fig. 1. The PSD of the cement, GCC and limestone are similar, while, in contrast, the ICC is coarser (Table 3).
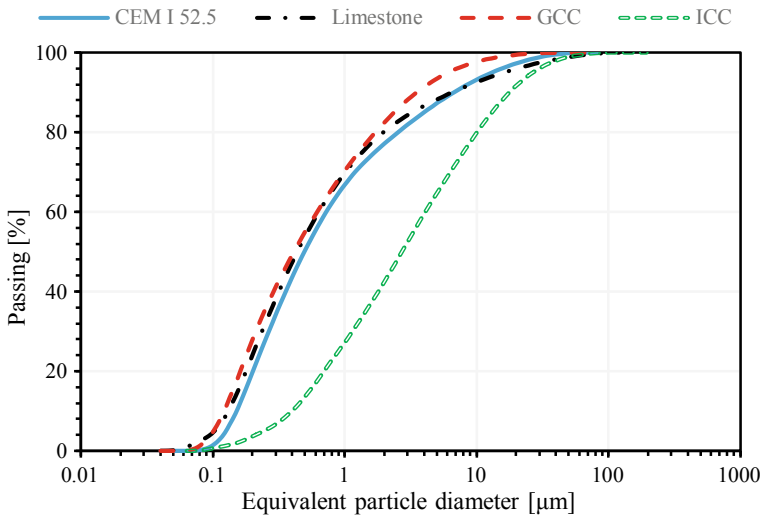
Fig. 1 Cumulative particle size distribution of cement, calcined clays and limestone

Table 3 Compositions of the cement pastes under investigation

Constituents	Density [kg/dm^3]	Ref mixture [kg/dm^3]	LC^3 mixture [kg/dm^3]
CEM I 52.5 R ft	3.10	1.140	0.599
Water	1.00	0.627	0.529
HRWRA (PCE)	1.01	0.009	0.009
Calcined clay	2.65	–	0.441
Limestone	2.31	–	0.221

Table 4 Preparation protocol for the cement pastes

Time [min:s]	Duration [min:s]	Speed [rpm]	Action
00:00–00:10	00:10	–	Adding water with the pre-dissolved HRWRA to the dry constituents
00:10–01:00	00:50	139	Mixing
01:00–02:30	01:30	–	Wall scraping
02:00–03:30	01:30	591	Mixing
03:30–04:00	00:30	–	Wall scraping
04:00–06:00	02:00	591	Final mixing

2.2 Paste Preparation

One liter (1 dm^3) of cement paste was prepared for each experiment following methodology given in Table 4, using a bench mounted planetary mixer. It was ensured that all pastes were dispersed well and had the same shear history during the mixing process.

2.3 Rheometry

Flow table test was employed to determine the spread diameter as a pragmatic, practical measure of the bulk rheological behaviour. Thereafter, the rheometer HAAKE MARS II was used with a so-called building materials' cell and a vane configuration. The paste was filled in the unit cell in three steps, making certain that no air remained entrapped. The test protocol following the single batch method was used to study the structural build-up. At first, the hysteresis loop test was performed at a paste age of 18 min to ensure the maximally deflocculated state in comparison with the successive ages of the paste [19]. The interpolation of the shear stress–shear rate lower curve to an intercept with the y-axis provided the Bingham yield stress while the slope yielded the Bingham plastic viscosity. The SYS was measured at the sample

Table 5 Testing profile for assessing the structural build-up

Time relative [mm:ss]	Shear rate [s^{-1}]	Action
18:00–18:30	0–100	Shear rate up
18:30–19:30	100	Constant shearing
19:30–20:00	100–0	Shear rate down
23:00	$0.08 < \dot{\gamma}_{ap}$	Stress growth test
45:00	$0.08 < \dot{\gamma}_{ap}$	Stress growth test
60:00	$0.08 < \dot{\gamma}_{ap}$	Stress growth test
90:00	$0.08 < \dot{\gamma}_{ap}$	Stress growth test
120:00	$0.08 < \dot{\gamma}_{ap}$	Stress growth test

ages of 23, 45, 60, 90 and 120 min following the strain-based approach [13]. The constant effective strain maintained was 0.2 for all measurements and was sufficient to ensure flow onset. In other words, the vane was rotated at a constant shear rate of 0.08 until an effective strain of 0.2 units was realized, and then, the vane was stopped. Stopping the measurement at 0.2 units enabled the prevention of excess disturbance of the specimen. Table 5 shows the test methodology of the experiments.

Each test was repeated thrice to ensure statistical reliability. The coefficient of variance with regards to the Bingham yield stress and plastic viscosity was less than 5%, underlining high reproducibility of the measurements.

3 Results and Discussion

In a set of preliminary experiments, it was observed that the pastes under investigation reached the maximum value of shear stress at a critical strain of 0.2 units, see also Sect. 2.3. The shear stress measured at the constant shear rate applied is plotted as a function of shear strain in Fig. 2. As the paste aged, the structural build-up evolved significantly and so did the response of shear stress to the shear strain. It is important to note that the ICC paste exhibited much more intense structural build-up than the GCC paste, and therefore, the *y*-axis limits of the plots in Fig. 2 vary by the factor of 10.

Literature suggests that static yield stress is the peak of the shear stress versus shear strain curves [18, 20]. However, the static yield stress may not always be read at a distinct point [13]. Hence, the static yield stress was calculated as the average of the shear stress values at the transition from the linear growth of shear stress and shear strain curve into the plateau (cf. Fig. 2). The calculated static yield stresses for various paste ages are plotted in Fig. 3a. The structuration rate is denoted with the parameter A_{thix} that is calculated by fitting the measured data to Perrot's model [15]. A_{thix} of the ICC is 7.5 times and 47.8 times higher than that of the GCC and reference paste, respectively. The flow table spread values showed a similar trend, see Table 6. These results confirm the anticipated increase in the structural build-up due
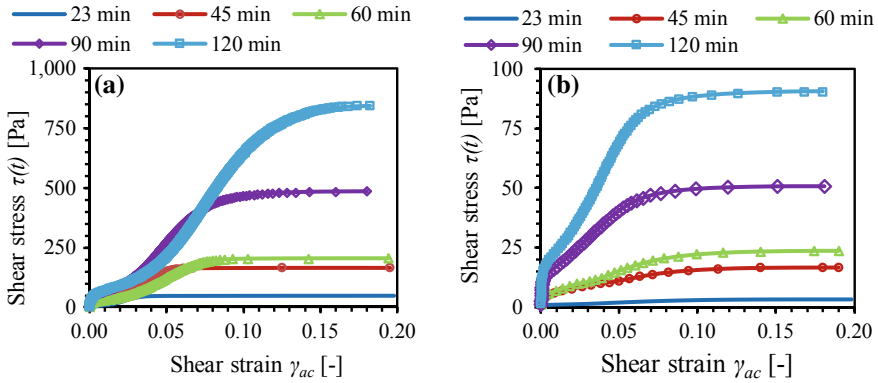
Fig. 2 Shear stress–shear strain curves for mixture under investigation at different ages: **a** ICC-based LC3 paste and **b** GCC-based LC3 paste
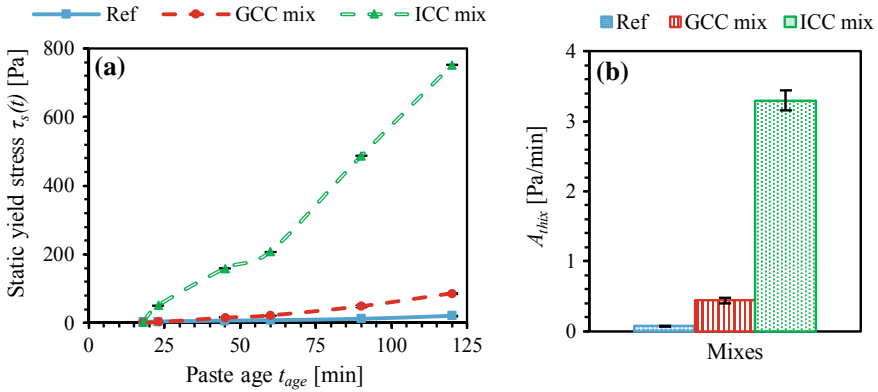
Fig. 3 a Static yield stress versus the paste age plot and **b** A_{thix} plot for the mixtures under investigation

Table 6 Flow spread diameter of the pastes under investigation

Mixture	Initial diameter at 18 min [mm]	Final diameter at 120 min [mm]
Ref. paste	303	301
GCC paste	270	190
ICC paste	180	130

to the substitution of cement using the combination of calcined clay and limestone powder. Both the GCC and ICC mixtures exhibited a considerably more intense structural build-up in comparison with the reference cement paste while having less than half of the Portland cement content. Since high A_{thix} values are usually regarded as beneficial for digital concrete construction, the use of LC^3 has a high potential as

a binder for 3PCs. It must be emphasized that among the CCs tested, the ICC with A_{thix} of 3.3 Pa/min leads to a significantly higher structural build-up in comparison with the 0.437 Pa/min of GCC. The origins of this behaviour are a matter of ongoing investigation. Differences in both the particle size distribution and the mineralogical composition could be probable causes. In addition to potential differences in the actions of the amorphous phase, the ICC had a rather high amount of kaolinite and some tricalcium aluminate. The latter is highly reactive in the presence of water and may result in a quick setting. Concerning the clay of kaolinite, the HRWRA may specifically react with this layered mineral. Ng et al. [21] have reported that the layered structure of clay minerals is prone to intensely interact with PCEs. Besides adsorption to their outer surfaces, clays can intercalate significant numbers of PCE molecules in their interlayer spaces. In this way, a high amount of PCE is bound within the mineral and is not available for plasticizing the paste any longer. This critical issue will be considered in further research by selecting the type and dosage of HRWRA depending on the mineralogical composition of CC materials.

4   Summary and Conclusions

The rheology of binder pastes made of LC^3 was investigated. Calcined clays from India (ICC) and Germany (GCC) were used. XRD analysis showed 66 and 58% amorphous phase in GCC and ICC, respectively. ICC contained a significant portion of kaolinite, which represents uncalcined, initial clay mineral, whereas the GCC sample did not contain layered clayey minerals. The structural build-up was measured using the strain-based, single batch approach. The structuration parameter A_{thix} of ICC was 7.5 times higher than that of GCC and 47.8 times higher than that of the reference paste. The much more intense surge in the structuration in case of ICC in comparison with the GCC behavior may be owing to the presence of the kaolinite. Extensive adsorption accompanied by intercalation of HRWRA molecules is most likely the reason for the loss of the plasticizing effect in LC^3 paste with ICC. With respect to the digital concrete construction, the obtained results confirm the suitability of limestone calcined clay cement as a more sustainable and rheological beneficial alternative to Portland cement.

References

1. Buswell, R.A., Leal de Silva, W.R., Jones, S.Z., Dirrenberger, J.: 3D printing using concrete extrusion: a roadmap for research. Cem. Concr. Res. **112**, 37–49 (2018)

2. Nerella, V.N., Näther, M., Iqbal, A., Butler, M., Mechtcherine, V.: Inline quantification of extrudability of cementitious materials for digital construction. Cem. Concr. Compos. **95**, 260–270 (2019)

3. A. Perrot, A. Pierre, S. Vitaloni, V. Picandet, Prediction of lateral form pressure exerted by concrete at low casting rates, Mater. Struct., 2315–2322 (2015).

4. Ferraris, C.F., Obla, K.H., Hill, R.: The influence of mineral admixtures on the rheology of cement paste and concrete. Cem. Concr. Res. **31**, 245–255 (2001)

5. Kazemian, A., Yuan, X., Cochran, E., Khoshnevis, B.: Cementitious materials for construction-scale 3D printing: laboratory testing of fresh printing mixture. Constr. Build. Mater. **145**, 639–647 (2017)

6. Saleh, R., Kemal, T., Ramyar, K.: Thixotropy and structural breakdown properties of self consolidating concrete containing various supplementary cementitious materials. Cem. Concr. Compos. **59**, 26–37 (2015)

7. F. Nazário Santos, S. Raquel Gomes de Sousa, A. José Faria Bombard, S. Lopes Vieira, Rheological study of cement paste with metakaolin and/or limestone filler using Mixture Design of Experiments, Constr. Build. Mater. 143, 92–103 (2017).

8. Chen, Y., Veer, F., Copuroglu, O., Schlangen, E.: Feasibility of using low CO_2 concrete alternatives in extrusion-based 3D concrete printing. In: RILEM International Conference on Concrete Digital Fabrication, pp. 269–276. Springer International Publishing (2018)

9. Chen, Y., Li, Z. Figueiredo, S.C., Copuroglu, O., Veer, F., Schlangen, E.: Limestone and calcined clay-based sustainable cementitious materials for 3D concrete printing: a fundamental study of extrudability and early-age strength development. MDPI Appl. Sci. Part B Eng. **9** (2019)

10. Scrivener, K., Martirena, F., Bishnoi, S., Maity, S.: Calcined clay limestone cement (LC3). Cem. Concr. Res. **114**, 49–56 (2018)

11. Fernandez, R., Martirena, F., Scrivener, K.L.: The origin of the pozzolanic activity of calcined clay minerals: a comparison between kaolinite, illite and montmorillonite. Cem. Concr. Res. **41**, 113–122 (2011)

12. Gunnelius, K.R., Lundin, T.C., Rosenholm, J.B., Peltonen, J.: Rheological characterization of cement pastes with functional filler particles. Cem. Concr. Res. **65**, 1–7 (2014)

13. Nerella, V.N., Beigh, M.A.B., Fataei, S., Mechtcherine, V.: Strain-based approach for measuring structural build-up of cement pastes in the context of digital construction. Cem. Concr. Res. **115**, 530–544 (2019)

14. Roussel, N.: A thixotropy model for fresh fluid concrete: theory, validation and applications. Cem. Concr. Res. **36**, 1797–1806 (2006)

15. Perrot, A., Rangeard, D., Pierre, A.: Structural built-up of cement-based materials used for 3D-printing extrusion techniques. Mater. Struct. Constr. **49**, 1213–1220 (2015)

16. Nguyen, Q.D., Khan, M., Castel, A.: Engineering properties of limestone calcined clay concrete engineering properties of limestone calcined clay concrete. J. Adv. Concr. Technol. **16**, 343–357 (2018)

17. British Standards Institution: Concrete—Complementary British Standard to BS EN 206-1. Part 2 Specification for Constituent Materials and Concrete (2006)

18. Mahaut, F., Mokéddem, S., Chateau, X., Roussel, N., Ovarlez, G.: Effect of coarse particle volume fraction on the yield stress and thixotropy of cementitious materials. Cem. Concr. Res. **38**, 1276–1285 (2008)

19. Roussel, N.: A thixotropy model for fresh fluid concretes: theory, validation and applications. Cem. Concr. Res. **36**, 1797–1806 (2006)

20. Roussel, N., Ovarlez, G., Garrault, S., Brumaud, C.: The origins of thixotropy of fresh cement pastes. Cem. Concr. Res. **42**, 148–157 (2012)

21. Ng, S., Plank, J.: Interaction mechanisms between Na montmorillonite clay and MPEG-based polycarboxylate superplasticizers. Cem. Concr. Res. **42**, 847–854 (2012)

Rheological Properties of Self-Compacting Lightweight Concrete with Metakaolin

C. D. Wagh, S. N. Manu and P. Dinakar

Abstract To escalate the structural efficiency of concrete is one of the best practices to achieve sustainability of concrete. Development of high strength lightweight aggregate self-compacting concrete has significant importance in this circumstance. Due to lower strength of the porous lightweight aggregate, it is very much necessary to improve the strength of the binder that is used in the concrete. Incorporation of metakaolin in the binder is one such practice to improve the strength of the binding material and to achieve these rheological properties of the concrete is very important. The present study evaluates the rheological and mechanical properties of high strength self-compacting lightweight aggregate concrete developed using metakaolin. SCCs were developed with binder content of 550 kg/m^3 and water-binder ratio of 0.28, having metakaolin replacement percentages of 7.5, 10, 12.5 and 15%. Fresh properties of all the developed concretes using metakaolin were satisfying the SCC criteria. The compressive strength of the concretes increased due to the addition of metakaolin. At higher replacement level of metakaolin, it was also observed that the yield stress and plastic viscosity of the concrete increased. All these evidences justify that metakaolin is a potential material for the development of high strength lightweight self-compacting concrete which not only improves the rheological properties but also the mechanical properties of SCCs.

Keywords LWA · SCC · Rheology · Metakaolin

C. D. Wagh
Department of Civil Engineering, IIT Guwahati, Guwahati, India

S. N. Manu
Department of Civil Engineering, ASTRA Hyderabad, Hyderabad, India

P. Dinakar (✉)
School of Infrastructure, IIT Bhubaneswar, Bhubaneswar, India
e-mail: pdinakar@rediffmail.com

1 Introduction

Achievements in modern concrete technology have led to the introduction of lightweight aggregate concrete (LWAC) and self-compacting concrete (SCC) as mass reducing structures and workable materials. Structural lightweight aggregate self-compacting concrete (LWASCC) only accepted by the construction industry as it must satisfy all characteristics pertaining to self-compactness while having a low density; the latter poses a challenging hindrance toward robust self-compacting behavior as it imparts low dynamic energy to the mixture during flow. Moreover, some unfavorable properties of lightweight aggregates (LWAs) such as high porosity (high water absorption), low crushing strength and tendency of buoyancy are additional factors that should be taken into consideration during mix proportioning. If successfully designed, produced and implemented LWASCC constitutes a high-performance material that combines the advantages of structural LWAC, with self-compacting characteristics.

In general, workability, strength and durability are considered as the three major characteristics of concrete. It is believed that workability properties are related to fresh state concrete characteristics, whereas strength and durability properties attributed to the hardened state of concrete. Fresh and hardened properties of the concretes are mainly governed by the properties of the materials and the mix proportions that were adopted [1]. The structural behavior of concrete relies on mixing proportions and material properties of the composite system and these factors do not change after hardening.

It is a well-known fact that the use of supplementary cementitious material will enhance the fresh and hardened properties of concretes. The present study evaluates the influence of metakaolin (MK) in the development of high strength lightweight aggregate SCC. Metakaolin differs from the most commonly used mineral admixtures, such as fly ash and silica fume, in that it is not a by-product. It is manufactured under controlled conditions by thermally activating purified kaolinite clay within a specific temperature range (650–800 °C) [2]. It has been reported that metakaolin is a poorly crystallized white powder with a specific surface of 12,000 m^2/kg with an average particle size between 1.5 and 2.5 μm [3]. The particle size of metakaolin lies between fly ash and silica fume. Therefore, it offers better workability and requires lesser amounts of high-range water-reducing admixture to obtain slump comparable to silica fume concrete [4]. Apart from this, MK has a number of other benefits as well; its texture is creamier, generates less bleed water, and does not darken the concrete as silica fume does and results in concrete color that are similar to the conventional exposed concretes [5]. There are very few studies reported on the development of SCC using metakaolin.

2 Materials and Methods

2.1 Materials

The materials adopted in the present experimental investigations are as follows. The ordinary Portland cement of 53 grade locally available is used conforming to IS 12,269 [6]. The class F fly ash used in this study conforms to Indian standard code, IS 3812 (Part I) [7]. The metakaolin used in this study was able to meet the requirements of ASTM: C 618. Commercially available water-reducing admixture from BASF, Master Glenium ACE 30 is used in this study. Well-graded natural river sand has been used as fine aggregate in the present study. It has saturated-surface dry (SSD) specific gravity of 2.61, absorption of 1.12% and fineness modulus of 2.3. The coarse aggregate used in the present study is artificially produced sintered fly ash lightweight aggregates. The mix proportions adopted for the present experimental investigation has been shown in Table 1. In Table 1, CL indicates control concrete without metakaolin produced using artificially manufactured sintered fly ash lightweight aggregate as coarse aggregates. MKL stands for concrete produced using lightweight aggregate having certain level of metakaolin replacement. The replacements levels are 7.5, 10, 12.5 and 15%, respectively.

2.2 Experimental Methods Adopted

To assess the rheological properties of the produced LWASCC tests such as slump flow test, T500 test, V funnel test, L box test and ICAR rheometer test were used and the mechanical properties were assessed through compressive strength test. Slump test and T500 test indicate the flowability and filling ability of the SCC. The V funnel test determines the filling ability and segregation resistance of the SCC. L box test is used to determine the passing ability of the SCC through a confined space. The ICAR rheometer is designed to characterize the static yield stress, the dynamic yield

Table 1 Mix proportions adopted in the present study

Mix code	Binder content (kg/m^3)	Cement (%)	Fly ash (%)	Metakaolin (%)	w/b ratio	Superplasticizer (%)
CL	550	75	25	0	0.28	0.80
MK L1	550	67.5	25	7.5	0.28	0.85
MK L2	550	65	25	10.0	0.28	0.90
MK L3	550	62.5	25	12.5	0.28	0.95
MK L4	550	60	25	15.0	0.28	1.00

stress and the plastic viscosity of the concrete [8]. Compressive strength of all the concretes was evaluated at 3, 7, 28 and 90 days.

3   Results and Discussion

3.1   *Slump Flow*

The obtained slump flow values were shown in Fig. 1. From the results, it can be seen that the slump flow of all the developed concretes varied between 670 and 690 mm, which belongs to SF2 according to EFNARC guidelines [9]. From Fig. 1, it is observed that as the replacement level of increases the flow values decreased. Though the dosage of the superplasticizer was fixed during the trial mixes in such a way that the slump flow values belong to 670 ± 10 mm. From Table 1, it can be noticed that as the dosage of metakaolin increases the superplasticizer dosage also increases correspondingly. This may be due to the fact that the higher surface area of the finer metakaolin particles increases the superplasticizer demand. The use of metakaolin may increase the cohesiveness of the binder. This could be the reason for the decrease in slump flow values. Slump flow values indicating the consistency of the SCC; the obtained values indicating that these concretes are highly consistent and possess good flowability. During the test it is also noticed that no sign of bleeding was observed at the outer edge of the spread. And the spread was even and uniform also. This indicates that all the developed SCCs were segregation and bleeding free.
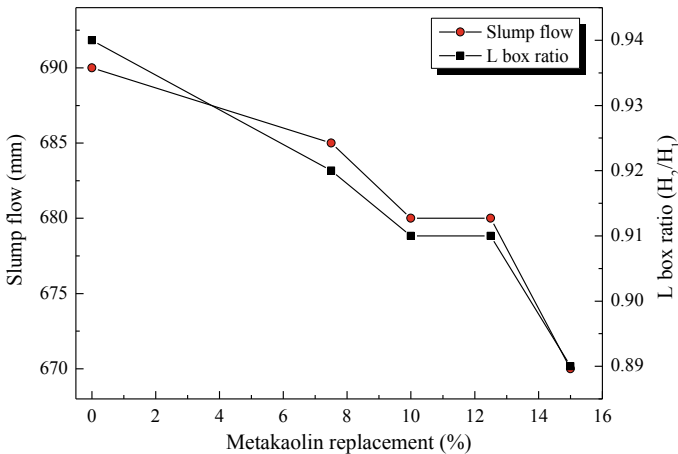
Fig. 1   Variation of flowability and passing ability at various replacements of metakaolin

3.2   L Box Ratio

Passing ability of the lightweight aggregate SCCs has been evaluated through L box test. And the obtained results indicate that the SCCs developed using sintered fly ash lightweight aggregates possess good passing ability. According to EFNARC, all the produced concretes belong to passing ability class 'PA1.' Except 15% replacement of metakaolin all the other concretes exhibited L box ratios more than 0.90. The spherical shape of the lightweight aggregate may reduce intergranular friction between the aggregate grains. Also, from Fig. 1, it is observed that as the replacement of metakaolin increases the passing ability decreases.

3.3 T_{500} Time and V Funnel Tests

Figure 2 shows the variation of T_{500} time and V funnel time at various replacement levels of metakaolin. Viscosity can be assessed by the T500 time during the slump flow test or assessed by the funnel flow time. The time value obtained does not measure the viscosity of SCC but is related to it by describing the rate of flow. Concrete with a low viscosity will have a very quick initial flow and then stop. Concrete with a high viscosity may continue to creep forward over an extended time. From the obtained results, it can be seen that as the percentage replacement of metakaolin increases the viscosity of the concrete also increases. The V funnel time is indicating the filing ability of the concrete, and from the results, it can be seen that all the concretes took more time to emptying the V funnel. This may be due to the fact that the mass (weight) of the SCC is less due to the inclusion of
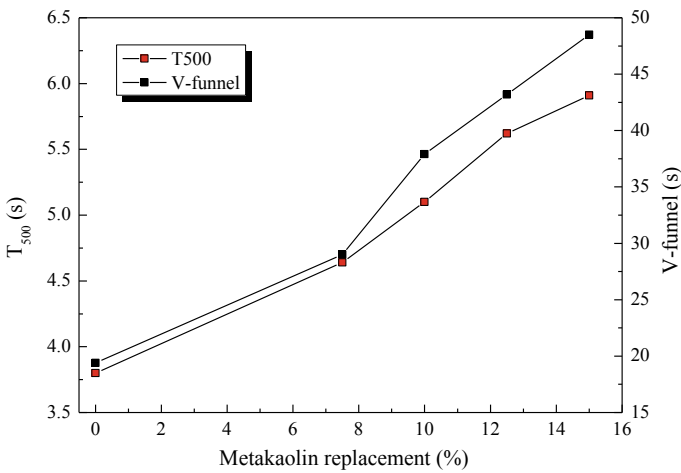
Fig. 2 Influence of metakaolin dosage on the viscosity of the SCC

lightweight aggregate as coarse aggregates. For higher flow time, it is more likely to exhibit thixotropic effects, which may be helpful in limiting the formwork pressure or improving segregation resistance. Negative effects may be experienced regarding surface finish (blowholes) and sensitivity to stoppages or delays between successive lifts.

3.4 Rheology of SCC

The SCC can be considered as a Bingham fluid. This complex interaction is described in several works [10, 11].

$$T = \tau_0 + \mu C \tag{1}$$

Here, the term τ_0 (yield stress) represents the solid phase contribution mainly dissipation by friction between the grains and the μ (plastic viscosity) represents the viscous dissipation in the paste phase in the case of angular aggregate concretes [12]. The results obtained from ICAR rheometer were shown in Fig. 3. The results indicate that as the metakaolin replacement increases both the yield stress and the plastic viscosity of the concrete increases. Though the coarse aggregate grains are spherical in shape the friction offered by the aggregate grains may be minimum. From T500 and V funnel test, it is already noticed that as the dosage of metakaolin increases the viscosity also increases. This reduced the workability with metakaolin inclusion is attributed to the higher surface area of finer grains of metakaolin that leads to a portion of water being absorbed on the surface which decreases workability [13].
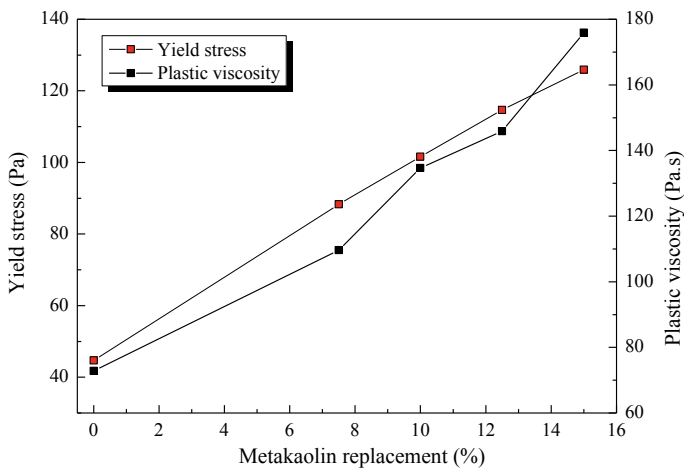
Fig. 3 Influence of metakaolin dosage on the rheological parameters

3.5 Compressive Strength

Compressive strength is the primary strength governing parameter. Compressive strength results obtained in the present experimental investigation have been depicted in Fig. 4. The compressive strength results obtained at 28 and 90 days are following the same trend, and from the results, it can be seen that 12.5% replacement of metakaolin is the optimum dosage for sintered fly ash lightweight aggregates. Also, from the results, it can be seen that the addition of metakaolin increase the compressive strength from 24 to 47% at 3 days. This indicates that inclusion of metakaolin facilitates the quick gain of compressive strength at early ages and this will be an advantage to the precast construction practices. This may be due to the micro-filling capability [14] of the finer metakaolin particles. 90 days compressive strength results show that the strength increment is only up to 11% even at the optimum dosage. This may be due to the 'strength ceiling' of the lightweight aggregates. The results also indicate that the optimum dosage is mainly associated with the compressive strength of the SCC. However, the flowability and the passing abilities decrease with the increase in metakaolin dosage. Also, the filling ability is found to be reduced as the metakaolin dosage increases. But these changes in fresh properties were not reflected in the compressive strengths results of the concretes. This may be due to the fact that all the concretes possess sufficient workability; so the micro-filling ability may dominate in the development of the compressive strength of SCCs produced with lightweight aggregates (Fig. 4).
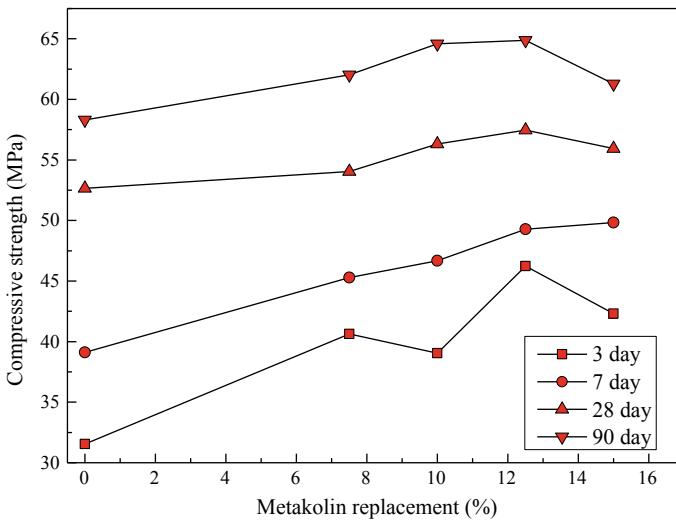
Fig. 4 Variation of compressive strength with replacement of metakaolin at different ages

4 Conclusions

- Addition of metakaolin increased the demand of superplasticizer.
- Slump flow and L box values decreased as the percentage replacement of metakaolin increases.
- T_{500} and V funnel times increased as the replacement of metakaolin increases. Rheological studies indicate that the yield stress and plastic viscosity also increases as the metakaolin dosage increases.
- 12.5% of metakaolin found to be the optimum dosage as far as the compressive strength is concerned in lightweight aggregate concretes.

References

1. Neville, A.M.: Properties of concrete, 5th edn, Trans-Atlantic Publications, Indian International Ed. (2012)
2. Dinakar, P.: High reactive metakaolin for high strength and high-performance concrete. Indian Concr. J. **85**(4), 28–34 (2011)
3. Caldarone, M.A., Gruber, K.A., Burg, R. G.: High reactivity metakaolin a new generation mineral admixture. Concr. Int. **16** (11), 37–40 (1994)
4. Caldarone, M.A., Gruber, K.A.: High reactivity metakaolin (HRM) for high performance concrete. In: Malhotra, V.M. (ed.) Fly Ash, Silica Fume, Slag, and Natural Pozzolans in Concrete, Fifth International Conference, Milwaukee, SP-153, pp. 815–827. American Concrete Institute, Farmington Hills, Mich. (1995)
5. Balogh, A.: High-reactivity metakaolin. Aberdeen's Concr. Constr. **40** (7), 604–606 (1995)
6. IS 12269: Indian standard: specification for 53 grade ordinary Portland cement. Bureau of Indian Standards, New Delhi (2013)
7. IS 3812-1: Specification for pulverized fuel ash, Part 1: for use as pozzolana in cement, cement mortar and concrete. Bureau of Indian Standards, New Delhi (2015)
8. Benaicha, M., Roguiez, X., Jalbaud, O., Burtschell, Y., Alaoui, A.H.: Influence of silica fume and viscosity modifying agent on themechanical and rheological behavior of self-compacting concrete. Constr. Build. Mater. **84**, 103–110 (2015)
9. EFNARC: Specification and guidelines for self-compacting concrete (2005)
10. Tatersall, G.H., Banfill, P.G.F.: The rheology of fresh concrete. Pitman, London (1983)
11. Roussel, N., Lemaître, A., Flatt, R.J., Coussot, P.: Cement and concrete research steady state flow of cement suspensions: a micro mechanical state of the art. Cem. Concr. Res. **40**, 77–84 (2010)
12. de Larrad, F.: Concrete mixture proportioning: a scientific approach. E& FN spon (1999)
13. Bai, J., Wild, S., Sabir, B.B., Kinuthia, J.M.: Workability of concrete incorporating pulverized fuel ash and metakaolin. Mag. Concr. Res. **51**, 207–216 (1999)
14. Wild, S., Khatib, J.M., Jones, A.: Relative strength, pozzolanic activity and cement hydration in superplasticised metakaolin concrete. Cem. Concr. Res. **26**(10), 1537–1544 (1996)

Comparing the Ecoefficiency of Cements Containing Calcined Clay and Limestone Filler

Pedro Cesar R. A. Abrão , **Rafael T. Cecel** , **Fábio A. Cardoso**
and **Vanderley M. John**

Abstract Calcined clay and fillers are materials with the best chance of scalability in cement industry. However, the addition of substantial amounts of SCMs affects the reactivity and water demand of blended cements, influencing their environmental impact in use as well as their performance. So, the aim of this work is to compare the influence of substituting clinker by calcined clay and limestone filler in the ecoefficiency of blended cements. For that, an ordinary Portland cement was replaced by calcined clay and limestone filler to produce two blended cements: LC3 and LFC. Regarding reactivity, LFC and LC3 presented higher relative combined water at 91 days compared to OPC. Water demand for constant workability was higher for LC3 compared to OPC and similar to LFC, but when superplasticizer was used, both cements demanded less water than OPC. Both parameters (reactivity and water demand) affected the binder's efficiency measured as *cwf* index which had a linear correlation with mechanical performance. In concern of environmental indicators, binder and carbon intensity, LFC presented the lowest indicators results for concretes with 20 and 30 MPa, LC3 for concrete with 50 MPa and OPC for concrete with 60 MPa.

Keywords Combined water fraction index · CO_2 emissions · Supplementary cementitious materials

1 Introduction

Fillers and calcined clays are materials with great potential to supply the cement industry demand to supplementary cementitious materials (SCMs), since they are two of the most abundant materials in the earth's crust [1]. Practically, any inert rock can be used as fillers, but mineralogy and particle shape can influence their technical viability [2]. On the other hand, clays must have an considerable amount of kaolinite

P. C. R. A. Abrão (✉) · R. T. Cecel · F. A. Cardoso · V. M. John
National Institute on Advanced Eco-Efficient Cement-Based Technologies, São Paulo, Brazil
e-mail: pedro.abrao@lme.pcc.usp.br

Department of Construction Engineering, Escola Politécnica, University of São Paulo, São Paulo 05508-070, Brazil

in their composition, around 40% are already sufficient to produce blended cements with technical feasibility [3]. Those clays are widely available on equatorial and subtropical regions as well as at stockpiled materials on quarries all over the world. In Brazil, calcined clays are being used in construction since 1960 and blended cements with this material are still being produced.

The use of both materials, calcined clays and fillers, to replace clinker in cement production reduces CO_2 footprint of blended compositions. However, incorporating substantial contents of new materials in blended cements affects their performance, which is generally associated with mechanical strength and durability, both significantly impacted by paste porosity. On the other hand, porosity is basically the difference between the mixing water for a specific rheological behavior and the chemically combined water. Both parameters were put together in a ratio to provide the combined water fraction index (*cwf*) [4, 5], that measures the binder's efficiency in terms of reactivity and water demand.

Nowadays, standards all over the world are classifying cements according to compressive strength, looking just to their reactivity since they use a fixed water/cement ratio in the tests. However, in real situations, cements can require more or less mixing water to achieve the desired rheological behavior, affecting their final performance and environmental impact in use. Thus, it is crucial to put the variable water demand to discuss the equation of cement's ecoefficiency.

The aim of this work is to compare the influence of substituting clinker by calcined clay and limestone filler in the ecoefficiency of blended cements. For that, an ordinary Portland cement was partially replaced by calcined clay and limestone filler to produce two blended cements: LC3 and LFC. Then, combined water, water demand, superplasticizer demand, and compressive strength were measured. These data were used to calculate the combined water fraction (*cwf*), porosity, binder, and carbon intensity indicators.

2   Experimental

The materials used in this work were an OPC from Brazilian market (similar to Europe's CEM I), a dilution limestone filler (Filler 3) with approximately the same particle-size distribution of OPC, an ultrafine performance filler (Filler 2), and a calcined clay from India gently provided by LC3 team. Filler 1 comes incorporated in the OPC from the factory. These materials were blended to produce LC3 and LFC. Codes, general description, and raw materials proportion in mass of each cement are shown on Table 1. Sulfate content of LC3 cement was corrected. It is important to note that the dilution of OPC by limestone filler to produce LFC was not adjusted by increasing the fineness of OPC or by reducing the packing porosity.

Table 1 Code, general description, and raw materials proportion in mass of each investigated cement

Code	Description	Clinker + CaSO$_4$ (%)	Calcined clay (%)	Filler (%)			
				Filler 1	Filler 2	Filler 3	Total
OPC	High early strength cement	94	–	6	0	0	6
LC3	Limestone calcined clay cement	52	30	3	5	10	18
LFC	Limestone filler cement	52	–	3	5	40	48

2.1 Characterization of Anhydrous Materials

Mineralogical composition of OPC and calcined clay were measured by X-ray diffraction. For phase quantification, a refinement was performed by the Rietveld method. OPC presented a regular mineralogical composition, with 60.8% of alite, 13.3% of belite, 3.5% of CaSO$_4$, 8.2% of C$_3$A, 8% of ferrite, and 6% of limestone filler. Calcined clay has a substantial amount of amorphous phase (82%), indicating an efficient calcination process. Calcined clay also presented quartz (9.4%) and kaolinite (5.2%) in their composition, as well as anatase and hematite in lower contents.

Physical properties of the materials are presented on Table 2. Shape factor is obtained by dividing the SSA$_{BET}$ by SSA$_{LD}$. All physical properties were evaluated for raw materials (OPC, fillers and calcined clay), and physical parameters of the blended cements (LC3 and LFC) were calculated according to weight percentage of raw materials in their composition. Cement LC3 presented a higher specific surface area, shape, factor and lower density compared to the others, which was expected

Table 2 Physical properties of the used raw materials and blended cements

Parameters	Filler 2	Filler 3	Calcined clay	OPC	LC3	LFC
ρ (g/cm^3)	2.76	2.74	2.32	3.08	2.76	2.92
D$_{10}$ (μm)	0.9	1.7	1.9	2.3	1.5	1.6
D$_{50}$ (μm)	3.0	10.5	13.4	14.4	10.5	10.6
D$_{90}$ (μm)	8.5	27.5	89.8	39.0	43.0	31.7
SSA$_{LD}$ (m^2/g)	1.13	0.50	0.51	0.36	0.46	0.42
SSA$_{BET}$ (m^2/g)	3.73	1.16	8.04	1.64	3.62	1.55
VSA$_{BET}$ (m^2/cm^3)	10.29	3.18	18.65	5.05	9.99	4.53
Shape factor (ξ)	3.3	2.3	15.7	4.6	7.9	3.7

True density (He pycnometry); particle-size distribution parameters (Laser diffraction); Specific surface area from laser diffraction; Specific surface area from BET method; Volumetric surface area; and shape factor

due to the addition of calcined clay. Also, LC3 has a greater volume of fine and coarse particles (broader particle-size distribution) than other cements, fine particles are probably associated with kaolinite nano-plates and coarse particles with quartz.

2.2 Studies on Paste

The determination of superplasticizer demand of each raw material was evaluated in pastes using rotational rheometry. Mixing was conducted by mechanical dispersion at 10.000 rpm for 90 s. Superplasticizer demand of the blended cements was calculated according to weight percentage of raw materials in their composition. Reactivity was assessed by measuring the combined water at 7, 28, and 91 days. Samples at the selected ages were submitted to hydration stoppage by solvent exchange, then combined water was measured by thermogravimetric test.

2.3 Studies on Mortar

Mortar composition (1:3 cement: sand, in mass) was elaborated according to Brazilian standard [6] for determination of cement strength class which agreed with European standards [7]. Therefore, the differences on densities of cements as higher as 10% in the case of LC3, were neglected. Mortars were mixed conforming EN 196-1. Flow table test was used to define the water demand of each cement. Mortars were tested with Brazilian standard water/cement ratio (0.48) and with water adjusted to achieve a constant spread of 240 ± 10 mm in the flow table test, with and without superplasticizer. Superplasticizer was used since it is an essential material in concrete industry. After the flow table test (according to ABNT NBR 13,276), mortars were molded and tested for evaluation of compressive strength at 7, 28, and 91 days according to EN196-1. The calculation of porosity was carried out according to Power's model, with combined water measured by TG.

2.4 Binder Efficiency and Environmental Indicators

Combined water fraction index (*cwf*) relates reactivity and water demand of each cement was calculated according to Eq. 1. The highest is the combined water and the lowest is the mixing water to reach desired rheological behavior, the higher is this *cwf*, indicated an overall more efficient binder.

$$\mathrm{cwf} = \frac{w_c}{w_m} \qquad (1)$$

where, w_c is the chemically combined water at the age of interest and w_m is the amount of mixing water used. In this case, mixing water was the one for spread of 240 ± 10 mm in flow table.

Binder (*bi*) and carbon intensity (*ci*) indicators [8] were also determined. The first measures the amount of binder per m^3 of concrete to achieve 1 MPa of compressive strength, similarly the second quantifies the CO_2 emitted per m^3 of concrete to achieve 1 MPa of compressive strength. CO_2 emissions from production of each cement were estimated as well. It was considered a CO_2 emission factor of 842 kg CO_2/t clinker [9], 271 kg CO_2/t calcined clay, and 5 kg CO_2/t limestone filler [10]. For *ci* and *bi* calculations, concretes were modeled with 300 dm^3 of paste. Strength of concrete was estimated by multiplying the strength of mortars by a factor of 0.8. For *ci* calculations, CO_2 footprint of aggregates was not considered since they were kept constant.

3 Results and Discussions

3.1 Demand of Superplasticizer

For the same water and superplasticizer content, cement LC3 presented a greater yield stress, due to its higher surface area and shape factor. The specific dispersant content for each cement stayed in a similar range, varied from 3.4 mg/m^2 for OPC and 2.8 mg/m^2 for LC3. However, cement LC3 with higher surface area, required 1%wt of dispersant to achieve the saturation content, a value about two times higher than OPC (0.55%wt) and LFC (0.5%wt). The higher demand for dispersants can represent significant cost but have almost negligible environmental impact.

3.2 Combined Water

Figure 1a shows the combined water of each cement. At 7 and 28 days, OPC presented a greater combined water compared to LC3 and LFC, which was expected due to its higher clinker content. However, at 91 days, cement LC3 had a similar result to OPC, associated with late pozzolanic reaction of clays.

In Fig. 1b, the line shows were combined water is a result of binder – clinker + pozzolan – dilution, considering OPC with 6% of filler as reference. As example, at 91 days combined water of LC3 was 4% above the expected from reference OPC with a dilution of 12% by filler. But at 7 days, LC3 combined water content was below the dilution line, illustrating that the contribution of calcined clay was increasing over time. On the other hand, cement LFC stayed close to the dilution line all over the period.
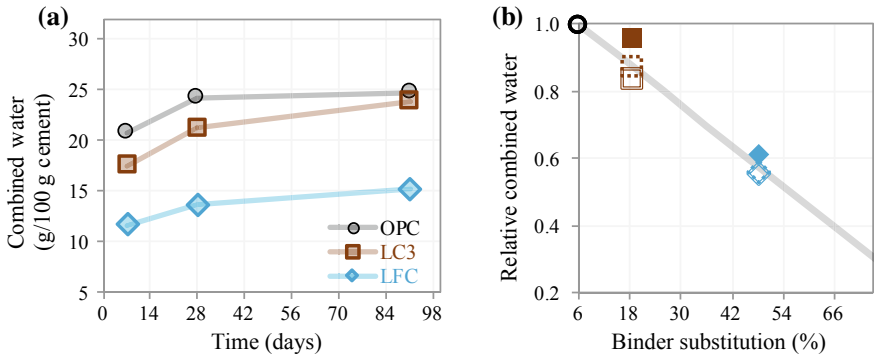
Fig. 1 **a** Combined water of each cement at 7, 28, and 91 days; **b** Relative combined water (OPC) versus binder substitution. Empty icons correspond to 7 days of hydration, dotted icons to 28, and filled icons to 91. The gray line corresponds to a direct dilution

3.3 Water Demand for Standard Mortars

Mortars made with 0.48 w/c ratio presented a very dry aspect (Fig. 2a and e) which is not the proper consistency for molding. Images from after the test (Fig. 2b and f) show that mortars did not spread but underwent fracturing due to the lack of cohesion between the cementitious matrix and the aggregates. Suspensions with superplasticizer and 0.48 w/c ratio also did not present a proper consistency for molding, with tendency to segregation (relevant images can be found in [5]). It seems desirable that mixing water to classify cements should be adjusted to the actual need for adequate rheological behavior for molding. In this work, a spread of 240 ± 10 mm was
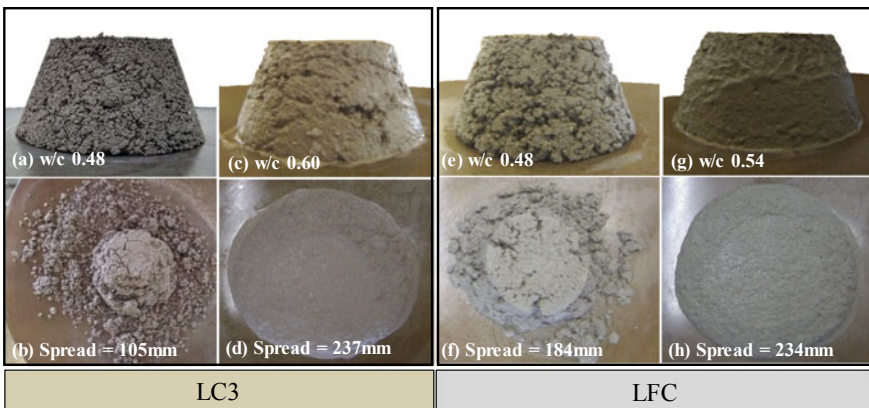
Fig. 2 Images before and after the flow table test for mortars without superplasticizer made with 0.48 w/c ratio and the water needed to achieve 240 ± 10 mm spread

Table 3 Effect of superplasticizer on water/cement ratio for constant flow spread of 240 ± 10 mm on the various cements tested

Materials	Water/cement ratio (cm^3/cm^3)			Relative water demand	
	noSP	SP	SP/noSP	noSP	SP
OPC	1.60	1.26	0.79	1	1
LC3	1.66	1.21	0.73	1.04	0.96
LFC	1.58	1.17	0.74	0.99	0.93

adopted, as mortars without (Fig. 2c–h) and with superplasticizer presented a better consistency.

For mortars without superplasticizer, cement LC3 demanded more water (Table 3) to achieve the 240 mm spread, followed by OPC and LFC. The higher water demand of LC3 is related to its higher specific surface area, that imply in more water to cover the cement particles plus the very high shape factor. Results between OPC and LFC are similar, an outcome expected, since for LFC, the OPC was substituted by a filler with similar particle-size distribution and surface area and was not adjusted to reduce the packing porosity [2].

For mortars with superplasticizer, cement OPC demanded more water than the others (Table 3), followed by LC3 and LFC. Cement with calcined clay had a great reduction on water demand when superplasticizer was used. This can be associated with a better dispersion of the agglomerates of kaolinite nano-plates, similar results were also found by Abrão et al. [5] for diatomaceous earth cements. LFC cement also had a considerable reduction on mixing water compared to noSP mortars, that is probably connected to surface properties and the small percentage of ultrafine fillers (filler 2). For mortars without superplasticizer, these ultrafine fillers were probably agglomerated, negatively affecting the rheological behaviour. The superplasticizer addition proportionated a reduction in the mixing water for all cements, with more pronounced results for LC3 and LFC (27 and 26%) followed by OPC (21%).

3.4 Combined Water Fraction Index—Mechanical Performance

The reactivity (combined water) and the water demand for a specific rheological behavior directly influenced porosity and the results of compressive strength. The combined water fraction index (*cwf*) relates both parameters and has a linear correlation with compressive strength (Fig. 3a) and an exponential correlation with capillary porosity (Fig. 3b) for mortars with and without superplasticizer, at any age. The superplasticizer reduces the mixing water increasing the binder efficiency (*cwf*) of 35% (LFC) and 37% (LC3), which is the cement that benefits more from dispersion. Aging between 7 and 91 days also improves the *cwf* by 19% (OPC) and 36% (LC3), again the best case.
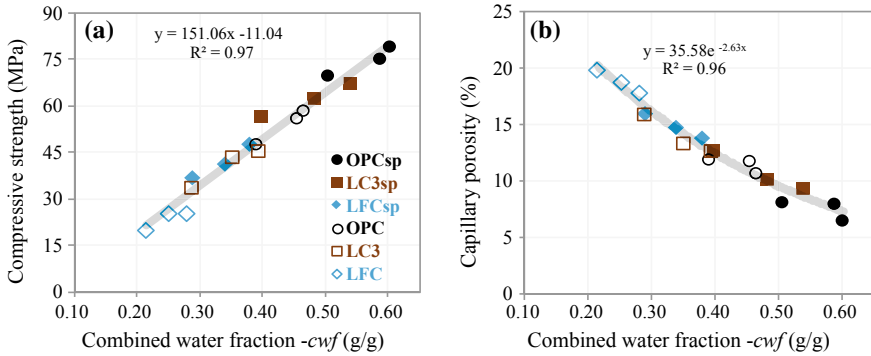
Fig. 3 **a** Compressive strength × *cwf*; **b** Mortar capillary porosity × *cwf*. Systems without super-plasticizer are represented by empty icons. Each composition has results for 7, 28, and 91 days (right to left)

The *cwf* is a practical tool to analyze and even classify cements. It ponders chemical reactivity with the mixing water (or even water demand) and allows to estimate strength for any given mixing water. Table 4 compares what will be the mechanical performance of all cements assuming being tested by the Brazilian cement standard, with constant w/c ratio (0.48). These values were produced by *cwf* equation and the combined water of each cement measured by TG (Fig. 1), which is not significantly affected by change in water/cement ratio, assuming a mixing water of 0.48 and entering this values in *cwf* equation (Fig. 3a). This is an estimation of the strength that neglects eventual molding defects expected due to poor workability of the 0.48 mortars (Fig. 2). Industry usually overcome workability problem of w/c 0.48 or 0.5 either by (i) applying a high-energy compaction; or (ii) adding a dispersant to achieve a better consistency.

The adoption of the Brazilian standard 0.48 w/c ratio causes an 13–22% increase of compressive strength in comparison for mortars with constant flow and noSP (Table 4). LC3 and OPC surpass 52 Mpa class strength, but the LFC remains below the minimum 32 Mpa. However, as observed in Fig. 2, w/c 0.48 produces a dry mortar and user will act to correct. A non-qualified user probably will increase water

Table 4 Comparison of the effect of mixing water for molding of Brazilian standard 0.48 versus 240 mm spread on 28 days compressive strength

Materials	Mixing water for molding (g/g)			28 days compressive strength (MPa)			Effect of mixing water on strength	
	Brazilian standard	Constant workability		Brazilian standard	Constant workability			
	noSP	noSP	SP	0.48	noSP	SP	noSP/0.48	SP/0.48
OPC	0.48	0.53	0.41	64.5	55.8	75.7	0.87	1.17
LC3	0.48	0.60	0.44	55.4	43.4	62.7	0.78	1.13
LFC	0.48	0.54	0.40	31.3	25.3	41.6	0.81	1.33

to reach suitable consistency. Therefore, the later value more representative of the in-field bagged cement performance. Without superplasticizer, but constant workability, the filler formulation still can be competitive in the mortar market, meanwhile the LC3 and OPC result in strength above 40 and 50 Mpa, respectively.

Reaching desirable workability by dispersant admixture and adjusting water is another feasible option. This is typical of professional concrete use (ready-mix concrete, precast…) but it is also possible to be part of a commercial Portland cement formulation since EN 197 allows add organic admixtures. In this case, the compressive strength increases between 13% for LC3 to 33% for LFC if compared with the fixed w/c 0.48 of the current standard. In this case, LFC almost reaches the 42 Mpa strength class, even with the binder diluted by 50% of limestone filler, without significant packing improvement or dilution compensation by finer grinding of clinker. The other two surpasses the 60 Mpa, a strength class above EN 197 limits.

3.5 Carbon and Binder Intensity Indicators

Figure 4a presents the results of binder intensity for modeled concretes at 28 days, with constant flowability. LFC presented the best result, staying below benchmark for the 250 kg of binder per m^3 of concrete, which is the best scenario with current technology [8]. All concretes from the various cements (LFC, LC3 and OPC) presented about the same range of binder intensity when mixed with superplasticizer. But since they have distinct strength classes, LC3 and OPC formulations will remain
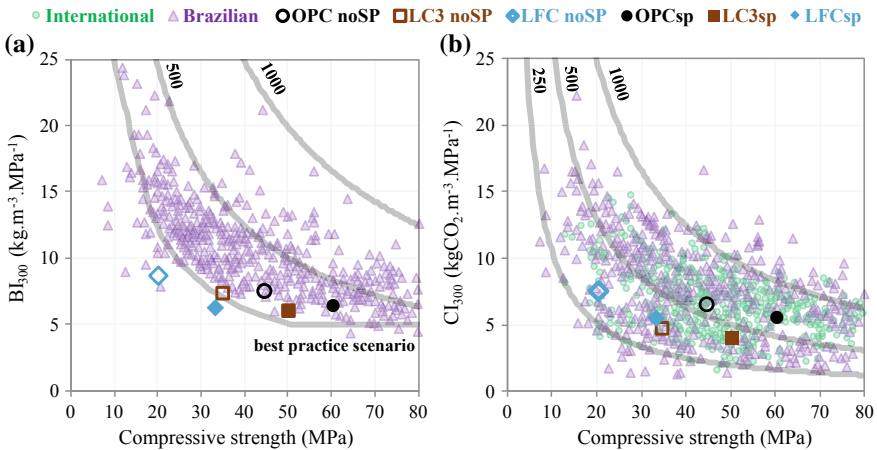
Fig. 4 a Binder intensity × compressive strength; **b** Carbon intensity × compressive strength of modeled concretes with 300 dm^3 of paste. Empty icons are without superplasticizer. Gray line represents concretes in the best practice scenario (250), 500 and 1000 kg of binder or CO_2 emitted per m^3 of concrete. The international and Brazilian data in the background were obtained by [8]

close but above the best practice scenario. Data show that for a 30 Mpa concrete, it is better to dilute OPC with limestone filler than increasing the amount of water in OPC, the traditional solution. Similarly, to produce a concrete with 50 Mpa, it is better to replace OPC with calcined clay and filler.

Figure 4b shows the results of carbon intensity. Concretes with LFC and LC3 stayed on the line of 350 kg CO_2 m^{-3} of concrete and OPC on the line of 550 kg CO_2 m^{-3}. Carbon intensities of concretes with LFCsp were drastically improved compared to LFC despite the material not being optimized for packing with mobility. For modeled concretes with 20–30 Mpa, the best results were found to LFCsp and LC3 noSP, concretes of 50 Mpa to LC3-SP and concrete with 60 Mpa to OPC-SP. Reducing the mixing water through the addition of superplasticizer reduces *bi* and *ci* indicators of all materials with greater improvements to LC3 and LFC. For this reason, superplasticizers are an important tool on environmental impact reduction in concrete production.

Emissions associated with the production of cements were lower for cement LFC (448 kg CO_2/t cement), followed by LC3 (528 kg CO_2/t cement) and OPC (814 kg CO_2/t cement). However, in our analyses, there is no correlation between the CO_2 footprint of cements cradle-to-gate and the carbon intensity indicator. The environmental impact of cement in use does not depend only on the CO_2 emissions in cement production, but also related to the binder efficiency (*cwf*), which influences cement demand needed to reach the desired mechanical strength.

4 Conclusions

Substituting OPC by calcined clay and filler (LC3) caused a higher demand of super-plasticizer to obtain the saturation content, opposite results were found when OPC was substitute only by filler. In terms of reactivity, cements LC3 and LFC presented better results of relative combined (in function of clinker content) water at 91 days compared to OPC. The water demanded for mortars without superplasticizer to achieve constant workability was higher for LC3 and similar for LFC compared to OPC. However, when superplasticizer was used, cements LC3 and LFC demanded less water than OPC. The *cwf* seems to be a better tool to classify cements compared to nowadays standards, because it considers the water demand. The replace of OPC by calcined clay and filler (LC3) would provide cements in the classes of 30–50 MPa depending on the use of superplasticizer. On the other hand, cements with just limestone filler (LFC) would be classified as 20–30 MPa. The choice of a blended cement by its ecoefficiency (*cwf*, binder and carbon intensities) must be made aware of the performance required in the technological application. In all cases, the use of superplasticizer increased the blended cements ecoefficiency.

References

1. Scrivener, K.L., John, V.M., Gartner, E.: Eco-efficient cements: Potential, economically viable solutions for a low-CO_2, cement-based materials industry. UNEP (2016)
2. John, V.M., Damineli, B.L., Quattrone, M., Pileggi, R.G.: Fillers in cementitious materials—experience, recent advances and future potential. Cem. Concr. Res. (2018). https://doi.org/10.1016/j.cemconres.2017.09.013
3. Scrivener, K., Martirena, F., Bishnoi, S., Maity, S.: Calcined clay limestone cements (LC3). Cem. Concr. Res. (2017). https://doi.org/10.1016/j.cemconres.2017.08.017
4. John, V.M. Quattrone, M., Cardoso, F.A., Abrão, P.C.R.A.: Rethinking cement standards: opportunities for a better future. Cem. Concr. Res. (Submitted) (2019)
5. Abrão, P.C.R.A., Cardoso, F.A., John, V.M.: Assessing the efficiency of Portland-pozzolana cements: reactivity, water demand and environmental indicators. Cem. Concr. Compos. (Submitted) (2019)
6. Brazilian Association of Technical Standards: Portland Cement: Determination of Compressive Strength (1996)
7. European Standards, EN196-1: Methods of testing cement—Part 1: determination of strength (2005)
8. Damineli, B.L., Kemeid, F.M., Aguiar, P.S., John, V.M.: Measuring the eco-efficiency of cement use. Cem. Concr. Compos. **32**, 555–562 (2010). https://doi.org/10.1016/j.cemconcomp.2010.07.009
9. WBCSD: Getting the Numbers Right, Project Emissions Report 2014. World Business Council for Sustainable Development (2016) https://www.gnr-project.org/
10. Miller, S.A., John, V.M., Pacca, S.A., Horvath, A.: Carbon dioxide reduction potential in the global cement industry by 2050. Cem. Concr. Res. (2017). https://doi.org/10.1016/j.cemconres.2017.08.026

Study of Concrete Made of Limestone Calcined Clay Cements (LC³)

François Avet and **Karen Scrivener**

Abstract This study investigates the feasibility of using LC³ concrete, in comparison with more conventional cements. LC³ provides better performance than slag concrete. Similar properties to plain cement concrete are obtained. LC³ even permits to catch silica fume concrete in terms of durability properties.

Keywords LC³ · Concrete · Rheology · Strength · Sustainability

1 Introduction

Among the alternatives to reduce the emissions related to construction materials, the reduction of the clinker content in cement is successful and efficient [1]. Among the supplementary cementitious materials (SCMs), calcined clay and limestone are the only widely available solutions to continue decreasing the clinker factor [2, 3]. Limestone calcined clay cements (LC³) combine these two SCMs. In LC³, clays with only 40% of kaolinite are sufficient to reach similar strength to reference cement [4], while providing better resistance to chloride ingress and alkali–silica reaction [5, 6]. Low-grade limestone improper for clinkerization can also be used as SCMs in LC³ [7]. Only few studies showed the performance of LC³ concrete [8]. In this work, the robustness of LC³ concrete is investigated and compared with plain cement and binders containing slag or silica fume. Fresh and mechanical properties are assessed, as well as the CO_2 footprint.

2 Materials and Methods

The LC³-50 binder consists of 50% clinker, 30% calcined clay, 15% limestone and 5% gypsum. The calcined clay contains 40% of calcined kaolinite, with quartz and anatase as main secondary phases. The clay was calcined using rotary kiln. LC³ was

F. Avet (✉) · K. Scrivener
Laboratory of Construction Materials, EPFL, 1015 Lausanne, Switzerland
e-mail: francois.avet@epfl.ch

Table 1 Physical and chemical characteristics of cement and SCMs

	Cement	Silica fume	Slag	Calcined clay	Limestone
$D_{v,50}$ (µm)	10.7	0.2	19.5	8.4	7.2
BET specific surface (m^2 g^{-1})	–	21.4	1.2	8.2	1.8
XRF composition (wt%)					
SiO_2	20.0	92.5	36.1	49.7	0.1
Al_2O_3	5.0	2.9	12.1	41.8	–
Fe_2O_3	2.9	0.2	0.8	2.3	–
CaO	63.4	–	42.0	0.2	55.0
MgO	1.8	–	7.1	0.1	0.2
SO_3	3.2	–	1.5	–	–
Na_2O	0.2	0.2	0.1	0.3	0.1
K_2O	0.8	0.1	0.3	0.1	–
TiO_2	0.3	–	0.5	3.4	–
P_2O_5	0.2	0.5	–	0.1	–
MnO	0.1	–	0.2	–	–
Others	0.2	2.8	–	0.1	–
LOI	–	0.6	−0.7	1.9	42.6

compared with plain cement (PC), a blend with 10% of cement replacement by silica fume (PPC10 SF) and a slag cement with a 1:1 ratio (PPC50 Slag). The physical and chemical characteristics of the cement, silica fume, slag, calcined clay and limestone are shown in Table 1.

The binder content was 375 kg m^{-3}, with water to binder ratio of 0.43. A PCE plasticizer (commercial PCE adapted for plain cement) was used to reach the same workability for all the systems. Compressive strength was measured at 2, 7 and 28 days. Life cycle analysis was also carried out on different systems.

3 Results

The amount of superplasticizer required to reach a slump of 4 cm is shown in Fig. 1. As expected, the demand for superplasticizer is lower for plain cement and slag compared with LC^3. However, LC^3 concrete requires less superplasticizer than silica fume, despite the much higher clinker substitution level used in LC^3.

The compressive strength values of the different concretes are shown in Fig. 2. For all ages, LC^3 reaches higher strength than slag concrete. Compared with PC, similar strengths are obtained for all ages. Finally, LC^3 even catches silica fume concrete at 7 days of hydration.

Fig. 1 Amount of superplasticizer for PC, PPC10 SF, PPC50 Slag and LC^3-50
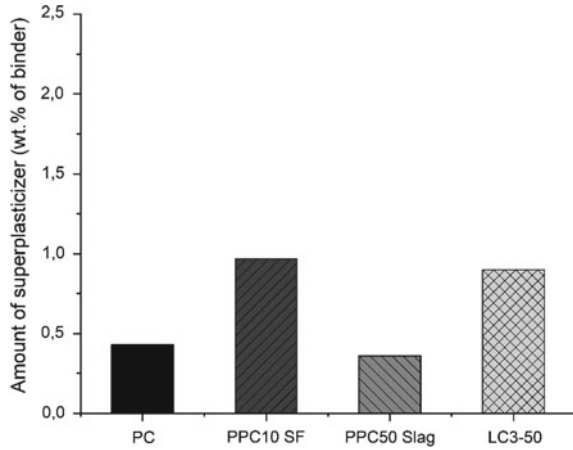
Fig. 2 Compressive strength for PC, PPC10 SF, PPC50 Slag and LC^3-50 at 2, 7 and 28 days
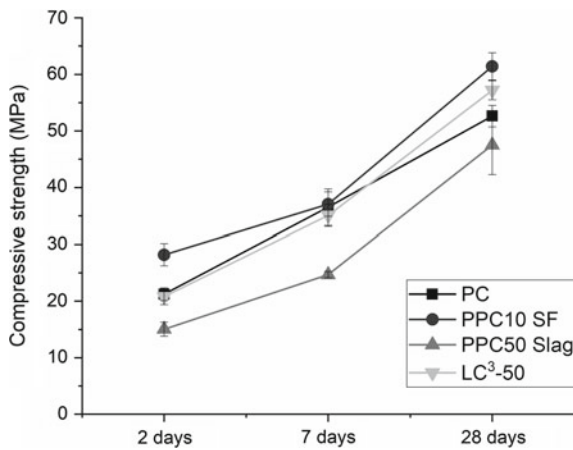
Concerning the CO_2 footprint related to the production of the different concretes, the emissions of the binders were obtained from [9]. The CO_2 emissions were calculated on a ground to gate approach, considering all the parameters involved from the extraction of the raw materials to the concrete mixing plant. To be consistent between the systems, the CO_2 emissions calculated are corrected based on the strength obtained at 28 days of hydration for the different systems. The CO_2 emissions are shown in Fig. 3. The lowest emissions are obtained for LC^3 blend. Despite lower absolute emission, the slag concrete suffers from lower strength compared with LC^3. The emissions are higher for the silica fume concrete. The higher strength obtained for the silica fume concrete compared with LC^3 is compensated by its much higher clinker content. Finally, the PC reference shows the highest level of emissions.

Fig. 3 CO_2 emissions normalized per MPa for PC, PPC10 SF, PPC50 Slag and LC^3-50 at 28 days of hydration
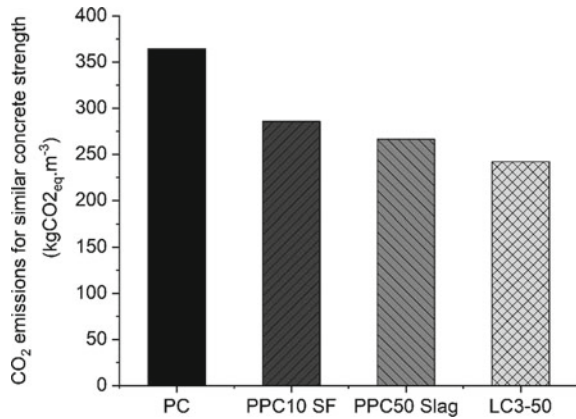
4 Conclusion

Excellent properties were obtained using LC^3-50 concrete. Compared with PC, LC^3 permits to get similar performance while improving sustainability. LC^3 requires less superplasticizer than silica fume, for comparable mechanical performance and a better environmental footprint. LC^3 also permits to get better performance than slag concrete.

References

1. Damtoft, J.S., Lukasik, J., Herfort, D., et al.: Sustainable development and climate change initiatives. Cem. Concr. Res. **38**, 115–127 (2008). https://doi.org/10.1016/j.cemconres.2007.09.008
2. IEA, World Business Council for Sustainable Development: Technology Roadmap Low Carbon Transition in the Cement Industry, 66 (2018)
3. Scrivener, K.L., John, V.M., Gartner, E.M.: Eco-efficient cements: potential economically viable solutions for a low-CO_2 cement-based materials industry (2016)
4. Avet, F., Scrivener, K.: Investigation of the calcined kaolinite content on the hydration of limestone calcined clay cement (LC^3). Cem. Concr. Res. **107**, 124–135 (2018). https://doi.org/10.1016/j.cemconres.2018.02.016
5. Scrivener, K., Avet, F., Maraghechi, H., et al.: Impacting factors and properties of limestone calcined clay cements (LC^3). Green Mater. **0**, 1–49 (2018). https://doi.org/10.1680/jgrma.18.00029
6. Maraghechi, H., Avet, F., Wong, H., et al.: Performance of limestone calcined clay cement (LC^3) with various kaolinite contents with respect to chloride transport. Mater. Struct. **51**, 125 (2018). https://doi.org/10.1617/s11527-018-1255-3

7. Krishnan, S., Bishnoi, S.: Understanding the hydration of dolomite in cementitious systems with reactive aluminosilicates such as calcined clay. Cem. Concr. Res. **108**, 116–128 (2018). https://doi.org/10.1016/j.cemconres.2018.03.010
8. Dhandapani, Y., Sakthivel, T., Santhanam, M., et al.: Mechanical properties and durability performance of concretes with limestone calcined clay cement (LC^3). Cem. Concr. Res. **107**, 136–151 (2018). https://doi.org/10.1016/j.cemconres.2018.02.005
9. Gettu, R., Patel, A., Rathi, V., et al.: Influence of supplementary cementitious materials on the sustainability parameters of cements and concretes in the Indian context. Mater. Struct. **52**, 10 (2019). https://doi.org/10.1617/s11527-019-1321-5

Impacts Assessment of Local and Industrial LC3 in Cuban Context: Challenges and Opportunities

Sofía Sánchez-Berriel, Yudiesky Cancio-Díaz, Inocencio R. Sánchez-Machado, José Fernando Martirena-Hernández, Elena R. Rosa-Domínguez and Guillaume Habert

Abstract The main goal of the paper is to compare the economic and environmental impacts of local production of low carbon cement based on a new mineral addition of calcined clay and limestone (LC2) versus industrial production of low carbon cement (LC3), considering particularities of Cuban context. First, a technical comparison is carried out comparing also with traditional OPC and PPC and considering standards applied in the island. Secondly, an economic assessment of production and investment costs is carried out using life cycle costing (LCC) technique. Afterwards, to assess environmental impacts a simplified life cycle assessment is performed to compare both cements, OPC and PPC. Cement based on LC2 reports economic advantages in comparison with the other cements: industrial LC3, OPC and PPC. Environmental results show a similar behaviour for local and industrial LC3 but a significant decrease of emissions and energy demand versus OPC and PPC. Technical comparison shows that local LC3 results are variable but complies with the standard for its use in mortars and non-structural applications. Finally, results show that LC3 introduction is a feasible option to reduce impacts of the cement industry in Cuba, and a combination of its local and industrial production is the best alternative to achieve sustainability goals in the short and mid-terms. Main opportunities of local LC3 are the reduction of costs, the easier storage, the use of local materials, amongst other. Main challenge is related to a correct use of the mineral addition in localities.

Keywords Low carbon cement · Mineral addition of calcined clay and limestone · Impacts assessment

S. Sánchez-Berriel (✉)
Faculty of Economy, UCLV, Carretera a Camajuaní km 51/2, 50100 Santa Clara, Cuba
e-mail: ssanchez@uclv.edu.cu

Y. Cancio-Díaz · I. R. Sánchez-Machado · J. F. Martirena-Hernández · E. R. Rosa-Domínguez · G. Habert
Center for Research and Development of Structures and Materials, UCLV, Santa Clara, Cuba

S. Sánchez-Berriel · Y. Cancio-Díaz · I. R. Sánchez-Machado · J. F. Martirena-Hernández · E. R. Rosa-Domínguez · G. Habert
Faculty of Chemistry and Farmacy, UCLV, Santa Clara, Cuba

ETH Zurich, 8093 Zurich, Switzerland

1 Introduction

Research associated with construction materials and its roll in sustainability is highly important in modern times [1, 2]. Production of cement, main component of several construction materials, is considered one of the higher industrial sectors that generates greenhouse gas emissions [3]. At the same time, cement and its derived are products with high cost of elaboration which need to be improved towards less economic and environmental cost [4].

Low carbon cement (LC^3) is a cement with high clinker substitution level with addition of 30% of calcined clay and 15% of limestone [5]. The new product has emerged as result of the innovative work of a multidisciplinary team with specialists from Switzerland, India and Cuba, as part of an international project (LC3). So far, technical, economic and environmental feasibility of industrial LC3 is been proven [6–9], but a new possibility as arisen: to produce LC3 locally. No matter if it is produced locally or industrially, LC3 advantages are strongly related to better use of existing capacities, reduction of energy consumption, capital and productive costs and emissions.

On 2018, an industrial trial was carried out in Siguaney cement factory, located in the centre of the island, to produce LC2. Previous industrial trials have been done to produce low carbon cement (LC3) in the same factory [10] showing satisfactory results that support first laboratory findings of LC3 [11]. The goal of this paper is to compare the economic and environmental impacts of local production of low carbon cement based on a new mineral addition of calcined clay and limestone (LC2) versus industrial production of low carbon cement (LC3), PPC and OPC; considering particularities of Cuban context.

2 Materials and Methodology

2.1 Low Carbon Cement (LC3) and the Mineral Addition LC2

Low carbon cement is a new cement based on a combination of calcine clay and limestone that permit to reduce clinker ratio to 50% (i.e. LC3: 50). Furthermore, a family of low carbon cements can be produced varying the percentage of substitution.

In Cuba, the Centre for Research and Development of Structures and Materials explores the feasibility of produce and use a new mineral addition based on calcined clay and limestone in 2:1 proportion called LC2. This mineral addition could be used to fabricate a large amount of low carbon cement-based products locally. Optimized mix design proposes the addition of 50% of LC2 to be mixed with 50% of OPC. First impact of this addition is the extension of productive capacities that could allow to satisfy a higher percentage of the local demand.

The production of both products is strongly related since LC2 can be considered as an intermediate product in LC3 production. Productive process begins with raw
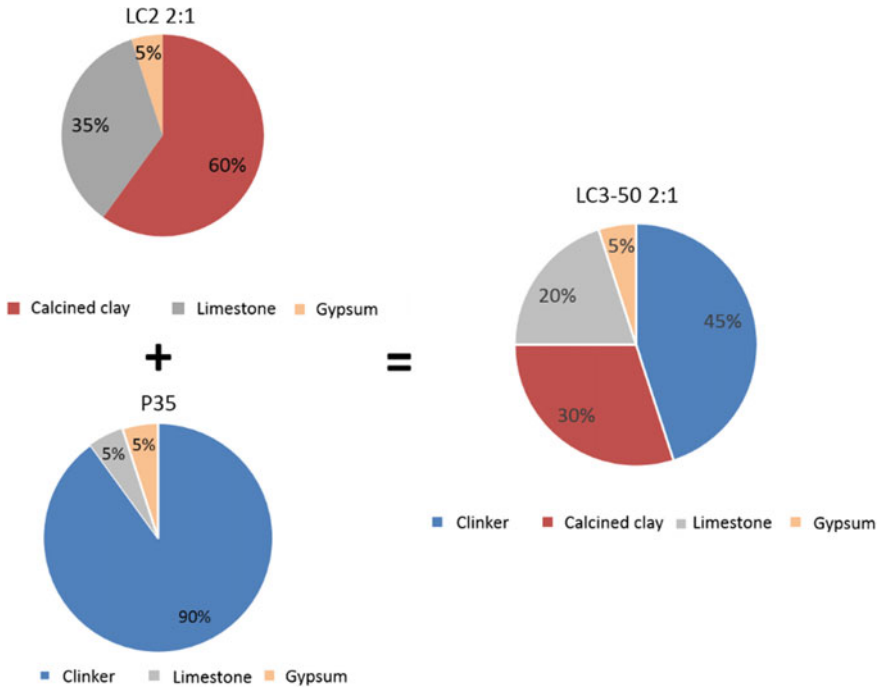
Fig. 1 Chemical composition of LC2 versus LC3: 50. *Source* [12]

materials extraction in the quarry. Afterwards these materials are transported to the factory to be calcined resulting in thermally activated clay and clinker (when producing LC3 industrially). The process ends with a grinding and mixing step followed by delivery in bags or in bulk. Figure 1 shows LC2 and LC3: 50 composition showing their technical relationship.

2.2 Impacts Assessment, Goal and Scope

The impacts assessment is performed through a life cycle assessment completed in harmony with ISO 14044:2006 [13]. This study focusses on the production and transport of the cement components. The analysis ends at an intermediate stage (cradle to gate) as shown in Fig. 2. Transport of final product to site has been excluded in the analysis since there are a vast variety of options for its destination. The functional unit used in the study is 1 ton of cement.

Life cycle inventory for productive process of the cements OPC, PPC and LC3_industrial is taken from [14]. Production of LC3_local combines data form OPC and LC2 production which is carried out in Siguaney cement factory following the next phases:
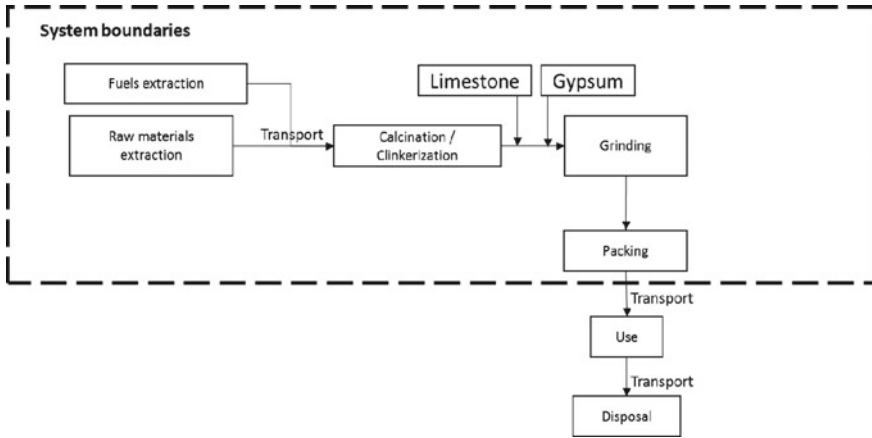
Fig. 2 System boundaries of impacts assessment performed

Extraction of clay. Previous analysis made to the quarry certifies that the kaolinite clay present has the needed quality to be reactive after calcination. Also a measurement of the reserves concluded there are enough resources to guarantee more than 35 years of production.

Transport to factory and homogenization. The quarry is located 60 km from the factory. Transport process was done with trucks of the cement factory. Due to the existence of different technological types of clay, a homogenization process was required before calcination. This process was performed in the factory using a frontal charger in the clay storage place of the factory.

Calcination of clay. This process was carried out in a wet process rotary clinker kiln. Thus, the material was first converted into paste and then calcined. Estimated consumption of energy reports a reduction of 40% respect to clinkerization process.

Grinding and blending with gypsum and limestone. During grinding process limestone and gypsum are incorporated to the mix. A closed circuit mill with high efficiency was used. Estimated energy consumption is around 45 Kwh per ton of LC2. It is assumed that 100% of the material is delivered in bulk.

Calculations are performed using the software Simapro vs- 8.0.3.14 and the Windows tool Microsoft Excel 2013. The environmental indicator category considered was global warming potential over 100 years (GWP100) [15]. This category measures emissions over a 100-year time period of any greenhouse gas, using CO^2 as an equivalence measure. For economic impact assessment, a life cycle costing technique is employed. Finally, a combined analysis is made through an eco-efficiency dispersion chart that allows to compare both dimensions.

3 Results and Discussion

Breakdown of life cycle costs from cradle to gate shows that low carbon cement, local and industrial, presents lower impact over economy and environment if they are compared with OPC and PPC. Figure 3 details costs composition of calcined clay. Main impacts are related to energy consumption for calcination, amortization and raw materials extraction and transport. High amortization costs are related to factory conditions where decapitalization process is high. LC2 cost reports a reduction of 50% when compared with OPC, product that could be substituted by this mineral addition.

Global warming potential results show higher impact related to OPC and PPC, as shown in Fig. 4. The higher the clinker ratio, the higher the costs and emissions. Comparison between local and industrial LC3 shows similar results with small reduction when industrial production is performed. This could be related with scale economies resulting from industrial production and extra transport involved to obtain LC3 locally. When LC3 is industrial, usually all raw materials are close to factory but LC3 local has transport costs for OPC and LC2 and all their constituents. This issue should be further studied.

LC2 is also presented in Fig. 4 showing an opposite location in comparison with OPC. OPC is located in the less eco-efficient quadrant of the figure and LC2 in the most sustainable one.
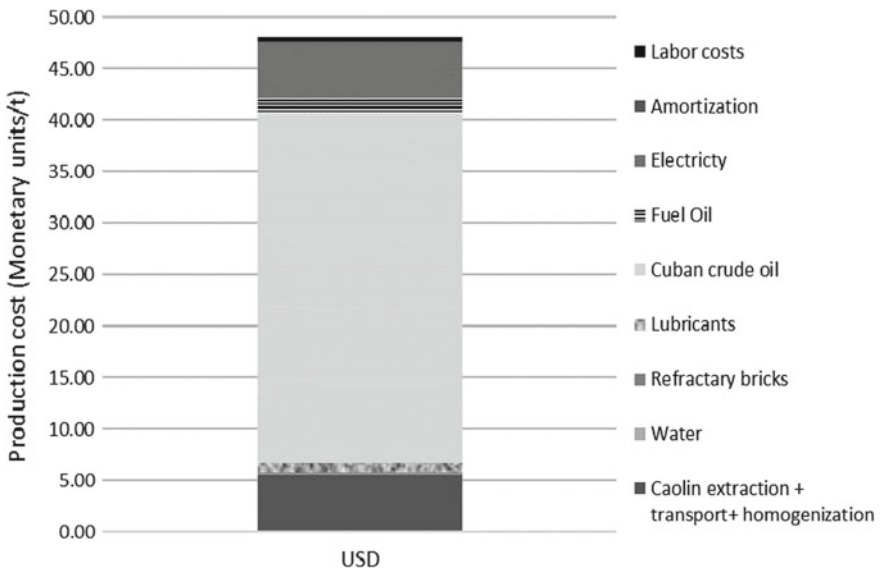
Fig. 3 Life cycle costing of calcined clay in Siguaney. Costs in USD
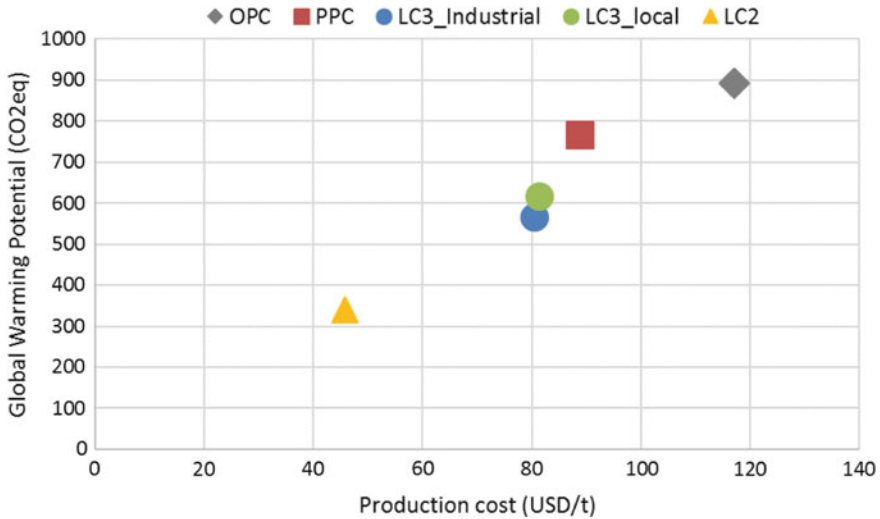
Fig. 4 Environmental versus economic impact. OPC, PPC, LC3 industrial and local

Despite of the minor differences in results between local and industrial LC3, it has been proven the feasibility of this type of cement in comparison with other traditional cements produced in Cuba.

Local production of LC3, through LC2, will allow to extend the use of available OPC, to adapt to construction needs and change mix-design accordingly reaching different clinker ratios depending on destination (e.g. mortars, concrete, blocks). No investment is needed in short term, but an investment should be considered to import an industrial rotary clay calciner in order to increase efficiency.

Another advantage is that LC2 can be stored for long periods and can survive to wet conditions with a drying process to revert humidity. As a strategy, this product could be produced in campaigns and stored. Its possible distribution and use need to be established.

However, a proper communication strategy should be designed once this product is approved to clarify its properties and ways of use. One big threat is the uncertainty on the correct mix-design; everywhere this product could be applied despite the fact of correct instructions available.

4   Conclusions

The assessment of environmental and economic impacts of LC3 production both locally and industrially shows that this cement reduces the production cost and carbon emissions in comparison with traditional OPC and PPC made in Cuba. Industrial

manufacture of LC3 increases efficiency in a small amount with respect to local production.

Local production is more viable in Cuban present conditions to introduce low carbon cement but the process has to be organized and well controlled. Industrial production could be considered in a mid-term period.

Existing technology accomplishes the needs to produce calcined clay but some efficiency reserves exists. To improve, efficiency investment is needed.

Results could be used to support communication strategies on this new product oriented to different stakeholders.

References

1. Damtoft, J.S., Lukasik, J., Herfort, D., Sorrentino, D., Gartner, Y.E.M.: Sustainable development and climate change initiatives. Cem. Concr. Res. **38**(2), 115–127 (2008)
2. Scrivener, K.L., John, V.M., Gartner, E.M.: Eco-efficient cements: potential economically viable solutions for a Low-CO^2 cement-based materials industry. Paris (2017)
3. IPCC: Summary for policymakers. In: Climate Change 2014: Mitigation of Climate Change. Contribution of Working Group III to the Fifth Assessment Report of the Intergovermental Panel on Climate Change. Cambridge University Press, United Kingdom and New York, USA (2014)
4. Flatt, R.J., Roussel, N., Cheeseman, C.R.: Concrete: an eco material that needs to be improved. J. Eur. Ceram. Soc. (2012)
5. Vizcaíno-Andrés, L.M.: Cemento de Bajo Carbono a partir del sistema cementicio ternario clínquer-arcilla calcinada-caliza. Universidad Central Marta Abreu de Las Villas (2014)
6. Fernandez, R., Martirena, F., Scrivener, K.L.: The origin of the pozzolanic activity of calcined clay minerals: a comparison between kaolinite, illite and montmorillonite. Cem. Concr. Res. **41**(1), 113–122 (2011)
7. Alujas, R., Fernández, R., Quintana, Scrivener, K.L., Martirena, F.: Pozzolanic reactivity of low grade kaolinitic clays: influence of calcination temperature and impact of calcination products in OPC hydration. Appl. Clay Sci. (2015)
8. Sánchez Berriel, S., Favier, A., Rosa, Domínguez. E., Sánchez Machado, I. R., Heierli, U., Scrivener, K., Martirena Hernández, F., Habert, G.: Assessing the environmental and economic potential of limestone calcined clay cement in cuba. J. Clean. Prod. **124**, 361–369 (2016)
9. Cancio-Díaz, Y., Sánchez Berriel, S., Heierli, U., Favier, A.R., Sánchez-Machado, I.R., Scrivener, K.L., Martirena, J.F., Habert, G.: Limestone calcined clay cement as a low-carbon solution to meet expanding cement demand in emerging economies. Dev. Eng. (2017) (Article in press)
10. Vizcaíno-Andrés, L.M., Sánchez-Berriel, S., Damas-Carrera, S., Pérez-Hernández, A., Scrivener, K.L., Martirena-Hernández, J.F.: Industrial trial to produce a low clinker, low carbon cement. Mater. Construcción **65**(317) (2015)
11. Antoni, M., Rossen, J., Martirena, F., Scrivener, K.: Cement substitution by a combination of metakaolin and limestone. Cem. Concr. Res. **42**(12), 1579–1589 (2012)
12. Martirena, J.F.: Advances in local production of Low Carbon Cement (2018)
13. ISO 14040:2006 Environmental management—life cycle assessment—principles and framework (2006)

14. Sánchez-Berriel, S.: Modelo de evaluación integrada de impactos aplicado al proceso de introducción del cemento de bajo carbono en la industria cementera en Cuba. UCLV (2018)
15. Goedkoop, M., Heijungs, R., Huijbregts, M., Schryver, A. De., Struijs, J., Van Zelm, R.: ReCiPe 2008. A life cycle assessment method which comprises harmonised category indicators at midpoint and the endpoint level (2009)

Service Life Modeling in Propagation Phase of Corrosion in Concrete Due to Carbonation

Yogendra Singh Patel, Lav Singh and Shashank Bishnoi

Abstract In this paper, a model is presented, which can predict propagation time due to carbonation-induced corrosion. This model is developed using existing models in the literature. Corrosion rate determination is a crucial step in modeling the propagation phase. An assembled model of corrosion rate is presented, which takes into account w/c ratio, relative humidity, temperature, pH, and cement-type effects into it. Corrosion rate model also considers effects coming due to the accumulation of rust products so as these products keep piling, corrosion rate reduces with time. This corrosion rate model shows good agreement with the experimental data, which is available for different scenarios in the literature for the OPC. From this corrosion rate model, a propagation time model is being developed using Faraday's law and critical mass for cracking model. The propagation time for the LC^3-added cement concrete is calculated.

Keywords Corrosion rate model · Propagation time · Carbonation-induced corrosion · LC^3

1 Introduction

In the carbonation, calcium hydroxide reacts with acid formed by carbon dioxide and forms calcium carbonate. Due to the consumption of alkalinity in reaction pH drops, this destabilizes the passivating film around the steel and active corrosion of the steel starts in the presence of oxygen and water. Corrosion is the electrochemical reaction in which one half of the reaction is oxidation in which iron dissolves and produces electrons; which are consumed by other half-cell reduction processes, in which oxygen and water combine to give hydroxyl ion. Service life due to corrosion can be divided into two phases: One is initiation, and the other is propagation phase. In this paper, propagation time is calculated by using a developed corrosion rate model. The mass loss of the steel is also taken into consideration in the corrosion rate model. The progress of rate of corrosion is simulated similar to the process of cracking in the concrete for carbonation-induced corrosion.

Y. S. Patel · L. Singh (✉) · S. Bishnoi
Department of Civil Engineering, Indian Institute of Technology Delhi, New Delhi, India

1.1 Summary of Some Existing Models

Different models for propagation are available. Some of the available models are Bazant's model [1], model by Liu [2], etc. After studying these models, it is clear that modeling of the corrosion rate is vital for the determination of propagation time. The corrosion rate is explored by many researchers. Alonso gave a relationship between the corrosion rate and resistance of the several cement types in carbonated concrete [3]. Li provided a model for the corrosion rate for the carbonation, which uses the basic formula of current density, and then, other models used to give reference potential gradient and resistivity of concrete [4].

2 Development of Corrosion Current Model

Current in general sense is voltage upon resistivity. Modifying this basic formula according to the impact of different parameters on voltage and resistivity, the final model for corrosion current is assembled. Different components which are assembled are as follows.

2.1 Assembly of the Model

Effect of the temperature and the time is taken directly on the corrosion current. Influence factor for water-to-cement ratio, relative humidity, and cement type is included, which are shown in Table 1 and multiplied to reference resistivity of concrete to obtain resistivity at different input factors. As corrosion continues, corrosion products form and deposit near the reinforcing bar with time; these products hinder the movement of the iron ions, so the mass of the rust is included in corrosion rate. M_{loss} is mass loss of the iron which can be converted to mass of rust by dividing by alpha (α). The final corrosion rate model which comes after the assembly is:

$$i_{\text{corr}}(t) = \left\{ \frac{V_0 K_{\text{pH}}}{\rho_0 K_{\text{cem}} K_{\text{w/c}} K_{\text{RH}}} e^{b_{i,\text{corr}}\left(\frac{1}{T} - \frac{1}{T_0}\right)} \right\} - 0.044 M_{\text{loss}} \tag{1}$$

where $V_0 K_{\text{pH}}$ combined is the potential in the carbonated concrete which is taken as 1 V/m, e = $\rho_0$250 Ωm, resistivity of carbonated concrete, $b_{i,\text{corr}} = -2283$ K, T = temperature at which corrosion rate is unknown; T_0 = reference temperature = 293 K; t is the time in years.

Table 1 All the influence factors and models used in the developed model

Influencing parameter	Models or influence factors used in the developed model	Remarks	References
Temperature	Arrhenius equation	Impact of temperature is positive on the corrosion rate	[5]
Time	Corrosionrate $= I_0 * e^{-0.2026t}$ where I_0 is corrosion rate at initiation of propagation phase	Data of corrosion rate from 3LP device from the Liu and Weyers are taken for 0% chloride addition in the samples and regression analysis is performed	[6]
Relative humidity	Influence factor K_{RH} taken from [7]	Resistance control mechanism	[7]
w/c ratio	Influence factor $K_{w/c}$ taken from [7]	Reducing the water-to-cement ratio reduces the permeability of the concrete, which increases the resistivity of the concrete	[7]
Cement type	Influence factor K_{cem} is derived from [8]	Influence factor for LC3-15 is 1.4 and for LC3-30 is 2.48	[8]
pH	Nernst equation is used for developing influence factor K_{pH} for pH	$K_{pH} = 1.3165 - 0.03957 pH$ Reference pH $= 8$	[1, 9]

3 Propagation Model

Time from initiation till cracking was mathematically calculated by Bazant [1]. This work was extended by Liu [2] by considering porous zone, which is part around the reinforcing bar where corrosion products deposit; after filling this part, products exert pressure on the concrete. This model is used in this paper for calculating critical weight of rust (W_{crit}). Mass loss of steel (M_{loss}) is calculated using Faraday's law of electrolysis. First law of Faraday states that the mass which will deposit due to passing of charge is proportional to the amount of charge passed. α is the ratio of steel molecular weight and corrosion products. Multiplying α with critical mass of rust will give the steel loss required to generate cracking. $\alpha = 0.57$.

$$M_{loss} = W_{crit}\, \alpha \tag{2}$$

Fig. 1 Different phases of corrosion rate and propagation time for OPC and LC^3
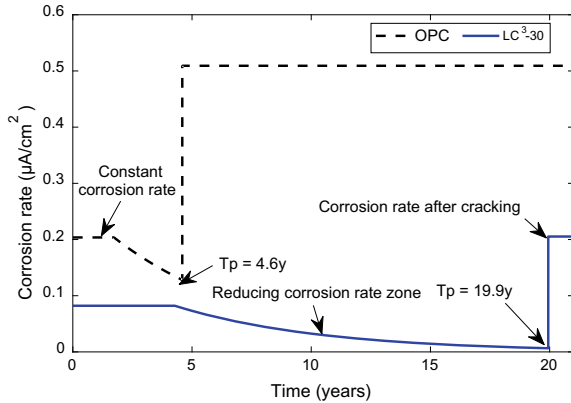
4   Results and Discussions from the Proposed Model

There are three phases of the corrosion rate in the execution of the model based on the cracking process. These three phases contribute to free expansion; stress build-up phase in which corrosion rate reduces due to corrosion products accumulation and the third phase is after cracking phase in which resistivity reduces substantially which increases the rate of corrosion suddenly. Figure 1 shows the change in the rate of corrosion with time for OPC and LC^3. Input parameters are diameter of bar = 16 mm, RH = 60%, pH = 8, cover $(C) = 30$ mm, $T = 300$ K, and w/c = 0.6.

The propagation time for the OPC is 4.6 years and for LC^3 is 19.9 years for the taken input parameters. Adding limestone increases the resistivity of the concrete, which causes a decrease in the corrosion rate. This results in the longer propagation time for the limestone calcined clay cement concrete.

5   Conclusions

- A model is developed by assembling the compatible models, which gives the propagation time for the corrosion in the carbonated concrete. Adding limestone calcined clay increases the resistivity of the concrete, which lowers the corrosion rate resulting in longer propagation time.

References

1. Bazant, Z.P.: Physical model for steel corrosion in concrete sea structures. J. Struct. Div. **105** (1979)
2. Liu, Y.: Modeling the time-to-corrosion cracking of the cover concrete in chloride contaminated reinforced concrete structures (1996)

3. Alonso, C., Andrade, C., González, J.A.: Relation between resistivity and corrosion rate of reinforcements in carbonated mortar made with several cement types. Cem. Concr. Res. **18**(5), 687–698 (1988)
4. Li, K.: Durability Design of Concrete Structures Phenomena, Modeling and Practice. Wiley, Singapore (2016)
5. Virmani, Y.P., Clear, K.C., et al.: Time-to-corrosion of reinforcing steel in concrete, vol. 5, FHWA/RD-83/012 (1983)
6. Liu, T., Weyers, R.W.: Modeling the dynamic corrosion process in chloride contaminated concrete structures. Cem. Concr. Res. **28**(3), 365–379 (1998)
7. Yu, B., Yang, L., Wu, M., Li, B.: Practical model for predicting corrosion rate of steel reinforcement in concrete structures. Constr. Build. Mater. **54**, 385–401 (2014)
8. Nguyen, Q.D., Khan, M.S.H., Castel, A.: Engineering properties of limestone calcined clay concrete. J. Adv. Concr. Technol. **16**(8), 343–357 (2018)
9. Ahmad, S.: Reinforcement corrosion in concrete structures, its monitoring and service life prediction—a review, **25**, 459–471 (2003)

Life Cycle Assessment of LC3: Parameters and Prognoses

Ravindra Gettu and Anusha S. Basavaraj

Abstract Life cycle assessment (LCA) has been conducted to obtain the potential reduction in the environmental impact due to the production of limestone calcined clay cement (LC3), with respect to ordinary portland cement (OPC) and fly ash-based portland pozzolana cement (PPC). A case study of a typical cement plant in South India is considered. It is found, for this particular case and the assumptions made, that the CO_2 emissions and the energy demand could decrease by 34% and 18%, respectively, if LC3 is used instead of OPC, with the corresponding reductions being 26% and 21% for PPC. A parametric study of some key factors that could influence the impact of LC3 showed that the CO_2 emissions and the energy demand could vary by 13% and 20%, respectively, with variations in the calcination energy requirement while the clay transportation distance did not have any significant influence.

Keywords Life cycle assessment · Cement · OPC · PPC · LC3 · Energy · Carbon footprint · Embodied energy

1 Introduction

Cement for concrete, one of the widely used materials in construction, accounts for about 5–8% of the man-made CO_2 emissions [1], and consequently, any reduction in the emissions would make a significant impact on global warming. It is evident that the use of blended binders with low portland cement clinker content can reduce the carbon footprint of concrete dramatically, with viable options including the now-common secondary cementitious materials (SCMs) such as slag and fly ash [1, 2]. Limestone calcined clay has been promoted as a promising clinker substitute [3], and considerable research and development effort have been dedicated to demonstrate its technical feasibility and advantages. One of the regions with kaolinitic clay reserves as well as a growing demand for cement is India, and consequently, there is a need to perform studies to rationally assess the potential reduction in CO_2 emissions and energy requirement or embodied energy for cement production with the use

R. Gettu (✉) · A. S. Basavaraj

Department of Civil Engineering, Indian Institute of Technology Madras, Chennai 600036, India
e-mail: gettu@iitm.ac.in

of limestone calcined clay cement (LC3). The present work considers the Indian scenario, with primary data being collected at a typical cement plant, and presents the impact assessment LC3, along with the more conventional ordinary portland cement (OPC) and fly ash-based portland pozzolana cement (PPC). The parameters that could influence the assessment significantly when LC3 production becomes prevalent are also discussed.

2 Life Cycle Assessment (LCA)

LCA is a widely-applied technique for analyzing the environmental impacts associated with a product or process [4, 5]. In the present work, the sustainability assessment employs this technique in four steps [6–8]: (i) definition of scope and system boundaries, (ii) collection of the inventory of raw materials, fuels, and electricity consumed, (iii) assessment of the impact in terms of CO_2 emissions and energy demand, and (iv) comparison of the impacts of different materials. The system boundary considered is cradle to gate or ground/mine to gate, i.e., all processes from the extraction of raw materials (limestone and fuels), production of electricity, transportation of fuels and raw materials and actual production processes are included. For transportation, the diesel consumed, road construction, truck manufacturing, repair of roads, etc., are considered. The primary data referred to here pertains to an integrated cement plant at Nandyal, in South India, and secondary sources of data are EPA [9], IPCC [10], and the ecoinvent database [11]. Suitable conversion factors are also taken from databases to relate to the actual case. All the cements are assumed to be manufactured in a cement plant having double-string six-stage pre-heater with pre-calciner. The main raw material used in manufacturing clinker is limestone, which is extracted from a quarry about 10 kms away. Other materials such as slag, flue dust, red mud, and laterite, which are waste materials form other industries are also used in the production of the clinker. Coal and petcoke along with alternate fuels, such as carbon black and pharmaceutical waste, are used as fuel in clinker production. Electricity is always supplied by the grid.

2.1 LCA of Clinker

Based on the amount of input materials, fuel, electricity, transportation distances for the materials, and infrastructure used per tonne of clinker, the total CO_2 emissions and energy consumed are calculated using the LCA framework. It is found that, in this case, the total CO_2 emission is 910 kg CO_2-eq. and energy consumed is 5300 MJ per tonne of clinker. Note that the energy consumed and CO_2 emissions can vary with type and amount of fuel used, type of raw material, amount of electricity, distance of transportation of fuels, and raw materials.

Table 1 LCA results of different cements considered in the study

Impact	OPC	PPC	LC3
Carbon footprint (kg CO_2 eq./tonne of cement)	930	690	610
Energy demand (MJ/tonne of cement)	5945	4690	4850

2.2 LCA of the Different Cements

Based on the actual production data, the assessment was done for OPC (95% clinker and 5% gypsum), along with the hypothetical production of PPC (65% clinker, 30% fly ash, and 5% gypsum), and LC3 (50% clinker, 30% calcined clay, 15% limestone, and 5% gypsum) at the same plant. The clinkerization, burning of fuel, electricity for grinding, blending and packing, and transportation of raw materials are the major processes that influence the results of the LCA of cement. Natural gypsum and phosphogypsum are used in equal proportions for the cement production. Class F fly ash is assumed to be brought from Vijayawada (325 km) and clay is assumed to be brought from Dharmapuri to Nandyal (540 km) by truck. Fly ash and phosphogypsum are considered to be waste and, therefore, no impact is assigned to them other than their transportation.

For the calcination of clay in the production of LC3, the energy consumed was taken to be 2.6 MJ/kg of clay based on the theoretical calculations done with the energy valued obtained by thermo gravimetric analysis (TGA) and differential scanning calorimetry (DSC) analysis. DSC values were obtained for different clays having kaolinite contents of about 30 to 90%, and a 13% mass loss was considered along with 30% losses of energy in the kiln. It is further assumed that the same fuel type used for the clinkerization is used for the clay calcination.

The values consequently obtained from the LCA are given in Table 1, where it can be seen that the impacts of OPC are much higher than that of the blended cements. LC3 has the least CO_2 emissions, even lower than PPC due to the higher replacement level of clinker. The main reason for the lower energy consumption for PPC is the additional energy required for clay calcination and the proximity of the fly ash source.

2.3 Parameters Influencing the LCA of LC3

2.3.1 Clay Calcination Energy

Clay becomes reactive after calcining it to a temperature of about 700 °C, and consequently, the energy-intensive process of calcination affects the LCA results significantly. Therefore, any change in the calcination energy demand and the type of fuel used will affect the total emissions, as well the energy demand of the cement.

As mentioned earlier, the energy requirement for the clay calcination was taken as 2.6 MJ/kg. However, from the analysis of a wide range of clays from various parts of

Table 2 Impact of LC3 with varying clay calcination energy requirement (per tonne of LC3)

Calcination energy (MJ/kg)	Emissions (kg CO_2-eq)	Energy demand (MJ)
1	560	4280
2.6	610	4850
3.5	640	5220

Table 3 Impact of LC3 with varying clay transportation distance (per tonne of LC3)

Transportation distance (km)	Emissions (kg CO_2-eq.)	Energy demand (MJ)
10	590	4580
540	610	4850
1000	620	5080

India, it was seen that the energy requirement in some cases could be as low 1 MJ/kg or rarely as high as 3.5 MJ/kg. The influence of this parameter is presented in Table 2, where it is seen that the CO_2 emissions can decrease by 8% if the calcination energy requirement goes down from 2.6 to 1.0 1 MJ/kg, whereas it can go up by 5% if the calcination energy is 3.5 MJ/kg. Similarly, the energy demand can go down by about 12% or go up by about 8% if the extreme cases occur.

2.3.2 Transportation Distance of Clay

In the results given in Sect. 2.2, it was assumed that the clay was brought from Dharmapuri, and calcined at the plant in Nandyal (540 km away). To study the influence of the transportation distance on the impacts of LC3, the calculations have been done assuming the cement plant to be located near the clay mines, say 10 km away (as is usually the case with the limestone mines) and a distance of 1000 km away. The results given in Table 3 show that the variation in the CO_2 emissions is small, going down by 3% or up by 2%.

3 Conclusions

The life cycle assessment framework has been followed to estimate the environmental impacts, i.e., CO_2 emissions and energy demand, of cement manufacturing in order to compare limestone calcined clay cement (LC3) with ordinary portland cement (OPC) and portland pozzolana cement (PPC). For the case study and the assumptions considered, it is clearly seen that both the blended cements have much lower CO_2 emissions than OPC, with LC3 giving the best prognosis. The energy demand of LC3 is also significantly lower than that of OPC though not lower than that of PPC due to clay calcination requirement. Parametric studies also show that the CO_2

emissions and the energy demand of LC3 could vary by 13 and 20%, respectively, depending on the clay calcination energy requirement, whereas the influence of the clay transportation distance is not significant.

References

1. Scrivener, K.L., John, V.M. Gartner, E.M.: Eco-efficient cements: potential, economically viable solutions for a low CO_2, cement-based materials industry. Report of a Working Group Initiated by Unep's Sustainable Building and Climate Initiative, United Nations Environment Programme (2016)
2. Gettu, R., Patel, A., Rathi, V., Prakasan, S., Basavaraj, A.S. Maity, S.: Sustainability assessment of cements and concretes in the Indian context: influence of supplementary cementitious materials. In: Ghafoori, N., Claisse, P., Ganjian, E., Naik, T.R. (eds.) Proceedings of the Fourth International conference on Sustainable Construction Materials and Technologies (SCMT4), paper S299, pp. 1142–1150. Las Vegas, USA (2016)
3. Scrivener, K.L.: Options for the future of cement. Indian Concr. J. **88**(7), 11–21 (2014)
4. ISO 14040: Environmental management—life cycle assessment—principles and framework. International Organization for Standardization, Geneva, p. 20 (2006)
5. ISO 14044: Environmental management—life cycle assessment—requirements and guidelines. International Organization for Standardization, Geneva, p. 46 (2006)
6. Gettu, R., Patel, A., Rathi, V., Prakasan, S., Basavaraj, A.S., Palaniappan, S., Maity, S.: Influence of supplementary cementitious materials on the sustainability parameters of cements and concretes in the Indian context. Mater. Struct. **52**(10), 1321–1325 (2019). https://doi.org/10.1617/s11527-019-1321-5
7. Gettu, R., Pillai, R.G., Santhanam, M., Basavaraj, A.S., Rathnarajan, R., Dhanya, B.S.: Sustainability-based decision support framework for choosing concrete mixture proportions. Mater. Struct. **51**(6), 16 (2018). https://doi.org/10.1617/s11527-018-1291-z
8. Pillai, R.G., Gettu, R., Santhanam, M., Rengaraju, S., Dhandapani, Y., Rathjnarajan, S., Basavaraj, A.S.: Service life and life cycle assessment of reinforced concrete systems with limestone calcined clay cement (LC3). Cem. Concr. Res. **18**, 111–119 (2018)
9. U.S. Environmental Protection agency: emission factors for greenhouse gas inventories, p. 5. http://www.epa.gov/sites/production/files/2015-12/documents/emission-factors_nov_2015.pdf (2015). Accessed 31 Jan 2016
10. Garg, A., Kazunari, K., Pulles, T.: IPCC Guidelines for National Greenhouse Gas Inventories, p. 29. http://www.ipcc-nggip.iges.or.jp/public/2006gl/vol2.html (2007)
11. PRé Consultants: SimaPro LCA software, version 8.0.5.13. https://www.pre-sustainability.com/simapro

Effect of Temperature on the Hydration of White Portland Cement–Metakaolin Blends Studied by ^{29}Si and ^{27}Al MAS NMR

Zhuo Dai and Jørgen Skibsted

Abstract Metakaolin can be considered as a model compound for an aluminosilicate-rich supplementary cementitious material (SCM) because of its composition and highly pozzolanic properties. This work presents a systematic investigation of the hydration of white Portland cement (wPc)–metakaolin (MK) blends cured at different temperatures by ^{29}Si and ^{27}Al MAS NMR with the main focus on the structure and composition of the C-(A)-S-H phase. White Portland cement–MK paste samples with wPc replacement levels of 0, 10, 20, and 30 wt% have been prepared and hydrated for 1–8 weeks at five different temperatures (5, 20, 40, 60, and 80 °C). Information on the degree of reaction for alite, belite, and MK is derived from the ^{29}Si NMR spectra and shows that the hydration of the wPc–MK blends is accelerated with increasing temperature except for the blend with the highest MK level (30 wt%). The Al_{IV}/Si ratio of the C-(A)-S-H phase is found to be independent on the hydration time but increases slightly with curing temperature. On the other hand, a significant increase in the average aluminosilicate chain lengths is observed for blends with increasing temperature, reflecting a decrease in the Ca/Si ratio for the C-(A)-S-H phase. Strätlingite is present in the wPc–MK blends at 20 °C and the fraction of this phase decreases with increasing curing temperature.

Keywords Metakaolin · C-(A)-S-H phase · Temperature

1 Introduction

The phase assemblages of hydrated Portland cement–metakaolin (MK) blends with different substitution levels have recently been studied in detail at ambient curing temperatures (see, for example, refs [1–8]). These studies have shown that high degrees

Z. Dai · J. Skibsted (✉)
Department of Chemistry and Interdisciplinary Nanoscience Center (INANO), Aarhus University, 8000 Aarhus C, Denmark
e-mail: jskib@chem.au.dk

Present Address:
Z. Dai
Aalborg Portland A/S, Cementir Holding S.p.A, 9100 Aalborg, Denmark

of MK reaction can be achieved as long as portlandite, formed by the cement hydration, has not been fully consumed by the pozzolanic reaction. Portlandite depletion may occur at replacement levels of 15–20 wt% pure MK where higher contents of MK will result in the formation of strätlingite along with a C-(A)-S-H phase with a reduced Ca/Si ratio [6]. Besides thermodynamic considerations, space availability during prolonged hydration may also have an effect, since the formation of the C-(A)-S-H phase results in pore structure refinement that can reduce the porosity to a critical size of pores which prevents formation of new hydration products. This effect has been observed in limestone-calcined clay cements with 50 wt% cement replacement, where the formation of carboaluminate hydrates was limited at a certain age by the absence of pores above a critical size [8]. After this age, a significantly higher amount of aluminum is incorporated in the C-(A)-S-H phase as a result of the higher aluminum concentration in the pore solution caused by the continued MK reaction.

The abovementioned results indicate that the composition, structure, and morphology of the C-(A)-S-H phase have crucial impact on the physical properties of blended cements including calcined clays. For this reason, it is of fundamental interest to study the microstructure of the C-(A)-S-H phase in blended cements at different temperatures, since elevated temperatures may result in the formation of C-(A)-S-H phases with different compositions (Ca/Si ratios), interlayer spacings, and a denser packing. Earlier ^{29}Si NMR studies have shown an increased polymerization of silicate chains with increasing temperature [9], whereas neutron scattering data have indicated that C-S-H pastes at 60 °C collapse into a denser material with fewer large gel pores [10]. The apparent density of C-S-H formed in cements has been estimated from XRD–Rietveld data and found to continuously increase with the curing temperature in the range 5–60 °C [11]. This significant increase in density results in a higher capillary porosity, which will have a negative impact on the durability and mechanical performance of the cured materials.

This study reports a systematic study of the impact of hydration temperature (5–80 °C) on the degrees of reaction and the C-(A)-S-H composition for binary Portland cement blends incorporating different levels of metakaolin (0–30 wt%), utilizing information gained from ^{29}Si and ^{27}Al MAS NMR spectroscopy.

2 Experimental

2.1 White Portland Cement–Metakaolin Blends

Four different white Portland cement (wPc)–metakaolin (MK) blends were prepared with wPc substitution levels of 0, 10, 20, and 30 wt% MK. The same sources of a commercial wPc from Aalborg Portland, Cementia Holding ApS, and kaolinite from Imerys Performance Minerals, UK, as used in an earlier study of wPc–MK blends [4], were employed. The wPc contains 4.1 wt% gypsum and MK was obtained by

calcination of kaolinite at 480 °C for 20 h. The elemental compositions of the wPc and MK are given in Ref. [4]. The paste samples used a water/solid ratio of 0.5, distilled water, and were mixed using a motorized stirrer. The pastes were cast into 25 mL polypropylene vials, demoulded after 24 h, and subsequently cured in plastic containers (75 mL) filled with water and stored in temperature-controlled climate chambers. At the selected hydration times, a small fraction of the sample was ground into a fine powder and stirred in 10 mL of isopropyl alcohol for approx. one hour. Afterwards, the samples were filtered and dried in a desiccator over silica gel. The cement blends were stored at 5, 20, 40, 60, and 80 °C and samples were taken after 1, 2, 4, and 8 weeks of hydration.

2.2 ^{27}Al and ^{29}Si MAS NMR Spectroscopy

The ^{29}Si MAS NMR spectra were obtained on a Varian INOVA-400 (9.39 T) spectrometer using a homebuilt CP/MAS NMR probe for 7 mm o.d. zirconia rotors, a spinning speed of $\nu_R = 6.0$ kHz, a 30-s relaxation delay and typically 2048 scans. The ^{27}Al MAS NMR spectra were acquired on a Varian Direct-Drive VNMR-600 spectrometer (14.1 T) using a homebuilt 4 mm CP/MAS probe, $\nu_R = 13.0$ kHz, a 2-s relaxation delay, and typically 4096 scans. Further experimental details on the acquisition and deconvolution analysis of the experimental spectra are given in Ref. [4].

3 Results and Discussion

3.1 Degrees of Reaction as Function of Temperature

The hydration of the silicate phases for the wPc blends with the four different MK substitution levels has been studied by ^{29}Si NMR at the different curing temperatures and hydration times, as illustrated in Fig. 1 for the wPc–MK 70:30 blend. A visual inspection of the spectra in Fig. 1 clearly reveals a low degree of belite hydration (-71.3 ppm peak) for all temperatures at this high substitution level and also a significant incorporation of tetrahedral Al in the C-(A)-S-H structure at all temperatures, as evidenced by the $Q^2(1Al)$ resonance at approx. -81 ppm. The individual spectra have been deconvolved using resonances from alite, belite, MK, and the Q^1, $Q^2(1Al)$ and Q^2 resonances of the C-(A)-S-H phase and the approach described earlier for similar wPc–MK blends at ambient temperature [4]. After prolonged hydration (8 weeks), the effect of curing temperature is smallest for alite (Fig. 2a) which shows degrees of hydration above 80% at all temperatures for the wPc blends with 0, 10, and 20 wt% MK. However, a small decrease in alite reaction with increasing temperature is observed for the highest substitution level. A pronounced effect of temperature is
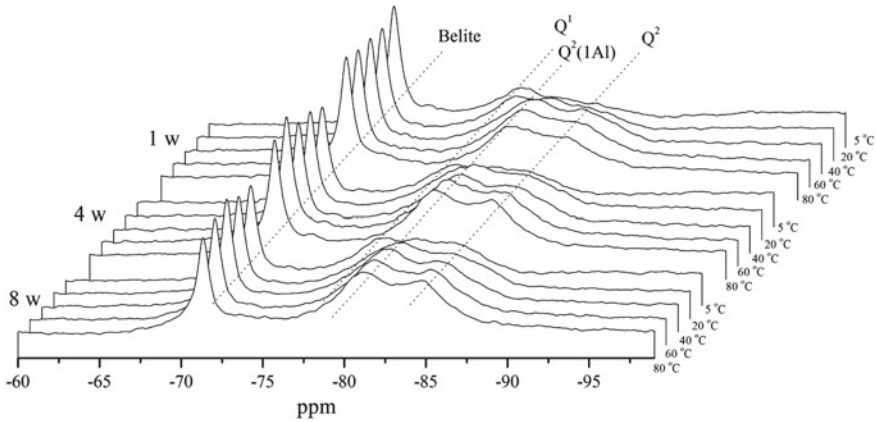
Fig. 1 ^{29}Si MAS NMR spectra following the hydration for the wPc–MK 70:30 blends hydrated at different temperatures for one, four, and eight weeks. The shown spectral range does not include the broad resonance from MK observed at approx. -90 to -110 ppm
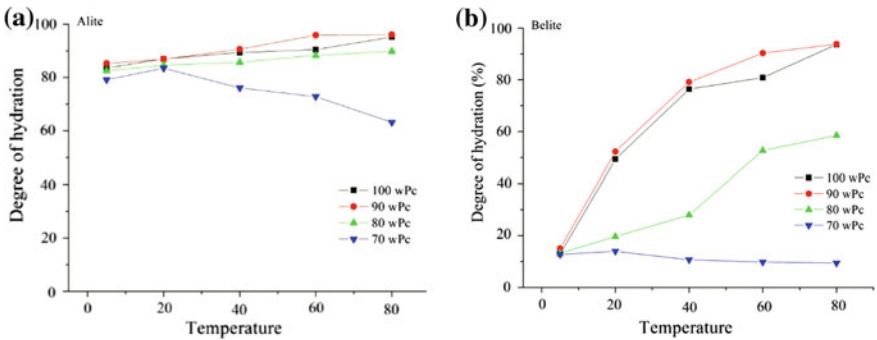
Fig. 2 Degrees of hydration for (a) alite and (b) belite in the wPc blends hydrated for 8 weeks at the different curing temperatures. The data results from deconvolution of the ^{29}Si NMR spectra

observed for the belite hydration, where the pure wPc and wPc–MK 90:10 blends show similar degrees of hydration which increases significantly with increasing temperature. A similar behavior is apparent for the 80:20 blends but with lower degrees of reaction. On contrary, only a small degree of belite reaction (~10%) is observed for the highest substitution level with no clear temperature variation. The lower reactivity of alite and belite at the highest substitution level may partly reflect an undersulfatization of these cement blends.

The corresponding degrees of MK reaction after one and 8 weeks of hydration (Fig. 3) range from 70–100% after 8 weeks of hydration for curing temperatures of 20 °C and above with a small decrease for increasing substitution levels. Also, a pronounced difference is apparent for the samples cured at 5 °C.
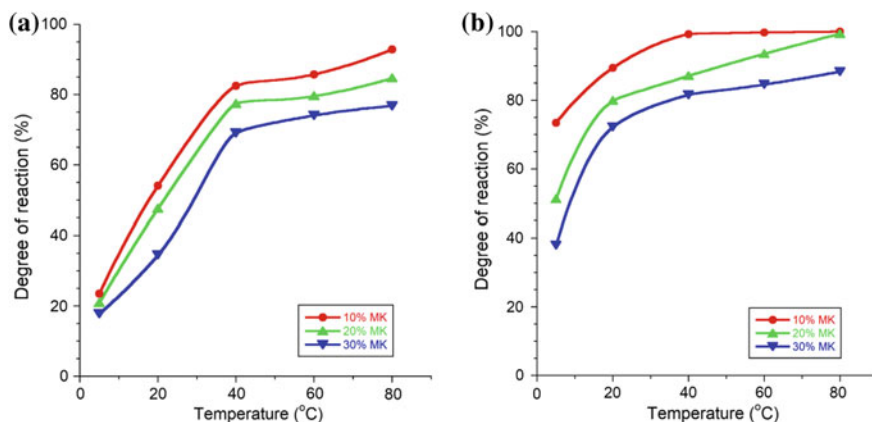
Fig. 3 Degrees of metakaolin reaction in the wPc blends hydrated for (a) one and (b) 8 weeks at the different curing temperatures. The data results from deconvolution of the ^{29}Si NMR spectra

The results show that after prolonged hydration, higher curing temperatures increase the degree of belite hydration at low substitution levels (10 wt% MK), which is ascribed to a temperature effect on the belite hydration kinetics. On the other hand, the lower degrees of belite reaction at higher MK levels may reflect a higher dissolution rate for MK as compared to belite, resulting in a consumption of portlandite by MK and a higher amount of aluminum ions in the pore solution which may slow down the silicate reaction. At the highest substitution level, the reaction of MK may even slow down the alite reaction at high curing temperature, as seen for the wPc–MK 70:30 blends above, indicating that MK reaction becomes increasingly important at higher temperature, despite the dissolution rate for alite is faster than for MK at ambient temperature [12].

3.2 The C-(A)-S-H Structure as Function of Temperature

The intensities for the Q^1, Q^2, and $Q^2(1Al)$ resonances of the C-(A)-S-H phase from the deconvolutions of the ^{29}Si NMR spectra allow calculation of the average chain length of aluminosilicate chains ($\overline{CL}$), the average chain length of pure silicate tetrahedra ($\overline{CL}_{Si}$), and the fraction of fourfold coordinated Al in the silicate chain (Al_{IV}/Si), using the well-known relations from earlier studies (*c.f.* Ref. [4] for further details). Our earlier study at ambient temperature [4] has shown that $\overline{CL}_{Si}$ increases with increasing MK content, whereas $\overline{CL}$ values are less affected, reflecting that the increase in $\overline{CL}_{Si}$ is mainly caused by the uptake of fourfold coordinated aluminum in the chains. The corresponding data for different cuing temperatures are illustrated in Fig. 4 for the blends hydrated for one week and show that $\overline{CL}_{Si}$ increases both with temperature and MK content. Moreover, a slight increase in the pure chain lengths
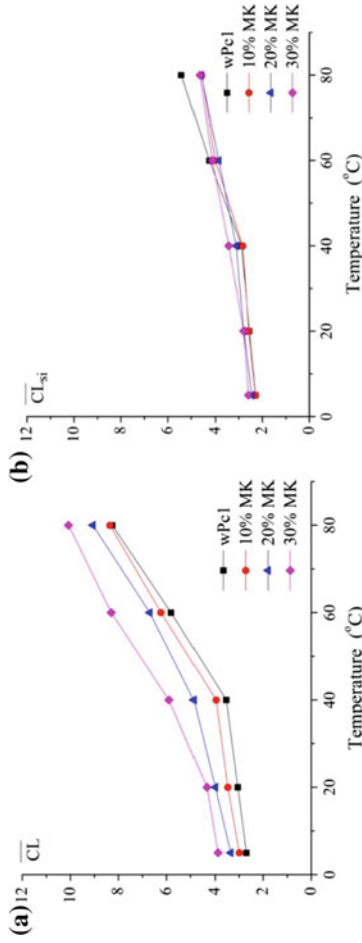
Fig. 4 Average (a) aluminosilicate ($\overline{CL}$) and (b) pure silicate ($\overline{CL}_{Si}$) chain lengths of the C-(A)-S-H phases formed in the wPc blends hydrated for one week

is also observed with temperature, demonstrating that the uptake of silicate species also contributes to the longer average aluminosilicate chain lengths, formed with increasing temperature. This agrees well with the observation of only a small increase in the Al_{IV}/Si ratios with temperature (Fig. 5a). Furthermore, at each temperature, the Al_{IV}/Si ratios are found to be nearly independent of the hydration time at the different temperatures, as illustrated in Fig. 5b for the blends hydrated at 80 °C. This is in accordance with several earlier studies of Portland cement blends hydrated at ambient temperature.

Consideration of all acquired data show that $\overline{CL}_{Si}$ increases with increasing MK content, temperature, and hydration time. After prolonged hydration, this reflects either a decalcification of the C-(A)-S-H phase by structural rearrangements at the atomic scale and/or the formation of secondary C-(A)-S-H gel with low Ca/Si ratio from the beginning. The Ca/Si ratio of the C-(A)-S-H phase may be estimated from the ^{29}Si NMR data, as shown in Fig. 6 for the blends hydrated for one week. This
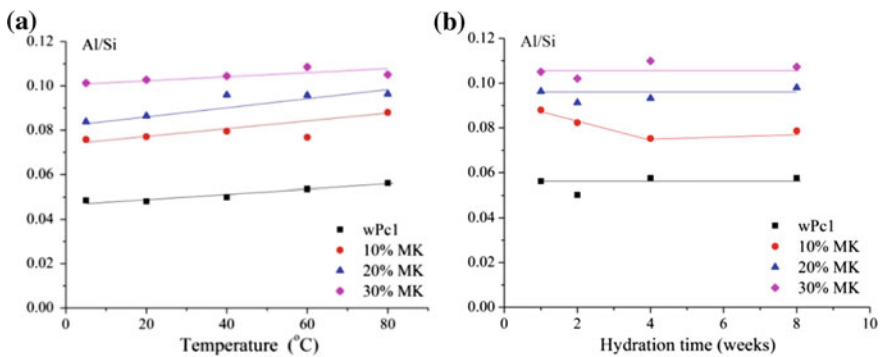
Fig. 5 Al_{IV}/Si ratios of the C-(A)-S-H phases as a function of (a) the temperature for the blends hydrated for one week and (b) as a function of hydration time for blends cured at 80 °C

Fig. 6 Calculated Ca/Si ratios for the C-(A)-S-H phase for the different wPc–MK blends after one week of hydration, using data estimated from the deconvolutions of the ^{29}Si NMR spectra
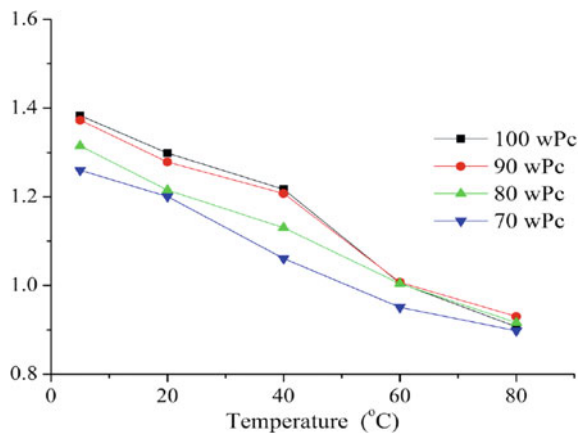
graph illustrates clearly that increasing MK levels and temperature result in C-(A)-S-H phases with lower Ca/Si ratios. More interestingly, the impact of different MK contents levels out at higher temperature, indicating that similar structures with a low Ca/Si ratio are reached for the C-(A)-S-H phase. This situation may reflect that portlandite is virtually depleted in the regions of C-(A)-S-H formation and that a continued hydration of MK (and belite) is driven by decalcification of the C-(A)-S-H phase. Decalcification of C-S-H phases by carbonation has shown that the basic tobermorite-like structure persists until a Ca/Si ratio of 0.67 is reached [13], corresponding to infinite silicate chains and no interlayer Ca^{2+} ions, and Ca/Si = 0.67 may also be the ultimate lowest ratio that can be achieved in hydrated blended Portland cements with high substitution levels.

3.3 Impact of Temperature on the Aluminate Phases

The ^{27}Al MAS NMR spectra of the wPc blend with 20 wt% MK hydrated for 8 weeks (Fig. 7) show that temperature also has a significant impact on the aluminate phases
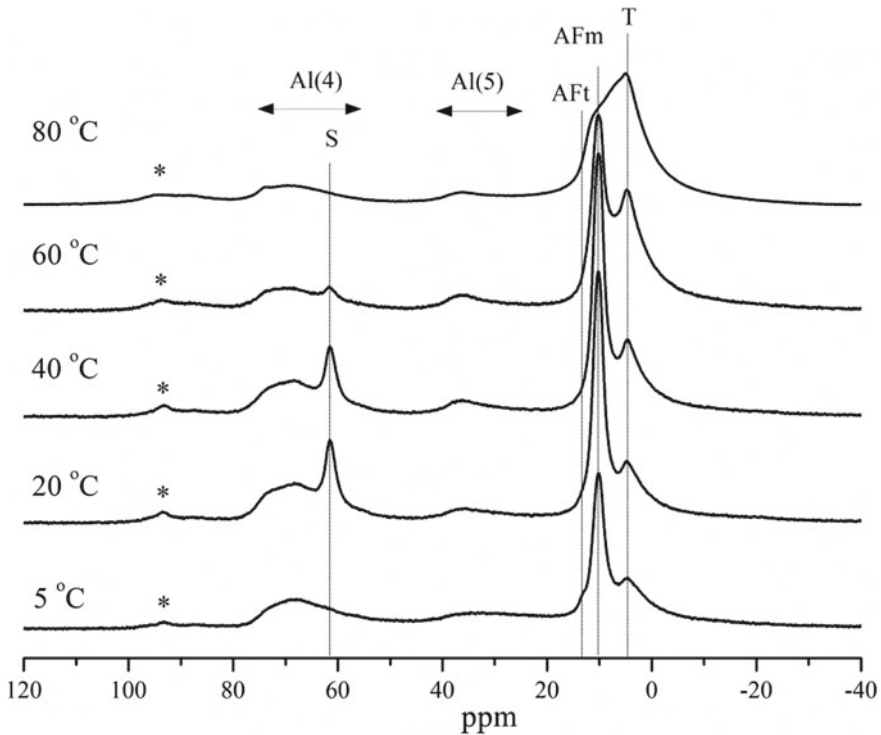
Fig. 7 ^{27}Al MAS NMR spectra of the wPc–MK 80:20 blends hydrated for 8 weeks

present after prolonged hydration. Ettringite is only detected at 5 °C, whereas an increasing amount of AFm phases are observed from 5 to 40 °C, which then decreases again at higher curing temperatures. Strätlingite is clearly detected by its resonance at 61 ppm from tetrahedral aluminum and it is only present in the samples cured at 20–60 °C. Strätlingite will form when portlandite is depleted and thus its absence at 5 °C may reflect the relative low degree of MK reaction at this temperature (i.e., 51% according to ^{29}Si NMR). The absence of strätlingite at 80 °C is not clearly understood as this system exhibits the lowest portlandite content, as observed for the wPc–MK 80:20 samples by TGA and powder XRD. However, it may potentially reflect an increased solubility of strätlingite at high temperatures. Finally, a clear increase in the intensity of the 4–5 ppm resonance from octahedral aluminum associated with the C-(A)-S-H phase is observed for increasing temperature, reflecting that a major part of the aluminum released from the MK reaction is taken up by the C-(A)S-H phase.

The wPc–MK samples 80:20 have also been characterized by TGA and powder XRD, allowing a more clear distinction of the different AFm phases that contribute to the resonance at approx. 10 ppm. In combination, the three techniques have shown that the main hydration products at 5 °C are ettringite, monosulphate, hemicarboate, portlandite, and C-(A)-S-H. At intermediate temperatures (20–40 °C) monosulphate, hemicarbonate, strätlingite, portlandite, and C-(A)-S-H are the dominating phases, whereas the primary hydration products at high curing temperatures (60–80 °C) are hydrogarnet and an aluminum-rich C-(A)-S-H phase.

4 Conclusions

A high degree of MK reaction has been observed at high curing temperatures, which results in a low degree of belite reaction, as a major part of portlandite has been consumed by MK. The average aluminosilicate chain length ($\overline{CL}$) increases with increasing MK content, temperature, and hydration time. The increase in $\overline{CL}_{Si}$ with temperature is caused both by the uptake of tetrahedral aluminum and silicate species. The impact of MK on $\overline{CL}$ levels out with increasing temperature, resulting in C-(A)-S-H phases with nearly the same $\overline{CL}$ value for all blends cured at 80 °C. This reflects a decalcification of the C-(A)-S-H phase, which may drive the continued MK and belite reaction when portlandite has been consumed.

References

1. de Silva, P.S., Glasser, F.P.: Hydration of cements based on metakaolin: thermochemistry. Adv. Cem. Res. **3**(12), 167–177 (1990)
2. Love, C.A., Richardson, I.G., Brough, A.R.: Composition and structure of C-S-H in white Portland cement-20% metakaolin pastes hydrated at 25 °C. Cem. Concr. Res. **37**(2), 109–117 (2007)

3. Fernandez, R., Martirena, F., Scrivener, K.L.: The origin of the pozzolanic activity of calcined clay minerals: a comparison between kaolinite, illite and montmorillonite. Cem. Concr. Res. **41**(1), 113–122 (2011)
4. Dai, Z., Tran, T.T., Skibsted, J.: Aluminum incorporation in the C-S-H phase of white portland cement–metakaolin blends studied by ^{27}Al and ^{29}Si MAS NMR spectroscopy. J. Am. Ceram. Soc. **97**(8), 2662–2671 (2014)
5. Alujas, A., Fernández, R., Quintana, R., Scrivener, K.L., Martirena, F.: Pozzolanic reactivity of low-grade kaolinitic clays: influence of calcination temperature and impact of calcination products on OPC hydration. Appl. Clay Sci. **108**, 94–101 (2015)
6. Kunther, W., Dai, Z., Skibsted, J.: Thermodynamic modeling of hydrated white Portland cement–metakaolin–limestone blends utilizing hydration kinetics from ^{29}Si MAS NMR spectroscopy. Cem. Concr. Res. **86**, 29–41 (2016)
7. Ferreiro, S., Herfort, D., Damtoft, J.S.: Effect of raw clay type, fineness, water-to-cement ratio and fly ash addition on workability and strength performance of calcined clay–limestone Portland cements. Cem. Concr. Res. **101**, 1–12 (2017)
8. Avet, F., Scrivener, K.: Investigation of the calcined kaolinite content on the hydration of limestone calcined clay cement (LC[3]). Cem. Concr. Res. **107**, 124–135 (2018)
9. Cong, X., Kirkpatrick, R.J.: Effects of the temperature and relative humidity on the structure of C-S-H gel. Cem. Concr. Res. **25**, 1237–1245 (1995)
10. Jennings, H.M., Thomas, J.J., Gevrenov, J.S., Constantinides, G., Ulm, F.J.: A multi-technique investigation of the nanoporosity of cement paste. Cem. Concr. Res. **37**(3), 329–336 (2007)
11. Gallucci, E., Zhang, X., Scrivener, K.L.: Effect of temperature on the microstructure of calcium silicate hydrate (C-S-H). Cem. Concr. Res. **53**, 185–195 (2013)
12. Lapeyre, J., Kumar, A.: Influence of pozzolanic additives on hydration mechanisms of tricalcium silicate. J. Am. Ceram. Soc. **101**, 3557–3574 (2018)
13. Sevelsted, T.F., Skibsted, J.: Carbonation of C-S-H and C-A-S-H samples studied by 13C, 27Al and 29Si MAS NMR spectroscopy. Cem. Concr. Res. **71**, 56–65 (2015)

The Effect of Curing Temperature on the Properties of Limestone Calcined Clay Cement (LC^3)

Wilasinee Hanpongpun and Karen Scrivener

Abstract The use of supplementary cementitious materials (SCMs) as partial clinker substitute permits to reduce the environmental impact of cement production. Calcined clay is one of the most attractive SCMs because it is widely available. Its combination with limestone in limestone calcined clay cement (LC^3) benefits from the synergy effect between metakaolin and calcite. This study investigates the effect of curing temperature between 20 °C and 30 °C on the properties of LC^3. Increasing temperature promotes the hydration of clinker and the pozzolanic reaction resulting in a boost of strength development of LC^3 at early ages. A coarser threshold pore diameter is observed on the samples cured at 30 °C for 28 days but it does not affect the strength of LC^3.

Keywords Calcined clay · LC^3 · SCMs · Curing temperature

1 Introduction

Limestone calcined clay cement (LC^3) is a new type of ternary blend made of limestone, calcined clay and clinker [1] and becomes very attractive for the cement industry to reduce CO$_2$ emissions from cement production. Although calcined clay and limestone have been used for several decades in blended cement, the novelty of LC^3 is to exploit the synergy of the combined use of calcined clay and limestone [2]. LC^3 has properties similar to or better than conventional Portland cement even using much lower levels of clinker. However, most of the previous tests were performed at a control temperature (20 °C) which is lower than the normal working temperature in the tropical zone countries. For example, in Thailand, the average temperature is around 30 °C. Therefore, the results obtained may show different effects on LC^3 in these countries. Thus, the aim of this work is to investigate the impact of curing temperature on the properties of LC^3.

W. Hanpongpun (✉) · K. Scrivener
Laboratory for Construction Materials, EPFL, Lausanne, Switzerland
e-mail: wilasinh@scg.com

2 Materials and Methods

In this work, the replacement of clinker with limestone and calcined clays from 15–45% was studied. LC^3-80(2:1), LC^3-65(2:1) and LC^3-50(2:1) correspond to blended cement with approximately 80%, 65% and 50% of clinker content, 5% of gypsum and with a replacement by calcined clay and limestone fixed ratio of 2:1 at 15%, 30% and 45%, respectively. Calcined clay used in this study contains approximately 50% of calcined kaolinite. The chemical composition of PC and calcined clay used are shown in [3].

The blended cement pastes were prepared using water to solid ratio of 0.4 and were cured at 20 °C and 30 °C until testing. The degree of clinker hydration was calculated from the mass fractions of the C_3S (Alite), C_2S (Belite), C_3A (Aluminate) and C_4AF (Ferrite) reacted. The phase quantification based on Rietveld analysis was carried out with X'Pert HighScore Plus program using rutile powder (Kronos–2300 titanium dioxide) as an external standard. The amount of reacted calcined clay (metakaolin) is calculated using mass balance calculation. The steps of the calculation are explained in [4]. The pore size distribution of cement paste samples at 28 days were measured by using mercury intrusion porosimetry (MIP). The compressive strengths of mortar were tested according to EN 196-1 at 1, 3, 7, 28 days.

3 Results and Discussion

3.1 Degree of Reaction

The degree of clinker hydration and the degree of metakaolin reaction are shown in Figs. 1 and 2, respectively. The hydration degree of clinker increases with increasing the addition of SCMs at early ages but the opposite is observed at later ages. Increasing the temperature from 20 °C to 30 °C means this turnover occurs earlier. For the degree of metakaolin reaction of LC^3 at 20 °C, there is no significant difference of metakaolin reaction among LC^3 blended cement at 3 days and 7 days but at 28 days the reaction degree of metakaolin of LC^3-50(2:1) is lower than the others. Not only the degree of clinker hydration is promoted by elevated temperature, but also the pozzolanic reaction. The degree of metakaolin reaction of LC^3-65(2:1) and LC^3-80(2:1) reaches 80% and 60% for LC^3-50(2:1) at 3 days. However, it can observe the slowdown of the degree of clinker hydration and the degree of metakaolin reaction at later age when increased the temperature. It is possible due to the lack of space for the growth of hydration products as it also found in the earlier work [5].

Fig. 1 Degree of clinker hydration of PC and LC^3 systems at **a** 20 °C and **b** 30 °C
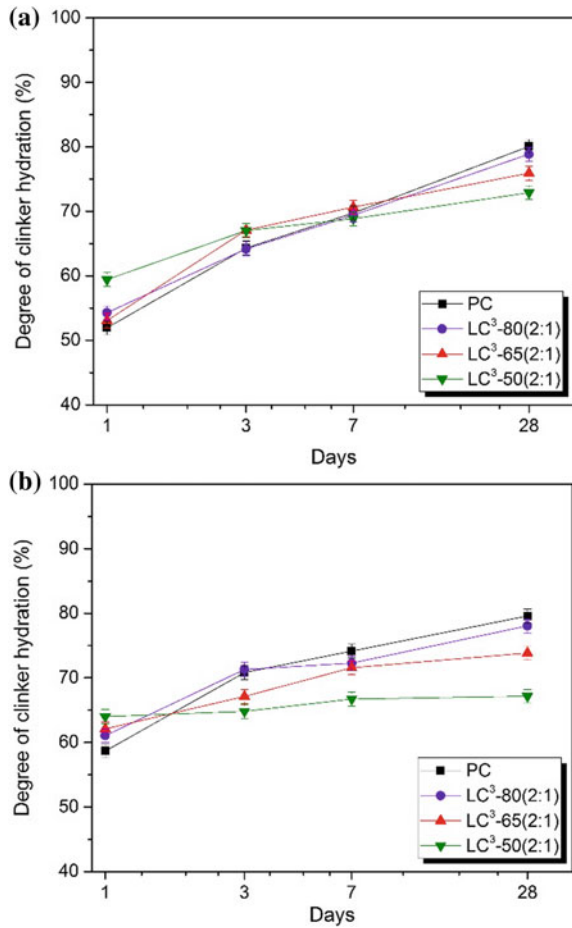
3.2 Compressive Strength

The compressive strength of PC and LC^3 cured at 20 °C and 30 °C shown in Fig. 3. The compressive strength of LC^3-80(2:1) and LC^3-65(2:1) is similar to PC from 7 days onwards at 20 °C. Increasing temperature up to 30 °C improves the strength development of PC and LC^3, especially at early ages. Similar strength of LC^3-80(2:1) and LC^3-65(2:1) to PC is obtained from 3 days onwards.

3.3 Porosity

Figure 4 shows the pore size distribution analyzed by MIP of PC and LC^3 systems at

Fig. 2 Degree of metakaolin reaction of LC^3 at **a** 20 °C and **b** 30 °C
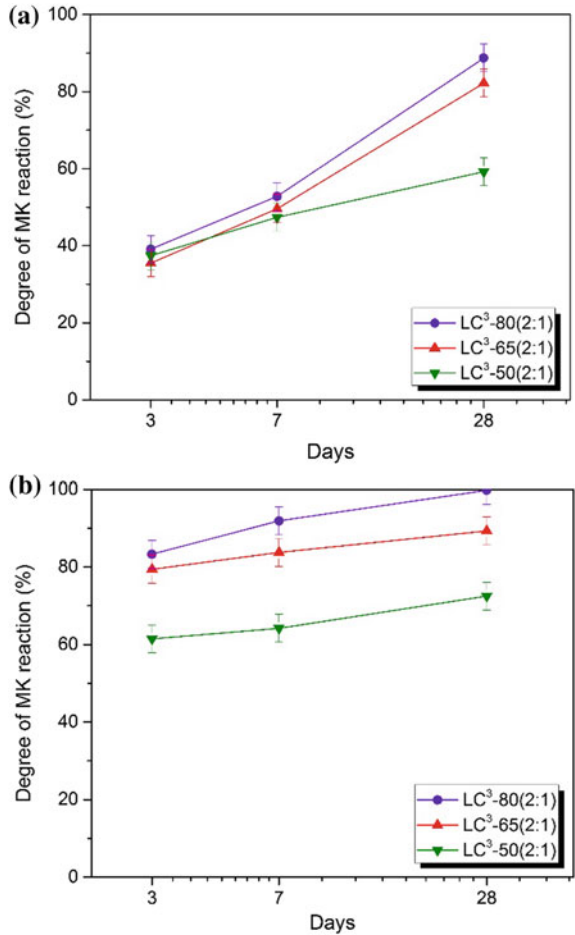
20 °C and 30 °C. A coarser threshold pore diameter is observed on the samples cured at 30 °C for 28 days, particularly, in the systems of PC and LC^3-80(2:1). However, it does slightly affect the compressive strength at 28 days because the hydration of clinker and pozzolanic reaction are promoted since the early ages of hydration.

4 Conclusions

Increasing temperature does affect the properties of LC^3. It promotes the hydration of clinker and the pozzolanic reaction resulting in an increase of strength development of LC^3 at early ages. Curing at 30 °C permits to reach comparable strength of LC^3-80(2:1) and LC^3-65(2:1) to PC from 3 days onwards. However, curing samples at

Fig. 3 Compressive strength of PC and LC^3 systems at **a** 20 °C and **b** 30 °C

(a) ■ PC ■ LC3-80(2:1) ■ LC3-65(2:1) ■ LC3-50(2:1)

(b) ■ PC ■ LC3-80(2:1) ■ LC3-65(2:1) ■ LC3-50(2:1)
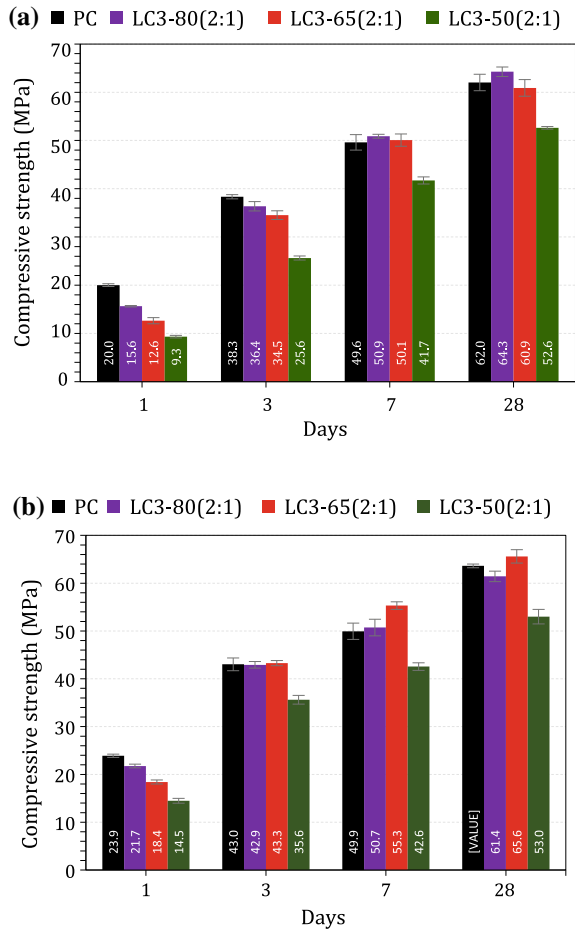
30 °C causes a coarser threshold pore diameter but it does not harm the strength of LC^3.

References

1. Scrivener, K., Martirena, F., Bishnoi, S., Maity, S.: Calcined clay limestone cements (LC^3). Cem. Concr. Res. **114**, 49–56 (2017)
2. Antoni, M., Rossen, J., Martirena, F., Scrivener, K.: Cement substitution by a combination of metakaolin and limestone. Cem. Concr. Res. **42**, 1579–1589 (2012)
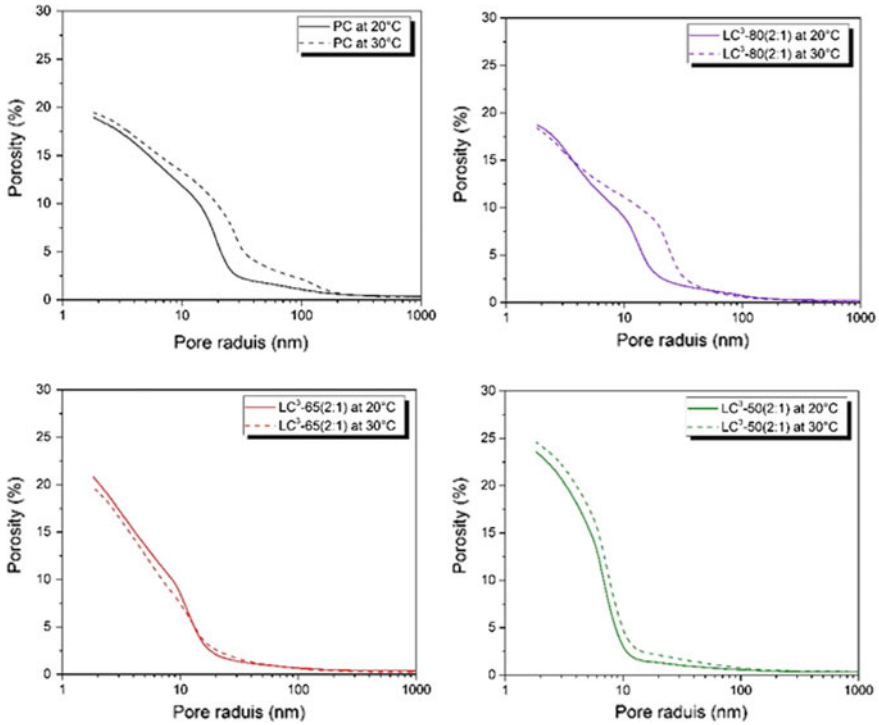
Fig. 4 Pore size distribution of PC and LC^3 cured at 20 °C and 30 °C for 28 days

3. Hanpongpun, W., Scrivener, K.: The effect of alkali on the properties of limestone calcined clay cement (LC^3). In: Martirena, F., Favier, A., Scrivener, K. (eds.) Calcined Clays for Sustainable Concrete, pp. 200–204. Springer, The Netherlands (2018)
4. Avet, F., Li, X., Scrivener, K.: Determination of the amount of reacted metakaolin in calcined clay blends. Cem. Concr. Res. **106**, 40–48 (2018)
5. Avet, F., Scrivener, K.: Investigation of the calcined kaolinite content on the hydration of limestone calcined clay cement (LC^3). Cem. Concr. Res. **107**, 124–135 (2018)

The Influence of Temperature Regime on Performance of Low Clinker Blended Cements

Arun C. Emmanuel[ORCID], Geetika Mishra and Shashank Bishnoi

Abstract An experimental work was conducted for studying the influence of early age curing temperature on the performance of low clinker blends. Three low clinker blends, limestone calcined clay cement (LC^3), Portland pozzolanic cement (PPC) using fly ash, and Portland slag cement (PSC) were used in this study. The clinker replacement level was kept at 50% by weight for all the blends. In addition to the isothermal curing conditions at 27 and 50 °C till 28 days, samples were also exposed to two different temperature regimes by changing the specimens from 27 to 50 °C at the age of 1 day and 3 days. Mortar compressive strength and X-ray diffraction were carried out at the age of 28 days. Strength and degree of hydration of clinker phases were compared. The later age performance of low clinker blends observed to be detrimental at a higher temperature (50 °C). It is observed that reduction in performance is relatively higher in LC^3 as compared to PSC and PPC. However, when the time of temperature exposure delayed by 24 h, the adverse effect of temperature on LC^3 was disappeared, and the blend has shown better performance than the other two blends.

Keywords Curing temperature · Calcined clay · Low clinker cements

1 Introduction

The production of cement is highly energy intensive emits a large amount of CO_2 mainly due to the decomposition of calcium carbonate. The industry account about 7% of global CO_2 emissions, and continuously looking for new technologies and

A. C. Emmanuel (✉) · G. Mishra · S. Bishnoi
Department of Civil Engineering, Indian Institute of Technology Delhi, New Delhi, India
e-mail: aruncemmanuel@gmail.com

G. Mishra
e-mail: geetika.mishra30@gmail.com

S. Bishnoi
e-mail: shashank.bishnoi@civil.iitd.ac.in

materials which could reduce environmental pollution. However, the industry currently uses highly efficient technology for clinker production and not much scope left to improve it [1]. The use of supplementary cementitious materials (SCM) for replacing clinker in ordinary Portland cement (OPC) considered as the best viable option to reduce the environmental pollution due to clinker production. The most popular SCMs are fly ash and slag, industrial byproducts from the coal-based thermal power plant and steel industry, respectively. However, the availability of these SCMs is not sufficient to meet the forecast demand for cement for the upcoming decades, which lead the industry to look at alternative options. The recent studies showed that calcined clay could be a potential option, and the optimum usage of calcined clay with limestone could potentially reduce the clinker factor up to 50% [2], and this ternary blend is known as limestone calcined clay cement (LC^3). Studies showed that raw materials with impurities such as dolomitic limestone as well as industrial waste products such as marble dust could also be used in LC^3 systems [3, 4].

Curing temperature is one of the critical factors which determine the early and later age performance of cement-based construction materials. In real field conditions, the curing temperature used to differ from the normal laboratory conditions significantly. The construction industry often uses various heat curing methods for maintaining the project schedule. Due to global warming, the rise in atmospheric temperature is also a concern, especially in tropical countries. During mass concreting, the temperature of the fresh concrete often rises due to the heat generation from cement hydration. Hence, it is imperative to understand how the temperature and time of exposure influence the performance of cement.

In general, the increase in temperature accelerates the cement hydration and subsequently increases the early strength. However, it is observed that the high-temperature curing adversely affects the later age performance [5, 6]. Although the ultimate degree of hydration (DoH) of clinker is found to be independent of curing temperature (within 5–60 °C), the density of the main hydration product: C–S–H increases with temperature which subsequently increases the porosity of the microstructure which lead to reduction in strength [7, 8]. The temperature regime also has a significant impact on the performance of the blend [9, 10].

In this study, three low clinker blends: limestone calcined clay cement (LC^3), Portland pozzolanic cement (PPC) and Portland slag cement (PSC) were prepared in the laboratory and cured in different temperature regimes. The strength and phase assemblages were obtained at 28 days and performance was compared.

2 Materials and Methods

2.1 Materials

Raw materials: clinker, calcined clay, limestone, fly ash, slag and gypsum were procured and ground individually in a laboratory ball mill. The particle size distribution of the raw materials is shown in Fig. 1. The phase composition of the raw materials was obtained from XRD-Rietveld analysis and is shown in Table 1. The blends were prepared by interblending the ground raw materials in a turbo blender. The composition of the blends is shown in Table 2. In order to keep the sulphate content same, the same amount of gypsum was added for all the blends.
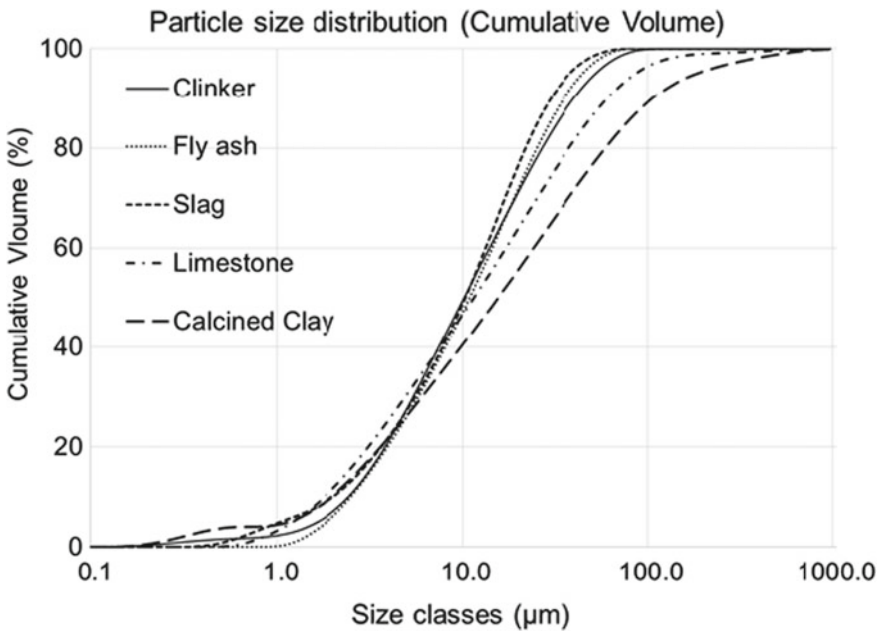
Fig. 1 Particle size distribution of raw materials

Table 1 Phase composition of the raw materials from XRD-rietveld analysis

Phase	Clinker	FA	Slag	CC	LS	G
C_3S	48.3	–	–	–	–	–
C_2S	31.3	–	–	–	–	–
C_3A	4.5	–	–	–	–	–
C_4AF	14.8	–	–	–	–	–
Calcite	–	–	–	–	85.1	–
Hematite	–	1.5	–	2.5	–	–
Kaolinite	–	–	–	4.2	–	–
Mullite	–	28.2	–	0.0	–	–
Quartz	–	15.9	0.7	17.6	7.3	–
Gypsum	–	–	–	–	–	86.0
Dolomite	–	–	–	–	–	14.0
Amorphous		54.7	99.4	75.7	7.6	–

FA fly ash, *CC* calcined clay, *LS* limestone, *G* gypsum (Unit: % weight)

Table 2 Composition of blends

Blend	Raw material composition (% weight)					
	Clinker	FA	Slag	CC	LS	G
PSC	50	–	45	–	–	5
PPC	50	45	–	–	–	5
LC^3	50	–	–	30	15	5

3   Methods

3.1   Temperature Regimes

Two temperature conditions: 27 and 50 °C were considered for constructing temperature regimes. The temperature regimes and respective notations are shown in Table 3.

Table 3 Temperature regime

Temperature regime	Notation
Samples cured at 50 °C till 28 days	h28
Samples cured at 27 °C for one day and exposed to 50 °C till 28 days	m1.h28
Samples cured at 27 °C for three days and exposed to 50 °C till 28 days	m3.h28
Samples cured at 27 °C till 28 days	m28

3.2   Mortar Compressive Strength

Mortar cubes of 7.06 cm size were prepared and tested as per Bureau of Indian Standards (132). Indian standard sand [11] was used for making the mix at the sand to cement ratio of 3 : 1. The water to cement ratio kept constant as 0.45 by weight. The materials: blend, standard sand, and distilled water were preconditioned at the specified temperature for 24 h before casting. The specimens were placed in an environmental chamber immediately after casting for one day, followed by demoulding the specimens and cured in lime saturated water in a temperature-controlled water bath till the time of testing.

3.3   X-Ray Diffraction and Rietveld Analysis

X-ray diffraction was carried out in at stipulated ages. The paste specimens were cast by mixing preconditioned dry blend and distilled water, using a paste mixer. The water to binder ratio kept as 0.45. The mix then poured into a plastic tube-like mould, and air bubbles were removed using a vortex mixer. The mould was then sealed and cured at temperature-controlled water baths which were set at 27 and 50 °C. One set of samples were shifted from 27 to 50 °C after one day and 3 days. XRD scanning was carried out in slices of 3 mm thick which were cut from the hardened cement paste specimens using a diamond cutter. In order to avoid carbonation, XRD scanning was carried out immediately after slicing. Scanning was done it in Bruker D8-Advance Eco at 40 and 25 mV with Cu target. Scanning was done in 2θ configuration with Cu-Kα source. The quantification of phases was carried out considering ASTM standard [12] and using TOPAS v5 software from Bruker using rutile as the external standard.

3.4   Results

The compressive strength of mortar cubes was tested at 28 days and is shown in Fig. 2. The average strength of 3 cubes was represented.

Though the strength of LC^3 specimens cured at isothermal conditions at 27 °C has shown a similar performance to that of PSC and PPC, the samples exposed to 50 °C isothermal condition observed a significant reduction in compressive strength by 28 days. However, it is seen that a delay in exposing to a higher temperature by one day or further could potentially improve the 28 days compressive strength of LC^3 significantly.
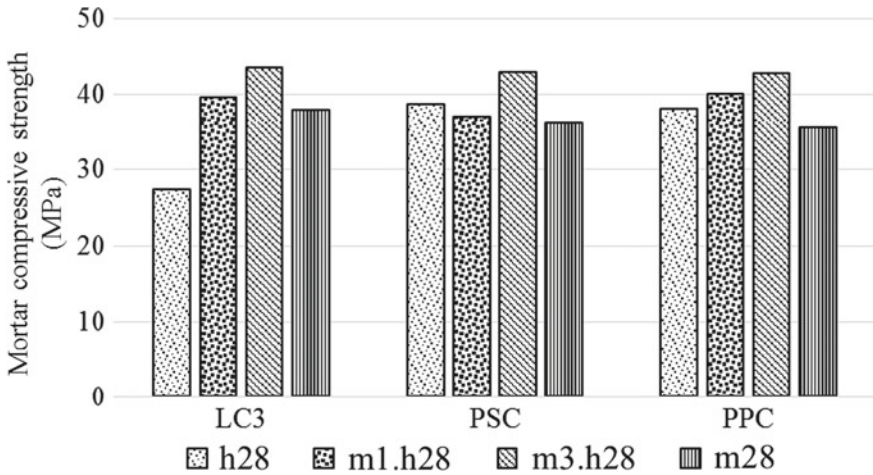
Fig. 2 Influence of temperature regime on compressive strength of blends at 28 days

3.5 The Degree of Hydration (DoH) of Clinker Phases

The DoH of clinker was calculated from the DoH of individual clinker phases as per the given equations

$$\text{DoH of clinker} = \sum \text{DoH of individual clinker phases(alite, belite, ferrite and aluminate)}$$
$$= w_1 - w_2/w_1$$

w_1 weight of clinker phases in 100 gm of the dry blend,
w_2 weight fraction of clinker phases remaining at the time of testing normalised to 100 gm of the dry blend.

The calculated DoH of clinker of the blends is shown in Fig. 3. The DoH of individual clinker phases; alite, belite and ferrite are shown in Figs. 4, 5, and 6 respectively.

It was observed that the 28 days clinker hydration at 50 °C isothermal conditions is lower than that cured at 50 °C isothermal condition. Irrespective of the temperature regime, the maximum DoH of clinker in LC^3 and PSC is about 70%, wherein the case of PPC, a better DoH was observed for m3.h28 and m28 (Fig. 4, 5 and 6).
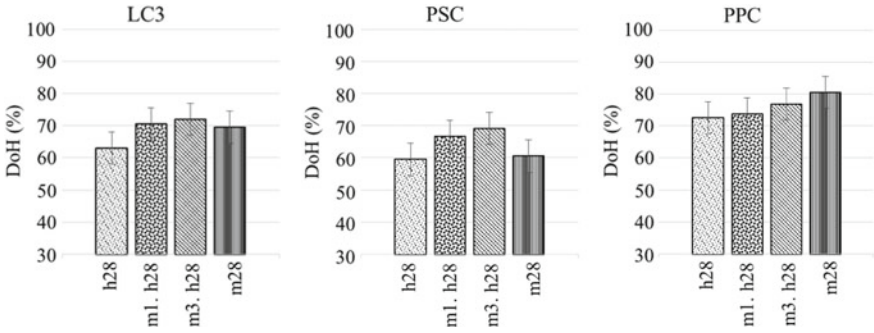
Fig. 3 Influence of temperature regime on DoH of clinker phases
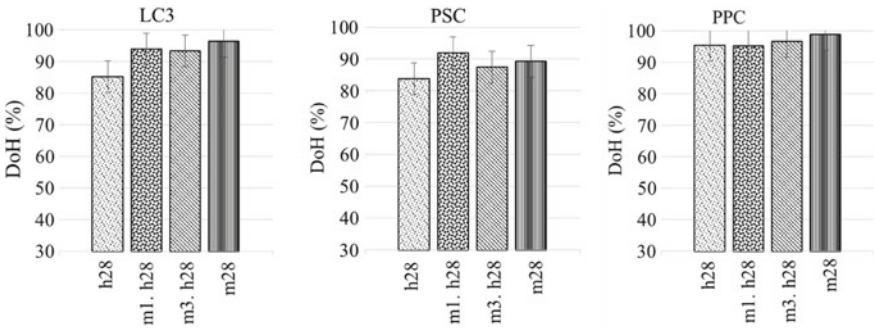
Fig. 4 Influence of temperature regime on hydration of alite at 28 days
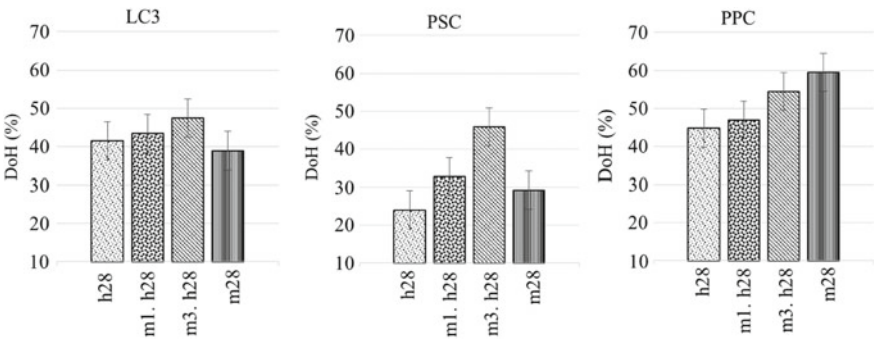
Fig. 5 Influence of temperature regime on hydration of belite at 28 days
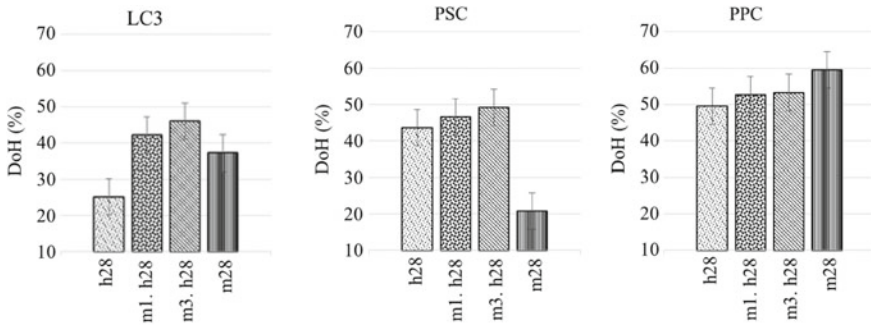
Fig. 6 Influence of temperature regime on hydration of ferrite at 28 days

4 Discussions

The influence of high curing temperature and temperature regime on the performance of low clinker blended cements with calcined clay limestone, fly ash and slag was compared at 28 days. The major observations are discussed below.

- While the 28 days compressive strength of low clinker blended cements with slag and fly ash have not shown a significant change between 27 and 50 °C, the LC^3 specimens have shown a lower strength at 50 °C. However, one day delay in high-temperature exposure could potentially eliminate the adverse effect of high-temperature curing for LC^3.
- Irrespective of the temperature regime, the maximum DoH of clinker in LC^3 and PSC was about 70%, wherein PPC the DoH was about 80% for 27 °C isothermal conditions. It is seen that the DoH is reduced for all the blends when the specimen is exposed to 50 °C immediately after casting.
- A delay in high-temperature exposure increases the DoH of clinker about 10% for both LC^3 and PSC. No significant improvement was observed for PPC.
- While comparing the DoH of clinker phases, a visible change in DoH of alite was observed for both LC^3 and PSC, no such change was observed for PPC.
- The early high-temperature exposure significantly influences the hydration of belite irrespective of the type of SCM. While the lower DoH of belite for 27 °C isothermal condition for LC^3 and PSC could be due to the slow rate of hydration, a significant reduction of belite hydration was observed for PSC and PPC when the specimen is cured at 50 °C isothermal conditions.
- The hydration of ferrite was observed to be much lower in LC^3 at h28 conditions. This could be due to the higher rate of aluminate dissolution from calcined clay. However, the DoH of ferrite significantly improves with a delay in high-temperature exposure.
- The increase in strength due to delay in high-temperature exposure in LC^3 can be attributed to better DoH of clinker phases particularly belite and ferrite. In the

case of PSC, the reduction in strength due to lower clinker hydration could have overcome with the increase in pozzolanic reaction due to the higher temperature. The increase in strength in PPC at 50 °C irrespective of the temperature regime could also be due to the higher temperature.

References

1. Gartner, E.: Industrially interesting approaches to "low-CO_2" cements. Cem. Concr. Res. **34**, 1489–1498 (2010). https://doi.org/10.1016/j.cemconres.2004.01.021
2. Scrivener. K.L.: 202 Special issue—options for the future of cement. Indian Concr. J. **88**:11–21 (2014). http://www.lc3.ch/wp-content/uploads/2014/09/0851_ICJ_Article.pdf
3. Krishnan, S., Kanaujia, S.K., Mithia, S., Bishnoi, S.: Hydration kinetics and mechanisms of carbonates from stone wastes in ternary blends with calcined clay. Constr. Build. Mater. **164**, 265–274 (2018). https://doi.org/10.1016/j.conbuildmat.2017.12.240
4. Krishnan, S., Bishnoi, S.: Understanding the hydration of dolomite in cementitious systems with reactive aluminosilicates such as calcined clay. Cem. Concr. Res. **108**, 116–128 (2018). https://doi.org/10.1016/j.cemconres.2018.03.010
5. Saul, A.G.A.: Principles underlying the steam curing of concrete at atmospheric pressure. Mag. Concr. Res. **2**:127–140 (1951). https://doi.org/10.1680/macr.1951.2.6.127
6. Kim, J.-K., Moon, Y.-H., Eo, S.-H.: Compressive strength development of concrete with different curing time and temperature. Cem. Concr. Res. **28**, 1761–1773 (1998). https://doi.org/10.1016/S0008-8846(98)00164-1
7. Escalante-García, J., Sharp, J.: The microstructure and mechanical properties of blended cements hydrated at various temperatures. Cem. Concr. Res. **31**:695–702 (2001). https://doi.org/10.1016/s0008-8846(01)00471-9
8. Gallucci, E., Zhang, X., Scrivener, K.L.: Effect of temperature on the microstructure of calcium silicate hydrate (C-S-H). Cem. Concr. Res. **53**, 185–195 (2013). https://doi.org/10.1016/j.cemconres.2013.06.008
9. Sajedi, F.: Effect of curing regime and temperature on the compressive strength of cement-slag mortars. Constr. Build. Mater. **36**, 549–556 (2012). https://doi.org/10.1016/j.conbuildmat.2012.06.036
10. Zhang, X. (2007) Quantitative microstructural characterisation of concrete cured under realistic temperature conditions, École Polytechnique Fédérale de Lausanne
11. IS: 650, Specification for Standard Sand for Testing of Cement (1991)
12. ASTM: C1365-06: Standard test method for determination of the proportion of phases in portland cement and portland-cement clinker using x-ray powder diffraction analysis. Am. Soc. Test. Mater. (2011). https://doi.org/10.1520/c1365-06r11.2

The Origin of the Increased Sulfate Demand of Blended Cements Incorporating Aluminum-Rich Supplementary Cementitious Materials

Franco Zunino and Karen L. Scrivener

Abstract It has been well established by several studies that LC^3 requires an additional amount of gypsum on top of the normal dosage contained in OPC. In this manner, the second (aluminate) peak does not overlap with the first (silicate) peak. This required adjustment of the system sulfate content is attributed to the additional aluminate phases introduced to the system by the addition of calcined clay. However, a correlation between metakaolin (aluminosilicate) addition and the amount of additional gypsum has not been found, and the relationship between these parameters and the position of the aluminate peak is not clear. This study explored in depth this issue in order to further understand the driving mechanism controlling the sulfate demand in LC^3. Our results show that there is no direct link between the aluminate phase content and the gypsum demand. On the contrary, the driving mechanism is linked to the specific surface area that the mineral additions (calcined clay and limestone) introduce to the system.

Keywords Gypsum · Ettringite · Kinetics

1 Introduction

Calcined clays are a promising opportunity to lower clinker levels in cements because of their widespread availability and their excellent reactivity in blended cements. The combination of metakaolin and limestone in OPC-based systems produces a synergy that enables the production of high-performance cement with a significantly lower clinker factor. Clays are mixtures of clay minerals (such as kaolinite, illite, and montmorillonite) and other impurities, such as quartz, iron oxide, and other rock-forming minerals. In some blended cements, such as limestone calcined clay cements (LC^3), undersulfation of the system is observed. This leads to the requirement to incorporate additional gypsum into the system to avoid the undesirable effects of undersulfation on the intensity of the silicate peak.

F. Zunino (✉) · K. L. Scrivener
Laboratory of Construction Materials, IMX, École Polytechnique Fédérale de Lausanne (EPFL), 1015 Lausanne, Switzerland
e-mail: franco.zunino@epfl.ch

The incorporation of gypsum in Portland cement has the goal of controlling the reaction of tricalcium aluminate (C_3A) and thus prevent flash setting [1] by retarding the reaction of this phase. In the presence of gypsum, the hydration reaction of C_3A changes and ettringite is formed [2]. As more gypsum is incorporated to the system, more retardation of the C_3A reaction can be achieved [3].

Despite the clear relationship between gypsum addition and C_3A, no clear relationship between the content of aluminates phases and the gypsum requirement for proper sulfation of a system has been established. Evidence of this is the fact that most standards require empirical measures like compressive strength or isothermal calorimetry to determine the optimum sulfate content of cement [4]. This study aimed to understand the mechanism behind the contribution of SCMs to the sulfate balance of blended cements.

2   Materials and Methods

A commercial ordinary Portland cement (OPC) conforming to EN 197-1 as CEM I 42.5R was used in this study. A commercial calcined clay from Burgess with 95% metakaolin content (referred onwards as metakaolin) was selected due to its high purity. Limestone powders (calcite) with two particle sizes were also used in this study: The coarser material is noted as LS and the finer one as fLS. The specific surface area (SSA) of each raw material was measured by nitrogen adsorption, using the BET method.

The influence of the additional SSA introduced by the incorporation of SCMs (filler effect) on the sulfate balance of the system was compared to the effect of the additional aluminates sourced from the addition of metakaolin. OPC blends with different limestone replacements were compared to LC^3 systems that incorporate metakaolin. A base LC^3 system containing 55% OPC plus additional gypsum, 15% limestone, and 30% metakaolin (LC^3-50) was taken as a reference. The water-to-binder ratio (w/b) was fixed at 0.4. Based on the computed SSA for the LC^3 system, an equivalent blend of OPC and fine limestone (fLS) was prepared, with a proportion intended to replicate the same binder surface area of each LC^3 system. As these systems do not contain any additional aluminates, the effect of the additional aluminates sourced from metakaolin can be decoupled from the contribution of the filler effect alone.

3 Results and Discussion

3.1 The Role of Sulfate in OPC

In pure OPC systems, C_3S dissolves quickly during the acceleration period of the silicate reaction and is therefore the main responsible of this peak. In addition, it can be noted that ettringite is detected from the first scan acquired. During the silicate peak, ettringite is precipitated continuously at a slower rate. In parallel, C_3A remains almost invariant during this period as it has been shown that the amount of C_3A that dissolves during the first minutes is enough to form the amount of ettringite observed during this period [5]. When gypsum is depleted, the rate of dissolution of C_3A increases, and consequently, the rate of precipitation of ettringite increases. This leads to the second (aluminate) peak, which is linked to the ettringite formation during this period (second ettringite formation as described in [6]).

3.2 Sulfation of LC^3: The Role of Specific Surface Area on Sulfate Depletion

The issue of undersulfation observed in LC^3 systems can be seen in Fig. 1, where a typical LC^3-50 blended system is compared to OPC. In this case, natural calcined clay with an SSA of 62 m^2/g was used. It can be seen that as the gypsum content is increased, the aluminate peak is retarded and the height of the silicate peak recovers.

Fig. 1 Sulfation of LC^3-50 system and the effect of gypsum incorporation on the aluminate peak position
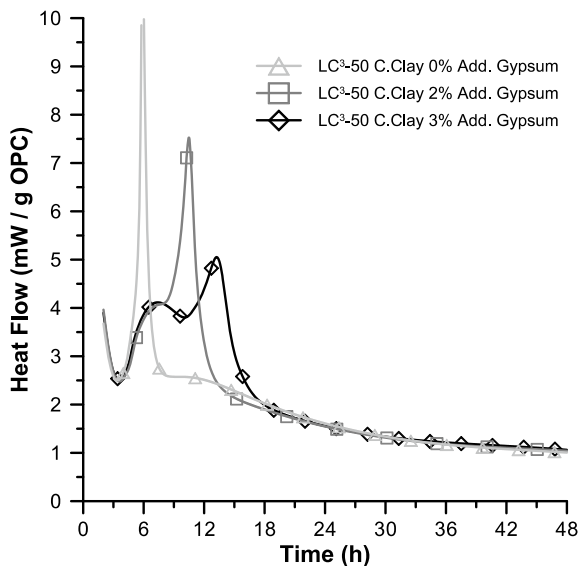
Figure 2 shows the heat flow profiles for the LC[3] system with 95% metakaolin on its calcined clay fraction with different gypsum additions. The incorporation of metakaolin provides another source of aluminum to the system in addition to C_3A. However, by comparing Figs. 1 and 2, it can be observed that this relationship is not systematic. While the system in Fig. 1 contains almost half the amount of metakaolin as compared to the system in Fig. 2, more acceleration of the aluminate reaction is observed in the first case. The main difference between these systems is the SSA of the clay fraction. While the 50% metakaolin clay has an SSA around 60 m^2/g, the clay with 95% metakaolin has an SSA of 13 m^2/g. This has consequences in the filler effect contribution of each clay. As seen, the finer clays lead to a higher silicate peak (Fig. 1) as compared to the coarser clay (Fig. 2), independent of their metakaolin content. This suggests that the filler contribution of the clay could be responsible for the observed acceleration and enhancement of the aluminate peak, rather than the additional aluminate phases introduced.

Figure 3 shows the heat flow curve of and OPC blended with fine limestone, where the specific surface area of the binder was match to the one measured for the LC[3]-50 system shown in Fig. 2. As seen, the same effect of acceleration and enhancement of the aluminate reaction is observed, despite the fact that no additional aluminum-bearing phases are incorporated into the system in this case. Thus, the mechanism of acceleration of the aluminate reaction in blended cements is linked to the specific surface area of the mineral additions and not to their chemical composition.

A link between the acceleration of the C_3S reaction due to the incorporation of additional nucleation sites (filler effect) and the enhancement and acceleration of the aluminate peak has been established based on the results presented. The acceleration of the silicate reaction leads to a faster precipitation of C-S-H, which can adsorb the

Fig. 2 Sulfation of LC[3]-50 system blend with synthetic calcined clay (95% metakaolin)
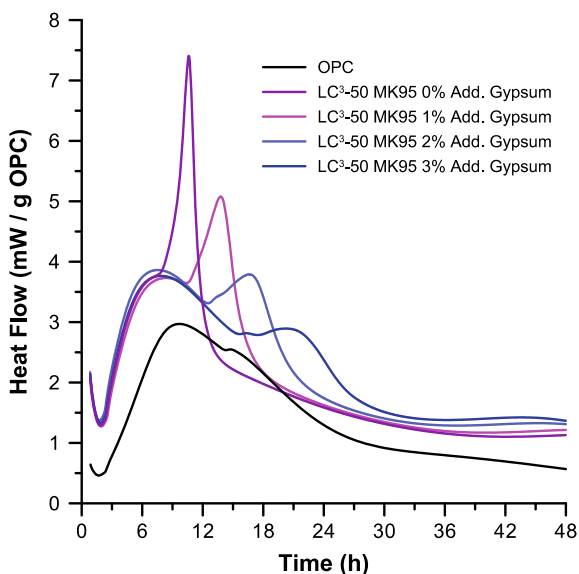
Fig. 3 Heat flow curve of an OPC + fLS system with the same SSA as the LC^3 systems in Fig. 2
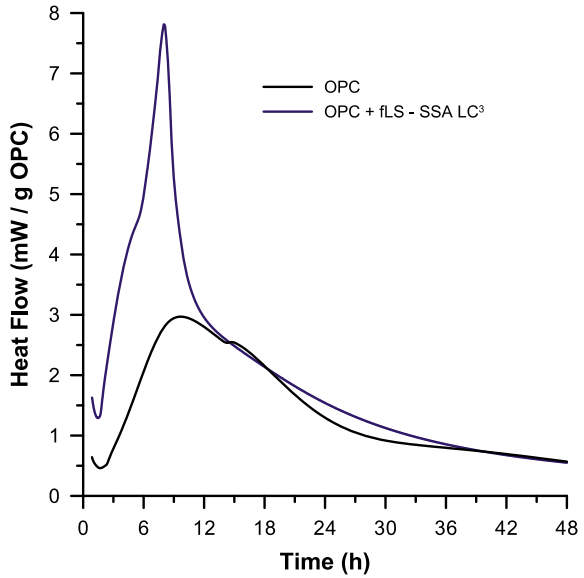
sulfate ions in solution. The higher the amount of C-S-H, the more sulfate ions that can be adsorbed and therefore, the earlier the gypsum depletion point is reached. As the aluminate peak is triggered by the depletion of sulfate from the system, the adsorption of sulfate into C-S-H can explain the results observed.

4 Conclusions

Based on the presented results, the following conclusions can be drawn:

- The acceleration and enhancement of the aluminate reaction observed in LC^3 is not related to the metakaolin content of the calcined clay used. On the contrary, the specific surface area of the mineral additions triggers the observed acceleration.
- The acceleration and enhancement of the aluminate peak is independent of the chemical composition of the mineral addition used.
- A mechanism of sulfate adsorption into C-S-H allows to link the filler effect contribution of mineral additions and the observed acceleration of gypsum depletion.

References

1. Lerch, W.: The influence of gypsum on the hydration and properties of portland cement pastes. Am. Soc. Test. Mater. J. (1946)
2. Rilem, T.C.: The hydration of tricalcium aluminate and tetracalcium aluminoferrite in the presence of calcium sulfate. Mater. Struct. **19**, 137–147 (1986). https://doi.org/10.1007/BF02481758
3. Quennoz, A., Scrivener, K.L.: Hydration of C3A–gypsum systems. Cem. Concr. Res. **42**, 1032–1041 (2012). https://doi.org/10.1016/j.cemconres.2012.04.005
4. ASTM C563, Standard guide for approximation of optimum SO3 in hydraulic cement (2018). https://doi.org/10.1520/c0563-18.2
5. Jansen, D., Goetz-neunhoeffer, F., Stabler, C., Neubauer, J.: A remastered external standard method applied to the quantification of early OPC hydration. Cem. Concr. Res. **41**, 602–608 (2011). https://doi.org/10.1016/j.cemconres.2011.03.004
6. Scrivener, K.L.: Development of the microstructure during the hydration of Portland cement, University of London (1984)

Influence of Calcium Sulphate on Hydration of Cements Containing Calcined Clay

Gopala Rao Dhoopadahalli , **Sreejith Krishnan** **and Shashank Bishnoi**

Abstract The present study tries to understand the effect of sulphates on the hydration of Portland cement—calcined clay systems. Calcined clay was obtained by calcining a clay having 95% kaolinite at temperatures ranging from 700 to 800 °C. The calcined clay was used to replace 30% of clinker. A clinker with low aluminate and low alkali content was used. Laboratory grade gypsum was used as the source of sulphates. In this study, the sulphate content in the cement system was varied as 2.5 and 5.0%. Mainly, the effect of sulphates on the hydration of cement was studied by conducting isothermal calorimetry on cement pastes for 48 h. In addition, the phase assemblage studies were done at 1 day and 3 days by performing X-ray diffraction on the paste samples. It was observed from calorimetry that the blends with higher sulphate content show a significant delay in aluminate hydration. It was again noticed that the main hydration peak was also affected with increase in sulphates. In calcined clay blend, the amount of ettringite formed was lesser than the normal OPC blend at similar sulphate content. In the other case where the dosage of sulphate was high, the ettringite continues to form till 3 days.

Keywords Calcined clay · Calcium sulphate · Hydration

1 Introduction

The manufacturing of cement contributes significantly to overall CO_2 emissions at various stages of its production, starting from quarrying to packing. Out of all the processes involved, the CO_2 emitted during limestone decomposition and burning of fuel in the kiln accounts to major portion of overall CO_2 emission, which are

G. R. Dhoopadahalli (✉) · S. Krishnan · S. Bishnoi
Department of Civil Engineering, Indian Institute of Technology Delhi, New Delhi, India
e-mail: gopalaraod@gmail.com

S. Krishnan
e-mail: sree1111@gmail.com

S. Bishnoi
e-mail: bishnoi@iitd.ac.in

unavoidable. In order to reduce the overall CO_2 emissions, cement industry is constantly undertaking huge efforts like improving the processes by adopting state of the art technologies, utilisation of alternative fuels, etc. The present trend in cement industry is to achieve lower clinker factors in cements without compromising on performance. Binary and ternary blended cements are prepared by replacing some portion of clinker with one or more supplementary cementitious material (SCM). Calcined clay or metakaolin is one such SCM that can be used for replacing cement.

Metakaolin is obtained from calcining a clay having high amount of kaolinite ($Al_2Si_2O_5[OH]_4$) mineral. These kaolinitic clays are calcined at temperatures ranging from 500 to 850 °C to make it a pozzolanic material [1–4]. The temperature up to which it should be calcined is still a question of debate. It is reported that highest pozzolanic reactivity is achieved by calcining at 800 °C [1]. However, beyond 850 °C, if calcined, clay may transform to less reactive crystalline material like cristobalite and mullite [5]. Furthermore, it must be noted that even the duration to which the clay is subjected to calcination can influence the properties of calcined clay.

Calcined clay rich in amorphous alumina and amorphous silica readily reacts with water and $Ca(OH)_2$ liberating enormous amount of heat. The reactivity of calcined clay depends largely on the type of cement and the same is delayed when used with low C_3A cement [6]. It has been reported that the pozzolanic reaction is more in clays containing lesser amount of kaolinite replaced at higher levels [7]. Calcined clay contains high alumina and is finer than ordinary Portland cement (OPC). Thus, sulphates are added in extra quantities in calcined clay blended cements to control the hydration reaction. In addition to controlling the aluminate hydration, sulphate can also influence other reactions. Hence, it becomes necessary to investigate the influence of sulphate in cements blended with calcined clay. The current study is mainly focused on isothermal calorimetry and phase assemblage studies during initials ages of hydration.

2 Materials and Methods

The oxide composition of clinker and calcined clay used in making the cements is presented in Table 1. Cement with low C_3A and low alkali content was intentionally chosen to better understand the reaction of calcined clay which is rich in aluminates.

Table 1 Chemical composition of clinker and calcined clay

Oxides (%)	CaO	SiO$_2$	Al$_2$O$_3$	Fe$_2$O$_3$	K$_2$O	Na$_2$O	SO$_3$	MgO	TiO$_2$	Cl
Clinker	65.02	19.83	5.06	5.46	0.52	0.00	1.48	1.16	0.71	0.00
Calcined clay	0.17	48.08	46.57	0.82	0.02	0.41	0.17	1.49	1.93	0.18

Precisely, the clinker contains 52.14% C_3S, 29.08% C_2S, 1.41% C_3A and 17.36% C_4AF.

The calcined clay procured from industry was not calcined properly as some amount of kaolinite was still left in it. Consequently, the calcined clay procured was again calcined at 800 °C in a muffle furnace for 1 h. The X-ray diffractograms of both originally procured calcined clay and the treated calcined clay are shown in Fig. 1 and their phase composition is shown in Table 2. The amorphous content has been increased drastically after calcination indicating the complete conversion of kaolinite to metakaolin (Table 2). The treated calcined clay and the clinker are then subjected to particle size analysis. The particle size distribution results are presented in Table 3.
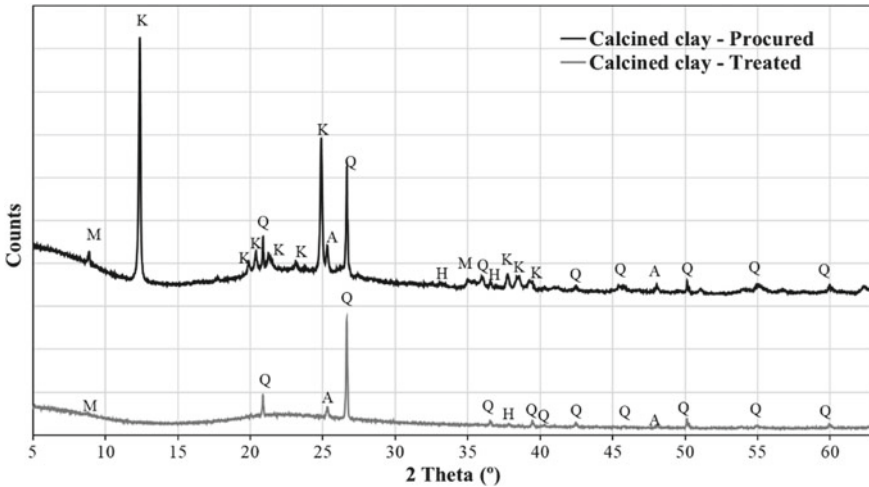
Fig. 1 XRD of calcined clay (K-Kaolinite, Q-Quartz, A-Anatase, M-Muscovite and H-Haematite)

Table 2 Phase composition of calcined clay before and after calcining in muffle furnace

Phase name	Calcined clay—procured	Calcined clay—treated
Kaolinite	15.63	0.16
Quartz	4.04	5.96
Muscovite	1.42	0.60
Hematite	0.80	0.26
Anatase	1.38	0.76
Total amorphous	76.73	92.27

Table 3 Physical properties of clinker and calcined clay

Parameter	Clinker	Calcined clay
Specific gravity	3.2	2.59
D_{10} (μm)	3.43	3.32
D_{50} (μm)	15.2	10.7
D_{90} (μm)	70.8	32.8

Table 4 Material proportions for blend preparation

Blend	Clinker	Calcined clay	Gypsum
OPC-2.5	94.63	–	5.38
CC-2.5	66.24	28.39	5.38
CC-5.0	62.48	26.78	10.75

Calcium sulphate dihydrate obtained from Merck which is of laboratory grade with 99% purity was used in all the blends. The sulphate content in cements was varied as 2.5 and 5.0%. The proportions of various materials required in the preparation of each blend are shown in Table 4. The blend OPC-2.5 was treated as the control blend to which the other blends were compared.

3 Tests Performed on Cement

3.1 Isothermal Calorimetry on Cement Pastes

Isothermal calorimetry test was conducted to know the effect of sulphate addition on heat evolution in cements at early stage. All the materials required for the test were stored in a closed chamber where temperature was maintained as 27 °C always. The pre-conditioning of materials was done for 24 h. A fixed water to cement ratio of 0.40 was used to make the cement paste. After thorough mixing, the paste was transferred to calorimeter cups immediately. The cups were closed properly and placed inside the isothermal calorimeter (Calmetrix I-cal 8000) for logging. And the logging was carried out for 48 h.

3.2 X-Ray Diffraction on Cement Pastes

The cement paste was made as described in Sect. 3.1. The paste was filled in 2 cm diameter cylindrical tubes and allowed to mature till the day of testing. At 1 day and 3 days, the hardened paste was taken out of the tube and 3 mm thick slices were cut with the help of precision saw. The slices made were scanned in X-ray diffractometer (Bruker D8 Advance Eco). The scan was performed from 5° to 65°

(2-theta) with a step size of 0.019° and 0.3 s per step. The scan files were analysed by performing Rietveld refinement by external standard method. High purity rutile was used as an external standard. The hydration products like ettringite and portlandite were quantified at 1 day and 3 days.

4 Results and Discussions

4.1 Hydration Studies

The rate of heat evolution curve for all the blends is shown in Fig. 2. The rate of heat evolution at induction period and at silicate peak and the slope of the curves at acceleration period are calculated and are presented in Table 5. The rate of heat evolved at induction period and at silicate peak is more for CC-2.5 compared to OPC-2.5 (Table 5). On the other hand, the rate of heat evolution at silicate peak is less for CC-5.0 compared to control blend. A clear aluminate peak is not observed in
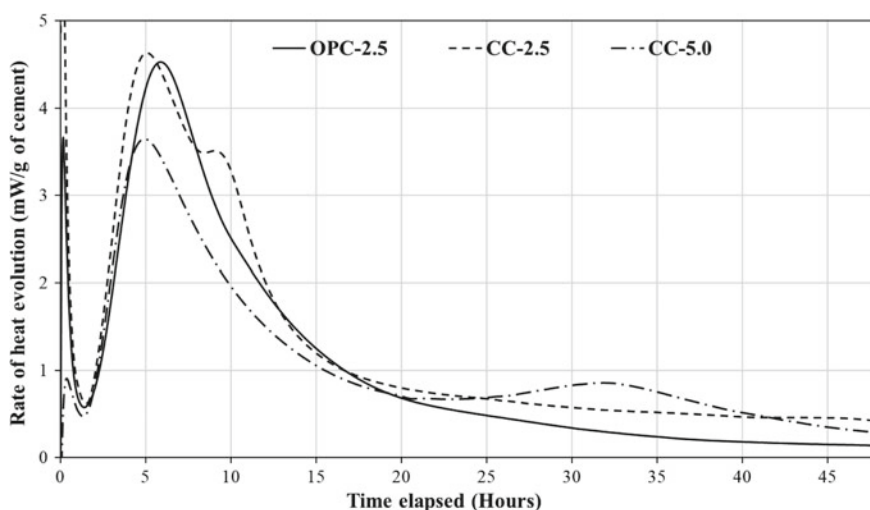
Fig. 2 Rate of heat evolution in blends OPC-2.5, CC-2.5 and CC-5.0

Table 5 Salient features from calorimetric curves

Blend	Rate of heat evolution at induction period (mW/g)	Rate of heat evolution at silicate peak (mW/g)	Slope of the curve during acceleration (mW/g-hour)
OPC-2.5	0.57	4.53	1.21
CC-2.5	0.62	4.63	1.55
CC-5.0	0.47	3.65	1.24

OPC-2.5 as it is a low C_3A cement. However, in CC-2.5 and CC-5.0 the aluminate peaks occur at 9 h and 32 h, respectively.

Among all the blends, the rate of heat evolution is more in CC-2.5 at induction period which indicates early onset of acceleration period. It is also evident from the slope of acceleration curve (Table 5) that the reaction occurs at a faster rate during the acceleration period in CC-2.5 blend indicating the early activity of aluminates. The higher rate of heat evolution in CC-2.5 blend during acceleration period is the combined effect of OPC hydration and pozzolanic reaction. The same is not observed in CC-5.0 blend because it has lower clinker content and due to significant delay in the hydration of aluminates. It is also seen that the reaction of aluminates is delayed significantly at higher dosage of sulphates. The aluminate hydration appears as a shoulder peak in CC-2.5 around 9 h and the same is observed as a broad hump in CC-5.0 with its peak occurring around 32 h (see Fig. 2).

The cumulative heat released curve for all the blends is shown in Fig. 3. It is clearly observed from the curves (see Fig. 3) that at the end of 48 h, calcined clay blends CC-2.5 and CC-5.0 are releasing more heat than the control blend OPC-2.5. At all times, the cumulative heat energy released is more in CC-2.5 compared to the other two blends. At initial stages, till 5 h the heat energy released is same for both OPC-2.5 and CC-5.0 but in OPC-2.5 the heat released increases gradually thereafter. However, after 30 h, the heat energy value increases rapidly because of delayed aluminate hydration in CC-5.0 blend. Also, the energy gap between OPC 2.5 and CC-5.0 goes on reduces. Finally, at 38 h, CC-5.0 curve crosses OPC-2.5 curve around 32 h indicating the delayed activity of aluminates. Overall, after 48 h, both calcined clay blends release more heat than the control one showing that the effect of reduction in clinker is well compensated by the calcined clay.
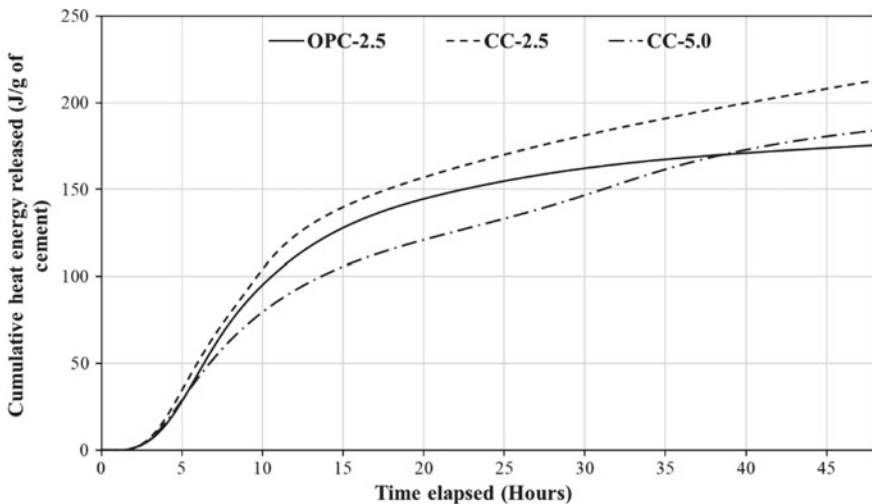
Fig. 3 Cumulative heat energy released in OPC-2.5, CC-2.5 and CC-5.0 blends

Table 6 Ettringite and portlandite formed in g per 100 g cement paste after 1 and 3 days

Blend	Ettringite at 1 day	Ettringite at 3 days	Portlandite at 1 day	Portlandite at 3 days
OPC-2.5	14.16	16.77	7.09	10.08
CC-2.5	10.90	10.10	3.55	4.71
CC-5.0	18.08	21.54	3.85	2.53

4.2 Phase Assemblage Studies

The phase assemblage studies are carried out on hardened cement paste specimens to know the effect of sulphate content on the formation of hydration products. The quantity of ettringite and portlandite formed at the end of 1 day and 3 days is presented in Table 6.

The quantity of portlandite is increased in OPC-2.5 from 1 day to 3 days due to hydration of silicates. Likewise, in CC-2.5 there is an increase in portlandite content from 1 day to 3 days. However, in CC-5.0 blend, a reduction in portlandite content is observed from 1 day to 3 days. It is reported that in properly sulphated cement, in the presence of gypsum, the dissolution of Ca^{2+} ions increase [8]. Also, it has been reported that C_3S hydration is increased when both C_3A and sulphates are present and the same is decreased when aluminium ions are present [9]. In CC-5.0 blend, the portlandite content is more at 1 day compared to CC-2.5 might be due to enhanced silicate reaction at higher sulphate content.

In low C_3A clinker, the reaction of calcined clay is slow [6] and hence there is an increase in portlandite content from 1 day to 3 days in CC-2.5 blend. However, the same trend is not observed in CC-5.0 blend. At higher sulphate dosages, i.e. in CC-5.0 blend, the rate of depletion of $CaOH_2$ is faster than its rate of formation. Thus, a reduction is observed from 1 day to 3 days in portlandite content which may be due to more pozzolanic reaction.

In control blend OPC-2.5 the sulphate to alumina ratio is high and thus the quantity of ettringite is increased from 1 day to 3 days (Table 6). However, a reduction in ettringite content is observed from 1 day to 3 days in CC-2.5 blend. In blend CC-2.5, the reactive alumina content is more, and the sulphate content is same as in OPC-2.5 leading to reduction in sulphate to alumina ratio which favours the AFm transformations. Furthermore, in CC-5.0 where there is ample amount of sulphates, ettringite quantity is increased from 1 day to 3 days. It is reported that the alumina uptake can take place in C-S-H resulting in C-(A)-S-H formation in calcined clay rich in kaolinite content [10]. However, at higher dosage of gypsum, where sulphate to alumina ratio is high ettringite formation is favoured instead of C-(A)-S-H.

5 Conclusions

The following conclusions were drawn based on hydration and phase assemblage studies conducted on calcined clay blends.

- Though, the aluminate peak is significantly delayed in Portland cement—calcined clay systems, overall heat is more than the control OPC blend at 48 h.
- The initial hydration of silicates may be affected due to higher sulphate contents.
- At higher dosage of sulphates, ettringite is formed at the expense of C-(A)-S-H.

References

1. Alujas, A., Fernández, R., Quintana, R., Scrivener, K.L., Martirena, F.: Applied clay science pozzolanic reactivity of low grade kaolinitic clays: influence of calcination temperature and impact of calcination products on OPC hydration. Appl. Clay Sci. **108**, 94–101 (2015). https://doi.org/10.1016/j.clay.2015.01.028
2. Almenares, R.S., Vizcaíno, L.M., Damas, S., Mathieu, A., Alujas, A., Martirena, F.: Case studies in construction materials industrial calcination of kaolinitic clays to make reactive pozzolans. Case Stud. Constr. Mater. **6**, 225–232 (2017). https://doi.org/10.1016/j.cscm.2017.03.005
3. Siddique, R., Klaus, J.: Applied clay science influence of metakaolin on the properties of mortar and concrete: a review. Appl. Clay Sci. **43**, 392–400 (2009). https://doi.org/10.1016/j.clay.2008.11.007
4. Murat, M., Comel, C.: Hydration reaction and hardening of calcined clays and related minerals. III. Influence of calcination process of kaolinite on mechanical strengths of hardened metakaolinite. Cem. Concr. Res. **13**, 631–637 (1983)
5. Moodi, F., Ramezanianpour, A.A., Safavizadeh, A.S.: Sharif University of Technology Evaluation of the optimal process of thermal activation of kaolins. Scientia Iranica **18**, 906–912 (2011). https://doi.org/10.1016/j.scient.2011.07.011
6. Cyr, M., Trinh, M., Husson, B., Casaux-Ginestet, G.: Effect of cement type on metakaolin efficiency. Cem. Concr. Res. **64**, 63–72 (2014). https://doi.org/10.1016/j.cemconres.2014.06.007
7. Tironi, A., Castellano, C.C., Bonavetti, V., Trezza, M.A., Scian, A.N., Irassar, E.F.: Blended cements elaborated with kaolinitic calcined clays. Proc. Mater. Sci. **8**, 211–217 (2015). https://doi.org/10.1016/j.mspro.2015.04.066
8. Ménétrier, D., Jawed, I., Skalny, J.: Effect of gypsum on C3S hydration. Cem. Concr. Res. **10**, 697–701 (1980)
9. Quennoz, A., Scrivener, K.L.: Interactions between alite and C3A-gypsum hydrations in model cements. Cem. Concr. Res. **44**, 46–54 (2013). https://doi.org/10.1016/j.cemconres.2012.10.018
10. Avet, F., Scrivener, K.L.: Hydration study of limestone calcined clay cement (LC3) using various grades of calcined kaolinitic clays. In: Calcined clays for sustainable concrete, pp. 35–40 (2018)

Sulfate Optimization for CCIL Blended Systems

Hai Zhu, Dhanushika Mapa, Brandon Lorentz, Kyle Riding and Abla Zayed

Abstract Limestone cements (IL) are becoming commonly available for structural applications. Calcined clays have great effect on performance enhancement of IL systems. Blending of those systems typically occurs in cement plants; however, for markets where blending occurs in concrete ready-mixed facilities, optimization of sulfate content is critical for the successful use of this new ternary blend. Optimum sulfate content for calcined-clay-limestone-cement systems was assessed using isothermal calorimetry, with hemihydrate as a sulfate source. The optimums are determined at 1, 2 and 3 days of hydration using both IL and ordinary portland cement (OPC) with two clay sources. Maximum heat of hydration was found to vary with age as well as the blended material sources. Less sulfate is required to optimize the limestone blended cement system. The replacement level of clay and the sulfate demand in the blended system are also examined. At the same replacement level, the optimum SO_3/Al_2O_3 ratio is similar, irrespective of cement type or clay type.

Keywords Sulfate optimization · IL cement · Calcined clay · Heat of hydration

1 Introduction

Calcined clay is a natural pozzolanic resource for use as a supplementary cementitious material with the advantages of reducing cost and carbon footprint. Limestone is found to enhance the performance of cementitious systems, and IL cement is becoming more commonly used in structural concrete [1]. Ternary blends of limestone, low-grade kaolin clay and portland cement clinker (with appropriate gypsum addition) show positive effects on concrete durability and performance [2, 3]. How-

H. Zhu · D. Mapa · B. Lorentz · A. Zayed (✉)
University of South Florida, Tampa, FL 33620, USA
e-mail: zayed@usf.edu

K. Riding
University of Florida, Gainesville, FL 32611, USA

ever, when materials with high alumina content are incorporated in cementitious systems, proper adjustment of the sulfate content is imperative to maintain good performance [4]. In this paper, sulfate optimization of IL cement as well as a Type I/II cement with two different clay sources are studied. The effect of several parameters such as limestone content, clay source and replacement level on the optimum sulfate content of the blended system is discussed.

2 Materials and Methods

2.1 Materials

An OPC (cement A) and two limestone cements of varying sulfate content (ILOP (optimized) and ILUS (under-sulfated)) were used for this study. Two types of clays from different sources (EM and CC) were used for blending with the cement. Hemihydrate was used as the external sulfate source to adjust the sulfate content in the blended system. The chemical oxide composition of the materials was determined using X-ray fluorescence spectroscopy (XRF) in accordance with ASTM C114 [5], Table 1.

2.2 Experimental Methods

Isothermal calorimetry following ASTM C1702, method A, internal mixing was used to measure the heat of hydration (HOH) [6]. The water-to-cementitious ratio (w/cm)

Table 1 Chemical oxide composition of cements, clays and hemihydrate

Analyte	Cements			Clays		Hemihydrate
	A	ILOP	ILUS	EM	CC	
SiO_2	21.2	18.43	19	68.68	63.49	0
Al_2O_3	5.15	4.56	4.6	20.81	19.89	0
Fe_2O_3	3.61	3.29	3.38	1	7.99	0.01
CaO	63.91	62.28	62.6	0	1.08	38.7
MgO	0.7	0.91	0.92	0.08	0.45	0
SO_3	2.59	2.93	2.41	0	0.23	55.34
Na_2O	0.14	0.18	0.14	0.18	0.09	0.02
K_2O	0.31	0.32	0.31	2.37	1.66	0
Na_2O_{eq}	0.35	0.4	0.35	1.74	1.19	0.02
Limestone	N/A	9.8	9.8	–	–	–

Table 2 Sulfate optimization mixtures

Mixes	Cement		Cement + clay			
	1	2	3	4	5	6
A	√	–	√	–	–	–
ILUS	–	√	–	–	–	–
ILOP	–	–	–	√	√	√
EM	–	–	20%	20%	30%	–
CC	–	–	–	–	–	30%

was maintained at 0.485 for all the mixes, and the testing was conducted at 23 °C. A polycarboxylate-based high-range water reducer was used for cement-clay mixtures to maintain constant flow similar to that of the cement mixtures while maintaining a constant w/cm, ASTM C563 [7]. A TAM air isothermal calorimeter was used. All mixtures contained hemihydrate in addition to the materials described in Table 2.

3 Results and Discussion

3.1 *Sulfate Optimization of OPC and IL Cements*

Figure 1 shows the effect of varying total sulfate content in the system on HOH for cement A and ILUS at 1, 2 and 3 days. The maximum in the HOH increases with age. At all ages, cement A shows a higher HOH as well as a higher optimum sulfate content. This could be because of the higher Al_2O_3 content, but could to some extent also be because of alkali solubility, or fineness. The optimum sulfate content for ILUS increased by 0.55% from 1 day to 2 days while for cement A it was 0.30%. The sulfate demand at 1 day for ILUS is lower than that for cement A.

3.2 *Optimization of Clay Blended Cements*

Sulfate optimization of the 20% clay blended systems is shown in Fig. 2. Although the optimum sulfate content increases with age, the increase in the optimum between 1 day and 2 days in the blended systems (0.78% for ILOP and 0.65% for cement A) is higher than in the plain cement paste for both cements. This clearly shows that the blended systems are under-sulfated when clays are blended without sulfate adjustment. However, when sulfate is added, the ILOP system reaches the optimum at a faster rate than cement A, thus indicating a lower sulfate demand in the former.

Sulfate optimization for the 30% clay blended system is shown in Fig. 3. It is interesting to note that increasing the clay content in the blended system increased the
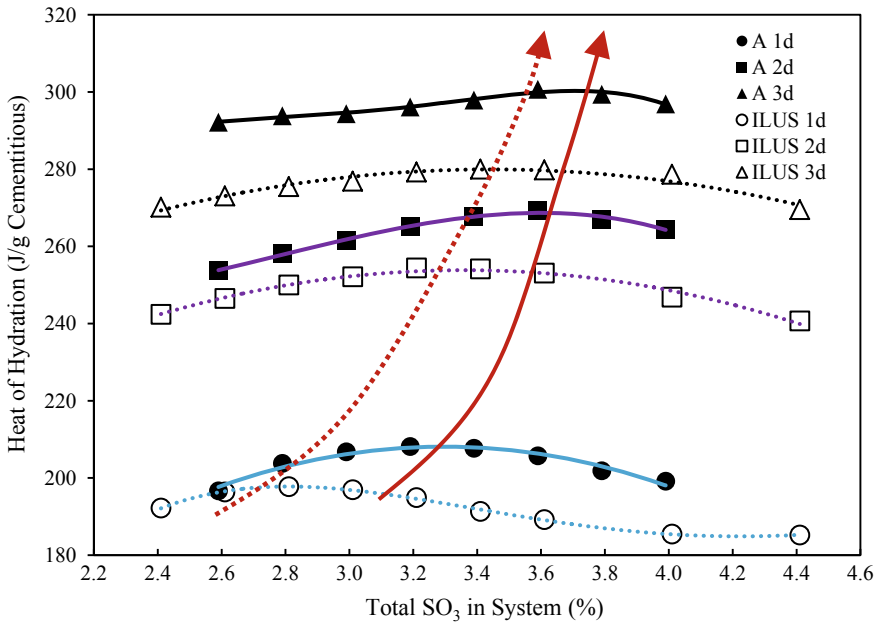
Fig. 1 Sulfate optimization for type I/II and IL cement pastes. Red solid arrow shows approximate path of optimum sulfate content with age for cement A. Red dashed arrow shows approximate optimum sulfate concentration with age for IL cement

HOH at 1 day but decreased it at longer hydration times. This is probably because the high reactive alumina in clay influences the early-age hydration kinetics. At 3 days, the HOH for 30% EM is lower than 20% replacement. The optimum SO_3 content at both replacement levels is similar. It is likely some amount of alumina from clay does not contribute to early-age hydration.

3.3 Optimization of Different Clay Mixtures

Another clay source (CC) was blended with ILOP cement and optimized for its sulfate demand, Fig. 4. Quantitative X-ray analysis indicates the presence of similar quartz content in both clays. The HOH is higher for EM blended systems at all sulfate levels examined here. This could be due to the finer particle size of EM clay. The results also indicate that the sulfate demand for the two clays studied here, which were collected from different mines, is variable. Further characterization of the clays is necessary to identify the parameters of significance on optimizing the sulfate demand.
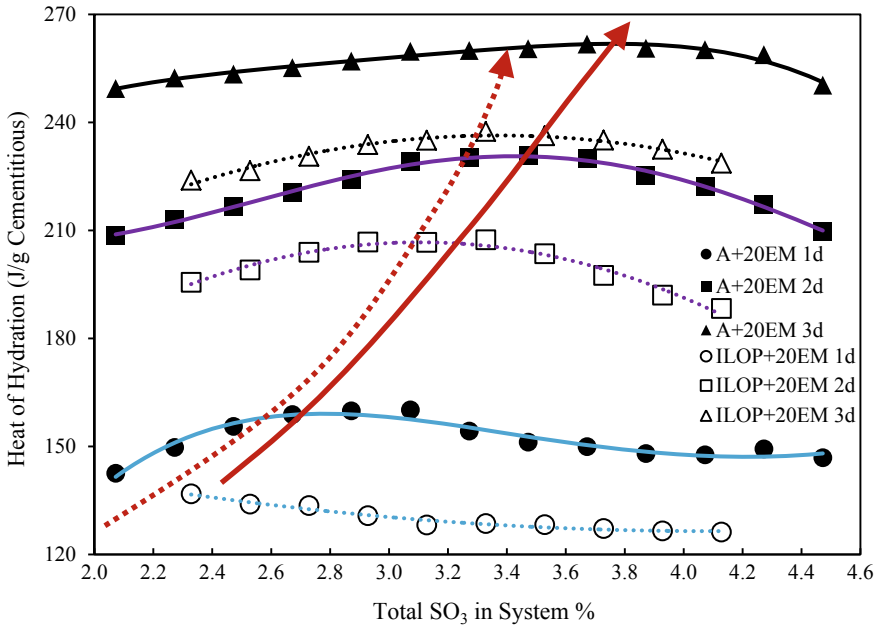
Fig. 2 Effect of cement type on sulfate optimization in clay blended cementitious systems. Red solid arrow shows approximate path of optimum sulfate content with age for cement A. Red dashed arrow shows approximate optimum sulfate concentration with age for IL cement

3.4 Optimum Value of Different Blended Systems

Optimum values of $SO_3\%$ in each blended system are calculated based on fitting curves. The corresponding alumina values and optimum SO_3/Al_2O_3 are also listed in Table 3. The variation in the optimum SO_3/Al_2O_3 with hydration time is depicted in Fig. 5. It is clear that the SO_3/Al_2O_3 ratio increases with hydration time for all cases. The ratio is highest for the as-received cements and decreases on blending with clays. Increasing clay substitution level from 20 to 30% did not seem to have a significant effect on the sulfate optimum in the system. Within the same replacement level, the ratio is similar, irrespective of cement type or clay type. However, the testing matrix needs to be expanded to verify this preliminary conclusion.

4 Conclusions

Three cements and two low-grade kaolin calcined clays are investigated for sulfate optimization of the blended systems at 23 °C. Sulfate optimization is critical for wider application of CCIL blended systems in structural concrete, especially since
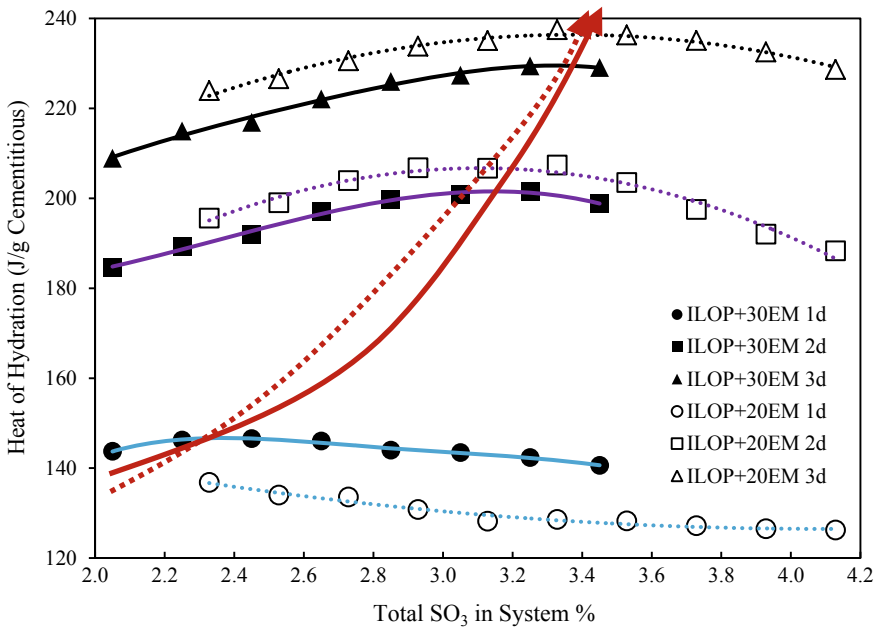
Fig. 3 Effect of clay replacement level on sulfate optimization. Red dashed arrow shows approximate path of optimum sulfate content with age for 20 EM. Red solid arrow shows approximate optimum sulfate concentration with age for 30 EM

undersulfating systems can reduce later age strength development. While numerous factors influence the optimum sulfate content in a clay blended system, only the effect of limestone content, type of clay and replacement level are studied here. The following conclusions can be drawn from the results:

- The optimum sulfate content varies with the age. Depending on the application, the appropriate optimum sulfate content can be specified.
- Higher replacement levels for the low-grade kaolin clays result in higher heat of hydration at one day but lower total heat at 3 days.
- Blending with low-grade kaolin clay in OPC and IL cement systems requires sulfate reoptimization.
- At the same clay replacement level, varying the cement type in a blended system requires sulfate reoptimization.
- At the two replacement levels considered here (20 and 30%), and using the same IL cement, the change in sulfate demand is negligible.
- The optimum sulfate content of a blended system varies with different clay sources. It is possible that the optimum value is affected by not only the chemical composition but also the particle size distribution and clay mineralogy.
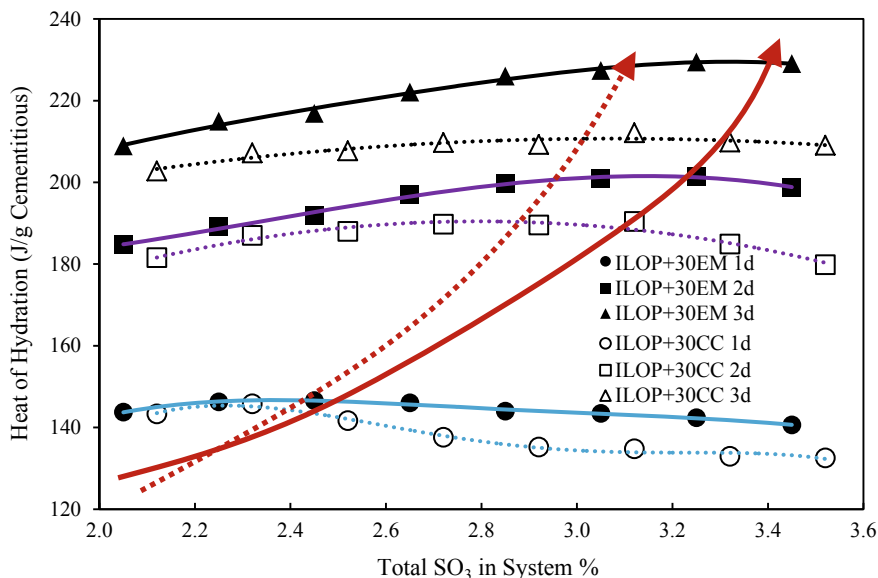
Fig. 4 Sulfate optimization for ILOP + 30% EM and ILOP + 30% CC blended systems. Red solid arrow is approximate optimum sulfate content with age for 30 EM. Red dashed arrow is approximate optimum sulfate content with age for 30 CC

Table 3 Optimum values for SO_3 and Al_2O_3

	Cement A			Cement ILUS			A + 20 EM		
	1d	2d	3d	1d	2d	3d	1d	2d	3d
Opt. SO_3	3.30	3.60	3.71	2.81	3.36	3.45	2.78	3.43	3.77
Al_2O_3	5.08	5.05	5.04	4.57	4.52	4.51	8.21	8.15	8.12
Opt. SO_3/Al_2O_3	0.65	0.71	0.74	0.62	0.74	0.77	0.34	0.42	0.46
	ILOP + 20 EM			ILOP + 30 EM			ILOP + 30 CC		
	1d	2d	3d	1d	2d	3d	1d	2d	3d
Opt. SO_3	2.33	3.11	3.37	2.38	3.15	3.32	2.27	2.80	3.08
Al_2O_3	7.81	7.74	7.72	9.31	9.02	8.96	9.15	9.10	9.08
Opt. SO_3/Al_2O_3	0.30	0.40	0.44	0.26	0.35	0.37	0.25	0.31	0.34

- Optimum SO_3/Al_2O_3 ratio increases with age for all mixtures. The ratios for clay blended systems are significantly lower than those of pure cement systems, but the reduction in the ratio becomes smaller with increasing the replacement level between 20 and 30%. Within the same replacement level, the ratio is similar irrespective of the type of cement (Type I/II or IL) or the clay source (kaolin content of approximately 45–65).
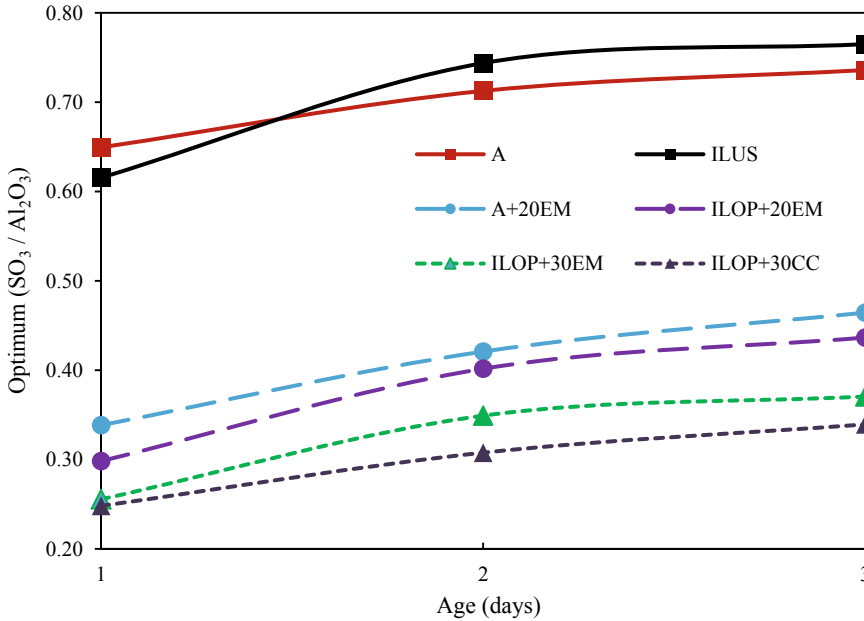
Fig. 5 Optimum SO_3/Al_2O_3 variation with hydration time

References

1. Lothenbach, B., Le Saout, G., Gallucci, E., Scrivener, K.: Influence of limestone on the hydration of portland cements. Cem. Concr. Res. **38**(6), 848–860 (2008)
2. Antoni, M., Rossen, J., Martirena, F., Scrivener, K.: Cement substitution by a combination of metakaolin and limestone. Cem. Concr. Res. **42**(12), 1579–1589 (2012)
3. Dhandapani, Y., Sakthivel, T., Santhanam, M., Gettu, R., Pillai, R.G.: Mechanical properties and durability performance of concretes with limestone calcined clay cement (LC3). Cem. Concr. Res. **107**, 136–151 (2018)
4. Avet, F.: Investigation of the calcined kaolinite content on the hydration of limestone calcined clay cement (LC3). École Polytechnique (2017)
5. ASTM C114 − 15: Standard test methods for chemical analysis of hydraulic cement. ASTM International, West Conshohocken, PA (2015)
6. ASTM C1702-17: Standard test method for measurement of heat of hydration of hydraulic cementitious materials using isothermal conduction calorimetry. In: Annual Book of ASTM Standards, pp. 1–9 (2017)
7. ASTM C563-18: Standard guide for approximation of optimum SO3 in hydraulic cement. ASTM International, West Conshohocken, PA (2018)

Influence of Kaolinite Content, Limestone Particle Size and Mixture Design on Early-Age Properties of Limestone Calcined Clay Cements (LC^3)

Franco Zunino and Karen L. Scrivener

Abstract This study explores the effect of kaolinite content from 20 to 95% on porosity refinement and mechanical properties of LC^3-50 and LC^3-65 (50% and 65% clinker factor, respectively) systems by dilution of pure metakaolin. The effect of metakaolin dilution was coupled with other factors that were observed to have a significant impact on hydration kinetics and strength. The effect of limestone particle size was studied in terms of packing optimization and workability enhancement. A detailed comparison between LC^3-50 and LC^3-65, currently allowed in the European standard, is provided showing that the main difference in mechanical properties occurs at 1 d for an equivalent kaolinite content. Finally, guidelines for effective and optimized utilization of clays of different grades (kaolinite contents) in LC^3 systems are given.

Keywords Sustainability · Clinker factor · Compressive strength

1 Introduction

Environmental concerns, such as energy consumption and CO_2 emission reductions, have become of increasing concern in the construction industry during the last decades [1, 2]. Supplementary cementitious materials (SCMs) are an effective means to reduce the cement content in concrete mixes [3–5] and enhance the durability of the material [6]. For these main reasons, they have become of increasing interest among researchers. The available amounts of commonly used SCMs (fly ash, blast furnace slags and natural pozzolan) are much lower than the worldwide demand for cement (OPC). Consequently, research interest has shifted toward alternative and more abundant sources of SCMs such as calcined clays and limestone.

Calcined clays provide a promising opportunity to lower clinker levels in cements because of their widespread availability and their excellent reactivity in blended

F. Zunino (✉) · K. L. Scrivener
Laboratory of Construction Materials, IMX, École Polytechnique Fédérale de Lausanne (EPFL), 1015 Lausanne, Switzerland
e-mail: franco.zunino@epfl.ch

cements. The combination of metakaolin and limestone in OPC-based systems produces a synergy that enables the production of high-performance cement with a significantly lower clinker factor. The reactive alumina supplied by metakaolin enhances the limestone reaction and allow higher replacement levels with improved performance, due to the increased formation of CO_3-AFm phases [7]. For this reason, LC^3 (limestone calcined clay cements) have become of great interest. This study explores the effect of calcined metakaolin content on the early-age performance of LC^3 by dilution of pure metakaolin using limestone. The effect of particle size of the limestone fraction and alkali content adjustment on strength is also discussed.

2 Materials and Methods

Portland cement classified as CEMI 42.5R was used for the preparation of blended cement pastes. The limestone powders were supplied from commercial manufacturers and were used as received. For the base mixtures of this study, a limestone with $D_{V50} = 4.1$ µm was used. A pure metakaolin (95% purity) was used in this study as calcined clay. Lower grades of clay were achieved by dilution of the pure metakaolin with limestone. A base mixture design of LC^3-50 with clay-to-limestone ratio of 2:1 was used (50% clinker, 30% calcined clay, 15% limestone and 5% gypsum). From there, different levels of dilution were explored by combining pure metakaolin and additional limestone in the 30% clay fraction of the binder, ranging from 95% metakaolin content (30% calcined clay and 15% limestone) down to 20% metakaolin (6.3% calcined clay and 38.7% limestone) content.

The LC^3-65 systems were designed by increasing the clinker factor up to 65% and keeping the relative proportions between limestone and clay constant in the remaining fraction for comparison with LC^3-50.

A constant w/b ratio of 0.4 by mass was used for all mixtures. Compressive strength was measured in mortar samples in conformity with EN 196-1 standard procedure. For the limestone particle size study, mortar samples were cast at w/b 0.4 in the same way as the base mixtures. Two additional limestone sizes were used: D_{15} (coarse limestone, with $D_{V50} = 17.5$ µm) and BUG (fine limestone, with $D_{V50} = 1.8$). The coarse and fine limestone replaced the limestone used to dilute down the 95% metakaolin down to the desired values (therefore, an increased amount of fine or coarse limestone is added as the metakaolin content goes down), while the initial 15% base limestone content of the LC^3-50 with clay-to-limestone ratio of 2:1 system was always kept constant with the $D_{V50} = 4.1$ µm limestone. For the mixtures where the alkali content was adjusted, KOH was used to achieve a total alkali content, expressed as a percentage of Na_2O_{EQ} of the total binder, of 0.8 and 1.0%. The particle size distribution of the raw materials used is shown in Fig. 1, measured by laser diffractometry.

Mercury intrusion porosimetry (MIP) was conducted on paste samples cast with analogous compositions to the mortar mixtures in selected systems. The aim of these experiments was to compare the effect of coarse and fine limestone inclusions in

Fig. 1 Particle size distribution of the raw materials used in this study
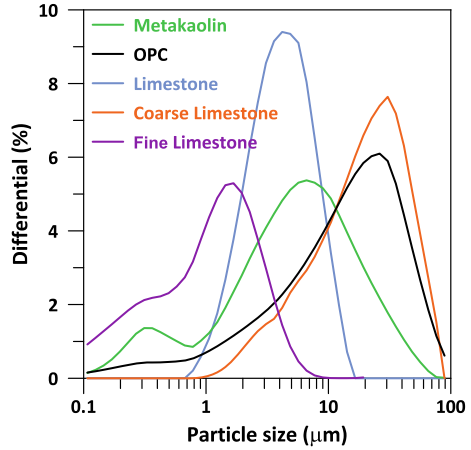
the porosity refinement profile. In addition, isothermal calorimetry at 20 °C was conducted to assess the hydration kinetics of the systems. Furthermore, it was used to study the effect of raw materials properties in the aluminate reaction of LC^3.

3 Results and Discussion

3.1 Effect of Calcined Clay Grade (Metakaolin Content) and Clinker Factor on Compressive Strength

Results for compressive strength of mortar with 50 and 65% clinker factors are presented in Fig. 2. In general, LC^3-65 exhibits a higher strength at one day as compared to LC^3-50. This is attributed to the higher clinker content. At this age, the hydration of clinker dominates the production of hydrates. However, this difference starts to disappear already at two days, starting from the systems with higher metakaolin content. At seven days, the difference is negligible across the whole range explored. LC^3-65 formulations are currently allowed in the European EN 197 standard as CEMII/B-Q-L, but not the LC^3-50 based formulations. From a strength point of view, it appears that the difference between both clinker factors is restricted to the very early stage of hydration. Furthermore, as it will be shown in the next section, this difference can be shortened even further by the refinement of the limestone fraction of the adjustment of the alkali content.
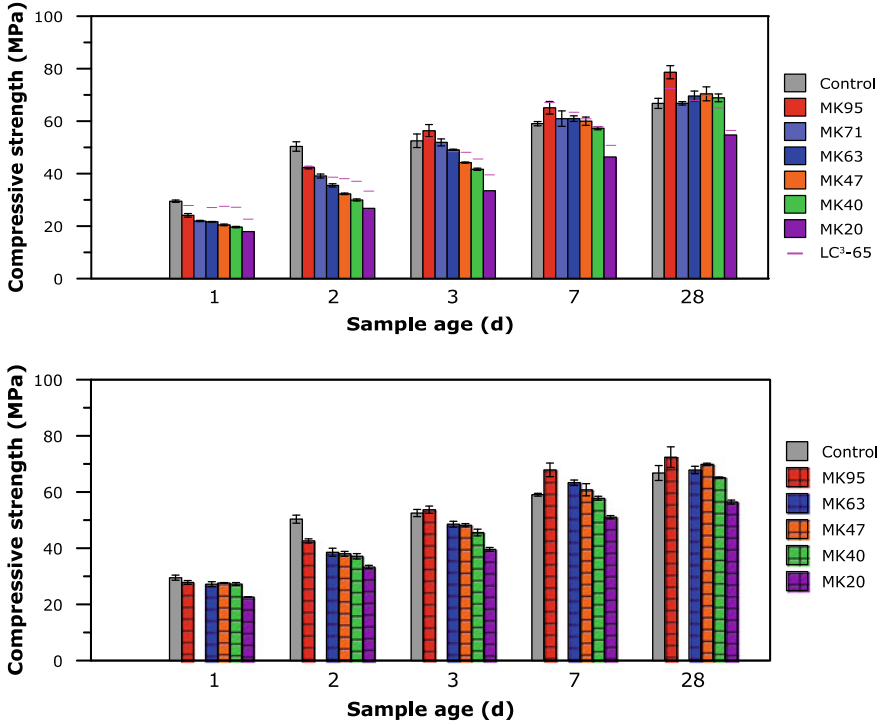
Fig. 2 Compressive strength of LC^3-50 (top) and LC^3-65 (bottom) mortar mixtures with different amounts of metakaolin. Eye guides are included in the top figure referring to the LC^3-65 strength at each metakaolin level

3.2 Effect of Limestone Particle Size Compressive Strength of LC^3-50 Formulations

Results of LC^3-50 mixtures where coarse (D15) or fine (BUG) limestone is incorporated are shown in Fig. 3. It can be observed that for the same metakaolin content, the surface area of limestone has a significant effect on compressive strength, especially at an early age. In fact, at one, two and three days, the effect of limestone refinement on strength is higher for a given mixture than the observed variation (Fig. 1) for a reduction in metakaolin content. Thus, limestone particle size is a relevant factor that influences the strength of LC^3 at an early age and could be used to increase the performance of binders in scenarios where only low-grade clays are available. Furthermore, the use of fine limestone allows approaching to the strength level of LC^3-65 formulations at one day.

Figure 4 shows the porosity profiles obtained after seven days of hydration by MIP of a group of LC^3-50 systems with normal size and coarse limestone. As observed, the incorporation of coarse limestone leads to a higher total porosity in both cases (MK63 and MK40). However, in the case of MK63, the difference is smaller and
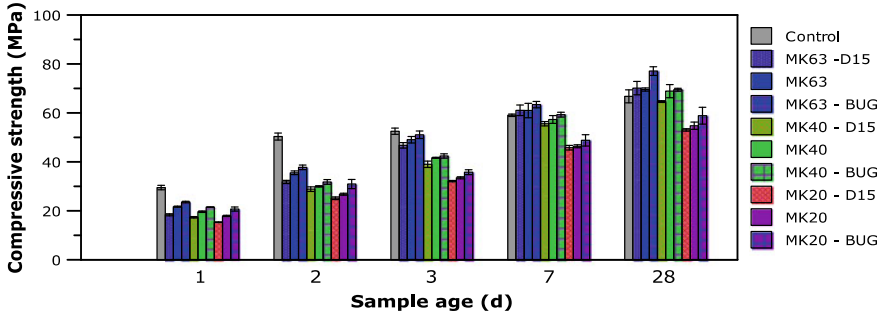
Fig. 3 Compressive strength of LC^3-50 mortar with coarse (D15) and fine (BUG) limestone

Fig. 4 Porosity profiles of LC3-50 systems at seven days measured by MIP (contact angle 120°)
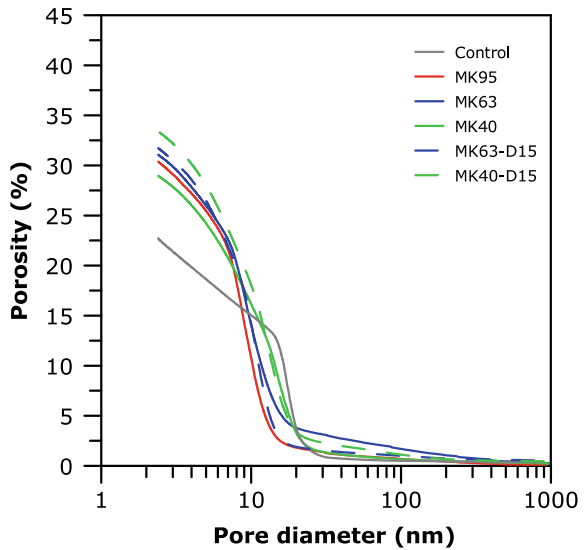
the critical entry radius with coarse limestone is slightly lower than the reference system, which could explain a similar result in strength at this age between the D15 and the reference system, as opposed to MK40.

3.3 Physical (Fine Limestone) and Chemical (Alkali Content) Strategies to Increase Strength

To explore the possibilities to increase the early-age strength of LC^3-50 systems using chemical strategies, alkali adjustment was used. Figure 5 shows the studied mixtures with 63 and 40% metakaolin content, with adjusted alkali content, fine limestone
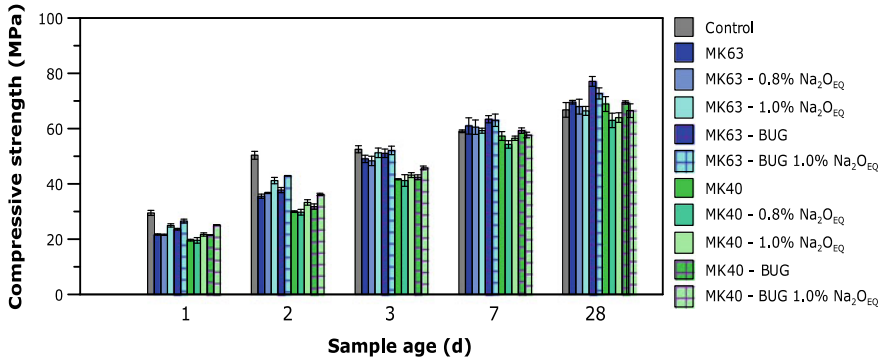
Fig. 5 Compressive strength of LC^3-50 mortar mixtures that incorporate different strategies to increase early-age strength (alkali adjustment, limestone refinement or a combination of both)

(BUG) addition or a combination of both. In addition, the reference values for the MK63 and MK40 with the reference limestone are also included for comparison. As seen, for the two metakaolin contents studied, the mixtures with an increased alkali content up to 1% Na$_2$O$_{EQ}$ shown higher strength at early age. A decrease of strength is observed at 7 and 28 days as compared to the reference system but within the error of the experiment. The combination of fine limestone and alkali adjustment exhibited an even higher increase of strength at one, two and three days.

4   Conclusions

Based on the presented results, the following conclusions can be drawn:

- Calcined kaolinite content is linked with compressive strength of LC^3 systems. However, other design parameters such as limestone fineness shown a strong influence in strength and therefore can be managed to achieve the desired performance of the mixture.
- The inclusion of fine limestone in LC^3-50 mixtures proved to be an effective way to increase early-age strength to levels comparable to LC^3-65 formulations.
- Further increase can be achieved by adjusting the alkali content of the binder, with no negative impact observed at later-age strength at the amounts below 1% Na$_2$O$_{EQ}$.

References

1. Schneider, M., Romer, M., Tschudin, M., Bolio, H.: Sustainable cement production—present and future. Cem. Concr. Res. **41**, 642–650 (2011). https://doi.org/10.1016/j.cemconres.2011.03.019
2. Scrivener, K.L., John, V., Gartner, E.M.: Eco-Efficient Cements: Potential, Economically Viable Solutions for a Low-CO_2, Cement-Based Materials Industry. United Nations Environmental Programme (UNEP) (2016)
3. Lothenbach, B., Scrivener, K., Hooton, R.D.: Supplementary cementitious materials. Cem. Concr. Res. **41**, 1244–1256 (2011). https://doi.org/10.1016/j.cemconres.2010.12.001
4. Jain, N.: Effect of nonpozzolanic and pozzolanic mineral admixtures on the hydration behavior of ordinary Portland cement. Constr. Build. Mater. **27**, 39–44 (2012). https://doi.org/10.1016/j.conbuildmat.2011.08.006
5. Karim, E., El-Hadj, K., Abdelkader, B., Rachid, B.: Analysis of mortar long-term strength with supplementary cementitious materials cured at different temperatures. ACI Mater. J. 323–331 (2010)
6. Mehta, P.: Durability—critical issues for the future. Concr. Int. **19**, 69–76 (1997)
7. Avet, F., Scrivener, K.: Investigation of the calcined kaolinite content on the hydration of limestone calcined clay cement (LC^3). Cem. Concr. Res. **107**, 124–135 (2018). https://doi.org/10.1016/j.cemconres.2018.02.016

Evaluation of Age Strengths of Metakaolin Blend Pastes with Varying Fineness of Grind

N. Dumani and J. Mapiravana

Abstract The objective of the study was to evaluate the effect fineness of grind of metakaolin (MK) on age strength development of metakaolin/cement blend pastes. Five batches of metakaolin designated MK1, MK2, MK3, MK4 and MK5 were investigated. The metakaolins were each ground to three different fineness—95% passing 75 µm, 95% passing 53 µm and 95% passing 45 µm. Cement pastes containing 0 and 30% of MK were prepared at a constant water/binder ratio of 0.3. The compressive strengths of the cement pastes were determined at 2, 7, 14 and 28 days. The results indicated that the compressive strengths of the cement pastes with MK were not significantly affected by the fineness of grind of the MK between 75 and 45 µm particle sizes. The results showed that the highest compressive strengths were achieved with cement pastes that contained MK3 and MK5 which had the highest metakaolinite contents. MK1 which had the lowest metakaolinite content but the highest mullite and cristobalite contents exhibited the lowest compressive strength at all ages. Based on this study, it was concluded that the coarser MK can be utilized for partial replacement of OPC reducing grinding costs and ultimately market prize of the MK/cement blends.

Keywords Compressive strength · Fineness · Grinding · Metakaolin · Ordinary portland cement

1   Introduction

Cement, the primary binding ingredient in concrete, is by far considered one of the most important and most produced materials in the world [1]. Ordinary Portland cement (OPC) production is a highly energy-intensive process and accounts for approximately 5–7% of global carbon dioxide (CO_2) emissions [2–6]. Production of one ton of OPC results in about one ton of CO_2 emissions [7]. Globally, the cement sector needs to find a solution to reduce CO_2 emission. One of the effective ways is the reduction of clinker content of OPC, via the use of cement extenders

N. Dumani (✉) · J. Mapiravana
Council for Scientific and Industrial Research Smart Places, Pretoria 0001, South Africa
e-mail: zdumani@csir.co.za

[8, 9]. The most widely used cement extenders are fly ash, ground granulated blast furnace (GGBS) and silica fume. However, the use of these materials is constrained by geographical availability and their quality. Therefore, there is a need to identify alternative cement extenders that are abundantly and ubiquitously available to meet the global demand. One of the most promising alternatives is metakaolin. Kaolinitic clays that are used to produce metakaolin are abundantly and ubiquitously available. In their natural form, kaolinitic clays are valuable materials used for ceramics and also as fillers for paper, paint, polymers and related materials [10–13]. However, when calcined under the right conditions, kaolinitic clays convert to metakaolin [5, 10, 13, 14].

The partial substitution of OPC by metakaolin reduces the energy consumption and CO_2 emissions to the environment [5]. Besides the environmental benefits, the use of metakaolin can also significantly enhance strength and durability of concrete in comparison to OPC alone [14, 15]. Metakaolin exhibits similar performance to that of silica fume and has the capability to replace silica fume as an alternative cement extender [16, 17].

Generally, an increase in fineness has a corresponding influence in the strength development [18]. There are limited studies on the effect of different fineness of metakaolin as a partial replacement in concrete. According to Wild et al. [19], there are three elementary factors influencing the contribution that MK makes to strength when it partially replaces OPC in concrete [19]. These are the filler effect, which is immediate, the acceleration of OPC hydration, which occurs within the first 24 h, and the pozzolanic reaction of metakaolin with calcium hydroxide (CH), which has its maximum effect somewhere between 7 and 14 days of age. Therefore, when dealing with role of filler effect, understanding the influence of fineness of metakaolin is very important.

Boháč et al. [20] studied the compressive strength and flexural strength of mortars containing different fractions of metakaolin. Jet mill classifying system was used to prepare the various fractions of metakaolin. OPC was replaced by 10% of different fractions of metakaolin. The compressive strength and flexural strength of the mortars were determined at 1, 2, 7 and 28 days with water/binder ratio of 0.5. The results showed that compressive strength development of mortars is rather slower for coarse fractions as compared with the control mixture; however, the finest fraction of MK showed higher 28-day compressive strength as compared to the reference sample. The results further showed that all fractions of MK showed higher 28-day flexural strength compared to the reference mixture.

Vizcaíno-Andrés et al. [21] carried out a study to examine the effect of fineness of three different components, i.e. the clinker, calcined clay and limestone on mechanical properties of the resulting blended cement. Ternary blends were produced by blending separately ground clinker, calcined clay, limestone and gypsum in different combinations of coarse and fine components. The blend contained 48.6% clinker, 29% calcined clay, 14.5% limestone and 7.8% gypsum. The compressive strength of the mortars was determined at 3, 7 and 28 days with water/binder ratio of 0.5. The

results showed that the higher fineness of both clinker and calcined clay can significantly enhance the compressive strength of all ages, while limestone only plays a role at early age.

Said-Mansour et al. [22] studied the effect of two different fineness of metakaolin on strength development of cement mortars. OPC was replaced by 10% of different fineness of metakaolin. The compressive strength of the mortars was determined at 1, 7 and 28 days with water/binder ratio of 0.36. The results showed the finer metakaolin gave a faster strength development than the coarse MK and reference mixture of all ages.

The objective of the study was to evaluate effect of the fineness of grind of metakaolin on the age strength development.

2 Experimental Method

Five batches of metakaolin were produced and investigated in this study. The semi-quantitative mineralogies of the materials obtained using XRD are shown in Table 1. These batches of metakaolin differed from each other primarily in the amounts of amorphous (metakaolinite), mullite and cristobalite contents present in each as shown in Table 1. The batches of metakaolin are referred as MK1, MK2, MK3, MK4 and MK5. High-grade kaolinitic clay containing 95% kaolinite, 4% quartz and 1% anatase was used to produce these batches of metakaolin.

The five batches of metakaolin were each ground to three different fineness of grind in order to evaluate the effect of fineness on the age strength development. The three different fineness of grind chosen were 95% passing 75 µm, 95% passing 53 µm and 95% passing 45 µm.

Ordinary Portland cement 52.5 N was used for blending. The OPC/MK blended pastes prepared had MK content of 30% with different degrees of fineness. The pastes were prepared using a water/binder (w/b) ratio of 0.3. A normal OPC paste with no MK was prepared as a reference. A polycarboxylate superplasticizer (SP) was used to produce an appropriate mortar paste consistency.

Table 1 Mineralogical composition of the batches of metakaolin obtained using XRD

Mineralogical composition	MK1	MK2	MK3	MK4	MK5
Amorphous phase	76.5	82.6	90.7	81.0	95
Quartz	4.00	4.00	4.00	4.00	3.02
Anatase	0.71	1.04	1.58	1.10	0.84
Mullite	6.35	3.65	1.40	3.80	0.39
Cristobalite	11.53	6.96	1.49	6.50	–
Rutile	0.94	0.70	0.84	0.80	0.75

The particle size distribution of materials after grinding was obtained by using laser diffraction technology. The Blaine fineness of each of the five batches of metakaolin was also measured after grinding to different degrees of fineness.

Cube specimens of $50 \times 50 \times 50$ mm in dimension were cast in steel moulds and compacted by vibration. The specimens were covered to prevent water loss and left overnight. The specimens were de-moulded and cured in water at ambient temperature. The compressive strengths of the pastes were determined at the ages of 2, 7, 14 and 28 days. For each age, three specimens of each mixture were tested for compressive strength and the mean value of these measurements was reported.

3 Results and Discussion

3.1 Particle Size Distribution and Specific Surface Area

Key parameters D_{10}, D_{50}, D_{90} and D_{95} and Blaine fineness are given in Table 2. The results for the 95% passing 75 µm, 53 µm, 45 µm obtained from physical screening for each MK sample were lower than results obtained using laser diffraction which assumes spherical geometry for the particles as shown in Table 2.

Table 2 Results from the Blaine fineness and particle size distribution of the five batches of metakaolin with different fineness

MK	D_{10} (µm)	D_{50} (µm)	D_{90} (µm)	D_{95} (µm)	Blaine fineness (cm^2/mg)
OPC	5.260	16.18	33.40	41.96	4500
MK1 75 µm	2.863	31.20	79.40	99.04	5750
MK1 53 µm	2.809	27.34	68.69	87.16	6750
MK1 45 µm	2.572	23.83	60.66	77.04	7300
MK2 75 µm	2.533	26.80	78.94	99.71	6750
MK2 53 µm	2.312	23.50	64.66	82.92	7300
MK2 45 µm	2.147	20.90	59.65	76.43	7900
MK3 75 µm	2.328	25.51	82.78	105.95	9150
MK3 53 µm	2.149	22.23	66.15	84.90	10,150
MK3 45 µm	2.004	18.35	58.05	75.06	10,650
MK4 75 µm	2.501	29.84	87.46	109.80	9300
MK4 53 µm	2.206	24.78	70.95	90.72	10,300
MK4 45 µm	1.973	19.76	59.14	75.81	11,500
MK5 75 µm	2.324	25.77	83.16	107.60	8800
MK5 53 µm	2.017	19.56	60.89	78.05	10,250
MK5 45 µm	1.919	17.86	56.88	73.30	10,750
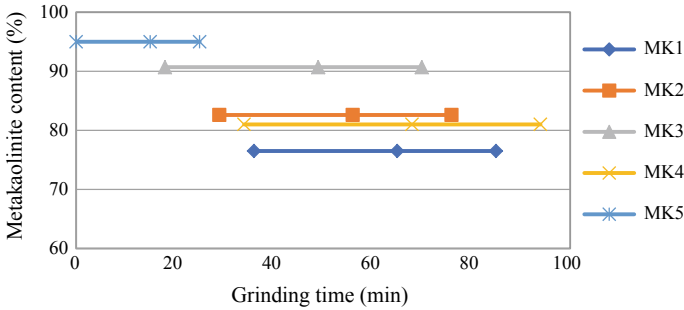
Fig. 1 Relationship between the grinding times required to obtain the target fineness of MK and metakaolinite content
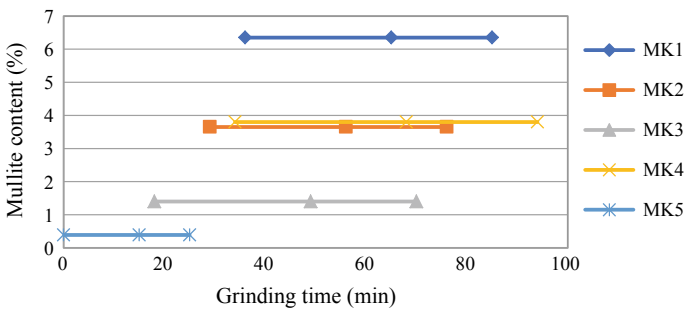
Fig. 2 Relationship between the grinding times required to obtain the target fineness of MK and mullite content

It was observed from Figs. 1 and 2 that the MK with high metakaolinite content and low mullite content was soft and required less grinding time while the MK with low metakaolinite content and high mullite content needed more grinding time.

3.2 Age Strength Development

The role of fineness of MK was examined on compressive strength development after 2, 7, 14 and 28 days. The results of compressive strength of the reference sample (OPC) and OPC/MK blended pastes are shown in Figs. 3, 4, 5, 6 and 7, where each value is the average of three measurements. The compressive strength of the reference samples ranged between 64 and 112 MPa while strengths of OPC/MK pastes ranged between 36 and 135 MPa.

It can be seen in Figs. 3, 4, 5, 6 and 7, increasing the fineness of MK from 75 μm to 53 μm, and finally, 45 μm does not increase the compressive strength development significantly at all ages. The increases in compressive strength were only 1–5%
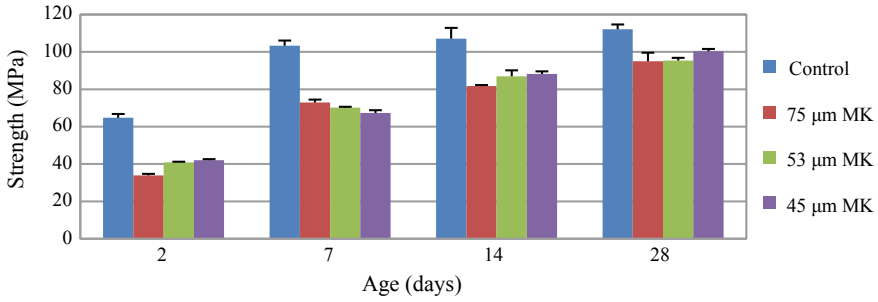
Fig. 3 Compressive strength as a function of age for cement pastes containing MK1 of different fineness
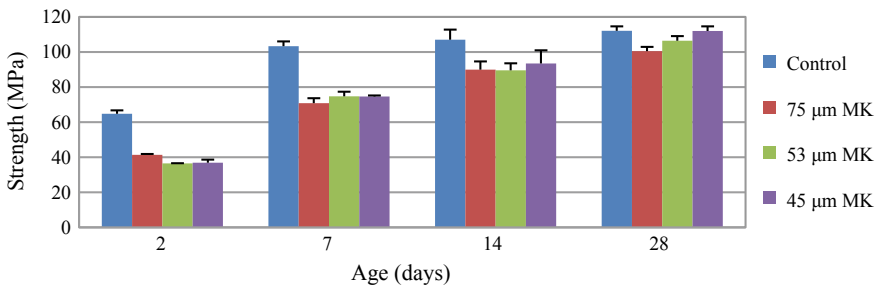
Fig. 4 Compressive strength as a function of age for cement pastes containing MK2 of different fineness
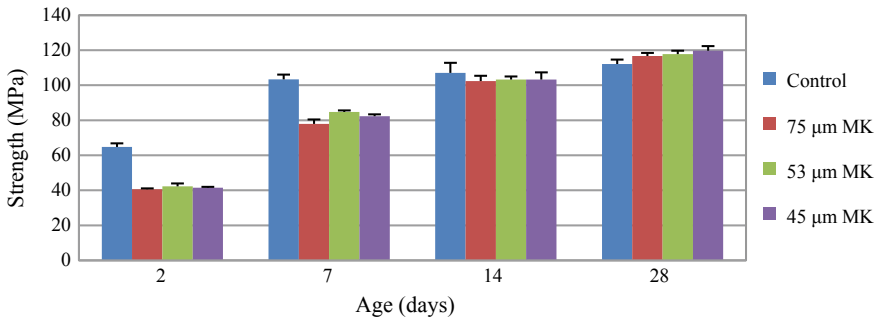
Fig. 5 Compressive strength as a function of age for cement pastes containing MK3 of different fineness

with the exception of MK2 which increased by 11%. These results show that when the particle sizes of MK were between 75 and 45 µm, insignificant variation in compressive strength was observed.

The batches of metakaolin investigated in this study differed in their mineralogical composition as shown in Table 1. At 28 days of curing, it was observed from
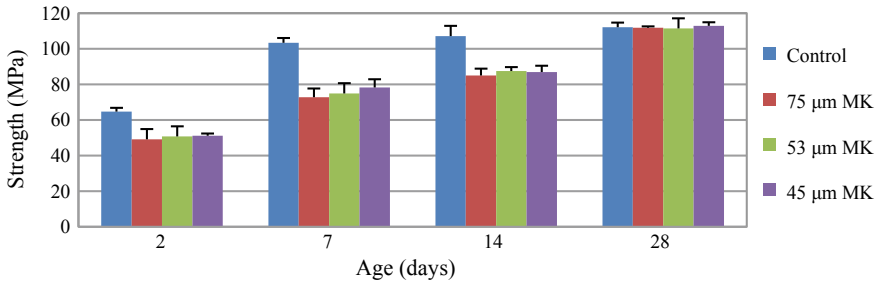
Fig. 6 Compressive strength as a function of age for cement pastes containing MK4 of different fineness
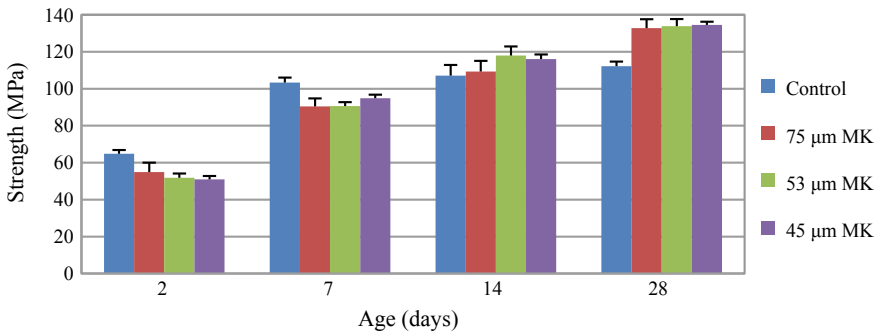
Fig. 7 Compressive strength as a function of age for cement pastes containing MK5 of different fineness

the compressive strength results that the cement pastes containing MK3 and MK5 exhibited higher strengths than the reference specimen due to their higher reactivity. MK5 and MK3 had the highest metakaolinite content, lowest mullite and cristobalite contents lower than MK1, MK2 and MK4. Cement pastes containing MK1 had the lowest metakaolinite content and highest mullite and cristobalite contents and had lower strengths in all cases due to their lower reactivity as compared to other OPC-MK blends. Over-burning of the clay as indicated by the presence of mullite and cristobalite phases caused a decline in pozzolanic reactivity of metakaolin [14, 23].

It follows from the results obtained that there is a possibility to use coarser MK and thus afford more economical grinding. On the market, MK is sold for more than OPC and supplementary cementitious materials such as fly ash and slags [8, 24]. Consequently, the market price of MK would be reduced if the cost of grinding can be neglected during the production of MK. Metakaolinite, mullite and cristobalite contents and reactivity of MK influenced the strength development results of the OPC-MK blended pastes.
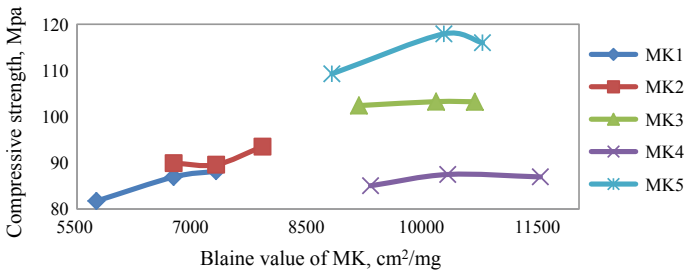
Fig. 8 Relationship between Blaine fineness of MK used in the cement blends and compressive strength of the OPC-MK blend pastes at 14 days
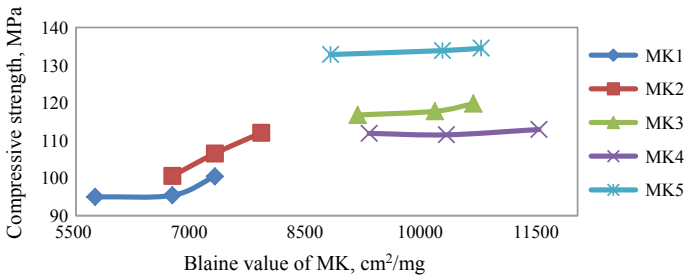
Fig. 9 Relationship between Blaine fineness of MK used in the cement blends and compressive strength of the OPC-MK blend pastes at 28 days

3.3 Grindability and Fineness Effects

The results obtained from the study were further confirmed by considering the relationship between the Blaine fineness of the MK used in the test blends and the compressive strength at 14 and 28 days (Figs. 8 and 9). Increasing the MK Blaine fineness did not necessarily increase the compressive strength of the OPC-MK blended pastes, especially at 14 days.

4 Conclusions

It can be concluded from the results that the fineness of MK between 95% passing 75 µm and 95% passing 45 µm did not significantly influence the compressive strength development of 30% MK/cement blends. The positive effect of the MK fineness on the compressive strength development may be observed for much finer MK. The compressive strength and reactivity of the OPC-MK blended pastes were influenced by their mineralogical contents. MK3 and MK5 that contained the highest metakaolinite but the lowest mullite and cristobalite contents exhibited the highest

grindabilities and compressive strengths. MK1, which had the lowest metakaolinite content but the highest mullite and cristobalite contents, exhibited the lowest grindability and compressive strength. Based on this study, coarser MK can be utilized for partial replacement of OPC reducing grinding costs and ultimately market prize of the MK/cement blends.

References

1. Hendriks, C.A., Worrell, E., de Jager, D., Blok, K., Riemer, P.: Emission Reduction of Greenhouse Gases From the Cement Industry. In: International Energy Agency (IEA), 1–11 (2004)
2. Torgal, F.P., Shasavandi, A., Jalali, S.: Using metakaolin to improve the compressive strength and the durability of fly ash based concrete. In: INVACO2: International Seminar, Innovation & Valorization Civil Engineering & Construction Materials (2011)
3. Juenger, M.C.G., Winnefeld, F., Provis, J.L., Ideker, J.H.: Advances in alternative cementitous binders. Cem. Concr. Res. **41**, 1232–1243 (2011)
4. Ramezanianpour, A.A., Jovein, H.B.: Influence of metakaolin as supplementary cementing material on strength and durability of concretes. Constr. Build. Mater. **30**, 470–479 (2012)
5. Krajči, L., Mojumdar, S.C., Janotka, I., Puertas, F., Palacios, M., Kuliffayová, M.: Performance of composites with metakaolin-blended cements. J. Therm. Anal. Calorim. **119**, 851–863 (2015)
6. Suryawanshi, Y.R., Kadam, A.G., Ghogare, S.S., Ingale, R.G., Patil, P.L.: Experimental study on compressive strength of concrete by using metakaolin. Int. Res. J. Eng. Technol. **2**(2), 235–239 (2015)
7. Rashad, A.M., Zeedan, S.R.: The effect of activator concentration on the residual strength of alkali-activated fly ash pastes subjected to thermal load. Constr. Build. Mater. **25**, 3098–3107 (2011)
8. Palomo, A., Blanco-Varela, M.T., Granizo, M.L., Puertas, F., Vazquez, T., Grutzeck, M.W.: Chemical stability of cementitious materials based on metakaolin. Cem. Concr. Res. **29**, 997–1004 (1999)
9. El-Diadamony, H., Amer, A.A., Sokkary, T.M., El-Hoseny, S.: Hydration and characteristics of metakaolin pozzolanic cement pastes. In: Housing and Building National Research Center, pp. 1–9 (2016) (in Press)
10. Justice, J.M.: Evaluation of metakaolins for use as supplementary cementitious materials. In: MSc Thesis. Georgia Institute of Technology (2005)
11. Huat, O.C.: Performance of concrete containing metakaolin as cement replacement material. In: MSc Thesis. Universiti Teknologi Malaysia (2006)
12. Rashad, A.M.: Metakaolin as cementitious material: history, scours, production and composition—a comprehensive overview. Constr. Build. Mater. **41**, 303–318 (2013)
13. Shan, C.S., Rijuldas, V., Aiswarya, S.: Effects of metakaolin on various properties of concrete—an overview. Int. J. Adv. Technol. Eng. Sci. **4**(1), 237–245 (2016)
14. Sabir, B.B., Wild, S., Bai, J.: Metakaolin and calcined clays as pozzolans for concrete: a review. Cem. Concr. Compos. **23**, 441–454 (2001)
15. Aiswarya, S., Arulraj, P.G., Dilip, C.: A review on use of metakaolin in concrete. Eng. Sci. Technol. Int. J. ESTIJ **3**(3), 592–597 (2013)
16. Dinakar, P., Sahoo, P.K., Sriram, G.: Effect of metakaolin content on the properties of high strength concrete. Int. J. Concr. Struct. Mater. **7**(3), 215–223 (2013)
17. Khatib, J.M., Negim, E.M., Yeligbayeva, G.Z.H.: Strength characteristics of mortar containing high volume metakaolin as cement replacement. Res. Rev. Mater. Sci. Chem. **3**(1), 85–95 (2013)

18. Makhdoom, O., Makhdoom, I.: Effect of components fineness of ground granulated blast furnace slag (GGBFS) on its strength efficiency in roller compact concrete mixes. Asian J. Nat. Appl. Sci. **2**(3), 82–89 (2013)
19. Wild, S., Khatib, J.M., Jones, A.: Relative strength, pozzolanic activity and cement hydration in superplasticised metakaolin concrete. Cem. Concr. Res. **26**(10), 1537–1544 (1996)
20. Boháč, M., Novotný, R., Frajkorová, F., Yadav, R.S., Opravil, T., Palou, M.: Properties of cement pastes with different particle size fractions of metakaolin. World Acad. Sci. Eng. Technol. Int. J. Mater. Metall. Eng. **9**(4), 301–305 (2015)
21. Vizcaíno-Andrés, L.M., Antoni, M.G., Alujas-Diaz, A., Martirena-Hernández, J.F., Scrivener, K.L.: Effect of fineness in clinker-calcined-limestone-limestone cements. Adv. Cem. Res. **27**(9), 546–556 (2015)
22. Said-Mansour, M., Kadri, E., Kenai, S., Ghrici, M.: Influence of fineness of active addition concrete equivalent. In: International Conference on Construction and Building Technology, pp. 539–547 (2008)
23. Teklay, A.: CFD modelling and experimental testing of thermal calcination of kaolinite rich clay particles: an effort towards green concrete. In: PhD Thesis. Aalborg University, Denmark (2015)
24. Velmelková, E., Pavlíková, M., Keppert, M., Keršner, Z., Rovnaníková, P., Ondráček, M., Sedlmajer, M., Černý, R.: High performance concrete with Czech metakaolin: experimental analysis of strength, toughness and durability characteristics. Constr. Build. Mater. **24**, 1404–1411 (2010)

The Effect of Composition of Calcined Clays and Fly Ash on Their Dissolution Behavior in Alkaline Medium and Compressive Strength of Mortars

Satya Medepalli [ID]**, Anuj Parashar and Shashank Bishnoi**

Abstract There is a wide scope for use of calcined clays in cement as kaolinitic clays are available in huge quantities around the world. Similarly, fly ashes are also available in substantial quantities, though the quality of fly ash is still a major concern. One is used in large quantities, and the other has the potential and the resources to be utilized. The difference in their physical and chemical properties and their behavior in alkaline medium are studied in this work. One class F fly ash and one calcined clay with 60% kaolinite are selected for this study. The materials are characterized using X-ray fluorescence (XRF), X-ray diffraction (XRD) and scanning electron microscopy (SEM) to find chemical composition, mineral composition and morphology. The difference in their solubility behavior in alkaline medium was determined using ICP-MS to find the dissolution of silica, alumina and calcium ions in NaOH solution at 20 °C. Though the hydration behavior of calcined clays and fly ash in cement systems are very distinct, their solubility behavior was found to be similar. Calcined clays exhibited higher dissolution of Si and Al ions in the solution compared to fly ash. The effect of dissolution of Si and Al on the compressive strength of mortars is also studied. Strength activity index of mortars increases quickly starting from day 1 for calcined clay and reaches a maximum at 7 days, while for fly ash it increases steadily and reaches a maximum at 28 days.

Keywords Calcined clay · Fly ash · ICP-MS · XRD · XRF · SEM

1 Introduction

The use of supplementary cementitious materials (SCMs) to reduce the usage of clinker by replacing a portion of cement is an effective way to reduce the CO_2 footprint. SCMs contain a significant quantity of amorphous silica and alumina that can react with calcium hydroxide in the hydrating cement to form secondary cementitious products [1]. Industrial by-products such as fly ash, slag and silica fume have been used as SCMs from many decades; however, the quantity of some of these SCMs such

S. Medepalli (✉) · A. Parashar · S. Bishnoi
Civil Engineering Department, Indian Institute of Technology Delhi (IIT Delhi), Hauz Khas, New Delhi 110016, India

349

as slag and silica fume is not sufficient to replace a significant quantity of clinker. There is an abundant supply of fly ashes through the generation of coal-fired power plants, as coal is a major fuel source in many countries [2, 3]. However, there is a huge variation in the quality of fly ash generated posing a serious challenge in its utilization for high-volume replacements in cement [4]. Calcined clay is thought to be the next best alternative to fly ash, as it is available in huge quantities all over the world.

The metakaolin as a pozzolan for cement at lower replacements has been used for a long time. A lot of research is being carried out in the last few decade on the use of calcined clays to increase the replacement levels of clinker in cement [5–7]. Recent works include its usage to replace nearly 50% of clinker through the introduction of a new type of cement known as limestone calcined clay cements [8–11].

Both fly ashes and kaolinitic clays are available in substantial quantities and can be used effectively in high-volume replacement of clinkers. Even though, there is a huge availability of fly ash, its utilization is limited due to the quality of fly ash. Although, calcined clay has a great potential, it is still not being used on a large scale for partial replacement of cement. The demand for cement is expected to increase in the coming decades, especially for developing infrastructure in Third World countries. Both fly ash and calcined clay have the potential to replace high volumes of clinker in cement and reduce the CO_2 footprint due to clinker production. To increase the utilization of these SCMs, it is important to understand their role in cement systems and how they contribute to strength development. Their role as a pozzolan in cement systems depends on the solubility of silica and alumina ions in alkaline medium which is prevalent in the pore solution of cement systems. The current study is therefore focussed on finding out the dissolution of these ions from SCMs and their contribution to the strength development in cement systems.

2 Materials and Methods

2.1 Materials and Mixes

One fly ash and one calcined clay are used in this study. The fly ash was procured from a thermal power plants near Jamshedpur in India. Clay sourced from Rajasthan with a kaolinite content of 60% was calcined in a rotary kiln.

The oxide composition of the SCMs was analyzed using X-ray fluorescence and is listed in Table 1. Fly ash can be categorized as ASTM class F as calcium content is less than 10% [12]. Both fly ash and calcined clay have a major portion of silica and alumina content with minor phases of iron oxide, calcium oxide and alkalis. Similarity in the chemical composition makes it difficult to distinguish the nature of these SCMs based on the oxide content. Calcined clays, however, has slightly higher alumina content than the fly ash.

Table 1 Oxides composition of raw materials

SCM	SiO_2	Al_2O_3	Fe_2O_3	CaO	MgO	Na_2O	K_2O	SO_3	Cl
Fly ash	61.20	29.20	3.32	1.37	0.26	0.20	1.26	0.17	0.03
Calcined clay	57.70	38.14	4.00	0.09	0.02	0.18	0.17	0.10	–
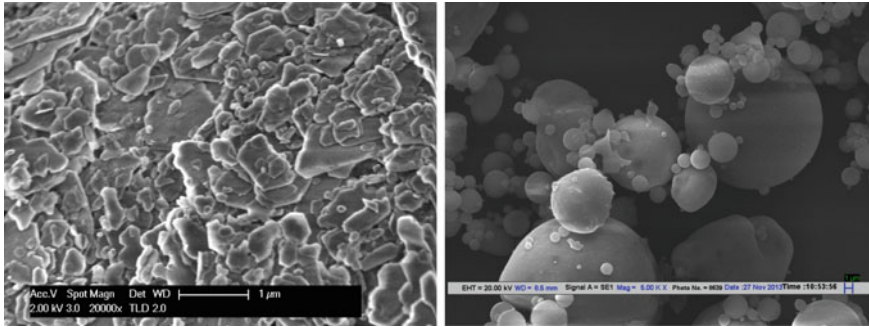
Fig. 1 SEM image of calcined clay (left) and fly ash (right)

SEM images of these two SCMs are shown in Fig. 1. Even though, both calcined clay and fly ash have amorphous silicates and aluminates, the morphology of these two SCMs is quite different. It can be observed that clay has a sheet structure while fly ash particles are mostly spherical. Such different morphologies affect the rheology of concrete while using these two SCMs. As fly ashes are spherical, it reduces the water demand in concrete due to its ball-bearing effect while the calcined clay has an opposite effect [13].

2.2 Experimental Methods

Inductively coupled plasma technique was used to find the ionic concentrations of these elements in NaOH solution. As no standardized method was established to study fly ash using dissolution experiments, the procedure followed by Durdzinski et al. (2015) to study dissolution of synthetic glasses is followed in this work. 1 g SCM is added to 1 L of 0.14 M NaOH solution. The test was conducted at 20 °C. The solution was not disturbed by stirring after adding the SCM to avoid any abrasion to the sample. 5 ml of the solution was taken out at designated time intervals to measure the dissolution of ions into the solution. NaOH solution of a known molarity was replenished by the same amount after each sampling to maintain the pH of the solution.

7.06 cm cubes were cast for compressive strength tests on mortar samples using binder-to-sand ratio of 1:3. After keeping for 1 day in moist environment, the cubes are demolded for curing in a temperature-controlled water bath maintained at 27 °C till testing. Testing was carried out at 1, 3, 7 and 28 days. A water-to-binder ratio of 0.4 was used for casting mortar. Strength activity index was calculated as the strength of the SCM blended mortar to the strength of OPC at corresponding ages.

Fig. 2 Dissolution of Si, Al and Ca in NaOH solution for fly ash at 20 °C
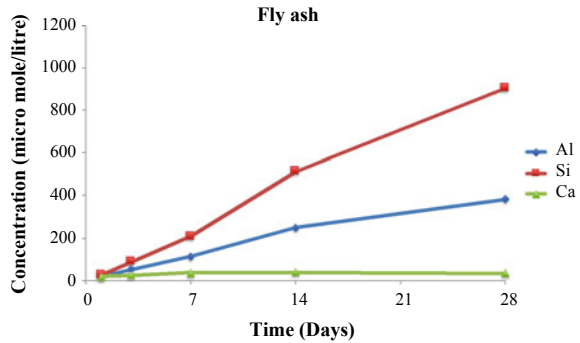
Fig. 3 Dissolution of Si, Al and Ca in NaOH solution for calcined clay at 20 °C
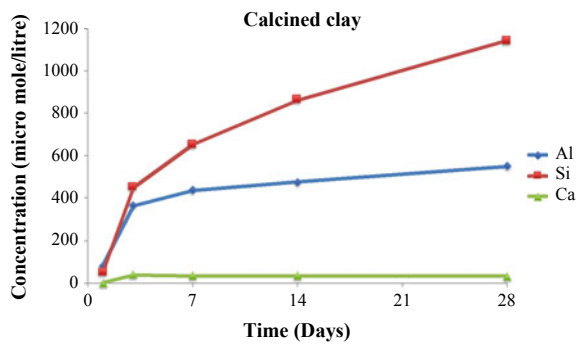
3 Results and Discussion

3.1 Dissolution of Ions

The dissolution of silica, alumina and calcium ions in NaOH solution for fly ash and calcined clay is shown in Figs. 2 and 3. Both these SCMs have low calcium content and as such there is no dissolution of calcium ions into the solution. However, alumina and silica concentration in the solution increases from day 1. Silica concentration in the solution is higher than alumina at all ages in both the SCMs. Alumina concentration steadily increases for fly ash till 28 days, while in the case of calcined clays it rapidly increases till 7 days, and thereafter, its dissolution gets slow.

3.2 Compressive Strength

The strength activity index of mortars for fly ash and calcined clay is plotted in Fig. 4. It can be observed that the strength activity index of calcined clays quickly increases reaching nearly 90% at 1 day and attaining a maximum value at 7 days.

Fig. 4 Strength activity
index of mortar for fly ash
and calcined clay
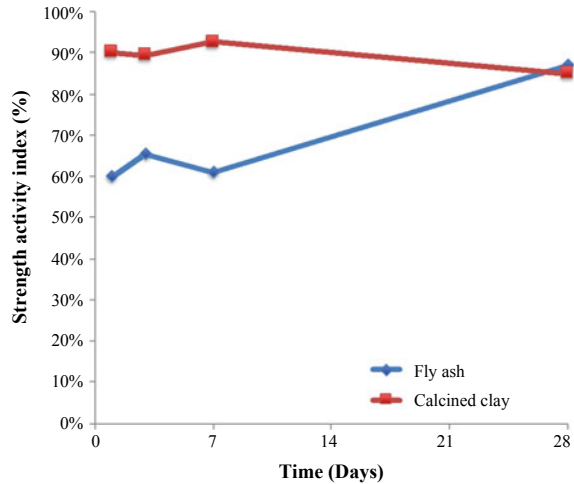
These results complement the results from the dissolution experiment, wherein Si
and Al ions dissolved rapidly with the first 7 days in case of calcined clays. The
strength activity index of fly ashes steadily increases from 60% at 1 day to 90% at
the age of 28 days similar to its dissolution behavior.

4 Conclusions

This study tried to compare the properties of fly ash and calcined clay based on their
dissolution behavior in alkaline medium. The following conclusions are made.

- Although, both fly ash and calcined clay exhibited similar oxide composition, their
  behavior and reactivity are completely different.
- The morphology obtained from SEM images clearly suggests that while fly ash
  has spherical glassy particles, kaolinitic clays have sheet like structure.
- Both calcined clay and fly ash have low calcium content and as such their behavior
  is purely pozzolanic and are activated in alkaline medium that is prevalent in the
  pore solution of cement paste.
- Dissolution tests in alkaline medium show that Si and Al ions dissolve rapidly in
  calcined clays attaining a substantial value at the end of 7 days. Fly ashes, however,
  dissolve slowly attaining a maximum value at 28 days.
- Strength activity index of calcined clays and fly ashes complements the results
  obtained from dissolution tests. It can be observed that strength activity index of
  calcined clays reaches 90% within 1 day and a maximum value at 7 days, while
  fly ashes attain a maximum at 28 days.

References

1. Lothenbach, B., Scrivener, K., Hooton, R.D.: Supplementary cementitious materials. Cem. Concr. Res. **41**, 1244–1256 (2011)
2. Shafiee, S., Topal, E.: When will fossil fuel reserves be diminished? Energy Policy **37**, 181–189 (2009). https://doi.org/10.1016/j.enpol.2008.08.016
3. Central Electrical Authority: Report on fly ash generation at coal/lignite based thermal power stations and its utilization in the country for the year 2017–18 (2018)
4. Kaur, A., Bishnoi, S., Bhattacharjee, B.: Characteristics of fly ashes in India for use in cement and concrete. Adv. Cem. Res. **618**, 1–11 (2017)
5. Murat, M.: Hydration reaction and hardening of calcined clays and related minerals. I. Preliminary investigation on metakaolinite. Cem. Concr. Res. **13**, 259–266 (1983). https://doi.org/10.1016/0008-8846(83)90109-6
6. Sabir, B., Wild, S., Bai, J.: Metakaolin and calcined clays as pozzolans for concrete: a review. Cem. Concr. Compos. **23**, 441–454 (2001). https://doi.org/10.1016/S0958-9465(00)00092-5
7. Ambroise, J., Murat, M., Péra, J.: Hydration reaction and hardening of calcined clays and related minerals V. Extension of the research and general conclusions. Cem. Concr. Res. (1985). https://doi.org/10.1016/0008-8846(85)90037-7
8. Scrivener, K.L.: Options for the future of cement. Indian Concr. J. **88**, 11–21 (2014)
9. Medepalli, S., Shah, V., Bishnoi, S.: Production of lab scale limestone calcined clay cements using low grade limestone. 7th Int. Conf. Sustain Built. Environ. (2016)
10. Antoni, M., Rossen, J., Martirena, F., Scrivener, K.: Cement substitution by a combination of metakaolin and limestone. Cem. Concr. Res. **42**, 1579–1589 (2012). https://doi.org/10.1016/j.cemconres.2012.09.006
11. Emmanuel, A.C., Haldar, P., Bishnoi, Shashank, Maity, S.: Second pilot production of limestone calcined clay cement (LC 3) in India: The experience. Indian Concr. J. **90**, 57–64 (2016)
12. ASTM C618: Standard specification for coal fly ash and raw or calcined natural pozzolan for use in concrete. ASTM International, West Conshohocken, USA (2012)
13. Ferreiro, S., Herfort, D., Damtoft, J.S.: Effect of raw clay type, fineness, water-to-cement ratio and fly ash addition on workability and strength performance of calcined clay—limestone portland cements. Cem. Concr. Res. **101**, 1–12 (2017)
14. Durdzinski, P.T., Snellings, R., Dunant, C.F., et al.: Fly ash as an assemblage of model Ca–Mg–Na-aluminosilicate glasses. Cem. Concr. Res. **78**, 263–272 (2015)

The Effect of Calcite and Gibbsite Impurities in Calcined Clay on Its Reactivity

Franco Zunino and Karen L. Scrivener

Abstract This study explored the effect of calcite (calcium carbonate) and gibbsite (aluminum hydroxide) impurities on the reactivity of a model calcined clay. Pure metakaolin was combined with calcite and gibbsite to prepare model raw clays, which were then calcined in a furnace at 800 °C for 1 h. The R^3 test was used to assess reactivity of the calcined materials, and physical and mineralogical characterizations were performed. It was observed that calcite forms a layer of granular deposit over kaolinite particles, reducing its specific surface area. However, the impact on reactivity is relatively minor if the effect of dilution is accounted. In the case of gibbsite, it completely dehydrates upon calcination and transforms into inactive crystalline alumina. The effect of its presence was compared to quartz, and no significant differences were found. Thus, natural clays with calcite and gibbsite impurities are suitable for LC^3 applications.

Keywords Calcination · Surface area · Isothermal calorimetry

1 Introduction

Supplementary cementitious materials (SCMs) are widely used in blended cements to reduce the carbon emissions associated with the production of the material [1]. Clays are unique among the supplementary cementitious materials because of their worldwide availability [2]. The three clay types of major abundance are kaolinite, illite and montmorillonite [3]. Heat treatment of kaolinitic clays between 600 and 800 °C leads to the dehydroxylation of its crystalline structure to give a state of more structural disorder known as metakaolin [4].

In some regions, clays are naturally combined with limestone in the quarries. Kaolinite is dehydroxylated between 600 and 800 °C [5]. While there is clear understanding of the process governing the transformation and recrystallization of the system kaolinite–calcite at temperatures above 1000 °C, there is lack of systematic

F. Zunino (✉) · K. L. Scrivener
Laboratory of Construction Materials, IMX, École Polytechnique Fédérale de Lausanne (EPFL), 1015 Lausanne, Switzerland
e-mail: franco.zunino@epfl.ch

357

studies exploring these interactions at temperatures of 800 °C or lower, which are of interest for metakaolin production.

Another common impurity found in kaolinitic clays is forms of aluminum hydroxide, in particular gibbsite. Gibbsite will dehydrate upon heating and transform into different forms of Al_2O_3 until the most stable mineral corundum is crystallized at high temperature [6]. As this transformation occurs in the same range of temperatures required for the dehydroxylation of kaolinite and consequent production of metakaolin, there is a question regarding the possible interference that gibbsite might have in the formation of metakaolin. Furthermore, there is an open question regarding the possible competition during dissolution between the dehydrated gibbsite phase and metakaolin.

2 Materials and Methods

An experimental design aimed to assess the effect of 2 and 8% calcite impurities on calcined clay reactivity was designed. The calcination temperatures were established at 600 and 800 °C, above and below the decarbonation threshold of calcite. Furthermore, the effect of residence time was explored at a low (20 min) and high (60 min) level.

Raw clay (kaolinite) content of 71% as measured by thermogravimetric analysis (TGA) and Durcal 5 calcium carbonate (calcite) were used. 250 g of material (uncalcined clay and calcite) were weighted in individual 1 L plastic containers for each experimental point. Powders were blended together using a turbular blender for 20 min. Homogeneity of the obtained powder samples was checked with TGA on selected samples. Calcination was carried out on 300 mL alumina crucibles. Calcined samples were then stored in sealed containers until analysis.

For the assessment of the gibbsite effect, pure $Al(OH)_3$, which was confirmed to correspond to gibbsite as shown in Fig. 1, was intermixed with pure metakaolin (MK), with a content of reactive material of 95%. The minerals were combined in
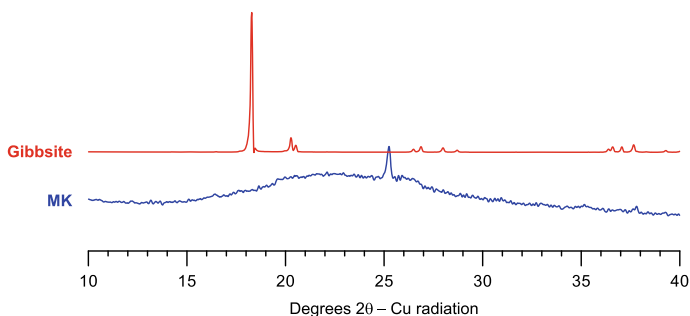
Fig. 1 XRD pattern of the pure gibbsite and metakaolin used in this study

proportions of 100:1, 50:50 and 25:75 MK to gibbsite ratios. In addition, in the 50:50 point, the effect of gibbsite was compared to one of the quartz. The blends were homogenized in the same manner as the systems containing calcite. Afterward, calcination was performed at 800 °C for 1 h.

Isothermal calorimetry was used to assess the pozzolanic reactivity of calcined clays. For this purposes, the R^3 test proposed by Avet et al. [7] was selected due to its reliability and ease of interpretation for calcined clay benchmarking purposes. The test considering pozzolanic and interaction with calcium carbonate (simulated LC^3-50) was selected. In this procedure, calcined clay is mixed with portlandite, calcium carbonate, potassium sulfate, potassium hydroxide and water at 40 °C and put into glass ampoules inside the calorimeter under the same temperature conditions.

The R^3 test procedure was applied to both calcined clays with calcite and gibbsite impurities to assess their effects on reactivity.

3 Results and Discussion

3.1 The Effect of Calcite Impurities on Calcined Clay Reactivity

Isothermal calorimetry tests were performed over the obtained materials using the R^3 method, in order to assess and compare the reactivity of the different calcined clays in a quick and reliable manner. As a general trend, the highest increase in reactivity is observed in all of the materials when increasing the calcination temperature from 600 to 800 °C. Figure 2 shows the heat flow (left) and total heat (right) plots for materials calcined at 600 and 800 °C, with low (2%) and high (8%) calcite contents, all of them calcined for low residence time (20 min).
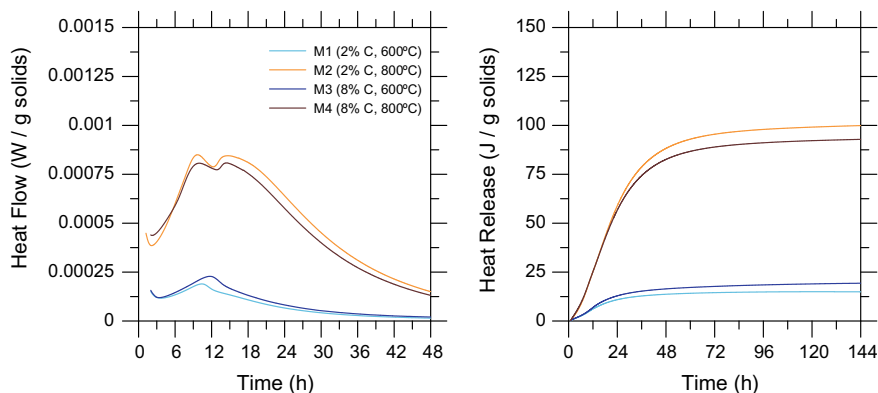
Fig. 2 Isothermal calorimetry results for materials calcined for 20 min, at high and low temperature and with different initial calcite content

At 600 °C, there is little impact of the calcite, and increased contents produce a slight increase in reactivity. At 800 °C, higher contents of calcite seem to have a negative effect on clay reactivity; however, the difference between 2 and 8% initial calcite materials is small (<10 J/g solids at 6 days of hydration).

Figure 3 shows the heat flow (left) and total heat (right) plots for materials calcined at 600 and 800 °C, with low (2%) and high (8%) calcite contents, all of them calcined for high residence time (60 min).

At 600 °C and after increasing the residence time to 60 min, the effect is similar to the one observed at 800 °C and low residence time (20 min). Reaction kinetics does not seem to be significantly affected during the first 24 h of hydration. At 800 °C, the difference in heat evolved at 6 days (144 h) is more significant. Hydration kinetics seems also to be affected (sample M8 exhibits a slight acceleration during the first 12 h), suggesting that the nature of the metakaolin may have changed.

Specific surface area measurements were performed on the calcined clay samples to try to elucidate the origin of the observed decrease in reactivity. It was seen that in the materials with calcite, the specific surface area after calcination was lower as compared to the materials without the impurity, even considering the originally different surface of calcite and raw clay itself. SEM micrographs of the calcined clay with 8% calcite are allowed to observe the formation of a granular deposit on top of the kaolinite particles, which may explain the measured decrease in surface and reactivity (Fig. 4).

3.2　The Effect of Gibbsite Impurities on Calcined Clay Reactivity

Figure 5 shows the results for the R^3 test of the different mixtures of metakaolin
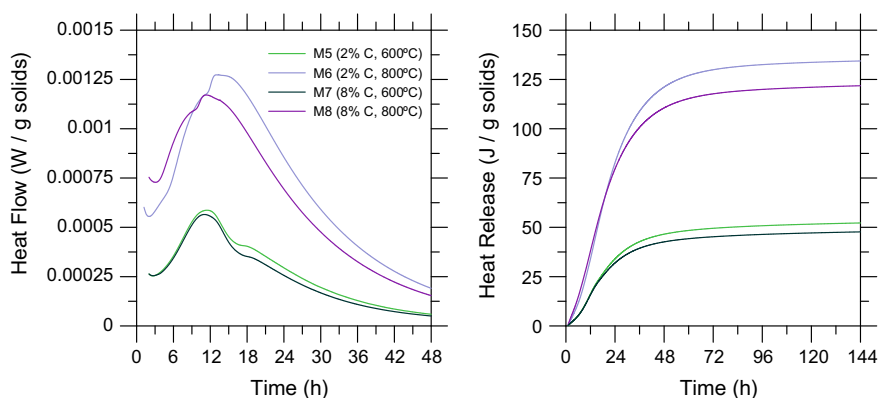
Fig. 3 Isothermal calorimetry results for materials calcined for 60 min, at high and low temperature and with different initial calcite content

Fig. 4 SEM micrograph of kaolinite particle calcined with 8% calcite, showing the deposition of a granular residue in part of its surface
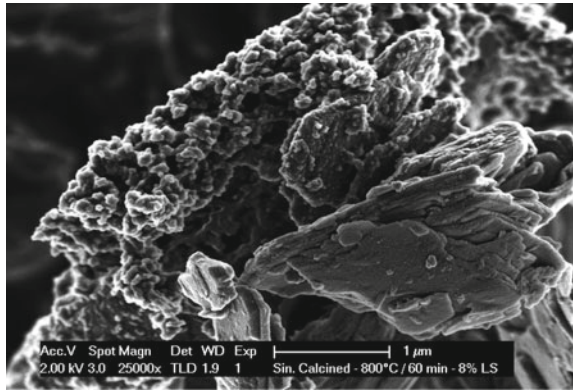
Fig. 5 Reactivity of metakaolin with calcined gibbsite impurities measured using the R^3 test
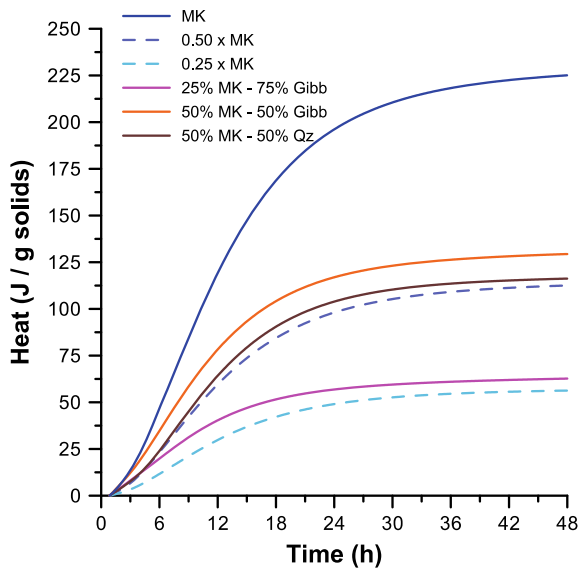
and calcined gibbsite, and the comparison system blended with quartz. As observed, the systems containing calcined gibbsite (obtained by thermal treatment in the same conditions normally used for metakaolin production) show a decrease in reactivity, but not below what would be expected for the level of dilution of metakaolin. This shows that, while calcined gibbsite does not appear to be a reactive phase, it certainly does not interfere with the normal dissolution of metakaolin.

The system with quartz provides another reference standard to benchmark the behavior of the systems with initial gibbsite impurities. As seen, the heat release is higher for the system with gibbsite, which can be attributed to the higher surface area of the material used in comparison with quartz.

4 Conclusions

- Based on the presented results, the following conclusions can be drawn.
- Calcite impurities in clay form a granular deposit on the surface of kaolinite which reduces surface area and slightly impact reactivity. However, the effect is minor, and therefore, calcite contaminated clays can be used as SCMs if the content of impurities is in the range explored in this study.
- The presence of gibbsite in raw clays does not interfere with the normal reactivity of the metakaolin available. Therefore, these clays are also suitable for production of metakaolin and use as SCM.

References

1. Lothenbach, B., Scrivener, K., Hooton, R.D.: Supplementary cementitious materials. Cem. Concr. Res. **41**, 1244–1256 (2011). https://doi.org/10.1016/j.cemconres.2010.12.001
2. Fernandez Lopez, R.: Calcined Clayey Soils as a Potential Replacement for Cement in Developing Countries. École Polytechnique Fédérale de Lausanne (2009). https://doi.org/10.5075/epfl-thesis-4302
3. Fernandez, R., Martirena, F., Scrivener, K.L.: The origin of the pozzolanic activity of calcined clay minerals: a comparison between kaolinite, illite and montmorillonite. Cem. Concr. Res. **41**, 113–122 (2011). https://doi.org/10.1016/j.cemconres.2010.09.013
4. Antoni, M.: Investigation of Cement Substitution by Combined Addition of Calcined Clays and Limestone. École Polytechnique Fédérale de Lausanne (2011)
5. Antoni, M., Rossen, J., Martirena, F., Scrivener, K.: Cement substitution by a combination of metakaolin and limestone. Cem. Concr. Res. **42**, 1579–1589 (2012). https://doi.org/10.1016/j.cemconres.2012.09.006
6. Ingram-Jones, V.J., Slade, R.C.T., Davies, T.W., Southern, J.C., Salvador, S.: Dehydroxylation sequences of gibbsite and boehmite: Study of differences between soak and flash calcination and of particle-size effects. J. Mater. Chem. **6**, 73–79 (1996). https://doi.org/10.1039/jm9960600073
7. Avet, F., Snellings, R., Alujas Diaz, A., Ben Haha, M., Scrivener, K.: Development of a new rapid, relevant and reliable (R^3) test method to evaluate the pozzolanic reactivity of calcined kaolinitic clays. Cem. Concr. Res. **85**, 1–11 (2016). https://doi.org/10.1016/j.cemconres.2016.02.015

High Performance Illitic Clay-Based Geopolymer: Influence of the Mechanochemical Activation Duration on the Strength Development

Baptiste Luzu, Myriam Duc, Assia Djerbi and Laurent Gautron

Abstract Demonstrate the feasibility of an illitic clay-based geopolymer is the purpose of this study. If the thermal activation of standard precursors such as kaolin is a well-known process, the reactivity of illitic precursors required the combination of thermal and mechanochemical activation. The structural changes of the precursor material submitted to various grinding durations were followed by X-ray diffraction (XRD), and Fourier transform infrared spectroscopy (FTIR) and the amorphous phase rate calculated from XRD analyses were correlated with this parameter as well as the compressive strength (Rc) of the manufactured geopolymers. Mechanical properties increased with the grinding time and the decrease of L/S ratio of the geopolymer paste. Illitic clay-based geopolymers may reach high performance as demonstrated with a Rc at 28 days reaching 102 MPa. Finally, the relations between the amorphization rate and the compressive strength of the geopolymers have been highlighted.

Keywords Illitic clay-based geopolymer · Mechanochemical activation · Amorphous rate · Compressive strength

1 Introduction

In order to develop new alternatives to ordinary Portland cement (OPC) with low CO_2 emission and optimized cost, the research works during the last ten years focused on geopolymers which are well-known inorganic binders produced by the reaction between an aluminosilicate raw material and an alkaline solution. In the alkaline environment, the aluminosilicate material is quickly dissolved and monomers are

B. Luzu (✉) · A. Djerbi · L. Gautron
Laboratory Geomaterials and Environment, University Paris-Est Marne la Vallée, 77420 Champs sur Marne, France
e-mail: baptiste.luzu@iffstar.fr

B. Luzu
University Paris-Est, IFSTTAR, MAST/FM^{2}D, 77420 Champs-sur-Marne, France

M. Duc
University Paris-Est, IFSTTAR, GERS/SRO, 77420 Champs-sur-Marne, France

formed (silicate and aluminate species) before the polycondensation reactions at the origin of the formation of a tri-dimensional aluminosilicate network [1].

On one hand, many studies dealt with alkali activated materials like ground granulated blast furnace slag (GGBFS), fly ash-based geopolymers and metakaolin-based geopolymers characterized by simple implementation because of their easy dehydroxylation [2]. However, several clay minerals could be used as aluminosilicate precursors like illite. Indeed, illite (close to muscovite) is one of the most abundant clayey minerals of the earth's crust, and its chemical composition is (K, H_30) (Al, Mg, Fe)$_2$ (Si, Al)$_4$ O$_{10}$ [(OH)$_2$, (H$_2$O)]. Activation of illitic clay and geopolymerization with such precursor were the purpose of few papers [3, 4], but the performance of the manufactured geopolymers remained far from one of the metakaolin-based geopolymers because of the difficult dehydroxylation of illite [2].

On the other hand, the metakaolin reactivity was improved by coupling a mechanochemical activation (dry grinding) with a thermal one, in order to reach the most advanced degradation of kaolinite structure. The mechanochemical activation leads finally to the decrease of the activation temperature [5, 6].

This study proposes to improve the reactivity of illitic raw materials by coupling thermal and mechanochemical activations. The aim is to make amorphous the precursor and to remove OH from its structure. The structural changes after the precursor treatment are studied through both XRD and FTIR analysis, and several geopolymerization tests have been realized in order to confirm the feasibility of an illitic clay-based geopolymer with high mechanical performances.

2 Materials and Methods

2.1 Materials

The natural Romainville green clay (labeled AV) from parisian basin was used to synthesize illite-based geopolymer. This material is partially composed of illite/muscovite whose content may vary naturally in the clay-rich geological formation. The tested material contained around 53 wt% of such clay assemblage. This material is considered as a waste for engineering companies working on the Paris Express Trainline construction sites and several thousand tons of these wastes will be produced in the next five years.

The sodium silicate solution used for geopolymerization is realized from a sodium silicate solution (Na$_2$O/SiO$_2$ = 0.31) supplied by VWR. The molar ratio was adjusted with added sodium hydroxide pellets (VWR, 97% purity) in order to obtain a final molar ratio Na$_2$O/SiO$_2$ = 0.54.

2.2 Characterization of the Precursor

The precursor material was characterized at different steps of the activation process by thermogravimetric analysis (TGA/DTA), X-ray diffraction (XRD), Fourier transform infrared spectroscopy (FTIR) and inductively coupled plasma–optical emission spectrometry (ICP-OES). The TGA/DTA analysis has been carried out with a NETZSCH STA 409 CD thermobalance under classical conditions and the XRD patterns with a Bruker D8 Advance X-ray diffractometer (*type* $\theta - \theta$). The EVA software coupled with the ICDD pdf-2 database enables the identification of the major phases present in the material. The quantitation of minerals was realized using the Rietveld method using Topas 4.2 software. For the quantification of amorphous phase, the internal method required the 15 wt% corundum addition to the ground tested sample. The background has been described with a Chebyshev polynomial of the fifth-order accompanied with the term 1/X. The FTIR spectrometer was a Nicolet 380 FTIR spectrometer from Thermo Scientific. The resulting spectra were analyzed with the OMNIC software from Nicolet. We used the device in the middle infrared to visualize the absorption bands from 400 to 4000 cm^{-1}.

2.3 The Protocol of Precursor Activation

The precursor material was calcined during 2 h at 850 °C in a Nabertherm LE 114/11/B150 muffle furnace. This optimized calcination temperature was obtained from the TGA/DTA analysis. Such temperature is positioned between 820 °C (temperature corresponding to the end of the dehydroxylation of the clayey minerals) and 870 °C (corresponding to the beginning of the peak of structural reorganization of illite until the appearance of mullite). The dehydroxylation corresponds to the diffusion of the crystalline hydroxyl OH groups belonging initially to the clay structure, followed by a progressive elimination under H$_2$O form when the calcination time increases [7].

The thermal activation has been coupled with a mechanochemical activation. A high energetic planetary mill PM100 from Retsch has been used. Tungsten carbide crucible and balls were used for grinding. The balls have a diameter of 30 mm and a density equal to 14.8 g cm^{-1}, while the quantity of material introduced into the crucible is very small (around 100 g of illitic clay). The speed rotation of grinder was 400 rpm, the ball/powder mass ratio was 7.7, the grinding duration varies from 30 to 300 min. The materials obtained at the end of the activation processes are called PX, where P indicates the planetary milling and X corresponds to the grinding time in minutes.

2.4   The Process of Geopolymer Manufacture

The alkaline solution ($Na_2O/SiO_2 = 0.54$) was mixed mechanically during 3.5 min in a pale mixer with the activated precursor by respecting a liquid/solid mass ratio (L/S) from 0.5 to 1.0. Geopolymer pastes were casted in 33 mm per 50 mm cylinders before a 3 min vibration on a vibrating table in order to remove air bubbles. Formulations were done for 3 to 9 specimens for the estimation of test repeatability. After this step, the samples were placed successively in an oven at 40 °C during 24 h and at 70 °C during 24 h more. After curing the specimens were unmolded and stored in hermetically sealed plastic bags to prevent micro-cracking due to low moisture content until they were tested in compression.

2.5   Geopolymers Characterization

A Controlab automatic press was used for mechanical test conducted with a constant charging speed of 2400 N/s. The compressive strength values (Rc in MPa) presented in the results section are the average values from three test pieces formulated under the same conditions. The compressive strength (Rc) of the samples was measured at 2, 7 and 28 days after the end of the manufacturing.

3   Results and Discussion

3.1   Characterization of Raw Material and Thermally Activated Precursor

The chemical analysis of the precursor before and after thermal activation shows in Table 1 high SiO_2/Al_2O_3 mass ratios, equal to 3.7 and 3.5 for AV and AV850, respectively. The large quantities of K_2O and Fe_2O_3 confirm the presence of illite and the low amounts of CaO and MgO indicate the minor presence of calcite and dolomite.

The XRD quantification in Table 2 confirms the presence of illite + muscovite (I + M) in high quantity. The other clay minerals are montmorillonite (Mtm) and chlorite (Ch) while in the un-clayey minerals a large quantity of quartz and a smaller amount of feldspar, calcite, diopside and hematite can be observed.

Once calcined at 850 °C, the amount of illite + muscovite decreases from 53 to 40 wt% but does not disappear while the quantity of amorphous phase increases from about 0 to 20 wt%. So, the clay calcination at 850 °C is not enough for complete amorphization of illite/muscovite clay mineral. It can be noted that the intensity of the main peaks of the carbonate phases (calcite and dolomite) decrease considerably

Table 1 Chemical composition of clayey precursors before and after activation

Precursor	Chemical composition (wt%)							
	SiO$_2$	Al$_2$O$_3$	CaO	Fe$_2$O$_3$	K$_2$O	Na$_2$O	MgO	TiO$_2$	LOI
AV	57.5	15.6	5.8	5.5	3.8	0.1	2.3	0.6	8.8
AV850	62.4	17.7	6.5	6.0	3.6	0.1	2.5	0.6	0.6

LOI loss on ignition

Table 2 Mineralogical composition of clayey precursor before and after thermal activation

Precursor	Clay minerals (wt%)			Other minerals (wt%)						Amorpous phase (wt%)
	I + M	Mtm	Ch	Q	F	C	D	A	H	
AV	53	6	2	22	7	8	–	1	–	–
AV850	40	–	–	25	10	2	1	1	1	20

I + M illite + muscovite, *Mtm* montmorillonite, *Ch* chlorite, *Q* quartz, *F* feldspar, *C* carbonates, *D* diopside, *A* anatase, *H* hematite

after the calcination at 850 °C due to decarbonation which starts at 400 °C and ends at about 650 °C.

3.2 Determination of the Optimal Grinding Time for Mechanochemical Activation

On Fig. 1, the six diffraction patterns show the evolution of the mineral composition of the precursor, while the grinding is processed from 30 to 500 min. First, the firing of the green clay at 850 °C is not enough to amorphize illitic clay because of the persistence of the illite + muscovite peak at 10° 2θ. With increasing grinding times, all peaks display a decreasing intensity and illite + muscovite almost disappears after 3 h of grinding. The amount of amorphous phase increases from 20 wt% for AV 850 to 49 wt% (see Fig. 2) which is the maximum reached after 180 min. After 3–4 h of grinding, the remaining crystalline phases are mainly quartz and feldspar.

The presence of illite/muscovite in the precursor was confirmed by the FTIR analysis (Fig. 3) with the presence of the broad OH-stretching band at 3620 cm^{-1} coupled with the band at 915 cm^{-1}. Firing the precursor at 850 °C causes the disappearance of the OH bands for clay minerals. The FTIR study evidences a shift of
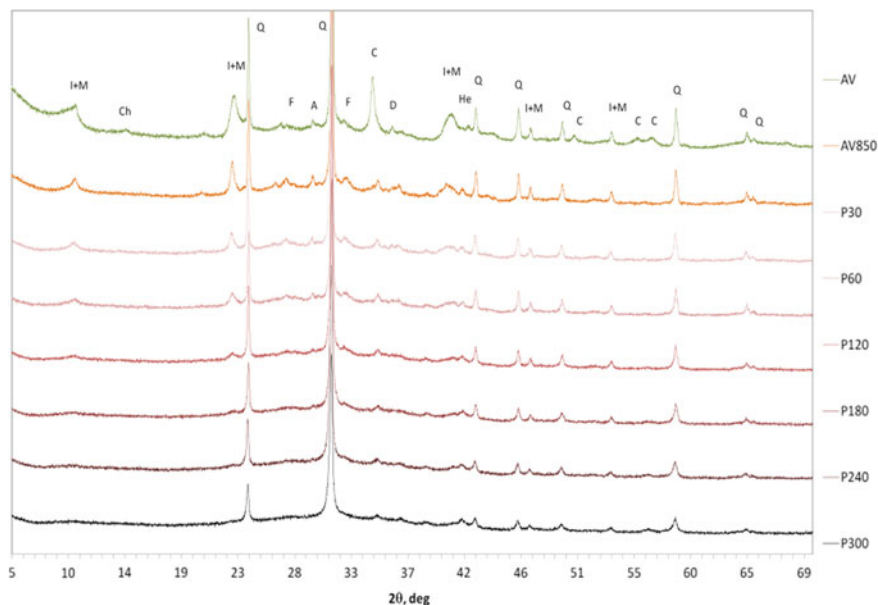
Fig. 1 XRD of Romainville green clay AV before and after various activations. AV: initial green clay, AV850: green clay calcined at 850° C, PX: green clay calcined and mechanochemical activated in a planetary mill during X minutes. I + M: illite + muscovite, Ch: chlorite, Q: quartz, F: feldspar, C: calcite, D: dolomite, A: anatase
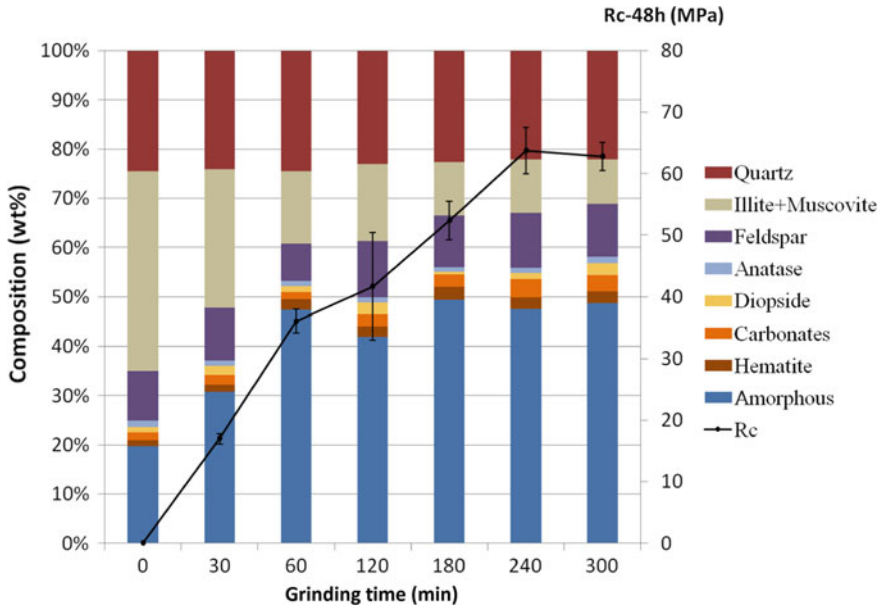
Fig. 2 Comparison of the mineralogical composition of thermo-mechanically activated precursor and the Rc at 48 h after geopolymerization versus the grinding time of green clay previously calcined at 850 °C

the band corresponding to the Si-O-Si bond from 1030 cm^{-1} for the initial green clay to 1090 cm^{-1} after thermal and mechanochemical activation (for the samples P240 and P300). In general, changes in the Si-O stretching bands (1113, 1030 and 1090 cm^{-1}) coupled with the disappearance of the Al-O-Si band at 529 cm^{-1} involve a distortion in tetrahedral and octahedral layers of the clay minerals [8]. This band displays also a shape enlargement after 3 h grinding. After that, the band centered at 1090 cm^{-1} seems refined. This change of shape indicates a stacking disorder in clay minerals [9]. After thermal activation, the band at 550 cm^{-1} that corresponds to Al(VI)-O-Si, vanishes after 1 h grinding and one other band appears at 512 cm^{-1} from 2 h grinding. This shift involves the environmental modification of the Al(VI). Furthermore, the higher area for this band is measured for 4 h of grinding.

In the highest wavelengths, the broadband centered at 3425 cm^{-1} relative to hydroxyl groups is divided into two bands (3590 and about 3300 cm^{-1}) after 30 min grinding time. This means that all the dehydroxylated OH groups are removed from calcined clay but when the grinding time increases (above 30 min), some water molecules from atmosphere are probably re-absorbed and leads to the appearance of bands at about 3430 and 1635 cm^{-1} [10].

In order to fix the grinding time, a first geopolymerization test was realized for each grinding times. The liquid/solid (L/S) mass ratio chosen was 1.0 and 3 specimens were manufactured for each type of activated precursor. Their compressive strength displayed in Fig. 2 was tested at 48 h and coupled with the XRD quantification. The
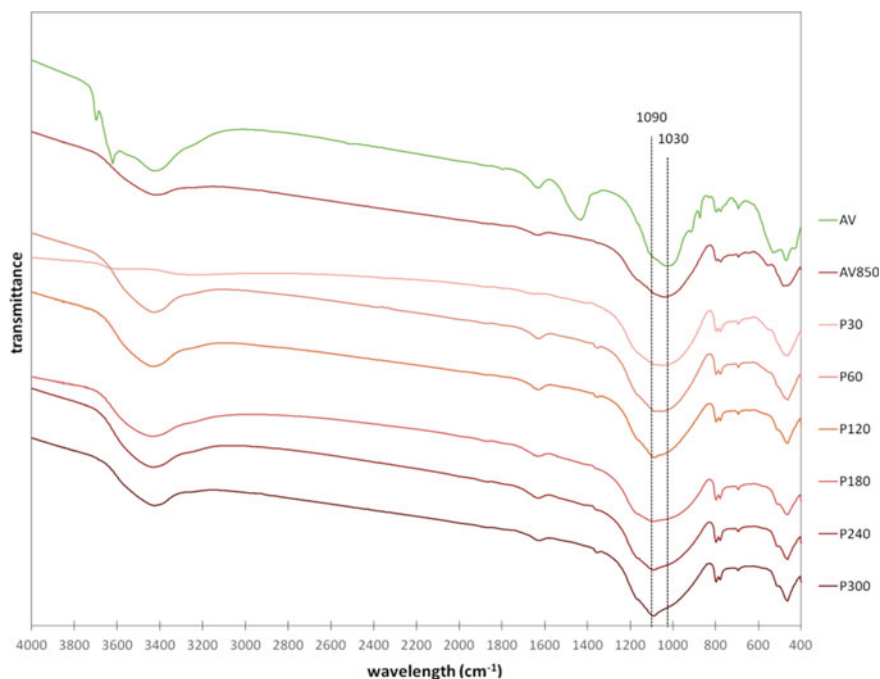
Fig. 3 FTIR spectra of the Romainville green clay before and after various activations

value of the Rc for AV850 is zero because the geopolymer paste was not hardened after 48 h (despite the cure protocol). If the maximum amorphous amount is reached after a 180 min grinding (about 49 wt%) and the decrease of the illite + muscovite quantity stops from this milling time, the maximum compressive strength (Rc = 63 MPa) is reached for 240 min. After this milling time, Rc does not increase anymore. In conclusion, the amorphous rate does not pretend to be the only parameter to make a good geopolymer precursor. Indeed, the mechanochemical activation involves significant structural changes and after several hours, the particles aggregate and the specific surface area decreases but these aggregates are composed of spherical nano-particles, whereas before grinding the particles were angular [11]. After 4 h grinding, the particles should be too compact and the reactivity does not increase anymore [6, 8, 10].

3.3 The Effect of L/S Ratio on the Compressive Strength of Geopolymers

The grinding time was fixed at 4 h while values of L/S mass ratio varied (L/S = 1.0, 0.75 and 0.5). Nine samples were manufactured for each L/S mass ratio. When
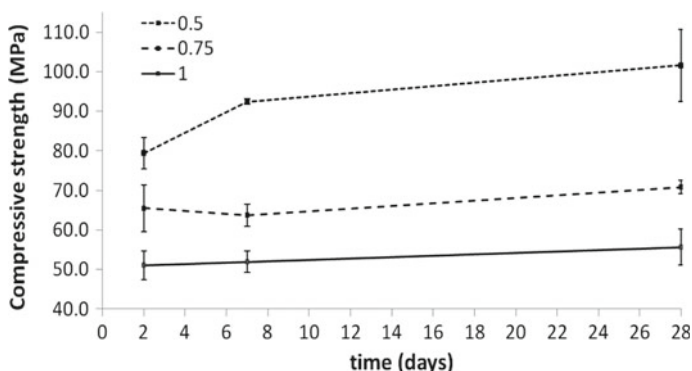
Fig. 4 Compressive strength Rc of AV850P4.0 at 2, 7 and 28 days with L/S mass ratios equal to 0.5, 0.75 and 1, respectively

the L/S ratio is decreasing in Fig. 4, the compressive strength displays a slightly increase versus time. The best Rc measured in the present study is about 102 MPa and is reached for a L/S mass ratio of 0.5 after 28 days, with a coupled thermo-mechanochemical activation (calcination at 850 °C followed by a 4 h planetary grinding). For the higher L/S, the Rc changes little over time, thereby the cure protocol allows the development of 92% of the maximum compressive strength at 48 h.

4   Conclusions

This study demonstrated that illitic geopolymers can be manufactured with high mechanical strengths. A thermo-mechanochemical activation allows the improvement of the precursor reactivity and the optimal grinding time with a planetary mill is 4 h. The L/S mass ratio equal to 0.5 leads to a high performance geopolymer with a compressive strength up to 102 MPa after 28 days. These results need to be complemented by microstructural and durability studies on the tested samples. In addition, there is still 13 wt% of illite + mucovite after the complete activation process, the amorphous content could be increased with the optimization of mechanochemical activation parameters such as the ball: powder mass ratio.

References

1. Davidovits, J.: Geopolymer chemistry and applications, 4th edn. Institut Géopolymère, Saint Quentin (2015)
2. Gualtieri, A.F., Ferrari, S.: Kinetics of illite dehydroxylation. Phys. Chem. Mineral **33**(7), 490–501 (2006)

3. Buchwald, A., Hohmann, M., Posern, K., Brendler, E.: The suitability of thermally activated illite/smectite clay as raw material for geopolymer binders. Appl. Clay Sci. **46**(3), 300–304 (2009)
4. Hu, N., Bernsmeier, D., Grathoff, G.H., Warr, L.N.: The influence of alkali activator type, curing temperature and gibbsite on the geopolymerization of an interstratified illite-smectite rich clay from Friedland. Appl. Clay Sci. **135**, 386–393 (2017)
5. Hamzaoui, R., Muslim, F., Guessasma, S., Bennabi, A., Guillin, J.: Structural and thermal behavior of proclay kaolinite using high energy ball milling process. Powder Technol. **271**, 228–237 (2015)
6. Balczár, I., Korim, T., Kovács, A., Makó, É.: Mechanochemical and thermal activation of kaolin for manufacturing geopolymer mortars—comparative study. Ceram. Int. **42**(14), 15367–15375 (2016)
7. Shvarzman, A., Kovler, K., Grader, G.S., Shter, G.E.: The effect of dehydroxylation/amorphization degree on pozzolanic activity of kaolinite. Cem. Concr. Res. **33**, 405–416 (2003)
8. Makó, É., Frost, R.L., Kristóf, J., Horváth, E.: The effect of quartz content on the mechanochemical activation of kaolinite. J. Colloid Interface Sci. **244**(2), 359–364 (2001)
9. D'Elia, A., Pinto, D., Eramo, G., Giannossa, L.C., Ventruti, G., Laviano, R.: Effects of processing on the mineralogy and solubility of carbonate-rich clays for alkaline activation purpose: mechanical, thermal activation in red/ox atmosphere and their combination. Appl. Clay Sci. **152**, 9–21 (2018)
10. Frost, R.L., Makó, É., Kristóf, J., Horváth, E., Kloprogge, J.T.: Mechanochemical treatment of kaolinite. J. Colloid Interface Sci. **239**(2), 458–466 (2001)
11. Vdović, N., Jurina, I., Škapin, S.D., Sondi, I.: The surface properties of clay minerals modified by intensive dry milling—revisited. Appl. Clay Sci. **48**(4), 575–580 (2010)

Performance and Properties of Alkali-Activated Blend of Calcined Laterite and Waste Marble Powder

Luca Valentini, Ludovico Mascarin, Maria Chiara Dalconi, Enrico Garbin, Giorgio Ferrari and Gilberto Artioli

Abstract This contribution reports on some preliminary studies on the use of lateritic soils from Cameroon as raw materials for the production of alkali-activated binders. These soils contain about 40–60% kaolinite and variable amounts of quartz, hematite, and other minor phases. After calcination at 800 °C, this material is blended with up to 30% waste marble powder, which is produced in large amounts during quarrying, cutting, and processing of marble. The results of our tests show that a careful mix design allows a good mechanical performance to be achieved, with the values of the cubic compressive strength larger than 30 MPa after 28 days. The role of Fe on the performance of this material is investigated by comparison with Fe-free blends of commercial metakaolin, waste marble powder, and quartz. Calorimetric data suggest that the use of alkanolamines as Fe chelating agents may accelerate the early-age reactivity, depending on dosage, although the effect on the development of mechanical properties is minor. It is argued that alkali-activated calcined laterite represents a viable option for the development of sustainable binders, especially for the African market, where it could be used, for example, to produce compressed stabilized earth blocks, in substitution of masonry units based on Portland cement or fired clay bricks. The use of waste marble powder adds further environmental value to this material.

Keywords Laterite · Alkali activation · Marble powder

1 Introduction

Research into sustainable cement materials based on calcined clays is gaining consensus, as it has now become clear that abundant, worldwide available, and relatively low-cost raw materials are necessary for a scenario of rising demand of building

L. Valentini (✉) · L. Mascarin · M. C. Dalconi · E. Garbin · G. Artioli
University of Padua, 35131 Padua, Italy
e-mail: luca.valentini@unipd.it

G. Ferrari
Mapei S.p.A, 20158 Milan, Italy

materials. Clay minerals are abundant in soils (Fig. 1), particularly in tropical regions and, more in general, in developing countries (Fig. 2).

Lateritic soils consist of impure, iron-rich kaolinite deposits, which are particularly abundant in the subequatorial areas of the African continent. Laterites may potentially represent a viable raw material for the production of sustainable cement in the African continent, where urbanization is increasing at a fast pace. Recent estimations envisage that in 2100, three African cities (Lagos, Kinshasa, Dar-es-Salaam)
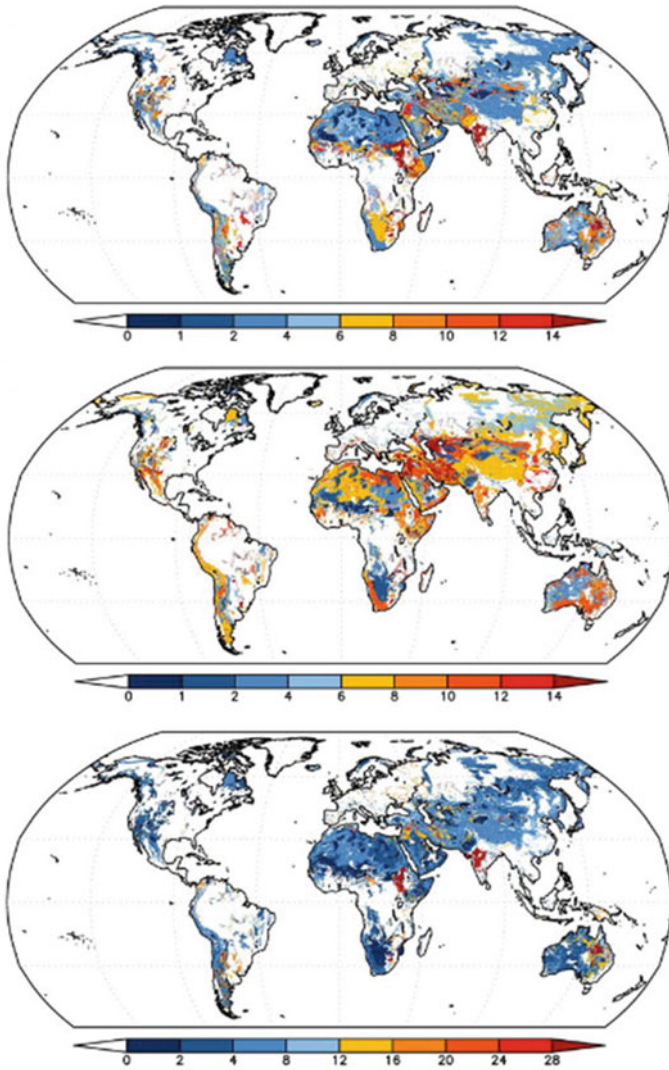
Fig. 1 Global distribution of kaolinite (top), illite (middle), and smectite (bottom) in soils. Modified from [1] CC Attribution 3.0 License
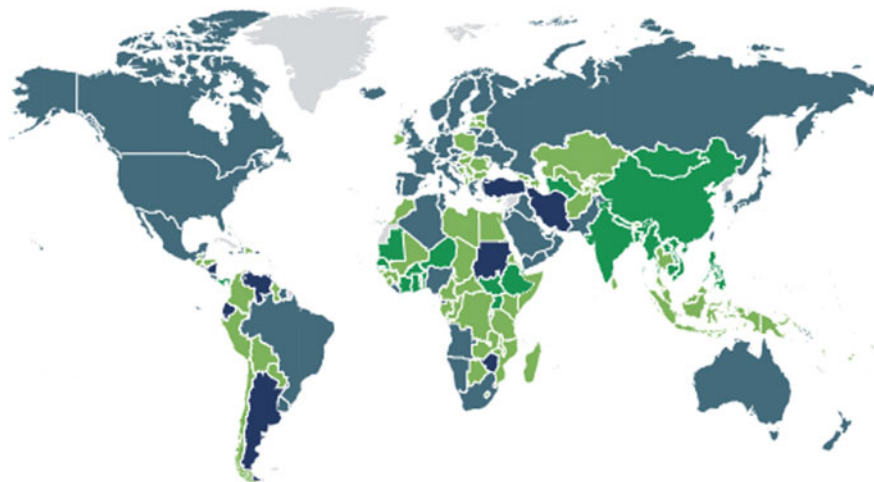
Fig. 2 Real GDP growth in 2019. Growth proportional to the intensity of the green color (compare with clay distribution in Fig. 1). Data from the International Monetary Fund (www.imf.org)

will become the most highly populated settlements in the world, each with over 70 million inhabitants [2]. Given the current dramatic backlog in providing adequate and affordable housing in the continent, producing sustainable and reliable building materials based on locally available and cheap raw materials, in order to relieve the economic and environmental burden associated with import from other continents, will represent a key technological and societal challenge.

In this study, we test the behavior of alkali-activated calcined clays produced from laterites sampled in Cameroon. Prior to alkali activation, the calcined laterite is blended with marble powder, a waste material produced during marble quarrying, cutting, and polishing. The disposal of this material poses severe environmental issues [3, 4], hence the further environmental value of its reuse in cement binders. Previous studies suggested that the addition of waste marble powder may enhance the properties of alkali-activated calcined clays [5].

In the present study, a series of analyses are performed to assess the role of Fe in the processes associated with the alkali activation of calcined clays.

2 Materials and Methods

Laterite soil samples were collected in Yaoundé (Cameroon) and consist of kaolinite, quartz, Fe-hydroxide (goethite), Fe-oxide (hematite), Ti-oxide (anatase), and traces of Al-hydroxide (gibbsite). This material was ground and thermally treated at 800 °C for 5 h. Upon calcination, goethite is converted to hematite and kaolinite is converted to metakaolinite, as testified by the disappearance of the basal peak at 14.32° 2θ
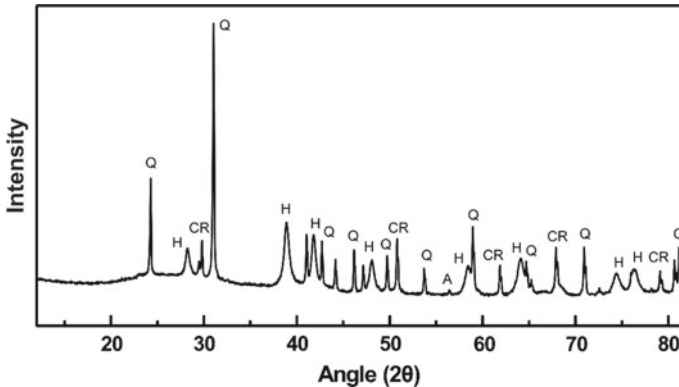
Fig. 3 Calcined laterite XRD pattern. Phase labels: Q = quartz; H = hematite; CR = corundum (internal standard); A = anatase

and of the 020 peak at 23.12° 2θ in the diffraction pattern (Fig. 3). The starting mix consisted of 70 wt% calcined laterite and 30 wt% marble powder. The latter consists of 100% calcite with Mg impurities. Sodium silicate pentahydrate was used as alkaline activator.

Compressive strength tests were performed on the above mix, as well as on a Fe-free mix consisting of commercial metakaolin blended with marble powder and fine quartz. Quartz was added with the aim of diluting the amount of metakaolinite, to match the weight fraction contained in the calcined laterite, in order to separate the effect of Fe with that of metakaolinite content. Moreover, additions of 0.2 wt% alkanolamines were performed with the aim of testing the effect of such additives acting as Fe chelating agents. The amount of this additive was calibrated on the XRF concentration of Fe in the laterite, which is about 20%.

3   Results

The phase composition of the reacted mix after 20 days, as obtained by XRD combined with the PONKCS method [6, 7], shows that approximately half of the initially present metakaolinite has been dissolved. Calcite (present in the marble powder) and hematite are also partially dissolved. The formation of an X-ray amorphous phase is testified by the presence of a diffuse scattering hump at 30° 2θ in the diffraction pattern (Fig. 4).

The maximum measured compressive strength is 29.0 MPa at 7 days and 32.2 MPa at 28 days. The compressive strength of the Fe-free metakaolin sample is approximately 15% higher.

The results of semi-adiabatic calorimetry show that the early-age reaction kinetics is accelerated in the presence of 0.2% alkanolamines (Fig. 5). However, only minor
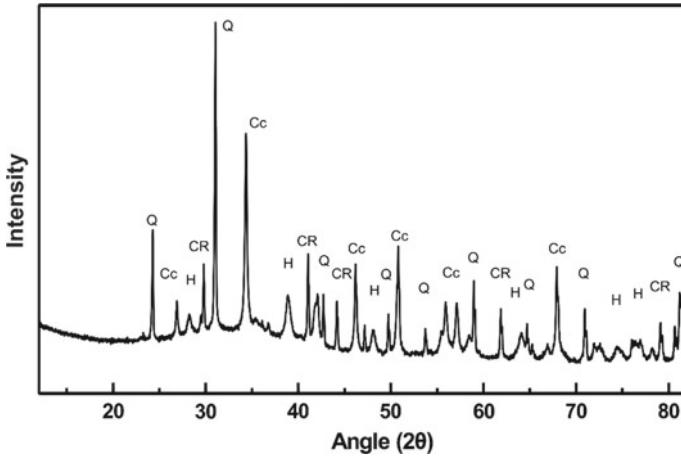
Fig. 4 XRD pattern of the alkali-activated blend. Phase labels: Q = quartz; H = hematite; CR = corundum (internal standard); Cc = calcite
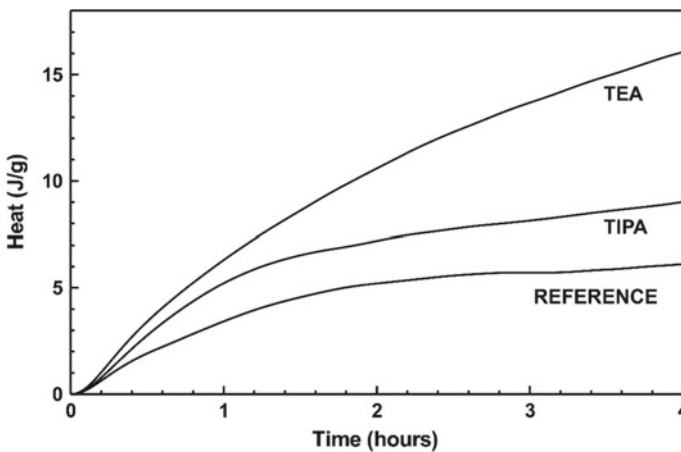
Fig. 5 Heat released by the reference alkali-activated blend of calcined laterite and marble powder and by the samples with additions of alkanolamines (TIPA: Triisopropanolamine; TEA: Triethanolamine)

changes in the 7 days compressive strength were detected in the samples containing these additives.

SEM-EDX spot analyses suggest that the composition of the matrix of the reacted material is compatible with that of a N-A-S-H phase, in which non-negligible amounts of Ca and Fe are present. Further research will be needed to clarify the exact nature of the reaction product and whether Fe may play a structural role in it.

4   Conclusions

The results of this study show that alkali-activated cement with an appropriate mechanical performance can be produced using a blend of calcined laterite, a cheap raw material that is particularly abundant in Africa, and waste marble powder, a secondary raw material that is also available in this continent [8, 9]. The use of commercial sodium silicate as alkaline activator may pose limitations due to high cost and environmental impact. However, combinations of primary and secondary raw materials rich in Na and Si, such as sodium carbonates present in geological deposits and vegetable ashes or waste glass, could be used as an alternative cheap and less impacting solution. These materials are promptly available in the African continent.

The presence of Fe seems to affect the development of mechanical strength only to a minor extent. The use of small amounts of Fe chelating agents in the mix improves the early-stage reactivity, although no significant variations in the 7 days compressive strength are observed. Further research will be necessary to understand the exact role of Fe on the dissolution–precipitation pathways.

We conclude that laterite soils represent a promising raw material for the production of sustainable binders in specific geographical locations and encourage additional studies on their exploitation to be performed.

References

1. Nickovic, S., Vukovic, A., Vujadinovic, M., Djurdjevic, V., Pejanovic, G.: Technical note: high-resolution mineralogical database of dust-productive soils for atmospheric dust modeling. Atmos. Chem. Phys. **12**, 845–855
2. Hoornweg, D., Pope, E.: Population predictions for the world's largest cities in the 21st century. Environ. Urban. **29**, 195–216 (2017)
3. Adewole, M.B., Adesina, M.A.: Impact of marble mining on soil properties in a part of Guinea Savanna zone of Southwestern Nigeria. Ethiop. J. Environ. Stud. Manag. **4**, 1–8 (2011)
4. Mulk, S., Azizullah, A., Korai, A.L., Khattak, M.N.K.: Impact of marble industry effluents on water and sediment quality of Barandu River in Buner District. Pakistan. Environ. Monit. Assess. **187**, 8–30 (2015)
5. Valentini, L., Contessi, S., Dalconi, M.C., Zorzi, F., Garbin, E.: Alkali-activated calcined smectite clay blended with waste calcium carbonate as a low-carbon binder. J. Clean. Prod. **184**, 41–49 (2018)
6. Scarlett, N.V.Y., Madsen, I.C.: Quantification of phases with partial or no known crystal structures. Powder Diffr. **21**, 278–284 (2006)
7. Snellings, R., Salze, A, Scrivener, K.L.: Use of X-ray diffraction to quantify amorphous supplementary cementitious materials in anhydrous and hydrated blended cements. Cem. Concr. Res. **64**, 89–98
8. Okagbue, C.O., Onyeobi, T.U.S.: Potential of marble dust to stabilise red tropical soils for road construction. Eng. Geol. **53**, 371–390 (1999)
9. Boukhelkhal, A., Azzouz, L., Belaidi, A.S.E., Benabed, B.: Effects of marble powder as a partial replacement of cement on some engineering properties of self-compacting concrete. J. Adhes. Sci. Technol. **30**, 2405–2419 (2016)

Identification and Activation of Coal Gangue and Performance of Limestone Calcined Gangue Cement

Bin Wang, Tongbo Sui and Hao Sui

Abstract Gangue, a typical waste associated with the coal mining process in northern China, was characterized before and after thermal treatment by XRF, XRD, TGA-DSC, and SEM. The pozzolanic reactivity of calcined gangue with different calcined temperature was tested by standard mortar strength and R^3 calorimetry test. The performance of blended cement was evaluated by mortar strength and flow. The XRD and TGA-DSC analyses showed that the main minerals that present in the raw gangue were kaolinite, and a small amount of carbon-based compounds and metakaolin were almost the only phase in calcined gangue. After thermal treatment and depending on the temperature, it showed very high reactivity especially combined with limestone. The strength property of limestone calcined gangue cement with 45% replacement of clinker was higher than reference cement (CEM I 42.5 N) on 7 and 28 days. Furthermore, it is found that the calcined gangue has less influence on the workability of LC^3 according to particle morphology compared with a typical calcined clay, based on the results of SEM observation.

Keywords Coal gangue · Reactivity · Blended cement · Performance

1 Background

Coal gangue is a rock mixed with organic and inorganic compounds co-deposited with coal during coal formation. Usually in a thin layer and in the coal seam or in the top and bottom of the coal seam, gangue is typical solid waste discharged when coal is excavated and washed in the production. In China, the total of accumulative stockpile

B. Wang (✉)
College of Materials Science and Engineering, Beijing University of Technology, Beijing 100124, People's Republic of China
e-mail: wangbin@sinoma.com.cn

B. Wang · T. Sui
Sinoma Research Institute, Sinoma International Engineering Co. Ltd, Beijing 100102, People's Republic of China

H. Sui
ARC Nanocomm Hub, Civil Engineering, Monash University, Victoria 3168, Australia

of coal gangue has been reached 4.5 billion metric tons. Such large quantities of the solid waste have not only occupied a great deal of land but also become harmful in initiating geologic hazards and land degradation [1].

Many studies have been carried out to investigate the abundantly utilize coal gangue in building materials, such as to replace ordinary sand or calcined with additional lime as cementitious materials [2–4]. Considering the fact that China is a country with more than half of world cement production, utilization of calcined coal gangue with the LC^3 solution is expected to lead to a significant disposal capacity of solid waste and contribution to CO_2 mitigation of cement industry.

This article aims to study the pozzolanic reactivity of gangue in the Inner Mongolia after calcination, and the mechanical performance of limestone calcined gangue cement.

2 Raw Materials and Experiment

2.1 Raw Materials

The coal gangue sample was separated to reduce coal content based on the density by calculating volume and weight of the ores. The other raw materials used for this study include PI cement (CEM I 42.5 N), gypsum, and limestone with their chemical component and were shown in Table 1.

2.2 Experiment

The chemical composition measured by Bruker S8 TIGER XRF analysis; the mineralogical composition measured via Bruker D8 ADVANCE XRD analysis; thermal analysis conducted with Mettler Toledo analyzer in a temperature range of 30–1000 °C at a heating rate of 10 °C/min and N_2 or O_2 atmosphere.

Mortar strength test: prismatic mortar specimens with dimensions of 40 × 40 × 160 mm were prepared with w/c ratio of 0.50 and sand/cement ratio of 3.0 and 20 °C standard curing (equal to ISO standard) at targeted ages from 1d, 3d, 7d, 28d to 90d.

The reactivity test—mortar strength method: comparison measurement of 28-day age mortar strength for reference cement and targeted samples prepared by reference cement with 30% replacement by calcined gangue.

The reactivity test—R^3 calorimetry method: heat released by isothermal calorimetry for a paste prepared with calcined gangue: $Ca(OH)_2$ = 1:3, w/b = 1.2, etc., tested under 40 C°C which has been detailed on basis of RILEM TC TRM-Protocol for R^3 model paste preparation and test procedure [5].

Table 1 Chemical component of raw materials

Sample	Loss	SiO$_2$	Al$_2$O$_3$	Fe$_2$O$_3$	CaO	MgO	SO$_3$	K$_2$O	Na$_2$O	Total
Coal gangue	15.5	45.4	37.4	0.7	0.1	0.3	0.1	0.2	0	99.7
PI cement	1.5	22.6	5.1	3.2	61.7	2.8	1.9	0.6	0.1	99.5
Limestone	36.4	13.1	0.6	0.2	46.0	1.0	0.5	0.1	0	97.9
Gypsum	21.4	6.7	2.2	0.8	29.3	1.8	38.0	0.4	0.1	100.7
Calcined clay	0.9	56.8	35.1	2.1	0.2	0.4	0.1	3.6	0.1	99.5

3　Results and Discussion

3.1　Mineralogical Composition of Coal Gangue

The chemical composition of coal gangue sample by XRF analysis was shown in Table 1. The results show that the main chemical elements in the samples are silicon and aluminum, and the total amount of other elements is less than 1.5%. The mineralogical composition measured via XRD analysis shown in Fig. 1. It is shown that kaolinite is almost the only mineral phase in raw gangue from the XRD pattern.

Thermal analysis (TGA-DSC) was also conducted to identify the purity of kaolinite both in nitrogen and in oxygen atmosphere. From Fig. 2, the gangue sample has
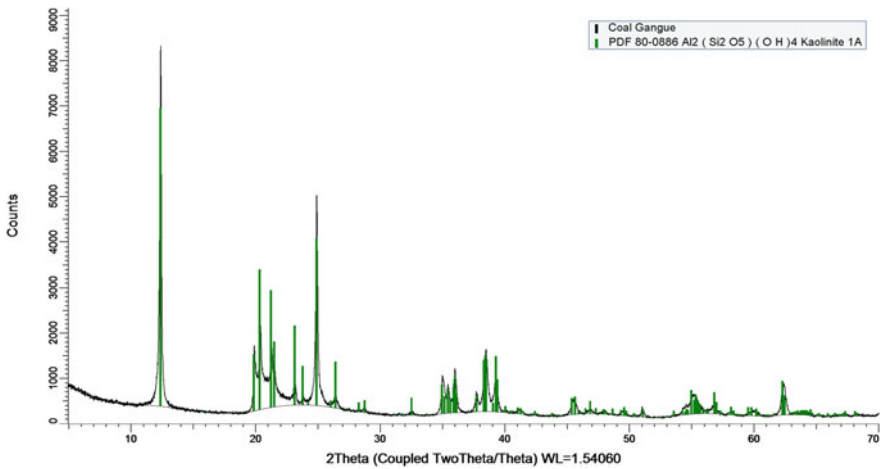
Fig. 1　X-ray diffract pattern of raw gangue
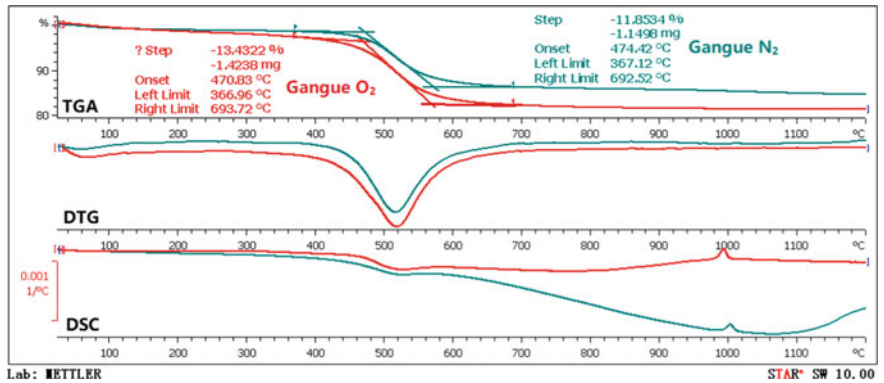
Fig. 2　Thermal analysis curve of raw gangue

an obvious weightlessness step between the temperature range from 350 to 700 °C on the TGA curve and a corresponding endothermic peak on DSC curve in N_2 atmosphere. This can be considered to be due to the dehydration of kaolinite. Comparing with the curves in O_2, it can be found that the weight loss mass increases with a weak exothermic peak during the same temperature range due to the oxidation of carbonyl compounds. Therefore, thermal analysis results show that the main components of the gangue sample are kaolinite, and a small amount of coal and the kaolinite content can be calculated through the weight loss in N_2 atm. which is 84.93%.

3.2 Thermal Activation

The bulk raw gangue sample was crushed into small pieces of 1–3 mm and then calcined in electric furnace under designated thermal activation history (various calcined temperature and same two-hour holding time). After calcined, the samples were cooled under ambient temperature and ground in a laboratory ball mill for 30 min. Residue of the ground calcined gangue after passing through 45 μm square mesh sieve was controlled below 5%. XRD analysis was also conducted for the 5 calcined samples with the results shown in Fig. 3. It is found from the pattern that the diffraction of the samples is generally amorphous and the characteristic diffraction peak of kaolinite around $2\theta = 12°$ and $25°$ is remarkably reduced and after calcination, it completely disappears at 800 °C. And the crystallization of θ-Al_2O_3 can be found in 900 °C calcined sample from the red pattern in Fig. 3.
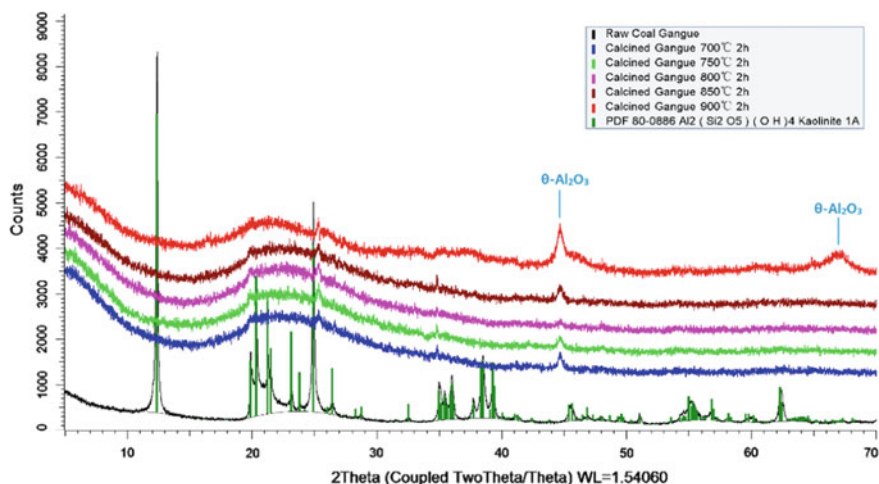
Fig. 3 X-ray diffract pattern of different temperature calcined gangue

3.3 Reactivity of Calcined Gangue

Raw gangue was thermally treated in laboratory furnace at different temperature for 2 h and then cooled down in air to produce calcined gangue (CG). The burning temperature and physical performance of cement mixtures with 30% CG used as SCM can be seen in Fig. 4. It shows that thermal activation has an important influence on the reactivity of CG. And the best burning temperature as can be seen is between 800 and 850 °C.

Heat release by isothermal calorimetry for a paste based on R^3 model was also measured to characterize the effect of calcination temperature on the activity of CG that shown in Fig. 5. It can be seen that R^3 calorimetry test can well demonstrate the reactivity of calcined gangue with its results in agreement with mortar strength test, and the cumulative heat release from 75 min to 3 days of the CG samples calcined at
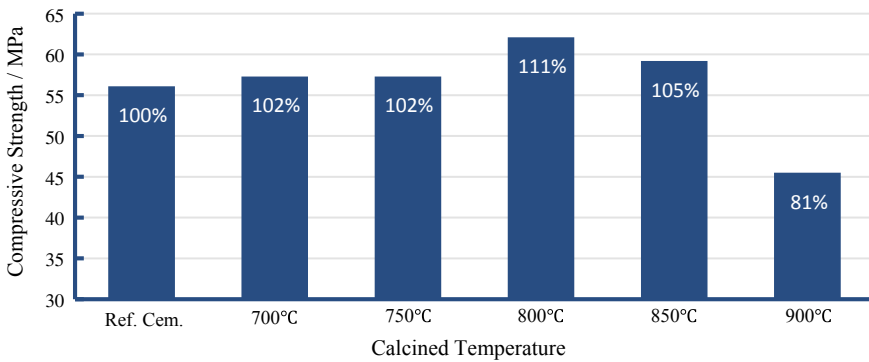
Fig. 4 Mortar strength and reactivity index of different temperature calcined gangue

Fig. 5 Three days of cumulative heat of different temperature calcined gangue with R^3 calorimetry test
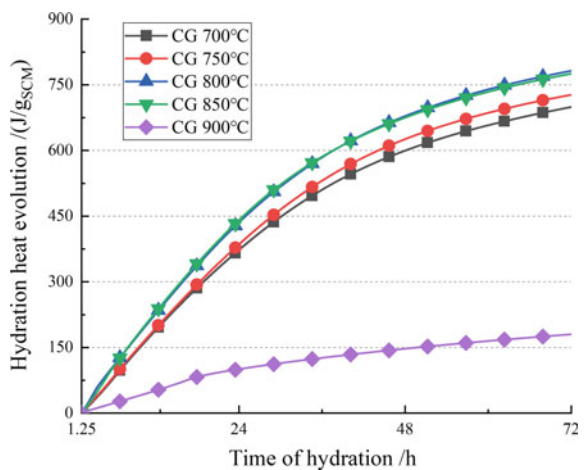
800 °C and 850 °C is the largest, indicating that the reaction activity of those is the highest. The 28-day mortar strength and pozzolanic reaction heat release of gangue calcined at 900 °C are both the lowest, which should be related to the decomposition of metakaolin and the crystallization of alumina. The 800 °C calcined gangue with the highest reactivity was selected for the following LC^3 performance test.

3.4　Performance of LC^3 Materials

Three LC^3 cement samples with the same clinker factor (0.50) and different ratios of calcined coal gangue and limestone were prepared to test the physical performance in comparison with reference cement and limestone calcined clay (CC) cement (Table 2). The clay is a typical kaolin clay with around 60% kaolinite and perfect calcined in rotary kiln (see Table 1). The results of mortar flow show that the negative effect of calcined coal gangue on the workability of cement is much less than that of calcined clay.

Mortar strength test was conducted for LC^3-50 in Fig. 6. It is found that the early age strength prior to 7-day of all samples is lower than the reference, except the LC^3-CG with 2 to 1 ratio has a little bit higher strength at 7 days. While at 28-day and 90-day, the samples of LC^3-CG with 2:1 and 1:1 ratio show excellent performance which is significantly higher than the reference cement. And the samples of LC^3-CG with 15% CG and 30% limestone exhibit similar strength to the reference and LC^3-CC cement with 30% CC and 15% limestone.

Table 2 Component of LC^3 materials

No.	Cement component w.t %					W/C	Flow/mm
	Clinker	Calcined gangue	Calcined clay	Limestone	Gypsum		
Control	95	–	–	–	5	0.50	225
LC^3-CC 2:1	50	–	30	15	5	0.50	160
LC^3-CG 2:1	50	30	–	15	5	0.50	192
LC^3-CG 1:1	50	22.5	–	22.5	5	0.50	197
LC^3-CG 1:2	50	15	–	30	5	0.50	204
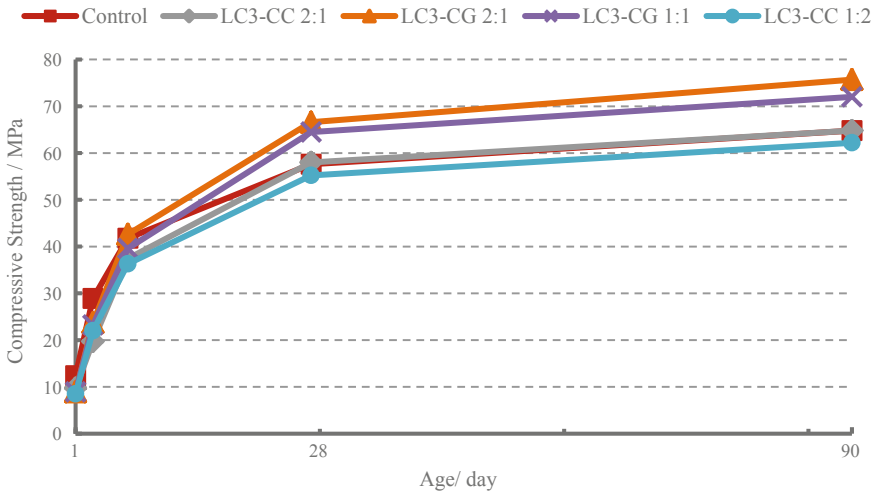
Fig. 6 Mortar strength of LC^3-50 materials

3.5 Micromorphology of Calcined Gangue

Scanning electron microscopy (SEM) was used to observe the micromorphology of powder particles and to analyze the influence on physical properties. As can be seen in Fig. 7, the typical calcined kaolin clay (see Fig. 7b) retains the layered kaolinite structure. Therefore, the large number of interlayer spaces will absorb water, resulting in a significant increase in water demand of LC^3-CC. In contrast, kaolinite minerals

(a) Calcined gangue   (b) Calcined kaolin clay
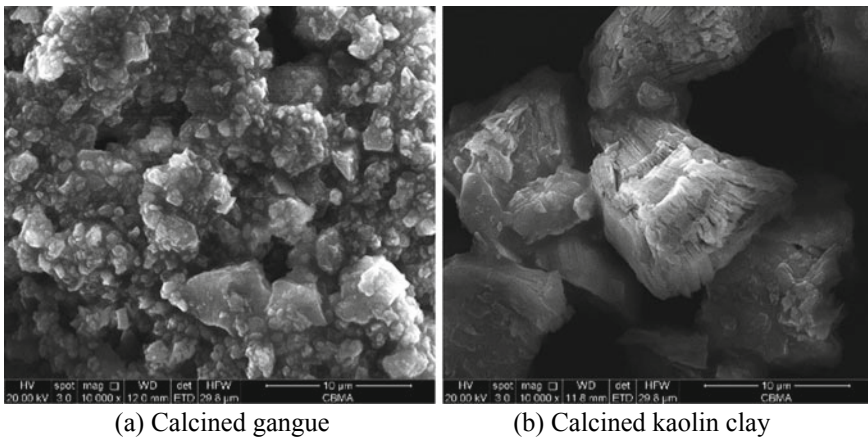
Fig. 7 Micromorphology of calcined gangue

in coal gangue do not have layered structure, and the surface of calcined and grinded particles is smooth (Fig. 7a), so it has less influence on the workability of LC^3-CG.

4 Conclusion

(1) A kind of Chinese waste material, coal gangue was identified via XRD and TGA for quantitative analysis. The reactivity of the calcined gangue was characterized by both mortar strength test and isothermal calorimetry test.

(2) LC^3-50 with 15% calcined gangue and 30% limestone was proved to give equivalent 28-day and 90-day compressive strength when compared with reference cement while 30% calcined gangue and 15% limestone can make the strength higher after 7 days.

(3) Calcined gangue has less influence on the workability of LC^3 compared with calcined clay due to the difference of particle morphology.

References

1. Ye, J.W., Shen, G.D., Lu, L.: Hazards and comprehensive utilization of coal gangue. Hazards Compr. Util. Coal Gangue **28**, 32–42 (2010)
2. Dong, Z., Xia, J., Fan, C., et al.: Activity of calcined coal gangue fine aggregate and its effect on the mechanical behavior of cement mortar. Constr. Build. Mater. **100**, 63–69 (2015)
3. Li, Y., Yao, Y., Liu, X., et al.: Improvement on pozzolanic reactivity of coal gangue by integrated thermal and chemical activation. Fuel **109**, 527–533 (2013)
4. Li, D.X., Song, X.Y., Gong, C.C., Pan, Z.H.: Research on cementitious behavior and mechanism of pozzolanic cement with coal gangue. Cem. Concr. Res. **36**, 1752–1759 (2006)
5. Li, X., Snellings, R., Antoni, M., et al.: Reactivity tests for supplementary cementitious materials: RILEM TC 267-TRM phase 1. Mater. Struct. **51**, 151–164 (2018)

Activation of Early Age Strength in Fly Ash Blended Cement by Adding Limestone Calcined Clay (LC^2) Pozzolan

Anuj Parashar, Satya Medepalli, Vineet Shah and Shashank Bishnoi

Abstract The low early age strength gain of fly ash-based Portland pozzolana cement (PPC) poses a challenge in many applications. This study tries to improve the early age strength gain of fly ash-based PPC by blending it with limestone calcined clay pozzolan (LC^2). Ordinary Portland cement was blended with a typical low calcium fly ash (FA) at replacement levels of 30 and 40% termed as PPC-30% and PPC-40%, respectively. To enhance the mechanical performance of PPC-30% and PPC-40%, the fly ash was blended with LC^2 in 1:1 mix proportion. Hydration and strength gain were evaluated using isothermal calorimetry and strength activity tests. Heat evolution results show that the addition of LC^2 pozzolana has increased the early age hydration of the blended pastes. Strength activity index of mortar showed improvement in early age performance in both the mixes compared to PPC. Moreover, 30% replacement by LC^2 is found to be more beneficial and can achieve strengths comparable to that of OPC.

Keywords Fly ash · LC^2 · Strength improvement

1 Introduction

Pozzolans have been used in the cement for many centuries to increase the performance of cements [1]. In the last many decades, the use of supplementary cementitious materials in cement has gained prominence due to the increasing concern of global warming and CO_2 emissions from the cement industry. Many industrial by-products such as fly ash, slag, silica fume were used as a partial replacement of cement to replace as much as 30% in case of fly ash to 80% in case of slags. The quantity of these by-products such as slags, silica fume is less compared to volumes required to replace a part of the cement, and hence, almost all of it is used. Fly ash is generated in substantial quantities as coal is a major fuel source in many countries [2, 3]. Due to the vast amount of fly ash generated, its usage has also increased and is now standardized everywhere [4, 5]. It is also well known that the use of fly ash in

A. Parashar (✉) · S. Medepalli · V. Shah · S. Bishnoi
Civil Engineering Department, Indian Institute of Technology Delhi (IIT Delhi), Hauz Khas, New Delhi 110016, India

cement has increased the performance of cements [6–8] apart from environmental and economic benefits. However, the early age strength development in these blended cements is still a concern for many applications.

Calcined clay is also becoming popular in the last few decades due to the availability of vast resources of kaolinitic clay in many parts of the world. Research has already been carried out to show that the use of calcined clay increases the overall performance of cement [9–11]. It is also used in combination with limestone to make limestone calcined clay pozzolana which has proved to be an effective pozzolana due to the synergy effect between these two materials [9, 12]. It was also used for high volume replacement of clinker as in the case of limestone calcined clay cements [13, 14]. The current study focusses on the use of limestone calcined clay pozzolana to reduce the shortcoming of fly ash by blending these two materials in equal proportions.

2 Materials and Methods

2.1 Materials and Mixes

A class F fly ash and LC^2 from industrial production [14] are used in this study along with OPC 43 grade cement [15]. Table 1 lists the chemical composition of the raw materials. LC^2 pozzolana has limestone and calcined clay in 1:2 proportions. Low-grade limestone and 60% kaolinitic clay were used in the production of LC^2. The mix proportion of the different blends with fly ash and LC^2 is listed in Table 2. Usual clinker replacement of 30% along with high volume replacement of 40% is studied. 5% gypsum by weight is added in all the mixes.

Table 1 Oxides composition of raw materials

Oxides (weight %)	OPC	Fly ash	LC^2
Loss on ignition	2.46	1.74	10.18
Silica (SiO_2)	21.84	67.66	36.41
Iron (Fe_2O_3)	3.62	5.32	3.58
Aluminum (Al_2O_3)	4.37	22.18	29.20
Calcium (CaO)	60.49	0.32	16.35
Magnesium (MgO)	2.50	0.18	1.44
Sulphate (SO_3)	3.18	0.02	–
Sodium (Na_2O)	0.54	0.43	–
Potassium (K_2O)	0.57	1.60	–

Table 2 Mix proportions of different blends in this study	Mix	OPC (%)	Fly ash	LC^2
	OPC	100	–	–
	PPC-30% FA	70	30%	–
	PPC-40% FA	60	40%	–
	PPC-30% LC^2 + FA (1:1)	70	15%	15%
	PPC-40% LC^2 + FA (1:1)	60	20%	20%

2.2 Experimental Methods

An isothermal calorimeter was used in this study to rate of heat flow during cement hydration at a standard temperature of 27 °C till 7 days for all the blends in this study. Water to binder ratio of 0.45 was used for all mixes. 7.06 cm cubes were cast for compressive strength tests on mortar samples using binder to sand ratio of 1:3. After keeping for 1 day in a moist environment, the cubes are de-molded for curing in a temperature-controlled water bath maintained at 27 °C till testing. Testing was carried out at 1, 3, 7, and 28 days.

3 Results and Discussion

3.1 Heat of Hydration

The cumulative rate of heat evolution per gram of OPC for all the mixes is shown in Fig. 1. It is well known that the fly ash addition helps in the reduction of heat
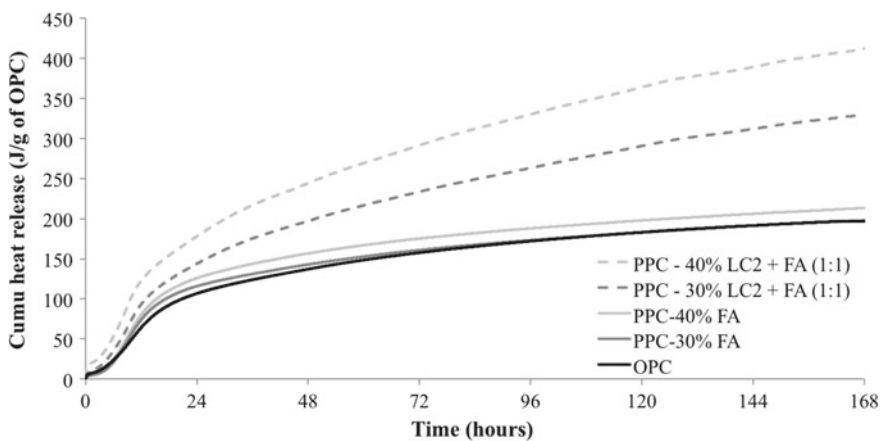
Fig. 1 Cumulative heat release plot for blended cements

release, which can also be observed in the results. A small increase in case of PPC 40% could be due to the filler effect which also increases the cumulative heat release during cement hydration.

In case of FA + LC^2, results clearly show a significant acceleration in the hydration reaction which was due to addition of LC^2 pozzolan. Due to the high solubility of clay in comparison with fly ash, the hydration reaction of LC^2 occurs at early ages, while fly ash behaves as a filler. This early age hydration results in the increase of cumulative heat release. This behavior also contributes due to the formation of additional hydration products such as carboaluminates and helps in stabilizing the ettringite in hydrated cement system [9, 12]. This acceleration in hydration also helps in strength gain even at early ages as will be observed in the next section.

3.2   Compressive Strength

The compressive strength of all mixes was compared with the help of strength activity index. The results are plotted with respect to the strength of OPC mortar at each testing age (see Fig. 1). Results indicate that the blending of fly ash with OPC at both the replacement levels (30 and 40%) affect the early age strength development. This effect was increased with an increase in the replacement level. However, in both cases, the strength gain has improved at later ages. In the case of higher replacement content such as in PPC 40%, the strength gain is affected significantly leading to poor strength gain at early ages. Blending of limestone calcined clay pozzolana along with fly ash has significantly improved the early age strength. In both cases, PPC 30% (LC^2 + FA) and 40% (LC^2 + FA), strength improvement was seen at all the ages corresponding to PPC 30 and PPC 40. Especially at the age of 3 days and 7 days, the strength activity index for PPC 40% (LC^2 + FA) was 81% and 103%, respectively. Similarly, for PPC 30% (LC^2 + FA) strength activity index at the age of 3 days as well as at 7 days was 98%. In both cases, the acceleration in strength gain at early age was conformed from the result (Fig. 2).

4   Conclusions

This study tried to improve the low strength gain behavior at early ages of fly ash-based PPC made in the laboratory by blending OPC with 30 and 40% fly ash. By maintaining fixed replacement levels, the fly ash and LC^2 were blended in 1:1 mix proportion with OPC at 30 and 40% replacement levels.

- The fly ash blends at 30% and 40%, only acts as an inert filler, and does not enhance the hydration at early ages as observed from the calorimetry results. A slight increase in the total heat is a result of availability of additional water for
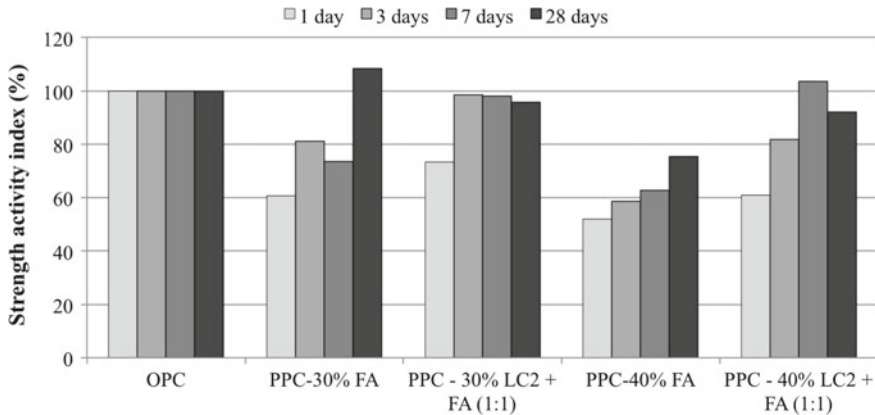
Fig. 2 Strength activity index of blended cements

hydration of OPC. Also, fly ash during this stage provides additional nucleation sites for hydration products of OPC.

- The calorimetry results indicate that the addition of LC^2 significantly accelerated the hydration as a higher amount of heat was released. This behavior helps in the formation of hydration products at an early age due to rapid dissolution of LC^2.
- The addition of LC^2 has a positive effect on the early age strength gain in the case of fly ash-based PPC. The strength activity index data showed an acceleration in strength gain at both the replacement levels. This behavior was confirmed with the help of the heat of hydration results also.

References

1. Massazza, F.: Pozzolanic cements. Cem. Concr. Compos. **15**, 185–214 (1993). https://doi.org/10.1016/0958-9465(93)90023-3
2. Central Electrical Authority: Report on fly ash generation at coal/lignite based thermal power stations and its utilization in the country for the year 2017–18 (2018)
3. Shafiee, S., Topal, E.: When will fossil fuel reserves be diminished? Energy Policy **37**, 181–189 (2009). https://doi.org/10.1016/j.enpol.2008.08.016
4. ASTM C618: Standard Specification for Coal Fly Ash and Raw or Calcined Natural Pozzolan for use in Concrete. ASTM International, West Conshohocken, USA (2012)
5. IS 3812 (2013) Specification for Pulverized fuel ash, Part-1: For Use as Pozzolana in Cement, Cement Mortar and Concrete. Bureau of Indian Standards, India
6. Mehta, P.K.: Influence of fly ash characteristics on the strength of portland-fly ash mixtures. Cem. Concr. Res. **15**, 669–674 (1985). https://doi.org/10.1016/0008-8846(85)90067-5
7. Malhotra, V.M.: Durability of concrete incorporating high-volume of low-calcium (ASTM Class F) fly ash. Cem. Concr. Compos. **12**, 271–277 (1990). https://doi.org/10.1016/0958-9465(90)90006-J
8. Erdoğdu, K., Türker, P.: Effects of fly ash particle size on strength of portland cement fly ash mortars. Cem. Concr. Res. **28**, 1217–1222 (1998)

9. Antoni, M., Rossen, J., Martirena, F., Scrivener, K.: Cement substitution by a combination of metakaolin and limestone. Cem. Concr. Res. **42**, 1579–1589 (2012). https://doi.org/10.1016/j.cemconres.2012.09.006

10. Murat, M.: Hydration reaction and hardening of calcined clays and related minerals. I. Preliminary investigation on metakaolinite. Cem. Concr. Res. **13**, 259–266 (1983). https://doi.org/10.1016/0008-8846(83)90109-6

11. Sabir, B., Wild, S., Bai, J.: Metakaolin and calcined clays as pozzolans for concrete: a review. Cem. Concr. Compos. **23**, 441–454 (2001). https://doi.org/10.1016/S0958-9465(00)00092-5

12. Shah, V., Parashar. A., Mishra, G., et al.: Influence of cement replacement by limestone calcined clay pozzolan on the engineering properties of mortar and concrete. Adv. Cem. Res. 1–11 (2018). https://doi.org/10.1680/jadcr.18.00073

13. Medepalli, S., Shah, V., Bishnoi, S.: Production of lab scale limestone calcined clay cements using low grade limestone. 7th Int. Conf. Sustain Built Environ. **6** (2016)

14. Emmanuel, A.C., Haldar, P., Bishnoi, Shashank, Maity, S.: Second pilot production of limestone calcined clay cement (LC 3) in India: the experience. Indian Concr. J. **90**, 57–64 (2016)

15. IS-8112: Indian Standard Ordinary Portland cement, 43 grade-Specification. Bur Indian Stand (2013)

Density of C-A-S-H in Plain Cement and Limestone Calcined Clay Cement (LC³)

François Avet and **Karen Scrivener**

Abstract The density of C-A-S-H was investigated by [1]H-nuclear magnetic resonance (NMR) on white plain cement and LC³. Despite the high variations in binder composition, the density of the C-A-S-H is found similar between all the systems, also being independent of the calcined kaolinite content of calcined clay in LC³.

Keywords C-A-S-H · Density · Hydration

1 Introduction

The combination of limestone and calcined clay in Limestone Calcined Clay Cements (LC³) permits to continue decreasing the clinker factor in cement. This will overcome the issue of global shortage of traditional SCMs such as fly ashes or slags [1, 2]. The hydration of LC³ benefits from additional reactions compared with plain cement. The pozzolanic reaction of metakaolin in calcined clay mainly leads to the formation of C-A-S-H [3]. The calcite from limestone reacts with the aluminate from the clinker to form carboaluminate hydrates [4, 5]. This reaction is limited by the amount of aluminate of clinker. In LC³, the metakaolin provides extra aluminate, which enhances the formation of carboaluminates [6]. Most of hydration products are well-characterized due to their fixed stoichiometric composition and density. However, the main hydration product, C-A-S-H, faces changes in composition and possibly in terms of morphology depending on the binder composition [7–10]. In this study, the objective is to investigate the density of C-A-S-H. The density will be determined by [1]H-nuclear magnetic resonance (NMR) combined with mass and volume balance. LC³ blends with various kaolinite contents in clay are compared with plain cement.

F. Avet (✉) · K. Scrivener

Laboratory of Construction Materials, EPFL, 1015 Lausanne, Switzerland

e-mail: francois.avet@epfl.ch

2   Materials and Methods

The use of ^{1}H-NMR requires materials with low iron content. A white cement was used. Due to the very low alkali content of the white cement, the alkali and sulfate content was adjusted in order to ensure similar hydration to gray cement. Most of the clays contain relatively high amount of iron as well. Two calcined clays were used, with 95.0 and 39.0% of calcined kaolinite. Two other systems were studied, by diluting the 95.0% kaolinitic clay with 50 and 75% of quartz. The calcined kaolinite content of these two mixes was 47.5 and 23.8%. The characteristics of the cement, limestone and clay used are shown in Table 1. WLC^3-50 was cast, with about 55 parts of adjusted white cement, 30 parts of calcined clay and 15% of limestone. Cement pastes were cast using water to binder ratio of 0.4. The fresh pastes were directly injected in the ^{1}H-NMR glass tubes and sealed. The samples were then tested at 28 days of hydration.

For ^{1}H-NMR experiments, the Carr-Purcell-Meiboom-Gill (CPMG) sequence was run on the different systems to measure the signals of the liquid water in capillaries, gel pores and C-A-S-H interlayer. The amount of "solid" water bound to portlandite, ettringite and AFm phases is detected by the quad-echo (QE) sequence. A combination of mass balance and volume permits to determine the density of the C-A-S-H phases, following the procedure described by Muller in [11].

Table 1 Physical and chemical characteristics of the calcined clays, quartz, white cement and limestone used

	Calcined clays		Quartz	White cement	Limestone
Calcined kaolinite content (wt%)	95.0	39.0	0	–	–
$D_{v,50}$ (μm)	5.1	10.8	11.2	7.4	7.2
BET specific surface (m^2/g)	9.6	10.7	1.2	1.3	1.8
SiO$_2$	52.0	71.0	99.8	24.2	0.1
Al$_2$O$_3$	43.8	23.4	–	1.9	–
Fe$_2$O$_3$	0.3	1.0	–	0.3	–
CaO	–	0.3	–	69.2	55.0
MgO	–	0.4	–	0.7	0.2
SO$_3$	0.1	–	–	2.0	–
Na$_2$O	0.3	0.2	–	0.2	0.1
K$_2$O	0.1	1.4	0.1	0.1	–
TiO$_2$	1.5	1.2	–	0.1	–
P$_2$O$_5$	0.2	0.2	–	0.3	–
MnO	–	–	–	–	–
Others	0.1	–	–	0.3	–
LOI	1.5	0.9	0.1	0.9	42.6

3   Results

The water distribution at 28 days for the different systems is shown in Fig. 1. The classes of water are classified from the shortest to the longest relaxation time of the hydrogen spins. The solid water is higher for the reference plain white cement (WPC). This is explained by the pozzolanic reaction of the metakaolin in calcined clay. This leads to the consumption of portlandite. However, the decrease is only about 20%, while the portlandite is almost fully consumed, as shown in [12]. This relatively low decrease can be explained by the dominance of ettringite, a water-rich phase, in the solid water signal, combined with the higher formation of AFm phases in WLC^3-50 systems. The amount of C-A-S-H interlayer water is the lowest for WLC^3-50 (23.8%). This is due to the low metakaolin content for this blend, leading to a lower amount of C-A-S-H formed during the pozzolanic reaction. The amount of interlayer is similar for the other WLC^3-50 blends, which is in agreement with the reaction degree of metakaolin observed in [12]. The ratio of gel to interlayer water is globally higher for the WLC^3-50 blends compared with WPC. Finally, the amount of capillary water is higher for WLC^3-50 blends. This can be explained by the significant refinement of porosity observed for these blends [13]. Still a high amount of water is present in the pores, but the pores are too fine for the growth of hydration products, leading to a slowing down of clinker hydration [12]. Moreover, the finer porosity also means that a higher fraction of capillaries is water-saturated. The empty pores are not detected by ^{1}H-NMR, and this would impact to a greater extent the WPC system, containing a coarser porosity.

Based on the results obtained in Fig. 1 combined with mass and volume balance, the density of the C-A-S-H was determined in Fig. 2. Similar bulk density (including gel pores) of about 1.9 g cm^{-3} is obtained for WPC and the different WLC^3-50 blends. The solid density, excluding gel water, is also very close for all systems. The slight variations are in the range of error. A value of about 2.8 g cm^{-3} is determined.

Fig. 1 Signal fraction of the different water populations for WPC (white Portland cement) and the WLC^3-50 with various calcined kaolinite content in calcined clay
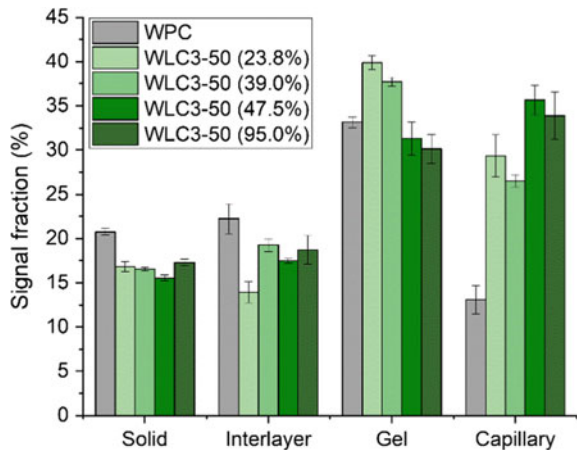
Fig. 2 Bulk and solid densities of C-A-S-H for WPC and the WLC^3-50 with various calcined kaolinite content in calcined clay. The bulk and solid densities include and exclude gel water, respectively
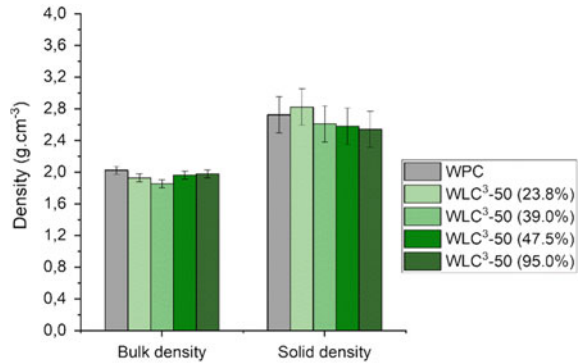
4 Conclusion

The distribution of water in WPC and WLC^3-50 blends shows some differences. The amount of capillary pores remaining is much higher for WLC^3-50 blends, the solid water is slightly lower than WPC and the gel to interlayer ratio is also slightly higher. Despite the change of binder composition and the large decrease in the clinker factor in WLC^3-50 blends, the density of C-A-S-H is found very similar.

References

1. IEA IEA, World Business Council for Sustainable Development: Technology roadmap low carbon transition in the cement industry 66 (2018)
2. Scrivener, K.L., John, V.M., Gartner, E.M.: Eco-efficient cements: potential economically viable solutions for a low-CO$_2$ cement-based materials industry
3. Ambroise, J., Murat, M., Pera, J.: Hydration reaction and hardening of calcined clays and related minerals. IV. Experimental conditions for strength improvement on metakaolinite minicylinders. Cem. Concr. Res. **15**, 83–88 (1985)
4. Péra, J., Husson, S., Guilhot, B.: Influence of finely ground limestone on cement hydration. Cem. Concr. Compos. **21**, 99–105 (1999). https://doi.org/10.1016/S0958-9465(98)00020-1
5. Lothenbach, B., Le Saout, G., Gallucci, E., Scrivener, K.: Influence of limestone on the hydration of Portland cements. Cem. Concr. Res. **38**, 848–860 (2008). https://doi.org/10.1016/j.cemconres.2008.01.002
6. Antoni, M., Rossen, J., Martirena, F., Scrivener, K.: Cement substitution by a combination of metakaolin and limestone. Cem. Concr. Res. **42**, 1579–1589 (2012)
7. Love, C.A., Richardson, I.G., Brough, A.R.: Composition and structure of C-S-H in white Portland cement-20% metakaolin pastes hydrated at 25 C. Cem. Concr. Res. **37**, 109–117 (2007). https://doi.org/10.1016/j.cemconres.2006.11.012
8. Rossen, J.E., Scrivener, K.L.: Optimization of SEM-EDS to determine the C-A–S–H composition in matured cement paste samples. Mater. Charact. **123**, 294–306 (2017). https://doi.org/10.1016/j.matchar.2016.11.041

9. Mota, B., Matschei, T., Scrivener, K.: The influence of sodium salts and gypsum on alite hydration. Cem. Concr. Res. **75**, 53–65 (2015). https://doi.org/10.1016/j.cemconres.2015.04.015
10. Avet, F., Boehm-Courjault, E., Scrivener, K.: Investigation of C-A-S-H composition, morphology and density in Limestone Calcined Clay Cement (LC3). Cem. Concr. Res. **115**, 70–79 (2019). https://doi.org/10.1016/j.cemconres.2018.10.011
11. Muller, A.C.A, Scrivener, K.L., Gajewicz, A.M., Mcdonald, P.J.: Densification of C−S−H Measured by 1 H NMR Relaxometry. J. Phys. Chem. 1–43 (2012). https://doi.org/10.1021/jp3102964
12. Avet, F., Scrivener, K.: Investigation of the calcined kaolinite content on the hydration of Limestone Calcined Clay Cement (LC3). Cem. Concr. Res. **107**, 124–135 (2018). https://doi.org/10.1016/j.cemconres.2018.02.016
13. Dhandapani, Y., Santhanam, M.: Assessment of pore structure evolution in the limestone calcined clay cementitious system and its implications for performance. Cem. Concr. Compos. **84**, 36–47 (2017). https://doi.org/10.1016/j.cemconcomp.2017.08.012

Microstructural Modelling of the Microstructural Development of Limestone Calcined Clay Cement

Meenakshi Sharma, Sreejith Krishnan and Shashank Bishnoi

Abstract This paper investigates the microstructural development of limestone calcined clay cements (LC3) using microstructural modelling. The microstructure of ternary blended cements containing 15, 30 and 45% limestone and calcined clay is simulated using microstructural modelling platform μic. It is found that replacing cement with limestone and calcined clay significantly increases the porosity of pastes. The increase in the porosity is observed to depend on the percentage replacement of cement with limestone and calcined clay. It is also observed that just the addition of fine limestone and calcined clays is not sufficient to explain the reduction in experimentally observed threshold pore diameter in pastes containing limestone and calcined clay. The results suggest that it is important to consider the modification in the hydration product (CASH) in order to explain the reduced threshold pore diameter of LC3 systems.

Keywords Limestone · Calcined clay · Microstructure · Model

1 Introduction

Pore structure and porosity of cementitious materials significantly influence their durability and service life [1]. The complex pore network in cementitious materials develops by the reaction of cement with water, which depends on the water to cement ratio (w/c), temperature, curing conditions and supplementary cementitious materials [2]. Supplementary cementitious materials (SCMs) react with the portlandite produced from cement hydration and refine the pore structure [3]. SCMs are added in cements to reduce the amount of clinker and consequently to reduce the anthropogenic CO_2 emissions. The addition of limestone and metakaolin as SCMs is reported to significantly reduce the clinker factor without significantly influencing the compressive strength [4]. Literature report that limestone and metakaolin reduce the conductivity and permeability of cementitious materials [5]. The reduction in the conductivity and permeability is attributed to the refinement of the pore

M. Sharma (✉) · S. Krishnan · S. Bishnoi
Indian Institute of Technology Delhi, New Delhi, India
e-mail: meenakshi1783@gmail.com

structure by the addition of fine particles of limestone and metakaolin. It has also been reported that limestone and metakaolin significantly reduce the threshold pore diameter of pastes due to the precipitation of low-density hydration products such as hemi-carboaluminates and mono-carboaluminates [6]. The addition of limestone and calcined clay modifies the morphology of the major hydration product, CSH, due to increased alumina uptake [7]. It has been reported that limestone and calcined clay change the alumina to silica ratio (A/S) of CSH gel from 0.047 (in OPC paste) to 0.12 (in LC3 paste) [8]. Based on the comparison of gel–space ratio versus strength curves for OPC and LC3. Krishanan [8] suggested that the alumina uptake in the CASH reduces the density of CASH from 2.0 g/cc to as low as 1.4 g/cc. The low-density CASH will occupy more space, which may have influence on the pore structure and threshold pore diameter of LC3 pastes. In the present work, an attempt is made to explain the reduction in threshold pore diameter of LC3 pastes. The influence of two main factors that may influence the pore structure of LC3 systems, the filler effect and formation of low-density hydration products by the addition of limestone and calcined clay and the change in the density of CASH due to higher alumina uptake, is studied using microstructural modelling.

The microstructure simulations of three limestone calcined clay cements (LC3) having different clinker factors are carried out using the microstructural modelling platform μic.

2 Microstructure Simulation

2.1 Properties of Materials Used

Figure 1 shows the particle size distribution of the raw materials used. The largest particle size is kept at 40 μm for the simulations, by truncating the particle size distribution of the raw materials, to reduce the size of the three-dimensional simulation volume. However, in order to study the influence of filler effect of these particles on

Fig. 1 Particle size distribution of raw materials used in simulations
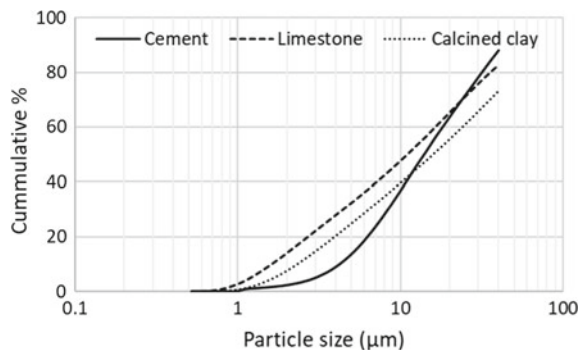
Table 1 Mix proportions of pastes simulated in the study

Sr. No.	Mix ID	w/c	Cement	Gypsum	Calcined clay	Limestone
1	OPC	0.4	95	5	–	–
2	LC3-85	0.4	80	5	10	5
3	LC3-70	0.4	65	5	20	10
4	LC3-55	0.4	50	5	30	15

microstructure development, the finer particles sizes are not truncated. The chemical composition and specific gravity of the raw materials, used in the simulations, can be found elsewhere [8]. The limestone to calcined clay ratio is kept constant at 1:2, and the w/c ratio is kept constant at 0.4. Three different LC3 having clinker factors 0.55, 0.70 and 0.85 are used for simulations. Table 1 shows the mix proportions of pastes simulated in the study.

2.2 Simulation Parameters

In the present work, the microstructure of hydrated cement systems are simulated using the microstructural modelling platform μic. This platform is used as the pixel size is not restricted, and the microstructure for a realistic particle size distribution of raw materials having finer particles can be generated. This platform can simulate hydration of different phases of cement and mineral additives. The size of the simulation volume is kept constant at 100 μm, and the voxel size is kept 0.25 μm, which is found sufficient to simulate the influence of the smallest size (around 0.60 μm) of the raw materials used in the study. The particles were placed using a random packing algorithm to place particles according to their descending diameters.

The degree of hydration (DoH) of the cement phases used for simulating the microstructure of OPC and LC3 pastes [8] are given in Tables 2 and 3, respectively.

The hydration reactions, suggested by Krishnan [8] for the hydration of cement phases, limestone and calcined clay in OPC systems and LC3 systems are used for the simulations. The reactions were suggested based on the experimental microstructural changes observed [8].

Table 2 Degree of hydration of phases used for the hydration of OPC paste

Days	Alite	Belite	Ferrite
1	0.72	0.18	0.25
3	0.85	0.24	0.28
7	0.90	0.37	0.40
28	0.91	0.51	0.56
90	0.97	0.85	0.57

Table 3 Degree of hydration of phases used for the hydration of LC3 paste

Days	Alite	Belite	Ferrite
1	0.75	0.20	0.49
3	0.80	0.30	0.60
7	0.83	0.31	0.61
28	0.84	0.33	0.62
90	0.85	0.35	0.63

Table 4 Density of CASH used for simulations

Density of CASH	LC3-85	LC3-70	LC3-55
Case 1	2	2	2
Case 2	1.95	1.85	1.4

2.3   Simulated Microstructure

For LC3 systems, two cases are simulated, as mentioned in Table 3. In case 1, it is assumed that the addition of limestone and calcined clay has no influence on the density of CASH. In case 2, the density of CASH is modified LC3 systems in order to match the gel–space ratio vs strength curves of OPC [8] (Table 4).

Figure 2 shows the two-dimensional snapshots of the simulated microstructure of LC3-55 at 90 days. The change in density of CASH seems to significantly reduce the porosity of LC3-55, as for case 1 the proportion of black colour, which represents pores, is higher compared to case 2.

The mercury instruction porosimetry measurements are simulated on the generated microstructures in order to simulate the pore size distribution of the pastes.
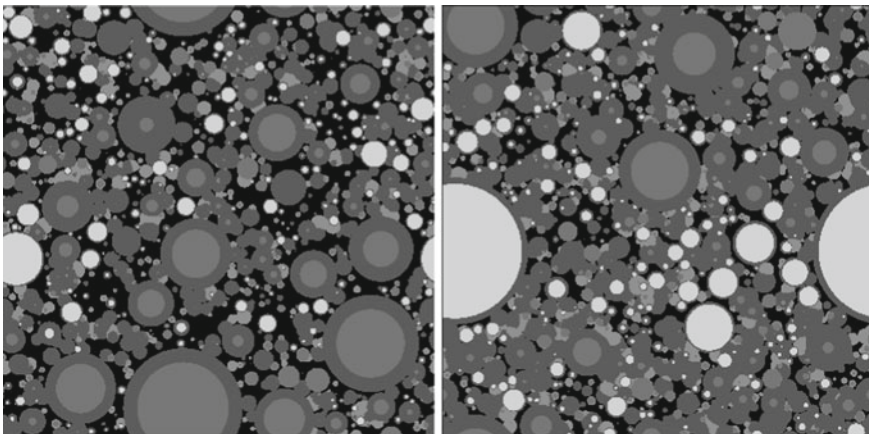
Fig. 2 Simulated microstructure of LC3-55 at 90 days for (left) case 1 and (right) case 2 with pores in black colour and cement, clay, limestone and hydration products in different grey shades

These simulations are carried at a voxel size of 0.1 µm in order to get information of pore size as small as 100 nm.

3   Results and Discussion

Figures 3 and 4 show the simulated pore size distribution of pastes at 28 days and 90 days for case 1 and case 2, respectively. It is shown in Fig. 3 that the addition of fine limestone and calcined clay slightly reduces the threshold pore diameter of the cement paste at 28 days for the cements containing 15 or 30% of limestone calcined clay. However, the same is not observed for the cement containing 45% limestone calcined clay (LC3-55). The replacement of 45% cement with limestone calcined clay significantly increases the threshold pore diameter of the cement paste and forms a coarser pore structure. As the hydration continues to 90 days, it is observed that the porosity and the threshold pore diameter reduces significantly in OPC system. However, the same is not observed for LC3 systems due to little hydration in LC3. In fact, it is observed that OPC system has significantly finer pore structure and smaller threshold pore diameter compared to LC3 systems.

For case 2, where the structure of the hydration product CASH is modified by changing the specific gravity of CASH to match the porosity suggested by Krishnan

Fig. 3 Simulated pore size distribution of pastes for case 1 at (**a**) 28 days and (**b**) 90 days
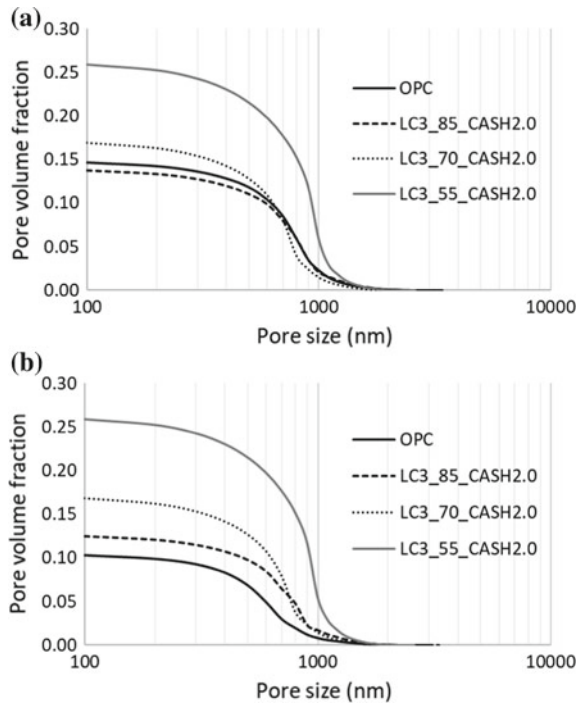
Fig. 4 Simulated pore size
distribution of pastes for case
2 at (**a**) 28 days and
(**b**) 90 days
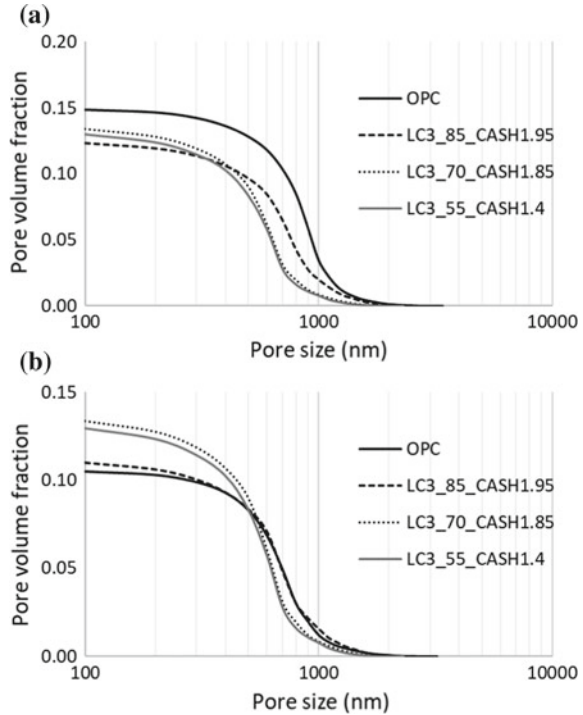
[8], a significant reduction in the threshold pore diameter is observed in LC3 systems, especially the systems having high replacement of limestone and calcined clay. However, most of the advantage of reduced threshold pore diameter is lost at 90 days, and the threshold pore diameter of the LC3-85 (containing 15% limestone and calcined clay) is found similar to the OPC systems. A slight reduction in the threshold pore diameter of LC3 system containing high proportions of limestone and calcined clay is observed compared to OPC system. This suggests that just the addition of fine limestone and calcined clay cannot explain the reduction of threshold pore diameter and the significant reduction in permeability of LC3 systems. A significant modification of hydration production CASH in LC3 systems must be considered to explain the reduction in the permeability of LC3 systems.

4   Conclusions

This paper investigates the microstructural development of limestone calcined clay cements using microstructural modelling. The microstructure of paste samples, made with normal OPC and with LC3 containing different proportions of limestone and clay, is simulated using μic. The pore size distribution of the microstructures is

simulated by performing mercury intrusion porosimetry simulation. The following conclusions are drawn:

- The filler effect and the reaction of limestone and calcined clay with portlandite are not sufficient to reduce the threshold pore diameter of LC3 pastes compared to OPC pastes.
- It is important to consider the modification in the hydration product CASH to explain the reduced threshold pore diameter, which can explain the significant reduction in permeability of LC3 pastes.

References

1. Mehta, P.K., Monterio, P.J.: Concrete: microstructure, properties and materials. McGraw Hill, New York (1993)
2. Taylor, H.F.W.: Cement chemistry, 2nd edn. Thomas Telford, London (1997)
3. Duan, P., et al.: Effects of metakaolin, silica fume and slag on pore structure, interfacial transition zone and compressive strength of concrete. Constr. Build. Mater. **44**, 1–6 (2013)
4. Antoni, M., Rossen, J., Martirena, F., Scrivener, K.: Cement substitution by a combination of metakaolin and limestone. Cem. Concr. Res. **45**, 1579–1589 (2012)
5. Dhandapani, Y., Santhanam, M.: Assessment of pore structure evolution in the limestone calcined clay cementitious system and its implications for performance. Cement. Concr. Compos. **84**, 36–47 (2017)
6. Krishnan, S., Bishnoi, S.: Understanding the hydration of dolomite in cementitious systems with reactive aluminosilicates such as calcined clay. Cem. Concr. Res. **108**, 116–128 (2018)
7. Wilson, W. et al.: Micro-chemo-mechanical characterization of a limestone-calcinated-clay cement paste by statistical nanoindentation and quantitative SEM-EDS. In: Martirena, F, Favier, A., Scrivener, K. (eds.) Proceedings of the 2nd International Conference on Calcined Clays for Sustainable Concrete 2018, pp. 494–499. Springer Netherlands, Dordrecht (2018)
8. Krishnan, S.: Hydration and microstructure development in limestone calcined clay cement. Ph.D. Dissertation, IIT Delhi (2019)

Hydration of Tricalcium Silicate Blended with Calcined Clay

Shiju Joseph, Ahmed Khalifa and Özlem Cizer

Abstract Hydration of triclinic tricalcium silicate (C_3S) blended with three different natural clays was investigated in this work. Pure C_3S, C_3S blended with metakaolin and fine quartz was used as references. Blends were made with 1:2 ratio of calcined clay/quartz and C_3S. A water-to-solid ratio of 2/3 was used. The samples were cured at 20 °C for 7 days of hydration. The total heat release was measured using isothermal calorimetry, and the degree of hydration of C_3S was determined using XRD/Rietveld analysis and portlandite content using TGA analyzed by tangent method. The results show that there is a higher heat release with higher kaolinitic content. The degree of hydration of C_3S in blends with calcined clay was found to be lower after 7 days of hydration compared to the reference systems.

Keywords Natural clay · Kaolinite · Kinetics

1 Introduction

Blending ordinary Portland cement (OPC) with supplementary cementing materials can improve the performance of concrete with regard to mechanical properties and durability [1]. With the reducing availability of traditional supplementary cementitious materials such as blast furnace slag and fly ash and rising demand for cement, it is necessary to look for sustainable alternatives. With large quantities of clay deposits available globally, calcined clay is currently considered as a high potential option [2, 3]. In this paper, the pozzolanic reactivity of natural calcined clays is investigated till 7 days of hydration when blended with C_3S, the primary phase of OPC.

S. Joseph (✉) · A. Khalifa · Ö. Cizer
Department of Civil Engineering, KU Leuven, 3001 Heverlee, Belgium
e-mail: shiju.joseph@kuleuven.be

411

Table 1 Chemical composition of the raw clay

Raw clay	SiO$_2$	Al$_2$O$_3$	CaO	Fe$_2$O$_3$	TiO$_2$	MgO	LOI
C1	49.3	33.89	0.09	0.97	0.87	0.25	12.8
C2	59.89	23.53	0.22	1.22	1.34	0.34	8.3
C3	52.37	27.06	0.68	2.87	1.12	0.61	9.5

Table 2 Mineralogical composition of the raw clay

Raw clay	Kaolinite	Illite	Pyrophyllite	Quartz	Anatase
C1	75	16	–	8	1
C2	34	35	–	30	1
C3	13	30.4	43.6	13	1

2 Materials and Methods

Triclinic tricalcium silicate (C$_3$S) purchased from SARL minerals (France) and three natural clays were used in this study. The chemical composition of the raw clays is given in Table 1, and the mineralogical composition is given in Table 2. These clays were calcined using laboratory muffle furnace at 800 °C.

Pastes were prepared in a climate-controlled room of 20 °C with water-to-solid (w/s) ratio of 2/3. A ratio of 1:2 is used for calcined clay blended with C$_3$S. For reference, pure C$_3$S paste and blends of C$_3$S-fine quartz and C$_3$S-metakaolin with 1:2 ratio were also used.

Isothermal calorimetry (8-channel TAMair) was performed on these mixes till 7 days of hydration at 20 °C. X-ray diffraction (XRD) and thermogravimetric analysis were performed on samples after hydration stoppage after 7 days of hydration. Hydration of the samples was arrested using a freeze dryer (0.025 mbar pressure) for 2 h. XRD was performed using D2 phaser (5–55°2θ, Cu anode), and TGA was performed at a heating rate of 10 °C/min under N$_2$ flow (60 ml/min) for 30–1000 °C. The degree of hydration of C$_3$S was determined using Rietveld analysis (Topas academic), and portlandite content was determined from TGA using tangent method [4].

3 Results and Discussions

Figure 1 shows the rate of heat release per g of C$_3$S from isothermal calorimetry. It could be seen that there is a significant acceleration associated with filler effect for the blended pastes [5]. Metakaolin and quartz have higher fineness than the calcined clays. The high surface area of metakaolin resulted in the highest peak intensity for the sample with metakaolin (MK). The pastes with C$_3$S blended with fine quartz (Qf)
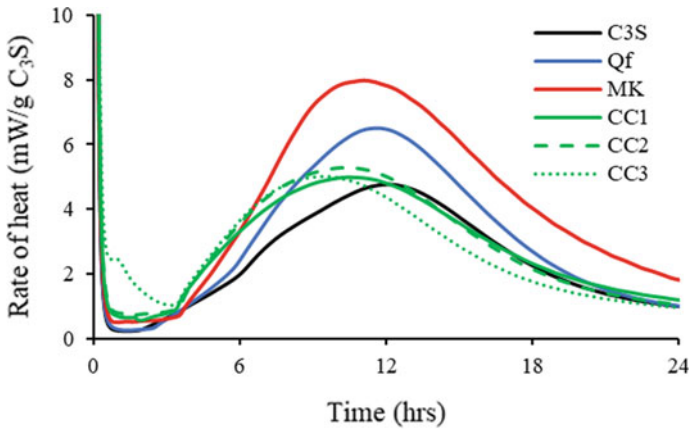
Fig. 1 Rate of heat release per gram of C_3S

also show an increased intensity of main peak of hydration. For mixes with calcined natural clays, there is a reduction in the induction period and a faster occurrence of the main peak of hydration. Previous studies indicated that alumina dissolved in pore solution from SCMs such as fly ash could increase the induction period of alite [6]. This effect is not seen in the studied calcined clays.

Figure 2 shows the cumulative heat per gram of C_3S, and Fig. 3 shows the cumulative heat release per gram of solids measured till 7 days using isothermal calorimetry. It could be seen from Fig. 2 that there is an increase in heat release compared to the reference C_3S paste for all the blended samples. This shall be attributed to a combination of filler effect and pozzolanic reaction. It could be seen that the cumulative heat
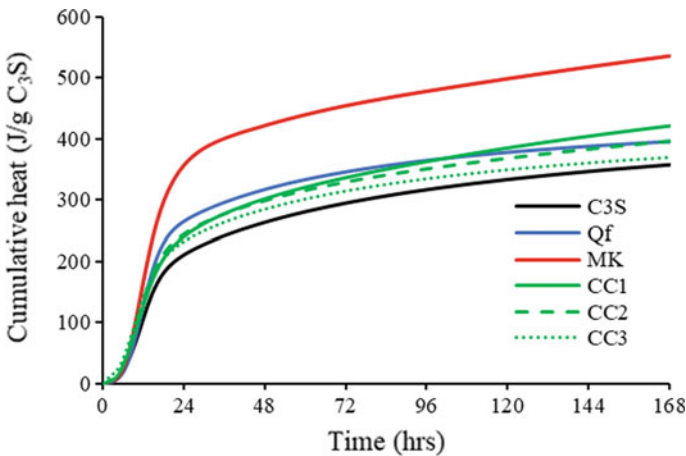
Fig. 2 Cumulative heat release per gram of C_3S
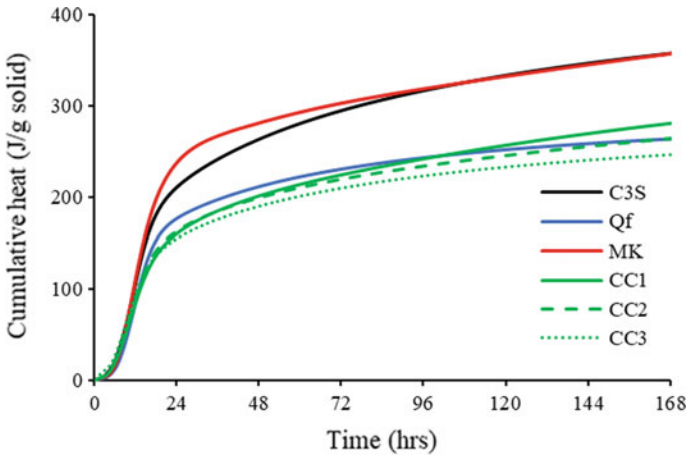
Fig. 3 Cumulative heat release per gram of solid

was higher for Qf compared to CC1 after 1 day of hydration, while by 7 days CC1 has a higher heat release. This is due to the increased pozzolanic reaction of CC1 although the filler effect is lower. While comparing with the three natural calcined clays, there is a direct positive correlation of the total heat released with the kaolinitic content.

Table 3 shows the portlandite content per 100 g paste and the degree of hydration of C_3S determined from TGA and XRD, respectively. It could be seen that there is an increase in the degree of hydration of C_3S with quartz filler (Qf) and metakaolin (MK) which are finer compared to the calcined clays which shall be attributed to the increased surface area available for nucleation of C-S-H. On the other hand, with the calcined natural clays, there is a slight decrease in the degree of hydration of C_3S. For blended systems, lower portlandite content refers to higher portlandite consumption. The portlandite content was found to be much lower than that of Qf, which shows the contribution from pozzolanic reaction as well. The results further show that the portlandite consumption is higher for clay with higher kaolinite content.

Table 3 Portlandite content determined from TGA and the degree of hydration of C_3S determined from XRD

Sample	Portlandite (per 100 g paste)	C_3S degree of hydration
C_3S	21.8	0.81
Qf	15.1	0.88
MK	8.8	0.91
CC1	9.7	0.77
CC2	11.0	0.77
CC3	13.1	0.80

4 Conclusion

In this work, hydration of C_3S blended with natural calcined clays was investigated. Blends with fine quartz and metakaolin were used as references. The results show that for blends with clay, there is an increase in overall heat release by 7 days with increasing kaolinitic content. They also corroborate that calcined clays reduce the degree of hydration of C_3S by 7 days.

References

1. Lothenbach, B., Scrivener, K., Hooton, R.D.: Supplementary cementitious materials. Cem. Concr. Res. **41**(12), 1244–1256 (2011)
2. Scrivener, K.L., Martierena, F., Bishnoi, S., Maity, S.: Calcined clay limestone cements (LC^3). Cem. Concr. Res. **114**, 49–56 (2018)
3. Hollanders, S., Adriaens, R., Skibsted, J., Cizer, O., Elsen, J.: Pozzolanic reactivity of pure calcined clays. Appl Clay Sci **132**, 552–580 (2016)
4. Taylor, H.: Cement Chemistry. Thomas Telford, London (1997)
5. Joseph, S., Bishnoi, S., Van Balen, K., Cizer, O.: Modeling the effect of fineness and filler in early-age hydrationof tricalcium silicate. J. Am. Ceram. Soc., 1–17 (2016)
6. Lothenbach, B., Winnefeld, F., Ben Haha, M., Zajac, M., Ludwig, H.M.: Early hydration of SCM-blended Portland cements: a pore solution and isothermal calorimetry study. Cem. Concr. Res. **93**, 71–82 (2017)

Weibull Probabilistic Analyses on Tensile Strength of Limestone Calcined Clay (LC^3) and Portland Cement Pastes

Fábio C. de Oliveira [ID]**, Sérgio C. Angulo** [ID]**, Marcos K. Pires** [ID]
and Pedro C. R. A. Abrão [ID]

Abstract The tensile strength of limestone calcined clays (LC^3) and Ordinary Portland Cement (OPC) pastes was determined by a point load test (PLT). Testing was carried out on reduced size cubic specimens ($10 \times 10 \times 10$ mm), and the results were analysed using the Weibull probabilistic distribution. Mercury intrusion porosimetry (MIP) was also carried out to complement the investigation. Results showed that, despite being slightly more porous, LC^3 has higher tensile strength than OPC due to the pore refinement caused by pozzolanic reactions. The data variability was three times lower for LC^3 in comparison to OPC, which may be related to the slightly higher fracture energy of the LC^3 samples.

Keywords Point load test · Tensile strength · Weibull

1 Introduction

Supplementary cementitious materials (SCMs) have been used to replace clinker Portland in the last decades and have proven to be useful tools to reduce CO_2 emission from the cement industry [1, 2]. A recent report [3] has indicated that limestone and calcined clays are the most prominent SCMs in terms of availability of resources and may help to achieve the CO_2 emission reduction target for future scenarios. Moreover,

limestone calcined clay cements (LC^3) have great potential to be used as binder for structural concrete, resulting in mechanical properties (strength and elastic modulus) comparable to those of an ordinary Portland cement binder [4].

Most of the standard methods to evaluate the strength of Portland cements makes use of standard sand [5]. Adding sand to a cement paste changes its intrinsic properties since the interfacial transition zone (ITZ) between the cement paste and the aggregate is characterized by a higher porosity [6]. Thus, the mechanical properties of the cement are altered by the addition of sand.

© RILEM 2020
S. Bishnoi (ed.), *Calcined Clays for Sustainable Concrete*, RILEM Bookseries 25,
https://doi.org/10.1007/978-981-15-2806-4_50

Furthermore, the mechanical performance of cementitious materials is usually measured in a small number of samples [7], which are insufficient to determine characteristic values or represent the variability of the results; on the other hand, testing a large number of standard size samples is labour and material intensive. Using alternative methods, such as the point load test (PLT) [8], to characterize small-sized samples can reduce experimental time and material costs. PLT is often used to estimate the strength of irregular rock particles, but it has also been applied to cementitious materials [9, 10].

In this context, the present paper aims to determine the tensile strength of limestone calcined clays (LC^3) and ordinary Portland cement (OPC) pastes using an adaptation of PLT. Testing was carried out on 200 reduced size cubic specimens (10 × 10 × 10 mm), and the variability of the tensile strength was investigated using the Weibull probabilistic analysis. Mercury intrusion porosimetry (MIP) was also carried out to complement the interpretation of the results.

2 Materials and Methods

In this study, Portland cement and LC^3 pastes were prepared. The Portland cement was an ordinary Portland cement (OPC) similar to a CEM I 42.5 N (<5% g/g of SCMs). The LC^3 was composed of the same Portland cement, calcined clay and limestone filler of different particle sizes: finer (Profine 1) and similar (Procarb 5) to that of OPC. The compositions of the cements are presented in Table 1, and their particle size distributions, obtained by laser diffraction, are shown in Fig. 1. Densities for OPC and LC^3, determined by helium pycnometer, were 3.08 and 2.76 g/cm³, while their specific surface area, obtained by N_2 adsorption (BET), was 1.64 and 3.62 m²/g, respectively.

The cement pastes were cast using a water/solids ratio of 0.3 (g/g); the aim was to have different microstructures after hardening. The optimum content of superplasticizer was determined based on the minimum values of viscosity and yield stress of the cement pastes determined by paste rheometer. This condition ensured the particles' dispersion. Contents were 0.4% and 1.0% for OPC and LC3, respectively, in % of cement mass.

Water, superplasticizer and cement were mixed manually for 30 s and then mechanically for 60 s at 10,000 rpm. Pastes were poured into cubic forms (10 × 10 × 10 mm) and vibrated on a vibration table. In the first 24 h, the specimens

Table 1 Cements compositions in mass percentage

Cement	Clinker + CaSO$_4$ (%)	Calcined clay (%)	Filler (%)			
			Filler in OPC	Profine 1	Procarb 5	Total
OPC	95	0	5	0	0	5
LC^3	52	30	3	5	10	18
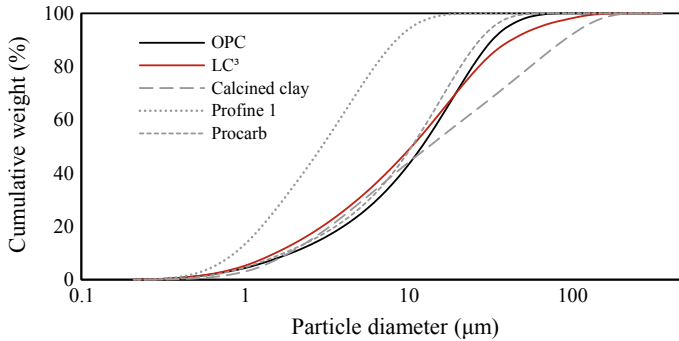
Fig. 1 Particle size distribution of OPC, LC^3 and its constituents

were sealed. After that, curing was carried out by immersion in water for 22 days. Finally, the specimens were oven-dried at 45 °C for five days (enough time until the cessation of mass loss due to water evaporation) and submitted to the mechanical characterization, at 28 days.

2.1 Mechanical Characterization: PLT-LVDT

One-hundred specimens of each paste were submitted to a point load test (PLT) based on ASTM D 5731 [7]. The test was performed in an Instron double-column universal test machine (model 5569) with a 50 KN load cell and a deformation rate of 0.2 mm/min. The apparatus consisted of two devices with semi-spherical tips of tungsten carbide (Fig. 2a), one coupled to the load cell and the other fixed in the bottom, serving as load applicators (Fig. 2c). A sponge ring was placed under the brass ring that served as a sample holder (Fig. 2b); so, when compressed during loading, the contact between the sample and the bottom semi-sphere was ensured. Also, an LVDT was coupled to the apparatus to measure the displacement (Fig. 2c). As output, the test provides a load–displacement curve.

The tensile strength was determined by the Hiramatsu and Oka [10, 11] formula, which states that the tensile strength (σ_t) depends on the compressive breakage force (P) and the distance between the load applicators (R) as shown in Eq. 1.

$$\sigma_t = \frac{0.9P}{R^2} \tag{1}$$

The described method was named PLT-LVDT by our research group, and it was validated using glass as reference material [12].

Weibull probabilistic analysis. The Weibull distribution is useful to statistically describe the tensile strength of brittle materials [13–15]. The analysis consists in ranking the data in ascending order so that an experimental cumulative distribution
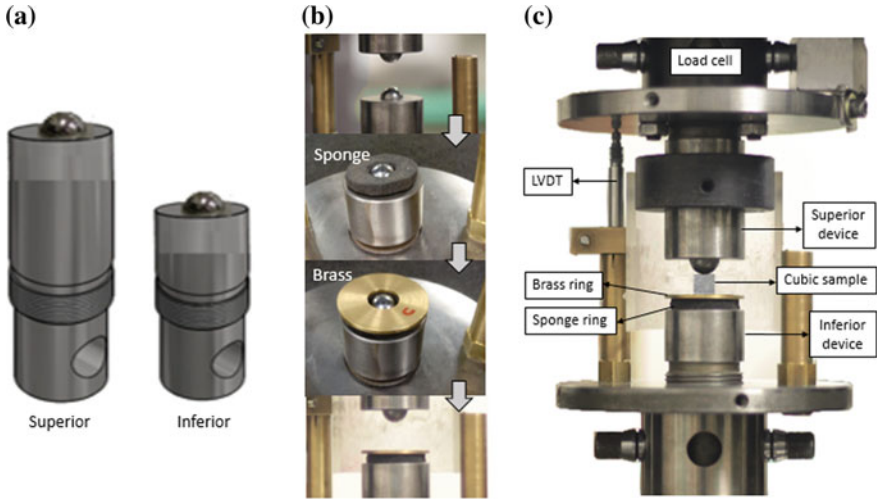
Fig. 2 PLT-LVDT apparatus. **a** Devices for load application, **b** Placement of the sponge and brass rings for sample holding and **c** Apparatus set-up

can be obtained by Eq. 4 [14], where P_s is the survival probability, N is the total number of samples, and n is the position of the sample (in ascending order of tensile strength).

$$P_s = 1 - \left(\frac{n}{N+1}\right) \tag{2}$$

Once the experimental cumulative distribution is known, it can be used in the linearized Weibull cumulative distribution (Eq. 5 [14]) to determine the Weibull parameters by linear regression. In the equation, $\sigma_{t,0}$ is the characteristic tensile strength (where the probability of failure = 36%), and m is the Weibull modulus, which serves as a measurement of the samples' relative variability, where a higher value of m indicates a lower variability.

$$\ln\left[\ln\left(\frac{1}{P_s}\right)\right] = m\left[\ln(\sigma_t) - \ln(\sigma_{t,0})\right] \tag{3}$$

A Kolmogorov–Smirnov nonparametric test was held to ensure that the Weibull distribution is valid to describe the set of data.

2.2 Porosity Analyses

Two methods were used to determine the specimens' porosity: (1) Archimedes's principle, before mechanical characterization and for all specimens and (2) MIP, after mechanical characterization and for two specimens of each paste. The samples submitted to MIP were the fragments of the specimens that showed the highest and lowest tensile strength. Testing was carried out in a micromeritics porosimeter (Autopore III). The test parameters were evacuation time of 5 min, evacuation pressure of 50 μm Hg and equilibrium time of 30 s.

3 Results

3.1 Mechanical Characterization

Results for the mechanical characterization are given in Table 2 and Fig. 3, in the form of histogram and failure probability, together with the respective Weibull analysis.

Table 2 PLT-LVDT results of the OPC and LC^3 pastes at 28 days. Here, m is the Weibull modulus, σ0 is the characteristic tensile strength, and K–S is the goodness of fit of the data

Parameter	OPC	LC^3
Mean (MPa)	8.81	11.44
Coeff. var.	0.34	0.11
m	3.27	9.18
σ0 (MPa)	9.83	11.96
K–S (Kolmogorov–Smirnov test)	0.08	0.06
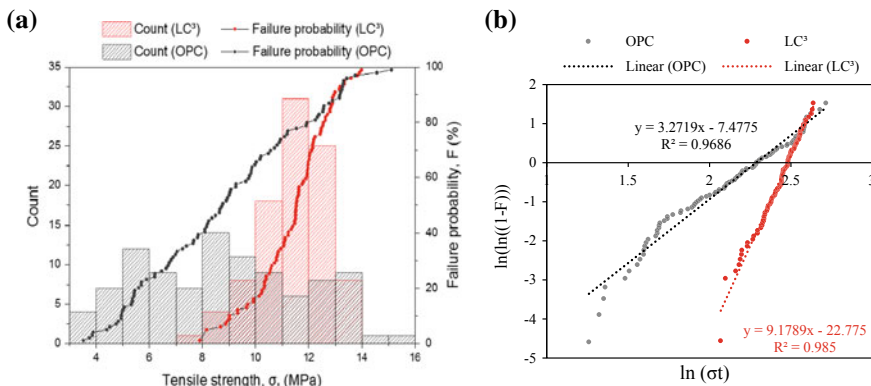
Fig. 3 PLT-LVDT results for tensile strength. **a** Histogram (left axis) and failure probability (right axis) versus tensile strength curve. **b** Weibull analysis
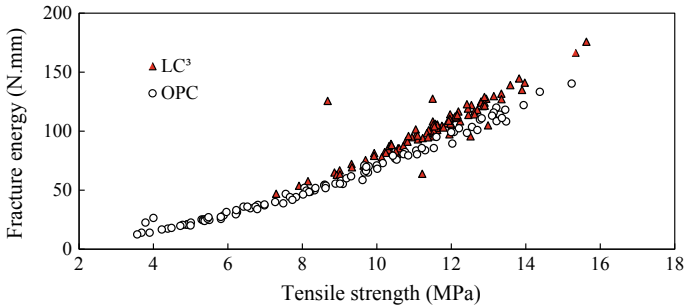
Fig. 4 Tensile strength versus fracture energy of OPC and LC^3 samples

The data showed an acceptable goodness of fit (lower than the critic K–S of 0.14), which means that the Weibull distribution is good to describe the tensile strength observations. LC^3 presented a higher tensile strength than OPC. The failure probability at around 10 MPa is 70% for OPC, while for LC^3 it is only 20%.

The data variability is about three times lower for LC^3 ($m = 9.2$) in comparison with OPC ($m = 3.3$), which goes against what was expected. According to Griffith [15, 16], the strength of brittle materials depends on defects in its microstructure, such as large pores. Once the pores sizes in LC^3 are finer than those in OPC (as will be shown in the next section), a large pore is expected to have greater influence on LC^3 than on OPC. Thus, we presumed that the tensile strength would be more variable for LC^3, contrary to what was observed.

The low variability of the LC^3 paste (in comparison to OPC) may be related to the limestone filler. According to Das et al. [17], the use of limestone filler in binary and ternary cementitious systems hinders the propagation of cracks and increases the energy dissipation during loading. This statement corroborates the observations presented in Fig. 4, which indicates that for a given value of tensile strength the LC^3 samples absorb more energy before rupture than the OPC samples. The enhancement of crack-tolerance caused by the limestone filler reduces the susceptibility of the samples to defects and, consequently, lowers the data variability.

It is worth mentioning that the fracture energy was assumed to be the area under the load–displacement curve obtained by the PLT-LVDT test. The authors are aware that there are specific methods to determine the fracture energy [18] and that the obtained values may not be accurate; however, the results may be used by way of comparison.

3.2 Porosity Characterization

Table 3 shows the porosity determined by Archimedes' principle, where LC^3 presented a total porosity slightly higher than OPC (concluded by statistical analysis using a 95% confidence interval). The coefficient of variation was low for both pastes,

Table 3 The porosity of the OPC and LC^3 samples determined by Archimedes' principle

Paste	Number of samples	Mean (%)	Stand. Dev. (%)	Coeff. Var.
OPC	100	24.9	2.01	0.08
LC^3	100	25.9	0.9	0.03
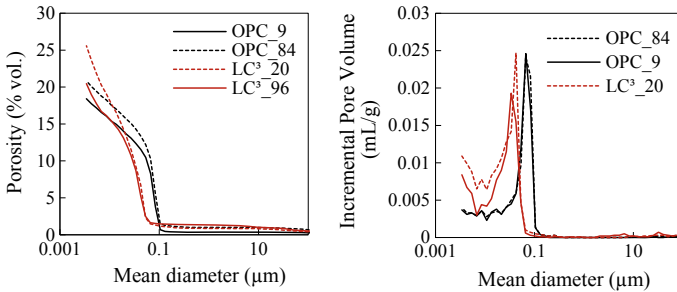
Fig. 5 MIP results of the hardened OPC and LC^3 pastes at 28 days. Solid lines indicate the samples that showed the highest values for tensile strength, and dashed lines indicate the samples that showed the lowest values

which means that the porosity does not vary much from one sample to another sample (in the same paste).

MIP results (Fig. 5) showed a more significant difference between the OPC and LC^3 total porosities and confirmed that LC^3 is more porous. However, LC3 presented a pore refinement due to the calcined clay pozzolanic reaction, which explains its higher tensile strength (Fig. 3). As shown by Kendall et al. [19], the tensile strength of cementitious materials is governed by large and capillary pores and not by the total porosity itself.

4 Conclusion

The tensile strength of OPC and LC^3 samples was determined by a simple method based on the point load test, and the data variability was analyzed using the Weibull distribution.

Despite being slightly more porous, LC^3 presented a higher tensile strength in comparison with OPC as a result of the pore refinement caused by pozzolanic reactions. Furthermore, the data variability was three times lower for LC^3, which is probably due to its slightly higher fracture energy that makes the LC^3 samples less susceptible to defects in the microstructure.

References

1. Gartner, E., Hirao, H.: A review of alternative approaches to the reduction of CO_2 emissions associated with the manufacture of the binder phase in concrete. Cem. Concr. Res. **78**, 126–142 (2015)
2. Technology Roadmap—Low-Carbon Transition in the Cement Industry, p. 66
3. Scrivener, K.L., John, V.M., Gartner, E.M.: Eco-efficient cements: potential economically viable solutions for a low-CO_2 cement-based materials industry. Cem. Concr. Res. **114**, 2–26 (2018)
4. Dhandapani, Y., Sakthivel, T., Santhanam, M., Gettu, R., Pillai, R.G.: Mechanical properties and durability performance of concretes with Limestone Calcined Clay Cement (LC3). Cem. Concr. Res. **107**, 136–151 (2018)
5. C01 Committee: Test Method for Compressive Strength of Hydraulic Cement Mortars (Using 2-in. or [50-mm] Cube Specimens). ASTM International
6. Scrivener, K.L., Crumbie, A.K., Laugesen, P.: The interfacial transition zone (ITZ) between cement paste and aggregate in concrete. Interface Sci. **12**(4), 411–421 (2004)
7. C09 Committee: Test Method for Compressive Strength of Cylindrical Concrete Specimens. ASTM International
8. D18 Committee: Test Method for Determination of the Point Load Strength Index of Rock and Application to Rock Strength Classifications. ASTM International
9. Richardson, D.N.: Point load test for estimation of concrete compressive strength. Mater. J. **86**(4) (1989)
10. Selçuk, L., Gökçe, H.S.: Estimation of the compressive strength of concrete under point load and its approach to strength criterions. KSCE J. Civ. Eng. **19**(6), 1767–1774 (2015)
11. Hiramatsu, Y., Oka, Y.: Determination of the tensile strength of rock by a compression test of an irregular test piece. Int. J. Rock Mech. Min. Sci. Geomech. Abstr. **3**(2), 89–90 (1966)
12. Silva, N.: Método de determinação de resistência à tração e módulo de elasticidade de partículas de agregados naturais. Master's dissertation, University of São Paulo, São Paulo (2018)
13. Askeland, D.R.: Essentials of materials science and engineering, Third edition, SI. Cengage Learn., Stamford, CT (2014)
14. Lim, W.L., McDowell, G.R., Collop, A.C.: The application of Weibull statistics to the strength of railway ballast. Granul. Matter **6**(4), 229–237 (2004)
15. Danzer, R., Supancic, P., Pascual, J., Lube, T.: Fracture statistics of ceramics—Weibull statistics and deviations from Weibull statistics. Eng. Fract. Mech. **74**(18), 2919–2932 (2007)
16. Griffith, A.A.: The phenomena of rupture and flow in solids. Philos. Trans. R. Soc. Math. Phys. Eng. Sci. **221**(582–593), 163–198 (1921)
17. Das, S., Aguayo, M., Sant, G., Mobasher, B., Neithalath, N.: Fracture process zone and tensile behavior of blended binders containing limestone powder. Cem. Concr. Res. **73**, 51–62 (2015)
18. Tavares, L.M., King, R.P.: Single-particle fracture under impact loading. Int. J. Miner. Process. **54**(1), 1–28 (1998)
19. Kendall, K., Howard, A.J., Birchall, J.D., Pratt, P.L., Proctor, B.A., Jefferis, S.A.: The relation between porosity, microstructure and strength, and the approach to advanced cement-based materials [and discussion]. Philos. Trans. R. Soc. Lond. Ser. Math. Phys. Sci. **310**(1511), 139–153 (1983)

Quantifications of Cements Composed of OPC, Calcined Clay, Pozzolanes and Limestone

S. Galluccio and H. Pöllmann

Abstract Alternative and supplementary cementitious materials originate from different sources in nature and also from industrial productions. These materials came into focus again as their use can contribute substantially in the reduction of CO_2 during the manufacturing of cementitious materials. Also, the aspect of reducing the industrial residues by recycling is of substantial importance. As the addition of supplementary cementitious materials leads to different composite cements, it is highly necessary to determine the reaction behavior and their part during the hydration of the interground or interblended components. The different natural occuring materials from volcanic and sedimentary sources like clays and pozzolanic materials are available in high quantities and can be used. Due to their formation, the natural materials differ in their mineralogical and chemical composition and should be optimized for this application. Therefore, clays are often thermally treated to be activated, whereas other products are used without treatment with their original composition. Natural and industrial pozzolans also contain high amounts of amorphous phases which should be determined as they are partially reactive. As these materials do not contain typical cement minerals as calcium silicates and calcium aluminates, their reaction behavior is often caused by their amorphous contents. Other basic sources of mineral additions are coming of artificial sources and are mainly based on industrial residues coming from the processing of ores and include slags ore coming from energy production like fly ashes and bottom ashes. As these materials showing different compositions, their chemical and mineralogical phase relations must be determined also. Some of these supplementary cement additions are known for long times, and like latent hydraulic slags, others must be investigated and characterized newly. As these components vary in their reaction behavior, it is highly likely that their mineralogical quantification relates to their various properties and can be determined by different methods:

S. Galluccio · H. Pöllmann (✉)
Institute of Geosciences and Geography, Mineralogy/Geochemistry, Martin Luther University Halle-Wittenberg, Von-Seckendorff-Platz 3, 06120 Halle, Germany
e-mail: herbert.poellmann@geo.uni-halle.de

S. Galluccio
e-mail: sabrina.galluccio@geo.uni-halle.de

- Rietveld method of these complex systems, including determination of amorphous contents
- Set up and application of a referenced file using **P**artial **or n**ot **k**nown **c**rystal **s**tructure (PONKCS) method for further quantification
- Cluster analysis including the various 2–4 component systems and summarizing similar phase contents and properties
- Set up and determination of phases and contents by **p**artial **l**east **s**quares **r**efinement (PLSR) method.

Different artificial mixtures based on various OPCs with different additions of pozzolans, metakaolinite, limestone, anhydrite, and the quantification of their crystalline and amorphous contents will be demonstrated.

Keywords Mineral quantification · PONKCS · Rietveld method · Cluster analysis · PLSR · XRD · PCA

1 Introduction

CO_2 reduction during the fabrication process of cementitious materials plays a very important role, as tremendous amounts of carbon dioxide are produced during the decarbonation processes of limestone. For this reason, many carbonate-free raw materials are investigated as replacement and supplementary raw materials coming from industry, processing industry, and also from primary industries, but also natural raw materials are under investigation [1, 2, 5, 6, 15, 18–22, 26, 28–30]. These inorganic-based materials are composed of many different crystalline and amorphous components. To understand their reaction behavior and the overall compositions, different mixtures of supplementary cementitious materials (metakaolin, fly ash, and limestone) and other cements are under investigation [12, 27]. All these different and very complex mixtures must be characterized to ensure optimal quality of these cementitious mixtures [10, 11]. For these mineralogical quantifications, different determination methods were applied to quantify the different mineralogical phases [4]. These methods include the determination of amorphous contents [9, 17]. The methods include Rietveld analysis, partial least squares regression (PLSR) [3, 8, 13], cluster analysis [14, 16] with principal component analysis (PCA) and the partial or not known crystal structure method (PONKCS) [25, 32–34]. Using a definite way of investigation starting with the X-ray data and transforming these with cluster analysis and the relevant principal component analysis (PCA) by developing the regression and obtaining a model for these mixtures is highly recommended to use these data for correlation with the properties of these samples.

2 Materials and Methods

2.1 Materials

Using an ordinary Portland cement (OPC, CEM I 42.5 R from Dyckerhoff company), binary mixtures were prepared with the supplementary cementitious materials and industrial residues metakaolin from IMERYS Performance Additives, fly ash from Sasol and calcium carbonate. The OPC is composed of alite (C_3S; $3CaO \cdot SiO_2$), belite (C_2S; $2CaO \cdot SiO_2$), brownmillerite (C_4AF; $4CaO \cdot Al_2O_3 \cdot Fe_2O_3$), tricalcium aluminate (C_3A; $3CaO \cdot Al_2O_3$), and anhydrite. The fly ash contains in addition to the main amorphous content the minerals quartz, hematite, and mullite. The granulated blast furnace slag shows only amorphous component by XRD. Metakaolin contains, besides a large amorphous portion, the minerals anatase, quartz, and illite. The chemical composition of the materials can be seen in Fig. 1. The mixtures with OPC were made by additions of the different supplementary materials in 5 or 10 weight percent steps (5, 10, 20, 30, 40, 50, 60, 70, 80, 90, 95%).
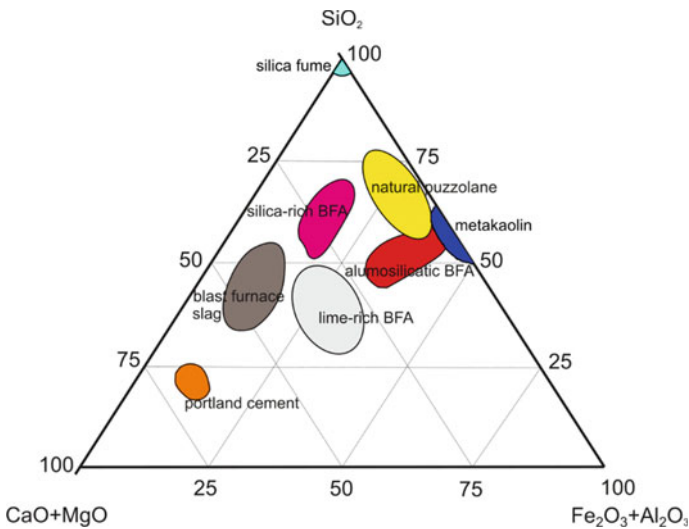
Fig. 1 Chemical constitution of OPC, wastes, and major supplementary cementitious materials groups in the ternary diagram SiO_2–$CaO + MgO$–$Fe_2O_3 + Al_2O_3$ (wt% based)

2.2 X-Ray Fluorescence Spectrometry

The chemical composition was analyzed using the wavelength dispersive X-ray fluorescence spectrometer SRS 3000 with Rh-tube from Siemens company. The measurement was performed using wax discs, prepared from 2 g paraffin wax and 8 g dried sample (40 °C, 24 h).

2.3 Powder X-Ray Diffraction

Powder X-ray diffraction analyses were performed using a PANalytical X'Pert[3] Powder diffractometer equipped with a PIXcel[1D] Detektor and a copper anode (CuKα$_1$ $\lambda = 1.5418$ Å, 45 kV, 40 mA), positioned in the θ/θ Bragg–Brentano geometry. The measured 2θ angle range was 5–70° with a step width of 0.0131 °2θ and counting time per step of 20.4 s. The samples were prepared by the backloading method in a standard sample carrier (diameter: 27 mm) and measured with 15 mm beam mask, 0.04 rad soller slits and fixed slits (0.25° and 0.5°). The measured data were afterward treated for interpretation and quantification using the HighScore suite programs [7].

2.4 Rietveld Method

The Rietveld method [23, 24] was used for the quantification of the total phase composition including the amorphous content [32–34]. For the analysis, the 4.8 version of HighScore Plus from Malvern Panalytical was used [3]. Scale factors, zero shift, and cell and peak shape parameters were refined. The peak shapes were fitted by pseudo-Voigt functions. A rutile standard (10%) (Kronos 2900-TiO$_2$, supplied by KRONOS TITAN GmbH) was added to the samples to determine the amorphous content. The crystallographic information files were taken from the Inorganic Crystal Structure Database and are shown in Table 1.

Table 1 Crystallographic information files used for the Rietveld method

Mineral phase	ICSD collection code
Anatase	200392
Illite	166965
Quartz	79634
Rutile	009161

2.5 Partial Or Not Known Crystal Structure

With the partial or not known crystal structure method (PONKCS), an hkl file is created by fitting a random cell and symmetry to an unknown crystal structure like, for example, an amorphous phase [31]. After calibrating with another method like Rietveld by fitting the pseudo-formula mass, the hkl file can be used for quantitative determinations of samples with similar phase contents without establishing the use of further admixtures with internal standards. Therefore, the actually observed phase peak intensity is used, instead of the data of a crystal structure, that could be based on slightly different substances, that do not really represent the actual occurring phase.

2.6 Partial Least Square Regression

The partial least square regression method (PLSR) can be used for a fast and reliable quality control of several sample sets. For this purpose, a calibration curve with several admixtures must first be prepared. With a statistical method, a regression is performed with relation to the principal component of the sample. The linear regression model is found by projecting the predicted variables and the observable variables to a new space area. The calculated regression model can then be applied to unknown samples for quantifying the principal component very quickly and easily without further admixtures or calculation fittings.

2.7 Cluster Analysis

With the cluster analysis, closely related scans are sorted automatically into separate clusters. Thus, samples with similar phase contents and properties are divided into groups. It thus simplifies the analysis of large amounts of data which can be quantified, even in complex mixtures within seconds after the XRD measurement. These quantifications even can be automated very easily, which can be of high interest for industrial applications. Principal component analysis (PCA) was also performed using the statistical data.

3 Results and Discussion

3.1 PLSR Method Applied on Fly Ash/OPC Mixtures

The artificial supplementary cementitious material fly ash was mixed with Portland cement. The Portland cement is a CEM I of strength class 42.5 with rapid hardening
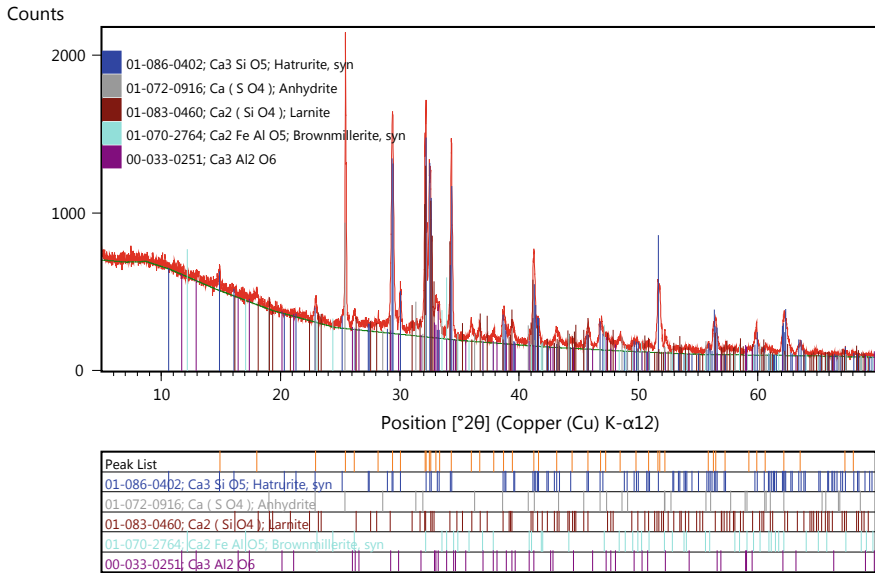
Fig. 2 XRD diagram and phase composition of a CEM I 42.5 R

and is composed like described in Chapter "Potential of Selected South African Kaolinite Clays for Clinker Replacement in Concrete". The mineralogical phase characterization was performed using X-ray diffraction, and the results are shown in Fig. 2. The main OPC phases are alite (hatrurite), belite (larnite), and celite phases as brownmillerite and tricalciumaluminate. During the milling process, anhydrite was added to the clinker.

The fly ash shows amorphous humps in the X-ray diffractogram and the crystalline phases quartz, mullite, and hematite (Fig. 3). OPC was added to the fly ash in 5% resp. 10% steps (5, 10, 20, 30, 40, 50, 60, 70, 80, 90, 95%). With increasing OPC content can be seen how the amorphous humps in the X-ray diffractogram decrease (Fig. 4).

From these series of mixtures, a regression model was created with the PLSR method (Fig. 5). The linear regression was performed with relation to fly ash as main component. Thus, the fly ash content rises in the direction of the right upper side and the OPC content rises in the opposite direction in the diagram. The blue squares mark the initial weights in weight percentages, and the red squares show the fly ash content predicted by the model. The two squares should therefore lie on top of each other as exactly as possible in a good regression line, as it is in the regression model of the fly ash/OPC. The predicted fly ash content does not correspond to the weighed content at one point only (20% fly ash, 80% OPC). This may be due to weighing or preparation mistakes. The model can also be quickly rewritten to use OPC as the main component. Depending on the used main component, the regression model can be applied to determine the unknown fly ash resp. OPC content in other samples.
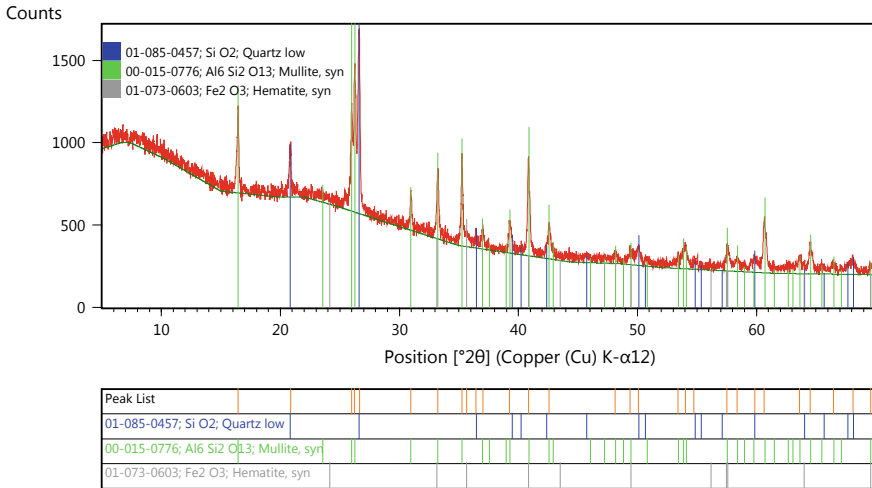
Fig. 3 XRD diagram and phase composition of the used fly ash
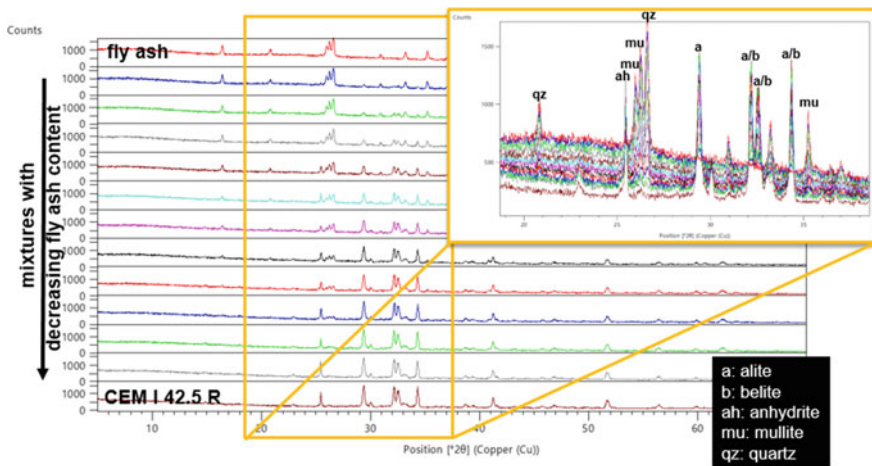
Fig. 4 XRD diagrams showing the change of phase composition of binary mixtures composed of CEM I 42.5 R and fly ash

Figure 6 shows the X-ray diffractogram of a mixture of 90% OPC and 10% fly ash. If the previously created regression model is applied, the predicted fly ash content appears in a blue window. This is 10.09% and thus corresponds to the actual content.
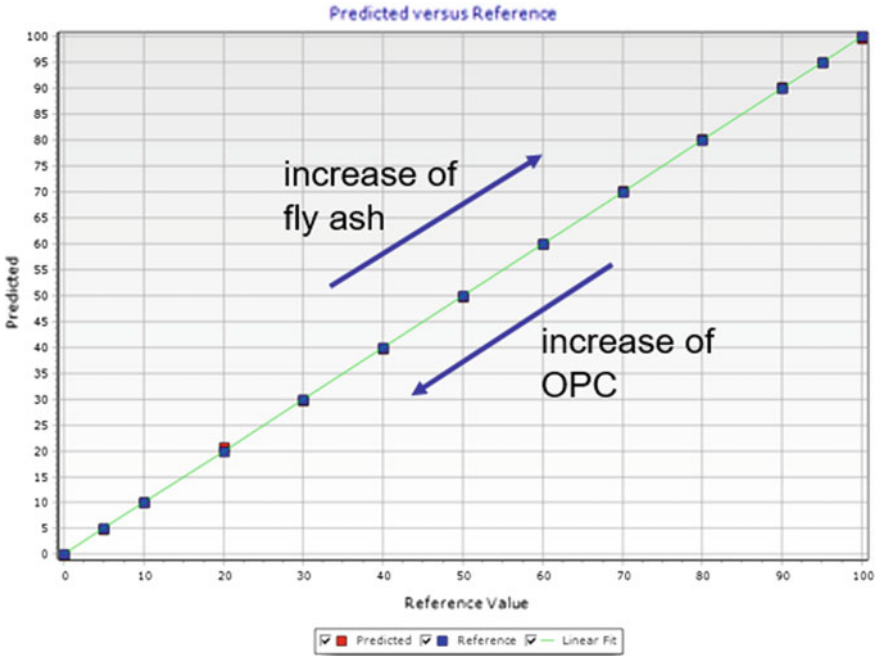
Fig. 5 Partial least squares regression of binary mixtures of OPC (CEM I 42.5 R) and fly ash
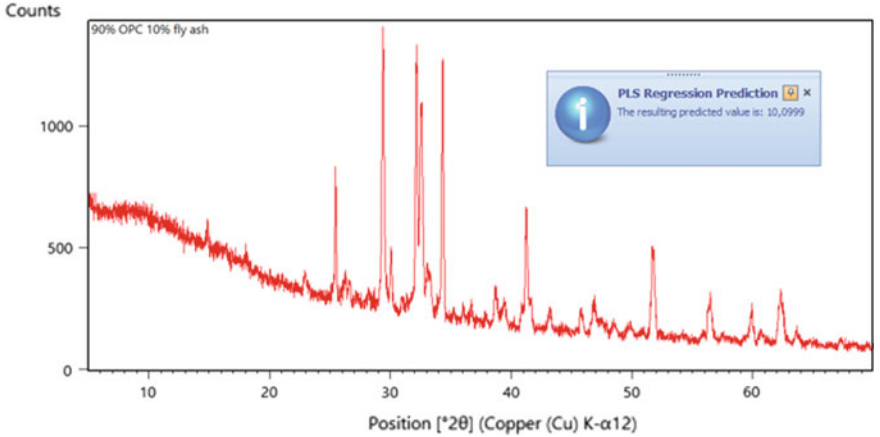
Fig. 6 XRD diagram showing the application of the regression model for quantification of fly ash in a mixture composed of 90% OCP and 10% fly ash. In the blue window is shown the predicted value of 10.09%

3.2 Cluster Analysis Applied on Limestone/OPC Mixtures

For the mixtures of limestone with OPC, the same CEM I was used as in Chapter "Potential for Selected Kenyan Clay in Production of Limestone Calcined Clay Cement". The X-ray diffractogram of the limestone can be seen in Fig. 7 and shows only the crystalline phase of calcite. OPC was added to the limestone in 5% resp. 10% steps (5, 10, 20, 30, 40, 50, 60, 70, 80, 90, 95%). With increasing OPC content, it can be seen how the main peak of calcite in the X-ray diffractogram decreases (Fig. 8). Figure 7 shows five different materials which can be quantified in these mixtures, depending on their compositional variety and on the available calibration curves.

These 13 mixtures were divided by the cluster analysis into four groups with similar phase compositions and thus similar properties (Fig. 9). Closely related scans can be sorted automatically in definite clusters. This helps to analyze large amounts of data sets. In an additional view, the separate X-ray diffractograms of the mixtures can be seen (Fig. 10). Cluster 2 contains the mixtures with intermediate contents of OPC and intermediate contents of limestone, cluster three contains the mixtures with high contents of OPC and therefore low amounts of limestone, and cluster four contains the mixtures with limestone and contents of up to 10% of OPC. With the help of a dendogram, it can be decided whether a more detailed classification with more clusters should be calculated or less classification with fewer clusters, based on only limestone or only OPC. These decisions can be influenced manually, depending on the properties to be installed from these mixtures.

Fig. 7 Compositional variety in five component mixtures important in complex cementitious supplementary materials
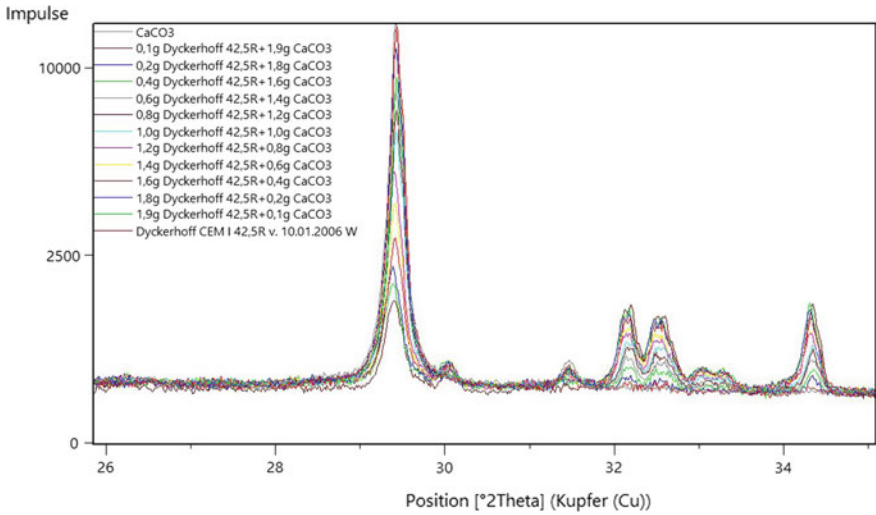
Fig. 8 Change of phase composition of binary mixtures of CEM I 42.5 R and limestone
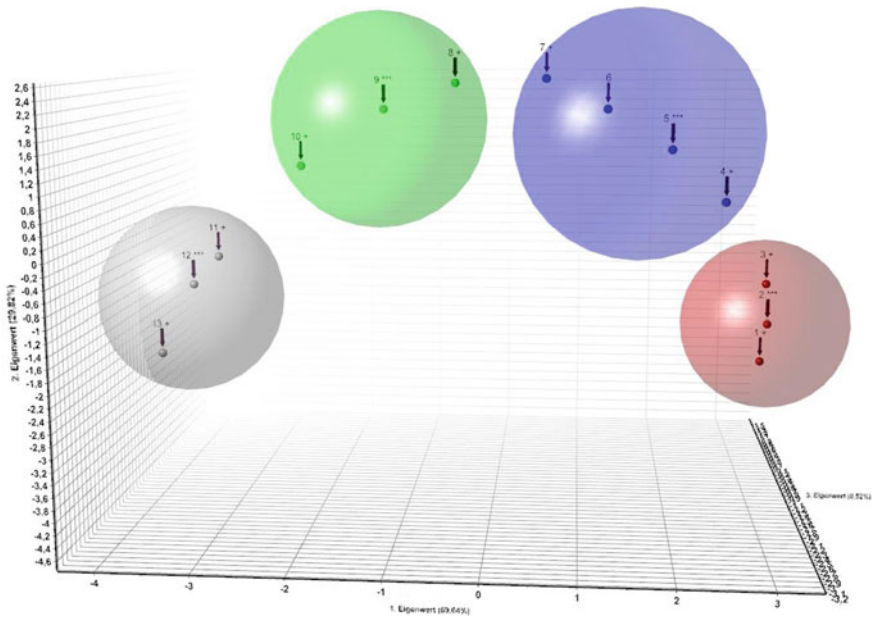
Fig. 9 Thirteen mixtures of limestone and OPC were sorted into four clusters by the cluster analysis
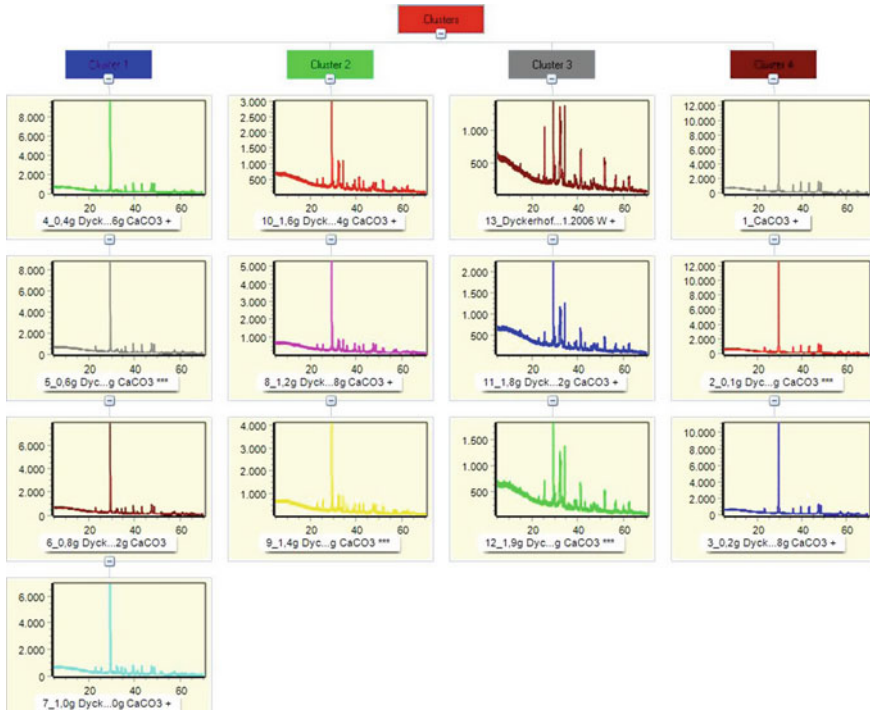
Fig. 10 X-ray diffractograms of the eleven mixtures of limestone and OPC sorted into four clusters according to their compositional changes. In this vcase, limestone-rich, OPC-rich, and two intermediate clusters were separated

The different XRD diagrams of the four different calculated clusters from initially 13 mixtures are shown in Fig. 10.

3.3 Rietveld Analysis Applied on Metakaolin Sample

The Rietveld method was applied to determine the total phase composition of metakaolin including the amorphous content. To determine the amorphous content, 10% rutile was added to the metakaolin as an internal standard. The metakaolin consists of 1% anatase, >1% quartz, 3.4% illite, and 95% amorphous phase (Fig. 11). The Rietveld mineralogical analysis was verified by an XRF measurement for chemical composition. The metakaolinite sample contains mainly amorphous phase, but also impurities of 1% of anatase, 0.7% quartz, and 3.4% of illite. Assuming that illite has a content of K0.5 in its structural formula, then this illite contains 5.08% K resp. 6.12% K_2O. In a metakaolin with 3.4% illite, this corresponds to 0.21% K_2O as given in the results of chemical analysis in Table 2. In Eq. 1, the simple calculation
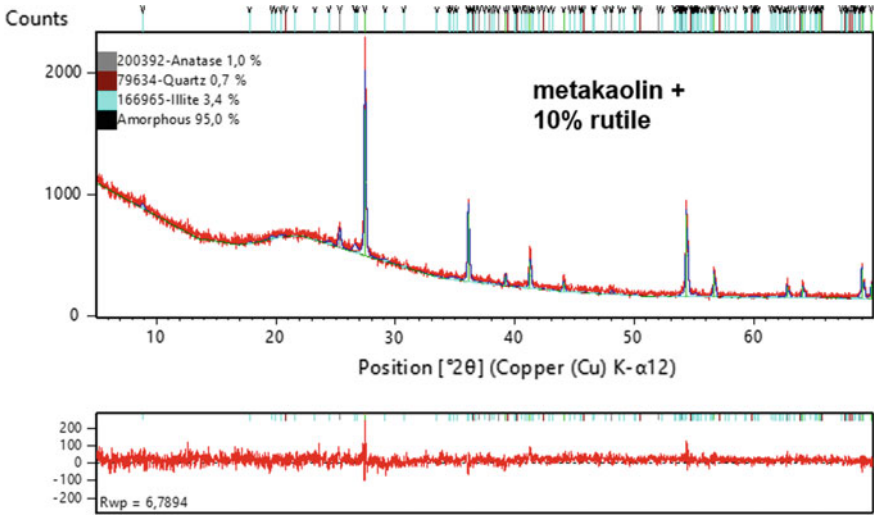
Fig. 11 XRD diagram showing Rietveld analysis of metakaolin with 10% rutile as internal standard in order to determine the amorphous content

Table 2 Results of chemical analysis by X-ray fluorescence spectroscopy and LOI of the metakaolin sample

Oxides and LOI	wt%	Oxides	wt%
LOI	0.94	TiO_2	1.01
SiO_2	52.45	Fe_2O_3	0.55
Al_2O_3	44.30	Na_2O	0.33
K_2O	0.22	$P_2O_5 + SO_3 + CaO + V_2O_5 + Cr_2O_5 + NiO + ZnO + Ga_2O_3$	0.2

of illite from the available potassium content is given.

$$\frac{6.12\% \ K_2O}{0.21\% \ K_2O} \ \hat{=} \ \frac{100\% \ \text{illite}}{3.4\% \ \text{illite}} \tag{1}$$

This result is consistent with the data obtained from XRF analysis (Table 2).

From Rietveld refinement, the mineralogical composition of the metakaolin was determined as 1.0% anatase, 0.7% quartz, 3.4% illite, and 95% amorphous phase.

3.4 Comparison of Rietveld Analysis and PLSR for the Determination of Amorphous Contents

Different amounts of the internal standard (10, 20, 30% rutile) were added to the metakaolin. Since the amorphous portion is reduced by the same value corresponding to the rutile admixture, the amorphous portion of only one of the samples was determined using the Rietveld method. Then, a partial least square regression of the mixtures and the pure materials (metakaolin, rutile) was made with reference to the amorphous portion as main component (Fig. 12). The predicted amorphous contents correlate very well with the amorphous portion determined with Rietveld (Fig. 13; Table 3).

The results obtained from the determinations of the amorphous contents derived from Rietveld analysis and PLSR method lead to an almost perfect correlation and confirm the contents obtained by both methods. Table 3 shows the definite contents of the used samples.
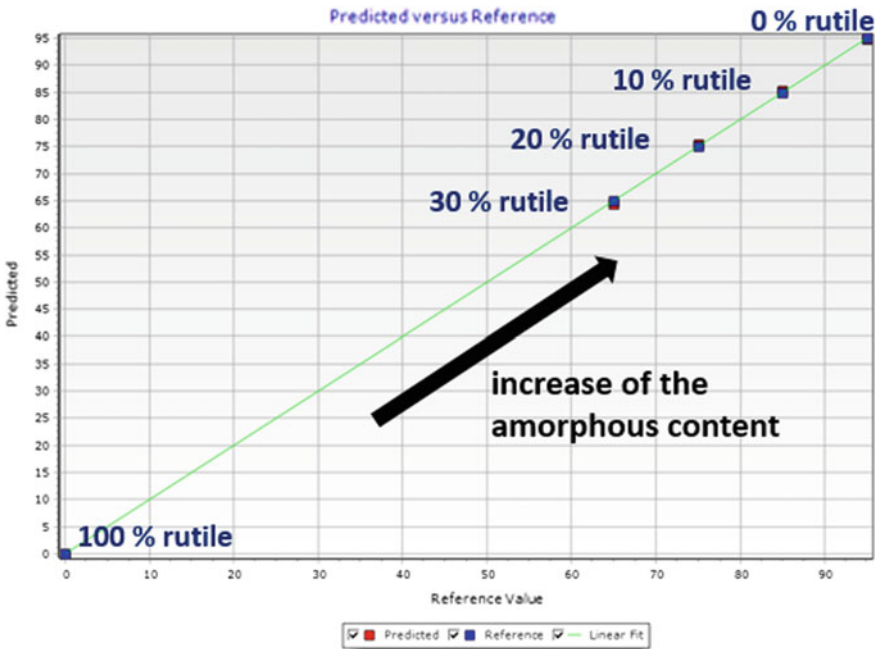
Fig. 12 PLSR model of rutile and metakaolin with 0, 10, 20, and 30% rutile with correlation to the amorphous portion as main component
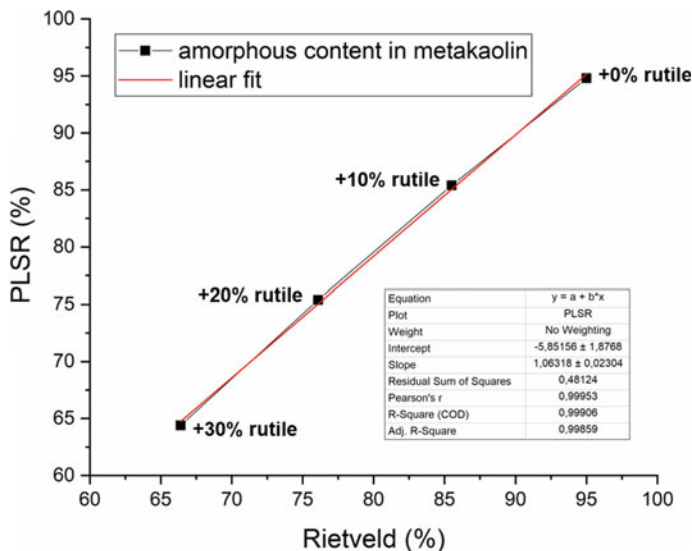
Fig. 13 Comparison of the analysis results for the amorphous content in metakaolin with the addition of 10, 20, and 30% rutile calculated with Rietveld and with the PLSR method

Table 3 Comparison of results of PLSR and Rietveld method: amorphous portion in metakaolin with admixture of different amounts of rutile

Rutile (%)	PLSR method (%)	Rietveld analysis (%)
0	94.8	95.0
10	85.4	85.5
20	75.4	76.1
30	64.4	66.4
100	0.08	0

3.5   PONKCS Method Applied on Metakaolin/OPC Mixtures

With the PONKCS method, an hkl file was created by fitting the XRD diagram with a random tetragonal unit cell ($a = b = 22.4969(8)$ Å, $c = 1.5$ Å, $\alpha = \beta = \gamma = 90°$) and crystal symmetry (tetragonal, P 4) for the amorphous hump of metakaolin (Fig. 14). Therefore, the Pawley fit was used to simulate a diagram from which all, except two remaining peaks, were deleted. The remaining two peaks were directly at the amorphous hump. The background was fitted using the Chebyshev method. In the next step, the scaling factors and the peak profile variable w of the remaining peaks were refined, using the hkl-fit method. Finally, the pseudo-formula mass of the hkl file was calibrated with the result of the Rietveld analysis of metakaolin (95% amorphous, Fig. 11). The crystalline phases were also refined for quantification with Rietveld. Thus, the quantification results correspond to those as obtained by Rietveld calculation (1% anatase, <1% quartz, and 3.4% illite).
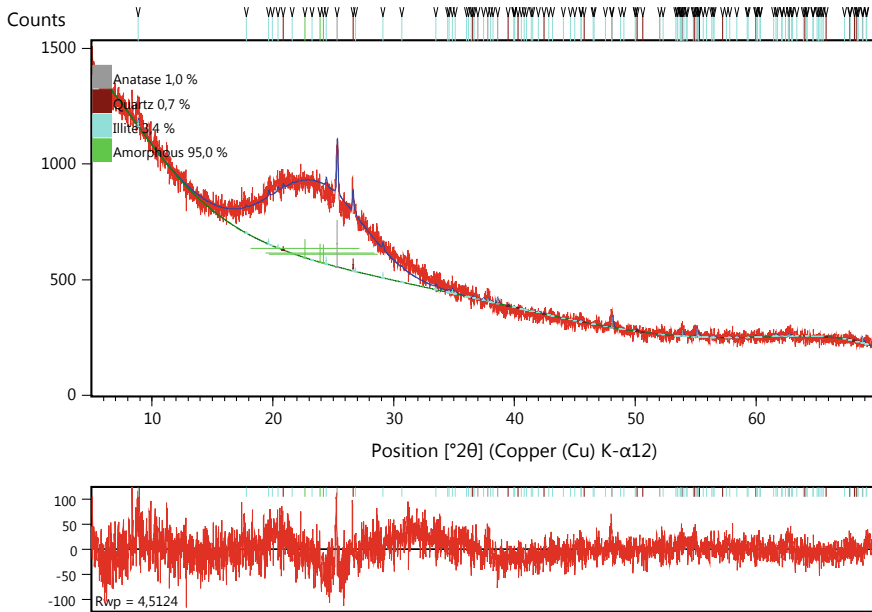
Fig. 14 X-ray diffractogram of metakaolin phase

The PONKCS method was used to create an hkl file by fitting a random cell and symmetry to the amorphous phase (green). The hkl file was calibrated with the Rietveld result (95% amorphous). The metakaolin sample consists mineralogical of 1.0% anatase, 0.7% quartz, 3.4% illite, and 95% amorphous components.

The hkl file can be used to quantify the amorphous content of other samples as long as this amorphous hump has similar dimensions. Figure 15 shows a mixture of 90% metakaolin with 10% OPC. With the previously created hkl file, the amorphous phase was refined using hkl-fit and the crystalline phases were refined using Rietveld-fit. The background was again fitted using the Chebyshev method. The mineralogical composition of this mixture was determined to 0.9% anatase, <1% quartz, 3.3% illite, 9.6% alite, and 85.6% amorphous components. This corresponds to the following calculation:

$$90\% \text{ metakaolin} \times 95\% \text{ amorphous content metakaolin}$$
$$= 85.5\% \text{ amorphous content in mixture} \tag{2}$$

Using this calculated hkl file for an amorphous phase, it is not necessary in further measurements to use an internal standard for the determination of the amorphous contents of a sample.

PONKCS method was used to quantify a mixture of 90% metakaolin and 10% CEM I 42.5 R with Rietveld. This mixture was determined to 0.9% anatase, 0.6% quartz, 3.3% illite, 9.6% alite, and 85.6% amorphous components.
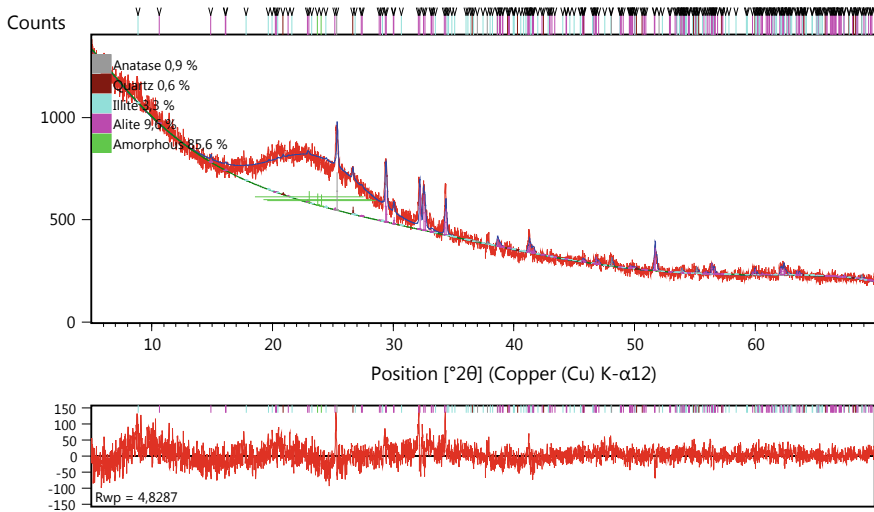
Fig. 15 XRD diagram showing the hkl file created with PONKCS

4 Conclusions

The cluster and PLSR analysis can be used easily to control compositions of binary cementitious mixtures. For the PLSR analysis, a calibration curve must be created for every different phase composition and mixtures in that cementitious materials field. This is slightly time-consuming at the beginning, but in case of many samples during a quantitative evaluation, the very rapid quantitative method can then easily be automatized. However, additionally, these newly created regression models are very good and reliable, as the comparison with Rietveld analyses shown. Once the regression model has been created, the quantification of other samples is very fast. Therefore, it is mainly used in applications with many samples available as it is the case for industrial operations. The cluster analysis simplifies the evaluation and sorting of large data sets, also under the aspect of different properties of the relevant mixtures. Apart from the XRD scans, no further information of admixtures is required.

After the setup of a quantitative model and a calibration curve, this type of quantification can be automized easily.

The quantification by the Rietveld analysis method is more complex, but gives more detailed information, such as the total phase composition, including the amorphous content. For the determination of the amorphous content, a crystalline internal standard must be added. In addition, crystallographic information files are required to refine the crystalline phases. With the PONKCS method, it is also possible to determine the amorphous content or in case, data from unknown crystalline compounds. However, this method must be calibrated with another method like Rietveld. After calibration, the created hkl file can be used for the quantification of other samples

without having to add an internal standard. Therefore, it is also interesting for rapid applications with many samples involved. While Rietveld and PONKCS methods are only for advanced users, the cluster analysis and PLSR method are easier to handle, but providing excellent data very fast on samples.

References

1. Barata, M.S., Angelica, R.S., Poellmann, H., Costa, M.L.: The use of wastes derived from kaolinite processing industries as a pozzolanic material for high-performance mortar and concretes. Eur. J. Mineral. **17**(1), 10 (2005)
2. Barthel, M., Rübner, K., Kühne, H.-C., Rogge, A., Dehn, F.: From waste materials to products in the cement industry. Adv. Cem. Res. 1–11 (2016). (ICE Publishing)
3. Beckers, D., Degen, T., König, U.: Analysis of hidden information—PLSR on XRD raw data. Acta Cryst. Sect. A **70** (2014)
4. Bish, D.L., Howard, S.A.: Quantitative phase analysis using the Rietveld method. J. Appl. Cryst. **21**, 86–91 (1988)
5. Costa, M.L., Moraes, E.L.: Mineralogy, geochemistry and genesis of kaolins from the Amazon region. Miner. Deposita **33**, 283–297 (1998)
6. Costa, M.L., Souza, D.J.L., Angélica, R.S.: The contribution of lateritization processes to the formation of the kaolin deposits from eastern Amazon. J. S. Am. Earth Sci. **27**, 219–234 (2009)
7. Degen, T., Sadki, M., Bron, E., König, U., Nénert, G.: The high score suite. Powder Diffr. **29**, 13–18 (2014). https://doi.org/10.1017/S0885715614000840
8. Degen, T., Koenig, U., Norberg, N.: PLSR as a new XRD method for downstream processing of ores: case study: Fe^{2+} determination in iron ore sinter. Powder Diffr. **29** (2014)
9. Dinnebier, R.E., Kern, A.: Quantification of amorphous phases—theory. PXRD-13 Workshop, Bad Herrenalb, May 2015
10. Galluccio, S., Pöllmann, H.: Usage of secondary raw materials (residual bauxite, laterite and residual kaolin) for the synthesis of CSA-based cements, DMG-Tagung, Jena, CD (2014)
11. Galluccio, S., Beirau, T., Pöllmann, H.: Maximization of the reuse of industrial residues for the production of eco-friendly CSA-belite clinker. Constr. Build. Mater. **208**, S.: 250–257 (2019) (ScienceDirect)
12. Kakali, G., Perraki, T., Tsivilis, S., Badogiannis, E.: Thermal treatment of kaolin: the effect of mineralogy on the pozzolanic activity. Appl. Clay Sci. **20**, 73–80 (2001)
13. König, U., Norberg, N.: Partial least square regression (PLSR)—a new alternative XRD method for process control in aluminium industries. Conference Paper (2014)
14. König, U., Degen, T.: Cluster analysis of XRD data for ore evaluation. Conference Paper (2013)
15. Korndörfer, J., Pöllmann, H., Costa, M.L., Angelica, R.: Mine tailings from the lateritic gold mine Igarape Bahia (Carajas region)—a basis for active hydraulic binders. Econ. Geol. ZAG SH **1**, 187–192 (2000)
16. Liao, B., Chen, J.: The application of cluster analysis in X-ray diffraction phase analysis. J. Appl. Cryst. **25**, 336–339 (1992)
17. Madsen, I.C., Scarlett, N.V.Y., Kern, A.: Description and survey of methodologies for the determination of amorphous content via X-ray powder diffraction. Z. Kristallogr. **226** (2011)
18. Maia, A.A.B., Saldanha, E., Angélica, R.S., Souza, C.A.G., Neves, R.F.: Utilização de rejeito de caulim da Amazônia na síntese da zeólita A. Cerâmica **53**, 319–324 (2007)
19. Maia, A.A.B., Angélica, R.S., Neves, R.F.: Estabilidade Térmica da Zeólita A - Sintetizada a partir de um Rejeito de Caulim da Amazônia. Cerâmica **54**, 345–350 (2008)
20. Maia, A.A., Angelica, R.S., De Freitas Neves, R., Pöllmann, H., Straub, C., Saalwächter, K.: Use of ^{29}Si and ^{27}Al MAS NMR to study thermal activation of kaolinites from Brazilian Amazon kaolin wastes. Appl. Clay Sci. 189–196 (2013)

21. Mestdagh, M.M., Vievoye, L., Ilerbillon, A.J.: Iron in kaolinite: II the relationship between kaolinite crystallinity and iron content. Clay Miner. **15**, 1–13 (1980)
22. Pöllmann, H., Da Costa, M.L., Angelica, R.: Sustainable secondary resources from Brazilian kaolin deposits for the production of calcined clays. In: Calcined Clays for Sustainable Concrete, pp. 21–26. Springer, Berlin (2015)
23. Rietveld, H.M.: Line profiles of neutron powder-diffraction peaks for structure refinement. Acta Crystallogr. **22**, 151–152 (1967)
24. Rietveld, H.M.: A profile refinement method for nuclear and magnetic structures. J. Appl. Crystallogr. **2**, 65–71 (1969)
25. Scarlett, N.V.Y., Madsen, I.C.: Quantification of phases with partial or no known crystal structure. Powder Diffr. **21**(4), 278–284 (2012)
26. Scrivener, K., Favier, A.: Calcined Clays for Sustainable Concrete. Springer, Berlin (2015)
27. Scrivener, K.L., Vanderley, M.J., Gartner, E.M.: Eco-efficient cements: potential economically viable solutions for a low-CO_2, cement-based materials industry. UNEP (2016)
28. Setzer, F.: Investigations on supplementary cementitious materials. Univ. Halle, Mineralogy. https://www.geologie.uni-halle.de/igw/mingeo/mingeo.html
29. Siddique, R., Cachim, P. (ed.): Waste and Supplementary Cementitious Materials in Concrete. Elsevier, WP (2018)
30. Snellings, R., Mertens, G., Elsen, J.: Supplementary cementitious materials. In: Broekmans, M.A.T.M., Pöllmann, H. (eds.) Applied Mineralogy in Cement & Concrete, pp. 211–278. Chantilly (Mineralogical Society of America) (2012)
31. Stetsko, Y.P., Shanahan, N., Deford, H., Zayed, A.: Quantification of supplementary cementitious content in blended Portland cement using an iterative Rietveld–PONKCS technique. J. Appl. Cryst. 50, 498-507, (2017)
32. Walenta, G., Füllmann, T.: Advances in quantitative XRD analysis for clinker, cements, and cementitious additions. Adv. X-ray Anal. **47**, 287–296 (2004)
33. Whitfield, P.S., Mitchell, L.D.: Quantitative Rietveld analysis of the amorphous content in cements and clinkers. J. Mater. Sci. **38**, 4415–4421 (2003)
34. Westphal, T., Füllmann, T., Pöllmann, H.: Rietveld quantification of amorphous portions with an internal standard—mathematical consequences of the experimental approach. Powder Diff. **24**, 239–243 (2012)

Investigation on Limestone Calcined Clay Cement System

S. K. Agarwal, Suresh Palla, S. K. Chaturvedi, B. N. Mohapatra, Shashank Bishnoi and Soumen Maity

Abstract The use of supplementary cementitious materials (SCMs); fly ash and granulated BF slag, by lowering clinker content in cement is a viable strategy to bring down CO_2 emission during cement manufacture. Due to the large availability of clay and limestone all over the world, a new ternary cementitious cement system containing calcined clay and limestone could increase clinker substitution to about 50% without significantly influencing cement performance due to the synergy between aluminates from calcined clay and carbonates from limestone. In the present study, mechanical properties of different limestone calcined clay cement blends, prepared maintaining clinker substitution of 0.40, 0.45, 0.50, 0.55 and 0.60 was measured as per Indian standard IS:4031 and showed compressive strength comparable to the minimum strength requirements for blended cements as specified in Indian standard, in case of cement having clinker substitution rate of 0.50. Comparative evaluation of compressive strength of OPC and limestone calcined clay cement showed substantial increase in strength at later ages in case of limestone calcined clay cement as compared to OPC. The heat evolution of limestone calcined clay cement using isothermal calorimeter showed higher heat evolution with early attainment at all ages as compared to OPC. The limestone calcined clay cement showed its resistivity to different aggressive solutions such as seawater, sulfate and chloride solution salts along with lean water up to the period of 12 months.

Keywords Limestone · Raw clay · Calcination · Compressive strength · Aggressive environment

S. K. Agarwal (✉) · S. Palla · S. K. Chaturvedi · B. N. Mohapatra
National Council for Cement and Building Materials, Ballabgarh, Haryana, India
e-mail: satishncb@gmail.com

S. Bishnoi
Indian Institute of Technology, New Delhi, India

S. Maity
Technology and Action for Rural Advancement, New Delhi, India

1 Introduction

Indian cement industry today stands second after China with installed capacity of around 502 MTPA, about 10% of global installed capacity with production stands at about 300 MTPA. The cement production is known to contribute about 9% of global CO_2 emissions. The decomposition of the raw material, limestone, creates most (~60%) of the cement industry's direct CO_2 emission; the rest comes from coal burning and power generation [2]. Recognizing the need to lower its carbon and energy footprints, the cement industry actively pursues four practices that can help reduce the industry's carbon footprint: (i) investment in more efficient kiln technology, (ii) increasing use of alternative fuels, (iii) clinker substitution and (iv) mastering heat consumption during production. With these efforts, the CO_2 emission in India is targeted to be reduced to 0.35 tonne CO_2/tonne cement by 2050 [3]. In cement production, limestone is being the primary raw material and the growth of the industry depends on the availability of cement grade limestone. In India, total limestone resources estimated by Indian Bureau of Mines is 124,539.55 million tonnes out of which, 30% falls under the forest cover, restricted area and eco-sensitive zone. Therefore, from the available remaining about 89,862 million tonnes limestone resources, cement grade limestone reserves are only around 8948 million tonnes that sustain for another 40 years (in case of 100% pet coke utilization as fuel) with anticipated clinker production of 500 million tonnes by the end of 2020.

Therefore, in order to address twin issues of CO_2 emission during clinker production and conserving limestone resources, use of supplementary cementitious materials (SCMs) represents a more promising approach associated with Portland cement production. Moreover, the average percentage of clinker in cement is decreasing which in combination with the worldwide increase in consumption of cement leads to increasing demands for SCMs [5, 6]. However, high demand of SCMs cannot be met only by conventional SCMs, such as silica fume, fly ashes and granulated blast furnace slag, which is further accentuated as the global production of some of these industrial by-products may significantly decrease in the near future. Recently, significant research efforts have focussed on calcined clays as alternative source of SCMs, as they are produced by thermal treatment of clay minerals which have the immediate advantage that they are naturally abundant in very large quantities almost all over the world. In India, total reserves/resources of clay are estimated to be around 2941 million tonnes out of which 2039 million tonnes falls under mixed grade/unclassified class [4]. The thermal activation of clays takes place at 500–900 °C and normally it does not involve the direct release of CO_2 from the raw clay material, in contrast to the de-carbonation of limestone, in the production of Portland clinker. Thus, the production of calcined clays is less energy demanding and considerably less CO_2 intensive than production of Portland clinkers. More importantly, the replacement level of the Portland cement with calcined clays in combination with limestone can be as high as 50% without causing significant loss in compressive strength compared to pure Portland cement [1].

This present paper highlights the physical characteristics of limestone calcined clay cement up to the period of 12 months and long-term compressive strength developments of cement mortars cured under different aggressive conditions.

2 Experimentation

The chemical analysis of calcined clay, limestone, ordinary Portland cement and limestone calcined clay cement samples provided by IIT-Delhi was carried out according to the procedures described in various Indian standards. Mineralogy of raw and calcined clay was studied by X-ray diffraction. The amount of kaolinite present in the clay is measured through DTA/TGA. The morphology and granulometry of calcined clay were investigated on temporary mount by optical microscopy (NIKON). The lime reactivity of calcined clay was determined according to test procedure IS:1727 (method of tests for pozzolanic materials). The limestone calcined clay cement (LC^3) blend was prepared by mixing 52 wt% of ordinary Portland cement (OPC) and 48 wt% of limestone calcined clay (LC^2) keeping target proportions as 50 wt% Portland clinker, 30 wt% calcined clay, 15 wt% limestone and 5 wt% gypsum. The mechanical characteristics of LC^3 blend were measured according to various test methods described in Indian standard IS:4031. The effect of curing under aggressive media was studied by immersing the hardened cement mortar cubes in solutions containing sulfate (0.33N Na_2SO_4, pH-5.99), chloride (0.5N NaCl, pH-6.43) salts and seawater along with distilled water (pH-7.45) for the period up to 12 months and evaluated for compressive strength developments.

3 Characterization of Materials

3.1 Raw and Calcined Clay

Mineralogy of the raw clay showed the predominance of mineral constituents, K-kaolinite [$Al_2Si_2O_5(OH)_4$] with diffraction peaks at $2\theta = 12.4$ and $24.8°$ and Q-α-quartz [SiO_2] along with minor phases, M-muscovite [KAl_2 (Al,Si_3O_{10}) $(F,OH)_2$] and H-hematite [Fe_2O_3] (Fig. 1). The raw clay sample was calcined at the temperature of 800 °C and diffraction pattern of calcined clay showed the presence of amorphous material indicating loss in crystallinity of kaolinite. The amount of kaolinite present in the clays can be determined by measuring the mass loss between 450 and 700 °C and the complete dihydroxylation of pure kaolinite mineral results in a mass loss of about 14%. TGA curves of raw clay sample showed ~59% kaolinite in raw clay sample (Fig. 2a). TGA curve of calcined clay showed no further mass loss indicating complete dihydroxylation of kaolinite (Fig. 2b) (XRD and DTA/TGA study carried

Fig. 1 X-ray diffraction pattern of raw clay and calcined clay (K: kaolinite, M: muscovite, Q: quartz, H: hematite)

(a)

(b)
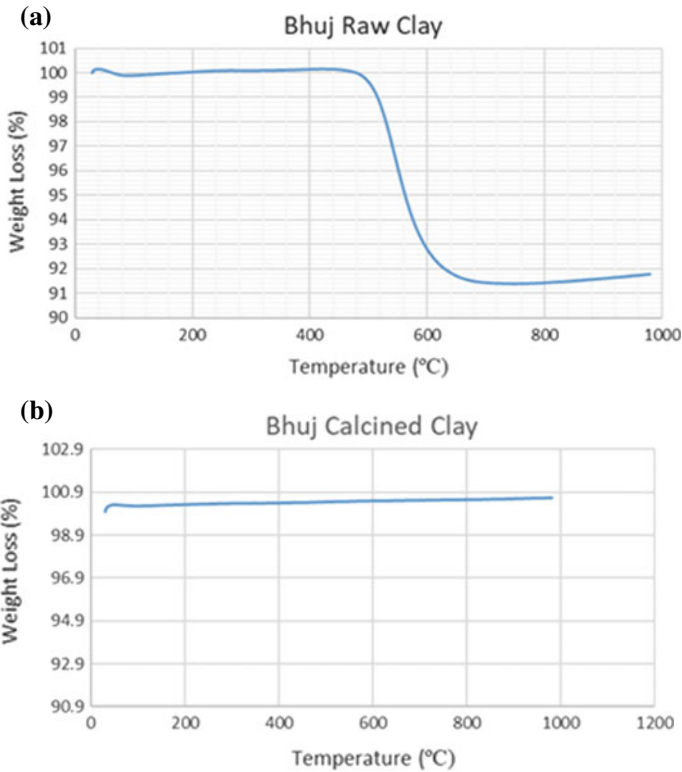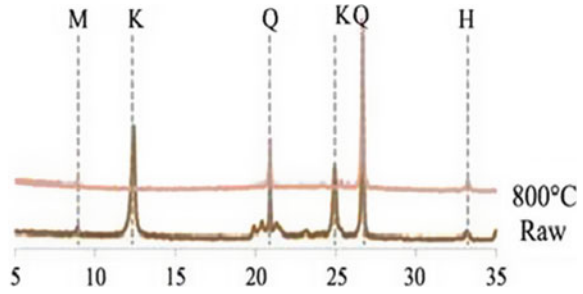
Fig. 2 **a** TGA curve of raw clay. **b** TGA curve of calcined clay

out by TARA). Chemical analysis of calcined clay showed the presence of 0.53% CaO, 49.50% SiO_2, 41.52% Al_2O_3, 1.88% Fe_2O_3, 41.48% reactive silica (Table 1).

Optical micrograph of calcined clay showed the presence of quartz, calcite, opaque minerals and iron oxide (Fig. 3a). The percentage of glass content was ~54%. Glass grains with both sharp angular and rounded grain margins were uniformly distributed in the sample (Fig. 3b). Grain size of glass varies from 2 to 75-μm with an average of

Table 1 Chemical analysis of materials used

Constituent oxides	Calcined clay	Limestone	Limestone calcined clay (LC^2)	OPC	Limestone calcined clay cement (LC^3)
LOI	2.42	24.87	9.21	1.56	5.37
CaO	0.53	28.11	28.29	61.54	45.89
SiO_2	49.50	30.03	34.28	21.78	27.03
Al_2O_3	41.52	8.93	19.45	5.20	12.34
Fe_2O_3	1.88	4.66	3.43	4.84	4.29
MgO	0.38	1.69	1.38	1.35	1.79
SO_3	0.03	–	1.58	2.25	1.99
Na_2O	0.22	0.34	0.31	0.19	0.27
K_2O	0.05	0.98	0.27	0.59	0.31
Chloride	–	–	0.03	0.03	0.02
IR	87.82	–	49.03	1.94	23.42
Reactive silica	41.48	–	24.12	–	–
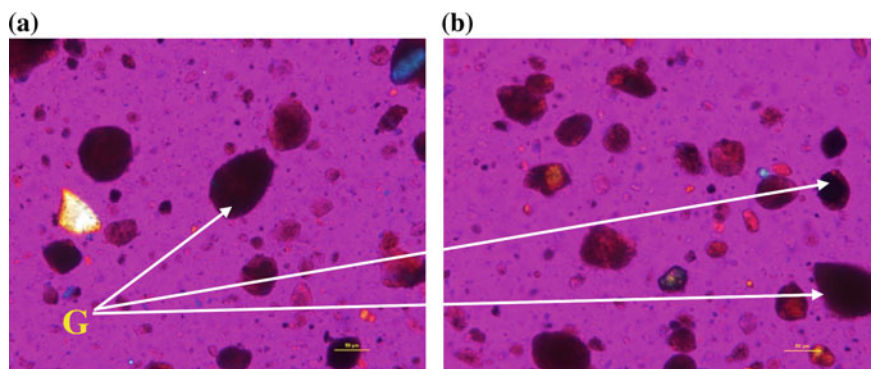
Fig. 3 Plate 1: photomicrograph of calcined clay **a** distribution of mineral grains (20x, x-nicols), **b** distribution of glass grains (20x, x-nicols) (G: glass gains)

14-μm. The majority of glass grains were in the size range of 2 to 15-μm. Subhedral to anhedral quartz grains with sharp grain margins were randomly distributed. Microglobular calcite grains were present as clusters in the sample. Opaque minerals with rounded grain margins were also observed. Anhedral to subhedral iron oxide grains were randomly distributed (Fig. 3b).

The lime reactivity of the samples was determined to be 8.0 MPa when measured according to Indian test procedure IS:1727 (methods of tests for pozzolanic materials).

3.2   Limestone Calcined Clay (LC²)

Chemical analysis of limestone showed 28.11% CaO, 30.03% SiO_2, 8.93% Al_2O_3, 4.66% Fe_2O_3 and 1.69% MgO (Table 1) and was categorized as low-grade limestone with $CaCO_3$ content was about 50%. Chemical analysis of limestone calcined clay (LC²) sample indicated 28.29% CaO, 34.28% SiO_2, 19.45% Al_2O_3, 3.43% Fe_2O_3, 1.38% MgO and 24.12% reactive silica. The mineral constituents in the sample were calcite [$CaCO_3$], quartz [SiO_2], kaolinite [$Al2Si_2O_5 (OH)_4$], dickite [$Al_2Si_2O_5(OH)_4$] and hematite [Fe_2O_3]. The Blaine's fineness of the sample was >600 m²/kg with lime reactivity of 7.0 MPa.

3.3   Limestone Calcined Clay Cement (LC³)

The chemical analysis of ordinary Portland cement (OPC) showed 61.54% CaO, 21.78% SiO_2, 5.20% Al_2O_3, 4.84% Fe_2O_3, 1.35% MgO and 2.25% SO_3 as major oxide constituents. The Blaine's fineness of OPC was 317m²/kg. Compressive strength of OPC at 1, 3, 7 and 28-days were determined to be 23.0, 27.5, 33.0, 50.5 MPa, respectively. Calcined clay cement blend was prepared by mixing 52 wt% of ordinary Portland cement (OPC) and 48 wt% of limestone calcined clay (LC²). The chemical analysis of cement blend showed the presence of 45.89% CaO, 27.03% SiO_2, 12.34% Al_2O_3, 4.29% Fe_2O_3, 1.79% MgO and 1.99% SO_3.

3.4   Particle Size Distribution of Limestone Calcined Clay (LC²), OPC and Limestone Calcined Clay Cement (LC³)

Particle size distribution of limestone calcined clay (LC²), OPC and limestone calcined clay cement (LC³) was analyzed using Microtrac S3500 particle size analyzer. The size distribution of limestone calcined clay (LC²) showed its finer nature as 44.22% particles were found to be below 10-µm against 8.86 and 31.40% particles were found to be below 10-µm in ordinary Portland cement (OPC) and limestone calcined clay cement (LC³), respectively (Fig. 4). Comparative evaluation of size distribution of limestone calcined clay and limestone calcined clay cement showed the finer nature of limestone calcined clay as 25.56, 11.64, 3.73 and 0.32% fraction passed through 5, 3, 2 and 1.156-µm, respectively, in case of limestone calcined clay as compared to 15.02, 5.57, 1.43 and nil percent size fraction passed through 5, 3, 2 and 1.156-µm in case of limestone calcined clay cement, as evident from Fig. 4.
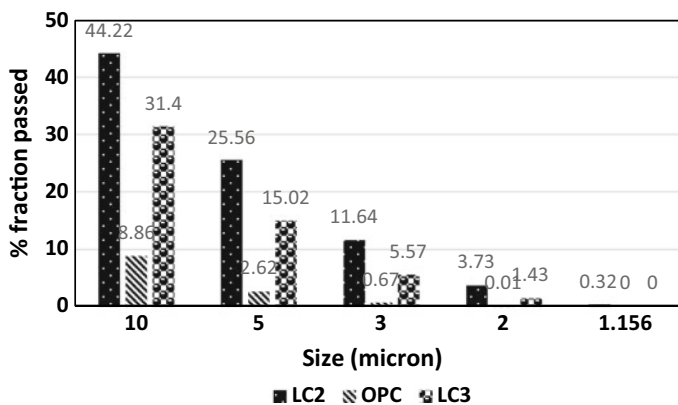
Fig. 4 Particle size distribution of limestone calcined clay (LC^2), OPC and limestone calcined clay cement (LC^3)

4 Results and Discussions

4.1 Mechanical Properties Vis-à-Vis Clinker Content in Limestone Calcined Clay Cement

Different limestone calcined clay cement blends LC-A-1, LC-A-2, LC-A-3, LC-A-4 and LC-A-5 were prepared maintaining different clinker contents at 0.40, 0.45, 0.50, 0.55 and 0.60, respectively, as per the designed composition given in Table 2 and evaluated for compressive strengths at 1, 3, 7 and 28-days as per the Indian test procedure IS:4031. Water requirement to prepare consistent paste of normal consistency was found to be in the range of 29.5–31.5%. The initial and final setting times of all cement blends were ranging from 100–160 and 150–205 min, respectively. The compressive strength of cement prepared with as low as 40 wt% clinker content met all the minimum strength requirements as specified in Indian standard for blended cements (i.e., ≥16 MPa for 3-days, ≥22.0 MPa for 7-days and ≥33.0 MPa

Table 2 Designed composition of limestone calcined clay cement blends

Cement code	Weight proportion (%)				Clinker factor
	Clinker	Limestone	Calcined clay	Gypsum	
LC-A-1	40.0	19.0	38.0	3.0	0.40
LC-A-2	45.0	17.5	34.5	3.0	0.45
LC-A-3	50.0	16.0	31.0	3.0	0.50
LC-A-4	55.0	14.0	28.0	3.0	0.55
LC-A-5	60.0	12.0	24.0	3.0	0.60

Table 3 Physical characteristics of limestone calcined clay cement blends prepared using different clinker contents

Properties	LC-A-1 (0.40)	LC-A-2 (0.45)	LC-A-3 (0.50)	LC-A-4 (0.55)	LC-A-5 (0.60)
Consistency (%)	31.3	31.5	30.5	30.5	29.5
Setting time (min)					
Initial	100	100	140	150	160
Final	155	150	190	200	205
Compressive strength (MPa)					
$24 \pm \frac{1}{2}$ h	11.0	12.0	14.0	15.5	16.5
72 ± 1 h	31.0	31.5	33.0	35.0	35.5
168 ± 2 h	36.5	37.0	41.0	42.5	43.0
672 ± 4 h	42.0	42.0	47.0	51.0	53.0

for 28-days) as given in Table 3. The trend of compressive strength of cements LC-A-1 to LC-A-5 showed gradual increase in strength of cement blends LC-A-1 to LC-A-5 due to the higher percentage of clinker content in the cement blend LC-A-5 in comparison with LC-A-1 (Fig. 5).

Blaine's fineness: 400–450m^2/kg.
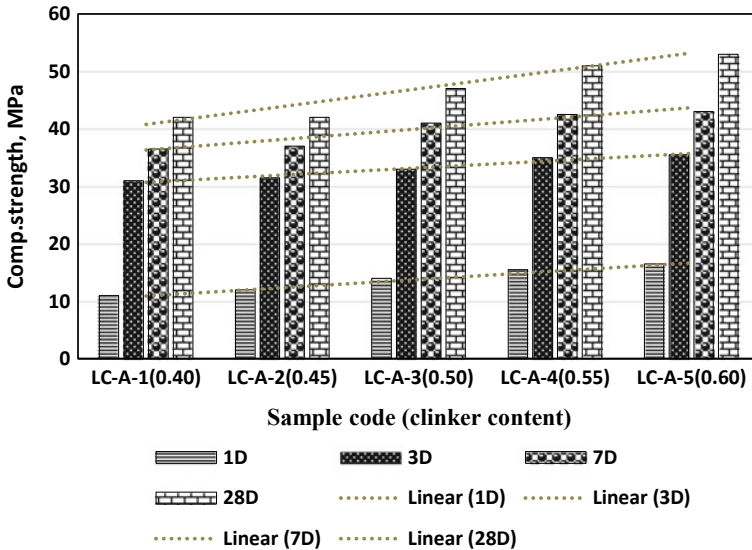
Fig. 5 Compressive strengths of limestone calcined clay cements prepared maintaining clinker content 0.40, 0.45, 0.50, 0.55 and 0.6

4.2 Performance Evaluation of Limestone Calcined Clay Cement Via-Vis OPC

Physical characteristics of ordinary Portland cement (OPC) and limestone calcined clay cement, in terms of Blaine's fineness, consistency, setting time, compressive strength at different intervals and soundness was carried out by using different testing procedures as described in Indian standard IS:4031 and results are given in Table 4. Blaine's fineness of OPC and limestone calcined clay cement, measured as per IS:4031(2)-1999, were found to be 317 and 443 m^2/kg, respectively, indicating finer nature of limestone calcined clay cement as evident from particle size distribution of cements (Fig. 4). Water requirement to prepare consistent paste of normal consistency, as per IS:4031(4)-1998, was determined to be higher in case of limestone calcined clay cement (33.0%) as compared to OPC (31.0%) owing to higher fineness of limestone calcined clay cement. The limestone calcined clay cement exhibited marginal faster setting as compared to OPC, when measured according to IS:4031(5)-1988. The compressive strength of limestone calcined clay cement at different intervals, measured as per IS:4031(6)-1993 up to the period of 12 months were found to be substantially higher at all ages particularly beyond 28-days (25% enhancement at 12 months cured sample) in comparison with OPC, whereas compressive strength of 1-day cured sample was found to be lowered by about 30% in comparison with OPC. The limestone calcined clay cement fulfilled the minimum strength requirements under compression as specified in Indian standard for blended

Table 4 Physical characteristics of OPC and limestone calcined clay cement

Property	OPC	Limestone calcined clay cement
Blaine's fineness (m^2/kg)	317	443
Consistency (%)	31.0	33.0
Setting time (min)		
Initial	150	115
Final	210	170
Compressive strength (MPa)		
24 ± ½ h	23.0	15.5
72 ± 1 h	27.5	33.5
168 ± 2 h	33.0	42.5
672 ± 4 h	50.5	52.0
90-days	53.0	61.5
180-days	55.0	69.0
365-days	58.0	79.0
Soundness		
Le-chatlier (mm)	1.0	2.0
Autoclave (%)	0.06	0.03
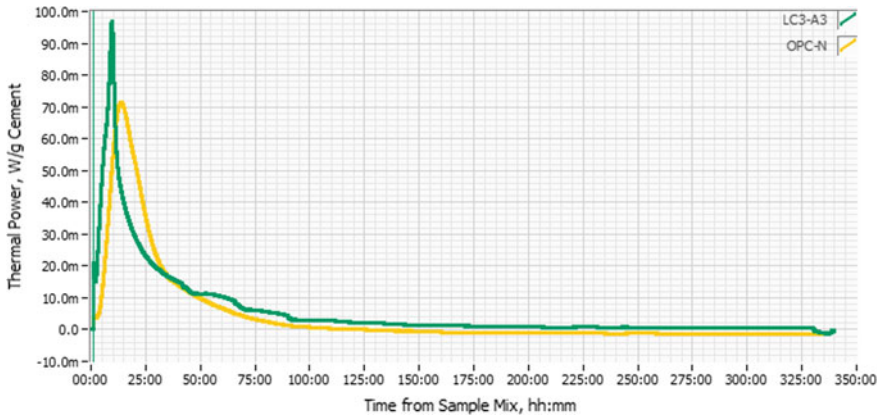
Fig. 6 Isothermal calorimeter curve of limestone calcined clay cement vis-à-vis OPC

cements. The limestone calcined clay cement showed dimensional stability as the values of linear and autoclave expansion were within permissible limit.

The heat evolution of limestone calcined clay cement using isothermal calorimeter showed high heat evolution with early attainment as compared to OPC (Fig. 6). Acceleration of limestone calcined clay cement blend starts early compare to OPC. This could be attributed to the synergetic effect between calcined clay and limestone [1, 7], mainly resulting from the formation of calcium monocarboaluminate hydrate $[Ca_4(Al(OH)_6)_2(CO_3)0.5H_2O]$. Deceleration period of limestone calcined clay cement shows similar trend with comparison of heart evolution of OPC.

4.3 Effect of Curing Under Different Mediums on Compressive Strengths of Limestone Calcined Clay Cement

The compressive strength developments of hardened limestone calcined clay cement mortars cubes cured for 1, 3, 6 and 12 months under the influence of different solutions; sulfate and chloride and seawater were found to be comparable to strength development of cement mortar cubes cured under lean water (Table 5), thus, showing that limestone calcined clay cement was resistant to different aggressive mediums.

5   Conclusion

1. The mineralogy of raw clay sample showed predominance of kaolinite mineral (~59%) and calcined at the temperature of 800 °C owing to loss in crystallinity

Table 5 Compressive strength of limestone calcined clay cement mortar samples cured under different aggressive medium

Curing medium	Compressive strength, MPa after curing at			
	1-month	3-month	6-month	12-month
Water	56.0	62.0	67.0	70.0
Seawater	54.0	58.0	56.0	60.0
Sulfate solution	52.0	61.0	63.0	64.0
Chloride solution	56.0	61.0	69.0	72.0

of kaolinite. Glass content calcined clay was estimated to be ~54% with lime reactivity of 8.0 MPa.

2. The compressive strength of limestone calcined clay cement blends prepared with clinker content as low as 0.40 met the minimum strength requirements of Indian standard specified for blended cements.
3. Comparative evaluation of physical characteristics of OPC and limestone calcined clay cement blend prepared using clinker content at 0.5 indicated.

   i.   Finer nature of limestone calcined clay cement as compare to OPC as evident from particle size distribution of cements.
   ii. Higher water demand in case of limestone calcined clay cement.
   iii. Slightly faster setting in case of limestone calcined clay cement.
   iv. Reduction in compressive strength by ~30% at 1-day of limestone calcined clay cement and afterward, there is fair gain in strength development under compression in comparison with OPC.
   v.   Substantial increase by ~25% in compressive strength development of limestone calcined clay cement mortar up to the curing period of 12 months.

4. Compressive strength of limestone calcined clay cement mortar cubes cured under sulfate and chloride solutions and seawater was found to be comparable to cement mortar cubes cured in lean water showing its resistivity to different aggressive solutions.

References

1. Antoni, M., Rossen, J., Martirena, F., Scrivener, K.: Cement substitution by a combination of metakaolin and limestone. Cem. Concr. Res. **42**, 1579–1589 (2012)
2. Bapat, J.D.: Cement industry-moving towards sustainable growth. Indian Cem. Rev. 61–63 (2013)

3. Fonta, P.: New data for cement industry shows reduction in CO_2 emissions. World Cem. 19–26 (2013)
4. IBM, Indian Bureau of Mines: Indian Minerals Handbook (2017)
5. Juenger, M.C.G., Siddique, R.: Recent advances in understanding the role of supplementary cementitious materials in concrete. Cem. Concr. Res **78**, 71–80 (2015)
6. Schneider, M., Romer, M., Tschudin, M., Bolio, H.: Sustainable cement production: present and future. Cem. Concr. Res **41**, 642–650 (2011)
7. Steenberg, M., Herfort, D., Poulsen, S.L., Skibsted, J., Damtoft, J.S.: Composite cement based on portland cement clinker, limestone and calcined clay. In: 13th International Congress on the Chemistry of Cement, Madrid, Spain (2011)

Heat Generation and Thermal Properties of Limestone Calcined Clay Cement Paste

Yanapol Thitikavanont and Raktipong Sahamitmongkol

Abstract In mass concrete construction, huge amount of cement is usually used and normally creates high temperature gradient across the thick section. Replacing suitable supplementary cementitious materials (SCMs) to ordinary Portland cement (OPC) is one of the potential strategies to reduce temperature rise of concrete. Although many benefits on the durability of concrete using limestone calcined clay cement (LC2 cement) have reported, very few studies have been published regarding the risk of thermal cracking when LC2 cement is used. Heat of hydration and thermal properties of LC2 cement are necessary parameters of the thermal cracking analysis and must be clarified before its application to the mass concrete construction. In this study, the calorimetric heat flow and cumulative heat of hydration are tested with isothermal calorimetry. The intensity of aluminum peak from calorimetric heat flow is the main hydration peak of LC2 cement pastes. The intensity of aluminum peak increases with higher LC2 cement replacement due to high Al_2O_3 content of LC2 cement. After the age of 12 h, the cumulative heat generation of LC2 cement pastes becomes lower than that of OPC pastes. Moreover, thermal properties which are specific heat (c), thermal conductivity (k) and coefficient of thermal expansion (CTE) of LC2 cement pastes are also investigated. The results showed that the specific heat of LC2 cement pastes decreases for 8% and 14% with 30% and 45% replacements, respectively, compared with OPC pastes. With higher LC2 cement replacement, the thermal conductivity decreases while the coefficient of thermal expansion increases. These changes are believed to be related to the pore structure development of LC2 cement pastes. Moreover, semi-adiabatic temperature rise is tested to observe the temperature rise. The peaks of temperature are 66.9 °C and 60.6 °C in the case of 30% and 45% LC2 concrete, respectively, which are lower than that of OPC concrete.

Keywords Heat of hydration · Limestone calcined clay cement · Temperature rise · Thermal cracking · Thermal properties

Y. Thitikavanont · R. Sahamitmongkol (✉)
King Mongkut's University of Technology Thonburi (KMUTT), Bangkok, Thailand
e-mail: raktipong.sah@kmutt.ac.th

1   Introduction

Mass concrete normally generates high level of temperature rise due to the hydration reactions. Since the thermal conductivity of concrete and the rate of heat transfer from concrete surface to environment are quite low, high temperature difference between center and surface of mass concrete section is frequently experienced [1]. Thermal cracking will occur if the self-restrained strain from unequal concrete thermal expansion exceeds tensile strength of concrete at early age [2, 3]. Therefore, the knowledge about heat generation and thermal properties of concrete is necessary because it could help engineers to evaluate risk of cracking and to design appropriate geometry, mix proportions of mass concrete or to plan suitable construction procedure to avoid the thermal crack.

One of the strategies to prevent thermal cracking in mass concrete is replacing suitable supplementary cementitious materials (SCMs) to clinker because the incorporation of some SCMs in concrete generates lower heat of hydration at the early age due to lower cement content [4].

Clay containing kaolinite becomes reactive after 600–850 °C calcination and has proved to be highly pozzolanic. Many studies report that pozzolanic component of calcined kaolinite clay, which is known as metakaolin, helps reducing the heat of hydration [5]. The ternary blended cement is developed to provide higher rate of clinker replacement by combining calcined clay and limestone powder [4, 6] and this binder system is called 'limestone calcined clay cement (LC2 cement)' [4].

Knowledge about complex hydration due to reactions of various mineral components in LC2 cement system is required to comprehend the temperature rise in LC2 concrete [2]. Therefore, in this study, the heat of hydration of LC2 cement paste is tested by isothermal calorimeter at the early age of paste. Moreover, the thermal properties which are specific heat, thermal conductivity and coefficient of thermal expansion of LC2 cement paste with a different replacement rate are also tested. Additionally, the temperature development in LC2 concrete is investigated using the semi-adiabatic experimental method.

2   Materials and Mix Proportions

2.1   Materials

The ordinary Portland cement (OPC) used in this study was produced from cement plant in Thailand. Calcined clay (CC) and limestone powder (LS) were ground to be 15 and 5 micron average particle size, respectively. All of these binder components were locally produced in Thailand. The weight ratio between calcined clay and limestone powder was controlled to be 2:1 which is the recommended ratio from previous researches [7]. Gypsum was added at 5% by weight of calcined clay in

Table 1 Chemical composition of materials

Oxide composition	SiO_2	Al_2O_3	Fe_2O_3	CaO	MgO	SO_3	Na_2O	K_2O	LOI
Ordinary Portland cement (%)	20.90	4.80	3.40	63.30	1.30	2.70	0.30	0.40	2.90
Limestone calcined clay (%)	27.97	23.67	10.31	18.40	0.77	1.60	0.01	0.29	15.55

order to prevent flash set cause by aluminous component in the binder. The chemical compositions of OPC and LC2, in this study, were examined by using X-ray fluorescence and shown in Table 1.

2.2 Mix Proportions

Cement Paste The control sample (CT) was prepared by using 100% of OPC. LC2 cement samples were prepared by 30 and 45% replacement of limestone calcined clay by weight. The water to binder ratio (w/b) was set at values of 0.5 and 0.6 as shown in Table 2.

Concrete Three mix proportions of concrete were prepared in this study. The weight proportions of limestone calcined clay in binder were 30 and 45%, in similar manner to the paste samples, but the water to binder ratio was fixed at only 0.5. The volumetric proportion of fine aggregate to the total aggregate (s/a) was 44% as shown in Table 3.

Table 2 Mix proportions of paste samples

Mix	w/b	Binder (% by weight)			
		Cement	Calcined clay	Limestone powder	Gypsum
W50CT	0.5	100.0	–	–	–
W50LC30	0.5	69.0	20	10	1.0
W50LC45	0.5	53.5	30	15	1.5
W60CT	0.6	100.0	–	–	–
W60LC30	0.6	69.0	20	10	1.0
W60LC45	0.6	53.5	30	15	1.5

Table 3 Mix proportions of concrete samples for semi-adiabatic temperature test

Mix	w/b	Binder (kg/m^3)				Water (kg/m^3)	Fine agg (kg/m^3)	Coarse agg (kg/m^3)
		OPC	CC	LS	GS			
W50CT	0.5	400	–	–	–	200	770	980
W50LC30	0.5	276	80	40	4	200	770	980
W50LC45	0.5	214	120	60	6	200	770	980

3 Experiment Program

3.1 Isothermal Calorimetry

In this study, an isothermal calorimeter was used to measure early age heat of hydration, the paste specimens were mixed and instantaneously placed in an ampoule that is in contact with a heat flow sensor [8]. When the hydration process occurred, a temperature gradient across the specimen and reference heat flow sensor was developed. The voltage that was proportional to the heat flow was continuously recorded for 3 days.

3.2 Specific Heat (**c**)

Specific heat was the parameter required to calculate temperature change from a specified amount of heat. From many studies, the constant specific heat was used to predict the temperature rise in model but specific heat actually changes with respect to time. Because the specific heat of water was highest compared to other ingredients and the free water in paste was consumed by hydration reaction [9]. Therefore, the specific heat of paste specimen would dramatically decrease at early age. In this study, the test method for the value of specific heat was modified from the previous publications.

The paste samples were casted into 25.4-mm diameter and 50-mm height PVC cylindrical mold. A thermocouple was installed at the center of specimen. Immediately after the cement paste samples get hardened, they were wrapped with aluminum foil in order to avoid the moisture loss while minimizing the change of thermal condition at the surfaces of the samples. The specimens were kept in insulated container and tested when the age of samples was 1, 3 and 7 days. At the age of testing, specimens with aluminum foil were submerged into water at 90 ± 1 °C in the insulated container. The energy from hot water was transferred into specimens. Consequently, the temperature of specimen and water increased and decreased, respectively. Both specimen temperature change (ΔT_{sp}) and water temperature change (ΔT_w) were recorded until the temperatures became equal. In the calculation, the heat loss to environment (ΔT_{loss}) is also considered as another cause of the reduction of water

temperature. The heat loss to environment was measured from the case in which the cement paste sample is not inserted into the test system. Moreover, since the cement paste specimen was generating heat of hydration during the test period; the heat from hydration process of cement (Q_{hyd}) was also included in the calculation. The amount of heat during the test period could be calculated from results of isothermal calorimetric test. The specific heat was then determined by using Eq. 1.

$$c_{sp} = \frac{m_w c_w (\Delta T_w - \Delta T_{loss}) - Q_{hyd}}{m_{sp} \Delta T_{sp}} \tag{1}$$

where

m_w	Mass of water, g
m_{sp}	Mass of specimen, g
c_w	Specific heat of water, J/(g °C)
c_{sp}	Specific heat of specimen, J/(g °C)
ΔT_w	Temperature change of water, °C
ΔT_{sp}	Temperature change of specimen, °C
ΔT_{loss}	Temperature loss of insulated container, °C
Q_{hdy}	Cumulative heat generation of specimen during testing, J.

3.3 Thermal Conductivity (k)

Thermal conductivity is a main parameter to describe the heat transfer behavior inside solid concrete. If thermal conductivity becomes higher, the temperature difference between surface and center of concrete section will be reduced. Hot-disk thermal constant analyzer was used to test for thermal conductivity in this study. The transient plane source (TPS) method which was suitable for porous material [10] is applied. The paste samples were casted into a 20-mm thick disk with 50-mm diameter PVC cylindrical mold. The upper and lower surface of specimens must be as smooth as possible. The specimens were kept at room temperature until ages of test which were 1, 3 and 7 days.

At the date of testing, two pieces of samples of the same cement paste each mixture were fitted on both sides of the hot-disk sensor. To obtain the accurate results, sensor was perfectly fitted between the two pieces of samples. The heating power and time measurement were set at 70 mW and 40 s, respectively. The measurement results were collected only if value of probing depth indicated by the system was within the thickness of the sample (approximately 20 mm).

3.4 Coefficient of Thermal Expansion (CTE)

The coefficient of thermal expansion was the length change per unit length with respect to change in temperature. The coefficient is required to compute the self-restraint stress due to temperature difference in mass concrete [2]. The results from previous publication [11] reported that CTE dramatically increased from the age of 10–24 h and to minimize the effect of shrinkage on the measurement of thermal expansion, the measurement duration must be as short as possible. The paste samples were prepared in $25 \times 25 \times 285$ mm mold. A thermocouple was installed at the center of specimen to measure temperature inside specimen. Specimens were immediately wrapped by aluminum foil after de-molding to avoid any moisture loss. The specimens were kept at temperature room and tested at the age of 10, 24, 72 and 168 h.

The range of temperature in this study was 10–50 °C. The length of specimen was measured using digital length comparator when the temperatures of specimen were 10, 30 and 50 °C. There were three containers with water at 10 ± 1 °C, 30 ± 1 °C and 50 ± 1 °C. The cooling and heating processes were performed by submerging specimen at room temperature into the 10 ± 1 °C, 30 ± 1 °C and 50 ± 1 °C water, respectively. Subsequently, the specimen stored at 50 ± 1 °C was removed and submerged into 30 ± 1 °C and 10 ± 1 °C water again. Each mixture was tested according to the prescribed procedures twice. Whole procedures and all readings for each sample were completed within 30 min. The coefficient of thermal expansion can then calculated as shown in Eq. 2.

$$\text{CTE} = \frac{\Delta L / L_0}{\Delta T} \qquad (2)$$

where

CTE   The coefficient of thermal expansion, strain/°C
ΔL The length change of specimen by temperature change, mm
L_0 The initial length of specimen, mm
ΔT The temperature change of specimen, °C.

3.5 Semi-adiabatic Temperature Test

The concrete specimens were casted into a shape of $350 \times 350 \times 350$ mm block. Polystyrene foam plates with 50-mm thickness were used as insulating material and installed at all of concrete surfaces. In each mixture, three thermocouples were installed at different locations which were center, bottom and side of concrete [12]. The locations of thermocouple are demonstrated in Fig. 1. The additional thermocouple was installed outside the samples to measure the ambient temperature in the
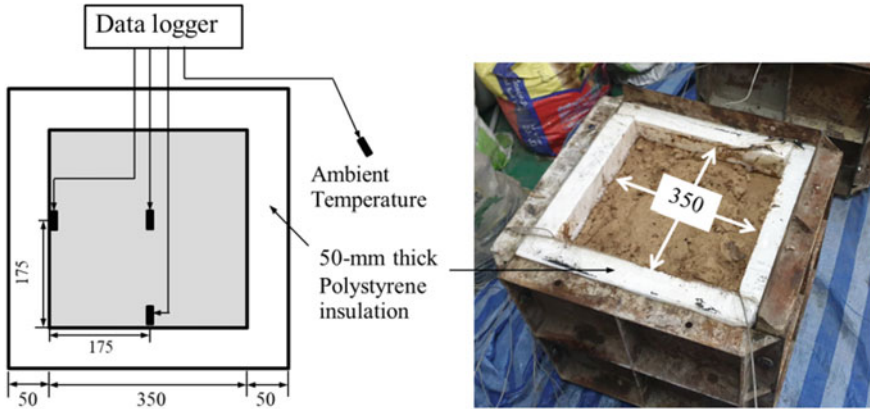
Fig. 1 Location of thermocouples in concrete for semi-adiabatic temperature test
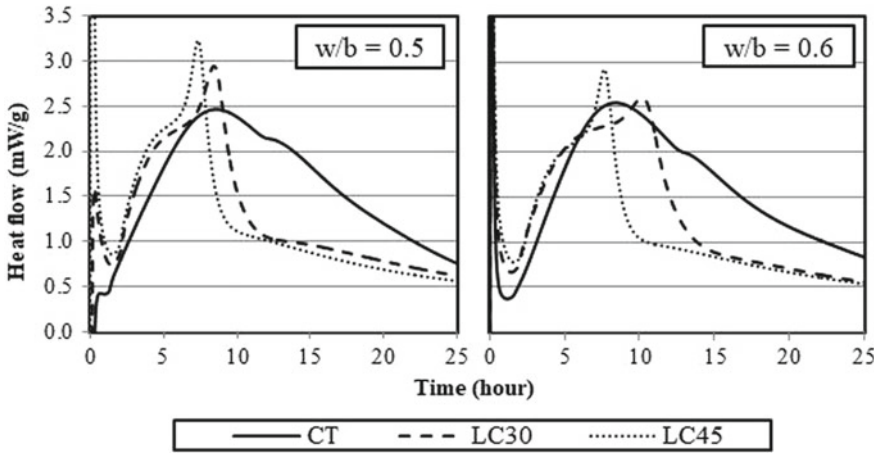
Fig. 2 Calorimetric heat flow of samples with $w/b = 0.5$ and 0.6

experimental room. The semi-adiabatic temperature rise was recorded continuously for 7 days.

4 Results and Discussion

4.1 *Heat of Hydration of Paste Mixtures*

The results from isothermal calorimetric test shown in Fig. 2 indicate that the incorporation of limestone calcined clay in LC2 cement pastes accelerated hydration compared to that of OPC paste. For LC2 cement pastes, the significant peak of heat flow was aluminum peak that represented aluminate phase's reaction due to high Al_2O_3 content in LC2 cement [4]. The aluminum peak could not be easily differentiated from the main peak of cement hydration. The peak intensity of LC2 cement pastes slightly decreased with increase of *w/b*. The possible reason was higher degree of dilution of cement in the cement–water solution, which affected lower rate of hydration [8]. The aluminum peaks of W50LC30, W50LC45, W60LC30 and W60LC45 occurred at the age of 8.4, 7.3, 10.2 and 7.6 h, respectively.

The cumulative heat released from hydration for 70 h was shown in Table 4. At the age of 10 h, all of LC2 cement pastes had higher cumulative heat than OPC pastes. However, the cumulative heat generation of LC2 cement pastes became lower than OPC paste at the age of 20 h and later. In the cases that *w/b* is 0.5, W50LC30 had lower cumulative heat of hydration than W50LC45 for the first three days because W50LC45 had very high rate of hydration at the age of 30 min. On the contrary, W60LC45 had lower 3-day cumulative heat generation than that of W60LC30.

4.2 *Specific Heat (*c*)*

LC2 cement pastes had lower specific heat than OPC paste. At the age of 1 day, the reductions were up to 8% and 14% for LC30 and LC45, respectively. The specific heat of cement paste decreased at the early age as shown in Fig. 3. The specific heat of OPC paste decreased at the rate of 0.03 J/(g °C day) from the age of 1 day to 3 days. The decreasing rates of specific heat of LC2 cement pastes were higher than that OPC pastes. It was found that the reductions were 0.07 and 0.05 J/(g °C day) when replacement was 30% and 45%, respectively. The faster change of specific heat found in the cases of LC2 cement pastes might be caused by faster consumption of free water by LC2 cement in mixtures since the hydration rate of LC2 cement seems to be faster at the early age. This tendency is very well in line with the results of specific heat reported by the previous study [9] in which the mixtures with higher water content was found to provide higher specific heat.

Table 4 Cumulative heat generation of OPC and LC2 cement pastes

Age	Cumulative heat generation									
	W50CT	W50LC30		W50LC45		W60CT	W60LC30		W60LC45	
Hour	J/g	J/g	%diff	J/g	%diff	J/g	J/g	%diff	J/g	%diff
10	53.9	65.4	+21	76.7	+42	63.6	71.6	+13	69.2	+9
20	118.8	100.8	−15	108.5	−9	126.8	113.3	−11	99.4	−22
30	147.4	123.5	−16	129.2	−12	157.1	133.5	−15	118.9	−24
40	163.2	138.9	−15	145.1	−11	172.8	147.3	−15	133.3	−23
50	175.6	151.3	−14	158.4	−10	183.6	158.4	−14	145.7	−21
60	185.7	162.6	−12	168.3	−9	192	168.4	−12	156.2	−19
70	193.8	172.7	−11	175.5	−9	198.8	177.6	−11	164.3	−17
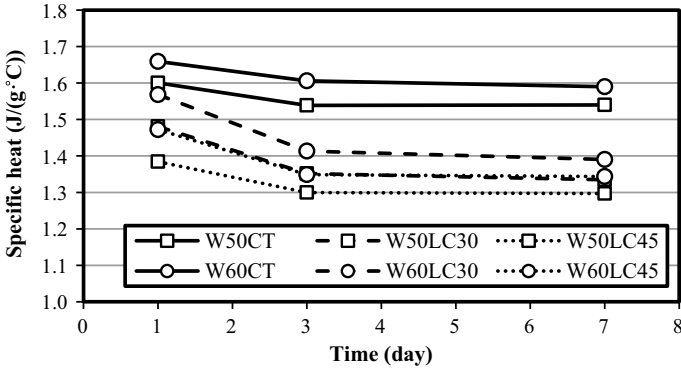
Fig. 3 Specific heat of samples at the age of 1, 3 and 7 days

4.3 Thermal Conductivity (k)

The results of thermal conductivity of OPC and LC2 cement pastes shown in Fig. 4 indicate that the thermal conductivity of all cement pastes did not significantly change with respect to the age of pastes. The water to binder ratio of pastes did not show a significant impact on thermal conductivity as well. These findings are similar to the observations in the previous research [9]. OPC paste had thermal conductivity in the range of 0.45–0.51 W/(m °C). LC30 and LC45 had lower thermal conductivity than OPC pastes at early age which were in rage of 0.44–0.50 and 0.42–0.47 W/(m °C), respectively. The reason for less thermal conductivity is probably an increase of total porosity in LC2 cement pastes at early age [13]. Because the thermal conductivity of air is 0.0262 W/(m °C) which is much lower than that of cement (0.29 W/(m °C)), water (0.606 W/(m °C)) or other hydrated products [14].
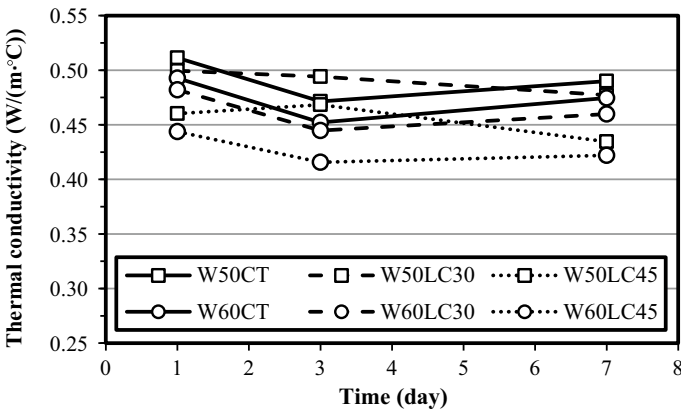
Fig. 4 Thermal conductivity of samples at the age of 1, 3 and 7 days
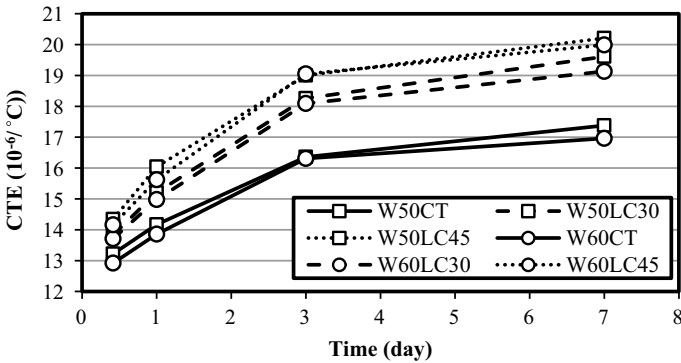
Fig. 5 Coefficient of thermal expansion of samples at the age of 10 h, 1, 3 and 7 days

4.4 Coefficient of Thermal Expansion (CTE)

The results of CTE test shown in Fig. 5 indicate that the CTE dramatically increase within 3 days after beginning of hydration reaction. After the age of 3 days, CTE of pastes was still increasing but the rate of increasing became lower. CTE increased up to 11% and 16% with 30% and 45% replacement of limestone calcined clay, respectively. The reason for higher CTE pastes is probably the refined pore structure in LC2 cement pastes [15]. Many researchers reported than the combination of limestone and calcined clay had a potential to refine pore structure since early age [15] and the thermal expansion of fluid in the pores smaller than 15 nm was anomalously higher than the bulk fluid [16].

4.5 Semi-adiabatic Temperature

The semi-adiabatic temperature of OPC and LC2 concrete is shown in Fig. 6. The water to binder ratio of all samples was 0.5 and the initial temperature was around 31 °C for all concretes. The temperature rise of LC2 concretes were less than that of OPC concrete. The temperatures at side and bottom of testing mold were not significantly different from the measured temperature at center. The peak temperatures of W50CT, W50LC30 and W50 LC45 concrete were 67.1, 66.9 and 60.6 °C, at the age of 13, 10.7 and 9.7 h, respectively.
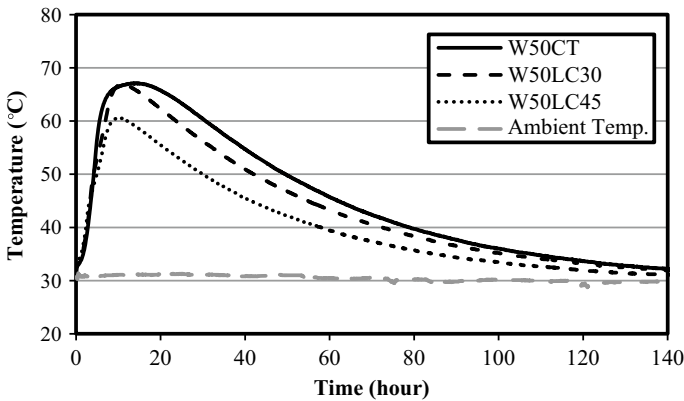
Fig. 6 Semi-adiabatic temperature of concrete samples with $w/b = 0.5$

5 Conclusions

1. The cumulative heat of hydration of LC2 cement pastes was higher than OPC pastes at the age of 10 h and became significantly lower at the age of 30 h. W60LC45 had 24% less cumulative heat generation than W60CT at the age of 30 h.
2. LC2 cement pastes had lower specific heat with higher proportion of limestone calcined clay. Specific heat of LC2 cement pastes also rapidly decreased from the age of 1 day to 3 days and then became quite constant.
3. The thermal conductivity of LC2 cement pastes was slightly lower than OPC pastes due to higher total porosity. The replacement rates of 30 and 45% lead to average thermal conductivities of 0.476 and 0.441 W/(m °C), respectively.
4. The CTE of LC2 cement pastes became higher proportionally with limestone calcined clay content in mixture due to the refined pore structure. The 30% LC2 cement and 45% LC2 cement had 11 and 16% increase of CTE.
5. The semi-adiabatic temperature of LC2 concrete was decreased with higher replacement rate of LC2 cement.

References

1. Wang, X.: Simulation of temperature rises in hardening Portland cement concrete and fly ash blended concrete. Mag. Concr. Res. **65**(15), 930–941 (2013)
2. Wang, X.: Modeling the hydration of concrete incorporating fly ash or slag. Cem. Concr. Res. **40**, 984–996 (2010)
3. Dabarera, A.: Models for predicting hydration degree and adiabatic temperature rise of mass concrete containing ground granulated blast furnace slag. Eng. J. **21**(3), 157–171 (2017)
4. Karen, S.: Calcined clay limestone cements (LC3). Cem. Concr. Res. **114**, 49–56 (2018)
5. Shah, V.: Influence of cement replacement by limestone calcined clay pozzolan on the engineering properties of mortar and concrete. Adv. Cem. Res. **30**(8), 1–11 (2018)
6. Karen, S.: Impacting factors and properties of limestone calcined clay cements (LC3). Green Mater. **7**(1), 3–14 (2018). https://doi.org/10.1016/j.chiabu.2004.01.005
7. Antoni, M.: Investigation of cement substitution by blends of calcined clays and limestone. Thesis EPFL (2014)
8. Hu, J.: Influence of cement fineness and water-to-cement ratio on mortar early-age heat of hydration and set times. Constr. Build. Mater. **50**, 657–663 (2014)
9. Bentz, B.P.: Transient plane source measurements of the thermal properties of hydrating cement pastes. Mater. Struct. **40**(10), 1073–1080 (2007)
10. Hanizam, A.: Effect of additives on mechanical and thermal properties of lightweight foamed concrete. Adv. Appl. Sci. **3**(5), 3326–3338 (2012)
11. Choktaweekarn, P.: A model for predicting the coefficient of thermal expansion of cementitious paste. ScienceAsia **35**(1), 57–63 (2009). https://doi.org/10.1016/j.brat.2017.09.009
12. Alhozaimy, A.: Heat of hydration of concrete containing powdered scoria rock as a natural pozzolanic material. Constr. Build. Mater. **81**, 113–119 (2015)
13. Investigation of the grade of calcined clays used as clinker substitute in Limestone Calcined Clay Cement (LC3), EPFL Thesis (2017)
14. https://www.engineeringtoolbox.com/thermal-conductivity. Last accessed 20 Apr 2019
15. Yuvaraj, D., Vignesh, K.: Development of the microstructure in LC3 systems and its effect on concrete properties. In: 2nd International Conference on Calcined Clays for Sustainable Concrete, RILEM Bookseries 16 (2018)
16. Siavash, G.: Micromechanics analysis of thermal expansion and thermal pressurization of a hardened cement paste. Cem. Concr. Res. **41**(5), 520–532 (2011). https://doi.org/10.1037/0022-006X.75.4.629

Study on the Efficacy of Natural Pozzolans in Cement Mortar

Ashish Shukla and Nakul Gupta

Abstract With the advent of the Industrial Revolution, science and technology grew rapidly with the producing era coming into view. The early industrial sectors engaged in small scale production of the major pollutant, smoke. Owing to the emergence of numerous factories and large scale jobs, the problems of industrial contaminating activities began to assume much importance. These issues made the burning up of industrial as well as agricultural waste products from industrial activities become the main focus of waste eradication study for environmental, economical, as well as technical reasons. Discarding of waste techniques became the problem emerging from constant industrial and technological development. Partial replacement of pozzolans by manufacturing waste product is not just efficient but an improvement to features of clean as well as cynical concrete. This is because it involves reducing the shrinkage, minimizing the cracks, as well as enhancing the sturdiness. Besides, the safe removal of waste substances serves as a means of shielding the surroundings from contamination. The main purpose of this research is to observe the ability and strength of the mortar by mixing the calcined clay in a mortar mix in the proportion of 0, 4, 8, 12, 16 and 20% and with this, the effect of mortar on HCl and acetic acid mixed in water in a proportional proportion has been studied.

Keywords Carbon emission · Pollution · Calcined clay · HCl · Acetic acid · Compressive strength · Water absorption test · Sorptivity test

1 Introduction

In today's era, concrete/cement mortar is proving to be the most commonly used component in the field of construction. Cement mortar are not environmentally friendly materials, either for production purposes, for utilization, or for disposal. The need for concrete in the construction sector is increasing ever increasing due

A. Shukla (✉)
Structural Engineering, GLA University, Mathura, India
e-mail: as302389@gmail.com

N. Gupta
Department of Civil Engineering, GLA University, Mathura, India

to which the main component of the concrete is also increasing the requirement of cement [1, 2]. Researchers replaced calcined clay in the form of wastes with cement to reduce pollution of the construction area in their constant search so that both the production and consumption of cement could be reduced [3]. To obtain suitable raw materials for making these materials substantial amount of water and energy are involved. Also, sand quarrying with other aggregates results into environmental pollution and annihilation. Concrete mortar therefore is affirmation for the large supply of carbon discharges into the environment. Researchers affirm that concrete causes the emission of approximately 5% of global overall quantity of carbon release which brings greenhouse gases. Due to continuous production of component cement used mainly in the construction sector, there is a very harmful effect in the environment as CO_2 and other harmful gases emit during cement production [2]. In order to reduce the need for cement instead of cement in concrete, supplementary cementitious material (i.e., pozzolans) is partly replaced with cement. These pozzolans are added to reduce the permeability of concrete and mortar, to increase strength, make cheaper or to influence other properties [4]. For this reason, "calcined clay" has been used on mortar in this research work, and the mixing of this supplemental material has been studied in response to mortar [5].

Components like cement mortars and concrete play important roles in the development of all the countries around the world in the construction sector. Concrete and cement mortars are used on the second number after water consumption across the world [6]. According to his research, Mehta informed that by 2050, these components of the manufacturing sector will be produced in such a large quantity which will affect the environment and economic situation [7]. According to researcher's research, around 1.6 billion metric tonnes of cement are produced in the whole world [8]. Many researchers have used calcined clay and other pozzolans to study their research in which they found that the calcined clay gets a parallel strength of cement on partial mixing with cement [9–14]. Mining as well as processing of calcined Kaolin in the industries generates huge volume of waste. Kaolin is a vital raw substance for utilization in different manufacturing sections. There are two types of wastes produced by the kaolin industrial sector that processes the primary kaolin. The first Kaolin waste is derived from the premium processing step which involves the partitioning of river sand from the ore. Another form of waste product is seen during the next production stage consisting of liquid filtrate to segregate the improved particles as well as cleansing [15]. Apart from water, concrete is another material used globally. It hardens and solidifies after combination with water as well as after placement because of the chemical process called hydration. Water mixes with cement to bind other particles together and they form sturdy resources [16].

The main purpose of this research is to observe the ability and strength of the mortar by mixing the calcined clay in a mortar mix in the proportion of 0, 4, 8, 12, 16 and 20% and with this, the effect of mortar on HCl and acetic acid mixed in water in a proportional proportion has been studied. And their results have been detected in 7, 28 and 90 days intervals.

2 Literature Review

2.1 Leonard (1991)

As stated by Leonard John Murdock, a neat pieced good quality brick offers satisfactory aggregates, with great strength as well as concreteness if the brick is from good quality rock; a well-engineered as well as connected brick if graded gives good concrete option for average strength. When second-hand blocks are utilized, it is imperative to get rid of every plaster so that the calcium sulfate content will not prevent setting or lead to disintegration within a short period. Always make sure to avoid blocks with sulfates soluble of more than or up to 0.50%. It is advisable to utilize brick aggregates that are highly saturated due to comparatively soaring absorbency level. It is also not advisable to use porous kind of block as aggregates in non-breakable concrete activities due to the problem of diffusion of dampness that might cause decomposition of steel fortification [17].

2.2 Al Saffar (2018)

In his paper, he told that the cement mortar reports on the effectiveness of the calcined clay (CC) on the strength characteristics of the calcining temperature (800 for 1 h). A set of eight different mortar blends was inserted and tested with different cement replacement levels (2.5–20% from the weight of cement). Based on the results of these tests, the impact on the aspects of strength in the cement mortar was discussed and analyzed. Tested mortar tests have identified tensile strength, compressed power, coefficient of water absorption, water absorption and the results of softness. FTIR and XRF tests were made to identify chemical composition and minerals. The result of this investigation is clear by the power test and shows significant improvement in the mechanical properties [18].

2.3 Sabir (1996)

He has replaced metakaolin with cement in proportion to 0, 5, 10, 15, 20, 25 and 30% in his experimental research work. (I) According to their experiment, they showed that metakaolin reacted with liberated lime and acted as a resistant to chloride. (II) He found that compression strength is good on the replacement of 25% metakaolin. (III) The microstructure of mixed mortar composed of metakaolin displays the compact structure and a homogeneous structure [19].

Table 1 Chemical properties of cement

S. No.	Chemical properties	Percentage
1	SiO_2	20.98
2	Al_2O_3	5.42
3	Fe_2O_3	3.92
4	CaO	62.85
5	MgO	1.76
6	Na_2	0.28
7	K_2O	0.53
8	SO_3	2.36
9	Loss on ignition	1.90

Table 2 Physical properties of cement

S. No.	Physical properties	Test result
1	Normal consistency	32%
2	Final setting time	255 min
4	Initial setting time	75 min
5	Color	Gray
6	Specific gravity	3.14

3 Raw Materials Used

3.1 Ordinary Portland Cement (OPC)

Concretes mortar or cements are described as substances having cohesive and adhesive characteristics that enable it to bind mineral pieces in a compressed solid when mixed with water. The cement bought for this test and use was of forty-three (43) grade. The attributes are as in Tables 1 and 2.

3.2 Fine Aggregate

Sand. Example of the form of sand used is river sand. The dimension of the fine aggregate used is less than or equal to 4.75 mm. The characteristics of the river sand testing are shown in Table 3.

Table 3 Physical properties of sand

S. No.	Physical properties	Test result
1	Specific gravity	2.60
2	Water absorption	1.10%
3	Fineness modulus	3.30%
4	Compacted bulk density	1644 kg/m^3
5	Zone	II

3.3 Calcined Clay

Calcined clay cement is a kind of low carbon cement. The main components of calcined clay are selected stone, clinker and gypsum. The chemical component of calcined clay used in this experimental work is stated in Table 4. And Fig. 1 illustrates calcined clay in the example [20].

Table 4 Chemical component of calcined clay

S. No.	Chemical properties	Percentage
1	Al_2O_3	22.34
2	SiO_2	70.42
3	Fe_2O_3	2.34
4	MgO	0.16
5	CaO	0.49
6	TiO_2	1.1
7	Na_2O	0.1
8	SO_3	0.02
9	K_2O	0.19
10	Loss on ignition	2.84
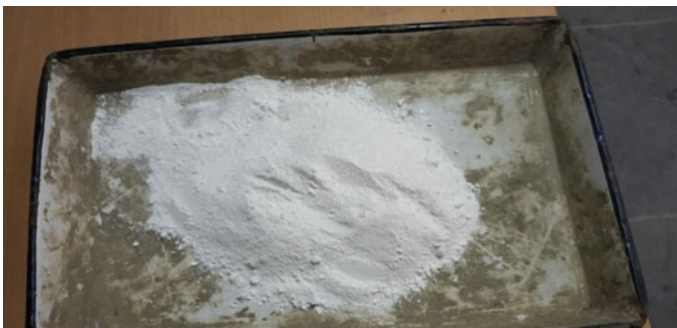
Fig. 1 Calcined clay

4 Methodology and Result

See Fig. 2.

4.1 Water Absorption Test for Cement Mortar

The experimentation technique is utilized for examining the frequency of absorption or water sorptivity using hydraulic cement. The test is carried out by measuring the increment in the weight of the sample from the water absorption as related to the time when just one section of the sample is in water.

Test technique. In this test, the samples are dried using oven device at a specific temperature and for a particular period of time. Then, they are kept in the desiccators for cooling effect. The water sorptivity is a porous substance which explains the capillary assimilation frequency of the porous substance that is exposed to the water surface. This is the standard parameter which defines the reinforced concrete covering quality. The entire experimental table given shows the ratio of calcined clay to CC0 to CC20 (Fig. 3 and Table 5).

4.2 Sorptivity Test

In this test, the results of the water increase absorption rate of cement mortar samples have been detected [21–24]. For the first time, cement mortars have been molded in
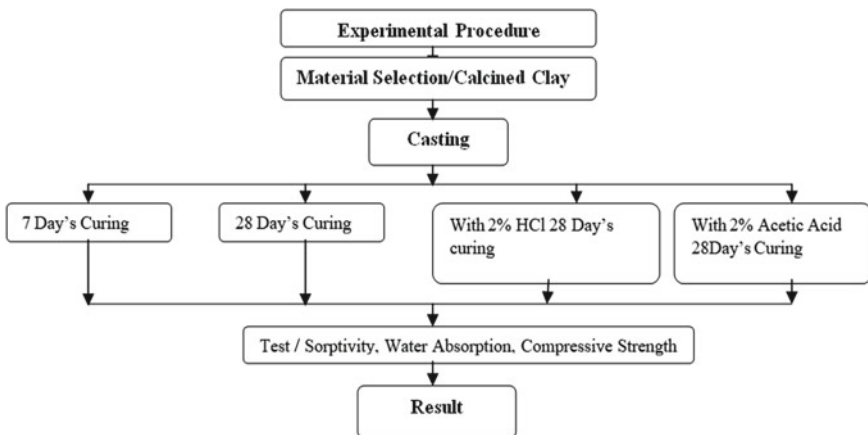
Fig. 2 Experimental methodology

Fig. 3 Graph 1: Water absorption test value
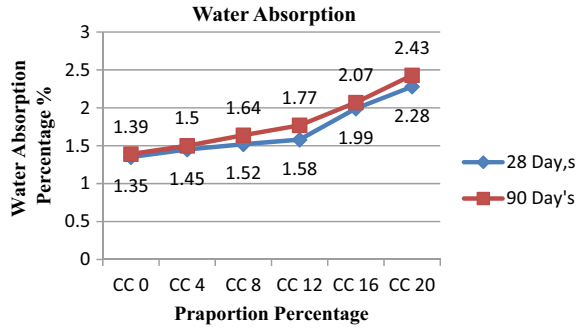
Table 5 Water absorption test

S. No.	Addition proportion	Mix	Water absorption (%)	
			28 days	90 days
1	Calcined clay 0%	CC0	1.35	1.39
2	Calcined clay 4%	CC4	1.45	1.5
3	Calcined clay 8%	CC8	1.52	1.64
4	Calcined clay 12%	CC12	1.58	1.77
5	Calcined clay 16%	CC16	1.99	2.07
6	Calcined clay 20%	CC20	2.28	2.43

mortar samples and their results have been detected in 7 and 28 days intervals. The results of this test are shown in Table 6 (Fig. 4).

Table 6 Sorptivity test

S. No.	Addition proportion	Mix	Sorptivity test (%)	
			28 days	90 days
1	Calcined clay 0%	CC0	0.45	0.43
2	Calcined clay 4%	CC4	0.48	0.46
3	Calcined clay 8%	CC8	0.53	0.5
4	Calcined clay 12%	CC12	0.57	0.52
5	Calcined clay 16%	CC16	0.67	0.6
6	Calcined clay 20%	CC20	0.92	0.87

Fig. 4 Graph 2: Sorptivity test
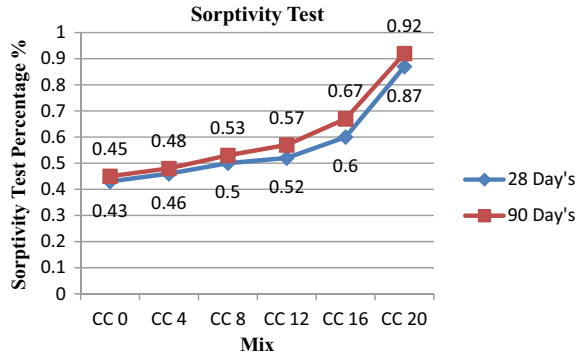
Table 7 Compressive strength test on cement mortar

S. No.	Addition proportion	Mix	Compressive strength (N/mm^2)		
			7 days	28 days	90 days
1	Calcined clay 0%	CC0	34.67	43.33	46.14
2	Calcined clay 4%	CC4	34.11	44.97	49.24
3	Calcined clay 8%	CC8	33.26	42.16	50.15
4	Calcined clay 12%	CC12	33.11	40.21	51.97
5	Calcined clay 16%	CC16	31.16	37.67	48.94
6	Calcined clay 20%	CC20	28.24	36.55	47.86

4.3 Compressive Strength Experiment

Hydration process is a key factor for the strength of concrete and cement mortar. Due to the hydration process in cement mortar and concrete, the strength is very good [25, 26]. During this test, samples of cement mortar have been found to be the result of compression strength in the interval of 7 and 28 days. To achieve the results of the compression strength test, samples have been kept wet for 7 and 28 days in water. And then the cement mortar samples were taken out of the water and the results were obtained by CTM machine. The results of the compression strength are shown in Table 7 (Fig. 5).

4.4 Compressive Strength for Cement Mortar After 2% HCl Curing

HCl acid is a simple chlorine-based acid system with water. This is a confluence of water and hydrogen chloride. HCl is an important industrial chemical and chemical reagent. It is used in the production of polyvinyl chloride in plastic. HCl acid is also

Fig. 5 Graph 3: Compressive strength of cement mortar
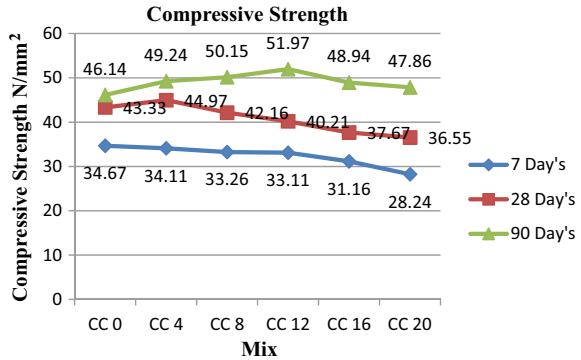
Fig. 6 Graph 4: Compressive strength and weight loss
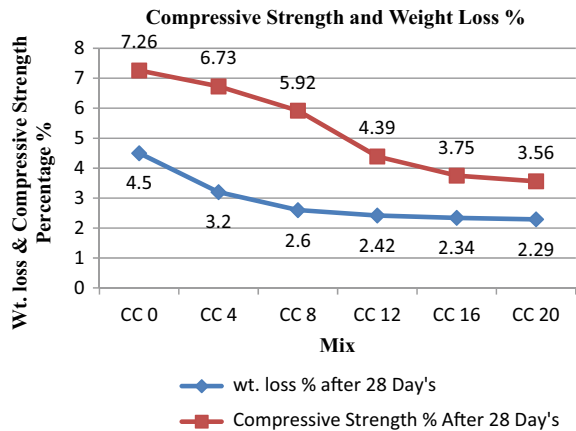
used as a leather processing [27]. Cement mortar samples are soaked in mixed water for 28 days. The amount of 2% hydrochloric acid (HCl) in this water has been added. In this research, the effect was studied due to HCl acid on cement mortar and after the 28 days of HCl mixed water, the result of the compression strength of these samples was detected (Fig. 6 and Table 8).

4.5 Compressive Strength with Acetic Acid

After the formic acid, the second simplest carboxylic acid is acetic acid. It is an industrial chemical and chemical reagent. It is mainly used for polyvinyl acetate for wood glue, cellulose acetate for clothing, photographic film and synthetic fiber [28]. Cement mortar samples are soaked in mixed water for 28 days. The amount of 2% acetic acid in this water has been added. In this research, the effect was studied due

Table 8 Weight loss and compressive strength after HCl curing

S. No.	Addition proportion	Mix	Wt. loss percentage after 28 days	Compressive strength percentage after 28 days
1	Calcined clay 0%	CC0	4.5	7.26
2	Calcined clay 4%	CC4	3.2	6.73
3	Calcined clay 8%	CC8	2.6	5.92
4	Calcined clay 12%	CC12	2.42	4.39
5	Calcined clay 16%	CC16	2.34	3.75
6	Calcined clay 20%	CC20	2.29	3.56

to acetic acid on cement mortar and after the 28 days of acetic acid mixed water, the result of the compression power of these samples was detected (Fig. 7 and Table 9).

Fig. 7 Graph 5: Compressive strength and weight loss
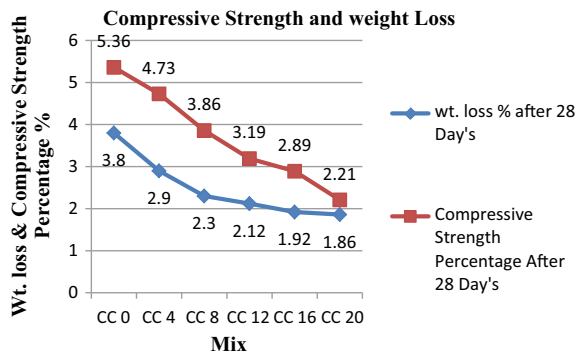
Table 9 Weight loss and compressive strength after acetic acid curing

S. No.	Addition proportion	Mix	Wt. loss percentage after 28 days	Compressive strength percentage after 28 days
1	Calcined clay 0%	CC0	3.8	5.36
2	Calcined clay 4%	CC4	2.9	4.73
3	Calcined clay 8%	CC8	2.3	3.86
4	Calcined clay 12%	CC12	2.12	3.19
5	Calcined clay 16%	CC16	1.92	2.89
6	Calcined clay 20%	CC20	1.86	2.21

5 Conclusion

Based on current experimental analysis on partial replacement of calcined clay with cement mortar are as follows:

- As a result of the water absorption test, the water absorption has increased in every proportion for 28 and 90 days.
- As a result of the sorptivity test, there has been an increase in water absorption in every proportion for 28 and 90 days.
- Cement mortar affects the compression strength of mortar on increasing or decreasing the proportion of calcined clay in the mixture.
- In compression strength test, it was found that 90 days result in higher strength at 12% ratio.
- The compression strength test also found that during the 7 days interval the result is reduced continuously.
- Due to soaking of cement mortar in HCl and acetic acid mixed water for 28 days, mortar starts losing weight.

References

1. Al saffar, D.M.: Influence of pottery clay in cement mortar and concrete mixture: a review. Int. J. Eng. Technol., 67–71 (2018)
2. Bhimani, P.: Performance of concrete with china clay (kaolin) waste. Int. J. Latest Trends Eng. Technol. **2**(3) (2013)
3. O'Farrell, M.: Strength and chemical resistance of mortars containing. Cem. Concr. Compos. **28**(9), 790–799 (2006)
4. Vijaya Sekhar Reddy, M.: Experimental investigations on flexural strength and durability properties of mortars containing cement replacement materials. Int. J. Eng. Comput. Sci. **4**(4), 11588–11596 (2015)
5. Seeni, A.: Experimental study of partial replacement of fine aggregate with waste. Material from China clay Industries. Int. J. Comput. Eng. Res., 167 (2012)
6. Plenge, W.H.: The U.S Concrete Industry Technology Roadmap. Concrete Research & Education Foundation (2002)
7. Mehta, P.K.: Concrete Structure, Properties and Materials. Prentice Hall, New Jersey (1993)
8. Lee, K.-C.: Red clay composites reinforced with polymeric binders. Constr. Build. Mater. **22**, 2292–2298 (2008)
9. Vu, D.D.: Strength and durability aspect of calcined kaolin-blended Portland cement mortars and concrete. Cem. Concr. Res. **27**(1), 471–478 (2001)
10. Osborne, G.J.: Durability of Portland blast-furnace slag cement concrete. Cem. Conc. Compos. **21**, 11–15 (1999)
11. Fragoulis, D.: The physical and mechanical properties of composite cements manufactured with calcareous and clayey greek diatomite mixtures. Cem. Concr. Compos. **27**, 205–209 (2005)
12. Al-Dulaijan: Sulfate resistance of plain and blended cements exposed to magnesium sulfate solutions. Constr. Build. Mater. **21**, 1792–1802 (2007)
13. Shehata, H.M.: Long-term durability of blended cement against sulphate attack. ACI Mater. J. 105, pp. 594–602, 2008.
14. Thomas, M.D.A.: Performance of slag concrete in marine environment. ACI Mater. J. **105**(M71), 628–634 (2008)

15. Sing, G., Siddique, A.R.: Effect of waste foundry sand [WFS] as partial replacement of sand on the strength, ultrasonic pulse velocity and permeability of concrete. Int. J. Constr. Build. Mater. **26**, 4 (2011)
16. Naikin, T.R.: Replacement of fine aggregate with foundry sand. Milwaukee J. **3**, 18 (2007)
17. Leonard, J.M., Brook, K.M.: Concrete materials and practise, 6th edn. London, Melbourne, Auckland (1991)
18. Sudha, P.: Intensification of calcined clay as a pozzolanic material in cement mortar. Int. J. Appl. Eng. Res. **10**, 35640–35644 (2015)
19. Sabir, B.B.: On the workability and strength development of metakaolin concrete. Concr. Environ. Enhancement Prod., 651–656 (1996)
20. Calcined Clay Cement Wikipedia, Google, 23 01 2019. [Online]. Available: https://en.wikipedia.org/wiki/Limestone_Calcined_Clay_Cement. Accessed 20 April 2019
21. Pitroda, J.: Assessment of sorptivity and water absorption of concrete with partial replacement of cement by fly ash and hypo sludge. IJARESM **1**(2), 33–42 (2015)
22. Sabir, B.B.: A water sorptivity test for martar and concrete. Mater. Struct. (1998)
23. Joshi, G.: Evaluation of sorptivity and water captivation of concrete with partial replacement of cement by hypo sludge. Mater. Sci. Eng. **431**, 1–6 (2018)
24. Shah, R.A.: Assessment of sorptivity and water absorption of mortar with partial replacement of cement by fly ash (class-f). Int. J. Civil Eng. Technol. (IJCIET) **4**(5), 15–21 (2013)
25. Kumar, S.: Experimental study on partial replacement of cement with marble powder. Int. J. Pure Appl. Math. **119** (2018)
26. Shukla, A.: Experimental study on partial replacement of cement with marble dust powder in m25 and m30 grade concrete. Int. J. Res. Appl. Sci. Eng. Technol. (IJRASET) **7**(4), 440–448 (2019)
27. HCL Acid Wikipedia, Google, 18 04 2019. [Online]. Available: https://en.wikipedia.org/wiki/Hydrochloric_acid. Accessed 30 April 2019
28. Acetic Acid Wikipedia, Google, 29 04 2019. [Online]. Available: https://en.wikipedia.org/wiki/Acetic_acid. Accessed 30 April 2019

Comparison of Strength Activity of Limestone-Calcined Clay and Class F Fly Ash

Dhanada K. Mishra, Jing Yu and Christopher K. Y. Leung

Abstract This study aims to investigate the pozzolanic strength activity of three kinds of supplementary cementitious materials (SCMs)—a limestone-calcined clay from India and class F fly ashes from China as well as India. Using the ASTM C311 strength activity index test method, the effect of the different pozzolan replacement levels of cement (0, 20, 50 and 80%, by weight) was investigated. Compressive strength at 3, 7, 14, 28 and 90 days under standard curing was recorded. It was observed that the effectiveness of the pozzolan in mortars depends on particle size distribution, glassy or amorphous nature, surface area and replacement level. The results in this study provide insights into the mix design and applications of high-volume pozzolanic cementitious materials that promote solid waste recycling in construction industry.

Keywords Limestone-calcined clay pozzolan · Fly ash · Compressive strength · Strength activity index

1 Introduction

Sustainable development is a kind of development that meets the needs of the present without compromising the ability of future generations to meet their own needs [1]. The exponential increase in greenhouse gas emissions even after Kyoto protocol and Paris agreement having come to effect indicates serious potential consequences of climate change. Unlike developed countries, China and India with their much higher economic growth rates are likely to continue to increase in their share of greenhouse gas emissions in coming decades. As shown in Fig. 1a, cement industry accounts for 6–7% of the global greenhouse gas emissions [2]. Figure 1b shows that China (30%) and India (7%) account for 37% of the total carbon emissions as of 2014

D. K. Mishra (✉)
KMBB College of Engineering and Technology, Bhubaneswar, Odisha 751003, India
e-mail: dhanadam@ust.hk

D. K. Mishra · J. Yu · C. K. Y. Leung
Department of Civil and Environmental Engineering, Hong Kong University of Science and Technology, Hong Kong SAR, PR China
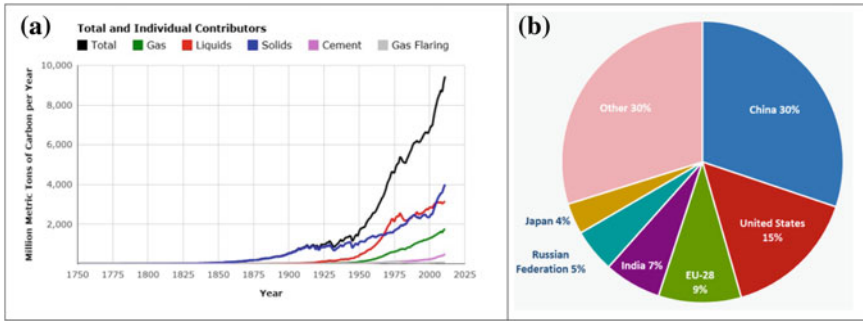
Fig. 1 **a** Global carbon emissions from fossil fuels and **b** emissions by countries in 2014 [2]

[2]. Concrete being the most consumed man-made material and Portland cement, the primary manufactured component of concrete, is particularly polluting as OPC contributes almost a metric ton (MT) of CO_2 per MT of cement produced.

There is a global effort to produce greener cement and reduce the consumption of the materials by using alternative binders and supplementary cementitious materials (SCMs) to produce blended cement as well as concrete with lower cement content [3–5]. Coal combustion ash or pulverized fuel ash, simply known as fly ash (FA), is a by-product of thermal power production in coal-fired plants. This industrial waste has proven to be an effective pozzolanic material with properties suitable to be used in cement production and as a mineral admixture in concrete [6]. The annual generation of fly ash is around 600 million MT in China and around 220 million MT in India, out of which only approximately 70 and 60% of the fly ash is reused in these countries [7, 8].

It is likely the total amount of SCM such as fly ash and blast furnace slag (by-product of steel making) available globally is inadequate to satisfy the likely demand from the construction industry [9, 10]. In this context, limestone-calcined clay (LC2) has been proposed as a low cost, readily available and green substitute that can be used both for making cement as well as in concrete as a pozzolanic mineral admixture or SCM [10, 11]. The green cement known as limestone-calcined clay cement (LC3), which is a blend of ordinary Portland cement (OPC) clinker and LC2 is being actively promoted by a consortium of researchers from Switzerland, Cuba and India. It is estimated that if all Portland cement can be replaced by a green LC3 cement with 50% clinker, 30% calcined clay, 15% limestone and 5% gypsum, the carbon emission from cement manufacturing can be reduced by up to 30% [10, 12, 13].

2 Research Significance

This paper reports strength development of high-volume pozzolanic cementitious materials with LC2 and fly ash. This would help substitute up to 80% of cement by

pozzolans in concrete and achieve 28-day compressive strength of 45 MPa as well as required early strength [14, 15]. Such low carbon mortar compositions can also be used in practical green concrete and strain-hardening cement composite (SHCC) mixes which can address the major weaknesses of conventional concrete, viz. its environmental sustainability and brittle fracture under tension [16–18].

3 Experimental Investigation

3.1 Materials

Type I 52.5N Portland cement manufactured by the Green Island Cement Co., Ltd in Hong Kong which met all the requirements of BS EN 197-1 [19] was used. Two different class F fly ashes—one supplied by the China Power and Light Co., Ltd in Hong Kong, China; another obtained from NTPC Thermal power plant in Kaniha in the eastern state of Odisha in India [20] were used. The limestone-calcined clay (LC2) material was also sourced from India from a batch of pilot production described in Bishnoi et al. [21]. Standard silica sand per ASTM C778 [22] was used as the fine aggregate.

Table 1 shows the chemical composition procured by X-ray fluorescence (XRF) analysis of the two fly ashes and the LC2 as compared to that of Type I Portland cement. SEM images of Indian fly ash and LC2 material are shown in Fig. 2, and the morphology of the Chinese fly ash is very similar to that of the Indian fly ash. Figure 3a presents the particle size distributions of the cement, fly ashes and LC2 material obtained from a Microtrac Bluewave Laser particle size analyzer. The X-ray diffraction (XRD) analysis of the three powder materials is shown in Fig. 3b. The

Table 1 XRF data of Portland cement (PC), fly ash (FA) and limestone-calcined clay (LC2)

Material	OPC	Chinese FA	Indian FA	LC2
LOI[a] (%)	1.2	2.5	1.7	1.2
Al_2O_3 (%)	4.4	18.9	27.5	31.3
SiO_2 (%)	20.2	49.8	64.6	45.8
Fe_2O_3 (%)	3.4	11.4	3.5	3.4
CaO (%)	63.9	9.3	1.1	14.5
SO_3 (%)	4.7	2.1	–	1.7
MgO (%)	2.1	3.6	–	0.0
Na_2O (%)	0.1	1.6	–	0.0
K_2 (%)	0.4	1.8	1.3	0.7
TiO_2 (%)	–	–	1.9	2.6

[a]Loss on ignition
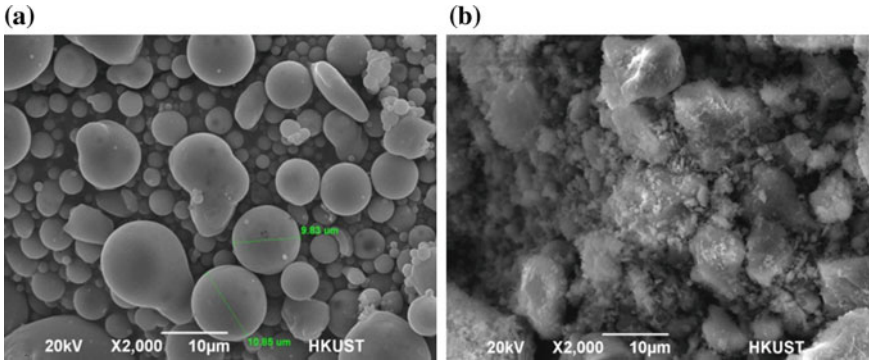
Fig. 2 Scanning electron microscope (SEM) images of **a** Indian fly ash and **b** limestone-calcined clay
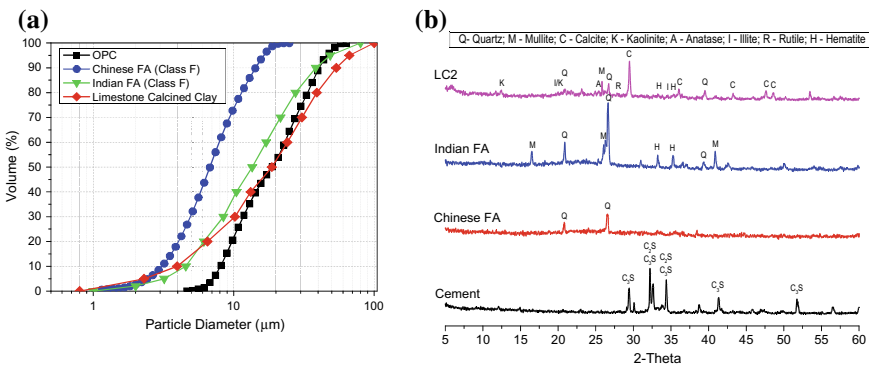
Fig. 3 **a** Particle size distribution of Portland cement (PC), fly ash (FA) and limestone-calcined clay (LC2); **b** X-ray diffraction (XRD) results of Portland cement (PC), fly ash (FA) and limestone-calcined clay (LC2)

loss on ignition for LC2 is the highest due to the decomposition of $CaCO_3$ into CaO and CO_2.

From the chemical compositions of the materials listed in Table 1, the two fly ashes are both categorized as class F as per ASTM C618 [23]. The Chinese fly ash has significantly higher calcium oxide compared to the Indian fly ash, which can result in higher pozzolanic strength activity. This is particularly important in ultrahigh-volume pozzolan cementitious materials, where calcium hydroxide produced from cement hydration may not be adequate to react with all the pozzolanic material in the mix.

3.2 Mix Design and Testing Procedure

A series of mortar mixes were designed as shown in Table 2. The experimental plan was to test the mortar samples with 0, 20, 50 and 80% replacement of cement by the three pozzolans under standard curing [24], and study their effects on strength development. No superplasticizer was used during mixing although the workability was significantly affected by the use of different pozzolans particularly LC2, given its rather irregular particle geometry (Fig. 3). A Hobart HL800 mixer was utilized to prepare the mortars. For each mortar mix in Table 2, the fresh property was measured using the flow table test according to ASTM C1437 [25]. A characteristic deformability factor, denoted by Γ, was calculated as:

$$\Gamma = (D_1 - D_0)/D_0 \tag{1}$$

where D_1 is the average of two orthogonal diameter measurements after dropping and D_0 is the diameter of the bottom of the slump cone.

Cubic samples measuring 40 mm × 40 mm × 40 mm prepared and cured for comparison purposes. Compressive tests were performed with a standard sample holder to ensure a 40 mm × 40 mm loading area, with the test procedure following ASTM C109/C109M [26]. The loading rate for compressive tests was 0.35 MPa/s. For each data point, a minimum of three test results were averaged and reported along with the coefficient of variation. The strength activity index (SAI) for the mixes with different contents of pozzolans can be calculated as per ASTM C311/C311M [27]

Table 2 Mix proportions (weight ratio)

Mix	Pozzolan	Cement/Binder	Pozzolan/Binder	Sand/Binder	Water/Binder
C100 (control)	–	1.0	0.0	2.75	0.484
C80FA20(C)	Chinese FA	0.8	0.2	2.75	0.484
C50FA50(C)	Chinese FA	0.5	0.5	2.75	0.484
C20FA80(C)	Chinese FA	0.2	0.8	2.75	0.484
C80FA20(I)	Indian FA	0.8	0.2	2.75	0.484
C50FA50(I)	Indian FA	0.5	0.5	2.75	0.484
C20FA80(I)	Indian FA	0.2	0.8	2.75	0.484
C80L20	LC2	0.8	0.2	2.75	0.484
C50L50	LC2	0.5	0.5	2.75	0.484
C20L80	LC2	0.2	0.8	2.75	0.484

as follows:

$$SAI = \left(f_c^{\text{pozz}} / f_c^{\text{control}} \right) \times 100\% \tag{2}$$

where f_c^{pozz} = compressive strength of the mix with pozzolan at a specific age, MPa; f_c^{control} = compressive strength of the control mix at the same age, MPa.

4 Experimental Results and Discussion

The results of the study are discussed in two parts, viz. the basic characteristics of the pozzolanic materials and the fresh and hardened properties.

4.1 *Characterization of Pozzolans*

The SEM images of the fly ash contrast sharply against the image of the LC2 (Fig. 2). The fly ash consists of spherical smooth particles, LC2 is characterized by angular particles of random shapes. This difference is expected to affect the workability of the mix. From the particle size distribution shown in Fig. 3a, the median particle size of Type I PC, Chinese FA, Indian FA and the LC2 are 18.86 µm, 6.76 µm, 13.56 µm and 18.68 µm, respectively. The Chinese fly ash has the finest particle size and would be expected to have better pozzolanic strength activity as compared to the Indian fly ash. The BET surface area measurement yields values of 2.328 m^2/g for Chinese fly ash, 0.696 m^2/g for the Indian fly ash and 8.353 m^2/g for the LC2. From the X-ray diffraction (XRD) results for the three pozzolanic materials as well as the Portland cement shown in Fig. 3b, the peaks corresponding to the Quartz (SiO$_2$) and CaO are visible to different degrees of intensity.

4.2 *Fresh Property of Mortars*

The characteristic deformability factors (Γ) for all the mixes listed in Table 2 are summarized in Table 3. Compared to the control mix ($\Gamma = 1.10$), the mixes with Chinese fly ash showed improved workability, from $\Gamma = 1.15$ for C80FA20(C) to $\Gamma = 1.35$ for C20FA80(C), and the mixes with India fly ash had a similar trend. However, the mixes incorporating LC2 had lower workability with a Γ no more than 1.05. As mentioned earlier, the water/binder ratio was constant and superplasticizer was not used to compensate for the variation in workability. The lower workability of LC2 mixes was compensated by its much higher surface area and calcium content resulting in comparable strength development.

Table 3 Summary of characteristic deformability factor (Γ) and comp. strength (in MPa)

Mix	Characteristic deformability factor	3-day comp. strength	7-day comp. strength	14-day comp. strength	28-day comp. strength	90-day comp. strength
C100 (control)	1.10	27.0(1.3)	32.4(0.7)	36.6(1.8)	43.6(0.8)	45.6(1.4)
C80FA20(C)	1.15	23.6(2.1)	28.7(2.2)	30.9(3.4)	38.3(1.9)	39.2(1.4)
C50FA50(C)	1.21	14.3(0.7)	20.6(1.3)	23.6(0.9)	30.6(2.7)	38.8(1.2)
C20FA80(C)	1.35	3.4(0.4)	5.8(0.4)	6.5(0.5)	8.3(1.4)	12.0(0.4)
C80FA20(I)	1.10	19.1(1.9)	24.7(2.8)	28.6(3.5)	32.0(1.5)	41.2(2.5)
C50FA50(I)	1.19	11.3(0.7)	14.5(0.3)	15.6(1.8)	20.3(1.4)	31.9(1.6)
C20FA80(I)	1.31	4.4(0.2)	5.1(0.1)	5.8(0.4)	7.0(0.4)	12.9(0.5)
C80L20	1.05	22.2(2.2)	29.6(2.5)	33.0(4.7)	35.4(2.3)	38.3(5.6)
C50L50	1.03	10.5(1.4)	15.8(2.4)	16.4(0.4)	18.7(0.5)	18.9(0.8)
C20L80	1.00	4.7(0.1)	5.5(0.3)	5.9(0.1)	6.7(0.2)	6.9(0.2)

Note Data in brackets is the standard deviation

4.3 Compressive Strength and Pozzolanic Strength Activity Index

Table 3 summarizes the compressive strength of all the mixes at 3-day, 7-day, 14-day, 28-day and 90-day ages under standard curing conditions. The coefficients of variation of the results are 3.5–10.3% for different mixes, which indicates reasonable uniformity among samples. The 28-day compressive strength of control sample is lower than expected due to variation in manual casting procedure and inadequate compaction. However, since the identical procedure is used for all mixes, the relative strengths are reasonable and can be used to understand the effect of pozzolan addition on strength as shown in Fig. 4.

The overall trend of strength development with increasing age is reasonable. According to Eq. 2, the pozzolanic strength activity indices for the mixes with different replacement levels of pozzolan at different ages can be calculated, and the results are shown in Fig. 4. For the mixes with Chinese fly ash, the index is about 88% for C80FA20(C), about 70% for C50FA50(C) and 19% for C20FA80(C). In other words, the index is decreased with increasing replacement level of pozzolan. The same trend can be observed for the mixes with Indian fly ash and LC2, and the indices are 73% and 81% for Indian fly ash and LC2, respectively. It is interesting to note that while there is not much increase in strength after 28 days for the control and LC2 mixes unlike the mixes with both fly ashes. These results indicate that in order to use LC2 in place of fly ash in ultra high-volume pozzolanic concrete (17, 18), a similar approach of low water binder ratio and liberal use of superplasticizer can be adopted. However, the long term strengths may not be as high as fly ash concrete.
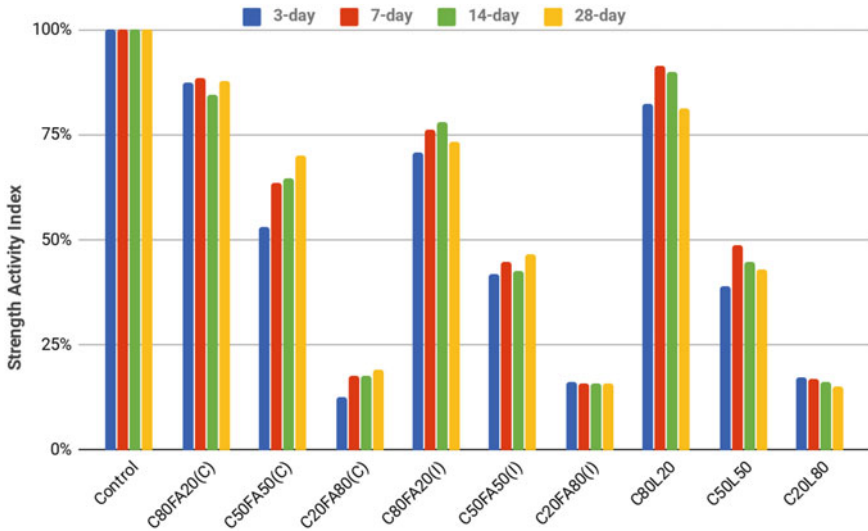
Fig. 4 Strength activity indices of mortars with different pozzolan substitutes

5 Conclusions

The following conclusions can be made according to the materials used and the test results from current phase of this study:

1. The workability of the standard mortar when using fly ash showed increased flow unlike in case of LC2, which resulted in significantly reduced flow properties. In spite of the reduced workability, LC2 seems to have a comparable strength activity index given its much higher BET surface area compared to the two fly ashes studied.
2. When tested according to pozzolanic strength activity tests recommended by ASTM C311/C311M, the strength activity index was found to be 88, 73 and 81% for the Chinese fly ash, Indian fly ash and LC2, respectively.
3. It is postulated that the higher amorphous nature, finer particle size distribution, higher calcium content and surface area of the Chinese fly ash give comparatively better performance.

References

1. McManus, P.: Defining sustainable development for our common future: a history of the World Commission on Environment and Development (Brundtland Commission). Aust. Geogr. **45**, 559–561 (2014)
2. Boden, T.A., Marland, G., Andres, R.J.: Global, Regional, and National Fossil-Fuel CO_2 Emissions. Carbon Dioxide Information Analysis Center, Oak Ridge National Laboratory, U.S. Department of Energy, Oak Ridge, Tenn., U.S.A. (2017)
3. Mehta, P.K.: Sustainable cements and concrete for the climate change era—a review. In: Second International Conference on Sustainable Construction Materials and Technologies (2010)
4. Lothenbach, B., Scrivener, K., Hooton, R.D.: Supplementary cementitious materials. Cem. Concr. Res. **41**, 1244–1256 (2011)
5. Scrivener, K.L.: Options for the future of cement. Indian Concr. J. **88**, 11–21 (2014)
6. Zhang, G., Wei, Q., Ding, Q., Wang, A., Liu, K.: Effect of curing temperature and fly ash content on the hydration and microstructure of fly ash–cement pastes. J. Sustain. Cem. Based Mater. **7**, 372–383 (2018)
7. National Development and Reform Commission of China (NDRCC): Annual Report on Comprehensive Utilization of Resources 2014 (2014) (in Chinese)
8. Yao, Z.T., Ji, X.S., Sarker, P.K., Tang, J.H., Ge, L.Q., Xia, M.S., Xi, Y.Q.: A comprehensive review on the applications of coal fly ash. Earth Sci. Rev. **141**, 105–121 (2015)
9. Monteiro, P.J.M., Miller, S.A., Horvath, A.: Towards sustainable concrete. Nat. Mater. **6**, 698–699 (2017)
10. Scrivener, K., Martirena, F., Bishnoi, S., Maity, S.: Calcined clay limestone cements (LC3). Cem. Concr. Res. **114**, 49–56 (2018)
11. Scrivener, K.L., John, V.M., Gartner, E.M.: Eco-efficient cements: potential economically viable solutions for a low-CO_2 cement-based materials industry. Cem. Concr. Res. **114**, 2–26 (2018)
12. Avet, F., Scrivener, K.: Investigation of the calcined kaolinite content on the hydration of limestone calcined clay cement (LC3). Cem. Concr. Res. **107**, 124–135 (2018)
13. Dhandapani, Y., Sakthivel, T., Santhanam, M., Gettu, R., Pillai, R.G.: Mechanical properties and durability performance of concretes with limestone calcined clay cement (LC3). Cem. Concr. Res. **107**, 136–151 (2018)
14. Yu, J., Li, G., Leung, C.K.Y.: Hydration and physical characteristics of ultrahigh-volume fly ash-cement systems with low water/binder ratio. Constr. Build. Mater. **161**, 509–518 (2018)
15. Yu, J., Lu, C., Leung, C.K.Y., Li, G.: Mechanical properties of green structural concrete with ultrahigh-volume fly ash. Constr. Build. Mater. **147**, 510–518 (2017)
16. Yu, J., Leung, C.K.Y.: Strength improvement of strain-hardening cementitious composites with ultrahigh-volume fly ash. J. Mater. Civ. Eng. **29**, 05017003 (2017)
17. Yu, J., Li, H., Leung, C.K.Y., Lin, X., Lam, J.Y.K., Sham, I.M.L., Shih, K.: Matrix design for waterproof engineered cementitious composites (ECCs). Constr. Build. Mater. **139**, 438–446 (2017)
18. Yu, J., Yao, J., Lin, X., Li, H., Lam, J.Y.K., Leung, C.K.Y., Sham, I.M.L., Shih, K.: Tensile performance of sustainable strain-hardening cementitious composites with hybrid PVA and recycled PET fibers. Cem. Concr. Res. **107**, 110–123 (2018)
19. BSI. Cement Part 1: Composition, specifications and conformity criteria for common cements. EN 197-1:2011: British Standards (2011)
20. Yu, J., Mishra, D.K., Wu, C., Leung, C.K.Y.: Very high volume fly ash green concrete for applications in India. Waste Manage. Res. **36**, 520–526 (2018)
21. Bishnoi, S., Maity, S., Mallik, A., Joseph, S., Krishnan, S.: Pilot scale manufacture of limestone calcined clay cement: the Indian experience. ICJ **88**, 22–28 (2014)
22. ASTM: Standard Specification for Standard Sand. C778. ASTM International, West Conshohocken, PA, USA (2017)
23. ASTM: Standard Specification for Coal Fly Ash and Raw or Calcined Natural Pozzolan for Use in Concrete. C618. ASTM International, West Conshohocken, PA, USA (2012)

24. ASTM. Standard Practice for Making and Curing Concrete Test Specimens in the Field. C31/C31M. ASTM International, West Conshohocken, PA, USA (2012)
25. ASTM: Standard Test Method for Flow of Hydraulic Cement Mortar. C1437. ASTM International, West Conshohocken, PA, USA (2007)
26. ASTM: Standard Test Method for Compressive Strength of Hydraulic Cement Mortars. C109/C109M. ASTM International, West Conshohocken, PA, USA (2013)
27. ASTM: Standard Test Methods for Sampling and Testing Fly Ash or Natural Pozzolans for Use in Portland-Cement Concrete. C311/C311M. ASTM International, West Conshohocken, PA, USA (2013)

Limestone Calcined Clay as Potential Supplementary Cementitious Material—An Experimental Study

Revanth Kumar Kandagaddala, Vikas Manare and Prakash Nanthagopalan

Abstract The present study aims to explore the potential of using limestone calcined clay (LC^2) blend as a supplementary cementitious material. The cement was replaced with LC^2 blend (by volume), and experiments were carried out at the same solid volume concentration. Initially, the influence of LC^2 particles on cement was assessed through wet packing density studies. Further, fresh properties were evaluated using rheological studies, setting time for all the experimental combinations. Also, the compressive and flexural strengths for different combinations were determined at various ages (up to 56 days). The results are discussed in the light of optimal and maximum replacement levels based on the performance of cementitious mortars in the fresh and hardened state.

Keywords Limestone calcined clay · Rheology · Packing studies · Compressive strength

1 Introduction

The use of supplementary cementitious materials (SCM) in cement is strongly prompted to reduce the clinker factor in the manufacturing of cement, which in turn reduces the CO_2 emissions. However, most of the SCMs such as pulverised fuel ash, ground-granulated blast-furnace slag, silica fume, and bagasse ash are either industrial by-products or agro-based residues. Due to their limited availability [1] and logistical issues, the need for alternative materials with technical and economic feasibility becomes essential. Materials such as fly ash, silica fume, and limestone powder are being used up to 5% as performance improvers in the manufacturing of ordinary Portland cement [2]. Research [3] shows that the addition of limestone powder to cement is beneficial in terms of filler effect, providing additional nucleation sites for hydration, stabilising ettringite, and the formation of carboaluminates, thus improving the fresh (workability) and hardened properties and durability of concrete [3–5]. From the viewpoint of availability, clay is abundant in nature [6], and

R. K. Kandagaddala (✉) · V. Manare · P. Nanthagopalan
Indian Institute of Technology Bombay, Mumbai, India
e-mail: revanthkumar@iitb.ac.in

dehydroxylation of kaolinite clay by thermal treatment around 600–800 °C produces metakaolin, which has pozzolanic properties due to the presence of amorphous alumina and silica. Addition of metakaolin to cement has been beneficial in terms of mechanical properties and durability of concrete [6–9]. Recent investigations on the combination of limestone powder and metakaolin were found to have a synergistic effect. Calcite in limestone reacts with alumina in metakaolin and produces hemi-carboaluminates and monocarboaluminates, leading to pore refinement [10]. This study is focussed on utilising the potential of limestone calcined clay (LC^2) blend as a suitable supplementary cementitious material in cementitious mortar.

2 Materials

2.1 Cement and Limestone Calcined Clay

Ordinary Portland cement (OPC) of 53 grade conforming to IS 269 [2] and LC^2 were used in the investigation. The ratio of calcined clay to limestone was kept as 2:1 (by weight) based on the earlier studies [11, 12]. The physical properties of materials and the chemical composition of the materials are given in Tables 1 and 2, respectively. The morphology of cement and LC^2 are shown in SEM pictures in Fig. 1.

2.2 Fine Aggregates

The fine aggregates (FA) were standardised to eliminate the subjectivity owing to minor variation in particle-size distribution while taking from the storage area. The fine aggregates were sieved according to each size fractions and stored in separate bins. The aggregates from each bin were selected based on gradation corresponding

Table 1 Physical properties of materials

Property	OPC	LC^2
Specific gravity	3.14	2.68
Specific surface area (Blaine's), m^2/kg	342.00	577.48

Table 2 Chemical composition of materials (wt%)

Oxide	CaO	SiO_2	Al_2O_3	Fe_2O_3	MgO	Na_2O	K_2O	SO_3	TiO_2	LOI
Cement	61.7	22.5	5.7	3.0	1.4	0.3	0.4	2.5	–	2.5
LC^2	28.29	34.28	19.45	3.43	1.38	0.31	0.27	1.58	1.63	9.21
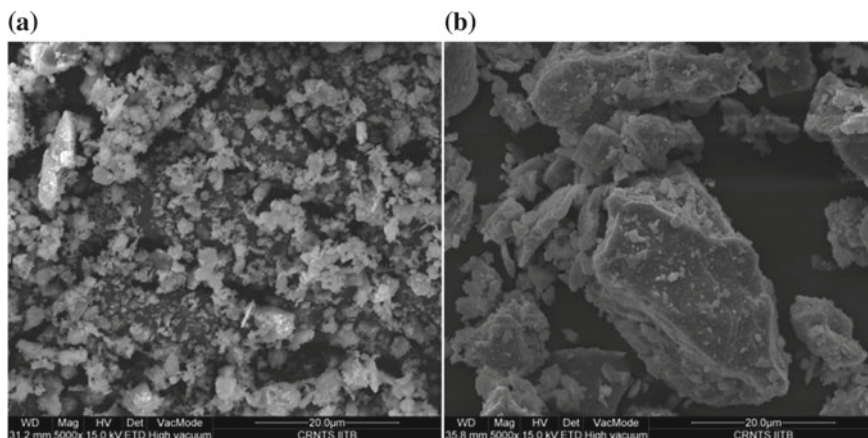
Fig. 1 Scanning electron microscope (SEM) images of **a** cement and **b** LC^2

to Zone-II of IS 383 [13]. The specific gravity and water absorption of FA were 2.69 and 2.73%, respectively.

2.3 High-Range Water-Reducing Admixture (HRWRA)

A polycarboxylate-ether-based water reducer with a specific gravity of 1.10 and 45% solid content was used in the investigation.

3 Experimental Work

3.1 Pozzolanic Reactivity of Limestone Calcined Clay

Limestone calcined clay was evaluated for its pozzolanic reactivity by lime reactivity test. Mortar cubes of 50 mm size were prepared as per IS 1727 [14], and the specimens were kept in a moist environment for the first two days and stored in a chamber at 50 °C and 90% RH for the next eight days. RH was maintained in the chamber using saturated potassium sulphate solution. The compressive strength of the mortars determined at the age of ten days is an indication of the reactivity of pozzolana.

3.2 Packing Density Studies

Cement was replaced with LC^2 blend (by volume) at 0, 5, 10, 20, 30, 50, 70, and 90%, and experiments were carried out to determine the wet packing density by Puntke test [15].

Sample Preparation—Rheological Studies The pastes were prepared with 0, 5, 10, 20, and 30% volume replacement of cement with LC^2 at a constant w/p of 0.45. The powders were initially dry blended in a turbular mixer for better homogenisation. The cementitious pastes were prepared using planetary mixer, and mixing was carried out for three minutes. All the rheological measurements were made at the 8th minute after the addition of water.

3.3 Rheology

Rheology is the study of flow and deformation of matter under the action of shear stress [16]. Generally, during pumping, the flow of concrete in a pipe occurs as a plug surrounded by a thin layer of paste called lubrication layer. This lubrication layer facilitates the movement of concrete. In the case of plug flow, the pumping pressure is dictated by the rheological properties of the lubrication layer rather than bulk concrete [17]. Hence, rheological investigations were carried on paste level targeting the pumping applications of concrete. Rheological studies were carried at the same solid volume concentration using a controlled shear rate rheometer. The adopted geometry is a cup and bob with the outer and inner cylinder as 28.8 mm and 26.6 mm, respectively.

Shearing protocol. The shearing protocol for evaluating the rheological parameters is shown in Fig. 2a. The shear profile needs to be formulated in such a way that it should resemble the velocity profile of the lubrication layer [18] and achieve a steady
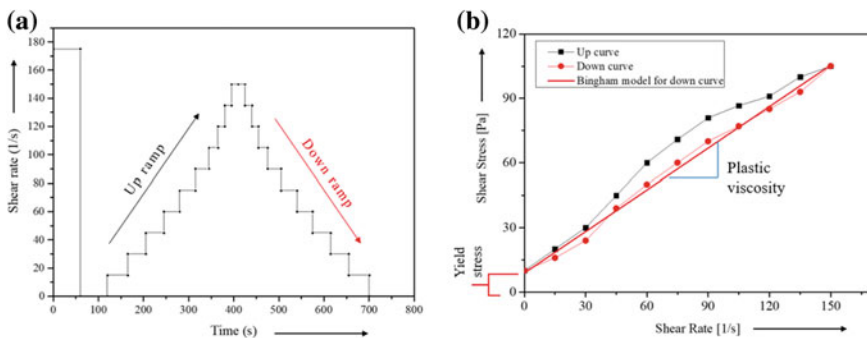
Fig. 2 a Shearing protocol and **b** typical flow curve for the rheological evaluation

state at each measuring point. To satisfy the requirement, the following assumptions were made to determine the maximum shear rate in the shear profile.

1. The thickness of the lubrication layer is around 2 mm [19].
2. The velocity profile is uniform throughout the cross-section of the pipe.
3. The diameter of the pipe and discharge of concrete are 125 mm and 12 m^3/h, respectively. These suit the requirement of general pumping operations carried out in Mumbai region, India.

$$\text{Shear rate, } \gamma' = \frac{Q}{Ah} = \frac{12 \times 1000 \times 4}{\pi \times 0.125^2 \times 3600 \times 2} = 135{-}150\left(\frac{1}{s}\right)$$

The shearing cycle consists of two parts. First part is pre-shearing, performed at $175\ s^{-1}$, to have a consistent shear history before each measurement. The second part is for data recording, in which the down curve is selected for analysis to get robust data. For the applied shear rate, the corresponding shear stress was measured. A plot (flow curve—Fig. 2b) was made between the shear stress and shear rate. The dynamic yield stress (intercept on Y-axis) and plastic viscosity (slope) were determined by analysing the flow curve using the Bingham model.

3.4 Mortar Preparation

Mortars were prepared with 0, 5, 10, 20, and 30% volume replacement of cement with LC^2 and fine aggregates using the planetary mixer as follows: two minutes of dry blending for homogenisation and three minutes of intense mixing after the addition of water. The mixture proportions were given in Table 3.

Table 3 Details of mortar mixture proportions

Mixture ID	LC^2—0%	LC^2—5%	LC^2—10%	LC^2—20%	LC^2—30%
Cement: LC^2 (by vol.)	1:0	0.95:0.05	0.9:0.10	0.80:0.20	0.70:0.30
Water-to-binder ratio	0.45	0.45	0.45	0.45	0.45
HRWRA (%)	0.3	0.3	0.3	0.3	0.3
Binder: fine aggregate (by wt.)	1:3	1:3	1:3	1:3	1:3

3.5 Mini-Slump Cone Test—Flowability

In this study, the flow properties of mortar were determined by using a mini-slump cone for cement mortar as described in IS 4031: Part 7 [20]. The spread is measured in two perpendicular directions.

3.6 Fresh and Hardened Properties of Mortar

Setting time of mortars was determined as per ASTM C 807 [21]. Specimens were cast in $40 \times 40 \times 160$ mm moulds for compressive strength and flexural strength and cured in saturated lime water (0.3% concentration) until testing. The specimens were tested as per EN 196-1 [22].

4 Results and Discussion

4.1 Pozzolanic Reactivity of Limestone Calcined Clay

As per IS 1727 [14], LC^2 showed a lime reactivity of 9.2 MPa, satisfying the minimum requirements of 4.0 MPa as per IS 1344 [23].

4.2 Packing Density Studies

From Fig. 3a, it is evident that the packing density of powders increased up to 5% replacement of LC^2. Further increment in the replacement leads to a reduction in the packing density. The packing system depends upon the particle size/gradation, shape, compaction, wall effect, or loosening effect [24]. The size, shape, and compaction effort are same for all the combinations. Depending on the dominant percentage of particles in the system, the gradation of particles and the wall effect/loosening effect will change. Therefore, while replacing cement with LC^2, the packing system of cement particles is dominant, and LC^2 particles are packed based on the voids between the cement particles. In the case of higher replacement levels (i.e., above 50% LC^2), LC^2 particles will be the dominant fraction, in turn, dictate the packaging. If the size of the cement particles exceeds the size of voids between the LC^2 particles, the packing structure is disturbed, leading in more voids in the system. This is evident from Fig. 3a. Finally, the packing of 100% LC^2 is more than 100% of cement particles. Although LC^2 particles are relatively large in size, as shown in Fig. 3b, the higher
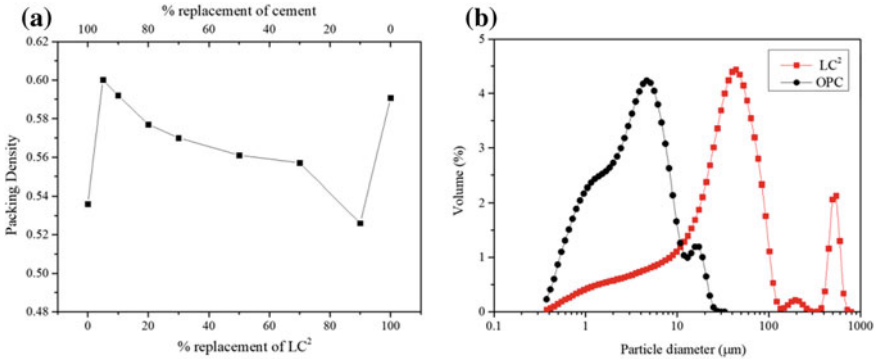
Fig. 3 **a** Wet packing density of cement blended with LC^2 and **b** particle-size distribution of LC^2 and OPC

packing density of LC^2 particles could be due to the presence of suitable size fractions of fine particles in LC^2 getting packed between the voids of larger particles compared to cement particles.

4.3 Rheology

Lower yield stress implies that it requires less resistance to flow, and can be understood with high workability. From Fig. 4a, it is observed that yield stress of cementitious paste decreased slightly at 5% replacement of LC^2. This could be attributed to the better packing density (refer Fig. 3a) of cement and LC^2 blend, leading to enhanced flow properties. This is in line with the observations in the past research [25]. As all the paste combinations are with same solid volume fraction, the increase
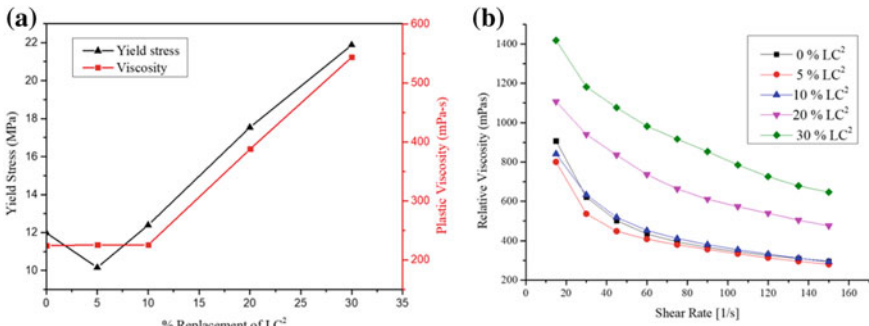
Fig. 4 Rheological behaviour of pastes substituted with LC^2. **a** Variation of yield stress and plastic viscosity at different replacement levels and **b** viscosity curve for various replacement levels

Table 4 Spread of mortars blended with LC^2

Mixture ID	LC^2—0%	LC^2—5%	LC^2—10%	LC^2—20%	LC^2—30%
Spread (mm)	195	235	230	155	130

in yield stress beyond 5% replacement can be attributed to the higher specific surface area of LC^2, which is 40% higher than cement which demands higher water content.

From Fig. 4a, it is observed that the viscosity of pastes remains same up to 10% replacement level and increased for higher replacement levels. This could be attributed to the increased cohesion of pastes with LC^2. From the viscosity curve, as shown in Fig. 4b, it is observed that all the pastes exhibit shear-thinning behaviour, which is beneficial from a pumping perspective, which otherwise may demand high pressures. The rate of shear thinning decreases as the replacement level increases, and the rate of shear thinning is lower for 5% replacement. The shear-thinning behaviour might be due to the preferred orientation of particles and deagglomeration due to the application of high shear rates [26].

4.4 Flowability

The results of the flowability of mortars for the different combinations are reported in Table 4. From the results, it is evident that, with the increase in LC^2 proportions, the spread decreased, except at 5% replacement of LC^2. The decrease in spread could be attributed to the higher surface area and angular nature of LC^2 particles. The highest spread for LC^2-5% combination can be understood due to the high packing density.

4.5 Fresh and Hardened Properties of Cementitious Mortar

From Table 5, it is clear that the setting time of mortar decreases as the replacement level of LC^2 blend increases. The decrement could be due to limestone powder accelerating the reaction kinetics in the form of providing the nucleation sites [27].

From Fig. 5a, it is observed that at the age of 7 days the compressive strength of all the LC^2 combinations (up to 30%) is more than OPC-based mortar. This indicates that the synergetic effect due to the presence of limestone and calcined clay in cement systems forming calcium carboaluminates [10] leading to pore refinement

Table 5 Setting time of mortars blended with various percentages of LC^2

Mixture ID (min.)	LC^2—0%	LC^2—5%	LC^2—10%	LC^2—20%	LC^2—30%
Initial setting time	165	142	135	100	80
Final setting time	205	215	180	135	100
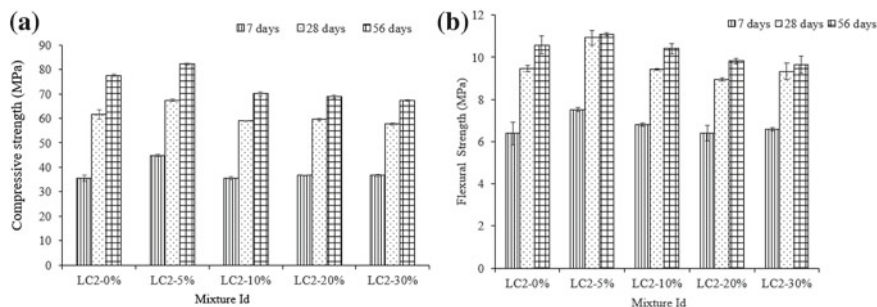
Fig. 5 **a** Compressive strength and **b** flexural strength of LC^2-based mortars at the age of 7, 28, and 56 days

is much pronounced until seven days. However, post seven days and upto 28 days, the contribution from LC^2 towards strength reduced slightly. This is evident from Fig. 5. At 28 and 56 days, for 5% LC^2 replacement, highest compressive strength (~5 MPa more than LC^2—0%) was achieved w.r.t OPC-based mortar due to the relatively better packing density of the particles. For LC^2 combinations (10–30%), the compressive strengths are lower than OPC-based mortars at 28 and 56 days. This could be attributed to the lesser packing density of mortar. With the increase in age, all the combinations resulted in higher strengths. It is interesting to note that, post 28 days, 16 MPa (approx. 20% of 56 days strength) gained with OPC mortar (LC^2—0%). Similar strength increments of 8–14 MPa for LC^2-based combinations were observed at 56 days. It is well established in the literature [12] that the contribution of LC^2-based reaction products on strength requirement is negligible beyond 28 days. This could be attributed to the contribution from OPC-based reaction products' formation beyond 28 days. This is also clear with a decrease in the strength gain with an increase in % replacement of LC^2. From this observation, it is clear that the LC^2 contribution towards strength beyond 28 days is insignificant. A similar trend was observed for the flexural strength of all the combinations. Considering the fact that most of the construction sites rely on compressive strength at the age of 28 days for acceptance, it is evident from Fig. 5 that the optimal replacement level of LC^2 for maximising the strength is 5% and the maximum replacement of LC^2 for obtaining almost equal performance of OPC mortar is 20%.

5 Conclusions

The following conclusions were drawn from this investigation in evaluating LC^2 as a potential pozzolana.

a. LC^2 qualified as a pozzolanic material showing higher lime reactivity.

b. With increased replacements beyond 10%, due to the higher surface area, the yield stress and viscosity increased. This may demand higher water content or water reducer for given workability in comparison with OPC mortar.

c. 5% (by vol.) replacement of LC^2 exhibited better hardened properties due to relatively higher packing density. Maximum of 20% LC^2 replacement with cement is possible without compromising on the strength w.r.t OPC mortar.

It can be concluded that LC^2 can be regarded as a potential pozzolana. However, the durability aspect needs to be evaluated for maximum replacements.

References

1. Miller, S.A., John, V.M., Pacca, S.A., Horvath, A.: Carbon dioxide reduction potential in the global cement industry by 2050. Cem. Concr. Res. **114**, 115–124 (2018)
2. IS 269: Ordinary Portland Cement—Specification, pp. 1–10. Bur Indian Stand, New Delhi, India (2015)
3. Wang, D., Shi, C., Farzadnia, N., Shi, Z., Jia, H., Ou, Z.: A review on use of limestone powder in cement-based materials: mechanism, hydration and microstructures. Constr. Build. Mater. **181**, 659–672 (2018)
4. González, M., Irassar, E.F.: Effect of limestone filler on the sulfate resistance of low. Cem. Concr. Res. **28**, 1655–1667 (1998)
5. Sawicz, Z., Heng, S.S.: Durability of concrete with addition of limestone powder. Mag. Concr. Res. **48**, 131–137 (2009)
6. Scrivener, K.L.: Options for the future of cement. Indian Concr. J. **88**, 11–21 (2014)
7. Al-Akhras, N.M.: Durability of metakaolin concrete to sulfate attack. Cem. Concr. Res. **36**, 1727–1734 (2006)
8. Badogiannis, E.G., Sfikas, I.P., Voukia, D.V., Trezos, K.G., Tsivilis, S.G.: Durability of metakaolin self-compacting concrete. Constr. Build. Mater. **82**, 133–141 (2015)
9. Dinakar, P., Sahoo, P.K., Sriram, G.: Effect of Metakaolin content on the properties of high strength concrete. Int. J. Concr. Struct. Mater. **7**, 215–223 (2013)
10. Antoni, M., Rossen, J., Martirena, F., Scrivener, K.: Cement substitution by a combination of metakaolin and limestone. Cem. Concr. Res. **42**, 1579–1589 (2012)
11. Bishnoi, S., Maity, S., Mallik, A., Joseph, S., Krishnan, S.: Pilot scale manufacture of limestone calcined clay cement: the Indian experience. Indian Concr. J. **88**, 22–28 (2014)
12. Emmanuel, A.C., Haldar, P., Maity, S., Bishnoi, S.: Second pilot production of limestone calcined clay cement in India: the experience. Indian Concr. J. **90**, 57–64 (2016)
13. IS 383: Coarse and Fine Aggregate for Concrete—Specification, pp. 1–18. Bur Indian Stand, New Delhi, India (2016)
14. IS 1727: Methods of Test for Pozzolanic Materials, pp. 1–49. Bur Indian Stand, New Delhi, India (1967)
15. Nanthagopalan, P., Haist, M., Santhanam, M., Müller, H.S.: Investigation on the influence of granular packing on the flow properties of cementitious suspensions. Cem. Concr. Compos. **30**, 763–768 (2008)
16. Howard, A.B.: A Handbook of Elementary Rheology. University of Wales, Institute of Non-Newtonian Fluid Mechanics, Aberystwyth, Wales (2000)
17. Kaplan, D., De Larrard, F., Sedran, T.: Design of concrete pumping circuit. ACI Mater. J. **102**, 110–117 (2005)
18. Khatib, R.: Analysis and prediction of pumping characteristics of high-strength self-consolidating concrete. PhD Thesis (2013)

19. Choi, M., Roussel, N., Kim, Y., Kim, J.: Lubrication layer properties during concrete pumping. Cem. Concr. Res. **45**, 69–78 (2013)
20. IS: 4031 (Part 7): Methods of Physical Tests for Hydraulic Cement-Part 7: Determination of Compressive Strength of Masonry Cement, pp. 1–4. Bur Indian Stand, New Delhi, India (1988)
21. ASTM C807: Standard Test Method for Time of Setting of Hydraulic Cement Mortar by Modified Vicat Needle, pp. 1–3. Am Soc Test Mater, West Conshohocken, PA (2018)
22. BS EN-196-1: Methods of Testing Cement—Part 1: Determination of Strength, pp. 1–22. Br Stand Inst, London, UK (1995)
23. IS 1344: Indian Standard Specification for Calcinated Clay Pozzolana, pp. 1–9. Bur Indian Stand, New Delhi, India (1981)
24. Andersen, P.J., Johansen, V.: Particle packing and concrete properties. Mater. Sci. Concr. II 111–146 (1995)
25. Chen, J.J., Kwan, A.K.H.: Superfine cement for improving packing density, rheology and strength of cement paste. Cem. Concr. Compos. **34**, 1–10 (2012)
26. Mezger, T.G.: The Rheology Handbook: For Users of Rotational and Oscillatory Rheometers. Vincentz Network GmbH & Co KG, Hannover, Germany (2006)
27. Lothenbach, B., Le Saout, G., Gallucci, E., Scrivener, K.: Influence of limestone on the hydration of Portland cements. Cem. Concr. Res. **38**, 848–860 (2008)

Sustainable PVA Fiber-Reinforced Strain-Hardening Cementitious Composites (SHCC) with Ultrahigh-Volume Limestone Calcined Clay

Jing Yu and **Christopher K. Y. Leung**

Abstract Strain-hardening cementitious composites (SHCC) exhibiting tensile strain-hardening and multiple-cracking behaviors are attractive for many construction applications. Compared to conventional concrete, typical SHCC are cost-, energy- and carbon-intensive. Specifically, the cement content of typical SHCC mixtures can be as high as 600–1200 kg/m^3. To reduce the material cost and improve the sustainability of SHCC, one possible approach is to replace cement with supplementary cementitious materials (SCM). It has been shown in the literature that the limestone calcined clay (LC2) system is a promising source of SCM for conventional concrete. This paper presents an attempt to use ultrahigh-volume LC2 (80% by weight of binder) to produce polyvinyl alcohol (PVA) fiber-reinforced SHCC with adequate compressive strength and excellent tensile performance. This version of sustainable SHCC is applicable for many practical applications, and the substitution of high percentages of cement with LC2 can reduce the environmental impact significantly.

Keywords Engineered cementitious composite · Fiber-reinforced concrete · Supplementary cementitious material · Limestone calcined clay · Polyvinyl alcohol fiber · Tensile performance · Crack pattern

1 Introduction

Strain-hardening cementitious composites (SHCC) are a class of special fiber-reinforced concrete (FRC) exhibiting strain-hardening and multiple cracking under tension, and their compressive strength can be designed to range from 20 to 150 MPa [1]. According to the micromechanical theory, the fiber, matrix and fiber/matrix interfacial properties can be designed to achieve tensile strain-hardening by incorporating around 2 vol.% of high-performance polymeric fibers (e.g., polyvinyl alcohol (PVA) and polyethylene (PE)) [2–5]. The ultimate tensile strain of SHCC is typically 1–8% (Fig. 1), which is several hundred times the tensile strain capacity of ordinary FRC

J. Yu (✉) · C. K. Y. Leung
Hong Kong University of Science and Technology, Hong Kong SAR, PR China
e-mail: jyuad@connect.ust.hk
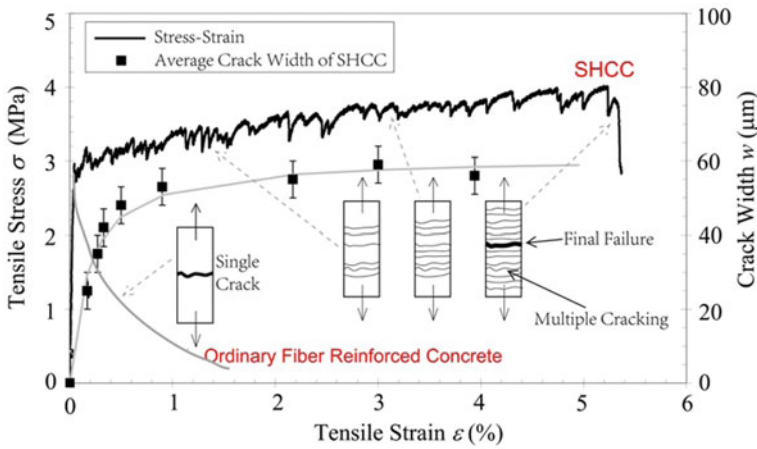
Fig. 1 Typical tensile stress–strain curve and crack width development of SHCC (adapted from [1])

and concrete; at the same time, the crack width can be controlled to less than 100 μm (Fig. 1) [1]. On account of the aforementioned excellent mechanical and durability properties, SHCC are attractive materials for durable and resilient infrastructures and buildings [6–8].

However, the commercial development of SHCC imposes additional considerations, as the adoption of a new technology must be justified with advantages in the cost–benefit ratio. In contrast with conventional concrete, while typical SHCC materials are cost-, energy- and carbon-intensive, the long term benefits may be sufficient to potentially drive this technology into the commercialization stage in the near future in a number of countries [9]. Nevertheless, the cost reduction of SHCC materials remains very important. Specifically, the material cost of typical PVA fiber-reinforced SHCC (PVA-SHCC) is more than 9 times that of ordinary concrete [10]. To reduce the material cost and/or environmental impact of SHCC, one possible approach is to replace cement with supplementary cementitious materials (SCM) [11–16], while another approach is to partially or even totally replace the commonly used PE/PVA fibers by other alternatives with lower cost [17–22].

It is likely the total amount of SCM including fly ash and blast furnace slag available globally is inadequate to satisfy the likely demand from the construction industry in the near future [23, 24]. Recently, limestone calcined clay (LC2) has been proposed as a low-cost, readily available and green substitute that can be used for making cement as well as in concrete as a SCM [23, 24]. It has been estimated that if all Portland cement can be replaced by a green LC2 cement with 50% clinker, 30% calcined clay, 15% limestone and 5% gypsum, the carbon emission from cement manufacturing can be reduced by up to 30% [23, 25].

So far, no studies on using LC2 to develop sustainable SHCC have been reported. Based on the previous experience of the authors on developing sustainable PVA-SHCC [10, 16] and Grade 45 structural concrete [26–28] with ultrahigh-volume fly ash, the authors aim to explore the feasibility of making sustainable PVA-SHCC with ultrahigh-volume LC2 (80% by weight of binder) in the present study. To achieve high ultimate tensile strain, using lightweight fillers to lower the matrix fracture toughness was also explored. Compressive strength after 7/28/90 days standard curing as well as uniaxial tensile performance after 28 days standard curing were evaluated.

2 Experimental Program

2.1 Materials and Mix Proportion

Totally 6 mixes as listed in Table 1 were tested. Type I 52.5N Portland cement, silica fume and limestone calcined clay (LC2, limestone:calcined clay = 1:2) sourced from India were used as the binder materials. The chemical compositions of the received cement, silica fume and LC2 materials are listed in Table 2. Silica sand with particle sizes of 120–180 μm was used. To maintain the workability of the mix (slump flow of 200 mm) and guarantee the uniform fiber dispersion, powder-form polycarboxylate-based super-plasticizers (SP) were added. The nominal physical properties of the Kuraray K-II REC15 polyvinyl alcohol (PVA) fibers are given in

Table 1 Mix proportions of sustainable PVA-SHCC with ultrahigh-volume LC2 (by weight)

Mix ID	Binder		Sand/Binder	Filler/Binder	Water/Binder	SP/Binder (%)	PVA fiber (vol.%)
	Cement	LC2					
Control	0.2	0.8	0.2	0	0.40	0.24	2
AG-1				0.01		0.64	
AG-2				0.02		1.10	
FAC-2				0.02		0.28	
FAC-4				0.04		0.32	
FAC-6				0.06		0.37	

Table 2 Chemical compositions of cement and limestone calcined clay

Materials	LOI[a] (%)	SiO_2 (%)	Al_2O_3 (%)	Fe_2O_3 (%)	CaO (%)	MgO (%)	SO_3 (%)	Na_2O (%)	K_2O (%)
Cement	1.2	20.2	4.4	3.4	63.9	2.1	4.7	0.1	0.4
LC2	12.0	45.8	31.3	3.4	14.5	0.0	1.7	0.0	0.7

[a]*LOI* loss on ignition

Table 3 Nominal properties of Kuraray K-II REC15 polyvinyl alcohol (PVA) fiber

Length (mm)	Diameter (μm)	Aspect ratio	Elastic modulus (GPa)	Fiber strength (MPa)	Fiber density (g/cm^3)
12	39	308	42.8	1600	1.30

Table 3. To achieve high ultimate tensile strain by lowering matrix fracture toughness, two kinds of lightweight fillers were explored, namely fly ash cenosphere (FAC) and aerogel (AG). FAC is a by-product of coal burning during electricity production process, which is lightweight (550 kg/m^3) and cost-effective. Aerogel is an extremely light (100 kg/m^3) nano-porous material composed of silica having a major volume (94–95%) being the air voids.

2.2 Sample Preparation and Test Method

A Hobart HL200 mixer was used to mix the material. Specimens were cast in greased steel molds on a vibrating table. After finishing the surface, the specimens were covered with a polyethylene sheet to prevent moisture loss and kept under room temperature for 24 h prior to demolding. After demolding, specimens were cured up to 7/28/90 days in a fog room at the temperature of 23 ± 2 °C and relative humidity of $95 \pm 5\%$.

The compressive test was carried out with cube specimens measuring 50 mm × 50 mm × 50 mm. An automatic compression testing machine was utilized to perform the compression tests, with a loading rate of 0.6 MPa/s.

The uniaxial tension test was performed with the dumbbell specimen recommended by JSCE [29], with a middle part measuring 30 mm × 13 mm (Fig. 2). Two external linear variable displacement transducers (LVDT) were attached to both
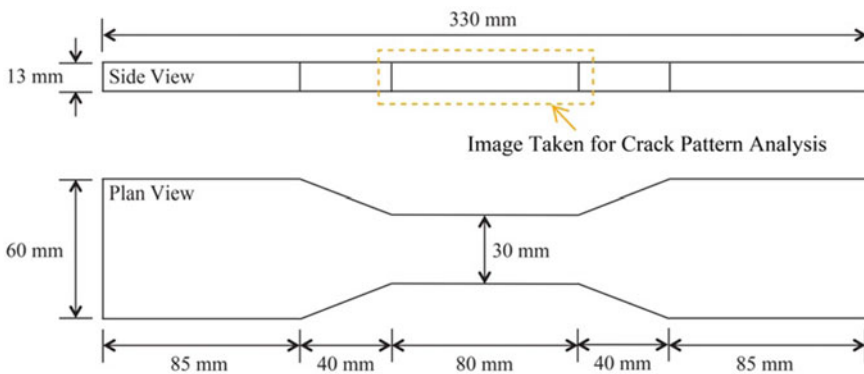
Fig. 2 Dimensions of dumbbell tensile specimen recommended by JSCE

sides of the middle part of the tensile specimen to measure the elongation over a gauge length of 80 mm. A 25 kN servo-hydraulic MTS testing system was used, with the grips providing fixed support to both ends of the specimen (rotations and transverse displacements were restrained). The displacement-controlled loading rate was 0.5 mm/min [29].

3 Results and Discussion

3.1 Compressive Strength

The 7-day, 28-day and 90-day compressive strengths for the 6 mixes given in Table 1 are graphically shown in Fig. 3. The overall trend of strength development of these mixes with ultrahigh-volume LC2 is different from that of ultrahigh-volume fly ash mixes, as the ratios between the 7-day and 28-day compressive strengths can reach 75–82%. This is due to the higher reactivity of calcined kaolinite (the major pozzolan in LC2) than common glassy SCM (e.g., fly ash) [23, 24]. In other words, using ultrahigh-volume LC2 in cementitious materials does not significantly reduce the early strength and delay the construction processes.

As shown in Fig. 3, the control mix achieved 26.89 MPa at 7-day age, 32.89 MPa at 28-day age and 35.39 MPa at 90-day age, which should be adequate for many non-structural or semi-structural applications as well as some structural applications in rural areas. As expected, the addition of 1 wt% and 2 wt% aerogels lowered the compressive strength by about 13% and 52%, respectively. On the other hand, adding 2 wt% FAC had negligible effect on the compressive strength, while incorporating 4 wt% and 6 wt% FAC increased the 28-day compressive strength by about 4% and 20%, respectively.

Fig. 3 Compressive strength of different PVA-SHCC mixes in Table 1
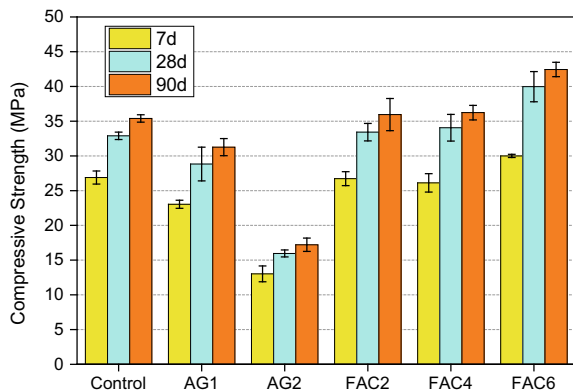
3.2   Uniaxial Tension Performance

The 28-day uniaxial tensile stress–strain curves for the 6 mixes in Table 1 are graphically shown in Fig. 4, and the major tensile characteristics are graphically shown in Fig. 4.

Compared to the control mix, the addition of 1 wt% aerogels had negligible effects on the first-cracking strength and tensile strength, but significantly increased the ultimate tensile strain (from 1.41 to 4.21%) and the crack width (as indicated from the curves). Additionally, the incorporation of 2 wt% aerogels significantly improved the ultimate tensile strain (from 1.41 to 4.69%) and the crack control capacity (i.e., smaller crack width), but extremely lowered the tensile strength to 2.2 MPa. In a
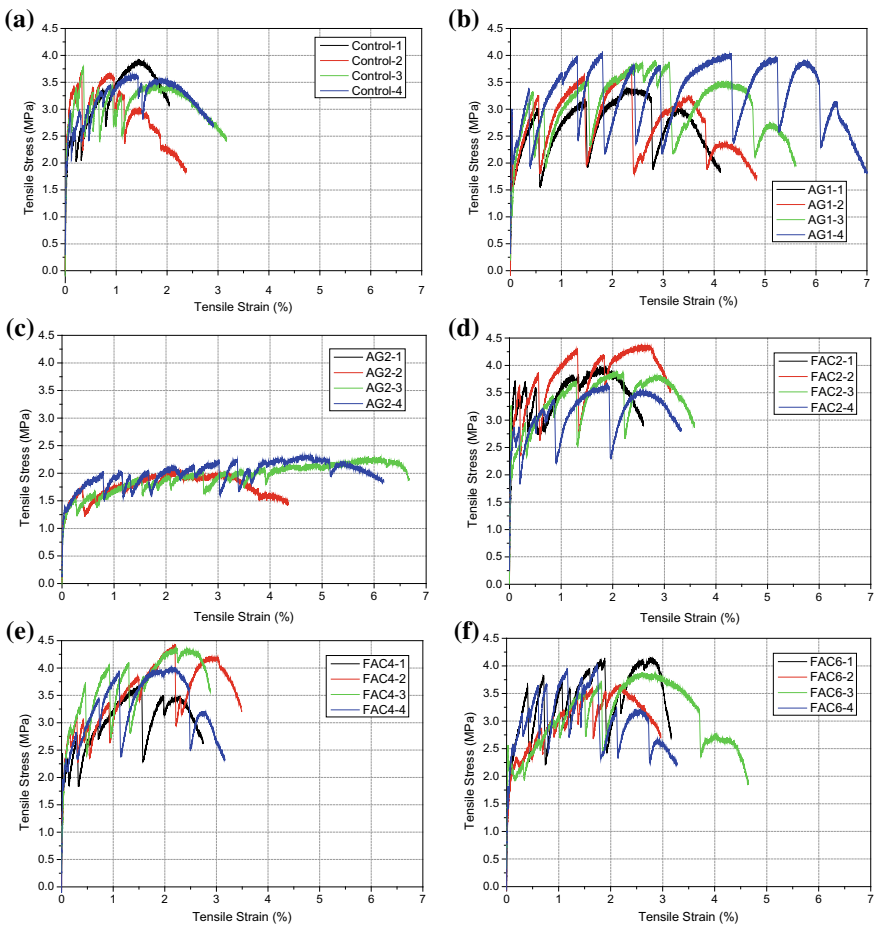
Fig. 4 28-day tensile stress–strain curves of different SHCC mixes: **a** control; **b** AG1; **c** AG2; **d** FAC2; **e** FAC4; and **f** FAC6

Table 4 Summary of major tensile characteristics of different PVA-SHCC mixes in Table 1

Mix ID	First-cracking strength (MPa)	Tensile strength (MPa)	Ultimate tensile strain (%)
Control	2.83 ± 0.25	3.77 ± 0.12	1.41 ± 0.37
AG-1	2.80 ± 0.15	3.75 ± 0.31	4.21 ± 1.11
AG-2	1.54 ± 1.17	2.21 ± 0.19	4.69 ± 1.49
FAC-2	2.47 ± 0.54	3.95 ± 0.29	2.51 ± 0.46
FAC-4	2.02 ± 0.42	4.11 ± 0.36	2.49 ± 0.38
FAC-6	1.96 ± 0.28	3.91 ± 0.22	2.54 ± 0.26

word, using aerogels in PVA-SHCC with ultrahigh-volume LC2 can increase the ultimate tensile strain, but the optimal dosage for different applications should be verified with the considerations of tensile strength and crack width control Table 4.

On the other hand, adding 2–6 wt% FAC slightly lowered the first-cracking strength, slightly increased the tensile strength and significantly improved the ultimate tensile strain (from 1.4% to about 2.5%). Though a higher dosage of FAC did not increase the ultimate tensile strain, the crack control capacity was improved (Fig. 4d–f).

4 Conclusions

This paper presents an attempt to use ultrahigh-volume LC2 (80% by weight of binder) to produce polyvinyl alcohol (PVA) fiber-reinforced SHCC with adequate compressive strength and excellent tensile performance. According to the results in this study, the following conclusions can be drawn:

(1) SHCC with 80 wt% LC2 in the binder system achieved 26.89 MPa at 7-day age, 32.89 MPa at 28-day age and 35.39 MPa at 90-day age. This SHCC mix showed tensile strength of 3.77 MPa and ultimate tensile strain of 1.41% at 28-day age.
(2) While maintaining comparable compressive strength to the control mix, adding 1 wt% aerogels or 2 wt% FAC as lightweight fillers in SHCC ultrahigh-volume LC2 significantly improved the ultimate tensile strain from 1.41 to 4.21% and 2.51%, respectively.

This study offers an approach to develop sustainable SHCC. Future studies on improvement of the ultimate tensile strain and the reduction of crack width are recommended.

References

1. Li, V.C.: Engineered Cementitious Composites (ECC)—Bendable Concrete for Sustainable and Resilient Infrastructure. Springer, Berlin, Heidelberg, Germany (2019)
2. Li, V.C., Leung, C.K.Y.: Steady-state and multiple cracking of short random fiber composites. J. Eng. Mech. **118**(11), 2246–2264 (1992)
3. Li, V.C.: From micromechanics to structural engineering—the design of cementitous composites for civil engineering applications. J. Struct. Mech. Earthq. Eng. **10**(2), 37–48 (1993)
4. Leung, C.K.Y.: Design criteria for pseudoductile fiber-reinforced composites. J. Eng. Mech. **122**(1), 10–18 (1996)
5. Zhang, D., Yu, J., Wu, H., Jaworska, B., Ellis, B.,Li, V.C.: Discontinuous micro-fibers as intrinsic ductile reinforcement for engineered cementitious composites (ECC). Comp. Part B Eng. **184**, 107741 (2020)
6. Rokugo, K., Kanda, T., Yokota, H., Sakata, N.: Applications and recommendations of high performance fiber reinforced cement composites with multiple fine cracking (HPFRCC) in Japan. Mater. Struct. **42**(9), 1197–1208 (2009)
7. Mechtcherine, V.: Novel cement-based composites for the strengthening and repair of concrete structures. Constr. Build. Mater. **41**, 365–373 (2013)
8. Li, V.C.: Bendable concrete. Innov. Constr. Hong Kong CIC Res. J. (Special Issue: CIC Inavation Award), 11–17 (2016)
9. Li, V.C.: On engineered cementitious composites (ECC)—a review of the material and its applications. J. Adv. Concr. Technol. **1**(3), 215–230 (2003)
10. Yu, J., Leung, C.K.Y.: Strength improvement of strain-hardening cementitious composites with ultrahigh-volume fly ash. J. Mater. Civ. Eng. **29**(9), 05017003 (2017)
11. Yang, E.-H., Yang, Y., Li, V.C.: Use of high volumes of fly ash to improve ECC mechanical properties and material greenness. ACI Mater. J. **104**(6), 620–628 (2007)
12. Zhou, J., Qian, S., Sierra Beltran, M.G., Ye, G., Breugel, K., Li, V.: Development of engineered cementitious composites with limestone powder and blast furnace slag. Mater. Struct. **43**(6), 803–814 (2010)
13. Huang, X., Ranade, R., Zhang, Q., Ni, W., Li, V.C.: Mechanical and thermal properties of green lightweight Engineered Cementitious Composites. Constr. Build. Mater. **48**, 954–960 (2013)
14. Ohno, M., Li, V.C.: A feasibility study of strain hardening fiber reinforced fly ash-based geopolymer composites. Constr. Build. Mater. **57**, 163–168 (2014)
15. Nematollahi, B., Sanjayan, J., Shaikh, F.U.A.: Matrix design of strain hardening fiber reinforced engineered geopolymer composite. Compos. B Eng. **89**, 253–265 (2016)
16. Yu, J., Li, H., Leung, C.K.Y., Lin, X., Lam, J.Y.K., Sham, I.M.L., Shih, K.: Matrix design for waterproof engineered cementitious composites (ECCs). Constr. Build. Mater. **139**, 438–446 (2017)
17. Choi, W.-C., Yun, H.-D., Kang, J.-W., Kim, S.-W.: Development of recycled strain-hardening cement-based composite (SHCC) for sustainable infrastructures. Compos. B Eng. **43**(2), 627–635 (2012)
18. Felekoglu, B., Tosun-Felekoglu, K., Ranade, R., Zhang, Q., Li, V.C.: Influence of matrix flowability, fiber mixing procedure, and curing conditions on the mechanical performance of HTPP-ECC. Compos. B Eng. **60**, 359–370 (2014)
19. Yu, J., Yao, J., Lin, X., Li, H., Lam, J.Y.K., Leung, C.K.Y., Sham, I.M.L., Shih, K.: Tensile performance of sustainable Strain-Hardening Cementitious Composites with hybrid PVA and recycled PET fibers. Cem. Concr. Res. **107**, 110–123 (2018)
20. Lin, X., Yu, J., Li, H., Lam, J.Y.K., Shih, K., Sham, I.M.L., Leung, C.K.Y.: Recycling polyethylene terephthalate wastes as short fibers in strain-hardening cementitious composites (SHCC). J. Hazard. Mater. **357**, 40–52 (2018)
21. Yu, J., Chen, Y., Leung, C.K.Y.: Mechanical performance of Strain-Hardening Cementitious Composites (SHCC) with hybrid polyvinyl alcohol and steel fibers. Comp. Struct. **226**, 111198 (2019)

22. Ahmed, S.F.U., Maalej, M.: Tensile strain hardening behaviour of hybrid steel-polyethylene fibre reinforced cementitious composites. Constr. Build. Mater. **23**(1), 96–106 (2009)
23. Scrivener, K., Martirena, F., Bishnoi, S., Maity, S.: Calcined clay limestone cements (LC3). Cem. Concr. Res. **114**, 49–56 (2018)
24. Scrivener, K.L., John, V.M., Gartner, E.M.: Eco-efficient cements: potential economically viable solutions for a low-CO2 cement-based materials industry. Cem. Concr. Res. **114**, 2–26 (2018)
25. Gettu, R., Pillai, R.G., Santhanam, M., Rathnarajan, S., Basavaraj, A.S., Rengaraju, S., Yuvaraj, D.: Service life and life-cycle assessment of reinforced concrete with fly ash and limestone calcined clay cement. In: Sixth International Conference on Durability of Concrete Structures, pp. 27–35. University of Leeds, Leeds, United Kingdom (2018)
26. Yu, J., Lu, C., Leung, C.K.Y., Li, G.: Mechanical properties of green structural concrete with ultrahigh-volume fly ash. Constr. Build. Mater. **147**, 510–518 (2017)
27. Yu, J., Mishra, D.K., Wu, C., Leung, C.K.Y.: Very high volume fly ash green concrete for applications in india. Waste Manage. Res. **36**(6), 520–526 (2018)
28. Yu, J., Li, G., Leung, C.K.Y.: Hydration and physical characteristics of ultrahigh-volume fly ash-cement systems with low water/binder ratio. Constr. Build. Mater. **161**, 509–518 (2018)
29. JSCE: Recommendations for design and construction of high performance fiber reinforced cement composites with multiple fine cracks (HPFRCC). Tokyo (2008)

Using Limestone Calcined Clay to Improve Tensile Performance and Greenness of High-Tensile Strength Strain-Hardening Cementitious Composites (SHCC)

Jing Yu and Christopher K. Y. Leung

Abstract High-tensile strength strain-hardening cementitious composites (HTS-SHCC) can reduce the size of structural members, enhance the flexibility of architectural design and make 3-D printed structures without steel reinforcements possible. To produce HTS-SHCC, high-performance polyethylene (PE) fiber is widely used, due to its high-tensile strength of about 3 GPa. However, PE fiber has a hydrophobic and smooth surface, which limits the fiber/matrix interfacial bond strength. Therefore, a large dosage of very fine powders (e.g., micro silica) has been generally included in the matrix to densify the fiber/matrix interface and ensure sufficient fiber-bridging capacity. Recently, it has been proved in the literature that limestone calcined clay (LC2) system has a strong porosity refinement effect in cementitious materials. Thus, LC2 has the potential to ensure sufficient fiber/matrix frictional bond strength by replacing a fraction of cement by LC2 in HTS-SHCC, which can also reduce the material cost and the environmental impact of the materials. This paper presents a feasibility study of incorporating different dosages of LC2 (0, 20, 40, 60 and 80% of binder) in HTS-SHCC, with the focus on the tensile performance in terms of tensile strength, ultimate tensile strain and crack pattern. The findings in this study provide a new, low-cost and sustainable approach to produce HTS-SHCC.

Keywords Engineered cementitious composite · Fiber-reinforced concrete · Supplementary cementitious material · Limestone calcined clay · Polyethylene fiber · High-tensile strength · Crack pattern · Environmental impact

1 Introduction

To overcome the brittle fracture nature of conventional concrete, a family of fiber-reinforced cementitious composites with compressive strength ranging from 20 to 150 MPa—strain-hardening cementitious composites (SHCC) have been developed [1]. Based on the design theory, the properties of the matrix, fiber and fiber/matrix interface can be selected or tailored to achieve pseudo-ductile behavior with the

J. Yu (✉) · C. K. Y. Leung
Hong Kong University of Science and Technology, Hong Kong SAR, PR China
e-mail: jyuad@connect.ust.hk

addition of about 2% (volume fraction) of polyvinyl alcohol (PVA) or polyethylene (PE) fibers [2–5]. The deformation capacity of SHCC under uniaxial tension can reach 1–8%, and typically the crack width of multiple fine cracks can be controlled to less than 100 μm [1]. Because of these outstanding properties, SHCC are clearly superior to conventional concrete for resilient, durable and sustainable buildings and infrastructures [6–9].

To achieve high-tensile strength (typically > 7 MPa) in SHCC, the following approaches have been widely used: (1) using high strength polyethylene (PE) fiber (about 3 GPa); (2) reducing the water/binder ratio to obtain a strong matrix; (3) incorporating fine particles (e.g., micro silica, nano silica) to densify the microstructure of fiber/matrix interface for improving the interfacial frictional bond and (4) treating the surface of PE fibers to reduce the hydrophobicity for improving the interfacial chemical and frictional bonds. Additionally, the high cement content (typically 1000–1600 kg/m^3) in high-tensile strength SHCC (HTS-SHCC) is a consequence of rheology control for uniform fiber dispersion as well as matrix toughness control (i.e., to reduce matrix toughness by reducing sand/cement ratio) for strain-hardening behavior [1]. To improve the sustainability of HTS-SHCC, one possible approach is to substitute cement with supplementary cementitious materials (SCM) in the matrix [10–16], while a more effective solution is to partially or even totally replace the PE fibers by more cost-effective alternatives [17–20]. This study only focuses on the first approach dealing with the matrix.

Recently, limestone calcined clay (LC2) has been proposed as a low cost, readily available and green substitute that can be used both for making cement as well as in concrete as a SCM [21, 22]. Specifically, it has been reported that LC2 has a strong porosity refinement effect in cementitious materials [21, 22]. Thus, LC2 has the potential to ensure sufficient fiber/matrix frictional bond strength by replacing a fraction of cement by LC2 in HTS-SHCC, which can also reduce the cost and the environmental impact of the materials.

So far, no studies on using LC2 to develop sustainable SHCC have been reported. The aim of this study is to explore the benefits of partially replacing the cement by LC2 in HTS-SHCC, with the LC2/binder ratios of 0, 20, 40, 60 and 80% by weight. Compressive strengths at 7-day and 28-day ages, as well as uniaxial tensile performance at 28-day age were evaluated.

2 Experimental Program

2.1 Materials and Mix Proportion

Type I 52.5N Portland cement and limestone calcined clay (LC2, limestone:calcined clay = 1:2) sourced from India were used as the binder materials. Totally, five mixes as listed in Table 1 were tested, where the LC2/binder ratios range from 0 to 80%. The chemical compositions of the received cement and LC2 materials are listed in Table

2, and their particle size distributions are presented in Fig. 1. Silica sand with particle sizes of 120–180 µm was used. The nominal physical properties of the polyethylene (PE) fibers are given in Table 3. To maintain the workability of the mix (slump flow of 150–180 mm) with a low water-to-binder ratio (i.e., 0.2) to guarantee uniform fiber dispersion, powder form polycarboxylate-based superplasticizers were added.

Table 1 Mix proportions (by weight)

Mix ID	Binder		Sand/binder	Water/binder	Superplasticizers/binder (%)	PE fiber (vol%)
	Cement	LC2				
C100	1.00	0	0.3	0.2	0.645	2.0
C80LCC20	0.8	0.2			0.800	
C60LCC40	0.6	0.4			1.205	
C40LCC60	0.4	0.6			2.554	
C20LCC80	0.2	0.8			4.287	

Table 2 Chemical compositions of cement and limestone calcined clay

Materials	LOI[a] (%)	SiO_2 (%)	Al_2O_3 (%)	Fe_2O_3 (%)	CaO (%)	MgO (%)	SO_3 (%)	Na_2O (%)	K_2O (%)
Cement	1.2	20.2	4.4	3.4	63.9	2.1	4.7	0.1	0.4
LC2	12.0	45.8	31.3	3.4	14.5	0.0	1.7	0.0	0.7

[a]LOI Loss on Ignition

Fig. 1 Particle size distributions of cement and limestone calcined clay

Table 3 Nominal properties of polyethylene (PE) fiber

Length [mm]	Diameter [μm]	Aspect ratio	Elastic modulus [GPa]	Fiber strength [MPa]	Fiber density [g/cm^3]	Surface coating
12	24	500	110	2850	0.97	N/A

2.2 Sample Preparation and Test Method

A Hobart HL200 mixer was used to mix the material. Specimens were cast in greased steel molds on a vibrating table. After finishing the surface, the specimens were covered with a polyethylene sheet to prevent moisture loss and kept under room temperature for 36 h prior to demolding. An exception was C20LCC80, which was demolded after 84 h from casting, due to the significant retarding effect caused by a large dosage of superplasticizers. After demolding, specimens were cured up to 7 or 28 days in a fog room at the temperature of 23 ± 2 °C and relative humidity of $95 \pm 5\%$.

The compressive test was carried out with cube specimens measuring 50 mm × 50 mm × 50 mm. An automatic compression testing machine was utilized to perform the compression tests, with a loading rate of 0.6 MPa/s.

The uniaxial tension test was performed with the dumbbell specimen recommended by JSCE [23], with a middle part measuring 30 mm × 13 mm (Fig. 2). Two external linear variable displacement transducers (LVDT) were attached to both sides of the middle part of the tensile specimen to measure the elongation over a gauge length of 80 mm. A 25 kN servo-hydraulic MTS testing system was used, with the grips providing fixed support to both ends of the specimen (rotations and transverse displacements were restrained). The displacement-controlled loading rate was 0.5 mm/min [23].
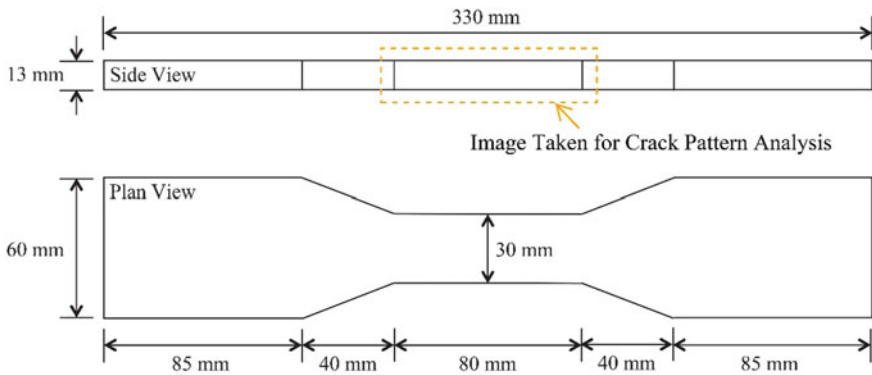
Fig. 2 Dimensions of dumbbell tensile specimen recommended by JSCE

The single fiber pull-out test was performed on PE fibers to determine the fiber/matrix interfacial properties. The general profile of single fiber pull-out performance consists of two obvious stages: a debonding/pre-peak stage and a pull-out/post-peak stage. After complete debonding, the entire embedded part of the fiber undergoes pulling-out against the friction bond with continuously reduced embedment length. Therefore, the fiber/matrix interface frictional bond (τ_0) can be obtained as follows [24]:

$$\tau_0 = \frac{P_b}{\pi d_f l_e} \tag{1}$$

where P_b is the peak load of the single fiber pull-out curve; d_f is the fiber diameter; l_e is the fiber embedment length (2 mm in this study). Details on the sample preparation can refer to Curosu et al. [25] and Yu [17]. The pull-out tests were conducted at a speed of 0.02 mm/s on a universal testing system MTS (Model E44.104). A 50-N load cell was used to measure the pull-out forces, and the pull-out displacement was obtained from the displacement of the actuator. At least six single fiber pull-out tests were performed for each mix in Table 1.

3 Results and Discussion

3.1 Compressive Strength

Both 7-day and 28-day compressive strengths for the five mixes in Table 1 are graphically summarized in Fig. 3. The 28-day compressive strengths for the first four mixes are about 100–135 MPa for 50-mm cubic specimens, which is equivalent to around 90–125 MPa for 100 mm cubic specimens [26]. Additionally, even when 80% of the cement was replaced by LC2 in C20LCC80, 28-day compressive strength of 53.6 MPa (equivalent to 49.5 MPa for 100-mm cubic specimens) was achieved, which is still attractive for many practical applications.

Compared to the control C100, both the 7-day and 28-day compressive strengths increase for C80LCC20 and C40LCC60, and then decrease with increasing LC2/binder ratios. The strength improvement in C80LCC20 and C40LCC60 should be due to the strong porosity refinement effect of LC2 in cementitious materials [21, 22].

Additionally, the ratio between 7-day and 28-day compressive strengths is shown in Fig. 3, which indicates an interesting trend that the ratio increases at first, and then decreases with increasing LC2 dosages. Actually, it was reported that calcined kaolinite (the major pozzolan in LC2) is much more reactive than glassy SCM and was expected to react rapidly at an early stage [21, 22], so why significant strength improvement was still observed for mixes with ultra-high volume LC2 (C40LCC60 and C20LCC80)? As discussed in Yu et al. [27], for mixes with SCM, the Ca(OH)$_2$
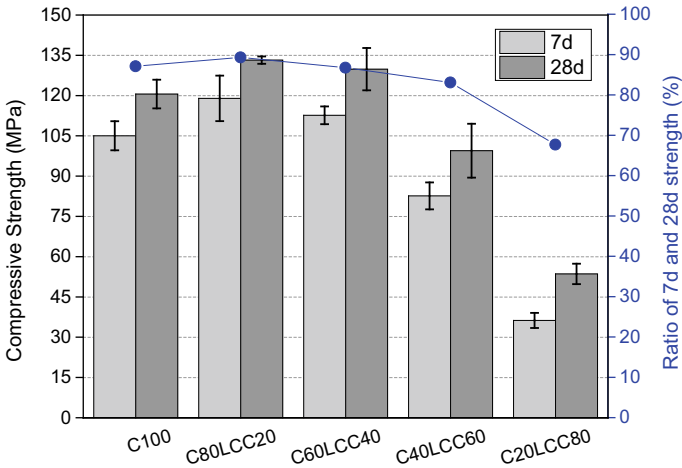
Fig. 3 Compressive strength of different HTS-SHCC mixes in Table 1

content is affected by both the generation rate of the cement hydration as well as the consumption rate by the pozzolanic reaction. Therefore, for C40LCC60 and C20LCC80, the insufficiency of Ca(OH)$_2$ due to the low cement content at early stage (e.g., 7 days in this study) results in a relatively low degree of pozzolanic reaction of LC2, while further pozzolanic reaction occurs with subsequent Ca(OH)$_2$ from further hydration of cement at later stage.

3.2 Uniaxial Tension Performance

The uniaxial tensile stress–strain curves for the five mixes in Table 1 are graphically shown in Fig. 4, and the major tensile characteristics are summarized in Table 4.

All the five mixes showed outstanding tensile strain-hardening behavior with the ultimate tensile strain no less than 5% (Table 4), which is sufficient for almost all construction applications. Compared to the control C100 (8.45 MPa), the tensile strength was improved by about 36%, 55%, 51% and 3% for LC2/binder ratios of 20%, 40%, 60% and 80%, respectively. The fiber/matrix interfacial frictional bond for different mixes is also summarized in Table 4. As discussed before, LC2 has a strong porosity refinement effect in cementitious materials [21, 22], which means LC2 can improve the fiber/matrix frictional bond and then the tensile strength of SHCC in this study. Specifically, though the compressive strength of C40LCC60 (99.5 MPa) is about 1/4 less than that of C60LCC40 (130.0 MPa), their tensile strengths are very close to each other.

Additionally, the ratios between the 28-day tensile strength and compressive strength are summarized in Table 4, which shows an interesting trend that the ratio
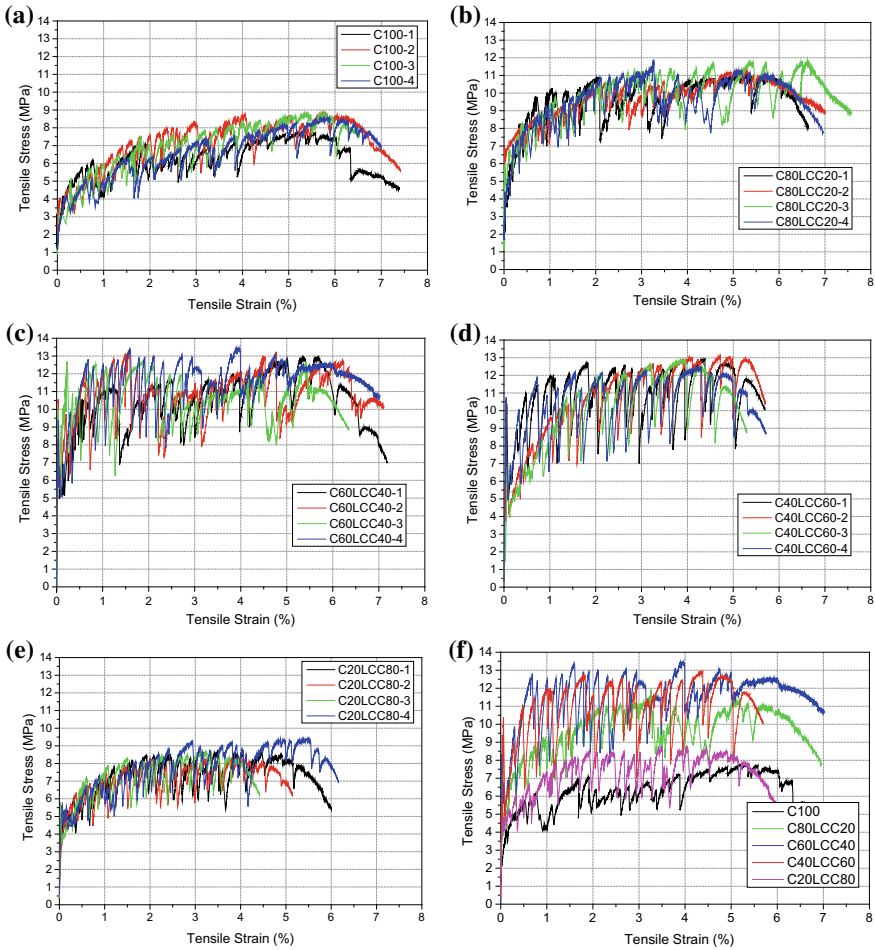
Fig. 4 28-day tensile stress–strain curves: **a** C100; **b** C80LCC20; **c** C60LCC40; **d** C40LCC60; **e** C20LCC80 and **f** summary of typical curves

Table 4 Summary of major tensile characteristics of different HTS-SHCC mixes in Table 1

Mix ID	Fiber/matrix frictional bond (MPa)	Tensile strength (MPa)	Ultimate tensile strain (%)	Tension strength/compressive strength (%)
C100	1.46	8.45 ± 0.49	6.29 ± 0.30	7.01
C80LCC20	1.67	11.47 ± 0.45	6.02 ± 0.46	8.61
C60LCC40	2.25	13.09 ± 0.39	6.34 ± 0.51	10.08
C40LCC60	2.18	12.78 ± 0.29	5.18 ± 0.26	12.85
C20LCC80	1.43	8.70 ± 0.44	5.00 ± 0.84	16.24
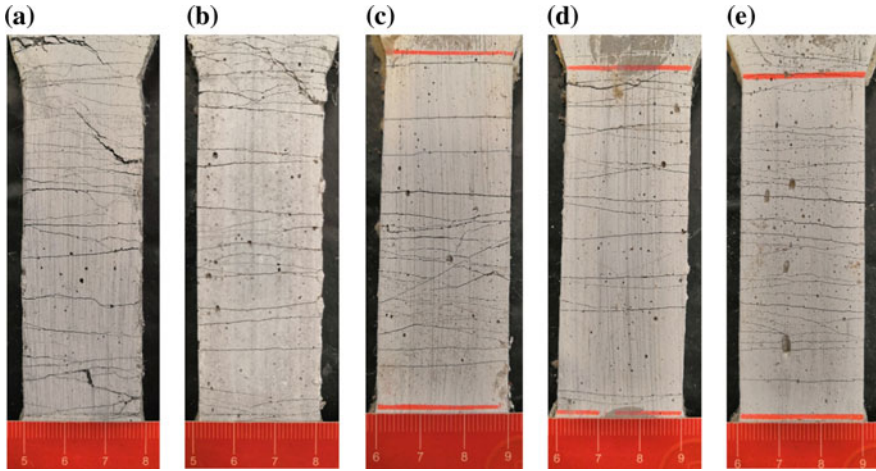
Fig. 5 Typical crack patterns after tension tests: **a** C100; **b** C80LCC20; **c** C60LCC40; **d** C40LCC60 and **e** C20LCC80

increases with increasing LC2 dosages, from 7% for C100 to 16% for C20LCC80. In other versions of PE fiber-reinforced SHCC without fiber surface treatments, high-tensile strength is generally achieved by improving the compressive strength of the materials to more than 100 MPa or even 150 MPa, by reducing the water/binder ratio to an extremely low value of about 0.15 and/or incorporating a remarkable dosage of fine particles (e.g., micro silica, nano silica). These approaches significantly increase the material cost as well as the environmental impact. The incorporation of LC2 offers a new, low cost and sustainable approach to achieve high-tensile strength in SHCC.

The typical residual crack patterns for the five mixes in Table 1 are graphically shown in Fig. 5. Further analysis on the crack width development with increasing tensile strain is in progress.

4 Conclusions

This paper explores the benefits of partially replacing the cement by limestone cal-cined clay (LC2) in high-tensile strength strain-hardening cementitious composites (HTS-SHCC), with the LC2/binder ratios of 0%, 20%, 40%, 60% and 80% by weight. According to the results in this study, the following conclusions can be drawn:

(1) All the five mixes showed outstanding tensile strain-hardening and multiple-cracking behaviors, with the ultimate tensile strain no less than 5%. Compared to the control mix without LC2 (8.45 MPa), the tensile strength was improved by about 36%, 55%, 51% and 3% for LC2/binder ratios of 20%, 40%, 60% and 80%, respectively. The strong porosity refinement effect of LC2 improves the fiber/matrix frictional bond and the resulting tensile strength of SHCC.

(2) High compressive strengths of 100–135 MPa were achieved in SHCC with LC2/binder ratios no more than 60 wt%. The mix with an ultra-high LC2/binder ratio of 80 wt% achieved 28-day compressive strength of about 55 MPa.

(3) Compared to other versions of PE fiber-reinforced SHCC where the high-tensile strength is generally achieved by reducing the water/binder ratio to an extremely low value and/or incorporating a remarkable dosage of fine particles, the incorporation of LC2 in the binder offers a new, low-cost and sustainable approach to achieve high-tensile strength in SHCC.

References

1. Li, V.C.: Engineered Cementitious Composites (ECC)—Bendable Concrete for Sustainable and Resilient Infrastructure. Springer, Berlin, Heidelberg, Germany (2019)
2. Li, V.C., Leung, C.K.Y.: Steady-state and multiple cracking of short random fiber composites. J. Eng. Mech. **118**(11), 2246–2264 (1992)
3. Li, V.C.: From micromechanics to structural engineering—the design of cementitous composites for civil engineering applications. J. Struct. Mech. Earthq. Eng. **10**(2), 37–48 (1993)
4. Leung, C.K.Y.: Design criteria for pseudoductile fiber-reinforced composites. J. Eng. Mech. **122**(1), 10–18 (1996)
5. Zhang, D., Yu, J., Wu, H., Jaworska, B., Ellis, B., Li, V.C.: Discontinuous micro-fibers as intrinsic ductile reinforcement for engineered cementitious composites (ECC). Compos. Part B Eng. **184**, 107741 (2020)
6. Rokugo, K., Kanda, T., Yokota, H., Sakata, N.: Applications and recommendations of high performance fiber reinforced cement composites with multiple fine cracking (HPFRCC) in Japan. Mater. Struct. **42**(9), 1197–1208 (2009)
7. Mechtcherine, V.: Novel cement-based composites for the strengthening and repair of concrete structures. Constr. Build. Mater. **41**, 365–373 (2013)
8. Li, V.C.: Bendable concrete. Innovation Constr. Hong Kong CIC Res. J. (Special Issue: CIC Inavation Award) 11–17 (2016)
9. Huang, B., Li, Q., Xu, S., Zhou, B.: Strengthening of reinforced concrete structure using sprayable fiber-reinforced cementitious composites with high ductility. Comp. Struct. **220**, 940–952 (2019)
10. Yang, E.-H., Yang, Y., Li, V.C.: Use of high volumes of fly ash to improve ECC mechanical properties and material greenness. ACI Mater. J. **104**(6), 620–628 (2007)
11. Zhou, J., Qian, S., Sierra Beltran, M.G., Ye, G., Breugel, K., Li, V.: Development of engineered cementitious composites with limestone powder and blast furnace slag. Mater. Struct. **43**(6), 803–814 (2010)
12. Zhang, Z., Qian, S., Ma. H.: Investigating mechanical properties and self-healing behavior of micro-cracked ECC with different volume of fly ash. Constr. Build. Mater. **52**, 17–23 (2014)
13. Ohno, M., Li, V.C.: A feasibility study of strain hardening fiber reinforced fly ash-based geopolymer composites. Constr. Build. Mater. **57**, 163–168 (2014)
14. Nematollahi, B., Sanjayan, J., Shaikh, F.U.A.: Matrix design of strain hardening fiber reinforced engineered geopolymer composite. Compos. B Eng. **89**, 253–265 (2016)

15. Yu, J., Li, H., Leung, C.K.Y., Lin, X., Lam, J.Y.K., Sham, I.M.L., Shih, K.: Matrix design for waterproof engineered cementitious composites (ECCs). Constr. Build. Mater. **139**, 438–446 (2017)
16. Yu, J., Leung, C.K.Y.: Strength improvement of strain-hardening cementitious composites with ultrahigh-volume fly ash. J. Mater. Civ. Eng. **29**(9), 05017003 (2017)
17. Yu, J.: Multi-scale Study on Strain-Hardening Cementitious Composites with Hybrid Fibers (PhD Thesis). Department of Civil and Environmental Engineering, Hong Kong University of Science and Technology, Hong Kong (2017)
18. Yu, J., Yao, J., Lin, X., Li, H., Lam, J.Y.K., Leung, C.K.Y., Sham, I.M.L., Shih, K.: Tensile performance of sustainable strain-hardening cementitious composites with hybrid PVA and recycled PET fibers. Cem. Concr. Res. **107**, 110–123 (2018)
19. Lin, X., Yu, J., Li, H., Lam, J.Y.K., Shih, K., Sham, I.M.L., Leung, C.K.Y.: Recycling polyethylene terephthalate wastes as short fibers in strain-hardening cementitious composites (SHCC). J. Hazard. Mater. **357**, 40–52 (2018)
20. Zhou, Y., Xi, B., Yu, K., Sui, L., Xing, F.: Mechanical properties of hybrid ultra-high performance engineered cementitous composites incorporating steel and polyethylene fibers. Materials **11**, 1448 (2018)
21. Scrivener, K., Martirena, F., Bishnoi, S., Maity, S.: Calcined clay limestone cements (LC3). Cem. Concr. Res. **114**, 49–56 (2018)
22. Scrivener, K.L., John, V.M., Gartner, E.M.: Eco-efficient cements: potential economically viable solutions for a low-CO_2 cement-based materials industry. Cem. Concr. Res. **114**, 2–26 (2018)
23. JSCE: Recommendations for design and construction of high performance fiber reinforced cement composites with multiple fine cracks (HPFRCC), Tokyo (2008)
24. Lin, Z., Li, V.C.: Crack bridging in fiber reinforced cementitious composites with slip-hardening interfaces. J. Mech. Phys. Solids **45**(5), 763–787 (1997)
25. Curosu, I., Liebscher, M., Mechtcherine, V., Bellmann, C., Michel, S.: Tensile behavior of high-strength strain-hardening cement-based composites (HS-SHCC) made with high-performance polyethylene, aramid and PBO fibers. Cem. Concr. Res. **98**, 71–81 (2017)
26. Mehta, P.K., Monteiro, P.J.M.: Concrete: Microstructure, Properties, and Materials, 4th edn. McGraw-Hill Education, New York (2013)
27. Yu, J., Li, G., Leung, C.K.Y.: Hydration and physical characteristics of ultrahigh-volume fly ash-cement systems with low water/binder ratio. Constr. Build. Mater. **161**, 509–518 (2018)

Basic Creep of LC^3 Paste: Links Between Properties and Microstructure

Julien Ston and Karen Scrivener

Abstract This study investigates the creep properties of limestone calcined clay cement. A series of paste samples using limestone and calcined clays as replacement materials were tested under basic compressive creep. The ternary mixes showed lower creep compliance than the plain cement references, even when using low reactivity clays or lower replacement fraction. A finite element model was used to back-calculate the visco-elastic properties of the C-S-H matrix and C-S-H gel. Whereas the elastic properties of C-S-H were found to be similar between LC^3 and plain cement, the viscous behaviour of C-S-H gel appeared to be noticeably different for LC^3.

Keywords Calcined clay · Creep · Modelling

1 Introduction

Traditional supplementary cementitious materials (SCM), such as blast furnace slag, fly ash or silica fume, present many advantages in cement technology, such as improved fresh and hardened properties or cost and energy reduction. However, they come in limited quantities that cannot meet the actual demand for clinker substituents. Recent studies showed the potential of calcined kaolinitic clays as a reliable source of pozzolanic metakaolin. In addition, such activated clays can replace up to 50% of the clinker in a binder when used together with limestone, while keeping mechanical properties comparable or superior to most blended cements [1]. Such binders are named limestone calcined clay cement, or LC^3.

LC^3 has proven to have mechanical properties close to that of plain cement, along with good durability against chlorides [2]. However, the volume stability of such mixes has not been extensively studied yet. This is the reason why this research investigates the visco-elasticity of these ternary blends. In particular, this work focuses on creep in sealed conditions. Creep without the exchange of water with the environment and at constant temperature is called basic creep. Creep is believed to be

J. Ston · K. Scrivener (✉)
Laboratory of Construction Materials, EPFL, Lausanne, Switzerland
e-mail: karen.scrivener@epfl.ch

a consequence of the viscous properties of the amorphous C-S-H present in cement microstructure.

There is a very important interest in studying this property when aiming at engineered structures. For instance, many important structures require low creep in order to remain safe with minimum maintenance during their lifetime, such as bridges, skyscrapers or containment buildings. Creep is an intrinsic characteristic of the materials; moreover, mitigation of this phenomenon is difficult or expensive, and it occurs anyway on top of other phenomena, such as drying. Therefore, investigating the proper behaviour of LC^3 is a necessary step for widespread application.

This research project investigates the basic compressive creep behaviour of mature cement paste of LC^3 binders. The main variable is the calcined kaolinite content of the clays used to prepare the blends. A finite elements model is also used to back-calculate the viscous properties of the C-S-H gel via a self-consistent homogenization scheme.

1.1   The Effect of SCM on Creep

There have been a few investigations on the impact of metakaolin and limestone on creep, but they yielded only some specific results. In a binary mix, metakaolin is a very efficient, yet expensive pozzolan. Its influence on creep of cementitious binders has only been slightly investigated. The work from Brooks and Johari [3] offers a good review of the knowledge concerning metakaolin substitution in concrete.

In summary, a modest replacement of clinker with metakaolin (5–10%) increases compressive strength at the expense of workability, if mix design remains unchanged. Concerning delayed strains, the use of metakaolin was found to reduce both autogenous and drying shrinkage of concrete and lower compressive creep compliance. This study did not give any precise mechanism leading to the change in visco-elastic behaviour, but proposed a list of potential reasons, such as a refinement of the pore structure [4] or better interface between cement and aggregates, both thanks to the extra hydrates from the pozzolanic reaction and the filler effect of metakaolin.

From a chemical point of view, metakaolin is an important source of aluminium ions. This supplementary aluminium will enrich C-S-H into C-A-S-H, while consuming portlandite. Aluminium-rich strätlingite(C_2ASH_8 in cement shorthand) will also precipitate if metakaolin is the only replacement material.

Many studies reported a decrease in creep compliance when using metakaolin [3], or other SCMs, such as slag, fly ashes or glass powder [5, 6]. SCM in general will affect the chemical composition of C-S-H [7], but none of the cited works reported a direct link between C-S-H composition and creep compliance, as the incorporation of SCM has other very important effects on the microstructure that can affect creep.

According to a study carried out on mixtures of white cement and metakaolin [8], incorporation of metakaolin in the mix increases both the average alumino-silicate chain length and the Al/Si of C-S-H. Unfortunately, they did not compare mechanical properties against the evolution of C-S-H morphology and composition.

Limestone is mostly considered on its own as an inexpensive filler. It provides extra surface for hydrate nucleation and even shows some reactivity with the aluminium present in the cement [7, 9, 10], Little knowledge is available on the effect of limestone filler on the creep properties of concrete or cement. Wang et al. [11] reported a decrease of the compressive creep compliance in drying conditions when replacing cement with limestone in concrete. Unfortunately, they did not examine the microstructure of the different samples, nor did run any basic creep tests. Belov and Kuliaev [12] attributed the decrease in creep compliance to a denser microstructure in their short communication about concrete using limestone powder replacement.

Finally, He et al. [6] reported a lower basic creep compliance in concrete using metakaolin and limestone as replacement materials (a mix design equivalent to LC^3-70 1:2 (95%) in the present study, containing 70% clinker, 10% metakaolin and 20% limestone. See next section for more details).

2 Experimental Method

2.1 Materials and Mix Designs

This study focuses on a two LC^3 mix designs, using calcined clays of various origin and chemical purity. The grade of a kaolinitic clay is defined by its content in kaolinite, which will turn into metakaolin after full calcination. The mix designs were either LC^3-50 or LC^3-65, meaning 50% or 65% by mass of clinker (ignoring gypsum from cement). The replaced fraction consisted of 60% calcined clay, 30% limestone and 10% gypsum (including gypsum from cement and extra addition) for the 2:1 variant, or 46% calcined clay, 46% limestone and 8% gypsum for the 1:1 variant. As an example, the LC^3-50 2:1 (45%) mix contains in total 50% clinker, 30% calcined clay (itself containing 45% of calcined kaolinite), 15% limestone and 5% gypsum. All mixes were prepared at a water to binder ratio of 0.4 and are summarized on Table 1.

2.2 Sample Preparation and Creep Frames

After weighing, powders and water were mixed in a vacuum mixer for 2 min at 450 rpm. Paste was then cast into eight $25 \times 25 \times 80$ mm moulds. The samples were cured for 24 h in a moist environment. Right after demoulding, the paste prisms were wrapped in a polyethylene film and two layers of adhesive aluminium sheet, to ensure autogenous conditions. The top and bottom square faces were covered only with a single layer of aluminium, in order to have as little material as possible between the sample and the loading plates.

The samples were then left to cure at 20 °C, until they reached their loading age, 28 days in this study. Sealed prisms were weighed right after wrapping, at the end of

Table 1 Summary of the mix designs. All mixes cast at a W/B of 0.4

Sample	Clinker (%)	Calcined clay (%)	Limestone (%)	Gypsum (%)	Metakaolin content in clay (%)
PC	97	–	–	3	–
LC3 (15%)	50	30	15	5	15
LC3 (25%)	50	30	15	5	25
LC3 (45%)	50	30	15	5	45
LC3 1:1 (45%)	50	30	15	5	45
LC3 (50%)	50	30	15	5	50
LC3 (60%)	50	30	15	5	60
LC3 (95%)	50	30	15	5	95
LC3-65 2:1 (45%)	70	19	10	<2	45
LC3-65 1:1 (45%)	70	14	14	<2	45

the cure and after the creep test. The weight loss was always very low, between 0 and 0.2%. Between 6 and 24 h before the beginning of creep loading, two prisms were unwrapped and each cut down to three cubes of 25 mm and tested for compressive strength. The creep test load was then adjusted so that the stress on the sample corresponded to 10–15% of its strength at loading age, with a maximum of 50 kg (without considering the 10-fold amplification from the lever arm). The environment was kept at 20 °C and 70% RH in the testing rooms. The compressive creep tests lasted for 28 days. This duration is sufficient to reach a logarithmic regime on paste samples [13, 14].

2.3 Autogenous Shrinkage Measurement

Autogenous shrinkage measurements were carried out according to ASTM C1698-09 [15], using a silicon oil bath for controlling temperature and submersible linear variable differential transformers (LVDT) for continuous monitoring. A volume of about 700 mL was then prepared using a vacuum mixer at a mixing speed of 450 rpm for 2 min. The mix was then carefully poured into a tube held in a vertical position with a steel tube or a specifically designed plastic holder. The operation is carried out on a vibrating table to ensure proper flow of the paste. The tube is then sealed with a pristine plug, weighted and placed on the bench in the silicone oil bath. One end of the tube is fixed to the bench, and submersible LVDT is placed at the free end. Automatic logging is achieved thanks to an autonomous logger. Most measurements

started between 30 and 60 min after mixing. All mixes were replicated twice or thrice and showed little deviation within a given mix.

2.4   Creep Modelling

A two-dimensional finite element (FE) model using the framework XFEM-AMIE was adopted for this study. It consists of a 100 by 100 μm 2D mesh describing a square section of composite material undergoing uniaxial load. Round inclusions representing crystalline anhydrous or hydrated phases are embedded in a visco-elastic matrix of C-S-H. The inclusions only possess elastic properties and are defined by their Young's modulus, Poisson's ratio, abundance and particle size distribution. Phases were regrouped by similar mechanical properties, summing their amount. In total, five elastic phases were used to represent the different families of minerals present in cement or LC3 mixes. Their mechanical properties are summarized in Table 2. The inclusions were randomly spread in the domain (without overlap) and their diameters varied from 15 nm to 2 μm, according to a normal distribution. All the phase amounts come from a volume balance calculation, from XRD-Rietveld and SEM-EDS data. The amount of matrix corresponds to the space not occupied by the crystalline inclusions, that is to say C-S-H gel, capillary water and air voids from chemical shrinkage, all obtained from the mass (or volume) balance calculation.

The first run of the simulation only considers elasticity and is used to adjust the Young's modulus of the C-S-H matrix so that the model output is similar to the measured Young's modulus of the material. The second run models the visco-elasticity of the matrix, calculating the strain over 28 days. The visco-elastic behaviour of the matrix is modelled with a Kelvin-Voigt chain composed of six elements, fitted to the macroscopic behaviour of the material. A coefficient of proportionality is then applied to the stiffness of the springs to minimize the difference between the output of the FE model and the experimental data. Plasticity and cracking are not considered in this model.

After adjusting the visco-elastic properties of the matrix, an analytical, poromechanical approach was used to calculate the expected properties of the C-S-H gel, considered as the solid part of the porous visco-elastic matrix. The relation between

Table 2 Mechanical properties of the elastic phases used in the finite element model

Phases	Young's modulus (GPa)	Poisson's ratio
C3S, C2S, C3A, C4AF	130	0.3
CH, monocarboaluminate	38	0.305
Ettringite, metakaolin, other clayey phases	22.4	0.255
Monosulfoaluminate, hemicarboaluminate, hydrotalcite, hydrogarnet	42.3	0.324
Quartz, limestone	80	0.25

porosity, properties of the porous material and properties of the bulk material comes from the work of Roberts and Garboczi [16]. The two-cut Gaussian random field was used here to interpret the results, as it approaches best the geometry of cement pores—especially compared to simpler models such as growing spheres of solid. This approach is solely used to back-calculate the strain of the C-S-H gel. Thermodynamic effects are not explicitly modelled, although their contribution is contained in the experimental data and is also implicitly included in the Kelvin-Voigt chain.

3 Results

3.1 Experimental Data

This section presents the experimental results of basic creep compliance over loading time for the samples being studied. Creep compliance is defined as the creep strain divided by the applied stress. Creep strain is obtained by subtracting the autogenous shrinkage to the total creep strain measured from the creep set-up.

Figure 1 shows the evolution of compressive creep compliance for mature LC3-50 2:1 samples, using various calcined clays as replacement material. All the ternary blends exhibit a lower compliance than the plain cement reference. One of the most striking features is the apparent independence of the grade of the clay on the resulting compliance of the mix. For a clay grade from 45–95%, the effect on compliance is quite similar. This could indicate that a threshold value exists for the initial metakaolin content to have a significant effect on the creep compliance. These results indicate
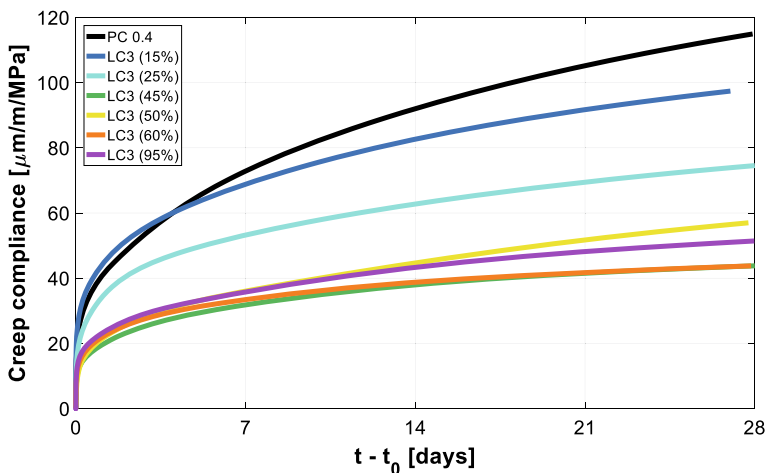
Fig. 1 Creep compliance over loading time for paste samples with varying clay grade
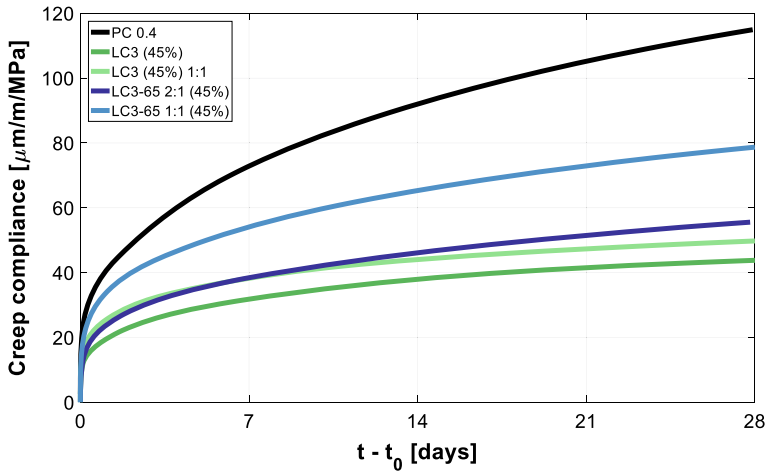
Fig. 2 Creep compliance over loading time for paste samples with varying mix design

that even clay with only 25% of calcined kaolinite causes a reduction in basic creep compliance of mature paste.

Figure 2 presents the results for the LC3-50 and LC3-65 series with the same calcined clay but different calcined clay to limestone ratios. For the LC3-50, the change in calcined clay to limestone ratio did not affect compliance significantly. This is in line with the previous observations, as changing this ratio is equivalent to using a lower grade clay. The metakaolin content of this mixture is still sufficient to affect compliance. This is not the case in LC3-65, where further blending of the clay limits the compliance reduction, but still being lower than the plain cement.

3.2 Modelling Results

Results from the finite element model reached a good agreement with the experimental data for all simulated systems. A summary of the Young moduli of C-S-H matrix and gel obtained after the poromechanical interpretation of the modelling outputs is presented in Table 3. A noticeable result from the elasticity modelling is the narrow range of stiffness found for the C-S-H gel. The Young's modulus of C-S-H gel back-calculated using the analytical approach is estimated to be in the range of 20–25 GPa for most mixes. This corresponds to the published values for the Young's modulus of C-S-H, ranging from about 20 GPa for the so-called low density C-S-H to 30 GPa for "high density C-S-H" [17–19]. In spite of the fact that the stiffness of the C-S-H matrix can double between the softest and the hardest one, the varying solid fraction of this porous matrix and the adopted model suggest that the solid forming said matrix has similar mechanical properties in all situations.

Table 3 Young's modulus of C-S-H back-calculated from the FE model (matrix) and the poromechanical approach (gel)

Sample	C-S-H matrix (GPa)	C-S-H gel (GPa)
PC	11.6	23.0
LC3 (15%)	6.9	26.7
LC3 (25%)	8.9	26.6
LC3 (45%)	10.3	23.9
LC3 1:1 (45%)	9.1	21.9
LC3 (50%)	8.3	21.1
LC3 (60%)	8.8	21.4
LC3 (95%)	8.9	23.5
LC3-65 2:1 (45%)	9.6	20.2
LC3-65 1:1 (45%)	9.5	22.5

Modelling of the visco-elastic behaviour of C-S-H gel is carried out using the same analytical tools as for elasticity. It was supposed that the visco-elastic response was affected in the same way as the elastic one. Compliance of the different simulated microstructures is shown in Fig. 3.

A remarkable result from these simulations is the prediction of a different C-S-H compliance between plain cement samples and LC3, combined with a very consistent prediction within the plain cement or the LC3 groups of samples. Notably, the samples of LC3-50 15 and 25%—previously showing higher creep strains at the macroscopic level than the other LC3-50 mixes—can be modelled using a C-S-H gel with similar visco-elastic properties as the other LC3. It appears that the changes in abundance and porosity of the matrix are enough to explain most of the visco-elastic variations among samples. The model also indicates that the C-S-H gel present in plain cement could be less viscous than that of LC3. As the simulation is not carried out at the nanometric scale, the difference in viscous behaviour cannot be attributed to specific mechanisms without further investigation.
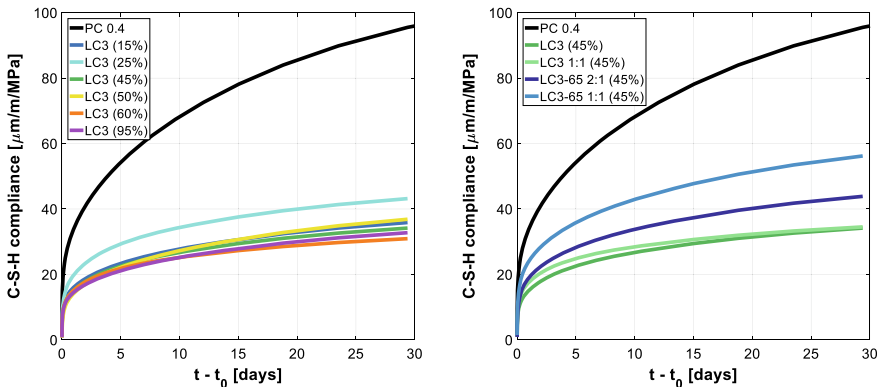
Fig. 3 C-S-H gel compliance calculated from the poromechanical approach

4   Conclusions

This study explored the compressive creep behaviour of mature, sealed cured LC3 and plain cement paste samples. A first qualitative assessment of the data indicated a lower compliance for the ternary blends. The extent of this reduction is not dependent on the calcined kaolinite content of the clay if it is above about 40%, and a noticeable compliance reduction in mature samples was observed with a clay containing only 25% of metakaolin. This is a clue indicating that all the clayey phases, including inert phases or unreacted metakaolin, and the carboaluminates typical of LC3 can be considered as elastic phases, as their proportions varied but the viscous response was similar among the samples. Specifically, their volume amount can double between the lowest or highest grade clays and the middle grade clays, which give rise to the highest amount of carboaluminates in the microstructure [20].

To push the investigation deeper, a 2D finite elements model was used to simulate creep via a two-scale model. The larger scale considered the C-S-H matrix containing solid inclusions of anhydrous and hydrated phases as a continuous medium. The visco-elastic properties of the matrix were adjusted so that the simulation results fell close to the experimental data. The second scale used an analytical, poromechanical approach to take the porosity of the matrix into account and estimate the mechanical properties of the C-S-H gel alone.

The output of the simulations pointed towards a less compliant C-S-H in the LC3, with a similar viscous behaviour among all the samples containing limestone and calcined clay, regardless of the clay grade. The model also indicated that the differences observed at the macroscopical level could be explained by a different amount of C-S-H in the structure and a different amount of porosity.

As the model considers C-S-H gel as a whole, modelling its visco-elasticity through a generic rheological model, it cannot explain the exact mechanisms at the origin of the decrease of compliance. However, from our current knowledge of the specific LC3 microstructure, some hypothesis regarding the causes of this change in compliance can be proposed or ruled out:

- The proportion of outer to inner C-S-H product seems higher in LC3 than PC [21], indicating that the C-S-H gel is likely to be more intermixed with dispersed filler particles and hydrates present in LC3. Specifically, thin clay platelets could physically limit the viscous flow of the material. This effect was observed in polymers reinforced with graphene [22], although creep mechanisms are different. The mere filler effect of limestone and clay could also provide more interfacial surface between the variety of hydrates formed in LC3 and a finer phase mixing. In their recent study, Wyrzykowski et al. [23] observed a very different creep behaviour between their real and equivalent systems. One of the microstructural disparities between these mixes is the proportion of outer and inner product.
- The addition of limestone and calcined clay will affect the chemical composition of C-S-H. In particular, the more metakaolin present in the clay , the more C-S-H

will incorporate aluminium. However, the similar compliance found for C-S-H gel formed in LC3 does not point towards a strong influence of the chemistry on creep properties.

References

1. Scrivener, K., Martirena, F., Bishnoi, S., Maity, S.: Calcined clay limestone cements (LC3). Cem. Concr. Res. **114**, 49–56 (2018)
2. Scrivener, K.L., John, V.M., Gartner, E.M.: Eco-efficient cements: Potential economically viable solutions for a low-CO2 cement-based materials industry. Cem. Concr. Res. **114**, 2–26 (2018)
3. Brooks, J.J., Megat Johari, M.A.: Effect of metakaolin on creep and shrinkage of concrete. Cem. Concr. Compos. **23**(6), 495–502 (2001)
4. Neville, A.M.: Creep of concrete as a function of its cement paste content. Mag. Concr. Res. **16**(46), 21–30 (1964)
5. Li, J., Yao, Y.: A study on creep and drying shrinkage of high performance concrete. Cem. Concr. Res. **31**(8), 1203–1206 (2001)
6. He, Z., Zhan, P., Du, S., Liu, B., Yuan, W.: Creep behavior of concrete containing glass powder. Compos. Part B Eng. **166**, 13–20 (2019)
7. Lothenbach, B., Le Saout, G., Gallucci, E., Scrivener, K.: Influence of limestone on the hydration of portland cements. Cem. Concr. Res. **38**(6), 848–860 (2008)
8. Dai, Z., Tran, T.T., Skibsted, J.: Aluminum incorporation in the c-s-h phase of white portland cement-metakaolin blends studied by 27Al and 29Si MAS NMR Spectroscopy. J. Am. Ceram. Soc. **97**(8), 2662–2671 (2014)
9. Péra, J., Husson, S., Guilhot, B.: Influence of finely ground limestone on cement hydration. Cem. Concr. Compos. **21**(2), 99–105 (1999)
10. Matschei, T., Lothenbach, B., Glasser, F.P.: The role of calcium carbonate in cement hydration. Cem. Concr. Res. **37**(4), 551–558 (2007)
11. Wang, Y.H., Xu, Y.D., He, Z.H.: Effect of limestone powder on creep of high-strength concrete. Mater. Res. Innov. **19**(9), S9-220-S9-223 (2015)
12. Belov, V., Kuliaev, P.: Limestone filler as one of the cheapest and best additive to concrete. IOP Conf. Ser. Mater. Sci. Eng. **365** (2018)
13. Delsaute, B., Torrenti, J.-M., Staquet, S.: Modeling basic creep of concrete since setting time. Cem. Concr. Compos. **83**, 239–250 (2017)
14. Irfan-ul-Hassan, M., Pichler, B., Reihsner, R., Hellmich, C.H.: Elastic and creep properties of young cement paste, as determined from hourly repeated minute-long quasi-static tests, Cem. Concr. Res. **82**, 36–49 (2016)
15. ASTM C1698-09, Standard test method for autogenous strain of cement paste and mortar, as of 2014
16. Roberts A.P., Garboczi, E.J.: Computation of the linear elastic properties of random porous materials with a wide variety of microstructure. In: Proceeding of the Mathematical, Physical and Engineering Sciences, vol. 458, no. 202 (2002)
17. Vandamme, M., Ulm, F.-J.: Nanoindentation investigation of creep properties of calcium silicate hydrates. Cem. Concr. Res. **52**, 38–52 (2013)
18. Moon, J., Yoon, S., Wentzcovitch, R.M., Monteiro, P.J.M.: First-principles elasticity of monocarboaluminate hydrates. Am. Mineral. **99**(7), 1360–1368 (2014)
19. Hlobil, M., Šmilauer, V., Chanvillard, G.: Multiscale micromechanical damage model for compressive strength based on cement paste microstructure. In: CONCREEP, vol. 10, pp. 1211–1218 (2015)

20. Avet, F.H.: Investigation of the grade of calcined clays used as clinker substitute in limestone calcined clay cement (LC3) (2017)
21. Avet, F., Boehm-Courjault, E., Scrivener, K.: Investigation of C-A-S-H composition, morphology and density in limestone calcined clay cement (LC3). Cem. Concr. Res. **115**, 70–79 (2019)
22. Bhattacharyya, A.: Graphene reinforced ultra high molecular weight polyethylene with improved tensile strength and creep resistance properties. Express Polym. Lett. **8**(2), 74–84 (2013)
23. Wyrzykowski, M., Scrivener, K., Lura, P.: Basic creep of cement paste at early age—the role of cement hydration. Cem. Concr. Res. **116**, 191–201 (2019)

Study on Fresh and Harden Properties of Limestone Calcined Clay Cement (LC^3) Production by Marble Stone Powder

S. M. Gunjal and **B. Kondraivendhan**

Abstract In this paper, the utilization of waste marble powder for the production of limestone calcined clay cement is investigated. Limestone calcined clay cement is an advanced ternary blended cement made by using the combination of low grade calcined clay, limestone and gypsum. It can be replaced by 50% of clinker which is beneficial for the reduction of carbon dioxide (CO_2) emission at the time of production of cement. In the existing paper, the physical and chemical characteristics, chemical analyses carried out by X-ray fluorescence, lime reactivity test for pozzolanic behaviours, mechanical properties of LC^3 using marble powder, i.e. compressive strength and spilt tensile strength are checked and compared to the Portland pozzolana cement (PPC) and ordinary Portland cement (OPC).

Keywords Marble powder · Calcined clays · Limestone · Blended cement · Compressive strength

1 Introduction

Day by day the demand of concrete is increasing due to industrialization, globalization and infrastructure development. Developing countries require a large quantity of concrete. Concrete is the heterogeneous mixture of cement, coarse aggregate, fine aggregate and water. For the production of 1 ton of cement, it emits nearly 1 ton of carbon dioxide (CO_2) into the atmosphere [1]. As compared to the world, India is the second-highest cement producer, in which near about 280 million tons of cement is produced in India [2]. Annually from cement production nearly about 1.35 billion tons of greenhouse gas releases, which is represented in the 2013 World Business Council for Sustainable Development Energy Agency (WBCSDEA) [3]. So for minimizing the demand of ordinary Portland cement, a new ternary blended cement is produced [4] called limestone calcined clay cement (LC^3). It contains 50% ordinary

S. M. Gunjal (✉) · B. Kondraivendhan
Applied Mechanics Department, S.V. National Institute of Technology, Surat 395007, India

S. M. Gunjal
Department of Civil Engineering, Sanjivani College of Engineering, Savitribai Phule Pune University, Kopargaon, Maharashtra 423603, India

Portland cement (OPC), 30% calcined clay, 15% limestone powder and 5% gypsum. Similarly, marble stone calcined clay cement (MC^3) is produced and checked the physical and chemical properties of these cement.

Cement substitution by a combination of metakaolin and limestone [5] in this research is 30% of metakaolin and 15% of limestone in Portland cement give better result as compare to other mixture. Higher kaolin clay content gives good strength than ordinary Portland cement (OPC) in concrete mortars. Similarly, the compressive strength of higher kaolin clay nearly equal to ordinary Portland cement and lower kaolin content nearly equal to Portland pozzolana cement (PPC) [6]. Production of limestone calcined clay cement (LC^3) is economical as compare to Portland pozzolana cement where the source of fly ash is located at a farther distance than clay also the quantity of fly ash is low and cost of fly ash is high [7]. The higher fineness of both clinker and calcined clay can considerably improve compressive strength at all ages, while limestone fineness only plays a role at an early age [8].

Concretes produced with limestone calcined clay cement shows equivalent strength development characteristics with Portland pozzolana cement and enhances strength development than 70% ordinary Portland cement + 30% fly ash called FA30 in all the concrete mixes [9]. When ordinary Portland cement is replaced by 2.5, 5.0, 7.5 and 10% with waste marble dust tensile and compressive strength decrease because of marble dust act as only filler material [10]. But workability increases when marble powder used in concrete [11].

In India, the annual production of marble is nearly 17 million tonnes [12] and formed by the metamorphic rocks. Millions of tonnes of waste dust are generated during the process of stones which hazards for health, environmental problem and productivity of the land. The aim of this study was to investigate whether marble waste powder utilizes as a replacement for limestone to produce marble stone calcined clay cement.

2 Materials and Methods

A 43 grade of ordinary Portland cement (OPC) conforming to BIS 8112-2013 [13] was used for this study. Chemical composition of the material used for the preparation of limestone calcined clay and marble stone calcined clay cement using X-ray fluorescence was shown in Table 1. The material used for the preparation of cement is calcined clay over that lime reactivity test is carried out as per IS 1727-1967 and shows that it is 9.11 MPa which is good in agreement. The X-ray diffraction (XRD) of materials limestone powder, marble powder and calcined clay shown in Figs. 1, 2 and 3, respectively.

The details of blends used such as limestone calcined clay cement (LC^3) in that OPC-50%, calcined clay-30%, lime powder-15%, gypsum-5% for marble stone calcined clay cement (MC^3) in that OPC-50%, calcined clay-30%, marble powder-15%, gypsum-5% is used for preparation of cement shown in Table 2.

Table 1 Chemical composition of raw materials

Oxide (%)	OPC	Calcined clay	Marble powder	Limestone powder
SiO_2	22.07	53.75	5.366	5.073
Al_2O_3	3.6	44.32	0.8546	0.6834
K_2O	0.7	0.0455	0.0012	0.0012
CaO	63.25	0.4838	33.17	32.45
TiO_2	0.007	1.707	0.0184	0.0179
Na_2O	0.3	0.447	0.014	0.014
MgO	1.08	0.19	20.06	19.39
P_2O_5	0.008	0.0784	0.00069	0.00069
MnO	–	0.0049	0.02587	0.0263
Fe_2O_3	4.69	0.4156	0.2043	0.1946
LOI	1.14	0.3	40.66	39.45

Fig. 1 XRD Pattern for limestone powder
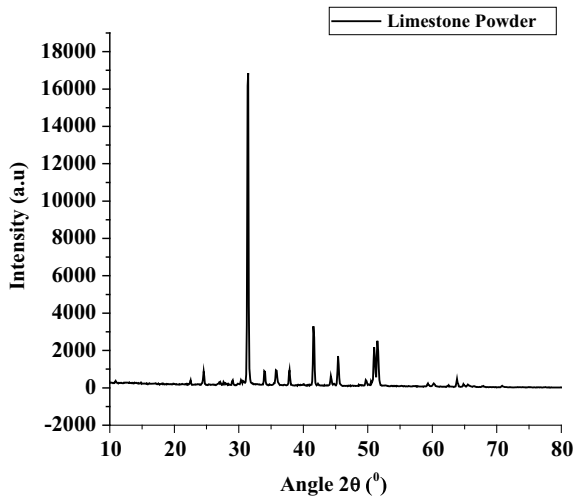
2.1 Test on Cement

Laboratory prepared cement such as limestone calcined clay, marble stone calcined clay cement and ordinary Portland cement over that standard consistency in percentage, initial setting time (min), final setting time (min) and soundness (mm) test is carried out as per IS 4031-1988 [14] shown in Table 3. Similarly, the compressive strength of cement for 3 days, 7 days, 28 days and 56 days carried out on compressive testing machine shown in Table 4 and prepared mortar cube of OPC, LC^3 and MC^3 as shown in Fig. 4.
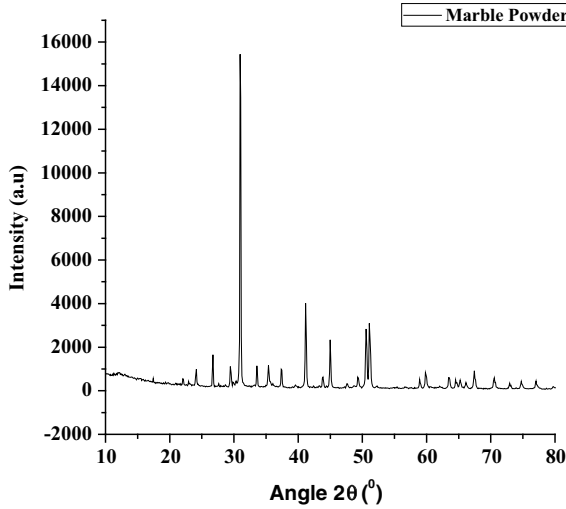
Fig. 2 XRD pattern for marble powder
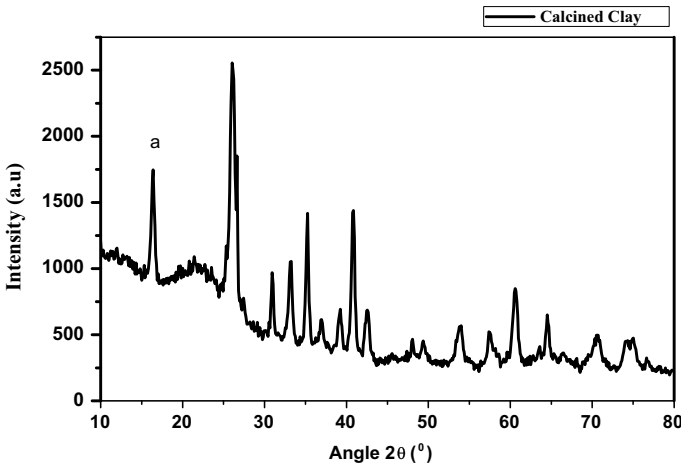
Fig. 3 XRD pattern for calcined clay

2.2   Test on Concrete

M25 grade of concrete is prepared using IS 10262-2009 [15] such that water to cement ratio is taken as 0.5, cement content 380 kg/m^3, the fine aggregate confirming zone-I which has fineness modulus 3.11 and ratio of coarse aggregate such as 12.5 mm:20 mm taken as 0.3:0.7, respectively. The mix proportion and workability by slump shown in Table 5. Compressive strength of different mix at 3 days, 7 days,

Fig. 4 Mortar cube of OPC, LC^3 and MC^3

Fig. 5 Concrete cube and cylinder of OPC, LC^3 and MC^3

28 days and 56 days and spilt tensile strength at 28 days has shown in Tables 6 and 7, respectively. Prepared cube of different blend mix for M25 grade of concrete as shown in Fig. 5. Similarly compressive and spilt tensile strength for M25 grade of concrete as shown in Figs. 6 and 7.

3   Result and Discussions

The physical characteristics such as standard consistency of limestone calcined clay cement and marble stone calcined clay cement are more than ordinary Portland cement because of calcined clay is present in this cement [16], and similarly initial setting time, final setting time and soundness satisfies the requirements given by Indian standard. The compressive strength of limestone calcined clay cement and
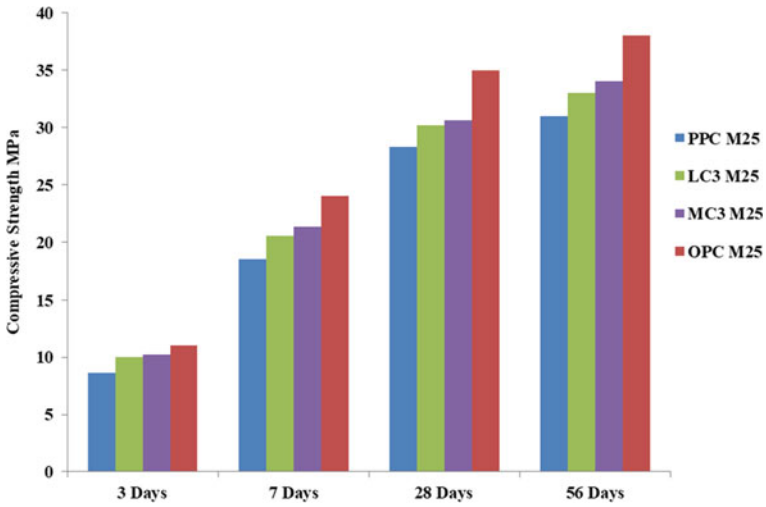
Fig. 6 Compressive strength of M25 grade of concrete
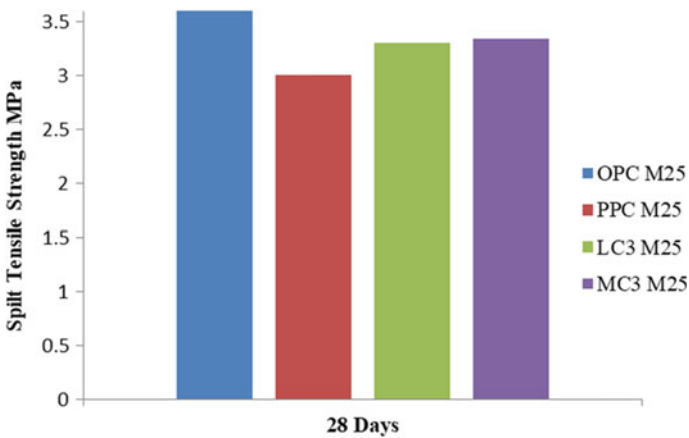
Fig. 7 Spilt tensile strength of M25 grade of concrete

Table 2 Details of blends used in this study

Blend name	OPC (%)	PPC	Calcined clay (%)	Limestone powder	Marble waste powder	Gypsum
LC^3	50	–	30	15%	–	5%
MC^3	50	–	30	–	15%	5%
OPC	100	–	–	–	–	–
PPC	–	100%	–	–	–	–

Table 3 Physical properties of limestone calcined clay cement; marble stone calcined clay, ordinary Portland cement

Description	LC^3	MC^3	OPC
Standard consistency (%)	33	33.67	29.5
Initial setting time (min)	90	96	100
Final setting time (min)	240	255	270
Soundness (mm)	2	2.1	2
Specific gravity (g/cc)	2.85	2.95	3.15

Table 4 Mortar compressive strength of OPC, PPC, LC^3 and MC^3 blends

S. No.	Mix	Compressive strength (N/mm^2)			
		3 days	7 days	28 days	56 days
1	OPC	15	34	49	50.5
2	PPC	10	25	35.5	38
3	LC^3	12	28	36	40
4	MC^3	13	29.6	39	42

Table 5 Mix design of M25 grade of concrete

S. No.	Concrete grade	W/C	Cement (kg/m^3)	Fine aggregate (kg/m^3)	Coarse aggregate (kg/m^3)		Slump (mm)
					12.5 mm	20 mm	
1	M25	0.5	380	738.72	334.85	781.36	90

Table 6 Compressive strength of different mix of concrete

S. No.	Mix	W/C	Compressive strength (N/mm^2)			
			3 days	7 days	28 days	56 days
1	OPC-M25	0.5	11	24	35	38
2	PPC-M25	0.5	8.6	18.5	28.3	31
3	LC^3-M25	0.5	10	20.5	30.2	33
4	MC^3-M25	0.5	10.2	21.3	30.6	34

Table 7 Spilt tensile strength of different mix concrete

S. No.	Mix	W/C	Spilt tensile strength for 28 days (N/mm^2)
1	OPC-M25	0.5	3.6
2	PPC-M25	0.5	3.1
3	LC^3-M25	0.5	3.3
4	MC^3-M25	0.5	3.34

marble stone calcined clay cement satisfies the Indian standard for Portland pozzolana cement. The compressive strength of ordinary Portland cement is more than LC^3 and MC^3 because of the amount of clinker in OPC (100%) greater than LC^3 and MC^3. The reactivity of the calcined clay is dependent on the kaolinite content present in the clay. Clays containing about 40% kaolin or above give strengths comparable to plain Portland cement when used in LC^3-50 (50% clinker, 30% calcined clay, 15% limestone and 5% gypsum) [17]. With more substitution, it is possible to obtain good mechanical performance, at early ages, at higher levels of substitution than other pozzolana. Because the clay is finely divided, it can react faster and to a higher degree than fly ash. Similar, levels of substitution are possible with slag, which is a hydraulic material rather than a pozzolana.

When calcined clay $AS_2 + 3CH + 6H \rightarrow C\text{-}A\text{-}S\text{-}H + C_2ASH_8$ is added in clinker calcium aluminium silicate hydrate, (C-A-S-H) are formed and further addition of limestone formation of carboaluminates which is an enhancement of carboaluminate $A_{(\text{from calcined clay})} + Cc + 3CH + H \rightarrow C_3ACcH_{11}$ [4] formation and contribute to the strength. The addition of calcined clay and marble stone which content carbonate source form carboaluminates enhanced ettringite contribute towards the strength.

The M25 concrete prepared by limestone calcined clay cement and marble stone calcined clay cement compressive and spilt tensile strength is less than ordinary Portland cement but more than Portland pozzolana cement satisfies by the Indian standard for Portland pozzolana cement.

4   Conclusion

Based on experimental studies conducted on physical and mechanical properties study on limestone calcined clay cement and marble stone calcined clay cement the following conclusion can be drawn.

1. Cement prepared by limestone calcined clay cement and marble stone calcined clay cement has comparable physical properties of the ordinary Portland cement.
2. The presence of carbonate stone dust studied leads to the stabilization of ettringite and the formation of carboaluminates.
3. Mortar compressive strength prepared by LC^3 and MC^3 is more than Portland pozzolana cement at all curing ages investigated in this study.
4. Compressive strength of M25 grade prepared by OPC is more than limestone calcined clay cement; marble stone calcined clay cement and Portland pozzolana cement. The similar mixture prepared by LC^3 and MC^3 has more compressive strength than Portland pozzolana cement at all days.

References

1. Gartner, E.: Industrially interesting approaches to 'low-CO_2' cements. Cem. Concr. Res. **34**, 1489–1498 (2004). https://doi.org/10.1016/j.cemconres.2004.01.021
2. Planning Commission: Low Carbon Strategies for Inclusive Growth. Government of India (2011)
3. Initiative, WBCSD Cement Sustainability Getting the Numbers Right, Project Emissions 2014, Report (2016)
4. Scrivener, K.L.: Options for the future of cement. Indian Concr. J. **88**, 11–21. https://www.lc3.ch/wp-content/uploads/2014/09/0851_ICJ_Article.pdf (2014)
5. Antoni, M., Rossen, J., Martirena, F., Scrivener, K.: Cement substitution by a combination of metakaolin and limestone. Cem. Concr. Res. **42**, 1579–1589 (2012). https://doi.org/10.1016/j.cemconres.2012.09.006
6. Bishnoi, S., Maity, S., Mallik, A., Joseph, S., Krishnan, S.: Pilot scale manufacture of limestone calcined clay cement: the Indian experience. Indian Concr. J. **88**, 22–28 (2014)
7. Joseph, S., Bishnoi, S., Maity, S.: An economic analysis of the production of limestone calcined clay cement in India. Indian Concr. J. **90**, 22–27 (2016)
8. Vizcaíno Andrés, L.M., Antoni, M.G., Alujas Diaz, A., Martirena Hernández, J.F., Scrivener, K.L.: Effect of fineness in clinker calcined clays limestone cements. Adv. Cem. Res. **27**, 546–556 (2015)
9. Dhandapani, Y., Sakthivel, T., Santhanam, M., Gettu, R., Pillai, R.G.: Mechanical properties and durability performance of concretes with limestone calcined clay cement (LC^3). Cem. Concr. Res. **107**, 136–151 (2018). https://doi.org/10.1016/j.cemconres.2018.02.005
10. Technical Report: Utilization of waste marble dust as an additive in cement production. **31**, 4039–4042 (2010). https://doi.org/10.1016/j.matdes.2010.03.036
11. Shah, V., Bishnoi, S.: Use of marble dust as clinker replacement in cements. Indian Concr. J. **89**, 27–32 (2015)
12. Krishnan, S., Kanaujia, S.K., Mithia, S., Bishnoi, S.: Hydration kinetics and mechanisms of carbonates from stone wastes in ternary blends with calcined clay. Constr. Build. Mater. **164**, 265–274 (2018). https://doi.org/10.1016/j.conbuildmat.2017.12.240
13. Bureau of Indian Standard (BIS), IS 8112 (2013): Ordinary Portland cement 43 grade-specifications (2013)
14. Bureau of Indian Standard (BIS), IS 4031-5 (1988): Methods of physical tests for hydraulic cement, part 5 (1988)
15. Bureau of Indian Standard (BIS): Concrete mix proportioning guideline, IS 10262-2009, pp. 1–11 (2009)
16. Snelson, D., Wild, S., O'Farrell, M.: Setting times of Portland cement-metakaolin—fly ash blends. J. Civ. Eng. Manag. **17**, 55–62 (2011). https://doi.org/10.3856/13923730.2011.554171
17. Scrivener, K., Martirena, F., Bishnoi, S., Maity, S.: Calcined clay limestone cements (LC^3). Cem. Concr. Res. **114**, 49–56 (2018). https://doi.org/10.1016/j.cemconres.2017.08.017

Performance and Durability of High Volume Fly Ash Cementitious System Incorporating Silica Nanoparticles

L. P. Singh, D. Ali and U. Sharma

Abstract This paper presents the beneficial role of silica nanoparticles (SNPs) in high volume fly ash (HVFA) cementitious system. The dosages of fly ash (FA) replaced with cement in the present study were 40% (40 FA) and 50% (50 FA). The dosages of SNPs were first optimized in mortar, and the optimized dosages were used in the concrete study. The fresh stage properties of mortar show that delay in setting time in HVFA system can address using SNPs as the initial final setting time gets shorten in the presence of SNPs. In addition to this, mechanical strength improves significantly especially at an early age of hydration. Compressive strength of the concrete containing 3% SNPs resulted in the speedy construction because we can achieve maximum compressive strength in 7 days in spite of 28 days, which is around four times faster. Long-term carbonation results revealed that SNPs incorporated mixes show a reduction of carbonation depth up to 45% with respect to control specimens containing 40 FA, while with 50 FA mix, the reduction was ~38%. Similarly, SNPs incorporated specimens show significant resistance towards the sulphate attack of about 41% with 40 FA and 34% with 50 FA samples and as compared to control specimens. Therefore, the incorporation of SNPs in concrete leads to the improvement of its durability and service life.

Keywords Cement · Silica nanoparticles · Fly ash

1 Introduction

In the recent years, rapid urbanization in the construction sector led to an increased demand for concrete, owing to its benefits like cost-effectiveness, mouldability, ease of transportation and good engineering properties. As it utilizes cement as a sole binder for its different constituents, its production usually contributes 5–7% of total CO_2 emission to the atmosphere which is a toxic Green House Gases (GHG) [1, 2]. Therefore, cement industries are focusing on techniques and substituents materials

L. P. Singh (✉) · D. Ali · U. Sharma
CSIR-Central Building Research Institute, Roorkee, India
e-mail: lpsingh@cbri.res.in

that will be led to the significant reduction in CO_2 emissions. For the same, miscellaneous solutions, i.e. eco-friendly green concrete with low carbon content will be used as replacement (supplementary cementitious materials (SCM)) like fly ash, without compromising the performance of cement concrete [3, 4]. Fly ash (FA) is a by-product of the thermal power plant, and it may be an excellent replacement for cement due to its similar mineral composition, abundant availability and compatibility. In the last decades, FA is enormously used as a limited replacement (15–35%) of cement in mortar and concrete system [5, 6]. Although FA can be used as replacement in cement-based materials, it led to several issues in early age properties, i.e. setting time, strength gain, etc. [7]. Keeping in view the same, scientific community is looking nanotechnological intervention as one of the best solutions for addressing these issues [8–10]. Various nanomaterials, i.e. silicon dioxide (SiO_2), titanium oxide (TiO_2), aluminium oxide (Al_2O_3), calcium carbonate ($CaCO_3$), zirconium oxide (ZrO_2), ferric oxide (Fe_2O_3), clay and carbon nanotube (CNTs) have been explored [11, 12] for their application in cement-based materials in order to enhance the early age strength and hydration of cement concrete.

Among all the materials, silica nanoparticles (SNPs) have received widespread attention for achieving high performance and enhanced durability in the cement-based materials [13, 14] due to its high specific surface area. SNPs react with portlandite, leads to the formation of additional C–S–H due to their high pozzolanic activity, which improves the microstructure and sustainability of cementitious material. In addition to this, it also improves the interfacial transition zone in the concrete system [15, 16]. Several researchers used SNPs for the improvement of early age properties, i.e. setting time, strength, with the replacement of HVFA. Zhang et al. [17] studied the impact of SNPs in HVFA concrete and its incorporation results in reduced initial and final setting times as compared to control by 90 and 100 min, respectively, while in terms of compressive strength significant enhancement of ~30 and ~25% at 3 and 7 days, respectively, as compared to control was observed. Although a lot of studies have been carried out to investigate the effect of different dosage of SNPs on the engineering properties in HVFA cement concrete. However, an optimized effect of SNPs and the durability of SNPs incorporated HVFA system are still a grey area for research. In the present paper, the optimized dosage of laboratory synthesized SNPs in HVFA mortar system was investigated first on the basis of rheology and compressive strength. These optimized dosages were used in HVFA concrete system, and its effect on engineering properties and durability was monitored systematically.

2 Experimental Details

2.1 Materials and Methods

The ordinary Portland cement (OPC) 43-grade was used in the present study with Blaine fineness 390 m^2/kg, approving to IS 8112:1989, and its chemical composition

Table 1 Chemical composition of cement, silica nanoparticles and fly ash

Minerals (%)	Cement	Fly ash	SNPs
CaO	63.38	1.61	
SiO_2	19.00	55.27	99.8
Al_2O_3	3.90	26.69	
Fe_2O_3	4.36	8.14	
K_2O	1.41	1.76	
Na_2O	0.83	0.13	
SO_3	3.14	0.25	
MgO	3.31	0.39	
LOI	0.50	1.33	
Density (g/cm^3)	3.15	2.25	1.40

is shown in Table 1. Siliceous FA (Class F) was used with a specific gravity of 2.22 and the fineness of 410 m^2/kg and is conforming to the specifications of ASTM C618 and IS 3812 [18, 19]. The chemical composition is given in Table 1. Powdered SNPs were prepared in the laboratory, using water glass (sodium silicate solution) as a precursor through the sol-gel technique. The powdered SNPs are amorphous in nature with particles size in the range of 30–70 nm and a specific surface area of 116 m^2/g as reported previously [20, 21]. As per IS 650 [22], the standard sand having the specific gravity 2.60 and fineness modulus 2.77 for mortar was used for the entire study, and polycarboxylate-based superplasticizer (Glenium 52) was used for maintaining the workability of mortar samples.

The coarse aggregate used for the concrete mix has a maximum size of 12.5 mm, fineness modulus of 7.49 and specific gravity of 2.63. The fine aggregate is the natural river sand with fineness modulus of 2.72 and specific gravity of 2.64 [23]. Both the coarse and fine aggregates were found to be satisfying the specification of IS 383:1970 [24], and the details are given in Table 2. The FA concrete mix (Table 3) was prepared at a constant w/b (water/binder) ratio of 0.30 with varying dosages of polycarboxylate-based superplasticizer for maintaining the desired workability (targeting slump 25–50 mm) of the FA concrete. The FA concrete casting was carried out as per IS 10086: 1982 [25]. Casted samples were demoulded after 24 h and cured in tap water at room temperature for 28 days as per IS 516:1959 [26].

2.2 Specimen Preparation for the Compressive Strength

For the optimization of SNPs' dosage in HVFA cement mortar, mix containing 40% and 50 FA with incorporation of 1, 2, 3, 3.5 and 4% SNPs dosages with respect to cement was cast (50 × 50 × 50 mm) at constant water/cement ratio of 0.30 using standard sand with cement/sand ratio of 1:3 as shown in Table 2. The compressive strength studies of mortar samples were carried out at 3, 7 and 28 days of curing

Table 2 Mortar mixes with different dosages of SNPs

Binder	SNPs (%)	Notation	w/b ratio
60% cement + 40% FA	0.0	Control	0.30
	1.0	40 FA1SNPs	–
	2.0	40 FA2SNPs	–
	3.0	40 FA3SNPs	–
	3.5	40 FA3.5 SNPs	–
	4.0	40 FA4 SNPs	–
50% cement + 50% FA	0.0	Control	–
	1.0	50 FA1SNPs	–
	2.0	50 FA2SNPs	–
	3.0	50 FA3SNPs	–
	3.5	50 FA3.5 SNPs	–
	4.0	50 FA4 SNPs	–

Table 3 Mix proportion use for concrete casting

Mix	Cement (kg/m^3)	SNPs (kg/m^3)	Fly ash (kg/m^3)	Fag (kg/m^3)	CAg (kg/m^3)	Water (L/m^3)	SP (L)
40FA	282	–	188	676	1278	136.7	0.98
40FA3SNPs	282	8.46	188	676	1278	136.7	1.27
50FA	235	–	235	676	1278	136.7	0.70
50FA3SNPs	235	7.05	235	676	1278	136.7	0.94

as per ASTM C109 [27]. For concrete samples, the compressive strength test was carried out on cubes having size of $100 \times 100 \times 100$ mm and tested at 3, 7, 28, 56 and 90 days according to IS 456 [28].

2.3 Carbonation

The carbonation depth and carbonation rate were investigated as per RILEM CPC-18 [29], and the prism specimens of size $100 \times 100 \times 500$ mm were cast and demoulded after 24 h and cured in water. After 6 days of water curing, samples were dried at 20 °C and 65% relative humidity for 21 days in the environmental chamber. Then, the specimens were placed in a carbonation chamber using 2.0% CO_2 concentration, at 20 °C and 65% relative humidity. After exposure of 28, 90 and 180 days, slices of specimens ($50 \times 100 \times 100$ mm) were tested for the determination of carbonation depth using phenolphthalein solution (1% phenolphthalein in 70% of ethanol v/v). In exposed specimens, the non-carbonated region is shown by purple-red colour due to high alkalinity; whereas, the carbonated region of the specimen is colourless.

The carbonation depth 'X_{CO_2}' is determined by taking the average of depth of colourless region [30].

The carbonation rate of exposed specimens was determined by using the equation:

$$\text{Carbonation rate } (R) = \left(\frac{X_{CO_2}}{\tau}\right)^2 \tag{1}$$

where X_{CO_2} is the carbonation depth in m, and τ is the time constant in [(s/kg $CO_2/m^3)^{0.5}$] [29].

2.4 Sulphate Attack

Sulphate attack in the prism specimens ($100 \times 100 \times 500$ mm) was investigated as per ASTM C1012 [31]. After seven days of water curing, the prism specimens were placed in the sulphate solution, containing 5% magnesium sulphate at room temperature and at a pH range of 6.0–8.0 was maintained throughout the period of exposure. For determining sulphate ion concentration, split slice ($50 \times 100 \times 100$ mm) from the prism was used and tested at 28, 90 and 180 days of exposure. Sulphate ion concentration was determined by the chemical analysis as per IS 4032 [32].

3   Results and Discussion

3.1 Setting Time of SNPs Incorporated HVFA Cement Mortar

The initial and final setting time studies of SNPs incorporated HVFA cement mortars were carried out using the Vicat's apparatus. The result obtained reveals that as the FA content increases in the cementitious system, the initial and final setting time also increase (Fig. 1). The addition of 3% dosage of SNPs reduced both of initial and final setting time by 50% and 36%, respectively. Further, 40 and 50% FA containing with 3% SNPs reduced initial setting time by 54% and 58%, respectively, while final setting time reduced by 28% only in all mixes. Hence, the incorporation of SNPs in HVFA system results in the reduction of initial and final setting time. Thus, the delay in the initial and final setting time in HVFA cementitious system can be addressed by incorporating SNPs.
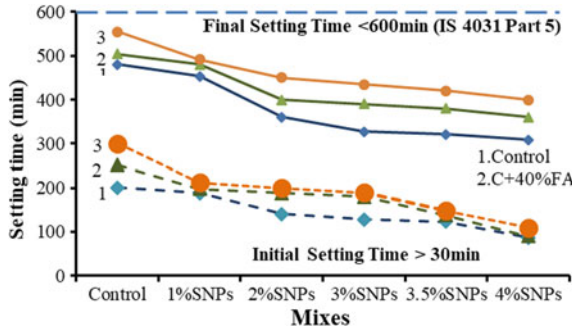
Fig. 1 Effect of SNPs on setting time in HVFA mortar

3.2 The Effect of SNPs on Compressive Strength in HVFA Cementitious System

The effect of varying the dosages of SNPs on 3, 7 and 28 days strength of HVFA mortar specimens is shown in Fig. 2a, b. From the results obtained, it is observed that
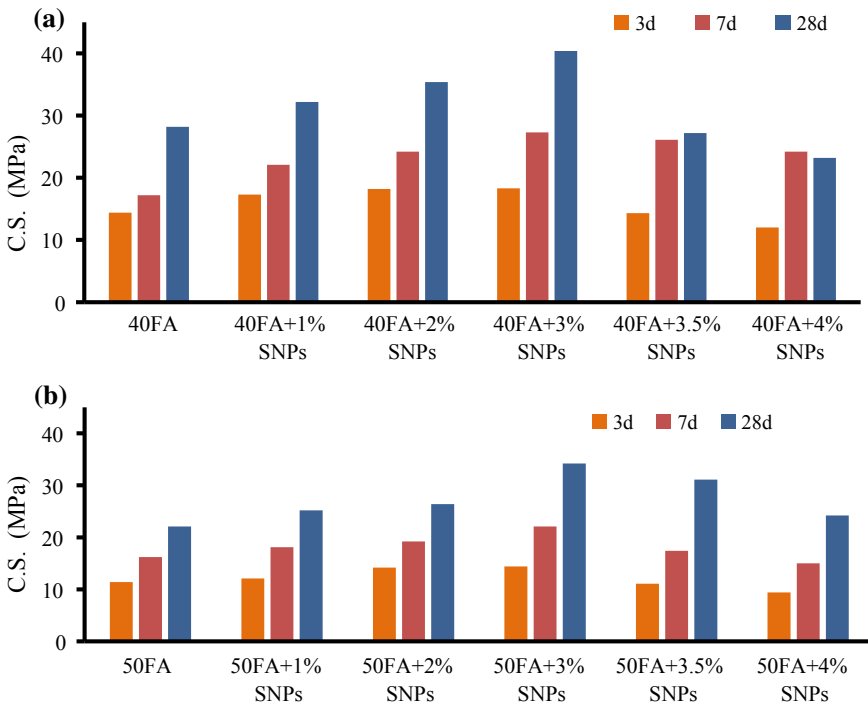
Fig. 2 Compressive strength results 40FA, **a** and 50 FA, **b** mixes with different dosages of SNPs

Table 4 Compressive strength results of SNPs (3%) incorporated FA concrete specimens

Days	Compressive strength (MPa)			
	40 FA	40 FA3SNPs	50 FA	50 FA3SNPs
3	20.8	24.9	18.8	24.3
7	26.4	33.7	22.6	32.4
28	38.6	47.4	32.5	41.7
56	45.9	55.2	41.6	48.9
90	50.1	57.3	46.5	52.3

the strength of mortar samples containing SNPs increases with the increasing dosages of SNPs up to 3%, and further increase in the dosages of SNPs (e.g. at 3.5 and 4%) results in the decrement of the compressive strength. The reason behind strength decrement beyond optimized dosages of SNPs is due to the formation of dense compact microstructure around the hydrated, which may slow down the hydration process [7, 10]. The compressive strength of concrete specimens containing 40 and 50% FA with SNPs (3%) was determined up to 90 days, and the results are presented in Table 4. Results show that SNPs contribute to higher strength at an early stage; however, at later ages (56 and 90 days) strength enhancement exhibits more or less similarity (Table 4).

3.3 Carbonation Rate

The variation in carbonation rate with respect to time is shown in Fig. 3a, b. The reduction in the carbonation rate with respect to time was determined by using RILEM CPC-18 [29]. Figure 3a results show the significant reduction in carbonation rate between 90 and 180 days of exposure from the initial carbonation rate. This reduction in carbonation rate attributes to deposition of the calcium carbonate at exposed surface of concrete during the carbonation [30, 33]. 40FA3SNPs mix shows that carbonation rate reduces at 90 days of exposure from their initial carbonation rate and same results found from 50% FA containing SNPs mix (Fig. 3b).

3.4 Sulphate Attack

The SO_4^{2-} ions accelerate the formation of gypsum crystals and ettringite in the interfacial transition zone of the concrete system, which can be associated with cracking, cohesion decrease and spalling.

The effect of SO_4^{2-} ions on concrete was experimentally determined by measuring SO_4^{2-} ions concentration after 28, 90 and 180 days of exposure in magnesium sulphate solution by gravimetric analysis. The concrete mix containing 40 and 50%
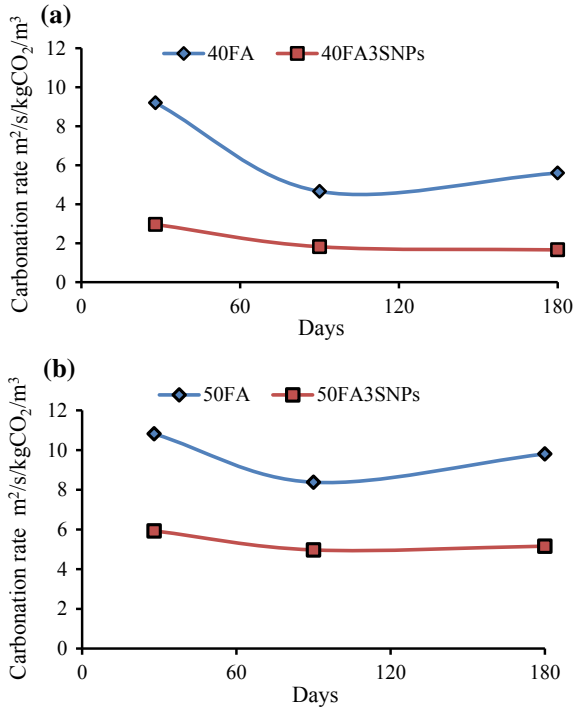
Fig. 3 Compressive strength of FA concrete specimens having 40 and 50% FA concrete, **a** 40 and 50% FA with 3% SNPs, **b** at 28, 56 and 90 days

FA with and without incorporation of 3% SNPs was exposed in magnesium sulphate solution. Figure 4 reveals that with the incorporation of 3% SNPs in 40% FA concrete (40FA3SNPs), ~38% reduction in SO_4^{2-} ions concentration is observed as compared to control (40FA) after 28 days of exposure. Figure 4 indicates that 50FA3SNPs concrete mix reduces SO_4^{2-} ions concentration by ~35% than those of control (50FA) after 28 days of exposure.

4 Conclusions

The modification of the hydration products of cement-based material would be expedient for the completion of the entire mechanical properties of FA concrete, and it reduces the penetration of harmful substances, which enhanced the durability properties. In this study, several durability parameters were evaluated, and significant observations are as follows:

1. The mix containing 40% and 50% FA with 3% of SNPs shows ~29% and 37% reduction in initial setting time, while in terms of final setting time it shows
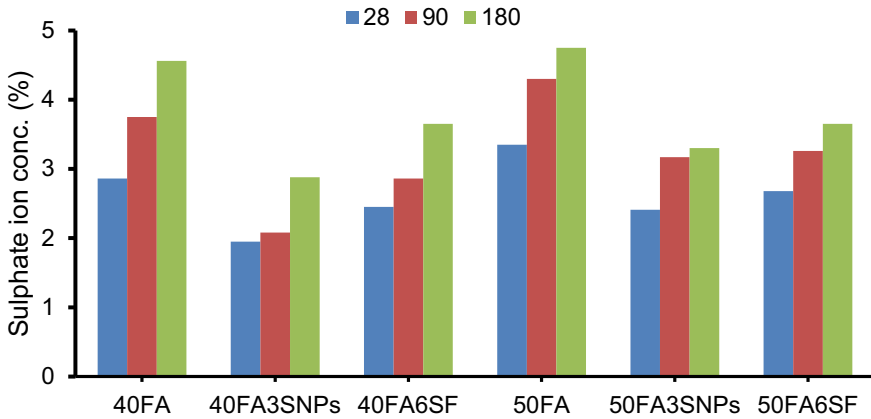
Fig. 4 Sulphate ion concentration in FA concrete specimens having 3% SNPs with varying the amount fly ash 40 and 50% at 28, 90 and 180 days

~23% and 22% reduction was observed, respectively, as compared to control specimens.

2. SNP' dosage more than 3%, i.e. 3.5 and 4%, results in the reduction of the compressive strength of HVFA mortar showing the optimized dosages of SNPs.

3. SNPs incorporated specimens show the significant reduction in carbonation depth as well as in SO_4^{2-} attack in the FA concrete. This reduction indicates that in the presence of SNPs formed hydration product enhanced the resistance against aggressive ions and which helps to improve the durability of FA concrete during the service environment.

4. The incorporation of SNPs in concrete leads to the improvement of its durability and service life, in addition to this, the performance of SNPs incorporated concrete is significantly improved as compared to control specimens.

References

1. Singh, L.P., Karade, S.R., Bhattacharyya, S.K., Yousuf, M.M., Ahalawat, S.: Beneficial role of nanosilica in cement based materials–a review. Constr. Build. Mater. **47**, 1069–1077 (2013)
2. Monteiro, P.J.M., Mehta, P.K.: Concrete Microstructure, Properties, and Materials (2006)
3. Hemalatha, S.S.T., Mapa, M., George, N.: Physico- chemical and mechanical characterization of high volume fly ash incorporated and engineered cement system towards developing greener cement. J. Clean. Prod. **125**, 268–281 (2016)
4. Hemalatha, A.R.T.: A review on fly ash characteristics—towards promoting high volume utilisation in developing sustainable concrete. J. Clean. Prod. **147**, 546–559 (2017)
5. Shaikh, F.U.A., Supit, S.W.M.: Compressive strength and durability properties of high volume fly ash (HVFA) concretes containing ultrafine fly ash (UFFA). Constr. Build. Mater. **82**, 192–205 (2015)

6. Supit, S.W.M., Shaikh, F.U.A.: Durability properties of high volume fly ash concrete containing nano-silica. Mater. Struct. **48**, 2431–2445 (2014)
7. Singh, L.P., Ali, D., Tyagi, I., Sharma, U., Singh, R., Hou, P.: Durability studies of nano-engineered fly ash concrete. Constr. Build. Mater. **194**, 205–215 (2019)
8. Sanchez, F., Sobolev, K.: Nanotechnology in concrete—a review. Constr. Build. Mater. **24**, 2060–2071 (2010)
9. Sobolev, K., Shah, S.P.: Nanotechnology in Construction (2015)
10. Singh, L.P., Ali, D., Sharma, U.: Studies on optimization of silica nanoparticles dosage in cementitious system. Cem. Concr. Compos. **70**, 60–68 (2016)
11. Hou, P., Kawashima, S., Kong, D., Corr, D.J., Qian, J., Shah, S.P.: Modification effects of colloidal nano SiO_2 on cement hydration and its gel property. Compos. Part B Eng. **45**, 440–448 (2013)
12. Kong, D., Su, Y., Du, X., Yang, Y., Wei, S., Shah, S.P.: Influence of nano-silica agglomeration on fresh properties of cement pastes. Constr. Build. Mater. **43**, 557–562 (2013)
13. Singh, L.P., Agarwal, S.K., Bhattacharyya, S.K., Sharma, U., Ahalawat, S.: Preparation of silica nanoparticles and its beneficial role in cementitious materials regular paper. Nanom. Nanotechnol. **1**, 44–51 (2011)
14. Singh, L.P., Zhu, W., Howind, T., Sharma, U.: Quantification and characterization of C–S–H in silica nanoparticles incorporated cementitious system. Cem. Concr. Compos. **79**, 106–116 (2017)
15. Kawashima, S., Hou, P., Corr, D.J., Shah, S.P.: Modification of cement-based materials with nanoparticles. Cem. Concr. Compos. **36**, 8–15 (2013)
16. Hou, P., Qian, J., Cheng, X., Shah, S.P.: Effects of the pozzolanic reactivity of nanoSiO_2 on cement-based materials. Cem. Concr. Compos. **55**, 250–258 (2014)
17. Zhang, M.H., Islam, J., Peethamparan, S.: Use of nano-silica to increase early strength and reduce setting time of concretes with high volumes of slag. Cem. Concr. Compos. **34**, 650–662 (2012)
18. ASTM C618: Standard Specification for Coal Fly Ash and Raw or Calcined Natural Pozzolan for Use in Concrete. Standard, pp. 1–5 (2015)
19. IS-3812: Specifications for Pulverized Fuel Ash. Indian Standard, p. 3812 (2013)
20. Singh, L.P., Goel, A., Bhattachharyya, S.K., Ahalawat, S.: Effect of morphology and dispersibility of silica nanoparticles on the mechanical behaviour of cement mortar. Int. J. Concr. Struct. Mater. **9**, 207–217 (2015)
21. Singh, L.P., Bhattacharyya, S.K., Shah, S.P., Sharma, U.: Studies on hydration of tricalcium silicate incorporating silica nano-particles. Nanotechnol. Constr. 151–159 (2015)
22. IS 650: Standard sand for testing cement specification. Bur. Indian Stand. **4**–11 (1991)
23. Kumar, R., Singh, S., Singh, L.P.: Studies on enhanced thermally stable high strength concrete incorporating silica nanoparticles. Constr. Build. Mater. **153**, 506–513 (2017)
24. IS-383: Specification for coarse and fine aggregates from natural sources for concrete. Standard 1–24 (1970)
25. IS-10086: Specification for Moulds for Use in Tests of Cement and Concrete, pp. 1–29 (1982)
26. IS-516: Method of tests for strength of concrete. Indian Stand. 1–30 (1959)
27. ASTM C109: Standard test method for compressive strength of hydraulic cement mortars (using 2-in. or [50-mm] cube specimens). Am. Soc. Test. Mater. **1**, 1–9 (2010)
28. IS-456, Plain and Reinforced Concrete, pp. 1–100 (2000)
29. Gehlen, C., RILEM CPC 18, Measurement of hardened concrete carbonation depth, RILEM Tech. Comm. TDC, pp. 1–11 (2011)
30. Chang, C., Chen, J.: The experimental investigation of concrete carbonation depth. Cem. Concr. Res. **36**, 1760–1767 (2006)
31. ASTM-C1012: Standard Test Method for Length Change of Hydraulic-Cement Mortars Exposed to a Standard, pp. 1–8 (2015)
32. IS-4032: Method of chemical analysis of hydraulic cement. Indian Stand. 1–47 (1985)
33. Palacios, M., Puertas, F.: Effect of carbonation on alkali-activated slag paste. J. Am. Ceram, Soc (2006)

Monitoring Strength Development of Cement Substituted by Limestone Calcined Clay Using Different Piezo Configurations

Tushar Bansal and Visalakshi Talakokula

Abstract Recently developed limestone calcined clay cement (LC^3) with low clinker factor is growing rapidly in the construction industry because of its several benefits over ordinary Portland cement (OPC) and Portland pozzolana cement (PPC). In this paper, monitoring strength development of cement substituted by (LC^3) using different piezo configurations was studied. The experimental study was carried out on concrete cube specimens of OPC and LC^3, in which different piezo configurations such as embedded piezo sensor (EPS), surface-bonded piezo sensor (SBPS), jacketed piezo sensor (JPS) and non-bonded piezo sensor (NBPS) are installed to the specimen to acquire data in the form of conductance and susceptance signatures via electro-mechanical impedance (EMI) technique. The sensitivity of the different piezo configurations was calibrated with the compressive strength, based on the results, it can be concluded that the compressive strength of OPC and LC^3 is comparable to each other. All the piezo configurations were effective in monitoring the compressive strength; however, the embedded sensors, EPS and JPS, perform the best in LC^3 and OPC, respectively.

Keywords Limestone calcined clay cement (LC^3) · Piezo sensor · Compressive strength · Structural parameters

1 Introduction

In today's world scenario, the demand for cement is continuously increasing day by day due to the construction boom. According to the Indian Brand Equity Foundation report 2018 [1], the production capacity of the cement is 502 tons per year, in which India is the second largest producer in the world, but the production of cement is considered as an environmentally unfriendly because it emits the high amount of carbon dioxide (CO_2) in the atmosphere. For this purpose, many researchers used the supplementary cementitious materials (SCMs) such as fly ash, rice husk ash, pond ash,

T. Bansal (✉) · V. Talakokula
Department of Civil Engineering, Bennett University, Greater Noida, India
e-mail: tb6292@bennett.edu.in

agro-industrial and natural waste material and ground steel slag as a partial replacement for cement for reducing the (CO_2) emissions. The primary issue with SCMs is that it does not fulfill the production demand because it is not abundantly available in the world. To meet the demand for sustainable development and application of cement, it is necessary to develop new SCMs that can meet the good mechanical performance of concrete. In this regard, limestone calcined clay cement (LC^3) has been developed which is a latest technological development in the cement industry to reduce the carbon dioxide emission and provide similar strength as compared to the ordinary Portland cement (OPC). According to the preliminary analysis done Bishnoi et al. [2] and Shiju et al. [3], it is found that the LC^3 is economical than OPC and PPC and more suitable where there is a shortage of locally available fly ash (FA). It reduces the clinker factor by 0.5, CO_2 emissions by 0.5 kg per m^2 of floor area [4], production cost 15–25% and greenhouse gas emissions up to 20–23% as compared to the conventional solutions. The mechanical properties, shrinkage and durability performance of different blended concrete such as OPC, FA-blended cement (FA30) and LC^3 were studied by Dhandapani et al.[5] and concluded that LC^3 has either comparable/better properties. All the above studies were based on destructive evaluation; hence, the authors felt the need for studying the mechanical properties of the newly developed LC^3 concrete non-destructively using piezo sensors.

Piezo sensors are the smart materials used for monitoring the structural health based on its unique property of sensing and actuating. Soh and Bhalla [6] presented new impedance-based monitoring using piezo sensors for non-destructive evaluation (NDE) of concrete strength prediction and damage assessment and found that equivalent structural parameters identified by piezo sensors were effective in monitoring the strength development and diagnosing the damage progression. Providakis et al. [7] introduced the cost-effective, reusable and non-destructive wireless monitoring device system to monitor the early age strength of the concrete using electromechanical impedance (EMI) technique via piezo sensors and found that EMI signatures gradually shift to the right with the increase in strength. Talakokula et al. [8] monitored the early age hydration of concrete and derived a non-dimensional parameter based on equivalent stiffness identified by a piezo sensor via EMI technique. Based on their results, they found that the piezo-based non-dimensional hydration parameter was effective in monitoring the early age hydration of concrete. All the above studies monitored the strength of conventional concrete using surface-bonded piezo sensors (SBPS); the present study is focused on using different piezo configurations for monitoring the strength development in LC^3 concrete system.

2 Monitoring the Strength Development of LC^3 Using Different Piezo Configurations

Four different piezo configurations such as embedded piezo sensor (EPS), SBPS, jacketed piezo sensor (JPS) and non-bonded piezo sensor (NBPS) are used to monitor
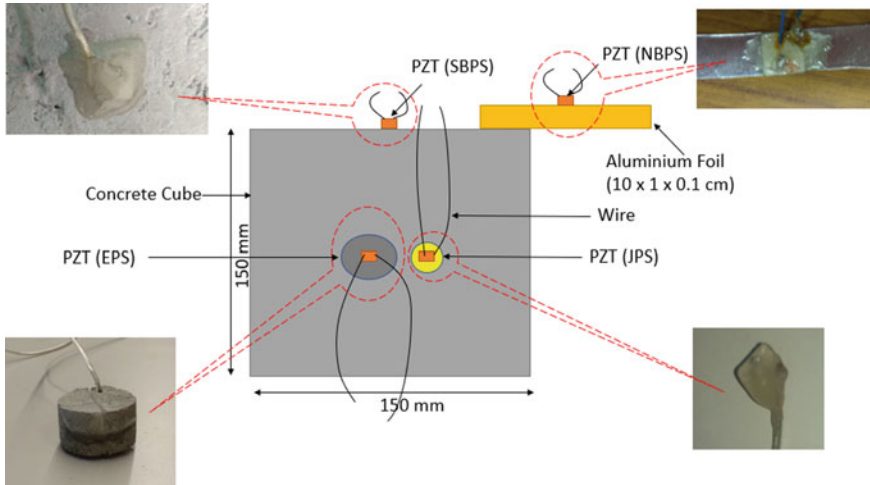
Fig. 1 Schematic diagram of specimen with different piezo configurations

the compressive strength. EPS is the one in which the sensor is sandwiched between the mortar layers (see Fig. 1), JPS is the sensor which is jacketed by epoxy coating, SBPS is the surface bonded on the top surface on the specimen, and NBPS is the sensor which is bonded on the thin aluminum foil and in turn non-directly bonded to the top surface of the specimen in a reusable form [9]. All the piezo configurations are based on the effective impedance model developed Bhalla and Soh [10] using EMI technique in which both the direct and the converse effects of the piezo sensors are utilized. The sensors are first excited using an impedance analyzer such as LCR meter, and its interactions with the host structures are acquired in the form of electrical admittance signature containing the conductance (the real part) and the susceptance (the imaginary part). Any changes such as mass, damping and stiffness of the host structure are reflected in the admittance signature in the form of shifting/occurrence of new peaks.

2.1 Experimental Program

In this study, total fifty-eight concrete cube specimens were cast with OPC and LC^3-50 (using clinker replacement level of 50%) cement in which twenty-seven specimens of each OPC and LC^3-50 are utilized to check the compressive strength destructively and the remaining specimens of OPC and LC^3-50 are installed with different piezo configurations as shown in Fig. 1 to monitor the compressive strength non-destructively. The admittance signatures were acquired from all the piezo configurations during the curing process.

3 Results and Discussion

The variation of conductance signature with strength derived from destructive testing for LC^3-50 specimens installed with different piezo configurations is shown in Fig. 2; it is observed that the resonance peaks and magnitude of the conductance signature increase as the strength increases. It is due to the changes inside the concrete such as gain in stiffness which can be detected by all the sensors well. Out of all the sensors, EPS shows appreciable changes because the sensor is embedded inside the concrete and can effectively sense the changes occurring during the hydration process. Figure 3 shows the variation of compressive strength with curing time; it is observed that the strength increases as the curing time increases; it is due to gain in stiffness. The magnitude of the conductance spectra at first resonance peak with curing time in different piezo configurations in LC^3-50 is shown in Fig. 4; it can be seen that the magnitude of EPS with respect to curing time is higher as compared to the other piezo configurations, but in case of JPS, it shows lower magnitude which needs to be further studied because JPS is the sensor which is jacketed by epoxy coating, so its sensing capability should be more as compared to EPS which is sandwiched between the mortar layers due to which the EPS peaks and magnitude were damped out.

In the case of OPC specimens, the variation of conductance signature with respect to strength in different piezo configurations is shown in Fig. 5; it is observed that
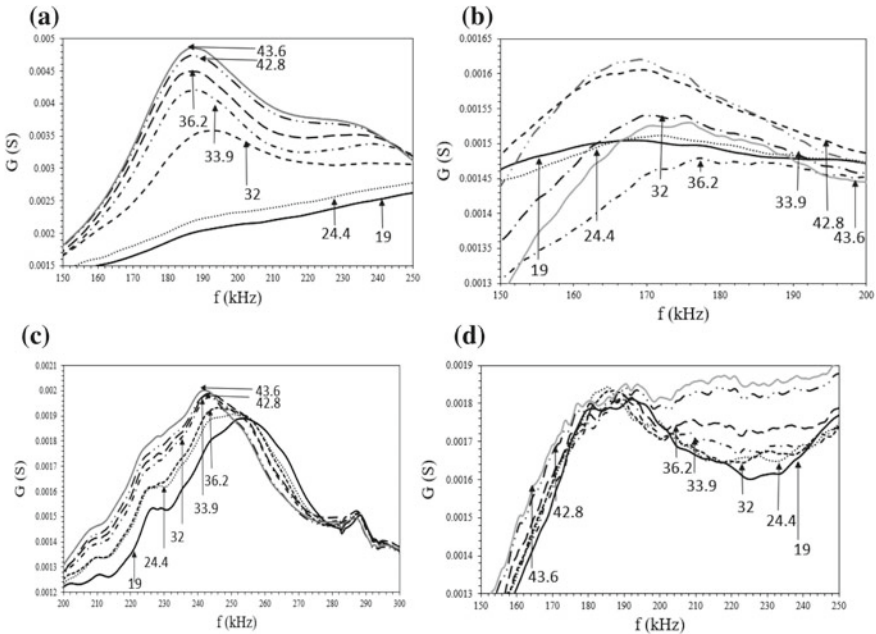
Fig. 2 Variation of conductance signature with strength for LC^3-50 specimens with different piezo configurations: **a** EPS, **b** SBPS, **c** NBPS and **d** JPS
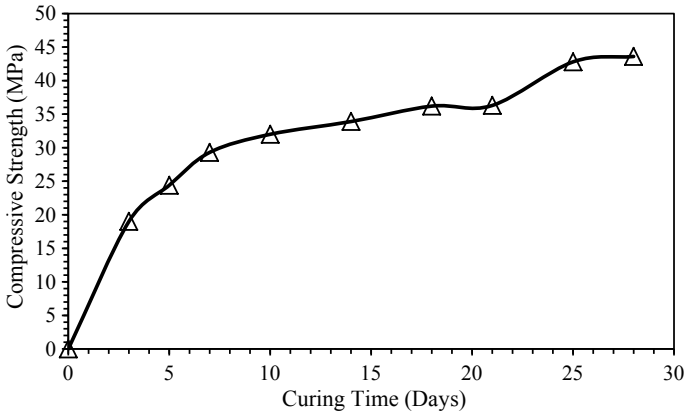
Fig. 3 Variation of compressive strength with curing time of LC^3
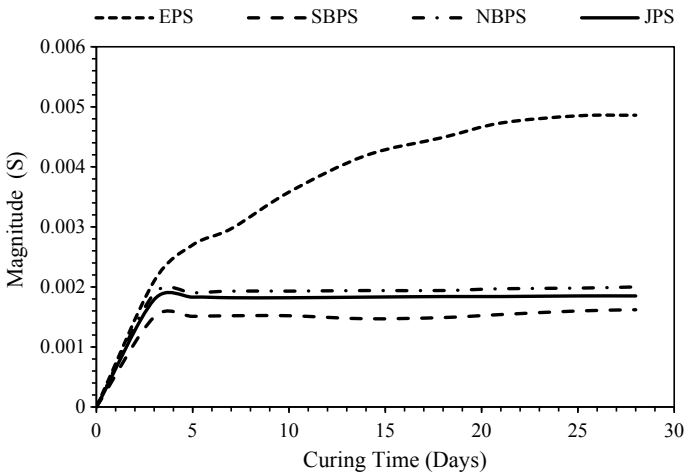
Fig. 4 Magnitude of the conductance spectra at first resonance peak with curing time in the different piezo configurations in LC^3

EPS and JPS show appreciable changes, SBPS shows lesser changes because it is bonded on the top surface of the specimen, and NBPS shows not much appreciable changes because it is non-directly bonded to the structure. The same increase in compressive strength with curing time is seen from OPC specimens as shown in Fig. 6. But on comparing the compressive strength of OPC and LC^3-50, it is found that in an equivalent grade category, it is comparable to each other. From Fig. 7, it is observed that the magnitude conductance spectra at first resonance peak of JPS show higher as compared to other different piezo configurations because the sensor
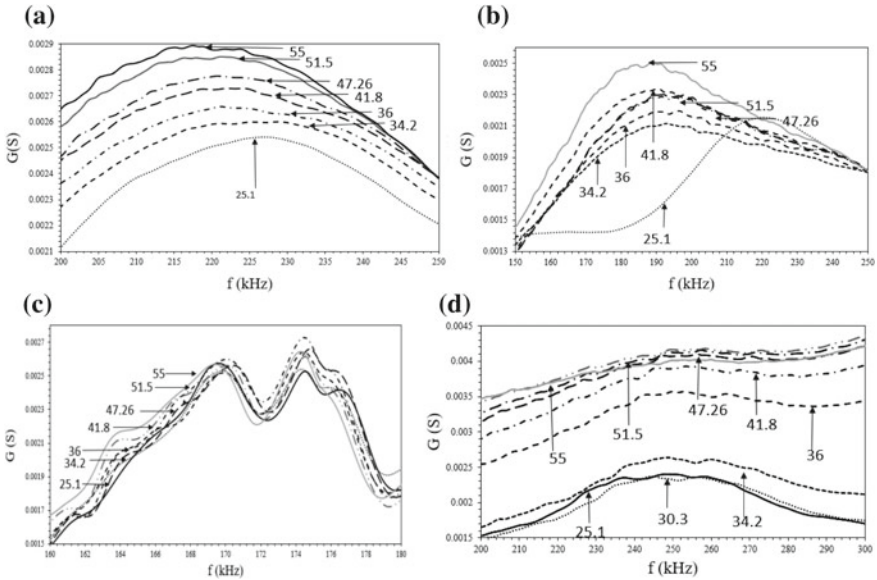
Fig. 5 Variation of conductance signature with strength for OPC specimens with different piezo configurations: **a** EPS, **b** SBPS, **c** NBPS and **d** JPS

Fig. 6 Variation of compressive strength with curing time of OPC
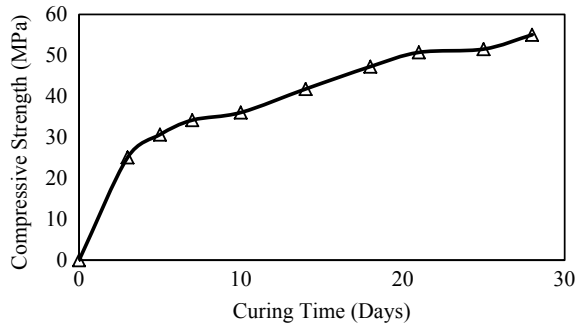
is jacketed inside the epoxy layer and can effectively sense the changes occurring during the hydration process.

4 Conclusions

In this study, different piezo configurations such as EPS, JPS, NBPS and SBPS were used to monitor the strength development of LC^3. All piezo configurations proved to be suitable for monitoring the compressive strength. It was observed that the
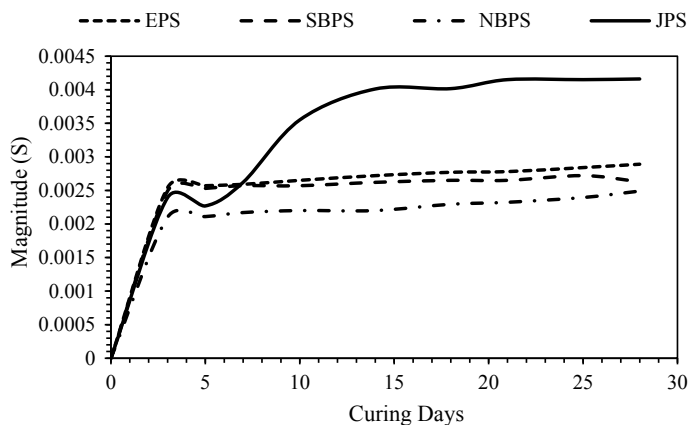
Fig. 7 Magnitude of the conductance spectra at first resonance peak with the different piezo configurations in OPC

embedded sensors EPS and JPS perform the best in LC^3-50 and OPC, respectively, because it is embedded inside the concrete, but the behavior of the JPS in LC^3-50 needs to be further study. NBPS shows lesser appreciable changes because it is non-directly bonded to the structure, but it is used when there will be a problem of embedded or surface-bonded sensor. SBPS shows better results than NBPS because it the bonded on the top surface of the concrete specimens, so it can sense the changes occurring inside the concrete, and it is used when there will be a problem of embedded sensor. The destructive study was carried out to understand the compressive strength of LC^3-50 and OPC.

References

1. IBEF: Indian Cement Industry Analysis. [Online]. Available https://www.ibef.org/industry/cement-presentation (2018). Accessed 04 June 2019
2. Bishnoi, S., Maity, S., Mallik, A., Joseph, S., Krishnan, S.: Pilot scale manufacture of limestone calcined clay cement: the Indian experience. Indian Concr. J. **88**(7), 22–28 (2014)
3. Shiju, J., Aneeta, M.J., Shashank, B.: Economic Implications of Limestone Clinker Calcined Clay Cement (LC3) in India. Calcined Clays Sustain. Concr. **10**, 11–19 (2015)
4. Soumen, M., Shashank, B., Arun, K.: Field Application of Limestone-Calcined Clay Cement in India. Calcined Clays Sustain. Concr. **10**, 11–19 (2015)

5. Dhandapani, Y., Sakthivel, T., Santhanam, M., Gettu, R., Pillai, R.G.: Mechanical properties and durability performance of concretes with Limestone Calcined Clay Cement (LC3). Cem. Concr. Res. **107**(March), 136–151 (2018)
6. Soh, C.K., Bhalla, S.: Calibration of piezo-impedance transducers for strength prediction and damage assessment of concrete. Smart Mater. Struct. **14**(4), 671–684 (2005)
7. Providakis, C.P., Liarakos, E.V., Kampianakis, E.: Nondestructive Wireless Monitoring of Early-Age Concrete Strength Gain Using an Innovative Electromechanical Impedance Sensing System. Smart Mater. Res. **2013**, 1–10 (2013)
8. Talakokula, V., Bhalla, S., Gupta, A.: Monitoring early hydration of reinforced concrete structures using structural parameters identified by piezo sensors via electromechanical impedance technique. Mech. Syst. Signal Process. **99**, 129–141 (2018)
9. Srivastava, S., Bhalla, S., Madan, A.: Assessment of human bones encompassing physiological decay and damage using piezo sensors in non-bonded configuration. J. Intell. Mater. Syst. Struct. **28**(14), 1977–1992 (2017)
10. Bhalla, S., Soh, C.K.: Structural health monitoring by Piezo-impedance transducers. I: modeling. J. Aerosp. Eng. **17**(4), 154–165 (2004)

Bond Behavior Between Limestone Calcined Clay Cement (LC^3) Concrete and Steel Rebar

Zhenyu Huang, Youshuo Huang, Lili Sui, Ningxu Han, Feng Xing and Tongbo Sui

Abstract To investigate the mechanical properties of the localized LC^3 concrete and interfacial bond behavior between LC^3 concrete and steel rebar, different design mixtures of LC^3 concrete and normal concrete were prepared. The compressive strength in different curing ages was evaluated experimentally compared with that of normal concrete with the same W/B ratio. The interfacial bond strength was evaluated by pullout test on the steel rebar from the concrete block. The test results show that rebar–LC^3 concrete has comparable good bond strength and has higher secant stiffness in bond-slip curve than that of rebar–normal concrete.

Keywords Limestone calcined clay cement · Metakaolin · Bond behavior · Compressive strength

1 Introduction

Calcined clays combined with limestone (LC^3 blends) can be used to achieve blended cements with good performance at much lower levels of clinker. Such blends can make a significant contribution to the reduction of CO_2 emission associated with cement production. Calcined clay as a pozzolanic material has been successfully used in concrete production. The use of clays with modest kaolinite content is very promising for a massive use in cement due to their good performance and low cost [1]. The previous studies show that LC^3 exhibits good strength behavior and dense microstructure compared to normal cements [2]. The concrete and steel reinforce-

Z. Huang (✉) · Y. Huang · L. Sui · N. Han · F. Xing
Guangdong Provincial Key Laboratory of Durability for Marine Civil Engineering, Shenzhen University, Shenzhen 518060, People's Republic of China
e-mail: huangzhenyu@szu.edu.cn

T. Sui
Sinoma Research Institute, Sinoma International Engineering Co. Ltd, Beijing 100102, People's Republic of China

ment are widely used materials in civil construction. Their superior bond behavior allows the reinforced concrete to resist the outer loading by using their composite action. Therefore, it is quite interesting to understand the fundamental behavior of such new material and interaction with reinforcement. Therefore, the purpose of this paper is to evaluate the bond behavior between the LC^3 concrete and steel rebar, which is the key issue to promote the application of LC^3 concrete in structural engineering.

2 Experimental Program

2.1 Materials

LC^3 was produced in the laboratory by using ordinary Portland cement 42.5, limestone, gypsum and calcined clay. The calcium clay used in this study was calcined kaolin tailings provided by the Sinoma International Engineering Co. Ltd. Table 1 shows the chemical composition percentage of each raw material.

To prepare the LC^3 concrete, the experimental program started from preparing the cement paste, cement mortar and then concrete. Therefore, six mixtures including the OPC paste, LC^3 paste, OPC mortar, LC^3 mortar, normal concrete and LC^3 concrete were considered. Table 2 shows the mixture proportions for each paste, mortar and

Table 1 Chemical compositions of materials

Oxides	OPC (%)	Limestone (%)	Calcined clay (%)	Gypsum (%)
SiO_2	17.00	0.30	52.70	6.76
Al_2O_3	3.58	0.10	36.90	1.29
K_2O	–	–	3.49	–
Fe_2O_3	4.07	0.08	1.99	–
MgO	2.31	0.64	0.28	7.49
TiO_2	0.25	–	0.18	0.09
SO_3	3.64	–	0.12	16.60
CaO	62.92	81.13	0.04	53.24
Rb_2O	–	–	0.03	–
SrO	0.04	0.02	–	0.23
MnO	0.14	–	–	0.08
ZnO	0.13	–	–	0.02
P_2O_5	0.12	–	–	–
CuO	0.03	–	–	–
ZrO_2	0.02	–	–	–
Others	5.75	17.73	4.27	14.2

Table 2 Mixture proportion

Mixture	W/B	OPC	Limestone	Calcined Clay	Gypsum	CAgg	Sand	SP	Slump flow (mm)
OPC paste	0.4	1	–	–	–	–	–	–	280
LC^3 paste-1	0.4	1	0.6	0.3	0.1	–	–	0.012	275
OPC mortar	0.4	1	–	–	–	–	3.0	0.004	200
LC^3 mortar-1	0.4	1	0.6	0.3	0.1	–	6.0	0.03	198
OPC concrete	0.4	1	–	–	–	2.2	1.4	0.004	100
LC^3 concrete-1	0.4	1	0.6	0.3	0.1	4.4	2.8	0.03	100

*CAgg = coarse aggregates; SP is the percentage of OPC weight

concrete. The matrix had a water-to-binder ratio of 0.4. For mortar and concrete, finely graded sand and coarse aggregates with maximum size of 20 mm were used. A polycarboxylate-based superplasticizer (SP) with 30% solid content by mass was used to improve the workability of mixtures, especially for LC^3 mixtures. Before casting, the slump flow value of all the pastes and mortar mixtures was measured based on ASTM C1611 [3], while for concrete the slump measurement was based on GB 50164-92 [4]. The concrete samples were divided into two groups. The first group was demoulded after 24 h curing in a standard fog room with temperatures of 28–30 ºC and a relative humidity (RH) of >98% for 28 days, while for the second group they were cured at room temperature with the pullout test specimens until the test day. Three $100 \times 100 \times 100$ mm concrete cubes and three $50 \times 50 \times 50$ mm paste/mortar cubes were tested for each mixture according to GB/T 50081-2002 [5].

The steel rebar used was HRB 400 with the yield strength and ultimate strength of 392 and 577 MPa, respectively, based on the coupon tests.

2.2 Specimen Preparation and Test Method

The pullout test specimens were prepared to investigate the bond behavior of steel rebar embedded in the LC^3 concrete and normal concrete block. The detailed geometric information and material property of specimens are presented in Table 3. In the test, a cube size of $150 \times 150 \times 150$ mm was selected for concrete block embedded with HRB 400 rebar. The embedded length of rebar was 50 mm. Figure 1a shows the dimension of specimens, while Fig. 1b shows the test setup and instrumentations for pullout test. The pullout test was performed in a 300 kN testing machine operated in displacement-control mode. A specially designed steel frame was used to support the concrete part in the test. Steel rebar was claimed in the top grip. In this case, the load was applied from the top of the exposed steel rebar which was transferred to the concrete via the shear stress distributed along the interface between the two parts so that the rebar can deform along the path when the slippage occurred.

Table 3 Geometric information of pullout specimens

Specimen	B × D × H (mm)	d (mm)	l (mm)	Concrete type	Compressive strength (MPa)
PNC-1	150	16	50	Normal	59.0
PLC3-1	150	16	50	LC3	54.6

BxDxH = length, width and height of the concrete block; d = rebar diameter; l = embed length of rebar. The compressive strength was obtained from the cubes cured with pullout specimens

Fig. 1 Dimension of specimen (**a**) and test setup (**b**) for pullout test
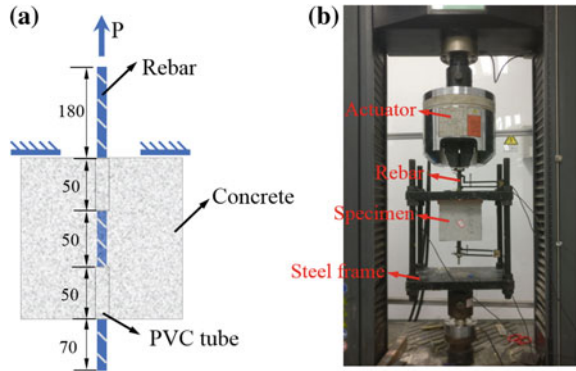
3 Results and Discussion

3.1 Compressive Strength

Figures 2 and 3 show the compressive strength of all the mixtures for different curing ages. For paste with W/B of 0.4, OPC paste had higher compressive strength compared to that of LC3 paste for all curing age. For mortar with W/B of 0.4, OPC mortar had higher early compressive strength, while the 7-day and 28-day compressive strength of LC^3 mortar both exceeded that of OPC mortar. However, for concrete series with W/B of 0.4, the compressive strength of OPC concrete always was higher than that of LC^3 concrete for different curing ages. Basically, the produced LC^3 concrete has comparable compressive strength to the normal concrete, which had sufficient structural strength.

Fig. 2 Compressive strength of cement paste and mortar for different curing ages
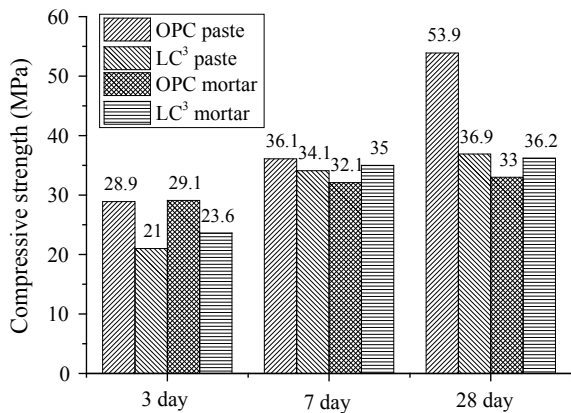
Fig. 3 Compressive strength
of concrete for different
curing ages
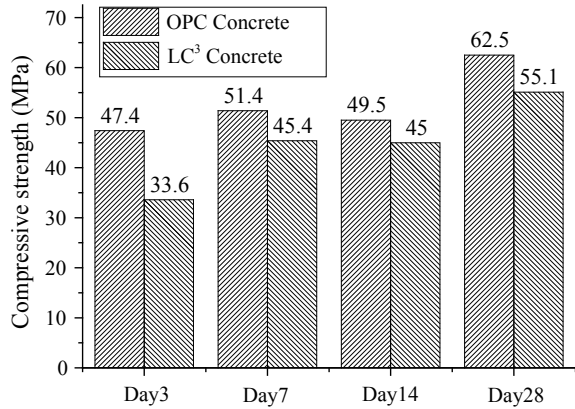
3.2 Bond-Slip Behavior

Two pullout specimens were tested to totally debonding failure of rebar–concrete interface. The slippage was approximately 8–13 mm when the test ended. Figure 4a shows the failure modes of the specimens after pullout tests. Figure 4b depicts the relation between the bond strength and slip. The maximum peak load for PLC3-1 achieved 28.7 MPa, which was approximately 16.6% lower than that of PNC-1, which was 34.4 MPa. It was corresponding to the concrete strength of PLC3-1 and PNC-1. The strain in the rebar did not yield for these two specimens. It was found that the main failure mode, namely 'debond', occurred in these two specimens. The rebars were pulled out slowly from the concrete block. No cracks or microcrack width of less than 0.1 mm were observed after the test. The secant stiffness of the bond-slip curve of PLC3-1 was higher than that of PNC-1. It may be due to the denser microstructure of LC^3 concrete than that of PNC-1 which has more macropores in

(a) failure aftertest   (b) bond-slip curves
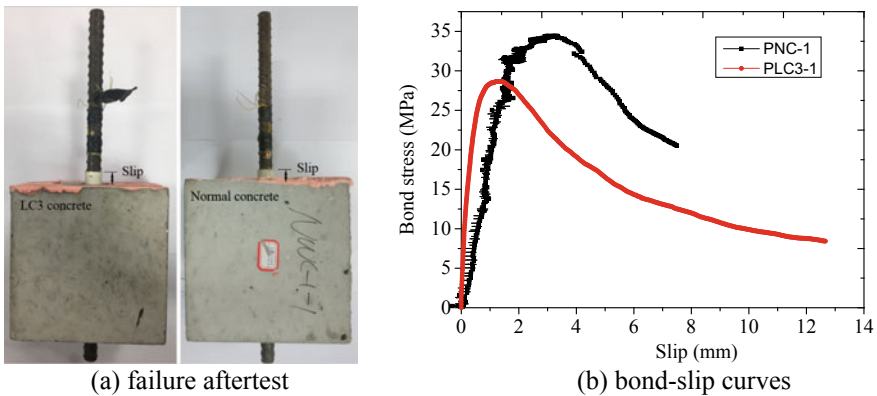
Fig. 4 Failure mode and bond-slip curves of pullout test

the concrete, showing that the rebar was easier to be pulled out from the concrete. Therefore, specimens using LC^3 concrete exhibited comparable good bond behavior compared to that using normal concrete.

4 Conclusion and Further Outlook

This paper presents the production of LC^3 concrete based on local OPC, limestone and calcined clay materials and conducts experimental investigation on the bond-slip behavior of steel rebar embedded in the concrete. The test program investigates the failure modes and bond stress-slip curve behavior of the rebar–concrete interface. The following conclusions are derived based on the investigations:

- This paper successfully produces the LC^3 concrete with 28-day compressive strength about 50 MPa under normal curing condition for structural application, which is though slightly lower than that of normal concrete using the same W/B ratio.
- The bond strength of rebar–LC^3 concrete is 16.6% lower than that of the rebar–normal concrete, but the secant stiffness of bond-slip curve is higher than normal concrete. It may be because the second hydration of using metakaolin improves the porosity of concrete, resulting in denser microstructure of the LC^3 concrete.
- The experimental program conducts the bond-slip tests on rebar embedded with LC^3 or normal concrete considering limited parameters. Further study should extend to investigate a wider range of parameters, e.g., different rebar diameter, different concrete strength, embed length to generate a more unified analytical model for bond strength prediction.

References

1. Avet, F., Snellings, R., Diaz, A.A., Haha, M.B., Scrivener, K.: Development of a new rapid, relevant and reliable (R3) test method to evaluate the pozzolanic reactivity of calcined kaolinitic clays. Cem. Concr. Res. **85**, 1–11 (2016)
2. Scrivener, Karen, Martiren, Fernando, Bishnoi, Shashank, Maity, Soumen: Calcined clay limestone cements (LC3). Cem. Concr. Res. **114**, 49–56 (2018)

3. ASTM C1611/C1611M-14: Standard test method for slump flow of self-consolidating concrete, West Conshohocken, PA, USA (2014)
4. GB 50164-92: Standard of quality control of concrete, Beijing, P.R. China (1992)
5. GB/T 50081-2002: Standard for test method of mechanical properties on ordinary concrete. Beijing, P.R. China (2002)

Evaluating the Hydration of Cement Mortar Blended with Calcined Clay Using Piezoelectric-Based Sensing Technique

Kamal Anand, Divya Aggarwal, Shweta Goyal and Naveet Kaur

Abstract This paper aims to study the possibility of using piezoelectric-based patches to characterize the hydration of cement-based mortar mix blended with calcined clay (CC). An embedded piezoelectric-based sensor is used for monitoring for the early age as well as long-term hydration of binder paste. Progressive changes in hydration of mortar were studied in terms of admittance signatures recorded over a period of 28 days. This study examines the behavior of cement mortar with CC as partial replacement of cement at various substitution levels of 4–12%. 70.6 mm mortar cubes of 1:3 (cement:sand) were cast for the study. Setting time, compressive strength and hydration of cement-based mortar mix were studied on formulated binder paste. The experimental results with 6% replacement of cement showed maximum compressive strength as compared to other mixes, and similar trend of results has been noted by electromechanical impedance (EMI) technique. Delay in setting time and approximately linearly decrease in flow value have been observed with rising the percentage of CC replacement as cement in cast mortar mixes. To study the hydration of cement mortar mixes, signatures were recorded from 0 to 28 days on the prepared cubes of 70.6 mm with different percentages of CC. To relate the EMI spectra, statistical metrics such as root mean square deviation (RMSD) has been used for all cement mortar mixes. RMSD was found to be reasonably effective in estimating the hydration in terms of compressive strength gain of cement mortar over the time.

Keywords Calcinated clay · Electro-mechanical impedance · Cement mortar · Piezo

K. Anand (✉) · D. Aggarwal · S. Goyal
Department of Civil Engineering, Thapar Institute of Engineering and Technology, Patiala 147004, India
e-mail: sayhitokamal@yahoo.co.in

N. Kaur
Bridge Engineering and Structures Division, CSIR-Central Road Research Institute (CRRI), New Delhi 147004, India

1 Introduction

With the infrastructure development globally, concrete is widely used in modern-day construction due to various reasons like cheap availability, more durability and easy to use in different civil engineering applications [1]. Monitoring real-time development is not only important to determine the mechanical properties of the structure but also important to ensure the safety of the structure [2]. During the course of chemical process, there is significant increase in stiffness and real-time monitoring of strength gain which is termed as hydration [3]. In the initial phase of hydration, cement-based material behaves like a fluid, but after a specific time frame, it starts gaining strength persistently. To monitor and symbolizing hydration of hard cementitious materials, numerous non-destructive techniques (NDTs) have been reported such as the penetrating technique, pulling-out test, surface hardness method, rebounding hammering, resonant frequency, ultrasonic pulse velocities, scanning of electron microscopy, X-ray diffraction techniques and thermal analysis [3, 4], but strength prediction methodology has some limitations too. It is often found that most of the calibration charts of the penetrating technique, the rebounding method and surface hardening method, are effective only for specific kind of cement, aggregates, moisture content and age of the sample [4]. In addition, these methods require a monotonous arrangement of the laboratory tests and cannot give ceaseless data about early age properties. All things considered, these tests containing mechanical estimation and compound investigation are not appropriate for observing in situ enormous scale concrete structure, and results are vigorously affected by the drying process and test preparation [5]. Earlier literature has analyzed the employability of lead zirconate titanate (PZT)-based EMI to examine the feasible and most significant applications for monitoring civil structures [6]. The EMI technique had been used by various researchers for structural health monitoring of reinforced concrete (RC) structure, corrosion detection, hydration of cementitious materials and so on [7]. For quality control and work scheduling, information related to beginning and ending of the hydration is extremely noteworthy. The EMI technique involves procurement of conductance and susceptance response over a frequency range, either surface bonded or embedded inside the structure which is to be monitored [8]. The EMI technique has been proven as a paramount technique which can be applied under the well-controlled environment as well as in the laboratory. Durability and repeatability are being continuously examined. To make progressively precise and compelling monitoring, various researchers are keen on creating inventive EMI techniques and developing different assessment indices. Authors presented the results of gain in compressive strength of cement paste comprising the supplementary cementitious materials (SCMs) and investigated that root mean square deviation correlated better results than CC [5]. Researchers worked on short-term monitoring of mortar while embedded the PZT patch in the cube of size 100 mm. The structural resonance peak was identified at 8 h, and it indicated the setting in the material [9]. Authors found the RMSDs plots and proved that an embedded EMI technique was sensitive for removing the formwork [10]. Shin et al. (2008) had done almost similar work

related to EMI technique [11]. Yang et al. (2010) extended the application of PZT patch by reuse for the future purpose [3]. Their results showed the initial hydration of concrete and PZT patch is bonded to be fenced in area with two bolts tightened inside the holes drilled in the enclosure and related the results of signature with RMSD value. Moreover, they found that higher sensitivity can be predicted by thicker PZTs. Authors proposed the active sensing method for monitoring the early age of hydration in which smart aggregate with waterproof layer was sandwiched between the two marble blocks [12]. For quantitative assessment of strength gain and structural health, RMSD has been demonstrated as dependable indices. To monitor the initial hydration of cement-based material, EMI has been demonstrated as an effective and accurate technique. For long-term monitoring, embedded PZT patches inside the concrete give better observing predictions rather than surface bonded. However, the literature available on strength gain of cement-based material containing CC has not been examined by EMI technique. The hydration rate of cement is changed by addition of supplementary cementitious materials (SCMs) and with different water-to-cement ratios which result in the distinctive strength gain process from that of a plain concrete [5, 9]. This present study aims to examine the possibility of using EMI technique for in situ assessment of hydration of mortar paste containing CC a well as correlates the results of setting characteristics and compressive strength with conductance signature which is acquired from the raw data (real and imaginary components) of PZT patch. The outcome of the present works can serve in the evaluation of using piezoelectric-based NDT method to study the hydration process of cement mortar.

2   Experimental Program

The experimental study was conducted on mortar specimens of cement paste materials with different mix proportions comprising ordinary Portland cement (OPC) of grade 43 and CC. Ordinary Portland cement confirming to BIS 8112-2013 was used in investigation [13]. The mortar proportion was efficiently balanced by varying CC from 4 to 10% and 12% while keeping the water content ratio as 0.47. Table 1 shows the composition of various mixes. The compressive strength of mortar paste was evaluated using the 70.6 mm cube samples. As the CC percentage is increased, the calculated proportions of cement content are decreased accordingly. A total of 96 cubes were cast, and compression strength tests were conducted at 1 day, 3 days, 7 days and 28 days. Setting time test was done to examine the quality of mortar as per IS 4031 (Part 5).

Strength and workability characteristics of 1:3 cement mortar using natural sand as fine aggregate and CC were used at various replacement levels of cement and compared. Slump test on mortar is depicted in BIS 4031 (Part 6)-1988 and conducted on different percentages of CC substitution [14]. Fine aggregate of zone II (confirming to IS 383:2016) was used with specific gravity of 2.6 and water absorption of 0.20% [15].

Table 1 Mix proportions of all cement mortar mixes

Mix designation	CC (%)	Embedded PZT patch number	Cement content (kg/m^3)	CC (kg/m^3)	Sand (kg/m^3)	Water-cement ratio
C0	0	PZT-1	479	0	1878.29	0.47
C4	4	PZT-2	460	19	1878.29	0.47
C6	6	PZT-7	450	29	1878.29	0.47
C8	8	PZT-8	441	38	1878.29	0.47
C10	10	PZT-9	431	48	1878.29	0.47
C12	12	PZT-10	422	57	1878.29	0.47

2.1 Casting of Mortar Cubes for Fixing PZT Sensors

The specimens utilized for the EMI measurements were each introduced with circular PZT sensor (procured from Central Electronics Limited, New Delhi) which had a diameter 10 mm and thickness 1 mm having properties listed in Table 3. The PZT sensors were implanted in the mortar specimen with two-part of an epoxy adhesive of Araldite. An embedded PZT-based sensor comprises of PZT patch, protective layer and lead wire for electrical connection [6]. In order to study the EMI measurements, cured electro-conductive adhesive was connected to impedance analyzer (LCR meter) by means of Kelvin clip as shown in Fig. 1. Typical measurements of electrical admittance from PZT were conducted utilizing E4980AL LCR meter of key sight at 201 discrete frequencies varying 20 Hz to 500 kHz.

The PZTs admittance (Y) was illustrated to be the inverse of the impedance [16]. Bhalla et al. [4] proposed the underneath equation for the electrical admittance of PZT patch model by presenting the concept of "effective mechanical impedance" as pursues:
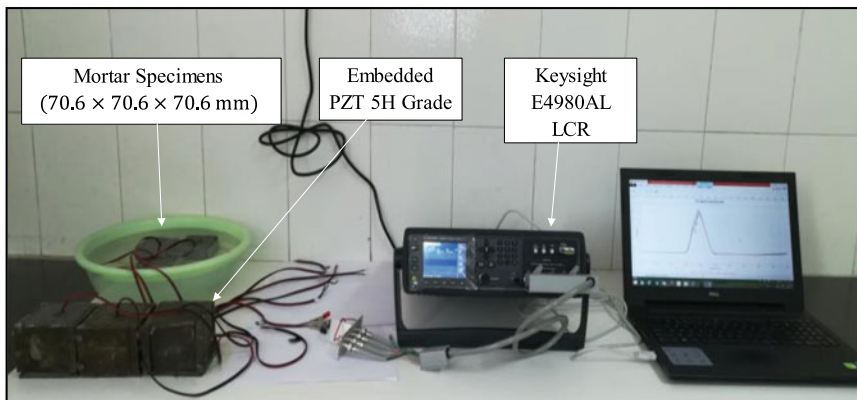
Fig. 1 Experimental setup of EMI technique

Table 2 Setting time of various mortar mixes

Mixes	Initial setting time (IST) (min.)	Final setting time (FST) (min.)	Initial time–final time (min.)	Slump (mm)
C0	85	196	111	70
C4	90	204	114	65
C6	95	210	115	60
C8	101	222	121	55
C10	105	231	126	40
C12	112	240	128	35

$$Y = G + Bj = 4W\frac{l^2}{h}\left[\varepsilon_{33} - \frac{2d_{31}^2 Y^E}{(1-v)} + \frac{2d_{31}^2 Y^E}{(1-v)}\left(\frac{Z_a}{Z_a + Z_s}\right)\frac{tankl}{kl}\right] \quad (1)$$

where Y is the electrical admittance, Y^E is Young's modulus, G is conductance, B is susceptance, j is the imaginary unit, ε_{33} is electrical permittivity, d_{31} is a piezoelectric coefficient, v is Poisson's ratio, η is mechanical loss, δ is dielectric loss, κ is the wave number, Z_a is the impedance of the PZT patch and Z_s is impedance of the structure. Therefore, impedance signature of PZT patch can be monitored and analyzed by using the above formula and simultaneously visualizing the change in properties of the specimen.

3   Results and Discussions:-

3.1   Initial and Final Setting Time Cement Mortar

Initial, final setting time and workability of various mixes of CC are given in Table 1. Due to high surface area of CC and increase in the demand of water in accordance with their interlayer absorption, it is reported that there is increase in initial and final setting time of CC mortar mixes as compared to C0 [17]. Decreasing trend of slump flow has been noticed due to increase in water demand for CC mixes [18] Table 2.

3.2   Compressive Strength of Cement Mortar

Compressive strength results of different mix proportions are shown in Fig. 2. With curing time, the strength of cement mortar is increased both for control mix as well as for different percentages of CC mortar mix due to chemical activation [19].

Maximum percentage rise is observed in compressive strength of cement mortar by 6% replacement of cement at different ages of mortar cube. At 1 day, there

Fig. 2 Results of compressive strength versus curing time of all mixes
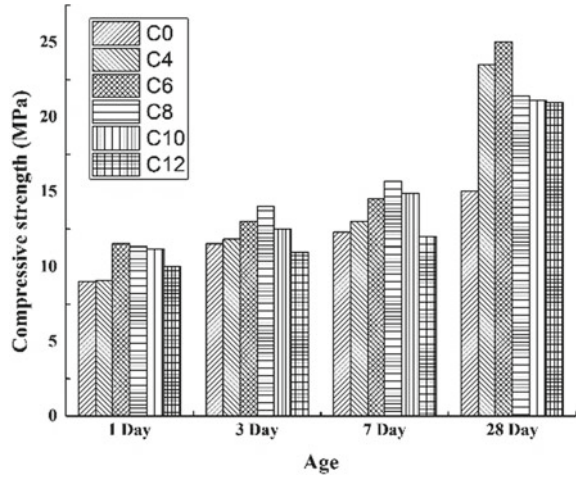
is periodical increase in strength up to 6% replacement then a decrease up to 12% replacement. Similar patterns have been observed for all other curing days. Moreover, increase in strength at all percentage levels of CC has been noticed as compared to reference mix proportion.

In short-term study, the less gain in the strength of cement mortar has been observed for all the mix proportions. Therefore, long-term study (i.e., 28 days) is more important to compare the results and for achieving the positive outcomes [18]. The drop in the strength after 6% replacement of cement by CC showed that beyond this percentage CC acts as mere filler in the mortar cube as the percentage of SiO_2 and Al_2O_3 is increased upto 6% [20].

3.3 Spectra of EMI Resonance

It is noticed that there is decrease in the conductance value after applying epoxy layer over the PZT sensor. This may be due to softening and damping effect of epoxy [20]. After analyzing the data (as shown in Fig. 3), it is observed that in initial days, maximum upward shift in first resonance peak at 4% (0 h and 3 days), but suddenly the maximum upward shift in first resonance peak at 6% (3 days, 7 days, 21 days and 28 days) due to gain in strength of mortar paste at an early age, and formation of C3S and C2S leads to upward shift in signature. Figure 6 shows the conductance signature of all PZT patches at different days. Maximum resonant peak occurred at 200 kHz and upward increase in resonant frequency over the time [6].
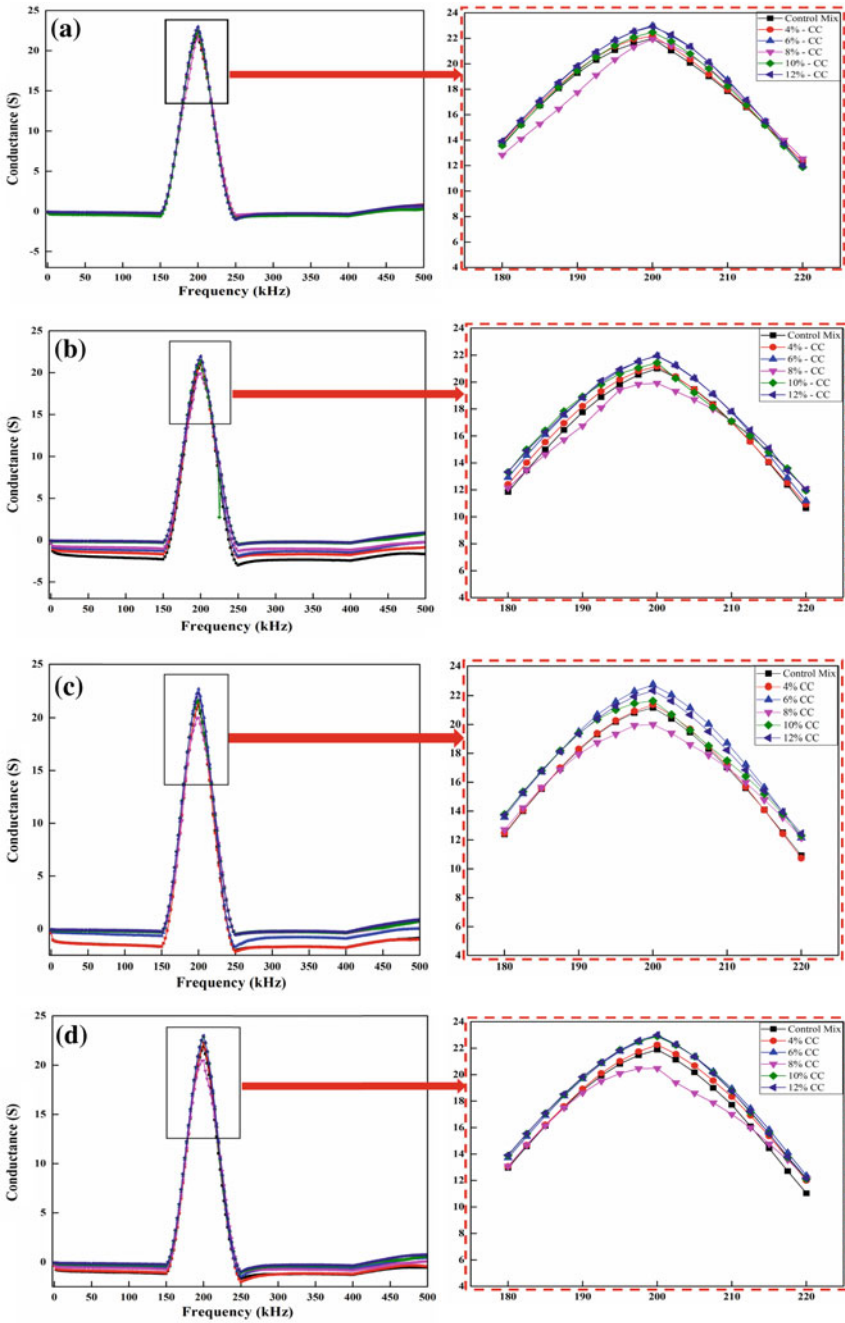
Fig. 3 EMI signatures of PZT patch at different curing ages **a** 1 day **b** 3 days **c** 7 days **d** 28 days
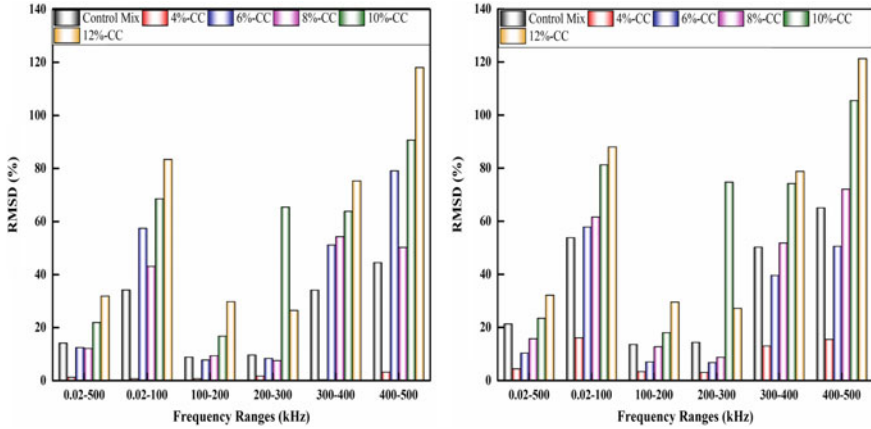
Fig. 4 RMSD plots over the different frequency ranges of **a** 7 days and **b** 28 days

Gain in strength is recognized by clear shifts in frequency over the time interval and that clearly occurred at 6%. To monitor the cement hydration, conductance signature can be successfully used. All conductance signatures show the similar trends as reported by authors [8].

The change in conductance signature can be monitored in two different intervals of time, i.e., early age of monitoring and long-term monitoring. Early age monitoring refers to the time interval between 0 h and 24 h, and long-term monitoring refers to the time interval from 1 day to 28 days.

In the first 24 h, maximum upward shift in conductance value at all the CC percentage which means that maximum hydration has done in first 24 h. Suddenly, there is reduction in conductance value at 3 days and then again proceeds toward the upward. Almost, similar resonance peak has been observed at 24 h and 28 days. As the hydration process continues and mortar cube becomes stiffer, the conductance signature gradually shifts in the rightward direction [8].

In the present study, statistical technique is utilized, i.e., RMSD, to correlate the results of hydration with PZT conductance signature. The RMSD plots over a different sub-frequency range are shown in Fig. 4 at testing ages. In control mix, there is regular increase in RMSD value with curing age. Between 0.02 and 100 kHz, the large variation in RMSD plots (C4) for monitoring the hydration process is noted. The relationship between compressive strength of various mixes cast with CC of cement mortar cubes with bonded PZT patch has approximately similar results at 28 days as shown in Fig. 3. The RMSD plots at different interval of time have been identified which is clay due to maximum rise in RMSD value at full frequency range.

4 Conclusion

This study presents the effect of rate of hydration of cement mortar with embedded PZT patch by utilizing EMI technique and depicts the gain in compressive strength through EMI technique. In initial stage of hydration, embedded PZT patch was able to commendably give the changes during early age of hydration process. In initial hours, there was a major shift in frequency toward the rightward side. In spite of that, it is very effective in long-term hydration because it shows the minimal change in frequency shifts from 7 days to 28 days. To check the reliability of EMI technique, correlate the conductance signature shifts with compressive strength test for monitoring the strength gain. Moreover, an approximately same compressive strength of cement mortar with bonded PZT patch at 28 days. It is concluded that 6% replacement of cement by CC is the optimum percentage. Shift in conductance value toward rightward side indicates the gain in stiffness in cement mortar and provides the real-time information about hydration process. The effect of initial stiffening occurred due to filling of cement pores by CC. There is retardation in initial and final setting time of various mix proportions with the addition of CC. Decrease in slump flow of cement mortar has been observed with increase in percentage of CC as compared to control mix.

References

1. Lim, Y.Y.: Monitoring of concrete hydration using electromechanical impedance technique. In: 23rd Australasian Conference on the Mechanics of Structures and Materials, pp. 1155–1160 (2014)
2. Baek, J., Na, WS.: A review of the piezoelectric electromechanical impedance based structural health monitoring technique for engineering structures. Sensors (Switzerland) **18** (2018). https://doi.org/10.3390/s18051307
3. Yang, Y., Divsholi, B.S., Soh, C.K.: A reusable PZT transducer for monitoring initial hydration and structural health of concrete. Sensors **10**, 5193–5208 (2010). https://doi.org/10.3390/s100505193
4. Bhalla, S., Soh, C.K.: Structural health monitoring by piezo–impedance transducers. II: applications. J. Aerosp. Eng. **17**, 166–175 (2004). https://doi.org/10.1061/(ASCE)0893-1321(2004)17:4(166)
5. Ghafari, E., Yuan, Y., Wu, C., Nantung, T., Lu, N.: Evaluation the compressive strength of the cement paste blended with supplementary cementitious materials using a piezoelectric-based sensor. Constr. Build. Mater. **171**, 504–510 (2018). https://doi.org/10.1016/j.conbuildmat.2018.03.165
6. Negi, P., Chakraborty, T., Kaur, N., Bhalla, S.: Investigations on effectiveness of embedded PZT patches at varying orientations for monitoring concrete hydration using EMI technique. Constr. Build. Mater. **169**, 489–498 (2018). https://doi.org/10.1016/j.conbuildmat.2018.03.006

7. Paper, C., Negi, P., Bhalla, S., Chakraborty, T.: Experimental strain sensitivity investigations on embedded PZT patches in varying orientations (2014). https://doi.org/10.1007/978-81-322-2187-6

8. Visalakshi, T., Bhalla, S., Gupta, A.: Monitoring early hydration of reinforced concrete structures using structural parameters identified by piezo sensors via electromechanical impedance technique. Mech. Syst. Signal Process. **99**, 129–141 (2018). https://doi.org/10.1016/j.ymssp.2017.05.042

9. Narayanan, A., Subramaniam, K.V.L.: Early age monitoring of cement mortar using embedded piezoelectric sensors. Health Monit. Struct. Biol. Syst. 98052W (2016). https://doi.org/10.1117/12.2219655

10. Quinn, W., Kelly, G., Barrett, J.: Development of an embedded wireless sensing system for the monitoring of concrete. (2015). https://doi.org/10.1177/1475921711430438

11. Shin, S.W., Qureshi, A.R., Lee, J.Y., Yun, C.B.: Piezoelectric sensor based nondestructive active monitoring of strength gain in concrete. Smart Mater. Struct. **17** (2008). https://doi.org/10.1088/0964-1726/17/5/055002

12. Kong, Q., Hou, S., Ji, Q., Mo, Y.L.: Very early age concrete hydration characterization monitoring using piezoceramic based smart aggregates. Smart Mater. Struct. 085025 (2013). https://doi.org/10.1088/0964-1726/22/8/085025

13. IS 8112, 2013. Ordinary Portland Cement, 43 Grade-Specification, Bureau of Indian Standards, New Delhi

14. IS: 4031 (Part 6)-1988. Methods of physical tests for hydraulic cement—determination of compressive strength of masonry cement

15. IS: 383, Coarse and Fine Aggregate for Concrete-Specification. Bureau of Indian Standards, New Delhi (2016)

16. https://doi.org/10.1177/1045389X08100384

17. Nehdi, M.L.: Clay in cement-based materials: critical overview of state-of-the-art. Constr. Build. Mater. **51**, 372–382 (2014). https://doi.org/10.1016/j.conbuildmat.2013.10.059

18. Opoku Amankwah, E.: Influence of calcined clay pozzolana on strength characteristics of portland cement concrete. Int. J. Sci. Eng. Appl. Sci. 3, 410 (2015). https://doi.org/10.11648/j.ijmsa.20140306.30

19. Mwiti, M.J., Karanja, T.J., Muthengia, W.J.: Properties of activated blended cement containing high content of calcined clay. Heliyon **4**, e00742 (2018). https://doi.org/10.1016/j.heliyon.2018.e00742

20. Kaur, K., Singh, J., Singh, D.: Determination of optimum percentage of metakoalin by compressive strength and XRD analysis. Int. J. Sci. Eng. Appl. Sci. **1**, 2395-3470 (2015). www.ijseas.com

Perspectives on Durability of Blended Systems with Calcined Clay and Limestone

Manu Santhanam, Yuvaraj Dhandapani, Ravindra Gettu and Radhakrishna Pillai

Abstract In the light of the increasing demand for cement in construction and dwindling reserves of cement-grade limestone, the blend of ground limestone and lower grade calcined clay has emerged as a potential candidate for large volume cement replacement. Studies of such ternary blended systems in paste and concrete reveal very interesting physical and chemical effects on the structure development, strength and durability performance. This paper describes the results of durability studies conducted at IIT Madras on concretes prepared with limestone calcined clay Cement, in comparison with ordinary Portland cement and fly ash-based cement. The focus of the study was to delineate the chemical and physical effects caused by the binder composition on durability indicators for chloride-induced corrosion. The experimental strategy involved the assessment of the pore structure evolution and electrical properties on cementitious pastes, along with measurement of the durability parameters based on moisture absorption, chloride migration and diffusion. The results from the study reveal the complex interplay of the various factors that lead to improved performance of the blended cementitious systems. The synergistic interactions of the blend of calcined clay and limestone impact the physical structure positively at early ages as opposed to fly ash systems, which require prolonged curing to realize their potential.

Keywords Calcined clay · Limestone · Ternary blends · Microstructure · Formation factor

1 Introduction

It is widely accepted that the path forward for the production of sustainable concrete involves the reduction of the clinker factor in the binder, which is made possible by the use of suitable alternative or supplementary cementitious materials (SCMs) [1, 2]. With the low availability of good quality fly ash and slag and the uncertainty of tapping

M. Santhanam (✉) · Y. Dhandapani · R. Gettu · R. Pillai
Department of Civil Engineering, IIT Madras, Chennai, India

into the natural pozzolan sources, calcined clay has emerged as the most promising alternative for the extender in blended cements [3, 4]. Another development over the last 15 years or so has been increased by the use of ground limestone as an additive in the binder, either up to 5% as a performance improver or up to 15% in Portland limestone cement (PLC) formulations [5, 6]. More recent literature has indicated the synergistic effects of using limestone in combination with other SCMs as part of a ternary binder system with Portland cement [7–10].

A major international collaborative project between leading universities such as EPFL (Switzerland), UCLV (Cuba), IITs Delhi, Bombay and Madras (India) in partnership with an Indian non-governmental organization called development alternatives has resulted in a systematic scientific study this type of binder, termed as limestone calcined clay cement (LC 3), which has contributed vastly to the development of such binders [11].

The studies on hydration, microstructure and concrete performance with LC 3 binder systems have led to significant insights into the structure–property relationships. The aim of the current paper is to throw light on the understanding of pore structure and durability of concrete with ternary binder systems involving limestone and calcined clay. The paper mainly relies on the results already published in [12–14], in conjunction with some new studies.

2   Materials and Methods

Ordinary Portland cement (OPC) of 53 grade conforming to IS 269, type F fly ash from North Chennai, and limestone calcined clay cement (LC 3) from an industrial production (reported in [15, 16]) were used as the binders in this study in Phase 1. The fly ash and cement were blended together in the ratio of 30:70 to produce the binder termed as FA30. The complete description of material characteristics is provided in Dhandapani and Santhanam [12]. In an extension of some of the investigations (Phase 2), calcined clay from Bhuj, Gujarat (with 50–60% kaolinite content) and limestone from a cement plant in Ariyalur (with CaO content of 42%) were used to produce the ternary blended systems, with the formulations indicated in Table 1. Gypsum amount was adjusted for the calcined clay—admixed binder to ensure that the aluminate peak was pushed beyond the main silicate hydration peak based on isothermal calorimetry profiles.

A major part of this paper reports the results of three types of concrete produced with the three binder systems: (i) concrete of grade M30 (i.e. characteristic compressive strength of 30 MPa), (ii) concrete of grade M50 (i.e. characteristic compressive strength of 50 MPa) and (iii) concrete with binder content of 360 kg/m^3 and w/b of 0.45 (designated as C-mix). A second investigation reports the results of binary and ternary blended mixtures with the binders indicated in Table 1. In all these mixes, the binder content and w/b were maintained at 360 kg/m^3 and 0.45, respectively.

For all concrete mixes, the coarse aggregate was crushed granite with a maximum size of 20 mm, and fine aggregate was well-graded river sand. The coarse to fine

Table 1 Binder systems investigated in the study

	SMC type	Mix id	OPC (Clinker) (%)	SCM (%)	Limestone[a] (%)	Gypsum (%)
Phase 1	OPC	OPC	100	–	–	–
	FA30	FA30	70	30	–	–
	LC 3	LC 3	50	31	15	4
Phase 2	OPC	OPC	100	–	–	–
	Class F	FAF30	66	30	3.5	0.5
		FAF42	55	42	3	0.5
		FAFL10	55	34	10.5	0.5
		FAFL15	54.5	30	15	0.5
		FAFL20	54.5	25	20	0.5
	Calcined clay	CC30	65.0	30	3.5	1.5
		CC42	53.5	42	3	1.5
		CCL10	53.5	34	10.5	1.5
		CCL15	53.5	30	15	1.5
		CCL20	53.5	25	20	1.5

Note [a]inclusive of limestone contributed from 5% calcite present in OPC

aggregate ratio was maintained at 60:40 by weight, and a polycarboxylic ether (PCE)-based superplasticizer was used to obtain a slump of 80–120 mm.

3 Results

3.1 Mechanical Properties

Figure 1 presents the evolution of compressive strength for the concrete mixes. Figure 1a shows the results from Phase 1 [13], while Fig. 1b shows the results from Phase 2. It is evident from Fig. 1a that the rates of strength development of LC 3 concrete are similar to OPC concrete and significantly higher than FA30 concrete (which needs extended curing to achieve similar ultimate strengths). On the other hand, the Phase 2 results in Fig. 1b indicate that it is possible to produce concrete strengths with calcined clay–limestone combinations on par with OPC strengths, when the calcined clay is at 30% replacement level, and limestone is used up to 15% replacement level. Even in CCL20 with limestone substitution of 20%, there is a steady development of strength up to 180 days. In CC42, with 42% binary substitution of calcined clay, there was stagnation in the strength development beyond 28 days as cementitious matrix could have possibly reached a portlandite-deficient state at higher substitution levels of calcined clay.
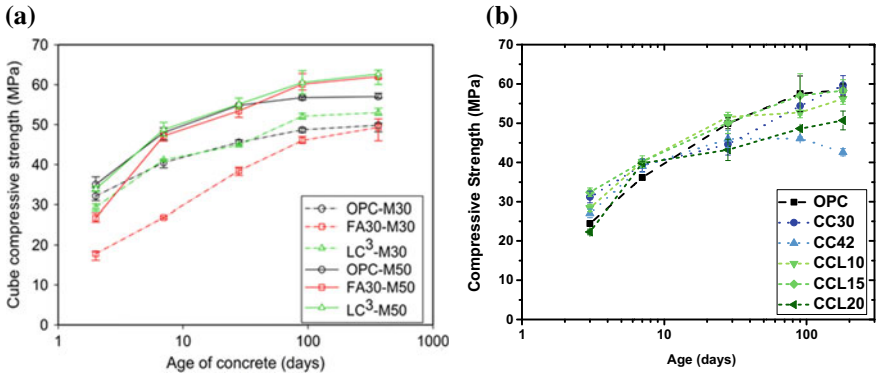
Fig. 1 Results for compressive strength evolution: **a** comparison of strength evolution from Phase 1 concrete made with OPC, FA30 and LC 3 and **b** influence of calcined clay-limestone ratio on strength development of LC 3 concrete from Phase 2 studies

3.2 Durability Characteristics

The detailed results of durability tests from the Phase 1 study are presented in Dhandapani et al. [13]. For the purpose of this discussion, the formation factor is computed as a means of assessing the influence of the pore structure development on the durability results. The concept of formation factor has been extensively explored in [17–19]. In simple terms, the formation factor is the ratio of the conductivity of the pore solution to the effective conductivity of the bulk concrete. The use of formation factor helps in understanding the influence of pore structure (volume and connectivity) on durability, without the concomitant effects of the pore solution conductivity.

The variation of formation factor with age for the Phase 1 mixes are presented in Fig. 2a based on Dhandapani and Santhanam [12]. The result clearly shows that pore tortuosity (or disconnectedness), as represented by the formation factor, rapidly
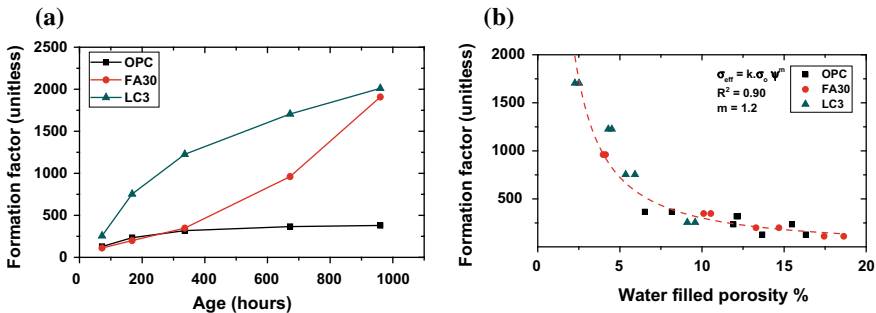
Fig. 2 **a** Change in formation factor with curing age for the Phase 1 'C-mix' concretes, **b** exploring relationships between formation factor and durability (in terms of water-filled porosity) for all Phase 1 from [12]

increases for LC 3 concretes. In the case of FA30, extended curing is essential to get the same level of increase in formation factor. The OPC concrete, on the other hand, does not show much increase in formation factor beyond 7 days. From the same paper, the results of the relationship between formation factor and the water-filled porosity (as determined by vacuum saturated process on thin slices of cement paste) are presented in Fig. 2a. The plot in Fig. 2b clearly indicates that the formation factor can be a unifying approach to compare the structure development and durability characteristics across cementitious systems with different binder chemistry.

The results of the non-steady state chloride migration coefficient (as determined from the NT BUILD 492 test [20]), plotted against formation factor, are presented in Fig. 3. Migration coefficient and formation factor were measured over different curing ages up to 1 year. Migration coefficient is a reliable test for chloride penetrability than ASTM C1202 as the estimate is based on depth of penetration of chloride and also the parameter has found acceptability in performance-based design approaches for service life estimates as suggested in fib 34 [21]. The influence of the binder type is clearly evident, with the results from the LC 3 concretes showing a much lower migration coefficient and higher formation factor as compared to FA30, which in turn shows a significantly better result than OPC. At the equivalent formation factor, concretes made with different mixture proportion and binder chemistry have similar chloride penetration resistance. This confirms the generic adoption of formation factor as a representative microstructure-based factor which can be related to durability characteristics across different binder chemistry by deconvoluting the impact of pore structure and pore solution from the bulk electrical response.

The results for secondary rate of water absorption from ASTM C1585 [22] also indicate a superior performance for the LC 3 concretes (results in Fig. 4 presented here are for the C-mix). In other words, the superlative performance of LC 3 is evident not just in migration-based experiments, but also in direct moisture movement by a measure of absorption rate in unsaturated concrete.

Fig. 3 Non-steady state migration coefficient expressed against the formation factor
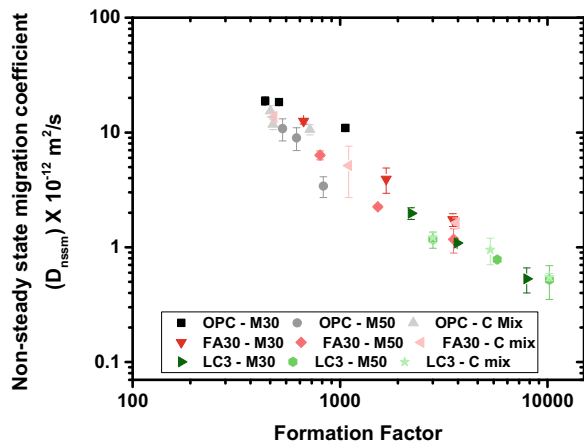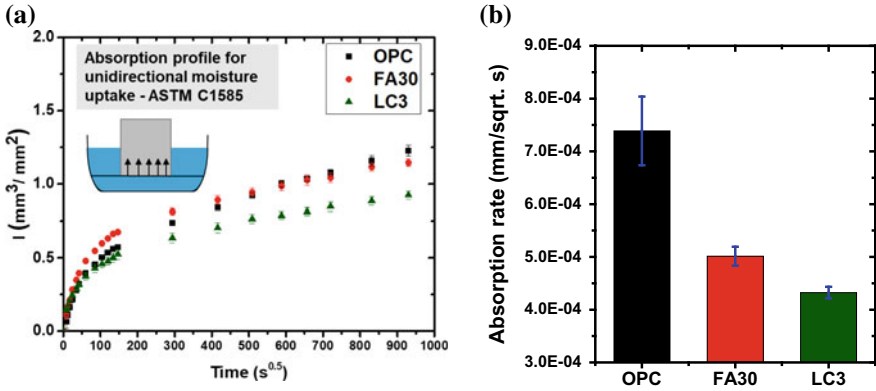
Fig. 4 Results of the sorptivity test as per ASTM C1585

It is clearly shown by the published works of Dhandapani and Santhanam [12] and Avet and Scrivener [23] that this edge in performance comes from the rapid development of a disconnected pore structure in the LC 3 systems. An evidence of this phenomenon is presented in Fig. 5 from [12], where the results clearly indicate the shift in pores towards finer sizes as early as 7 days for the LC 3 systems. The results presented are for pastes with 0.35 w/b. These trends seem to indicate that LC 3 systems would not be significantly affected by the curing duration, with respect to the development of the durability characteristics. Indeed, it was confirmed with the result in Fig. 6 for the C-mix, which shows that LC 3 concretes had a very low non-steady state chloride migration coefficient irrespective of the moist curing duration (varied between 3 and 28 days). The OPC concretes also did not show a major dependence on curing duration, but their performance was significantly lower than LC 3 concretes. On the other hand, fly ash concrete showed a clear dependence on the age of curing.
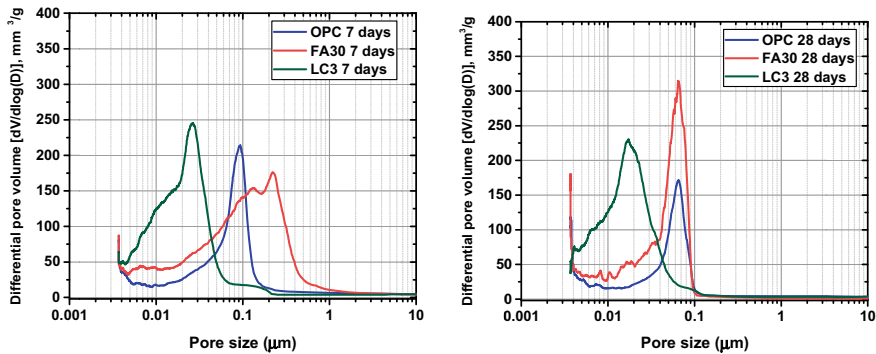
Fig. 5 Pore size distribution from mercury intrusion porosimetry, as presented in Dhandapani and Santhanam [12]

Fig. 6 Influence of curing age on durability properties
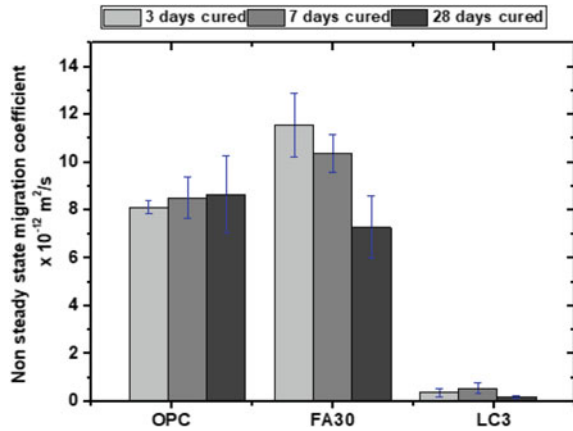
4 Discussion—Impact on Chloride-Induced Corrosion

The results in the preceding section give every reason to believe that the performance of LC 3 concretes is expected to be superior in chloride environments. However, this aspect is also affected to some extent by the binder composition. Literature indicates that the chloride threshold is lowered in blended binder systems [24, 25]. Indeed, results from the study conducted in the IIT Madras project (reported in Pillai et al. [14]) also indicate the same, as seen in Fig. 7a. The determination of the chloride threshold was as per the method suggested by Rengaraju et al. [26]. Pillai et al. [14] used the chloride threshold data along with the transport characteristics (chloride diffusion coefficient) reported in Dhandapani et al. [13]—shown in Fig. 7b—to predict the service life with respect to chloride-induced corrosion as per the probabilistic modelling approach suggested by LIFE-365. The results of the analysis shown in Fig. 8 indicate that despite the lower chloride threshold, the service life of LC 3
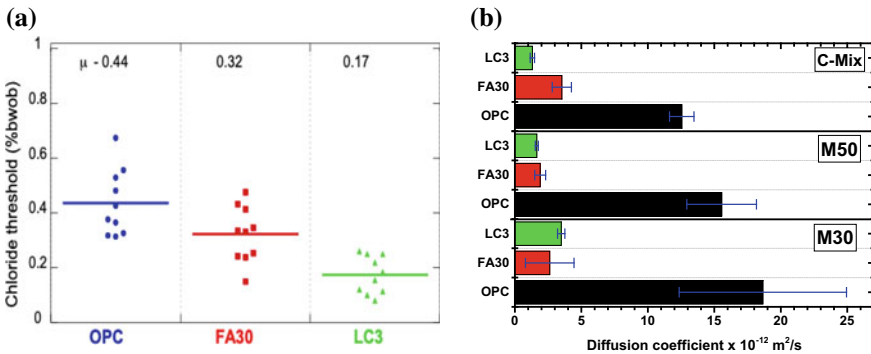
Fig. 7 **a** Chloride threshold values for the different binder systems and **b** comparison of chloride diffusion coefficients for all mixes from Phase 1

Fig. 8 Comparison of
service life calculations for
the concretes with the three
binder systems as presented
in [14]
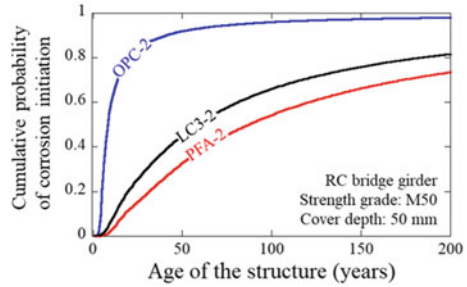
concretes is on par with FA30, and much superior to OPC systems in a chloride
environment.

The chloride corrosion performance was also directly assessed using the accelerated corrosion cracking test, based on the method suggested by FM 5-522 [27].
The results presented in Fig. 9 for M50 concrete clearly show that the concrete with
LC 3 does not crack at all in the test, despite a long time of 500 h. This could be
partially attributed to the extremely high resistivity of LC 3 concretes—an order of
magnitude higher than for OPC and significantly higher than FA30, as seen in the
results presented in Fig. 10.

The higher resistivity of LC 3 concretes is also expected to play a major role in the
slowing down of corrosion propagation—post initiation. Current work at IIT Madras
looks at the role of the CSH chemistry in addition to the pore structure characteristics
with respect to the development of resistivity.
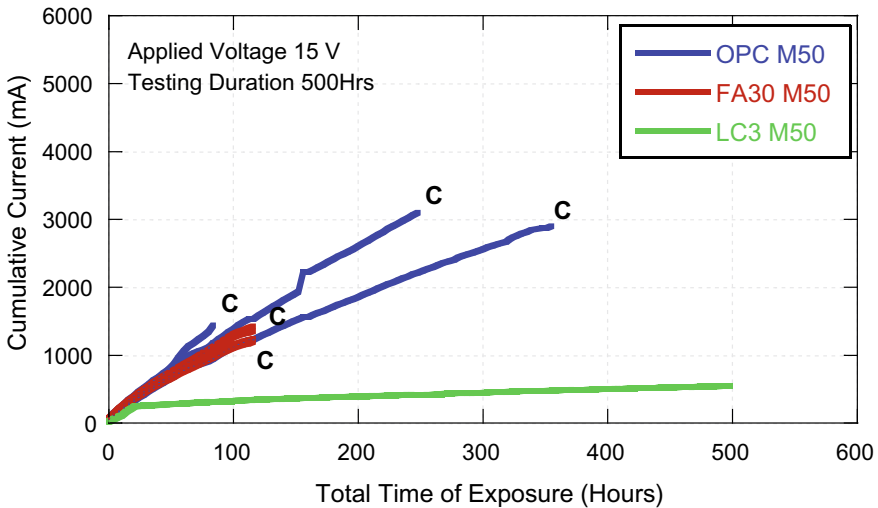
Fig. 9 Results of the accelerated corrosion cracking test

Fig. 10 Surface resistivity of concretes measured using Wenner 4-probe test [13]
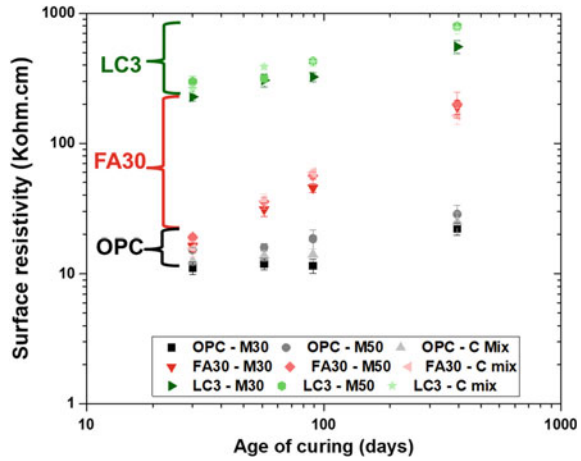
5 Synergy of Limestone Calcined Clay Binder Systems

The concretes from Phase 2 are used to determine compositional robustness of the calcined clay binders and to investigate the influence of limestone—calcined clay ratio on the resistivity development of concretes. Figure 11 shows the change in resistivity of concretes with fly ash and calcined clay (as binary binders with cement, as well as ternary binder with limestone). In order to evaluate the synergistic performance from limestone addition in conjunction with a particular SCM, the resistivity value of the concretes including L10, L15, L20 and SCM42 were normalized with the resistivity of their corresponding 30% binary mixes (i.e. FAF30 and CC30) at the respective age. This was done to assess the influence of increasing SCM or limestone or a combination of limestone-SCM as substituent in place of clinker. For instance, the value of SCM42 indicates the change in resistivity at a given age with increasing substitution of calcined clay or fly ash (SCM42) from 30 to 42%. Similarly, L10,
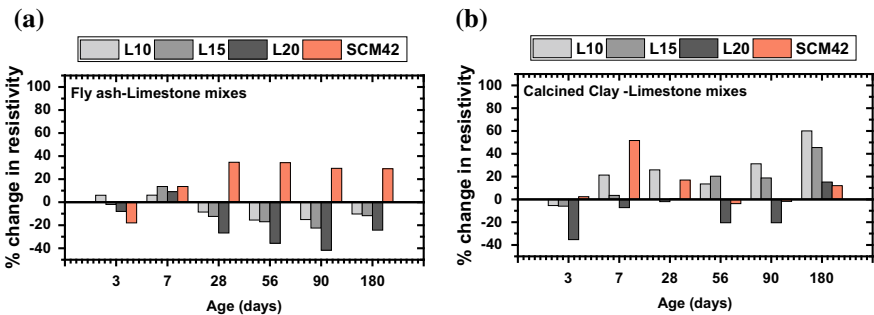
Fig. 11 Resistivity development for fly ash and calcined clay concretes in combination with limestone

L15 and L20 indicate the change in the resistivity with respect to limestone addition at the expense of clinker and/or SCM.

It is evident from Fig. 11a that increase in fly ash dosage positively improves resistivity beyond 7 days. However, limestone addition along with fly ash reduces resistivity indicating a more porous structure in comparison with FAF30 at corresponding ages with an exception at 7 days. This can be due to early interaction of limestone which is seen to show beneficial effect at 7 days at the expense of clinker. However, lower reactivity of fly ash cannot mask the dilution of hydrates due to limestone addition. On the contrary, Fig. 11b show the positive influence of calcined clay-limestone combination on the resistivity development compared to binary calcined clay concretes. At 180 days, all calcined clay-limestone combinations had higher resistivity than binary calcined clay binders (i.e. CC30 and CC42). CCL10 with 10% limestone addition had shown nearly 20% higher resistivity at 7 days and the performance extends to nearly 50% increase at 180 days. The resistivity development clearly points out to a distinct synergy in the performance characteristics of limestone calcined clay combination as cement replacement.

6　Conclusions

The durability performance of concrete with ternary binder systems prepared with combinations of cement and limestone along with fly ash or calcined clay was explored in this paper. Results from the study clearly indicate the superior durability performance—with respect to chloride-induced corrosion—of limestone—calcined clay combinations as cement replacement. The ternary system with cement-limestone-calcined clay offers an excellent alternative cement for the future.

References

1. Schneider, M., Romer, M., Tschudin, M., Bolio, H.: Sustainable cement production—present and future. Cem. Concr. Res. **41**, 642–650 (2011). https://doi.org/10.1016/j.cemconres.2011.03.019
2. Scrivener, K.L., John, V.M., Gartner, E.M.: Eco-efficient cements: Potential, economically viable solutions for a low-CO_2, cement-based materials industry (2016)
3. Scrivener, K.L.: Options for the future of cements. Indian Concr. J. **88**, 11–21 (2014)
4. Fernandez, R., Martirena, F., Scrivener, K.L.: The origin of the pozzolanic activity of calcined clay minerals: a comparison between kaolinite, illite and montmorillonite. Cem. Concr. Res. **41**, 113–122 (2011). https://doi.org/10.1016/j.cemconres.2010.09.013
5. Tennis, P.D., Thomas, M.D.A., Weiss, W.J.: State-of-the-art report on use of limestone in cements at levels of up to 15%. Portl. Cem. Assoc. 1–78 (2011)
6. Hooton, R.D., Nokken, M., Thomas, M.D.A.: Portland-limestone cement : state of the art report and gap analysis for CSA A 3000. Cem. Assoc. Canada. 0–59 (2007)
7. Men, G., Bonavetti, V., Irassar, E.F., Menéndez, G., Bonavetti, V., Irassar, E.F., Men, G., Bonavetti, V., Irassar, E.F.: Strength development of ternary blended cement with limestone

filler and blast-furnace slag. Cem. Concr. Compos. **25**, 61–67 (2003). https://doi.org/10.1016/S0958-9465(01)00056-7

8. De Weerdt, K., Ben Haha, M., Le Saout, G., Kjellsen, K.O.O., Justnes, H., Lothenbach, B.: Hydration mechanisms of ternary Portland cements containing limestone powder and fly ash. Cem. Concr. Res. **41**, 279–291 (2011). https://doi.org/10.1016/j.cemconres.2010.11.014

9. Antoni, M., Rossen, J., Martirena, F., Scrivener, K.: Cement substitution by a combination of metakaolin and limestone. Cem. Concr. Res. **42**, 1579–1589 (2012)

10. Vance, K., Aguayo, M., Oey, T., Sant, G., Neithalath, N.: Hydration and strength development in ternary portland cement blends containing limestone and fly ash or metakaolin. Cem. Concr. Compos. **39**, 93–103 (2013). https://doi.org/10.1016/j.cemconcomp.2013.03.028

11. Scrivener, K., Martirena, F., Bishnoi, S., Maity, S.: Calcined clay limestone cements (LC3). Cem. Concr. Res. 1–22 (2017). https://doi.org/10.1016/j.cemconres.2017.08.017

12. Dhandapani, Y., Santhanam, M.: Assessment of pore structure evolution in the limestone calcined clay cementitious system and its implications for performance. Cem. Concr. Compos. **84**, 36–47 (2017). https://doi.org/10.1016/j.cemconcomp.2017.08.012

13. Dhandapani, Y., Sakthivel, T., Santhanam, M., Gettu, R., Pillai, R.G.: Mechanical properties and durability performance of concretes with limestone calcined clay cement (LC3). Cem. Concr. Res. **107**, 136–151 (2018). https://doi.org/10.1016/j.cemconres.2018.02.005

14. Pillai, R.G., Gettu, R., Santhanam, M., Rengaraju, S., Dhandapani, Y., Rathnarajan, S., Basavaraj, A.S.: Service life and life cycle assessment of reinforced concrete systems with limestone calcined clay cement (LC3). Cem. Concr. Res. 1–9 (2018). https://doi.org/10.1016/j.cemconres.2018.11.019

15. Bishnoi, S., Maity, S., Amit, M., Joseph, S., Krishnan, S.: Pilot scale manufacture of limestone calcined clay cement: the Indian experience. Indian Concr. J. **88**, 22–28 (2014)

16. Emmanuel, A.C., Haldar, P., Bishnoi, S., Maity, S., Bishnoi, S., Shashank, Maity, Maity, S., Bishnoi, S., Maity, S.: Second pilot production of limestone calcined clay cement (LC 3) in India: the experience. Indian Concr. J. **90**, 57–64 (2016)

17. Archie, G.E.: The electrical resistivity log as an aid in determining some reservoir characteristics. Trans. AIME. **146**, 54–62 (1942). https://doi.org/10.2118/942054-G

18. Snyder, K.A., Feng, X., Keen, B.D., Mason, T.O.: Estimating the electrical conductivity of cement paste pore solutions from OH−, K+ and Na+ concentrations. Cem. Concr. Res. **33**, 793–798 (2003). https://doi.org/10.1016/S0008-8846(02)01068-2

19. Nokken, M.R., Hooton, R.D.: Using pore parameters to estimate permeability or conductivity of concrete. Mater. Struct. **41**, 1–16 (2007)

20. NT Build 492: Concrete, mortar and cement-based repair materials: chloride migration coefficient from non-steady-state migration experiments. NordTest, 1–8 (1999)

21. International Federation for Structural Concrete, MC-SLD: Model Code for Service Life Design (2006)

22. ASTM C1585–13: American society for testing and materials—ASTM, ASTM C1585-13, C1585-13, standard test method for measurement of rate of absorption of water by hydraulic-cement concretes. ASTM Int. **41**, 1–6 (2013). https://doi.org/10.1520/c1585-13.2

23. Avet, F., Scrivener, K.: Investigation of the calcined kaolinite content on the hydration of limestone calcined clay cement (LC 3). Cem. Concr. Res. **107**, 124–135 (2018)

24. Lollini, F., Redaelli, E., Bertolini, L.: Investigation on the effect of supplementary cementitious materials on the critical chloride threshold of steel in concrete. Mater. Struct. **49**, 4147–4165 (2016). https://doi.org/10.1617/s11527-015-0778-0

25. Azad, V.J., Suraneni, P., Trejo, D., Jason Weiss, W., Burkan Isgor, O.: Thermodynamic investigation of allowable admixed chloride limits in concrete. ACI Mater J **115**, 727–738 (2018). https://doi.org/10.14359/51702349

26. Rengaraju, S., Neelakantan, L., Pillai, R.G.: Investigation on the polarization resistance of steel embedded in highly resistive cementitious systems—an attempt and challenges. Electrochim. Acta **308**, 131–141 (2019). https://doi.org/10.1016/j.electacta.2019.03.200

27. F. 5-522: Florida Method of Test for An accelerated Laboratory Method for Corrosion Testing of Reinforced Concrete Using Impresse.pdf, 1–6 (2000)

Tortuosity as a Key Parameter of Chloride Diffusion in LC³ Systems

**William Wilson, Julien Nicolas Gonthier, Fabien Georget
and Karen Scrivener**

Abstract In the context of climate changes, limestone calcined clay cement (LC³) represents a very promising alternative to ordinary Portland cement (OPC), not only to reduce by up to 30% the CO_2 emissions but also to dramatically increase service life. Notably, the resistance to chloride ingress is significantly higher in LC³ systems, although understanding and quantifying the mechanisms responsible remain a challenge. In this study, the effect of porosity on chloride diffusion was investigated by comparing at water-to-binder ratios w/b = 0.3–0.5, OPC pastes and LC³-50 pastes (50% clinker, 30% calcined clay, 15% limestone and 5% gypsum). Chloride diffusion was measured using a mini-migration test developed for paste samples. The microstructure was further characterized in terms of porosity and diffusion tortuosity as obtained from the formation factor. The results showed how increasing the tortuosity of the porous network (by changing the binder type) led to a higher reduction of the chloride diffusion coefficient compared to decreasing the total porosity with lower water-to-binder ratios. These results strengthened the importance of the tortuosity as one of the key microstructure features to explain and model the chloride diffusion in alternative cementitious systems (along with the chloride binding and the composition of the pore solution).

1 Introduction

Building a sustainable future requires sustainable construction materials such as concrete made of limestone calcined clay cement (LC³), which enables both significant reduction in embodied CO_2 and significant increase of service life (compared to conventional ordinary Portland cement [OPC]). Notably, previous studies have shown

W. Wilson (✉) · J. N. Gonthier · F. Georget · K. Scrivener
École Polytechnique fédérale de Lausanne (EPFL), Lausanne, VD, Switzerland
e-mail: william.wilson@epfl.ch

the very high resistance to chloride ingress of LC^3 systems [1, 2], and this improvement of properties was related to the combined effects of porosity, chloride binding and pore solution composition.

The latter is particularly important when using electricity-accelerated tests measuring chloride penetration potential (in terms of charge passed, resistivity, migration current, etc.) as the conductivity of the pore solution will affect the results and may vary significantly in blended systems, by factors up to 2–4 [3]. Thus, the diffusion tortuosity obtained from the formation factor (initially developed for diffusion in rocks, [4]) may represent a better indicator for chloride ingress resistance as it takes into account the conductivity of the pore solution [5, 6]. However, estimating service life requires a chloride diffusion coefficient, which may be obtained in a more straightforward way by measuring chloride flow or profiles of chloride ingress (e.g. [7, 8]).

In this study, chloride diffusion was measured on LC^3 and OPC systems at different water-to-binder ratios (w/b = 0.3, 0.4 and 0.5) using a mini-migration test adapted for paste samples. The study further aimed to understand the mechanisms responsible for the high resistance to chloride ingress of LC^3 systems; thus, the samples were also characterized with respect to their porosity and diffusion tortuosity.

2   Materials and Methods

With the objective to limit variables and enable direct comparison between complementary analyses, the experimental set-ups and procedures were adapted to analyse the same paste samples after 28-day curing in pore solution. The materials and sample preparation are described below along with the experimental approaches employed—the mini-migration test and the characterization of porosity using the formation factor.

2.1   Materials and Sample Preparation

The raw materials employed in this study include an industrial cement CEM I 42.5, an Indian calcined clay containing 45% calcined kaolinite, fine limestone powder and gypsum of chemical grade.

The first series of OPC systems was prepared by mixing cement with variable amounts of distilled water to obtain water-to-binder ratios of 0.3, 0.4 and 0.5, by mass. The second series of LC^3-50 systems was prepared by mixing 53% cement with 30% calcined clay, 15% limestone and 2% gypsum at the same water-to-binder ratios. To ensure homogeneity of the pastes, LC^3-50 powders were pre-homogenized with a paint mixer for 10 min before beginning the paste mixing procedure.

The pastes were mixed for 2 min in a high-shear mixer at 1600 RPM followed by 1 min of vacuum mixing at 450 RPM to remove entrapped air and obtain a

homogeneous consistency. A polycarboxylate-based superplasticizer was employed to obtain similar workability for all mixes. The mixtures were then carefully cast in cylindrical polypropylene moulds of 33 mm diameter with a funnel to avoid entrapping air bubbles. The moulds were sealed for the first 24 h of curing before demoulding. The samples were then transferred into slightly larger containers for 28 days of water curing in minimal amount of water. To further avoid any leaching, an additional specimen was cast and finely ground for each series; this powder was then added to each curing container to act as a leaching buffer protecting the sample.

2.2 Mini-migration Test for Cement Pastes

The mini-migration set-up employed for this investigation was developed using the same principles as the chloride migration set-up developed by Marchand et al. [9]. As illustrated in Fig. 1, the main difference is the size of the set-up which was designed about 30 times smaller for the investigation of cement paste discs of 33 mm diameter by 10 mm thickness (similarly as in [10]).

After coating the sides of the sample with silicon and fixing it to the set-up, the downstream reservoir was filled with 0.3 M NaOH solution (to limit leaching of alkalis during the test) and the upstream reservoir with a solution of 0.5 M NaCl and 0.3 M NaOH. The chlorides were then forced through the sample with an electrical potential provided by the power supply, while the migration current was measured during the test with a data logger. In order to optimize the signal and the length of the test, the voltage was adjusted to obtain an initial current between 10 and 20 mA.

To follow the migration of chloride through the sample, the downstream reservoir was sampled each 2–4 days and the chloride content was titrated using a TitroLine® 5000 automatic titrator with a 0.05 M $AgNO_3$ solution. When reaching a constant migration regime, these periodic measurements were used to estimate the flux J_{down} [mol/m^2/s]:

Fig. 1 The mini-migration set-up: the cement paste disc (33 mm diameter and 10 mm thickness) is placed between the upstream and downstream reservoirs in which electrodes provide a potential difference forcing the migration of chloride through the sample

$$J_{\text{down}} = \frac{1}{S} \frac{\dot{m}_{\text{Cl}^-}}{M_{W,\text{Cl}^-}} \qquad (1)$$

where S is the surface area of the sample [m^2], $\dot{m}_{\text{Cl}^-}$ is the chloride mass rate [g/s], and M_{W,Cl^-} is the chlorine molar mass [g/mol]. The effective diffusion coefficient D_{eff} was then calculated from the electrically-accelerated migration results using a simplified Nernst–Plank equation [7, 11]. By assuming a constant electrical field across the sample, the saturation of the paste, and a concentration equal to the activity of chlorides, the equation could be simplified into

$$D_{\text{eff}} = \frac{1}{c_{\text{up}}} \frac{RT}{F} \frac{J_{\text{down}}}{E} \qquad (2)$$

where c_{up} is the upstream cell concentration [mol/m^3], E is the electrical field through the sample [V/m], T is the temperature [K], R is the gas constant [J/mol/K], and F is Faraday's constant [J/V/mol].

2.3 Characterization of Porosity with the Formation Factor

The total porosity ϕ was first estimated in terms of free-water relative volume. Slices of saturated-surface-dry samples were weighted and their dimensions precisely measured. Free-water was removed by freeze-drying, and the dried samples were finally reweighted. The diffusion tortuosity τ_D of the porous network was then estimated based on the following definition of the formation factor:

$$F = \frac{\rho_b}{\rho_0} = \rho_b \sigma_0 = \frac{\tau_D}{\phi} \qquad (3)$$

where ρ_b is the bulk resistivity (Ω m), ρ_0 is the pore solution resistivity (Ω m), and σ_0 is the pore solution conductivity (Ω^{-1} m^{-1}). The bulk resistivity of the pastes was directly measured with a Giatec RCON^2 instrument on cylindrical specimens of 33 mm diameter by ~50 mm length. Pore solutions were extracted using an experimental set-up similar to that proposed by Barneyback and Diamond [12] and the conductivity of these solutions was directly measured with a METTLER TOLEDO conductivity probe.

3 Results and Discussion

3.1 Chloride Diffusion Coefficients

Figure 2 shows a typical evolution of the chloride mass in the downstream reservoir as a function of time (shown here for the OPC system at w/b = 0.4). After an initial delay t_0, a constant migration regime was reached and the chloride mass in the downstream reservoir increased at a constant rate $\dot{m}_{Cl^-}$. The time lag t_0 represents the breakthrough time, i.e. the time needed for chloride ions to migrate into the whole thickness of the sample. The chloride mass rate $\dot{m}_{Cl^-}$ was used to calculate the effective chloride diffusion coefficient D_{eff} with Eqs. (1) and (2).

The calculated D_{eff} for both OPC and LC³-50 systems is shown in Fig. 3. For each type of binders, D_{eff} decreases with a decrease of the water-to-binder ratios (i.e. as expected with an increase of the density of the cement paste matrix). However, changing the type of binder from OPC to LC³-50 had a much higher impact, with fivefold to tenfold reductions of D_{eff} for the same water-to-binder ratio. These impressive results indicate the potential of using LC³-50 for reinforced concrete structures

Fig. 2 Typical characterization of the flux of chlorides with the mini-migration set-up as measured from sampling and titration of the downstream reservoir; after an initial breakthrough time t_0, a constant migration regime is reached with a characteristic mass rate $\dot{m}_{Cl^-}$
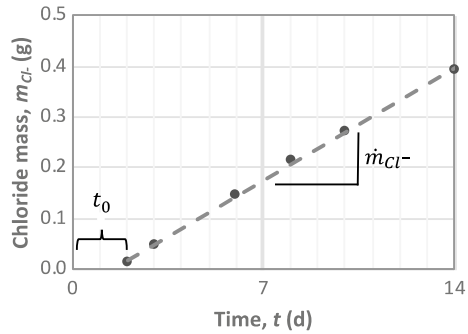
Fig. 3 Chloride diffusion coefficients obtained from downstream titration of the mini-migration set-up for OPC systems (100% ordinary Portland cement) and LC³-50 systems (50% clinker, 30% calcined clay, 15% limestone and 5% gypsum) at water-to-binder ratios w/b = 0.3–0.5
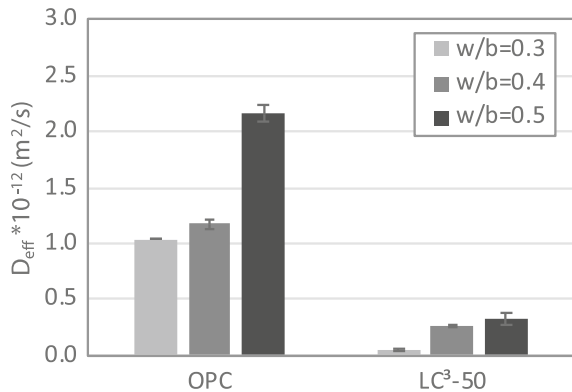
exposed to chlorides and trigger the need to better understand the microstructural differences between OPC and LC^3-50 systems.

3.2 Characterization of the Porous Network

As the migration and diffusion of chloride ions occur through the porous network of the cement pastes, a first parameter of interest is the total porosity. As shown in Fig. 4, the free-water porosity is directly related to the water initially provided to the system (i.e. to the water-to-binder ratio). Moreover, for the same w/b, similar or higher porosity was measured for LC^3-50 systems compared to OPC systems. Thus, even if the reduction in porosity with w/c could explain the differences of D_{eff} for each type of binders separately, it does not provide a valid explanation for the lower D_{eff} of LC^3-50 systems.

On the other hand, the diffusion tortuosity values presented in Fig. 5 are in very good agreement with the diffusion coefficients of Fig. 3. Thus, reducing the

Fig. 4 Free-water porosity for the investigated systems as obtained by weight difference of saturated-surface-dry specimens before and after freeze-drying
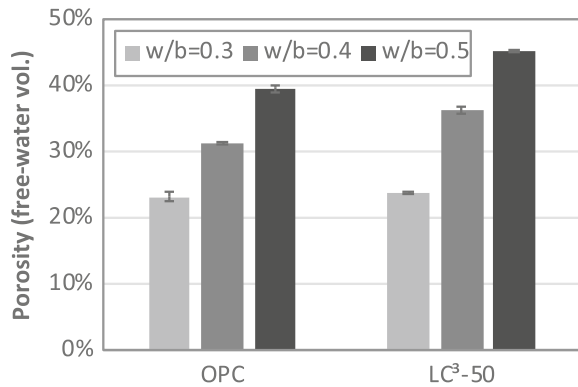
Fig. 5 Diffusion tortuosity of the porous network as obtained from the formation factor, showing the important difference between the two types of binders, for w/b = 0.3–0.5
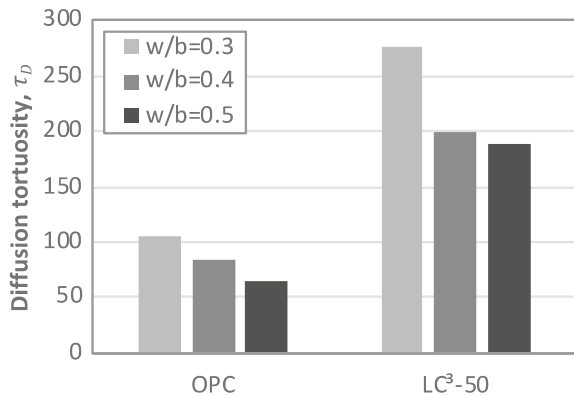
water-to-binder ratio not only reduces the porosity, but it also increases its "tortuosity". Moreover, LC^3-50 system microstructures are significantly different from those of OPC, leading to tortuosities 2–3 times higher. The diffusion tortuosity describes the difficulty for ions to diffuse in the porous network (relatively to their diffusion in water). However, it is difficult to explain the very high values obtained for both types of systems only by the geometrical tortuosity of the porous network. The measured diffusion tortuosity is likely to include other mechanisms, which are currently under further investigation.

4 Conclusion

In conclusion, this study showed that the tortuosity of the porous network has a much higher impact on chloride diffusion than the porosity itself, based on a comparison of 28-day samples of conventional OPC pastes with LC^3-50 systems at w/b = 0.3–0.5. The findings can be summarized as follows:

- Firstly, reducing the water-to-binder ratio resulted in lower total porosity and thus lower chloride diffusion coefficients;
- Secondly, at the same water-to-binder ratio, LC^3-50 systems (with 50% clinker, 30% calcined clay, 15% limestone and 5% gypsum) exhibited much lower chloride diffusion coefficient than OPC systems;
- Thirdly, the diffusion tortuosity measured using the formation factor was found to be closely correlated to the chloride diffusion coefficients, showing the same trends when comparing OPC and LC^3-50 systems.

Thus, in order to increase the service life of concrete structures exposed to chloride ions, using LC^3-50 systems with high tortuosity of the porous network seems to be a very promising approach. Following this study focusing mainly on chloride migration and on diffusion tortuosity, ongoing work includes in-depth investigations and modelling of the same systems to consider the three key parameters of chloride ingress in cementitious systems (i.e. porosity, chloride binding and composition of pore solution).

References

1. Maraghechi, H., Avet, F., Wong, H., Kamyab, H., Scrivener, K.: Performance of limestone calcined clay cement (LC3) with various kaolinite contents with respect to chloride transport. Mater. Struct. Constr. **51** (2018). https://doi.org/10.1617/s11527-018-1255-3
2. Sui, S., Georget, F., Scrivener, K.: Developing a generic approach to durability: factors affecting chloride transport in binary and ternary cementitious materials. Cem. Concr. Res. Under Revi (2019)
3. Wilson, W., Labattaglia, V., Tagnit-Hamou, A., Sorelli, L.: Will blended-cement systems with similar chloride penetration potentials resist similarly to corrosion. In: Proceedings of Sixth International Conference Durability Concrete Structures, pp 587–591 (2018)

4. Katz, A., Thompson, A.: Quantitative prediction of permeability in porous rock. Phys. Rev. B. **34**, 8179–8181 (1986). Accessed 17 July 2014
5. Nokken, M.R., Hooton, R.D.: Using pore parameters to estimate permeability or conductivity of concrete. Mater. Struct. **41**, 1–16 (2007). https://doi.org/10.1617/s11527-006-9212-y
6. Qiao, C., Coyle, A.T., Isgor, O.B., Weiss, W.J.: Prediction of chloride ingress in saturated concrete using formation factor and chloride Binding isotherm. Adv. Civ. Eng. Mater. **7**, 20170141 (2018). https://doi.org/10.1520/acem20170141
7. Truc, O., Ollivier, J.P., Carcassès, M.: New way for determining the chloride diffusion coefficient in concrete from steady state migration test. Cem. Concr. Res. **30**, 217–226 (2000). https://doi.org/10.1016/S0008-8846(99)00232-X
8. ASTM C1556: Standard Test Method for Determining the Apparent Chloride Diffusion Coefficient of Cementitious Mixtures by Bulk Diffusion. ASTM International, West Conshohocken, PA (2011)
9. Marchand, J., Samson, E., Maltais, Y.: Method for modeling the transport of ions in hydrated cement systems, United States Patent US6,959,270B2 (2005)
10. Henocq, P.: Modélisation des interactions ioniques à la surface des Silicates de Calcium Hydratés. Ph.D. Thesis, Université Laval, Quebec, QC, Canada (2005)
11. Andrade, C.: Calculation of chloride diffusion coefficients in concrete from ionic migration measurements. Cem. Concr. Res. **23**, 724–742 (1993). https://doi.org/10.1016/0008-8846(94)90067-1
12. Barneyback, R.S., Diamond, S.: Expression and analysis of pore fluids from hardened cement pastes and mortars. Cem. Concr. Res. **11**, 279–285 (1981). https://doi.org/10.1016/0008-8846(81)90069-7

Chloride Resistance of Cementitious Materials Containing Calcined Clay and Limestone Powder

Raktipong Sahamitmongkol, Narith Khuon and Yanapol Thitikavanont

Abstract Durability of reinforced concrete in marine environment depends largely on chloride resistance of concrete which should be always ascertained. In this article, an effect of limestone calcined clay (LC2) on chloride resistance is, thus, investigated. Limestone calcined clay cement with 7.5, 15, and 30% replacement by weight was tested with various methods. Rapid chloride penetration test (RCPT) was performed by measuring the total charge passed value according to ASTM C1202. The age of samples for RCPT was 60 and 90 days. At the age of 90-day, control sample had the charge passed of 4284 coulombs. The 7.5%, 15%, and 30% LC2 replacement samples had the charge passed of 3490, 2486, and 926 coulombs, respectively. Replacing cement with limestone calcined clay could decrease chloride ion penetrability of concrete. Moreover, the chloride binding capacity of LC2 cement paste was also tested by 42-day exposure in different concentration of NaCl solution. For 0.3 M concentration of NaCl solution, the bound chloride contents of 30% LC2 cement paste and control cement paste were 25.40 and 12.09 mg/g, respectively. The results significantly showed that LC2 cement paste had higher bound chloride content than control paste for any rate of replacement. Cement paste samples were submerged in NaCl solution for 168 days. Total and free chloride contents of pastes at different distance from exposed surface were tested according to ASTMC1152 and ASTMC1218, respectively, to compare apparent chloride diffusion coefficients of LC2 cement pastes and that of control cement paste. The results clearly showed that total chloride content of LC2 cement pastes was lower control paste. The chloride diffusion coefficient and surface chloride content of 30% LC2 was 150.05 mm^2/year and 0.67% by weight, respectively. The cement paste with 30% LC2 had lower chloride diffusion coefficient and surface chloride content than control cement paste up to 50%

Keywords Calcined clay · Chloride binding · Choride penetrability · Diffusion coefficient · Limestone

R. Sahamitmongkol (✉) · N. Khuon · Y. Thitikavanont
King Mongkut's University of Technology Thonburi (KMUTT), Bangkok, Thailand
e-mail: raktipong.sah@kmutt.ac.th

1 Introduction

Chloride-induced corrosion of embedded reinforcing steel is recognized as a major problem affecting durability of reinforced concrete structures. Chloride ions may exist in concrete by many reasons. They may be added during mixing or penetrate into concrete from exposed environment during service period. Chloride ions in concrete can be categorized into two types, i.e., bound chloride and free chloride [1]. The bound chloride is either chloride ions bounded by chemical reactions with aluminate phases to form Friedel's salt ($3CaO \cdot Al_2O_3 \cdot CaCl_2 \cdot 10H_2O$) or physically adsorbed to surface of calcium-silicate-hydrate gel (C–S–H) [2]. The remaining chloride ions in pore solution refer to free chloride. Only free chloride is responsible for depassivation of steel reinforcement. Because when the concentration of free chloride in pore solution is higher than the chloride threshold level, it can possibly destroy the passive film with the presence of oxygen and water, leading to steel corrosion [1–3].

The use of supplementary cementitious materials (SCMs) such as calcined clays has a potential to improve the chloride resistance of concrete. Recently, a ternary blended cement with the substitution of limestone and calcined clay has been developed [4]. It is also called limestone calcined clay cement (LC2 cement or LC3).

Some researches showed that replacing limestone or alumina-rich components in cement may largely influence the rate of chloride migration in concrete [5, 6]. It is necessary to determine how this may influence the corrosion of steel reinforcement in concrete. Moreover, little research investigated the chloride resistance of LC2 cement; especially, the LC2 cement produced in Southeast Asia or Thailand.

This study aims to evaluate the effect of LC2 cement on chloride resistance of cementitious materials in terms of chloride penetration depth, chloride diffusion coefficient, and chloride binding capacity. Two finenesses of limestone powder are also considered.

2 Materials and Methods

2.1 Material

The ratio of calcined clay (CC) and limestone (LS) is 2:1 by weight and mixed with ordinary Portland cement (OPC) type I as a binder. Thai raw clay was calcined at temperature around 800 °C to obtain calcined clay and also ground to get average particle size approximately equal to 15 μm. Two different sizes; 5 and 10 μm, of local limestone powder with high calcium carbonate ($CaCO_3$) content were used in this study.

The gypsum was added into LC2 cement for 5% by weight of calcined clay. Crushed limestone with a maximum size of 19 mm was used as coarse aggregate in concrete, while natural river sand is used as fine aggregate.

The chemical composition of OPC and limestone calcined clay (LC2) is shown in Table 1. It was found that LC2 consists primarily of 27.97% and 23.67% of silica dioxide and aluminum oxide, respectively. Both of these oxides are components of calcined clay and have pozzolanic nature, while 18.4% of CaO and 15.55% loss of ignition indicate the portion of limestone power in the LC2.

2.2 Details of Mix Proportions

Seven mix proportions were tested to evaluate chloride resistance of both LC2 concretes and LC2 cement pastes as shown in Table 2. Control (CT) mix proportion was cast by using 100% of OPC, while the limestone calcined clay cement (LC2 cement) were cast by LC2 replacement rates of 7.5, 15, and 30% by weight of binder. In this mix proportion, all specimens contain 5% gypsum (GS) by weight of calcined clay and the water to binder ratio (w/b) is 0.5 for all specimens. The ratio of paste: fine aggregate: coarse aggregate was controlled by 0.276:0.315:0.409 by weight. In Table 2, the terms 'LC5' and 'LC10' indicate the use of limestone calcined clay (LC2) with the average size of 5 and 10 micron, respectively.

Concrete samples were mixed in drum mixing machine and casted into cylindrical molds with 100-mm diameter and 200-mm height. At 24 h after mixing, the samples were demolded and cured in tap water until the date of testing.

Cement paste samples were mixed and casted in 55-mm diameter and 110-mm height PVC cylindrical molds. At 24 h, the samples were removed from the molds and cured in tap water.

2.3 Test Method

Chloride penetration depth: After the curing period of 28 days, the concrete samples were cut at middle height to get two pieces of concrete samples. The sample with 100-mm diameter and 100-mm height was used to evaluate the chloride penetration depth. All surfaces of the concrete samples except the cut surface were coated with epoxy, so that the chloride ion can penetrate into sample only in one direction. Subsequently, all of the samples were submerged in 5% NaCl solution for 60 and 90 days.

After 60-day and 90-day of exposure, the concrete samples were vertically split off and sprayed with 0.1 M $AgNO_3$ solution in order to measure the chloride penetration depth from the formation of AgCl with white color.

Rapid chloride penetration: The rapid chloride penetration test (RCPT) was performed by measuring the total charge passed value. According to ASTM C1202, chloride ion penetrability of samples were classified and compared by the value of charge that passed through the concrete samples. After the concrete samples reached

Table 1 Chemical composition of materials

Oxide composition	SiO$_2$	Al$_2$O$_3$	Fe$_2$O$_3$	CaO	MgO	SO$_3$	Na$_2$O	K$_2$O	LOI
OPC (%)	20.90	4.80	3.40	63.30	1.30	2.70	0.30	0.40	2.90
LC2 (%)	27.97	23.67	10.31	18.40	0.77	1.60	0.01	0.29	15.55

Table 2 Mix ratios of binder for concrete and cement paste

Mix	Binder (% by weight)					w/b
	OPC	CC	LS-5	LS-10	GS	
CT	100	–	–	–		0.5
7.5LC5	92.25	5	2.5	–	0.25	0.5
15LC5	84.5	10	5	–	0.50	0.5
30LC5	69	20	10	–	1	0.5
7.5LC10	92.25	5	–	2.5	0.25	0.5
15LC10	84.5	10	–	5	0.50	0.5
30LC10	69	20	–	10	1	0.5

the curing age of 60 and 90 days, the samples were horizontally cut to get the height of 50-mm. Subsequently, silicon sealant was used to coat the curve side surface of samples. Next, the samples were assembled with the rapid chloride penetration test cells. A direct current with voltage of 60 V is maintained across the exposed flat surfaces of the sample. Negative pole is connected to 3.0% NaCl solution and positive pole is connected to 0.3 M NaOH solution. The current (I) was recorded continuously by computerized measuring system for 6 h.

The total charge passed in unit of coulombs was calculated by using the value of electric current (I) as shown in Eq. (1).

$$Q_x = 900(I_0 + 2I_{30} + 2I_{60} + \cdots + 2I_{300} + I_{360}) \tag{1}$$

where

Q_x Charge passed which passed through the x-mm diameter sample, coulomb
I_0 Initial current when the voltage is applied, ampere
I_t Current at t(min) after the voltage is applied, ampere.

Chloride binding capacity: The paste samples were cured in water for a period of 24 weeks. At the end of the curing period, the pastes were cut, ground, and sieved to obtain particles size ranging from 250 to 841 µm (passing through sieve No. 20 and retaining on No. 60). The samples were then dried under a vacuum (0.75 bar) in a desiccator containing silica gel for three days in order to remove most of the water. After that, the dried samples were stored in a desiccator with decarbonized air and kept at 11% RH by saturated LiCl solution for 7 days.

The equilibrium method developed by Luping and Nilsson [2, 7] was used to determine chloride binding capacity in this study. As the first step, 20 g of the sample dried at 11% RH was placed in plastic bottle and filled with approximately 50 ml of NaCl solution.There are four different cases of NaCl concentrations (0.3, 0.5, 1.0, and 3.0 M). The bottle was sealed and stored for 6 weeks to allow the solution to reach equilibrium. After equilibrium was reached, the chloride concentration of host solution was then determined by means of potentiometric titration using 0.05 M

AgNO$_3$. Since the samples stored under 11% RH contained some moisture content, weight of dry sample was calculated by drying in oven at 105 °C. Then, knowing the initial and final concentrations of the NaCl solution, the weight of dry sample, and the volume of the external solution, the content of bound chloride was determined by using Eq. (2).

$$C_b = \frac{35.45 \, V(C_i - C_f)}{W} \tag{2}$$

where

C_b Amount of bound chloride of sample, mg/g
V   Volume of the external solution, ml
C_i Initial chloride concentration of external solution, mol/l
C_f Equilibrium concentration of the chloride solution, mol/l
W   Weight of the dry sample, g.

Chloride diffusion coefficient: The paste samples were prepared and coated by epoxy onto all surface area except exposure surface in order to allow chloride penetration to penetrate in only one direction. The samples were exposed to 5% NaCl solution for 168 days.

At the end of exposure, the specimen was dry-cut into 10-mm thick disks. At least 4 disks were cut from the exposed surface of each specimen and each disk was ground into powder. Next, 10 g of the paste powder in each disk was prepared for chloride tests according to ASTM C1218 [8] and ASTM C1152 [9] in order to determine free and total chloride contents, respectively.

Free chloride content: 2 g of the powder from each cement paste disk was put in the 250-ml beaker. 50 ml of reagent water was added to beaker. Then, the mixture was heated to boil for 5 min and allowed to stand for 24 h. The sample was filtered through a fine-textured filter paper. 3 ml of 1:1 ratio diluted nitric acid (HNO$_3$) solution by volume was poured. After allowing the solution to stand for 1–2 min, the process of boiling sample was repeated for a few seconds. Sample was left at room temperature. Make a blank using 75 ml of distilled water. 2 ml of 0.05 M NaCl solution were filled into cooled sample beaker. The cooled sample was placed to auto-titration machine and started titrating with 0.05 M AgNO$_3$.

Total chloride content: About 2 g of sample and 75 ml of distilled water were put in the beaker. 25 ml of 1:1 ratio diluted nitric acid (HNO$_3$) solution by volume was slowly poured. The sample was stirred with a glass rod to break up any lumps of sample and then 3 drops of methyl orange indicator were added. The mixture was heated to boil for 10 s and subsequently removed from hot plate. The sample was filtered through a coarse-textured filter paper. Next, 2 ml of 0.05 M NaCl solution were filled into the cooled sample. The cooled sample was then placed to auto-titration machine and titrated with 0.05 M AgNO$_3$. The content of chloride was determined by using Eq. (3).

$$\% \, Cl = \frac{3.545 \, N(V_1 - V_2)}{W} \qquad (3)$$

where

V₁ Volume of 0.05 N AgNO₃ solution used for sample titration, ml
V₂ Volume of 0.05 N AgNO₃ solution used for blank titration, ml
N   Exact normality of 0.05 N AgNO₃ solution, mol/l
W   Mass of sample, g.

After the total chloride profile of samples was determined, Fick's second law of diffusion as shown in Eq. (4) was applied to fit the total chloride penetration profile.

$$C_{x,t} = C_s\left[1 - \mathrm{erf}\left(\frac{x}{2\sqrt{D_c t}}\right)\right] \qquad (4)$$

where

$C_{x,t}$ Total chloride content at distance x from the surface at time (year), %
C_s Chloride content at exposure surface, %
x Distance from concrete surface, mm
D_c Chloride diffusion coefficient, mm²/year
t Time, year.

A best-fit value of surface chloride content (C_s) and chloride diffusion coefficient (D_c) was determined by the least-square error between calculated chloride content and the experimental results.

3 Results and Discussion

3.1 Chloride Penetration Depth of Concrete

Chloride penetration depths of LC2 concrete with any sizes of LS are lower than that of CT concrete. And, higher rates of LC2 replacement lead to lower chloride penetration depth of concrete as shown in Table 3. The sample "30LC5" had the lowest chloride penetration depths among of all concrete samples. The lower penetration depth clearly indicates that the use of LC2 cement as a binder effectively

Table 3 Chloride penetration depth of OPC and LC2 concretes at 60 and 90 days

Chloride penetration depths (mm)	CT	7.5LC5	15LC5	30LC5	7.5LC10	15LC10	30LC10
60 days	23.1	17.1	14.1	8.3	21.0	18.5	13.1
90 days	28.0	19.2	16.1	9.0	25.2	23.1	17.2

provides better chloride resistance. Moreover, the penetration depth of 30LC10 is almost double of that found in 30LC5 after 90-day exposure. This strongly indicates that the 5-μm limestone powder is better than 10-μm one to be used as a part of LC2 when the chloride resistance is considered.

3.2 Chloride Binding Capacity

Figure 1 shows the bound chloride of LC2 cement pastes submerged in 0.3M, 0.5M, 1M, and 3M NaCl solution. The results show that the use of LC2 to partially replace OPC could improve the chloride binding capacity. This is in line with several researches [2, 10, 11] which showed that replacing OPC with high alumina content material increases chloride binding capacity since Al_2O_3 content in LC2 used in this study was also high. The result implies that that reactive Al_2O_3 in the LC2 has an ability to chemically react with chloride to form Friedel's salt. Moreover, LC2 cement paste might influence an increase of chloride binding capacity in term of physical bound chloride because LC2 cement pastes also contain more C–S–H. Considering the case of 3 M concentration, 35 and 80% increase of bound chloride could be obtained with 7.5 and 15% LC2 replacement. Apparently, 30LC5 bound the most (25.40 mg/g) and CT bound least amount of chloride (12.09 mg/g), respectively. That means 30LC5 has more than double chloride binding capacity than the CT paste.
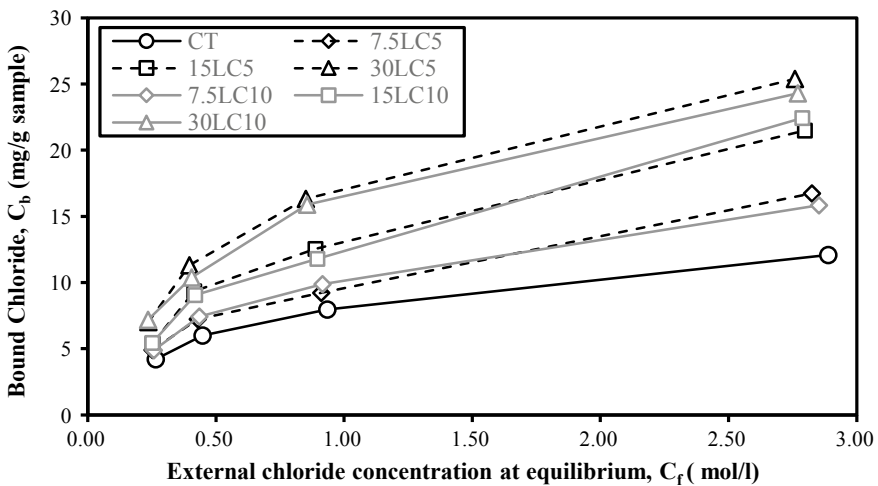
Fig. 1 Chloride binding relationships for OPC and LC2 cement pastes

3.3 Rapid Chloride Ion Penetration

The replacement rate of LC2 in concrete was the major factor for reducing the charge passed values of LC2 concrete.

The chloride ion penetrability CT sample is 4445 and 4284 coulombs at the concrete age of 60-day and 90-day, respectively. According to ASTM C1202 [12], these values can be classified as "high" level. With LC2 replacement percentage of 7.5% and 15%, the charge passed in concrete could be reduced for 18% and 40%, respectively, as shown in Fig. 2. When the replacement rate of LC2 is at 15% by weight, chloride ion penetrability of concrete is classified in "moderate" level. In the case of 30% LC2 replacement, the excellent resistance of chloride could be observed. The value of charge passed could be reduced for 75% when compared to CT sample and can be classified to a "very low" level. It was also found that the sample incorporating 30% LC2 with 5-μm limestone powder (30LC5) has the lowest charge passed in concrete among all samples. The remarkable low charge passed value of LC2 concrete is believed to be related to the higher chloride binding capacity of LC2 concrete and the refined microstructure.

It should be noticed from the results as well that all samples with 5 μm LS have slightly less charge passed than the case of 10-μm LS. The results are similar to other studies which suggest that chloride ingress in limestone concrete decreases with increasing limestone fineness [6]. The charge passed values of the samples tended to decrease in all concrete mix proportion when the curing age increased from 60 to 90 days. This is natural because the concrete samples became denser due to higher degree of hydration and pozzolanic reaction.
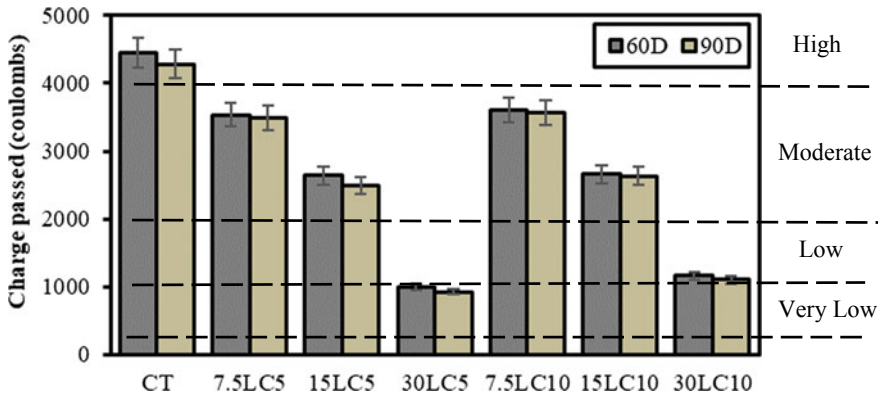
Fig. 2 Charge passed of concrete by using rapid chloride penetration test (RCPT) at 60 and 90 days of curing period of concrete samples

3.4 Distribution of Total Chloride and Free Chloride

The results in Fig. 3 demonstrate that the LC2 cement pastes with any rate of replacement provide lower total and free chloride contents than CT paste at the same distance from exposure surface.

The chloride contents are high near the exposed surface and decrease with more distance from the surface for both CT and LC2 cement pastes. The total chloride content at distance 5 mm from exposure surface could be reduced for 25%, 36%, and 50% for 7.5%, 15%, and 30% LC2 replacement, respectively. The sample "30LC5" has lowest chloride content at any distances which are 0.45%, 0.12%, and 0.04% at distance of 5, 15, and 25 mm from exposure surface, respectively.

The trend of free chloride content profile is similar to total chloride content profile. Comparing free chloride contents of all types of samples at the depth of 25 mm, 30LC5 exhibited the lowest chloride content. Furthermore, the LC2 cement pastes with 10-µm LS have higher free chloride content than the case with 5-µm LS as shown in Fig. 3.
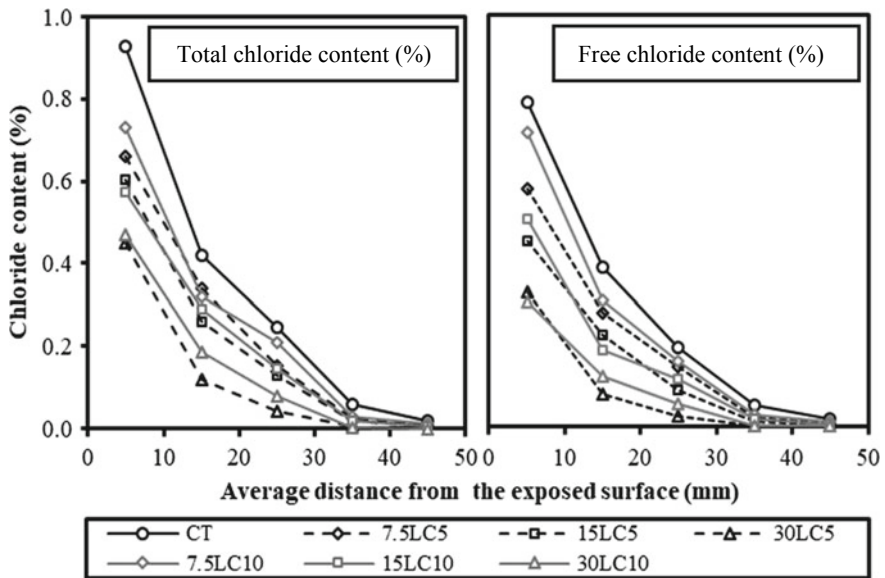
Fig. 3 Total and free chloride content of OPC and LC2 cement pastes after 168-day exposure in 5% NaCl solution

Table 4 Diffusion coefficient and surface chloride content of CT and LC2 cement pastes

Mix	Diffusion coefficient (mm^2/year)	Surface chloride content (%)
CT	345.55	1.17
7.5LC5	344.45	0.86
15LC5	292.50	0.79
30LC5	150.05	0.67
7.5LC10	351.90	0.92
15LC10	346.40	0.75
30LC10	241.05	0.63

3.5 Chloride Diffusion Coefficient

Table 4 illustrates effect of LC2 replacement on apparent chloride diffusion coefficient (D_c) of cement pastes after being exposed to 5% NaCl solution. The results revealed that chloride diffusion coefficient (D_c) decreased with more LC2 replacement. It can be explained that both the refinement of pore structure and enhanced chloride binding capacity of LC2 cement pastes reduce the chloride diffusion coefficient. 30LC5 cement paste has the lowest apparent diffusion coefficient which is 150.05 mm^2/year (approximately half of CT paste). As a results, the surface chloride content decreases with higher replacement of LC2. Considering the effect of particle size of LS, the LC2 cement pastes containing 5-µm LS have lower D_c than that with 10-µm LS.

4 Conclusions

1. The results of chloride penetration depths from concrete in fully immersion reveal that the penetration depths of LC2 concrete with all types of LS particle sizes were lower than that of CT concrete and more LC2 replacement increased the chloride resistance of LC2 concrete. The samples containing 5-µm limestone powder had lower chloride ion penetration than the case of 10 µm.
2. Chloride binding capacity of cement paste could be significantly improved by utilizing limestone calcined clay (LC2) to partially replace Portland cement. Higher LC2 replacement results in higher binding capacity.
3. The results of rapid chloride penetration show that the use of LC2 to replace OPC in concretes reduces effectively the charge passed of LC2 concretes. In addition, the higher LC2 replacement; the lower chloride ion penetrability.
4. For chloride penetration profile, the results demonstrated that the pastes with LC2 had lower chloride content than conventional cement paste at the same distance from the surface of paste.

References

1. Dousti, A., Shekarchi, M.: Relationship between free and total chloride profiles for optimization of service life prediction in chloride exposed RC structures. In: The Third International Conference on Modeling Simulation and Applied Optimization. ICMSAO, Sharjah (2009)
2. Ogirigbo, O.R., Black, L.: Chloride binding and diffusion in slag blends: influence of slag composition and temperature. Constr. Build. Mater. **149**, 816–825 (2017)
3. Yang, Z., Gao, Y., Mu, S., Chang, H., Sun, W., Jiang, J.: Improving the chloride binding capacity of cement paste by adding nano-Al_2O_3. Constr. Build. Mater. **195**, 415–422 (2019)
4. Dhandapani, Y., Sakthivel, T., Santhanam, M., Gettu, R., Pillai, R.G.: Mechanical properties and durability performance of concretes with limestone calcined clay cement (LC3). Cem. Concr. Res. **107**, 136–151 (2018)
5. Thomas, M.D.A., Hooton, R.D., Scott, A., Zibara, H.: The effect of supplementary cementitious materials on chloride binding in hardened cement paste. Cem. Concr. Res. **42**, 1–7 (2012)
6. Abdurrahman, A.E., Ravindra, D., Gurmel, G.: Chloride ingress in concrete: limestone addition effects. Mag. Concr. Res. **70**, 292–313 (2018)
7. Luping, L., Nilsson, L.: Chloride binding capacity and binding isotherms of OPC pastes and mortars. Cem. Concr. Res. **23**, 247–253 (1993)
8. ASTM C1218: Standard test method for water-soluble chloride in mortar and concrete. ASTM International. West Conshohocken (2015)
9. ASTM C1152: Standard test method for acid-soluble chloride in mortar and concrete. ASTM International. West Conshohocken (2012)
10. Ukpata, O.J., Basheer, P.A.M., Black, L.: Slag hydration and chloride binding in slag cements exposed to a combined chloride-sulphate solution. Constr. Build. Mater. **195**, 238–248 (2019)
11. Qiao, C., Suramemi, P., Ying, T.N.W., Choudhary, A., Weis, J.: Chloride binding of cement pastes with fly ash exposed to CaCl2 solutions at 5 and 23 °C. Cem. Concr. Res. **97**, 43–53 (2019)
12. ASTM C1202: Standard test method for electrical indication of concrete's ability to resist chloride ion penetration. ASTM International. West Conshohocken (2017)

Chloride-Induced Corrosion Resistance of Steel Embedded in Limestone Calcined Clay Cement Systems

Sripriya Rengaraju, Radhakrishna G. Pillai, Lakshman Neelakantan, Ravindra Gettu and Manu Santhanam

Abstract Nowadays, various concrete systems with fly ash, slag, limestone calcined clay, etc. exhibiting high ionic resistivity are used to enhance the resistance against chloride-induced corrosion. This study deals with the corrosion assessment of steel in three cementitious systems, namely (i) Ordinary Portland Cement (OPC), (ii) OPC + 30% fly ash, and (iii) limestone calcined clay cement (LC3) exhibiting 'low to moderate', 'moderate to high', and 'very high' resistivities, as per AASHTO T358 (2017). Results from the ASTM G109 and impressed current corrosion (ICC) tests were evaluated. It was found that LC3 systems have excellent resistivity against the ingress of chlorides and provide better corrosion resistance. It was also found that the corrosion products formed on steel in LC3 systems are different and less expansive than that found in the OPC systems.

1 Introduction

Most structures built with Ordinary Portland Cement (OPC) systems are showing premature corrosion (say before reaching the anticipated design life) due to high permeability and poorly developed microstructure. Hence, nowadays, cements with pulverized fly ash (PFA), limestone calcined clay cement (LC3), etc. with very high ionic resistivity are used to enhance the resistance against the ingress of moisture and chlorides, and thereby delay the onset of corrosion. Figure 1 shows the surface resistivity of concrete made with different binders classified as per AASHTO T358 (2017) [1, 2]. In this study, the long-term corrosion performance of OPC, PFA, and LC3 systems was assessed using ASTM G109 [3]. Also, the performance of these systems under impressed current corrosion (ICC) test, as per FM5-522 [4], was assessed. Following this, the corrosion-induced cracking in these systems was also

S. Rengaraju · R. G. Pillai (✉) · L. Neelakantan · R. Gettu · M. Santhanam
Indian Institute of Technology Madras, Chennai, India
e-mail: pillai@iitm.ac.in
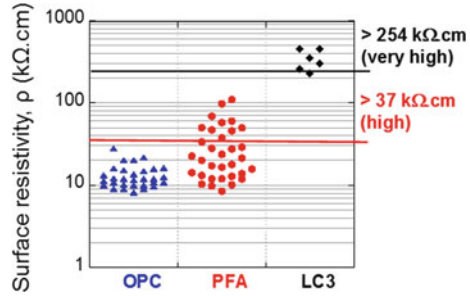
evaluated. It was also found that the resistivity and chemistry of cementitious system
used to play a significant role in the type of corrosion products formed and resulting
in expansive stresses and cracking of concrete cover. It was found that some of these
tests are not suitable to evaluate the steel-cementitious systems with high resistivity
(say, LC3).

2 Experimental Programme

Three binders, namely OPC, 70% OPC + 30% replacement with class F fly ash (PFA),
and 50% OPC clinker + 50% limestone calcined clay (LC3), were studied. Thermo-
mechanically treated (TMT) rebar was used for all the tests. The performance of
binders in delaying the onset of corrosion was assessed using the following long-term
and short-term electrochemical test methods, namely (i) ASTM G109 test method
and (ii) ICC test method. The details of each test method are explained next.

ASTM G109 test method

Figure 2 shows the schematic of the G109 test specimen. M25 concrete mix was
used for the study. See Table 1 for the mix design. The size of the coarse aggregate
was restricted to 10 mm to have a reduced cover depth of 19 mm, as per the standard.
Three specimens were cast for each combination. The specimens were subjected to
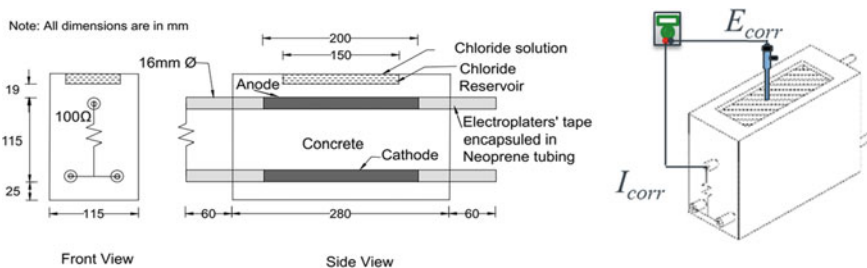
Fig. 2 Schematic diagram of macrocell corrosion test specimen

Table 1 Concrete mix design used for the ASTM G109 tests

Ingredients	Quantity (kg/m^3 of concrete)
Water–binder ratio	0.5
Binder	360
Fine aggregate	877
Coarse aggregate	954

alternate wet-dry cycle with 3% NaCl solution. Macrocell corrosion current between the top bar (anode) and the two bottom bars (cathode), I_{corr}, was monitored as per ASTM G109, and half-cell potential of the top bar (anode), E_{corr}, was monitored as per ASTM C876 [5] at the middle of the wet cycle. The time to corrosion initiation (i.e. time taken for the total charge to reach 150 C) was calculated as per ASTM G109 procedure.

Impressed current corrosion test method

Figure 3 shows the schematic of the impressed current corrosion (ICC) test specimen. Each ICC test specimen consisted of a concrete cylinder (200 mm long x 100 mm diameter) with a 16-mm-diameter TMT rebar (100 mm long) embedded at the centre with a side cover of 42 mm and an end cover of 50 mm. M35 grade concrete was used for the study. The rebar in the specimen was connected to the positive terminal of the DC power supply system. A nickel-chromium (Nichrome) mesh placed in the electrolyte was connected to the negative terminal. An external potential gradient of 15 V was applied for 10 hours a day until failure (visible crack) occurred. At the end of testing, the oxide composition of the corrosion products on the steel was analysed with Raman spectroscopy for all types of concrete.

Test specimen   Test setup
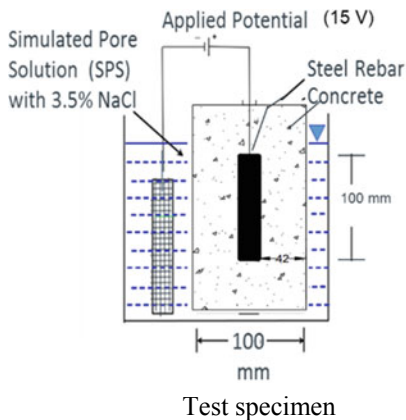
Fig. 3 Schematic diagram of impressed current corrosion test specimen and set-up

3   Results and Discussion

ASTM G109 test method

Figure 4 shows the half-cell potential, $E_{corr,}$ and Fig. 5 shows the macrocell current exhibited by the ASTM G109 type specimens with OPC, PFA, and LC3 concrete, respectively. The cumulative charge of 150 C was observed early in OPC when compared to the corresponding LC3 specimens with higher resistivity. The refined pore structure and high ionic resistance in early age enhance the corrosion resistance in LC3 specimens. Hence, the macrocell corrosion current measured in Circuit 1 (see Fig. 6) as per ASTM G109 standard was very less in LC3 specimens. However, due to higher resistivity in LC3, macrocell corrosion within the same rebar (Circuit 2) was found to be predominant, as observed by Hansson et al. [6] and Rengaraju et al. [7], as shown in Fig. 7.

Impressed current corrosion test method

Figure 7 shows three distinct ranges of instantaneous corrosion current (I) observed in the ICC test specimens. OPC concrete has lesser resistivity, and hence, higher I in the range of (40–80 mA) was observed. In PFA, the I observed was lower (10–30 mA) due to medium resistivity, whereas LC3 has the lowest range of I (say, 0–3 mA) due to very high resistivity. The potential was applied until all the OPC specimens cracked. When the OPC specimens cracked, the application of voltage on the companion specimens of PFA and LC3 was terminated. All the specimens were tested for a maximum of 160 h, because all the OPC specimens cracked within that time duration.

The corrosion products tend to move to the capillary pores accessible near the interface and start accumulating. When these products fill the pore space, they create radial stress and induce cracking. Since OPC has less resistivity and higher capillary
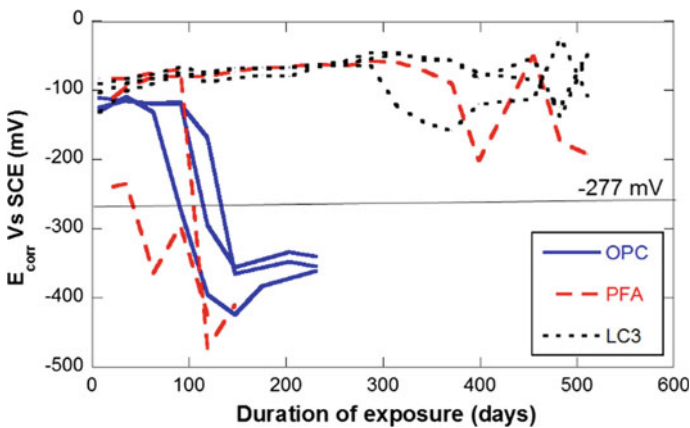
Fig. 4 E_{corr} as a function of time (as per ASTM C876)
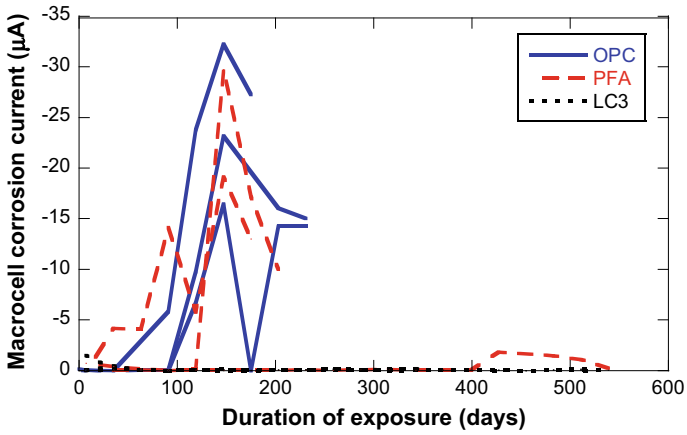
Fig. 5 Macrocell corrosion current as a function of time (as per ASTM G109)
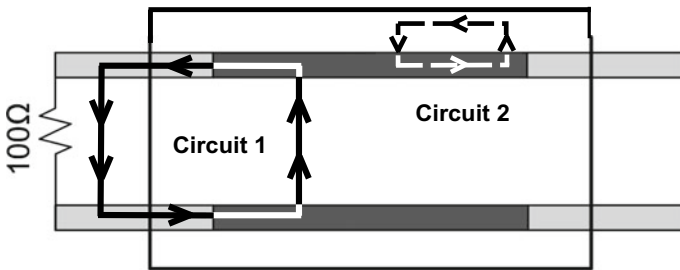
Fig. 6 Possible macrocell corrosion current circuits in ASTM G109 test specimen (Rengaraju et al. [7])
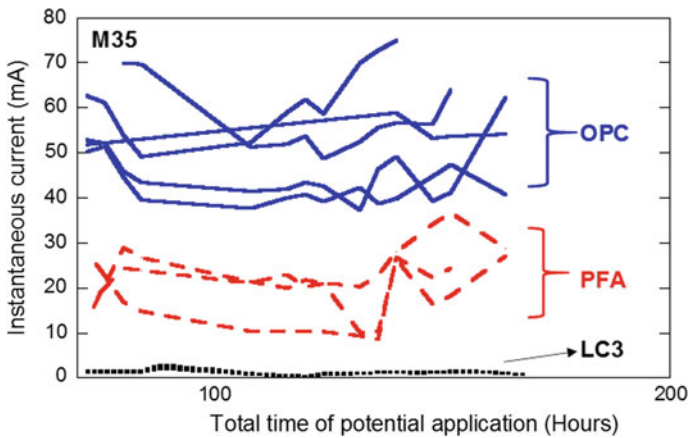
Fig. 7 Instantaneous current in OPC, PFA, and LC3 systems as a function of time

porosity [8], the instantaneous corrosion current is much higher than that in the PFA and LC3 concrete. This led to earlier cracking in OPC specimens. In PFA specimens, small hairline cracks were observed in one of the specimens. This could be due to low resistivity in the early age of hydration in PFA specimens. No cracks were observed in any of the LC3 specimens. The reason for this lack of cracking in LC3 systems was found by understanding the difference in the nature of corrosion products and resulting expansive stresses in OPC, PFA, and LC3 systems.

Figure 8 shows the Raman spectra obtained from the specimens with OPC, PFA, and LC3 specimens (after the ICC tests). In OPC and PFA specimens, the corrosion products formed are lepidocrocite and feroxyhyte, respectively (as indicated by the peaks at 248, 300, 668, and 1311 for OPC and at 297, 392, and 666 for PFA), which are expansive in nature (say, by about three times). Due to higher corrosion current in OPC and PFA specimens, the amount of corrosion products formed is also greater. This leads to significant expansive stresses in concrete and results in cracking of the cover. However, the corrosion products formed on steel in LC3 specimens had hematite and magnetite (as indicated by the peaks at 292 and 410 for LC3), which are not as expansive as lepidocrocite and feroxyhyte. Also, the dense microstructure restricts the movement of ions in the cementitious matrix and thus restricts the current flow leading to lower current and maintenance of the passive film. Because of these two reasons, the LC3 specimens did not crack. In general, the corrosion current data indicate that LC3 can exhibit higher corrosion resistance than OPC and PFA systems.
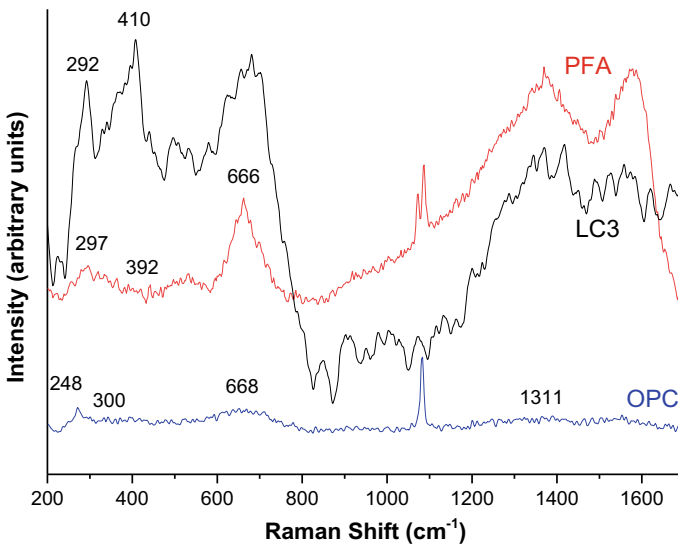
Fig. 8 Raman spectra of corrosion products of steel in OPC, PFA, and LC3 systems

4   Conclusions

Based on the long-term ASTM G109 and short-term ICC testing, the following conclusions are made

(1) The chloride ingress could be very slow in LC3 specimens due to higher resistivity, and thus, it provides longer durability against chloride-induced corrosion.

(2) LC3 system has higher resistance against impressed current corrosion compared to OPC and PFA systems. Due to higher resistivity in the early age itself, the LC3 specimens have denser microstructure and lead to better corrosion resistance by protecting the passivity of the steel.

(3) The nature of corrosion products formed on steel in LC3 systems is less expansive than that formed on steel in OPC and PFA systems—resulting in less corrosion-induced cracking in the former systems.

References

1. AASHTO T 358: Standard Method of Test for Surface Resistivity Indication of Concrete's Ability to Resist Chloride Ion Penetration. American Association of State Highway and Transportation Officials, Washington, D.C., U.S.A (2017)
2. Rengaraju, S., Neelakantan, L., Pillai, R.G.: Investigation on the polarization resistance of steel embedded in highly resistive cementitious systems—an attempt and challenges. Electrochim. Acta **308**, 131–141 (2019)
3. ASTM G109-07: Standard Test Method for Determining Effects of Chemical Admixtures on Corrosion of Embedded Steel Reinforcement in Concrete Exposed to Chlorides. ASTM International, West Conshohocken, PA, USA (2013)
4. FM5-522.: Florida Method of Test for an accelerated Laboratory Method for Corrosion Testing of Reinforced Concrete Using Impressed Current. Florida Department of Transportation, USA (2000)
5. ASTM C876-15: Standard Test Method for Corrosion Potentials of Uncoated Reinforcing in Concrete. ASTM International, West Conshohocken, PA, USA (2015)
6. Hansson, C.M., Poursaee, A., Laurent, A.: Macrocell and microcell corrosion of steel in ordinary Portland cement and high performance concretes. Cem. Concr. Res. **36**(11), 2098–2102 (2006)
7. Rengaraju, S., Godara, A., Alapati, P., Pillai, R.G.: Macrocell corrosion mechanisms of prestressing strands in various concretes. Mag. Concr. Res. **109**, 1–13 (2018)
8. Dhandapani, Y., Santhanam, M.: Assessment of pore structure evolution in the limestone calcined clay cementitious system and its implications for performance. Cem. Concr. Compos. **84**, 36–47 (2017)

Influence of Carbonation on Mechanical and Transport Properties of Limestone Calcined Clay Blend Mortar Mix

Tarun Gaur, Lav Singh and Shashank Bishnoi

Abstract When calcium bearing phases of hydration products react with carbon dioxide, it results in formation of calcium carbonate. The consumption of alkaline compounds leads to reduction in the pH of concrete, thereby affecting the stability of hydration product and increasing the risk of steel corrosion in low alkaline environment. The reaction of pozzolans with calcium hydroxide reduces the reserve alkalinity in the hydrated cement paste which accelerates the rate of carbonation. The main objective is to determine the change in mechanical and transport properties of carbonated and non-carbonated samples. In this investigation, a cement blend mix has been prepared using OPC and limestone calcined clay. Mortar specimens were prepared for using blend to sand ratio as 1:3 to prepare samples for testing compressive strength, sorptivity and porosity using boiling water test. Paste samples were cast to measure reserve alkalinity and carry out thermogravimetric analysis. Some specimens were kept in carbonation chamber for 90 days at 3% CO_2 concentration and 60% relative humidity for carbonation to occur at an accelerated rate while the other samples were sealed to avoid carbonation. The results show that after carbonation, there is slight decrease in the compressive strength and increase in sorptivity after carbonation of LC^3.

Keywords Carbonation · Boiling water test · Thermogravimetric analysis

1 Introduction

Carbonation is one of the major factors which affect the durability of concrete. This is usually a cause of concern in the areas where carbon dioxide concentration is higher

T. Gaur (✉) · L. Singh · S. Bishnoi
Indian Institute of Technology Delhi, New Delhi, India
e-mail: tarun.tg94@gmail.com

L. Singh
e-mail: singh.lav1987@gmail.com

S. Bishnoi
e-mail: bishnoi@iitd.ac.in

such as in railway tunnels (where diesel locomotives are used to haul trains) or any other industrial area where CO_2 emission is higher than normal. Carbonation is one of the major reasons for corrosion of reinforcement. Carbonation is the conversion of calcium bearing phases into calcium carbonates when it reacts with carbon dioxide. In this reaction, calcium hydroxide is also consumed; therefore, the pH of concrete reduces to below 8.3. Thus, the alkaline passivating film on the reinforcing steel gets deteriorated, and the steel gets exposed to outer environment. [1] pointed out that the presence of even a small amount of chloride in carbonated concrete enhances the corrosion rate resulted from carbonation of concrete.

$$Ca(OH)_2 + CO_2 \rightarrow CaCO_3 + H_2O$$
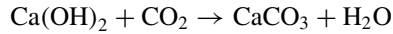
Many researches state that when OPC is carbonated, its porosity gets reduced as conversion of calcium hydroxide to calcium carbonate increases its volume. Carbonation of $Ca(OH)_2$ causes expansion and thus a decrease in porosity, while carbonation of C–S–H causes shrinkage, thus an increase in porosity [2]. The carbonation of C–S–H results in leaching of calcium ions from C–S–H leads to formation of amorphous silica gel. This reaction is accompanied by an overall reduction in the volume of solids in concrete. This reduction in volume results in increase in porosity of concrete and pore sizes, known as carbonation shrinkage [3, 4]. In case of blended cement paste, the amount of free calcium hydroxide is very low while the amount of CSH is high. CH and CSH both release calcium ions into the solution simultaneously, but it has been seen that CH reacts faster than CSH [5]. There in OPC more of CSH reacts with carbon dioxide thereby increasing the porosity of mortar as conversion of CSH to $CaCO_3$ reduces the product volume and increases the porosity.

GGBS, SF, FA, Metakaolin, etc. contribute to the improvement of various other properties. They improve strength of concrete and results in reduction of carbonation depth [6]. This is true up to a certain level of replacement of OPC clinker. The degree of carbonation and change in various properties depends upon the type of mineral admixture and its proportion in the mix composition.

2 Experimental Work

2.1 Materials and Specimens

Limestone calcined clay (LC^2) was used in this experiment with limestone: calcined clay as 1:2. LC^2 was mixed thoroughly with OPC in a ball mill with LC^2: OPC as 45:55. Various tests performed on the raw materials to determine physical and chemical properties. The results of various tests are as follows (Tables 1, 2 and 3).

Mortar specimens of cement: sand ratio as 1:3 were prepared for determining compressive strength, sorption, porosity and carbonation depth. The w/c ratio was

Table 1 Specific gravity of various materials

Material	Sp. Gravity
Clinker	3.17
Sand	2.61
Limestone calcined clay	2.78

Table 2 Lime reactivity of limestone calcined clay

Material	Compressive strength (MPa)
Limestone calcined clay	11.59

Table 3 Particle size distribution of materials

Material	D_{10} (µm)	D_{50} (µm)	D_{90} (µm)
OPC	4.58	18.2	48.6
LC^2	3.42	20.6	84.3

taken as 0.45 for all the mortar specimens. To perform reserve alkalinity and thermogravimetric analysis, paste samples were prepared. Paste samples were crushed and powdered to carry out TGA and titration.

To determine compressive strength, 7.07 * 7.07 * 7.07 cm^3 cubical mortar specimens were prepared whereas to perform sorptivity and boiling water test, cylindrical samples with 100 mm dia and 50 mm thickness were prepared. All the samples were cured in potable water for 28 days at 27 °C in the curing tank.

2.2 Environmental Conditions

Two types of environmental conditions were created to simulate non-carbonation condition and accelerated carbonation condition. For creating no carbonation condition, the samples were kept in three layers of zip-lock plastic packets so as stop the ingress of carbon dioxide into the specimens.

For creating accelerated carbonation condition, the specimens were kept inside a carbonation chamber with 3% CO_2 concentration, 27 °C and 65% relative humidity for 90 days. The specimens were kept fairly apart from each other so that carbonation can occur uniformly.

2.3 Experiments

Conditioning. All the mortar specimens were kept for 90 days under respective environmental conditions after which they were tested for determining various properties.

Compressive strength. Compressive strength test was used to determine the influence of carbonation on mechanical properties on carbonated and non-carbonated mortar specimens. The specimens were tested as per the provision of IS 4031—Part 6—1988.

Sorptivity test. Sorptivity test was used to determine the connectivity pores in the mortar specimens. This test was performed according to codal provisions of ASTM: C 1585—13. This test was conducted after completion of 90 days of environmental conditions. The surface was grinded after epoxy coating beacuse during applying the epoxy, sometimes it gets stick to the plane surface also. This epoxy can block the pores and the results for porosity can be misleading. Hence we grind the surface to remove the epoxy coating from plane surfaces. The samples were kept in a tray at 27 °C containing water such that the bottom of specimens is immersed in water up to a height of 1–3 mm.

Boiling water test. Boiling water test was used to determine the influence of carbonation on porosity of the specimens. This test was performed in accordance with the code ASTM C 642—13. After 90 days of conditioning, the specimens were kept in oven at 100 ± 5 °C until the decrease in mass of specimen is less than 0.5% on the consecutive day of oven drying. The mass was noted, and the specimens were kept in normal water at 27 °C for saturation until the increase in the mass is less than 0.5% on the consecutive day. The mass of specimens was noted, and they were kept in boiling water for 5 h at 100 °C. After 14 h, the mass of specimens was noted. After this, the specimens were submerged in water to determine their buoyant weight.

Carbonation depth. Carbonation depth was determined by spraying phenolphthalein indicator on freshly split mortar samples. The phenolphthalein indicator changes its color in presence of hydroxyl ions which indicates the presence of $Ca(OH)_2$ in case of cement blends. The portion of specimen which remains colorless indicates the carbonated region and the portion which turns pink indicates the uncarbonated region.

Reserve alkalinity. Reserve alkalinity was determined to quantify the amount of remaining OH^- ion in the paste sample. The powdered sample of hydrated paste sample was prepared by slicing and crushing the paste specimen on a mortar pestle. Powder was sieved through 150 μm sieve. 1 g of powder was mixed with 100 ml of water to form the solution. This solution was titrated against 0.1M H_2SO_4 until the pink color completely disappears. The solution was stirred continuously using magnetic stirrer so that the OH^- ions from the powder can easily dissolve in the solution.

Thermogravimetric analysis. Thermogravimetric analysis was carried out to quantify the amount of $CaCO_3$ in the paste after carbonation. In this study, TGA was carried out on powder sample in the temperature range of 30–1000 °C under a flow of 30 mL/min of N_2 and with a step rate of 20 °C/min. Samples for TGA were prepared by drying and grinding the disk samples. The disk samples were dried in isopropanol for 7 days. Isopropanol was changed at the end of 1 h, 1 day and 3 days.

Fig. 1 Non-carbonated and carbonated specimens after 90 days

They were subsequently stored in a desiccator under vacuum to evaporate the iso-propanol. The disk samples were ground to a fine powder using a pestle and mortar. Approximately 40 mg of the powder was used for each TGA analysis.

3 Result and Discussion

3.1 Carbonation Depth

After 90 days of carbonation, the average depth of carbonation was found to be 7 mm in LC^3 blend. This depth is very small because of the smaller duration of carbonation. If the duration of carbonation had been extended to 120 or 150 days, the carbonation would have been much more (Fig. 1).

3.2 Compressive Strength

The result shows that the compressive strength of mortar gets reduced after carbonation. Since the carbonation depth is very small, the difference in compressive strength is not very significant to drive a concrete conclusion. These results still give a fair idea that the strength is getting reduced upon carbonation. This may be due to the fact that more of CSH would have been carbonated and carbonation of CSH results in reduction of product volume. This reduction in volume results in decrease in compressive strength (Fig. 2).

Fig. 2 Test results for
compressive strength

Compressive strength of LC³
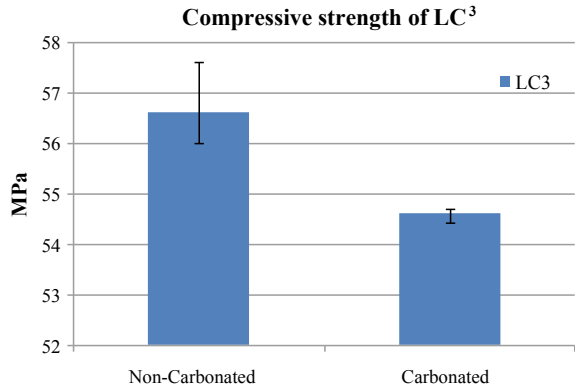
Fig. 3 Initial and final
sorption of carbonated and
non-carbonated mortar
specimens

Sorptivity in LC³
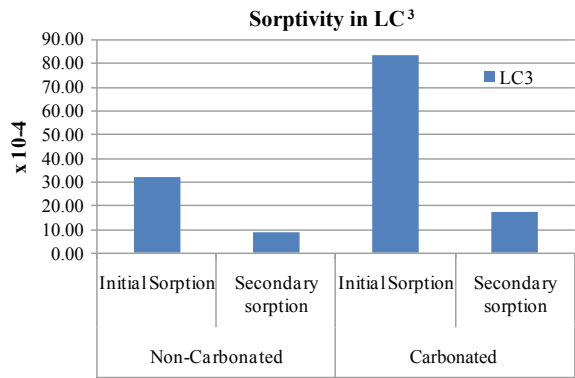
3.3 Test for Sorption

The results show that the rate of sorption is increased upon carbonation. This indicates that the pore connectivity is improved due to carbonation. Better pore connectivity is not a good sign from durability perspective as it becomes easier for foreign materials to ingress into the mortar (Fig. 3).

3.4 Boiling Water Test

The results show that there is no significant difference in the porosity of mortar. Therefore, nothing can be concluded regarding the influence of carbonation on porosity. We must try to increase the duration of carbonation to derive better conclusion (Fig. 4).

Fig. 4 Results for boiling water test

Porosity % in LC³
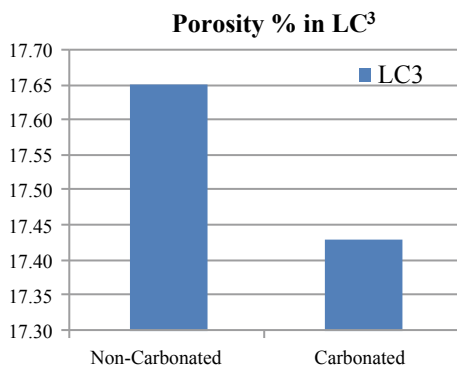
3.5 Thermogravimetric Analysis

The TGA curve shows that the mass drop in the range of 600–800 °C is more in case of carbonated samples when compared to non-carbonated sample. This indicates the presence of calcium carbonate which is formed after carbonation of calcium hydroxide and CSH (Fig. 5; Table 4).

Similarly, we see that the mass drop in the temperature range of 400–500 °C is more in non-carbonated samples than in carbonated samples. This indicates the presence of more calcium hydroxide present in the non-carbonated specimens.

Fig. 5 TGA curve for non-carbonated and carbonated paste samples

TGA curve for LC³
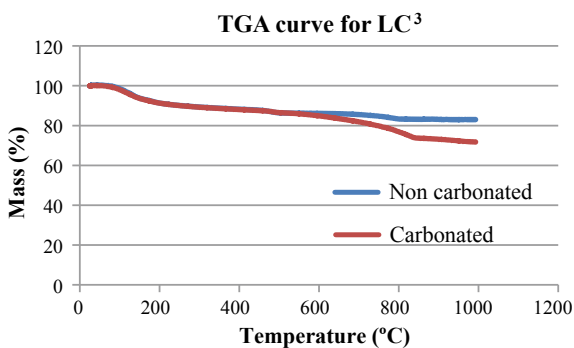
Table 4 Percentage mass loss due to decomposition in TGA

Decomposing material	Non-carbonated	Carbonated
$CaCO_3$	2.782	7.96
$Ca(OH)_2$	1.839	1.548

Fig. 6 Reserve alkalinity of
LC^3 paste samples

Reserve Alkalinity in LC^3
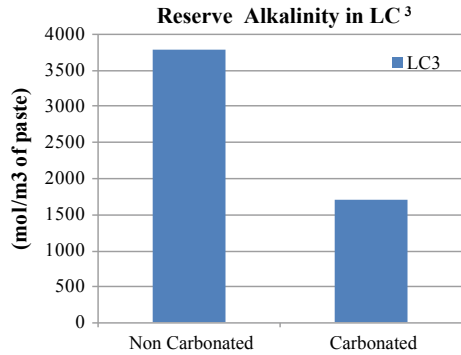
3.6   Reserve Alkalinity

The result shows that the alkalinity of paste is significantly reduced when subjected to carbonation. This indicates that the pH of paste drops when calcium bearing phases of hydrated paste are converted to calcium carbonates (Fig. 6).

4   Conclusion

The durability of LC^3 is reduced after carbonation. This is because of the better pore connectivity and low pH in the hydrated paste. These conditions allow more impurities to enter into the concrete, and the steel reinforcement gets deteriorated at a faster rate.

The effect of carbonation on compressive strength is not very significant as the difference in compressive strength of carbonated and non-carbonated specimens is very small. Further research must be conducted for determining the effect.

The carbonation is a very slow process in natural conditions. Even in accelerated conditions, the rate was very slow due to which the fractional volume that got carbonated is very small. To derive better conclusions, the duration should be 120–150 days such that a major fraction of volume gets carbonated.

Therefore, we conclude that the carbonation is a concern for durability in blended cements. It does not affect the mechanical properties to create a cause of concern.

References

1. Glass, G.K., Buenfeld, N.R.: Presentation of the chloride threshold level for corrosion of steel in concrete. Corros. Sci. **39**(5), 1001–1013 (1997)
2. Bertolini, L., Bernhard, E., Redaelli, P., Polder, R.: Corrosion of Steel in Concrete, 2nd edn. WILEY-VCH Verlag GmbH & Co. kGaA, Germany (2013)

3. Borges, P.H.R., Costa, J.O., Milestone, N.B., Lynsdale, C.J., Streatfield, R.E.: Carbonation of CH and C–S–H in composite cement pastes containing high amounts of BFS. Cem. Concr. Res. **40**(2), 284–292 (2010)
4. Chen, J.J., Thomas, J.J., Jennings, H.M.: Decalcification shrinkage of cement paste. Cem. Concr. Res. **36**(5), 801–809 (2006)
5. Phung, Q.T., Maes, N., Jacques, D., Bruneel, E., Van Driessche, I., Ye, G., De Schutter, G.: Effect of limestone fillers on microstructure and permeability due to carbonation of cement pastes under controlled CO_2 pressure conditions. Constr. Build. Mater. **82**, 376–390 (2015)
6. Venkat Rao, N., Meena, T.: A review on carbonation study in concrete. Mater. Sci. Eng. **263**(2017), 032011 (2017)

Durability of Concrete Containing Calcined Clays: Comparison of Illite and Low-Grade Kaolin

Gisela P. Cordoba, Silvina Zito, Alejandra Tironi, Viviana F. Rahhal and Edgardo F. Irassar

Abstract In this paper, durability parameters (water sorptivity, water penetration, chloride penetration and natural carbonation) are studied on conventional mixtures (w/cm = 0.50). Concretes were elaborated with Portland cement (PC) and blended Portland cements, containing 25% replacement by illitic calcined clay (ICC) and low-grade kaolinitic calcined clay (KCC). They were characterized by slump, compressive and tensile strengths and bulk porosity. Water sorptivity (ASTM C 1585) was determined on concretes cured 2, 7 and 28 days; water penetration test (EN 12390) and chloride penetration (ASTM C 1556) were determined on concretes cured 28 days. Carbonation depth undergoing a good and very good curing was assessed using a phenolphthalein indicator at 3 and 6 months of natural exposition. Results show that water sorptivity is reduced when concrete is curing for 2, 7 and 28 days for all concretes. KCC has a significantly lower sorptivity than PCC and ICC. At 28 days, the water penetration is deeper for ICC and lower for KCC concrete. All concretes have similar apparent chloride diffusion coefficients. After six months, the natural carbonation of all concretes is less than 2 mm, with a slightly lower performance of ICC and KCC than PCC.

Keywords Calcined clays · Concrete · Durability

1 Introduction

Nowadays calcined clays are one of the most studied materials for their use as supplementary cementitious material (SCM). Metakaolin (MK) has been the most studied calcined clay in the last time. Due to its high pozzolanic activity, the inclusion of MK improves the mechanical properties and durability of concrete [1]. According to Toledo Filho et al. [2], the incorporation of ceramic brick waste, with a chemical composition similar to the illitic calcined clay, improves sorptivity and reduces the

G. P. Cordoba · S. Zito · A. Tironi · V. F. Rahhal · E. F. Irassar (✉)
Facultad de Ingeniería—CIFICEN (UNCPBA-CICPBA-CONICET), B7400JWI Olavarría, Argentina
e-mail: firassar@fio.unicen.edu.ar

diffusion of chlorides. In addition, the total volume of pores increases, although their diameter decreases.

The durability of cement-based materials is greatly influenced by the transport properties, principally by the difficulty of aggressive agents (chlorides, sulfates, etc.) to penetrate into the concrete. These concrete properties depend strongly on the pore structure of the material, and the design of durable concrete requires the reduction of the porosity and permeability [3].

The penetration of aggressive ions by diffusion and capillary absorption is also governed by the same parameters that the porosity and permeability of concrete (the water–binder ratio, the cement content and the curing time). Chloride diffusion depends strongly on the open porosity and pore tortuosity of the cement paste. A decrease in the former and an increase in the latter tend to reduce the diffusion coefficient [3].

The carbonation of concrete is usually slowed down by the reaction of CO_2 with CH. It means that SCM that consumes the CH could lead to an increase in the carbonation depth, especially if the permeability of the concrete is not reduced by the pozzolanic reaction [4]. For example, MK reacts rapidly with the calcium hydroxide (CH) released by cement hydration and also accelerates the cement hydration, causing the reduction of the average pore size and the increase of volume of smaller pores [1].

After 28 days, mortars containing ground calcined brick clay (GCBC) showed an increase in the pore size refinement and the strength gain, and after one year, both the compressive strength and the fineness of the pore structure were greater than that of the control even though the total pore volume remains above that of the control. These results were attributed to the pozzolanic reaction of the GCBC and their products blocking and segmenting the capillary pore of the cement paste [5].

In this paper, durability parameters (water sorptivity, water penetration, chloride penetration and natural carbonation) are studied on conventional concrete mixtures (w/cm = 0.50) using an ordinary Portland cement and blended cements with 25% of kaolinitic and illitic calcined clays as cement replacement.

2   Materials and Methods

2.1   Materials

Concretes were elaborated with Portland cement (PC) and blended cements containing 25% replacement by low-grade kaolinitic calcined clay (KCC) or illitic calcined clay (ICC). Cementitious content was 350 kg/m³, and the w/cm ratio was 0.50.

Silica natural sand was used as fine aggregate, with a fineness modulus of 2.35 and a relative density of 2.67. Granitic crushed stone was used as coarse aggregate, with a maximum size of 16 mm, relative density of 2.70 and a weight per unit of loose and compacted volume of 1430 and 1560 kg/m³, respectively. The granulometric curves of the aggregates were composed with fractions of commercial aggregates to

Table 1 Concrete mixture proportion and workability properties

Concrete	Materials (kg/m^3)					Slump (cm)	Flow (%)
	Cement	Water	Crushed stone	Natural silica sand	SP (#)		
PC	350	175	1050	807	0.06	7.0	1.73
ICC	350	175	1050	788	0.12	9.7	2.50
KCC	350	175	1050	805	0.36	9.0	2.13

(#) % by cement mass

accomplish the A and B curves for total aggregates established in DIN 1045 standard, which corresponds to a fine aggregate/total aggregate ratio of 0.43.

A polycarboxylate-based superplasticizer admixture (SP) with a 40% active ingredient proportion (BASF, Germany) was used. The SP dose was adjusted to obtain a plastic consistency of the concrete (K2 or E2 consistency of EN206). The density difference of blended cements was offset by slightly modifying the sand content.

Concrete mixture proportions, slump (ASTM C 143) and flow (DIN 1048, EN 12350-5) are reported in Table 1.

2.2 Methods

Concretes were characterized by compressive and tensile strengths and permeable pore volume. Tests were carried out according to procedure described by ASTM C 39, ASTM C 496 and ASTM C 642 standard, respectively. Compressive and tensile strengths were determined on cylinders of 100 mm diameter and 200 mm in height. Bulk porosity was determined on cylinders of 100 mm diameter and 50 mm in height. Specimens for concrete characterization were cured 28 days in water.

The water capillary absorption (sorptivity) was determined according to Argentine standard IRAM 1871 on cylinders of 100 mm diameter and 50 mm in height. The specimens were water-curing for 2, 7 and 28 days. For the sorptivity rate determination, the specimens were dried at 50 °C up to a weight variation less than 0.1% and the lateral face was waterproofed. Then the underside of the specimen was submerged in water 3 mm in depth. At regular time, specimens were weighted to register the water suction. The sorptivity rate was determined as the straight line that best fits the water absorbed per unit area as a function of the square root of the time corresponding to the water absorbed between 10 and 80% of the sorptivity capacity (IRAM 1871 standard).

According to Villagrán, Alderete and De Belie [6], the straight line does not present a good fit when considering the square root of time. Therefore, a variation is introduced, considering the capillary absorption rate determined as the straight line that best fits the water absorbed per unit area as a function of the fourth root of the time ($t^{0.25}$). Hence, this procedure is used in this paper to achieve better adjustments

(adjustment higher than 0.98 is obtained, being lower for the most impermeable concretes).

Water penetration test was carried out according to EN 12390. It was determined on the mold side of 150 mm cubes curing 28 days in water.

Chloride penetration and profile were determined according to ASTM C 1556. Chloride diffusion was determined on cylinders of 100 mm diameter and 50 mm in height at 28 days of curing.

Carbonation was determined after three and six months of natural exposition in a rural area with a CO_2 concentration ranging from 350 to 400 ppm on prismatic specimens, 100 mm high and 70 mm side. The specimens were subjected to good and very good curing (7 and 28 days, respectively) and placed on exposing site with the molding and lateral surfaces of prism exposed to air and rain. Carbonation depth was assessed on saw sections of prims using solution of phenolphthalein indicator.

3 Results and Discussion

3.1 Concrete Characterization

At 28 days, compressive strength was 32.4, 28.6 and 37.4 MPa for PC, ICC and KCC, respectively. The ICC compressive strength is 91% with respect to PC. While the KCC compressive strength is 15% higher than the corresponding for PC. Concerning the tensile strength, PC, ICC and KCC reach 3.4, 2.8 and 3.6 MPa, respectively. The ICC's tensile strength was 83% of that PC's strength. The KCC's tensile strength surpasses the PC, being about 7% higher. Both compressive and tensile strength indexes exceed 75%, so the stimulation effect and the pozzolanic reaction generated by these calcined clays are confirmed.

The volume of permeable pore at 28 days is higher for the concretes ICC and KCC than PC. It is about 7 and 2% higher than PC for ICC and KCC, respectively. Previous studies made on similar materials and proportions using MIP show that ICC and KCC cements have a large porosity at 28 days, in accordance with the pore volume determined in concrete. Marchetti et al. [7] show that the volume of large (0.1–10 µm) and finer pores (0.01–0.1 µm) increased for cement with illitic calcined clay comparing with PC. On the other hand, Tironi et al. [8] for KCC reported that the volume of large pores (0.05–10 µm) was reduced and the volume of finer pores (0.01-0.05 µm) increased at 28 days. For KCC, the filler effect and the pozzolanic reaction are more significant earlier and the dilution effect can be compensated at 28 days, while more time could be necessary for calcined illitic clay. The increase of finer pores volume is attributed to the pore size refinement caused by the pozzolanic reaction of calcined clays. The large porosity of ICC could be attributed to the increase of volume in larger pores. The presence of calcined clays alters the pore structure, increasing the total porosity. However, the pore size distribution and their

connectivity differ with the calcined clay reactivity. For KCC, the pore tortuosity is higher, and the volume of larger pores is lower than for ICC.

3.2 Sorptivity

Figure 1 shows the results of sorptivity at 2, 7 and 28 days of curing for studied concretes. For all cases, the sorptivity decreases from 2 to 28 days. The KCC's sorptivity is notably lower than PC and ICC. The first sorptivity index of HKC is 67% lower than PC at 2 days, 55% at 7 days and 61% at 28 days. The first sorptivity index of HIC is 10% lower PC at 2 days, and it is higher than that the PC at 7 and 28 days (28% and 13%, respectively).

Even though KCC has a higher volume of permeable pores than PC, it shows a notably lower sorptivity rate and the water capillary rise was lesser than 50 mm. The
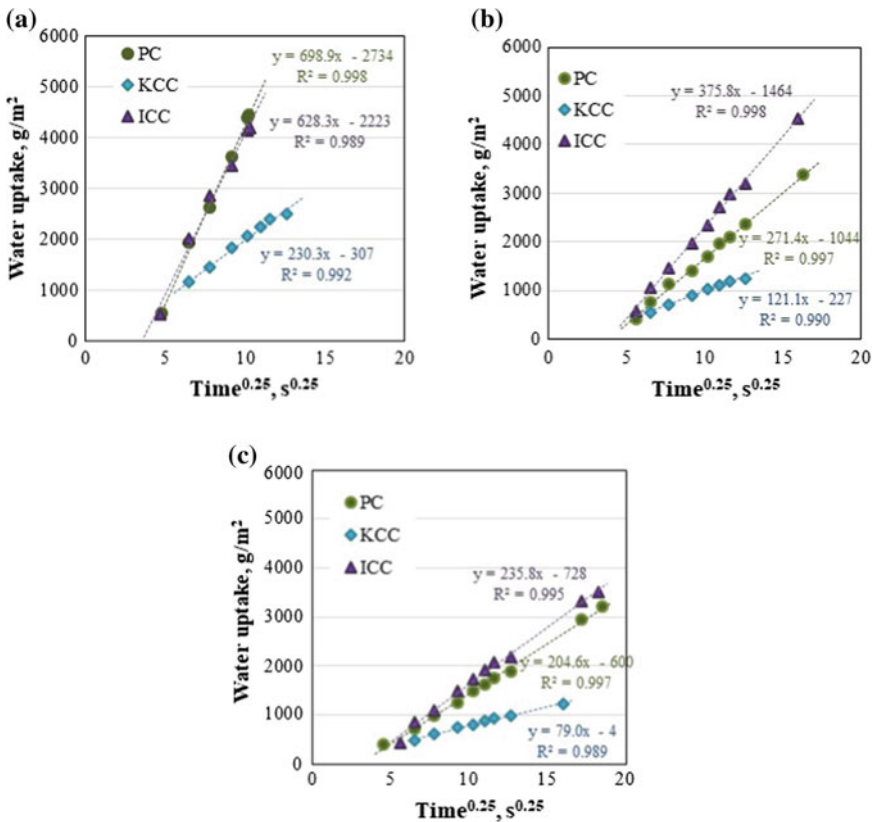
Fig. 1 Sorptivity test at **a** 2 days, **b** 7 days and **c** 28 days of curing

Table 2 Water penetration

		Concrete		
		PC	KCC	ICC
Penetration (mm)	Average	19.5	11.1	39.4
	Maximum	26.0	15.8	52.6
	Minimum	12.0	6.0	26.5

excellent results obtained are attributed to the disconnection of the total porosity due to the pozzolanic reaction of metakaolinite that appears at early ages reducing the larger pores.

The Argentine Code (CIRSOC 201) establishes a limit value of 4 $g/m^2/s^{0.5}$ for concrete to be used in structures with durable requirements. This limit is only applicable if the experimental data are analyzed with $t^{0,5}$. Villagrán et al. [9] propose a limit of 127 $g/m^2/s^{0.25}$ as equivalent to the limit established in CIRSOC 201 when the data are analyzed with $t^{0.25}$. According to this limit, only KCC cured at 7 and 28 days would satisfy the regulations for concretes exposed to severe environments.

3.3 Water Penetration

The average, maximum and minimum water penetration at 28 days for PC, ICC and ICC are shown in Table 2. It is observed that ICC presents a water penetration average 100% higher than PC, while for KCC, the water penetration was 43% lower than PC.

Water penetration results agree with the sorptivity results. The ICC porosity at 28 days is still high because the pozzolanic reaction of calcined illite is slow. KCC presents low larger pore volume due to the pozzolanic activity of MK after 7 days. Therefore, in spite of the higher porosity that shown KCC, it could appear as disconnected allowing to reduce water penetration. For PC and ICC, it would be convenient to perform the sorptivity and water penetration tests at 90 days to assess the influence of the later pozzolanic activity of the IC.

3.4 Chloride Diffusion

Figure 2 shows the total chloride (TC) profiles for PC, ICC and KCC curing 28 days in water immersed during 35 days in NaCl solution. It is clearly observed that the total chloride concentration decreases as the distance to the exposed surface increases.

The results for the bulk diffusion tests were also analyzed to obtain the best fit to calculate the diffusion coefficients using the solution to Fick's second law. Each diffusion curve was characterized by its equivalent apparent diffusion coefficient (Da) and the surface concentration (Cs). The results of Da and Cs are shown in

Fig. 2 Chloride profile for HPC, HKC and HIC concretes
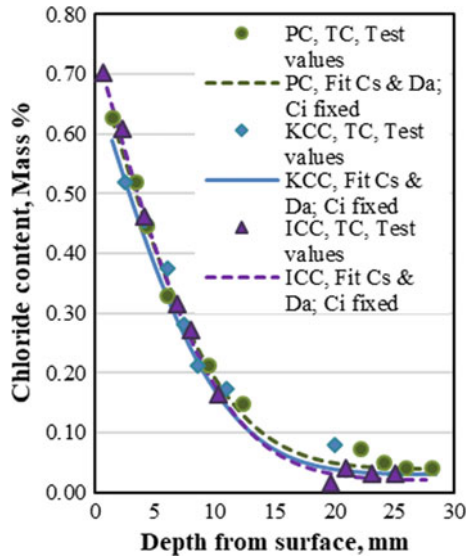
Table 3 Surface concentration (Cs) and equivalent apparent diffusion (Da)

Concrete	Cs (mass%)	Da (m²/seg)
HPC	0.72	11.2×10^{-12}
HIC	0.75	10.9×10^{-12}
HKC	0.68	12.9×10^{-12}

Table 3. Da has similar order in all concretes in spite of the incorporation of the KCC and ICC. Calcined clays effectively prevent the penetration of chloride ions into the concrete mass. Both KCC and ICC improved the pore structure by the filler effect. In addition, the pozzolanic reaction, resulting in a decrease of $Ca(OH)_2$, leads to more compact hydration products.

3.5 Natural Carbonation

Figure 3 shows the carbonation depth of PC, KCC and ICC cured 7 and 28 days in water and then exposed 3 and 6 months to natural carbonation conditions. Reported carbonation depth is the average depth for the molding face and the two lateral faces of the specimen. PC concrete with 7 days' water-curing has the lowest carbonation depth of reaching to 0.7 and 0.9 mm at 3 and 6 months of exposure. For PC cured during 28 days, the carbonation depth decreases slightly (0.4 and 0.8 mm at 3 and 6 months, respectively). For concretes containing calcined clays cured 7 days, ICC has the highest carbonation depth (1.7 mm) at 3 months. KCC and ICC have the same carbonation depth (1.9 mm) at 6 months. For concretes with 28 days of curing,

Fig. 3 Carbonation depth
for concretes cured 7 and
28 days, after 3 and 6 months
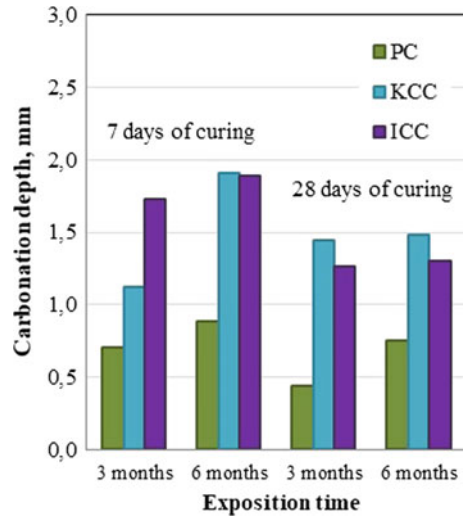
KCC has the highest carbonation depth at 3 and 6 months of exposure (1.4 and 1.5 mm, respectively). On the other hand, ICC has a carbonation depth of 1.3 at both exposure ages. Therefore, the presence of calcined clays as SCM decreases carbonation resistance both for poor and suitable curing. This is due to the fact that the replacement of cement by calcined clays increases the concrete porosity and reduced the calcium hydroxide availability, favoring the carbonation process.

It is observed that the carbonation depth for KCC concretes cured 7 days increases significantly between 3 and 6 months of exposure (70%), while for PC and ICC, the carbonation depth did not advance significantly (27% and 10%, respectively). For 28 days cured concretes, the most significant increases in carbonation depth between 3 and 6 months occurred for the PC (72%), while KCC and ICC show very little increases (3%). These results reveal the importance of proper curing for concretes containing calcined clays as SCM.

Carbonation does not dominate by porosity and pore connectivity, especially not for MK blended cements. This process also depended on the chemical composition, i.e., the amount of portlandite [10]. It is confirmed by the fact that although KCC has very low sorptivity, it has the highest carbonation penetration. It could be attributed to the low alkaline reserve of KCC caused by the pozzolanic reaction of MK consuming large proportion of CH. It allows the ingress of CO_2 without calcite forming and blocking the pore networks. In spite of KCC and ICC have a greater carbonation depth, these values are still acceptable as they do not exceed 2 mm and the carbonation rate is expected to decrease over time.

4   Conclusions

In this study, low-grade kaolin (KCC) and illite (ICC) calcined clays were used in concrete. These calcined clays have different water demand and pozzolanic reactivity causing a different hydration kinetic of paste that affects the development of porosity in concretes. The main conclusions on durable performance of conventional concrete are as follows:

- The volume of permeable pores at 28 days was higher for concretes with ICC and KCC than the corresponding to PC. However, the compressive strength of ICC was lower than that PC, and it was higher for the KCC.
- At early ages, ICC concrete performs worse than PC against capillary absorption and water penetration. It is attributed to the pozzolanic contribution of ICC that appears after 28 days. However, the later hydration causes a comparable performance against carbonation and chloride penetration to the obtained for PC.
- KCC concrete has good performance against capillary absorption and water penetration and the worse performance against carbonation. It is due to the pozzolanic activity after 7 days that consume large amount of calcium hydroxide, giving a more compact structure, but with low calcium reserve. Regarding the chloride penetration, its performance is comparable with the PC concrete.

References

1. Paiva, H., Silva, A.S., Velosa, A., Cachimc, P., Ferreira, V.M.: Microstructure and hardened state properties on pozzolan-containing concrete. Constr. Build. Mater. **140**, 374–384 (2017)
2. Toledo Filho, R.D., Gonçalves, J.P., Americano, B.B., Fairbairn, E.M.R.: Potential for use of crushed waste calcined-clay brick as a supplementary cementitious material in Brazil. Cem. Concr. Res. **37**(9), 1357–1365 (2007)
3. Cyr, M.: Eco-Efficient Concrete, 1st edn. Woodhead Publishing, Cambridge (2013)
4. Bucher, R., Cyr, M., Escadeillas, G.: Carbonation of blended binders containing metakaolin. In: Scrivener, K., Favier, A. (eds.) Conference on Calcined Clays for Sustainable Concrete, RILEM Bookseries, vol. 10, pp. 27–33. Springer, Heidelberg (2015)
5. Wild, S., Khatib, J.M., O'Farrell, M.: Sulphate resistance of mortar, containing ground brick clay calcined at different temperatures. Cem. Concr. Res. **27**(5), 697–709 (1997)
6. Villagrán Zaccardi, Y.A., Alderete, N.M., De Belie, N.: Improved model for capillary absorption in cementitious materials: progress over the fourth root of time. Cem. Concr. Res. **100**, 153–165 (2017)
7. Marchetti, G., Pokorny, J., Tironi, A., Trezza, M.A., Rahhal, V.F., Pavlík, Z., Černý, R., Irassar, E.F.: Blended cements with calcined illitic clay: workability and hydration. In: Martirena, F., Favier, A., Scrivener, K. (eds.) Conference on Calcined Clays for Sustainable Concrete, RILEM Bookseries, vol. 16, pp. 310–317. Springer, Heidelberg (2018)
8. Tironi, A., Scian, A.N., Irassar, E.F.: Blended cements with limestone filler and kaolinitic calcined clay: Filler and pozzolanic effects. J. Mater. Civ. Eng. **29**(9), 04017116 (2017)
9. Villagrán Zaccardi, Y.A., Alderete, N.M., Maio, Á.D.: La ganancia de peso por absorción capilar evoluciona linealmente con la raíz cuarta del tiempo. In: Bonavetti, V. (ed.) VIII Congreso Internacional—22ª Reunión Técnica de la AATH 2018, pp. 335–344. Asociación Argentina de Tecnología del Hormigón (2018)

10. Shi, Z., Geiker, M.R., De Weerdt, K., Lothenbach, B., Kaufmann, J., Kunther, W., Ferreiro, S., Herfort, D., Skibsted, J.: Durability of portland cement blends including calcined clay and limestone: Interactions with sulfate, chloride and carbonate ions. In: Scrivener, K., Favier, A. (eds.) Conference on Calcined Clays for Sustainable Concrete, RILEM Bookseries, vol. 10, pp. 133–141. Springer, Heidelberg (2015)

Assessment of the Efficacy of Waterproofing Admixtures Using Calcined Clay and SCMs

Nitin Narula, Lav Singh and Shashank Bishnoi

Abstract Waterproofing of concrete is important to prevent deterioration of concrete due to corrosion and carbonation. Integral waterproofing admixtures give varied results, in terms of strength of concrete and transport properties, with the change of cementitious materials. Presently, there is a lack of substantiated data for blended cement in terms of their efficacy with waterproofing admixtures especially Limestone Calcined Clay Cement (LC^3), which is a relatively new cement blend. This paper presents an experimental study on transport properties of mortar with the use of integral waterproofing admixtures. In this study, mortar mixes were prepared with LC^3 using different waterproofing admixtures, and the results have been compared with OPC and other blended cement as well. The effects on transport properties were determined by carrying out various tests, including the sorptivity test and boiling water test. The results were found to be useful in understanding the influence on capillary pores and pore volume due to the action of various waterproofing compounds in different cement blends.

Keywords Integral waterproofing chemicals · LC^3 · Capillarity · Sorptivity

1 Introduction

Concrete is a very durable material, and concrete structures have lasted numerous centuries without much deterioration. However, the durability issues increase manifold with the introduction of rebar in the concrete which gets deteriorated, primarily because of the presence of water. The property of concrete which makes it most susceptible to deterioration is its porosity and permeability. This is because concrete as a structure is very porous and hence allows water and gases to penetrate in various forms by various transport processes [1]. The solution lies in the prevention of ingress

N. Narula (✉) · L. Singh · S. Bishnoi
Indian Institute of Technology Delhi, Delhi, India

S. Bishnoi
e-mail: shashank.bishnoi@civil.iitd.ac.in

641

of liquids, to stop ions ingress, and gaseous materials by using certain admixtures [2].

Integral waterproofing admixtures refer to the compounds which are added to the concrete raw ingredients at the time of preparation of concrete. These compounds function within the pores of the concrete and are believed to grow in the pores structure. This admixture type of waterproofing treatment has an advantage over surface coating in terms of puncture, tear, or abrasion and hence said to have a long-lasting effect on the durability of concrete.

Waterproofing could be achieved by using both hydrophobic and hydrophilic reagents. Hydrophobic materials work by repelling the water, while hydrophilic material used in waterproofing admixtures works mostly by blocking the transportation of water by crystallization in the network of pores [3]. Most of the research till date has been focused on surface protection of concrete, and there is an existing research gap in integral compounds and their efficacy. Due to these reasons, the study is based on integral waterproofing agents.

2   Experimental Methods

The transport properties were tested by conducting various experiments like sorptivity test and boiling water test.

The present study is a comparison of the efficacy of IWAs with four types of cement blends to include a unary blend OPC, a binary blend of OPC + 30% FA (PPC), a binary blend of OPC + 50% slag (PSC), and a ternary blend of OPC + 30% CC + 15% LS (LC^3). The mix design was prepared by keeping the water content and total cementitious material (TCM) constant. The water to binder ratio was kept at 0.4 and binder to sand as 1:3. The admixtures were added as per the recommended dosage, and water correction was also incorporated in the mix.

2.1   Integral Waterproofing Admixtures

In the present study, three different integral waterproofing admixtures were used. The details are shown in Table 1.

2.2   Casting, Curing, and Conditioning

The casting was carried out for four types of cement blends and with three admixtures for each blend. For each mix, eight cubes (of 70.6 mm side) and three cylinders (diameter 100 mm, height 200 mm) were cast. After casting, the moulds were kept in the conditioning room and were de-moulded after 24 h. OPC and LC^3 samples were

Table 1 Brief description of integral waterproofing admixtures

Abv.	Type and description	Dosage
IW1	Hydrophobic pore-blocking ingredient (HPI) for concrete. It is a colourless, clear to slightly cloudy viscous liquid	2.0 L per 100 Kgs of cementitious binder
IW2	Integral crystalline waterproofing admixture in powder form. The active chemicals in the admixture react with moisture in the concrete resulting in crystalline formation within the pores and capillary tracts of concrete	Dosage of 1% by weight of the cementitious binder
IW3	Integral crystalline waterproofing admixture of a different industrial brand	Dosage of 1% by weight of the cementitious binder

cured for 28 days whereas PPC and PSC samples were cured for 56 days. During curing, the samples were kept in a temperature controlled room with temperature controlled at 25 ± 2 °C.

After curing, the samples were kept in the conditioning chamber for 45 days of conditioning at 25 ± 2 °C temperature and 65 ± 2% of humidity.

2.3 Sorptivity and Boiling Water Tests

Sorptivity test is used to determine the rate of absorption (sorptivity) of water by measuring the increase in the mass of specimen due to the water absorbed. The experiment was conducted as per the procedure mentioned in ASTM C 1585-13.

Boiling water test is used to determine the density, percent absorption, and percentage voids in the hardened mortar or concrete samples. The calculation for obtaining the volume of permeable voids was done as per ASTM C642-13.

3 Results and Discussions

The results of experiments conducted to analyze various transport properties of mortar have been discussed in this section.
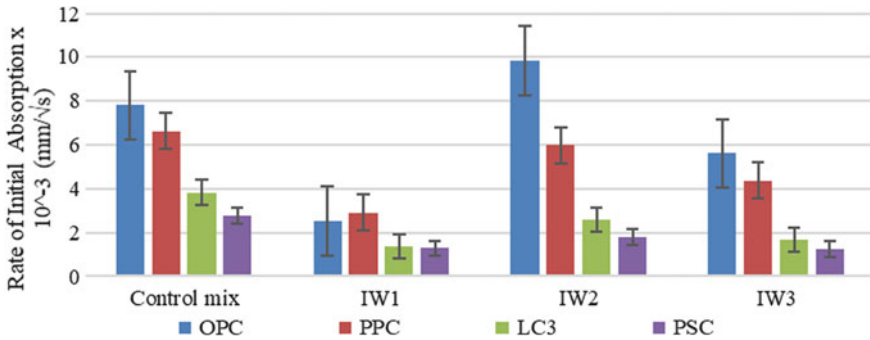
Fig. 1 Sorptivity of various admixtures—initial absorption

3.1 Assessment of Capillary Action—Sorptivity Test

It can be inferred from Fig. 1 that there is a substantial drop in sorptivity with the use of IW1 in all types of cement blends. For OPC, the reduction in initial sorptivity is 67% and the reduction in secondary sorptivity is 43%.

For LC^3 samples, there is a substantial reduction in the initial rate of absorption in comparison with OPC and PPC as the calcium carbonate supplied through limestone and the extra alumina provided by calcined clay will further react to form alumina phases [4]. This alumina phase reacts vigorously in comparison with pozzolanic cement, and hence, there is densification of microstructure which reduces porosity. The reduction in LC^3 in initial sorption amounts to 50% while the reduction in secondary sorption is 66%.

3.2 Evaluation of Pore Volume—Boiling Water Test

The results of porosity have also been analyzed with the usage of various admixtures. Hydrophobic admixture IW1 has given the maximum reduction in porosity in comparison with OPC. Porosity in case of OPC was reduced by 50% for IW1, 17% for IW2, and 27% for IW3 as shown in Fig. 2. These results are in confirmation with sorptivity results obtained for the same admixtures. Both the crystalline admixtures have given a reduction in porosity but the maximum reduction is obtained in hydrophobic admixtures.
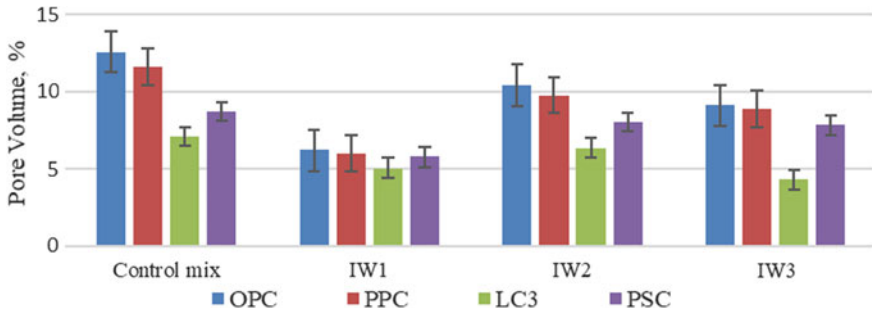
Fig. 2 Results of boiling water test done on various admixtures with different percentage of clinker replacements

4 Conclusion

LC^3 an emerging cement blend showed similar or in some cases better results when compared with conventional cement blends made with OPC and other pozzolanic cement in terms of transport properties. Its usage along with the addition of integral waterproofing admixtures enhances its properties with regard to the durability of concrete. The study can be summarized with the following conclusions.

- LC^3 has substantially less porosity and capillarity as compared to OPC and other cement blends like PPC and PSC as well.
- PPC blend has a marginal reduction in sorptivity and porosity whereas PSC has a substantial reduction in the same. The reduction in PSC is almost similar to that achieved in LC^3 blend.
- Use of integral waterproofing admixtures reduces the porosity and sorptivity with all cement blends commonly used in the construction industry to include OPC, PPC, PSC, and LC^3.
- Hydrophobic admixtures give better results than crystalline admixtures in aspects of reduction of sorptivity and porosity.

References

1. Mehta, P.K., Monteiro, P.J.: Concrete Microstructure, Properties and Materials (2017)
2. Bertolini, L., Pedeferri, P., Redaelli, E., Polder, R.: Corrosion of Steel in Concrete
3. Pan, X., Shi, Z., Shi, C., Ling, T.-C., Li, N.: A review on concrete surface treatment part I: types and mechanisms. Constr. Build. Mater. **132**, 578–590 (2017)
4. Díaz, Y.C., et al.: Limestone calcined clay cement as a low-carbon solution to meet expanding cement demand in emerging economies. Devel. Eng. **2**, 82–91 (2017)

Corrosion Properties of Self-Compacting Lightweight Concrete Using Metakaolin

Santosh K. Patro, S. N. Manu and P. Dinakar

Abstract Combining the advantages of both lightweight concrete and self-compacting concrete in a single entity will be highly beneficial in offshore structures. Due to the addition of porous lightweight aggregate durability of these structures in adverse environment will be a matter of great concern. From the earlier studies, it was clear that the inclusion of metakaolin in normal aggregate concrete exhibits superior durable performance. The present study evaluates the effect of metakaolin in the corrosion performance of the high strength self-compacting lightweight aggregate concrete. The corrosion properties were accessed using various experimental techniques such as rapid chloride penetration test, surface resistivity, alkalinity and corrosion rate. All the concretes were developed with binder content 550 kg/m^3 and water-binder ratio maintained as 0.28. The metakaolin replacement percentages have been varied as 7.5, 10, 12.5 and 15%. The results indicate that all the durable parameters of concretes have been improved due to the inclusion of metakaolin. Also pH level of all the concretes is well above the threshold value. This evidence justifies that metakaolin is potential material for the development of high performance lightweight self-compacting concrete.

Keywords LWA · SCC · HPC · Metakaolin

1 Introduction

Structural lightweight concrete has been used in several structural applications for thousands of years and now its use is rapidly increasing due to its economic and technical potentials [1]. In the early 90s, the development of self-compacting concrete

S. K. Patro
Works Department Govt. of Odisha, Bhubaneswar, India

S. N. Manu
Department of Civil Engineering, ASTRA Hyderabad, Hyderabad, India

P. Dinakar (✉)
School of Infrastructure, IIT Bhubaneswar, Bhubaneswar, India

(SCC) enabled the execution of concrete structures without the need for vibration due to its flow ability and self-consolidating capabilities [2]. In recent years, some efforts have been made to couple the advantages of both lightweight concrete and self-compacting concrete in one package which is called as self-compacting lightweight aggregate concrete (SCLWAC). Even though a great deal of investigations has been made till date to study the properties of self-compacting concrete using variety of lightweight aggregate, characterization and behavior of sintered fly ash lightweight aggregates for development of high strength self-compacting concrete are still limited.

The most significant potential advantage of the use of sintered fly ash lightweight aggregates for SCC is the environmental value [3]. For several decades' utilization of fly ash as a cement substitution material has been practiced by many researchers. Coal-fired thermal power plants generate large quantities of fly ash (FA), but only a small amount can be used in concrete industry. Utilization of FA in production of artificial aggregate has attracted the attentions of investigators and practitioners as an alternative way for larger consumption. Since aggregate is the main occupant of concrete (about 50–75% of total concrete volume), it may be considered as an effective solution to use such waste materials as artificial aggregate in concrete. Fly ash lightweight aggregates when used not only acts as a substitute for natural coarse aggregates but also helps in the utilization. Also the use of sintered fly ash lightweight aggregates can be advantaged for the structures due to significant reduction in dead loads, high thermal insulation and enhanced fire resistance provided that the fresh mechanical and durability characteristics of SCLWAC are comparable to normal weight SCC. Inclusion of supplementary cementitious material is one of the ways to improve the mechanical and durability properties. Apart from the most commonly used mineral admixtures, such as fly ash, slag and silica fume, metakaolin is not a by-product. It is mostly manufactured by thermally activating purified kaolinite clay within a specific temperature range (650–800 °C) [4]. The main objective of the present study is to investigate experimentally the influence of metakaolin in the corrosion characteristics of high strength lightweight aggregate self-compacting concrete.

2 Materials and Methods

2.1 Materials and Mix Design

Ordinary Portland cement (53 grade) confirming to IS: 12269 [5] was used as the primary binding material, and metakaolin (MK) is used as supplementary cementitious materials (SCMs). The different size fractions of sintered fly ash aggregates (20,12.5 and 6.3 mm) were taken as coarse aggregates and well-graded natural river sand having a maximum size of 4.75 mm were used as fine aggregates, to attain a well-packed

Table 1 Mix proportions adopted in the present study

Mix ID	TCM (kg/m^3)	Cement (kg/m^3)	FA (%)	MK (%)	Coarse aggregate (kg/m^3)			Sand (kg/m^3)	w/b
					20 mm	12.5 mm	6.3 mm		
Control	550	412.5	25	0	110	123	259	775	0.36
7.5 MK	550	371.25	25	7.5	111	122	258	772	0.36
10 MK	550	357.5	25	10	110	122	257	771	0.36
12.5 MK	550	343.75	25	12.5	109	122	257	769	0.36
15 MK	550	330	25	15	109	122	256	768	0.36

aggregate matrix. Commercially, available polycarboxylate ether (PCE)-based superplasticizer was used in the present study. The mix proportion adopted in the present investigation has been given in Table 1. The number in the mix designation indicates the percentage replacement of the metakaolin and MK stands for metakaolin. In the mix design, the SCCs were designed in such a way that the control mix was designed with binary (Portland Cement + Fly Ash (FA)) in which a 25% of Portland cement was replaced with fly ash only, and subsequently four SCC mixtures with metakaolin (7.5, 10, 12.5 and 15 MK) were designed in which a proportion of Portland cement was replaced with varying percentage of metakaolin. The mix design procedure established earlier by Dinakar and Manu [6] for SCC was used in this present investigation.

2.2 Experimental Methods

The experimental program was formulated in such a way that the strength of the concretes was assessed by compressive strength. The corrosion properties were accessed using various experimental techniques such as rapid chloride penetration test, surface resistivity, alkalinity and corrosion rate. Rapid chloride penetration test was conducted in accordance with ASTM C 1202 [7]. The alkalinity of the concretes was determined using the powdered sample. To determine the ionic conductivity of the concrete, surface resistivity has been conducted using the Wenner four probe apparatus on a cylindrical sample. To understand the status of the reinforcement steel embedded within the concrete, corrosion rate was monitored using potentiodynamic polarization technique. Corrosion currents were determined by electrochemical potentiodynamic polarization technique (Tafel extrapolation) methods. Three electrodes were used: reinforcing steel as a working electrode, saturated calomel electrode as standard reference electrode and guard ring as the auxiliary or counter electrode.

3 Results and Discussions

3.1 Fresh Properties and Compressive Strength

All of the five concrete mixtures were designed to give a slump flow diameter of 650 ± 10 mm, which was acquired by adjusting the dosage of superplasticizer (SP) used. Targeted slump flow diameter was attained in all the SCC mixtures. Similarly, the L-Box passing abilities ratios and the V-funnel flow times varied between 0.86–0.82 and 17–25 s as the metakaolin replacements increased from 7.5 to 15%. Therefore, all the fresh SCC mixtures have confirmed to EFNARC-2005 [8] guidelines and can be considered as SCCs. It was observed that the SP demand increased with increase of MK replacement in SCC. This may be due to the higher surface area of the binder, thus its higher reactivity than control mix.

The compressive strengths obtained in various age of curing has been depicted in Fig. 1. As noted from the results, it has been observed that there is a general trend of increasing strength with age for all the concrete mixtures with and without addition of MK. For SCC with MK mixes, the highest rate of strength development over control concrete was observed in 3, 7 days, respectively, and this is because the pozzolanic reaction starts at very early stages of hydration, and hence the contribution of MK toward strength is more significant at early ages. This finding is similar to earlier studies [9]. According to literature, it was suggested that there are three elementary factors influencing the contribution that MK makes to strength when it partially replaces cement in concrete. These are the filler effect, the acceleration of
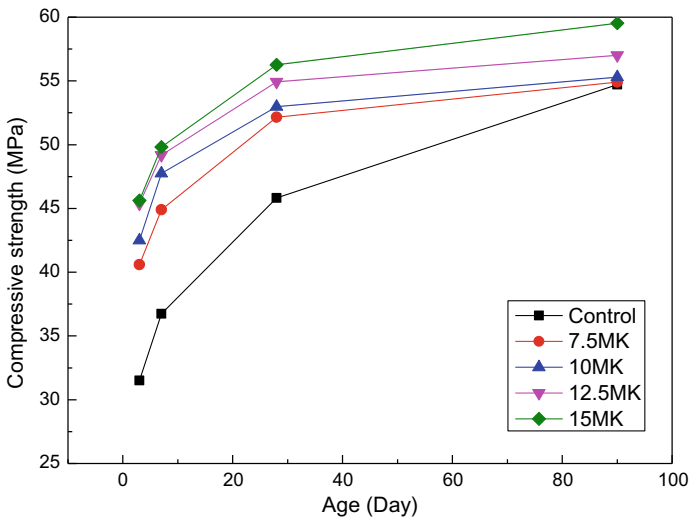
Fig. 1 Variation of compressive strength with age of all mixtures

OPC hydration and the pozzolanic reaction of MK with calcium hydroxide (CH) [10]. The compressive strength was the highest for the 15 MK mixtures achieving strength of nearly 60 MPa at 90 days.

3.2 Rapid Chloride Penetration Test (RCPT)

The results of the rapid chloride test of all SCLWACs measured after 90 days of curing are shown in Fig. 2. The results of test are compared in accordance with ASTM 1202 [7] to assess the concrete quality. From the results, it can be seen that all the concrete specimens showed "very low" chloride permeability. It is well established that the binary and ternary incorporation of fly ash and metakaolin in SCC results in drastic reductions in the Coulomb charges. Sintered fly ash lightweight aggregates transported chloride ions more quickly due to their high open porosity, but in case of high strength concrete which is rich with cementitious materials and pores are expected to be discontinuous, will limit the ingress of chloride ions into the concrete. The reason for "very low" chloride ion penetrability in control mix may be use of fly ash probably resulted in a denser matrix, by reducing the pore size and thickness of transition zone between aggregate and surrounding cementitious matrix. The effect of fly ash on the chloride ion penetration of concretes was also studied by other researchers. It can be seen that the total charge passed for the MK concrete mixes from 7.5 to 15 MK is lower than the control concrete. The results indicate that SCCs having metakaolin exhibited more resistance toward chloride ion penetration than control concrete. This can be attributed to three primary actions, which are the filler effect, acceleration of cement hydration and by means of pozzolanic reaction. A similarly enhancing effect of MK as a replacement material was also reported earlier by Dinakar et al. [11].
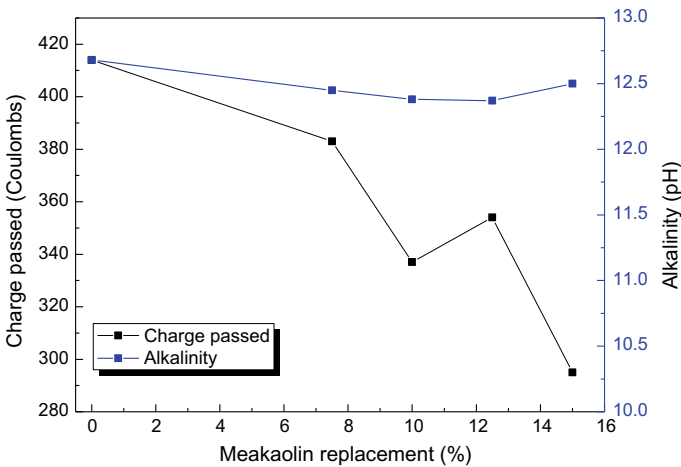
Fig. 2 Charge passed in RCPT and alkalinity with respect to metakaolin dosage

3.3 Alkalinity

The results of pH values of all SCLWACs measured at 90 days are presented in Fig. 2. The pH values of MK concretes were measured for various replacement levels and these ranges between 12.37 and 12.50 at 90 days and these values are marginally lower than that of control mix, but the reduction is insignificant. Since the reduction in pH is not significant, it can be inferred that addition of MK up to 15% does not adversely affect the alkalinity of concrete. All the SCCs had pH values around 12.0, which is above the threshold value of 9.5 mentioned earlier by Hobbs for de-passivation of steel [12].

3.4 Surface Resistivity

The results of the surface resistivity of investigated concretes and variation of surface resistivity with age are shown in Fig. 3. All the concrete mixes show an increase in resistivity as a function of time, owing to the micro-structural changes in the hydrated paste and the consequent reduction in porosity of the concrete. It can be seen from the results that the resistivity of self-compacting concretes increases with age may be due to pore refinement induced by the pozzolanic reaction. The resistivity also increases with increase in metakaolin. In addition, for all the concretes resistivity values were more than 20 kΩ-cm at 90 days which indicates "low corrosion" as per the assessment criteria suggested by ASHTO TP 95 [13].
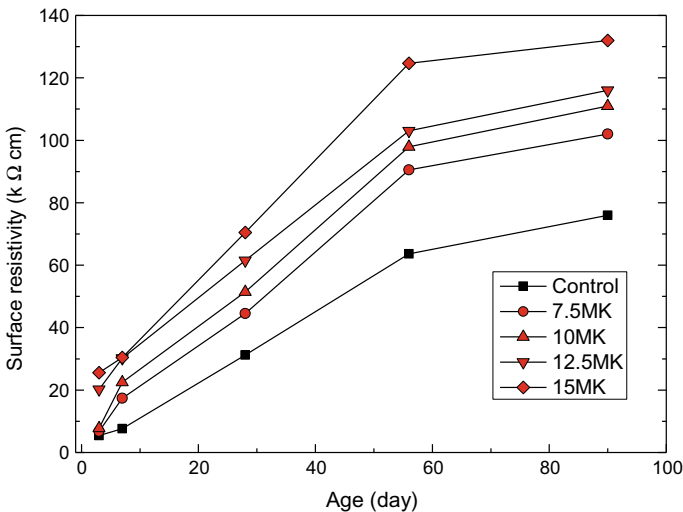
Fig. 3 Variation of surface resistivity with age of all mixtures
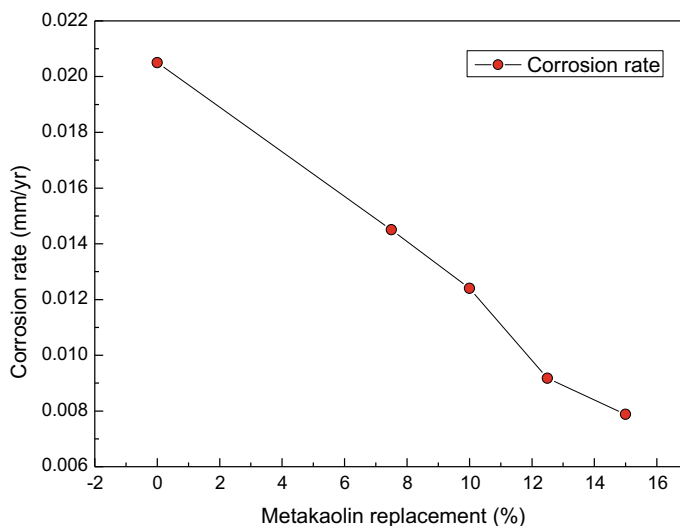
Fig. 4 Variation of corrosion rates with respect to metakaolin dosage

3.5 *Corrosion Rate*

The corrosion rates calculated based on the Tafel plots for self-compacting concretes are presented in Fig. 4. From these results, it can be seen that in the control mix concrete the corrosion rate is in the intermediate range but as the metakolin replacement increased from 7.5 to 15% (7.5–15 MK mixes) the corrosion rate decreases correspondingly showing negligible corrosion rates. This improved corrosion resistance of SCCs with MK may be attributable to the pore filling effect of metakaolin during cement hydration reaction. Also the alkalinity near the steel anode perfectly maintained throughout the time as shown in the previous section.

4 Conclusions

- The strength increase by MK SCC is effective only at the early age in the long term; the strength increase is only marginal.
- All SCLWACs show chloride ion penetration values less than 1000 coulombs of total charge passing which assessed them to be "very low."
- The resistivity increases with age and with increase in percentage of metakaolin in all lightweight aggregate SCCs. All the concretes were seen to be very good in terms of the resistivity.
- It was also observed that due to addition of mineral admixtures such as fly ash and metakaolin the alkalinity of concrete was not significantly affected.

- The corrosion rates measured from potentiodynamic polarization studies indicate rate of corrosion varies from "intermediate" to "negligible" in lightweight aggregate SCCs. Also, as the metakaolin replacement increased the corrosion rates decreased.

References

1. ESCSI: Lightweight Concrete—History, Application, Economics. Expanded Shale, Clay, and Slate Institute, Salt Lake City, UT (1971)
2. Okamura, H.: Self-compacting high-performance concrete. Concr. Int. **19**(7), 50–54 (1997)
3. Chandra, S., Berntsson, L.: Lightweight Aggregate Concrete: Science, Technology, and Applications. Noyes Publications, Norwich, New York, U.S.A (2002)
4. Dinakar, P.: High reactive metakaolin for high strength and high performance concrete. Indian Concr. J. **85**(4), 28–34 (2011)
5. IS: 12269, Indian Standard: Specification for 53 Grade Ordinary Portland Cement. Bureau of Indian Standards, New Delhi (1987)
6. Dinakar, P., Manu, S.N.: Concrete mix design for high strength self-compacting concrete using metakaolin. Mater. Des **60**, 661–668 (2014)
7. ASTM C1202-12 Standard Test Method for Electrical Indication of Concrete's Ability to Resist Chloride Ion Penetration. ASTM International, West Conshohocken, PA (2012)
8. Self-Compacting Concrete European Project Group. The European Guidelines for Self-Compacting Concrete. BIBM, CEMBUREAU, EFCA, EFNARC and ERMCO. 2005. http://www.efnarc.org. Accessed 27/01/2012
9. Caldarone, M.A., Gruber, K.A., Burg, R.G.: High reactivity metakaolin a new generation mineral admixture. Concr. Int. **16**(11), 37–40 (1994)
10. Kadri, E.H., Kenai, S., Ezziane, K., Siddique, R., De Schutter, G.: Influence of metakaolin and silica fume on the heat of hydration and compressive strength development of mortar. Appl. Clay Sci. **53**(4), 704–708 (2011)
11. Dinakar, P., Sahoo, P.K., Sriram, G.: Effect of metakaolin content on the properties of high strength concrete. Int. J. Concr. Struct. Mater. **7**(3), 215–223 (2013)
12. Hobbs, D.W.: Carbonation of concrete containing PFA. Mag. Concr. Res. **40**(143), 69–78 (1988)
13. AASHTO TP 95: Standard Method of Test for Surface Resistivity of Concrete's Ability to Resist Chloride Ion Penetration. American Association of State Highway and Transportation Officials, Washington, DC (2011)

Performance of Blended Cements with Limestone Filler and Illitic Calcined Clay Immediately Exposed to Sulfate Environment

Agustin Rossetti, Tai Ikumi, Ignacio Segura and Edgardo F. Irassar

Abstract The use of ternary blended cements with limestone filler and calcined clays can improve the durability of concrete structures exposed to aggressive environments and extend their service life. In sulfate-rich environments, the effects of supplementary cementitious materials depend on the replacement level and the progress of hydration. Low level of limestone filler contributes to the stabilization of AFt due to formation of monocarboaluminate. However, high replacement increases the effective w/c ratio and the capillary porosity, favoring the sulfate penetration. The use of active pozzolans improves sulfate resistance by reducing portlandite content and the permeability, which minimize ettringite and gypsum formation and sulfate penetration. It is generally assumed that curing prior to sulfate exposure should be extended to allow the pozzolanic reaction to progress. It is currently uncertain the effectiveness of calcined clay in combination with limestone filler when the cement is exposed immediately to aggressive environments. Typical structures affected by sulfate attack are commonly built in situ, thus being exposed to the aggressive environment since casting. This paper analyzes external sulfate attack of blended cements with 30% replacement by combinations of limestone filler and/or calcined clay exposed to Na_2SO_4 solution at two days after casting. For that, expansions, mass variation, visual appearance and compressive strength are monitored in mortars and pastes during 6 months. The evolution of microstructure was evaluated with XRD. Despite the lack of curing prior to sulfate exposure, cement with calcined clay showed an excellent resistance to external sulfate attack, while limestone cements presented a worse performance.

A. Rossetti (✉)
Comisión de Investigaciones Científicas de la Provincia de Buenos Aires, CICPBA-LEMIT, La Plata, Argentina

T. Ikumi · I. Segura
Department of Civil and Environmental Engineering, Universitat Politècnica de Catalunya Barcelona Tech, Jordi Girona 1-3, C1, E-08034 Barcelona, Spain

E. F. Irassar
Facultad de Ingeniería, CIFICEN (UNCPBA-CICPBA-CONICET), B7400JWI Olavarria, Argentina
e-mail: firassar@fio.unicen.edu.ar

1 Introduction

Illite is one of the most abundant clayed minerals of the earth's crust coming from the alteration of feldspars and micas of rocks due to the weathering process. Illite clays develop pozzolanic properties when clays are thermally treated at 950 °C [1] causing dehydroxylation and collapse of structure to form a metastable or amorphous aluminosilicate [2]. These pozzolanic properties combined with the large availability of this mineral place illite calcined clays as a key supplementary material for the future mineral admixtures used in concrete.

Despite the promising characteristics of calcined clays described, a safe introduction of these materials in the concrete technology requires the assessment of other aspects, such as the durability against different aggressive environments. External sulfate attack (ESA) has been recognized as a complex degradation phenomenon that may cause severe damage in cement-based materials [3]. High resistance to ESA in Na_2SO_4 solutions is normally associated with a segmented pore structure and low levels of portlandite (CH) and aluminate phases available to limit sulfate ingress and ettringite formation [4]. Another important issue hardly ever evaluated for ESA resistance is the early sulfate exposure. In reality, the source of external sulfate ions is usually found in sulfate-rich soils and underground waters in contact with concrete. Therefore, ESA is especially significant in underground structures like foundations, tunnels or waste containers. Due to their large size, these structures are usually built in situ, hence being exposed to sulfates since casting. However, most studies about the ESA in laboratory rely on testing of specimens cured several days in limewater prior to immersion in the aggressive sulfates solution [5].

The aim of this paper is to make a comparative study of the performance of blended cements with the addition of filler and illitic calcined clay against sulfate attack without previous curing that commands the standards to evaluations of the sulfate attack when supplementary materials are used. Three paste and mortar compositions with different contents of limestone filler and illitic calcined clay were cast to evaluate the mineralogical changes (X-ray diffraction) and the evolution of physical and mechanical properties (mass variation, visual aspect, expansion and compressive strength) during ESA.

2 Materials and Methods

Portland cement (CEM I 52.5 R) with high C3A-content (8.2%), limestone filler composed by high purity calcite (LF) and illitic calcined clay (ICC) were used in these experiences. Their chemical composition determined by XRF is reported in Table 1.

Table 1 Chemical composition and loss on ignition of cement, filler and ICC, %

Material	CaO	SiO$_2$	Al$_2$O$_3$	Fe$_2$O$_3$	MgO	SO$_3$	K$_2$O	Na$_2$O	LOI
Cement	60.92	16.58	4.21	1.80	2.16	1.77	0.67	0.28	2.05
Filler	59.53	<0.01	1.10	0.52	0.48	0.06	0.060	<0.01	39.98
ICC	0.33	66.30	16.28	9.23	1.46	<0.01	5.60	0.08	0.58

The illitic clay from quarry near to Olavarría city (Province of Buenos Aires, Argentine) was calcined in oven at 950 °C and ground in laboratory ball mill until 90% of particles were less than 45 µm. XRD analysis reveals that the clay is completely dehydroxylated and the formation of hematite, while the quartz remains as the main impurity. The illitic calcined clay (ICC) meets the chemical requirements for Class N pozzolan (ASTM C 618): S + A + F > 70%; SO$_3$ < 4% and LOI < 10%. For this ICC, the Frattini test was positive after 14 days also strength test was made in another paper [1].

Physical characteristic of the materials, density (ASTM C 188), retained on 75 and 45 µm sieves (ASTM D 422 and C 618), Blaine specific surface (ASTM C 204) and the particle size distribution (PSD) determined using the laser granulometer (Malvern Mastersizer 2000) are reported in Table 2. The particle size distribution by volume of materials is shown in Fig. 1.

For this study, the SCM replacement in all binders was set to 30% by cement weight. By this way, all compositions present the same initial C3A content and thus, the different behaviors observed can be solely attributed to the effects of the SCMs introduced. Three different blended cements were prepared: a binary filler cement (70% CEM + 30% LF), a binary calcined clay cement (70% CEM + 30% Calcined clay) and a ternary blended cement (70% CEM + 15% Calcined clay + 15% LF). The nomenclature adopted is C30F, C30CC and C15F15CC, respectively.

Pastes were prepared using water to binder ratio of 0.485 (as prescribed by ASTM C1012) and mixed using high-speed mixer, and remixed every 30 min during six hours to prevent bleeding and segregation. Eighteen cubes of 20 mm-edge were cast for each blended cement and cured in moist cabinet. After 24 h, cubes were demolded and separated into two groups. Twelve cubes were immersed in 50 g/l Na$_2$SO$_4$ solution and the remaining cubes in water at 20 °C.

Table 2 Physical characteristic of cement, cements and filler

Property/material		Cement	Filler	ICC
Density		3.10	2.70	2.63
Particle size distribution	Dv10 (µm)	1.8	1.7	1.6
	Dv50 (µm)	20.1	6.6	8.8
	Dv90 (µm)	65.1	72.2	33.7
Specific surface area	BET (m^2/g)	1.10	3.74	
	Blaine (m^2/kg)			522

Fig. 1 Particle size distribution of materials
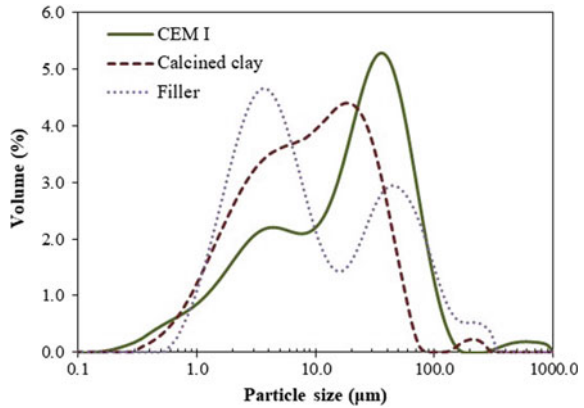
At 7, 14, 28, 56, 96 and 204 days, the change of mass and the visual appearance was evaluated. The sulfate solution and water were replaced after each determination. Changes in phase composition were examined using X-ray diffraction (XRD) at 28 and 204 days. Surface and core samples of the same size were cut from the paste cubes, dried by solvent exchange with acetone, crushed and the powder was pressed in cylindrical standard sample holders of 16 mm diameter and 2.5 mm height. XRD measurements were made using a PANalytical X'Pert PRO MPD Alpha $\theta/2\theta$.

The evaluation of expansions during sulfate exposure was based on the mortar bar expansion tests defined by the ASTM C 1012. Mortar specimens of $25 \times 25 \times 297$ mm elaborated with w/c = 0.485 and cement:graded sand = 1:2.75 were cast. Before sulfate immersion, the standard proposes a 24 h curing in molds at 38 °C and further curing after demolding in limewater until the compressive strength reaches 20 MPa. For this experience, the initial curing was made in the molds during 24 h in a moist cabinet at 20 °C. After one day, the specimens were demolded and immersed in limewater at 20 °C during 24 h. Finally, the initial length was measured and the bars were immersed in the 0.352 M Na_2SO_4 solution (50 g/l) at 20 °C. The expansion was determined at 7, 14, 21, 28, 56, 91, 105, 120 and 180 days and the solution was renewed after each measurement period. Reported expansions are the average of six specimens. According to ASTM C 1157, blended cement is sulfate resistant (HS) when the expansion does not exceed 0.05% at 6 months.

For compressive strength, mortars bars were cast following the procedure described above and cut with diamond saw in 25 mm-cubes before immersion in the sulfate solution. Complementary, a set of 12 cubes continues curing in limewater. These cubes allow comparing change length and compressive strength on the specimens with the same dimension when they were exposed to sulfate solution.
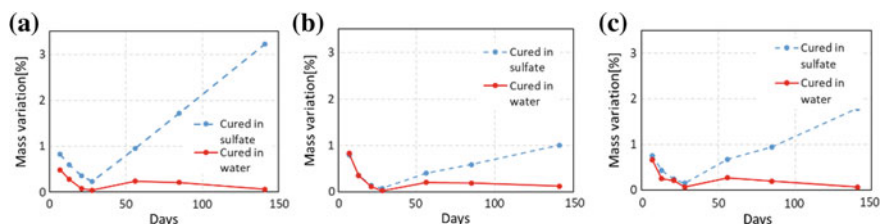
Fig. 2 Mass variation rate of paste cured in water (solid line) and in sulfate solution (dashed line): **a** C30F; **b** C30CC and **c** C15F15CC

3   Results and Discussion

3.1   Mass Variation of Paste

Figure 2 shows the relative mass variation rate for each blended cement immersed in sulfate solution (dotted line) and in water (solid line) during 6 months. As can be seen, all pastes presented positive relative mass variations throughout the period evaluated, which indicates increments of mass during the attack. However, this mass increment is produced at different rates depending on the binder composition. During the first 28 days, all specimens follow similar trends, with a gradual decrease on mass gain over time, regardless of the binder and the exposure condition. This behavior is associated with the pore filling caused by normal hydration processes, which are especially relevant here as the samples were immersed only 2 days after casting.

After 28 days, the specimens submerged in non-aggressive conditions maintain similar mass variation rates until the end of the test, as the main hydration reactions occur during the first weeks. However, the samples stored in aggressive conditions show an increase of mass gain from this age, which is more significant in the composition C30F, followed by the C15F15CC and C30CC. This mass gain observed after 28 days of aggressive curing is associated with the sulfate uptake and the progressive formation of sulfate attack compounds such as gypsum and ettringite. These results suggest that the use of calcined clay reduces the amount of sulfate ions penetrating the matrix and delays the formation of expansive phases.

3.2   Visual Appearance of Paste

Figure 3 shows the evolution of visual appearance of paste cubes immersed in sulfate solution and some selected photographs at 28, 90 and 180 days. It can be observed that the integrity of cubes for all blended cements is not compromised during the first 28 days of sulfate exposure. At 90 days, the composition with 30% of limestone filler (C30F) presents a remarkable cracking along the edges of the cube, which is the typical cracking pattern associated with the ESA. The composition C15F15CC

Fig. 3 Visual appearance of paste: photographs of cubes at 28, 90 and 180 days
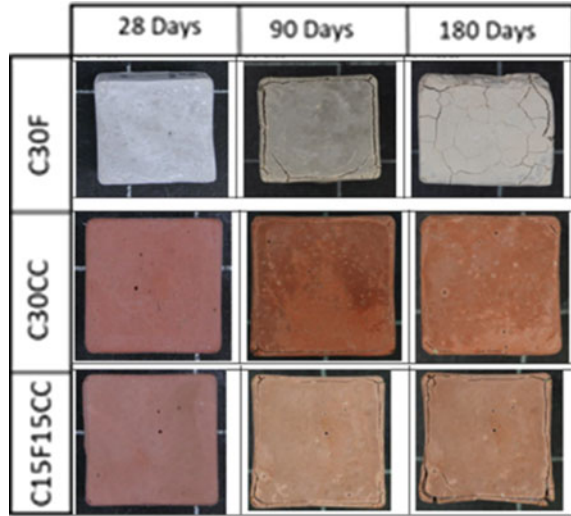
shows a slight cracking near the corners of the cubes, being its intensity considerably lower than for C30F. On the other hand, the composition with 30% of calcined clay (C30CC) presents no signs of damage after 90 days of sulfate exposure. At 180 days, C30F cubes are completely cracked as the external layers and regions close to the corners can be easily shelled by hand. The damage in the composition C15F15CC has progressed after 180 days of exposure and the initial cracks observed at 90 days are now connected throughout the entire external edges of the cube. On the other hand, the C30CC cubes only developed very slight and fine cracks along the edges. These results suggest that the incorporation of calcined clays limits the amount of cracking developed during the ESA.

3.3   XRD Analysis of Pastes

Figure 4 shows the XRD patterns of surface samples of paste curing in water and in sulfate solution at 28 days and 6 months.

For C30F, the hydrated compounds identified in water are calcium hydroxide, monocarboaluminate and a small peak of ettringite at both 28 days and 6 months. This sample immersed in sulfate solution shows high intensity peaks of ettringite and the incipient gypsum formation identified by peak at 20.7° 2θ and the doublet peak at 22.8° 2θ. At six months, the gypsum is the main attack compound and the calcium hydroxide peaks present a high reduction of intensity.

For C30CC, the compounds of hydrated samples were calcium hydroxide, ettringite, hemicarboaluminate and monocarboaluminate. These remain at six months with the reduction of intensity of CH-peaks. For paste immersed in sulfate solution, the
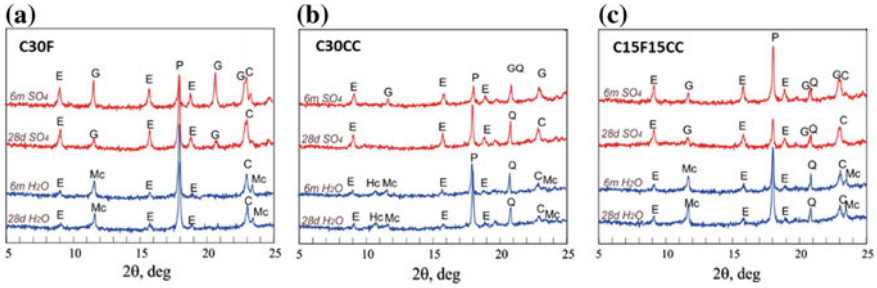
Fig. 4 XRD pattern of specimens cured in water and sulfate solution: **a** C30F; **b** C30CC and **c** C15FC15CC. (E = ettringite, G = gypsum, P = portlandite, Hc = hemicarboaluminate, Mc = monocarboaluminate, C = calcite and Q = quartz)

Fig. 5 Expansion of mortars bars without previous water curing and exposed to sulfate solution
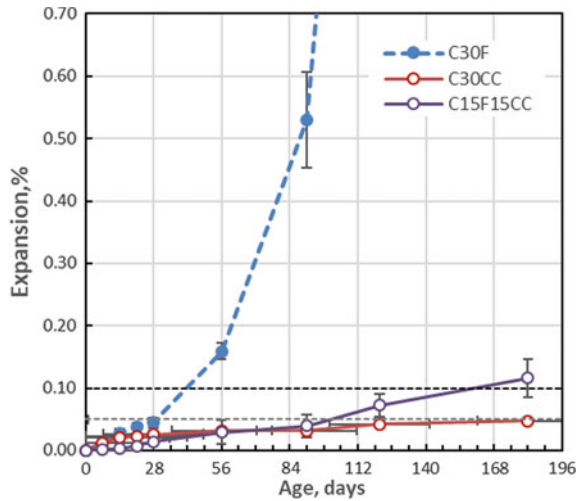
AFm peaks disappear and the ettringite peak is more intense reveling the sulfate attack on the surface. After six months, ettringite appears accompanied by a low intensity peak of gypsum and a high reduction of CH-peaks.

For the ternary blended cement, the limestone filler promotes the formation of monocarboaluminate as the only AFm and the calcined clay reduces the CH-peaks intensity at six months. In sulfate solution, the formation of gypsum is incipient at 28 days and it grows later.

3.4 Expansion of Mortar

Expansion of mortar bars in sulfate solution is shown in Fig. 5. During the initial exposure up to 28 days, the expansions of the three blended cements present a similar rate, being slightly higher for C30F. After 28 days, the C30F expansion rate increases exponentially reaching the limit of 0.10% at 38 days. At 90 days, the attack has been so severe that it is no longer possible to measure the length variations in this composition since the specimens are practically disintegrated.

On the other hand, C30CC mortars show a very slow expansion rate and the limit of 0.05% is only reached at 252 days, which is after the threshold of 6 months established by the ASTM standard to be considered as a sulfate resistant cement. The low expansion is attributed to the pozzolanic reaction of the calcined clay with the calcium hydroxide released during hydration of cement that generates secondary compounds reducing the calcium hydroxide needed for ettringite formation and specially blocking the pores to prevent the ingress of sulfates into the matrix. This pozzolanic reaction progresses after the immersion in the sulfate solution as occurred in water curing.

For C15F15CC mortar, the expansion is similar to C30CC up to 90 days, but from this point, the slope increases and exceeds the limit of 0.10% at 161 days, qualifying this cement as not sulfate resistant. The expansion behavior is in agreement with the formation of ettringite in C30F, which causes cracking and sulfate penetration. On the other hand, the C30CC mortar has little expansion due to the low ettringite formation and less sulfate penetration. The ternary blended cement has an intermediate behavior.

3.5 Compressive Strength

Figure 6 shows the compressive strength of mortar for blended cements immersed in sulfate solution (Fig. 6a) and in distilled water (Fig. 6b). For C30CC and C15F15CC, the compressive strength of mortar cubes cured in water increases from 28 to 90 days confirming the pozzolanic reaction. On the other hand, C30F shows a slight increase due to the dilution caused by limestone filler addition.

Compressive strength of the cubes immersed in sulfate solution shows that the strength of C30F from 7 to 28 days remains constant and then the strength drops quickly due to the cracking of matrix caused by sulfate attack. At 90 days, this mortar has practically lost its compressive strength. For C30CC cubes cured in sulfate solution, the compressive strength increases up to 90 days and their compressive strength overcomes the strength of cubes stored in water. This shows that curing of blended cement with 30% replacement of calcined clay prevents the sulfate attack and improves the compressive strength. This is an important finding for some applications of underwater concrete and additionally could be an indication of unnecessary curing at 38 °C and water curing as prescribed by the ASTM 1012 standard for mortars with mineral additions. For C15F15CC cubes cured in the sulfate solution, the compressive
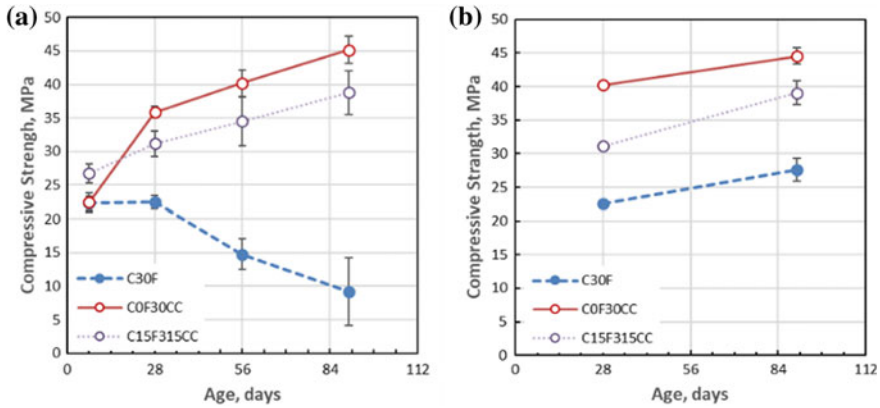
Fig. 6 Compressive strength of mortar immersed in: **a** sulfate solution, **b** water

strength increases continually up to 90 days as occurred for C30CC. At 90 days, the compressive strength is similar to the strength of samples exposed to the non-aggressive curing, but the greater dispersion in these measures could be an indication of the internal deterioration of mortar due to sulfate attack in agreement with the large expansion.

4   Conclusions

Preliminary results of this study related to the sulfate attack with limestone filler and illitic calcined clay exposed immediately to the aggressive environment show that:

Limestone filler addition to Portland cement causes the formation of monocarboaluminate, which is unstable in sulfate environment and rapidly forms ettringite causing cracking and massive influx of sulfate ions promoting the gypsum formation, expansion and compressive strength reduction.

The pozzolanic reaction of calcined clay in mortars is similarly developed in aggressive and non-aggressive curing conditions, consuming the CH and blocking the sulfate ingress due to pore size refinement. The AFm phases formed during hydration in water were converted to ettringite when pastes are exposed to sulfate solution, but the mortar shows no expansion and retains the compressive strength at 6 months.

These experiences show that despite the lack of curing prior to sulfate exposure, cement with the replacement of 30% of an illitic calcined clay becomes an excellent resistance to ESA, while limestone cements presented a worse performance.

References

1. Lemma, R., Irassar, E.F., Rahhal, V.: Calcined illitic clays as portland cement replacements. In: Scrivener, K., Favier, A. (eds.) Calcined Clays for Sustainable Concrete, pp. 269–276. https://doi.org/10.1007/978-94-017-9939-3_33 (2015)
2. Ramachandran, V.S.: Concrete Admixtures Handbook: Properties, Science and Technology, 2nd edn. Noyer Publication, United States of America (1995)
3. Neville, A.: The confused world of sulfate attack on concrete. Cem. Concr. Res. **34** (2004)
4. Wild, S., Khatib, J.M., O'Farrell, M.: Sulphate resistance of mortar, containing ground brick clay calcined at different temperatures. Cem. Concr. Res. **27**, 697–709 (1997). https://doi.org/10.1016/S0008-8846(97)00059-8
5. Ikumi Montserrat, T., Segura Pérez, I., Cavalaro, S.: Influence of early sulfate exposure on the pore network development of mortars. Constr. Build. Mater. **143**, 33–47 (2017). https://doi.org/10.1016/j.conbuildmat.2017.03.081

Mitigation of Alkali–Silica Reaction in Limestone Calcined Clay Cement-Based Mortar

Quang Dieu Nguyen, Mohammad Khan, Arnaud Castel and Taehwan Kim

Abstract This work aims to assess the potential of limestone calcined clay cement (LC3) in mitigating alkali–silica reaction (ASR). Two General Purpose (GP) cement substitution rates using calcined clay and limestone were tested: 20 and 30% with a ratio 2:1 by mass of calcined clay and limestone. Silica ions dissolution of rhyodacite rock used as reactive aggregate, expansion of mortar specimens using the accelerated mortar bar test (AMBT) and the initial chemical composition of the mortars pore solution were investigated. The combination of calcined clay and limestone significantly reduced the expansion of mortar bars compared to reference mortar using 100% GP cement. The reduction in mortar bar expansion correlates well with the reduction in alkalis ions concentration and pH of the pore solution of LC3 mortars compared to reference mortar. 30% OPC substituted by calcined clay and limestone seems to be able to mitigate the risk of ASR in concrete using alkali-reactive aggregate.

Keywords Alkali-aggregate reaction · Calcined clay · Limestone · AMBT

1 Introduction

The use of supplementary cementitious materials (SCMs) to partially replace Ordinary Portland Cement (OPC) in concrete has been a rational approach over the last decades to limit CO_2 emission. Among the promising SCMs, calcined clays have received a considerable attention nowadays due to its global availability. Calcined clay is essentially composed of silica and alumina (more than 90%) and has a SiO_2/Al_2O_3 ratio between 1.5 and 2.5, depending on the purity of raw materials used in the production [1]. Calcined clay provides fine pore networks and is able to increase packing of cementitious particles due to its pozzolanic nature [2, 3].

Q. D. Nguyen · M. Khan · T. Kim
Centre for Infrastructure Engineering and Safety, School of Civil and Environmental Engineering, The University of New South Wales, Sydney, NSW 2052, Australia

A. Castel (✉)
School of Civil and Environmental Engineering, University of Technology Sydney, PO Box 123, Broadway, Sydney, NSW 2007, Australia
e-mail: a.castel@unsw.edu.au

665

OPC blend with calcined clay and limestone is referred to as limestone calcined clay cement (LC3) [4]. It has been reported that the synergic between calcined clay and limestone can lead to an improvement of the mechanical performance of LC3-based concrete [5]. LC3 blends present an extremely promising option to the increasing demand for cement in coming decades without increasing CO_2 emissions and costs [4]. This work aims to assess the potential benefit in using calcined clay and limestone as SCMs to mitigate the risk of alkali–silica reaction (ASR). Silica ions dissolution of rhyodacite rock used as reactive aggregate, expansion of mortar specimens using the accelerated mortar bar test (AMBT) and the initial chemical composition of the mortars pore solution were investigated.

2 Materials and Mix Design

Binder is the ternary combination of General Purpose (GP) cement, flash calcined clay and limestone. With the aim of accelerating the utilization of LC3 concrete in the current industry, flash calcined clay and limestone are sourced from large-scale production, replacing directly GP cement in binder without any gypsum optimization. Limestone identified as Stone Dust from Boral Construction Materials Limited (New South Wales, Australia) and flash calcined clay is provided by Argeco (Fumel, France). The chemical composition, mineralogical composition and physical properties such as particle size distributions of all binder components were reported in a previous paper of the authors [5]. Quartz and calcite observed from X-ray diffraction (XRD) were identified as the only crystalline phases in calcined clay and limestone, respectively. The flash calcined clay is categorized as low-graded calcined clay due to its low amorphous phase content of 50.9%. The reactive coarse aggregate used is rhyodacite rock supplied from Culcairn, New South Wales, Australia. The rhyodacite rock was crushed to obtain the required gradation in Australia Standard AS 1141.60.1 for accelerated mortar bar test (AMBT) [6].

Three mix designs of mortars have been considered to evaluate the effect of calcined clay and limestone on alkali–silica reaction. 20 and 30% of the mass of GP were substituted by a combination of calcined clay and limestone with the ratio 2:1 by mass, which are defined as LC3-20 and LC3-30 mixtures, respectively. The third mix is the reference mix labelled OPC with binder being 100% GP cement. The mix designs complying with Australia Standard AS 1141.60.1 [6] for testing potential alkali–silica reactivity are given in Table 1. Cylinder paste specimens with 50 mm of diameter and 100 mm of height were prepared using the same mix design (without aggregate) and same curing condition as for the mortars to analyse the pore solution in paste and to determine hydration phases using X-ray diffraction (XRD).

Table 1 Mortar's mix designs

Materials (kg/m^3)	Concrete		
	OPC	LC3-20	LC3-30
Aggregate	1346.4	1346.4	1346.4
Total binder	598.4	598.4	598.4
OPC	598.4	478.7	418.9
Calcined clay	0	79.8	119.7
Limestone	0	39.9	59.8
Water/binder ratio	0.47	0.47	0.47
Water	281.2	281.2	281.2

3 Experimental Programme

3.1 Compressive Strength

The compressive strength of mortars was measured at 1, 7, 14, 21 and 28 days by using 50 mm cubes in accordance with Australian Standard AS 1012.9.

3.2 Accelerated Mortar Bar Test

Accelerated mortar bar test method based on AS1141.60.1 [6], similar to ASTM C1260 [7], was employed to monitor the alkali-aggregate reaction of rhyodacite rock in LC3-based system. At least four mortar bar specimens were fabricated for each mix design. After demoulding, the specimens were immersed into 80 °C water for 24 h and then the zero reading of each specimen was recorded. Thereafter, the mortar bars were placed on a container with 1 mol/L sodium hydroxide and stored at 80 °C. The ratio volume of solution to specimens was 4:1. The length change in the specimens was measured at 1, 3, 7, 10, 14 and 21 days and then weekly using the comparator.

3.3 Pore Solution Composition and pH

The pore solution analysis was performed to determine the effect of LC3 on the pore solution chemistry. To focus on the effect of LC3 on the paste system, the paste samples were prepared with similar binder composition as the mortars. A well-established method published by Barney Back and Diamond [8] was employed to extract the pore water from the cylindrical specimens. Subsequently, the pore solution
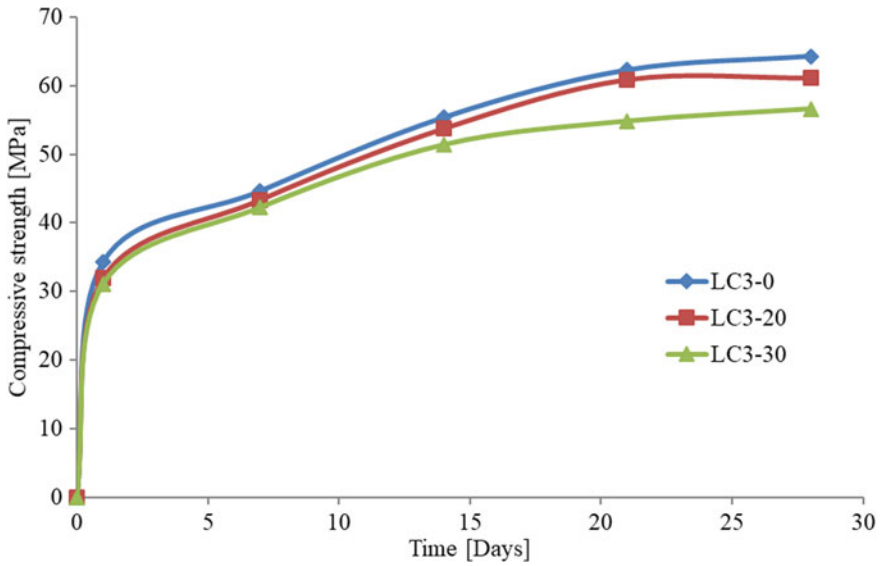
Fig. 1 Compressive strengths of mortars

composition and its concentration were measured by ICP-OES analysis. In addition, a calibrated pH probe was used to directly measure the pH of pore solution.

4 Experimental Results

4.1 Compressive Strength

The development of the compressive strength versus time of all mortars is given in Fig. 1. All mortars presented similar compressive strength up to 7 days. The compressive strength of the LC3 mortars declined only marginally in comparison with reference LC3-0 mortar from 14 to 28 days.

4.2 Accelerated Mortar Bar Test

Figure 2 presents the average expansion of all mortar bars up to 100 days. Without calcined clay and limestone in binder, the expansion rate of LC3-0 reference mortar was 0.22% and 0.4% at 10 days and 21 days, respectively, which classifies rhyodacite rock as reactive aggregate as stipulated in AS1141.60.1 [6]. The length expansions of mortar bars significantly decreased with the increase in calcined clay
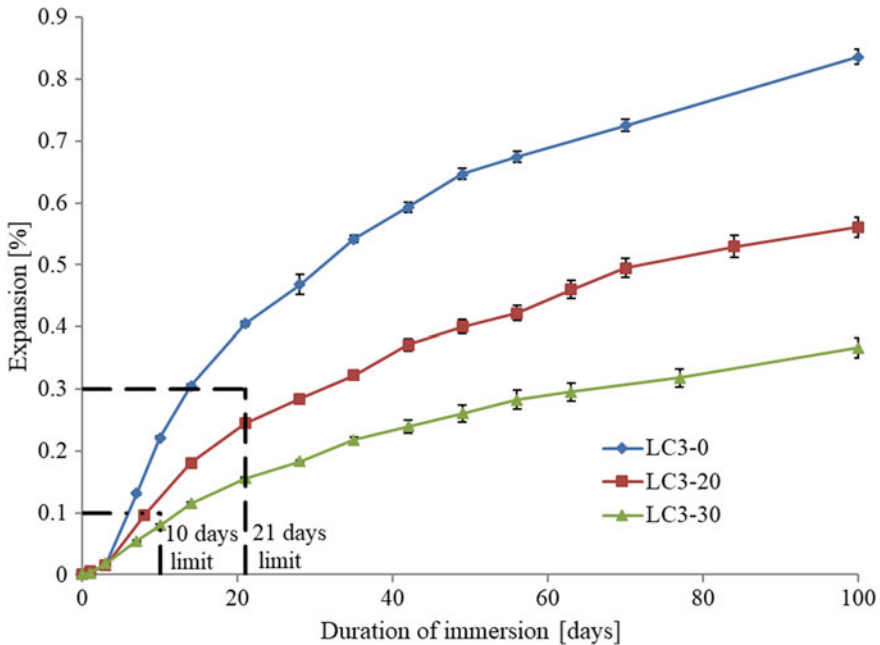
Fig. 2 ASR expansion of mortar bars

and limestone contents in both binders (LC3-20 and LC3-30). After 100 days of immersion in sodium hydroxide 1 M at 80 °C, the reduction in length expansion of mortar bars containing 20% and 30% combination of calcined clay and limestone was approximately 33% and 56% in comparison with reference mortar bars (LC3-0), respectively. Noticeably, both 10-day and 21-day expansions of LC3-30 mortar bars were less than 10-day and 21-day limits of AS1141.60.1 [6]. Blending OPC with 30% (or more) calcined clay and limestone seems to be effective to mitigate the risk of alkali–silica reaction when using reactive aggregate.

4.3 Pore Solution Composition and PH

The pH and the pore solution composition of all pastes tested at 28 days are given in Table 2. The pH of LC3 pastes decreases consistently with the increase in calcined clay and limestone content. Flash calcined clay and limestone are poor in alkalis, which leads to a reduction in alkali concentrations in pore solution. A decrease in sulphate ion was observed due to the decrease in GP cement content in the mix design as sulphate ions are dominantly derived from the gypsum in GP cement.

Figure 3 presents the initial pH of the paste versus the 21 days expansion measured using the standard AMBT. It is acknowledged that the initial pore solution

Table 2 pH and chemical composition (mg/l) of pore solution of pastes at 28 days

LC3 Pastes	pH	Ca	Na	Mg	K	Al	Si	S
LC3-0	13.35	76.5	1831	0	6929	1.26	3.06	209
LC3-20	13.15	139	1039	0	3937	1.53	4.69	73.2
LC3-30	12.89	259	1799	0.02	2955	0.78	1.9	83.3
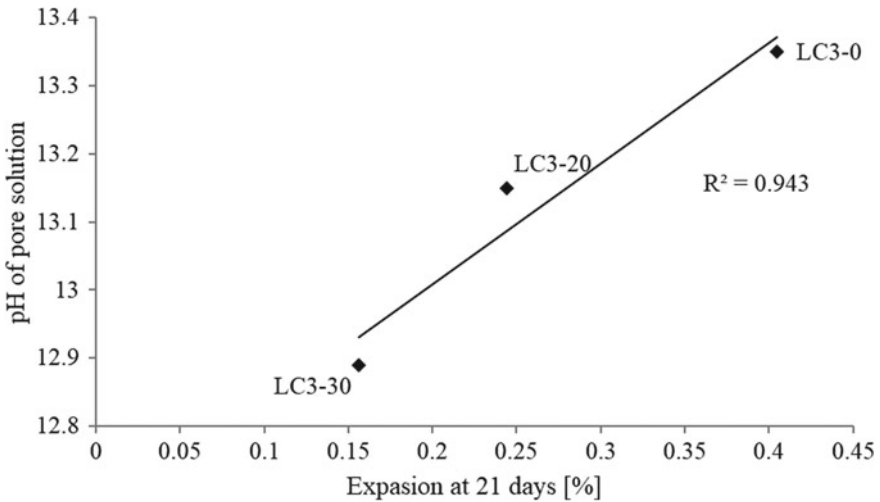
Fig. 3 Correlation between initial pH of pore solution and expansion of mortar bars at 21 days

composition and pH of mortar bars are greatly affected by the exposure condition in the AMBT (i.e. 1 mol/L sodium hydroxide solution at 80 °C). However, a clear correlation appears between the initial pore solution pH and the 21 days expansion of the mortar bars showing that mortar bars expansion is drastically decreasing with the decrease in initial pore solution pH.

Dissolution of rhyodacite aggregate was assessed using four different solutions of sodium hydroxide: 1 M, 0.03 M, 0.003 M and 0.0003 M, corresponding to four different pH levels, pH 14, pH 12.5, pH 11.5 and pH 10.5, respectively. 10.5 g of rhyodacite rock in each set were utilized in this test. All aggregates were washed thoroughly by distilled water and then dried in the oven at 100 °C for over 24 h-period in order to eliminate all impurity and unexpected particles on the surface of test aggregates. Solutions were prepared using 98% purity from Ajax Finechem was dissolved to distilled water. Aggregates were submerged in 450 ml sodium hydroxide solution and stored in the controlled room at a fixed temperature of 23 ± 2 °C and relative humidity of 50% for 21 days. Si dissolution was monitored by sampling 10 ml of solution periodically. Si concentration was measured by using an inductively coupled plasma-optical emission spectrometry (ICP-OES) in the Mark Wainwright Analytical Centre at UNSW Sydney. Figure 4 shows the results obtained for the 4

Fig. 4 Si ion dissolution from rhyodacite aggregate exposed to NaOH solution
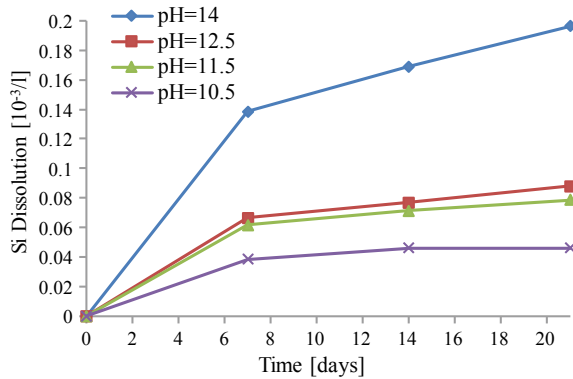
pH tested. Figure 4 shows that aggregate dissolution is greatly increasing with the increase of the pH of the solution particularly from pH 12.5 (which is close to LC3-30 pore solution pH) and pH 14 which can be assumed close to LC3-0 pH during the first 48 h after batching (before exposure to AMBT solution). This significant reduction in aggregate dissolution (an Si ions supply) at early age (before exposure to AMBT solution) can be a first reason for the lower expansion observed on mortar bars with LC3 compared to reference OPC mortar bars. Another reason could be that incorporating calcined clay and limestone cement contributes to the refinement of the pore structure [5, 9, 10], delaying the diffusion of species from the AMBT solution into the mortar bars. Microstructural and chemical analysis is in progress at the UNSW Sydney in order to better understand the mechanisms governing ASR in LC3-based mortars.

5 Conclusions

The substitution of calcined clay and limestone up to 30% of OPC mass did not cause a significant reduction in compressive strength of mortars at early age or at 28 days. The accelerated mortar bar test results showed that the ternary combination of OPC, calcined clay and limestone significantly reduced the expansion of mortar bars immersed in sodium hydroxide at 80 °C. In plain OPC mortar, the specimens expanded over the limit of 10-day and 21-day expansion, which indicates that rhyodacite rock is reactive aggregate in traditional cement-based system. The expansion of mortar bars decreased with increasing replacement of calcined clay and limestone: 21-day expansions were 0.4%, 0.24% and 0.15% for LC3-0, LC3-20 and LC3-30, respectively. 30% OPC substituted by calcined clay and limestone seems to be able to mitigate the risk of ASR in concrete using alkali-reactive aggregate.

References

1. Nicolas, R.S., Cyr, M., Escadeillas, G.: Characteristics and applications of flash metakaolins. Appl. Clay Sci. **83–84**, 253–262 (2013)
2. Siddique, R., Klaus, J.: Influence of metakaolin on the properties of mortar and concrete: a review. Appl. Clay Sci. **43**, 392–400 (2009)
3. Shi, Z., Lothenbach, B., Geiker, M.R., Kaufmann, J., Leemann, A., Ferreiro, S., Skibsted, J.: Experimental studies and thermodynamic modeling of the carbonation of Portland cement, metakaolin and limestone mortars. Cem. Concr. Res. **88**, 60–72 (2016)
4. Scrivener, K.L.: Options for the future of cement. Indian Concr. J. **88**(7), 11–21 (2014)
5. Nguyen, Q.D., Khan, M.S.H., Castel, A.: Engineering properties of limestone calcined clay concrete. J. Adv. Concr. Technol. **16**(8), 343–357 (2018)
6. AS 1141.60.1: Methods for Sampling and Testing Aggregates Potential Alkali-Silica Reactivity—Accelerated Mortar Bar Method. Standards Australia (2014)
7. ASTM C1260-14: Standard Test Method for Potential Alkali Reactivity of Aggregates (Mortar-Bar Method). ASTM International, West Conshohocken, PA (2014)
8. Barneyback, R.S., Diamond, S.: Expression and analysis of pore fluids from hardened cement pastes and mortars. Cem. Concr. Res. **11**(2), 279–285 (1981)
9. Antoni, M., Rossen, J., Martirena, F., Scrivener, K.: Cement substitution by a combination of metakaolin and limestone. Cem. Concr. Res. **42**(12), 1579–1589 (2012)
10. Tironi, A., Scian, A.N., Irassar, E.F.: Blended cements with limestone filler and kaolinitic calcined clay: filler and pozzolanic effects. J. Mater. Civ. Eng. **29**(9), 04017116 (2017)

Hydration and Durability of Ternary Binders Based on Metakaolin and Limestone Filler

Emmanuel Roziere, Gildas Medjigbodo, Laurent Izoret and Ahmed Loukili

Abstract The combination of Portland cement and mineral additions allows reducing the carbon footprint of cement-based materials and improving their resistance to several environmental actions. The development of binary binders is limited by the reactivity of pozzolanic materials at high substitution levels and the availability of industrial by-products such as slags and fly ash. Thus, it is necessary to develop new cements from natural raw materials such as clay and limestone and to combine them to design ternary binders with higher hydraulic activity. The study is focused on mortar based on binary and ternary binders (Portland cement, metakaolin, limestone filler) with a maximum substitution level of 45%. Two sets of mortar mixtures with different water-to-cement ratios were designed. The experimental program includes the determination of strength, porosity, hydration heat, portlandite content, shrinkage and natural carbonation. The analysis of data aimed at correlating the evolution of mechanical properties with hydration degree and reactivity of calcined clays. The results actually showed that the performances of ternary binders closely depend on the properties of the three studied metakaolins, especially their production process and physical properties. For a given substitution level, the studied ternary binders clearly showed better performances than other mineral additions. The reduction of water-to-cement ratio resulted in an acceleration of pozzolanic reaction. This allowed an improvement of short-term strength as well as potential durability.

Keywords Hydration · Shrinkage · Carbonation

E. Roziere (✉) · A. Loukili
Institut de Recherche en Génie Civil et Mécanique (GeM), Centrale Nantes, Nantes, France
e-mail: emmanuel.roziere@ec-nantes.fr

G. Medjigbodo
UMR Ecologie Des Forêts de Guyane (EcoFoG), Université de Guyane, Kourou, France

L. Izoret
Association Technique de L'Industrie Des Liants Hydrauliques (ATILH), Paris, France

1   Introduction

The use of calcined clay and limestone filler now appears as a promising alternative to plain Portland cement (PC) and industrial by-products. The raw materials are relatively abundant, and the calcination process mainly consists in de-hydroxylation, which results in lower CO_2 emission than clinker production.

Metakaolin-based binders have been widely studied. The reactive phase of metakaolin (AS_2) consists of aluminates Al_2O_3 (A) and silicates SiO_2 (S). They allow the production of C(A)SH [1], which improves the strength and durability of obtained cement-based materials. The optimum metakaolin (MK) proportion depends on its properties and mix-design parameters but generally remains lower than 30% [2].

Higher replacement thus lower carbon footprint can be reached by combining MK or calcined clay with limestone filler [3]. Besides its pozzolanic activity, MK actually reacts with limestone filler (LF) and portlandite to produce carboaluminates and stabilize ettringite. However, the CO_2 emissions should only be compared at equivalent durability, and the performances of ternary binders depend on several parameters, especially the physicochemical properties of raw materials.

The studies on the durability of ternary systems are still relatively scarce. For a given water-to-binder ratio, a high replacement of Portland cement affects early-age strength and durability. Reducing the water-to-binder ratio improves both properties [4] and influences shrinkage [5], but there are still very few references on calcined clay [6]. The experimental study presented in this paper investigates binary and ternary binders based on Portland cement (PC), metakaolin, limestone and siliceous fillers (SFs). The results are analyzed in order to understand the behavior of PC-MK-LF binders and to identify the relevant parameters allowing to improve their strength and durability.

2   Materials and Procedures

The results presented here are a part of a comprehensive study [11] described in Table 1. A Portland cement CEM I 52.5 N (PC) was combined with three different metakaolins (MKi), two limestone fillers (LF) and two siliceous fillers, at different PC replacement levels at water-to-cement ratios (W/C$_0$).

The mixtures CX$_L$ include L% (in mass) of material X, with X = {MK1; MK2; MK3; LF; µLF, SF1; SF2}. The mixtures CX$_M$Y$_N$ include M% of X and N% of Y, with W = {LF; µLF, SF1; SF2}. The workability was assessed using a 150 mm high mini-cone. The workability of mixtures including MK2 and MK3 was adjusted by adding superplasticizer TEMPO11 to reach a slump of 50 mm in order to make the casting of mortar samples easier. Limestone fillers had a beneficial effect on the workability of MK-based mixtures due to its lower water demand.

Table 1 Experimental program

Parameter	Mineral addition	Metakaolin properties	Water-to-binder ratio
Binary binders	$CMK1_{30}$ CFC_{30} $C\mu FC_{30}$ $CFS1_{30}$ $CFS2_{30}$	$CMK1_{30}$ $CMK2_{30}$	$CMK3_{15}$ $CMK3_{30}$
Ternary binders	$CMK1_{30}LF_{15}$ $CMK1_{30}\mu LF_{15}$ $CMK1_{30}SF1_{15}$ $CMK1_{30}SF2_{15}$	$CMK1_{30}FC15$ $CMK2_{30}FC15$	$CMK3_{30}FC15$
Water-to-binder ratio	0.50	0.50	0.42 and 0.50 for each binder
Characterization	Compressive strength Hydration degree Portlandite content		Porosity Shinkage Carbonation

2.1 Materials and Mixtures

The physical and chemical properties of studied materials are given in Table 2. Metakaolin 1 results from the flash calcination [1] of clay extracted in Fumel, France. It showed relatively high quartz content, and its reactive material content ($Al_2O_3(SiO_2)_2$ or AS_2) of 53% was deduced from X-ray diffraction. Metakaolins

Table 2 Chemical and physical properties of constituents

	PC	Metakaolin			Limestone filler		Siliceous filler	
		MK1	MK2	MK3	LF	μLF	SF1	SF2
Chemical composition								
SiO_2	20.6	68	55	55	0.0005	0.3	99.1	99
Al_2O_3	5.3	25	40	39	–	–	0.0048	0.0052
CaO	66.3	0.4	0.3	0.6	98.8	99.6	0.0003	0.0003
Physical properties								
Density (g/cm^3)	3.12	2.5	2.4	2.2	2.71	2.7	2.65	2.65
Specific surface BET (m^2/g)	0.34	16	17	19	0.88	2.2	0.29	0.47
Water demand	0.34	0.56	0.90	1.65	0.31	0.10	0.29	0.52
Pozzolanic index (mg $Ca(OH)_2/g$)	–	754	1000	1400	–	–	–	–
d_{50} (μm)	12	31	15	1.5	8.5	3.7	34	17

MK2 and MK3 with AS_2 of 68% were obtained from the calcination (in rotary and flash kiln respectively) of kaolinite-rich clay from the Charentes Basin, France [6]. They only contain traces or original kaolinite. Limestone filler LF comes from Orgon, France, and microfiller µFC from Arboç, Spain. The mortar mixtures were designed keeping the volume of 0–2 mm crushed quartzite sand constant (47%). The studied mixtures were derived from the initial PC composition with constant water-to-binder ratio.

2.2 Experimental Procedures

Compressive strength. Compression tests were performed on three $40 \times 40 \times 80$ mm^3 specimens after 1, 2, 7 and 28 days of water curing. The activity index i is defined as the ratio of the strength f_p of the mortar with the replacement of PC p% (in mass) to the strength of the plain PC mortar specimens f_0 (Eq. 1).

$$i = \frac{f_p}{f_o} \tag{1}$$

Hydration. The studied materials are likely to influence the hydration kinetics as well as the type of hydration products. This was investigated using isothermal calorimetry and thermogravimetric analysis (TGA).

Isothermal calorimetry was performed on mortar samples at 20 °C according to the method described by Lenormand et al. [10]. The technique allows determining the heat flow $q(t)$ and by integration the cumulated heat release $Q(t)$ (in Joule per gram of cement). The hydration degree is assumed proportional to this value; thus, the time evolution of hydration degree $\alpha(t)$ can be estimated through Eq. (2).

$$\alpha(t) \approx \frac{Q(t)}{Q_{\text{tot}}} = \frac{\int_0^t q(\tau)\mathrm{d}\tau}{Q_{\text{tot}}} \tag{2}$$

Q_{tot} is the long-term value of heat release estimated by the extrapolation of experimental data using the $1/\sqrt{t}$ function. The evolution is almost linear for the lowest values of $1/\sqrt{t}$, and the intersection of this linear function with the y-axis gives an estimation of Q_{tot}.

Durability. The actual durability of cement-based materials depends on many factors. Three properties have been investigated: water porosity, drying shrinkage and carbonation. The water porosity has been assessed according to French standard NF P18-459. Cylindrical mortar samples were saturated with water under vacuum then dried under constant mass. Total shrinkage and mass loss were measured on $20 \times 20 \times 160$ mm^3 mortar prisms stored at 20 °C and 50% relative humidity from the age of $t_0 = 1$ day. The shrinkage data $\varepsilon(t)$ were analyzed using the hyperbolic function (3) in order to deduce the long-term shrinkage magnitude ε_∞ and the shrinkage halftime

N_S. $40 \times 40 \times 160$ mm^3 mortar prisms were exposed to natural carbonation in the laboratory conditions at 0.04% CO_2, 20 °C and 50% relative humidity from the age of 1 day. Carbonated depth was estimated by spraying phenolphthalein indicator at 28 days.

3 Results and Discussion

3.1 Activity Index and Hydration of Binary and Ternary Binders

The activity indices are plotted as a function of PC replacement (in mass) in Fig. 1. The binary binders clearly show the difference between metakaolin and fillers. The four fillers lead to the same values of activity index. The drop in 28-day strength is actually due to the clinker dilution effect [10]. These materials, especially limestone filler, accelerate hydration at early age through nucleation effect [11], but this effect vanishes at 28 days as the degree of hydration of Portland cement becomes closer to its ultimate value. The higher activity index of MK-based binders indicates its chemical reactivity.

The relatively high pH and high calcium content provided by Portland cement foster the hydration of MK, which produces C(A)SH and hydrated aluminate phases contributing to strength. This corresponds to pozzolanic reactivity resulting from the progressive activation of the aluminates and silicates from the amorphous fraction of MK [1]. However, the quantitative results differ from the values reported by Antoni et al. [2]. Their 30% MK mortars reached 120–130% of 28-day strength of reference
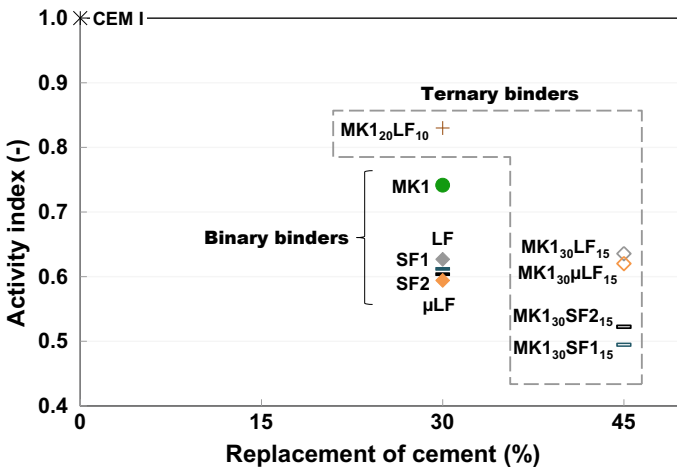
Fig. 1 Activity indices at 28 days ($W/C_0 = 0.50$)

mortar, whereas they did not exceed 74% here. This discrepancy could mainly come from the properties of cements and metakaolins. Antoni et al. [2] used a CEM I 42.5 cement and a metakaolin with a significantly higher content of reactive phase. Avet et al. [3] actually showed a linear increase of compressive strength with calcined kaolinite content. From their results, the strength decreases by 30% when this content is reduced by 50%. As a consequence, the optimum replacement of Portland cement strongly depends on metakaolin properties [13].

Figure 1 also allows highlighting the synergistic effect of metakaolin and limestone filler. The CMK1$_{20}$LF$_{10}$ mixture reached the highest activity index of 0.83 at 30% replacement. The activity index of PC-MK-LF binders did not exceed 0.65 at 45% replacement, but it was significantly higher than PC-MK-SF binders, which confirm the interaction between the three constituents and the beneficial effect of formed phases on compressive strength. TGA results (not shown here) actually showed a higher portlandite consumption in PC-MK-LF binders. XRD analyses performed by Antoni et al. [3] showed the formation of hemi- and monocarboaluminate. Carbonate phases are more stable than corresponding sulfates; thus, the addition of limestone filler favors the stability of ettringite, whereas it would transform into monosulfoaluminate without calcium carbonate.

Ternary binders are likely to influence the hydration kinetics as well as the hydration products and their contribution to strength. In order to distinguish both effects, the activity index has been plotted against hydration degree in Fig. 2. The difference between the ternary binders with limestone and siliceous fillers increases between 1 and 7 days. The increase of specific surface area provided by microfiller did not result in significant accelerating of hydration, but the activity index was higher at early age. This can be attributed to higher initial packing density of cement paste due to particle size distribution of μLF. This allows optimizing short-term strength this durability (see Sect. 3.2).
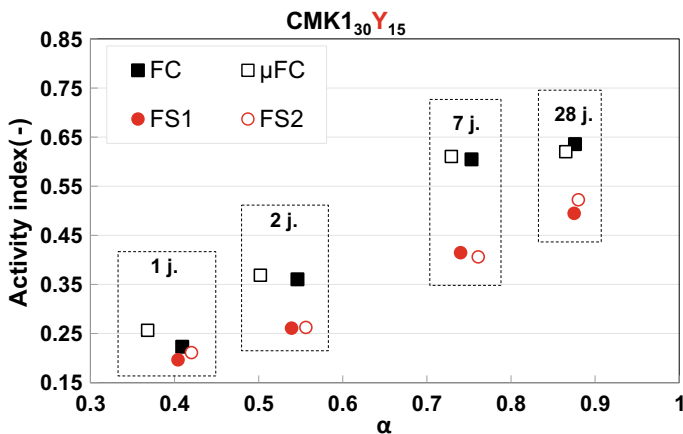
Fig. 2 Activity index and hydration degree of ternary binders ($W/C_0 = 0.50$)

Table 3 Shrinkage magnitude, hydrous compressibility factor (K) and water porosity

W/C_0		CEM I	$CMK3_{15}$	$CMK3_{30}$	$CMK3_{30}LF3_{15}$
0.50	Ultimate shrinkage (μm/m)	978	833	558	890
	K	270	237	140	189
	Porosity (%)	22	24.5	25.2	26.6
	1-day strength (MPa)	17.4	14.4	8	6.2
	28-day carbonated depth (mm)	2.5	3.0	4.1	5.8
0.42	Ultimate shrinkage (μm/m)	773	572	522	488
	K	276	199	–	132
	Porosity (%)	19.9	23.0	23.3	25.0
	1-day strength (MPa)	23.5	19.5	13.2	9.5
	28-day carbonated depth (mm)	1.7	1.7	2.7	3.4

3.2 Durability-Related Properties

The parameters deduced from water porosity and shrinkage tests are given in Table 3. For a given replacement, the shrinkage magnitude increased with W/C_0 ratio. This trend has already been reported in previous studies. Higher W/C_0 actually results in coarser pores, thus lower capillary tensions according to Kelvin–Laplace equation, but lower elastic modulus decreases and higher creep strain, thus shrinkage finally increases.

At both W/C_0 ratios, the replacement of cement by the studied materials led to lower ultimate shrinkage. This could be due to higher capillary tension induced by the finer pores of plain Portland cement paste. In order to confirm this assumption, the shrinkage versus mass-loss curves was analyzed. The second stage of this evolution shows a linear increase that can be characterized by a coefficient K. The PC mortar actually had higher K values; in other words, a given mass loss induces higher shrinkage. The hydration of plain Portland cement is actually faster than binary or ternary binders; thus, the porosity of these mortars was finer when exposed to drying at 1 day.

The porosity increased with W/C_0 ratio, which was attributed by Bredy et al. [14] to unreacted MK particles. Ambroise et al. [2] reported a decrease of porosity, but at W/C_0 ratios lower than 0.3. This confirms the strong influence of MK properties and mix-design parameters on the behavior of these materials.

For a given water-to-binder ratio, the carbonated depth increased due to coarser porosity and lower portlandite content. However, reducing the W/C_0 resulted in an acceleration of hydration [7] at early age, which was beneficial for strength and carbonation [8].

4 Conclusion

The study aimed at understanding the behavior of ternary binders based on Portland cement, metakaolin and limestone filler. The experimental results were promising in terms of strength and potential durability. Advanced characterization based on isothermal calorimetry and thermogravimetric analysis allowed correlating the development of strength, hydration and durability parameters such as porosity, shrinkage and carbonation.

The compressive strength of studied mortars confirmed the synergistic effect of metakaolin and limestone filler used as a substitution of Portland cement. These ternary binders actually induced higher portlandite consumption during hydration. The activity index closely depends on metakaolin properties.

Mortars with binary and ternary binders had lower ultimate shrinkage but lower shrinkage halftime. The analysis of shrinkage versus mass-loss curves showed a coarser porosity at short-term resulting from the coupling between hydration and drying, especially for the water-to-binder ratio of 0.50.

For the given water-to-binder ratio, the porosity and carbonated depth increased. However, for a given replacement, reducing the water-to-binder ratio allowed mitigating carbonation as well as increasing compressive strength.

References

1. Ambroise, J., Maximilien, S., Pera, J.: Properties of metakaolin blended cements. Adv. Cem. Based Mater. **1**(4), 161–168 (1994)
2. Antoni, M., Rossen, J., Martirena, F., Scrivener, K.: Cement substitution by a combination of metakaolin and limestone. Cem. Concr. Res. **42**(12), 1579–1589 (2012)
3. Avet, F., Snellings, R., Alujas, D.A., Ben, H.M., Scrivener, K.: Development of a new rapid, relevant and reliable (R3) test method to evaluate the pozzolanic reactivity of calcined kaolinitic clays. Cem. Concr. Res. **85**, 1–11 (2016)
4. Darquennes, A., Roziere, E., Khokhar, M.I.A., et al.: Long-term deformations and cracking risk of concrete with high content of mineral additions. Mater. Struct. **45**(11), 1705–1716 (2012)
5. Bredy, P., Chabannet, M., Pera, J.: Microstructure and porosity of metakaolin blended cements. MRS Proc. **136**, 275 (1988)
6. Cassagnabère, F., Diederich, P., Mouret, M., Escadeillas, G., Lachemi, M.: Impact of metakaolin characteristics on the rheological properties of mortar in the fresh state. Cem. Concr. Compos. **37**, 95–107 (2013)
7. Ferreiro, S., Herfort, D., Damtoft, J.S.: Effect of raw clay type, fineness, water-to-cement ratio and fly ash addition on workability and strength performance of calcined clay–Limestone Portland cements. Cem. Concr. Res. **101**, 1–12 (2017)
8. Khokhar, M.I.A., Roziere, E., Turcry, P., Grondin, F., Loukili, A.: Mix design of concrete with high content of mineral additions: optimisation to improve early age strength. Cem. Concr. Compos. **32**(5), 377–385 (2010)

9. Lawrence, P., Cyr, M., Ringot, E.: Mineral admixtures in mortars effect of type, amount and fineness of fine constituents on compressive strength. Cem. Concr. Res. **35**(6), 1092–1105 (2005)
10. Lenormand, T., Rozière, E., Loukili, A., Staquet, S.: Incorporation of treated municipal solid waste incineration electrostatic precipitator fly ash as partial replacement of Portland cement: Effect on early age behaviour and mechanical properties. Constr. Build. Mater. **96**, 256–269 (2015)
11. Medjigbodo, G., Rozière, E., Charrier, K., Izoret, L., Loukili, A.: Hydration, shrinkage, and durability of ternary binders containing Portland cement, limestone filler and metakaolin. Constr. Build. Mater. **183**, 114–126 (2018)
12. Poon, C.S., Kou, S.C., Lam, L.: Compressive strength, chloride diffusivity and pore structure of high performance metakaolin and silica fume concrete. Constr. Build. Mater. **20**(10), 858–865 (2006)
13. San Nicolas, R., Cyr, M., Escadeillas, G.: Characteristics and applications of flash metakaolins. Appl. Clay Sci. **83**, 253–262 (2013)
14. Ye, G., Liu, X., De Schutter, G., Poppe, M., Taerwe, L.: Influence of limestone powder used as filler in SCC on hydration and microstructure of cement pastes. Cem. Concr. Compos. **29**(2), 94–102 (2007)

Calcined Clay—Limestone Cements: Hydration and Mechanical Properties of Ternary Blends

Guillemette Cardinaud, Emmanuel Rozière, Ahmed Loukili, Olivier Martinage and Laury Barnes-Davin

Abstract Through the study of binary and ternary blends, the work is focused on the influence of the substitution of the cement by calcined clay and/or limestone filler on the mechanical properties. Besides of an ordinary Portland cement, three binders were analyzed: one binary blend where 30% of the cement is replaced by calcined clay and two ternary blends—one with 15% of calcined clay and 15% of limestone filler and the other with 30% of calcined clay and 15% limestone filler. First, the results show that the substitution rate does not influence the overall degree of reaction determined with the cumulated heat evolution. Then, we notice that the behaviors of the 30% substitution blends (binary and ternary) are similar when the ternary blend with only 55% of Portland cement is clearly different. Finally, the mechanical properties brought back to substitution rate seem to be enhanced for the ternary blend with only 55% of Portland cement. This shows that the limestone filler allows to keep, and even to enhance, the mechanical properties of a binary blend by increasing the level of substitution.

Keywords Metakaolin · Ternary blend · Supplementary cementitious materials

1 Introduction

Cement substitution by materials such as fly ash [1], blast furnace slag or silica fume [2] is nowadays widely spread. This replacement allows enhancing the resistivity of such materials toward aggressive environments while reducing CO_2 emissions related to the production of clinker. However, these substitution materials, most of the time by-products of other industries, are less and less available. Their decreasing availability tends to limit their utilization in cementitious matrix, and other solutions must be found.

G. Cardinaud (✉) · E. Rozière · A. Loukili
GeM, UMR-CNRS 6183, Ecole Centrale de Nantes, Nantes, France
e-mail: guillemette.cardinaud@ec-nantes.fr

G. Cardinaud · O. Martinage · L. Barnes-Davin
VICAT, Centre Technique Louis Vicat, L'Isle d'Abeau, France

Several studies have shown for decades now that the substitution of cement by calcined clays (and specifically calcined kaolinite) gives interesting results concerning the mechanical properties [3]. Indeed, calcined kaolinite, called metakaolin, reacts with the portlandite formed by the hydration reaction between cement and water. New hydrates are formed from the reaction between metakaolin and portlandite [4] which enhance, in some cases, the mechanical properties. Besides, these binary blends (cement and calcined clay) have been rapidly spread to ternary blends—combination between cement, calcined clay and limestone filler [5]. Some studies highlight the fact that limestone filler increases the development of hydration process at an early age and favors the insertion of aluminates brought by the calcined clay in the hydration products at longer ages [3].

In this study, we focus on the mechanical properties of hydraulic binders in which two or three components are combined. We remind that binary blends contain cement and calcined clay while ternary blends are composed of cement, calcined clay and limestone filler.

2 Methods and Materials

2.1 Characterization of Materials

The cement used in this study is a Portland cement type CEM I 52,5 R. The calcination temperature of the calcined clay used in the blend is 850 °C. In Table 1, chemical compositions of the main materials are given.

Table 1 Characteristics of the materials

	Cement (PC)	Calcined clay (MK)	Limestone filler (LF)
Chemical compositions (wt%)			
SiO_2	20.1	54.5	4.2
Al_2O_3	5.5	23.9	1.5
Fe_2O_3	3.2	7.0	0.8
CaO	62.5	4.5	51.4
LOI	0.9	2.4	40.8
Physical properties			
d_{50} [μm]	11.5	11	6.0

Table 2 Blend compositions (in wt%)

Blend	Cement	Calcined clay	Limestone filler
PC	100	–	–
CMK$_{30}$	70	30	–
CMK$_{15}$LF$_{15}$	70	15	15
CMK$_{30}$LF$_{15}$	55	30	15

2.2 Experimental Procedure

Fabrication mix design

The properties of three blended cements and one reference cement are studied through compressive strength tests and isothermal calorimetry. In the rest of the document, the reference refers to a 100% CEM I 52,5 R and is called PC. One binary and two ternary blends are investigated as well. Table 2 gives the compositions of the studied blends (in wt%).

Compressive strengths were determined following the EN 196-1 standard [6]. The results are translated into the Bolomey activity coefficient calculated in the next section and defined at Eq. (2).

Isothermal calorimetry tests are performed on cement pastes with a water-to-cement ratio of 0.5. Heat flow $q(t)$ and cumulated heat $Q(t)$ are recorded for seven days on a TAM Air 3 channels device. Tests are made on 60 g of powder at 20 °C. Powder and water are mixed in a glass pot which is then closed and put inside the chamber. Such tests allow us to determine the degree of reaction, calculated below.

Bolomey activity coefficient

One can link the compressive strength of a mortar to its water-to-cement ratio thanks to the relation of Bolomey [7]. We have:

$$f_0 = K_B \left(\frac{C_0}{E + V} - 0.5 \right) \tag{1}$$

where f_0 is the compressive strength of the reference cement, K_B is a coefficient which depends on the sand (and gravels if any), C_0 is the mass of cement in the reference mortar, E is the mass of water and V is the mass of water occupied by air.

Lawrence and Ringot [8] have adjusted this relation for blends containing mineral additions in order to characterize their effect in the blend. The compressive strength of a blend containing p% of the addition A is given by:

$$f_p = K_B \left(\frac{C + \chi_B \times A}{E + V} - 0.5 \right) \tag{2}$$

where C represents the quantity of cement in the blend, A is the quantity of the mineral addition and χ_B is the Bolomey activity coefficient.

The value of χ_B for each blend is determined with the activity index defined by the ratio between f_p and f_0 at different stages of the reaction. The Bolomey coefficient is needed to qualify the effect of the addition and substitution rate on the mechanical properties. When χ_B is 0, the addition has no effect on the blend; when it is 1, we are in the same case as the reference cement (i.e., to say that the addition allows the blend to reach the same mechanical properties as the cement taken as a reference). If χ_B is negative, the addition impairs performances; if χ_B is between 0 and 1, the effect is "normal," and if it is above 1, the activity of this blend is better than the reference cement activity (the addition has a positive effect on the mechanical properties of the blend).

Degree of reaction

The degree of reaction is determined with the help of the cumulated heat measured over time by isothermal calorimetry. We define the degree of reaction by the ratio between the heat of hydration and the maximal heat of hydration at an infinite time [9]. If we plot the heat of hydration with respect to the quantity $1/\sqrt{t}$, we can extrapolate the curve in 0 (when t tends to ∞) and then determine the maximal heat of hydration, Q_∞. The graphical method for the determination of Q_∞ is shown in Fig. 1.

The degree of hydration is then calculated by the following Eq. (3) below.

$$\alpha(t) \approx \xi(t) = \frac{Q(t)}{Q_\infty} = \frac{\int_0^t q(t)\mathrm{d}t}{Q_\infty} \tag{3}$$
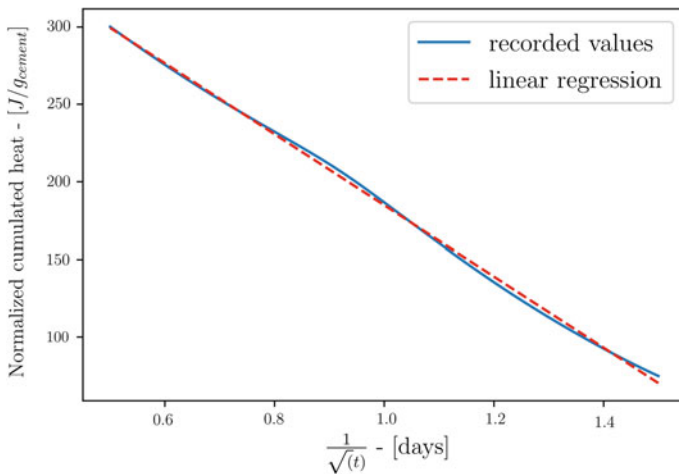
Fig. 1 Linear regression method to determine Q_∞

3 Results and Discussion

Normalized heat flow and normalized cumulated heat for all the blends are plotted below on the Fig. 2. Heat flow and cumulated heat are normalized by the quantity of cement CEM I 52,5 R contained in the blend (and not the quantity of total binder).

Intensity and position of the first peak of heat flow, as known as silicate reaction peak, are quite similar for all the mix. Though, we notice the apparition of a second peak for the heat flow of blends in which the cement is substituted. This peak is often called the sulfate depletion peak [3, 10]. The shape of this peak depends on the substitution rate of the cement. Indeed, the second peak is more intense and occurs earlier for $CMK_{30}LF_{15}$ than for the other two blended cements CMK_{30} and $CMK_{15}LF_{15}$.

The higher the substitution rate, the higher the normalized cumulated heat. CMK_{30} and $CMK_{15}LF_{15}$ have nearly the same shape all along the hydration reaction. However, cumulated heat increases when the substitution rate is increased from 30 to 45%. Table 3 gives the value of the maximal cumulated heat normalized for every mix.
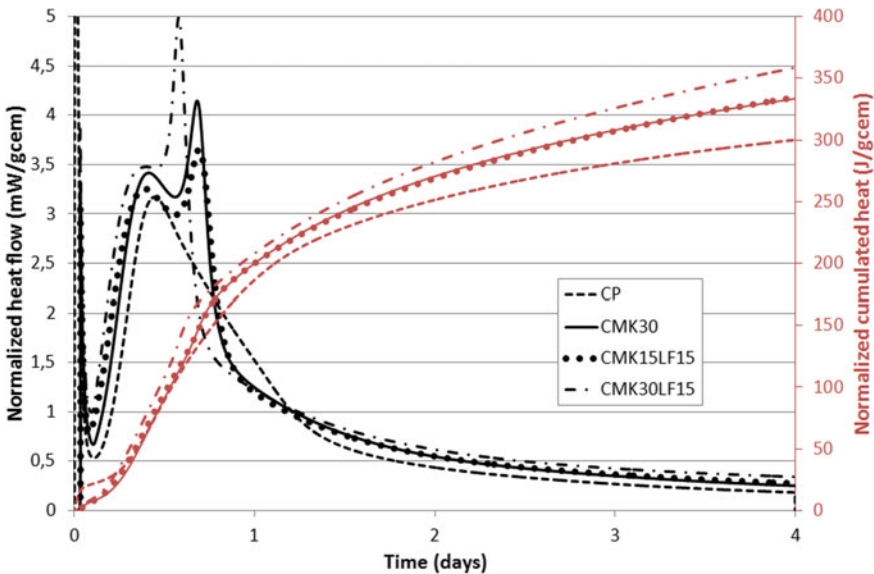
Fig. 2 Normalized heat flow and cumulated heat evolution over time

Table 3 Maximal cumulated normalized heat Q_∞

	PC	CMK_{30}	$CMK_{15}LF_{15}$	$CMK_{30}LF_{15}$
Q_∞ (J/g$_{cem}$)	414.0	475.6	481.2	522.5
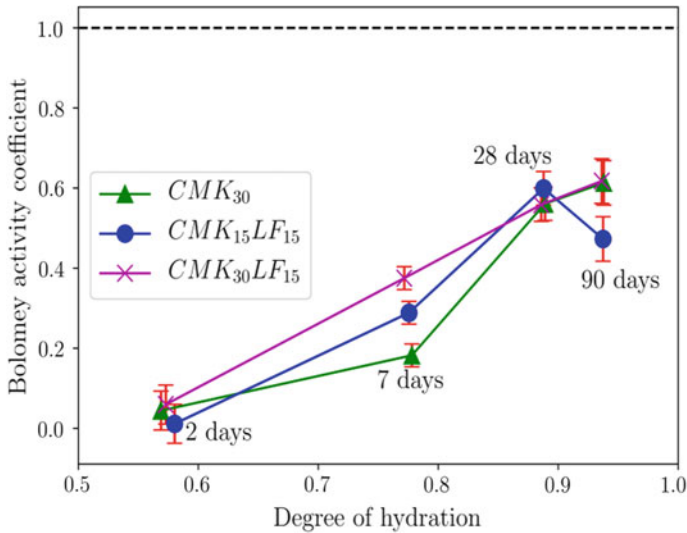
Fig. 3 Bolomey activity coefficient over hydration

In Fig. 3, here, we represent the evolution of the Bolomey activity coefficient in over the hydration reaction.

Even though the activity coefficient of all the blended cements is below 1, we still notice that it is never negative; so, the addition is not detrimental for the blend.

Besides, the behavior observed in Fig. 3 is different for the three blended cements. Indeed, when the substitution rate of the cement is 30% (both binary and ternary blends), we observe a change in slope at 7 days, and the evolution of the activity coefficient changes. However, this change in slope is not observed for the 45% substitution blend.

For almost every age of test, the Bolomey activity coefficient of $CMK_{30}LF_{15}$ is higher than the other two. This result does not demonstrate that the mechanical properties are enhanced when the substitution rate is higher, but it shows that the activity of the mineral addition, brought back to the substitution rate, is more efficient in this case from a mechanical point of view. Limestone filler in the case of $CMK_{30}LF_{15}$ has a positive effect for a higher substitution rate. Indeed, limestone filler in such a cementitious matrix with calcined clay can have different ways to interact. The nucleation effect enhances the formation of hydrates at an early age of the reaction. A chemical effect can also help to enhance the reaction by creating new hydrates, called the carboaluminates, and develop the mechanical properties of the blend at later ages [3].

4   Conclusion

The addition of limestone filler to binary blends (cement–calcined clay blends) increases the overall substitution rate while enhancing the contribution of the supplementary cementitious materials toward the mechanical performances. The opposite is often noticed because of the dilution effect. Indeed, the blend where 45% of the cement is replaced shows higher cumulative heat (normalized by the quantity of cement) and Bolomey activity coefficient than the blend where only 30% of the cement is substituted. Many hypotheses can explain this phenomenon. In one hand, thanks to the nucleation effect, limestone filler favors formation of hydrates at the beginning of the reaction. In the other hand, the presence of limestone allows the formation of new hydrates, called carboaluminates, which are probably responsible for the enhancement of the properties over time. A precise analysis of the microstructure (by TGA, XRD and NMR) will help understand and validate these hypotheses.

References

1. Younsi, A.: Performance-based design and carbonation of concrete with high fly ash content. Cem. Concr. Compos. (2011)
2. Khokhar, M.I.A.: Optimisation of concrete mix design with high content of mineral additions: effect on microstructure, hydration and shrinkage. In: Ecole Centrale de Nantes (2010)
3. Antoni, M.: Cement substitution by a combination of metakaolin and limestone. Cem. Concr. Res. (2012)
4. Cassabagnère, F.: Metakaolin, a solution for the precast industry to limit the clinker content in concrete: mechanical aspects. Constr. Build. Mater. (2010)
5. Mounanga, P.: Improvement of the early-age reactivity of fly ash and blast furnace slag cementitious systems using limestone filler. Mater. Struct. (2011)
6. NF EN 196-1: Méthodes d'essais des ciments—Détermination des résistances mécaniques (2006)
7. Bolomey, J.: Granulation et prévision de la résistance probable des bétons. Bulletin technique de la Suisse romande (1936)
8. Lawrence, P., Ringot, E.: Prise en compte des additions minérales dans le calcul des résistances de mortiers. Rev. Fr. Génie Civ. **4**(4), 525–542 (2000)
9. Lenormand: Cendres volantes d'électrofiltres d'incinérateur d'ordures ménagères : traitement et incorporation dans des matériaux cimentaires. Université Libre de Bruxelles, Ecole Centrale de Nantes (2013)
10. Lerch, W.: The influence of gypsum on the hydration and properties of Portland cement pastes. Res. Lab. Portland Cem. Assoc. (1946)

Assessment of Sorptivity and Porosity Characteristics of Self-Compacting Concrete from Blended Cements Using Calcined Clay and Fly Ash at Various Replacement Levels

Harshvardhan, Arun C. Emmanuel and Shashank Bishnoi

Abstract As limestone calcined clay cement (LC^3) is on the verge of commercialization around the world, it is becoming more and more important to understand its durability under various conditions. It has been shown that LC^3 is especially useful to achieve the cohesion required in self-compacting concrete. However, the influence of the higher paste content in the self-compacting concrete related to a regular workability concrete is not well understood. In this study, self-compacting concrete and normal vibrated concrete were prepared using fly ash and limestone calcined clay pozzolan, at various replacement levels of 20, 35 and 50%. The mixes were designed to have similar strengths, and their sorptivity and porosity were measured after curing for 28 days. The results indicate that self-compacting concrete has better durability characteristics than normal vibrated concrete made of similar strength grade.

Keywords LC^3 · Self-Compacting concrete · Durability · Sorptivity · Porosity

1 Introduction

Self-compacting concrete (SCC) was developed in Japan in 1980s by Prof. Okamura and his team at University of Tokyo to tide over acute shortage of skilled manpower that was affecting the durability of concrete structures. The development of self-compacting concrete has been referred to as "quite revolution" of the concrete industry with the potential to replace the labour-intensive normal vibrated concrete. A lot of research work has been carried out on mix design and mechanical properties of SCC [1, 2]. However, very limited research work has been carried out in the area of durability of SCC in comparison with normal vibrated concrete [3, 4]. Thus, it is quite ironical that SCC which came into existence to tide over the "durability crisis" in Japan was criticized for lack of information related to durability by RILEM technical committee in 2008 [5].

The SCC mix essentially contains a large amount of superplasticizers and powder materials. Superplasticizers are required to add fluidity to the concrete mix, while presence of large amount of powder material is required for the stability of the mix.

Harshvardhan (✉) · A. C. Emmanuel · S. Bishnoi
Department of Civil Engineering, IIT Delhi, New Delhi, India

The amount of course aggregate and its maximum size is strictly restricted in case of SCC to avoid any blocking tendency of the concrete. Due to so many constraints imposed on the mix design and compaction of SCC, there is need to conduct a comparative study in the area of transport properties of SCC in comparison with normal vibrated concrete (NVC).

Hence, the main objective of this study is to assess the durability of SCC in comparison with NVC. For the purpose of the study, eco-friendly materials like fly ash and calcined clay are used for the preparation of concretes of similar strength grads, and their transport properties are assessed using boiling water and sorptivity tests after 28 days of curing.

2   Materials and Methods

In order to satisfy the project objective, SCC and NVC were designed for similar strength keeping the w/c ratio constant at 0.4. The total water content for SCC and NVC was fixed at 186 lit/cum and 164 lit/cum. The total cementitious content for SCC and NVC was calculated as 463 and 405 kg/m^3. The content of superplasticizers was varied from 0.7 to 1.5% for SCC, considering higher dosage required to obtain flowability and 0.2–0.3% for NVC. The values of slump flow, V funnel test of SCC were kept in conformity with EFNARC 2002 [6] guidelines by varying the dosage of superplasticizer content.

Based on the mix design shown in Tables 1 and 2, the samples for SCC and NVC were cast. Table 3 indicates the slump flow values for SCC and slump values of NVC made of different fillers.

Each sample of SCC and NVC was cast in six cubes of 15 cm $\times$ 15 cm $\times$ 15 cm and four cylinders 100 mm diameter and 200 mm depth for measuring transport properties. Concrete was prepared by mixing in a concrete batch mixer, and a mixing time of 5 and 3 min was kept for SCC and NVC, respectively. A Table Vibrator was used to provide proper compaction to samples corresponding to NVC mix only, while SCC mix is not compacted but levelled from the top so as to get a smooth surface finish.

Table 1 Mix Design adopted for Self-Compacting Concrete (SCC)

Mix proportions (kg/m^3)	Notations	Cement blend	Sand	10 mm	Admix dosage
OPC (100%)	O	463	917	866	2.87
OPC (80%) + LC^2 (20%)	L20	463	909	858	3.79
OPC (65%) + LC^2 (35%)	L35	463	902	852	4.39
OPC (50%) + LC^2 (50%)	L50	463	896	846	5.55
OPC (80%) + FA (20%)	F20	463	898	847	3.24
OPC (65%) + FA (35%)	F35	463	870	803	3.93
OPC (50%) + FA (50%)	F50	463	855	789	6.94

Table 2 Mix Design adopted for Normal Vibrating Concrete (NVC)

Mix proportions (kg/m^3)	Notations	Cement Blend	Sand	10 mm	20 mm	Admix dosage
OPC (100%)	O	405	674	490	736	1.01
OPC (80%) + LC^2 (20%)	L20	405	669	487	730	1.62
OPC (65%) + LC^2 (35%)	L35	405	665	484	726	1.82
OPC (50%) + LC^2 (50%)	L50	405	661	481	721	2.22
OPC (80%) + FA (20%)	F20	405	662	482	723	1.01
OPC (65%) + FA (35%)	F35	405	653	475	713	1.01
OPC (50%) + FA (50%)	F50	405	645	469	703	1.21

Table 3 Basic Fresh Properties and Compressive Strength of Hardened Concrete

Concrete	Slump test	Slump flow test	V funnel test	28 days strength
SCC OPC	–	700	10	47.70
SCC 20% FA	–	700	8	50.37
SCC 35% FA	–	720	12	41.48
SCC 50% FA	–	740	14	29.96
SCC 20% LC^2	–	600	12	41.11
SCC 35% LC^2	–	650	12	41.33
SCC 50% LC^2	–	650	13	45.77
NVC OPC	80	–	–	47.63
NVC 20% FA	70	–	–	44.14
NVC 35% FA	50	–	–	38.07
NVC 50% FA	80	–	–	27.11
NVC 20% LC^2	70	–	–	46.66
NVC 35% LC^2	75	–	–	45.77
NVC 50% LC^2	80	–	–	41.33

Subsequently, concrete samples are kept in a temperature and humidity-controlled room with a temperature $25 \pm 2°$ C and humidity of 65%. Samples are demoulded after 24 h of casting and cured in water saturated with lime. After curing of 7 days and 28 days, cylindrical samples were cut into discs of 50 ± 2 mm depth with a diamond saw cutter discarding the top or bottom 20 mm.

2.1 Testing of Transport Properties

The transport of liquid into concrete takes place through the presence of interconnected voids in the matrix, paste-aggregate interface. Depending on the driving force,

the transportation of liquid into the concrete happens by the mechanism of capillary sorption, diffusion and permeation. In the current study, a comparison of transport properties is carried out using the results obtained from sorptivity and boiling water test.

2.2 Sorptivity Test

This test method measures the absorption of water by hydraulic cement by measuring the increase in weight of the specimen. The resultant absorption of water is plotted against time. This test gives the susceptibility of an unsaturated concrete to penetration of water (ASTM C 1585-13). This test provides us with information regarding the pore structure and interconnectivity amongst the pores which have a great influence on the penetration resistance of concrete against aggressive ions. This test is performed over a disc of 100 ± 6 mm and depth 50 ± 3 mm. The discs are conditioned in a conditioning chamber maintained at a temperature of 50 ± 2 °C and relative humidity of 70% for 3 days. The specimen is removed from the chamber, and the sides of the specimen are sealed using an epoxy coating. After the drying of epoxy coating, the top surface of the specimen is sealed with a plastic sheet so as to prevent evaporation or wicking action. Weight and diameter of the specimen are measured. A supporting device is placed at the bottom of the container in which the sorptivity test is performed. The container is filled with water such that the level of water is 1–3 mm above the support device. The sealed specimen is then placed on the supporting device. The stopwatch is started as soon as the surface of the specimen comes in contact with water. Mass of the specimen is recorded at intervals specified in the ASTM code.

The amount of water absorbed is given by the following formula:

$$I = \frac{Mt}{a * d} \tag{1}$$

I absorption.
Mt change in mass of specimen with reference to time t.
a exposed area of the specimen in mm^2.
d density of water in g/mm^3.

The initial rate of water absorption is slope of the best fit line to I plotted against square root of time. This slope is obtained by performing the linear regression analysis. The correlation coefficient obtained should not be less than 0.95 for the purpose of the experiment.

2.3 Boiling Water Test

Boiling water test is used to measure the porosity of the concrete. It was conducted as per the guidelines stipulated in ASTM C642-13. This test is performed over a disc of 100 ± 6 mm and depth 50 ± 3 mm. The sample to be used for test should be free from observable cracks, fissures and shattered edges. The specimen is then kept in an oven at a temperature of 110 ± 5 °C for a period not less than 24 h. Then, the sample is taken out and allowed to cool to 20–25 °C, and weight is measured. The sample again kept in the oven for another 24 h, and the mass of the sample is measured. If the difference between first and second mass is less than 0.5%, then the lesser mass is oven-dry mass of the sample. In case, the difference is more than 0.5%, then the sample is again placed in an oven for another 24 h, and the above process is repeated until the mass difference is less than 0.5%.

Once the oven-dry mass of the sample is calculated, it is immersed in water at a temperature of 21 °C for not less than 48 h until the two successive values of the mass of surface dried sample at an interval of 24 h show a variation less than 0.5%. Here, we obtain the saturated mass after immersion.

After calculation of the saturated mass of the sample, it is placed in a container with heating facility and boiled for 5 h. It is then allowed to cool by natural heat loss for not less than 14 h to a temperature of 20–25 °C. The surface moisture is removed with a cloth and surface dried mass of specimen that is the saturated mass after boiling is determined.

The specimen obtained after immersion and boiling is further immersed in water by mode of a wire, and apparent weight of specimen is measured.

The volume of permeable voids is calculated using the following formula:

$$\text{Porosity}(\%) = \frac{(C - A)}{(C - D)} \tag{2}$$

A   Mass of oven-dried sample in air, gm.
B   Mass of saturated surface dry sample, gm.
C   Mass of saturated surfaces dry sample after boiling, gm.
D   Apparent weight of sample in water after immersion and boiling, gm.

3 Results and Discussions

3.1 Sorptivity–Capillary Water Absorption

The results of sorptivity test are shown in Figs. 1 and 2. The results indicate that the primary sorptivity and secondary sorptivity of SCC are less than NVC at different filler replacement levels for both fly ash and LC^2 after 28 days of curing. Irrespective
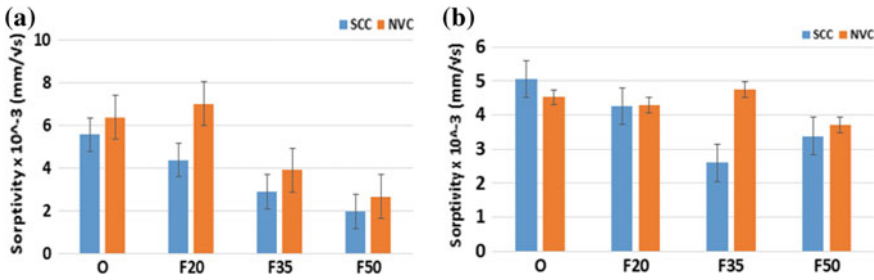
Fig. 1 28 days initial sorptivity of SCC versus NVC **a** OPC + fly ash and **b** OPC + LC^2
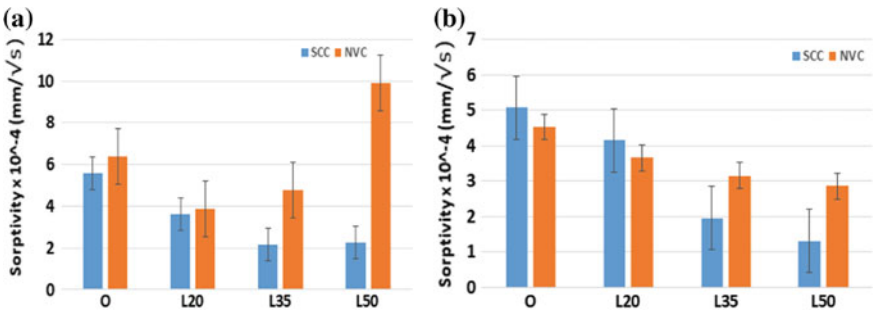
Fig. 2 28 days secondary sorptivity results SCC versus NVC **a** OPC + fly ash and **b** OPC + LC^2

of having a higher amount of paste content, reason for lower sorptivity values in case of SCC in comparison with corresponding NVC may be due to denser ITZ in SCC due to use of lesser amount of course aggregates and more amount of fine in comparison with NVC. Reduced amount of course aggregate and increased fines content make the ITZ stronger and thereby can be a justification of decrease in sorptivity values of SCC in comparison with corresponding NVC values. Another factor that may have had a negative impact on sorptivity values of NVC is the process of vibration associated with it. Vibration of concrete is an important process to remove the air voids, but the process of vibration leads to the accumulation of pore fluids around the aggregate particles which further impacts the transport properties of NVC in a negative way.

3.2　Boiling Water Test Results

The total volume of permeable voids obtained for SCC and NVC is compared in this section. Figure 3 represents the porosity values of SCC with corresponding NVC after 28 days of curing.
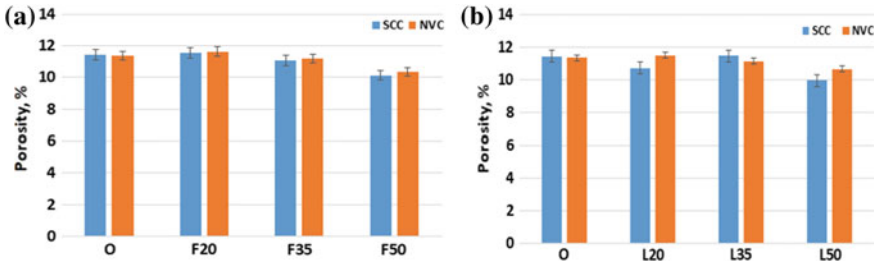
Fig. 3 28 days porosity results SCC versus NVC **a** OPC + fly ash and **b** OPC + LC^2

In case of samples of SCC and NVC cast with LC^2, there is a decrease in overall porosity with increase in LC^2 content, indicating better filling ability and faster hydration reaction for both SCC and NVC. On comparing individual mix designs of SCC and NVC, it is observed that the porosity value of SCC is still lower than corresponding NVC sample values reinforcing the idea behind stronger ITZ structure of SCC in comparison with NVC.

3.3 Summary

LC^2 is fast emerging an eco-friendly alternative to slow-reacting conventional pozzolans which based on requirement can lead to high early strength and durability gain of concrete in contrast to conventional pozzolans like fly ash. The positive effect of incorporation of LC^2 is not only restricted to conventional NVCs but can be extended to SCC as well.

SCC inherently has a denser microstructure in comparison with corresponding NVC, and incorporation of LC^2 further densified the microstructure of SCC leading to all-round better performance of SCC in comparison with NVC, incorporated with fly ash or LC^2. Hence, the degree of sorptivity and total volume of permeable voids reported from SCC tend to be lower than corresponding NVC values.

The results obtained and the analysis of the results have been successful in fulfilment of important research gap that was highlighted in RILEM technical committee report in 2008 [6] with respect to lack of durability-related studies on use of SCC.

4 Conclusions

The objective of the study was to assess the effect of fines on transport properties of SCC and to compare the durability of SCC with corresponding NVC designed for similar strength using different fillers like fly ash and LC^2. The conclusion derived from results and analysis has been summarized as follows:

- The incorporation of LC^2 leads to lower sorptivity values for both SCC and NVC concrete. However, in case of NVC, due to insufficient compaction, there may be some mixes where the sorptivity values obtained for LC^2 might be more than usual. However, in case of SCC, the problem pertaining to compaction is absent. Hence, the SCC samples give results indicating a common trend of sorptivity with the incorporation of LC^2.
- A comparative study on the sorptivity of SCC and NVC showed that for 28 days cured samples, the sorptivity of SCC tends to be lower than corresponding NVC samples. This leads us to conclude that the microstructure of SCC is denser in comparison with NVC. The densified microstructure is result of absence of compaction, use of excessive fines, strong ITZ which negates the negative impact of a higher amount of paste content leading to lower sorptivity values of SCC in comparison with NVC.
- For samples of SCC and NVC using LC2, the values of porosity obtained for both SCC and NVC are lower than equivalent samples using fly ash under similar curing conditions. This leads us to reinforce our conclusion stated in the sorptivity test that LC2 makes the microstructure of the concrete dense due to faster reaction of alumina phase and filling ability of clay.
- Comparison of the porosity values of SCC and NVC irrespective of the filler used shows that the amount of permeable voids in SCC is less than NVC as problem of accumulation of liquid in pores due to vibration or wall effect due to course aggregates is reduced as SCC does not require vibration and has less course aggregate content and higher fines content.

References

1. Okamur, H., Ozawa, K.: Mix Design of Self Compacting Concrete. Concrete Library of JSCE (1995)
2. Khayat K.H., Guizani, Z.: Use of viscosity-modifying admixture to enhance stability of fluid concrete. ACI Mater. J. **94**(4) (1997)
3. Kanellopoulos, A., Petrou, M.F., Ioannou, I.: Durability performance of self-compacting concrete. Constr. Build. Mater. **37**, 320–325 (2012)
4. Dharmaraj, R., Malathy, R.: Rapid chloride permeability test for durability studies on corrosion inhibiting self-compacting concrete. J. Chem. Pharm. Sci. ISSN: 0974-2115 (2016)
5. Final report of RILEM TC 205-DSC: durability of self-compacting concrete; Mater. Struct. **41**, 225–233 (2008)
6. EFNARC: Specification and guidelines for self compacting concrete (2002)
7. Okamura, H., Ouchi, M.: Self compacting concrete. J. Adv. Concr. Technol., Japanese Concrete Institute (2003)
8. Boström, L.: Self-compacting concrete exposed to fire. In: International RILEM Symposium on Self-Compacting Concrete (2003)
9. Turka, K., Karatasb, M.: Abrasion resistance and mechanical properties of self-compacting concrete with different dosages of fly ash/silica fume. Indian J. Eng. Mater. Sci. **18** (2011)

10. Ryan, P.C., O'Connor, A.: Comparing the durability of self-compacting concretes and conventionally vibrated concretes in chloride rich environment. Constr. Build. Mater. **120** (2016)
11. King, D.: The effect of silica fume on the properties of concrete as defined in concrete. In: 37th Conference on Our World in Concrete & Structures, 29–31 August 2012, Singapore

Utilization of Limestone Powder and Metakaolin as Mineral Fillers in High-Performance Self-Compacting Concrete

Shamsad Ahmad and Saheed Kolawole Adekunle

Abstract In the present work, limestone powder (LSP) and calcined clay (metakaolin, MK) were used as mineral fillers in two different mixtures of high-performance self-compacting concrete (SCC). In the first mixture, LSP was used alone as the mineral filler, whereas in the second one, the mineral filler consisted of the blend of LSP and MK. For both SCC mixtures, dune sand was used as fine aggregate and crushed limestone particles were used as coarse aggregate. Both SCC mixtures were prepared using a total powder content of 500 kg/m^3 (400 kg/m^3 Portland cement and 100 kg/m^3 mineral filler), a water/powder ratio of 0.3, and a fine/total aggregate ratio of 0.4. Dosages of superplasticizer and stabilizer were optimized through trials satisfying the self-compactability requirements. Performance of the SCC mixtures was evaluated in terms of selected mechanical properties, durability characteristics, and resistance against reinforcement corrosion that included compressive and splitting tensile strengths, modulus of elasticity, water penetration depth, rapid chloride permeability, electrical resistivity, and reinforcement corrosion monitoring. Both SCC mixtures achieved 28-day compressive strength (above 60 MPa), splitting tensile strength (above 5 MPa), and modulus of elasticity (above 40 GPa), *low* water permeability, very low chloride permeability, and negligible corrosion risk, indicating suitability of using LSP and MK as mineral filler for producing high-performance SCC. The self-compactability and mechanical properties of the mixture with the blend of LSP and MK were slightly better than the mixture with LSP alone; however, both mixtures showed the same durability characteristics and resistance against reinforcement corrosion.

Keywords Limestone powder · Calcined clay · Metakaolin · Self-compacting concrete · Mechanical properties · Durability characteristics

S. Ahmad (✉) · S. K. Adekunle
Civil & Environmental Engineering Department, King Fahd University of Petroleum & Minerals, Dhahran 31261, Saudi Arabia
e-mail: shamsad@kfupm.edu.sa

1   Introduction

Self-compacting concrete (SCC) basically developed for placing concrete in the formworks without the need for compaction using external means such as vibration and rodding. It has ability to flow under its self-weight without segregation or bleeding problems and take the shapes of the formworks without vibration or rodding that is required especially for concrete placement in structural members having narrow sections and/or congested reinforcement. The filling ability and segregation resistance of SCC reduce the risk of honeycombing that result in the production of strong and durable concrete [1].

The ingredients of SCC are very much similar to that for conventional vibrated concrete (CVC) that include cement, fine and coarse aggregates, water, mineral, and chemical admixtures. However, as compared to CVC mixtures, SCC mixtures are produced keeping the quantities of fine aggregate and superplasticizer (SP) higher besides using mineral admixture and viscosity modifying admixture (VMA) as essential ingredients. These compositional changes are made in SCC mixtures to achieve flow ability, filling ability, and resistance against segregation. The higher dosage of SP helps in improving the flow ability and filling ability, and the use of VMA provides required cohesion to prevent segregation due to high degree of workability. Higher amount of fines provides better lubrication for coarse aggregates that enhances the deformability of the SCC mixture [2]. The ingredients of SCC mixtures should be properly proportioned to achieve self-compactability that is controlled by three properties of the fresh SCC mixture, as follows: high deformability, good cohesion (i.e., restrained flowability), and a high resistance against segregation [3]. The mechanical properties and durability characteristics of SCC mixture are reported to be better than that of CVC mixtures [4–12], except for the modulus of elasticity that may be slightly lower as a result of the lower coarse aggregate content [13, 14]. However, these problems could be solved by proper mix proportioning and incorporation of appropriate additives.

Fly ash or silica fume has been commonly used as a mineral filler in producing the SCC mixtures. In recent years, the usage of limestone powder (LSP) and calcined clay, as alternative supplementary cementitious materials, is being frequently reported [15, 16]. LSP is produced as a result of crushing the limestone rocks for obtaining coarse aggregates; it contains the calcium oxide as its main constituent. When LSP is used in concrete as a mineral filler, it helps in achieving higher workability, densification of concrete microstructure, early strength, and control on bleeding [17–20]. When LSP is used in SCC, it enhances the deformability and cohesion and reduces the porosity of SCC. Due to these advantages of LSP, it is being used to produce SCC mixtures with technical and economic benefits. Metakaolin (MK), which is produced through calcination of kaolinitic clays, mainly consists of silica and alumina with a negligible amount of lime. MK falls under the category of highly pozzolanic materials that has the filler effect and accelerates the hydration of OPC and the pozzolanic reaction. While the MK provides immediate filling effect, its effect on pozzolanic reaction comes within first two weeks. The use of MK in

concrete or mortar as a strong pozzolanic material results in the improvements in strength and durability properties of concrete [21–28]. A study conducted by Mohsen and El-maghraby [29] has indicated that the MK produced by calcination of clays sourced from different parts of Saudi Arabia can be utilized as pozzolanic material in producing concrete and other construction materials.

In the present work, an attempt was made to explore the possibility of producing high-performance SCC mixtures using LSP and MK (available in Saudi Arabia) as mineral fillers with an intent to show the utility of local raw materials for strong, durable, economical, and environment-friendly SCC. Two high-performance SCC mixtures consisting of LSP and MK were prepared using optimal levels' water/cementitious material ratio, fine/total aggregate ratio, cementitious materials content. The dosage of SP and VMA was optimized satisfying the self-compactability criteria for both SCC mixtures. The performance of the SCC mixtures was evaluated in terms of selected mechanical properties, durability characteristics, and resistance against reinforcement corrosion.

2 Experimental Program

2.1 Materials

Powders. The blend of ordinary Portland cement (OPC) and mineral fillers is termed here as 'powder'. The OPC used in the present work was ASTM C 150 Type I. The LSP used in the present work was sourced from a quarry involved in producing coarse aggregate by crushing limestone rocks, located in Abu Hadriyah, Eastern Province of Saudi Arabia. The clay obtained from Hufoof, Eastern Province of Saudi Arabia, was calcined to prepare MK. The raw clay was thermally activated in a furnace at 850 °C and then ground with laboratory pulverizer to a fineness of passing #100 (150 µm) sieve. Table 1 shows the chemical compositions and specific gravities of OPC, LSP, and MK.

Coarse and fine aggregates. Crushed limestone sourced from a local quarry in Abu Hadriyah, Eastern Province of Saudi Arabia, was used as coarse aggregate. Coarse aggregate had a maximum aggregate size of 20 mm, specific gravity of 2.60, and water absorption of 1.4%. Dune sand, available in abundance in Saudi Arabia, was used as fine aggregate. It had a specific gravity of 2.56, and water absorption was 0.4%. Table 2 shows the particle size distribution of coarse and fine aggregates.

SP, VMA, and water. A new-generation polycarboxylic-based ether hyperplasticizer, commercially available with the trade name (Glenium 51®), was used as superplasticizer (SP). An aqueous solution of a high-molecular-weight synthetic copolymer that consists of a water-soluble polymer and commercially available with the trade name (RheoMATRIX®) was used as the stabilizer/viscosity modifying admixture (VMA). The technical data of SP and VMA are shown in Table 3.

Table 1 Chemical compositions and specific gravities of OPC, LSP, and MK

Oxide	Weight (%)		
	OPC	LSP	MK
CaO	64.35	45.70	0.10
SiO_2	22.00	11.79	48.29
Al_2O_3	5.64	2.17	35.58
Fe_2O_3	3.80	0.68	0.95
K_2O	0.36	0.84	0.88
MgO	2.11	1.80	0.50
Na_2O	0.19	1.72	0.87
Loss on ignition	0.70	35.1	12.60
Specific gravity	3.15	2.60	2.00

Table 2 Particle size distributions of coarse and fine aggregates

Size (mm)	% passing	
	Coarse aggregate	Fine aggregate
19.0	100	–
12.5	65	–
9.5	30	–
4.75 mm	10	100
2.36 mm	–	100
1.18 mm	–	100
600 µm	–	76
300 µm	–	10
150 µm	–	4

Table 3 Technical data of SP (Glenium 51®) and VMA (RheoMATRIX®)

Material	Appearance	Specific gravity @ 20 °C	pH @ 20 °C	Chloride content	Alkali content
SP	Brown	1.08 ± 0.02 g/cm^3	7.0 ± 1.0	≤0.1%	≤5.0%
VMA	Brown	1.0–1.02 g/cm^3	6–9	≤0.1%	–

The normal sweet water available in the laboratory tap was used throughout the trial mixing and preparation of test specimens for the evaluation of hardened properties of successful mixtures.

2.2 Proportioning of the Ingredients of the SCC Mixtures

It can be seen from Table 4 that two SCC mixtures with same powder content ($500 \, kg/m^3$ comprising $400 \, kg/m^3$ OPC and $100 \, kg/m^3$ mineral filler), water/powder ratio (0.3 by weight), fine/total aggregate ratio (0.5 by weight) but with different types of mineral fillers were considered. The mixture, M1, contained $100 \, kg/m^3$ of LSP alone as mineral filler, whereas the mixture M2 contained $75 \, kg/m^3$ of LSP and $25 \, kg/m^3$ of MK as combined mineral filler. The proportioning of the ingredients of the SCC mixtures was carried out using absolute volume equation based on the selected mixture parameters and the specific gravities of the ingredients. Weights of the ingredients, calculated for producing $1 \, m^3$ of the SCC mixtures (M1 and M2), are shown in Table 4.

The dosages of SP and VMA for both SCC mixtures were optimized through trials based on achieving the self-compactability in terms of slump flow, V-funnel flow time, U-box, and segregation resistance according to the test procedure and self-compactability criteria available in the literature [15, 16, 30]. The optimal dosages of SP and VMA, as shown in Table 4, were selected based on the satisfactory results of self-compactability tests on both SCC mixtures, as presented in Table 5.

Table 4 Weights of the constituent materials for $1 \, m^3$ of the SCC mixtures

Materials	Weight (kg)		Note
	M1 (LSP)	M2 (LSP and MK)	
Cement	400	400	OPC = 400 kg
LSP	100	75	Mineral filler(s) = 100 kg
MK	–	25	Total powder content = 500 kg
w/p ratio	0.3	0.3	Water/powder ratio = 0.3 by weight
Water	165	165	
Coarse aggregate	837	829	Particle size distribution, as shown in Table 2
Fine aggregate	837	828	Fine/total aggregate ratio = 0.50 by weight
SP	10	16.3	Optimum dosages satisfying self-compactability: 2% of powder for M1 3.25% of powder for M2
VMA	6.3	5	Optimum dosages satisfying self-compactability: 1.25% of powder for M1 1% of powder for M2

Table 5 Self-compactability test results of the SCC mixtures

SCC mixtures	Flow table (mm) minimum required: 650 mm	V-funnel time (s) acceptable range: 6–12 s	U-box (mm) acceptable range: 0–30 mm	Bleeding (visual)	Segregation (visual)
M1 (LSP)	680	11	5	None	Negligible
M2 (LSP and MK)	760	9	3	None	None

2.3 Test Standards and Test Specimens

Table 6 shows the details of test standards and test specimens used for evaluating the mechanical properties of the SCC mixtures. The test standards and test specimens, used for the evaluation of selected durability characteristics and resistance against reinforcement corrosion, are presented in Table 7. The detailed procedure for each test in Tables 6 and 7 is widely reported in the literature [15, 16].

The corrosion resistance of SCC specimens was evaluated by exposing them to 5% sodium chloride (NaCl) solution. Reinforced SCC specimens, measuring 75 mm in diameter and 150 mm high, were prepared with a 12-mm-diameter steel bar placed at the center. A cover of 25 mm was provided at the bottom. The reinforcing steel bars were coated with cement paste followed by an epoxy coating at the bottom of the bar and at the concrete–air interface to avoid crevice corrosion. Reinforcement corrosion was monitored by measuring the corrosion potentials using the saturated calomel

Table 6 Test standards and specimens for mechanical properties of SCC mixtures

Property	Test standard	Specimen shape and size	Test age (days)
Compressive strength	ASTM C 39	100 mm cube	3, 7, 14, 28, 90
Splitting tensile strength	ASTM C 496	75 × 150 mm cylinder	28
Modulus of elasticity	ASTM C 469	75 × 150 mm cylinder	28

Table 7 Test standards and specimens for durability characteristics of SCC mixtures

Characteristic	Test standard	Specimen shape and size	Test age
Water permeability	DIN 1048	100 mm cube	28 days
Chloride permeability	ASTM C 1202	75 × 150 mm cylinder	28 days
Electrical resistivity	2-electrode method	75 × 150 mm cylinder	28 days
Corrosion (potentials and rate)	LPR Method	12 mm bar centralized in 75 × 150 mm cylinder	28 days cured, then exposed to 5% NaCl

electrode (SCE), according to ASTM C 876, and the corrosion current density by the linear polarization resistance method.

2.4 Casting and Curing of Specimens

Casting of the specimens of the SCC mixtures was carried without vibrating the mixtures, unlike the casting of CVC mixtures that involves vibration after each layer is placed in the molds. The specimens were cured in water for a period of 28 days at a fairly constant laboratory temperature of 25 °C. After curing, they were used for testing for the evaluation of their mechanical properties and durability characteristics. The specimens for 90-day compressive strength test were left in the curing tanks until 90 days.

3 Results and Discussion

3.1 Mechanical Properties

The plots of the compressive strength data pertaining to both SCC mixtures, as shown in Fig. 1, indicate a significant increase in the compressive strength with age. The increase in compressive strength is continued up to the age of 90 days confirming the
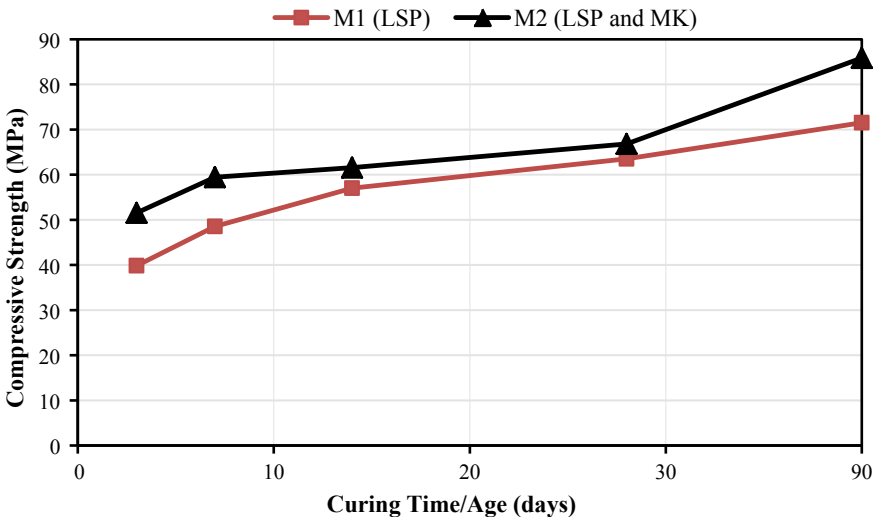
Fig. 1 Variation of compressive strength of SCC mixtures with age

Table 8 Mechanical properties of the SCC mixtures after 28 days of curing

SCC mixtures	Compressive strength (MPa)	Splitting tensile strength (MPa)	Modulus of elasticity (GPa)
M1 (LSP)	64	5.9	40
M2 (LSP and MK)	67	6.2	42

pozzolanic effects of both LSP and MK. At all ages, the compressive strength of the mixture M2, having the blend of both LSP and MK as mineral admixture, showed a higher strength than M1 with LSP alone as mineral filler. Further, it can be seen from the data presented in Table 8 that the 28-day tensile strength and modulus of elasticity values of the mixture M2 are also higher than that of the mixture M1. The reason behind beneficial effect of incorporating MK on the mechanical properties of the SCC mixture may be attributed to the high pozzolanic action of MK because of its high silica and alumina contents [24, 26, 31, 32].

The 28-day compressive strength, splitting tensile strength, and modulus of elasticity of both SCC mixtures (M1 and M2) are comparable with that of the high-performance CVC mixtures with approximately similar cement content and water/cement ratios. Kadri et al. [33] reported 28-day compressive strength in the range of 55–95 MPa for high-performance CVC mixtures prepared using cement content in the range of 310–550 kg/m^3 and water/cement ratio in the range of 0.25–0.45 (by weight). 28-day splitting tensile strength of 5.25 MPa was reported by Singla [34] for a high-performance concrete prepared with a cement content of 563 kg/m^3 and water/cement ratio of 0.3 (by weight). 28-day modulus of elasticity of a high-performance CVC mixture, with a cement content of 483 kg/m^3 and water/cement ratio of 0.41 (by weight), was found to be 34.8 ± 2.1 GPa by de Abreu et al. [35]. Therefore, the data presented in Table 8 show that both SCC mixtures satisfy the mechanical properties of a high-performance concrete. Further, the mechanical properties of the SCC mixtures, given in Table 8, are in the close agreement with the empirical equations developed by Awati and Khadiranaikar [36] for correlating compressive strength with splitting tensile strength and modulus of elasticity values of high-performance concrete mixtures.

3.2 Durability Characteristics and Resistance Against Reinforcement Corrosion

The data pertaining to the durability characteristics of the SCC mixtures after 28 days of curing, as shown in Table 9, indicate that the both mixtures have high degree of durability. Mixtures M1 and M2, having a water penetration depth of 7 and 12 mm, respectively, are less than 30 mm that corresponds to a 'low' water permeability of

Table 9 Durability characteristics of the SCC mixtures after 28 days of curing

SCC mixtures	Water penetration depth (mm)	Rapid chloride permeability (C)	Resistivity (kΩ-cm)
M1 (LSP)	7	399	34
M2 (LSP and MK)	12	315	43

concrete [37]. The values of rapid chloride permeability of both mixtures as shown in Table 9 are in the range of 100–1000 C that correspond to a 'very low' chloride permeability [38]. The electrical resistivity of both SCC mixtures, being greater than 20 kΩ-cm, indicates a 'low to negligible' likelihood of reinforcement corrosion [39].

Corrosion potential, E_{corr}, and corrosion current density, I_{corr}, were monitored for a period of three months by exposing the reinforced concrete specimens to 5% NaCl solution. Figures 2 and 3 show the variations of E_{corr}, and I_{corr}, respectively, with exposure duration. The E_{corr} values of both SCC mixtures, being far passive than the threshold value of −270 mV (SCE), as can be observed from Fig. 2, indicate that the probability of initiation of reinforcement corrosion is very low after an exposure period of three months. The I_{corr} values of both SCC mixtures, being far below the threshold value of I_{corr}, i.e., 0.3 µA/cm^2, that can be seen from Fig. 3 also confirm that both SCC mixtures have a high degree of resistance against reinforcement corrosion.
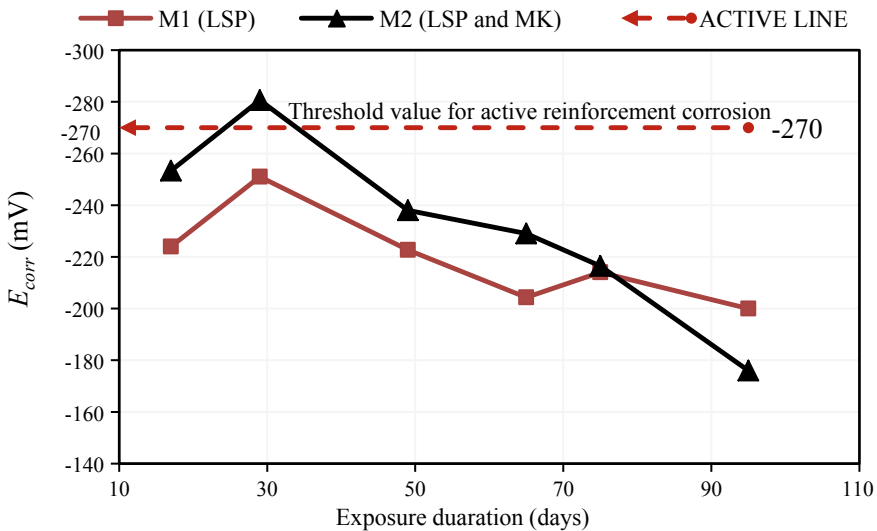
Fig. 2 Variation of corrosion potential, E_{corr}, of SCC with exposure time
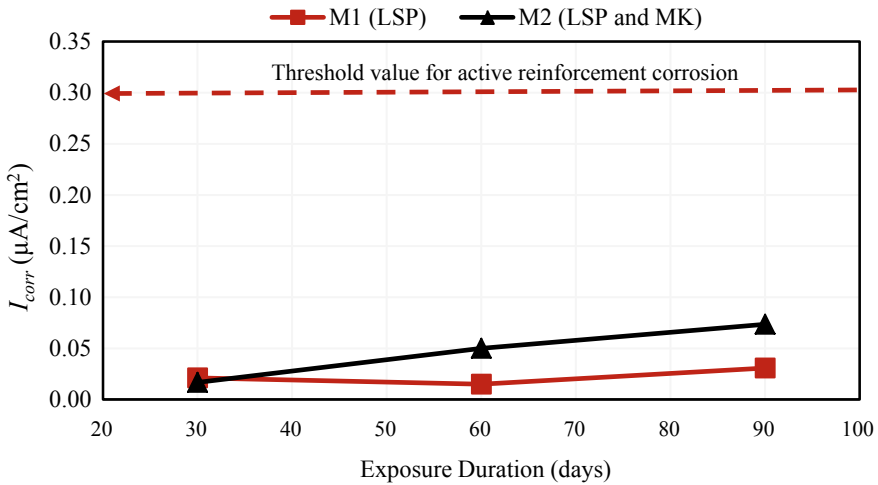
Fig. 3 Variation of corrosion current density, I_{corr}, with exposure time

4   Conclusions

Based on the experimental data obtained in this study, the following conclusions can be drawn:

1. Limestone powder alone as well as the blend of limestone powder and metakaolin can be used to produce the mixtures of high-performance self-compacting concrete with 28-day compressive strength above 60 MPa, splitting tensile strength above 5 MPa, and modulus of elasticity above 40 GPa, *low* water permeability, *very low* chloride permeability, and *negligible* risk of reinforcement corrosion.
2. The self-compactability and mechanical properties of the mixture with the blend of limestone powder and metakaolin were slightly better than the mixture with limestone powder alone; however, both mixtures showed the same durability characteristics and resistance against reinforcement corrosion.
3. The performance of both SCC mixtures was comparable with the high-performance CVC concrete mixtures produced with similar cement content and water/cement ratio.

References

1. Su, N., Hsu, K.-C., Chai, H.-W.: A simple mix design method for self-compacting concrete. Cem. Concr. Res. **31**(12), 1799–1807 (2001)
2. Dehn, F., Holschemacher, K., Weibe, D.: Self-compacting concrete time development of the material properties and the bond behavior. In: LACER, pp. 115–124 (2000)
3. Khayat, K.H., Assaad, J., Daczko, J.: Comparison of field-oriented test methods to assess dynamic stability of self-consolidated concrete. ACI Mater. J. **101**(2), 168–176 (2004)
4. Ouchi, M., et al.: A quantitative evaluation method for the effect of superplasticizer in self-compacting concrete. Trans. JCI, 15–20 (2001)
5. Kapoor, Y.P., Munn, C., Charif, K.: Self-compacting concrete—an economic approach. In: 7th International Conference on Concrete in Hot & Aggressive Environments, pp. 509–520. Manama, Kingdom of Bahrain (2003)
6. Zhu, W., Bartos, P.J.M.: Permeation properties of self-compacting concrete. Cem. Concr. Res. **33**(6), 921–926 (2003)
7. Ramsburg, P., et al.: Durability of self consolidating concrete in precast applications. In: ISHPC (www.oldcastle-precast.com), pp. 1–7 (2003)
8. Patel, R., et al.: Development of statistical models for mixture design of high-volume fly ash self-consolidating concrete. ACI Mater. J. **101**(4), 294–302 (2004)
9. Nehdi, M., Pardhan, M., Koshowski, S.: Durability of self-consolidating concrete incorporating high-volume replacement composite cements. Cem. Concr. Res. **34**(11), 2103–2112 (2004)
10. Persson, B.: Chloride migration coefficient of self-compacting concrete. Mater. Struct. **37**(2), 82–91 (2004)
11. Assie, S., et al.: Durability properties of low-resistance self-compacting concrete. Mag. Concr. Res. **58**(1), 1–7 (2006)
12. Assié, S., Escadeillas, G., Waller, V.: Estimates of self-compacting concrete 'potential' durability. Constr. Build. Mater. **21**(10), 1909–1917 (2007)
13. Holschemacher, K., Klug, Y.: A database for the evaluation of hardened properties of SCC. In: Leipzig Annual Civil Engineering Report, vol. 7, pp. 123–134 (2002)
14. Leemann, A., Hoffmann, C.: Properties of Self-compacting and Conventional Concrete: Differences and Similarities. ROYAUME-UNI, Telford, London (2005)
15. Adekunle, S., et al.: Properties of SCC prepared using natural pozzolana and industrial wastes as mineral fillers. Cem. Concr. Compos. **62**, 125–133 (2015)
16. Ahmad, S., et al.: Properties of self-consolidating concrete made utilizing alternative mineral fillers. Constr. Build. Mater. **68**, 268–276 (2014)
17. Bonavetti, V., et al.: Limestone filler cement in low w/c concrete: a rational use of energy. Cem. Concr. Res. **33**(6), 865–871 (2003)
18. Bosiljkov, V.B.: SCC mixes with poorly graded aggregate and high volume of limestone filler. Cem. Concr. Res. **33**(9), 1279–1286 (2003)
19. Hallal, A., et al.: Combined effect of mineral admixtures with superplasticizers on the fluidity of the blended cement paste. Constr. Build. Mater. **24**(8), 1418–1423 (2010)
20. Liu, S., Yan, P.: Effect of limestone powder on microstructure of concrete. J. Wuhan Univ. Technol. Mater. Sci. Ed. **25**(2), 328–331 (2010)
21. Bai, J., Wild, S., Sabir, B.B.: Chloride ingress and strength loss in concrete with different PC-PFA-MK binder compositions exposed to synthetic seawater. Cem. Concr. Res. **33**(3), 353–362 (2003)
22. Behfarnia, K., Farshadfar, O.: The effects of pozzolanic binders and polypropylene fibers on durability of SCC to magnesium sulfate attack. Constr. Build. Mater. **38**, 64–71 (2013)
23. Güneyisi, E., et al.: Strength, permeability and shrinkage cracking of silica fume and metakaolin concretes. Constr. Build. Mater. **34**, 120–130 (2012)
24. Melo, K.A., Carneiro, A.M.P.: Effect of Metakaolin's finesses and content in self-consolidating concrete. Constr. Build. Mater. **24**(8), 1529–1535 (2010)
25. Mobasher, B., et al.: Transport properties in metakaolin blended concrete. Constr. Build. Mater. **24**(11), 2217–2223 (2010)

26. Ramezanianpour, A.A., Bahrami Jovein, H.: Influence of metakaolin as supplementary cementing material on strength and durability of concretes. Constr. Build. Mater. **30**, 470–479 (2012)
27. Sabir, B., Wild, S., Bai, J.: Metakaolin and calcined clays as pozzolans for concrete: a review. Cem. Concr. Compos. **23**(6), 441–454 (2001)
28. Morsy, M.S., et al.: Mechanical properties, phase composition and microstructure of activated Metakaolin-slaked lime binder. KSCE J. Civ. Eng. **21**(3), 863–871 (2017)
29. Mohsen, Q., El-maghraby, A.: Characterization and assessment of Saudi clays raw material at different area. Arab. J. Chem. **3**(4), 271–277 (2010)
30. EFNARC: The European Guidelines for Self Compacting Concrete. EFNARC, UK (www.efnarc.org): United Kingdom, pp. 1–68 (2005)
31. Khatib, J.M.: Performance of self-compacting concrete containing fly ash. Constr. Build. Mater. **22**(9), 1963–1971 (2008)
32. Sabir, B.B., Wild, S., Bai, J.: Metakaolin and calcined clays as pozzolans for concrete: a review. Cement. Concr. Compos. **23**(6), 441–454 (2001)
33. Kadri, E.H., et al.: The compressive strength of high-performance concrete and ultrahigh-performance. Adv. Mater. Sci. Eng. **2012** (2012)
34. Singla, S.: Mechanical properties of high strength high performance concrete. In: International Conference on Advances in Civil Engineering, pp. 169–172. ACEE, Noida, India (2012)
35. de Abreu, G., et al.: Mechanical properties and microstructure of high performance concrete containing stabilized nano-silica. Rev. Mater. **22**(2) (2017)
36. Awati, M.M., Khadiranaikar, R.B.: Mix design and some mechanical properties of high performance concrete. J. Inf. Knowl. Res. Civil Eng. **4**(1) (2016)
37. The concrete society: permeability testing of site concrete—a review of methods and experience. In: Technical Report No. 31, 75 (1987)
38. American society for testing and materials: standard test method for electrical indication of concrete's ability to resist chloride ion penetration. In: ASTM C 1202, Annual Book of ASTM Standards, 4.02. Philadelphia (1994)
39. Broomfield, J.P.: Corrosion of Steel in Concrete: Understanding, Investigation and Repair. Spoon Press (2003)

Experimental Investigation on Strength and Durability of Concrete with Partial Replacement of Cement Using Calcined Clay

Payal Dubey and Nakul Gupta

Abstract Concrete has never been an environmental amiable substance neither for make nor for its use, or to dispose. Huge amount of water and energy is being used to get the raw material to make concrete and excavating for sand and other aggregates which cause ecological annihilation and air contamination. Concrete is also an assertion to be the colossal cause of carbon emission in the earth's atmosphere. Some assert that concrete is accountable for up to 5% of the world's cumulative carbon secretion which contributes greenhouse gases. Mixing of water in cement and cement production generate a huge amount of CO_2 gases realizing in environment seriously detrimental ozone layer causing high temperature increasing seasonal temperature variation. This paper is a probe with partial replacement of cement by calcined clay in concrete collected from two cities. The work deals with compressive strength, split tensile strength, water absorption. Data therefore presents over a maximum curing of 28 days. The substitutions proportions used were 4, 8, 12, 16 and 20% by weight of cement.

1 Introduction

The flexibility of concrete allows it to take any shape. The primary quality of strength and durability makes concrete the most favourable material to be used worldwide for constructions and building works. Concrete is a composition of cement, aggregate (both coarse and fine), admixtures and water. Over the last two decades, the demand for cement and concrete has seen an exponential growth throughout the world. The growth of the population complemented the increased needs for housing and infrastructure, and intensive economic activities as a result of emerging economies also

P. Dubey (✉) · N. Gupta
Department of Civil Engineering, GLA University, Mathura, India

N. Gupta
e-mail: nakul.gupta@gla.ac.in

lead to higher usage of cement [1–3]. The cement industry, after power, is the largest source of anthropogenic CO_2 emissions. This constitutes 5–7% of the worldwide CO_2 emissions taking place as a result of any human activities and causing adverse effects on earths' climate [2, 4, 5]. 95% of this carbon dioxide is the by-product of the cement production process, and 50% of it is released when carbonic acid is being removed from limestone during cement manufacturing. Surprisingly, cement is the second most-consumed product after water. The rate of production of normal raw resources is getting scarce, while globally, millions of masses of inert waste products are dominating the world through mining, industrial activities as well as mineral processing industrial performances, whose removals are subject to stricter ecological legislation [5, 6]. Nonetheless, the majority of the wastes products are analogous in the constitution to their original raw materials utilized in the production industries. As a result, the improvement of wastes products to substitute raw resources is technologically, economically and environmentally interesting. Mineral and mining processing of wastes has been traditionally abandoned in landfills as well as cast-off openly into environment without satisfactory treatment. Nonetheless, potential recycling or reuse options ought to be investigated and put into practice. Today, recycling and reuse of waste product after its potentiality have been noticed and measured as what could add up to the well-being of the society, add to the reduction of production costs, offer a substitute raw material for use in various industrial activities and preserve community well-being [5, 7]. The rapid urbanization in developing nations will further push forward this demand for cement, and according to a recent study, it has been estimated that by 2023, the contribution of global CO_2 emissions as a result of cement production will be around 10–15%. This environmental urgency to lessen the CO_2 secretion during the cement manufacturing method has propelled the researchers to propose different approaches to cement compositions [8]. A practically feasible option to reduce the consumption of cement, thereby reducing its environmental effects is to replace it by supplementary cementitious materials (SCMs). Among different available SCMs like fly ash and slag, calcined clay is considered to be a more favourable option, mainly due to its wide availability in huge capacity [7, 9, 10]. Calcined clays are usually mixed with clinker to create Portland cement that is being used as an alternative for a portion of Portland cement while making concrete [11]. Calcined clay is a suitable entry for concrete and cement applications, which can improve many specific characteristics. While calcined clay is processed and cooled down to the temperature range of 600–800 °C, it reacts properly in the concrete as partial replacement of the cement [12]. Generally, instead of Portland cement, 8–20% (according to the weight) is replaced by calcined clay. This type of concrete reveals engineering-friendly properties [13, 14].

1.1 Objective of Study

- Our main objective was to research the impact of partial replacement of cement by calcined clay on various levels according to the weight of cement.

- Initially, the compressive strength, split tensile strength, acid attack and water absorption of an ordinary grade M25 concrete are observed.

2 Literature Review

Vipat A. R and Kulkarni P. M et al.: This research showcases the outcome of an inquiry over the use of metakaolin as an added cementitious material for concrete's performance improvement. The study consists of three levels of MK replacements in the concrete—10, 15 and 20%—by weight of Portland cement's usage. The main characteristics of concrete are evaluated by measuring compressive strength, splitting tensile strength and bond stress. The results have revealed that, depending on the replacement levels of metakaolin, its inclusion in concrete remarkably increases the strength properties of concrete Out of the three levels given above, the maximum compressive strength is being observed at 15%. The inclusion of metakaolin improves tensile and bond strength.

Priyank Bhimani and Chetna M. Vyas et al.: This paper deals with studying the impact on partially replacing cement with industrial waste from china clay industries. Once the procedure is completed, water absorption test and compressive strength tests were conducted on both original concrete and concrete created by replacing cement with china clay, and results were recorded. China clay, also known as kaolin is available in abundance in India and also in various parts of the world. 9 ton of waste is generated to produce 1 ton of kaolin. The procedure involves replacing kaolin waste in concrete by 10, 20 and 30%. However, it was observed that the replacement of OPC by china clay materials provides maximum compressive strength at 10%. Furthermore, the maximum water absorption achieved when 20% replacement of cement happens in concrete. People will give the usage of china clay preference as it provides strength to buildings at an economical price. This will also help in making the environment green by reducing the problem of waste disposal.

John [15]: States that as per the weight of metakaolin the cement replacement levels were 5, 10, 15, 20%. The strength development of concrete overshoot by metakaolin admixed concrete mix. Other mixes are inferior when compared to 15% mixture of metakaolin. The compressive, split tensile and flexural strength have been enhanced up to 15% replacement with an increase in metakaolin content. The outcome emboldens the use of metakaolin as pozzolanic substance for partial cement replacement in manufacturing high strength concrete. The presence of metakaolin brings quicker age strength growth of concrete. The usage of add-on cementitious material like metakaolin concrete can pay-off for environment, technical and ecological issues initiated by cement manufacturing.

3 Material Study

3.1 Materials

Cement: The cement of 43 grades ordinary Portland cement manufactured by. ACC Cement Company confirming to IS 8112-1989 is used in this investigation (Table 1).

Aggregates: Aggregate is a vital component of concrete. Coarse aggregates with a maximum size of 20 mm from a local source. Conforming to IS 383-1970 used in this research. Fine aggregates locally available river sand passing through 4.75 mm IS sieve (Table 2).

Calcined Clay: Calcined clay is retrieved from Astro Chemicals, Chennai, and from Jain Chemicals, Faridabad (Kutch). The calcined clay Chennai has a specific gravity of 2.31, and calcined clay Kutch has a specific gravity of 2.6 and is used in replacing the cement. The clay's colour is super white and off-white. It acts as a Pozzolanic material. The grinding activity of calcined clay to a finer particle size may also affect its reactivity. The properties of clay are given as follows (Table 3).

Water: Using fresh portable water, concrete is mixed and cured as it is free from the concentration of acids and organic matter. Water is an important component of concrete. It produces chemical reactions with water (hydration) to produce the desired properties of concrete.

Mix Design: Design of concrete mix adopted in this research was as per guiding principle in IS-10262-2009. Guide for concrete mix is in proportions. All the specimens were processed using the design mix. M25 grade of concrete was used for the analysis. Mix proportion of concrete is in kg/m^3 (Table 4).

Table 1 Physical properties of cement

S. No.	Physical properties	Test result
1	Initial setting time	76 min
2	Final setting time	265 min
3	Consistency	32%
4	Specific gravity	3.12
5	Colour	Grey

Table 2 Physical properties of aggregates

S. No.	Specification	Coarse aggregate	Fine aggregate
1	Specific gravity	2.76	2.62
2	Water absorption	1.60%	1.20%
3	Bulk density	1580 kg/m^3	1654 kg/m^3
4	Fine modulus	6.61%	3.40%

Table 3 Properties of calcined clay Kutch and Chennai

S. No.	Properties	CCK	CCC
1	Colour	Super white	Off-white
2	Specific gravity	2.6	2.31
3	Physical form	Powder	Powder
4	SiO_2	47%	45%
5	Al_2O_3	40%	37.85%

Table 4 Mix proportions of M25 grade

S. No.	Material	Quantity (kg/m^3)
1	Cement	437.7
2	Fine aggregate	703.4
3	Coarse aggregate	1067.1
4	Water	197
5	Water–cement ratio	0.45

4 Experimental Program

4.1 Casting of Specimens

The program involves the casting and testing of cubic specimens of concrete of 150 mm edge length and a cylinder of 150 × 300 mm. The moulding was a cast of M25 grade concrete created using OPC, sand and crushed stones (20 and 10 mm) mixed with calcined clay from Kutch and Chennai. Each of the three specimens was created to obtain the average value. The specimens created were de-moulded after 24 h.

Testing of Specimen: To obtain and record the result of compressive strength, split tensile strength, and acid attack and water absorption levels.

Compressive Strength: Six cubes of size 150 mm were casted for each mix (7 days, 28 days and 90 days) and were tested on universal testing machine (UTM). The samplings were individually placed on the platform of machine, and load was applied gradually, till the mould structure compromises. The ultimate load was documented, and the compressive strength of the corresponding sample was calculated.

Split Tensile Strength: For every mixture, 6 cylinders of size 150 × 300 mm were casted and tested using the same machine universal testing machine (UTM) on 7, 28 and 90 days. This time specimens were placed at 90 degrees to platform's axis of universal testing machine (UTM). Load was applied until the mould structure failed.

Acid Attack: The hydrochloric acid attack test was conducted on 150 mm cubes. The proportion taken for hydrochloric acid attack (HCL acid) was 2%. For each mix, six numbers of cubes were casted.

Hydrochloric Acid: The chemicals formed in the form of reaction products between hydrochloric acid and hydrated cement phases are some soluble salts and some insoluble salts. Soluble salts, mostly with lectures, are later leached out, while insoluble salts, along with amorphous hydrogel, together the layers remain in the layer. In addition to dissolution, some Fe–Si, Al–Si, Ca–Al–Si complex can also be formed as a result of the interaction between hydrogel which appears to be stable in the pH range above 3.5.

$$Ca(OH)_2 + 2HCl \Rightarrow CaCl_2 + 2H_2O$$
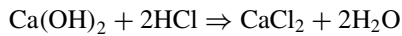
The reaction essentially causes the leaching of $Ca(OH)_2$ from set cement. Hydrochloric acid attack is a specific acidic erosion that may characterize the formation of the layer structure [16].

Water Absorption: Water absorption test provides amendment of overall zero space in concrete. When applied on the samples removed from cubes during production, the inconsistency of the test process is quite small. While the absorption value is partly dependent on the condition of the mixture, it is also significantly influenced by the initial treatment and the effectiveness. Thus makes it challenging to find whether there is a high outcome due to the content or cube making/treatment problems. Cubes of 150 mm after casting were submerged for 28 days in water. Then the wet weight of the cube is being noted and also gets weaved. By the time, the mass was not stable and weighed again; the dry weight of the cube was being noted by drying these samples in the oven at 105 °C.

$$\%\text{Water absorbed} = [(WW_C - WD_C)/WD_C] \times 100$$

where WW_C = Wet Cube Weight and WD_C = Dry Weight of Cube [17].

5 Results

The test results of concrete specimen are given below:

5.1 Compressive Strength

See Figs. 1 and 2.
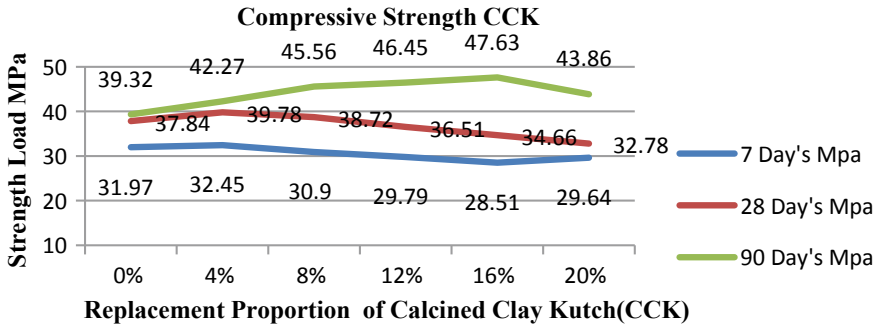
Fig. 1 Compressive strength of CCK
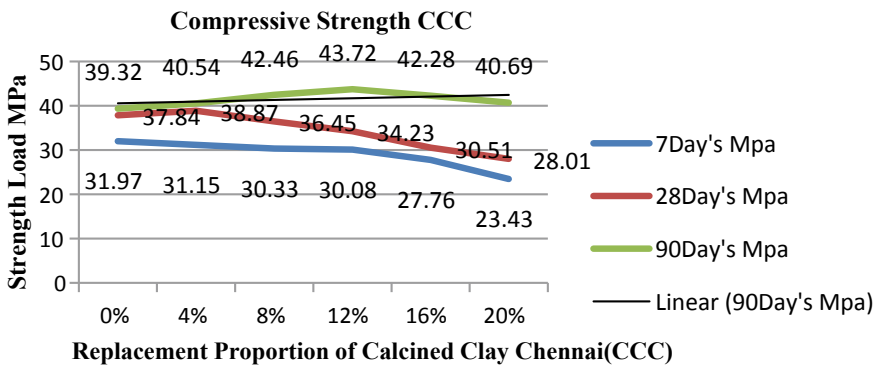
Fig. 2 Compressive strength of CCC

5.2   Split Tensile Strength

See Figs. 3 and 4.

5.3   Acid Attack

See Figs. 5 and 6.

5.4   Water Absorption Test

See Fig. 7.
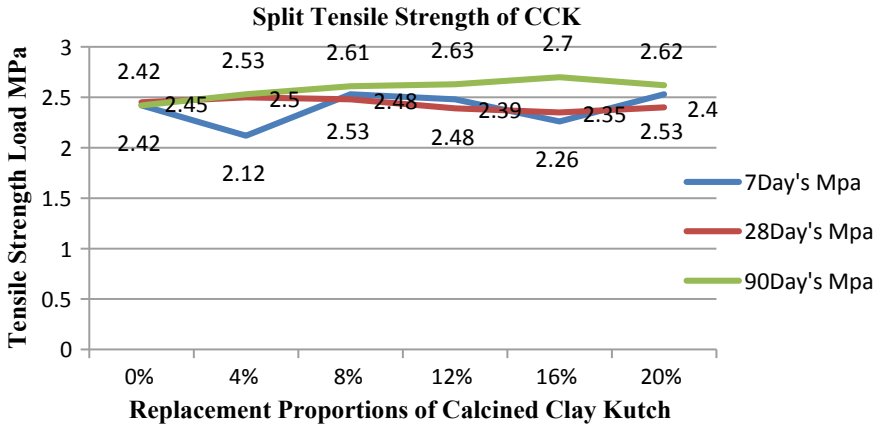
Fig. 3 Split tensile strength of CCK
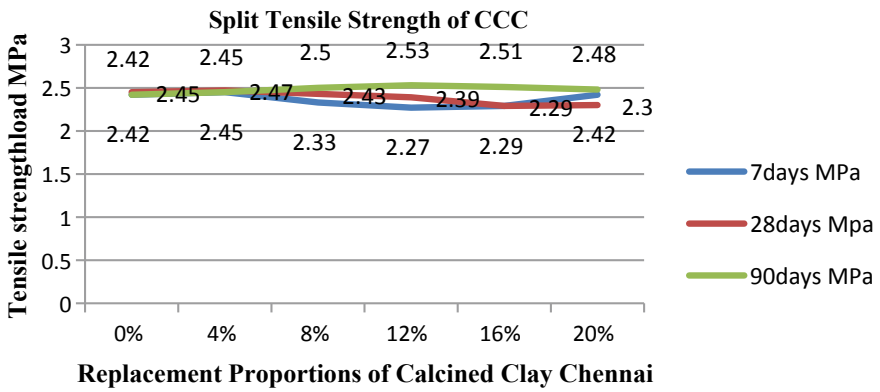
Fig. 4 Split tensile strength of CCC
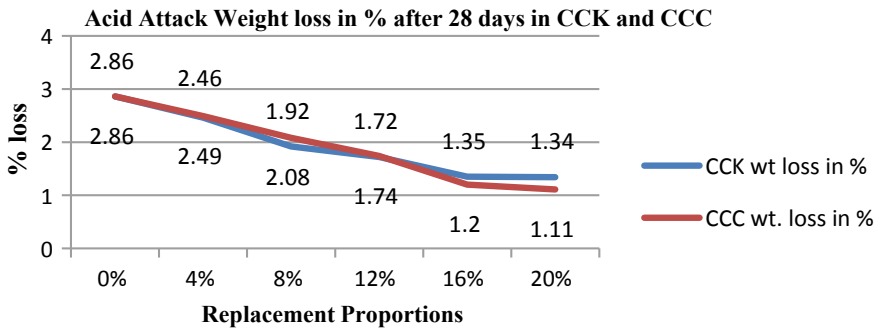
Fig. 5 Acid attack percentage weight loss of CCK and CCC

Acid attack Compressive strength after 28 days in CCK and CCC
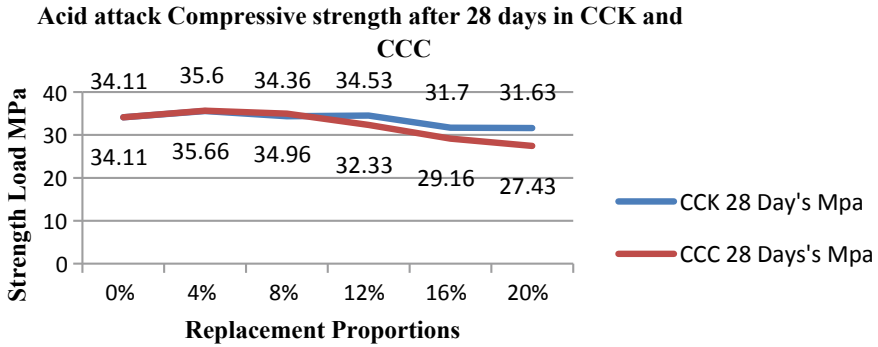
Fig. 6   Acid attack compressive strength of CCK and CCC

Water absorption after 28 days in CCK and CCC
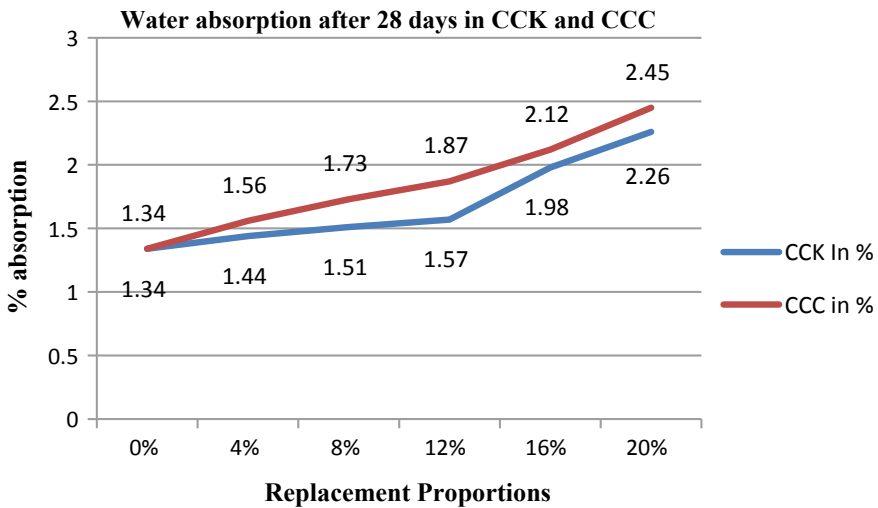
Fig. 7   Water absorption

6   Conclusion

Based on the present experimental analysis on the partial replacement of calcined clay with cement in concrete, the following conclusions were made:

1. In this experiment used calcined clay from Kutch and calcined clay from Chennai, the best results were from calcined clay Kutch.
2. On 16% cement replacement by calcined clay Kutch, compressive strength on 90 days is superior and gave the maximum value when compared with calcined clay Chennai on 16%.
3. The increase in calcined clay content improves the split tensile strength up to 16% cement replacement.

4. On 20% cement replacement by calcined clay Chennai, the test of water absorption provides a maximum percentage.
5. As per the analysis of HCL acid attack improves in concrete the 1.11% weight loss at 20% cement replacement by calcined clay Chennai and the compressive strength on CCK 35.60 at 4% cement replacement and compressive strength on CCC 35.66 at 4% from standard conventional is 34.11 so it was improved.
6. The problem of waste disposal and environmental issues on waste can be reduced through this research, and the environment can be made green.

References

1. Sánchez Berriel, S., et al.: Assessing the environmental and economic potential of limestone calcined clay cement in Cuba. J. Clean. Prod. **124**, 361–369 (2016)
2. Pavithra, O., Gayathri, D., Kumar, T.N.: Experimental analysis on concrete with partial replacement of cement with metakaolin and fine aggregate with quartz sand. Int. J. Adv. Eng. Res. Dev. **4**(12), 448–455 (2018)
3. Tironi, A.: Assessment of pozzolanic activity of different calcined clays. Cem. Concr. Compos. **37**, 319–327 (2013)
4. Cancio Díaz, Y., et al.: Limestone calcined clay cement as a low-carbon solution to meet expanding cement demand in emerging economies. Dev. Eng. **2**, 82–91 (2017)
5. Bhimani, P.: Performance of concrete with China clay (kaolin) waste. Int. J. Latest Trends Eng. Technol. **2**(3), 49–54 (2013)
6. Aishwaryalakshmi, V., Kumar, N., Seshachalam, H.: Experimental study on strength of concrete by partial replacement. **3**, 310–311 (2017)
7. Chari, K.S., Rao, M.N.: Study on mechanical and durability characteristics of concrete on partial replacement of cement with metakaolin and fine aggregate with quarry dust. Int. J. Eng. Res. **6**(1) (2018). ISSN: 2321-7758
8. Murat, M.: Hydration reaction and hardening of calcined clays and related minerals. I. Preliminary investigation on metakaolinite. Cem. Concr. Res. **13**(2), 259–266 (1983)
9. Du, H., Pang, S.D.: Value-added utilization of marine clay as cement replacement for sustainable concrete production. J. Clean. Prod. **198**, 867–873 (2018)
10. Lothenbach, B., Scrivener, K., Hooton, R.D.: Supplementary cementitious materials. Cem. Concr. Res. **41**(12), 1244–1256 (2011)
11. Juenger, M.C.G., Siddique, R.: Recent advances in understanding the role of supplementary cementitious materials in concrete. Cem. Concr. Res. **78**, 71–80 (2015)
12. Kalaignan, R., Reddy, S.S.M.: Control compressive strength, split tensile strength. Comparative study on mechanical properties of concrete with partial replacement of cement using. Int. J. Civ. Eng. Technol. **9**(13), 503–511 (2018)
13. Sabir, B., Wild, S., Bai, J.: Metakaolin and calcined clays as pozzolans for concrete: a review. Cem. Concr. Compos. **23**(6), 441–454 (2001)
14. Jian Tong, D., Zongjin, L.: Effects of metakaolin and silica fume on properties of concrete. ACI Mater. J. **99**(4), 393–398 (2002)
15. John, N.: Strength properties of metakaolin admixed concrete. Int. J. Sci. Res. Publ. **3**(6), 2250–3153 (2013)
16. Amudhavalli, N.K., Mathew, J.: Effect of silica fume on strength and durability parameters of concrete. Int. J. Eng. Sci. Emerg. Technol. **3**(1), 2231–6604 (2012)
17. Kulkarni, M.P., Vipat, A.R.: Performance of metakaolin concrete in bond and tension. Int. J. Eng. Sci. Res. Technol. **5**(762–765), 762–765 (2016)

Study of Durability Aspects of Limestone Calcined Clay Cement Using Different Piezo Configurations

Tushar Bansal and Visalakshi Talakokula

Abstract The present research focuses on durability aspects of limestone calcined clay cement (LC^3) using different piezo configurations specifically aimed at acid attack. The experimental study was carried out on concrete cylindrical specimens of ordinary Portland cement (OPC) and LC^3, which were immersed into the sulphuric acid (H_2SO_4) and hydrochloric acid (HCl) solution. Different piezo configurations were installed to acquire the data in the form of conductance and susceptance signatures via electro-mechanical impedance (EMI) technique. From the acquired data, the equivalent structural mass parameter was extracted which was then validated with actual mass obtained by physical measurement. Based on the results, it can be concluded that the equivalent mass parameter is able to identify the mass loss in the specimens subjected to acidic environment non-destructively.

Keywords Limestone calcined clay cement (LC^3) · Piezo sensor · Acid attack

1 Introduction

A durable concrete is one that performs satisfactorily in the working environment when exposed to various atmospheric conditions, water, soil and many other chemical exposures. Concrete is highly alkaline in nature with pH values normally ranging from 12.5 to 13.5 depending upon the mixture proportion. Since it has high alkalinity, it is readily attacked by various chemicals which have a pH value less than 7. However, some chemicals such as sulphuric acid (H_2SO_4) and hydrochloric acid (HCl) are the most destructive acids which cause degradation and damage to concrete when come into contact with it. Both these acids are produced either from sewage, acid rain, seawater or from the sulphur dioxide present in the atmosphere of industrial cities. H_2SO_4 attack causes the extensive formation of gypsum or ettringite in the regions close to the surfaces and tends to cause expansion which ultimately leads to spalling.

T. Bansal · V. Talakokula (✉)
Department of Civil Engineering, Bennett University, Greater Noida, India
e-mail: basavishali@gmail.com

T. Bansal
e-mail: tb6292@bennett.edu.in

The chemical reaction involved in H_2SO_4 attack on cement-based materials can be given in Eq. 1.

$$Ca(OH)_2 + H_2SO_4 = CaSO_4 \cdot 2H_2O \tag{1}$$
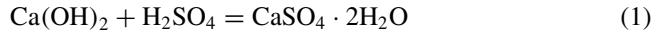
In hydrochloric acid attack, the chemicals formed as the products of the reaction between hydrochloric acid and hydrated cement phases are some soluble salts and some insoluble salts. Soluble salts, mostly with calcium are subsequently leached out, whereas insoluble salts along with amorphous gels remained in the corroded layer. Eq. 2 shows the leaching of calcium hydroxide. After leaching out of calcium hydroxide, ettringite and C-S-H start to decompose with the release of Ca^{2+} to counteract the loss of calcium hydroxide, and the set cement starts to disintegrate accelerating the dissolution as shown in Eqs. (3 and 4).

$$Ca(OH)_2 + 2HCl = CaCl_2 + 2H_2O \tag{2}$$

$$Ca_6Al_2(SO_4)_3(OH)_{12} \cdot 26H_2O = 3Ca^{2+} + 2[Al(OH)_4]^- + 4OH^- + 26H_2O \tag{3}$$

$$3Ca^{2+} + 2[Al(OH)_4]^- + 4OH^- + 12HCl = 3CaCl_2 + 2AlCl_3 + 12H_2O \tag{4}$$
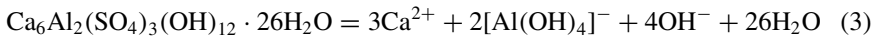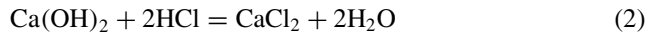
From the above issue, it is concluded that the acid attack on concrete is a major problem. To solve this issue, many authors replaced the OPC with supplementary cementitious (SCMs) material to increase the resistance of concrete against acids attack. Chang et al. [1] investigated the concrete's resistance against H_2SO_4 attack using limestone aggregates and different types of cement such as ground granulated blast furnace slag, silica fume and fly ash and found that limestone aggregates and the ternary cement containing silica fume and fly ash has excellent acid resistance in 1% sulphuric acid solution. Romanova et al. [2] assessed the corrosion process on concrete circular pipe exposed to H_2SO_4 solution with different temperature and found that the concrete mass and density increases during the early stage of corrosion process which become quicker in the presence of higher temperature. Siad et al. [3] investigated the effect of mineral admixture on the resistance of H_2SO_4 and HCl acid attacks in self-compacting concrete (SCC) and found that on the addition of natural pozzolana in SCC demonstrates positive influence against H_2SO_4 and HCl acid. The mechanical properties, shrinkage and durability performance of different blended concrete such as OPC, FA blended cement (FA30) and limestone calcined clay (LC^3) were studied by Dhandapani et al. [4] and concluded that LC^3 has either comparable/better properties. All the above studies investigate the durability of concrete by subjecting the specimen to acid attack destructively, and hence, the authors felt the need of studying the same non-destructively using piezo configurations.

2 Durability Aspects of LC³ Using Different Piezo-Configurations

The durability aspects of LC³ studies by using three different piezo configurations such as embedded piezo-sensor (EPS), surface-bonded piezo sensor (SBPS) and non-bonded piezo sensor (NBPS). EPS is the one in which the sensor is sandwiched between the mortar layers, SBPS is the surface bonded on the top surface on the specimen and NBPS is the sensor which is bonded on the thin aluminium foil and in turn non-directly bonded to the top surface of the specimen in a reusable form. All the piezo-sensors are based on the effective impedance model developed by Bhalla and Soh [5] using EMI technique, in which, both the direct and the converse effects of the piezo-sensors are utilized. The sensors are first excited using an impedance analyser such as LCR metre and its interactions with the host structures are acquired in the form of conductance (the real part) and the susceptance (the imaginary part) signatures. Any changes such as mass, damping and stiffness of the host structure are reflected in the admittance signature in the form of shifting/occurrence of new peaks. After that, an impedance technique was used to understand the correlation between change in signatures and the corresponding change in the equivalent mass parameter. This technique is outlined by Talakokula and Bhalla [6], Talakokula et al. [7, 8] to determine the mechanical impedance of the structure, $Z_{s,\text{eff}} = x + yj$, at a particular frequency, ω, from the conductance and susceptance signature. The identified mechanical system is a series combination of spring-mass-damper system (k-c-m) when examined in the frequency range 270–300 kHz as shown in Fig. 1. The 'x' and 'y' for the identified system was given by Hixon [9] as shown in Eqs. (5 and 6) and mass parameter can be determined by algebraic manipulations as shown in Eq. (7).

$$x = \frac{C^{-1}}{C^{-2} + (\omega/k - 1/\omega m)^2} \tag{5}$$

$$y = \frac{-(\omega/k - 1/\omega m)}{C^{-1} + (\omega/k - 1/\omega m)^2} \tag{6}$$

$$m = \frac{(\omega_o^2 - \omega^2)(x^2 + y^2)}{\omega \omega_o^2 y} \tag{7}$$

where $y = 0$, then $\omega = \omega_o$.

Fig. 1 Identified system (a series combination of spring-mass-damper)
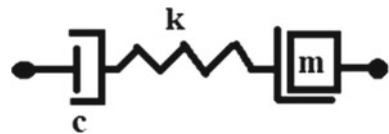
Table 1 Mix design details of OPC and LC^3-50

Concrete	Materials				
	Cement (kg/m^3)	Fine aggregate (kg/m^3)	Coarse aggregate (kg/m^3)	Water (kg/m^3)	Limestone calcined clay (kg/m^3)
OPC	386.36	672.84	1196.16	170	–
LC^3-50	193.18	672.84	1196.16	170	193.18
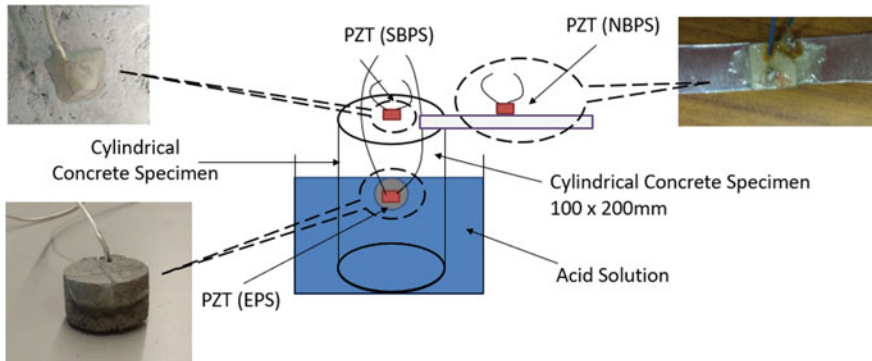
Fig. 2 Experimental set-up

2.1 Experimental Programme

In this study, eight concrete cylindrical specimens were cast with OPC and LC^3-50 (using clinker replacement level of 50%) cement. The concrete mix data of OPC and LC^3-50 are shown in Table 1. The specimens were subjected to hydrochloric acid and sulphuric acid solution (see Fig. 2) for 30 days. To check the durability of the specimen, the mass of the concrete is measured at the interval of 2 days by weighing the specimen after 1 h of drying, at the same time data were acquired in the form of electric admittance signature using different piezo configurations. After that actual mass loss in percentage was computed after 30 days of exposure of acid attack with respect to original mass.

3 Results and Discussion

From Figs. 3 and 4, it is observed that the thirty-day conductance signature resonance peaks shift from its baseline position in all the different piezo-configurations when subjected to H_2SO_4 and HCl environment, respectively. In H_2SO_4 attack, it is because of exposure of sulphate when react with hydrated cement paste, it forms gypsum or

(a)

(b)

(c)
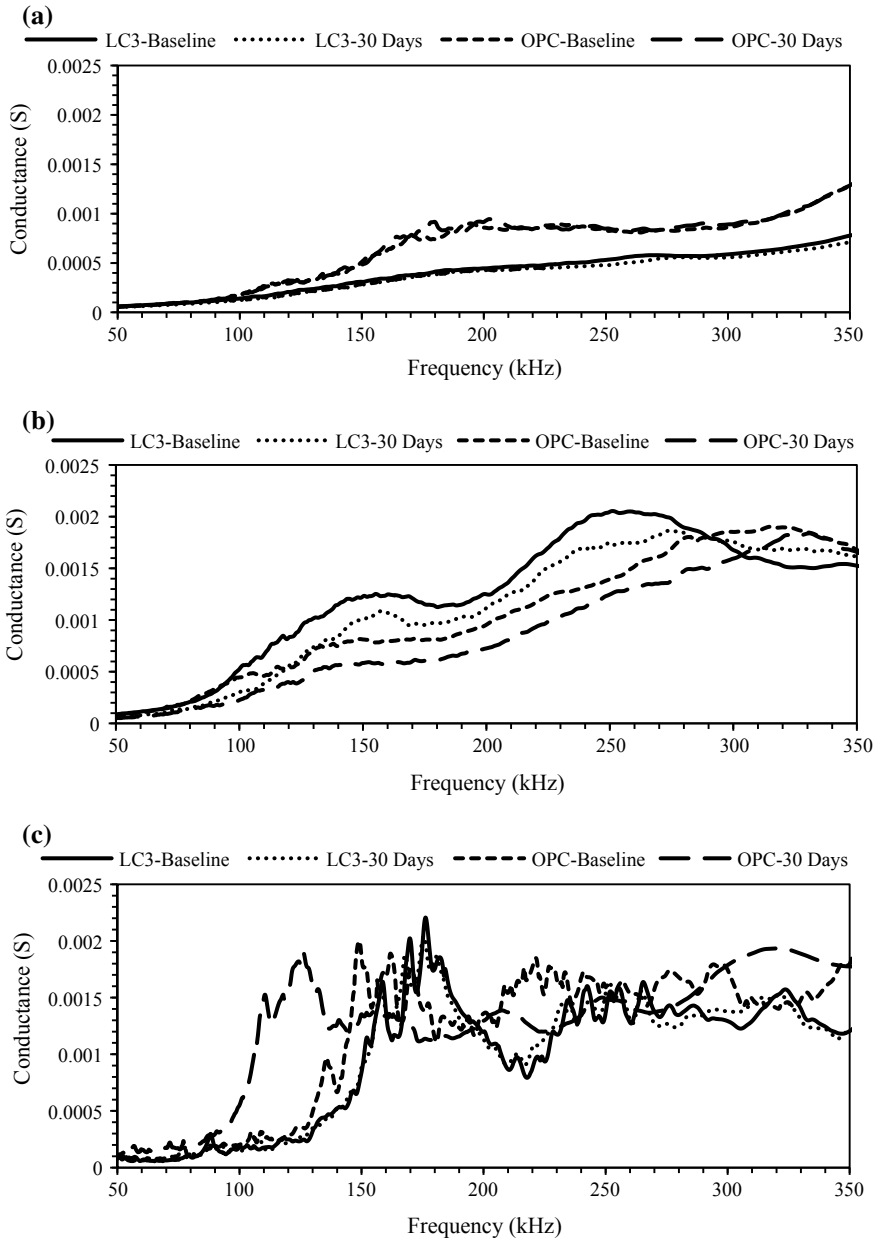
Fig. 3 Variation of baseline conductance signature with exposure of H_2SO_4 attack on OPC and LC^3-50 specimens with different piezo configuration: **a** EPS, **b** SBPS and **c** NBPS

(a) ── LC3-Baseline ⋯⋯ LC3-30 Days ----- OPC-Baseline ── OPC-30 Days

(b) ── LC3-Baseline ⋯⋯ LC3-30 Days ----- OPC-Baseline ── OPC-30 Days

(c) ── OPC-Baseline ⋯⋯ OPC-30 Days ----- LC3-30Days ── LC3-Baseline
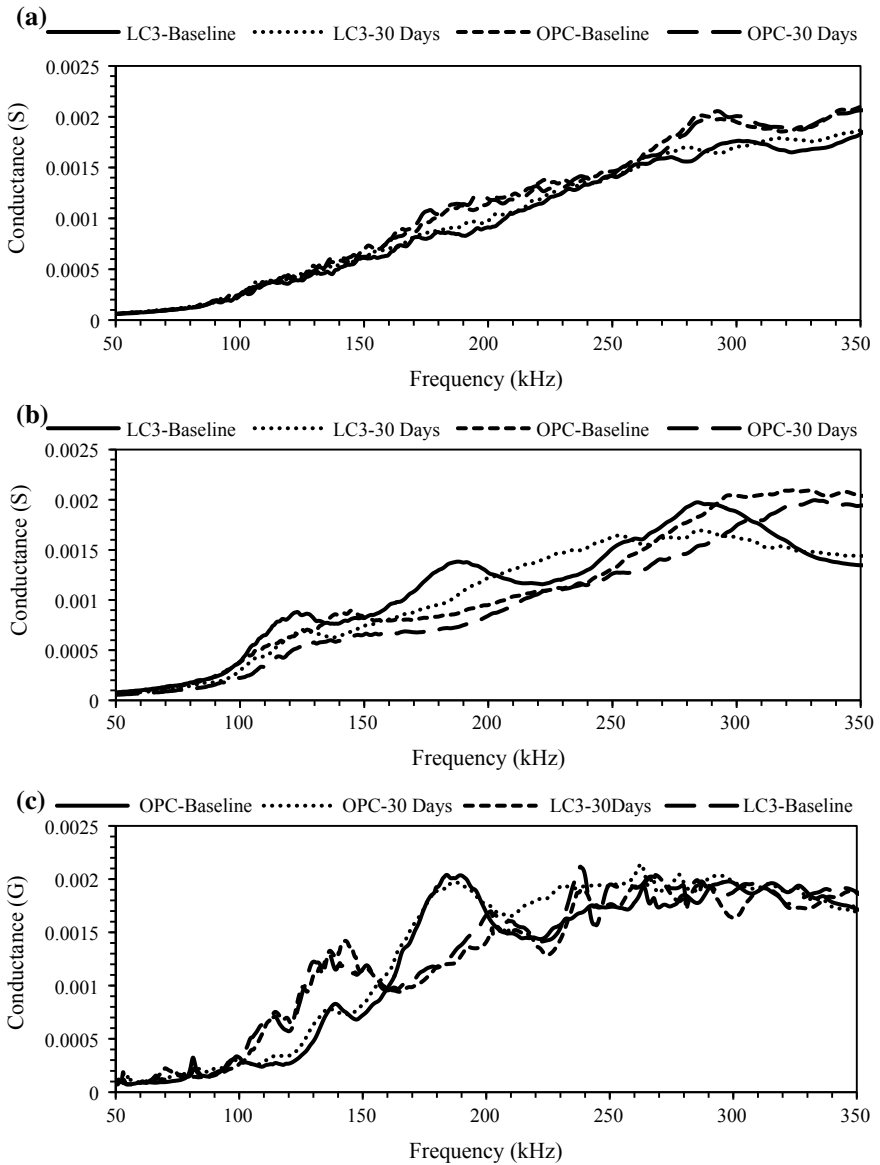
Fig. 4 Variation of baseline conductance signature with exposure of HCl attack on OPC and LC^3-50 specimens with different piezo configuration: **a** EPS, **b** SBPS and **c** NBPS

Table 2 PZT Identified equivalent mass loss in percentage after 30 days with exposure of H_2SO_4

	EPS (%)	SBPS (%)	NBPS (%)
OPC	1.1	0.76	1.9
LC^3-50	9.6	2.4	5.8

Table 3 PZT identified equivalent mass loss in percentage after 30 days with exposure of HCl

	EPS (%)	SBPS (%)	NBPS (%)
OPC	0.41	0.13	0.13
LC^3-50	2.65	0.49	1.14

Table 4 Actual mass loss in percentage after 30 days of exposure

	H_2SO_4 (%)	HCl (%)
OPC	0.064	0.10
LC^3-50	0.119	0.114

ettringite that becomes more than doubles the volume which causes the deterioration in the structure. In the case of the HCl attack, when the chloride reacts with hydrated cement paste, it forms soluble and insoluble salts, in which the soluble salts are leached out whereas, insoluble salts along with amorphous gel remain in the corroded layer which causes deterioration in the structure. When the properties of the structure are changed, the mechanical impedance of the structure will be changed resulting in a deviation of signature. Tables 2 and 3 show the PZT identified equivalent mass loss in percentage of OPC and LC^3-50 concrete due to exposure of H_2SO_4 and H_2SO_4, respectively. It is observed that the identify equivalent mass loss in LC^3-50 is higher than OPC because of higher water–binder ratio and lower binder content in concrete mixes of LC^3-50 than OPC [4]. Actual mass loss is calculated by physical measurement as shown in Table 4, it is found that the LC^3-50 concrete shows a higher reduction in mass than OPC. On comparing the exposure of H_2SO_4 and HCl attack, it is observed that H_2SO_4 attack cause greater degradation than HCl attack.

4 Conclusion

This paper presented a new way to identify the mass loss in LC^3 concrete subjected to the acidic environment using different piezo-configurations. It is observed that all the sensors sense the changes well. The reduction in mass is higher in LC^3 concrete than OPC when subjected to acidic environment and exposure of H_2SO_4 causes greater degradation than HCl exposure.

References

1. Chang, Z.T., Song, X.J., Munn, R., Marosszeky, M.: Using limestone aggregates and different cements for enhancing resistance of concrete to sulphuric acid attack. Cem. Concr. Res. **35**(8), 1486–1494 (2005)
2. Romanova, A., Mahmoodian, M., Chandrasekara, U., Alani, M.A.: Concrete sewer pipe corrosion induced by sulphuric acid environment. Int. J. Civ. Environ. Struct. Constr. Archit. Eng. **9**(4), 467–470 (2015)
3. Siad, H., Mesbah, H.A., Khelafi, H., Kamali-Bernard, S., Mouli, M.: Effect of mineral admixture on resistance to sulphuric and hydrochloric acid attacks in self-compacting concrete. Can. J. Civ. Eng. **37**(3), 441–449 (2010)
4. Dhandapani, Y., Sakthivel, T., Santhanam, M., Gettu, R., Pillai, R.G.: Mechanical properties and durability performance of concretes with limestone calcined clay cement (LC3). Cem. Concr. Res. **107**, 136–151 (2018)
5. Bhalla, S., Soh, C.K.: Structural health monitoring by piezo-impedance transducers. I: Modeling. J. Aerosp. Eng. **17**(4), 154–165 (2004)
6. Talakokula, V., Bhalla, S.: Reinforcement corrosion assessment capability of surface bonded and embedded piezo sensors for reinforced concrete structures. J. Intell. Mater. Syst. Struct. **26**(17), 2304–2313 (2015)
7. Talakokula, V., Bhalla, S., Gupta, A.: Corrosion assessment of reinforced concrete structures based on equivalent structural parameters using electro-mechanical impedance technique. J. Intell. Mater. Syst. Struct. **25**(4), 484–500 (2014)
8. Talakokula, V., Bhalla, S., Gupta, A.: Monitoring early hydration of reinforced concrete structures using structural parameters identified by piezo sensors via electromechanical impedance technique. Mech. Syst. Signal Process. **99**, 129–141 (2018)
9. Hixon, E.L.: In: Harris, C.M. (ed.) Mechanical Impedance Shock and Vibration Handbook, 3rd edn. Mc Graw Hill Book Co, New York (1988)

Influence of Calcined Clay-Limestone Ratio on Properties of Concrete with Limestone Calcined Clay Cement (LC3)

Yuvaraj Dhandapani and Manu Santhanam

Abstract In this study, the compositional robustness of limestone-calcined clay combination as clinker replacement in cement, and its effect on concrete performance was assessed in detail. The ratio of limestone-calcined clay in the LC3 with 55% clinker was varied from 1:1.25, 1:2 and 1:3.5 with increasing limestone dosage from 10 to 20%. Additionally, binary binders with calcined clay at 30% (CC30) and 42% (CC42) replacement were studied for benchmarking and dissociating limestone's contribution to the performance of LC3 binder. Concretes were prepared with 360 kg/m^3 and 0.45 with fly ash-limestone and calcined clay-limestone combinations. Early hydration benefits from limestone ensured that binders with a combination of limestone-calcined clay showed higher compressive strength than the binary substitution of 45% calcined clay binder up to 180 days. The higher reactivity of calcined clays resulted in a tremendous rise in resistivity for all calcined clay binders by early curing duration, i.e. 7 days. Resistivity development confirmed the synergistic impact of limestone-calcined clay combination, which reaffirms the potential ability of the calcined clay to complement the utilization of higher amount of less energy-intensive limestone in the cementitious materials. Additionally, the influence of varying limestone-calcined clay ratio on time-dependent change in chloride resistance by migration test was probed, and the impact of chloride build-up at the steel surface during service life is also discussed.

Keywords Limestone · Calcined clay · Microstructure · Resistivity

1 Introduction

The importance of low-grade calcined clay as an alternative supplementary cementitious material (SCM) is a relevant exploration in the context of reducing carbon footprint in cement production [1, 2]. Furthermore, the direct use of uncalcined powdered forms of limestone along with calcined clay can lead to substantial impact on the phase assemblages and the early age properties [3, 4]. Limestone addition can

Y. Dhandapani (✉) · M. Santhanam
Department of Civil Engineering, IIT Madras, Chennai, India

reduce the burden on the clinker and bring down greenhouse emissions associated with cement production. The contribution of limestone to the evolving microstructure can be limited primarily due to the lower solubility of calcite phases. The co-substitution of low-grade calcined clay with fine limestone was found to produce strength equivalent to a plain Portland cement [5]. The durability performance of these composite cements with limestone-SCM composition is affected by the ability of the limestone to compensate for the dilution and produce a conceivably synergistic interaction with the aluminosilicate based SCM [6]. Aluminosilicates such as fly ashes, slags and calcined clay are the widely recognized alternatives that can be utilized as binder component [7]. Limestone addition can produce a varying influence on concrete properties depending on the characteristics of SCM used for co-substitution. Several key characteristics such as reactivity, the composition of reactive content present in SCMs, particle size and proportioning of SCM can govern the properties of limestone-SCM composite cement.

This study reports experimental characterization on hydration and hardening properties on cement paste with binary and ternary mixes involving limestone. The influence of calcined clay-limestone ratio on strength development and durability performance was also investigated.

2 Research Design

An ordinary Portland cement (OPC) was used as a control mix. Limestone and calcined clay sourced from Bhuj, Gujarat (with 50–60% kaolinite content) and Ultratech plant, Ariyalur (with CaO content of 42%) were used to produce the ternary binder with a combination of OPC, limestone, calcined clay and gypsum as given in Table 1.

Table 1 Binder composition used in the study

SCM type	Mix ID	OPC	SCM	Limestone*	Gypsum
OPC	OPC	100	–	–	–
Class F	FAF30	66	30	3.5	0.5
	FAF42	54.5	42	3	0.5
	FAFL10	54.5	34	11	0.5
	FAFL15	54.5	30	15	0.5
	FAFL20	54.5	25	20	0.5
Calcined clay	CC30	65.0	30	3.5	1.5
	CC42	53.5	42	3	1.5
	CCL10	53.5	34	11	1.5
	CCL15	53.5	30	15	1.5
	CCL20	53.5	25	20	1.5

*Limestone content includes calcite content in OPC + limestone amount added

For comparison, a similar combination was prepared with fly ash and limestone. In all concretes, the binder content and w/b were maintained at 360 kg/m³ and 0.45, respectively.

Concretes were prepared with crushed granite as coarse aggregate with a maximum size of 20 mm and well-graded river sand as fine aggregate. The coarse to fine aggregate ratio was fixed at 60:40 by weight and a polycarboxylic ether (PCE) based superplasticizer was used to obtain a slump of 80–120 mm.

3   Results and Discussion

3.1   Hydration, Hardening and Compressive Strength

Hydration heat and setting characteristics of the cement paste (w/b: 0.4) for all binder compositions are presented in Fig. 1. The cumulative heat release in these binder systems shows the difference between binary and ternary combinations. An increase in the amount of SCM, i.e. fly ash or calcined clay reduces the total heat release by 7 days. The reduction was significantly higher for increasing dosage of fly ash than calcined clay as shown in Fig. 1a, b. The early interaction and consequential acceleration in the hydration process contribute to the heat release with increasing
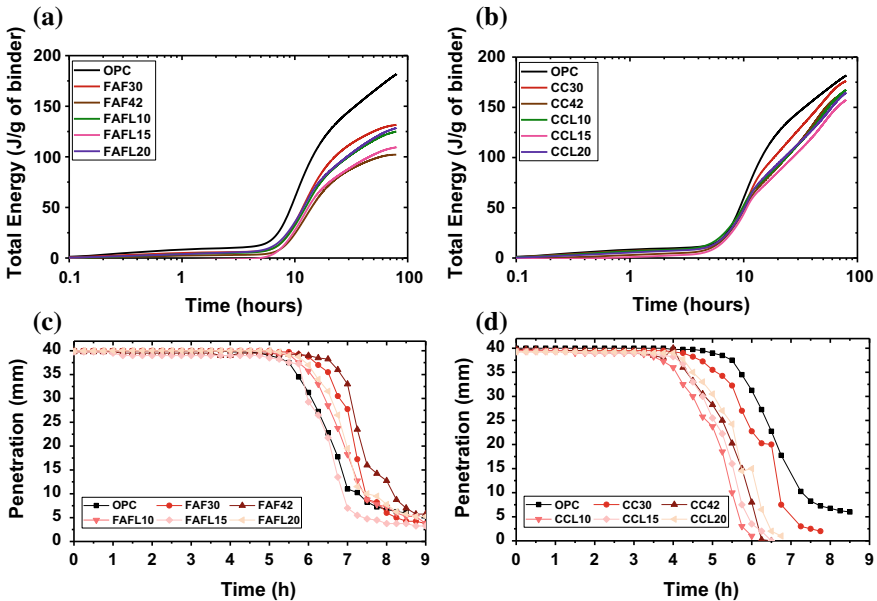
Fig. 1 Hydration heat of fly ash (**a**) and calcined clay (**b**) mixes and setting characteristics of fly ash (**c**) and calcined clay (**d**) mixes

dosage of calcined clay as opposed to fly ash. Limestone-fly ash combinations showed higher heat release than FAF42. This shows the positive influence of limestone on early hydration characteristics. The change in heat release was not significant between CC30 and CC42, and only a marginal variation was observed in the cumulative heat release due to limestone addition in calcined clay binders.

Setting characteristics of all binder compositions with fly ash and calcined clay are presented in Fig. 1c, d, respectively. The penetration resistance reduces with increasing dosage of fly ash (see FAF30 and FAF42 in Fig. 1c). The acceleration in hydration characteristics due to limestone addition was able to shift the setting characteristics of fly ash binders close to plain Portland cement. Similar results were previously reported for high-volume fly ash concretes with a minor dosage of limestone in [8]. Unlike fly ash mixes, an increase in calcined clay dosage from CC30 to CC42 resulted in early hardening, and the Vicat resistance was further accelerated in the presence of limestone. The combined early contribution of calcined clay and limestone collectively accelerates the setting characteristics of calcined clay-limestone binders. In fly ash mixes, limestone addition was found to be beneficial in reducing delay in setting characteristics caused by a higher dosage of fly ash addition as a cement substitute.

The compressive strength development (up to 180 days) in concretes reaffirmed the influence of limestone on the early age properties (see Fig. 2). This can be identified from the comparable strength development of ternary mixes with limestone with binary mixes even at the expense of a more reactive component such as clinker and SCM. Compressive strengths at 7 days and 28 days were marginally higher for ternary mixes than binary mixes with 42% SCMs. The lack of strength development from 28 to 90 days in CC42 can be due to lack of portlandite and limited progressive hydration due to the high dosage of calcined clay.
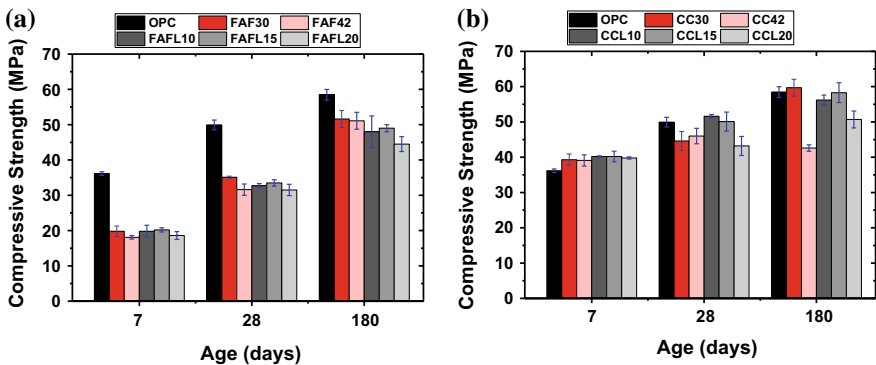
Fig. 2 Comparison of compressive strength for binary and ternary concretes with **a** fly ash and **b** calcined clay

3.2 Chloride Resistance

Chloride resistance of concretes with all binder compositions was studied using non-steady-state migration experiment at 28, 90 and 180 days as per NT Build 492 [9]. The results confirm that fly ash-limestone mixes showed a consistent increase in chloride migration coefficient with limestone dosage, as seen in Fig. 3. This reduction in chloride resistance was evident by 28 days due to the impact of dilution and a lack of dominant interaction between fly ash and limestone. Also, the low reactivity state of fly ash particles was not able to subsidize for the reduction in the amount of hydrates due to limestone addition. All calcined clay concretes attains higher resistance to chloride ingress despite the dosage of limestone. This indicates that the driving factor for such performance characteristics can be due to the early interaction of calcined clay binders to form a compact microstructure with the LD (low density) CASH produced in such systems. This phenomenon of LD CASH in calcined clay binder is discussed in [10]. The early interaction was captured by the significant rise in resistivity for all calcined clay binders. Notably, the resistivity value of CCL10 and CCL15 were higher compared to CC30 and CC42 due to benefit from the complementary interaction of calcined clay-limestone.

The time dependency parameter, also known as an ageing coefficient, can be obtained as the slope of the chloride resistance parameter and time on a log–log plot. For this purpose, the chloride migration rate was measured at 28, 90 and 180 days. Figure 4 shows the ageing coefficient for all binary and ternary mixes of fly ash and calcined clay. The delayed contribution of fly ash to pore structure and chloride resistance is well captured with the higher ageing coefficient for all concretes with fly ash. The ageing coefficient was lower for all concretes with calcined clay due to the rapid development of microstructure with calcined clay binders [3]. This study demonstrates that calcined clay binders attain lower chloride ingress rate at an early
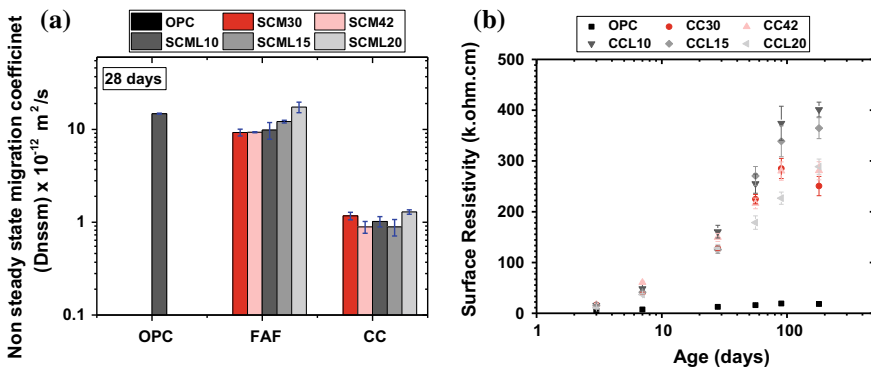
Fig. 3 **a** Chloride resistance of concretes at 28 days. **b** Resistivity development in binary and ternary binders with calcined clay

Fig. 4 Range of ageing
coefficient for concretes with
fly ash and calcined clay
binders
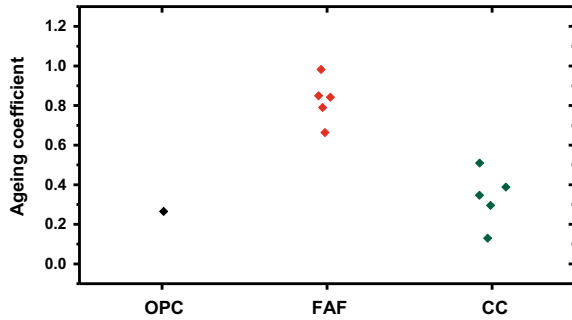
age. However, the change in the transport parameter over time was lower compared
to fly ash concretes.

The combined effect of the initial difference in the chloride transport parameter
and time-dependent change captured in the form of the ageing coefficient on the
service life can be estimated by calculating chloride content at the surface of steel
based on error function solution to Fick's second law of diffusion as given Eq. (1).

$$C(x = X, t) = C_0 + (C_\mathrm{s} - C_0) \cdot \left[1 - \mathrm{erf}\left(\frac{X}{2\sqrt{D_{\mathrm{app_{Temp}}} \cdot \left(\frac{t_{\mathrm{ref}}}{t}\right)^a \cdot t}} \right) \right] \quad (1)$$

where C_s is the surface chloride concentration, C_x is the chloride content at the
depth X (cover depth of 60 mm used in this case), C_0 is the initial chloride content
in concrete and t_{ref} is the reference time. D_{app} is the apparent chloride diffusion
coefficient in m^2/s and t is the exposure time.

To estimate the chloride content at the surface of steel over the service life, C_s was
considered to rise linearly to represent a slow deposition of chlorides on the concrete
surface over 15 years to reach a maximum chloride at the surface of 1% by weight
of concrete (bwoc). The D_{app} was considered as time-dependent and temperature-
dependent. A temperature variation from 30 to 38 °C (annual temperature cycle
similar to Chennai, India) was considered and corresponding suitable change in
chloride diffusion rate was computed at every time step (say one day) using Arrhenius
function as suggested in FIB-34 [11]. Also, the ageing coefficient was used to account
for the time-dependent reduction in the chloride resistance for 10 years. Using Eq.
(1), the chloride content at the surface of steel ($X = 60$ mm was used in this case) was
computed. Figure 5 shows the amount of chloride accumulated at the surface of the
steel in binary and ternary binders with fly ash (Fig. 5a) and calcined clay (Fig. 5b)
considering the combined effect of chloride resistance and ageing coefficient.

In OPC concrete, the higher chloride ingress rate results in a steady rise in chloride
content at the steel surface in a short duration. Beyond a certain duration, the chloride
build rate slows down (see Fig. 5, OPC curve) as chloride content reaches close to
the concentration at the exposure surface (1% as considered for this computation).
As concentration variation narrows down between steel surface and concrete surface,
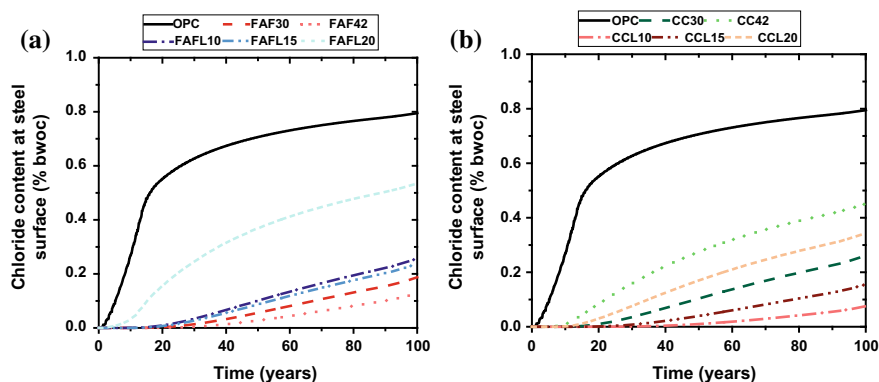
Fig. 5 Development of chloride content at the steel surface over the exposure time for **a** fly ash concretes and **b** calcined clay concretes

the diffusion flux, which leads to the continuous rise in chloride content at the surface of the steel, is reduced. This results in faster chloride build-up initially which slows down over the period of time.

In fly ash concretes, the binary mixes, FAF30 and FAF42, have lower chloride build-up rate than ternary mixes. FAFL20 has reduced the resistance to chloride build-up at the steel surface despite similar ageing coefficient. This is because of a higher value in the chloride transport parameter by 28 days. In calcined clay concretes, the ternary binders with 10 and 15% limestone had lower chloride build-up at the steel surface during the exposure time compared to the binary mixes, i.e. CC30 and CC42. This further reiterates the beneficial influence of limestone co-substitution with calcined clay on the durability performance of concrete systems.

4 Conclusion

The study put forward the compositional robustness of the calcined clay-limestone in producing durable concrete. The influences of calcined clay-limestone ratio on hydration setting and strength development showed the impact of minor variation of the dosage limestone content. The positive role of limestone on heat release and setting due to acceleration of hydration process with calcined clay and fly ash binder was evident.

The alteration in strength development due to limestone addition was limited and a major influence of the choice of SCM (i.e. calcined clay or fly ash) on the strength development potential can also be noted. The calcined clay-limestone binders could accommodate up to 15% limestone and produce comparable strength development to OPC at all ages.

The variations in chloride resistance were limited for calcined clay binders irrespective of limestone dosage. In fly ash-limestone combination, the 28 days transport

properties were consistently reduced with the addition of limestone powder. The combined influence of both initial transport resistance and the higher ageing coefficient can be rationalized a slower chloride build-up at steel surface for fly ash and calcined clay concretes compared to OPC.

References

1. Schneider, M., Romer, M., Tschudin, M., Bolio, H.: Sustainable cement production—present and future. Cem. Concr. Res. **41**, 642–650 (2011)
2. Scrivener, K.L., John, V.M., Gartner, E.M.: Eco-efficient cements: potential, economically viable solutions for a low-CO_2, cement-based materials industry. United Nations Environ Program, Paris (2016)
3. Dhandapani, Y., Santhanam, M.: Assessment of pore structure evolution in the limestone calcined clay cementitious system and its implications for performance. Cem. Concr. Compos. **84**, 36–47 (2017)
4. Krishnan, S., Bishnoi, S.: Understanding the hydration of dolomite in cementitious systems with reactive aluminosilicates such as calcined clay. Cem. Concr. Res. **108**, 116–128 (2018)
5. Dhandapani, Y., Sakthivel, T., Santhanam, M., et al.: Mechanical properties and durability performance of concretes with limestone calcined clay cement (LC3). Cem. Concr. Res. **107**, 136–151 (2018)
6. Avet, F., Scrivener, K.: Investigation of the calcined kaolinite content on the hydration of limestone calcined clay cement (LC3). Cem. Concr. Res. **107**, 124–135 (2018)
7. Li, X., Snellings, R., Antoni, M., et al.: RILEM TC 267-TRM report: performance of reactivity tests for supplementary cementitious materials. Mater. Struct. **51**, 1–17 (2018)
8. Bentz, D.P., Sato, T., de la Varga, I., Weiss, W.J.: Fine limestone additions to regulate setting in high volume fly ash mixtures. Cem. Concr. Compos. **34**, 11–17 (2012)
9. NT Build 492: Concrete, mortar and cement-based repair materials: chloride migration coefficient from non-steady-state migration experiments. NordTest 1–8 (1999)
10. Dhandapani, Y., Santhanam, M. (2019) Characterisation of microstructure in limestone calcined clay cementitious systems. In: RILEM Spring Convention and Sustainable Materials, Systems and Structures Conference, Rovinj, Croatia, 18–22 Mar 2019
11. International Federation for Structural Concrete (2006) MC-SLD:2006. Model Code for Service Life Design

Volumetric Deformations at Early Age on Portland Cement Pastes with the Addition of Illitic Calcined Clay

Agustín Rossetti, Graciela Giaccio and Edgardo Fabián Irassar

Abstract With the aim of reducing the environmental impact associated with cement production, during the last decade, different percentages of clinkers have been replaced in cement by supplementary cementitious materials (SCMs). When new SCMs are incorporated in concrete, it is necessary to evaluate, not only the mechanical properties (as strength and stiffness) and the durability but also the deformations that can generate cracking and decrease the service life of the structures. This paper is focused on the study of volumetric changes at the early ages of pastes made with blended cements with the addition of illitic calcined clays from the Buenos Aires province, Argentina. The objective of this work is to present preliminary studies on the effect of illitic calcined clays on the autogenous and chemical shrinkage of pastes. The studies were made on pastes (water/cementitious material ratio equal to 0.275) using a Portland cement type II/A-L, with the incorporation of different percentages (10%, 20% and 30%) of illitic calcined clays. A device for direct deformation measurement was used to register linear dimensional changes; the general guidelines of ASTM C 1608 were applied for the determination of chemical and autogenous shrinkage. The volumetric changes measured with direct device are the sum of the chemical and autogenous shrinkage accompanied with the expansion due to the heat released during hydration. It was found that pastes incorporating calcined clays had early deformations similar to or lower than reference paste without clay.

Keywords Illitic calcined clays · Paste · Autogenous and chemical shrinkage

A. Rossetti · G. Giaccio
LEMIT, CIC, Av 52 e/ 121y122, B1900AYB La Plata, Provincia de Buenos Aires, Argentina

E. F. Irassar (✉)
Facultad de Ingeniería, CIFICEN (UNCPBA-CICPBA-CONICET), B7400JWI Olavarría, Argentina
e-mail: firassar@fio.unicen.edu.ar

1 Introduction

In the last years, in the cement industry, the tendency to use cementitious supplementary materials (SCMs) has grown. The most commonly used being blast furnace slag, calcareous filler and natural pozzolans. Its use is justified by economic and environmental issues. Studies have shown that the projections of cement consumption in the coming years will be very high and, on the other hand, the production of these SCMs will not be enough to cover the demands of the world market, mainly in the developing countries. In this circumstance, calcined clays with an adequate content of aluminum in their structure to react with the cement-like kaolinite, illite and montmorillonite appear as a promissory alternative. There are several studies on kaolinite calcined clays and their performance in concrete, but there are few references to illitic calcined clays.

Illitic clays are one of the most abundant clay minerals in the earth's crust. They come from the alteration of feldspars and micas in rocks due to weathering processes. The illitic clays acquire pozzolanic properties when they are thermally activated at 950 °C [1] causing dehydroxylation and the collapse of their structure to form an amorphous aluminosilicate compound [2]. Knowing the pozzolanic capacity of the addition, to prevent cracking, other technological aspects of the fine materials such as the volumetric stability in paste, mortar and concrete must be studied.

Autogenous shrinkage refers to an apparent volume or length reduction of hydrated cement under isothermal conditions and without interchange of water to the medium [3]. This phenomenon is caused by the continuous hydration of the cement after the formation of a resistant initial structure and can be explained by the theory of capillary pressure that is generated in pastes of low w/c ratio [4].

Generally, the autogenous shrinkage manifests itself at an early age within the first 24 h after the paste is mixed, but the matrix of the paste is more prone to cracking during the first 12 h [5]. During this period, the tensile strength of the paste is too low to resist the stresses caused by the volumetric deformation. The addition of supplementary cementitious materials modifies these behaviors. Mineral additions tend to produce densification and refinement of the internal structure of pores and then mechanical characteristics, durables and volumetric changes are modified [6]. To study the autogenous shrinkage, it can be measured as volumetric or length changes. Beyond the selected method, during the measuring of deformations, generally what is measured is a combination of autogenous, chemical, drying shrinkage and volumetric deformations by thermal processes that must be able to be identified separately [7].

Chemical shrinkage refers to volume changes the at early ages of hydration, which occur when the hydrated cement compounds are formed, as they have smaller volumes than the original compounds (cement and water) before being combined [8]. After the initial structure of the paste is formed during hydration, the continuous hydration generates the formation of voids in the matrix of the solid skeleton. At this point, the value of the autogenous shrinkage is lesser than the chemical, since the first one measures the apparent reduction of the volume, while the accumulated value of the vacuum is considered to be the chemistry. In the plastic state, the terms

"chemical shrinkage" and "autogenous shrinkage" could be used interchangeably, but studies by Holt [9] have shown that autogenous shrinkage and chemistry are not equivalent in concretes with w/c ratio less than 0.30.

The objective of this work is to analyze the influence of illitic calcined clays incorporation on the autogenous and chemical shrinkage of pastes at an early age after casting. The studies were done on pastes (w/c = 0.275) using a Portland cement type II/A-L, with the incorporation of different percentages (10%, 20% and 30%) of an illitic calcined clay. A device for direct deformation measurement was implemented to register linear dimensional changes and the general guidelines of ASTM C 1608 were applied for the determination of chemical and autogenous shrinkage.

2　Materials and Methods

2.1　Materials and Mixtures

Portland cement type II/A-L 42.5 R (UNE-EN-197) with 10% of calcareous filler and an illitic calcined clay from a quarry of Olavarría (Argentina) identified as ICC was used. The clay stones were reduced to 5 mm particles and calcined in an oven. The temperature increased at 10.5 °C/min up to 950 °C and the maximum temperature was maintained for 90 min and then samples were cooled slowly in the oven according to previous test [1]. Finally, calcined clays were ground in a laboratory ball mill until obtaining 90% of the particles smaller than 45 μm. XRD analysis reveals low-intensity peaks of dehydroxylated illite and the associated minerals are quartz, hematite, oligoclase and spinel. Chemical composition of the cement and the clay determinate by XRF are reported in Table 1. The calcined clay meets the chemical requirements for Class N pozzolan (ASTM C 618): S + A + F > 70%; SO_3 < 4% and LOI < 10%. For this illitic calcined clay, the Frattini test was positive after 14 days, and also, the compressive strength development was reported in previous paper [1].

The physical characteristic of the materials, density (ASTM C 188), retained on 75 and 45 μm sieves (ASTM D 422 and C 618), the Blaine specific surface (ASTM C 204) and the particle size distribution (PSD) determined using the laser granulometer (Malvern Mastersizer 2000) are reported in Table 2.

This study was performed on pastes with 0.275 water/cement + ICC ratio; the pastes incorporated 0, 10, 20 and 30% of calcined clay as cement replacement (percentages by weight) and they are identified as PC, ICC10, ICC20 and ICC30, respectively.

Table 1 Chemical composition and loss on ignition of the cement and the ICC (%)

Material	CaO	SiO$_2$	Al$_2$O$_3$	Fe$_2$O	MgO	SO$_3$	K$_2$O	Na$_2$O	TiO$_2$	P$_2$O$_5$	LOI
Cement	60.92	16.58	4.21	1.80	2.16	1.77	0.67	0.28	0.29	0.19	2.05
ICC	1.13	63.43	18.32	7.89	2.71	0.04	4.29	1.52	0.90	0.06	0.19

Table 2 Physical characteristics of ICC and cement

Property/material		ICC	Cement
Density		2.65	3.05
Retained on sieve, %	75 μm	4.02	–
	45 μm	5.68	–
Particle size distribution	d10, μm	1.29	2.39
	d50, μm	7.34	15.7
	d90, μm	36.95	48.0
Specific surface Blaine, m²/kg		724	
Specific surface BET, m²/g			1.88

2.2 Direct Linear Deformations

Linear deformations were measured using a device that automatically recorded length changes of the pastes after casting ($t = 0$). The device used (Fig. 1) consists of steel mold of $40 \times 40 \times 160$ mm (Fig. 1a) with a mobile end in contact with a LVDT (Fig. 1b) that measures the longitudinal deformation.

This device can measure the longitudinal deformations in both directions, as a screw of ~4 cm long was incorporated into the mobile part so the paste can drag the head. To avoid friction and adhesion of the paste with the faces of the mold, this was covered with a layer of Teflon and oil. After filling and compaction, the test paste was covered with a waterproof film and a thermocouple was introduced to measure the temperature inside the paste (Fig. 1c). The device was placed in a container with water in the base and was covered with a lid to control the temperature (22 °C) and humidity (>95%) (Fig. 1d). During the test, data acquisition (LVDT and thermocouple) occurred every 2 min until 48–72 h.
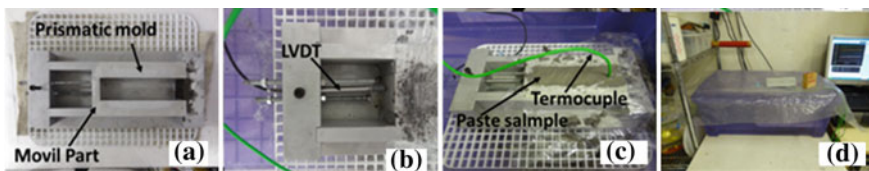
Fig. 1 **a** Device used to measure longitudinal deformations; **b** LVDT; **c** molded paste with thermocouple ready to measure internal temperature; **d** device in the container ready to start the test

2.3 Volumetric Determination of Chemical and Autogenous Shrinkage

Chemical shrinkage was determined based on the methodology proposed by ASTM C 1608; it was placed approximately 100 g of paste (w/cm = 0.275) in a glass cylindrical container, then it was carefully filled with water, and finally, a plug with a capillary tube to ensure a tight seal was placed, as shown in Fig. 2a. Then the container was introduced in isothermal medium, and in half-hour intervals, measurements of the water level in the capillary tube were made.

The autogenous shrinkage was studied with the same methodology described in the previous paragraph but with the main difference that the paste was isolated to avoid water interchange and moisture variations (condition of the autogenous shrinkage). To isolate the paste, it was placed and consolidated inside a latex membrane, and then, it was introduced in the glass container (Fig. 2b) ensuring that no air bubbles remain inside. Then the plug and graduated tube were placed and proceed to measure in the same way as the chemical shrinkage. In order to make continuous measurements, webcams programmed to monitor the whole experience filming the capillary tubes were implemented (Fig. 2c).

In addition, with these pastes, rings (2 cm thick) were cast to determine the times of cracking using the method of restrained contraction (Fig. 3). After 24 h of casting the pastes, the external part of the mold was removed and the rings were kept in laboratory environment (temperature 20 °C and relative humidity of 70%). The idea of this study was to determine qualitatively if the addition of the calcined clays increases the contraction which would mean that the fissures occur earlier.
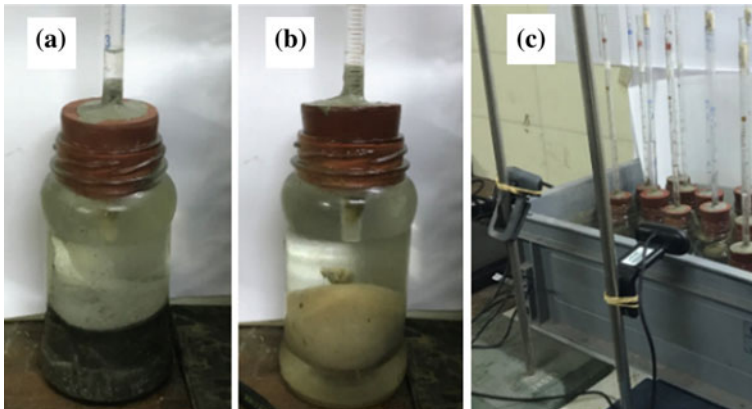
Fig. 2 **a** Chemical shrinkage; **b** autogenous shrinkage; **c** monitoring cameras

Fig. 3 Determination of restrained shrinkage in paste rings with the addition of illitic calcined clay

3 Results and Discussion

3.1 Longitudinal Deformations

The results of Direct Linear Deformation Experiment were analyzed taking into account the results from Holt thesis [10]. According to Holt, the curve of the longitudinal variation at early age is the sum of several processes: reabsorption of the bleeding water, growth of the ettringite crystals, growth of the portlandite crystals, topochemical reaction produced by the hydration of the C_3S, thermal expansion product of the exothermic reactions of the hydration of the cement, among others.

Figure 4 shows the results of the longitudinal deformations and the temperature for the reference pastes made only with cement (PC) and the pastes with the incorporation of the different percentages of illitic calcined clays (ICC10, ICC20, ICC30).

Analyzing the curve corresponding deformation to the PC control: from the beginning of the measurement (time 0) and up to ~90 min, shrinkage is observed reaching a maximum of 320 µm/m as a result of the chemical contraction while the temperature decreased slightly. After 90 min, both curves (deformation and temperature) present an inflection point that occurs in correspondence with the initial setting time, the rate of hydration heat increases and the solid skeleton of high connectivity develops where the water moves freely through the interior of the paste. This process generates an expansion of ~170 µm/m until 4 h (final setting) and it is attributed to the heat of hydration. Between 4 and 6 h after the formation of the solid skeleton by the setting process, capillary pressures begin because the continuous hydration makes a structure of pores that inhibit the free movement of water in the hardened paste.

From this point, a competition between capillary pressure and temperature starts, winning pressure and making small shrinkage until it stabilizes. Between 6 and 10 h, there is volumetric and thermal stability and the paste reaches the maximum temperature (~10 h). Then the curve deformation shows shrinkage lower than 60 µm/m attributed to the deceleration of the heat released by hydration and begins the cooling of the paste. Between 14 and 24 h, an expansion lower than 90 µm/m is developed, although the thermal curve indicates a continuous cooling of the paste until it stabilizes at room temperature for 36 h. In other words, the expansion process that takes
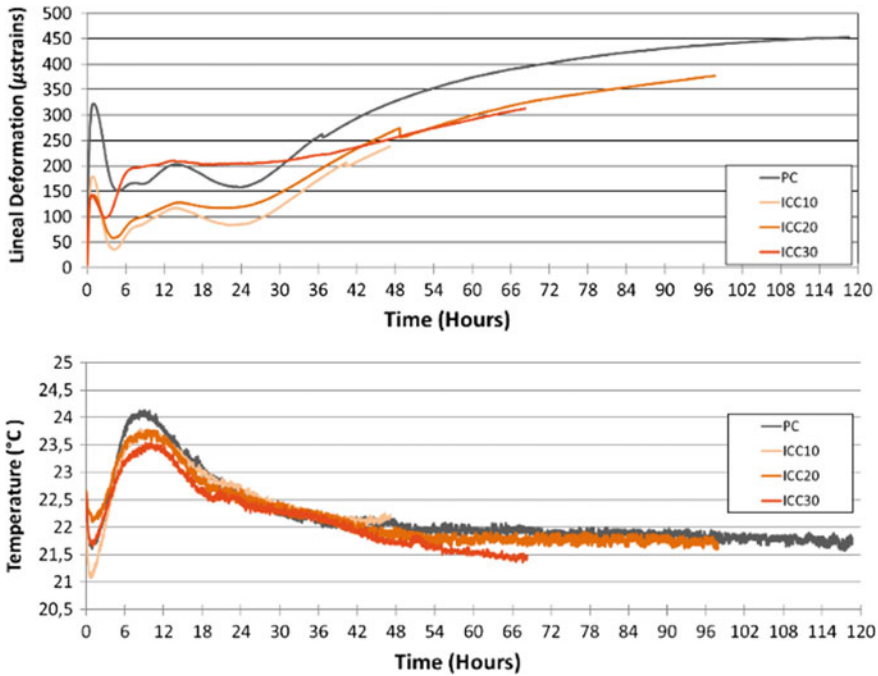
Fig. 4 Linear deformations and temperature variation measured in Portland cement paste with illitic calcined clays

place between 10 and 24 is independent of temperature. After 24 h, a combination of thermal, chemical and autogenous shrinkage is developed. After 36 h, the temperature stabilizes and only the autogenous and chemical shrinkage develops, reaching 300 μm/m at 120 h.

Analyzing the deformation curves corresponding to the cement with the addition of illitic calcined clays: at the beginning, the initial shrinkage is less than that one measured for the control cement. Then at the start of the setting time (90 min), the solid skeleton formation begins producing an expansion by the reabsorption of the free water and thermal expansion for the ICC10 and ICC20 pastes. This expansion is lower for the ICC30. The shrinkage by capillary pressure appears ~at 4 h and it is compensated by the thermal expansion until the system stabilizes at 14 h. At this time, there is no variation in volume due to the balance between the chemical–autogenous shrinkage and the cooling. From 14 to ~24 h, ICC10 and ICC20 samples have a slight expansion, where is more pronounced in the ICC10 which can be attributed to a lower effective ratio of water to cement (effective w/c = 0.34) making a high confined space where the free water wants to move. The paste ICC30 shows higher shrinkage between 4 and 7 h, and after that, the shrinkage remains constant until 36 h where the shrinkage increases (autogenous and chemical) without thermal influence

since the paste has reached equilibrium with the environment. At 48 h, final shrinkage of the pastes is less than that corresponding to the reference paste with a similar value (250 μm/m) for the three replacement percentages studied.

3.2 Volumetric Deformations. Chemical and Autogenous Shrinkage

Figure 5 shows the results of the chemical (Q) and autogenous (A) shrinkage measured following the guidelines of ASTM C 1608 of pastes PC, 10ICC, 20ICC and 30ICC with 0, 10, 20 and 30% of clay replacement, respectively. It can be seen that for all calcined clay replacements, both autogenous and chemical shrinkage are slightly lower than for the control paste. The differences in volume changes are not significant and there was not a clear effect produced by the clay content. Analyzing the chemical shrinkage curve at the age of 60 h, the values are practically the same reaching 3 cm^3/100 g. It is important to highlight that addition of different percentages of calcined clays did not increase the chemical or autogenous shrinkage.

During the restricted shrinkage ring test, it was possible to observe that the cracking occurred between 20 and 48 h after casting. It should be noted that the control paste PC was the first to crack, and as the percentage of addition increased the cracking took place in later time, this behavior is consistent with the deformations measured using the other methods described above.
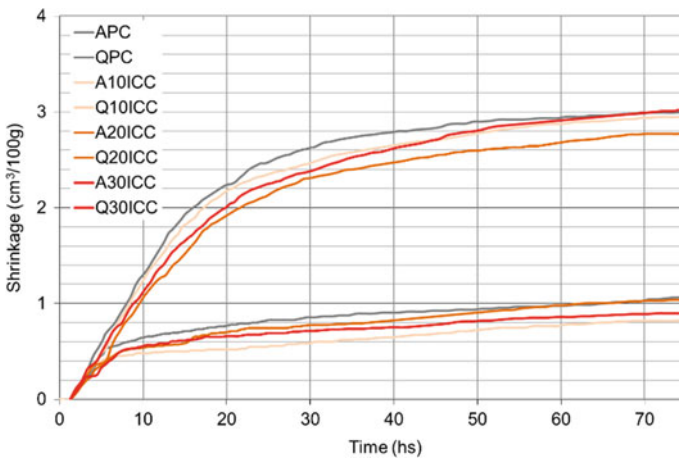
Fig. 5 Chemical and autogenous shrinkage curves with the addition of 10, 20 and 30% of illicit calcined clay according to ASTM C 1608

4   Conclusions

In the present work, first measurements of deformations were made in Portland cement pastes with the incorporation of different percentages of illitic calcined clays using a direct measurement method (linear deformations) and a modification of the ASTM C 1608 standard (volumetric deformations). The main conclusions are:

- The volumetric changes determined by an experimental device of direct measurement provide information on the different states of the paste as well as the thermal gradients in cements mixed with calcined clays.
- The deformation curve (direct measurement method) corresponding to the control cement presents a higher number of inflection points than those corresponding to the different percentages of illitic calcined clays pastes. The first explanation to this is that as the additional content grows, the effective water–cement ratio increases and this causes a less confined and less restrictive internal system.
- For all replacements of illicit calcined clay, volumetric deformations, both in terms of autogenous and chemical shrinkage, yield final values that are less than the control paste. This situation is also reflected when the pastes are analyzed with the direct measurement method.

References

1. Lemma, R., Irassar, E.F., Rahhal, V.: Calcined illitic clays as Portland cement replacements. In: Scrivener, K., Favier, A. (eds.) Calcined Clays for Sustainable Concrete, pp. 269–276 (2015). https://doi.org/10.1007/978-94-017-9939-3_33
2. Ramachandran, V.S. (ed.): Concrete Admixtures Handbook: Properties, Science and Technology, 2nd edn. Noyer Publication, United States of America
3. Williams, A., Markandeya, A., Stetsko, Y., Riding, K., Zayed, A.: Cracking potential and temperature sensitivity of metakaolin concrete. Constr. Build. Mater. **120**, 172–180 (2016)
4. Lura, P., Jensen, O.M., van Breugel, K.: Autogenous shrinkage in highperformance cement paste: an evaluation of basic mechanisms. Cem. Concr. Res. **33**(2), 223–232 (2003)
5. Van Breugel, K., Van Tuan, N.: Autogenous Shrinkage of HPC and Ways to Mitigate It. Trans Tech Publications, Switzerland (2015)
6. Recommendation, R.D., De La Rilem, P.D.R.: Creep and shrinkage prediction model for analysis and design of concrete structures-model B3. Mater. Struct. **28**, 357–365 (1995)
7. Bazant, Z., Chern, J.: Concrete creep at variable humidity: constitutive law and mechanism. Mater. Struct. **18**(1), 1 (1985)
8. Bullard, J.W., Jennings, H.M., Livingston, R.A., Nonat, A., Scherer, G.W., Schweitzer, J.S., Scrivener, K.L., Thomas, J.J.: Mechanisms of cement hydration. Cem. Concr. Res. **41** (2011)
9. Holt, E.: Contribution of mixture design to chemical and autogenous shrinkage of concrete at early ages. Cem. Concr. Res. **35**(3), 464–472 (2005)
10. Holt, E.: Early age autogenous shrinkage of concrete. PhD Thesis, University of Washington, VTT Technical Research Centre of Finland, 2001. (ISBN 951-38-6250-X)

Anomalous Early Increase in Concrete Resistivity with Calcined Clay Binders

Hareesh Muni, Yuvaraj Dhandapani, K. Vignesh and Manu Santhanam

Abstract The present study investigates the effect of concrete mixture proportioning on two major performance parameters which include compressive strength and surface resistivity for limestone calcined clay cement (LC3) and FA30 (70% OPC + 30% Class F fly ash) binders. The findings show that there was a significant early strength development of about 38–88% of the 28th-day strength by 3 days in the range of concrete studied, despite only 50% clinker in LC3 binder. In comparison, FA30 with 70% clinker had about 30–61% of 28th-day strength by 3 days. All LC3 concretes had higher resistivity than FA30 counterparts indicating higher resistance to ionic transport in the binding phase. By 90 days of curing, the surface resistivity values varied between 50–200 and 10–80 kΩ cm for LC3 and FA30 concretes, respectively. Furthermore, a dramatic rise in surface resistivity was seen by 7 days for LC3 concretes conforming to the early impact of calcined clay on the concrete physical structure. In the case of fly ash concretes, resistivity measurements showed a major increase only after 28 days. The pore structure refinement was found to be the significant factor controlling the early development of durability indices in LC3 concretes.

Keywords Limestone · Calcined clay · Surface resistivity · Ionic resistance · Microstructure

1   Introduction

Limestone calcined clay cement (LC3) is a ternary blended binder made with a combination of Portland cement and a mixture of limestone and calcined clay (denoted as LC2 hereafter) [1, 2]. LC2 is an alternative supplementary cementitious material (SCM) composed of the mixture of limestone, calcined clay and gypsum which can be blended with OPC to produce LC3 binder. LC2 combines two widely available materials to substitute the clinker—kaolinitic clays and limestone in calcined and uncalcined forms, respectively. Previous studies have found that replacement

H. Muni · Y. Dhandapani (✉) · K. Vignesh · M. Santhanam
Department of Civil Engineering, IIT Madras, Chennai, India

of cement with a blend of limestone and calcined clay can give a mechanical performance, on a par with plain Portland cement [2]. Also, concretes made with LC3 binder have shown promising concrete strength development and excellent resistance to chloride ingress [1].

The durability of concrete is partially controlled by the transport of aggressive ions through the microstructure. The ability of concrete to resistance transfer of ions relies on the electrical resistivity of the concrete bulk. Resistivity can also be used to indicate the physical structure development in concrete, connectivity of the pore system. Surface resistivity can be an ideal indicator for concrete quality and quick identification of concrete mixes for target durability performance in chloride exposure [3–5].

This study reports the viability of using LC2 at 45% clinker replacement for producing typical moderate to high-strength concretes. Two characteristics investigated in this study includes (i) the strength development potential in concretes made with LC2 and fly ash as admixture and (ii) the development of surface resistivity as a measure of durability characteristics in concretes made with LC2 and fly ash over a range of concrete mixes.

2   Materials and Methods

The experimental matrix was designed to determine the effect of different concrete components such as binder type (mainly LC3 and Class F fly ash as binder component), binder content and water–binder ratio. Table 1 gives the matrix with the variables used in the study. A total of 51 concrete mixes (marked as ↑ in Table 1) , 27 concrete with LC3 and 24 concretes with FA30, were fabricated.

Table 1 Different binder contents (kg/m3) and water–binder ratios used in the study

Binder type	Binder content (kg/m^3)	Water–binder ratio						No. of Mixes
		0.35	0.40	0.45	0.50	0.55	0.60	
LC3	280				↑	↑	↑	27
	310	↑	↑	↑	↑	↑	↑	
	360	↑	↑	↑	↑	↑	↑	
	400	↑	↑	↑	↑	↑	↑	
	450	↑	↑	↑	↑	↑	↑	
FA30	280				↑	↑	↑	24
	310	↑	↑	↑	↑	↑	↑	
	360	↑	↑	↑	↑	↑	↑	
	400	↑	↑	↑	↑	↑	↑	
	450	↑	↑	↑				

2.1 Materials Used in the Study

The binder materials used in this study are ordinary Portland cement (Grade 53 conforming to IS 269), and two SCMs considered include fly ash (Class F type from Ennore, Chennai) and an admixture made of limestone calcined clay (LC2 produced industrially by JK Lakshmi Cements Ltd). The fly ash and LC2 were used to produce binders named FA30 and LC3, respectively.

Crushed granite and graded river sand were used as coarse and fine aggregate, respectively. A PCE-based high-range water reducer was used to obtain the target slump between 80 and 160 mm. Notably, fly ash mixes were workable even at lower superplasticizer addition and LC3 mixes required higher superplasticizer dosage in most instances. The maximum dosage of superplasticizers required for FA30 and LC3 concretes was 0.33 and 1.18% of solids by weight of binder.

2.2 Testing Methodology

A 100 mm cubical concrete specimen was prepared for compressive strength assessment. The specimens were cast and moved to a moist room (>95 RH) after 24 h till the age of testing. Three specimens were tested by universal compression testing machine (Controls®-3000 kN) at 3, 7, 28 and 90 days curing in accordance with IS 516. Surface resistivity measurement was carried out on 100 mm-diameter cylindrical specimens. A four-point Wenner probe resistivity technique was used to determine the surface resistivity of the concretes. The resistivity measurements are sensitive to the surface condition of the concrete, including the presence of moisture and voids. Hence, 27 data measurements were made on three specimens to obtain a reliable average for the inherent resistivity of concrete.

3 Results and Discussion

3.1 Compressive Strength

Figure 1 presents the compressive strength results as a function of different water–binder ratios at different ages. From Fig. 1a and c, it is evident that LC3 concretes showed better strengths compared to FA30 across the range of binder contents at lower water–binder ratio. The strengths at 0.50, 0.55 and 0.60 water–binder ratios were also found to follow a similar trend with a major change due to binder content. In fly ash concrete, no major difference was found despite an increase in binder content. The early participation of calcined clay and limestone in LC3 complements to improve the strengths even at a higher water–binder ratio. In most FA30 concretes, strength was less than 15 MPa for mixes with a water–binder ratio above 0.45,
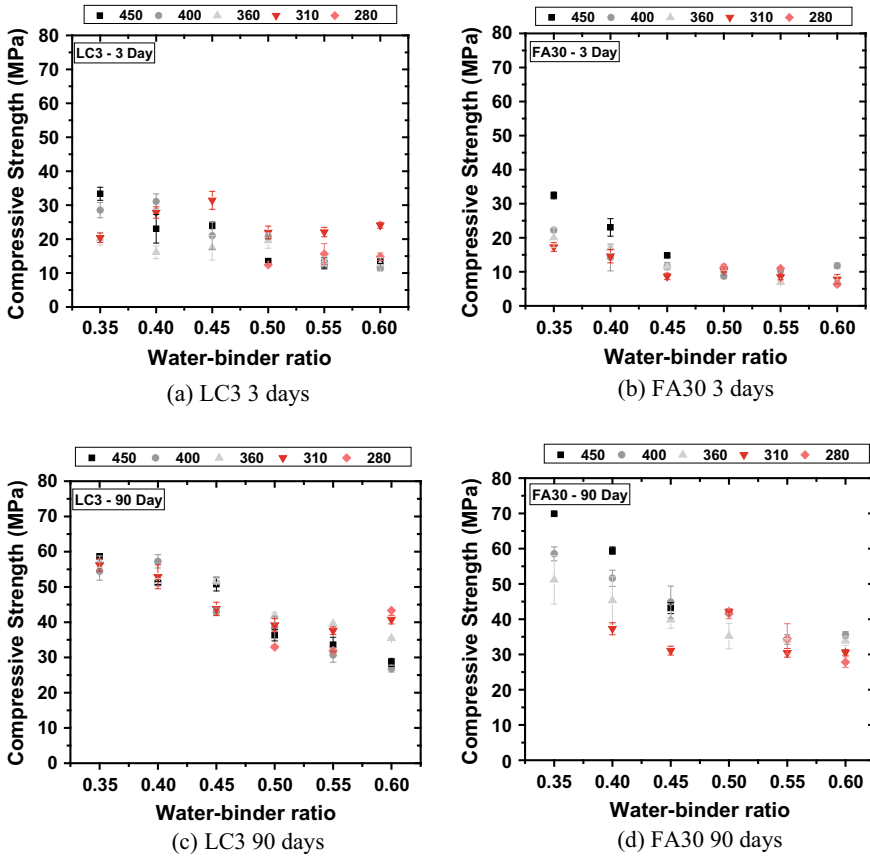
Fig. 1 Compressive strength as a function of water–binder ratio for concretes with varying binder content

irrespective of binder content. Also, FA30 mixes have a major shift in the strength occurring between 0.4 and 0.45. In the case of LC3 concretes, the shift was found between 0.45 and 0.5 water–binder ratio. This shows that LC3 concretes have a more pronounced strength development even at a marginally higher water–binder ratio despite 15% reduced clinker content compared to FA30 binder. Also, some variation in the 3 days strength for LC3 concretes can be due to the retardation effects due to higher dosage of superplasticizer which should also be noted.

Figure 1c presents 90 days compressive strengths of LC3 concretes, which gradually decreased from 0.35 to 0.60 w/b. Notably, all LC3 concretes with 0.45 or lesser water–binder ratio reached above 40 MPa signifying the strength potential of LC3. The strengths of FA30 concretes also decreased from 0.35 to 0.60 with binder content showing an influence on strength at a lower water–binder ratio. In the case of FA30, concretes made with w/b ratio up to 0.4 attained 40 MPa. Typically, there will be a higher amount of free capillary porosity for cementitious systems made with

water–binder ratio above 0.45. The free capillary porosity can delay the time taken for the hydration product to densify the cementing matrix and further delay the onset of the influence of binder content to impact the strength development. In the case of an LC3 system, the free capillary pore space gets densified at an early age due to better filling characteristics of the pozzolanic hydrate and additionally produces hydrates in limestone-calcined clay interaction. In fly ashes, the difference due to binder content and the water–binder ratio is significant, and fly ash-based systems require more time to densify the matrix due to lower intrinsic reactivity.

3.2 Surface Resistivity

Surface resistivity of concrete is used to assess the ability of concrete to withstand/resist the transfer of ions when subjected to an electrical field. Table 2 gives the concrete quality classification based on surface resistivity as suggested by ACI 222R and FM 5-578.

The electric current flows through the fluid-filled pores in concrete indicating the nature of the pore network. In this context, resistivity measurement can be used to assess the extent of the interconnectivity of pores and can be related to several transport properties of concrete such as chloride diffusion coefficient, water absorption and corrosion rate of embedded steel.

The resistivity of both LC3 and FA30 concretes increases with curing duration due to continuous pozzolanic interaction from calcined clay and fly ash. The absolute values of resistivity of LC3 concretes were always higher than FA30 mixes at all curing periods. Previous studies on cement paste also found similar trends [6]. Also, the average resistivity of LC3 specimens is higher than their FA30 counterparts at any given water–binder ratio. This difference can be due to the significant reduction in the pore size of the LC3 binder as reported in [6]. From the data presented in Fig. 2a and b, resistivity is predominantly sensitive to the binder type than the water–binder ratio at a specified age. There is a limited but steady reduction in the resistivity with increasing water–binder ratio. However, this difference is insignificant compared to the difference between the absolute resistivity of LC3 and FA30 concrete across

Table 2 Classification of concrete based on surface resistivity

ACI 222-R		FM 5-578	
Resistivity (kΩ cm)	Corrosion rate classification	Resistivity (kΩ cm)	Risk of chloride ingress
<5	Very high	<12	High
5–10	High	12–21	Moderate
10–20	Low to moderate	21–37	Low
>20	Low	37–254	Very low
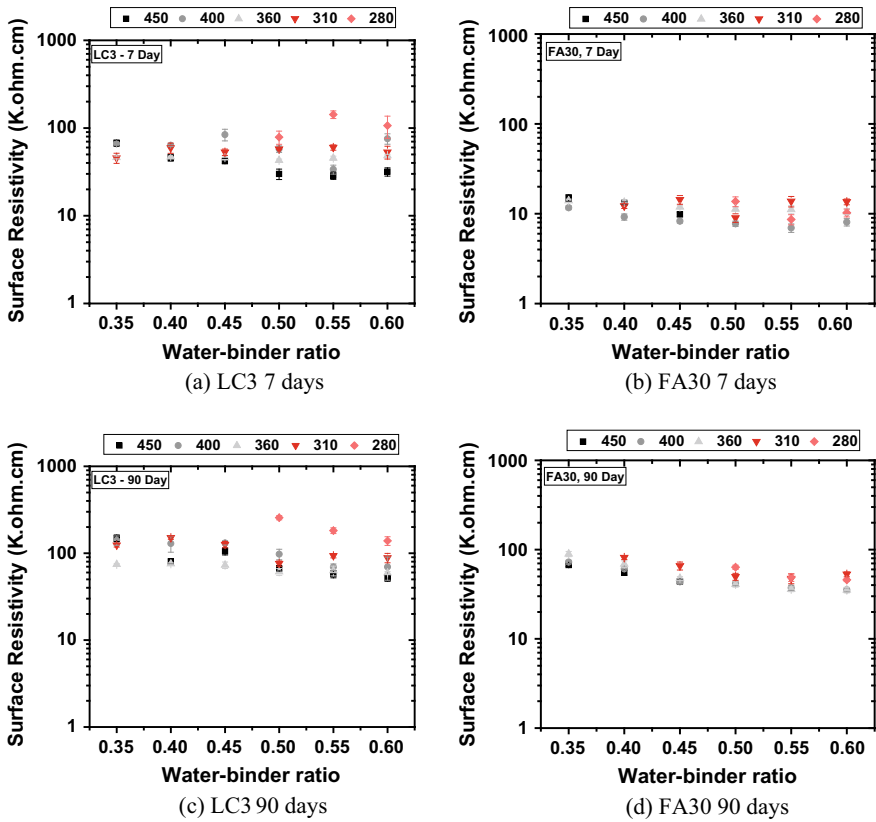
Fig. 2 Surface resistivity as a function of water–binder ratio for concretes with varying binder content

water–binder ratios. In some instances, for concretes with lower binder content had higher resistivity value. This was due to the reduction in the paste content, which reduces the permeable medium in the concrete and explains such variations.

Figure 2c and d confirms that there is a permanent effect of water–binder ratio on the resistivity value. This is because the water–binder ratio governs the initial distribution of the solid particles in the cementitious matrix per unit volume. At lower water–binder ratios, more solid particles are packed tightly in a unit volume of cementing matrix. This reduces the capillary space for hydrates to evolve, and ultimately, there will be a lesser amount of porous hydrates in a unit volume. Based on the difference seen in the LC3 and FA30 concretes, the nature of the pore network or the interconnectivity of the pores can be primarily controlled by characteristics of the hydrates formed in the capillary pore space. The low packing-density pozzolanic CASH with reduced Ca/Si ratio (discussed later in Fig. 6) due to the high reactivity of calcined clay can explain such early rise in durability indices of LC3 systems.
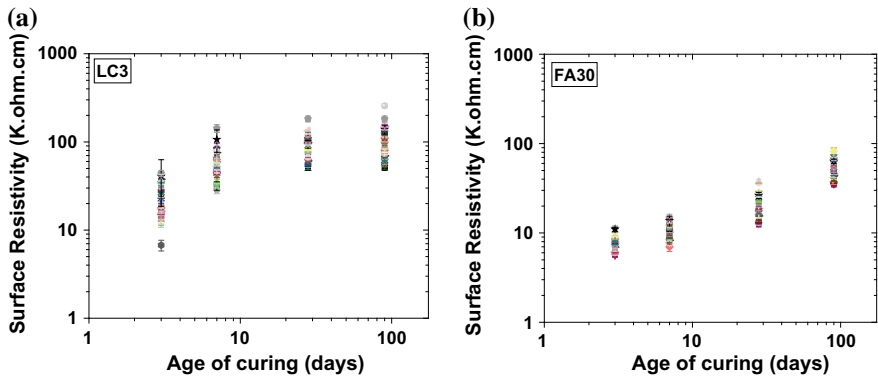
Fig. 3 Resistivity development in all **a** LC3 and **b** FA30 concretes

3.3 Resistivity Development Characteristics

Figure 3 shows the temporal change of resistivity in LC3 concretes, which confirms a consistent early interaction of calcined clay with a marked increase in the resistivity between 3 and 7 days for all 27 concretes. Beyond 7 days, the resistivity value increases at a lower rate to 90 days. In contrast, FA30 concretes shows major rise in resistivity between 7 and 28 days, and also further increase beyond 28 days till a period of 90 days. This distinct difference in the kinetics of resistivity development is in agreement with the findings on cement paste by Dhandapani and Santhanam [6] where an early decrease in the electrical conductivity in LC3 binder phase as a consequence of refined pore structure at the similar period was noted.

3.4 Discussion on the Resistivity of Concretes Made with LC3 Binder

The resistivity of LC3 concretes was above 10 kΩ cm by 3 days of curing. The change in mixture proportioning parameters such as water–binder ratio and binder content was able to produce a broad range of values between 10 and 50 kΩ cm for concretes made with LC3 binder (as seen in Fig. 4a). The slow interaction of fly ashes resulted in a narrow range of values, predominantly less than 10 kΩ cm by 3 days. Figure 4b shows that the resistivity value increased further above 50 kΩ cm for all LC3 concretes by 28 days. The range of values for LC3 concretes was between 50 and 250 kΩ cm. On the contrary, FA30 concretes had a resistivity range between10 and 50 kΩ cm.
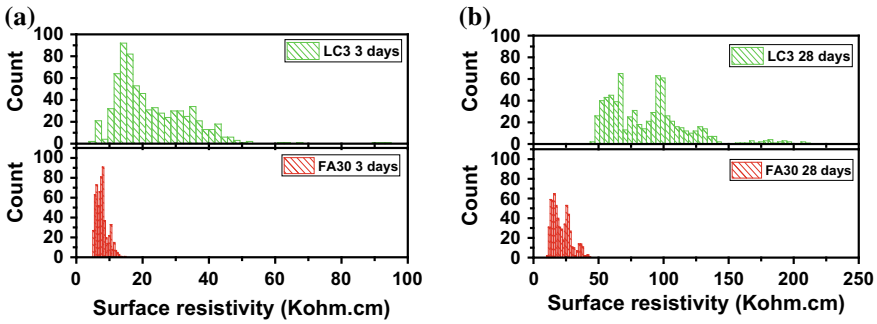
Fig. 4 Range of resistivity values for the two binder types at **a** 3 days and **b** 28 days

3.5 Microstructure

All concrete made with LC3 binder showed an early rise in resistance in the ionic transport, confirming the significance of microstructure development of the binder phase. Figure 5 shows the pore size development (as measured by mercury intrusion porosimetry) in LC3 and FA30 paste at 7 days of curing age. LC3 paste with all water–binder ratios showed a significant reduction in critical pore sizes as early as 7 days as seen in Fig. 5a. The critical pore size of FA30 binder reduced drastically across all water–binder ratios between 7 days of curing indicating the delayed interaction of fly ash in refining the capillary porosity.

(a) Pore sizes of LC3 at 7 days   (b) Pore sizes of FA30 at 7 days
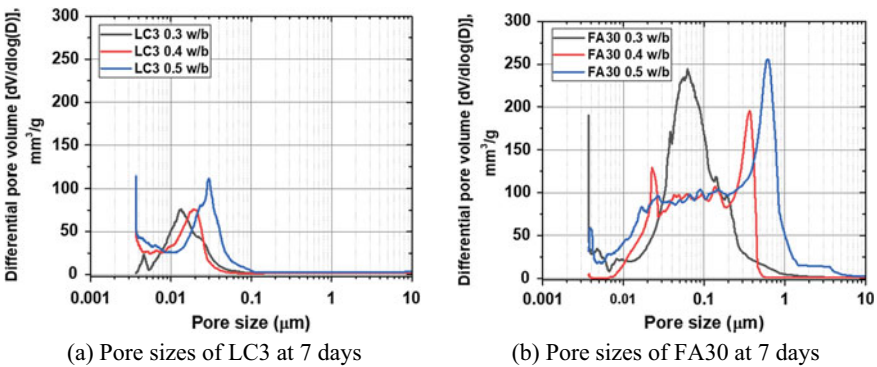
Fig. 5 Pore sizes of FA30 and LC3 at 7 days and 28 days

4 Conclusion

Limestone-calcined clay can be used as an admixture for a range of structural grade concretes with the required strength and durability parameters. The assessment of strength and durability of concretes prepared with LC3 and FA30 binders showed the following trends:

- **Strength development in LC3 and FA30**: LC3 specimens showed consistent strength development even at high water–binder ratio, whereas FA30 specimens showed a low rate of strength development at water–binder ratio above 0.45. The early strengths of LC3 specimens for all binder contents were higher than FA30 counterparts. Major strength evolution takes place at an early age in LC3 system as opposed to FA30 concretes. LC3 consisting of 50% clinker content can be efficiently utilised to make structural grade concretes with conventional mixture proportioning schemes.
- **Surface resistivity development in LC3 and FA30**: The surface resistivity values of LC3 specimens varied between 50 and 200 kΩ cm, while the resistivity values of FA30 specimens varied between 10 and 80 kΩ cm. This indicates that LC3 specimens offer more resistivity to the ingress of ionic species such as chlorides and sulphates. The significant importance of the binder composition on resistivity development was identified from a consistent increase in resistivity by 7 days, indicating that calcined clay gains control and has a prominent impact on concrete properties at an early age. In fly ash concretes, a similar increase in resistivity was observed only between 28 and 90 days due to the delayed interaction of the fly ashes despite modification in concrete mixture proportioning.

References

1. Dhandapani, Y., Sakthivel, T., Santhanam, M., et al.: Mechanical properties and durability performance of concretes with limestone calcined clay cement (LC3). Cem. Concr. Res. **107**, 136–151 (2018)
2. Antoni, M., Rossen, J., Martirena, F., Scrivener, K.: Cement substitution by a combination of metakaolin and limestone. Cem. Concr. Res. **42**, 1579–1589 (2012)
3. Sanchez, J., Andrade, C., Torres, J., et al.: Determination of reinforced concrete durability with on-site resistivity measurements. Mater. Struct. (2017)
4. Feliu, S., Gonzalez, J.A., Andrade, C.: Electrochemical methods for on-site determinations of corrosion rates of rebars. ASTM Int. STP **1276**, 107–118 (1996)
5. Nadelman, E., Kurtis, K.E.: A resistivity-based approach to optimizing concrete performance. Concr. Int. **36**, 50–54 (2014)
6. Dhandapani, Y., Santhanam, M.: Assessment of pore structure evolution in the limestone calcined clay cementitious system and its implications for performance. Cem. Concr. Compos. **84**, 36–47 (2017)

Properties of Calcined Clay-Based Geopolymer Mortars in Presence of Alccofine Powder and Recron Fiber

N. B. Singh, S. K. Wali, S. K. Saxena and Mukesh Kumar

Abstract Geopolymer mortars were prepared by treating calcined clay (CC) with sodium hydroxide and sodium silicate solutions in the presence of alccofine powder (AF) and recron fiber (RF). Alccofine powder increased the compressive strength of geopolymer mortar due to increased geopolymerization and filling of the pores. Recron fiber on the other hand decreased the strength. This was due to water absorption by the fiber. SEM was used to study the morphology. Rapid chloride permeability test showed that geopolymer mortar in the presence of AF is much more durable as compared to other mortars in the absence of AF. Durability of mortars in sulfuric acid indicated that geopolymer mortar containing AF is quite durable as compared to that containing RF. The overall results have shown that calcined clay of high surface area on reaction with concentrated NaOH (14 M) in the presence of AF gives mortar of high strength even at room temperature curing.

Keywords Calcined clay · Geopolymer mortar · Alccofine powder · Recron fiber · Durability

1 Introduction

Portland cement (OPC) is one of the most important ingredients of concrete, the most important construction material. OPC manufacture emits considerable amount of CO_2 gas in the atmosphere. There are number of ways to reduce CO_2 emissions from cement industry. One of the most important ways is to use geopolymer cements. When aluminosilicate (Al_2O_3–$2SiO_2$)-based materials are allowed to react with concentrated alkali hydroxide and alkaline silicate solutions, geopolymers are formed [1–4]. These have amorphous to semi-crystalline three-dimensional aluminosilicate

N. B. Singh (✉) · S. K. Saxena
Department of Chemistry and Biochemistry SBSR & RTDC, Sharda University, Greater Noida, India
e-mail: nbsingh43@gmail.com

S. K. Wali · S. K. Saxena · M. Kumar
JK Lakshmi Cement Ltd, Jhajjar, Haryana, India

framework structures formed by the combination of $[SiO_4]^{4-}$ and $[AlO_4]^{5-}$ tetrahedra [5]. In general substances like metakaolin (MK), fly ash (FA), rice husk ash (RHA), granulated blast furnace slag (GBFS) and red mud (RM) contain aluminosilicate materials, which when allowed to react with concentrated alkali hydroxide and alkali silicate and cured at about 90 °C, form geopolymers. FA and GBFS are more frequently used precursors for the preparation of geopolymers, but the availability of these materials is much less as compared to the demand. Therefore, attempts are being made to find some alternative materials. Raw clays (RC) are reported to be an alternative precursor. RC, when heated between 750 and 850 °C, is converted to calcined clay (CC) and shows higher reactivity when treated with alkaline solutions [2]. It is further reported that if CC is converted to higher surface area by grinding, the process of geopolymerization is enhanced [5]. In general, the strength development in geopolymer mortars is enhanced in the presence of certain fine materials. Combination of suitable precursor, fine additive and optimum concentration of alkali solutions can give high compressive strength even at room temperature. To save energy and improve mechanical properties of geopolymers, detailed investigations in the presence of fine additives on room temperature curing are important [6].

In this paper, raw clay was converted to calcined clay and ground to fine powder of different Blaine. Calcined clay when allowed to react with $NaOH/Na_2SiO_3$ in the presence of alccofine powder (microfine material based on low calcium silicate slag) (AF), high compressive strength geopolymer mortar was obtained on room temperature curing. The mortar was found to be quite durable in acidic atmosphere. However, in the presence of recron fiber (RF) (polyester and polypropylene monofilament fiber), the compressive strength and durability were decreased. The results have been discussed in detail.

2 Experimental

2.1 Materials

Raw clay was taken from Shriram Minerals, Bhuj, Gujarat India. Alccofine powder (ultrafine slag) (AF) is a microfine material was obtained from Ambuja cement ltd, Mumbai, by grinding of GGBFS in closed circuit vertical roller mill. It was stored in a set of twin cyclone and named as alccofine powder (AF). Due to high content of SiO_2, it acts as pozzolanic material. Being fine powder, it acts as filler also. It is not hydraulic. Sodium hydroxide (NaOH) (SH) and sodium silicate solution ($Na_2O = 16.84\%$, $SiO_2 = 35.01\%$ and water $= 46.37\%$ by mass) (SS) were used as alkaline liquid. The Ennor sand, a brand name of Tamil Nadu Corporation, India, was used. Recron 3S fiber (RF) (polyester and polypropylene monofilament fiber), made from polymerization of pure teraphthalic acid and mono ethylene glycol using catalyst, a reinforcing material in construction industry, was procured from Reliance Industries, India. The chemical composition of raw clay, calcined clay and AF is given in Table 1.

Table 1 Chemical composition of raw clay, calcined clay and alccofine powder (%)

Compounds	SiO_2	Al_2O_3	Fe_2O_3	CaO	MgO	K_2O	SO_3	Na_2O	LOI
Raw clay	47.34	36.58	3.60	12.37	0.00	0.03	0.00	0.08	–
Calcined clay	61.93	22.95	3.22	10.12	0.00	0.01	0.02	0.11	1.2
Alccofine powder	32.84	22.00	2.50	36.10	4.00	0.74	0.30	0.34	0.49

Calcination of raw clay was done between 750 and 800 °C in a rotary kiln for 15–20 min. Calcined clay was ground to obtain powders of different Blaine surface area.

2.2 Mix Design

Molds with size $7.5 \times 7.5 \times 7.5$ cm^3 were made. Mortars using calcined clay were made with Ennor sand. First, they were dry mixed for 1 min and then with alkaline activator (14 M NaOH + Na_2SiO_3) for another 1 min. The mixes were put into molds and vibrated with vibrating machine for 2 min with RPM $12,000 \pm 400$. The cubes were then demolded after 12 h. Compositions of different mixes are given in Tables 2 and 3.

All the experiments were carried out by taking calcined clay of Blaine area 591 m^2/kg in the presence of 14 M NaOH (Table 4).

Table 2 Calcined clay (different Blaine)-based geopolymer mortars (g)

Mix detail	Calcined clay (CC)	Ennor sand	Specific gravity of CC	Blaine of CC m^2/kg	Na_2SiO_3	NaOH	Extra water
Mix-1	200	600	2.63	487	80	40	0
Mix-2	200	600	2.90	529	80	40	0
Mix-3	200	600	2.84	591	80	40	0

Table 3 Geopolymer mortar mix with Ennor sand (g), fiber and AF

Mix detail	Calcined clay	Ennor sand	RF	Alccofine powder	Na_2SiO_3[a]	NaOH[b] 14 M	Extra water
Mix-4	200	600	0	0	80	40	0
Mix-5	200	600	0	64	80	40	10 ml
Mix-6	200	600	2	0	80	40	10 ml
Mix-7	200	600	2	64	80	40	10 ml

[a]Sodium silicate was 10%, and
[b]Sodium hydroxide was 5%

Table 4 Compressive strengths of different mixes in sulfuric acid

Mix No	Compressive strength at RT curing 28 days (Mpa)	Compressive strength after 24 h in 5% Sulfuric Acid (MPa)	% wt loss
Mix-4	52.4	40.3	23.1
Mix-5	77.6	73.1	5.8
Mix-6	45.8	34.2	25.3
Mix-7	71.1	64.0	10.0

2.3   Methods

Setting times and compressive strengths of geopolymer mortar (1:3) (Mix-4–Mix-7) cured at 27 ± 2 °C for different periods were measured. Rapid chloride permeability test (RCPT) was performed as per ASTM C 1202.

Calcined clay-based geopolymer mortar specimens of 28 days room temperature curing were immersed in 5% sulfuric acid for 24 h, and compressive strengths were measured. SEM pictures of selected samples were also taken.

3   Results and Discussions

Compressive strengths of geopolymer mortars made from calcined clay of different surface area and cured for 28 days at room temperature were determined. The results showed that compressive strength increased with increase of surface area of calcined clay, and the values were highest when surface area was highest (591 m^2/kg). Therefore, detailed investigations were carried out by taking calcined clay of 591 m^2/kg surface area only.

Both the initial setting time (IST) and final setting time (FST) decreased in the presence of AF (Mix-5) indicating that it accelerates the process of geopolymerization. Setting of geopolymers is related with the early formation of sodium aluminosilicate hydrate gel, and this gel at later stages is responsible for strength development. Setting time of geopolymer depends on several factors such as composition of the precursor, alkaline solutions and their concentrations, silica modulus, Na$_2$O content, w/s ratio, curing temperature and heat liberated during geopolymerization [7]. During the setting period in alkaline medium, dissolution of alumina and silica from the precursor takes place. During the process of setting, nucleation, gel formation and growth occur. Dissolution and polycondensation occur simultaneously. However, at the end, the major reaction shifts to polycondensation. In the presence of RF alone (Mix-6), setting times (IST & FST) increased and became almost equal to that of Mix-4. It appears that RF plays a very little role in the geopolymerization process. However, when both AF and RF were added, the setting times were found to be the lowest. This indicated that AF in combination with RF enhances the process of

geopolymerization. This may be due to surface area, morphology and heat evolution during the process of geopolymerization.

In the presence of alkalies, the dissolution and hydrolysis of aluminosilicate materials can be schematically expressed by the Eqs. (1) and (2) [8].

$$Al_2O_3 + 3H_2O + 2OH^- \rightarrow 2\left[Al(OH)_4\right]^- \tag{1}$$

$$SiO_2 + H_2O + OH \rightarrow \left[SiO(OH)_3\right]^- \tag{2}$$

The condensation reaction between $[Al(OH)_4]^-$ and $[SiO(OH)_3]^-$ may be written by the Eqs. (3) and (4) [9].

$$\tag{3}$$

$$\tag{4}$$
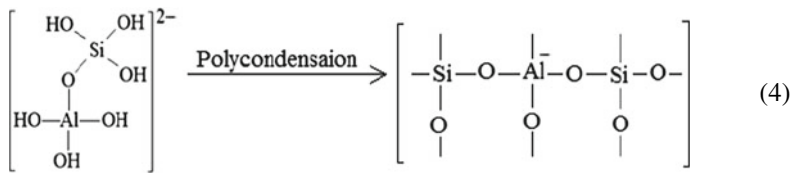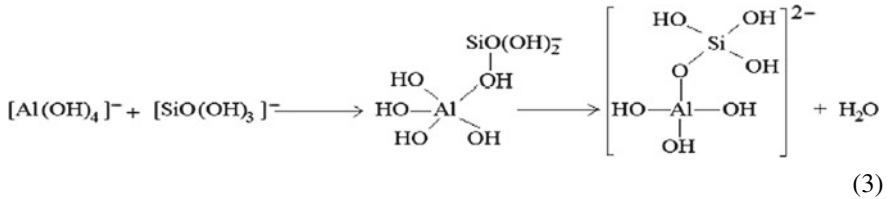
The optimum compressive strength is obtained when the NaOH is sufficient to ensure a charge balance for the substitution of tetrahedral Si by Al. In the present case, this optimum compressive strength appears to be at 14 M NaOH.

The compressive strengths of different mixes at different curing times are shown in Fig. 1. The results show that compressive strengths increased with curing time in all the mixes. In the presence of AF (Mix-5), the compressive strengths were found to be much higher at all the times as compared to that without AF (Mix-4). It appears that AF increases the geopolymerization and also fills the pores. Due to filling of pores, the matrix of the specimens became dense.

In the presence of RF (Mix-6), the compressive strengths decreased considerably. It is just possible that in the presence of RF, porosities are created, and the strength is decreased. Short hybrid polymeric fibers added to geopolymer mortars also reduced the compressive strength. The influence of fibers in geopolymer depends on quantity and properties of fiber, nature of geopolymer precursors, curing temperature and curing duration. However, fiber/matrix interface plays an important role in the mechanical properties of composite structures. Mix-7 containing both RF and AF
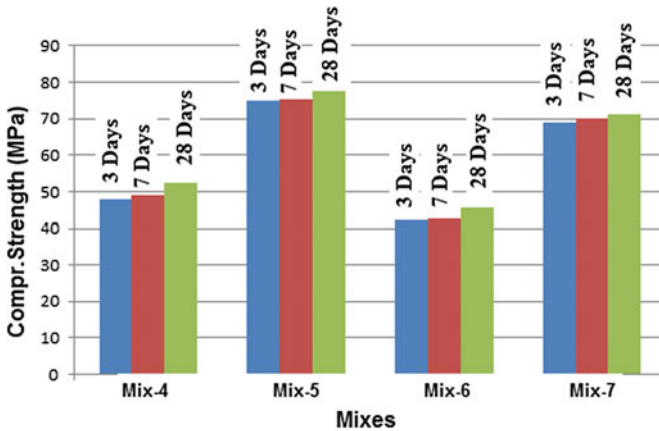
Fig. 1 Compressive strength of different mixes at different intervals of time

showed higher compressive strength. This indicated that AF enhanced the geopolymerization and decreased the porosity. As a result, the compressive strength of Mix-7 is much higher than that of Mix-6.

SEM pictures of different geopolymer mortars (Mix-4–Mix-7) are given in Fig. 2. SEM picture of Mix-4 (Fig. 2a) shows blocks of geopolymers separated from each other, whereas SEM picture of Mix-5 shows lot of smaller particles distributed in the structure (Fig. 2b). These particles may be of AF, and as a result, the compressive strengths are high. The SEM picture of Mix-6 containing RF (Fig. 2c) shows porous structure with small fibers distributed in the structure. The porosity of the structure may be the reason for decrease of compressive strength. The SEM picture of Mix-7 (Fig. 2d) shows comparatively compact structure as compared to that of Mix-6. Because of this, the compressive strength of Mix-7 is higher than that of Mix-6.

RCPT was conducted on all the mixes (Mix-4–Mix-7), and the values are given in Fig. 3. It is noted that less amount of charge passed through geopolymer mortar with AF (Mix-5) than that of geopolymer mortar without AF. This indicated that the diffusion coefficient was less due to dense structure in AF modified geopolymer mortar, thereby improving the durability. Highest amount of charge passed through geopolymer mortar containing RF (Mix-6). The results suggested that mortar with AF (Mix-5) is much more durable as compared to other mortars.

Effect of 5% sulfuric acid on the durability of mortars. Effect of 5% sulfuric acid on the compressive strength is given in Table 4. Results show that the minimum loss in compressive strength (5.8%) is in the case of mortar containing AF (Mix-5), whereas the maximum loss in compressive strength (25.3%) is in the case of mortar (Mix-6) containing RF. In other words, it can be said that AF decreases the pore size and number of pores making the mortar more compact, whereas RF increases the pore size, and as a result, the diffusion of sulfuric acid in the mass increases and deteriorates the structure.
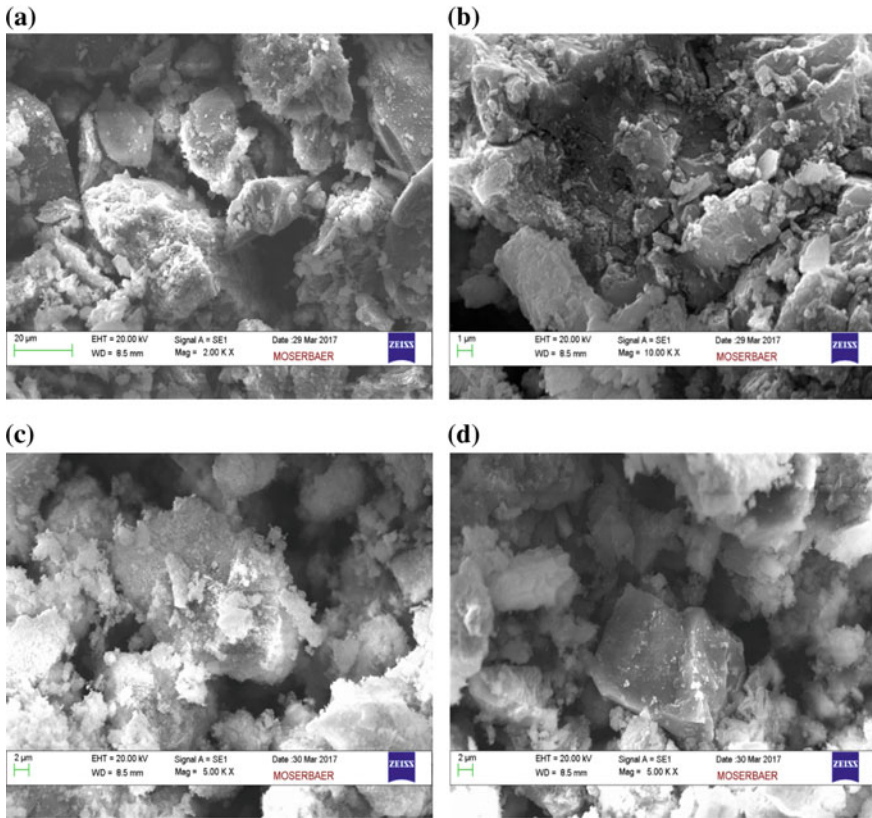
Fig. 2 SEM pictures of **a** MIX-4 **b** MIX-5 **c** MIX-6 **d** MIX-7

4 Conclusions

Calcined clay-based geopolymer mortars in the presence of AF and RF were made at room temperature. Geopolymerization process increased with increase of surface area of CC. Compressive strength increased in the presence of AF. AF being very small in size enhanced the geopolymerization and entered in the pores giving high compressive strength and high durability. Recron fibers absorb water and become porous, increase porosity, and as a result, the compressive strengths and durability are decreased. Room temperature cured clay-based geopolymer mortar in the presence of AF may offer several economic and environmental benefits over Portland cement mortars. It can be inferred that clay of high surface can be a suitable precursors for making geopolymer mortar of high strength on room temperature curing.
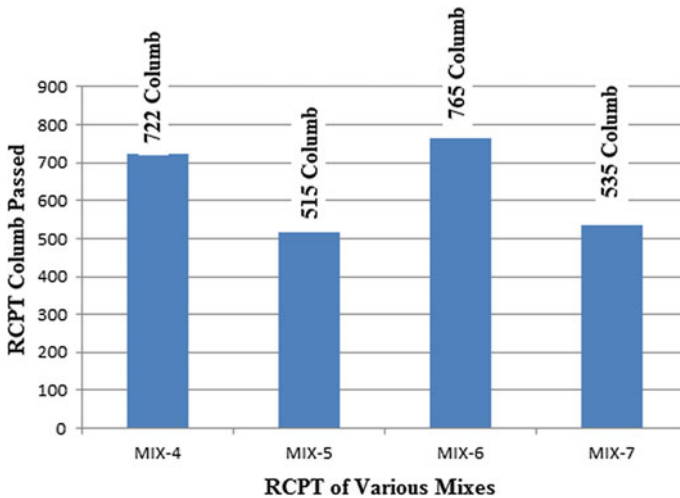
Fig. 3 RCPT test of various mixes

References

1. Yun-Ming, L., Cheng-Yong, H., Al Bakri, M.M., Hussin, K.: Structure and properties of clay-based geopolymer cements: a review. Progr. Mater. Sci. **83**, 595–629 (2016)
2. El Hafid, K., Hajjaji, M., El Hafid, H.: Influence of NaOH concentration on microstructure and properties of cured alkali-activated calcined clay. J. Build. Eng. **11**, 158–165 (2017)
3. Mohd Salahuddin, M.B., Norkhairunnisa M., Mustaphaa, F.: A review on thermophysical evaluation of alkali-activated geopolymers. Ceram. Int. **41**, 4273–4281 (2015)
4. Kaur, M., Singh, J., Kaur, M.: Synthesis of fly ash based geopolymer mortar considering different concentrations and combinations of alkaline activator solution. Ceram. Int. **44**, 1534–1537 (2018)
5. Dietel, J., Warr, L.N., Bertmer, M., Steudel, A., Grathoff, G.H., Emmerich, K.: The importance of specific surface area in the geopolymerization of heated illitic clay. Appl. Clay Sci. **139**, 99–107 (2017)
6. Oderji, S.Y., Chen, B., Ahmad, M.R., Shah, S.F.A.: Fresh and hardened properties of one-part fly ash-based geopolymer binders cured at room temperature: effect of slag and alkali activators. J. Cleaner Prod. **225**, 1–10 (2019)
7. Kupaei, R.H., Johnson Alengaram, U., Jumaat, M.Z.: The effect of different parameters on the development of compressive strength of oil palm shell geopolymer concrete. Sci. World J. **2014**, 1–16
8. Nmiri, A., Hamdi, N., Yazoghli-Marzouk, O., Duc, M., Srasra, E.: Synthesis and characterization of kaolinite-based geopolymer: alkaline activation effect on calcined kaolinitic clay at different temperatures. J. Mater. Environ. Sci. **8**(2), 676–690 (2017)
9. Hounsi, A.D., Lecomte-Nana, G., Djétéli, G., Blanchart, P., Alowanou, D., Kpelou, P., Napo, K., Tchangbédji, G., Praisler, M.: How does Na, K alkali metal concentration change the early age structural characteristic of kaolin-based geopolymers. Ceram. Int. **40**, 8953–8962 (2014)

Calcined Clays and Geopolymers for Stabilization of Loam Structures for Plaster and Bricks

Klaus-Juergen Huenger and David Kurth

Abstract Loam is a very ecological building material with a great potential. It is found worldwide and completely recyclable. Under dry conditions, loam develops high strength values. However, loam is not moisture-resistant. Permanently acting moisture reduces the strength dramatically. The idea to improve the water resistance of loams is adding materials to the loam with the same basic structure. Therefore, metakaolin, calcined clay, here, so-called metaclay and a specially developed geopolymer were selected. Blends of four different loams with different amounts of these additives were produced and tested. Criteria for an evaluation are the dynamical modulus of elasticity and the water resistance. These studies were supplemented by structural investigations using a light and a scanning electron microscope and XRD. The results are very interesting, and the effects depend strongly on the kind of loam too. Not all additives lead to an improvement of the mechanical properties. Nevertheless, not the samples with the highest mechanical values show the best water resistance behavior. Obviously, a balanced structure between loam and additive particles is necessary. Such structures are not so dense but enough resistant to water to guarantee the positive property of fast water absorption and delivery of natural loams. The service lives of the loam prisms could be increased from certain minutes to several days. The best results are obtained with geopolymer-based materials as an additive. This is not so surprising because both the loam and the geopolymer form aluminosilicate structures during hardening.

Keywords Loam bricks · Geopolymer · Calcined clays · Water resistance · Service live

1 Introduction

Loam is an ancient building material and was used over the millennia all over the world. The reasons therefore are very simple, because loam has many positive properties. Loam can be found in all regions of the world, requires little energy for

K.-J. Huenger (✉) · D. Kurth
Brandenburg University of Technology Cottbus-Senftenberg, 03046 Cottbus, Germany
e-mail: huenger@b-tu.de

production and processing and is completely recyclable. Under dry conditions, loam develops high compressive strength, and the tensile strength can be improved by addition of fibers. Fat loam can be emaciated by the addition of sand or other aggregates. The production of insulation materials is possible too by the addition of lightweight aggregates to the mixtures. It is logical that not so much literature exist. Some patents [1, 2] deals with the improvement of loam properties by the addition of cementitious materials. The focus here was to increase the strength, of course, the water resistance and other durability values. Already in [3], mixtures between loam and concrete to attach airfields and temporary roads were investigated. However, this is not the favorite solution for the loam worker today.

It is to take into account that loam has an important negative behavior, namely it is not moisture-resistant. Permanently acting moisture reduces the strength dramatically. Most of all discussed solutions and materials added to the loam to solve this problem lead to a compression of the natural loam structure. Needless to say is that the addition of cement to loam and vice versa give problems in the workability of mortars and concretes. Additionally, a further point of view is that ecologically orientated people will not accept a combination between loam and cement. Another research direction was described in [4], namely the stabilization of clay structures by the addition of natural polymers and wood fibers.

That is why the idea was born to combine materials with approximately the same basic structure elements. Loam is a natural mortar and consists of clay minerals as the binding part and quartz grains with different sizes as a structural scaffold. Clays have aluminum and/or aluminosilicate structures, which can form sheets and networks. The hardening process bases on physical interactions to form van der Waals bonds. If moisture escapes, the particles can be very close to each other. On the other hand, if moisture is taken again, the structures can swell and the distance between the particles is increased. The influence of water and moisture is not a chemical dissolution but a physical destruction process.

The search for materials, which are available and from a structural point of view suitable too, results in testing of geopolymers and other similar substances. There is not so much information on this combination in the literature. In [5], a combination of hydrothermal burnt clay with a lightweight aggregate was discussed to form clay bricks with an improved insulation behavior. The aim "strong and heat insulating" could be reached. In [6], a combination of loam with other additives is mentioned. For these investigations, an activated loam, called as an aluminosilicate compound, was mixed with different mineral additives to improve mechanical and durability properties. The activated loam binder is made up of clay and a reactive aluminosilicate compound, namely a geopolymer produced with metakaolin and a highly alkaline solution. In comparison with a conventional loam, the activated loam binder has achieved a higher strength and water resistance while maintaining the water vapor permeability. Exactly, this is the aim of this research project, however, without any use of highly alkaline activator substances (sodium hydroxide).

2 Materials Used

The investigations were performed with four different loams. Loam 1 (L1) is a swamp loam with a medium to strong binding behavior. Loam 2 (L2) is a glacial loam with a high amount of sand and silt, loam 3 (L3) is a loess loam with a relatively high lime content and loam 4 (L4) represents a sandy loam with a high amount of quartz and feldspars. Because of the different formations, the loams have also different compositions (chemical and mineralogical composition, grain sizes and grain size distributions).

The following Tables 1 and 2 give an overview on the chemical and mineralogical compositions of loams selected for the investigations. Figure 1 shows the distribution curves of grain sizes of the loam materials; differences between the loams can be clearly seen. Dry material was measured what means that agglomerates may have formed.

An important criteria of the loams used here is the grain size distribution, and it gives information on the contents of sand, silt and clay particles.

Data of the geopolymer, metakaolin and metaclay used as special additives are summarized in Table 3.

All additives are very fine grained, and therefore, they should contribute to the density increase of the loam samples.

Table 1 Chemical composition of loams chosen

Charge	L1 (wt%)	L2 (wt%)	L3 (wt%)	L4 (wt%)
SiO_2	64.39	84.17	77.01	81.55
Al_2O_3	16.16	7.76	10.89	10.16
CaO	0.98	0.31	0.60	0.17
Fe_2O_3	6.90	2.77	3.95	1.21
MgO	1.28	0.43	0.78	0.37
Na_2O	0.66	0.44	0.86	0.11
K_2O	2.06	1.66	2.47	1.73
TiO_2	0.91	0.47	0.81	0.81
Loss on ignition	6.66	2.01	2.62	2.62

Table 2 Mineralogical composition of loams chosen

Charge	L1 (wt%)	L2 (wt%)	L3 (wt%)	L4 (wt%)
Quartz	37.5	69.1	54.5	64.8
Clay	32.5	13.3	17.2	20.5
Feldspar	17.8	13.5	21.9	11.1
Oxide	8.8	3.9	6.2	2.5
Carbonate	2.7	0	0	0
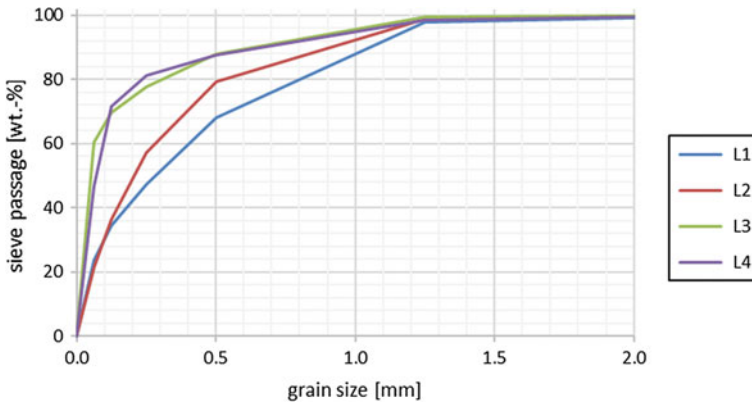
Fig. 1 Grain size distribution of loams investigated

Table 3 BET-surfaces of additional components

Additive	A (m^2/g)	Density (g/cm^3)
Metakaolin (MK)	18.94	2.605
Calcined Clay (MT)	14.73	2.615
Geopolymer (GP)	30.40	2.17

3 Performance

Samples for the investigations contain certain amounts of loam and additives. Of course, pure loam samples were also produced. The ratio loam/additive was varied between 10/1, 5/1 and 3/1. The last relationship is based on a typical mortar composition; however in difference to this, all components are binder materials, and the aggregate is the quartz content of the loam. The selected Si/Al ratio of the geopolymer is 2/1 and based on preliminary investigations to create a geopolymer mortar for special uses [7]. The geopolymer consists of two components, a siliceous residue with a high reactivity and an aluminate substance from the detergent production. The Si component accumulates as a slurry with a defined water content. In contact with the water from the slurry, the aluminate component reacts to an alkaline solution, in which the Si part can be dissolved. The result is the formation of an aluminosilicate network, a little bit similar to the loam structures. This formation process can be determined by using NMR investigations. Figure 2 shows the structure development of the geopolymer compound.

The metakaolin used is a common material called PowerPozz. It consists of approximately 55 wt% SiO_2 and 41 wt% Al_2O_3. The metaclay material is a mixture of two clays with different compositions. It was burnt at 650–680 °C in a rotary kiln. Characteristical values are summarized in [8].

The production procedure consists of several parts. In the first step, the loam and the aluminate component are mixed, grinded and homogenized dry. Because of the
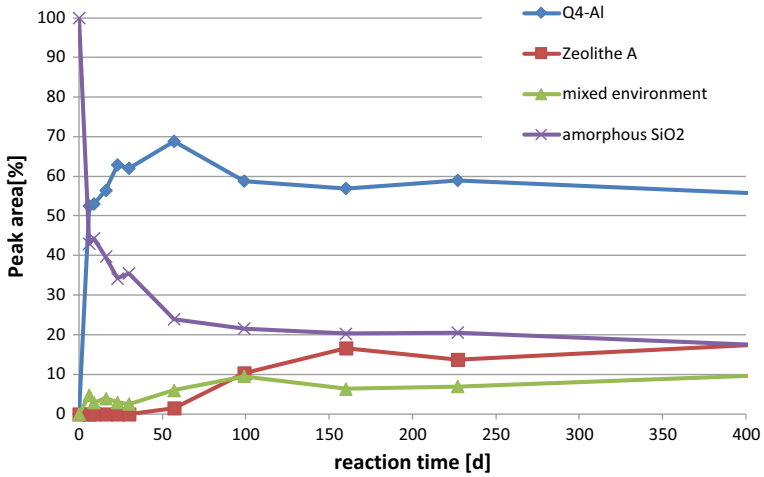
Fig. 2 NMR investigation results to demonstrate the different structures formed at different times in the geopolymer compound

fact that the siliceous component is a suspension with a certain water content, the dry compound was added to the slurry, and both were intensively mixed. Based on a brick technology for roof tiles, the material was pressed to 5–10-mm-thick plates with a defined shape. The pressure was 80 kN, converted to the test specimen surface 20 N/mm^2. The so-produced samples can be seen in Fig. 3.

This is what all test specimens look like. They are the basis for the further investigations.

Fig. 3 Loam samples produced in the laboratory
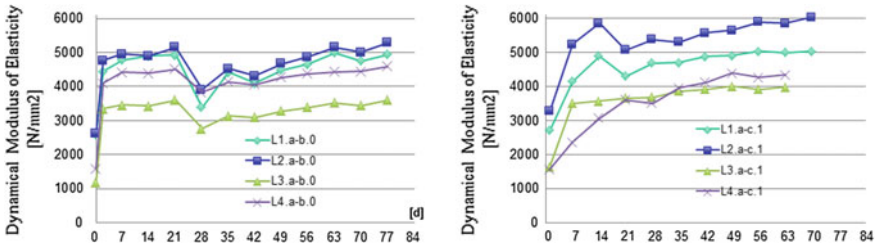
Fig. 4 Development of the modulus of elasticity of loam samples (left original, right 10/1)

4 Results

4.1 Dynamical Modulus of Elasticity

Figure 4 shows the results of the development of the dynamical modulus of elasticity. The values were determined by using a nondestructive method called Grindosonic. There are differences between the loam samples because of their different compositions. It can be observed that an addition of geopolymer in a ratio 10/1 leads not in all cases to an increase of the modulus. L2 indicates a raise, L4 even a decrease. Loam L3 produced with a ratio of 3/1, what means a higher amount of geopolymer in the mixture, gives a strong increase of the modulus. Loam–metakaolin and loam–metaclay mixtures have a lower strength in general in comparison with the starting materials. The results are very complicated and cannot be clearly discussed in this way that an addition of geopolymer or other additives leads under all conditions to an improvement of mechanical properties. However, this was not also the aim of the investigations.

4.2 Water Resistance

The German standard DIN 18945 from 2018 contains requirements for the water resistance depending on the use of loam bricks. There are different test methods to determine the water resistance. One of them is the so-called immersion test. Geometrical defined samples are stored in a water bath so that the water has always contact to the sample. The samples soak up the water until destruction. Bricks, which should be used outside, have to withstand this procedure for at least 10 min.

Soak investigations were performed with many samples and with different compositions. The time until destruction was measured automatically. The experimental setup is shown in Fig. 5. Some samples especially the original ones were destroyed after a very short period of time; in general, mixtures with additives stand longer. Very good results were obtained with an addition of geopolymer in a ratio 10/1 loam:GP (in Fig. 6 marked with **I**). The ratio 5/1 (in Fig. 6 marked with **II**) gives good results

Fig. 5 Investigation setup for the determination of the water resistance
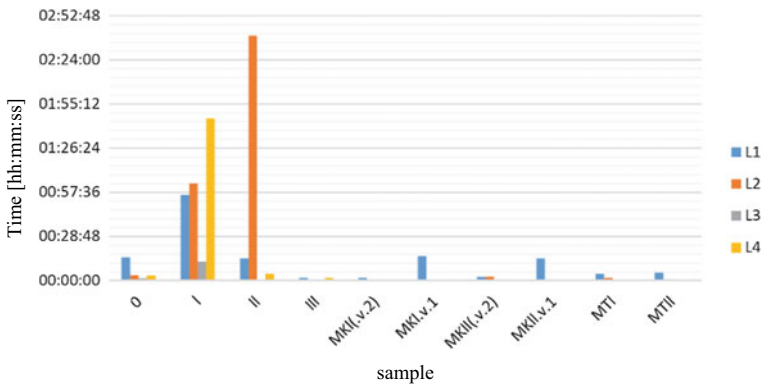
Fig. 6 Resistance against water uptake (the time of standing is shown)

for the standing time of loam L2, but the suction height here is too large. The ratio 3/1 loam:GP (**III**) provides the worst results, what is a little bit surprising. Metakaolin and metaclay are not so suitable because of the fact that such materials cannot lead a contribution for the structure formation process under neutral loam conditions.

Figure 6 summarizes the results. In this figure, the time of standing of the different mixtures is shown. MK stands for metakaolin, MT for metaclay. I, II and III represent the ratio between the loam and the additives, respectively (I = 10/1; II = 5/1; III = 3/1).

4.3   Structural Investigations

The question here is: Is it possible to find reasons for the observed water resistance behavior? XRD and SEM investigations were made to determine the mineralogical compositions with and without addition of Geopolymer. SEM investigations were performed to describe the structure of loam samplesformed.

Differences between the loam compositions were already mentioned in Tables 1 and 2 in Sect. 2. Changes of loam or clay structures shall only be demonstrated with L2 as an example. The next, Fig. 7 contains XRD pattern of L2 with geopolymer (10/1) at the beginning, after 14 and 28 days of reaction. The pattern demonstrates the decrease of 2-, 3- and mixed layer clay minerals. However, it can clearly be seen that a broad peak is formed during the reaction between loam and GP. The interpretation is not so clear; it could be a zeolite or an intercalated layer silicate (illite, vermiculite). In both cases, obviously this phase leads to a stabilization of the loam structure L2.

SEM investigations support this result. Figure 8 documents the structure of L2 with GP under $1100\times$ Mag (left) and under $3000\times$ Mag (right). In the right picture, swelling clay structures (in the middle) can be observed, what indicates that the XRD pattern can be interpreted in this direction.
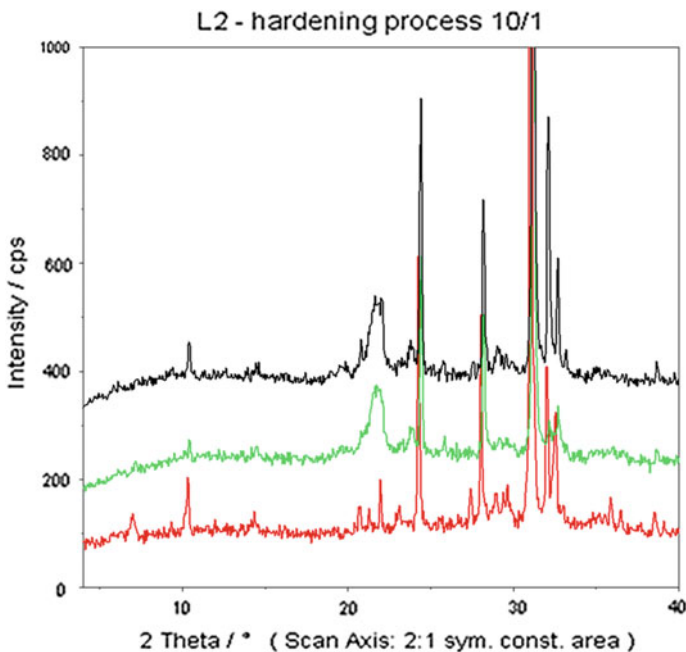
Fig. 7 XRD investigation results of L2 during reaction with geopolymer (L2/GP = 10/1)
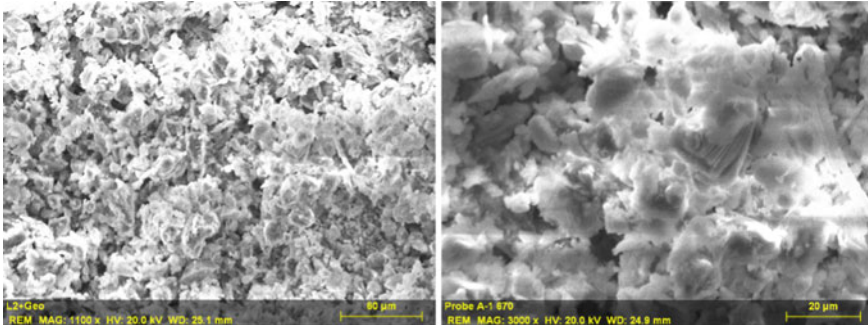
Fig. 8 SEM micrographs of loam–GP samples (here L2/GP = 10/1)

5 Conclusions

1. Loam as an ancient building material and a special geopolymer as a new one can be mixed to create stabilized loam structures.
2. The properties depend on the loam (composition and grain size) and, of course, on the geopolymer (here, Si/Al ratio).
3. Important is to guarantee that only water is added to the system because of the ecological basis of the loam material.
4. Best results for structure development, modulus of elasticity and water resistance are obtained with a glacial loam (L2) in combination with a geopolymer (Si/Al = 2/1) with a ratio of 10 parts loam to 1 part geopolymer.

References

1. EP 1 118 600 B1: Building material comprising clay and method of producing the same, 11p (2005)
2. EP 1 108 697 A1: Loam Building material, 10p (2001)
3. Graf, O.: Beton aus Zement und Lehm. In: Die Eigenschaften des Betons. Springer, Berlin, Heidelberg (1950)
4. Galán-Marí, C., Rivera-Gómez, C., Petric, J.: Clay-based composite stabilized with natural polymer and fibre. Constr. Build. Mater. **24**, 1462–1468 (2010)
5. Kaps, C., Hohmann, M.: Mineral polymerbinder produced from hydrothermal burnt clay. In: Proceedings of the 14. Ibausil, pp. 1-0415-0424, Bauhaus-Universität Weimar (2000)
6. DE10129873C1: Light building material used in the production of molded bodies for walls, ceilings and roofs consists of plant or mineral additives, and activated aluminosilicate compounds in the form of a reactive mixture (2001)

7. Brigzinsky, M., Huenger, K.-J.: An alternative alumino-silicate Binder based on the "justadd water method". In: 10th ACI/RILEM International Conference on Cementitious Materials and Alternative Binders for Sustainable Concrete, SUPP-320-23, Montreal (2017)
8. Huenger, K.-J., Gerasch, R., Sander, I., Brigzinsky, M.: On the reactivity of calcined clays from lower Lusatia for the production of durable concrete structures. In: Martirena, F. et al. (eds.) Calcined Clays for Sustainable Concrete, RILEM Bookseries, vol. 16, pp. 205–211, Habana (2017)

The Dissemination of the Technology "LC³" in Latin America. Challenges and Opportunities

Fernando Martirena and Adrian Alujas

Abstract The technology for the manufacture of a ternary cement based on Portland cement, calcined clay and limestone has gained interest in the region Latin America. Several cement companies have embraced the technology, and many of them are moving toward industrial production within the next 2–3 years. The introduction process must overcome a series of challenges associated with: (i) the choice of clay deposits rich in kaolinitic clays that are accessible to cement plants. Depending on the geological origin, several accompanying mineral can come with the clay, and some of them can compromise the reactivity of the activated clay; (ii) the choice of technology for clay calcination. Since this is a CAPEX dependent issue, each company has its own strategy for implementing the technology. The main trends are refurbishing old clinker kilns to convert them into calciners; opting for rotary kilns for the calcination and alternatively for flash calciners; (iii) The grinding strategy, which can opt for separate grinding or co-grinding, each with benefits and setbacks. Issues like grinding aids can be crucial in terms of achieving the best particle size distribution and avoiding excess grinding of some components and (iv) The strategy for the use of the ternary cements in mortar and concrete. The high specific surface of the calcined clays poses a challenge to the manufacture of concrete, since water demand is high. The strategy for the use of plasticizers differs from ordinary practices with Portland cement, but good flowing concrete can be achieved with a relatively high amount of calcined clay in its cement. Most of the results discussed in this paper are produced through the interaction of the Cuban Technical Resource Center with clients in the region.

Keywords Manufacture · Cement · Investment costs · Grinding · Calcination

F. Martirena (✉) · A. Alujas
CIDEM, Universidad Central de las Villas, Carretera de Camajuani km 5, Santa Clara, Villa Clara, Cuba
e-mail: fmartirena@ecosur.org

1 Introduction

Cement demand in Latin America (South America, including Brazil, Central America and the Caribbean) exceeds 250 million tonnes per year; this demand is planned to grow to 350–400 million in 2050 [1].

Cement production in the region was around 120 million tpy in 2016. Average clinker factor in the region is around 68–69%, and the main supplementary cementitious materials (SCM) used are limestone, fly ash, slag and natural pozzolans [2]. Carbon emissions in the region are close to 70 million tonnes per year, approximately 14% of global CO_2 emissions in the cement industry [2].

The availability of SCM will decrease in the forthcoming years in the region, especially fly ash and slag. New alternatives will have to be sought to keep the current clinker replacement levels [3].

Kaolinitic clays are widely available in vast regions of the continent, often coinciding with limestone reserves [4]. Many companies in the region have started to consider moving to the production of a new type of ternary binder known as limestone calcined clay cement "LC³" to cope with the challenge of low availability of SCM. This paper will discuss some of the issues related to the dissemination of the technology in the region.

2 Challenges in the Introduction of the Technology

2.1 Identifying the Clay Deposit

Kaolinitic clay deposits are abundant in the region; however, they must fulfill certain conditions. LC³ does not require a high purity clay for reasonably good results; thus, a minimum content of kaolinite clay minerals of 40% has been proposed by several authors [5–7], based on the minimum content of reactive material needed to achieve a mechanical performance comparable to OPC by a 30% substitution of OPC by calcined clay.

A first screening of candidates can be made by comparing mineralogical and chemical composition. Chemical composition is easier to use when dealing with most of the existing local geological databases, due to the fact that they often include quantitative chemical composition of sampling points, while just qualitative mineralogical description is offered in most cases.

Minerals of the kaolinite group are distinguished from other clay or non-clay minerals by their high contents of Al_2O_3, high Al/Si ratio, relatively high lost of ignition (LOI), associated with the dehydroxylation process of the clay minerals and low alkali content, since these elements are normally eliminated during primary kaolinitization process [8, 9]. The relation between the above-mentioned chemical parameters and the content of clay minerals from the kaolinite group, calculated on dry weight basis, is depicted in Fig. 1. From this comparison, the following chemical
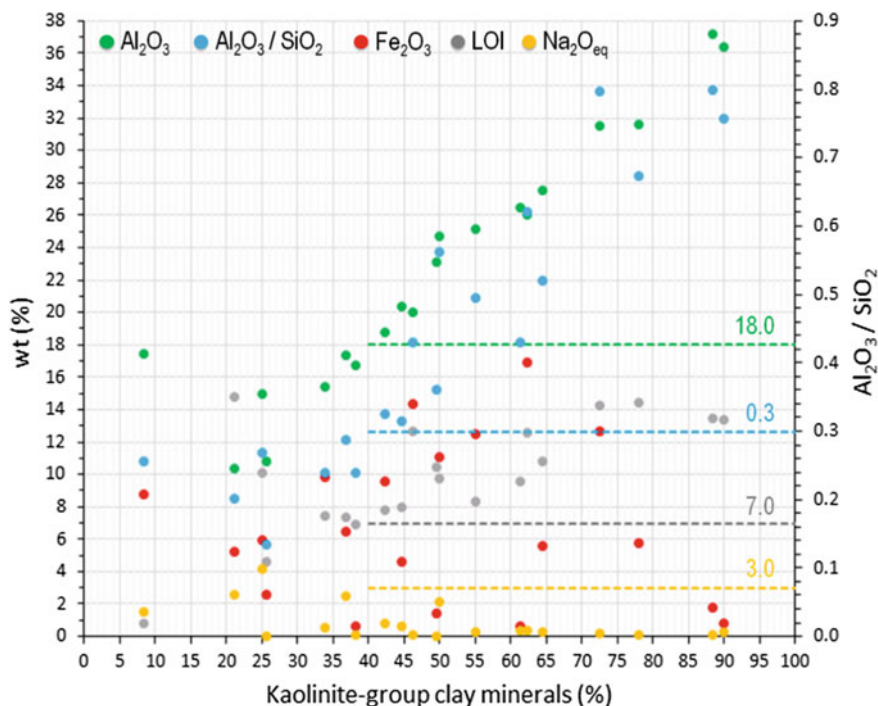
Fig. 1 Relationship between chemical composition and content of clay minerals from the kaolinite group

constraints could be established for the selection of a suitable kaolinitic clay likely to contain at least 40% of kaolinite clay minerals:

- % $Al_2O_3 > 18.0$,
- Al/Si > 0.3,
- % LOI > 7.0,
- % $Na_2O_{eq} < 3.0$.

It is important to point out that, for a successful selection process, all the above-mentioned criteria should be fulfilled as a whole, and not just individually.

2.2 Choice of the Calcination Technology

Calcination of kaolinitic clay should guarantee a total dehydroxilation of the material. This process takes place at a temperature range between 350 and 650 °C; however, for industrial purposes, the kiln operates at slightly higher temperatures, always below 950 °C, when recrystallization occurs [10, 11].

Table 1 Options for calcination technology

	Advantage	Disadvantage
Refurbished clinker rotary kilns	Low CAPEX	Low efficiency Little flexibility fuels Difficult to control color
Clay rotary calciners	Attractive CAPEX Reliable technology Possible to control color High productivity	High maintenance costs
Flash calciners	High energy efficiency Good use of space	High CAPEX Low productivity
Fluidized bed boilers	High homogeneity	No commercial technology available

There are technological options available. Table 1 presents some of the current alternatives evaluated in some of the ongoing projects. Preparation of the raw materials is crucial in terms of the choice of technology; for rotary kilns, for instance, the material demands little preparation, and it can enter the kiln with a 20% moisture content and in clumps of up to 50 mm. In flash calciners, the material must be completely dried and grounded to a maximum size of 150 μm. This has an impact on CAPEX, because the equipment for preparation is expensive and the energy consumption is relatively high.

2.3 Grinding Strategy

Multicomponent grinding is a great challenge for cement production. Softer materials such as calcined clay and limestone can get ground finer, while harder components such as clinker can be ground coarse, thus limiting the reactivity and increasing water demand.

For co-grinding, the use of grinding aids is very much recommended, and there are reports of their impact on particle size distribution and also on strength of mortars [12, 13]. Separate grinding is also recommended. A common practice is to grind calcined clay, limestone and gypsum together, to produce a mineral addition called "LC^2". It can be blended on the site or ready mix plant directly with Portland cement.

2.4 Water Demand in Concrete

The production of concrete with binders containing calcined clay has to overcome the challenge of the higher water demand caused by the high specific surface of the calcined clay [14]. Practical experiences prove that chemical admixtures of the family

Poly Carboxylate Ether, PCE, work very well with concrete made with LC3 cement. Practical trials made with concrete prove that despite the increase of consumption of superplasticizer, flowable concrete can be produced.

3   Applications of LC^3 in the Region

Industrial trials for the industrial production of LC^3 or LC^2 have taken place in Cuba (Cementos Siguaney 2013 and Cementos Siguaney 2018) [15], India, in 2017 [16] and Guatemala 2018. Kaolinitic clays used have had an average kaolinite content around 40–55%. Figure 2 presents some results of strength in standard mortars which are carried out, and the reference values of the standards for general use cement (GU) and high early strength cement (HE). As a general trend, most LC^3 cements produced comply with prescriptive values for high early strength cements (HE), despite its low clinker content, under 50%.

Concrete trials made with LC^3 also prove that it is possible to produce high-strength concrete (Strength > 45 MPa at 28 days) with a cement having less than 50% of clinker. Table 2 presents some of the results obtained.

Compressive strength MPa	LC3-50 2:1 CUB	LC3-50 2:1 GUA	LC3-50 2:1 ECU	LC3-50 2:1 IND	Standard GU	Standard HE
3d	12.50	22.12	19.96	25.00	13.00	11.84
7d	22.50	33.56	34.14	35.00	20.00	23.67
28d	42.08	40.61	41.12	46.00	28.00	
% clinquer	47%	50%	50%	50%		
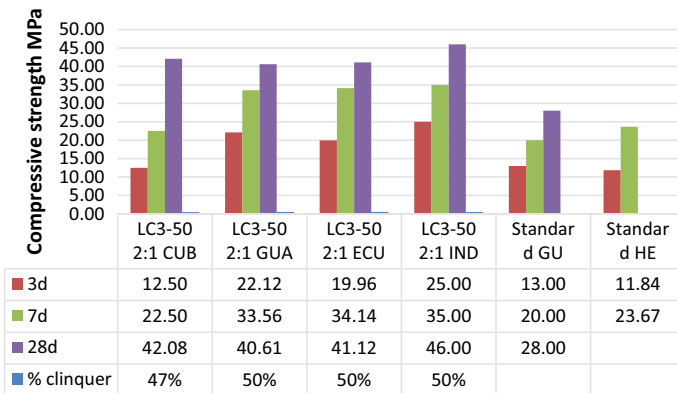
Fig. 2   Compressive strength results in standard mortars (EN-196) made with cement produced in industrial trials

Table 2 Strength in concrete made with LC^3 produced at industrial trials

	Cement (kg/m^3)	SP (%)	Water/cement	Slump (cm)	Str. 7d (MPa)	Str. 28d (MPa)
ECU concrete	412	2.00	0.34	7.50	26.57	47.00
CUB concrete	410	1.5	0.45	16.00	30.63	39.93
GUA concrete	290	2	0.4	7.00	39.59	53.37
IND concrete 1	400	0.7	0.4	19.00	39.2	44.7
IND concrete 2	450	1.2	0.3	20.00	45.4	61.7

Source Results of trials in Cuba, Guatemala (Cementos Progreso), India (Indian Institute of Technology Madras, and Ecuador (Cementos Atenas)

4 Conclusions

Sustainability of cement production and use in Latin America demands decreasing clinker content in cement. The combined use of calcined clays and limestone presents as an attractive alternative to achieve this. There are large reserves of kaolinitic clays. The new cement LC^3 shows a similar performance to traditional type I Portland cement. Industrial trials carried out in Cuba, Guatemala and India prove the robustness of the process and the possibility of adapting the existing equipment to the production of the new cement.

References

1. de P. de Cemento, A.A.D.: perspectiva del crecimiento mercado de cemento en América Latina y el Caribe, El Nuevo D. (2019) (2019)
2. WBCSD Cement Sustainability Initiative, Getting the Numbers Right Project Emissions Report 2016 (2016). https://www.wbcsdcement.org/GNR-2016/
3. Scrivener, K.L., John, V.M., Gartner, E.M.: Eco-efficient cements: potential, economically viable solutions for a low CO_2. Cement Based Materials Industry (2016)
4. Ito, A., Wagai, R.: Global distribution of clay-size minerals on land surface for biogeochemical and climatological studies (2017)
5. Scrivener, K., Martirena, F., Bishnoi, S., Maity, S.: Calcined clay limestone cements (LC^3). Cem. Concr. Res. **1** (2017). https://doi.org/10.1016/j.cemconres.2017.08.017
6. Avet, F., Li, X., Scrivener, K.: Determination of the amount of reacted metakaolin in calcined clay blends. Cem. Concr. Res. **106**, 40–48 (2018). https://doi.org/10.1016/j.cemconres.2018.01.009
7. Avet, F., Scrivener, K.: Hydration study of limestone calcined clay cement (LC^3) using various grades of calcined kaolinitic clays. In: Martirena, F., Aurélie Favier, K. Scrivener (eds.) Calcined Clays for Sustainable Concrete: Proceedings of the 1st International Conference on Calcined

Clays for Sustainable Concrete, pp. 35–41. Springer, France (2017). https://doi.org/10.1007/978-94-024-1207-9

8. Fernández, R.: Calcined Clayey Soils as a Potential Replacement for Cement in Developing Countries. École Polytechnique Federale de Lausanne (2009)

9. Alujas, A., Fernández, R., Quintana, R., Scrivener, K.L., Martirena, F.: Pozzolanic reactivity of low grade kaolinitic clays: influence of calcination temperature and impact of calcination products on OPC hydration. Appl. Clay Sci. **108**, 94–101 (2015). https://doi.org/10.1016/j.clay.2015.01.028

10. Tironi, A., Trezza, M.A., Scian, A.N., Irassar, E.F.: Kaolinitic calcined clays: factors affecting its performance as pozzolans. Constr. Build. Mater. **28**, 276–281 (2012). https://doi.org/10.1016/j.conbuildmat.2011.08.064

11. Fernandez, R., Martirena, F., Scrivener, K.L.: The origin of the pozzolanic activity of calcined clay minerals: a comparison between kaolinite, illite and montmorillonite. Cem. Concr. Res. **41**, 113–122 (2011). https://doi.org/10.1016/j.cemconres.2010.09.013

12. Garcés-Vargas, J.F., Espinosa, M., Diaz-Cardenas, Y., Hereira-Diaz, A., Martirena-Hernandez, J.F.: Use of grinding aids for grinding ternary blends Portland cement-calcined clay-limestone. In: Proceedings of the International Conference of Sustainable Production and Use of Cement and Concrete, ICSPCC 2019 (2019)

13. Zunino, F., Scrivener, K.L.: Processing of calcined clays for applications in cementitious materials: the use of grinding aids and particle classification after grinding. In: Proceedings of the International Conference of Sustainable Production and Use of Cement and Concrete, ICSPCC 2019 (2019)

14. Vizcaíno-Andrés, L., Antoni, M., Martirena-Hernández, F., Scrivener, K.L.: Effect of fineness in clinker-calcined clays-limestone cements. Adv. Cem. Res. (2015)

15. Vizcaíno-Andrés, L., Sánchez-Berriel, S., Damas-Carrera, S., Pérez-Hernández, A., Scrivener, K., Fernando, M.-H.: Industrial trial to produce a low clinker, low carbon cement. Mater. Construcción **65** (2015). http://dx.doi.org/10.3989/mc.2015.00614

16. Bishnoi, S., Maity, S., Mallik, A., Joseph, S., Krishnan, S.: Pilot scale manufacture of limestone calcined clay cement: the Indian experience. Indian Concr. J. **88**, 22–28 (2014)

What's Old Is New Again: A Vision and Path Forward for Calcined Clay Use in the USA

Kyle A. Riding and Abla Zayed

Abstract Calcined materials have a long history of use in concrete structures, with some now over 80 years old. Beginning in the 1950s, by-product supplementary cementitious materials (SCMs) began to replace natural pozzolans because of cost, availability, performance, and benefits of reuse. Specifications, mix designs, and performance data collected were built around an assumed continuous supply of these recycled SCMs. SCM availability, quality, and cost, especially for fly ash, is now in question. This has brought significant interest in alternative SCMs to provide durability in concrete structures. Calcined clay now appears to be a viable option going forward for concrete mixtures in the United States, especially when combined with ground limestone. This paper discusses the history of SCM use in the USA, potential for calcined clay use in concrete in the USA, barriers to use, and a path forward to overcome those barriers with only minimal changes in concrete specification, production, and placement methods. This paper will also discuss options to apply these and other potential strategies to other markets to speed adoption of concrete calcined clay use.

Keywords Supplementary cementitious materials · Specifications

1 Calcined Clay Historical Use in the USA

1.1 Early Use

Early use of supplementary cementitious materials (SCMs) in Portland cement concrete in the USA began in the early 1900s principally to improve concrete durability and reduce cost.

K. A. Riding (✉)
University of Florida, Gainesville, FL 32608, USA
e-mail: kyle.riding@essie.ufl.edu

A. Zayed
University of South Florida, Tampa, FL 33260, USA

A blended Portland-calcined Monterey shale cement was produced for several decades by the Santa Cruz Portland Cement Co. in California [1]. It was used in many highway structures in California and was used in the anchorage blocks of the Golden Gate Bridge and San Francisco–Oakland Bay Bridge because of sulfate resistance and low heat generation [1]. Recent inspections of the Golden Gate Bridge showed some limited areas of delaminations of spalling and some abrasion erosion, but overall in good structural condition [2]. An underwater inspection showed the concrete to be in excellent condition, proving the durability of reinforced concrete made with calcined pozzolans for harsh environments [3].

Much of the early pioneering work done on pozzolan use in massive structures in the USA was done by the US Bureau of Reclamation (USBR). The USBR is a federal water management agency that has been responsible for building and maintaining many of the dams and hydropower stations in the western half of the USA. The USBR built many of their large dams between the 1930s and 1960s. Heat generation, sulfate, and alkali-aggregate reaction (AAR) issues in these massive structures guided USBR research, which led them to use over 350,000 tons of natural pozzolans [4]. Calcined shale produced by the California Portland Cement Co. [5] was used in the Davis Dam in 1950 and calcined diatomaceous clay was used in the Monticello Dam in 1957. These calcined materials were used because they lowered the mixture cost and were found to reduce AAR and permeability. Heat of hydration was found to be similar to that of Class F fly ash, probably owing to the rather coarse grind used in the calcined shale [4]. The calcined shale used in the Davis Dam was also used successfully in concrete to line the San Jacinto Tunnel [1]. Calcined materials used in the 1930–1950s were much coarser than modern materials. For example, the Bonneville Dam Spillway used 25% calcined pozzolan in the mixture that had a minimum fineness of 1800 cm^2/g [1].

1.2   Shift to by-Product SCMs

SCMs began to be used not just for durability but for cost reduction. The introduction of fly ash into the concrete industry in the 1940s ushered in an era of expectations for cheap and plentiful fly ash in the USA. The first uses of fly ash in concrete in the USA were in the Hoover Dam in a tunnel spillway repair in 1942 and in Hungry Horse Dam from 1948 to 1952 [4]. Fly ash used in the Hungry Horse dam was shipped from Chicago to Montana at a cost of half of that paid for the Portland cement used in the project [1]. The seemingly endless supply of fly ash [4] and low cost led the industry to view fly ash as a cheap instead of as a value-enhancing product. Coal-fired power station numbers began to multiply and expand across the western USA in the late 1960s and 1970s [4]. This reduced shipping costs even more and allowed early adopters such as the USBR to begin routinely using it in projects. It began to displace other materials such as natural pozzolans from the market because of the low cost and abundance as the number and distribution of coal combustion electricity stations

increased. It is estimated that today half of all concrete used in the USA contains fly ash [6], with many specifications and approved mixtures requiring its use.

1.3 Modern Use of Calcined Clay

As fly ash displaced natural pozzolans on the low-cost end of the SCM spectrum, most of the calcined pozzolan use migrated to the high-performance end of the market. Highly reactive metakaolin (HRM) is marketed for use in high-performance and architectural concrete. HRM is made from clay sources with very high percentages of kaolin and is purified using sieving, cycloning, or other separation technique to remove sand, magnets to remove iron-bearing compounds and provide a material with a high whiteness, calcined, and ground to a very small particle size [6, 7]. Durability of HRM-containing concrete has been shown to be excellent, but as a premium product, HRM use has been lower than use before fly ash adoption.

Two companies in recent years have made calcined pozzolans for use in concrete. The first company was the Lehigh Cement Company, that made a calcined shale in the eastern USA from 1996 to 2004. This material was favored by precasters for helping improve the concrete flow and finishing properties [8]. Production of this material stopped, however, when production issues were encountered [7, p. 232]. Ashgrove Cement Co. made calcined pozzolans around the same timeframe as the Lehigh Cement Company in order to provide a material that could reliably mitigate alkali-aggregate reactions. Ashgrove made IP cement commercially from three different clay sources, but also suggested adding sulfates to the clay and using as an SCM blended at the plant. They designed the calcined clay system to still have CH to allow a user to add more fly ash to make the mix cheaper. All three clays showed improved strength, ASR mitigation, and sulfate attack compared to control mixtures. Permeability reductions with 25% mass replacement with these impure clays with Al_2O_3 contents as low as 19.6% produced permeability values similar to what would be seen with 10% silica fume [9]. Workability of mixtures made with these clays was not significantly impaired, as evidenced by one project superintendent who stated "The blended-cement concrete didn't set as fast and required less special attention because it finished more like ordinary concrete. Because of that, we didn't need as much labor to finish the concrete [10]." Eventually, production ceased because of economic reasons during a time when fly ash was very low cost.

2 Need for Calcined Clay in the USA

Recent advances in hydraulic fracking technology have dramatically lowered the cost of natural gas in the USA. These competitive pressures, combined with environmental regulation changes, have made coal-fired electricity less profitable in many locations, leading to plant closures. For example, coal combustion in Virginia was reduced by

50% between 2000 and 2016 [11]. The reduction in fly ash production has led to regional price increases and shortages even when aggregate numbers appear to show plentiful supply. This is especially true in the US southeast [12, 13]. Fly ash suppliers are currently importing fly ash into some US markets from foreign sources and are exploring use of landfilled fly ash. For example, in January and February 2019, fly ash was imported into Florida from Turkey, Portugal, and Italy [14]. Even with these imports, precasters in Florida are discussing rationing and changing mixture designs away from fly ash because of shortages. Plants to reclaim landfilled fly ash for use in cement production and concrete as SCMs have been built in South Carolina, North Carolina, and Maryland [11]. Beneficiation plants will supplement the supply of fly ash for the next couple of decades, but there is uncertainty as to how much is viable for use in concrete and at what cost. Much of the fly ash that is impounded is mixed with other materials such as bottom ash, or needs significant beneficiation to remove carbon, ammonia, or other undesirable materials.

As fly ash impoundments are removed and coal combustion continues to decline, alternative SCMs will be needed in some regions to provide durable concrete. Natural pozzolans are one of the few materials available in sufficient quantities in the USA to fill the gap that may be left by fly ash availability issues and cost increases.

3 Potential Calcined Clay Market Strategy for the USA

3.1 Material Availability

Volcanic natural pozzolans such as pumicite are available in the western USA, making them a likely source of SCMs in that portion of the country. In the eastern USA, non-calcined natural pozzolans are not readily available. Fortunately, large deposits of kaolin clay exist in the US southeast, coincidently where many of the fly ash shortages are occurring. Georgia produces 89% of the kaolin clay in the USA, with South Carolina producing 5.9%. This clay is found in the fall line centered around Macon, Georgia in central Georgia, and western South Carolina. Other suitable sources such as those used in the Midwest by Ashgrove Cement Co. and the mid-Atlantic region by Lehigh Cement Co. are available.

Because of the onerous regulations and permitting process involved in starting a new mine, the initial production of clay for pozzolan production will be simpler to obtain from already existing clay mining operations. As part of the kaolin mining process, clays that do not have the right color, size distribution, or purity level are often stockpiled or impounded. Figure 1 shows an example of a waste clay pile in the US southeast. A clay sample was recently obtained near the dam of a waste clay lagoon near the waste clay pile shown in Fig. 1. TGA measurements of the clay showed 66% kaolin content, sufficient to produce excellent calcined clay for use in concrete. Reuse of this clay material would not only provide income from its sale, but save the large cost of permitting and building additional lagoons in the future.

Fig. 1 Active kaolin mine with waste clays identified

Another option in the US southeast is to separate clay fractions from sand deposits. A recent study of Florida clay deposits at nine mines found that they were all mixed with significant quantities of sand, with only 10–35% of the material passing a #325 sieve (>45 µm). Of the material that did pass the #325 sieve (<45 µm), 75–94% was kaolin clay that showed satisfactory performance in concrete after calcination [15]. Since these mines currently extract and sell the sand, it may be economical to separate the two materials.

3.2 CCIL Concept

The majority of concrete made in the USA is made with cementitious materials added at the ready-mixed plant and not preblended at the cement plant. For example, in 2013 only 1.6% of all Portland cement made in the USA was blended cement [16]. Material customization to match specific project needs, as well as specifications and allowed materials that can differ significantly by owner, has led ready-mixed companies to prefer keeping cementitious materials separate until the concrete is made. The one exception to this is limestone fines. Cement companies are rapidly embracing use of ASTM C595 Type IL cements with up to 15% limestone fines blended in. Type IL cement production in the USA increased by 91% between 2012 and 2016 [17] and has continued to increase rapidly since then. The cement plant closest to the authors produces an excellent Type IL cement, and it is expected that in the near future Type IL cement will be the most common cement type produced.

The expanding availability of Type IL cement provides an opportunity to take advantage of the improved strength and durability properties found in limestone calcined clay cements (LC^3) from the formation of carboaluminate phases [18], while using the preferred method in North America of mixing the cementitious materials at the ready-mixed plant. This will also assist in the market transition of calcined clay. For example, an ASTM C618 Class N calcined clay could contain 95% calcined clay and 5% gypsum, used at a 25% cement replacement rate by mass. For use with Type IL cement, this combination of calcined clay—Type IL cement (CCIL) would give a similar material composition to 2-1 clay-to-limestone blended LC^3, as shown in Table 1.

Mortar compressive strength tests were performed according to ASTM C109 [19] for two different clays calcined at 850 °C in a benchtop electric furnace. Calcined clay 1 (CC1) had a kaolin content of 33%, and calcined clay 2 (CC2) had a kaolin clay content of 66%. Even without additional gypsum blended with the calcined clay, CC2 showed significant improvement of strength when used with a Type IL cement versus a Type I/II cement. CC1 did not have sufficient enough clay content to meet strength requirements. Current work is underway to determine appropriate methods for gypsum optimization for the calcined clay and its effects on strength and durability when optimized for one Type IL cement and used with another Type IL cement (Table 2).

Table 1 Example of CCIL composition

Material	(%)
Clinker	61.5
Limestone	10.5
Gypsum	4.25
Calcined clay	23.75

Table 2 CCIL mortar compressive strength

Materials	7-day hydration avg. strength (psi)	7-day percent of control strength (%)
Type IL	4600	
Type I/II	4650	
20% CC1, 80% Type IL	3380	73
20% CC1, 80% Type I/II	2680	58
20% CC2, 80% Type IL	5460	119
20% CC2, 80% Type I/II	3450	74

While some producers may eventually choose to use LC³ because of expected benefits of intergrinding and better sulfate balance, CCIL has some advantages over LC³ for the US market. These advantages can be summarized as follows:

- US market prefers blending at the ready-mixed plant. Ready-mixed producers are accustomed to blending materials and are familiar and comfortable with Type IL cement and metakaolin. Calcined clay has a long history of use in the construction of concrete structures with excellent field performance. Use of CCIL presents less product specification, adoption, and perception barriers.
- Customizable blends for the application. CCIL can be formulated to allow for the addition of fly ash for additional heat reduction or optimized for pumping. Applications with concerns about carbonation-related corrosion can be adjusted by decreasing slightly the calcined clay dosage to prevent complete portlandite consumption.
- Avoids any patent issues or royalties.
- Extends the distance calcined clay can be transported profitably. Transporting only 25% of the cementitious materials from the source reduces shipping costs considerably. Sufficient quality and quantities of kaolin clay may not be available near already existing plants. Mixing at the ready-mixed concrete plant could eliminate long-distance shipping from the mine to the cement plant and still allow for its use.

4   Conclusions

Calcined clay has a long history of use in concrete construction projects in the USA with excellent field performance. Its decline in use can be attributed mainly to lower-cost SCMs available, namely fly ash. As fly ash present and future availability becomes a concern, calcined clay presents a viable option in multiple geographical regions in the USA. Use of calcined clay, blended with gypsum, as an SCM blended with Type IL cement at the ready-mixed plant is proposed as a potential path for adoption. This calcined clay-Type IL cement strategy (CCIL) could speed adoption, provide flexibility in proportioning, avoid intellectual property issues, and reduce transportation issues.

References

1. Meissner, H.: Pozzolans used in mass concrete. In: Stanton, T., Blanks, R. (eds.) Symposium on Use of Pozzolanic Materials in Mortars and Concretes, pp. 16–30. ASTM International, West Conshohocken, PA (1950)
2. goldengate.org: Golden Gate Bridge Tower Rope Inspection April 2018, 26 Jul 2018

3. Stromberg, D.G.: Underwater Inspection of the Golden Gate Bridge: The Image of an Icon (2014) [Online]. Available: https://www.eiseverywhere.com/file_uploads/3837a86248438206715be8cb411669f1_9D_Stromberg.pdf. Accessed 13 Mar 2019

4. Elfert, R.J.: Bureau of reclamation experiences with fly ash and other pozzolans in concrete. In: Ash Utilization: Proceedings: Third International Ash Utilization Symposium, Pittsburgh, PA, pp. 80–93 (1973)

5. Davis, R.: A review of pozzolanic materials and their use in concretes. In: Stanton, T., Blanks, R. (eds.) Symposium on Use of Pozzolanic Materials in Mortars and Concretes, pp. 3–13. ASTM International, West Conshohocken, PA (1950)

6. Thomas, M.: Optimizing the Use of Fly Ash in Concrete, 24p. Portland Cement Association (2007)

7. ACI 232.1, Use of Raw or Processed Natural Pozzolans in Concrete, 33p. ACI International (2012)

8. Ramsburg, P., Neal, R.E.: The use of a natural pozzolan to enhance the properties of self-consolidating concrete. In: Conference Proceedings of the First North American Conference on the Design and Use of Self-Consolidating Concrete, pp. 401–405 (2002)

9. Barger, G., Hansen, E., Wood, M., Neary, T., Beech, D., Jaquier, D.: Production and use of calcined natural pozzolans in concrete. Cem. Concr. Aggreg. **23**(2), 73–80 (2001)

10. Malisch, W: Cement containing calcined shale and clay reduces concrete's chloride permeability. Concr. Constr. 2p (Oct 1998)

11. Gardner, K.H., Greenwood, S.: Beneficial Reuse of Coal Ash from Dominion Energy Coal Ash Sites Feasibility Assessment, 27p. University of New Hampshire (2017)

12. Rehana, S.J.: Where's the Fly Ash? Concr. Constr. (12 Nov 2015) [Online]. Available: https://www.concreteconstruction.net/producers/wheres-the-fly-ash_o. Accessed 14 Mar 2019

13. Rankin, S.: Despite glut of coal ash, U.S. is importing it from other countries. Lehigh Valley Business Cycle (23 Mar 2017) [Online]. Available https://www.mcall.com/business/energy/mc-despite-glut-of-coal-ash-u-s-is-importing-it-from-other-countries-20170323-story.html. Accessed 14 Mar 2019

14. SEAIR, Fly Ash Import Data and Price in USA (2019) [Online]. Available: https://www.seair.co.in/us-import/product-fly-ash.aspx. Accessed 14 Mar 2019]

15. Zayed, A., Shanahan, N., Sedaghat, A., Stetsko, Y.: Development of Calcined Clays as Pozzolanic Additions in Portland Cement Concrete Mixtures, FDOT Report BDV25-977-38, Final Report, 91p (2018)

16. PCA, 2016 U.S. Cement Industry Annual Yearbook, 62p. Portland Cement Association (2016)

17. Tennis, P.: Survey on US Production of Portland-Limestone Cements-2012 through 2016, 8p. Portland Cement Association, Skokie, IL (2017)

18. Zunino, F., Scrivener, K.: Reactivity and performance of limestone calcined-clay cement (LC^3) cured at low temperature. In: Martirena, F., Favier, A., Scrivener, K. (eds.) Calcined clays for sustainable concrete, vol. 16, pp. 514–520. Springer, Dordrecht, The Netherlands (2018)

19. ASTM C109, Test Method for Compressive Strength of Hydraulic Cement Mortars (Using 2-in. or [50-mm] Cube Specimens), 6p. ASTM International, West Conshohocken, PA (2016)

Limestone Calcined Clay Cement: Opportunities and Challenges

Shashank Bishnoi and Soumen Maity

Abstract Limestone calcined clay cement (LC^3) is being developed as a low-carbon alternative to conventional cements. The cement has the potential to reduce CO_2 emissions by up to 30%, at the same time, demonstrating a higher performance in many types of exposure conditions. Being a conservative industry, the introduction of a new cement is a challenging process with many technical, commercial, psychological and political hurdles. Additionally, it is understood that the solutions for the reduction of CO_2 emissions will be varied and will depend on various factors such as the availability of raw materials, the environmental conditions and the construction practices. It is, therefore, important to ensure that the engineering properties of concretes produced using any cement are well understood and that right type of cement is used for the right application. This article discusses the challenges that need to be overcome for the introduction of LC^3 and the applications where the cement is especially at an advantage or disadvantage.

Keywords Limestone calcined clay cement · Chloride · Carbonation · Economy · Workability

1 Introduction

Limestone calcined clay cement, or LC^3, has been developed as a low clinker alternative to conventional cements such as ordinary Portland cement (OPC) and Portland pozzolanic cements (PPC). Being a ternary cement that relies on the combined action of two supplementary cementitious materials (SCMs), calcined clay and limestone, the cement achieves similar mechanical properties as conventional cements despite the relatively lower clinker factor of 50% or less [1–3]. The cement also promises

S. Bishnoi (✉)
Department of Civil Engineering, Indian Institute of Technology Delhi, New Delhi 110016, India
e-mail: bishnoi@iitd.ac.in

S. Maity
Development Alternatives, Tara Crescent, Qutub Institutional Area, B-32, New Delhi 110016, India
e-mail: smaity@devalt.org

to reduce CO_2 emissions by as much as 30% compared to OPC. More details on the performance and the development of the cement can be found elsewhere [4]. Still, the acceptance of a new cement faces many hurdles due to the relatively conservative nature of the construction industry. Given the high risks involved, the demonstration of the usability, strength and durability of any new cement is important before it can be used for construction. Additionally, since the market potential of any new product is difficult to establish beforehand, the large investments required to start producing a new product may be difficult to justify. This article discusses the opportunities offered by the development of LC^3 as a new cement and the challenges being faced for its introduction to the market.

2 Opportunities

2.1 *Technical Opportunities*

From the results that have been obtained this far, it is apparent that LC^3 offers many technical benefits over the conventional cements. First, it has been shown that LC^3 develops its strength faster and is less sensitive to poor curing. This can be advantageous not only in precast applications, but also in site concreting applications since the faster removal of formwork would reduce cost and increase construction speed. Additionally, reduced curing durations will help in reducing the consumption of water, which is becoming more and more a precious resource. The presence of limestone in LC^3 also helps in improving the cohesion of mixes, which is especially useful for the production of self-compacting concrete.

The lower alkalinity of the cement will also be beneficial in preventing alkali silica reaction and in the consumption of reactive aggregates, especially in areas where non-reactive aggregates are difficult to obtain. Due to the nature of the composition of the cement, the resistance to sulphate attack also increases. The reduced permeability and sorptivity of concrete using LC^3 also make the cement suitable for use in foundations and locations that are susceptible to capillary rise of water from the ground. The lower heat of hydration of the cement, compared to OPC, also makes it suitable for application to mass concretes.

Perhaps the most important strength of LC^3 is that it offers a four-component system, which can be engineered to obtain different types of cements. For example, the gypsum content in the cement and the kaolinite content in the clay can be used to control the setting time and early strength development of concrete, making it suitable for application to repair applications. The calcined clay to limestone ratio and the clinker content can also be modified to control the heat of hydration.

2.2 Commercial Opportunities

Apart from various technical opportunities, LC^3 offers a variety of economic opportunities for the production of cement and concrete. The first opportunity comes from the quality of raw materials to be used. The clay that is calcined for blending in LC^3 contains around 50% to 60% kaolinite and is of a quality that cannot be used for other applications such as for the production of ceramics, paints, etc. It has been shown that pure clays that are used for such applications are less suitable in terms of workability and reactivity of LC^3 [4]. Additionally, clays with iron contents that are too high to allow the use of the clay in such applications can also be used in LC^3. The clays used in LC^3 should not be confused with fertile or agricultural soils. Given the requirements in composition, fertile agricultural soils cannot be used for the production of LC^3. Clays that are suitable for LC^3 are known to be present in large quantities, either as rejects from mines that produce purer kaolinitic or china clays, or around the areas where such pure clays are mined. This offers a unique opportunity for the consumption of such clays and the reduction of mine wastes.

The limestone that is grounded into LC^3 also offers an interesting economic opportunity for the consumption of limestones that have too low calcium content for the production of clinker or other applications. It has been shown that since the reactivity of carbonates in LC^3 is relatively low, lower grade limestones are also suitable [4]. It has also been shown that impurities such as quartz and clay minerals in the limestone do not negatively impact the performance of the cement. What is, perhaps, the most interesting opportunity for the cement industry is that limestones containing dolomite, which cause unsoundness in cements, and even pure dolomite, can be used in LC^3. Since limestone which is blended or grounded into LC^3 is not calcined, any dolomite present in it is not converted to periclase, which is known to react slowly and expand, causing unsoundness. In fact, studies have shown that LC^3 blends containing dolomite may be more robust under various conditions [5, 6]. LC^3, therefore, provides a unique opportunity for the consumption of rejected limestones from the mines of the cement companies.

Apart from the opportunity to utilise lower grade materials, LC^3 also offers the opportunity to reduce clinker content at locations where other suitable SCMs are either not available or are very expensive. Even in a country like India that has an overall abundance of fly ash, there are locations, such as in the north-east, that rely on fly ashes transported from several hundreds of km away, increasing their cost. The reduction of clinker factor achieved through the blending of limestone and calcined clay not only brings down the cost of the production of cement, but also allows a significant increase in the capacity of the cement plants with very small investment, without the need for installing new clinker production lines. This increase in capacity is advantageous even at locations where fly ash is available, since it is difficult to reduce clinker factors to levels possible with LC^3 by just using fly ash. A more detailed analysis of the factors that influence the relative cost of production of LC^3 can be found elsewhere.

Being different in performance from conventional cements, LC^3 also provides the opportunity to produce value-added cementitious products that can be used in niche markets. For example, the higher cohesion of the cement and its higher fineness may make it more suitable for plastering applications. It can also be used to produce lower cost binders for cement-based damp proof courses for brick walls. Given its high resistance to the flow of chlorides, the cement can be used for developing protective overlays for concretes exposed to marine conditions and groundwater.

The production of a blend of limestone and calcined clay as a pozzolanic material, also known as LC^2, for direct mixing in concrete also provides an opportunity for cement producers and ready-mixed concrete suppliers. LC^2 would provide concrete producers the flexibility to adjust the clinker content in concrete and would allow the production of specialised concretes depending on the application. The cost of production of concrete can also be reduced at locations where the supply of cement is difficult but suitable clays exist locally.

It can be seen from the above discussion that there are several commercial and technical opportunities that LC^3 offers.

3   Challenges

3.1   *Technical Challenges*

As is the case with any new product, there are many technical challenges that have to be overcome to allow the cement to be confidently used by engineers and the construction industry. The first challenge arises in the cement lacking a legacy of structures and experience that the conventional cements have. Although the relatively short life since the development of the cement has been significantly compensated by the vast research programme that has been implemented by a competent international research and application team, the results of accelerated durability tests are often not considered to be reliable by construction professionals. The first step in the acceptance of a new cement by the construction fraternity is the development of standards that permit its production and use. In the development and release of these standards, large committees of experts critically evaluate the performance of the cement and its suitability for use in structures. Confirmatory studies are often carried out by several research laboratories to validate results already available in the public domain. Although such testing work is important to ensure that the cement meets all technical requirements and the expectations of engineers, such work is often repetitive in nature, is costly and time consuming. Additionally, once the performance of the cement is established, it is difficult to obtain funding to repeat the same work in other laboratories. This is a major challenge that must be overcome by the cement industry, by making necessary investments so as to ensure timely and rigorous testing of the cement. However, given the absence of standards and the uncertainty involved in introducing new products in the market, such investments

may be difficult. Government and investment agencies must therefore play a role at this stage.

From the technical studies that are available of LC^3, it can be clearly seen that the cement is not without its demerits. The first obvious demerit of the cement is its higher water demand and the associated higher water-reducing admixture demand. This is due to the high surface area of clays and the adsorption of the admixture on this surface, reducing their efficacy. As much as twice the doses of admixtures required for OPC are required for similar mixture designs produced using LC^3. This must be overcome by carrying out better concrete mix designs and through the development of more suitable admixtures. Given the high surface area of LC^3 and the cohesion that it provides to concrete, a reduction in the fine aggregate content in concrete will reduce the water demand. This would require a change of the thumb rules that are often used in the design of concrete mixes. In the case of admixtures, it is understood that a significant quantity of admixtures is adsorbed on the internal surface of the clays. Development of larger molecules that cannot adsorb on these surfaces would significantly reduce admixture dosage. From this point of view, it is also important to ensure that clays with high purities are either not used in the production of LC^3 or are used with higher limestone to calcined clay ratios. Since the majority of the increased water or admixture demand is due to adsorption on metakaolin particles, the reduction of the quantity of metakaolin in cement will reduce this demand. It has also been shown that LC^3 blends containing lower metakaolin contents react more, especially at lower clinker factors [4].

LC^3 is known as a cement that emits lower quantities of CO_2 during its production. This also means that LC^3 has a lower capacity to bind CO_2 and, therefore, does not pose a significant barrier to the reduction of pH through the process of carbonation [7, 8]. This reduction in pH has been shown to be accompanied by a coarsening of the pore structure of the cement and a reduction in its resistivity [9]. Similar behaviour has been observed in most other cements as well that have a low calcium content due to their low clinker content. This implies that the steel reinforcement in concretes produced using these low clinker cements will be at a high risk of faster corrosion depending on the conditions to which the structure is exposed. Exterior reinforced concrete elements that are exposed to intermittent rain and indoor elements that may be exposed to seepage of water from natural or man-made sources would be especially susceptible to carbonation-induced corrosion. Special measures are required to be taken to prevent the ingress of moisture into such reinforced concrete elements. While research on the possible use of water-proofing compounds and protective overlays is ongoing, relatively expensive measures to prevent premature corrosion of such elements would be required.

Laboratory studies have shown that concretes produced using LC^3 and exposed to temperatures higher than 40 °C during the first 12–24 h of hydration are likely to develop lower strength in the long term due to the formation of hydration products that are known to be less space-filling. This has been seen to occur in both isothermal and semi-adiabatic curing conditions. This may lead to a significant structural risk, since although concrete mixture design is carried out at lower standard temperatures that range from 20 to 30 °C, the concrete in field may be exposed to significantly

higher temperatures depending on the climatic region and the casting conditions. Additionally, the coarsening of the microstructure while curing at higher temperatures would also reduce the durability of concrete. Although research on this subject is in a preliminary stage, it has been seen that LC^3 containing components with a certain composition may be more susceptible to a lower final strength development than others. Ensuring the right combination of materials to prevent a lower strength development in concrete is a challenge that must be overcome to allow a safe usage of the cement.

3.2   Commercial Challenges

The introduction of a new product to a market is always challenging. While one of the major strengths of LC^3 is that its use does not require special training and that it can be used almost in the same way as other conventional cements, it is also a challenge that the new cement will have to be marketed to consumers who are accustomed to conventional cements, without the opportunity to provide them additional training. Cost benefits are seen to be the most effective in inducing consumers to move to new products, and such cost benefits can only be provided in cases where the production cost of LC^3 is lower than the production cost of other cements.

One of the most important challenges for the production of LC^3 is locating, identifying and obtaining the rights to mine suitable clays. Since the composition of the clays that are the most suitable for use in LC^3 is significantly different from those used in most other applications, mapping of locations where they are available has not been carried out. Such a mapping is a large exercise where geologists collect samples from many locations on the surface and below using bore holes in order to determine the quality and the quantity of the minerals. This is an important hurdle for the production of LC^3 since significant investment is required in this process of prospecting, while the commercial suitability of production of LC^3 at a location can only be determined after the available quantities of suitable clays are established. Additionally, since these clays are significantly different from those usually sought by the cement industry, the geologists would require further training.

Although the cement industry is familiar with the technology required for the calcination of clays, the lower temperatures than those required for production of clinker and the difference in handling processes of the clays makes investment into new equipment necessary. Additionally, since the properties of the product, such as its hardness, fineness and cohesiveness, are different from the conventional cements, other handling equipment also requires modification. For example, ball mills that normally produce other cements would give larger throughputs of LC^3 due to the relatively softer nature of calcined clay and limestone. This would necessitate an increase in the capacity of the upstream and downstream handling systems. Given the lower temperature of calcination and the nature of the process, the options of using alternative fuels such as municipal solid wastes, rubber tires may not be available. Even the use of petcoke as a fuel, while keeping emissions within prescribed

environmental norms, may be difficult. It may be noted here that cement plant manufacturers are in the process of developing equipment that may help in reducing the cost of calcination and allowing the use of alternative fuels. Additionally, plants that adopt LC^3 may continue to produce the other varieties of cements that they currently produce and may require the construction of new cement storage silos. Being a ternary cement, the number of materials that would be required to be tested would increase, and additional staff and testing equipment may be required for this. The difference in the production process of the cement would also necessitate retraining of staff. The investments required in the addition and modification of equipment and the retaining of staff may pose an important hurdle to the adoption of the cement.

Market factors pose an important challenge to the adoption of the cement. Since properties of the cement, such as the fineness, feel and colour, are likely to be different from the other conventional cement, the conservative nature of the market may slow down the adoption of the cement by the users. Furthermore, given the risks involved in introducing a new product to the market, the cement companies may also prefer to take a conservative approach to marketing the cement, reducing the rate of return on the investment required for its production. Widespread marketing and user awareness programmes would be required to allow a faster adoption of the cement.

Currently, fly ash and blast furnace slag are the most widely used SCMs in cement. Both are by-products of other industries and are available at a low cost, without the need for much further processing before the addition to cement. The added costs of drying and calcining the clays reduce the commercial attractiveness of LC^3, compared to other cements where low clinker factors can be achieved using slag and fly ash. Additionally, since most cement plants are located near limestone deposits so as to reduce transportation costs, the additional costs of transporting the clays to the plant are also likely to pose a challenge. Setting up of grinding units at locations where suitable clays are available may be an interesting option in many cases. A more detailed analysis of the influence of transportation costs can be found elsewhere [10]. At locations where LC3 becomes a more commercially attractive option than other blended cements, the risk of increasing environmental pollution through a reduction in the consumption of fly ash is also important to consider for policy makers. This, however, is likely to be a temporary scenario as most economies would move to sources of power other than coal.

4 Conclusions

This article discusses the opportunities and challenges faced for the introduction of limestone calcined clay cement as a commercial product. It can be seen from the discussion that while the cement offers many technical and commercial opportunities for the cement and construction industry, there are challenges to be overcome for its introduction into the market. The environmental benefits offered by the production of LC^3 have been demonstrated widely, and it is imperative that these challenges be overcome as soon as possible to maximise the benefit from producing a more

environmentally friendly product. Since most of the challenges being faced by the cement are multifaceted in nature, researchers, consultants, policy makers and cement producers must work together to overcome these hurdles.

References

1. Antoni, M., Rossen, J., Martirena, F., Scrivener, K.: Cement substitution by a combination of metakaolin and limestone. Cem. Concr. Res. **42**, 1579–1589 (2012)
2. Bishnoi, S., Maity, S., Mallik, A., Joseph, S., Krishnan, S.: Pilot scale manufacture of limestone calcined clay cement: the Indian experience. Indian Concr. J. **88**(6), 22–28 (2014)
3. Emmanuel, A., Halder, P., Maity, S., Bishnoi, S.: Second pilot production of limestone calcined clay cement in India: the experience. Indian Concr. J. **90**, 57–64 (2016)
4. Krishnan, S., Emmanuel, A.C., Shah, V., Parashar, A., Mishra, G., Maity, S., Bishnoi, S.: Industrial production of limestone calcined clay cement (LC^3)—experience and insights. Green Mater. **7**, 15–27 (2018)
5. Krishnan, S., Bishnoi, S.: Understanding the hydration of dolomite in cementitious systems with reactive aluminosilicates such as calcined clay. Cem. Concr. Res. **108**, 116–128 (2018)
6. Krishnan, S., Kanaujia, S.K., Mithia, S., Bishnoi, S.: Hydration kinetics and mechanisms of carbonates from stone wastes in ternary blends with calcined clay. Constr. Build. Mater. **164**, 265–274 (2018)
7. Shah, V., Scrivener, K., Bhattacharjee, B., Bishnoi, S.: Changes in microstructure characteristics of cement paste on carbonation. Cem. Concr. Res. **109**, 184–197 (2018)
8. Shah, V., Bishnoi, S.: Carbonation resistance of cements containing supplementary cementitious materials and its relation to various parameters of concrete. Constr. Build. Mater. **178**, 219–232 (2018)
9. Shah, V., Bishnoi, S.: Analysis of pore-structure characteristics of carbonated low-clinker cements. Transp. Porous Media **124**, 861–881 (2018)
10. Joseph, S., Bishnoi, S., Maity, S.: An economic analysis of the production of limestone calcined clay cement in India. Indian Concr. J. **90**(11), 22–27 (2016)

LC^3 Cement Produced Using New Additives

S. K. Saxena, S. K. Wali and Mukesh Kumar

Abstract Portland cement is one of the most important binding materials in construction industry. It is manufactured at a very high temperature and thus consumes lot of energy. It consumes lot of good quality of limestone and at the same time it emits large quantity of CO_2 responsible for global warming. Number of measures is being made to reduce CO_2 emissions and decrease consumption of limestone and energy. One of the ways is to use waste natural materials like China clay, which is available many parts of India. Limestone calcined clay cement (LC^3) was produced on a pilot scale in a JK Lakshmi cement grinding unit (Jhajjar, Haryana, India). Due to high water consistency compare with OPC cement. JK Lakshmi cement had developed the improved version of LC^3 cement with low water consistency. LC^3 cement are being studied all over the world but some of problems persist. In this paper, we have studied the hydration and durability of improved version of LC^3 cement. Water consistency, setting times, non-evaporable water contents, compressive strength measurements, water percolation and X-ray diffraction studies were made to understand the hydration process.

Keywords Portland cement · LC^3 cement

1 Introduction

Manufacturing of Portland cement (OPC) is a resource exhausting, energy-intensive process and releases large amounts of the greenhouse gas (CO_2) into the atmosphere [1–3]. Greenhouse gases result in an increased temperature for the earth's troposphere. The intergovernmental panel on climatic change estimates that the average rise in temperature of the environment should reach between 1.9 and 5.3 °C in the next 100 years. The need to reduce the consumption of energy and the release of carbon dioxide increased the emphasis on the use of alternate raw materials like calcined clay waste mines reject for the production of LC^3 cement. LC^3 cement are the composition of Portland clinker, calcined clay, waste mines reject (JKLC-Sirohi)

S. K. Saxena (✉) · S. K. Wali · M. Kumar
JK Lakshmi Cement Ltd, Jhajjar, Haryana, India
e-mail: sksaxena@lc.jkmail.com

and gypsum. The LC^3 technology promises a suitable growth of economics around the world by reducing CO_2 emissions. Due to high water consistency compare with Indian OPC cement. JK Lakshmi cement had developed the improved version of LC^3 cement with low water consistency. LC^3 cement are being studied all over the world but some of problems persist. In this paper, we have studied the hydration and durability of improved version of LC^3 cement. Water consistency, setting times and compressive strength measurements were made to understand the hydration process.

2 Experiments

2.1 Materials

LC^3 and improved version (IV) LC^3 was taken from JK Lakshmi cement limited Haryana. The chemical compositions of LC^3 and IV-LC^3 are given in Table 1, respectively.

2.2 Methods

Determination of water consistency The water consistencies were determined with the help of Vicat apparatus (IS: 4031 part 4, 1988).

Determination of setting time Initial and final setting times were determined with the help of Vicat apparatus (IS: 4031 part 5, 1988).

Determination of heat of hydration 2 g each of LC^3 and improved version (LC^3) were mixed with 1 ml of water. Each vial was then vibrated for about 30 s and then placed into the calorimeter chamber immediately. The rate of heat evolution and total heat evolved were determined as a function of time.

Determination of compressive strength Mortar cubes were prepared in 7.5 × 7.5 × 7.5 cm 3 moulds and compressive strengths in presence of LC^3 and IV-LC^3 at different intervals of time were determined with the help of compressive strength testing machine.

Table 1 Chemical composition of IV-LC^3 and LC^3 (mass%)

Compounds	SiO_2	Al_2O_3	Fe_2O_3	CaO	MgO	K_2O	SO_3	Na_2O
IV-LC^3	33.25	14.47	4.31	39.64	2.71	0.47	2.12	0.41
LC^3	33.28	14.48	4.30	39.65	2.73	0.49	2.13	0.40

3 Results and Discussion

Water consistencies are given in Fig. 1. The results showed that improved version of LC^3 decrease the water consistency compare with LC^3. This indicated improved version LC^3 decreases the water requirement and as a result, compressive strength may increase.

Initial and final setting times are given in Fig. 2. The result showed that both the initial and final setting time is increased in the presence of IV-LC^3.

Hydration of LC^3 and IV-LC^3 is a complex and highly exothermic reaction. As soon as LC^3 and IV-LC^3 cement content comes in contact with water, a rapid heat evolution takes place. In the presence of LC^3 and IV-LC^3, the shape of the rate of heat evolution curve remained the same but the maxima shifted to longer time with higher rate of heat evolution. In the presence of IV-LC^3, hydrations were retarded to a considerable extent. Total heat evolved as a function of time is shown in Fig. 3.

Compressive strengths of IV-LC^3 increased with hydration time. This is as a result of increased amount of hydration products and decrease of porosity. The compressive strengths of LC^3 and IV-LC^3 were found to be comparable at all the times of hydration. However, IV-LC^3 gave highest compressive strengths at all times. This

Fig. 1 Water consistency of LC^3 and IV-LC^3
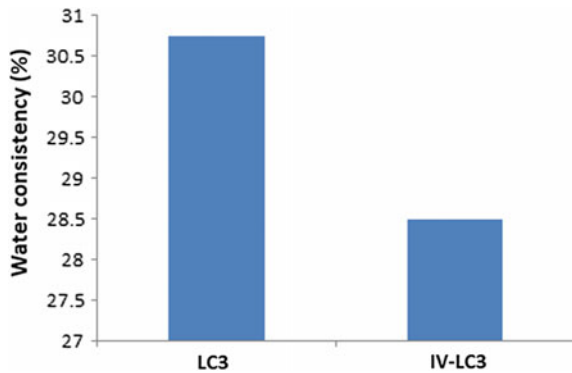
Fig. 2 Setting time of LC^3 and IV-LC^3
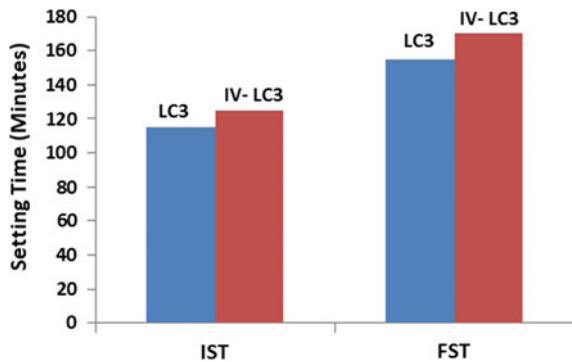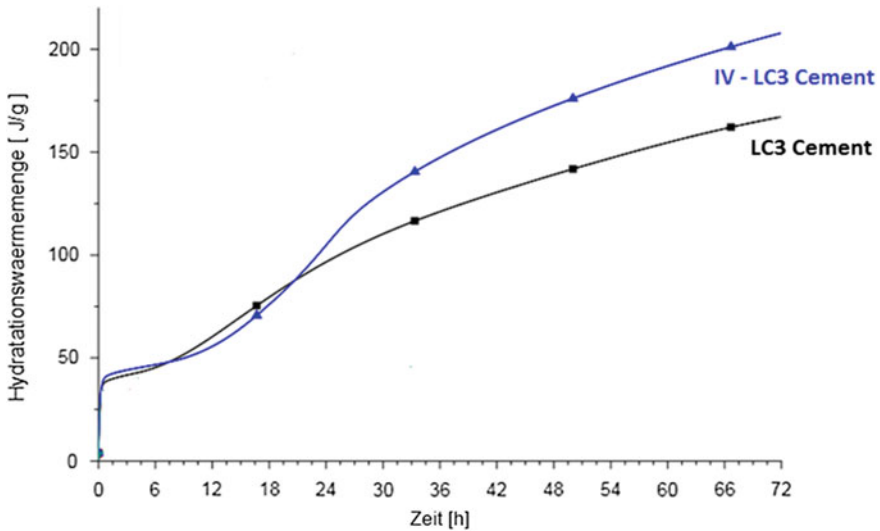
Fig. 3 Heat of hydration of LC^3 and IV-LC^3

Fig. 4 Compressive strength of LC^3 and IV-LC^3
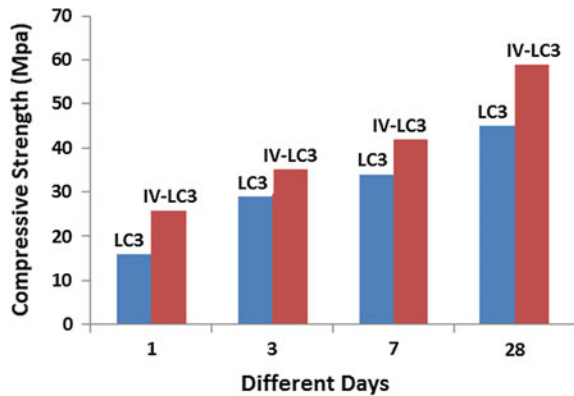
may be due to early pozzolanic reaction and forming larger amounts of C–S–H and reduction of water due to improved version of LC^3. As a result, the compressive strength is increased and shown in Fig. 4.

4   Conclusion

From the results, it is concluded that IV-LC^3 cement hydration were very compact with a dense structure. This reduced the pore size and pore size distribution. As a result, the compressive strength at all the times was higher.

References

1. Juenger, M.C.G., Siddique, R.: Recent advances in understanding the role of supplementary cementitious materials in concrete. Cem. Concr. Res. **78**, 71–80 (2015)
2. Saikia, N.J., Sengupta, P., Gogo, P.K., Borthakur, P.C.: Cementitious properties of metakaolin–normal portland cement mixture in the presence of petroleum effluent treatment plant sludge. Cem. Concr. Res. **32**, 1717–1724 (2002)
3. Siddique, R., Klaus, J.: Influence of metakaolin on the properties of mortar and concrete: a review. Appl. Clay Sci. **43**, 392–400 (2009)

Development of Green Additive for Cement and Concrete Industries

S. K. Wali, S. K. Saxena and Mukesh Kumar

Abstract New green additives are an innovative additive for concrete produced from widely available waste materials as a step towards sustainable infrastructure development. Being a versatile product it can be used as a direct additive during concrete production or as a partial clinker replacement. New green additives improve the properties of concrete by several simultaneous processes. The aluminosilicate of new green additives contributes in the pozzolanic reaction; smaller particle size of new green additives imparts filler effect providing extra sites for nucleation and growth of hydration products, the reaction of carbonates helps in improving efficiency.

Keywords OPC cement · PP+ additives

1 Introduction

The use of additives as cement supplementary materials in structural concrete is widely accepted by the construction industries in world [1]. Expenditure in construction and the growth of infrastructure are major indicators of the development of a nation. Rapid development in this sector faces crucial challenges in terms of economy and resources. Cement is one of the most expensive and resources and energy-intensive inputs to the construction sector [2]. Supplementary cementitious materials (SCMs) offer the most promising means of ensuring economical and resource-efficient construction. SCMs are materials that can partially replace cement and concrete, without a significant impact on its performance.

The usages of microfine materials like silica fume, metakaoline, rice husk ash, etc., are being used to obtain high strength concrete [3]. These micro materials work as pozzolanic materials. These materials fill up the inter particles spaces available between cement grains and react with $Ca(OH)_2$ produced during cement hydration process. Pozzolanic materials like fly ash, slag present in concrete react with $Ca(OH)_2$ and microfine materials work only as pore fillers.

S. K. Wali (✉) · S. K. Saxena · M. Kumar
JK Lakshmi Cement Ltd, Jhajjar, Haryana, India
e-mail: vvijay@jkmail.com

This paper presents the discussion on new developed green additives by JK Lakshmi Cement Ltd in the name of PP+ (Indian Patent Application No-201711019131 A, Published on 22/03/2019) for cement and concrete, which produced by using the waste materials from limestone mines. This invention provides a cost-effective green performance enhancing additive for cement, concrete, and mortar.

2 Experiments

2.1 Materials

Portland cement 43 grade (OPC) was obtained from JK Lakshmi Cement Ltd, Haryana, India. The oxide and mineral compositions of OPC 43 grade cement are given in Table 1. PP+ used for making the blended cement and particle size distribution is given in Fig. 1. Ennor sand were used from Tamil Nadu.

2.2 Experimental

Mix proportion of mortar using a different concentration of green cementing additives. The designs of mortars with OPC cement in that ratio of 1:3 (1 part cement and 3 part Ennor sand) are given in Table 2. Fixed W/C ratio was used during the cube casting. Different mixes of solid components were mixed in Hobart mixer for 1 min. Water was then added to the solid and mixing was done for 4 min. Control mix as MIX-1 were casted with ordinary Portland cement mortar and MIX-2, MIX-3, MIX-4 were casted with green cementing additives as replacement of 10, 15, and 20%.

Determination of heat of hydration. 2 g each of OPC and 10, 15, and 20% PP+ were mixed with 1 ml of water in different plastic vials. Each vial was then vibrated for about 30 s and then placed into the calorimeter chamber immediately. The rate of heat evolution and total heat evolved were determined as a function of time.

Determination of compressive strength. Compressive strength of cement mortars [OPC:sand—1:3] in the absence and presence of PP+ at different intervals of time were determined with the help of compressive strength testing machine.

Determination of water percolation by permeability apparatus. Following mixtures were mixed separately in order to have water/solid (w/c) ratio of 0.35.

 i.   140 g OPC + 700 g sand
 ii. 126 g OPC + 14 g PP+ + 700 g sand
 iii. 119 g OPC + 21 g PP+ + 700 g sand
 iv. 112 g OPC + 28 g PP+ + 700 g sand

Table 1 Chemical composition of ordinary Portland cement (OPC)

Constituents	SiO_2	Al_2O_3	Fe_2O_3	CaO	MgO	Na_2O	K_2O	SO_3	P_2O_5	L.O.I
OPC	20.50	5.05	2.99	62.0	2.07	0.48	0.09	2.40	–	3.10
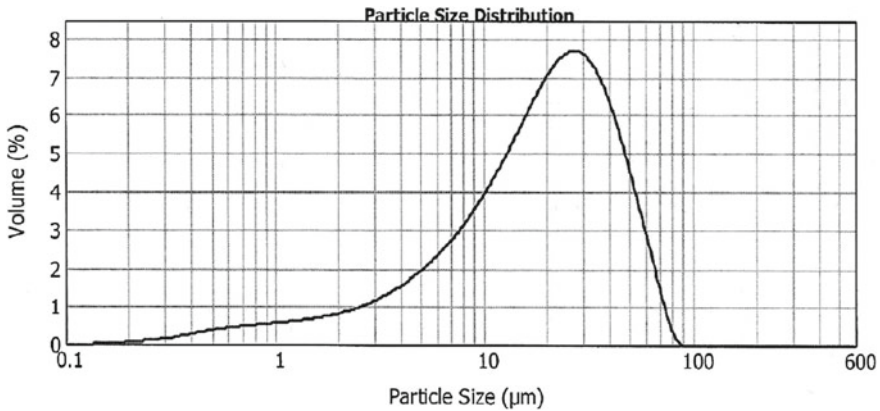
Fig. 1 Particle size of PP+

Table 2 Mix design of mortar using a different concentration of green cementing additive

Mix no.	MIX detail	Replacement PP+ green additives (%)	OPC 43 grade cement (kg)	Ennor sand (kg)	Water/cement ratio (%)	PP+ used (kg)
Mix-1	OPC	0	4.0	12	0.35	0.0
Mix-2	OPC+ PP+	10	3.6	12	0.35	0.4
Mix-3	OPC+ PP+	15	3.4	12	0.35	0.6
Mix-4	OPC+ PP+	20	3.2	12	0.35	0.8

The mortars were thoroughly mixed in Hobart mixer. Each mortar was placed in a mould as per IS 2645. After 24 h, the mortars were de moulded and immersed in water tanks separately for 20 days. The moulds were then fixed in a permeability apparatus where pressure of 2.0 kg/cm^2 was applied (pressure was slowly increased from 0.5 to 2.0 kg/cm^2). Water percolation was measured at every 1 h in terms of weight of percolated water for 8 h.

X-ray diffraction studies. Powder X-ray diffraction patterns were recorded with X-ray diffractogram using CuKα radiations.

3 Results and Discussion

Heat evolved during hydration as a function of time is illustrated in Fig. 2. It is clear that heat evolved increased with time and the value is maximum in the presence of green cementing additive (GCA) with 15% dosage. Green cementing additive
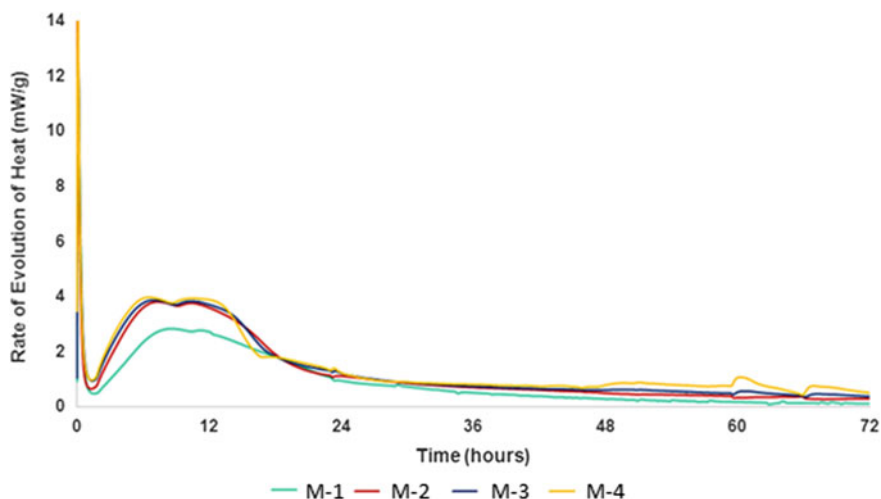
Fig. 2 Rate of heat evolution as a function of time

(GCA) powder having smaller size and crystalline in nature might be participating in hydration reaction, giving more heat and accelerating the process.

Mortars using by replacement of 10, 15, and 15% of green cementing additive (GCA) were made both with Ennor sand. The compressive strength is determined. Compressive strengths of green cementing additive mortars made from different dosages of green cementing additive and cured for 28 days at room temperature. The results showed that compressive strength increased with the increase of surface area of green cementing additive. Higher surface area means smaller particle size. Because of smaller size, the dissolution of green cementing additive in water was more, leading to the formation of a larger amount of C–S–H gel. This is responsible for higher compressive strength in the mortar (Table 3; Figs. 3 and 4).

The different mineral phases within the cement hydrate with different rates forming various reaction products. Some products deposit on the unreacted cement particle surfaces (surface products) while others form as crystals in the water-filled pore space between cement particles (pore products). For simplicity, cement paste can be thought of as consisting of four phases: (i) unreacted cement, (ii) surface products (like C–S–H), (iii) pore products (like calcium hydroxide), and (iv) capillary

Table 3 Compressive strength for various mixes

Detail	3 Days (In MPa)	7 Days (In MPa)	28 days (In MPa)
Mix-1	32.5	38.00	50.9
Mix-2	36.2	43.8	58.4
Mix-3	40.6	48.4	65.2
Mix-4	38.5	44.7	59.7
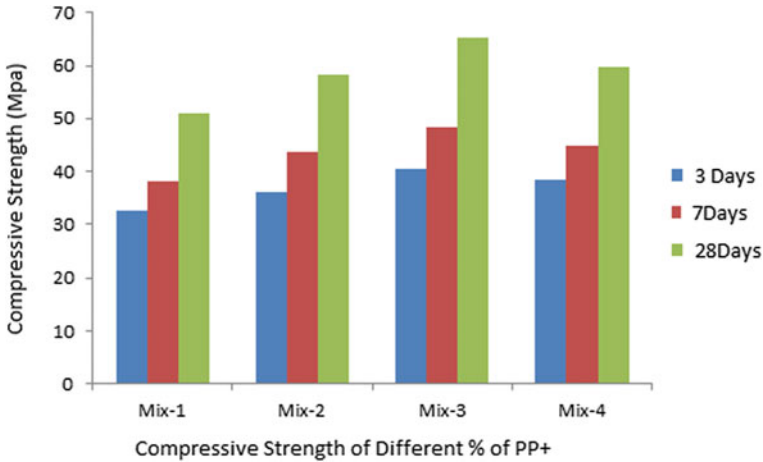
Fig. 3 Compressive strength of different mixes of PP+
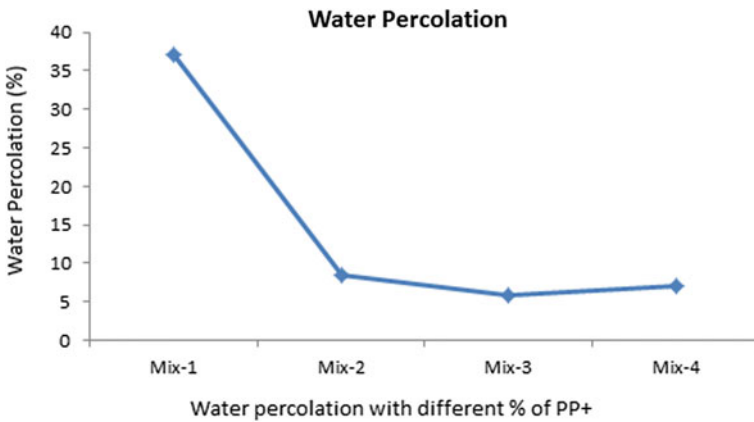
Fig. 4 Water percolations of different mixes

pore space. PP+ reduces CH and increases C–S–H. Surface products grow outward from the unreacted cement particles and contain connected (percolated) gel pores, while pore products are generally polycrystalline and fully dense, with no connected pores. The capillary pores are the water-filled space between solid phases and generally range from about 0.01 to 0.1 µm in size, in a reasonably well-hydrated cement paste, although during early hydration, they can range up to a few micrometres in size. These pores are responsible for water percolation in the mortar and concretes. The percent water percolation for mortars in the presence of PP+ is shown in Fig. 5. The presence of PP+ during hydration reduces the pore size, giving a dense structure. This is because of the formation of additional amount of C–S–H. The decrease in water percolation can be attributed to decrease in pore size. From Fig. 5, it is apparent
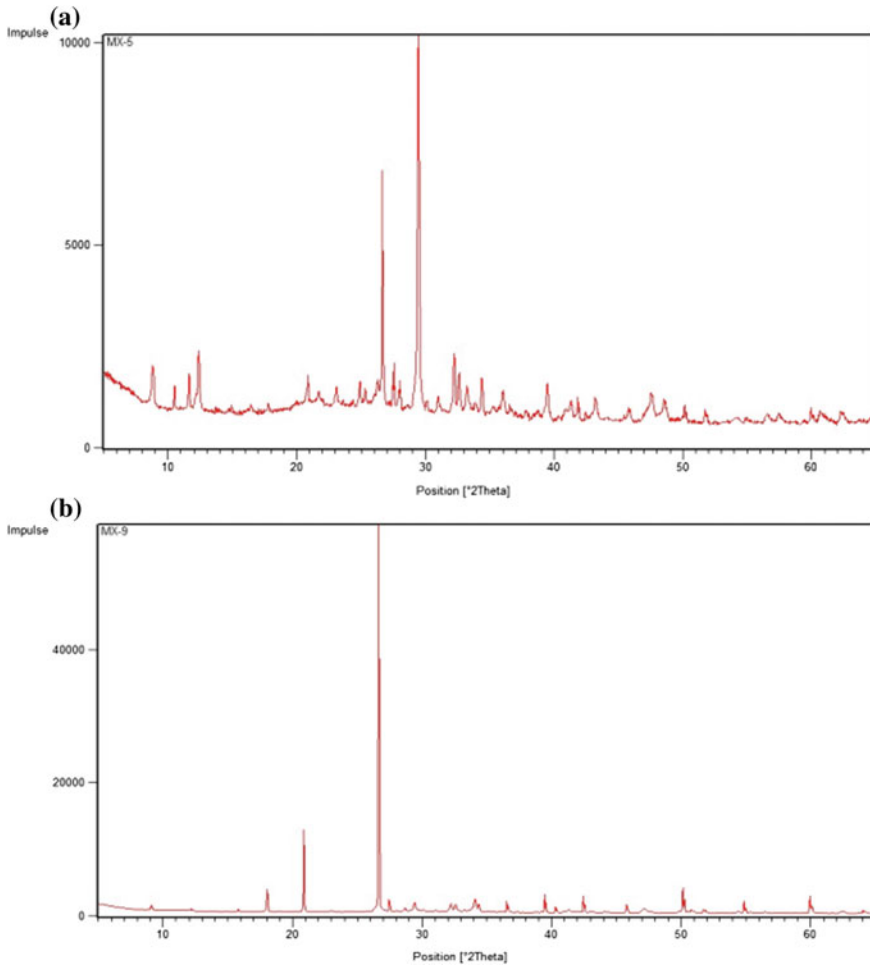
Fig. 5 **a** PP+ **b** OPC cement + PP+

that in the presence of PP+, the structure of hydration products is denser and as a result the water percolation is decreased.

Green cementing additive (PP+) hydrated with cement paste (OPC) were prepared and it is observed that the peaks of portlandite, mullite, as well as ettringite are clearly visible. Referring Fig. 5a, b clearly shows a number of crystalline phases due to quartz (Q) and kaolinite (K).

Green cementing additive (PP+) hydrated with OPC cement paste were prepared and cured at room temperature 27 ± 2 °C for 28 days were recorded. The SEM picture of green cementing additive (PP+) shows a comparatively compact structure with less porous, which increase the compressive strength with green cementing additive
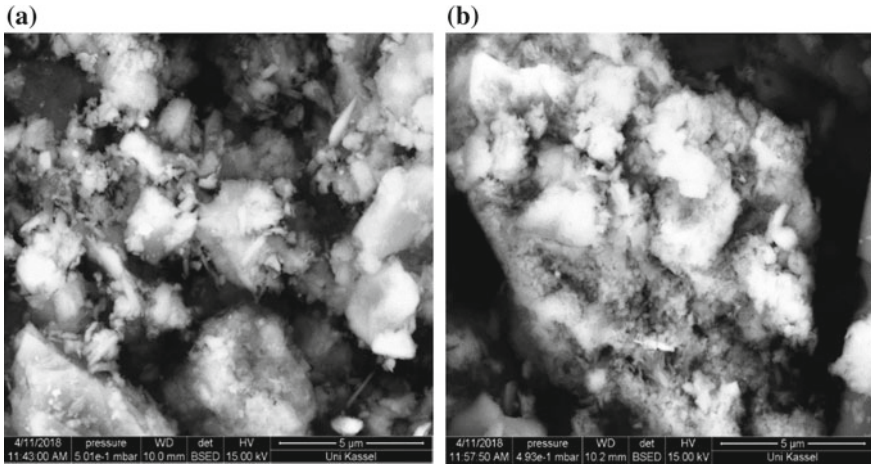
Fig. 6 **a** PP+ **b** OPC + PP+

(PP+). Referring Fig. 6a, b the SEM result shows the powder form of PP+ and hydrated PP+ clearly illustrates the good compact structure with reduced porosity.

4 Conclusions

PP+ materials will be a suitable and futuristic "green performance improver" for enhancement of performance of mortar and concrete, which has been developed by use of waste materials.

Their preliminary characteristic of this material ensure:

(a) PP+ replace the cement up to 15%.
(b) PP+ does not increase the water demand as other fine materials.
(c) Initial heat of hydration is higher in compare with OPC cement.
(d) Water percolation is less due packing density.

References

1. Khamchin Moghaddam, F., Sri Ravindrarajah, R., Sirivivatnan, V.: International Conference on Sustainable Structural Concrete, Properties of Metakaolin Concrete—A Review on School of Civil & Environmental Engineering, University of Technology Sydney, Australia (2015)
2. Ezema, I.C.: Sustainable Construction Technologies. Science Direct (2019)
3. Xu, W., Lo, T.Y., Wang, W., Ouyang, D., Wang, P., Xing, F.: Pozzolanic reactivity of silica fume and ground rice husk ash as reactive silica in a cementitious system: a comparative study. Materials (Basel) **9**(3), 146 (2016)

Use of Kaolin Clay as a Source of Silica in MgO–SiO$_2$ Binder

Vineet Shah and Allan Scott

Abstract Recent developments on the use of magnesium silicate (MgO–SiO$_2$) as a potential binder material have been promising. Brucite, produced from the hydration of magnesium oxide, reacts with amorphous silica to produce magnesium silicate hydrate (M-S-H). Currently, silica fume is used as the primary source of silica in the majority of research into the M-S-H binder system. With increasing emphasis on sustainable construction, the identification and use of practical silica sources on a global commercial scale are imperative. The use of calcined kaolinitic clays, as supplementary cementitious material, has been widely established in the Portland cement industry and can also be used in production of magnesium silicate-based binder. In this study, the feasibility of using calcined kaolinitic clay alongside magnesium oxide was investigated. The effect of clay on the mechanical properties and hydration characteristics of the binder system are reported.

Keywords Magnesium silicate hydrate · Metakaolin · Hydrotalcite

1 Introduction

MgO-based cements offer a promising alternative to Portland cement. The large reserves of magnesium minerals and the possibility of lower extraction costs make it an exciting future option [1, 2]. Recent developments on the use of magnesium silicate (MgO–SiO$_2$) as a potential binder material have been promising [3–5]. Brucite produced from hydration of magnesium oxide reacts with amorphous silica to produce magnesium silicate hydrate (M-S-H). Currently, silica fume or microsilica is used as the primary source of silica in the binder system [3, 6]. However, due to limited availability and relatively higher cost of the silica sources, MgO–SiO$_2$ binders will remain a niche cement until a more economical silica is found.

The use of kaolinitic clays, as supplementary cementitious material, has been extensively established in the cement industry [7–9]. Such clays are widely available

V. Shah (✉) · A. Scott
Department of Civil and Natural Resources Engineering, University of Canterbury, Christchurch, New Zealand
e-mail: vineet.shah9@gmail.com

in regions where the demand for cement is most likely to increase in the coming decades [10]. Clay can be also used as an alternative source of silica in MgO–SiO$_2$ binder due to its amorphous silica content and low environmental impact. Along with reactive silica, clay consists of significant amount of reactive alumina, which has a potential to react with magnesium oxide.

The main objective of this research is to investigate the feasibility of using calcined kaolinitic clay in the MgO–SiO$_2$ binder system in terms of hydration characteristics and mechanical properties.

2   Materials and Methodology

Light-burnt MgO was obtained from Calix Ltd., Australia. Clay (CC) with kaolinite content of approximately 40% was obtained from Canterbury region, NZ. The clay was calcined in a static furnace at a temperature of 800 °C for 2 h. Commercially available metakaolin (MK) was supplied from BASF NZ and with the silica fume (SF) and superplasticizer from Sika NZ. River sand was used as fine aggregate.

The MgO: silica source ratio was kept fixed at 1.5 for all the blends. Mortar samples were prepared at a water to cement ratio of 0.4 by mixing binder and sand in the ratio of 1:1. 3% superplasticizer by weight of binder was mixed with water to improve the workability of the mix. Cubes of $50 \times 50 \times 50$ mm and cylinders of diameter 50 mm and height 100 mm were cast using mortar. After casting, the samples were covered and left in the mould for 24 h at 20 °C and 60% relative humidity. Thereafter, the samples were cured in water at 20 °C until the age of testing. Paste samples were cast in plastic moulds at the water to cement ratio of 0.4 and were subsequently demoulded and cured under water after 24 h.

The compressive strength was measured on cube specimens at various ages. The cylindrical specimens were cut into discs having thickness of 30 mm. Porosity measurements were done on the disc samples. Thermogravimetric analysis (TGA) was carried out on paste samples.

3   Results and Discussion

3.1   TGA

Figure 1 shows the differential TGA curve of 7 days hydrated sample. The peak weight loss in the temperature range of 400–450 °C corresponds to decomposition of magnesium hydroxide formed on hydration of magnesium oxide. Irrespective of silica source, a definite decomposition peak of brucite is observed. However, in CC and MK blends, an additional decomposition peak is observed right before 400 °C. This peak may correspond with the decomposition of hydrotalcite [11], formed by the
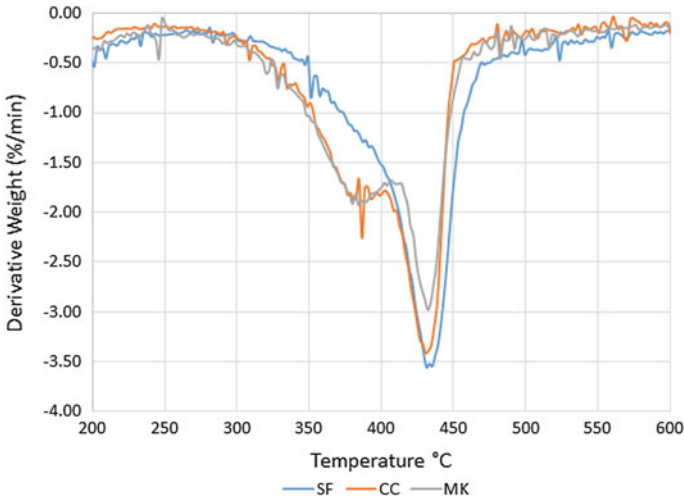
Fig. 1 Differential thermogravimetric curve of 7 days hydrated paste samples

reaction of alumina present in clay/metakaolin with magnesium. Scrivener et. al. [12] also reported decomposition of a peak around 400 °C corresponding to hydrotalcite.

3.2 Compressive Strength

The compressive strength was measured after 3, 7, 28 and 90 days of hydration as shown in Fig. 2 for the SF, CC and MK blends. An increase in strength is observed as hydration progresses. The 90 days compressive strength of SF and MK blends is similar. However, rate of strength gain was faster for the MK blend. This could be due to participation of alumina in the hydration reaction. The lower compressive strength

Fig. 2 Compressive strength at different ages for SF, CC and MK blends
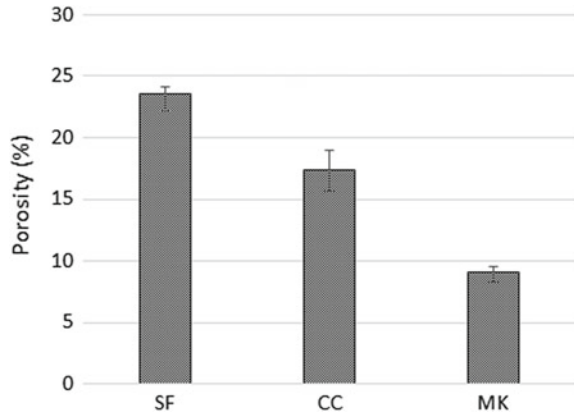
of CC blend is attributed to the overall lower content of reactive silica compared to SF or MK.

3.3 Porosity

The porosity of mortar samples was measured in accordance with ASTMC642 [13]. Vacuum saturation technique was used to saturate the samples. Figure 3 shows the 90 days porosity of all the three blends. Although the compressive strength of SF and MK blends was similar, the porosity for MK blend was 150% lower than the SF samples. Similarly, the porosity of CC blend was 50% lower than SF blend despite having a lower compressive strength. The lower porosity of CC and MK blends could be attributed to the formation of hydrotalcite, which is voluminous in nature. The higher solid volume helps to more effectively fill the space and thereby reduce the overall porosity.

4 Conclusions

This study investigated the possibility of using kaolinitic clays as a source of silica in the MgO–SiO$_2$ binder system. Compressive strengths similar to MgO-Silica fume blend were obtained on using clay. The reactivity of clay significantly affected the strength development of the mix. A substantial reduction in porosity was observed using clay compared to silica fume. The reduction in porosity was due to an additional reaction of alumina, present in clay, with the magnesium to form hydrotalcite which was absent in silica fume systems.

To ascertain the conclusions claimed, a further study investigating the microstructure characteristics and the products formed in MgO-Kaolinite system using scanning electron microscopy and X-ray diffraction is underway.

References

1. Walling, S.A., Provis, J.L.: Magnesia-based cements: a journey of 150 years, and cements for the future? Chem. Rev. **116**, 4170–4204 (2016). https://doi.org/10.1021/acs.chemrev.5b00463
2. Tonelli, M., Martini, F., Calucci, L., Fratini, E., Geppi, M., Ridi, F., Borsacchi, S., Baglioni, P.: Structural characterization of magnesium silicate hydrate: towards the design of eco-sustainable cements. Dalton Trans. **45**, 3294–3304 (2016). https://doi.org/10.1039/c5dt03545g
3. Tran, H.M., Scott, A.: Strength and workability of magnesium silicate hydrate binder systems. Constr. Build. Mater. **131**, 526–535 (2017). https://doi.org/10.1016/j.conbuildmat.2016.11.109
4. Sonat, C., Unluer, C.: Development of magnesium-silicate-hydrate (M-S-H) cement with rice husk ash. J. Clean. Prod. **211**, 787–803 (2019). https://doi.org/10.1016/j.jclepro.2018.11.246
5. Zhang, T., Vandeperre, L.J., Cheeseman, C.R.: Formation of magnesium silicate hydrate (M-S-H) cement pastes using sodium hexametaphosphate. Cem. Concr. Res. **65**, 8–14 (2014). https://doi.org/10.1016/j.cemconres.2014.07.001
6. Zhang, T.T., Du, Y.N., Sun, Y.J., He, Z.M., Wu, Z.L.: Development of magnesium-silicate-hydrate cement by pulverized fuel ash. Key Eng. Mater. **709**, 61–65 (2016). https://doi.org/10.4028/www.scientific.net/kem.709.61
7. Shah, V., Parashar, A., Mishra, G., Medepalli, S., Krishnan, S., Bishnoi, S.: Influence of cement replacement by limestone calcined clay pozzolan on the engineering properties of mortar and concrete. Adv. Cem. Res. 1–11 (2018)
8. Fernandez, R., Martirena, F., Scrivener, K.L.: The origin of the pozzolanic activity of calcined clay minerals: a comparison between kaolinite, illite and montmorillonite. Cem. Concr. Res. **41**, 113–122 (2011). https://doi.org/10.1016/j.cemconres.2010.09.013
9. Lopez, R.F.: Calcined clayey soils as a potential replacement for cement in developing countries, Ph.D. thesis. École Polytechnique Fédérale de Lausanne (2009)
10. Scrivener, K.L.: Options for the future of cement. Indian Concr. J. 11–21 (2014)
11. Ben Haha, M., Lothenbach, B., Le Saout, G., Winnefeld, F.: Influence of slag chemistry on the hydration of alkali-activated blast-furnace slag—part I: effect of MgO. Cem. Concr. Res. **42**, 74–83 (2012). https://doi.org/10.1016/j.cemconres.2011.08.005
12. Scrivener, K., Snellings, R., Lothenbach, B.: A Practical Guide to Microstructural Analysis of Cementitious Materials, First. Spon Press, Boca Raton (2016). https://doi.org/10.7693/wl20150205
13. ASTM C642-06: Standard test method for density, absorption, and voids in hardened concrete. Am. Soc. Test. Mater. 11–13 (2008). https://doi.org/10.1520/C0642-13.5

Fresh and Hardened Properties of Pastes and Concretes with LC³ and Its Economic Viability: Indian Ready Mix Industry Perspective

Pranav Desai and Amith Kalathingal

Abstract The study is focused on the evaluation of fresh and hardened properties of pastes and concrete with LC³. The plastic and hardened properties of LC³ are analyzed and compared with OPC 53. A comprehensive study is done on identifying the optimum admixture type for best LC³ paste fresh state properties and compared with OPC 53, PPC, PSC, OPC + 50% PFA (high-volume fly ash) and OPC + 70% GGBS (high-volume GGBS) pastes at varying water–binder ratios (w/b). Fresh and hardened properties of LC³ concretes are analyzed and compared with OPC, PPC, PSC, high-volume fly ash, and high-volume GGBS concrete. The concrete study is focused on achieving LC³ concrete fresh properties with regard to ready mix concrete industry requirements. The durability factors like resistance to chloride ion penetration, water permeability, and water absorption are studied on LC³ concrete and compared with OPC, PPC, PSC, high-volume fly ash and high-volume GGBS concrete. The study also compares material cost of M40 grade concrete in major Indian metro cities and arrives at a landed basic price for LC³ (in terms of percentage of OPC price) in these cities for commercial viability of LC³ use in Indian ready mix industry.

Keywords LC³ · Concrete properties · Durability · Ready mix industry · Cost

1 Introduction

The robust demand for cement in India aided by governments focus on infrastructure and housing for all is expected to enormously increase the per capita cement consumption in the country from the current 235 kg/person which will generate heavy stress on the usable raw material reserves in production of conventional OPC [1–3]. Even though a sustained approach of using other industry by or waste products like fly ash (PFA) and ground-granulated blast furnace slab (GGBS) in the form of PPC, PSC, and composite cement is undertaken in cement and concrete industry,

P. Desai (✉) · A. Kalathingal
Nuvoco Vistas Corp Ltd, Mumbai, India
e-mail: pranav.desai@nuvoco.in

an approach of utilizing unsuitable raw materials as per conventional cement production technology norms is rarely explored. Limestone calcined clay cement (LC^3) technology brings the potential of utilizing lower than cement grade limestone and widely available kaolinite clay at clinker factor as low as 40%, thus enhancing raw material sustainability and reducing CO_2 emission in the cement industry [4, 5].

The paper presents the results of the study on LC^3 and LC^3 concrete with a perspective of using the same in the Indian ready mix concrete industry. The laboratory data is used at arriving M40 grade concrete mixes with minimum binder with LC^3, OPC 53, OPC 53 + 25% PFA (PPC), OPC 53 + 50% PFA (high-volume fly ash), OPC 53 + 50% GGBS (PSC), and OPC 53 + 70% GGBS (high-volume GGBS) combinations, and the same is used for economic feasibility analysis of LC^3 concrete production from ready mix plants in major Indian cities of Delhi, Mumbai, Kolkata, Bengaluru, Ahmedabad, Chennai, and Hyderabad.

2 Experimental Program

2.1 Materials

Cement, fly ash, and GGBS

OPC 53 grade confirming to IS 269, LC^3 procured from Technology and Action for Rural Advancement (TARA) India, fly ash confirming to IS 3812, and GGBS confirming to IS 12089 are used throughout the study (Table 1). The OPC 53, LC^3, fly ash, and GGBS are stored in air tight containers during the entire duration of study.

LC^3 is prepared by TARA by blending 52% OPC 43 and 48% LC^2 (Tables 1 and 2). The LC^2 composed of 64% calcined clay, 32% raw limestone, and 4% gypsum (Tables 2 and 3).

Fine and Coarse Aggregates

Normal weight crushed stone sand (CSS), single-sized 10 mm and single-sized 20 mm conforming to IS 383 is used in the study (Table 4). Crushed stone sand is gaining prominence as preferred fine aggregate in the Indian ready mix concrete industry due to mining bans on river sand. Aggregates of the same lot are used in the entire duration of the study.

Chemical Admixtures

Polycarboxylate ether (PCE)-based non-retarding super-plasticizing admixture and retarding admixture is used in the study (Table 5). All admixture used complies with IS 9103. PCE with low solids and high solids are used in the study as PCE with low solids is gaining prominence as a replacement for sulphonated naphthalene formaldehyde (SNF) admixtures in the Indian ready mix industry.

Table 1 Physical properties of cements, fly ash, and GGBS

Cement type	OPC 53	LC³	OPC 43
Standard consistency (%)	29.0	35.3	29.3
Blaine fineness (m²/kg)	278	403	280
Initial setting time (minutes)	130	98	–
Final setting time (minutes)	215	128	–
Soundness—Le-Chatelier expansion (mm)	1	1	–
Loss on ignition, % by mass	2.52	9.16	–
Density (g/cc)	3.13	2.95	3.14
Compressive strength—3 days (MPa)	36.5	32.4	28.1
Compressive strength—7 days (MPa)	45.5	43.0	38.3
Compressive strength—28 days (MPa)	62.5	56.9	56.0
Pozzolana type		Fly Ash	GGBS
Blaine fineness (m²/kg)		335	480.1
45 micron retaining, % by mass		12.4	2.24
Soundness—autoclave expansion (%)		0.04	-1.08
Soundness—Le-Chatelier expansion (mm)		–	
Density (g/cc)		2.22	2.82
Compressive strength—28 days, % of control (MPa)		88.7	NA
Glass content. % by mass		NA	87.1

Table 2 Mixtures of basic materials for the production of LC² and LC³

LC³ composition, % by mass	
OPC 43	52
LC²	48
LC² composition, % by mass	
Calcined clay	64
Raw limestone	32
Gypsum	4

Water

Water complying with IS 456 section 5.4 is used for preparation of concrete and curing of specimens.

2.2 Study on Cement Admixture Compatibility

Marsh cone test is utilized to assess the compatibility and dosage of admixture with various combination of cement at varying w/b (Table 6). The marsh cone test gives

Table 3 Chemical composition and loss on ignition of LC^2 in comparison to calcined clay and limestone used in production of LC^2

Chemical composition of LC^2, calcined clay, and limestone			
Constituent, % by mass	LC^2	Calcined clay	Limestone
CaO	28.29	0.06	44.24
SiO^2	34.28	54.67	11.25
Al^2O^3	19.45	27.69	2.53
Fe^2O^3	3.43	4.93	1.55
MgO	1.38	0.13	1.96
SO^3	1.58	0.01	–
Na^2O	0.31	0.12	0.50
K^2O	0.27	0.25	0.28
TiO^2	1.63	1.68	–
Loss on ignition, % by mass	9.21	10.28	36.96

Table 4 Physical properties of fine and coarse aggregates

Property	Fine aggregate	Coarse aggregate	
	CSS	10 mm	20 mm
Physical properties			
Density (gm/cm^3)	2.79	2.76	2.84
Water absorption (%)	2.09	2.10	1.53
Bulk density loose (kg/m^3)	1800	1520	1540
Bulk density rodded (kg/m^3)	1980	1670	1640
Aggregate impact value (%)	–	16.8	11.8
Aggregate crushing value (%)	–	17.7	14.3
Combined flakiness and elongation index (%)	–	33.3	21.3
Particle size distribution			
IS sieve size (mm)	Percentage passing (%)		
40	100	100	100
20	100	100	94.2
12.5	100	100	15.8
10.0	100	88.1	2.7
4.75	97.1	4.2	0.4
2.36	73.4	0.8	–
1.18	58.7	–	–
0.6	38.6	–	–
0.3	26.3	–	–
0.15	14.0	–	–

Table 5 Properties of chemical admixtures

Admixture type	PCE—high solid	PCE—low solid	Retarder
Relative density at 25 °C	1.075	1.040	1.087
Solid content, % by mass	30.80	12.44	19.46
pH value at 25 °C	6.66	6.95	8.58
Chloride (Cl), % by mass	<0.01	<0.01	<0.01

fluidity of cement paste in terms of flow time with respect to incremental plasticizing admixture dosage; the data when plotted in a Marsh cone flow time curve helps in determining the saturation dosage of the plasticizing admixture [6].

It is observed that the LC^3 paste admixture saturation dosages are considerable higher than other paste saturation dosages. The fluidity measured as marsh cone flow time for LC^3 is comparable with other pastes at w/b of 0.50, but the LC^3 paste tends to exhibit lower fluidity at lower w/b of 0.38 and 0.32. The low- and high-solid PCE admixtures have not shown any significant difference in the behaviors of all paste combinations with respect to saturation dosage and fluidity at 0.50 w/b.

2.3 Study on Concrete

Concrete Mixes

Concrete mixes are designed as per IS 10262 for a volume of 1 m^3 (Table 7). All concrete mixes are designed considering high-rise pump ability with Nuvoco Vistas Corp Ltd industry experience.

Fresh concrete is prepared in batches of 0.050 m^3 in a central shaft-type laboratory mixer. Moisture corrections for all aggregates are done before concrete batching and added water corrected to maintain the design free water as in mix design. Cleaned and oiled, standard steel molds are used for specimen casting. The fresh concrete is casted in the molds as per recommendations of the test-specific code. Special care is taken to avoid any human error-induced segregation of concrete while casting. The specimens are demolded at 24 h and cured with complete immersion in water until testing.

Concrete Workability

Concrete workability is evaluated based on slump test as per IS 1199 method and slump flow test as per BS EN 12350-9 method (Table 8). The slump spread is measured as the diameter of concrete flow after the slump test.

Table 6 Mixture composition of pastes and marsh cone analysis summary

Cement classification	Binder composition	Water–binder ratio (w/b)							
		0.50	0.50	0.38	0.32	0.50	0.50	0.38	0.32
		PCE solid type				PCE solid type			
		Low	High			Low	High		
		Admixture saturation point — PCE dosage (%)				Paste fluidity as marsh cone flow time (s)			
OPC	100% OPC53	0.6	0.7	0.7	1.0	32	32	42	54
PPC	75% OPC53 + 25% PFA	0.6	0.6	1.0	1.2	32	32	43	54
High-volume fly ash	50% OPC53 + 50% PFA	0.6	0.4	0.8	1.3	32	32	42	49
PSC	50% OPC53 + 50% GGBS	0.5	0.6	1.1	1.1	34	34	45	70
High-volume GGBS	30% OPC53 + 70% GGBS	0.7	0.6	0.9	1.0	35	34	48	57
LC^3	100% LC^3	1.9	1.8	1.6	1.8	34	33	50	82

Table 7 Concrete mix design

Mixes	w/b	Total binder	Admixture dosage, % of binder			Aggregate proportions, %		
			PCE		Retarder	10 mm	20 mm	Sand
			High solids	Low solids				
OPC	0.45	365	0.70		0.20	29	29	42
	0.41	400	1.00		0.20	29	29	42
PPC	0.36	440		1.40	0.20	30	25	45
	0.36	450		1.50	0.20	32	25	43
	0.32	500		1.40	0.20	32	25	43
	0.30	530	0.90		0.20	32	26	42
High-volume fly ash	0.33	500	0.70		0.20	28	28	44
	0.28	590	0.62		0.20	28	28	44
PSC	0.38	420		1.30	0.20	30	25	45
	0.38	420	0.90		0.20	29	24	47
	0.35	460		1.45	0.20	31	25	44
	0.30	540	0.90		0.20	31	25	44
High-volume GGBS	0.41	400	0.90		0.20	29	29	42
	0.34	490	0.65		0.20	28	28	44
	0.29	576	0.76		0.20	29	29	42
LC^3	0.41	400	1.50		0.20	29	29	42
	0.38	440	1.60		0.20	29	29	42
	0.32	516	1.50		0.20	29	29	42

It is observed that the LC^3 concrete demands the highest admixture dosage to achieve a pumpable concrete workability. The admixture demand for LC^3 concrete is relatively stable at all tested w/b. It is also observed that the slump and slump spread that could be achieved with LC^3 concrete are relatively lower than concretes with OPC 53, fly ash, and GGBS combinations even with high-solid PCE.

Concrete Compressive Strength

Compressive strength is tested as per IS 516 method. It is observed that M40 grade of concrete can be achieved at 400 kg/m^3 of LC^3 at w/b of 0.41 compared to 365 kg/m^3 of OPC at a w/b of 0.45, 450 kg/m^3 of PPC at a w/b of 0.36, 500 kg/m^3 of high-volume fly ash at a w/b of 0.33, 420 kg/m^3 of PSC at a w/b of 0.38, and 576 kg/m^3 of high-volume GGBS at a w/b of 0.29 (Table 9). The early age strength gain of M40 grade LC^3 concrete is observed to be better than M40 grade concrete with OPC, PPC, high-volume fly ash, PSC, and high-volume GGBS mixes.

It is also observed that M55 grade LC^3 concrete can be achieved with 516 kg/m^3 of LC^3 at a w/b of 0.32 compared to 530 kg/m^3 PPC at a w/b of 0.30 and 540 kg/m^3 PSC at a w/b of 0.30.

Table 8 Comparison of workability of concretes produced

Mixes	W/b	Total binder	Admixture dosage, % of binder		Retarder	Workability test method	Workability (mm)	Slump spread (mm)
			PCE					
			High solids	Low solids				
OPC	0.45	365	0.70		0.20	Slump test	180	310
	0.41	400	1.00		0.20	Slump test	210	510
PPC	0.36	440		1.40	0.20	Slump test	240	–
	0.36	450		1.50	0.20	Slump test	230	–
	0.32	500		1.40	0.20	Slump test	240	–
	0.30	530	0.90		0.20	Slump flow test	690	NA
High-volume fly ash	0.33	500	0.70		0.20	Slump test	240	510
	0.28	590	0.62		0.20	Slump test	210	460
PSC	0.38	420		1.30	0.20	Slump test	230	–
	0.38	420	0.90		0.20	Slump flow test	710	NA
	0.35	460		1.45	0.20	Slump test	240	–
	0.30	540	0.90		0.20	Slump flow test	730	NA
High-volume GGBS	0.41	400	0.90		0.20	Slump test	200	490
	0.34	490	0.65		0.20	Slump test	200	410
	0.29	576	0.76		0.20	Slump test	220	480
LC^3	0.41	400	1.50		0.20	Slump test	150	290
	0.38	440	1.60		0.20	Slump test	140	270
	0.32	516	1.50		0.20	Slump test	130	280

From 28 days to 56 days strength gain of LC^3 concrete is observed to marginally lower than OPC, high-volume fly ash and high-volume GGBS mixes.

Concrete Durability Properties

Electrical indication of concretes' ability to resist chloride ion penetration (RCPT), hardened concrete depth of water penetration under pressure (water permeability), and water absorption under submersion tests are performed as per ASTM C 1202, BS EN 12390-8, and BS 1881 Part 122, respectively.

It is observed that LC^3 concrete exhibits considerably higher resistance to chloride ion penetration even at 28 days of age (Table 10). RCPT values of less than 500 °C are achieved for LC^3 mixes with 0.38 and 0.32 w/b. LC^3 concrete did not exhibit a significant reduction in water permeability and water absorption compared OPC, PPC, high-volume fly ash, PSC, and high-volume GGBS mixes.

Table 9 Comparison of compressive strength of concretes produced and grade classification as per IS10262

Mixes	w/b	Total binder	Average cube compressive strength (MPa)					Strength gain 28–56 days, %	Attained grade as per IS 10262
			1 Day	3 Days	7 Days	28 Days	56 Days		
OPC	0.45	365	14.6	27.7	35.0	49.6	60.2	21.4	M40
	0.41	400	12.4	28.0	35.5	57.4	64.7	12.7	M45
PPC	0.36	440	–	–	27.1	44.7	–	–	M35
	0.36	450	–	–	33.1	52.2	–	–	M40
	0.32	500	–	–	36.7	56.6	–	–	M45
	0.30	530	–	–	47.3	66.6	–	–	M55
High-volume fly ash	0.33	500	12.7	24.4	31.2	52.0	56.8	9.2	M40
	0.28	590	13.1	27.7	31.3	54.8	68.8	25.6	M45
PSC	0.38	420	–	–	29.8	50.9	–	–	M40
	0.38	420	–	28.3	36.3	51.8	–	–	M40
	0.35	460	–	–	34.2	56.5	–	–	M45
	0.30	540	–	29.3	45.7	66.5	–	–	M55
High-volume GGBS	0.41	400	3.5	15.5	22.0	33.2	38.5	16.0	M25
	0.34	490	8.0	20.7	30.6	46.1	56.0	21.5	M35
	0.29	576	9.3	24.6	36.4	52.9	62.7	18.5	M40
LC³	0.41	400	12.3	32.8	42.9	53.3	56.2	5.4	M40
	0.38	440	15.7	34.9	49.5	58.0	63.5	9.5	M45
	0.32	516	18.3	38.8	53.0	65.4	66.1	1.1	M55

Table 10 Comparison of resistance to chloride ion penetration (RCPT), water permeability, and water absorption of concretes produced

Mixes	w/b	Total binder	Durability tests				
			RCPT (Coulomb)		Water permeability (mm)		Water absorption (%)
			28 Days	56 Days	28 Days	56 Days	28 Days
OPC	0.45	365	5030	–	6	–	2.7
	0.41	400	6139	3320	12	–	2.7
PPC	0.36	440	–	3835	–	6	–
	0.36	450	–	2097	–	13	–
	0.32	500	–	2521	–	6	–
	0.30	530	–	1327	–	12	–
High-volume fly ash	0.33	500	3068	–	5	–	2.1
	0.28	590	2254	–	4	–	1.6
PSC	0.38	420	–	2157	–	11	–
	0.38	420	–	1819	–	8	–
	0.35	460	–	1234	–	10	–
	0.30	540	–	907	–	7	–
High-volume GGBS	0.41	400	957	620	5	–	2.1
	0.34	490	792	–	5	–	1.3
	0.29	576	779	–	5	–	1.5
LC^3	0.41	400	708	383	8	–	1.6
	0.38	440	340	–	5	–	1.6
	0.32	516	324	–	4	–	1.7

3 LC^3 Concrete Economic Viability of Use: Indian Ready Mix Industry

M40 grade concrete mixes achieved with OPC, PPC, high-volume fly ash, PSC, high-volume GGBS, and LC^3 are used for economic viability analysis (Tables 7 and 9).

The relative costs of PPC, high-volume fly ash, PSC, high-volume GGBS, and LC^3 M40 concrete mix pastes are evaluated with respect to M40 OPC mix paste cost (Fig. 1). The relative cost analysis is carried out for major Indian cities of Mumbai, Delhi, Kolkata, Bengaluru, Ahmedabad, Chennai, and Hyderabad. The average basic price of OPC, fly ash, GGBS, and admixtures for paste cost calculations is extracted for the financial year 2018–2019 from Nuvoco Vistas Corp Ltd as procured to its concrete business at various cities included in the study.
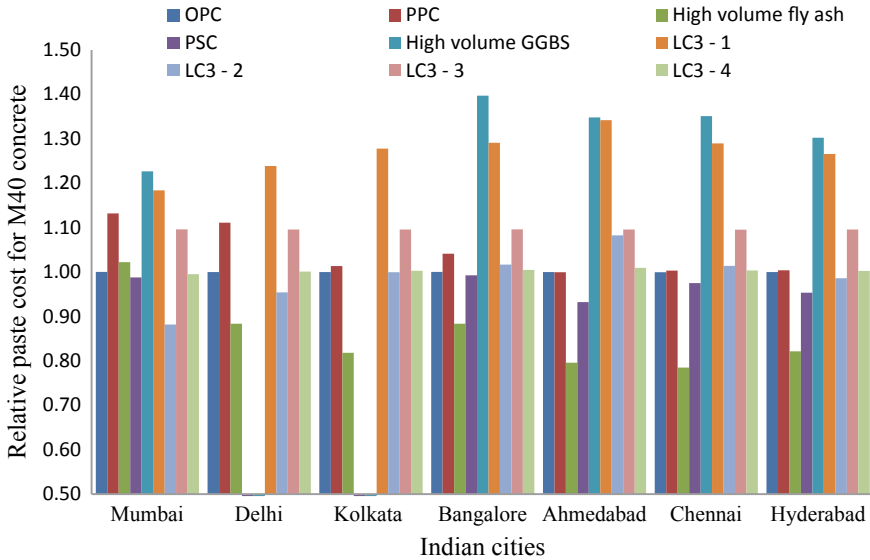
Fig. 1 Relative cost analysis of M40 concrete across Indian cities

It is observed that high-volume GGBS M40 mix is relatively the most expensive in all cities due to high binder content required to achieve the concrete grade, and high-volume fly ash M40 mix is the cheapest in all cities except Mumbai where PSC mix is the cheapest.

M40 concrete with LC^3, with LC^3 at the price of OPC (LC^3-1), is 18–34% more costly than OPC mixes and 20–55% more costly than the cheapest M40 grade mix in the given cities. M40 concrete with LC^3, with LC^3 at the price of 70% of OPC (LC^3-2), is relatively cheaper in cities of Mumbai, Delhi, and Hyderabad in comparison to OPC mixes and 7–23% more costly than the cheapest M40 grade mix in all given cities except Mumbai.

It is observed that the high admixture demand of LC^3 has hugely impacted the M40 concrete paste costing of LC^3 mixes; therefore, a costing is also arrived with LC^3 at the price of OPC with LC^3 admixture demand same as OPC (LC^3-3) and is observed that the cost impact of higher admixture demand of LC^3 is the range of 9–25% on LC^3 M40 mix across cities depending on the PCE cost in these cities. The impact of admixture cost is lowest in Mumbai and the highest in Ahmadabad. With LC^3 at the price of 90% OPC with LC^3 admixture demand same as OPC (LC^3-4), it is observed that the LC^3 mixes are costing same as OPC mixes.

4 Conclusion

From the study performed on pastes and concrete with LC^3, the following conclusions can be made:

1. LC^3 has compressive strength similar to OPC 53, the fineness and loss on ignition of LC^3 is considerable higher than OPC 53.
2. LC^3 pastes require considerably higher plasticizing admixture dosages to achieve saturation fluidity as assessed by marsh cone test.
3. LC^3 fluidity measured as marsh cone flow time at saturation dosage is comparable to OPC, PPC, and PSC at higher w/b of 0.50, but LC^3 paste tends to exhibit lower fluidity at lower w/b of 0.38 and 0.32.
4. M40 grade LC^3 concrete can be achieved with 400 kg/m^3 LC^3 at 0.41 w/b.
5. LC^3 concrete exhibits lower workability even at considerably high admixture dosages.
6. LC^3 concrete exhibits high resistance to chloride ion penetration.
7. LC^3 along with current plasticizing admixtures available in India is feasible to use in most cities through ready mix industry at a cost of 70% of OPC 53.
8. With development of plasticizing admixture compatible with LC^3 at the same dosage of OPC 53, LC^3 will be feasible to use in most cities of India through ready mix industry at a cost of 90% of OPC 53.

References

1. Commerce & Industry Minister Releases Compendium of Cement Industry. Press Information Bureau. Accessed 7 May 2019. http://pib.nic.in/newsite/PrintRelease.aspx?relid=188088
2. Business Opportunities in India: Investment Ideas, Industry Research, Reports | IBEF. Accessed 7 May 2019. https://www.ibef.org/download/cement-dec-2018.pdf
3. HOLTEC. Accessed 7 May 2019. http://www.holtecnet.com/holtecdocs/TechnicalPapers/p_2017_1.pdf
4. Bishnoi, S., Maity, S., Mallik, A., Joseph, S., Krishnan, S.: Pilot scale manufacture of limestone calcined clay cement: the Indian experience. Indian Concr. J. (July 2014)
5. Scrivener, K., Martirena, F., Bishnoi, S., Maity, S.: Calcined clay limestone cements (LC^3). Cem. Concr. Res. **114**, 49–56 (2018)
6. Jayasree, C., Gettu, R.: Experimental study of the flow behaviour of superplasticized cement paste. Mater. Struct. **41**(9), 1581–1593 (2008). https://doi.org/10.1617/s11527-008-9350-5

Reactivity of Clay Minerals in Intervention Mortars

S. Divya Rani, S. Mukil Prasath, Satvik Pratap Singh and Manu Santhanam

Abstract Historic lime binders were often modified by the addition of materials containing reactive silicates and aluminates. Roman builders utilized volcanic deposits from Pozzuoli near Naples, as the addition of this volcanic ash improved the performance of mortar. Pozzolans can be of natural or artificial origin; traditional artificial pozzolans were produced from natural materials, such as clay, after heat treatment. In India, pozzolan use was introduced by Mughals, and fired clay brick or '*surkh*i' was extensively used in medieval times to improve mortar consistency and strength. However, much attention may not have been given to the mineralogical composition and firing temperature of clay, which are critical in determining the pozzolanic activity. In the present study, three different types of clays—kaolinite, montmorillonite, and a sundried brick from the field—were fired to temperatures from 600 to 900 °C to assess pozzolanic activity. The clay crystal structures are disrupted, and an amorphous phase is produced by heating at a temperature range of 700–900 °C. The crushed sundried brick obtained from the field was not pozzolanically active at any of the temperatures. The maximum pozzolanic activity was obtained at 800 °C for the kaolinite and montmorillonite clays, and the fall of pozzolanic activity after this temperature can be attributed to the formation of new minerals such as mullite and hematite. These commercial clays can be used as pozzolans in intervention mortars if they are heated between 700 and 900 °C.

Keywords Pozzolanic reactivity · Lime mortar · Crushed brick · Historic binders · Intervention mortars

S. Divya Rani (✉) · M. Santhanam
Indian Institute of Technology Madras, Chennai, India

S. Mukil Prasath
National Institute of Technology Trichy, Trichy, Tamil Nadu, India

S. P. Singh
School of Technology, PDPU, Gandhinagar, Gujarat, India

1 Introduction

Lime mortar has been used as a popular binding material in historic buildings since ancient times. Roman builders utilized volcanic deposits from Pozzuoli near Naples, as the addition of this volcanic ash improved the performance of the mortar [1]. In certain parts of India, especially during the reign of Mughals in medieval times, there was a practice of adding crushed brick powder or '*surkhi*' as a pozzolana in lime mortar to ascertain hydraulic properties to the mortar. Usually, underburnt or overburnt bricks were crushed and added as brick dust or sometimes as pebbles of up to 40 mm size [1–3]. However, it is not known if the expected pozzolanic action was achieved from the brick dust or if it was just acting as a filler in the matrix. Characterization of the historic lime mortars of the Ganga canal system did not confirm the presence of hydraulic compounds or any evidence of pozzolanic action even though there is documentary evidence of adding brick dust during the preparation of the mortar [4]. The mortars obtained from Roman and Byzantine buildings revealed an increased strength and stiffness at the vicinity of the brick fragments as compared to the lime matrix, where crushed brick particles known as '*cocciopesto*' were used with lime binder [1, 5]. Even though the traditional builders used crushed brick, pottery, and fired clay tiles quite extensively in their mortars, it is unlikely that a scientific analysis of the pozzolanic activity would have been made before the preparation of the mortar. Mineralogical characteristics and firing temperature of clay are critical in determining the pozzolanic activity. The ability to bind calcium hydroxide in the presence of water in natural temperatures is determined by the amount of chemically active phases, and the intensity of this interaction depends upon the surface area and amorphous SiO_2 content of the pozzolans [6]. Clays containing silicates and aluminates as major phases are reported to be pozzolanically active around 500–1000 °C [7, 8]. In the present study, three different types of clays are analyzed to understand their mineralogical transformations with firing temperature and the subsequent effect on the pozzolanic activity so that they can be used in intervention mortars to repair the historic masonry.

2 Experimental Programme

For the experimental programme, three different types of clays, (i) a field soil, used for making clay bricks (obtained as sundried brick), and two commercially available clays, namely (ii) montmorillonite clay and (iii) kaolin clay were procured and fired at different temperatures of 600, 700, 800, and 900 °C, with a heating rate of around 10 °C/min. They were kept inside the furnace at the given temperature for 2 h and then allowed to naturally cool to ambient temperature. The fired clays were then pulverized to a size less than 75 µm.
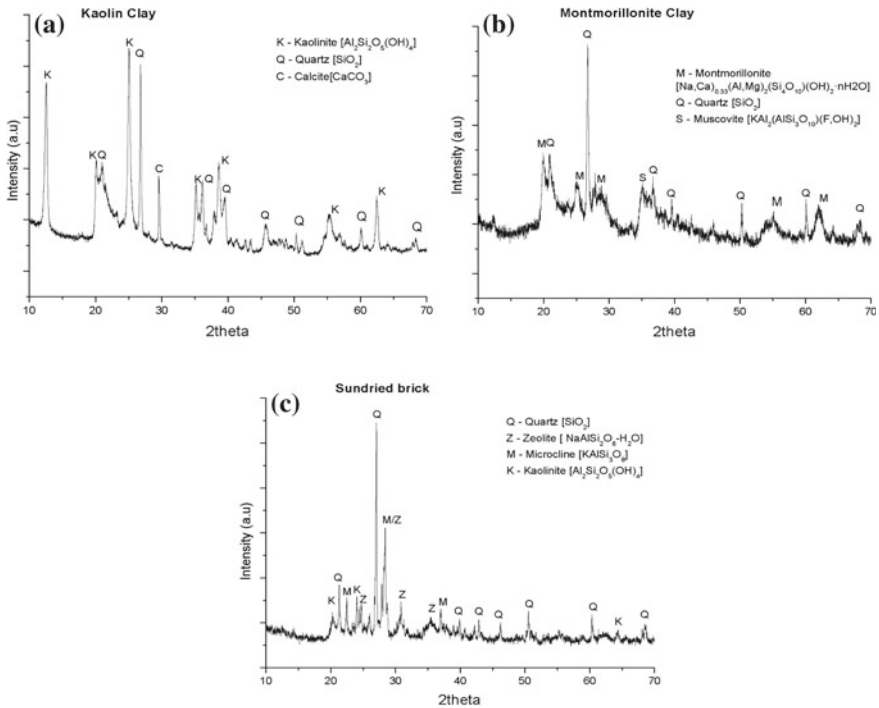
Fig. 1 Mineralogical composition of the raw clays

The mineralogical composition of the clay (presented in Fig. 1) was determined by X-ray diffraction at each of the temperatures. The diffraction data were collected using a PANalytical X'Pert PRO diffractometer with Cu-Kα radiation, 40 kV and 40 mA. A step size of 0.02° 2θ was chosen for a complete scan from 10° to 75° 2θ. The diffraction patterns were interpreted using X'Pert HighScore Plus 3.0 software by PANalytical, qualitatively matching the mineral profiles with standard database from International Centre for Diffraction Data (ICDD).

The pozzolanic activity was determined by conducting the lime reactivity test on 50-mm mortar cubes as specified in IS 1727 [9]. The amount of water was determined as that required to achieve a flow of 70 ± 5% with the flow table dropped for ten times in 6 s. The lime reactivity is expressed as the compressive strength after 8 days of curing at 50 °C and 90% RH, when tested at a loading rate of 35 kg/cm^2/min as per the guidelines.

3   Results and Discussion

3.1   Mineralogical Changes with Temperature

The change in composition of clay after heating at 600, 700, 800, and 900 °C for kaolin, montmorillonite, and sundried brick is shown in Figs. 2, 3, and 4, respectively. The loss of combined water in the structure of clay leads to the destruction of the crystal structure after heat treatment. The silica and alumina phases transform to an unstable amorphous state which is reactive and responsible for the pozzolanic action [7].

For kaolin clay, the crystalline structure is intact at 600 °C. The amorphous phases start forming at 700 °C, observed as a broad band between 20° and 30° 2θ at the expense of sharp crystalline peaks of kaolinite. The amorphous phases continue to exist at 800 and 900 °C, but the presence of less reactive mullite is observed at 900 °C. The dehydroxylation of the kaolinite and transformation to metakaolin at higher temperatures enhances the pozzolanic activity [10]. Quartz was not affected by heat treatment up to 900 °C, and the minor amount of calcite is completely decomposed by 900 °C.
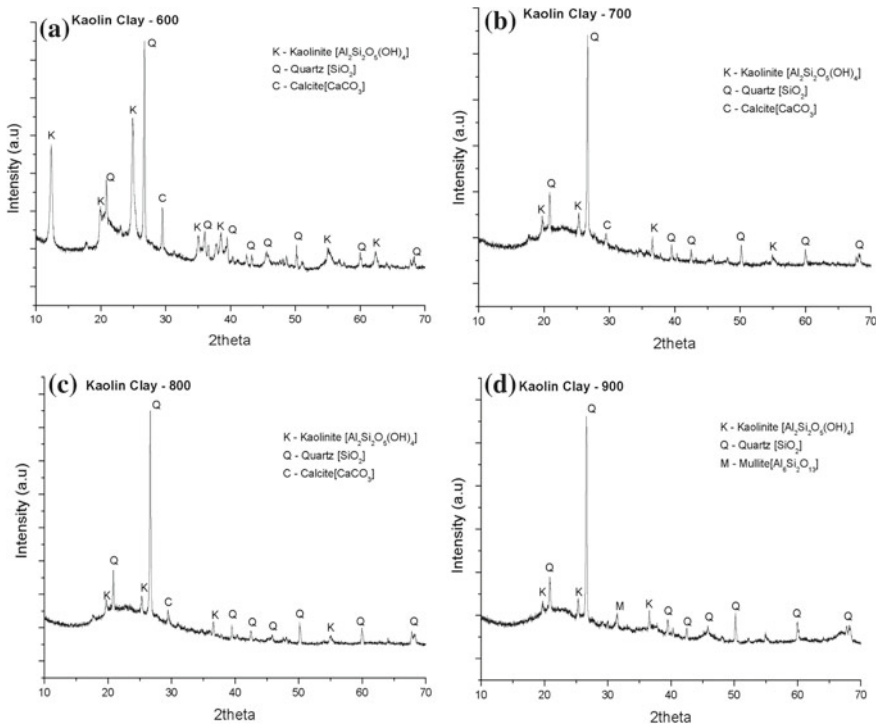

Fig. 2   a–d Mineralogical composition of kaolin clay with temperatures from 600 to 900 °C
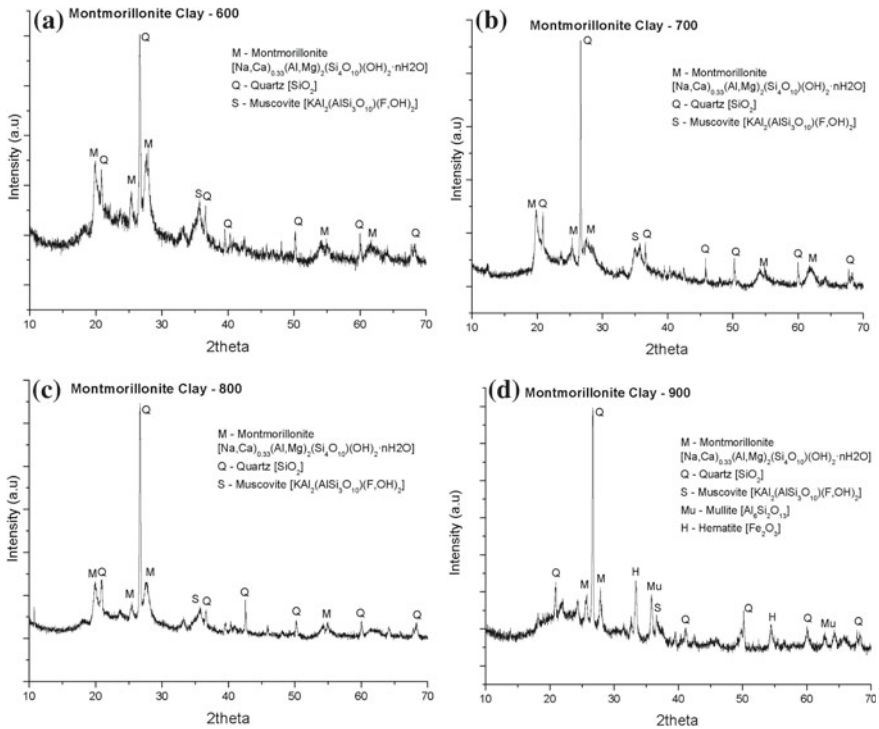
Fig. 3 **a–d** Mineralogical composition of montmorillonite clay with temperatures from 600 to 900 °C

For montmorillonite clay also, the crystalline structure is intact at 600 °C, and the amorphous phases start forming at 700 and 800 °C, which enhances pozzolanic activity; the presence of less reactive mullite and hematite [7, 8] is observed at 900 °C.

For the sundried brick, significant differences in the mineralogical composition could not be observed with an increase in temperature. The major composition is of crystalline quartz and microcline feldspar, which do not react with binders such as lime and cement. Minor amount of zeolite and kaolinite can be observed which transform with temperature. The kaolinite is completely transformed at 800 and 900 °C.

3.2 Pozzolanic Reactivity with Temperature

The specific gravity of lime used for the tests was 2.28, and that of sundried, montmorillonite, and kaolin clays were 2.09, 2.09, and 1.96, respectively. The specific gravities for all the heat treated clay samples were around 1.9–2.1. At 800 °C, the kaolin clay had a fineness (measured by Blaine air permeability) of about 563 m^2/kg,
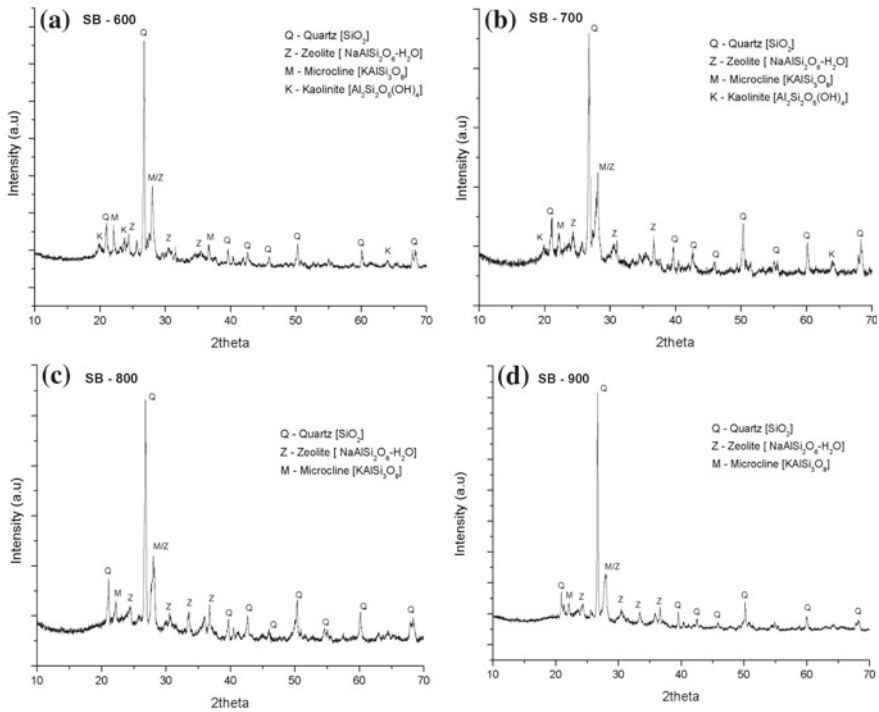
Fig. 4 a–d Mineralogical composition of sundried clay brick with temperatures from 600 to 900 °C

montmorillonite had a fineness of 333 m^2/kg, and sun dried brick was at a fineness of 148 m^2/kg. The pozzolanic reactivity of the clays was evaluated by the lime reactivity test and is represented as the compressive strength of the lime and pozzolan mortar (Fig. 5). Strength of the mixture is attained purely from pozzolanic activity between hydrated lime and brick dust. As per the guidelines, there should be a minimum of 4 MPa strength for the pozzolana to be considered as reactive.

The results show that the clay samples were not sufficiently reactive at 600 °C. At higher temperatures, the compressive strength increased for all the samples indicating an increase in pozzolanic activity. After 8 days curing in controlled temperature and humidity, compressive strengths of specimens from brick dust were less than 4 MPa at all the temperatures. These observations do not indicate sufficient pozzolanic activity between the lime and brick dust which can be attributed to the mineralogical composition of the field soil used for making the sundried brick. The major phases include less reactive quartz and microcline, whereas the reactive kaolin and zeolite phases are present in minor quantities. Kaolin and montmorillonite clays are reactive at 700–900 °C, and the higher reactivity of kaolin clay is attributed to the structure of the clay minerals and the higher surface area as compared to montmorillonite. Aluminosilicate minerals are stacked in two sheets in kaolinite clay, and two distinct interlayer surfaces with aluminate and silicate groups co-exist, linked with hydrogen
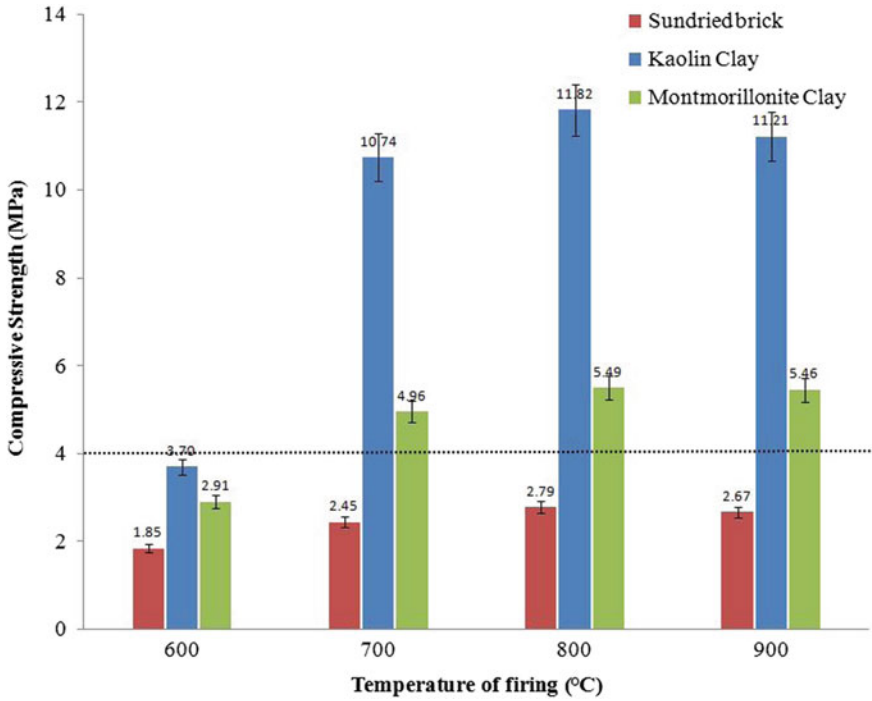
Fig. 5 Results from the lime reactivity test indicating the effect of temperature and clay mineralogy on their pozzolanic activity

bonding. The dehydroxilation process favors the exposure of Al groups at the surface of kaolinite clay, whereas montmorillonite seems to conserve the order of their structural layers, trapping Al groups between silicate tetrahedral, and hence are less able to react [11]. In both of these clays, the clay crystal structures are disrupted and an amorphous phase is produced by heating at a temperature range of 700–900 °C. The maximum pozzolanic activity was obtained at 800 °C, and the fall of pozzolanic activity after this temperature can be attributed to the formation of new minerals, mullite and hematite [7].

4 Conclusions

The paper discusses the pozzolanic reactivity of three types of clays with respect to their mineralogical composition and firing temperature. The results give valuable insights for the selection of pozzolanic materials for repair of historic masonry. The main conclusions drawn from the study are:

- The clay samples were not sufficiently pozzolanic at 600 °C
- The clay crystal structures are disrupted, and an unstable and reactive amorphous phase is produced by heating at a temperature range of 700–900 °C for kaolin and montmorillonite clays
- The brick dust produced originally from the field soil is not reactive at any of the temperatures. Hence, it is essential to identify the mineralogical composition of brick dust before its addition to an intervention mortar
- Kaolin and montmorillonite clays are reactive at 700–900 °C, and the higher reactivity of kaolin clay is due to the difference in crystal structure (exposure of reactive Al groups up on dehydroxylation) and higher surface area as compared to montmorillonite
- The maximum pozzolanic activity was obtained at 800 °C, and the fall of pozzolanic activity after this temperature can be attributed to the formation of new minerals, mullite and hematite.

References

1. Baronio, G., Binda, L., Lombardini, N.: The role of brick pebbles and dust in conglomerates based on hydrated lime and crushed bricks. Constr. Build. Mater. **11**(1), 33–40 (1997)
2. Hassan, M.Z.: Monuments of Delhi-Lasting Splendour of the Great Mughals and Others, 2nd edn. Om Books International, India (2008)
3. Bais, S., Santhanam, M., Rani, D.: Lime Manual for Conservation Works, 1st edn. National Centre for Safety of Heritage Structures, India (2018)
4. Dave, N.G., Malhotra, S.K.: Chemical composition of mortars from the Ganga canal system. Cement Concr. Compos. **14**, 235–238 (1992)
5. Nezerka, V., Nemecek, J., Slizkova, Z., Tesarek, P.: Investigation of crushed brick-matrix interface in lime-based ancient mortar by microscopy and nanoindentation. Cement Concr. Compos. **55**, 122–128 (2015)
6. Loganina, V.I., Simonov, E.E., Jezierski, W., Malaszkiewicz, D.: Application of activated diatomite for dry lime mixes. Constr. Build. Mater. **65**, 29–37 (2014)
7. Budak, M., Akkurt, S., Boke, H.: Evaluation of heat treated clay for potential use in intervention mortars. Appl. Clay Sci. **49**, 414–419 (2010)
8. Danner, T., Norden, G., Justnes, H.: Characterisation of calcined raw clays suitable as supplementary cementitious materials. Appl. Clay Sci. **162**, 391–402 (2018)
9. IS 1727-1967. Methods of test for pozzolanic materials. Bureau of Indian Standards, India (2004)
10. Danner, T., Justnes, H.: The influence of production parameters on pozzolanic reactivity of calcined clays. Nordic Concrete Research-Publ. No. NCR 59- 2(1), 1–12 (2018)
11. Fernandez, R., Martirena, F., Scrivener, K.L.: The origin of pozzolanic activity of calcined clay minerals: a comparison between kaolinite, illite and montmorillonite. Cem. Concr. Res. **41**, 113–122 (2011)

Performance of Limestone Calcined Clay Cement (LC³)-Based Lightweight Blocks

G. V. P. Bhagath Singh [ID] **and Karen Scrivener**

Abstract Current study explores the understanding of various parameters such as the role of aluminum powder dosage, water-to-binder ratio, and initial curing temperature on the production of lightweight blocks. Three different cementitious systems were used: limestone calcined clay cement (LC³), Portland pozzolana cement, and ordinary Portland cement. The aluminum powder dosage and the water-to-binder ratio clearly influence the hardened properties of blocks, whereas the initial curing temperature does not show much improvement to overall properties. Hardened properties such as dry density, compressive strength, and water absorption of blocks were evaluated. The required aluminum powder dosage varies from system to system, and it depends on the required density. To maintain lower density, OPC system required higher dosage of Al powder, and it showed lower strength compared to other systems. LC³-based lightweight blocks are produced with 3 MPa strength, and it showed good performance compared to other systems.

Keywords Light weight blocks · Limestone Calcined clay (LC³) · Portland Pozzolana Cement (PPC) · Ordinary Portland Cement (OPC) · Aluminum (Al) powder · Autoclave · Temperature

1 Introduction

In recent years, the utilization of lightweight concrete blocks in construction sector has increased significantly. Lightweight blocks also called as autoclaved aerated blocks are versatile material consisting of either Portland cement or blended cements with homogeneous pore structure created by air voids [1, 2]. Autoclaved aerated concrete (AAC) blocks show excellent sound and thermal insulation [3–5]. AAC blocks having high porosity result in a lower density and thermal conductivity compared to normal concrete [6]. Lightweight blocks bring few advantages to the construction

G. V. P. Bhagath Singh (✉) · K. Scrivener
Laboratory of Construction Materials, IMX, EPFL, 1015 Lausanne, Switzerland
e-mail: bhagath.gnagapatnam@epfl.ch

K. Scrivener
e-mail: karen.scrivener@epfl.ch

sector, such as quick and easy construction, improving housing affordability, and thermal insulating [2, 7].

Generally, AAC blocks will be produced using mechanical and chemical foaming methodologies by introducing air voids into the matrix. Typically, aluminum metal powder (chemical foaming) is used to produce lightweight blocks. The aeration level depends on the water-to-binder ratio and the aluminum powder dosage [8]. The fresh and hardened properties of blocks are dependent on the fineness of Al powder [9]. The strength was influenced by the size, shape, and formation of pores, age of sample, and method of curing process [10].

The current paper explores the development of LC^3-based lightweight blocks. Aluminum powder was used as a chemical agent to create the air voids in the system. Finally, LC^3 system performance was compared with other cementitious systems such as Portland pozzolana cement (PPC) and ordinary Portland cement (OPC).

2   Materials and Methods

PPC system consists of 30% siliceous fly ash (class F) and 70% OPC. LC^3-50 system with the typical composition as mentioned by previous authors was used [11]. The chemical composition of raw materials is shown in Table 1. The calcined clay contains 48% of kaolinite content. Commercially available aluminum power (<15 µm) was used as a chemical agent to generate air voids. The aluminum powder contains 99% metallic aluminum content.

Table 1 Chemical composition of raw materials (% by mass)

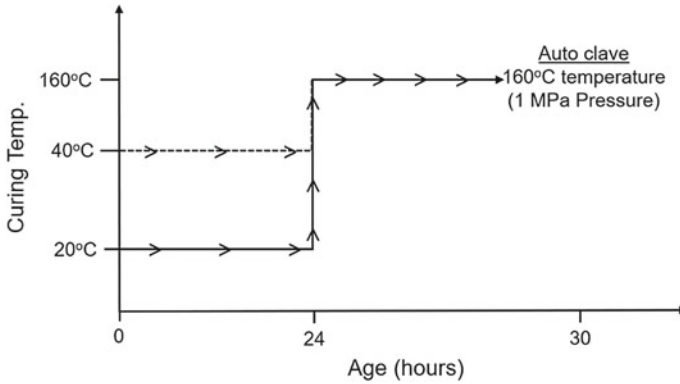| Composition	OPC	Calcined clay	Fly ash
SiO_2	19.27	49.74	50.54
Al_2O_3	5.65	41.78	24.70
Fe_2O_3	3.63	2.32	9.29
CaO	63.65	0.20	5.07
MgO	1.62	0.11	2.88
SO_3	3.16	0.04	0.71
Na_2O	0.15	0.26	1.05
K_2O	1.24	0.09	4.10
TiO_2	0.29	3.42	0.95
P_2O_5	0.19	0.09	0.00
Mn_2O_3	0.06	0.02	0.00
SrO	0.26	0.02	0.00
Cr_2O_3	0.02	0.03	0.00
LOI	0.75	1.85	0.71

Fig. 1 Schematic representation of curing conditions

2.1 Experimental Program

In all the systems, paste samples were prepared using two different water-to-binder (w/b) ratios: 0.40 and 0.60. The dry powder was mixed with the desired dosage of aluminum (Al) powder using paddle mixer for about 2 min to ensure the uniform distribution of Al powder; further mixing was done about 2 min after the addition of required water content. After the preparation of paste samples, samples were cured at initial curing temperature for 24 h. Two different initial curing temperatures (20 and 40 °C) were used in this study. Samples were demolded after 24 h further autoclaved it for 5 h at a temperature 160 °C. The detailed curing process is shown in Fig. 1. After the autoclave process, samples were removed from the autoclave chamber and allowed to cool down for 1 h. Finally, the hardened properties such as compressive strength, dry density, and water absorption (24 h) were determined on autoclave blocks.

3 Results and Discussion

3.1 Limestone Calcined Clay (LC³) Cement

Compressive strength

The influence of water-to-binder ratio and initial curing temperature on compressive strength development with Al powder dosage is shown in Fig. 2. The higher the Al powder content, the lower the strength. Besides, the higher the water-to-binder ratio, the lower the strength. The influence of temperature is not very significant on strength development.
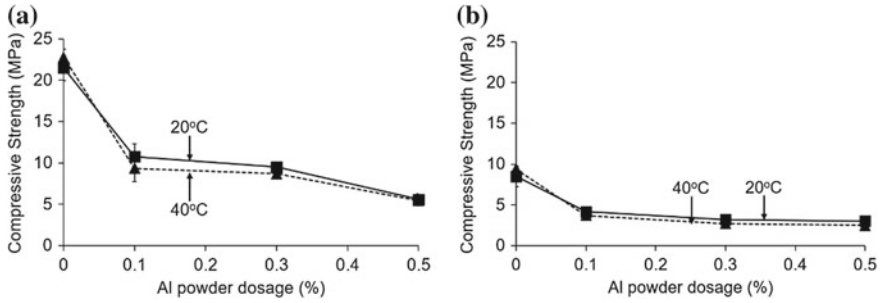
Fig. 2 Compressive strength variation with Al powder dosage. **a** w/b ratio 0.4 and **b** w/b ratio 0.6
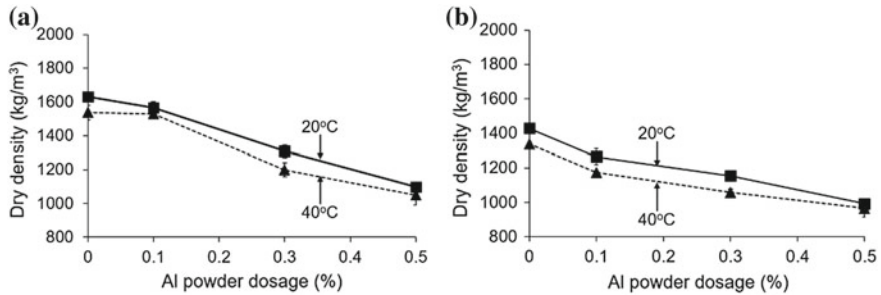

Fig. 3 Dry density variation with Al powder dosage at both the initial curing temperatures. **a** w/b ratio-0.4 and **b** w/b ratio-0.6

Dry density

The dry density variation with Al powder dosage at both water-to-binder ratio mixes is shown in Fig. 3. The role of initial curing temperature is also shown in the same figure. The effect of Al powder dosage clearly bought through dry density. The increase of the water content leads to a decrease of the dry density, as expected. Moreover, the higher the Al powder dosage, the lower the density. For constant Al powder dosage, higher the initial curing temperature, lower the density at both the water-to-binder ratio mixes.

Water absorption

The variation in water absorption of paste samples at both curing temperatures and water-to-binder ratio mixes is shown in Fig. 4. Water absorption content is increasing with the Al powder dosage. Initial curing temperature at 40 °C is slightly higher in the water absorption compared to initial curing temperature at 20 °C. The higher water-to-binder ratio shows higher water absorption at any Al powder dosage.
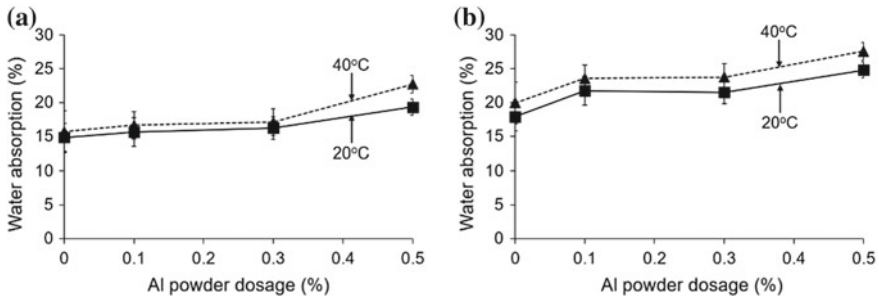
Fig. 4 Water absorption variation with Al powder dosage at both the initial curing temperatures. **a** w/b ratio-0.4 and **b** w/b ratio-0.6
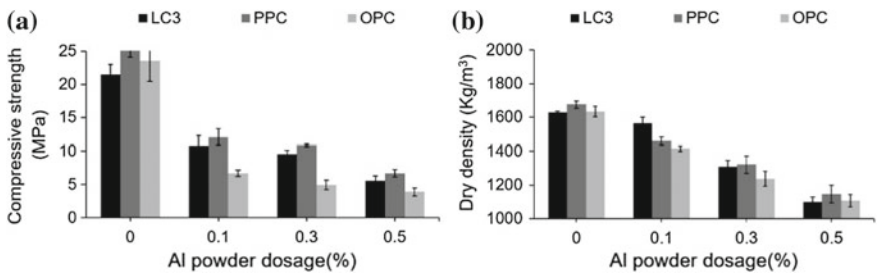
Fig. 5 **a** Compressive strength and **b** dry density variation in different systems with Al powder dosage at w/b ratio 0.4

3.2 Compressive Strength Variation in OPC, PPC, and LC^3 Systems

Figure 5 shows the strength and the dry density measured for PC, PPC, and LC^3 for various Al powder dosages. Systems using 0.4 water-to-binder ratio and 20 °C as initial curing temperature are shown. LC^3 and PPC show similar results in terms of strength and dry density. Both systems perform slightly better than PC.

3.3 Comparison of Similar Densities in OPC, PPC, and LC^3 Systems

Finally, two different densities such as 1300 and 1000 kg/m^3 are designed in all the systems by varying the Al powder dosage. In case of 1300 kg/m^3, the required amounts of Al powder dosage for LC^3, PPC, and OPC are 0.30, 0.32, and 0.21%. 1000 kg/m^3 dry density was obtained by utilizing the Al powder dosage in LC^3, PPC, and OPC which are 0.58, 0.68 and 0.61%. The designed and obtained densities

Fig. 6 Comparison of hardened properties in various systems at similar dry densities. **a** Dry density 1300 kg/m^3; **b** dry density 1000 kg/m^3

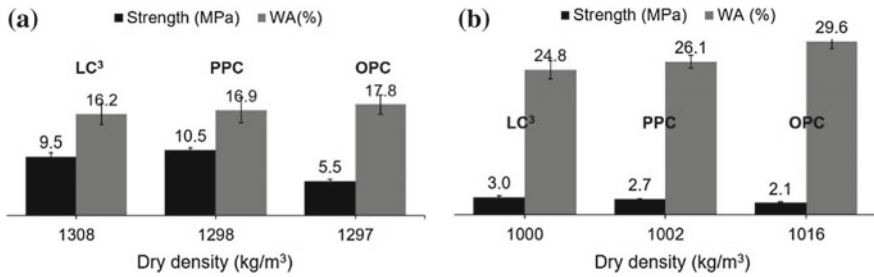in various systems are shown in Fig. 6. The strength and water absorption for each density in all the systems are also plotted in the same figure. Results clearly show that designed and obtained densities in all the systems are very close. Lower density leads to lower strength and higher water absorption. At higher density (1300 kg/m^3), LC^3 and PPC systems show almost similar strength and water absorption. OPC system reaches lower strength and higher water absorption. Coming to lower density (1000 kg/m^3), LC^3 performs better than the two other blends, as shown by the higher strength measured.

4 Conclusions

The following conclusions are drawn from this study.

1. LC^3-based lightweight blocks are produced with lower density with 3 MPa compressive strength.
2. LC^3 system required lesser Al powder dosage compared to PPC and OPC systems for low-density blocks.
3. LC^3 system shows good performance compared to PPC and OPC systems.
4. In all the systems, density is proportional to the compressive strength and inversely proportional to water absorption.
5. Higher initial curing temperature followed by autoclave process does not show much influence to the overall strength development.
6. Water-to-binder ratio plays a major role in strength development.

References

1. Nambiar, E., Ramamurthy, K.: Air-void characterisation of foam concrete. Cem. Concr. Res. **37**(2), 221–230 (2007)
2. Ramamurthy, K., Kunhanandan Nambiar, E.K., Indu Siva Ranjani, G.: A classification of studies on properties of foam concrete. Cem. Concr. Compos. **31**(6), 388–396 (2009)
3. Wongkeo, W., Thongsanitgarn, P., Pimraksa, K., Chaipanich, A.: Compressive strength, flexural strength and thermal conductivity of autoclaved concrete block made using bottom ash as cement replacement materials. Mater. Des. **35**, 434–439 (2012)
4. Amran, Y.M., Farzadnia, N., Ali, A.A.: Properties and applications of foamed concrete: a review. Constr. Build. Mater. **10**, 990–1005 (2015)
5. Jerman, M., Keppert, M., Vyborny, J., Cerny, R.: Hygric, thermal and durability properties of autoclaved aerated concrete. Constr. Build. Mater. **41**(4), 352–359 (2013)
6. Yang, K.H., Lee, K.H.: Tests on high-performance aerated concrete with a lower density. Constr. Build. Mater. **74**, 109–117 (2015)
7. Zhang, Z., Provis, J.L., Reid, A., Wang, H.: Mechanical, thermal insulation, thermal resistance and acoustic absorption properties of geopolymer foam concrete. Cem. Concr. Compos. **62**, 97–105 (2015)
8. Narayanan, N., Ramamurthy, K.: Structure and properties of aerated concrete: a review. Cem. Concr. Compos. **22**(5), 321–329 (2000)
9. Muthu Kumar, E., Ramamurthy, K.: Effect of fineness and dosage of aluminium powder on the properties of moist-cured aerated concrete. Constr. Build. Mater. **95**, 486–496 (2015)
10. Isu, N., Teramura, S., Ishida, H., Mitsuda, T.: Influence of quartz particle size on the chemical and mechanical properties of autoclaved aerated concrete (II) fracture toughness, strength and microstructure. Cem. Concr. Res. **25**, 249–254 (1995)
11. Avet, F., Scrivener, K.: Investigation of the calcined kaolinite content on the hydration of Limestone Calcined Clay Cement (LC^3). Cem. Concr. Res. **62**, 97–105 (2015)

Alternative Masonry Binders and Units Using LP Cement–Soil–Brick Powder Blend and Low-Molar Alkaline Solution

P. T. Jitha, Pooja Revagond and S. Raghunath

Abstract Small-scale production of low-cost cements can be an alternative to the conventional cement in the masonry applications. Lime-based products can potentially replace ordinary Portland cement (OPC) in the production of masonry mortar. Lime–pozzolana cement (LPC) is one such binder which can be produced using low capital-intensive infrastructure. They can be used as alternatives to conventional mortar in low-rise load-bearing masonry applications. A variety of locally available ingredients can be used along with LPC to produce moderate-to-high-strength mortars. This paper provides the details of the mortar mixes which have been produced using predominantly soil and brick powder. An attempt has been made to mobilize the strength gain not only through the hydration of the LPC and pozzolanic materials but also through low-molar alkaline activation. It is well known that alkaline solution can be used with reactive silica and/or alumina, and alkali activation can be achieved even at ambient tropical temperatures. This paper provides the details of how the alkaline solution was optimized. Mortars need to be evaluated for strength and workability. All the strength properties needed for classification of mortar have been evaluated. It is found that the strength development depends on the combination of pozzolanic reaction and geopolymerization. All the mixes achieved adequate strength for application in masonry construction. The masonry properties are comparable to cement mortar, and some values have outperformed.

Keywords Alternative mortar · Lime–pozzolana cement · Alkaline solution · Brick powder

P. T. Jitha (✉)
Research Scholar, Dept. of Civil Engineering, BMS College of Engineering, Bangalore, India
e-mail: jithapt@gmail.com

P. Revagond
Formerly PG Student, Central University of Karnataka, Gulbarga, India
e-mail: pooja.revagond@gmail.com

S. Raghunath
Professor, Dept. of Civil Engineering, BMS College of Engineering, Bangalore, India
e-mail: raghu.civ@bmsce.ac.in

1 Introduction

The acceptance of alternative building materials and technology in masonry building construction is still in a nascent stage. Currently used building materials are predominantly cement based and are capital- and energy-intensive. Limestone deposits that are not utilized by cement industry can be exploited to produce lime and lime-based cements, at a lower cost [1]. In the current scenario, the use of lime and lime-based materials in buildings are yet to cross the label 'local or rural material', and the benefits of these are under-explored. The practice of the blend of surkhi (burnt clay) and lime was popular till the twentieth century until the advent of cement. They are excellent for the masonry mortar and masonry units as the three-to-four-storied building seldom requires more than 10 MPa strength [2]. According to Yogananda et al., lime–pozzolana cement (LPC) can replace the ordinary Portland cement (OPC) in load-bearing masonry buildings [3].

The artificial and natural pozzolanas like ground-granulated blast furnace slag (GGBS), fly ash, burnt clay from bricks, clay tiles, etc., can be potentially utilized as supplementary cementitious materials. A major portion of the industrial by-products, GGBS and fly ash are generally consumed by concrete industry. Grist et al. [4] challenged the misconception that the lime-based construction materials are weak, slow setting and cannot replace the conventional cement in their study on lime-based mortars. Their study explored the possibilities to produce alternative mortar with compressive strength of 25 MPa using pozzolanas like silica fume, GGBS, etc.

Another emerging dimension in the current context relates to re-cycling or re-engineering of construction and demolition waste (CDW) that are available in large quantities. Brick masonry waste has a potential of being used as a pozzolanic material in lime-based products. The daily production of CDW is roughly 3200 tonnes per day in Bangalore [5]. Yet another study shows that in India, the bricks and masonry contribute 30–35% of the total CDW which is 3–4 million tonnes annually [6]. The utilization of this by a small percentage as fine or coarse aggregates in masonry products can reduce the material that goes to landfill. The recycled or crushed fine or coarse brick aggregates cannot be used in conventional concrete. There are very few studies in this regard.

Soil which is plentiful in nature can be potentially utilized for the masonry binders or blocks. There are extensive studies on stabilized mud blocks (SMB). The development of the block-making machine 'Mardini press' gave wider acceptance to SMBs [7]. Burnt clay as surkhi has been explored by many researchers [3, 8]. Metakaolin (MK)-based studies are in plenty, but soil remained as less explored material [9, 10]. It is reported that MK can be used as an additive, as pozzolanic material in Portland cement concretes or activated directly mixing with lime [11].

Geopolymer is emerging as an alternative to cement and is reported to be feasible for production of precast unit. It is well-known that geopolymer-based materials are better suited for precast products; nevertheless, masonry can be considered as 'precast' units. A study by Zhang et al. shows that metakaolin-based geopolymer can be effectively used as soil stabilizer for clayey soil [12]. A combination of

geopolymerization and pozzolanic reaction can be utilized in masonry production. As the alkaline solution is not available naturally, it may affect the cost factor, but low-molar alkaline solution can be taken into consideration. The low-molar alkali activation can be achieved even at ambient tropical temperatures. Solar curing along with locking of moisture can be achieved by sealing the samples in plastic covers and keeping it under sunlight [13].

There is a scope to develop low energy-intensive, cost-effective and sustainable alternative masonry products with LPC or pozzolana cement along with alkaline solution and other industrial by-products. In the current study, an attempt has been made to develop alternative masonry binders and blocks with locally available materials and low-molar alkaline solution as activators.

2 Objectives

The objectives of the experimental study are as follows:

- Bind the ingredients using low-molar alkaline solution
- Evaluate mortar strength and other masonry properties
- Evaluate the physical properties of bricks made using LPC, low-molar alkaline solution and brick masonry waste.

3 Experimental Program

The preliminary study involves production of LPC with locally available materials, low energy-intensive and in small scale by unskilled manpower. Further, the characterization of materials and the optimization of alkaline solution are done. Then, LPC–soil–brick aggregates geopolymer masonry products are developed, and the strength properties are evaluated.

A series of studies have been done to optimize the alkaline solution, i.e. 8–4 M, and then it further reduced to 2 M alkaline solution. Further, an attempt has been made to reduce the sodium hydroxide to sodium silicate ratio, i.e. from 1:2.5 to 1:1 [13, 14].

3.1 Materials

LPC: It is produced in custom-made kiln in laboratory conditions. Soil passing through 600 μm and calcium carbonate in 1:1 proportion are used in the production. They, along with water, are mixed thoroughly in pan mixer and spread on an acrylic sheet to a 10 mm thickness, cut into 100×100 mm to make briquettes. It is then
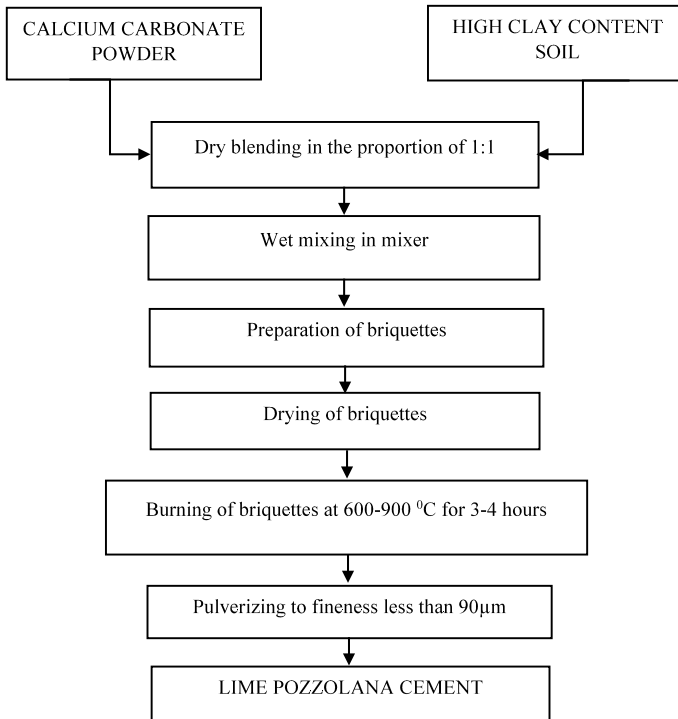
Fig. 1 Flowchart for LPC production

allowed to dry and stored. Further, it is burnt in the kiln at a temperature of 600–900 °C for 3–4 h. The burnt briquettes are then powdered to a size less than 90 μm and stored in air-tight containers [13]. The flowchart for the production of LPC is shown in Fig. 1. The physical characteristics of LPC as per IS 4098-1983 are provided in Table 1.

GGBS: Commercially available GGBS is used in combination with LPC. The specific gravity of GGBS is found to be 2.68 and fineness of 416 m^2/kg.

Cement: The OPC of 53 grades is used to replace LPC partially to compare the strength parameters. The specific gravity of GGBS is found to be 3.15 and fineness of 340 m^2/kg.

Soil: The soil procured locally is crushed and sieved through 2.36 mm sieve. The physical properties of soil are determined as per IS 1498-1970 [15] and provided in Table 2.

Brick powder: Surkhi can be used as substitute of sand for concrete and mortar, and almost the same function as of sand. In current study, the bricks are crushed in the ball mill and sieved through 2.36-mm sieve. The specific gravity is 2.5, and the water absorption is of 20%.

Table 1 Physical properties of the LPC [14]

SI. No.	Parameters tested	Values	Requirements
1	Specific gravity	2.58	–
2	Fineness by air permeability test	844.6 m^2/kg	Minimum 250 m^2/kg
3	Initial setting time	4 h	Minimum 2 h
4	Final setting time	24 h	Maximum 48 h
5	Normal consistency	80%	–
6	Soundness test	6–3 mm	<10 mm
7	7-day average wet compressive strength of mortar cubes of 50 mm size (1LPC:3Sand)	0.73 MPa	Minimum 0.3 MPa for LP7 grade LPC
8	28-day average wet compressive strength of mortar cubes of 50 mm size (1LPC:3Sand)	1.25 MPa	Minimum 0.7 MPa for LP7 grade LPC

Table 2 Physical properties of soil

SI. No.	Parameter tested	Values
1	Specific gravity	2.60
2	Liquid limit	34.00
3	Plastic limit	16.63
4	Shrinkage limit	14.84
5	Plasticity index	17.73
6	Free swell ratio	1.05
7	Sand content (%)	14
8	Silt content (%)	36
9	Clay content (%)	50
10	Type of soil based on IS classification	CH-fine grained, highly compressible clay

Brick aggregates: The bricks are crushed, and the material passing through 10 mm and retained on 4.75-mm sieve is collected as aggregates. The specific gravity is 2.2, and the water absorption is 15%.

Alkaline solution: Alkaline solution of 2 M, NaOH and Na_2SiO_3 in the ratio 1:1 is used.

3.2 Process

The materials are weighed according to their proportion and dry mixed thoroughly in planetary mixer. Next, the alkaline solution is added to get the desired consistency.

Fig. 2 Combination cured
samples

The mix is filled into the prepared moulds by 'adobe method' which can be achieved
without compaction energy. The adobe method is preferred since the mix is in plastic
form. The quantity of solution is on higher side compared to SMBs or rammed earth.
The mixes with alkaline solution settle quickly making compaction difficult. One of
the main advantages of adobe process is the non-usage of any compaction equipment
and thus can avoid capital cost.

The samples are demoulded once they are set and cured by 'combination curing'.
To achieve both geopolymerization and pozzolanic reaction, moisture-trapped heat
curing is availed. The combination of cured samples is shown in Fig. 2.

3.3 LPC–Brick Aggregates Alkaline Solution-Based Mortar Mixes

Different mortar mixes using LPC, cement, GGBS, brick powder (brick bats crushed
to sand size) in different proportion and geopolymer solution of 2 M 1:1 are studied.
Various mix proportions studied are shown in Table 3.

Results and Discussion

The mortar strength is mainly evaluated by its workability and bond strength. The
workability of mortar is significant to cater the aesthetics and workmanship in addi-
tion to the flow and cohesion. The adequate bond strength is important to resist wind
or earthquake or any other movement. In-plane shear stresses are developed due to

Table 3 LPC–brick aggregates alkaline solution-based mortar mixes

SI. No.	Mix	Proportion of materials used				
		LPC	Cement	GGBS	Soil	Brick powder
1	M1	1	–	–	1	2
2	M2	0.5	0.5	–	1	2
3	M3	0.5	–	0.5	1	2

lateral loads such as earthquake. There are different bond strength evaluation methods available. In the current study, the bond strength is found in two ways—tensile adhesion by cross-couplet and shear strength by triplet test.

All the strength and physical mortar characteristics are tested for all the mixes mentioned in Table 3. The respective results are compared with cement mortar 1:6 (CM) [16].

The burnt clay bricks of size 230 × 105 × 75 mm which are procured locally are used for tensile adhesion test and triplet test. The average compressive strength and water absorption of the brick are 7.5 Mpa and 18%, respectively.

The cross-couplet test set-up and tested sample are provided in Fig. 3. It is observed that the failure happened in the brick for few samples instead of the mortar joints because of high tensile strength of mortar and very good bond strength.

The shear strength of the mortar is found by triplet test. The set-up and the sample are shown in Fig. 4. The samples have outperformed, and the failure happened in
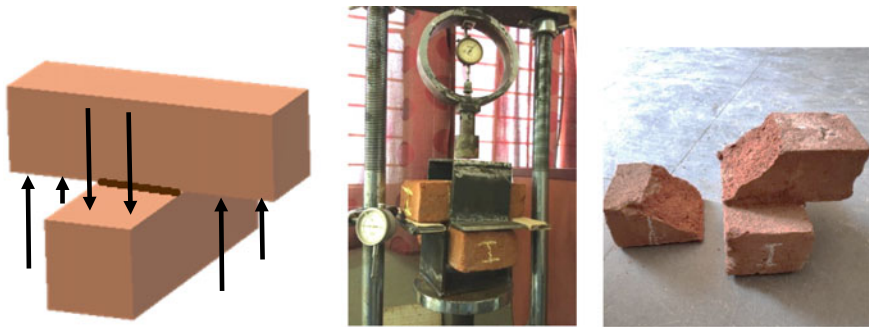

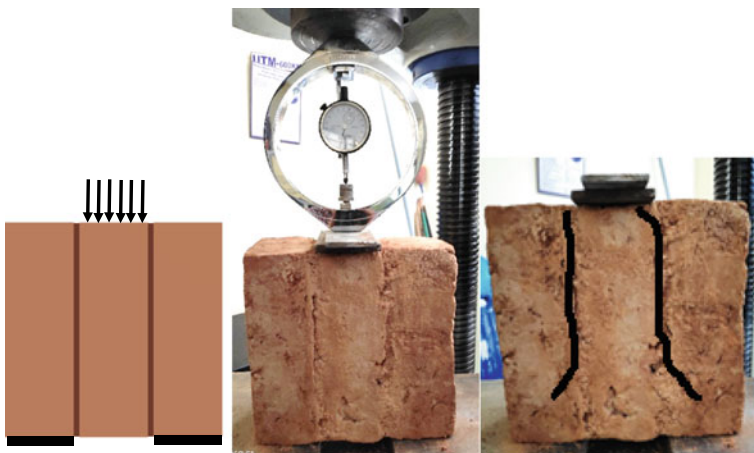**Fig. 3** Cross-couplet test set-up and tested sample

Fig. 4 Triplet shear test set-up and tested sample with failure pattern

Table 4 Test results on LPC–brick aggregates alkaline solution-based mixes

SI. No.	Tests	Mortar mixes			CM [16]
		M1	M2	M3	
Strength characteristics					
1	Wet compressive strength (MPa)	11.20	17.30	20.00	5.20
2	Flexural strength (MPa)	2.30	3.53	2.94	1.93
3	Tensile strength based on briquettes (MPa)	1.14	1.28	1.41	0.89
4	Tensile adhesion by cross-couple test (MPa)	0.09	0.12	0.11	–
5	Shear strength by triplet test (MPa)	0.30	0.34	0.40	0.023
Physical characteristics					
1	Water absorption (%)	14.50	14.80	10.00	–
2	Mortar density (kg/m^3)	1899	1927	1929	2100
3	Workability (% of solution)	35	28	27	45
4	Initial setting time (min)	6	12	18	30
5	Final setting time (min)	20	34	40	600

brick for few samples. The strength and physical characteristics' results are shown in Table 4.

The compressive strength of all the mixes has attained target strength and falls under the category of H1 grade as per IS 1905-1987 [2]. Tensile and flexure strength of the mixes are high compared to CM 1:6 [16]. Tensile and shear bond strength of the mixes are found to be high in all mixes. Initial setting time of the mixes is low compared to cement mortar and should find a way to delay the quick setting for better workability.

3.4 LPC–Soil–Brick Aggregates Alkaline Solution-Based Units

The mortar mixes with LPC, cement, GGBS, soil passing 2.36-mm sieve and brick aggregates are outperformed in all different mix varieties. An attempt has been made

to develop blocks using brick aggregates in addition to mortar mixes. The mixes are listed in Table 5.

Results and Discussion

The custom-made brick moulds of size 230 × 105 × 75 mm are used for casting bricks. The mould consists of a bottom plate with frog and two detachable side pieces which are screwed together for the ease of demoulding.

The compressive strength and water absorption tests are conducted for all the units. The test results are shown in Table 6.

The developed brick mould, brick with compression strength test set-up and the tested sample are shown in Fig. 5.

Table 5 LPC–brick aggregates alkaline solution-based units

GP Mix	Proportion of materials used					
	LPC	Cement	GGBS	Soil	Brick powder	Brick aggregates
SB-1	1	–	–	1	2	4
SB-2	0.5	0.5	–	1	2	4
SB-3	0.5	–	0.5	1	2	4

Table 6 Test results for LPC–brick aggregates alkaline solution-based units

Mix	Average compressive strength (MPa)	Water absorption (%)
SB-1	4.5	17.3
SB-2	4.6	17.1
SB-3	8.2	12.2

Fig. 5 Brick mould, compression test set-up and tested brick

The strength of all the brick samples is satisfying, and it is noticed that SB-3 outperformed of all other mixes. The failure pattern is of 'hourglass' failure, and the cracks through the brick aggregate indicate good interface bonding.

4 Concluding Remarks

- Locally available soil with high clay content can be used for producing mortar/units with less energy in an economic way.
- Surkhi/brick powder can be used as replacement of sand, since it adds more amount of silica and alumina and also acts as filler material.
- The combination of LPC and GGBS has given high compressive strength and less water absorption as compared to other mixes. It is found that it has good workability and could achieve high strength.
- Combination curing ensured the thermal activation without moisture loss which was required for hydration in all the mixes.

References

1. Rai, M.: Building Materials in India, 50 Years: A Commemorative Volume. Building Materials & Technology Promotion Council, New Delhi (1998)
2. IS: 1905–1987: Indian Standard Code of Practice for Structural Use of Unreinforced Masonry, 3rd edn. Bureau of Indian Standards, New Delhi, India, 1987 Reaffirmed (2002)
3. Yogananda, M.R., Jagadish, K.S., Kumar, R.: Studies on Surkhi and Rice Husk Ash Pozzolana. ASTRA, IISC, Bengaluru (1983)
4. Grist, E.R., Paine, K.A., Heath, A., Norman, J., Pinder, H.: Compressive strength development of binary and ternary lime–pozzolan mortars. Mater. Des. **52**, 514–523 (2013)
5. CSTEP, Vunnam, V., Ali, M.S., Singh, A., Asundi, J.: Construction and Demolition Waste Utilisation for Recycled Products in Bengaluru: Challenges and Prospects, New Delhi, India (2016)
6. TIFAC (ed.): Utilization of Waste from Construction Industry, Department of Science & Technology, New Delhi (2000)
7. Jagadish, K.S., Venkatarama Reddy, B.V., Nanjunda Rao, K.S.: Alternative Building Materials and Technologies. New Age International (P) Ltd Publishers, Bengaluru (2007)
8. Phalanetra, H.R., Sharada, R.H., Jagadish, K.S.: Building materials using fly ash and other pozzolana. Report submitted to KSCST, Department of science and technology, Government of India by Gramvidhya (1997)
9. Alonso, S., Palomo, A.: Calorimetric study of alkaline activation of calcium hydroxide-metakaolin solid mixtures. Cem. Concr. Res. **31**, 25–30 (2001)
10. Provis, J.L., Yong, S.L., Duxson, P.: Nanostructure/microstructure of metakaolin geopolymers. In: Geopolymers—Structure, Processing, Properties and Industrial Applications. Woodhead Publishing Ltd, UK (2009)
11. Sabir, B.B., Wild, S., Bai, J.: Metakaolin and calcined clays as pozzolana for concrete: a review. Cem. Concr. Compos. **23**, 441–454 (2001)
12. Zhang, M., Guo, H., El-Korchi, T., Zhang, G., Tao, M.: Experimental feasibility study of geopolymer as next generation soil stabilizer. Constr. Build. Mater. **47**, 1468–1478 (2012)

13. Jyothi, T.K., Jitha, P.T., Pattaje, S.K., Jagadish, K.S., Ranganath, R.V., Raghunath, S.: Studies on the strength development of lime-pozzolana cement-soil-brick powder based geopolymer composites. J. Inst. Eng. (India): Ser. A (2018)
14. Jitha, P.T., Kumar, B.S., Raghunath, S.: Studies on strength development of geopolymer stabilized soil-LPC (lime-pozzolana-cement) mortars. In: Earthen Dwellings and Structures, pp. 215–224. Springer Transactions in Civil and Environmental Engineering (2019)
15. IS: 4098-1983: Specification for Lime-Pozzolana Mixture. Bureau of Indian Standards, New Delhi, India, Reaffirmed (2009)
16. Keshava, M.: Behaviour of masonry under axial, eccentric and lateral loading. PhD Thesis, Department of Civil Engineering, B.M.S College of Engineering, Bengaluru, India (2012)